The RISING Project

Publications

GSI Helmholtzzentrum für Schwerionenforschung, Darmstadt

June 2012

Publications (fast beam campaign)

- Investigation of scintillation detectors for relativistic heavy ion calorimetry
  R. Lozeva, A. Banu, D. Balabanski, J. Gerl, M. Gorska, I. Kojouharov, Y. Kopatch, S. Mandal, H. Schaffner and H.J. Wollersheim;
  Nucl. Instr. Meth. B204 (2003) 678
- Rare isotope investigation at GSI (RISING) using gamma-ray spectroscopy at relativistic energies
  H.J. Wollersheim, D.E. Appelbe, A. Banu, R. Bassini, T. Beck, F. Becker, P. Bednarczyk, K.-H. Behr, M.A. Bentley, G. Benzoni, C. Boiano, U. Bonnes, A. Bracco, S. Brambilla, A. Brünle, A. Bürger, K. Burkard, P.A. Butler, F. Camera, D. Curien, J. Devin, P. Doornenbal, C. Fahlander, K. Fayz, H. Geissel, J. Gerl, M. Gorska, H. Grawe, J. Grebosz, R. Griffiths, G. Hammond, M. Hellström, J. Hoffmann, H. Hübel, J. Jolie, J.V. Kalben, M. Kmiecik, I. Kojouharov, R. Kulessa, N. Kurz, I. Lazarus, J. Li, J. Leske, R. Lozeva, A. Maj, S. Mandal, W. Meczynski, B. Million, G. Münzenberg, S. Muralithar, M. Mutterer, P.J. Nolan, G. Neyens, J. Nyberg, W. Prokopowicz, V.F.E. Pucknell, P. Reiter, D. Rudolph, N. Saito, T.R. Saito, D. Seddon, H. Schaffner, J. Simpson, K.-H. Speidel, J. Styczen, K. Sümmerer, N. Warr, H. Weick, C. Wheldon, O. Wieland, M. Winkler and M. Zieblinski;
  Nucl. Instr. Meth. A537 (2005) 637
- Spectroscopy of nuclei approaching the proton drip-line using a secondary fragmentation technique with the RISING detector array
  M.J. Taylor, G. Hammond, M.A. Bentley, F. Becker, J. Grebosz, A. Banu, C.J. Barton, T. Beck, P. Bednarczyk, A. Bracco, A.M. Bruce, L.C. Bullock, A. Bürger, F. Camera, C. Chandler, P. Doornenbal, J. Gerl, H. Geissel, M. Gorska, M. Hellström, D.S. Judson, I. Kojouharov, N. Kurz, R. Lozeva, A. Maj, S. Mandal, B. Mc Guirk, S. Muralithar, E.S. Paul, Z. Podolyak, W. Prokopowicz, D. Rudolph, N. Saito, T.R. Saito, H. Schaffner, J. Simpson, D.D. Warner, H. Weick, C. Wheldon, M. Winkler and H.J. Wollersheim;
  J. Phys. G: Nucl. Part. Phys. 31 S1527 (2005)
- Identification of heavy ion reaction channels with a new CAlorimeter TElescope within RISING
  R. Lozeva, J. Gerl, M. Gorska, S. Mandal, D. Balabanski, I. Kojouharov, F. Becker, J. Grebosz, A. Banu, P. Bednarczyk, P. Doornenbal and H.J. Wollersheim;
  J. Phys. G: Nucl. Part. Phys. 31 S1917 (2005)
- Status of the RISING project at relativistic energies
  P. Bednarczyk, A. Banu, T. Beck, F. Becker, M.A. Bentley, G. Benzoni, A. Bracco, A. Bürger, F. Camera, P. Doornenbal, C. Fahlander, H. Geissel, J. Gerl, M. Gorska, H. Grawe, J. Grebosz, G. Hammond, M. Hellström, H. Hübel, J. Jolie, M. Kmiecik, I. Kojouharov, N. Kurz, R. Lozeva, A. Maj, S. Mandal, W. Meczynski, B. Million, S. Muralithar, P. Reiter, D. Rudolph, N. Saito, T.R. Saito, H. Schaffner, J. Simpson, J. Styczen, N. Warr, H. Weick, C.

Wheldon, O. Wieland, M. Winkler and H.J. Wollersheim;
Acta Phys. Pol. B36 (2005) 1235

- Calorimeter telescope for identification of relativistic heavy ion reaction channels
  R. Lozeva, S. Mandal, J. Gerl, M. Gorska, J. Grebosz, I. Kojouharov, J. Adamczewski, A. Banu, F. Becker, T. Beck, P. Bednarczyk, A. Blazhev, P. Doornenbal, H. Geissel, M. Hellström, M. Kavatsyuk, O. Kavatsyuk, N. Kurz, M. Mutterer, S. Muralithar, G. Münzenberg, W. Prokopowicz, N. Saito, T.R. Saito, H. Schaffner, K. Sümmerer, H. Weick, M. Winkler, C. Wheldon and H.J. Wollersheim;
  Acta Phys. Pol. B36 (2005) 1245
- Relativistic Coulomb excitation of ^{54,56,58}Cr
  A. Bürger, T.R. Saito, A. Al-Khatib, A. Banu, T. Beck, F. Becker, P. Bednarczyk, G. Benzoni, A. Bracco, P. Bringel, F. Camera, E. Clement, P. Doornenbal, H. Geissel, J. Gerl, M. Gorska, A. Görgen, H. Grawe, J. Grebosz, G. Hammond, M. Hellström, H. Hübel, M. Kavatsyuk, O. Kavatsyuk, M. Kmiecik, I. Kojouharov, N. Kurz, R. Lozeva, A. Maj, S. Mandal, W. Meczynski, D. Mehta, B. Million, S. Muralithar, A. Neusser, Zs. Podolyak, T.S. Reddy, P. Reiter, N. Saito, H. Schaffner, A.K. Singh, H. Weick, O. Wieland, C. Wheldon, M. Winkler and H.J. Wollersheim;
  Acta Phys. Pol. B36 (2005) 1249
- Spectroscopy of T=3/2 mirror nuclei via two-step fragmentation using RISING
  G. Hammond, M.A. Bentley, F. Becker, J. Grebosz, M.J. Taylor, A. Banu, C.J. Barton, T. Beck, P. Bednarczyk, A. Bracco, A. M. Bruce, L.C. Bullock, A. Bürger, F. Camera, C. Chandler, P. Doornenbal, J. Gerl, H. Geissel, M. Gorska, M. Hellström, D. Judson, I. Kojouharov, N. Kurz, R. Lozeva, A. Maj, S. Mandal, B. Mc Guirk, S. Muralithar, E.S. Paul, Z. Podolyak, W. Prokopowicz, D. Rudolph, N. Saito, T.R. Saito, H. Schaffner, J. Simpson, D.D. Warner, H. Weick, C. Wheldon, M. Winkler and H.J. Wollersheim;
  Acta Phys. Pol B36 (2005) 1253
- Future RISING experiments at relativistic energies
  P. Reiter, F. Becker, M.A. Bentley, A. Bracco, G. de Angelis, C. Fahlander, J. Gerl, M. Gorska, H. Grawe, H. Hübel, J. Jolie, A. Maj, P. Mayet, T.R. Saito, K.-H. Speidel and H.J. Wollersheim;
  Acta Phys. Pol. B36 (2005) 1259
- Relativistic Coulomb excitation of neutron-rich ^{54,56,58}Cr: On the pathway of magicity from N=40 to N=32
  A. Bürger, T.R. Saito, H. Grawe, H. Hübel, P. Reiter, J. Gerl, M. Gorska, H.J.Wollersheim, A. Al-Khatib, A. Banu, T. Beck, F. Becker, P. Bednarczyk, G. Benzoni, A. Bracco, S. Brambilla, P.Bringel, F. Camera, E. Clement, P. Doornenbal, H. Geissel, A. Görgen, J. Grebosz, G. Hammond, M. Hellström, M. Honma, M. Kavatsyuk, O. Kavatsyuk, M. Kmiecik, I. Kojouharov, W. Korten, N. Kurz, R. Lozeva, A. Maj, S. Mandal, B. Million, S. Muralithar, A. Neußer, F. Nowacki, T. Otsuka, Z. Podolyak, N. Saito, A.K. Singh, H. Weick, C. Wheldon, O. Wieland, and M. Winkler;
  Phys. Lett. B622 (2005) 29

- Status of the RISING project at GSI
  F. Becker, A. Banu, T. Beck, P. Bednarczyk, P. Doornenbal, H. Geissel, J. Gerl, M. Gorska, H. Grawe, J. Grebosz, M. Hellström, I. Kojouharov, N. Kurz, R. Lozeva, S. Mandal, S. Muralithar, W. Prokopowicz, N. Saito, T.R. Saito, H. Schaffner, H. Weick, C. Wheldon, M. Winkler, H.J. Wollersheim, J. Jolie, P. Reiter, N. Warr, A. Bürger, H. Hübel, J. Simpson, M.A. Bentley, G. Hammond, G. Benzoni, A. Bracco, F. Camera, B. Million, O. Wieland, M. Kmiecik, A. Maj, W. Meczynski, J. Styczen, C. Fahlander and D. Rudolph;
  Euro. Phys. Jour. A25 (2005) 719
- Rare Isotopes investigations at GSI (RISING) using relativistic beams
  J. Jolie, G. Ilie, P. Reiter, A. Richard, A. Scherillo, T. Striepling, N. Warr, A. Banu, F. Becker, P. Bednarczyk, P. Doornenbal, J. Gerl, H. Grawe, M. Gorska, R. Grzywacz, I. Kojouharov, S. Mandal, N.Saito, T.R. Saito, H.J. Wollersheim, S. Mallion, G. Neyens, K. Turzo, P. van Duppen, N. Vermeulen, Z. Podolyak, W. Gelletly, P.H. Regan, P.M. Walker, W.N. Catford, Z. Liu, S. Williams, A. Blazhev, R. Lozeva, P. Detistov, L. Atanasova, G. Damyanova, D. Cortina Gil, J. Benlliure, T. Kurtukian-Nieto, E. Caserejos, J.M. Daugas, G. Belier, V. Meot, O. Roig, G. Simpson, I.S. Tsekhanovich, I. Matea, R. Schwengner, M. Hass, B.S. Nara Singh, S.K. Chamoli, G. Goldring, I. Regev, S. Vaintraub, D.L. Balabanski, G. Lo Bianco, K. Gladnishki, A. Saltarelli, C. Petrache, G. Benzoni, N. Blasi, A. Bracco, F. Camera, B. Million, S. Leoni, O. Wieland, A. Maj, M. Kmiecik, J. Grebosz, P. Bednarczyk, J. Styczen, M. Lach, W. Meczynski, K. Mazurek, M. Pfützner, A. Korgul, M. Ionescu-Bujor, A. Iordachescu, V. Zamfir and A. Jungclaus;
  Exotic nuclei and Nuclear/Particle Astrophysics, Proceedings of the Carpathian Summer School of Physics 2005, (ed. S. Stoica, L.Trache and R.E. Tribble, World Scientific 2006)
- ^{108}Sn studied with intermediate-energy Coulomb excitation
  A. Banu, J. Gerl, C. Fahlander, M. Gorska, H. Grawe, T.R. Saito, H.J. Wollersheim, E. Caurier, T. Engeland, A. Gniady, M. Hjorth-Jensen, F. Nowacki, T. Beck, F. Becker, P. Bednarczyk, M.A. Bentley, A. Bürger, F. Cristancho, G. de Angelis, Z. Dombradi, P. Doornenbal, H. Geissel, J. Grebosz, G. Hammond, M. Hellström, J. Jolie, I. Kojouharov, N. Kurz, R. Lozeva, S. Mandal, N. Marginean, S. Muralithar, J. Nyberg, J. Pochodzalla, W. Prokopowicz, P. Reiter, D. Rudolph, C. Rusu, N. Saito, H. Schaffner, D. Sohler, H. Weick, C. Wheldon and M. Winkler;
  Phys. Rev. C72 061305 (2005)
- A novel Calorimeter Telescope for identification of relativistic heavy-ion reaction channels
  R. Lozeva, J. Gerl, M. Gorska, I. Kojouharov, S. Mandal, H.J. Wollersheim, D. Balabanski, F. Becker, J. Grebosz, A. Banu, P. Bednarczyk, P. Doornenbal and H. Schaffner;
  Nucl. Instr. Meth. A 562, 298 (2006)
- Shell structure, collectivity and nuclear shapes – RISING in-beam experiments at relativistic energies
  P. Doornenbal; Int. Jour. Mod. Phys. E15 1495 (2006)

- RISING: Gamma-ray Spectroscopy with Radioactive Beams at GSI
  P. Doornenbal, A. Bürger, D. Rudolph, H. Grawe, H. Hübel, P.H. Regan, P. Reiter, A. Banu, T. Beck, F. Becker, P. Bednarczyk, L. Caceres, H. Geissel, J. Gerl, M. Gorska, J. Grebosz, M. Kavatsyuk, O. Kavatsyuk, A. Kelic, I. Kojouharov, N. Kurz, R. Lozeva, F. Montes, W. Prokopowicz, N. Saito, T.R. Saito, H. Schaffner, S. Tashenov, H. Weick, E. Werner-Malento, M. Winkler, H.J. Wollersheim, A. Al-Khatib, L.L. Andersson, L. Atanasova, D.L. Balabanski, M.A. Bentley, G. Benzoni, A. Blazhev, A. Bracco, S. Brambilla, C. Brandau, P. Bringel, J.R. Brown, F. Camera, S. Chmel, E. Clement, F.C.L. Crespi, C. Fahlander, A.B. Garnsworthy, A. Görgen, G. Hammond, M. Hellström, R. Hoischen, H. Honma, E.K. Johansson, A. Jungclaus, M. Kmiecik, W. Korten, A. Maj, S. Mandal, W. Meczynski, B. Million, A. Neußer, F. Nowacki, T. Otsuka, M. Pfützner, S. Pietri, Z. Podolyak, A. Richard, M. Seidlitz, S.J. Steer, T.Striepling, T. Utsuno, J. Walker, N. Warr, C. Wheldon and O. Wieland;
  AIP conference proceedings Vol.891 99 (2007)
- The Cracow Code – an Interactive method of sophisticated online analysis
  J. Grebosz;
  Comp. Phys. Comm. 176 (2007) 251
- The T=2 mirrors ^{36}Ca and ^{36}S: A test for isospin symmetry of shell gaps at the driplines
  P. Doornenbal, P. Reiter, H. Grawe, T. Otsuka, A. Al-Khatib, A. Banu, T. Beck, F. Becker, P. Bednarczyk, G. Benzoni, A. Bracco, A. Bürger, L. Caceres, F. Camera, S. Chmel, F.C.L. Crespi, H. Geissel, J. Gerl, M. Gorska, J. Grebosz, H. Hübel, M. Kavatsyuk, O. Kavatsyuk, M. Kmiecik, I. Kojouharov N. Kurz, R. Lozeva, A. Maj, S. Mandal, W. Meczynski, B. Million, Z. Podolyak, A. Richard, N. Saito, T.R. Saito, H. Schaffner, M. Seidlitz, T. Striepling, Y. Utsuno, J. Walker, N. Warr, H. Weick, O. Wieland, M. Winkler and H.J. Wollersheim; Phys. Lett. B647 (2007) 237
- Nuclear structure far off stability – Rising campaigns
  M. Gorska, A. Banu, P. Bednarczyk, A. Bracco, A. Bürger, F. Camera, E. Caurier, P. Doornenbal, J. Gerl, H. Grawe, M. Honma, H. Hübel, A. Jungclaus, A. Maj, G. Neyens, F. Nowacki, T. Otsuka, M. Pfützner, S. Pietri, Z. Podolyak, A. Poves, P.H. Regan, P. Reiter, D. Rudolph and H.J. Wollersheim;
  Acta Phys. Pol. B 38 (2007) 1219
- Coulomb excitation of ^{68}Ni at 600 AMeV
  A. Bracco, G. Benzoni, N. Blasi, S. Brambilla, F. Camera, F.C.L. Crespi, S. Leoni, B. Million, D. Montanari, M. Pignanelli, O. Wieland, A. Maj, P. Bednarczyk, J. Grebosz, M. Kmiecik, W. Meczynski, J. Styczen, T. Aumann, A. Banu, T. Beck, F. Becker, L. Caceres, P. Doornenbal, H. Emling, J. Gerl, H. Geissel, M. Gorska, O. Kavatsyuk, M. Kavatsyuk, I. Kojouharov, N. Kurz, R. Lozeva, N. Saito, T.R. Saito, H. Schaffner, H.J. Wollersheim, J. Jolie, P. Reiter, N. Warr, G. de Angelis, A. Gadea, D. Napoli, S. Lenzi, S. Lunardi, D. Balabanski, G. Lo Bianco, C. Petrache, A. Saltarelli, M. Castoldi, A.

Zucchiatti, J. Walker and A. Bürger;
Acta Phys. Pol. B 38 (2007) 1229

- Yrast and non-yrast 2^+ states of ^{134}Ce and ^{136}Nd populated in relativistic Coulomb excitation
  T.R. Saito, N. Saito, K. Starosta, J. Beller, N. Pietralla, H.J. Wollersheim, D.L. Balabanski, A. Banu, R.A. Bark, T. Beck, F. Becker, P. Bednarczyk, K.-H. Behr, G. Benzoni, P.G. Bizzeti, C. Boiano, A. Bracco, S. Brambilla, A. Brünle, A. Bürger, L. Caceres, F. Camera, F.C.L. Crespi, P. Doornenbal, A.B. Garnsworthy, H. Geissel, J. Gerl, M. Gorska, J. Grebosz, G. Hagemann, J. Jolie, M. Kavtsyuk, O. Kavatsyuk, T. Koike, I. Kojouharov, N. Kurz, J. Leske, G. Lo Bianco, A. Maj, S. Mallion, S. Mandal, M. Maliage, T. Otsuka, C.M. Petrache, Z. Podolyak, W. Prokopowicz, G. Rainovski, P. Reiter, A. Richard, H. Schaffner, S. Schielke, G. Sletten, N.J. Thompson, D. Tonev, J. Walker, N. Warr, O. Wieland and Q. Zhong;
  Phys.Lett. B 669 (2008) 19
- Search for pygmy dipole resonance in ^{68}Ni at 600MeV/u
  O. Wieland, A. Bracco, F. Camera, G. Benzoni, N. Blasi, S. Brambilla, F.C.L. Crespi, S. Leoni, B. Million, R. Nicolini, A. Maj, P. Bednarczyk, J. Grebosz, M. Kmiecik, W. Meczynski, J. Styczen, T. Aumann, A. Banu, T. Beck, F. Becker, L. Caceres, P. Doornenbal, H. Emling, J. Gerl, H. Geissel, M. Gorska, O. Kavatsyuk, M. Kavatsyuk, I. Kojouharov, N. Kurz, R. Lozeva, N. Saito, T.R. Saito, H. Schaffner, H.J. Wollersheim, J. Jolie, P. Reiter, N. Warr, G. de Angelis, A. Gadea, D. Napoli, S. Lenzi, S. Lunardi, D. Balabanski, G. Lo Bianco, C. Petrache, A. Saltarelli, M. Castoldi, A. Zucchiatti, J. Walker and A. Bürger;
  Phys.Rev.Lett. 102 (2008) 092502
- Lifetime effects for high-resolution gamma-ray spectroscopy at relativistic energies and their implications for the RISING spectrometer
  P. Doornenbal, P. Reiter, H. Grawe, T. Saito, A. Al-Khatib, A. Banu, T. Beck, F. Becker, P. Bednarczyk, G. Benzoni, A. Bracco, A. Bürger, L. Caceres, F. Camera, S. Chmel, F.C.L. Crespi, H. Geissel, J. Gerl, M. Gorska, J. Grebosz, H. Hübel, M. Kavatsyuk, O. Kavatsyuk, M. Kmiecik, I. Kojouharov, N. Kurz, R. Lozeva, A. Maj, S. Mandal, W. Meczynski, B. Million, Zs. Podolyak, A. Richard, N. Saito, H. Schaffner, M. Seidlitz, T. Striepling, J. Walker, N. Warr, H. Weick, O. Wieland, M. Winkler, H.J. Wollersheim;
  Nucl. Instr. Meth. A613 (2010) 218
- In-beam gamma-ray angular distribution and lifetime measurements-Experience from RISING and Perspectives at FAIR
  P.Bednarczyk, J.Grebosz, M.Kmiecik, A.Maj, W.Meczynski, S.Myalski, J.Styczen, C.Domingo-Pardo, P.Doornenbal, J.Gerl , M.Gorska, H.J.Wollersheim, J.Jolie, P.Reiter, A.Bracco, F.Camera
  Acta Phys. Pol. B 41 (2010) 505

Publications (g-RISING)

- g-factor measurements at RISING: The case of ^{127}Sn

  L. Atanasova, D.L. Balabanski, M. Hass, D. Bazzacco, F. Becker, P. Bednarczyk, G. Benzoni, N. Blasi, A. Blazhev, A. Bracco, C. Brandau, L. Caceres, F. Camera, S.K. Chamoli, F.C.L. Crespi, P. Detistov, P. Doornenbal, C. Fahlander, E. Farnea, G. Georgiev, J. Gerl, K. Gladnishki, M. Gorska, H. Grawe, J. Grebosz, R. Hoischen, G. Ilie, M. Ionescu-Bujor, A. Iordachescu, A. Jungclaus, G. Lo Bianco, M. Kmiecik, I. Kojouharov, N. Kurz, S. Lakshmi, R. Lozeva, A. Maj, D. Montanari, G. Neyens, M. Pfützner, S. Pietri, Z. Podolyak, W. Prokopowicz, S. Rudolph, G. Rusev, T.R. Saito, A. Saltarelli, H. Schaffner, R. Schwengner, G. Simpson, S. Tashenov, J.J. Valente-Dubon, N. Vermeulen, J. Walker, E. Werner-Malento, O. Wieland and H.J. Wollersheim;
  Nucl. Theo. 25, ed S. Dimitrova, Heron Press, Sofia, 2006
  The Twenty Fifth International Workshop on Nuclear Theory (Bulgaria)

- First results from the g-RISING campaign: The g-factor of the 19/2+ isomer in ^{127}Sn

  D. Balabanski, L. Atanasova, M. Hass, D. Bazzacco, F. Becker, P. Bednarczyk, G. Benzoni, N. Blasi, A. Blazhev, A. Bracco, L. Caceres, F. Camera, S.K. Chamoli, F. Crespi, P. Detistov, P. Doornenbal, C. Fahlander, E. Farnea, G. Georgiev, J. Gerl, K. Gladnishki, M. Gorska, H. Grawe, J. Grebosz, R. Hoischen, G. Ilie, M. Ionescu-Bujor, A. Iordachescu, A. Jungclaus, G. Lo Bianco, M. Kmiecik, I. Kojouharov, N. Kurz, S. Lakshmi, R. Lozeva, A. Maj, D. Montanari, G. Neyens, M. Pfützner, S. Pietri, Z. Podolyak, W. Prokopowicz, D. Rudolph, G. Rusev, T.R. Saito, A. Saltarelli, H. Schaffner, R. Schwengner, G. Simpson, S. Tachenov, J.J. Valente-Dubon, N. Vermeulen, J. Walker, E. Werner-Malento, O. Wieland, H.J. Wollersheim and M.Hjorth-Jensen;
  EPJ, conf. on Radioactive Nuclear Beams (RNB7) Cortina d'Ampezzo 2006

- g-factor measurements on relativistic isomeric beams produced by fragmentation and U-fission: the g-RISING project at GSI

  G. Neyens, L. Atanasova, D.L. Balabanski, F. Becker, P. Bednarczyk, L. Caceres, P. Doornenbal, J. Gerl, M. Gorska, J. Grebosz, M. Hass, G. Ilie, N. Kurz, I. Kojouharov, R. Lozeva, A. Maj, M. Pfützner, S. Pietri, Z. Podolyak, W. Prokopowicz, T.R. Saito, H. Schaffner, G. Simpson, N. Vermeulen, E. Werner-Malento, J. Walker, H.J. Wollersheim, D. Bazzacco, G. Benzoni, A. Blazhev, N. Blasi, A. Bracco, C. Brandau, F. Camera, S.K. Chamoli, S. Chmel, F.C.L. Crespi, J.M. Daugas, M. De Rydt, P. Detistov, C. Fahlander, E. Farnea, G. Georgiev, K. Gladnishki, R. Hoischen, M. Ionescu-Bujor, A. Iordachescu, J. Jolie, A. Jungclaus, M. Kmiecik, A. Krasznahorkay, R. Kulessa, S. Lakshmi, G. Lo Bianco, S. Mallion, K. Mazurek, W. Meczynski, D. Montanari, S. Myalsky, O. Perru, D. Rudolph, G. Rusev, A. Saltarelli, R. Schwengner, J. Styczen, K. Turzo, J.J. Valiente-Dobon, O. Wieland and M. Zieblinski;
  Acta Phys. Pol. B38 (2006) 1237

- A RISING g-factor measurement of the $19/2^+$ isomer in ^{127}Sn
  L. Atanasova, D.L. Balabanski, M. Hass, F. Becker, P. Bednarczyk, S.K. Chamoli, P. Doornenbal, G. Georgiev, J. Gerl, K.A. Gladnishki, M. Gorska, J. Grebosz, M. Kmiecik, S. Lakshmi, R. Lozeva, A. Maj, G. Neyens, M. Pfützner, G. Simpson, N. Vermeulen and H.J. Wollersheim;
  Progress in Particle and Nuclear Physics 59, (2007) 355
- Electromagnetic moments of isomers in exotic nuclei
  D. Balabanski et al. Proceedings of the 6th General Conf. of the Balkan Physics Union, Istanbul, Turkey (2006) ed. S.A.Cetin and I.Hikmet, AIP 889, (2007) 7
- New sub-μs isomers in ^{125,127,129}Sn and isomer systematics of $^{124\text{-}130}$Sn
  R.L. Lozeva, G.S. Simpson, H. Grawe, G. Neyens, L.A. Atanasova, D.L. Balabanski, D. Bazzacco, F. Becker, P. Bednarczyk, G. Benzoni, N. Blasi. A. Blazhev, A. Bracco, C. Brandau, L. Caceres, F. Camera, S.K. Chamoli, F.C.L. Crespi, J.-M. Daugas, P.Detistov, M. De Rydt, P. Doornenbal, C. Fahlander, E. Farnea, G. Georgiev, J. Gerl, K.A. Gladnishki, M. Gorska, J. Grebosz, M. Hass, R. Hoischen, G. Ilie, M. Ionescu-Bujor, A. Iordachescu, J. Jolie, A. Jungclaus, M. Kmiecik, I. Kojouharov, N. Kurz, S.P. Lakshmi, G. Lo Bianco, S. Mallion, A. Maj, D. Montanari, O. Perru, M. Pfützner, S. Pietri, J. A. Pinston, Z. Podolyak, W. Prokopowicz, D. Rudolph, G. Rusev, T.R. Saito, A. Saltarelli, H. Schaffner, R. Schwengner, S. Tashenov, K. Turzo, J.J. Valiente-Dobon, N. Vermeulen, J. Walker, E. Werner-Malento, O. Wieland and H.J. Wollersheim;
  Phys.Rev.C77 (2008), 064313
- g-factor of the 7^- isomer in ^{126}Sn and observation of spin-alignment in relativistic fission
  G. Ilie, G. Neyens, G.S. Simpson, J. Jolie, A. Blazhev, H. Grawe, R.L. Lozeva, N. Vermeulen, L. Atanasova, D.L. Balabanski, F. Becker, P. Bednarczyk, C. Brandau, L. Caceres, S.K. Chamoli, J.M. Daugas, P. Doornenbal, J. Gerl, M. Gorska, J. Grebosz, M. Hass, M. Ionescu-Bujor, A. Jungclaus, M. Kmiecik, I. Kojouharov, N. Kurz, A. Maj, S. Mallion, O. Perru, M. Pfützner, Zs. Podolyak, W. Prokopowicz, M. De Rydt, T.R. Saito, H. Schaffner, K. Turzo, J. Walker, E. Werner-Malento, H.J. Wollersheim ;
  Phys. Lett. B687 (2010), 305
- Spin-alignment and g-factor measurement of the $I^\pi=12^+$ isomer in ^{192}Pb produced in the relativistic-energy fragmentation of a ^{238}U beam
  M. Kmiecik, A. Maj, J. Gerl, G. Neyens, L. Atanasova, D.L. Balabanski, F. Becker, P. Bednarczyk, G. Benzoni, N. Blasi, A. Bracco, S. Brambilla, L. Caceres, F. Camera, M. Ciemala, F.C.L. Crespi, S.K. Chamoli, S. Chmel, J. M. Daugas, P. Detistov, P. Doornenbal, G. Georgiev, K. Gladnishki, M. Gorska, H. Grawe, J. Grebosz, M. Hass, R. Hoischen, G. Ilie, M. Ionescu-Bujor, J. Jolie, I. Kojouharov, A. Krasznahorkay, R. Kulessa, M. Lach, S. Lakshmi, S. Leoni, G. Lo Bianco, R. Lozeva, K. H. Maier, S. Mallion, K. Mazurek, W. Meczynski, B. Million, D. Montanari, S. Myalski, C. Petrache, M. Pfützner, S. Pietri, Zs. Podolyak, W. Prokopowicz, D. Rudolph, N. Saito, T.R.

Saito, A. Saltarelli, G.S. Simpson, J. Styczen, N. Vermeulen, E. Werner-Malento, O. Wieland, H.J. Wollersheim, M. Zieblinski;
Eur. Phys. J. A45 (2010), 153

- g-factor measurements at RISING: The case of ^{127}Sn and ^{128}Sn
  L. Atanasova, D.L. Balabanski, S.K. Chamoli, M. Hass, G.S. Simpson, D. Bazzacco, F. Becker, P. Bednarczyk, G. Benzoni, N. Blasi, A. Blazhev, A. Bracco, C. Brandau, L. Caceres, F. Camera, F.C.L. Crespi, P. Detistov, P. Doornenbal, C. Fahlander, E. Farnea, G. Georgiev, J. Gerl, K.A. Gladnishki, M. Gorska, J. Grebosz, R. Hoischen, G. Ilie, M. Ionescu-Bujor, A. Iordachescu, A. Jungclaus, G. Lo Bianco, M. Kmiecik, I. Kojouharov, N. Kurz, S. Lakshmi, R. Lozeva, A. Maj, D. Montanari, G. Neyens, M. Pfützner, S. Pietri, Zs. Podolyak, W. prokopowicz, D. Rudolph, G. Rusev, T.R. Saito, A. Saltarelli, H. Schaffner, R. Schwengner, S. Tashenov, J.J. Valiente-Dobon, N. Vermeulen, J. Walker, E. Werner-Malento, O. Wieland, H.J. Wollersheim, H. Grawe, M. Hjorth-Jensen;
  EPL 91 (2010), 42001

Publications (stopped beam campaign)

- Isomeric decay studies around ^{204}Pt and ^{148}Tb
  Zs. Podolyak, S.J. Steer, S. Pietri, E. Werner-Malento, P.H. Regan, D. Rudolph, A.B. Garnsworthy, R. Hoischen, M. Gorska, J. Gerl, H.J. Wollersheim, T. Kurtukian-Nieto, G. Benzoni, F. Becker, P. Bednarczyk, L. Caceres, P. Doornenbal, H. Geissel, J. Grebosz, A. Kelic, I. Kojouharov, N. Kurz, F. Montes, W. Prokopowicz, T.R. Saito, H. Schaffner, S. Tashenov, A. Heinz, M. Pfützner, M. Hellström, A. Jungclaus, L.L. Andersson, L. Atanasova, D.L. Balabanski, M.A. Bentley, B. Blank, A. Blazhev, C. Brandau, J. Brown, A.M. Bruce, F. Camera, W.N. Catford, I.J. Cullen, Z. Dombradi, E. Estevez, C. Fahlander, W. Gelletly, G. Ilie, E.K. Johansson, J. Jolie, G.A. Jones, M. Kmiecik, F.G. Kondev, S. Lalkovski, Z. Liu, A. Maj, S. Myalski, T.Shizuma, A.J. Simons, S. Schwertel, P.M. Walker, O. Wieland and B.A. Brown;
  Eur.Phys.J. Special Topics 150 (2007), 165, conf. on Radioactive Nuclear Beams (RNB7) Cortina d'Ampezzo, 2006
- Exciting isomers from the first stopped-beam RISING campaign
  D. Rudolph, S. Pietri, Z. Podolyak, P.H. Regan, A.B. Garnsworthy, R. Hoischen, S.J. Steer, F. Becker, P. Bednarczyk, L. Caceres, P. Doornenbal, H. Geissel, J.Gerl, M. Gorska, J. Grebosz, A. Kelic, I. Kojouharov, N. Kurz, F. Montes, W. Prokopowicz, T.R. Saito, H. Schaffner, S. Tashenov, E. Werner-Malento, H.J. Wollersheim, L.L. Andersson, L. Atanasova, D.L. Balabanski, M.A. Bentley, G. Benzoni, B. Blank, A. Blazhev, C. Brandau, J.R. Brown, A.M. Bruce, F. Camera, W.N. Catford, I.J. Cullen, Z. Dombradi, E. Estevez, C. Fahlander, W. Gelletly, A. Heinz, G. Ilie, E.K. Johansson, J. Jolie, G.A. Jones, A. Jungclaus, M. Kmiecik, F.G. Kondev, T. Kurtukian-Nieto, S. Lalkovski, Z. Liu, A. Maj, S. Myalski, M. Pfützner, T.Shizuma, A.J. Simons, S. Schwertel, P.M. Walker and O. Wieland;
  Eur.Phys.J. Special Topics 150 (2007), 173, conf. on Radioactive Nuclear Beams (RNB7) Cortina d'Ampezzo, 2006
- Experimental details of the Stopped Beam RISING Campaign
  S. Pietri, P.H. Regan, Z. Podolyak, A. Jungclaus, M. Pfützner, D. Rudolph, A.B. Garnsworthy, S.J. Steer, R. Hoischen, M. Gorska, J. Gerl, H.J. Wollersheim, I. Kojouharov, H. Schaffner, J. Grebosz, F. Becker, P. Bednarczyk, L. Caceres, P. Doornenbal, H. Geissel, A. Kelic, N. Kurz, F. Montes, W. Prokopowicz, T.R. Saito, S. Tashenov, E. Werner-Malento and W. Gelletly,
  Eur.Phys.J. Special Topics 150 (2007), 319, conf. on Radioactive Nuclear Beams (RNB7) Cortina d'Ampezzo, 2006
- Gamma spectroscopy with RIBs from RISING to AGATA
  J. Gerl, Eur.Phys.J. Special Topics 150 (2007),353 ; conf. on Radioactive Nuclear Beams (RNB7) Cortina d'Ampezzo, 2006
- First results from the stopped RISING Campaign at GSI: The mapping of

isomeric decays in highly exotic nuclei
P.H. Regan, A.B. Garnsworthy, S.J. Steer, S. Pietri, Z. Podolyak, D. Rudolph, M. Gorska, L. Caceres, E. Werner-Malento, J. Gerl, H.J. Wollersheim, F. Becker, P. Bednarczyk, P. Doornenbal, H. Geissel, H. Grawe, J. Grebosz, R. Hoischen, A. Kelic, I. Kojouharov, N. Kurz, F. Montes, W. Prokopowicz, T.R. Saito, H. Schaffner, S. Tshenov, A. Heinz, M. Pfützner, T. Kurtukian-Nieto, G. Benzoni, M. Hellström, A. Jungclaus, L.L. Andersson, L. Atanasova, D.L. Balabanski, M.A. Bentley, B. Blank, A. Blazhev, C. Brandau, J. Brown, A.M. Bruce, F. Camera, W.N. Catford, I.J. Cullen, Z. Dombradi, E. Estevez, C. Fahlander, W. Gelletly, G. Ilie, E.K. Johansson, J. Jolie, G.A. Jones, M. Kmiecik, F.G. Kondev, S. Lalkovski, Z. Liu, A. Maj, S. Myalski, S. Schwertel, T. Shizuma, A.J. Simons, P.M. Walker and O. Wieland;
AIP conf. proc. 899 (2007), 19, Istanbul (2006)

- Isomer Spectroscopy Using Relativistic Fragmentation at the N=Z Line for A≈80-90
P.H. Regan, A.B. Garnsworthy, S. Pietri, L. Caceres, M. Gorska, D. Rudolph, Z. Podolyak, S.J. Steer, R. Hoischen, J. Gerl, H.J. Wollersheim, J. Grebosz, H. Schaffner, W. Prokopowicz, I. Kojouharov, F. Becker, P. Bednarczyk, P. Doornenbal, H. Geissel, H. Grawe, A. Kelic, N. Kurz, F. Montes, T.R. Saito, S. Tashenov, E. Werner-Malento, A. Heinz, L. Atanasova, D.L. Balabanski, G. Benzoni, B. Blank, A. Blazhev, C. Brandau, A.M. Bruce, W.N. Catford, F. Camera, I.J. Cullen, E. Estevez, C. Fahlander, W. Gelletly, G. Ilie, A. Jungclaus, J. Jolie, T. Kurtukian-Nieto, Z. Liu, M. Kmiecik, A. Maj, S. Myalski, S. Schwertel, T. Shizuma, A.J. Simons, P.M. Walker and O. Wieland;
Nucl. Phys. A787 (2007), 491
- First Results from the Stopped Beam Isomer Rising Campaign at GSI
S. Pietri, P.H. Regan, Z. Podolyak, D. Rudolph, M. Gorska, A. Jungclaus, M. Pfützner, A.B. Garnsworthy, S.J. Steer, L. Caceres, E. Werner-Malento, R. Hoischen, J. Gerl, I. Kojouharov, H. Schaffner, H.J. Wollersheim, F. Becker, P. Bednarczyk, P. Doornenbal, H. Geissel, J. Grebosz, A. Kelic, N. Kurz, F. Montes, W. Prokopowicz, T.R. Saito, S. Tashenov, A. Heinz, T. Kurtukian-Nieto, G. Benzoni, M. Hellström, L.L. Andersson, L. Atanasova, D.L. Balabanski, M.A. Bentley, B. Blank, A. Blazhev, C. Brandau, J.R. Brown, A.M. Bruce, F. Camera, W.N. Catford, I.J. Cullen, Z. Dombradi, E. Estevez, C. Fahlander, W. Gelletly, G. ilie, E.K. Johansson, J. Jolie, G.A. Jones, M. Kmiecik, F.G. Kondev, S. Lalkovski, Z. Liu, A. Maj, S. Myalski, T. Shizuma, A. J. Simons, S. Schwertel, P.M. Walker and O. Wieland;
Acta Phys. Pol. B 38 (2007) 1255
- Isomeric States in the Light Tc Isotopes
A.B. Garnsworthy, P.H. Regan, S. Pietri, D. Rudolph, L. Caceres, M. Gorska, Z. Podolyak, S.J. Steer, A. Heinz, F. Becker, P. Bednarczyk, P. Doornenbal, H. Geissel, J. Gerl, H. Grawe, J. Grebosz, A. Kelic, I. Kojouharov, N. Kurz, F. Montes, W. Prokopowicz, T.R. Saito, H. Schaffner, S. Tashenov, H.J. Wollersheim, G. Benzoni, B. Blank, C. Brandau, A.M. Bruce, F. Camera, W.N. Catford, I.J. Cullen, Z. Dombradi, E. Estevez, W. Gelletly, R. Hoischen, G. Ilie, J. Jolie, G.A. Jones, A. Jungclaus, M. Kmiecik, F.G. Kondev, T.

Kurtukian-Nieto, S. Lalkovski, Z. Liu, A. Maj, S. Myalski, M. Pfützner, T. Shizuma, A. J. Simons, S. Schwertel, P.M. Walker and O. Wieland;
Acta Phys. Pol. B 38 (2007) 1265

- Identification of Excited States in the N=Z Nucleus ^{82}Nb
  L.S. Caceres, M. Gorska, A. Jungclaus, P.H. Regan, A.B. Garnsworthy, S. Pietri, Z. Podolyak, D. Rudolph, S.J. Steer, H. Grawe, D.L. Balabanski, F. Becker, P. Bednarczyk, G. Benzoni, B. Blank, C. Brandau, A.M. Bruce, F. Camera, W.N. Catford, I.J. Cullen, Z. Dombradi, P. Doornenbal, E. Estevez, H. Geissel, W. Gelletly, J. Gerl, J. Grebosz, A. Heinz, R. Hoischen, G. Ilie, J. Jolie, G.A. Jones, M. Kmiecik, I. Kojouharov, F.G. Kondev, T. Kurtukian-Nieto, N. Kurz, S. Lalkowski, L. Liu, A. Maj, S. Myalski, F. Montes, M. Pfützner, W. Prokopowicz, T.R. Saito, H. Schaffner, S. Schwertel, T. Shizuma, A.J. Simon, S. Tashenov, P.M. Walker, E. Werner-Malento, O. Wieland and H.J. Wollersheim;
  Acta Phys. Pol. B 38 (2007) 1271
- Isomeric ratio for the $I^{\pi}=8^{+}$ yrast state in ^{96}Pd produced in the relativistic fragmentation of ^{108}Ag
  S. Myalski, M. Kmiecik, A. Maj, P.H. Regan, A.B. Garnsworthy, S. Pietri, D. Rudolph, Z. Podolyak, S.J. Steer, F. Becker, P. Benarczyk, J. Gerl, M. Gorska, H. Grawe, I. Kojouharov, H. Schaffner, H.J. Wollersheim, W. Prokopowicz, J. Grebosz, G. Benzoni, B. Blank, C. Brandau, A.M. Bruce, L Caceres, F. Camera, W.N. Catford, I.J. Cullen, Z. Dombradi, P. Doornenbal, E. Estevez, H. Geissel, W. Gelletly, A. Heinz, R. Hoischen, G. Ilie, G.A. Jones, A. Jungclaus, A. Kelic, F.G. Kondev, T. Kurtukian-Nieto, N. Kurz, A. Lalkovski, Z. Liu, F. Montes, M. Pfützner, T.R. Saito, T. Shizuma, A.J. Simons, S. Schwertel, S. Tachenov, P.M. Walker, E. Werner-Malento and O. Wieland;
  Acta Phys. Pol. B 38 (2007) 1277
- Identification of isomeric states 'south' of ^{208}Pb via projectile fragmentation
  S.J. Steer, Z. Podolyak, S. Pietri, P.H. Regan, D. Rudolph, E. Werner-Malento, A.B. Garnsworthy, R. Hoischen, M. Gorska, J. Gerl, H.J. Wollersheim, F. Becker, P. Bednarczyk, L. Caceres, P. Doornenbal, H. Geissel, J. Grebosz, A. Kelic, N. Kurz, F. Montes, W. Prokopowicz. T.R. Saito, H. Schaffner, S. Tachenov, A. Heinz, M. Pfützner, T. Kurtukian-Nieto, G. Benzoni, A. Jungclaus, D.L. Balabanski, C. Brandau, A.M. Bruce, W.N. Catford, I.J. Cullen, Z. Dombradi, E. Estevez, W. Gelletly, G. Ilie, J. Jolie, G.A. Jones, M .Kmiecik, F.G. Kondev, S. Lalkovski, Z. Liu, A. Maj, S. Myalski, T. Shizuma, S. schwertel, P.M. Walker and O. Wieland;
  Acta Phys. Pol. B 38 (2007) 1283
- Simulation of the electromagnetic background radiation for the RISING experimental set-up
  P. Detistov, D.L. Balabanski and Z. Podolyak;
  Acta Phys. Pol. B 38 (2007) 1287
- Recent results in fragmentation isomer spectroscopy with RISING
  S. Pietri, P.H. Regan, Z. Podolyak, S. Steer, A.B. Garnsworthy, E. Werner-Malento, R. Hoischen, M. Gorska, J. Gerl, H.J. Wollersheim, I. Kojouharov, H.

Schaffner, F. Becker, P. Bednarczyk, L. Caceres, P. Doornenbal, H. Geissel, J. Grebosz, A. Kelic, N. Kurz, F. Montes, W. Prokopowicz. T.R. Saito, S. Tashenov, A. Heinz, M. Pfützner, T. Kurtukian-Nieto, G. Benzoni, M. Hellström, A. Jungclaus, J. Simpson, L.L. Andersson, L. Atanasova, D. Balabanski, M.A. Bentley, B. Blank, A. Blazhev, C. Brandau, J.R. Brown, A.M. Bruce, F. Camera, W.N. Catford, I.J. Cullen, Z. Dombradi, E. Estevez, C. Fahlander, W. Gelletly, G. Ilie, E.K. Johansson, J. Jolie, G.A. Jones, M. Kmiecik, F.G. Kondev, S. Lalkovski, Z. Liu, A. Maj, S. Myalski, T. Shizuma, A.J. Simons, S. Schwertel, P.M. Walker and O. Wieland;
Nucl. Instr. Meth. B261 (2007) 1079

- Observation of isomeric decays in the r-process waiting-point nucleus ^{130}Cd

  A. Jungclaus, L. Caceres, M. Gorska, M. Pfützner, S. Pietri, E. Werner-Malento, H. Grawe, K. Langanke, G. Martinez-Pinedo, F. Nowacki, A. Poves, J.J. Cuenca-Garcia, D. Rudolph, Z. Podolyak, P.H. Regan, P. Detistov, S. Lalkovski, V. Modamio, J. Walker, P. Bednarczyk, P. Doornenbal, H. Geissel, J. Gerl, J. Grebosz, I. Kojouharov, N. Kurz, W. Prokopowicz. H. Schaffner, H.J. Wollersheim, K. Andgren, J. Benlliure, G. Benzoni, A.M. Bruce, E. Casarejos, B. Cederwall, F.C.L. Crespi, B. Hadinia, M. Hellström, R. Hoischen, G. Ilie, J. Jolie, A. Khaplanov, M. Kmiecik, R. Kumar, A. Maj, S. Mandal, F. Montes, S. Myalski, G.S. Simpson, S.J. Steer, S. Tashenov and O. Wieland;
  Phys. Rev. Lett. 99 (2007), 132501
- Neutron-proton pairing competition in N=Z nuclei: Metastable state decays in the proton dripline nuclei ^{82}Nb and ^{86}Tc

  A.B. Garnsworthy, P.H. Regan, L. Caceres, S. Pietri, Y. Sun, D. Rudolph, M. Gorska, Z. Podolyak, S.J. Steer, R. Hoischen, A. Heinz, F. Becker, P. Bednarczyk, P. Doornenbal, H. Geissel, J. Gerl, H. Grawe, J. Grebosz, A. Kelic, I. Kojouharov, N. Kurz, G, Montes, W. Prokopowicz, T.R. Saito, H. Schaffner, S. Tashenov, E. Werner-Malento, H.J. Wollersheim, G. Benzoni, B.B. Blank, C. Brandau, A.M. Bruce, F. Camera, W.N. Catford, I.J. Cullen, Z. Dombradi, E. Estevez, W. Gelletly, G. Ilie, J. Jolie, G.A. Jones, A. Jungclaus, M. Kmiecik, F.G. Kondev, T. Kurtukian-Nieto, S. Lalkovski, Z. Liu, A. Maj, S. Myalski, M. Pfützner, S. Schwertel, T. Shizuma, A.J. Simons, P.M. Walker, O. Wieland and F.R. Xu;
  Phys. Lett. B660 (2008), 326
- Erratum to:Neutron-proton pairing competition in N=Z nuclei: Metastable state decays in the proton dripline nuclei ^{82}Nb and ^{86}Tc

  A.B. Garnsworthy, P.H. Regan, L. Caceres, S. Pietri, Y. Sun, D. Rudolph, M. Gorska, Z. Podolyak, S.J. Steer, R. Hoischen, A. Heinz, F. Becker, P. Bednarczyk, P. Doornenbal, H. Geissel, J. Gerl, H. Grawe, J. Grebosz, A. Kelic, I. Kojouharov, N. Kurz, G, Montes, W. Prokopowicz, T.R. Saito, H. Schaffner, S. Tashenov, E. Werner-Malento, H.J. Wollersheim, G. Benzoni, B.B. Blank, C. Brandau, A.M. Bruce, F. Camera, W.N. Catford, I.J. Cullen, Z. Dombradi, E. Estevez, W. Gelletly, G. Ilie, J. Jolie, G.A. Jones, A. Jungclaus, M. Kmiecik, F.G. Kondev, T. Kurtukian-Nieto, S. Lalkovski, Z. Liu, A. Maj, S.

Myalski, M. Pfützner, S. Schwertel, T. Shizuma, A.J. Simons, P.M. Walker, O. Wieland and F.R. Xu;
Phys. Lett. B668 (2008), 460

- From RISING to HISPEC/DESPEC
  Zs. Podolyak;
  Nucl. Instr. Meth. B266 (2008) 4589
- Evidence for an isomeric $3/2^-$ state in ^{53}Co
  D.Rudolph, R. Hoischen, M. Hellström, S. Pietri, Z. Podolyak, P.H. Regan, A.B. Garnsworthy, S.J. Steer, F. Becker, P. Bednarczyk, L. Caceres, P. Doornenbal, J. Gerl, M. Gorska, J. Grebosz, I. Kojouharov, N. Kurz, W. Prokopowicz, H. Schaffner, H.J. Wollersheim, L.L. Andersson, L. Atanasova, D.L. Balabanski, M.A. Bentley, A. Blazhev, C. Brandau, J.R. Brown, C. Fahlander, E.K. Johansson and A. Jungclaus;
  Eur. Phys.J. A36 (2008), 131
- Isospin symmetry and proton decay: Identification of the 10^+ isomer in ^{54}Ni
  D. Rudolph, R. Hoischen, M. Hellström, S. Pietri, Z. Podolyak, P.H. Regan, A.B. Garnsworthy, S.J. Steer, F. Becker, P. Bednarczyk, L. Caceres, P. Doornenbal, J. Gerl, M. Gorska, J. Grebosz, I. Kojouharov, N. Kurz, W. Prokopowicz, H. Schaffner, H.J. Wollersheim, L.L. Andersson, L. Atanasova, D.L. Balabanski, M.A. Bentley, A. Blazhev, C. Brandau, J.R. Brown, C. Fahlander, E.K. Johansson, A. Jungclaus and S.M. Lenzi;
  Phys. Rev. C78 (2008) 021301
- Single-particle behavior at N=126: Isomeric decays in neutron-rich ^{204}Pt
  S.J. Steer, Z. Podolyak, S. Pietri, M. Gorska, P.H. Regan, D. Rudolph, E. Werner-Malento, A.B. Garnsworthy, R. Hoischen, J. Gerl, H.J. Wollersheim, K.H. Maier, H. Grawe, F. Becker, P. Bednarczyk, L. Caceres, P. Doornenbal, H. Geissel, J. Grebosz, A. Kelic, I. Kojouharov, N. Kurz, F. Montes, W. Prokopowicz, T.R. Saito, H. Schaffner, S. Tashenov, A. Heinz, M. Pfützner, T. Kurtukian-Nieto, G. Benzoni, A. Jungclaus, D.L. Balabanski, C. Brandau, B.A. Brown, A.M. Bruce, W.N. Catford, I.J. Cullen, Z. Dombradi, M.E. Estevez, W. Gelletly, G. Ilie, J. Jolie, G.A. Jones, M. Kmiecik, F.G. Kondev, R. Krücken, S. Lalkovski, Z. Liu, A. Maj, S. Myalski, S. Schwertel, T. Shizuma, P.M. Walker and O. Wieland;
  Phys. Rev. C78 (2008) 061302
- First results with the RISING active stopper
  P.H. Regan, N. Alkhomashi, N. Al-Dahan, Z. Podolyak, S. Pietri, S.J. Steer, A.B. Garnsworthy, E.B. Suckling, P.D. Stevenson, G. Farrelly, I.J. Cullen, W. Gelletly and P.M. Walker;
  Int.Jour.Mod.Phys. E17 (2008) 8
- Testing of a DSSSD detector for the stopped RISING project
  R. Kumar, F.G. Molina, S. Pietri, E. Casarejos, A. Algora, J. Benlliure, P. Doornenbal, J. Gerl, M. Gorska, I. Kojouharov, Z. Podolyak, W. Prokopowicz, P.H. Regan, B. Rubio, H. Schaffner, S. Tashenov, H.J. Wollersheim;
  Nucl. Instr. Meth. A598 (2009) 754
- Spherical proton-neutron structure of the isomeric states in ^{128}Cd

L.Caceres, M. Gorska, A. Jungclaus, M. Pfützner, H. Grawe, F. Nowacki, K. Sieja, S. Pietri, D. Rudolph, Z. Podolyak, P.H. Regan, E. Werner-Malento, P. Detistov, S. Lalkovski, V. Modamio, J. Walker, K. Andgren, P. Bednarczyk, J. Benlliure, G. Benzoni, A.M. Bruce, E. Casarejos, B. Cederwall, F.C.L. Crespi, P. Doornenbal, H. Geissel, J. Gerl, J. Grebosz, B. Hadinia, M. Hellström, R. Hoischen, G. Ilie, A. Khaplanov, M. Kmiecik, I. Kojouharov, R. Kumar, N. Kurz, A. Maj, S. Mandal, F. Montes, G. Martinez-Pinedo, S. Myalski, W. Prokopowicz, H. Schaffner, G.S. Simpson, S.J. Steer, S. Tashenov, O. Wieland and H.J. Wollersheim;
Phys.Rev. C79 (2009) 011301

- Proton-hole excitation in the closed shell nucleus ^{205}Au

  Zs. Podolyak, G.F. Farrelly, P.H. Regan, A.B. Garnsworthy, S.J. Steer, M. Gorska, J. Benlliure, E. Casarejos, S. Pietri, J. Gerl, H.J. Wollersheim, R. Kumar, F. Molina, A. Algora, N. Alkhomashi, G. Benzoni, A. Blazhev, P. Boutachkov, A.M. Bruce, L Caceres, I.J. Cullen, A.M. Denis Bacelar, P. Doornenbal, M.E. Estevez, Y. Fujita, W. Gelletly, H. Geissel, H. Grawe, J. Grebosz, R. Hoischen, I. Kojouharov, S. Lalkovski, Z. Liu, K.H. Maier, C. Mihai, D. Mücher, B. Rubio, H. Schaffner, A. Tamii, S. Tashenov, J.J. Valiente-Dobon, P.M. Walker and P.J. Woods;
  Phys.Lett. B672 (2009) 116
- Evolution of the N=82 shell gap below ^{132}Sn inferred from core excited states in ^{131}In

  M.Gorska, L. Caceres, H. Grawe, M. Pfützner, A. Jungclaus, S. Pietri, E. Werner-Malento, Z. Podolyak, P.H. Regan, D. Rudolph, P. Detistov, S. Lalkovski, V. Modamio, J. Walker, T. Beck, P. Bednarczyk, P. Doornenbal, H. Geissel, J. Gerl, J. Grebosz, R. Hoischen, I. Kojouharov, N. Kurz, W. Prokopowicz, H. Schaffner, H. Weick, H.J. Wollersheim, K. Andgren, J. Benlliure, G. Benzoni, A.M. Bruce, E. Casarejos, B. Cederwall, F.C.L. Crespi, B. Hadinia, M. Hellström, G. Ilie, A. Khaplanov, M. Kmiecik, R. Kumar, A. Maj, S. Mandal, F. Montes, S. Myalski, G.S. Simpson, S.J. Steer, S. Tashenov, O. Wieland, Z. Dombradi, P. Reiter and D. Sohler;
  Phys.Lett. B672 (2009) 313
- Weak deformed oblate structures in ^{198}Os

  Zs. Podolyak, S.J. Steer, S. Pietri, F.R. Xu, H.L. Liu, P.H. Regan, D. Rudolph, A.B. Garnsworthy, R. Hoischen, M. Gorska, J. Gerl, H.J. Wollersheim, T. Kurtukian-Nieto, G. Benzoni, T. Shizuma, F. Becker, P. Bednarczyk, L. Caceres, P. Doornenbal, H. Geissel, J. Grebosz, A. Kelic, I. Kojouharov, N. Kurz, F. Montes, W. Prokopowicz, T.R. Saito, H. Schaffner, S. Tashenov, A. Heinz, M. Pfützner, A. Jungclaus, D.L. Balabanski, C. Brandau, A.M. Bruce, W.N. Catford, I.J. Cullen, Z. Dombradi, E. Estevez, W. Gelletly, G. Ilie, J. Jolie, G.A. Jones, M. Kmiecik, F.G. Kondev, R. Krücken, S. Lalkovski, Z. Liu, A. Maj, S. Myalski, S. Schertel, P.M. Walker, E. Werner-Malento and O. Wieland;
  Phys.Rev. C79 (2009) 031305
- A new simulation package to model detector systems with fragmentation reactions and ion separators

M. J. Taylor, M. A. Bentley, D. Rudolph, C. Fahlander, P. Golubev, R. Hoischen, P. Reiter, J. Gerl, M. Gorska;
Nucl. Instr. Meth. A606 (2009) 589

- Nuclear structure "southeast of ^{208}Pb: Isomeric states in ^{208}Hg and ^{209}Tl
  N. Al-Dahan, Zs. Podolyak, P.H. Regan, M. Gorska, H. Grawe, K.H. Maier, J. Gerl, S.B. Pietri, H.J. Wollersheim, N. Alkhomashi, A.Y. Deo, A.M. D. Bacelar, G. Farrelly, S.J. Steer, A.M. Bruce, P. Boutachkov, C. Domingo-Pardo, A. Algora, J. Benlliure, A. Bracco, E. Calore, E. Casarejos, I.J. Cullen, P. Detistov, Zs. Dombradi, M. Doncel, F. Farinon, W. Gelletly, H. Geissel, N. Goel, J. Grebosz, R. Hoischen, I. Kojouharov, N. Kurz, S. Lalkovski, S. Leoni, F. Molina, D. Montanari, A.I. Morales, A. Musumarra, D. R. Napoli, R. Nicolini, C. Nociforo, A. Prochazka, W. Prokopowicz, B. Rubio, D. Rudolph, H. Schaffner, P. Strmen, I. Szarka, T. Swan, J.S. Thomas, J.J. Valiente-Dobon, S. Verma, P.M. Walker, H. Weick;
  Phys. Rev. C80 (2009) 061302(R)
- Isomeric states in neutron-deficient A~80-90 nuclei populated in the fragmentation of ^{107}Ag
  A.B.Garnsworthy, P.H.Regan, S.Pietri, Y.Sun, F.R.Xu, D.Rudolph, M.Gorska, L.Caceres, Zs.Podolyak, S.J.Steer, R.Hoischen, A.Heinz, F.Becker, P.Bednarczyk, P.Doornenbal, H.Geissel, J.Gerl, H.Grawe, J.Gresbosz, A.Kelic, I.Kojouharov, N.Kurz, F.Montes, W.Prokopwicz, T.Saito, H.Schaffner, S.Tachenov, E.Werner-Malento, H.J.Wollersheim, G.Benzoni, B.Blank, C.Brandau, A.M.Bruce, F.Camera, W.N.Catford, I.J.Cullen, Zs.Dombradi, E.Estevez, W.Gelletly, G.Ilie, J.Jolie, G.A.Jones, A.Jungclaus, M.Kmiecik, F.G.Kondev, T.Kurtukian-Nieto, S.Lalkovski, Z.Liu, A.Maj, S.Myalski, M.Pfutzner, S.Schwertel, T.Shizuma, A.J.Simons1, P.M.Walker, and O.Wieland
  Phys. Rev. C80 (2009) 064303
- β-delayed spectroscopy of neutron-rich tantalum nuclei: Shape evolution in neutron-rich tungsten isotopes
  N.Alkhomashi, P.H.Regan, Zs.Podolyak, S.Pietri, A.B.Garnsworthy, S.J.Steer, J.Benlliure, E.Caserejos, R.F.Casten, J.Gerl, H.J.Wollersheim, J.Grebosz, G.Farrelly, M.Gorska, I.Kojouharov, H.Schaffner, A.Algora, G.Benzoni, A.Blazhev, P.Boutachkov, A.M.Bruce, A.M.Denis Bacelar, I.J.Cullen, L.Caceres, P.Doornenbal, M.E.Estevez, Y.Fujita, W.Gelletly, R.Hoischen, R.Kumar, N.Kurz, S.Lalkovski, Z.Liu, C.Mihai, F.Molina, A.I.Morales, D.Mucher, W.Prokopowicz, B.Rubio, Y.Shi, A.Tamii, S.Tashenov, J.J.Valiente-Dobon, P.M.Walker, P.J.Woods, and F.R.Xu;
  Phys. Rev. C80 (2009) 064308
- Structure of neutron-rich nuclei around the N=126 closed shell; the yrast structure of ^{205}Au up to spin-parity $19/2^+$
  Zs.Podolyak, S.J.Steer, S.Pietri, M.Gorska, P.H.Regan, D.Rudolph, A.B.Garnsworthy, R.Hoischen, J.Gerl, H.J.Wollersheim, H.Grawe, K.H.Maier, F.Becker, P.Bednarczyk, L.Caceres, P.Doornenbal, H.Geissel, J.Grebosz, A.Kelic, I.Kojouharov, N.Kurz, F.Montes, W.Prokopowicz, T.Saito, H.Schaffner, S.Tashenov, A.Heinz, T.Kurtukian-Nieto, G.Benzoni, M.Pfutzner,

A.Jungclaus, D.L.Balabanski, C.Brandau, B.A.Brown, A.M.Bruce, W.N.Catford, I.J.Cullen, Zs.Dombradi, M.E.Estevez, W.Gelletly, G.Ilie, J.Jolie, G.A.Jones, M.Kmiecik, F.G.Kondev, R.Krucken, S.Lalkovski, Z.Liu, A.Maj, S.Myalski, S.Schwertel, T.Shizuma, P.M.Walker, E.Werner-Malento, O.Wieland
Eur.Phys.J. A42 (2009) 489

- Isomeric ratios for nuclei with Z=62-67 and A=142-152 produced in the relativistic fragmentation of ^{208}Pb
  S. Myalski, A. Maj, Zs. Podolyák, F. Becker, P. Bednarczyk, G. Benzoni, B. Blank, C. Brandau, A.M. Bruce, L. Cáceres, F. Camera, W.N. Catford, I.J. Cullen, Zs. Dombradi, P. Doornenbal, E. Estevez, A.B. Garnsworthy, H. Geissel, W. Gelletly, J. Gerl, M. Górska, H. Grawe, J. Gręboszb, A. Heinz, R. Hoischen, G. Ilie, G.A. Jones, A. Jungclaus, A. Kelic, M. Kmiecik, I. Kojouharov, F.G. Kondev, T. Kurtukian-Nieto, N. Kurz, S. Lalkovski, Z. Liu, F. Montes, M. Pfützner, S. Pietri, W. Prokopowicz, P.H. Regan, D. Rudolph, T. Saito, H. Schaffner, S. Schwertel, T. Shizuma, A.J. Simons, S.J. Steer, S. Tashenov, P.M. Walker, E. Werner-Malento, O. Wieland and H.J. Wollersheim;
  Acta Phys. Pol. B40 (2009) 879
- Isomeric decay studies in neutron-rich N~126 nuclei
  S.J. Steer, ZS. Podolyák, S. Pietri, M. Górska, G.F. Farrelly, P.H. Regan, D. Rudolph, A.B. Garnsworthy, R. Hoischen, J. Gerl, H.J. Wollersheim, H. Grawe, K.H. Maier, F. Becker, P. Bednarczyk, L. Cáceres, P. Doornenbal, H. Geissel, J. Gręboszb, A. Kelic, I. Kojouharov, N. Kurz, F. Montes, W. Prokopowicz, T. Saito, H. Schaffner, S. Tashenov, A. Heinz, T. Kurtukian-Nieto, G. Benzoni, M. Pfützner, A. Jungclaus, D.L. Balabanski, C. Brandau, A. Brown, A.M. Bruce, W.N. Catford, I.J. Cullen, ZS. Dombrádi, M.E. Estevez, W. Gelletly, G. Ilie, J. Jolie, G.A. Jones, M. Kmiecik, F.G. Kondev, R. Krücken, S. Lalkovski, Z. Liu, A. Maj, S. Myalski, S. Schwertel, T. Shizuma, P.M. Walker, E. Werner-Malento and O. Wieland;
  Int. J. Mod. Phys. E18 (2009) 1002
- Isomer spectroscopy of ^{127}Cd
  F. Naqvi, M. Gorska, L. Caceres, A. Jungclaus, M. Pfuetzner, H. Grawe, F. Nowacki, K. Sieja, S. Pietri, E. Werner-Malento, P.H. Regan, D. Rudolf, Z. Podolyak, J. Jolie, K. Andgren, T. Beck, P. Bednarczyk, J. Benlliure, G. Benzoni, A.M Bruce, E. Casarejos, B. Cederwall, F.C.L. Crespi, P. Detistov, Zs. Dombradi,, P. Doornenbal, H. Geissel, J. Gerl, J. Grebosz, B. Hadinia, M. Hellstroem, R. Hoischen, G. Ilie, A. Khaplanov, I. Kojouharov, M. Kmiecik, N. Kurz, S. Lalkovski, A. Maj, S. Mandal, V. Modamio, F. Montes, S. Myalski, W. Prokopowicz, P. Reiter, H. Schaffner, G. Simpson, D. Sohler, S.J Steer, S. Tashenov, J. Walker, O. Wieland, and H.J Wollersheim;
  Phys. Rev C82 (2010) 034323
- Shape coexistence and isomeric states in neutron-rich ^{112}Tc and ^{113}Tc
  A.M. Bruce, S. Lalkovski, A.M.D. Bacelar, M. Gorska, S. Pietri, Zs. Podolyak, Y. Shi, P.M. Walker, F.R. Xu, P. Bednarczyk, L. Caceres, E. Casarejos, I.J. Cullen, P. Doornenbal, G.F. Farrelly, A.B. Garnsworthy, H. Geissel, W.

Gelletly, J. Gerl, J. Grebosz, C. Hinke, G. Ilie, G. Jaworski, I. Kojouharov, N. Kurz, S. Myalski, M. Palacz, W. Prokopowicz, P.H. Regan, H. Schaffner, S. Steer, S. Tashenov, H.J. Wollersheim;
Phys. Rev C82 (2010) 044312

- Observation of a new high-spin isomer in ^{94}Pd
  T.S. Brock, B. S. Nara Singh, P. Boutachkov, N. Braun, A. Blazhev, Z. Liu, R. Wadsworth, M. Gorska, H. Grawe, S. Pietri, C. Domingo-Pardo, S. Steer, A. Atac, L. Bettermann, L. Caceres, T. Engert, K. Eppinger, T. Faestermann, F. Farinon, F. Finke, K. Geibel, J. Gerl, N. Goel, A. Gottardo, J. Grebosz, C. Hinke, R. Hoischen, G. Ilie, H. Iwasaki, J. Jolie, I. Kojuharov, R. Kruecken, N. Kurz, E. Merchen, C. Nociforo, J. Nyberg, M. Pfutzner, A. Prochazka, Zs. Podolyak, P. Regan, P. Reiter, D. Rudolph, S. Rinta-Antila, H. Schaffner, C. Scholl, P.-A. Soderstrom, N. Warr, H. Weick, H.-J. Wollersheim, P. Woods;
  Phys. Rev C82 (2010) 061309
- Proton-rich nuclei studied with RISING
  D. Rudolph;
  Acta Phys. Pol. B 42 (2011) 567
- First observation of the decay of a 15^- seniority ν=4 isomer in ^{128}Sn
  S. Pietri, A. Jungclaus, M. Gorska, H. Grawe, M. Pfützner, L. Caceres, P. Detistov, S. Lalkovski, V. Modamio, Zs. Podolyak, P.H. Regan, D. Rudolph, J. Walker, E. Werner-Malento, P. Bednarczyk, P. Doornenbal, H. Geissel, J. Gerl, J. Grebosz, I. Kojouharov, N. Kurz, W. Prokopowicz, H. Schaffner, H.J. Wollersheim, K. Andgren, J. Benlliure, G. Benzoni, A.M. Bruce, E. Casarejos, B. Cederwall, F.C.L. Crespi, B. Hadinia, M. Hellström, R. Hoischen, G. Ilie, A. Khaplanov, M. Kmiecik, R. Kumar, A. Maj, S. Mandal, F. Montes, S. Myalski, G. Simpson, S.J. Steer, S. Tashenov, O. Wieland;
  Phys. Rev. C83 (2011) 044328
- High-spin isomers in ^{96}Ag: Excitations across the Z=38 and Z=50, N=50 closed shells
  P. Boutachkov, M. Gorska, H. Grawe, A. Blazhev, N. Braun, T.S. Brock, Z. Liu, B.S. Nara Singh, R.Wadsworth, S. Pietri, C. Domingo-Pardo, I. Kojouharov, L. Caceres, T. Engert, F. Farinon, J. Gerl, N. Goel, J. Grebosz, R. Hoischen, N. Kurz, C. Nociforo, A. Prochazka, H. Schaffner, S.J. Steer, H. Weick, H.-J. Wollersheim, T. Faestermann, Zs. Podolyak, D. Rudolph, A. Atac, L. Bettermann, K. Eppinger, F. Finke, K. Geibel, A. Gottardo, C. Hinke, G. Ilie, H. Iwasaki, J. Jolie, R. Krücken, E. Merchan, J. Nyberg, M. Pfützner, P.H. regan, P. reiter, S. Rinta-Antila, C. Scholl, P.-A. Söderström, N. Warr, P.J. Woods, F. Nowacki, K. Sieja;
  Phys. Rev. C84 (2011) 044311
- Isomeric states observed in heavy neutron-rich nuclei populated in the fragmentation of a ^{208}Pb beam
  S.J. Steer, Zs. Podolyak, S. Pietri, M. Gorska, H. Grawe, K.H. Maier, P.H. Regan, D. Rudolph, A.B. Garnsworthy, R. Hoischen, J. Gerl, H.J. Wollersheim, F. Becker, P. Bednarczyk, L. Caceres, P. Doornenbal, H. Geissel, J. Grebosz, A. Kelic, I. Kojouharov, N. Kurz, F. Montes, W. Prokopowicz, T. Saito, H. Schaffner, S. Tashenov, A. Heinz, M. Pfützner, T.

Kurtukian-Nieto, G. Benzoni, A. Jungclaus, D.L. Balabanski, M. Bowry, C. Brandau, A. Brown, A.M. Bruce, W.N. Catford, I.J. Cullen, Zs. Dombradi, M.E. Estevez, W. Gelletly, G. Ilie, J. Jolie, G.A. Jones, M. Kmiecik, F.G. Kondev, R. Krücken, S. Lalkovski, Z. Liu, A. Maj, S. Myalski, S. Schwertel, T. Shizuma, P.M. Walker, E. Werner-Malento, O. Wieland;
Phys. Rev. C84 (2011) 044313

- Isomeric mirror states as probes for effective charges in the lower pf shell
  R. Hoischen, D. Rudolph, H.L. Ma, P. Montuenga, M. Hellström, S. Pietri, Zs. Podolyak, P.H. Regan, A.B. Garnsworthy, S.J. Steer, F. Becker, P. Bednarczyk, L. Caceres, P. Doornenbal, J. Gerl, M. Gorska, J. Grebosz, I. Kojouharov, N. Kurz, W. Prokopowicz, H. Schaffner, H.J. Wollersheim, L.-L. Andersson, L. Atanasova, D.L. Balabanski, M.A. Bentley, A. Blazhev, C. Brandau, J.R. Brown, C. Fahlander, E.K. Johansson, A. Jungclaus;
  J. Phys. G: Nucl. Part. Phys. 38 (2011) 035104
- 16^+ spin-gap isomer in ^{96}Cd
  B.S. Nara Singh, Z. Liu, R. Wadsworth, H. Grawe, T.S. Brock, P. Boutachkov, N. Braun, A. Blazhev, M. Gorska, S. Pietri, D. Rudolph, C. Domingo-Pardo, S.J. Steer, A. Atac, L. Bettermann, L. Caceres, K. Eppinger, T. Engert, T. Faestermann, F. Farinon, F. Finke, K. Geibel, J. Gerl, R. Gernhäuser, N. Goel, A. Gottardo, J. Grebosz, C.Hinke, R. Hoischen, G. Ilie, H. Iwasaki, J. Jolie, A. Kaskas, I. Kojouharov, R. Krücken, N. Kurz, E. Merchan, C. Nociforo, J. Nyberg, M. Pfützner, A. Prochazka, Zs. Podolyak, P.H. Regan, P. Reiter, S. Rinta-Antila, C. Scholl, H. Schaffner, P.-A. Söderström, N. Warr, H. Weick, H.-J. Wollersheim, P.J. Woods, F. Nowacki, K. Sieja;
  Phys. Rev. Lett. 107 (2011) 172502
- Superallowed Gammow-Teller decay of the doubly magic nucleus ^{100}Sn
  C.B. Hinke, M. Böhmer, P. Boutachkov, T. Faestermann, H. Geissel, J. Gerl, R. Gernhäuser, M. Gorska, A. Gottardo, H. Grawe, J.L. Grebosz, R. Krücken, N. Kurz, Z. Liu, L. Maier, F. Nowacki, S. Pietri, Zs. Podolyak, K. Sieja, K. Steiger, K. Straub, H. Weick, H.J. Wollersheim, P.J. Woods, N. Al-Dahan, N. Alkhomashi, A. Atac, A. Blazhev, N.F. Braun, I.T. Celikovic, T. Davinson, I. Dillmann, C. Domingo-Pardo, P.C. Doornenbal, G. de France, G.F. Farrelly, F. Farinon, N. Goel, T.C. Habermann, R. Hoischen, R. Janik, M. Karny, A. Kaskas, I.M. Kojouharov, Th. Kröll, Y. Litvinov, S. Myalski, F. Nebel, S. Nishimura, C. Nociforo, J. Nyberg, A.R. Parikh, A. Prochazka, P.H. Regan, C.
  Nature 486 (2012) 341

Publications (slowed down beam campaign)

- Application of diamond detectors in tracking of heavy ion slowed down radioactive beams
  P. Bednarczyk P. Bednarczyk, E. Berdermann, J. Gerl, M. Gorska, I. Kojouharov, M. Pomorski, M. Rebisz, B. Voss, L. Acosta, R. Berjillos, I. Martel, M.A.G. Alvarez, J.M. Espino, J.L. Flores, I. Mukha, R. Wolski;
  Acta Phys. Pol. B 38 (2007) 1293
- Development of slowed down beams at the fragment separator for FAIR
  F. Naqvi, P. Boutachkov, M. Gorska, J. Gerl, F. Farinon, E.T. Gregor, K. Hadynska, A. Jhingan, R. Janik, I. Kojouharov, N.A. Kondratyev, M.A.G. Alvarez, I. Mukha, P. Napiorkowski, C. Nociforo, D. Pietak, W. Prokopowicz, S. Pietri, A. Prochazka, H. Schaffner, P. Strmen, H. Weik, H.J. Wollersheim;
  Acta Phys. Pol. B 42 (2011) 725

Available online at www.sciencedirect.com
SCIENCE DIRECT®
ELSEVIER
Nuclear Instruments and Methods in Physics Research B 204 (2003) 678–681
NIM B
Beam Interactions with Materials & Atoms
www.elsevier.com/locate/nimb

Investigation of scintillation detectors for relativistic heavy ion calorimetry

R. Lozeva [a,b,*], A. Banu [a], D. Balabanski [b], J. Gerl [a], M. Górska [a], I. Kojouharov [a], Y. Kopatch [a], S. Mandal [a], H. Schaffner [a], H-J. Wollersheim [a]

[a] *Gesellschaft für Schwerionenforschung mbH, GSI-Darmstadt, KP2, SB3, 160, Planckstr 1, Darmstadt D-64291, Germany*
[b] *Faculty of Physics, University of Sofia "St. Kl. Ohridski", 5 J. Bourchier blvd., 1164 Sofia, Bulgaria*

Abstract

The new $\Delta E/E$ detection system, calorimeter telescope (CATE), for charge and mass determination of heavy ions at high energies ($\geqslant$100 MeV/n) has been designed. CATE, a calorimeter telescope will consist of position sensitive Si detectors for ΔE determination and scintillators, readout by either PIN diode or PMT, for total-E determination. Different scintillation detectors were tested with ^{130}Sn, ^{186}Pb, ^{197}Au and ^{238}U beams of (100–300) MeV/n ion energy. By properly selecting the beam species from the FRS and applying position corrections, an energy resolution of $\simeq$0.5% FWHM was observed. The corresponding mass resolution of 1/200 is adequate for employment of CATE in the Fast Beam RISING campaign at GSI.

PACS: 07.20.F; 95.55; 25.75; 29.40.M; 29.40.G
Keywords: Calorimeter telescopes; Relativistic heavy ions; Energy resolution; Scintillators; Tracking and position sensitive detectors

1. Introduction and motivation

The RISING project [1] will make use of radioactive beam energies ~100 MeV/n for relativistic Coul-ex and fragmentation reactions with a secondary target in order to yield nuclear structure information. To distinguish the fragments resulting from the interaction with the secondary target, we have to determine their charge and mass with a resolution of ~1/100. This correlates with an energy resolution of 1% if a calorimeter is used for mass detection instead of the standard Bρ-measurement with a large dipole magnet. For that purpose a calorimeter telescope (CATE) system was developed, consisting of a ΔE-detector for charge and position determination and an E-detector for calorimetric mass determination.

2. Experimental conditions

The experimental set-up (Fig. 1) that was used during the tests of the CATE system and that will be used as a standard set-up during the Fast Beam Campaign of RISING [1] is described in the following: a high energetic heavy-ion beam, extracted from the synchrotron accelerator (SIS) at GSI, hits

* Corresponding author. Tel.: +49-6159-712484; fax: +49-6159-712809.
E-mail address: r.lozeva@gsi.de (R. Lozeva).

0168-583X/03/$ - see front matter
doi:10.1016/S0168-583X(02)02150-X

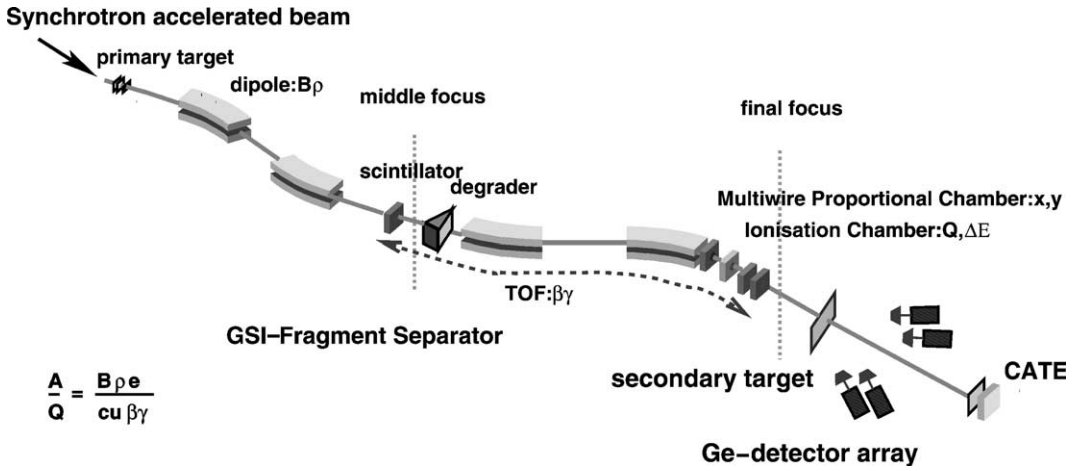

Fig. 1. The experimental set-up.

a primary target, and reaction products from fragmentation or fission are transported through the FRagment Separator, FRS [2]. Once the ions are separated by their Bρ, they reach the final focal plane, where a system of tracking detectors is placed to measure the particle position (MWPC), energy loss (IC) and time-of-flight (TOF). The selected heavy ions reach a secondary target, that will be surrounded in forward angles by the EUROBALL Ge-detectors for RISING. The secondary reaction products shall be identified in charge and mass by the CATE system placed down stream.

3. The CATE system

The complete CATE system (Fig. 2) will consist of Si-ΔE and of CsI(Tl)-E arrays. Nine Si-PIN

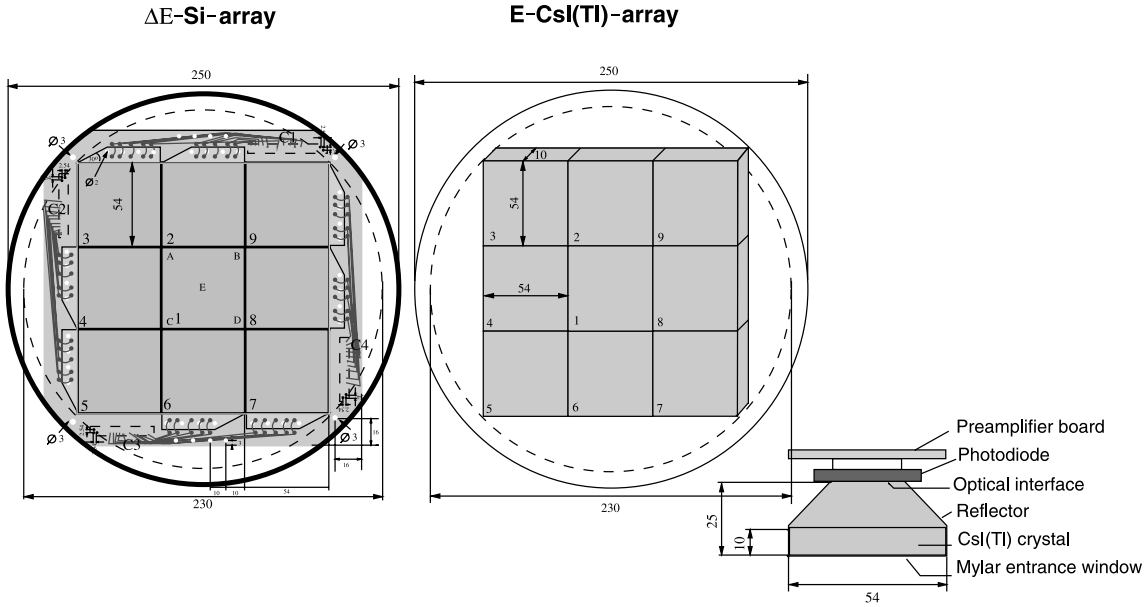

Fig. 2. The calorimeter telescope system.

diodes of 50×50 mm^2 size and 0.3 mm thickness will be used.The position of the impinging particle is detected through the charge division between the four contacts placed at the corners of the resistive layer back side. The following CsI(Tl) scintillator array will consist of nine crystals of 54×54 mm^2

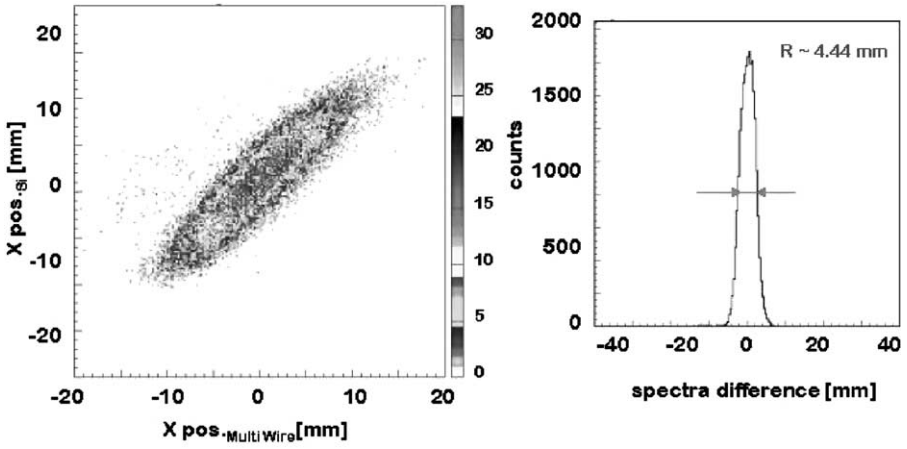

Fig. 3. Position resolution of the Si ΔE-detector.

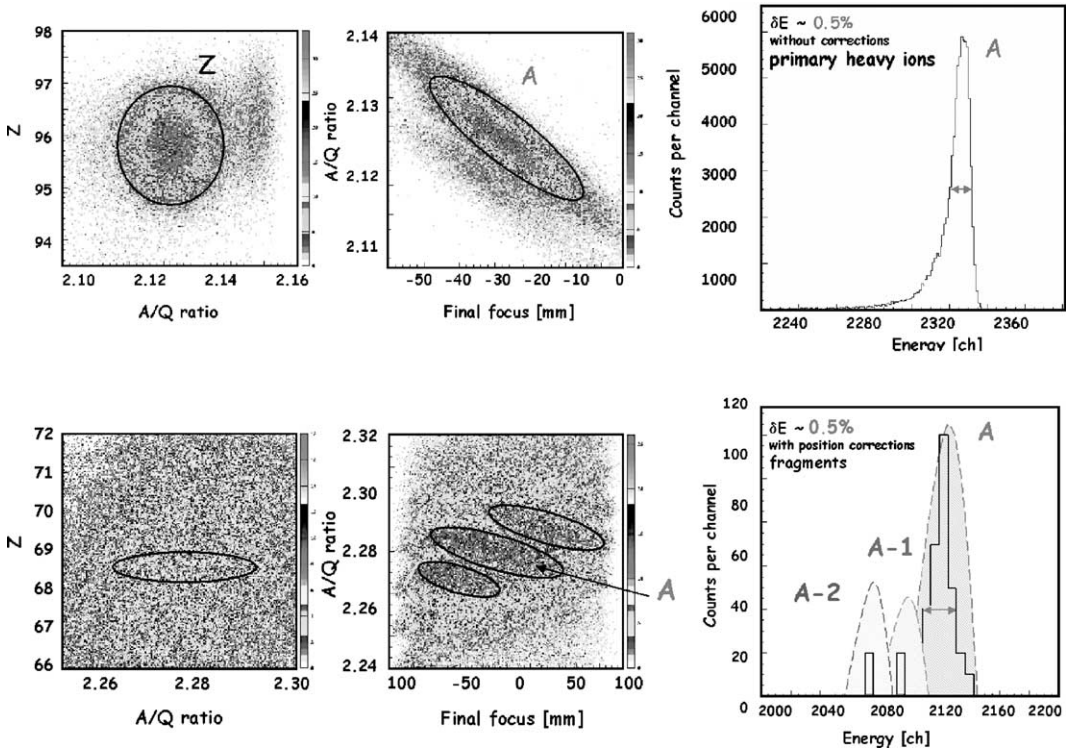

Fig. 4. Energy resolution of the CsI(Tl) E-detector.

size. The thickness of this array is 10 mm; that is enough to stop the high energetic heavy ions. The light collected in each crystal is read-out by a photo-diode.

4. $\Delta E - E$ behaviour

In an earlier investigation [3], the Si-PIN-diode ΔE-detector revealed a charge resolution of about 1/100. For the position resolution we determined a value of 4.4 mm (Fig. 3) by correlating the measured position to that of a MWPC (position resolution $\approx$1 mm) for a ^{238}U heavy-ion beam with an energy of 400 MeV/n. This result is sufficient for the intended use. In a first test the response of NaI(Tl) + PMT, CsI(Tl) + PIN, CsI(Tl) + PMT, CsI(Na) + PMT, BGO + PMT, Plastic + PMT scintillators to ^{197}Au heavy-ion beam with energies between 100 and 306 MeV/n was studied [4]. CsI(Tl) readout by either PMT or PIN-diode gave the best energy resolution determined to be up to 0.46% FWHM under appropriate analysis conditions [4]. The in-beam investigation of the prototype calorimeter system was performed, first, with a primary ^{238}U heavy-ion beam, with energies between 100 and 400 MeV/n, and second, with fragments. The energy resolution of the E-detector in case of primary beam was 0.46–0.52% FWHM without any correction (Fig. 4 top part). In case of ^{186}Pb fragments with energies between 130 and 150 MeV/n, and in case of ^{130}Sn fission fragments with an energy of 100 MeV/n, an energy resolution between 1.1% and 1.5% FWHM has been observed prior to any correction. By selecting charge and mass and by proper position correction, a remarkable energy resolution of 0.5% FWHM for fragments was reached with the calorimeter system (Fig. 4 bottom part). This corresponds to a mass resolution of 1/200 which is sufficient to select narrow mass regions and to determine masses for a given γ-transition. Therefore this method will be used in the coming experiments of the RISING campaign.

Acknowledgements

We would gratefully like to thank all people from GSI-Darmstadt, who participated and helped in this work!

References

[1] http://www-aix.gsi.de/~wolle/EB_at_GSI/rising.html.
[2] http://www-wnt.gsi.de/frs/index.asp.
[3] http://www-land.gsi.de/a_new_land/experiments/experiments.html.
[4] http://www-linux.gsi.de/~lozeva/index.html.

Available online at www.sciencedirect.com
SCIENCE DIRECT®
ELSEVIER
Nuclear Instruments and Methods in Physics Research A 537 (2005) 637–657
NUCLEAR INSTRUMENTS & METHODS IN PHYSICS RESEARCH Section A
www.elsevier.com/locate/nima

Rare ISotopes INvestigation at GSI (RISING) using gamma-ray spectroscopy at relativistic energies

H.J. Wollersheim[a], D.E. Appelbe[b], A. Banu[a], R. Bassini[c,d], T. Beck[a], F. Becker[a], P. Bednarczyk[a,d,e], K.-H. Behr[a], M.A. Bentley[f], G. Benzoni[c,d], C. Boiano[c,d], U. Bonnes[g], A. Bracco[c,d], S. Brambilla[c,d], A. Brünle[a], A. Bürger[h], K. Burkard[a], P.A. Butler[i], F. Camera[c,d], D. Curien[j], J. Devin[j], P. Doornenbal[a], C. Fahlander[k], K. Fayz[b], H. Geissel[a], J. Gerl[a], M. Górska[a,*], H. Grawe[a], J. Gręboszˊ[a,e], R. Griffiths[b], G. Hammond[f], M. Hellström[a], J. Hoffmann[a], H. Hübel[h], J. Jolie[l], J.V. Kalben[g], M. Kmiecik[e], I. Kojouharov[a], R. Kulessa[m], N. Kurz[a], I. Lazarus[b], J. Li[a,n], J. Leske[h], R. Lozeva[a,o], A. Maj[e], S. Mandal[a], W. Męczyński[e], B. Million[c,d], G. Münzenberg[a], S. Muralithar[p], M. Mutterer[g], P.J. Nolan[i], G. Neyens[q], J. Nyberg[r], W. Prokopowicz[a], V.F.E. Pucknell[b], P. Reiter[l], D. Rudolph[k], N. Saito[a], T.R. Saito[a], D. Seddon[i], H. Schaffner[a], J. Simpson[b], K.-H. Speidel[h], J. Styczeńˊ[e], K. Sümmerer[a], N. Warr[l], H. Weick[a], C. Wheldon[a], O. Wieland[c,d], M. Winkler[a], M. Zięblińˊski[e]

[a]*Gesellschaft für Schwerionenforschung, Planckstrasse 1, D-64291 Darmstadt, Germany*
[b]*CCLRC Daresbury Laboratory, Daresbury Warrington, Cheshire WA4 4AD, United Kingdom*
[c]*Department of Physics, University of Milano, Milano, Italy*
[d]*INFN sez. Milano Via G. Celoria, 16, I-20133 Milano, Italy*
[e]*Niewodniczańˊski Institute of Nuclear Physics, Polish Academy of Sciences, ul. Radzikowskiego 152, 31-342 Krakow, Poland*
[f]*Department of Physics, Keele University, Keele, Staffordshire ST5 5BG, United Kingdom*
[g]*Institut für Kernphysik, TU Darmstadt, Schlossgartenstrasse 9, D-64289 Darmstadt, Germany*
[h]*Helmholtz-Institut für Strahlen- und Kernphysik, Nußallee 14-16, D-53115 Bonn, Germany*
[i]*Department of Physics, University of Liverpool, Liverpool L69 7ZE, United Kingdom*
[j]*IReS, B.P. 28, F-67037 Strasbourg Cedex 2, France*
[k]*Department of Physics, Lund University, Box 118, SE-22100 Lund, Sweden*
[l]*Institut für Kernphysik, Univ. Köln, Zülpicher strasse 77, D-50937 Köln, Germany*
[m]*Nuclear Physics Division, Jagiellonian University, ul. Reymonta 4, 30-059 Krakow, Poland*

*Corresponding author.
E-mail addresses: h.j.wollersheim@gsi.de (H.J. Wollersheim), M.Gorska@gsi.de (M. Górska).

0168-9002/$ - see front matter
doi:10.1016/j.nima.2004.08.072

[n]Institute of Modern Physics, the Chinese Academy of Science, P.O. Box 31, Lanzhou 730000, China
[o]Faculty of Physics, University of Sofia "St. Kl. Ohridski", 5 J. Bourchier blvd., 1164 Sofia, Bulgaria
[p]Nuclear Science Center, New Delhi 110067, India
[q]Instituut voor Kern-en Stralingsfysica, K.U. Leuven, Celestijnenlaan 200D, B-3001 Leuven,Belgium
[r]Department of Radiation Sciences, Uppsala University, Box 535, SE-75121 Uppsala, Sweden

Received 13 April 2004; received in revised form 29 June 2004; accepted 10 August 2004
Available online 11 September 2004

Abstract

The Rare ISotopes INvestigation at GSI project combines the former EUROBALL Ge-Cluster detectors, the MINIBALL Ge detectors, BaF_2-HECTOR detectors, and the fragment separator at GSI for high-resolution in-beam γ-ray spectroscopy measurements with radioactive beams. These secondary beams produced at relativistic energies are used for Coulomb excitation or secondary fragmentation experiments in order to explore the nuclear structure of the projectiles or projectile like nuclei by measuring de-excitation photons. The newly designed detector array is described and the performance characteristics are given. Moreover, particularities of the experimental technique are discussed.

PACS: 13.40.Hq; 13.40.−f; 25.60.−t; 25.70.Mn; 25.75.−q; 29.30.Kv

Keywords: Radioactive beams; Relativistic heavy-ion beams; Electromagnetic interaction; Fragmentation reaction; Projectile excitation; γ-ray spectroscopy

1. Introduction

The SIS/FRS facility [1] at GSI provides secondary beams of unstable rare isotopes produced via fragmentation reactions or fission of relativistic heavy ions. Many of these unique radioactive beams have sufficient intensity to enable in-beam γ-ray spectroscopy measurements. In the first Rare ISotopes INvestigation at GSI (RISING) experiments such beams are being exploited at an energy of 100 A MeV to perform relativistic Coulomb excitation of radioactive projectiles and secondary nuclear reactions such as nucleon removal and fragmentation. The RISING set-up is optimised for the investigation of key subjects of nuclear structure research, namely:

- shell structure of known and predicted doubly magic nuclei and nuclei in their vicinity far off stability;
- isospin symmetry along the $N=Z$ line and mixed symmetry states;
- deformed shapes and shape coexistence;
- collective modes of nuclear excitation and E1 strength distribution.

High resolution γ-ray spectroscopy at relativistic beam energies is an experimental challenge. Limitations imposed by large Doppler effects and background caused by atomic processes and unwanted nuclear interactions have to be considered. Both the incoming and outgoing particles of the secondary target have to be identified in mass and charge and their energy and direction determined. The design of the germanium detector array and the heavy-ion tracking detectors were optimised to achieve the highest possible efficiency, energy resolution, and position resolution for heavy ions. In this paper, the experimental set-up for RISING experiments at beam energies of ~ 100 A MeV is described. The performance of the components and first results of Coulomb excitation and secondary fragmentation measurements are presented.

2. Atomic and nuclear processes at relativistic energies

2.1. Angular and energy-loss straggling

In relativistic heavy-ion reactions with secondary beams, thick targets can be used which partially compensate for the low beam intensity. The slowing-down of the fragments in the target layer contributes to the kinematics and results in an energy distribution. The distribution is further enlarged by multiple scattering in the target introducing angular straggling. Fig. 1 depicts the angular straggling [2,3] in a gold target for Ni, Sn and Pb projectiles at 100 A MeV as a function of the target thickness.

While the energy-loss straggling at relativistic energies is small ($<1\%$) even for relatively thick targets (600 mg/cm^2), the angular straggling shows a strong dependence on target thickness, which limits the impact parameter measurement for peripheral collisions.

2.2. Atomic background radiation

Atomic processes are the main source of background γ radiation in relativistic heavy-ion reactions. The main atomic processes contributing to this background are [4–6], (i) K and L shell X-rays from ionised target atoms, (ii) radiative electron capture (REC) of the target electrons into the projectile K and/or L shells, (iii) primary bremsstrahlung (PB) from target electrons produced by the collisions with the projectile, (iv) secondary bremsstrahlung (SEB) from energetic knock-out electrons re-scattering in the target and/or the surrounding material. The atomic cross-sections of all these processes depend strongly on the atomic number of the projectile and target. Based on experimental results, the double-differential cross-section $d^2\sigma/dE\,d\Omega$ of the four atomic processes given above can be calculated empirically [6]. The angle-integrated cross-section $d\sigma/dE$ is illustrated in Fig. 2 for ^{132}Sn fragments at different beam energies (left) and on Be, Sn and Au targets (right).

For small γ-ray energies the angle-integrated cross-section can reach several kb/keV, which is at least 4 orders of magnitude larger than typical Coulomb excitation and nuclear reaction cross-sections. To perform nuclear structure γ-ray spectroscopy (especially Coulomb excitation with heavy targets) down to 400 keV, the beam energy has to be limited to 100 A MeV. This energy of 100 A MeV will be fixed for the following discussion and is a basic quantity for the design of the Ge-Cluster detector array in RISING.

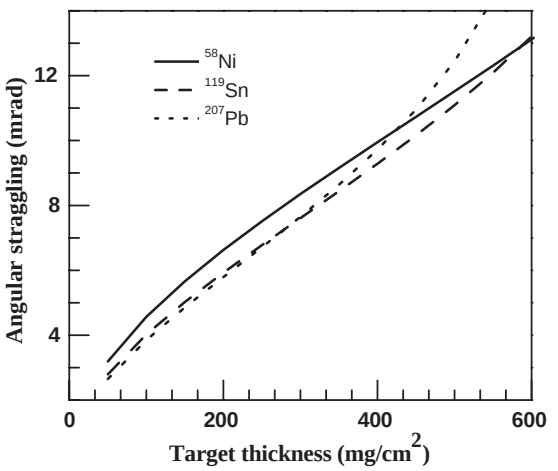

Fig. 1. Angular straggling (σ) in a gold target as a function of the target thickness for Ni (solid line), Sn (long-dashed line) and Pb projectiles (short-dashed line) at 100 A MeV.

2.3. Coulomb excitation at 100 A MeV

Coulomb excitation at a relativistic energy of 100 A MeV is a powerful spectroscopic method to study low-lying collective states of exotic nuclei produced at fast-beam facilities (for review see Ref. [7] and references therein). It takes advantage of the large beam velocities and allows the use of thick secondary targets (in the range of hundreds of mg/cm^2). Contributions to the excitation process by the nuclear force are excluded by selecting reactions at an extremely forward scattering angle, corresponding to a large impact parameter.

An important parameter for this measurement is the grazing angle and the distance of closest approach $D = R_{\mathrm{int}}$ at the nuclear interaction radius. For the present discussion we refer to the

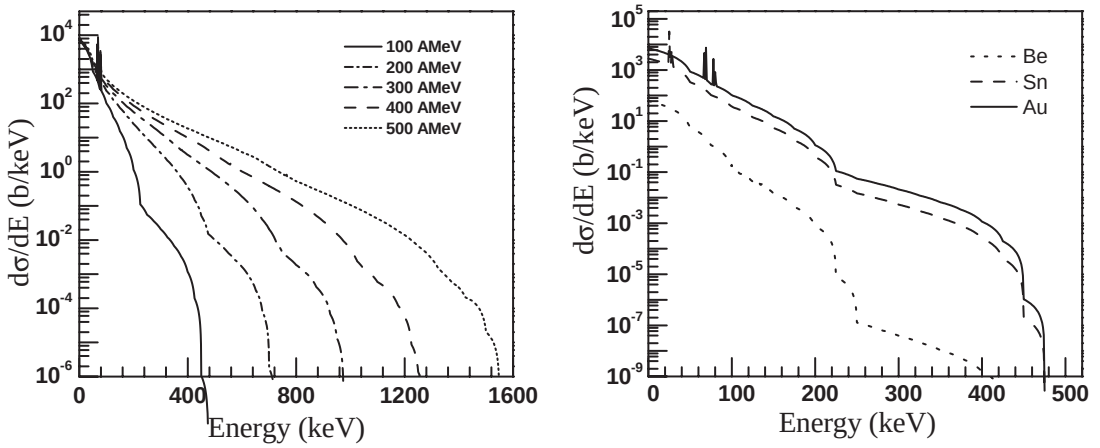

Fig. 2. Angle-integrated cross-section as a function of γ-ray energy for the atomic γ-ray background from ^{132}Sn on a Au target at different beam energies (left). The cross-section dependence on different target materials (Be, Sn, Au) for ^{132}Sn fragments at 100 A MeV (right).

definition of R_{int} following Wilcke et al. [8]:

$$R_{\mathrm{int}} = C_{\mathrm{p}} + C_{\mathrm{t}} + 4.49 - \frac{C_{\mathrm{p}} + C_{\mathrm{t}}}{6.35} \quad \mathrm{(fm)}$$

$$C = R(1 - 1/R^2)$$

$$R = 1.28A^{1/3} - 0.76 + 0.8A^{-1/3}$$

with the nuclear radius R for a homogeneous (sharp) mass distribution, the nuclear radius C for a diffuse Fermi mass distribution and the mass number, A, for the projectile, p, and target nucleus, t, respectively. For the beam-target combination ^{84}Kr + ^{197}Au the nuclear interaction radius is $R_{\mathrm{int}} = 14.2$ fm.

For small deflections ($\sin\theta \simeq \tan\theta \simeq \theta$) and including relativistic effects we obtain for the scattering angle ϑ in the laboratory frame [9]

$$\vartheta \simeq \frac{2Z_{\mathrm{p}}Z_{\mathrm{t}}e^2}{m_0c^2\gamma\beta^2 b} = \frac{2.88Z_{\mathrm{p}}Z_{\mathrm{t}}[931.5 + T_{\mathrm{lab}}]}{A_{\mathrm{p}}[T_{\mathrm{lab}}^2 + 1863T_{\mathrm{lab}}]}\frac{1}{b} \quad \mathrm{(rad)}$$

where T_{lab} is the laboratory beam energy in A MeV, b the impact parameter in fm, m_0 the rest mass of the projectile, γ the Lorentz contraction factor, and β the beam velocity in units of velocity of light. Since the scattering for $T_{\mathrm{lab}} = 100$ A MeV is confined to rather small angles, the projectile moves on a straight-line trajectory and the impact parameter b can be replaced by the distance of closest approach D. In this way we can calculate the grazing angle $\vartheta_{\mathrm{gr}}(b = R_{\mathrm{int}})$ which is the largest scattering angle in a Coulomb excitation experiment at relativistic energies.

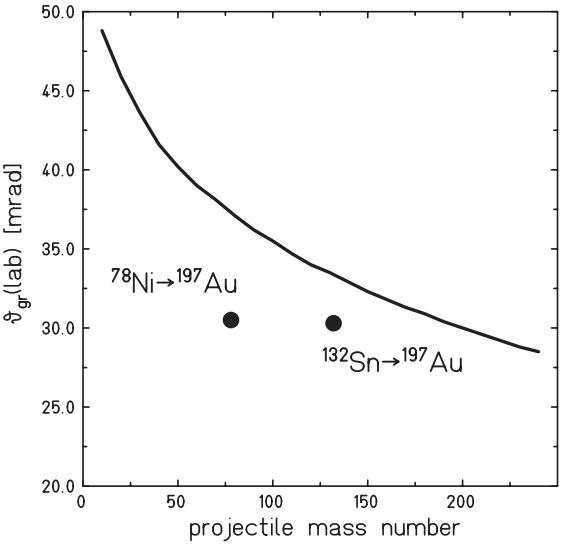

Fig. 3. The grazing angle ϑ_{gr}(lab) is displayed as a function of the projectile mass number for scattering on a ^{197}Au target. The solid line corresponds to projectiles in the valley of stability.

In Fig. 3 the grazing angle ϑ_{gr} is displayed as a function of the projectile mass number for scattering on a ^{197}Au target. For all projectile –

target combinations an angular range of about 3° (52 mrad) is important for Coulomb excitation.

2.4. Fragmentation reactions at the secondary target

Fragmentation reactions at the secondary target are powerful tools for producing exotic nuclear isotopes in excited states see e.g. Refs. [10–12]. Contrary to Coulomb excitation, states with higher spin transfer are populated. The latter can be described with the abrasion–ablation model using the Monte Carlo code ABRABLA [13], or by a simple analytical formula [14]. The average angular momentum calculated with both models is in qualitative agreement with the experimentally observed value.

Besides being an excellent tool for investigating radioactive fragments up to medium spin $4-10\,\hbar$, fragmentation reactions provide a selective trigger, in particular suppressing the huge background from atomic processes.

If the fragmentation cross-section for the isotope of interest is large compared to the competing cross-sections of other channels, this channel could be used directly. However, in most cases the fraction of the isotope in question is too small to be selectable within all isotopes produced. Moreover, even if the selectivity was sufficient, the γ-ray rate limitation would demand a rather low primary beam intensity and, hence, low yield of the reaction channel of interest. Therefore, an intermediate fragment is produced and selected by the FRS, which is directed to the secondary target to yield, in a secondary fragmentation step, the isotope of interest. The intermediate fragment is chosen with respect to its available intensity on one hand and the subsequent production cross-section and relative abundance in the produced isotope cocktail on the other hand. Another criterion is that the population of higher spin states requires more massive fragmentation processes. This optimisation is done by the above-mentioned EPAX calculations [15,16].

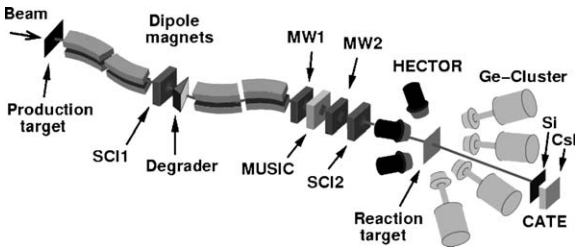

Fig. 4. Schematic layout of the RISING set-up at the FRS. The beam diagnostic elements consist of two multiwire detectors (MW1 and MW2), an ionisation chamber (MUSIC) and two scintillation detectors (SCI1 and SCI2). The γ rays are measured with BaF_2-HECTOR and Ge-Cluster detectors. The ions emerging from the reaction target are identified with the CATE array.

3. Rare isotope beam production, selection, and identification

3.1. Primary beam and target

At SIS/FRS secondary beams of radioactive nuclei are produced by fragmentation of a stable primary beam or fission of a ^{238}U beam on a ^{9}Be or ^{208}Pb target (with typical thicknesses of 1–4 g/cm^2) placed at the entrance of the fragment separator (FRS) (see Fig. 4). Typically, the primary beam energy ranges from 400 to 1000 A MeV for good optical transmission and minimum atomic charge state distribution (i.e. one charge state dominating). The present maximum beam intensity from the SIS synchrotron is $\sim 10^9$/s for medium heavy nuclei (e.g. ^{129}Xe) and $\sim 2\times10^8$/s for ^{238}U. The intensity of particular secondary beam species can be calculated from the luminosity and the production cross-section. For fragmentation reactions the production cross-sections and momentum distributions of the reaction products are rather well known [15,17,18]. The cross-sections are taken from the EPAX parametrisation [15,16], while experimental data are available for nuclear and electromagnetic fission yields [19–25].

3.2. Secondary beam selection

The FRS [1] is a zero-degree magnetic spectrometer and consists of four dipole stages and an

aluminium degrader at the intermediate focal plane, which provides high-energy, spatially separated isotopically pure exotic beams of all elements up to uranium. The nuclei of interest are selected via their magnetic rigidity, $B\rho$, and energy loss, ΔE, in the degrader, the so-called $B\rho$–ΔE–$B\rho$ method [1]. A specific property of the RISING experiments is the use of rather low beam energies (~ 100 A MeV) at the secondary target, which deteriorates the beam quality and transmission through the FRS due to large angular and energy loss straggling in the target and degrader. To simulate the experimental set-up and estimate the properties of the secondary beam with respect to luminosity, separation quality, implantation profiles, and transmission, the simulation programmes MOCADI [26] and LISE++ [27] were used. An example, calculated with MOCADI code, illustrates a radioactive beam quality dependence on its energy. A ^{56}Cr fragment impinging with 313 A MeV on the secondary target has 32% transmission through the FRS, a relative energy resolution, $\Delta E/E$, of 3.4%, and the horizontal beam size amounts to 2.1 cm (FWHM). By slowing down to 136 A MeV, the transmission is reduced to 19%, the relative energy resolution yields $\Delta E/E = 5.0\%$, and the horizontal beam size increases to 3.5 cm (FWHM). A comparison between simulation and measurement is shown in Fig. 5. The basic ion identification is given by plotting the atomic number Z versus A/Q (as the majority of light ions are fully stripped of electrons at ~ 100 A MeV, the measured Q represents Z of the ions). However, the ion identification procedure depends on the selected region of the nuclear chart. To get an optimum identification a more sophisticated analysis of correlations among the measured parameters such as TOF, energy loss and beam position is usually applied.

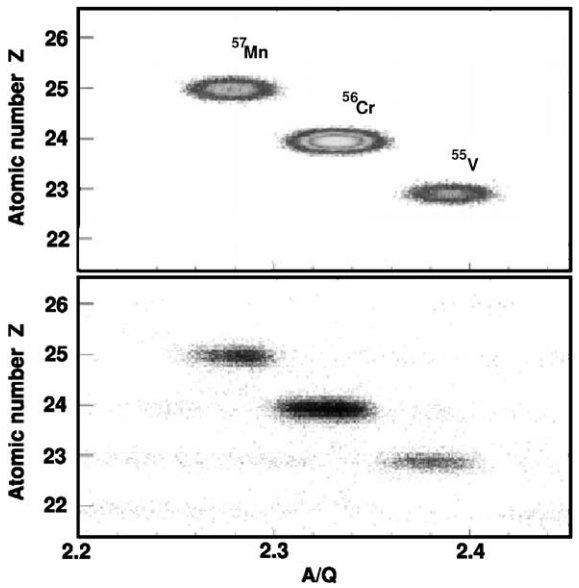

Fig. 5. Comparison of the calculations performed with the LISE++ code (top) with the experimental data (bottom) for the ^{56}Cr setting at a count rate of 10^4/s at SCI1. Plotting the intensity distribution of the atomic number Z versus A/Q gives an identification of the different ions.

3.3. Description of beam detectors, their location and performance

Various types of detectors were used to perform an A and Z identification of the secondary beam ions, including position tracking (see Fig. 4).

Two position-sensitive plastic scintillators (SCI1 and SCI2) were placed at the intermediate and close to the final focal planes providing time of flight (TOF) and position information. The location of the scintillator SCI2 was -1512 mm (upstream) from the target. The scintillation detectors with a thickness of 0.5 mm and a diameter of 250 mm have a typical intrinsic time resolution of about 100 ps (FWHM) [1]. Two Multi-Wire proportional chambers (MW1 and MW2) at -3251 and -2429 mm, respectively, provide the beam position and tracking information. The MW detectors have an active area of 200×200 mm^2 and operate with a mixture of Argon–CO_2 gas at the atmospheric pressure. Therefore thin Capton windows could be used. The readout of the wires representing the x and y planes is performed by the delay-line technique. The position resolution of the MW detectors is below 1 mm [28]. The TOF and $B\rho$ were used to determine the mass-to-charge ratio (A/Q).

The atomic number Z of the secondary beam nuclei is deduced by measuring their energy loss in a MUltiple Sampling Ionisation Chamber (MUSIC) [29] positioned at -2801 mm in front of the

target. The MUSIC consists of eight anode strips covering an active area of $200 \times 80\,mm^2$. The counting gas is CF_4 at the atmospheric pressure. Since the number of electrons generated in the gas are proportional to the square of the charge of the penetrating ion, the signal gives a measure of the atomic number Z of this ion. In addition, the TOF was used to obtain a velocity correction for the Z determination.

Since the secondary beam nuclei are slowed down in the FRS and the subsequent tracking detectors to about 100 A MeV before reaching the secondary target, the fragment identification is worse. While e.g. TOF resolution of 270 ps and a mass resolution of $\Delta A = 0.27$ (FWHM) could be reached during the calibration of the FRS with a stable ^{86}Kr at 419 A MeV, these numbers were increased significantly for the secondary nuclear beams. In addition, the TOF and the mass resolution are intensity dependent, such that for the ^{56}Cr beam a TOF resolution of 2.2 and 3.7 ns (FWHM) could be achieved at the counting rate of 10^4 and 10^6/s, respectively. The corresponding values of mass resolution are 0.59 and 0.89 (FWHM), respectively. For a unique mass identification the latter value therefore determines the count rate limit of SCI1. The identification of the atomic number Z was performed with the MUSIC detector. For the primary ^{86}Kr beam a Z resolution of $\Delta Z = 0.27$ (FWHM), while for the ^{56}Cr beam $\Delta Z = 0.24$ and 0.43 was obtained for the above-mentioned low and high count rates at SCI1, respectively.

4. Reaction channel determination with the CAlorimeter TElescope CATE

Following the reaction on a secondary target at the final FRS focal plane, the scattered particles and breakup products need to be identified in terms of A and Z, and the scattering angle has to be measured. The standard $B\rho$-TOF method for mass determination was not applicable for RISING, since the available space in the experimental area was not sufficient for placing a big magnet. Moreover, the broad charge state distribution of the heavy ions behind the secondary target would impede the mass determination. Therefore, a position-sensitive ΔE–E calorimeter was chosen. The required particle detector should be as efficient as possible and needs to accept the full available secondary beam intensity as it covers zero degree angle. Different beam particle detector designs have been used in the past and the latest generation devices are ΔE–E telescope systems. Energy loss is measured with thin position-sensitive Si detectors, whereas the residual-energy detectors are usually made of CsI(Tl) scintillators [30].

For the RISING project the CAlorimeter TElescope (CATE) array was designed [31] and consists of 3×3 modular ΔE–E telescopes covering the relevant opening angle of 58 mrad (see Section 2.3) at $+1426$ mm from the target and mounted in vacuum. Two types of transmission (ΔE) Si detectors were produced by the company EURISYS and CANBERRA (model: IPP 2D 50×50-300-SPE and PF-50×50-300EB, respectively). The detectors are position sensitive, which can be exploited for the impact parameter measurements in Coulomb excitation. The geometrical size and the active area of each 300 μm thick Si detector was 54×54 and $50 \times 50\,mm^2$, respectively, resulting in a geometrical efficiency of 92%. The central detector is positioned 3 mm behind the plane of the other eight Si detectors.

The energy deposition in the detector array was measured with the back contact, while a resistive layer (sheet resistance 2 kΩ) on the front side of each detector module served as a charge divider to the four corner contacts. The position of an incident ion was determined comparing relative heights of the four signals following a simple geometrical algorithm. Each corner contact is terminated by a 1 kΩ resistor to reduce non-linearities in the position determination as described, e.g. in Ref. [32]. The detector signals are integrated by charge-sensitive preamplifiers (model: CSTA2 made by the Institute of Nuclear Physics, Technical University, Darmstadt [33]). The Si detector prototype energy resolution, obtained with stopped α particles, was 80 keV for the 5.48 MeV ^{241}Am line. Additional tests with heavy ions of about 5 A MeV energy revealed a position resolution of <7 mm (FWHM) [34,35].

The CsI(Tl) detectors provided by the company SCIONIX (model: V502P25/18-E2-Cs-X SSX848) were mounted 40 mm behind the Si array. Each detector has a flat front face of $54 \times 54\,mm^2$ size, a thickness of 10–20 mm and a trapezoidal back shape. The thickness of detectors is sufficient to stop heavy ions with $Z \geqslant 7$ at 100 A MeV and with $Z \geqslant 28$ at 400 A MeV. This covers all possible secondary reaction products expected from the proposed RISING experiments. The detectors were mounted in an aluminium frame of 4 mm thickness between each two neighbours thus yielding the same geometrical efficiency of 92% as for the Si array. The scintillation light of each crystal is collected by a photo diode of $18 \times 18\,mm^2$ size mounted on the trapezoidal back side of the crystal. The signal of the PIN diode was amplified by integrated preamplifiers [36] and yields the residual energy of the fragments after passing through the Si detectors.

Several detector tests using relativistic heavy ions were performed to optimise the final design of the ΔE–E telescopes [35]. A ^{124}Sn beam of 450 A MeV gave values of ΔE corresponding to the resolution of $\Delta Z = 0.7$ (FWHM) for the Si detector. For the same detector a 5 mm (FWHM) position resolution was found in the measurement of the 400 A MeV ^{238}U beam. The CsI(Tl) test detector revealed an energy resolution of 1.0% for a ^{132}Xe beam. Considering the energy spread of the detected beam nuclei and applying a position-dependent energy correction, an intrinsic energy resolution of $\Delta E/E_{res} \approx 0.5\%$ is deduced. The latter correction accounts for the position dependence of the scintillation light production and collection in the detectors.

The CATE array with its nine ΔE–E_{res} telescopes was used in the first RISING experiments at $\sim$ 100 A MeV. Results from a fragmentation reaction and a Coulomb excitation experiment are displayed in Fig. 6. The two-dimensional ΔE–E_{res} plots of one telescope for ^{9}Be(^{55}Ni,xn,yp) and ^{197}Au(^{112}Sn,xn,yp) channels demonstrate the excellent Z resolution. The data were taken under the condition of a particle–γ coincidence. With this requirement one should note that for ^{55}Ni on ^{9}Be all reaction channels are almost equally populated, while for ^{112}Sn on ^{197}Au the inelastic (Coulomb excitation) channel dominates. The extracted Z resolution was 0.7 (FWHM) for the reaction with ^{55}Ni and 0.8 (FWHM) for the ^{112}Sn (a product of ^{124}Xe fragmentation) induced reactions. For the mass identification, which is the subject of a forthcoming paper [31], the combined $\Delta E + E$ information is used to extract from the total kinetic energy the mass number, thereby assuming the same velocity for all reaction products with a given charge.

In the RISING experiments, the accuracy of the position determination, measured with the Si detectors, is limited by the angular spread of the ions after the secondary target. It amounts at least

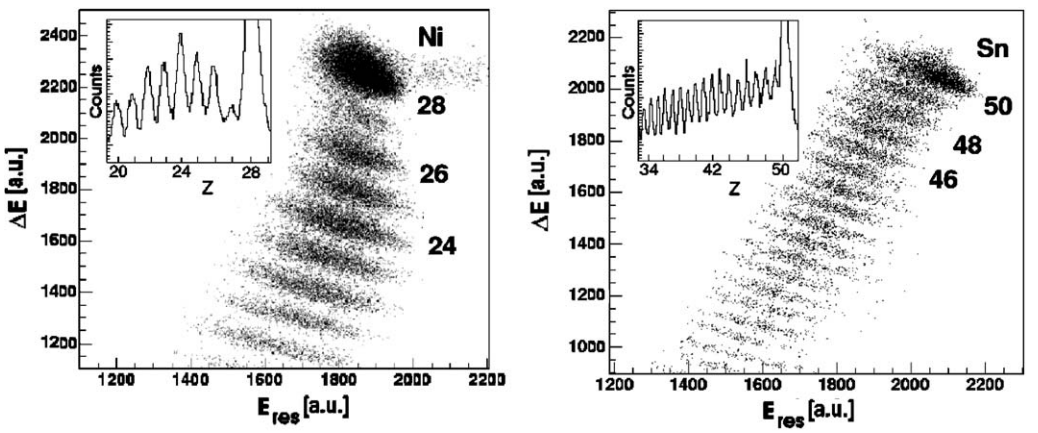

Fig. 6. Two-dimensional ΔE–E_{res} spectra from two RISING experiments exploring ^{9}Be(^{55}Ni,xn,yp) (left) and ^{197}Au(^{112}Sn,xn,yp) (right) reaction. The insets show the extracted element distribution.

to 7 mrad (FWHM)(see Fig. 1) corresponding to a circle of 20 mm diameter at the CATE position. This is large compared to the intrinsic position resolution. Beam intensities of several thousand ions per second could be accepted for the ΔE–E telescopes without deteriorating the detection characteristics. After an accumulated dose of $>10^9$ heavy ions on the central Si detector, the leakage current increased from originally 100 nA to 2 μA. Although the detector resolution did not deteriorate significantly, the detector was replaced at that stage.

5. High-resolution γ-ray detection with Ge-detectors

5.1. Doppler effect at relativistic energies

In the following section we will summarise the relevant formulas [37,38] for the Doppler effect, which are important for the design of the γ-detection array, since the photons from the excited projectiles are emitted in flight. Due to the large beam velocity of $\beta \geqslant 0.4$ at an energy around 100 A MeV, the observed γ-ray energies, E_γ, are strongly Doppler shifted relative to the de-excitation γ-ray energy, $E_{\gamma 0}$, for the projectile at rest according to the following formula:

$$\frac{E_\gamma}{E_{\gamma 0}} = \frac{\sqrt{1-\beta^2}}{1-\beta\cos\vartheta_\gamma}$$

with

$$\beta = \frac{\sqrt{(T_{\mathrm{lab}}/A_{\mathrm{p}})^2 + 1863(T_{\mathrm{lab}}/A_{\mathrm{p}})}}{931.5 + T_{\mathrm{lab}}/A_{\mathrm{p}}}.$$

Fig. 7 shows the Doppler shift for beam energies of 100 and 200 A MeV compared with an energy close to the Coulomb barrier, 6 A MeV. The quantity ϑ_γ denotes the angle between the γ ray and the projectile fragment in the laboratory frame. The small scattering angles of the fast moving projectile fragments ($\vartheta \leqslant 3^\circ$), means we can take the angle ϑ_γ as the γ-ray detection angle with respect to the beam axis in order to simplify the calculation. This approximation will be taken in the following discussion. At $\vartheta_\gamma = 0^\circ$ the γ-ray energy can reach $E_\gamma \approx 1.6E_{\gamma 0}$, while at $\vartheta_\gamma = 180^\circ$ $E_\gamma \approx 0.6E_{\gamma 0}$ for 100 A MeV beam energy.

To find the optimal positions for the γ-detectors, we also have to take the Lorentz boost of the γ

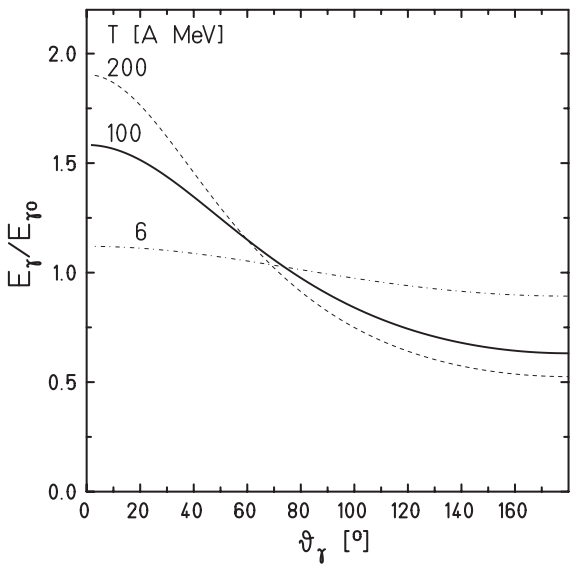

Fig. 7. The ratio of the photon energy E_γ measured in the laboratory frame, to the photon energy $E_{\gamma 0}$ in the rest frame of the projectile versus the laboratory angle ϑ_γ for bombarding energies of 6, 100 and 200 A MeV.

rays into consideration. Since in both laboratory and rest frame the z-axis is the beam direction, we obtain the following relations between the γ-ray emission angle and the solid angle:

$$\phi_\gamma^{\mathrm{rest}} = \varphi_\gamma^{\mathrm{lab}}$$

$$\cos\,\theta_\gamma^{\mathrm{rest}} = \frac{\cos\vartheta_\gamma - \beta}{1-\beta\cos\vartheta_\gamma}$$

$$\frac{\mathrm{d}\Omega_{\mathrm{rest}}}{\mathrm{d}\Omega} = \left(\frac{E_\gamma}{E_{\gamma 0}}\right)^2 = \frac{1-\beta^2}{(1-\beta\cos\vartheta_\gamma)^2}.$$

One should note that the relation between the solid angles is given by the square of the Doppler shift (see Fig. 7). This leads to a γ-ray intensity distribution which is peaked at forward angles and, hence, increases the γ-detection efficiency at small angles.

To correct for the Doppler shift, i.e. to get the γ-transition energy $E_{\gamma 0}$ from the detected E_γ, β and ϑ_γ must be determined precisely. The velocity, β, can usually be derived with an accuracy of better than 1% (TOF measurement), but the accuracy of ϑ_γ is worse in most cases because of the opening angle of standard γ-ray detectors. The Doppler broadening due to the opening angle is given by

$$\frac{\Delta E_{\gamma 0}}{E_{\gamma 0}} = \frac{\beta\,\sin\vartheta_\gamma}{1-\beta\cos\vartheta_\gamma}\Delta\vartheta_\gamma$$

where the opening angle can be estimated by

$$\Delta\vartheta_\gamma = 0.622\,\arctan\frac{d}{R+30}.$$

Here d(mm) denotes the diameter of the Ge crystal, R(mm) the distance to the target, 30 mm is the assumed interaction depth in a Ge crystal and the factor 0.622 which was determined empirically allows the calculation of the FWHM value. For the case of $d = 59$ mm (for crystals of a Cluster detector), $R = 700$ mm we obtain an opening angle of $\Delta\vartheta_\gamma = 2.9^\circ$ or 50 mrad and an energy resolution $\Delta E_{\gamma 0}/E_{\gamma 0} = 1\%$ (for $\beta = 0.43$) at a detection angle of $\vartheta_\gamma = 15^\circ$. Fig. 8 (left) shows the Doppler broadening for an opening angle of $\Delta\vartheta_\gamma = 3^\circ$ versus the laboratory angle ϑ_γ.

For very short-lived states in the pico-second range the expected γ-ray energy resolution $\Delta E_{\gamma 0}/E_{\gamma 0}$ depends also on the projectile velocity β. Since rather thick targets are used, the projectiles may decay within the target during the slowing down process. Therefore, the velocity of the projectile at the time of γ-ray emission is not known precisely. The relevant formula for the Doppler broadening is given below

$$\frac{\Delta E_{\gamma 0}}{E_{\gamma 0}} = \frac{\beta-\cos\vartheta_\gamma}{(1-\beta^2)(1-\beta\cos\vartheta_\gamma)}\,\Delta\beta.$$

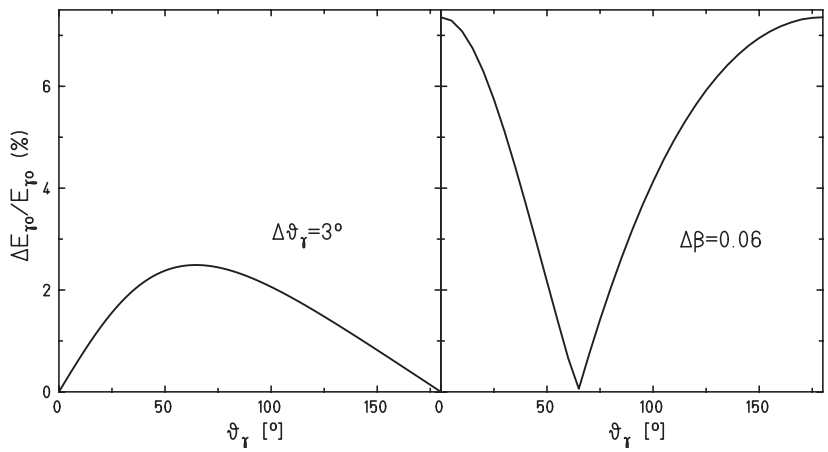

Fig. 8. The expected γ-ray energy resolution $\Delta E_{\gamma 0}/E_{\gamma 0}$ as a function of the laboratory angle ϑ_γ for a bombarding energy of 100 A MeV. For the Doppler broadening an opening angle of $\Delta\vartheta_\gamma = 3^\circ$ (left) and a spread in the beam velocity of $\Delta\beta = 6\%$ is assumed (right), respectively.

Fig. 8(right) shows an example of the Doppler broadening for a spread in the beam velocity of $\Delta\beta = 6\%$ versus the laboratory angle ϑ_γ.

In typical Coulomb excitation experiments, Au targets with a thickness of 400 mg/cm^2 are used. If we consider a fragment beam (100 A MeV) and a mean lifetime for a state of $\tau = 0.5$ ps, approximately 70% of the excited projectiles will decay within the target. The uncertainty in the beam velocity is $\Delta\beta = 6\%$ which effects the γ-ray energy resolution especially at forward and backward angles. Therefore, we have to consider effects on the γ-ray line shape due to energy losses of the excited nuclei in the target. For the example mentioned above, the mean lifetime $\tau = 0.5$ ps will not prevent the observation of the γ-ray transition, since $\approx 30\%$ of the γ-ray intensity remains in the sharp component of the γ-peak ($\Delta E_{\gamma 0}/E_{\gamma 0} = 1\%$).

5.2. Cluster array for experiments at relativistic energies

The γ-ray detectors used in the RISING experiment are the Cluster Ge detectors from the EUROBALL spectrometer [39] and the segmented Ge detectors from the MINIBALL spectrometer [40].

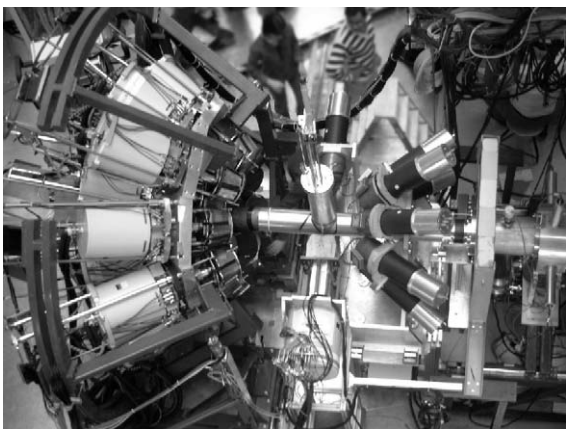

Fig. 9. A photograph of the set-up of the first phase of RISING. The beam comes from the right. BaF_2-HECTOR array, target chamber with one BaF_2 and one VEGA monitor detectors placed perpendicular to the beam axis, and the Ge-Cluster array are shown on the right, middle, and left, respectively.

In the first phase of the project the array was made up of 15 Cluster detectors. The photograph of the set-up is shown in Fig. 9. Each Cluster detector comprises seven closely packed tapered hexagonal Ge crystals [41] housed in a common cryostat. Each Ge crystal is encapsulated in a permanently sealed Al can. Due to the possibility to add back the energies measured in neighbouring crystals after Compton scattering a high full-energy efficiency is maintained up to γ-ray energies of several MeV [42]. Therefore, Cluster detectors are ideally suited for the fast beam RISING experiments where γ-ray energies are strongly Doppler shifted to higher energies.

For experiments with beam energies around 100 A MeV the Ge detectors have to be positioned at forward angles in order to maximise the effective solid angle affected by the Lorentz boost, and to minimise the Doppler broadening effect (see previous section). For optimum packing the crystals are arranged in three rings around the beam pipe, with the axis of the central detectors in each ring positioned at 15°, 33°, and 36°.

A design goal for the array was to obtain about 1% energy resolution for a γ transition, emitted from a nucleus moving at $\beta = 0.43$. This criterion defines the distance to the target.

Due to the Lorentz boost the main efficiency contribution comes from the detectors closest to the beam line in the forward direction. Using the formula given in Section 5.1, the efficiency and resolution of the detectors was estimated based on the known performance of the detectors at 445 mm (regular distance in EUROBALL spectrometer), using standard γ-ray sources ($\beta = 0$). At 15° a distance of 700 mm to the target was obtained. The mechanical constraint of the 16 cm diameter beam pipe defined this to be the most forward angle possible. In addition, due to the complexity of the downstream CATE detector, the distance of this first ring from the target could not be changed.

The resolution of the detectors in the 2nd and 3rd rings at a distance of 700 mm, at $\beta = 0.43$, would be significantly worse. Therefore, the array was designed such that these detectors could be positioned at a variable distance from the target (700–1400 mm). This various detector configurations to be chosen depending on the relative

Table 1
Detectors and their positions in the RISING γ-ray spectrometer

Ring	Detector type	Number	Angle (deg)	Distance (mm)
1	Cluster	5	15.9	700
2	Cluster	5	33.0	700–1400
3	Cluster	5	36.0	700–1400
4	MINIBALL	4	51.3	180–500
	MINIBALL	1	51.3	227–500
5	MINIBALL	2	86.0	180–500
	MINIBALL	1	86.0	232–500

The angles quoted for the Cluster detectors are between the beam direction and the axis of the central crystal, and for the MINIBALL detectors between the beam and the central axis of the triple cryostat.

importance of efficiency to energy resolution to achieve the physics goals of a particular experiment. A summary of the detectors and their positions is given in Table 1.

To allow access to the target position, maintenance of the spectrometer and the option of running non-RISING experiments with the detectors still in the experimental area, the array splits perpendicular to the beam direction, moving 1.4 m on one side and 3.2 m on the other side.

In the second phase, the existing three rings of Cluster detectors are maintained and the MINIBALL detectors [40] are added in two rings with the axis of centre of the triple cryostats at 51.3° and 86.0°. Each ring can consist of up to five detectors, although only a total of eight detectors will be available. Again a range of target to detector distances is permitted. These detectors are a further development of those used in the Cluster detectors. Each MINIBALL detector comprises three encapsulated Ge crystals, the same size as the Cluster capsules, mounted in one cryostat. Each of these capsules is electronically segmented six ways on its outer surface. The signals from each segment are read out independently and passed to a digital electronics system. The digital electronics is then used to determine the energy, time of interaction and, by complex pulse shape analysis, the position of interaction in the crystal. Information on the position of the main interaction in the crystal, supposed to be the first interaction, is extremely useful in these fast beam experiments since the correspondingly improved Doppler correction allows the detector to be placed significantly closer to the target. This increases the efficiency while maintaining good resolution. If a position resolution determination of 5 mm is assumed, a minimum distance smaller than the beam pipe diameter (130 mm) for a detector angle of 90° is derived for 1% energy resolution at $\beta = 0.43$.

However, the minimum distance is determined by the mechanical constraints of the beam pipe and target chamber (relaxing the position resolution requirement). There is an additional constraint imposed by the isolated hit probability and the intense atomic background. As discussed in Section 2.2 the dominant background from bremsstrahlung scales with the charge of projectile and target. For the worst case, corresponding to a ^{238}U beam incident on a ^{208}Pb target, the closest Ge detectors may be placed 400 mm distance from the target.

Table 2
Estimated performance of an array with Ge detectors at the closest position and at a position optimised for energy resolution considering the highest background from atomic radiation

Ring	Distance (mm)	Energy resolution (%)	Efficiency (%)
1	700	1.00	1.00
2	700	1.82	0.91
3	700	1.93	0.89
Total Cluster		1.56	2.81
4	180	0.70	2.75
	227	0.57	0.46
5	180	0.68	1.01
	232	0.56	0.32
Total MINIBALL		0.67	4.55
Total array		1.01	7.35
1	700	1.00	1.00
2	1295	1.01	0.28
3	1372	1.01	0.24
Total Cluster		1.00	1.52
4	400	0.36	0.82
5	400	0.37	0.36
Total MINIBALL		0.36	1.18
Total array		0.73	2.70

The given efficiencies include the Lorentz boost.

Table 2 shows the calculated performance of RISING assuming a 1.3 MeV γ ray emitted from a nucleus moving at $\beta = 0.43$. In these calculations the velocity spread in the target and the recoil cone were ignored. The total energy resolution is a weighted average of the energy resolution scaled by the efficiency.

All experiments so far were performed with the Cluster detectors in their closest position (700 mm). To reduce the contribution from the atomic background radiation, each Cluster detector was surrounded on the side by the lead shield of 2 mm thickness, and had in the front side a combination of Pb, Sn and Al absorbers of 5 mm thickness. The efficiency was determined experimentally with standard γ-ray sources. A comparison with corresponding simulation calculations revealed a very good agreement. Multiplying with the appropriate Lorentz factor results in 3% efficiency at 100 A MeV for 1.3 MeV γ ray. The preliminary energy resolution ranging from 1.2% to 1.5% is in agreement with the calculated value.

6. High-energy γ-ray detection with the HECTOR array

In order to have the possibility of measuring low and high energy γ rays with comparable efficiency, eight large-volume BaF_2 scintillators (part of the HECTOR array) are placed in the RISING set-up. These detectors have a good time resolution and high detection efficiency, complementing the Ge-Cluster detectors. The sub-nanosecond time resolution means that one can use the time information to identify sources of various background components. In addition, these detectors can be used to measure low-energy transitions when they correspond to well separated lines in the spectra resulting in an increase of the overall efficiency of the γ-ray detection system.

6.1. HECTOR array for experiments at relativistic energies

The HECTOR array consists of eight large scintillating crystals of BaF_2, 145 mm in diameter and 175 mm in length [43,44]. The crystals are tapered for half of the length in a hexagonal shape and have a cylindrical shape for the second half. Each crystal is coupled to a single fast photo-multiplier tube (EMI 9823QA, 125 mm in diameter) with a quartz window, selected for its stability in terms of counting rate and connected to an active voltage divider. Each BaF_2 detector works at an operating voltage set between −1500 and −1800 V to maximise the linearity of its response with respect of the incident energy. For the same purpose, the energy signal is taken from the 10th dynode of the photo-multiplier. Due to the very fast scintillation light of BaF_2 material, each detector has a sub-nanosecond intrinsic time resolution. The energy resolution is of the order of 10% for the 1173 and 1332 keV lines of ^{60}Co.

The gain fluctuations of each detector are monitored by a LED system that produces three light pulses of different intensity corresponding to three different energies detected in the crystal, spread over the range of interest of the experiment. The light pulses can be triggered either internally or externally by a NIM signal [45]. The internal radiation arising from radium contaminations in BaF_2 crystals is used to monitor the performance of the detectors.

In the RISING set-up, the BaF_2-HECTOR detectors are placed at 350 mm from the target at a backward angle of 142°. It is also possible to place two detectors at 90° without interfering with the Ge-Cluster detectors or with MINIBALL Ge detectors. This geometry represents a compromise to get the maximum solid angle, with a minimum

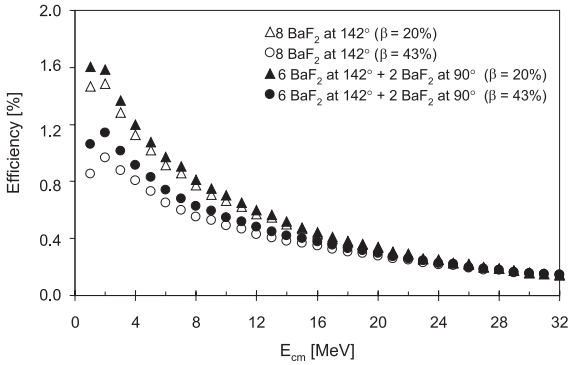

Fig. 10. Simulated HECTOR array efficiency as a function of γ-ray energy in the centre of mass frame.

Doppler broadening effect. To reduce the contribution from the atomic background radiation, each crystal is surrounded on the side by a lead shield of 6 mm thickness, and has on the front side selectable Pb-absorbers of 1, 3 or 6 mm thickness.

The performance of the BaF_2-HECTOR detectors in the RISING set-up and for the measurement of γ rays from relativistic beams has been simulated using the GEANT 3.21 programme [46]. Fig. 10 shows the absolute full-energy peak efficiency for the BaF_2 detectors placed at 350 mm at 142° or 90° and assuming a source velocity of $\beta = 0.2$ and 0.43.

6.2. Background investigation in the commissioning phase

In addition to the primary role of measuring high-energy γ rays emitted from the giant dipole resonance, the eight BaF_2 detectors have been shown to be very useful for the investigation of sources of disturbing background radiation in the RISING experiments.

Fig. 11 shows the time spectra measured with the 142° BaF_2-detector as obtained with a ^{84}Kr beam at 113 A MeV on an Au target and for an empty target frame. The spectra show a rather large contribution from background radiation (the broad distribution peaked at −5 ns). From the value of the centroid position of the broad

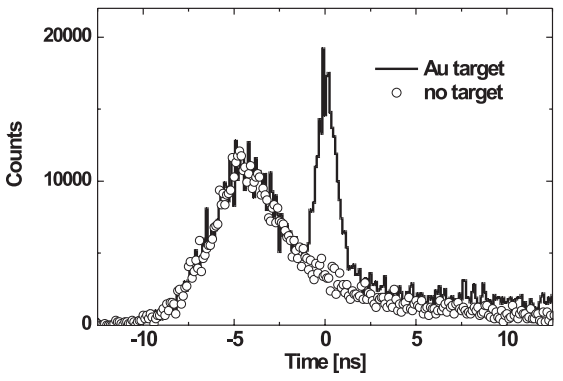

Fig. 11. Time spectra measured with a BaF_2 detector with respect to start signals from the plastic scintillator SCI2, using the relativistic ^{84}Kr beam and an Au-target (solid line), or an empty target frame (open circles).

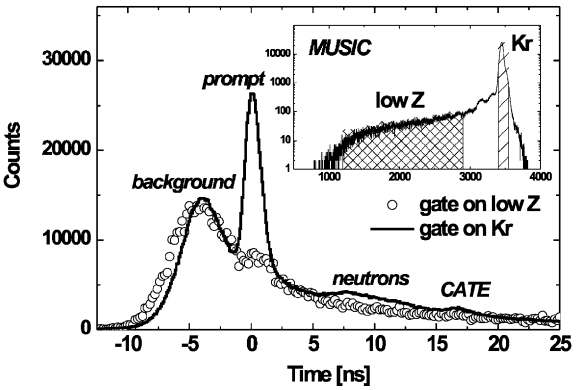

Fig. 12. Time spectra gated by the energy deposited in the MUSIC chamber (see inset), one gate corresponds to the low-Z fragments (open circles) and the other gate to the Z of the primary Kr beam (solid line).

structure it is deduced that this background radiation is originating from decays occurring at a distance of 1–4 m upstream from the target. The prompt radiation from the target gives rise to the narrow peak at $t = 0$.

Fig. 12 shows two time spectra gated by different values of the energy deposited in the MUSIC detector. The spectrum gated on the low-Z fragments has a shape very similar to that measured with the target frame only (see Fig. 12) and therefore it contains predominantly the background contribution. In contrast, the spectrum gated by the Z value of the ^{84}Kr beam clearly shows the prompt peak associated with events from the target. The background radiation, preceding the prompt peak from the target, still remains indicating that it is related to fragmentation reactions occurring behind the MUSIC chamber. In addition, different components of the radiation detected by the BaF_2 detector are seen. Delayed radiation and neutrons emitted from the target (7–12 ns after the prompt peak) and the γ radiation from reactions induced by the Kr beam hitting the CATE detector (17 ns after the prompt radiation), can be identified. Following this observation, a Pb absorber wall has been built to reduce the upstream background which cannot be separated by time conditions in the Ge detectors due to their limited time resolution.

7. Data acquisition and control system

As described in previous sections, RISING is a combination of three independent detector systems, the EUROBALL Ge-Cluster detectors, the HECTOR array and the FRS detectors including the CATE array. Each of these systems has an individual data acquisition systems (DAQ) producing independent events. To assemble them in common events, a time-stamping technique for event synchronisation, was developed in the framework of the GSI standard DAQ system, MBS [47]. Each sub-system is equipped with a newly developed VME time stamping module, TITRIS [48]. It produces a single-hit 48-bit time stamp with the least significant bit being 20 ns. As the hardware set-up is identical in all branches one TITRIS module is arbitrarily chosen to be a master, while all the others are slaves. All of them are connected in a line via a synchronisation bus, the length of which can exceed 100 m. The master module sends regularly synchronisation pulses to all slave modules and in this way keeps all modules on the same time base. Within this procedure, the signal cable delay of the calibration pulses is automatically taken into account by the slave modules. Tests and in-beam measurements revealed a precision better than 20 ns (RMS) for the complete timing system. Within the TITRIS module, the special daisy-chain readout is available, which is mandatory for the EUROBALL VXI system. The design of the time stamping system allows for the integration of up to 16 TITRIS modules in a system. Thanks to this new approach it is possible to keep most of the original components of the RISING sub-systems in operation. They still run independently and are fully operational DAQ systems with individual trigger sources and produce their local dead time for the readout. In addition, it is also possible to feed identical triggers into all sub-system and to combine their local dead times, as it was done for the RISING set-up. Upon receipt of each accepted trigger, the digitisers are read out and the event data are sent via a TCP socket to an event builder. The time-stamping module gets a signal

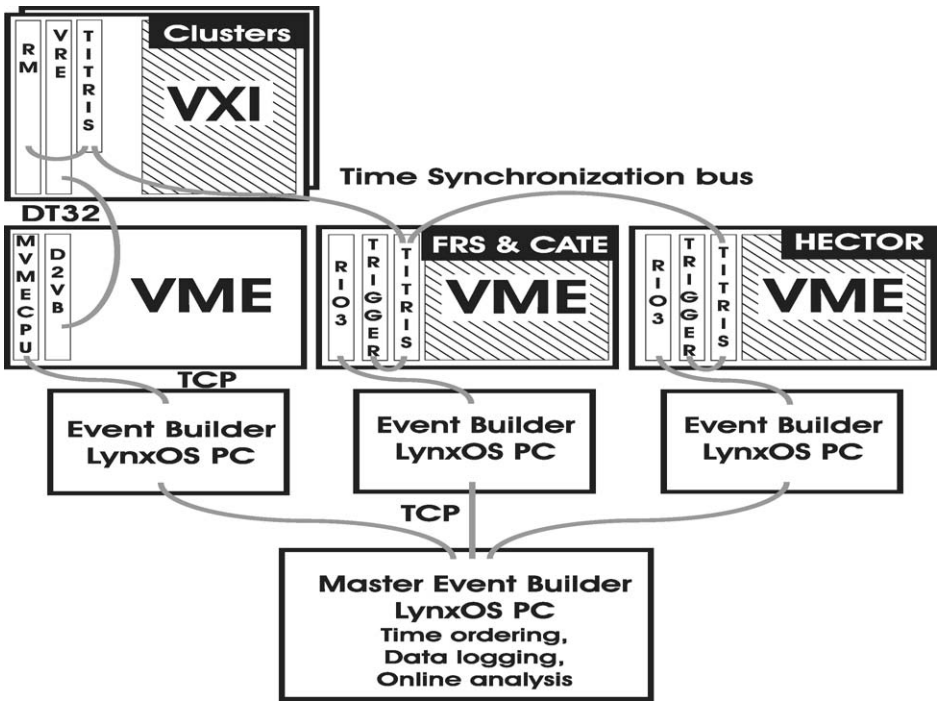

Fig. 13. Block diagram of the RISING data acquisition system.

from the Master Trigger Output signal for each accepted trigger. The time difference of the time stamps from the same trigger amounts to about 3 μs and is caused by various signal delay times of the VXI trigger card and the Master Trigger Output of the VME trigger module. This constant time offset must be taken into account for the time matching of events from different sub-systems. A schematic diagram of the RISING DAQ system is presented in Fig. 13.

The Cluster detector signals are processed and digitised by the VXI Ge-Cluster cards providing 4 and 20 MeV energy ranges and γ-ray time with respect to the VXI trigger. The cards are read out by the VXI Readout Engine (VRE) and then sent via the DT32 bus (10 MHz, 32-bit differential ECL) to a VME processor [49]. Up to this stage the procedure is identical to previous EUROBALL experiments [50]. The VXI modules and DAQ are controlled by the MIDAS software package [51]. On the VME processor a new programme developed for RISING sends event data in large data blocks via TCP sockets to an MBS event-builder PC. This event-builder receives the data, converts it into the MBS data format and provides it for further processing like data logging, online monitoring and most importantly as a data source for the RISING master event-builder described below. The DAQ system for FRS/CATE and HECTOR are structurally identical MBS systems. A VME crate contains a RIO3 readout processor, the GSI trigger module, the TITRIS time stamping module and digitisers, QDC, ADC, TDC, scaler and pattern unit. The energy and time signals from the BaF_2 detectors were collected for the HECTOR DAQ. For the fast component, a dedicated signal shaping and stretching module was developed to adopt the timing signal to the Ge branch. In order to set up and calibrate the BaF_2 array, a special data acquisition system, based on K-Max 7.2 [52] was employed.

The collecting and sorting of the data from all sub-systems is made by the RISING master event-builder running with an independent MBS system. For this purpose a new MBS programme has been developed. It has to fulfil three main tasks:

(1) Connect (and disconnect) rapidly to the sub-systems data output stream via TCP sockets. This allows for easy partitioning of the DAQ system, i.e. during set up phases.
(2) Sort all events from the connected systems according to their time stamps in ascending order into a single data output stream.
(3) Format all events into output buffers for data logging and online monitoring purposes.

It is the task of the data analysis, not the DAQ system, to select from the time-sorted event stream those which have to be combined into a real "physics" events. This allows the flexibility of using different criteria to compose events from identical data sets.

The basic trigger signal is derived from the SCI2 (see Section 3) providing a fast NIM signal, useful in defining local triggers and establishing the time reference. Two kinds of physics triggers are implemented with the help of the SCI2 signal:

(1) SCI2 and at least one γ ray in any Cluster detector in coincidence form a physics trigger, which is fed simultaneously to the Cluster detector—and the FRS/CATE DAQ system.
(2) SCI2 in coincidence with at least a single γ ray in the HECTOR array. This trigger initiates the readout of FRS/CATE and HECTOR.

In addition, a γ-ray singles trigger for calibration and control purposes is foreseen. A second type of a trigger is associated with generation of control LED pulses used to monitor the stability of the detector gains.

The on-line analysis of the combined RISING data was performed using the GO4 package developed at GSI [53]. An object-oriented programme picked up a portion of the data output stream from the MBS master event builder. Subsequently, it produced raw histograms and allowed for merging time sorted sub-events into complete physical events. Various conditions on the histograms could be set and combined in an unrestricted way using a graphical user interface [54], which also facilitated visualisation of the histograms. Among other plots, two-dimensional synchronisation matrices of control signals originating from different MBS branches were dis-

Table 3
Summary of experimental details of the first RISING measurements including the nucleus of interest, primary and secondary beams, secondary targets, excitation methods and γ-ray transitions of interest

Nucleus of interest	^{84}Kr	^{56}Cr	^{53}Ni	^{108}Sn
Primary beam (A MeV)	^{84}Kr	^{86}Kr	^{58}Ni	^{124}Xe
(SIS energy)	165	419	600	700
Secondary beam (A MeV)	—	^{56}Cr	^{55}Ni	^{108}Sn
(energy at target)	113	136	171	142
Secondary target	^{197}Au	^{197}Au	^{9}Be	^{197}Au
Thickness (g/cm^2)	0.4	1.0	0.7	0.4
Experimental method	Coul. ex.	Coul. ex.	Two-step. frag.	Coul. ex.
γ ray of interest (keV)	882	1006	Unknown	1206
$I_i^\pi \rightarrow I_f^\pi$	$2^+ \rightarrow 0^+$	$2^+ \rightarrow 0^+$		$2^+ \rightarrow 0^+$

played. Calibrated and Doppler-corrected γ-ray spectra, gated by the tracking detectors, were available on-line.

8. First experiments and data analysis

Four experiments have been performed with the RISING set-up so far. Table 3 summarises experimental details of the measurements including the nucleus of interest, primary and secondary beams, secondary target, experimental method and the γ-ray transition of interest. In all cases γ rays depopulating excited states were measured by the Ge-Cluster and BaF_2-HECTOR arrays. Preliminary results of the still on-going data analysis will be presented to illustrate the performance of the set-up.

In the first experiment, a primary beam of ^{84}Kr was impinging on a ^{197}Au target mounted in the final focal plane of the FRS in order to investigate the feasibility of Coulomb excitation measurements under the best beam conditions by measuring the $2^+ \rightarrow 0^+$ γ transition in ^{84}Kr and to study the particle–γ angular correlation at relativistic energies. Two relativistic Coulomb excitation experiments with secondary beams were performed to measure B(E2) values of transitions, depopulating the first 2^+ state in radioactive neutron-rich ^{56}Cr and neutron-deficient ^{108}Sn. In the case of ^{108}Sn, a thinner ^{197}Au target and higher energy of the secondary beam than in the case of ^{56}Cr were chosen because of the expected short lifetime (~ 0.4 ps) of the first 2^+ state of ^{108}Sn. Thus, the fraction of γ rays from decays in the target, causing large Doppler-shift uncertainties, as discussed in Section 5.1, is reduced.

A two-step fragmentation method was applied to identify the first excited states in ^{53}Ni. The goal of the measurement was to study the mirror symmetry between ^{53}Ni and ^{53}Mn. A secondary beam of ^{55}Ni was produced by fragmentation of a ^{58}Ni primary beam on a Be target, and was impinging on a secondary beryllium target mounted at the final focal plane of the FRS. The reaction fragments were detected by CATE using the ΔE–E correlation.

Data analysis was performed by software based on GO4 [53] and ROOT [55], developed for off-line analysis. The examples shown below are the first results of the RISING experiments on ^{84}Kr, ^{56}Cr and ^{53}Ni.

The selected particles, reaching the secondary target were identified in terms of A/Q and Z by TOF and MUSIC, respectively, as described in Section 3. Out-going particles after the target were identified and selected by CATE using ΔE–E correlations. Since the mass analysis of CATE is still in progress, only different elements can be selected at present. γ rays within a time range of ± 25 ns were selected with a further requirement of multiplicity $M_\gamma = 1$ for $E_\gamma \geqslant 500$ keV (in the laboratory frame). In- and out-going particles were tracked by the two Multi-Wire chambers before the target and by CATE behind the target.

The vertex on the target, the scattering angle between an in- and an out-going particle and the angle between an out-going particle and a γ ray were calculated event-by-event. A range of scattering angles was selected in order to enhance the Coulomb excitation events. The calculated angle between an out-going particle and a γ ray was used for Doppler correction. A velocity factor, β_t, behind the target, which is used for Doppler correction, was calculated event-by-event by using the TOF measurement with the two plastic scintillators together with the calculated energy loss in the target.

Since in the ^{84}Kr experiment the primary beam directly impinged on a gold target, selection of the in-coming projectile was not necessary and a fixed $\beta = 0.396$ was used for the Doppler correction. Out-going particles with $Z = 36$ were selected by CATE. A conservatively chosen range of scattering angles between 0.7° and 1.5° was demanded. Fig. 14(b) shows a Doppler-corrected γ-ray spectrum under the above conditions. The

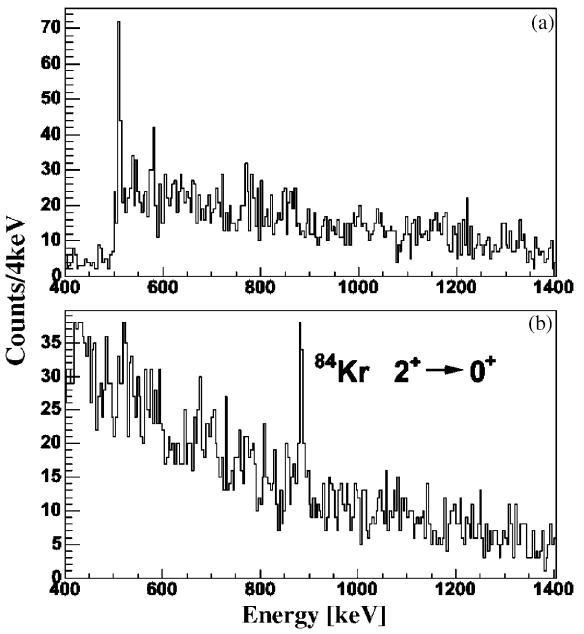

Fig. 14. Gamma-ray spectra for 113 A MeV ^{84}Kr projectile Coulomb excitation on a 0.4 g/cm^2 thick Au target, (a) without and (b) with Doppler correction. The $2^+ \rightarrow 0^+$ transition at 882 keV is marked.

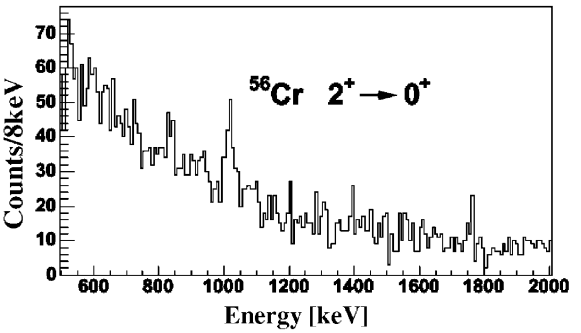

Fig. 15. Doppler-corrected γ-ray spectrum of ^{56}Cr Coulomb excitation at 136 A MeV on a 1.0 g/cm^2 gold target.

882 keV ($2^+ \rightarrow 0^+$) transition of ^{84}Kr is clearly visible. No background subtraction was applied. The FWHM and the significance of the peak are 1.5% and 8σ, respectively. For comparison, the same spectrum without Doppler correction is displayed in Fig. 14(a). Here, the γ-ray intensity corresponding to the ($2^+ \rightarrow 0^+$) transition is distributed between 1100 and 1400 keV leaving no indication of a peak.

For the analysis of the ^{56}Cr data similar method was applied. Out-going particles with $Z = 24$ and a scattering angle between 0.5° and 3.5° were selected by CATE to enhance Coulomb excitation events. The velocity, β_t, was determined event-by-event with the TOF measurements and corrected for energy loss in the target. In Fig. 15, the Doppler-corrected γ-ray spectrum under the above conditions is shown. The $2_1^+ \rightarrow 0^+$ transition at 1006 keV is clearly observed.

For the ^{53}Ni data only very preliminary results of the analysis performed during the experiment are currently available. As no information on tracking and TOF was used for the event reconstruction, the angle of Ge-detectors with respect to the target centre was used for the Doppler-correction with a fixed $\beta_t = 0.45$. The selection of scattering angles was not done. In Fig. 16, Doppler-corrected γ-ray spectra are shown for different element selection by CATE, (a) Co, (b) Fe, and (c) Cr. For these spectra only 10% of the data were analysed. In Fig. 16(a), the known γ-transitions ($2^+ \rightarrow 1^+$) at 509 keV and ($1^+ \rightarrow 0^+$) at 937 keV in ^{54}Co are indicated. In Fig. 16(b), the

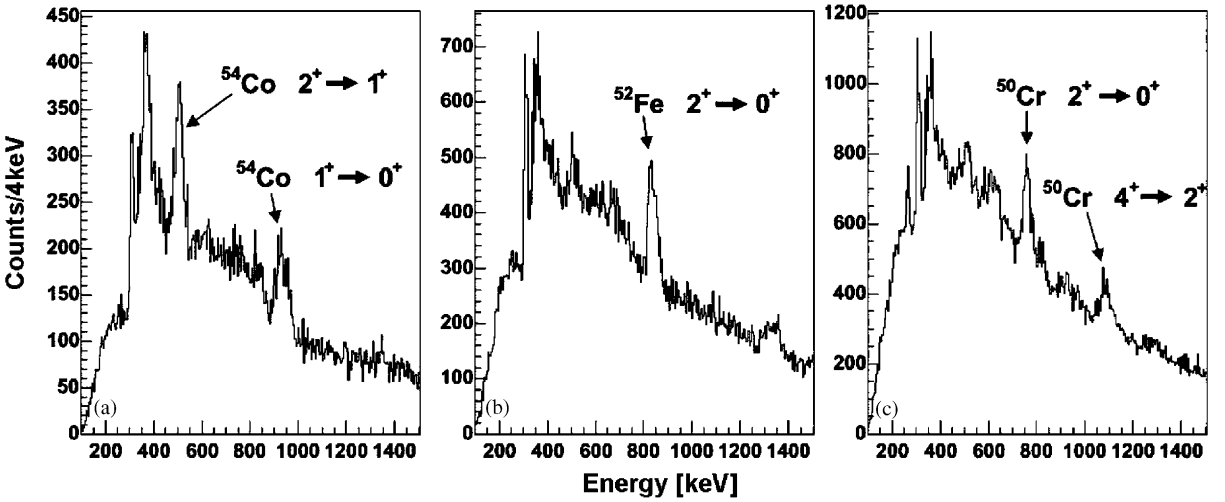

Fig. 16. Gamma-ray spectra of the fragmentation reaction ^{55}Ni on ^{9}Be with selection on different elements: (a) Co, (b) Fe, and (c) Cr.

($2^+ \rightarrow 0^+$) 849 keV transition of ^{52}Fe is shown, and in Fig. 16(c) the ($2^+ \rightarrow 0^+$) and ($4^+ \rightarrow 2^+$) transitions of ^{50}Cr at 783 and 1098 keV, respectively, are present, demonstrating that fragmentation reactions populate states with spins beyond $2\hbar$. Additional peak structures in all three spectra are due to the decay of higher lying states of the selected isotopes and transitions in other isotopes since no mass selection was applied. The γ-ray energies in Fig.16 are slightly shifted as compared to the literature values and the peaks are broader than expected. This results from the absence of tracking and β measurement in the on-line analysis. The event-by-event analysis which is now in progress will significantly improve the final result.

9. Summary and conclusion

The RISING set-up allows for high-resolution γ-ray spectroscopy experiments employing beams of short-lived isotopes at 100 A MeV energy from the SIS/FRS facility at GSI. It comprises heavy-ion tracking detectors for incoming beam nuclei impinging on a secondary target, the CATE detector for outgoing heavy ions and the EUROBALL Ge-Cluster detector and BaF_2-HECTOR detector arrays for γ-ray detection. A new data acquisition system with independent subsystems linked by time stamps was employed for the first time at GSI to connect three data branches.

The set of particle detectors is capable of uniquely determining the mass and charge of each beam nucleus with the necessary precision. In addition, they allow the measurement of the velocity and direction of the fast-moving nucleus, information necessary to perform the Doppler correction of the measured γ-ray energy. The first phase of the Cluster array has a full-energy efficiency of 3% with 1.2–1.5% energy resolution at 100 A MeV. The novel position-sensitive ΔE–E calorimeter, CATE, enables an accurate scattering angle determination, limited only by target angular straggling. The charge identification is unique and a mass identification with a resolution of $\Delta A/A \geqslant 0.5\%$ is expected, depending on further ongoing complex analysis steps. The excellent time resolution of the HECTOR array has been used to identify background sources, which were reduced during commissioning.

The first Coulomb excitation and secondary fragmentation experiments with RISING demonstrated that the set-up fulfils all requirements and provides a new powerful instrument for high-resolution in-beam γ spectroscopy at relativistic energies.

Acknowledgements

The collaboration would like to thank the EUROBALL Owners Committee, the MINIBALL Collaboration and the HECTOR collaboration for making the detectors available for the RISING campaigns at GSI. J.J., P.R. and N.W. acknowledge support of the BMBF under grant 06OK-167. H.H. and A.B. acknowledge support of the BMBF under grant 06BN-109. K.-H.S. and J.L. acknowledge support of the BMBF under grant 06BN-911. The Swedish coauthors acknowledge the Swedish Research Council. The Polish coauthors acknowledge the Polish State Committee for Scientific Research (KBN Grant No. 2P03B 118 22).

References

[1] H. Geissel, et al., Nucl. Instr. and Meth. B 70 (1992) 286.
[2] J.F. Ziegler, J.B. Biersack, U. Littmark, The Stopping and Range of Ions in Solids, vol.1, Pergamon Press, Oxford, 1985.
[3] http://www-linux.gsi.de/weick/atima/.
[4] R. Anhold, S.A. Andriamonje, E. Morenzoni, C.H. Stoller, J.D. Molitoris, W.E. Meyerhof, H. Bowman, J.-S. Xu, J.O. Rasmussen, D.H.H. Hoffmann, Phys. Rev. Lett. 53 (1984) 234.
[5] R. Anhold, et al., Phys. Rev. A 33 (1986) 2270.
[6] R. Holzmann, K. Grimm, R. Kulessa, E. Wajda, H. Xie, M. Zinser, the LAND Collaboration, GSI Annual Report, 1992, p. 48.
[7] T. Glasmacher, Annu. Rev. Nucl. Part. Sci. 48 (1998) 1.
[8] W.W. Wilcke, J.R. Birkelund, H.J. Wollersheim, A.D. Hoover, J.R. Huizenga, W.U. Schröder, L.E. Tubbs, At. Data Nucl. Data Tables 25 (1980) 391.
[9] J.D. Jackson, Classical Electrodynamics, Wiley, New York, 1974, p. 620.
[10] F. Azaiez, et al., Nuclear Structure 98, Gatlinburg, TN, AIP, Conference Proceedings, vol. 481, 1998, p. 243.
[11] S. Wan, et al., Eur. Phys. J. A 6 (1999) 167.
[12] K. Yoneda, et al., Phys. Lett. B 499 (2001) 233.
[13] J.-J. Gaimard, K.-H. Schmidt, Nucl. Phys. A 531 (1991) 709.
[14] M. de Jong, A.V. Ignatyuk, K.-H. Schmidt, Nucl. Phys. A 613 (1997) 435.
[15] K. Sümmerer, B. Blank, Phys. Rev. C 61 (2000) 034607 and references therein.
[16] K. Sümmerer, B. Blank, EPAX version 2.1 http://www-w2k.gsi.de/hellstr/asp/gsi/epaxv21m.asp.
[17] T. Enqvist, et al., Nucl. Phys. A 658 (1999) 47.
[18] J. Benlliure, K.-H. Schmidt, D. Cortina-Gil, T. Enqvist, F. Farget, A. Heinz, A.R. Junghans, J. Pereira, J. Taieb, Nucl. Phys. A 660 (1999) 87.
[19] C. Engelmann, et al., Z. Phys. A 352 (1995) 351.
[20] M. Bernas, et al., Phys. Lett. B 331 (1994) 19.
[21] M. Bernas, et al., Phys. Lett. B 415 (1997) 111.
[22] C. Donzaud, et al., Eur. Phys. J. A 1 (1998) 407.
[23] W. Schwab, et al., Eur. Phys. J. A 2 (1998) 179.
[24] J. Benlliure, et al., Eur. Phys. J. A 2 (1998) 193.
[25] H.J. Wollersheim, www-aix.gsi.de/~wolle/ISOMER/fission_cross.pdf.
[26] N. Iwasa, et al., Nucl. Instr. and Meth. B 126 (1997) 284.
[27] O. Tarasov, D. Bazin, Nucl. Instr. and Meth. B 204 (2003) 174; The LISE code web sites: http://groups.nscl.msu.edu/lise and http://dnr080.jinr.ru/lise.
[28] H. Stelzer, Nucl. Instr. and Meth. A 310 (1991) 103.
[29] R. Schneider, A. Stolz, Technical Manual Ionisation Chamber MUSIC80, 2000.
[30] N. Le Neindre, et al., Nucl. Instr. and Meth. A 490 (2002) 251.
[31] R. Lozeva, et al., to be published.
[32] T. Doke, J. Kikuchi, H. Yamagichi, S. Yamaguchi, K. Yamamura, Nucl. Instr. and Meth. A 261 (1987) 605.
[33] U. Bonnes, J. Foh, private communication.
[34] P. Doornenbal, Diploma Thesis, University of Frankfurt, Germany, 2003.
[35] R. Lozeva, et al., Nucl. Instr. and Meth. B 204 (2003) 678.
[36] A. Pullia, R. Bassini, C. Boiano, S. Brambilla, IEEE Trans. Nucl. Sci. NS-48 (3) (2001) 530.
[37] D. Pelte, D. Schwalm, In-beam Gamma-ray Spectroscopy with Heavy Ions, North-Holland, Amsterdam, 1982.
[38] D. Schwalm, A. Bamberger, P.G. Bizzeti, B. Povh, G.A.P. Engelbertink, J.W. Olness, E.K. Warburton, Nucl. Phys. A 192 (1972) 449.
[39] J. Simpson, Z. Phys. A 358 (1997) 139; Achievements with the EUROBALL spectrometer, in: W. Korten, S. Lunardi (Eds.), Scientific and Technical Report 1997–2003, 2003, http://www-dapnia.cea.fr/Sphn/Deformes/EB/eb-report-final.pdf.
[40] J. Eberth, et al., Prog. Part. Nucl. Phys. 46 (2001) 389.
[41] J. Eberth, et al., Nucl. Instr. and Meth. A 369 (1996) 135.
[42] M. Wilhelm, et al., Nucl. Instr. and Meth. A 381 (1996) 462.
[43] A. Maj, et al., Nucl. Phys. A 571 (1994) 185.
[44] F. Camera, Ph.D Thesis, University of Milano, Italy, 1992.
[45] A. Boiano, et al., to be published.
[46] CERN Geneva, GEANT—Detector Description and Simulation Tool [online]. pp. 1–430. Available: http://wwwinfo.cern.ch/asd/geant/geantall.ps.gz.
[47] H.G. Essel, J. Hoffmann, N. Kurz, R.S. Mayer, W. Ott, D. Schall, IEEE Trans. Nucl. Sci. NS-43 (1) (1996) 132; H.G. Essel, N. Kurz, IEEE Trans. Nucl. Sci. NS-47 (2) (2000) 337.
[48] J. Hoffmann, N. Kurz, GSI Scientific Report, 2002, p. 224.
[49] I. Lazarus, P. Coleman-Smith, N. Karkour, G.M. McPherson, A. Richard, C. Ring, IEEE Trans. Nucl. Sci. NS-39 (1992) 1352;

I. Lazarus, P.J. Coleman-Smith, IEEE Trans. Nucl. Sci. NS-42 (1995) 891;
I. Lazarus, P. Coleman-Smith, J. Thornhill, G. Bosson, N. Karkour, A. Richard, Z. Zojceski, C. Ring, IEEE Trans. Nucl. Sci. NS-42 (1995) 2288;
M.M. Aleonard, et al., IEEE Trans. Nucl. Sci. NS-39 (1992) 892;
J. Alexander, F.A. Beck, C. Ender, I. Lazarus, G.M. McPherson, E.C.G. Owen, J. Pauxe, A. Richard, C. Ring, IEEE Trans. Nucl. Sci. NS-39 (1992) 886.

[50] G. Maron, V. Pucknell, A data acquisition system for EUROBALL III, EDOC306, http://npg.dl.ac.uk/documents/edoc306/.
[51] V.F.E. Pucknell, The MIDAS Multi Instance Data Acquisition System, http://npg.dl.ac.uk/MIDAS.
[52] KMAX—Sparrow Corporation, 1901 Poppy Lane Port Orange, FL 32128, USA.
[53] http://www-w2k.gsi.de/go4/.
[54] J. Grębosz, private communication.
[55] http://root.cern.ch/.

INSTITUTE OF PHYSICS PUBLISHING JOURNAL OF PHYSICS G: NUCLEAR AND PARTICLE PHYSICS

J. Phys. G: Nucl. Part. Phys. **31** (2005) S1527–S1530 doi:10.1088/0954-3899/31/10/025

Spectroscopy of nuclei approaching the proton drip-line using a secondary-fragmentation technique with the RISING detector array

M J Taylor[1,16], G Hammond[2,16], M A Bentley[2,16], F Becker[3], J Grębosz[4], A Banu[5], C J Barton[6], T Beck[3], P Bednarczyk[4], A Bracco[7], A M Bruce[1], L C Bullock[2], A Bürger[8], F Camera[7], C Chandler[2], P Doornenbal[3], J Gerl[3], H Geissel[3], M Górska[3], M Hellström[3], D S Judson[1], I Kojouharov[3], N Kurz[3], R Lozeva[9], A Maj[4], S Mandal[3], B McGuirk[10], S Muralithar[11], E S Paul[10], Z Podolyák[12], W Prokopowicz[3], D Rudolph[13], N Saito[3], T R Saito[3], H Schaffner[3], J Simpson[14], D D Warner[14], H Weick[3], C Wheldon[15], M Winkler[3] and H J Wollersheim[3]

[1] School of Engineering, University of Brighton, Brighton, BN2 4GJ, UK
[2] School of Chemistry and Physics, Keele University, Staffordshire, ST5 5BG, UK
[3] Gesellschaft für Schwerionenforschung (GSI), Darmstadt, D-64291, Germany
[4] Institute of Nuclear Physics (IFJ), Kraków, 31-342, Poland
[5] Institut für Kernphysik, Universität Mainz, Mainz, 55099, Germany
[6] Department of Physics, University of York, York, YO10 5DD, UK
[7] Department of Physics, University of Milano and INFN, Milano, Italy
[8] Helmholtz-Institut für Strahlen- und Kernphysik, Bonn, D-53115, Germany
[9] Faculty of Physics, University of Sofia 'St Kl Ohridski', Sofia, 1164, Bulgaria
[10] Department of Physics, University of Liverpool, Liverpool, L69 7ZE, UK
[11] Nuclear Science Centre, New Delhi, 110067, India
[12] Department of Physics, University of Surrey, Guildford, GU2 7XH, UK
[13] Department of Physics, Lund University, Lund, S-22100, Sweden
[14] CCLRC Daresbury Laboratory, Warrington, Cheshire, WA4 4AD, UK
[15] Hahn-Meitner-Institut, Berlin, 14109, Germany

Received 21 March 2005
Published 12 September 2005
Online at stacks.iop.org/JPhysG/31/S1527

Abstract

An experiment utilizing a double fragmentation reaction was performed to study isobaric analogue states in $A \sim 50$ nuclei approaching the proton drip-line. γ-ray spectroscopy will be used to identify excited states in the neutron-deficient nuclei produced in the second fragmentation reaction. Excited state level schemes will be obtained, through comparison with states in their well-known mirror partners, along with information on Coulomb effects through measurements of the Coulomb energy differences between isobaric analogue excited states. The validity of isospin symmetry for nuclei approaching the proton drip-line can also be investigated and the information gained will aid in testing and improving fp shell model calculations. The analysis of the collected data is at a preliminary stage and current status of this work is reported.

[16] Present address: Department of Physics, University of York, York, YO10 5DD, UK.

1. Introduction

The study of exotic nuclei near to the proton drip-line has had renewed interest as more and more nuclei have become experimentally accessible, due to technological and accelerator improvements. Fragmentation reactions have proven their ability of producing $N \sim Z$, $A \approx 50$ nuclei with large cross-sections compared with fusion–evaporation reactions. The production of these neutron-deficient nuclei, along with their mirror partners, is of great interest as they provide ideal laboratories for investigating isospin symmetry and Coulomb effects for large proton excess and also probe the extent of nuclei bound to ground or excited state proton emission. Full fp shell model calculations have been shown to be successful when explaining the properties of nuclei in the upper half of the $f_{7/2}$ shell but fall short for nuclei in the lower half where excitations from the closed ^{40}Ca core contribute to the excited state wavefunctions. Spectroscopic information gained from this work on the produced neutron-deficient fp-shell nuclei can be used to test and improve shell model calculations in this region. Nuclei such as ^{45}Cr and ^{44}V for which no γ-ray transitions have yet been observed and ^{43}V which is the lightest bound V isotope with the last proton being bound by ~200 keV are of particular interest. It is expected for ^{43}V that a combination of the centrifugal and Coulomb barriers will strongly inhibit proton emission from the yrast excited states and that γ decays will be observed. In fact, γ decays have recently been observed from yrast states between $J^\pi = 3/2^-$ and $13/2^-$ in ^{61}Ga [1] where the proton binding energy is very similar.

2. Experimental details

The experiment was performed at the GSI laboratory in Darmstadt, Germany and utilized a two-step fragmentation reaction. A beam of ^{58}Ni (5×10^8 pps) was accelerated to 600 MeV A^{-1} and impinged on a ^{9}Be target (4 g cm^{-2}) located at the entrance of the FRagment separator (FRS) [2]. The FRS separated the fragments of interest which were then identified using a combination of inline detectors, multi-wire and scintillation detectors and an ionization chamber. The separated fragments (~4×10^5 pps), with energies ~170 MeV A^{-1}, then impinged on a second ^{9}Be target (700 mg cm^{-2}) where a second fragmentation reaction occurred. De-excitation γ rays emitted from these high velocity fragments ($v/c \approx 50\%$) were detected by the rising Ge detector array. References [3, 4] give a detailed description of the experimental setup. The fragments from the second reaction were detected downstream in a CAlorimeter TElescope (CATE) [5] which consisted of nine individual position sensitive Si detectors arranged in a square geometry behind which were nine CsI detectors arranged in the same geometrical configuration. The Si detectors provide an energy loss signal for the fragments passing through which can be used to provide Z identification and the residual energy deposited in the CsI detectors combined with the energy loss in the Si detectors can provide fragment mass identification. By correlating implanted and identified fragments with detected prompt γ rays, spectroscopy of exotic neutron-deficient nuclei can be performed.

3. Data analysis

The selection of primary fragments of ^{55}Ni (or ^{55}Co) and secondary fragments of Ni (or Fe) in CATE (without any isotopic selection), allows prompt γ-ray spectra to be produced. Figure 1(a) shows such a Doppler corrected γ-ray spectrum for all the Ni isotopes produced. Transitions at 1227 and 1392 keV can clearly be seen which correspond to the $4_1^+ \rightarrow 2_1^+$ and $2_1^+ \rightarrow 0_1^+$ transitions respectively, in ^{54}Ni [6], which has the largest production cross-section.

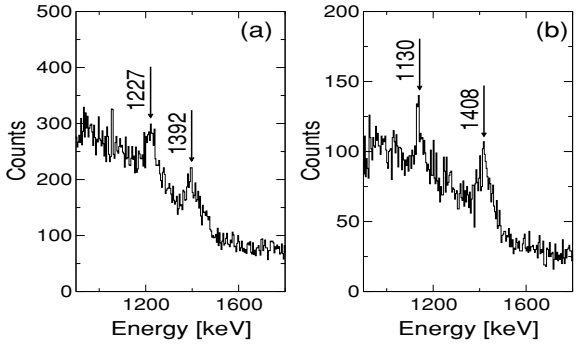

Figure 1. (a) Ni gated γ-ray spectrum showing clearly the 1227 keV $4_1^+ \rightarrow 2_1^+$ and 1392 keV $2_1^+ \rightarrow 0_1^+$ transitions in ^{54}Ni [6], the Ni isotope with the largest production cross-section. (b) Fe gated γ-ray spectrum showing the 1130 keV $4_1^+ \rightarrow 2_1^+$ and 1408 keV $2_1^+ \rightarrow 0_1^+$ transitions in ^{54}Fe [7], the mirror nucleus of ^{54}Ni.

Figure 1(b) shows the resulting spectrum for the mirror partner of ^{54}Ni, ^{54}Fe, with transitions $4_1^+ \rightarrow 2_1^+$ at 1130 keV and $2_1^+ \rightarrow 0_1^+$ at 1408 keV [7].

In order to produce similar spectra for fragments with smaller production cross-sections than that of ^{54}Ni such as ^{53}Ni, ^{45}Cr and ^{44,43}V, mass separation for the secondary fragments is required. Several signal corrections need to be applied to the CATE CsI detectors to achieve definitive fragment mass resolution, these are due to:

- the variation of energy signal with fragment implantation position,
- the energy resolution dependence on the velocity spread of the primary and secondary fragments,
- the energy resolution dependence on fragment implantation rate.

A correction for the variation in the detected energy signal with implantation position can be performed by determining the implantation position from the position sensitivity of the Si detectors. The (x, y) position of the interaction in a particular Si detector segment is calculated from the charge collected at the four corners of the front face of the Si wafer in a similar way to a two-dimensional potential divider. The charge collection points are attached to different amplifiers with different gains which need to be matched before a correction for the well-known 'pin cushion' effect can be applied. The 'pin cushion' effect, which arises from the $1/r$ dependence of the charge collection, is discussed in [8, 9] and a software method of correcting this effect has been developed by Lozeva *et al* [10].

The corrections performed in this work use a new and different approach that involves using the correlation between the charge collected at diagonally opposite collection points for each implantation signal. This new approach is required as the average charge collected at each corner is not the same due to the distribution of fragments being non-uniform across each segment. The correlation method is used to gain match the individual signals in a self-consistent way after which the resulting (x, y) position is mapped onto the results from a Monte Carlo simulation to recover the true geometrical implantation position. Although the fragment energy resolution in the CsI detector is dependent on implantation position, the main limiting factor to the achievable mass resolution is the spread in the velocity of the primary fragments. This contribution to the resolution can be improved somewhat by using time-of-flight and Bρ information from the FRS and the beam tracking detectors. An energy resolution of $\sim$1% FWHM is sought for this data set to have adequate mass separation and a

resolution of 2–3% [11] has already been achieved by Lozeva *et al* from a preliminary analysis of these data. The resolution dependence on the implantation rate into the CsI detectors is yet to be investigated as these complex detector correction procedures are still ongoing.

4. Summary

In summary, the analysis of the collected data is still at a preliminary stage. The spectra shown in figure 1 are a testament to the technique used and show that spectroscopy using this method to populate excited states in neutron-deficient nuclei in the $A \approx 50$ region is possible. The complexity of the experimental setup and the multi-array detection systems means that novel analysis techniques are being employed in order to obtain γ-ray spectra of exotic nuclei approaching the proton drip-line.

References

[1] Anderson L L *et al* 2005 *Phys. Rev.* C **71** 011303
[2] Geissel H *et al* 1992 *Nucl. Instrum. Methods* B **70** 286
[3] Wollersheim H J *et al* 2005 *Nucl. Instrum. Methods* A **537** 637
[4] Hammond G *et al* 2005 *Acta. Phys. Pol.* B **36** 1253
[5] Lozeva R *et al* 2003 *Nucl. Instrum. Methods* B **204** 678
[6] Gadea A *et al* 2003 *LNL Annual Report* p 8
[7] Rudolph D *et al* 1999 *Eur. Phys. J.* A **4** 115
[8] Doke T *et al* 1987 *Nucl. Instrum. Methods* A **261** 605
[9] Yanagimachi T *et al* 1989 *Nucl. Instrum. Methods* A **275** 307
[10] Lozeva R *et al* 2005 *Balkan Phys. Lett.* at press
[11] Lozeva R *et al* 2005 *Acta. Phys. Pol.* B **36** 1245

INSTITUTE OF PHYSICS PUBLISHING JOURNAL OF PHYSICS G: NUCLEAR AND PARTICLE PHYSICS

J. Phys. G: Nucl. Part. Phys. **31** (2005) S1917–S1920 doi:10.1088/0954-3899/31/10/101

Identification of heavy ion reaction channels with a new CAlorimeter TElescope within RISING*

R Lozeva[1,2], J Gerl[2], M Górska[2], S Mandal[2], D Balabanski[1,3], I Kojouharov[2], F Becker[2], J Grębosz[2,4], A Banu[2], P Bednarczyk[2,4], P Doornenbal[2] and H-J Wollersheim[2]

[1] University of Sofia "St. Kl. Ohridski", 1164-Sofia, Bulgaria
[2] Gesellschaft für Schwerionenforschung, 64291-Darmstadt, Germany
[3] University of Camerino, 62032-Camerino, Italy
[4] The Henryk Niewodniczanski Institute of Nuclear Physics, 31342-Krakow, Poland

E-mail: rady@phys.uni-sofia.bg and r.lozeva@gsi.de

Received 21 March 2005
Published 12 September 2005
Online at stacks.iop.org/JPhysG/31/S1917

Abstract

A newly developed CAlorimeter TElescope (CATE) is employed in the fast beam RISING γ-campaign with relativistic energies at the FRS at GSI. CATE consists of nine Si-CsI(Tl) detector telescopes for position and $\Delta E - E$ measurements. It registers the scattering angle and identifies the charge (Z) and the mass (A) of exotic heavy ions produced after secondary fragmentation or Coulomb excitation.

1. Introduction

Within the fast beam RISING [1] campaign at GSI, stable and radioactive heavy-ion beams at relativistic energies have been used, after separation by the FRS [2] and identification, to investigate fragmentation reactions and single step Coulomb excitation with secondary targets. To obtain information about the impact parameter and to distinguish the different reaction channels, a position sensitive CAlorimeter TElescope (CATE) [3] has been designed and employed. The detector system has been used for the detection of primary and secondary heavy ions from ^{54}Cr up to ^{132}Xe in the energy range between 90 and 400 MeV/u (at the detectors) with instantaneous rates between 1×10^2 and 5×10^4 p s^{-1}.

2. CATE

CATE is a chessboard-like array of nine $\Delta E - E$ telescopes. Each of them comprises a position sensitive Si-pin detector for position (x, y) and atomic number (Z) determination, and a corresponding CsI(Tl) detector coupled to a photodiode for particle mass (A) determination

* NUSTAR conference contribution.

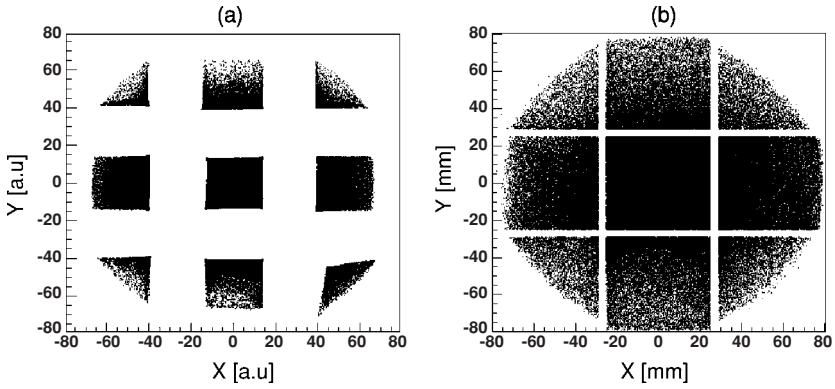

Figure 1. Position response of the CATE-Si array for ^{54}Cr ions with an energy of 170 MeV/u: (a) raw and (b) corrected spectra.

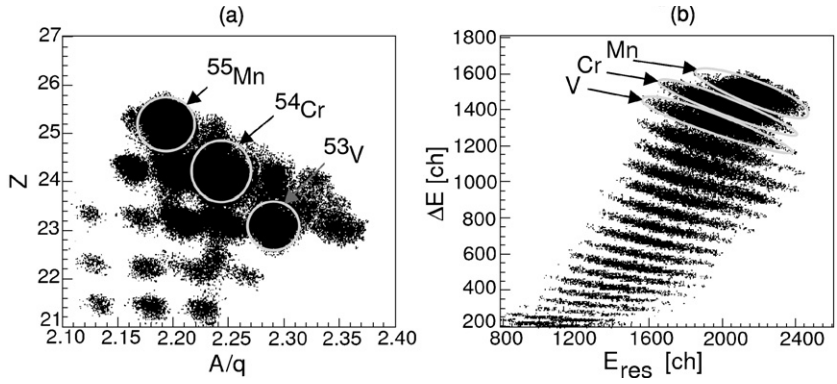

Figure 2. Identification of ^{55}Mn, ^{54}Cr and ^{53}V particles (a) before, and (b) after the secondary reaction (^{197}Au) target.

[3]. The CATE array is placed downstream from the secondary target, covering a solid angle $\theta \in [-3, 3]^{\circ}$, and having geometrical efficiency with respect to the incoming particles of 92%.

The position (x, y) is determined from the Si detectors via a charge division in its resistive layer (with a sheet resistance of 4–5 kΩ cm^{-2}). The resolution amounts to accuracy of better than (3×3) mm^2, tested with α-particles. The energy loss (ΔE) deposited in the Si transmission detectors, is a measure of the atomic number (Z), which is approximated to the particle charge (q) at relativistic energies [2]. The intrinsic energy resolution is about 1.5% (FWHM) for α-particles and about 2% (FWHM) for heavy ions (i.e. ^{86}Kr with an energy of 150 MeV/u and ^{58}Ni ions with an energy of 120 MeV/u). The residual energy ($E_{\rm res}$) is deposited in the 25 mm thickness of the CsI(Tl) scintillators. Combined with the ΔE signal in the Si semiconductors, it is a measure of the ion mass A, under the assumption that all particles with the same mass have the same velocity. The intrinsic heavy ion energy resolution of these stop detectors is about 0.8% (FWHM), found with primary ^{86}Kr beam at an energy of 145 MeV/u and for a ^{58}Ni beam at an energy of 113 MeV/u.

3. The position sensitivity

The position, determined with the Si detectors, gives a measure of the scattering angle, and hence of the impact parameter, of the particles from the RISING secondary target. The

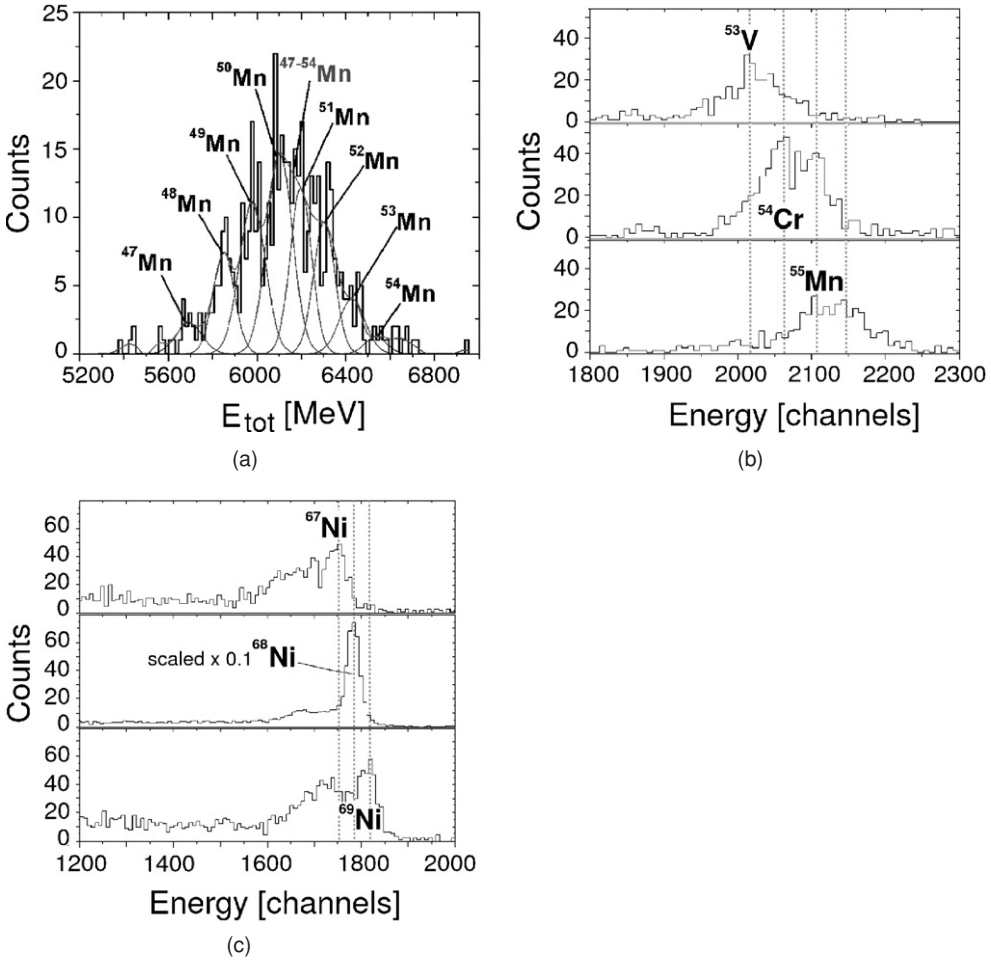

Figure 3. The mass spectra of CATE for (a) fragmentation ^{55}Ni(^{9}Be,xn,3p) of 100 MeV/u (b) Coulex ^{53}V, ^{54}Cr, ^{55}Mn(^{197}Au,0n,0p) of 170 MeV/u and (c) Coulex ^{67}Ni, ^{68}Ni, ^{69}Ni(^{197}Au,0n,0p) of 415 MeV/u.

thickness of the secondary target is usually chosen to keep the angular straggling of the order of 10 mrad, corresponding to a position uncertainty at CATE of about 1 cm [1]. Therefore, the intrinsic position resolution and the linearity are not critical. As demonstrated in figure 1(a), the position response of the Si detectors is almost linear. Since the efficiency with respect to the incoming particles is kept, only a simple calibration, using a normalization to the detector size [4] is required to obtain the real position as shown in figure 1(b).

4. The particle identification

The energy measurement of the CATE detectors is found to be influenced by (i) the particle position, (ii) the beam rate and (iii) the velocity. The first effect is connected to the nature of the detectors and their inhomogeneity, while the rest are effects connected to the beam and depend on its irradiation and distribution. Therefore, corrections are performed for all these effects [4].

In all in-beam studies the detector response revealed a unique Z identification with extracted Z resolution of the particle cocktail of $\Delta Z \sim 0.7$–$0.8\,Z$ (FWHM). A typical example is the system (^{55}Mn, ^{54}Cr, ^{53}V on a ^{197}Au target) at 170 MeV/u. For the selected ^{55}Mn, ^{54}Cr and ^{53}V ions, separated and identified by the FRS (see figure 2(a)), the reaction channels were detected by CATE as shown in figure 2(b).

In fragmentation processes, the momentum variation of the abraded nucleons leads to a spread of the momentum, respectively, the velocity of the final fragment [5]. Therefore, the assumption of constant velocity for all secondary ion species does not hold. Consequently, without a time-of-flight measurement after the secondary target, the possible mass resolution is typically 2–3% (FWHM) at energies of about 100 MeV/u. These values were also found from the total energy ($E_{\rm tot} = \Delta E + E_{\rm res}$) of CATE in the experimental data (^{55}Ni on ^{9}Be at 100 MeV/u). The energy is obtained after an absolute energy calibration and linearization of the $\Delta E - E$ distribution [4]. As an illustration, the $E_{\rm tot}$ spectrum for i.e. $Z = 25$ isotopes is presented in figure 3(a) with multiple fit and deconvolution to single distributions (with reduced $\chi^2 \leqslant 5$; $\chi^2 = \chi^2/n$, where n is the number of degrees of freedom). The identification is performed by comparison of the energy centroids with simulated single mass distributions using the LISE code [6], as indicated with arrows.

In relativistic Coulomb excitation it is important to distinguish the Coulex channel from knock-out channels. For the selected isotopes in figure 2(b) the masses are obtained from the $E_{\rm res}$ projection (in channels) and identified by their reaction probability with the secondary target (since no energy calibration is performed). The extracted mass resolution from the difference in the energy centroids is about 2% (FWHM), as shown in figure 3(b).

In another Coulex reaction of ^{67}Ni, ^{68}Ni, ^{69}Ni on ^{197}Au at 415 MeV/u, the high energetic ^{67}Ni, ^{68}Ni and ^{69}Ni isotopes are identified in the same way and their mass resolution is determined with an accuracy of about 1–2% (FWHM) (see figure 3(c)).

5. Summary

With the newly developed $\Delta E - E$ telescope, CATE, identification of relativistic heavy ions at energies $\geqslant$100 MeV/u can be performed. The system has a good position resolution (Δx, Δy) of (3×3) mm^2 for scattering angle reconstruction, a unique charge resolution of 0.7–0.8 Z (FWHM), a mass resolution of 2–3% (FWHM) for fragmentation and 1–2% (FWHM) for Coulex channels.

Taking into account the intrinsic energy resolution, with an additional time-of-flight measurement after the secondary target, the A resolution for fragments could be improved to about 1% (FWHM).

References

[1] Wollersheim H-J *et al* 2005 *Nucl. Instrum. Methods* A **537** 637
[2] Geissel H *et al* 1992 *Nucl. Instrum. Methods* B **70** 286
[3] Lozeva R *et al* 2003 *Nucl. Instrum. Methods* B **204** 678
[4] Lozeva R *et al* 2005 *Acta Phys. Pol.* B **36** 1245 and to be published
[5] Goldhaber A *et al* 1974 *Phys. Lett.* B **53** 306
[6] Tarasov O and Basin D 2003 *Nucl. Instrum. Methods* B **204** 174

STATUS OF THE RISING PROJECT AT RELATIVISTIC ENERGIES*

P. Bednarczyk[a,b], A. Banu[a], T. Beck[a], F. Becker[a], M.A. Bentley[c]
G. Benzoni[d], A. Bracco[d], A. Bürger[e], F. Camera[d], P. Doornenbal[a]
C. Fahlander[f], H. Geissel[a], J. Gerl[a], M. Górska[a], H. Grawe[a]
J. Grębosz[a,b], G. Hammond[c], M. Hellström[a], H. Hübel[e], J. Jolie[g]
M. Kmiecik[b], I. Kojouharov[a], N. Kurz[a], R. Lozeva[a], A. Maj[b]
S. Mandal[a], W. Męczyński[b], B. Million[d], S. Muralithar[a], P. Reiter[g]
D. Rudolph[f], N. Saito[a], T.R. Saito[a], H. Schaffner[a], J. Simpson[h]
J. Styczeń[b], N. Warr[g], H. Weick[a], C. Wheldon[a], O. Wieland[d]
M. Winkler[a] and H.J. Wollersheim[a]

[a]GSI, 64291 Darmstadt, Germany
[b]Institute of Nuclear Physics PAN, Kraków, Poland
[c]Department of Physics, Keele University, Keele, Staffordshire ST5 5BG, UK
[d]Department of Physics, Milano University and INFN Milano, Milano, Italy
[e]HISKP, Bonn University, 53115 Bonn, Germany
[f]Department of Physics, Lund University, 22100 Lund, Sweden
[g]IKP, Köln University, 50937 Köln, Germany
[h]CCLRC, Daresbury Warrington, Cheshire WA4 4AD, UK

(Received December 13, 2004)

The RISING project was designed to perform high-resolution γ-ray spectroscopy with radioactive beams at GSI. Unstable beams were produced by fragmentation of relativistic heavy ion projectiles provided by the SIS synchrotron. The fragment separator FRS was used to select and to focus the exotic fragments at about $100A$ MeV energy on a secondary target. Various charged particle detectors enabled an event-by-event tracking of the incoming radioactive projectiles and the reaction products, thus allowing for a selection of the nuclei of interest and their velocity vector reconstruction. The γ-ray detection system consisting of the EUROBALL Cluster Ge detectors and the large volume HECTOR BaF_2 detectors measured prompt γ-radiation from nuclei excited in the secondary target. Despite the huge Doppler shift due to the high recoil velocity ($\beta \approx 40\%$), RISING achieved a γ-energy resolution below 2%. The paper reviews the present status of the RISING project.

PACS numbers: 26.60.–t, 25.70.De, 29.30.–h, 29.30.Kv

* Presented at the XXXIX Zakopane School of Physics — International Symposium "Atomic Nuclei at Extreme Values of Temperature, Spin and Isospin", Zakopane, Poland, August 31–September 5, 2004.

1. Introduction, γ-spectroscopy studies with radioactive beams

Nuclei with an extreme N/Z ratio are expected to exhibit features not observed near the stability line. By studying the structure of unstable nuclei one can significantly extend the knowledge of nucleon–nucleon interactions, nuclear symmetries, and collective excitation modes. Therefore, the exploration of exotic regions of the nuclear chart becomes a key issue of current and future research projects in the nuclear γ-spectroscopy domain.

Nowadays, rare nuclei so far inaccessible by conventional fusion-evaporation or transfer reactions, can be created in-flight by peripheral nuclear collisions. Primary beams at intermediate energies ranging from a few ten to several hundred A MeV are of use. The relativistic projectile impinging on a primary-production target undergoes fragmentation. In this way, exotic fragments with a large proton or neutron excess are produced. More neutron rich nuclei originate from fission of heavy projectiles such as ^{238}U, induced by the Coulomb scattering on a heavy target.

The in-flight technique relies on a forward focusing of the reaction products and a high production yield due to the use of thick targets. Large acceptance electromagnetic separators selecting the exotic fragments of interest provide isotopically pure radioactive ion beams (RIB) [1].

The in-beam γ-decay of the excited rare projectiles can be studied [2]. On the other hand, the investigation of secondary nuclear reactions induced by the RIB is feasible [3].

Pioneering γ-spectroscopy experiments with RIB produced by the in-flight method were performed at GANIL [4] and GSI [5] in Europe, NSCL–MSU [6] in the USA, and RIKEN in Japan [7]. However, important limitations occurred due to the accelerator, the fragment separator, and the detector techniques applied so far.

GSI offers a wealthy choice of high-intensity heavy-ion beams, including uranium, at a wide range of energies. They can be used to produce secondary projectiles through either fragmentation or fission, suitable for in-beam investigations. This, together with the availability of the most powerful γ-ray detection system, the EUROBALL Ge array [9], could be considered as a breakthrough in the discipline. A large international collaboration involving over 40 institutions from 10 countries launched the RISING (Rare ISotope INvestigation at GSI) research program, aiming at high-resolution γ-ray spectroscopy with radioactive beams provided by the GSI facilities. Measurements with fast RIBs at $100A$ MeV energy, exploring γ-decays of rare nuclei excited via the Coulomb scattering or secondary fragmentation reactions are presently being carried out. In future experiments, beams slowed down to Coulomb barrier energies for investigations of states excited in nuclear reactions and stopped beams for decay studies will be used.

The three aforementioned campaigns require not only an efficient γ-ray detection system but also a dedicated set of ancillary detectors selecting the reaction channel of interest and tracking the decay products. In the forthcoming paragraphs, a general description of the experimental techniques used at RISING with fast beams is presented. This includes the secondary beam separation, tracking of the reaction products and the γ-ray detection. The in-beam performance of the system is discussed. The technical details on the RISING setup for fast beams can be found in Ref. [8].

2. Radioactive beams at GSI and the RISING heavy ion tracking detector system

The SIS synchrotron of GSI provides all the primary beams up to ^{238}U [11]. The heavy ions can be accelerated up to 1 A GeV and reach intensities of 10^9 particles per second. Depending on the requested secondary ion, the relativistic projectiles interacting with the production target nuclei may be fragmented or undergo fission.

The fully stripped fragments of interest produced in the reaction are separated in the fragment separator (FRS) by the $B\rho-\Delta E-B\rho$ technique [10]. The FRS consists of two mirror sets of dipole and quadrupole magnets. Each part selects heavy ions according to the A/Q ratio. A degrader placed in the intermediate focal plane of the separator introduces a fragment velocity dispersion due to the specific energy loss of different elements. Therefore, the fragments with the particular A and Q are focused onto a secondary target placed in the final focal plane of the FRS.

The exotic beams obtained in a projectile fragmentation reaction nearly retain the velocity vector of the primary ions. Thus, the typical transmission through the FRS is several ten per cent. In contrast, in fission reactions, the energy transferred to the fragments induces a spread of their velocity and direction, causing a reduction in the transmission to a few per cent maximum.

Due to low production cross sections, the intensities of radioactive beams may reach only 10^4 particles per second. Moreover, a momentum spread of the fragments makes the precise determination of the projectile trajectory and the energy difficult. Therefore, the optimization of the FRS settings and the online control is essential in obtaining a good quality radioactive beam.

In Fig. 1 a schematic plot of the FRS setup incorporating various particle detectors used for the secondary beam monitoring is shown. The ionization chamber MUSIC gives the proton number Z of the selected projectiles, whereas the fast plastic scintillator detectors provide the corresponding time of flight, allowing for a velocity and A/Q determination. The two position sensitive avalanche multiwire counters are used to determine the trajectory before the secondary target and to monitor the beam spot size and position.

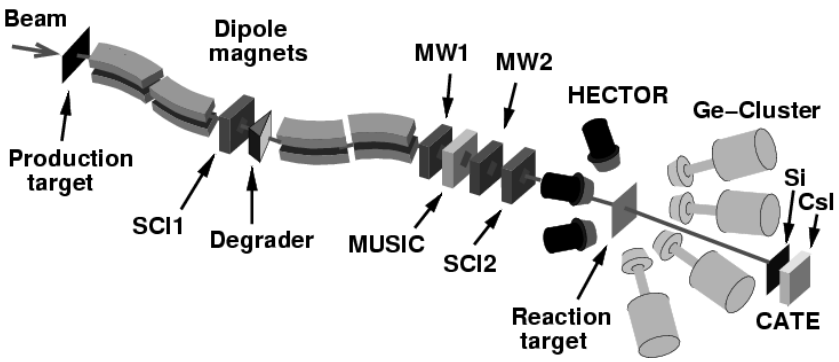

Fig. 1. Schematic layout of the RISING setup at the FRS fragment separator. The beam diagnostic elements consist of two multiwire detectors (MW1 and MW2), an ionization chamber (MUSIC) and two scintillation detectors (SCI1 and SCI2). The γ-rays are measured with the BaF_2-HECTOR and the Ge-Cluster detectors. The ions emerging from the reaction target are identified with the CATE array.

The full identification of the reaction products and their scattering angle after the secondary target plays a vital role in selecting the nucleus of interest from a dominating unwanted background. The high efficiency position sensitive $\Delta E - E$ telescope array CATE [12] was developed for RISING in order to determine A, Z and the position of detected heavy ions. CATE allows for measuring the full energy range of expected fragments with $Z > 7$. The detector angular acceptance from $\theta = 0^\circ$ to $\theta = 3^\circ$ is sufficient for detecting the Coulomb scattered nuclei up to the maximum grazing angle.

The interaction of heavy-ion beams at relativistic energies with matter causes electromagnetic radiation of the atomic origin such as bremsstrahlung, target-atom ionization, or radiative electron capture [13]. These atomic processes can be several orders of magnitude stronger than a nuclear level excitation. Depending on the projectile energy, the atomic background can extend up to several hundred keV. Therefore, to avoid the overlap with the energy range where γ-rays from excited nuclear levels are expected *i.e.*, $E_\gamma > 400$ keV, the secondary beam energy shall be limited to about $100A$ MeV.

3. RISING γ-ray detector arrays at the FRS focal plane

The $100A$ MeV energy fragments excited in the secondary reaction, emit γ-rays in flight with $\beta = 43\%$. In the laboratory coordinate system, due to the Lorentz velocity transformation, the electromagnetic radiation originating from the moving source is forward focused (Lorentz boosted). For this reason, the fifteen EUROBALL Cluster Ge detectors were placed at the forward angles between 15° and 36°, 70 cm from the secondary target. In order to increase the solid angle they were mounted without the anticompton shields. For the moving radiation source, such a geometry guarantees

a gain in efficiency by a factor of about 2.2 with respect to the isotropic photon emission at rest. Thus, taking into account the efficiency of 1.3% measured with the ^{60}Co source, the estimated overall value is about 2.8% at 1.3 MeV energy.

The very large recoil velocity induces the Doppler shift of $E/E_0 \approx 1.5$ and a significant broadening of γ-lines observed at the forward angles. Nevertheless, the use of the high-granularity encapsulated Cluster Ge detectors allows to maintain a good energy resolution of $\Delta E/E < 2\%$. Furthermore, the Cluster detectors enable the energy add-back that considerably increases the efficiency at high γ-energies [14]. For example, the measurement performed with a Pu-α-Be source giving gammas of 6.129 MeV energy, revealed a gain in the number of counts in the peak by a factor of two when using the add-back mode.

The RISING γ-detection system benefits from eight large volume BaF_2 counters from the HECTOR array [15]. The BaF_2 detectors are particularly suitable for measuring high-energy γ-rays, as originating from the GDR decay. Although HECTOR is installed at the backward angle of 142°, in the area not occupied by the Clusters, its high efficiency compensates the deficit due to the forward Lorentz boost of the γ-radiation emitted in flight. Consequently, γ-rays of a few MeV energy can be registered in the HECTOR array with an efficiency comparable to those of Clusters.

A photo of the RISING detector arrangement at the reaction target area is shown in Fig. 2.

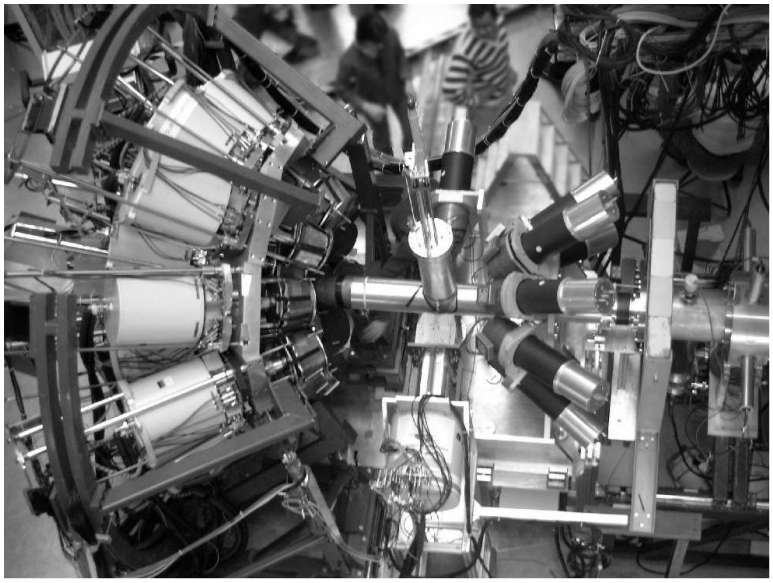

Fig. 2. The RISING γ-ray detectors placed around the reaction target. The BaF_2 HECTOR (right) and the Ge Cluster (left) arrays are shown.

4. In beam performance of the RISING system

The FRS/CATE heavy ion tracking detectors, the HECTOR array and the EUROBALL Cluster Ge detectors run as fully independent systems, with their original data acquisition being synchronized by time stamps.

Preparatory RISING measurements were done with the primary beams of ^{132}Xe, ^{84}Kr, and ^{40}Ar propagated through the FRS. The first in-beam tests permitted to adjust the subsystem settings and to elaborate the common particle-γ trigger selecting valid events in all the parts.

Further in-beam optimization of the RISING setup included suppression of the strong γ-radiation background arising from a beam scattering onto the beam-line components. Discrimination of gammas from the target and from a distant radiation source was possible due to a good time resolution of the HECTOR BaF_2 detectors. The most suitable arrangement of passive γ-ray detector shields was chosen.

Gamma rays from the Coulomb excited ^{84}Kr primary projectiles at $113A$ MeV hitting the 0.4 g/cm^2 Au target were detected in the Cluster detectors. A coincidence with the Kr ions selected by the CATE array was required. Using a fixed value of $\beta = 0.396$ for the Doppler correction, the measurement revealed an energy resolution of 1.5% for the 882 keV $2^+ \rightarrow 0^+$ transition in ^{84}Kr, as was expected from the setup design.

In contrast, when using a secondary beam, a fragment momentum spread occurs. However, it can be compensated by an event-by-event projectile tracking. The Coulomb excitation reaction of the secondary ^{54}Cr projectiles of $136A$ MeV energy on the Au target provides a good example, illustrating the tracking procedure.

The ^{54}Cr nuclei were obtained from the ^{86}Kr primary beam fragmentation and separated in the FRS. They were further selected before and after the reaction target by the MUSIC and the CATE detectors, respectively. The corresponding $Z-A/Q$ and $\Delta E-E$ scatter plots are presented in Fig. 3.

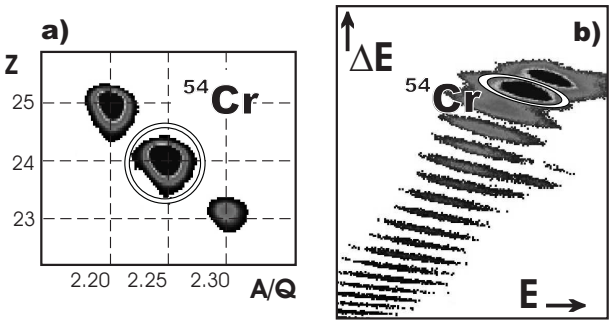

Fig. 3. The $Z - A/Q$ (a) and the $\Delta E - E$ (b) plots. The ^{54}Cr fragments were selected before and after the reaction target, respectively.

The projectile velocity used for event-by-event Doppler correction was determined from the time-of-flight measurement. The positions of a γ-ray detected by the Clusters and a scattered particle measured in CATE were recorded. However, due to the rather big size of the irradiated target area (see Fig. 4), in order to determine the actual γ-ray emission angle and the particle scattering angle, the trajectory of every incoming and outgoing Cr fragment had to be calculated.

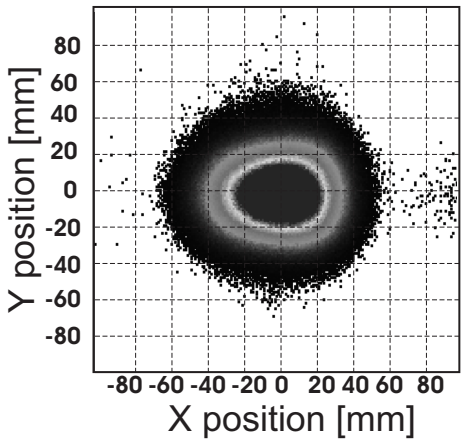

Fig. 4. Reconstruction of the secondary beam spot at the reaction target deduced from the multiwire position information. The irradiated area had a diameter of about 4 cm at FWHM.

The role of the projectile tracking in improving a γ-ray spectrum quality is illustrated in Fig. 5. For the measured 834 keV $2^+ \rightarrow 0^+$ transition in ^{54}Cr the overall energy resolution of FWHM = 2% was achieved when using the event-by-event particle tracking, whereas the average zero degree approximation resulted in resolution deterioration by a factor of nearly two.

The ^{54}Cr particle angular distribution measured in coincidence with the 834 keV gammas is shown in Fig. 6. The significance of the experimental points allows for comparison with the Coulomb excitation model calculations [16]. The plot clearly demonstrates an increase of the electromagnetic interaction cross section with increasing scattering angle up to the maximum grazing angle, where an absorption occurs.

A projectile scattering on the reaction target goes together with the Coulomb excitation of a target nucleus. The relative intensities of γ-transitions from the Coulomb excited levels in the target and the secondary beam nuclei can provide information on the decay probability of the studied projectile nuclei. In addition, a surveillance of the well known γ-rays emitted

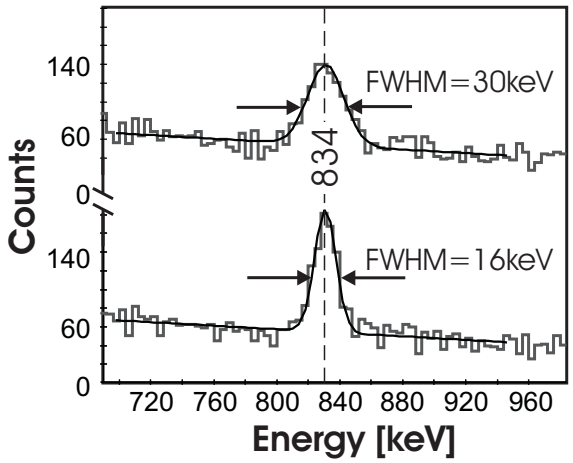

Fig. 5. The 834 keV γ-line from the ^{54}Cr Coulex after the Doppler correction using the event-by-event particle tracking (lower panel) and the zero degree scattering angle approximation (upper panel). In the lower spectrum the gain in energy resolution by a factor of about two is seen.

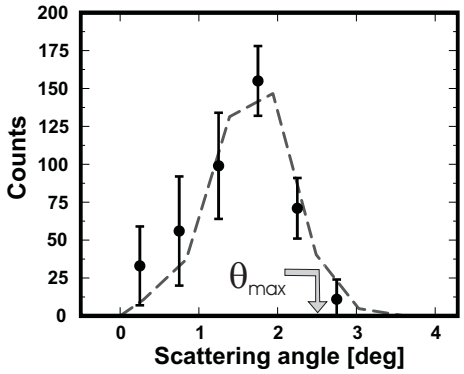

Fig. 6. The scattering angle of the ^{54}Cr fragments measured by the CATE array in coincidence with the 834 keV γ-rays. The experimental points follow the angular distribution predicted by the inelastic Coulomb scattering theory [16], normalized to the total number of counts, represented by the dashed line. The maximum Coulomb scattering angle $\theta_{\max}$ is indicated.

at rest from the target can help in choosing the optimal measurement conditions as particle selection criteria and background suppression. In Fig. 7, the in-beam non Doppler corrected γ-spectra are shown. When measured in coincidence with the ^{54}Cr fragments, the weak 547 keV line from the ^{197}Au $7/2^+ \rightarrow 3/2^+$ decay emerges from the huge γ-ray background. The intensity ratio $I(^{197}\mathrm{Au}; 547\,\mathrm{keV})/I(^{54}\mathrm{Cr};\ 834\,\mathrm{keV}) = 0.10 \pm 0.02$, determined from

the experiment, is in agreement with the relativistic Coulex code prediction [16]. In the calculation the reduced transition probabilities B(E2) were taken from [17] and [18] for ^{197}Au and ^{54}Cr, respectively.

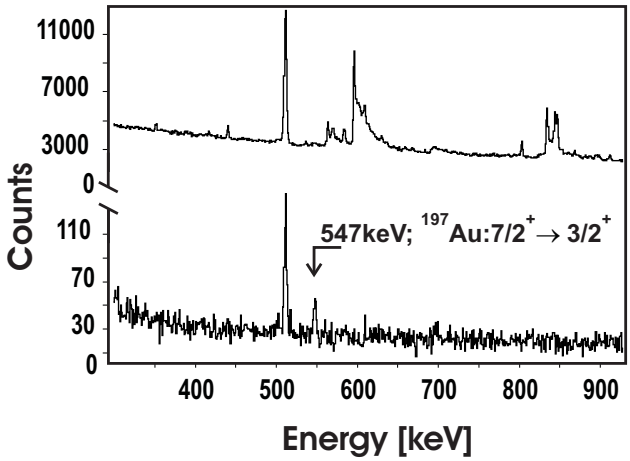

Fig. 7. In-beam non Doppler corrected γ-spectra measured without (upper panel) and with (lower panel) ^{54}Cr particle selection. The weak 547 keV γ-transition from the Coulomb excited ^{197}Au target nuclei appears due to a significant background suppression, when using the particle gate.

So far, in the course of the RISING fast beam campaign, mainly Coulomb excitation experiments were performed. They concerned the shell structure of neutron rich Cr isotopes [19] and Sn isotopes near the doubly magic ^{100}Sn nucleus [20]. An attempt at exciting the GDR resonance in the ^{68}Ni projectiles at $400A$ MeV kinetic energy initiated the study of decays from highly-excited collective states in nuclei with large neutron excess [21]. Furthermore, a two-step fragmentation reaction of ^{58}Ni was used to investigate high-spin states in the $T_z = \pm 3/2$ mirror pair ^{53}Mn and ^{53}Ni [22].

5. Further development of the setup

In the future RISING experiments, the efficiency of the γ-detection system will be significantly increased by the inclusion of eight MINIBALL segmented germanium cluster detectors [23]. The high position sensitivity of the MINIBALL detectors allows for placing them relatively close to the secondary target at large angles, while at the same time a very good energy resolution of 0.3% can be maintained. The expected overall EUROBALL and MINIBALL efficiency at the 1.3 MeV energy for a γ-ray emitted in flight will be between 4 and 10 per cent, depending on the adjustable detector distance to the target.

6. Conclusion

RISING made use of unique radioactive beams at relativistic velocities available at the SIS/FRS facilities at GSI. The setup demonstrated the feasibility of high resolution γ-ray spectroscopy studies of nuclei excited either by Coulomb scattering or by fragmentation of relativistic radioactive beams. The first physics results concerning exotic atomic nuclei were obtained.

This work was partially supported by the Polish State Committee for Scientific Research (KBN) Grants No. 2 P03B 118 22 and 620/E-77/SPB/GSI/P-03/DWM105/2004–2007.

REFERENCES

[1] G. Münzenberg *et al., Nucl. Instrum. Methods* **B70**, 265 (1992).
[2] T. Glasmacher *et al., Nucl. Phys.* **A693**, 90 (2001).
[3] K. Yoneda *et al., Phys. Lett.* **B499**, 233 (2001).
[4] M. Lewitowicz *et al., Nucl. Phys.* **A734**, 645 (2004).
[5] S. Wan *et al., Z. Phys.* **A358**, 213 (1997).
[6] W.F. Müller *et al., Nucl. Phys.* **A734**, 418 (2004).
[7] A. Ozawa *et al., Pramana J. Phys.* **57**, 525 (2001).
[8] H.J. Wollersheim *et al., Nucl. Instrum. Methods* **A**, in print.
[9] J. Simpson *et al., Z. Phys.* **A358**, 139 (1997).
[10] H. Geissel *et al., Nucl. Instrum. Methods* **B70**, 286 (1992).
[11] GSI accelerator service, `http://www-aix.gsi.de/accelerator`.
[12] R. Lozeva *et al.*, *Acta Phys. Pol. B* **36**, 1245 (2005), these proceedings.
[13] R. Anhold *et al., Phys. Rev.* **A33**, 2270 (1986).
[14] M. Wilhelm *et al., Nucl. Instrum. Methods* **A381**, 462 (1996).
[15] A. Maj *et al., Nucl. Phys.* **A571**, 185 (1994).
[16] C. Bertulani *et al., Comput. Phys. Commun.* **152**, 317 (2003).
[17] Z. Chunmei *Nucl. Data Sheets* **76**, 399 (1995).
[18] H. Junde *Nucl. Data Sheets* **68**, 887 (1993).
[19] A. Bürger *et al.*, *Acta Phys. Pol. B* **36**, 1249 (2005), these proceedings.
[20] A. Banu *et al.*, to be published.
[21] A. Bracco *et al.*, to be published.
[22] G. Hammond *et al.*, *Acta Phys. Pol. B* **36**, 1253 (2005), these proceedings.
[23] J. Eberth *et al., Prog. Part. Nucl. Phys.* **46**, 389 (2001).

CALORIMETER TELESCOPE FOR IDENTIFICATION OF RELATIVISTIC HEAVY ION REACTION CHANNELS*

R. Lozeva[a,b], S. Mandal[a], J. Gerl[a], M. Górska[a], J. Grębosz[a,c]
I. Kojouharov[a], J. Adamczewski[a], A. Banu[a], F. Becker[a]
T. Beck[a], P. Bednarczyk[a], A. Blazhev[a,b], P. Doornenbal[a]
H. Geissel[a], M. Hellström[a], M. Kavatsyuk[a], O. Kavatsyuk[a],
N. Kurz[a], M. Mutterer[d], S. Muralithar[a], G. Münzenberg[a]
W. Prokopowicz[a], N. Saito[a], T. Saitoh[a], H. Schaffner[a]
K. Sümmerer[a], H. Weick[a], M. Winkler[a], C. Wheldon[a]
and H.-J. Wollersheim[a]

[a]Gesellschaft für Schwerionenforschung mbH, GSI-Darmstadt
Planckstr. 1, 64291-Darmstadt, Germany
[b]Faculty of Physics, University of Sofia "St. Kl. Ohridski", Sofia, Bulgaria
[c]The H. Niewodniczański Institute of Nuclear Physics PAN, Kraków, Poland
[d]Institut für Kernphysik, TU Darmstadt, Darmstadt, Germany

(Received December 13, 2004)

A new ΔE–E CAlorimeter TElescope, CATE, has been developed to identify the reaction products from secondary fragmentation reactions or Coulomb excitation. Radioactive relativistic beams with energies between 90 and 400 MeV/u and instantaneous rates of up to 5×10^4 particles/s bombarded the detector system. CATE distinguishes the reaction channels in terms of charge (Z) and mass (A) and gives position information about the impinging ions, used for impact parameter determination.

PACS numbers: 07.20.Fw, 95.55.–n, 25.75.–q, 29.40.Mc

1. Introduction and motivation

During the recent RISING [1] campaign at GSI, stable and radioactive heavy-ion beams separated by the FRS [2] at relativistic energies between 90 and 410 MeV/u have been used to perform fragmentation reactions and Coulomb excitation on secondary targets. To identify the outgoing reaction

* Presented at the XXXIX Zakopane School of Physics — International Symposium "Atomic Nuclei at Extreme Values of Temperature, Spin and Isospin", Zakopane, Poland, August 31–September 5, 2004.

products and to get an information about their scattering angle, a new ΔE–E CAlorimeter TElescope (CATE [3]) has been designed. The CATE detector was so far employed for the detection of heavy ions from ^{55}Ni up to ^{132}Xe. The performance for ^{58}Ni primary beam particles and ^{55}Ni secondary fragments is described.

2. The CATE detectors

The CATE array consists of nine Si-CsI(Tl) ΔE–E telescopes. Downstream from the secondary target position, the array covers an opening angle from 0 to 3 degrees in θ. The size of each Si detector is (50×50) mm^2, the active thickness is 300 μm and the resistive sheet amounts to 2 kΩ/cm^2. The energy resolution of such a detector is typically 80 keV for 5.5 MeV ^{241}Am α particles. The intrinsic position resolution, measured with the same α-source $(\Delta x, \Delta y)$, is better than 3 mm in x and y. Each CsI(Tl) scintillator has a size of (54×54) mm^2 and a nominal thickness of 10 mm. It is read out by a photodiode with a size of (18×18) mm^2, attached to an integrated low gain preamplifier [4]. The nine telescopes are arranged in three by three configuration. Because of the dead layer of 4mm between each two telescopes the geometrical efficiency of the total array is 92 % with respect to the incoming particles.

3. The position measurement

When a reaction product impinges on the Si resistive sheet it creates charge carriers. They migrate to the four corners, where the contacts for the outgoing signals are located. By a relative comparison of the produced pulses the position of that particle can be obtained following a simple geometrical algorithm. As the detector response is not everywhere linear, several linearization procedures have to be performed in order to obtain the square geometrical shape from the detector response [3].

4. The energy measurement

The energy ΔE, deposited in the Si detector, is measured at the back contact. Therefore the atomic number Z of the impinging particle can be deduced. The CsI(Tl) measures the particle's residual energy, E_{res}, which together with ΔE is proportional to its mass, A, under the assumption that all particles with the same mass have the same velocity. Several effects influence the energy measurement, *i.e.* position, velocity distribution, beam intensity, and the reaction mechanism. The position dependence of the impinging particle is an effect connected to the nature of the detectors, while the velocity spread and the ion intensity are beam related effects. With

^{58}Ni primary beam, the measured mean energy resolution values of CATE of 2.0 % (FWHM) for the Si and 0.8% (FWHM) for the CsI(Tl) detectors were determined using only position corrections. In order to obtain a precise energy determination with a ^{55}Ni fragment beam and hence unambiguous identification, the effect of the velocity spread also needs to be corrected for. After applying an absolute energy calibration, the experimental data were compared with a simulation. Such ΔE–E spectra are shown in figure 1. A simulation (using the code LISE++[5]), corresponding to the experimental conditions, is plotted on the left and the experimental spectrum is plotted on the right. A unique Z identification can be expected from the simulation

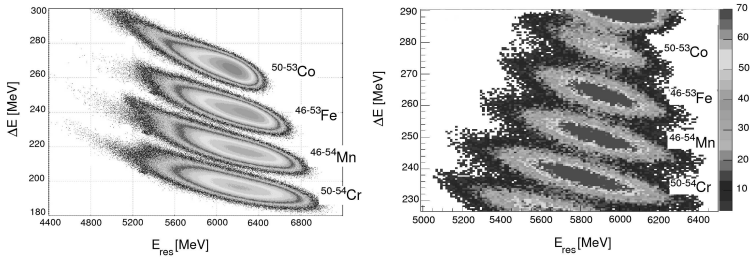

Fig. 1. Comparison of a simulation (left) and the experimental data (right) for the reaction ^{9}Be(^{55}Ni,xn, yp).

and is observed in the experimental data. For the ^{55}Ni beam the nuclear charge is determined with an accuracy $\Delta Z/Z = 0.7$ (FWHM). From the simulation no separation of two neighboring masses ($\Delta A/A \leq 1$) for this ($A \approx 55$) region can be expected, what is confirmed by the experimental spectrum. The reason is the reaction mechanism, an effect that in case of fragmentation reactions turns to be severe. When the ^{55}Ni fragment particle interacts with a target nucleus (in this case ^{9}Be) its momentum distribution is broadened. By removing nucleons the broadening of the energy distribution can reach up to several percent. This effect was described in the past by Goldhaber [6] and later parametrized to match experimental data by Tarasov [5,7]. Furthermore, the measured energy distribution of relativistic heavy ions according to the Universal parametrisation of Tarasov [7], does not follow a Gaussian shape, but is slightly asymmetric. For a single Z, *i.e.* $Z = 25$, the all produced isotopes are overlapping and creating one common ΔE–E distribution according to the simulation. When a separate calculation for each single isotope is performed, a clear shift in the centroid of the total ($\Delta E + E_{\mathrm{res}}$) energy distribution is observed. To compare the expected energy distributions with the experimental data, a linearization procedure is applied as described in reference [3]. Simulated total energy distributions for each Mn isotope are shown on the left of figure 2. The total mass dis-

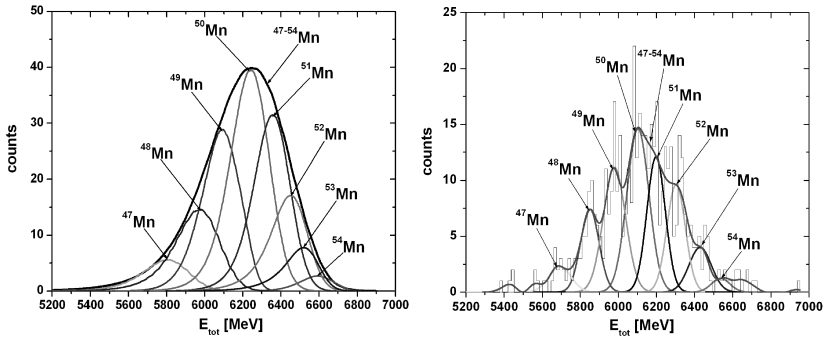

Fig. 2. A simulated single mass distribution spectrum (left), for the Mn isotopes, produced in the reaction ^{9}Be(^{55}Ni,xn, yp), is compared with the experimental single mass distribution spectrum (right). The total mass distribution for all $^{47-54}$Mn in both cases are plotted as top curves.

tribution for $Z = 25$ is plotted as an envelope curve. The corresponding experimental data are shown on the right. The total experimental mass distribution can be decomposed to single mass distributions by comparison of the peak positions and widths with the simulation. The different masses of Mn isotopes are indicated by the arrows. Obviously the measured resolution is significantly better compared to the theoretical model. The parametrization used in the model had been optimized for lower particle energies. Our new data allow now to improve the model parametrization.

5. Summary

The newly developed ΔE–E calorimeter telescope identifies relativistic heavy ions at energies around 100 MeV/u. It has a good position resolution of 3 mm for scattering angle reconstruction, an unique nuclear charge resolution $\Delta Z/Z$ of 0.7 (FWHM) and a mass resolution for fragmentation reactions of 2–3 % (FWHM).

REFERENCES

[1] H.-J. Wollersheim *et al.*, *Nucl. Instrum. Methods A*, in press.
[2] H. Geissel *et al.*, *Nucl. Instrum. Methods* **B70**, 286 (1992).
[3] R. Lozeva *et al.*, *Nucl. Instrum. Methods* **B204**, 678 (2003); and to be published.
[4] A. Pulia *et al.*, private communication.
[5] O. Tarasov, D. Bazin, *Nucl. Instrum. Methods* **B204**, 174 (2003).
[6] A. Goldhaber *et al.*, *Phys. Lett.* **B53**, 306 (1974).
[7] O. Tarasov *et al.*, *Nucl. Instrum. Methods* **A734**, 536 (2004).

RELATIVISTIC COULOMB EXCITATION OF ^{54,56,58}Cr* **

A. Bürger[a], T. Saito[b], A. Al-Khatib[a], A. Banu[b], T. Beck[b], F. Becker[b] P. Bednarczyk[b], G. Benzoni[c], A. Bracco[c], P. Bringel[a], F. Camera[c] E. Clement[d], P. Doornenbal[e], H. Geissel[b], J. Gerl[b], M. Górska[b] A. Görgen[d], H. Grawe[b] J. Grębosz[b], G. Hammond[f], M. Hellström[b] H. Hübel[a], M. Kavatsyuk[b,g], O. Kavatsyuk[b,g], M. Kmiecik[h] I. Kojouharov[b], N. Kurz[b], R. Lozeva[b,i], A. Maj[h], S. Mandal[b] W. Męczyński[h], D. Mehta[j], B. Million[c], S. Muralithar[k], A. Neusser[a] Zs. Podolyák[l], T.S. Reddy[m], P. Reiter[e], N. Saito[b] H. Schaffner[b] A.K. Singh[a,n], H. Weick[b], O. Wieland[c] C. Wheldon[o], M. Winkler[b] and H.J. Wollersheim[b]

[a]Helmholtz-Institut für Strahlen- und Kernphysik, Universität Bonn, Germany
[b]Gesellschaft für Schwerionenforschung, Darmstadt, Germany
[c]Dipartimento di Fisica, Universitá di Milano, and INFN sezione di Milano, Italy
[d]DAPNIA/SPhN, CEA Saclay, Gif-sur-Yvette, France
[e]Institut für Kernphysik, Universität zu Köln, Germany
[f]Department of Physics, Keele University, Keele, UK
[g]Taras Shevchenko Kiev National University, Ukraine
[h]The H. Niewodniczański Institute of Nuclear Physics PAN, Kraków, Poland
[i]Faculty of Physics, University of Sofia, Bulgaria
[j]Department of Physics, Panjab University, India
[k]Nuclear Science Centre, New Delhi, India
[l]Department of Physics, University of Surrey, UK
[m]Department of Nuclear Physics, Andhra University, India
[n]Indian Institute of Technology, Kharagpur, India
[o]Hahn-Meitner-Institut Berlin, Germany

(Received December 13, 2004)

The first excited 2^+ states in ^{54,56,58}Cr have been populated by relativistic Coulomb excitation using the FRS-RISING setup at GSI. The Cr ions were produced by fragmentation of a ^{86}Kr beam on a primary Be target and separated by the FRS. The ion beams impinged on a thick secondary Au target at an energy of around 135A MeV. Gamma-rays were observed by the Ge cluster detectors of the RISING setup and stored in coincidence with particle and position signals from a set of tracking detectors. The steps of the analysis and spectra showing the $2^+ \rightarrow 0^+$ transitions are presented.

PACS numbers: 27.40.+z, 25.70.De, 21.10.Ky

* Presented at the XXXIX Zakopane School of Physics — International Symposium "Atomic Nuclei at Extreme Values of Temperature, Spin and Isospin", Zakopane, Poland, August 31–September 5, 2004.

** Supported by the German BMBF (06 BN 109) and by DFG (Hu 325/10), and by the Polish State Committee for Scientific Research (KBN) Grant No. 2 P03B 118 22.

1. Introduction

Very neutron rich nuclei may exhibit new shell structures due to the monopole part of the effective nuclear interaction and an apparent modification of the spin-orbit interaction. For nuclei in the $Z = 20$–28 region, theoretical and experimental results suggest a possible subshell closure at $N = 32$ or 34 [1–3]. Figure 1 shows an overview of calculated and known

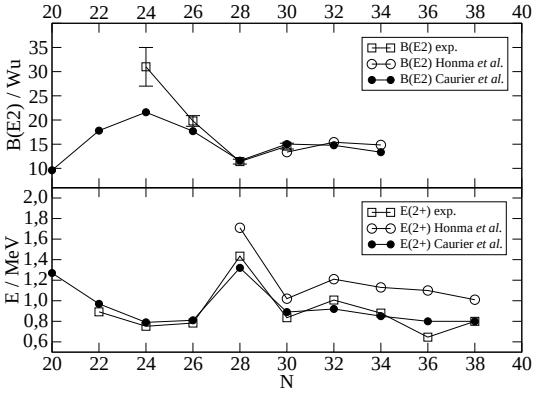

Fig. 1. Calculated and experimental values for $E(2^+)$ and $B(E2;2^+ \rightarrow 0^+)$ for Cr isotopes. The calculated values are from Honma *et al.* (open circles) [4] and Caurier *et al.* (filled circles) [5]. The open squares show experimental values from previous work [6].

experimental values in the Cr isotopes. Above the well-known shell closure at $N = 28$ the energies of the first excited 2^+ states show a maximum at $N = 32$. However, $B(E2)$ values which are a more crucial test of the nuclear wave function, are not known above $^{54}Cr_{30}$. In the present work, a report is given on a measurement of the $B(E2)$ values of the first 2^+ states in ^{56,58}Cr by relativistic Coulomb excitation.

2. Experiment

The experiment was performed using the RISING detector setup at GSI [7]. For the production of ^{54}Cr, ^{56}Cr and ^{58}Cr, ions of ^{86}Kr were accelerated to around $480A$ MeV and fragmented on a ^{9}Be target of $2.5\,\mathrm{g/cm^2}$ thickness. The fragment separator FRS was used to select and identify the ions of interest out of the secondary beam before it hit the secondary target. Behind that target, the ions were stopped in the CATE detector array [8]. Tracking before the target was done with two multiwire detectors. They were placed before and after the MUSIC ionisation chamber [7] which is used to identify the charges of the incoming ions. The masses before the

target were determined using the time of flight between two scintillators. The secondary target was a 7×7 cm^2 foil of ^{197}Au with 1 g/cm^2 thickness. Both, particle identification and tracking after the secondary target, were done with the calorimeter telescope CATE. The settings for the three runs for ^{54}Cr, ^{56}Cr and ^{58}Cr were chosen so that the beam energy after the secondary target was $100A$ MeV. The γ rays were detected using the Ge cluster detectors of RISING [7].

In the beam time of 22 h for ^{54}Cr an average intensity of 4×10^4 beam particles per spill was obtained. Around 45% of the beam particles were identified as ^{54}Cr before the target. The two other main beam components were ^{55}Mn and ^{53}V.

For ^{56}Cr in a beam time of 20 h the secondary beam intensity was around 2×10^4 particles per spill due to the lower production rate of this isotope. The main beam components were ^{56}Cr (35%), ^{57}Mn and ^{55}V.

In the case of ^{58}Cr the production rate was still lower so that only 2–4 $\times 10^3$ particles per spill hit the secondary target during 55 h of beam time. The beam contained mainly the three nuclides ^{58}Cr (25%), ^{59}Mn and ^{57}V.

3. Analysis and results

In the analysis the incoming particles were identified using the detectors mentioned above. Particles with impact parameters above ≈ 50 fm (atomic background) or below ≈ 10 fm (nuclear reactions) were excluded by a scattering angle selection. It was required that in the Ge detector array exactly one γ ray with an energy above 500 keV was registered within a narrow time window.

The Doppler-shift correction of the γ-ray energies takes into account the angle between the outgoing particle and the Ge detector as determined from tracking, and the velocity calculated from the measured time of flight. Simulation results from the MOCADI software [9] were used to obtain the relation between time of flight and velocity after the target. The resulting γ-ray spectra are shown in Fig. 2.

The $B(E2)$ values for ^{56}Cr and ^{58}Cr can be determined in two alternative ways. Absolute values may be derived from the number of incoming and outgoing Cr ions on the Au target and from the intensities of the γ-ray lines in the spectra. Alternatively, the $B(E2)$ values for ^{56}Cr and ^{58}Cr may be determined relative to the known value for ^{54}Cr, $B(E2) = 14.6(6)$ W.u. [6], since the Coulomb excitation of the three isotopes was performed under comparable conditions. The analysis is in progress.

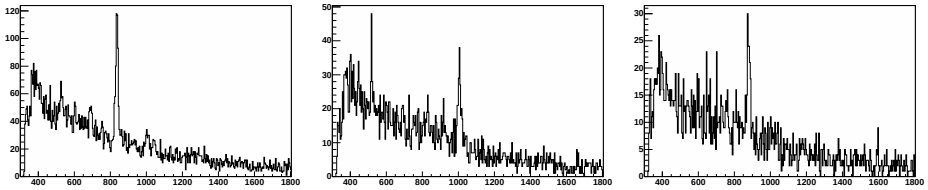

^{54}Cr, $E(2^+) = 835\,\mathrm{keV}$ ^{56}Cr, $E(2^+) = 1006\,\mathrm{keV}$ ^{58}Cr, $E(2^+) = 880\,\mathrm{keV}$

Fig. 2. Doppler-corrected spectra showing the $2^+ \rightarrow 0^+$ transitions in ^{54,56,58}Cr with 4 keV per bin. The other peaks in the spectra are assumed to originate from neighbouring nuclei which cannot currently be separated due to up to now insufficient mass resolution after the target.

4. Summary

To measure $B(E2, 2^+ \rightarrow 0^+)$ values for ^{56,58}Cr and to obtain information on a possible subshell closure at $N = 32$, the first 2^+ states of ^{54,56,58}Cr were populated by relativistic Coulomb excitation in a ^{197}Au target using the FRS-RISING setup at GSI. In a preliminary analysis γ-ray spectra were produced that clearly show the $2^+ \rightarrow 0^+$ transitions in the three Cr isotopes under investigation.

REFERENCES

[1] T. Otsuka *et al.*, *Phys. Rev. Lett.* **87**, 0852502 (2002).

[2] H. Grawe *et al.*, *Acta Phys. Pol. B* **34**, 2267 (2003).

[3] D.E. Appelbe *et al.*, *Phys. Rev.* **C67**, 034309 (2003).

[4] M. Honma *et al.*, *Phys. Rev.* **C69**, 034335 (2004).

[5] E. Caurier, F. Nowacki, A. Poves, *Eur. Phys. J.* **A15**, 145 (2002).

[6] ENSDF database, `http://www.nndc.bnl.gov/ensdf/`.

[7] H.J. Wollersheim *et al.*, *Nucl. Instrum. Methods Phys. Res.* **A537**, 637 (2004).

[8] R. Lozeva *et al.*, *Nucl. Instrum. Methods Phys. Res.* **B204**, 678 (2003).

[9] MOCADI Homepage, `http://www-linux.gsi.de/~weick/mocadi/`.

SPECTROSCOPY OF $T = 3/2$ MIRROR NUCLEI VIA TWO-STEP FRAGMENTATION USING RISING*

G. Hammond[a,b], M.A. Bentley[a], F. Becker[b], J. Grębosz[b,c]
M.J. Taylor[d], A. Banu[b,e], C.J. Barton[f], T. Beck[b], P. Bednarczyk[b,c]
A. Bracco[g], A.M. Bruce[d], L.C. Bullock[a], A. Bürger[h], F. Camera[g]
C. Chandler[a], P. Doornenbal[b], J. Gerl[b], H. Geissel[b], M. Górska[b]
M. Hellström[b], D. Judson[d], I. Kojouharov[b], N. Kurz[b], R. Lozeva[b,i]
A. Maj[c], S. Mandal[b], B. McGuirk[j], S. Muralithar[b,k], E.S. Paul[j]
Zs. Podolyák[l], W. Prokopowicz[b], D. Rudolph[m], N. Saito[b], T.R. Saito[b]
H. Schaffner[b], J. Simpson[n], D.D. Warner[n], H. Weick[b], C. Wheldon[b,o]
M. Winkler[b] and H.-J. Wollersheim[b]

[a]School of Chemistry and Physics, Keele University, Staffordshire ST5 5BG, UK
[b]Gesellschaft für Schwerionenforschung (GSI), 64291 Darmstadt, Germany
[c]The H. Niewodniczański Institute of Nuclear Physics PAN, Krakow, Poland
[d]School of Engineering, University of Brighton, Brighton BN2 4GJ, UK
[e]Institut für Kernphysik, Universität Mainz, 55099 Mainz, Germany
[f]Department of Physics, University of York, York YO10 5DD, UK
[g]Department of Physics, University of Milano and INFN, Milano, Italy
[h]Helmholtz-Institut für Strahlen- und Kernphysik, 53115 Bonn, Germany
[i]Faculty of Physics, University of Sofia "St. Kl. Ohridski", 1164 Sofia, Bulgaria
[j]Department of Physics, University of Liverpool, Liverpool L69 7ZE, UK
[k]Nuclear Science Center, New Delhi 110067, India
[l]Department of Physics, University of Surrey, Guildford GU2 7XH, UK
[m]Department of Physics, Lund University, 22100 Lund, Sweden
[n]CCLRC Daresbury Laboratory, Warrington, Cheshire WA4 4AD, UK
[o]Hahn-Meitner-Institut Berlin, 14109 Berlin, Germany

(Received December 13, 2004)

Two two-step fragmentation reactions were performed using RISING to populate excited states in $A \approx 50$ mirror nuclei near to the proton-drip line, in order to test isospin symmetry. The experiments were designed to observe gamma decays of excited states in the mirror nuclei $^{53}_{28}\mathrm{Ni}_{25}/^{53}_{25}\mathrm{Mn}_{28}$, which have a large value of total isospin ($T = 3/2$). In the continuing off-line analysis, gamma transitions have been observed in ^{54}Ni indicating that two-step fragmentation is a successful technique for spectroscopic investigations of proton-rich nuclear systems in this mass region.

PACS numbers: 21.10.Hw, 21.10.Sf, 23.20.Lv, 25.70.Mn

* Presented at the XXXIX Zakopane School of Physics — International Symposium "Atomic Nuclei at Extreme Values of Temperature, Spin and Isospin", Zakopane, Poland, August 31–September 5, 2004.

1. Introduction

Investigating fundamental symmetries is a principal aim of nuclear structure physics. Isospin is one of the most basic symmetries, occurring between protons and neutrons in the nucleus due to the charge independent nuclear force. In a pair of mirror nuclei, one can observe the difference in energy between isobaric analogue states, so-called *Coulomb energy differences* (CED), which are typically of the order of tens of keV. Two-body Coulomb matrix elements (CME) can be added to shell model calculations in order to reproduce the experimentally observed CED.

CME can also be extracted from experimental data. This was done by Williams *et al.* who studied the $T = 1/2$ mirror nuclei $^{53}_{27}\mathrm{Co}_{26}/^{53}_{26}\mathrm{Fe}_{27}$ [1]. Upon exciting a nucleus, pairs of like particles begin to align. The alignment of a pair of protons (proton holes in the case of ^{53}Fe) reduces the Coulomb self-energy of the proton (hole) pair. This, in turn, affects the CED, as the corresponding alignment in ^{53}Co is due to neutrons. Fig. 1 shows the CME extracted from the experimental CED, as a function of spin for a proton pair. One expects to see a decrease in the CME with increasing particle alignment. However, as is evident from Fig. 1, the CME increase at $J = 2$. This anomaly has been observed elsewhere in the $f_{\frac{7}{2}}$ shell but not explained.

Due to the current high level of experimental and theoretical interest in studies of isobaric analogue states, it is essential to push such investigations towards the largest accessible values of isospin. To do this, two two-step fragmentation reactions were performed as a part of the RISING (Rare Isotope Spectroscopic INvestigation at GSI) campaign [2].

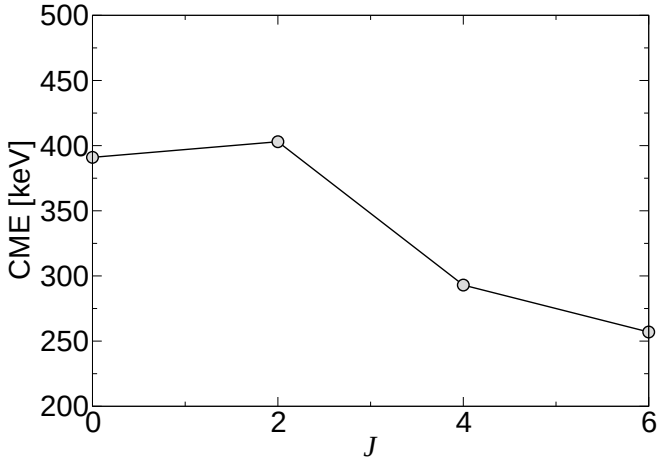

Fig. 1. CME *versus* particle alignment for the $T = 1/2$, $A = 53$ mirror nuclei ^{53}Co/^{53}Fe [1]. There is clearly an anomaly at $J = 2$.

2. Experimental details

A stable beam of ^{58}Ni was incident upon a $4.0\,\mathrm{g/cm^2}$ ^{9}Be target at the entrance to the GSI FRS (FRagment Separator) [3], with an energy of $600A\,\mathrm{MeV}$. This primary fragmentation reaction produced a wide range of fully-stripped nuclei, from which one of two radioactive fragments were selected by the FRS: either $^{55}_{28}\mathrm{Ni}_{27}$, for producing proton-rich mirror pair members, or its mirror, $^{55}_{27}\mathrm{Co}_{28}$, for producing the corresponding neutron-rich members. The radioactive intermediate beams were only a few nucleons away from the nuclei of interest, since previous fragmentation studies have shown that this provides the highest yield [4, 5].

The time-of-flight through the second stage of the FRS was measured, using two plastic scintillator detectors as start and stop signals. This allowed for the determination of the velocity of the intermediate beam. An ionisation chamber, MUSIC, was used to determine the Z of the intermediate beam particles. The A/Q of the intermediate beam was calculated and a combination of A/Q and Z allowed for perfect beam identification.

The nuclei of interest were produced at a second, $700\,\mathrm{mg/cm^2}$ ^{9}Be fragmentation target, located at the focal plane of the FRS. The emerging recoils had a v/c of approximately 0.45. Fifteen RISING cluster detectors were situated at forward angles to the secondary target, each detector comprising seven independent Ge crystals. The cluster detectors were arranged in two rings at approximately 16° and 34°. The positioning of the detectors provided maximum efficiency for the detection of gamma rays subject to the Lorentz boost, incurred by the high-recoil velocity. Additionally, the HECTOR (High Energy γ deteCTOR) array [6], consisting of eight large volume BaF_2 crystals, was arranged at backward angles to the secondary target.

Situated downstream of the secondary target was CATE (the CAlorimter TElescope) [7,8], consisting of nine individual elements arranged in a square, each of which comprised a thin silicon wafer for measuring recoil position and energy loss (ΔE) and a thick CsI wafer for measuring total recoil energy (E). The values of ΔE and E provided information about the Z and A of each recoil, respectively [7, 8].

The condition of beam tracking, provided by two multi-wire proportional chambers along with the position sensitivity of CATE allows for a full tracking Doppler shift correction to be applied.

3. Results

Although the analysis is still at a preliminary stage, some interesting results have already been gleaned from the data. The CATE detector currently gives clear $\Delta E(Z)$ separation for the recoils but so far only limited E (A) separation. Work done to resolve this issue is being carried out by Lozeva *et al.* (see Refs. [7, 8]).

By gating on Z and projecting out the coincident gamma rays, isotopic spectra for all produced masses are obtainable. The observed transitions are from the nuclei with the highest fragmentation cross-section, σ_{frag}. Fig. 2 shows two such spectra: part (a) was made by gating on nickel and is dominated by ^{54}Ni ($\sigma_{\text{frag}} \approx 5$mb); part (b) is dominated by ^{54}Fe ($\sigma_{\text{frag}} \approx 77$mb), the mirror nucleus of ^{54}Ni and was made by gating on all iron isotopes. Cross-sections quoted are predicted by the EPAX parameterization [9, 10].

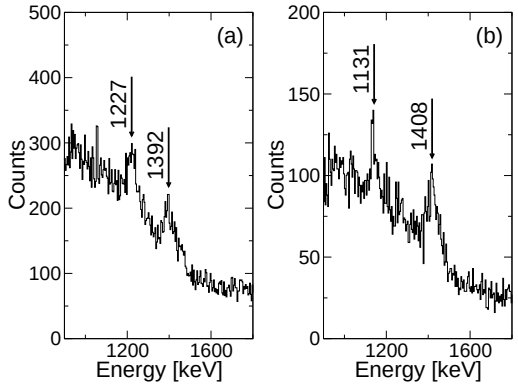

Fig. 2. (a) Nickel gated γ ray spectrum, showing the 1227 keV $4^+ \rightarrow 2^+$ and 1392 keV $2^+ \rightarrow 0^+$ transitions in ^{54}Ni [13, 14]. (b) Iron gated γ ray spectrum, showing the 1131 keV $4^+ \rightarrow 2^+$ and 1408 keV $2^+ \rightarrow 0^+$ transitions in ^{54}Fe, the mirror nucleus of ^{54}Ni [11]. Energies are taken from Gadea *et al.* [13, 14].

The spectra shown in Fig. 2 only have a basic Doppler shift correction algorithm applied; a full event-by-event tracked Doppler shift correction will be implemented to reduce the widths of the peaks. The value of v/c used in the Doppler shift correction was calculated in a simulation using LISE++ [12].

Even at this preliminary stage of the analysis, the $4^+ \rightarrow 2^+$ and $2^+ \rightarrow 0^+$ transitions in ^{54}Ni, which have only recently been identified by Gadea *et al.* [13, 14] using a heavy-ion fusion-evaporation reaction, are clearly visible in Fig. 2 (a). It can be clearly seen from these spectra that the energy shift of the 4^+ state is in the opposite direction to the 2^+ state, providing further evidence of the presence of the "$J = 2$ anomaly".

4. Conclusions

The observation of the mirrored $4^+ \rightarrow 2^+$ and $2^+ \rightarrow 0^+$ transitions in the $A = 54$ mirror nuclei shows that two-step fragmentation can be used successfully for populating excited states in proton-rich nuclear systems in the $A \approx 50$ mass region. Furthermore, the anomalous behavior of the CME at $J = 2$ has now been observed across the entire $f_{\frac{7}{2}}$ shell, with the same

effect being seen in the mirror pairs for $A = 42$, 47, 49, 53 (see, for example, Refs. [1, 15, 16]) and $A = 54$ (Refs. [13, 14] and this work). This would seem to indicate that the origin of the anomaly is not based around interactions with the ^{40}Ca core, but originates from elsewhere. Whether or not the anomaly is nuclear or electromagnetic in origin remains to be seen. Observing the anomaly at higher values of isospin will provide more insight into its origin.

The application of a fully tracked Doppler shift correction along with improved A resolution in the CATE spectrometer will allow for improved spectra to be created, in turn allowing for a more accurate determination of γ ray energies and separation of masses to allow discrimination between different isotopes. Judging from the analysis to date, it seems likely that spectroscopy at the level of 1mb or less is feasible within the data. This will allow spectroscopic investigations of unknown proton-rich systems, such as $^{52}_{27}\mathrm{Co}_{25}$ ($N = Z - 2$) and, hopefully, ^{53}Ni.

This work was partially supported by the Polish State Committee for Scientific Research (KBN) Grants Nos. 2 P03B 118 22 and 620/E-77/SPB/GSI/P-03/DWM105/2004-2007).

REFERENCES

[1] S.J. Williams *et al., Phys. Rev.* **C68**, 011301(R) (2003).
[2] H.-J. Wollersheim, M. Górska *et al., Nucl. Instrum. Methods* **A**, in press (2004).
[3] H. Geissel *et al., Nucl. Instrum. Methods* **B70**, 286 (1992).
[4] K. Yoneda *et al., Phys. Lett.* **B499**, 233 (2001).
[5] J. Enders *et al., Phys. Rev.* **C65**, 034318 (2002).
[6] A. Maj *et al., Nucl. Phys.* **A571**, 185 (1994).
[7] R. Lozeva *et al., Nucl. Instrum. Methods* **B204**, 678 (2003).
[8] R. Lozeva *et al., Acta Phys. Pol. B* **36**, 1245 (2005), these proceedings.
[9] K. Sümmerer, B. Blank, *Phys. Rev.* **C61**, 034607 (2000).
[10] K. Sümmerer, B. Blank, *EPAX version 2.1,* `http://www-w2k.gsi.de/hellstr/asp/gsi/epaxv21m.asp`.
[11] D. Rudolph *et al., Eur. Phys. J.* **A2**, 115 (1999).
[12] D. Bazin, O. Tarasov, M. Lewitowicz, O. Sorlin, *Nucl. Instrum. Methods* **A482**, 307 (2002).
[13] A. Gadea, private communication.
[14] A. Gadea *et al., LNL Annual Report 2003*, INFN (REP) 202/2004, p. 8.
[15] M.A. Bentley *et al., Phys. Lett.* **B437**, 243 (1998).
[16] C.D. O'Leary *et al., Phys. Rev. Lett.* **79**, 4349 (1997).

FUTURE RISING EXPERIMENTS AT RELATIVISTIC ENERGIES *

P. Reiter[a], F. Becker[b], M.A. Bentley[c], A. Bracco[d]
G. de Angelis[e], C. Fahlander[f], J. Gerl[b], M. Gorska[b], H. Grawe[b]
H. Hübel[g], J. Jolie[a], A. Maj[h], P. Mayet[i], T. Saito[b]
K.-H. Speidel[g] and H.J. Wollersheim[b]

[a]IKP University of Cologne, 50932 Cologne, Germany
[b]GSI Darmstadt, 64291 Darmstadt, Germany
[c]Keele University, Keele, Staffordshire ST5 5BG, UK
[d]University of Milan and INFN Milan, Milano, Italy
[e]Istituto Nazionale di Fisica Nucleare, Legnaro, Italy
[f]Lund University, 221 00 Lund, Sweden
[g]ISKP University of Bonn, 53115 Bonn, Germany
[h]The H. Niewodniczański Institute of Nuclear Physics PAN, Kraków, Poland
[i]University of Leuven, 3001 Leuven, Belgium

(Received December 16, 2004)

The proposed experiments for the first RISING (Rare ISotope INvestigations at GSI) campaign will exploit secondary unstable beams at relativistic energies in the range from 100 MeV/u to 400 MeV/u. The RISING spectrometer will be employed for relativistic Coulomb excitation and for high-resolution γ-spectroscopy experiments after secondary nucleon removal reactions and secondary fragmentation. New experimental methods for spectroscopy at relativistic energies will be investigated in order to measure nuclear structure observables beside the directly accessible level energies and quadrupole deformations. The future experiments will focus on: Shell structure of unstable doubly magic nuclei and their vicinity, symmetries along the $N = Z$ line and mixed symmetry states, shapes and shape coexistence, collective modes and E1 strength distribution.

PACS numbers: 25.70.De, 23.30.–g

* Presented at the XXXIX Zakopane School of Physics — International Symposium "Atomic Nuclei at Extreme Values of Temperature, Spin and Isospin", Zakopane, Poland, August 31–September 5, 2004.

1. Introduction

The SIS/FRS facility provides secondary beams of unstable rare isotopes after fragmentation reactions or secondary fission of relativistic heavy ions with sufficient intensity for in-beam γ-spectroscopy measurements. The proposed experiments for the first RISING (Rare ISotope INvestigations at GSI) campaign exploit these unique beams at relativistic energies in the range from 100 MeV/u to 400 MeV/u. Comparing with other fragmentation facilities the majority of the experiments depend on fragmentation products from heavy primary beams or the high secondary beam energy and are predestined for GSI. The RISING spectrometer is employed not only for relativistic Coulomb excitation but also for high-resolution γ-spectroscopy experiments after secondary nucleon removal reactions and secondary fragmentation. The latter may lead to rather high angular momentum states. Several experiments will focus on new methods and techniques in order to obtain important nuclear structure observables beside the level energies and quadrupole deformations. As special application they may allow g-factor measurements for short lived states, systematic studies of the spin alignment/polarisation and to determine life times of short lived states and spectroscopic factors.

The proposed γ-ray spectroscopy of nuclei from exotic beams will be performed after in-flight isotope separation. The exotic beams will be produced by fragmentation of a heavy stable primary beam or fission of a ^{238}U beam on a ^{9}Be or ^{208}Pb target in front of the fragment separator FRS. A maximal beam intensity from the SIS synchrotron of 10^{10}/s for medium heavy beams and 10^{9}/s for ^{238}U is expected. The secondary beam intensities take advantage of the primary target thickness of $\approx$ 1–4 g/cm^2 and the high cross section, for fragmentation reactions and fission given *e.g.* by the EPAX parameterisation [1] and measured data for the fission processes [2]. Experimental details related to the RISING spectrometer and its ancillary detectors [3] are presented by the contributions of Bednarczyk [4] and Lozeva [5] to this conference.

2. RISING physics program

The motivations to explore nuclear structure of exotic nuclei focus on the following subjects:

(i) shell structure of unstable doubly magic nuclei and their vicinity;

(ii) symmetries along the $N = Z$ line and mixed symmetry states;

(iii) shapes and shape coexistence;

(iv) collective modes and E1 strength distribution.

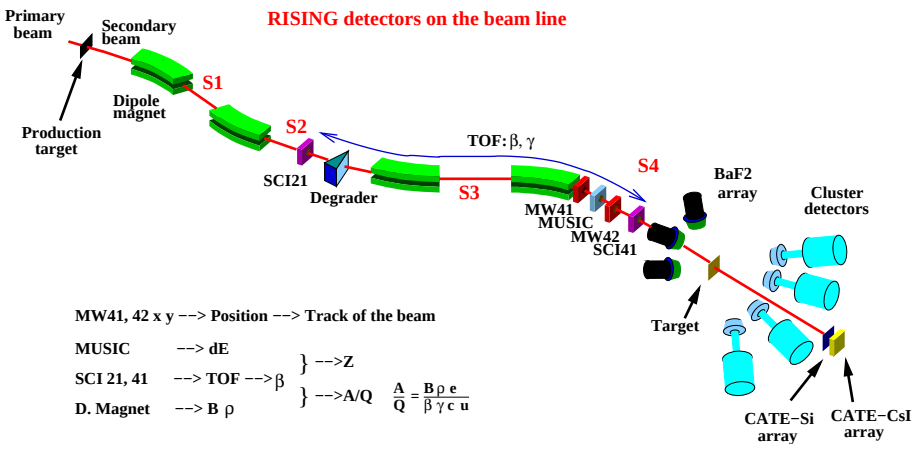

Fig. 1. Schematic layout of the RISING set-up at the FRS. The beam diagnostic and tracking elements consist of two multiwire detectors MW41, MW42, an ionisation chamber MUSIC and two scintillation detectors SC21, SC41. The γ-rays are measured with BaF2-HECTOR and Ge-Cluster detectors. The ions emerging from the reaction target are identified with the CATE array.

2.1. Shell structure

Spectroscopic data on the single particle structure of unstable doubly magic nuclei and their nearest neighbours are pivotal for theoretical description of the effective interactions in large-scale shell-model calculations. The proposed studies along the $N = Z$ line, passing doubly magic nuclei ^{56}Ni and ^{100}Sn, provide an excellent probe for single-particle shell structure, proton–neutron interaction and the role of correlations, normally not treated in mean field approaches. For example, the $B(\mathrm{E2},2_1^+ \rightarrow 0^+)$ values in semi-magic Sn nuclei provide a sensitive test for changing (sub)shell structure, the E2 polarisability and the shape response of the magic core. For several reasons conventional techniques, employing (HI,xn) reactions, are very difficult or even impossible and Coulomb excitation measurements with unstable beams are the most promising way to obtain the interesting $B(\mathrm{E2},2_1^+ \rightarrow 0^+)$ values.

The development of new shell structure at $N \gg Z$ as studied in light and medium-heavy neutron-rich nuclei around $N = 8, 20, 28$ [6–8] is generally ascribed to the weakening of the surface slope of the neutron potential due to the large neutron excess. As a consequence the familiar Woods–Saxon shape of the potential for nuclei close to stability is expected to change towards a harmonic oscillator type. This goes along with a reduction of the spin–orbit splitting, which is proportional to the potential slope, for orbitals probing in their radial extension the surface region and thus harmonic oscillator

magic numbers are expected to be reinforced [9]. Moreover, ^{78}Ni and ^{132}Sn are located close to the astrophysical rapid neutron capture process path and indirect evidence for an altered shell structure and shell quenching of magic gaps at $N = 82$ and $N = 126$ is derived from r-process network calculations [10].

Alternatively, the existing experimental evidence of changing shell structure along the $N = 8$, 20 and 28 isotonic sequences can be explained in terms of the monopole part of the nucleon–nucleon residual interaction. Schematically this is due to the $(\sigma\sigma)(\tau\tau)$ part of the interaction, which is binding and strongest in the $S = 0$ (spin-flip) and $T = 0$ (proton–neutron) channel of the two-body interaction. This causes large monopole shifts of neutron single-particle orbits due to their missing $S = 0$ proton partners at large neutron excess, and thus generates new shell gaps. The effect was first discussed for the *sd* shell [11, 12] and for the *pf* shell [12, 14]; see also contribution by Otsuka [13] to this conference.

To date the investigations concentrate on the region of neutron-rich Ca, Ni and Sn isotopes about the most significant matrix elements, the spectroscopic factors and the magnetic moments, which are sensitive indicators of their structure. It is known experimentally that the neutron $\nu f_{5/2}$ orbit from ^{57}Ni towards ^{49}Ca undergoes a large monopole shift due to the reduced binding with increasing removal of the proton $\pi f_{7/2}$ $S = 0$ spin–orbit partners [14]. Beyond $N = 28$ this opens a gap between the $\nu p_{3/2}, p_{1/2}$ and $\nu f_{5/2}$ orbits, which might be subject to change depending on the $2p_{1/2}$ position, as this also forms a $S = 0$ pair with $\pi 1f_{7/2}$ but with less radial overlap. In the Ca isotopes beyond $N = 28$ a possible (sub)shell closure at $N = 32, 34$ seems to develop in $E(2_1^+)$. It has been pointed out recently that the Cr isotopes show a maximum in $E(2_1^+)$ at $N = 32$. On the other hand within the $N = 34$ isotones $E(2_1^+)$ is increasing from Fe to Cr in contrast to the expected trend towards midshell, which supports a $N = 34$ closure [15]. Besides masses, which due to short half lives are difficult to measure, obviously B(E2) values are missing for a proof of the concept. A study of the $N = 30$–34 isotones of Cr would reveal such a change in shell structure and was started in one of the first RISING experiments; see contribution of Bürger to this conference [16].

2.2. Spectroscopic factors in ^{132}Sn

The spin–orbit splitting plays the crucial role in determining the binding and structure of nuclei. Depending on the relative orientation of the spin and the orbital angular momentum, the energy of the associated nuclear state is shifted up or down. According to certain model predictions [9], the energy splitting of the spin–orbit partners should decrease or even vanish

far from stability for very neutron-rich isotopes. Recently energy differences between pairs of high-j proton single-particle states and the spectroscopic factors of these states were measured following Sn(α, t) reactions for all seven stable even Sn isotopes [17]. A possible explanation of the changing energy separation is a decreasing overall spin–orbit splitting, proposed by [9]. Experiments with radioactive ion beams measuring spectroscopic factors in the vicinity of ^{132}Sn are, therefore, especially intriguing.

The determination of the spectroscopic factors in $A-1$ nucleus at the $N = 82$ shell closure will provide detailed information on the mixing of single particle states with more complicated configurations. The mixing is expected to occur mainly with configurations containing a low-lying surface vibrational mode [18]. Estimates of absolute one-particle removal cross sections for knock-out reactions indicate considerable cross sections of the order of a few mb/sr. The evolution of the single-particle levels, of which only a few are known, could be studied with knock out reactions by detecting the gamma rays deexciting the states in nuclei around the $Z = 50$ proton closed shell and the $N = 82$ neutron shell. The spectroscopic factors for ^{132}Sn obtained through Hartree–Fock calculations with SGII effective interaction, including the coupling to collective phonons, underline the doubly magic character of the ^{132}Sn.

A direct way to measure the ground state structure of ^{132}Sn, employing the RISING setup, is to determine the spectroscopic factors for the removal of a neutron. The observation of the decay of the $7/2^-$ level in the gamma spectrum of ^{131}Sn should directly probe the occupancy of the $2f_{7/2}$ orbit. The neutron closed shell configuration $(h_{11/2})^{12}$ would give spectroscopic factors of $12/(2j+1)$ for the $11/2^-$ and 0 for the $7/2^-$ states. The experimental determination of the single particle character of the $5/2^+$ state above the $\nu d_{3/2}$ ground state, should shed some light on the relatively low value of the $\nu d_{5/2} - \nu d_{3/2}$ spin orbit splitting.

2.3. Magnetic moments

Nuclei near closed shells are characterised by specific single particle components in the wave functions, which changes into collective structures when departing from shell closures. In comparison to the stable even-A Te isotopes $^{120-130}$Te, which are collective of vibrational nature, the structure of the unstable neutron-rich isotopes $^{132-136}$Te is strongly influenced by the $N = 82$ shell closure and the two protons outside the magic $Z = 50$ shell. This feature becomes evident already from their 2_1^+ excitation energies. For the stable ^{134,136}Xe nuclei g-factors were recently determined for the 2_1^+ and 4_1^+ states clearly exhibiting single proton excitations with dominant $\pi 1g_{7/2}$

configuration [19]. Large and positive g-factors of both states in ^{136}Xe and of the 4_1^+ state in ^{134}Xe unambiguously shows the dominant proton nature whereas the smaller $g(2_1^+)$ value in ^{132}Xe implies additional neutron hole configurations.

At present, for *ps* lifetimes of nuclear states only the technique of transient magnetic fields (TF) provides the necessary field strengths of several kTesla, to observe spin precessions with the method of perturbed γ-angular correlations (PAC). The TF are hyperfine fields, which are experienced in fast moving ions during their passage through ferromagnetic materials [20]. TF are described by empirical parameterisations [20] at intermediate ion velocities, $v \ll Zv_0$ (in units of the Bohr velocity v_0), whereby the field strength generally increases with velocity reaching a maximum at $v = Zv_0$ for single-electron ions with its maximum fraction at the $1s$ electron Bohr velocity. Hence, the largest TF are expected for H-like ions implying velocities of relativistic heavy ions available at GSI.

The technique proposed for future RISING g-factor measurements is projectile Coulomb excitation in combination with TF in ferromagnetic Gadolinium. The target, consisting of approximately 50 mg/cm^2 of ^{208}Pb and 50 mg/cm^2 of Gd, serves for excitation in Pb and Gd and spin precession in the Gd layer. After fragmentation reactions of stable ^{136}Xe and ^{164}Dy beams, the secondary ^{132,134,136}Te and ^{138}Xe ions will be focused onto the double-layered target polarised by an external field of 0.08 Tesla. The mean energy of the excited ions in Gd corresponds to a velocity of $v_{\rm ion} \simeq 60v_0$, implying a H-like ion fraction of $q_{1s} \simeq 0.5$. For the TF strength in these conditions one calculates a very high field strength of $B_{\rm TF} \simeq 23$ kTesla and effective interaction times of $t_{\rm eff} \approx 0.3$ps and 0.2 ps for excitation in Pb or Gd, respectively. Main advantage of the relativistic energy will be a huge precession angle of *e.g.* $\theta_{\rm exp}(2^+) \approx 240$ mrad assuming a positive g-factor in ^{134}Te of $g(2^+) = +0.8$. Its observation is based on a pronounced anisotropy of the angular correlation of the $(2^+ \rightarrow 0^+)$ γ-rays of ^{134}Te in the rest frame of the emitting nuclei. As the Te ions recoil out into vacuum, the anisotropy of the correlation will be attenuated by the strong hyperfine fields of $1s$ electrons in the dominant H-like ions, expressed by attenuation coefficients. The spin precession is observed via the rotation of the anisotropic angular correlation of γ-rays emitted from the excited states. The deexcitation γ-rays are measured with the RISING Ge-detectors — at fixed polar angles θ_γ, in and close to the reaction plane — in coincidence with the scattered ions, registered in the position sensitive Si detector array CATE [5]. In such a geometry previous TF measurements were successfully carried out at lower beam energies of 15 MeV/u [21] which will be extended now to higher energies.

2.4. Symmetries

Recently spectroscopy at high spin of even–even $T = 1 (T_z = \pm 1)$ mirror nuclei with $A = 50$ [22] and $A = 46$ [23] has been achieved, by identifying gamma decays in the most proton-rich ($N = Z - 2$) isobars. The Coulomb Energy Differences CED between these $T = 1$ mirror states showed that a very detailed understanding of the spatial correlations of pairs of particles can be gained. In these cases, it was also found necessary to include "one-body" effects in order to understand the CED. One such effect [22] is the Coulomb energy associated with nucleon orbitals of different radii, the occupation of which evolve as a function of spin, resulting in a contribution to the CED. These $A = 46$ and $A = 50$ even–even mirror nuclei described above represent the largest value of total isospin T, for which isobaric analogue states have been studied at high spin.

For mirror nuclei with larger values of isospin ($T \leq 3/2$) no detailed spectroscopic studies in medium-mass nuclei have been undertaken. The large proton excess for the proton-rich members of these isobaric multiplets may be expected to have an increasingly significant effect on the one-body part of the measured Coulomb energy. This includes the bulk Coulomb effect associated with the differences in radii of specific orbitals as well as the more subtle effect of the Coulomb distortion of the specific nucleon wave functions (the Thomas–Ehrman shift). The mirror pair ^{53}Ni/^{53}Mn is of particular interest, as these nuclei have a very simple $(f_{7/2})^{-3}$ structure — neutron holes in ^{53}Ni and proton holes in ^{53}Mn. This allows for a comparison of the $(f_{7/2})^{-3}$ proton and neutron multiplets, and the CED between these will give new information on the Coulomb two-body matrix elements in the upper $f_{7/2}$ shell — a vital ingredient for the shell model calculations that can only be derived from experimental data.

Therefore, in one of the first RISING experiments even Z, $T_z = -3/2$ nuclei in the $f_{7/2}$-shell were produced after secondary fragmentation reactions and a spectroscopic study of the energy levels up to 3–4 MeV excitation energy was started. The fragmentation reaction may populate low-spin non-yrast structures that are only weakly populated in the fusion–evaporation technique, allowing a more complete study of the Coulomb effects. For details of the status of the analysis of this experiment see contribution by Hammond [25] to this conference.

Spectacular shape effects are observed in the $A = 70$–80 mass region with extremely large oblate deformation for $N = Z = 36$ changing to a large prolate deformation for $N = Z = 38, 42$. Therefore, the light Se- to Zr-isotopes are amongst the best candidates for investigations of the origin and development of nuclear shapes and shape coexistence. Moreover, in the $N = Z$ odd–odd nucleus ^{70}Br [24] indication exist that the Coulomb

distortion of the nucleon wave functions may be important as the drip-line is approached. The CED between the $T = 1$ states and those in the neighbouring analogue nucleus ^{70}Se shows anomalous behaviour which has been interpreted in terms of the Thomas–Ehrman shift.

A proposed spectroscopic RISING investigation of excited states in the $T_z = -1/2$ nucleus ^{69}Br should reveal information on one of the accessible, heaviest mirror nucleus. Due to the location at the proton drip line or even beyond, extended proton distributions may become apparent from the break down of the mirror symmetry. The differences in proton radii should manifest themselves through differences in the behaviour of CEDs. A recent investigation of the Coulomb energy differences in ^{70}Br,^{70}Se has shown a similar effect possibly attributed to a decrease of the nuclear two-body residual interaction due to the different radial distributions of the wave functions for neutrons and loosely bound protons [24]. In case of ^{69}Br due to the very low binding energy major differences are expected with respect to the strongly bound ^{69}Se in the excitation energy of the low lying states.

The rapid-proton capture process (rp process), first proposed by Wallace and Woosley [26], proceeds via a sequence of proton capture and beta decays near and along the proton drip line. The path of the rp process is determined by the stability of the nuclei involved. Different predictions of the exact position of the proton drip line are related to possible termination points of the rp process. The odd-Z isotopes of ^{65}As and ^{69}Br are considered as possible termination points because the half-lives of their proton capture targets ^{64}Ge and ^{68}Se are supposed to be longer than the time scale of the explosion that provides the proton flux. With respect to ^{69}Br, a first evidence for the existence was reported [27]. However, follow-up experiments did not succeed to observe ^{69}Br. In particular, experiments at GANIL [28] and NSCL [29] could not attribute an event to ^{69}Br. The latter experiment indicates that ^{69}Br was not stable or had a very short half-life in the range below 24 ns. To overcome difficulties due to the flight path limit in a fragment separator, the RISING study of ^{69}Br will investigate the prompt gamma decay produced in a secondary fragmentation reaction.

2.5. Collective excitations

Collective excitations such as the giant dipole resonance (GDR), built from superpositions of single-particle excitations are necessarily influenced by the nuclear shell structure. In exotic nuclei like $^{68-78}$Ni the proton–neutron asymmetry may give rise to differing shell structure. Theoretical calculations predict a significant change in the GDR strength distribution as one progresses towards the doubly magic ^{78}Ni [30, 31]. The excitation function of the isovector GDR mode is expected to fragment substantially,

favouring a redistribution of the strength towards lower excitation energies (Pygmy resonance). Measurements of the GDR strength function provide access to the isospin dependent part of the in-medium nucleon–nucleon interaction and on dipole type vibrations of the excess neutrons. The predicted low-energy shift of the GDR strength was confirmed in neutron-rich oxygen isotopes by the LAND group at GSI by means of virtual photon absorption measurements [32]. A RISING GDR experiment in ^{68}Ni will apply a complementary method, virtual photon scattering, which relies on real projectile γ-ray emission following the virtual excitation. In order to observe discrete γ-transitions with high resolution and γ-decay from the GDR, the RISING array will be augmented the HECTOR array [33], 8 large volume BaF2 scintillator detectors positioned at very backward angles. With the scintillators the highest energy transitions up to ≈ 30 MeV can be measured efficiently.

3. Summary

As part of an extended physics program the first Coulomb excitation and secondary fragmentation experiments [16, 25] were successfully performed with the RISING spectrometer, a new instrument for high-resolution γ-ray spectroscopy experiments employing beams of short-lived isotopes at 100–400 MeV/u energy from the SIS/FRS facility at GSI. The experimental set-up comprises heavy-ion tracking detectors for incoming beam nuclei impinging on a secondary target, the CATE detector for outgoing heavy ions, the EUROBALL Ge-Cluster detector and the BaF2-HECTOR detector arrays for γ-ray detection. In the near future the remaining part of the relativistic RISING experiments will be performed hopefully contributing to a better understanding of several open nuclear structure problems.

RISING is supported by the German BMBF under grant 06OK-167, 06BN-109, 06BN-911; the Swedish Research Council; the Polish State Committee for Scientific Research (KBN) Grants No. 2 P03B 118 22 and 620/E-77 /SPB/GSI/P-03/DWM105/2004-2007).

REFERENCES

[1] EPAX Version 2, K. Sümmerer, B. Blank, *Phys. Rev.* **C61**, 034607 (2000).

[2] W. Schwab *et al.*, *Eur. Phys. J.* **A2**, 179 (1998); J. Benlliure *et al.*, *Eur. Phys. J.* **A2**, 193 (1998).

[3] H.J. Wollersheim *et al.*, accepted for publication in *Nucl. Instrum. Methods Phys. Res. A*.

[4] P. Bednarczyk *et al.*, *Acta Phys. Pol. B* **36**, 1235 (2005), these proceedings.

[5] R. Lozeva *et al.*, *Acta Phys. Pol. B* **36**, 1245 (2005), these proceedings.
[6] A. Navin *et al.*, *Phys. Rev. Lett.* **85**, 266 (2000).
[7] N. Orr *et al.*, *Phys. Lett.* **B258**, 29 (1991).
[8] O. Sorlin *et al.*, *Phys. Rev.* **C47**, 2941 (1997).
[9] J. Dobaczewski *et al.*, *Phys. Rev. Lett.* **72**, 981 (1994).
[10] B. Pfeiffer, K.-L. Kratz, F.-K. Thielemann, *Z. Phys.* **A357**, 235 (1997).
[11] T. Otsuka *et al.*, *Phys. Rev. Lett.* **87**, 082502 (2001).
[12] T. Otsuka *et al.*, *Eur. Phys. J.* **A13**, 69 (2002).
[13] T. Otsuka *et al.*, *Acta Phys. Pol. B* **36**, 1213 (2005), these proceedings.
[14] H. Grawe, *Acta Phys. Pol. B* **34**, 2267 (2003).
[15] J.I. Prisciandaro *et al.*, *Phys. Lett.* **B510**, 17 (2001).
[16] A. Bürger *et al.*, *Acta Phys. Pol. B* **36**, 1249 (2005), these proceedings.
[17] J. Schiffer *et al.*, *Phys. Rev. Lett.* **92**, 162501 (2004).
[18] F. Barranco, G. Colo', private communication.
[19] G. Jakob *et al.*, *Phys. Rev.* **C65**, 024316 (2002).
[20] K.-H. Speidel *et al.*, *Prog. Part. Nucl. Phys.* **49**, 91 (2002).
[21] U. Grabowy *et al.*, *Z. Phys.* **A359**, 377 (1997).
[22] S.M. Lenzi *et al.*, *Phys. Rev. Lett.* **87**, 122501 (2001).
[23] P.E. Garrett *et al.*, *Phys. Rev. Lett.* **87**, 132502 (2001).
[24] G. de Angelis *et al.*, *Eur. J. Phys.* **A12**, 51 (2001).
[25] G. Hammond *et al.*, *Acta Phys. Pol. B* **36**, 1253 (2005), these proceedings.
[26] R.K. Wallace, S.E. Woosley, *Astrophys. J. Suppl.* **45**, 389 (1981).
[27] M.F. Mohar *et al.*, *Phys. Rev. Lett.* **66**, 1571 (1991).
[28] B. Blank *et al.*, *Phys. Rev. Lett.* **74**, 4611 (1995).
[29] R. Pfaff *et al.*, *Phys. Rev.* **C53**, 1753 (1996).
[30] G. Giambrone *et al.*, *Nucl. Phys.* **A726**, 3 (2003).
[31] D. Vretenar *et al.*, *Nucl. Phys.* **A692**, 496 (2001).
[32] A. Leistenschneider *et al.*, *Phys. Rev. Lett.* **86**, 5442 (2001).
[33] A. Maj *et al.*, *Nucl. Phys.* **A571**, 185 (1994).

Available online at www.sciencedirect.com
SCIENCE DIRECT®
Physics Letters B 622 (2005) 29–34
PHYSICS LETTERS B
www.elsevier.com/locate/physletb

Relativistic Coulomb excitation of neutron-rich ^{54,56,58}Cr: On the pathway of magicity from $N = 40$ to $N = 32$

A. Bürger [a], T.R. Saito [b], H. Grawe [b], H. Hübel [a,*], P. Reiter [c], J. Gerl [b], M. Górska [b], H.J. Wollersheim [b], A. Al-Khatib [a], A. Banu [b], T. Beck [b], F. Becker [b], P. Bednarczyk [b,d], G. Benzoni [e], A. Bracco [e], S. Brambilla [e], P. Bringel [a], F. Camera [e], E. Clément [f], P. Doornenbal [c], H. Geissel [b], A. Görgen [f], J. Gręboszˊ [b,d], G. Hammond [g], M. Hellström [b], M. Honma [h], M. Kavatsyuk [b,i], O. Kavatsyuk [b,i], M. Kmiecik [d], I. Kojouharov [b], W. Korten [f], N. Kurz [b], R. Lozeva [b,j], A. Maj [d], S. Mandal [b], B. Million [e], S. Muralithar [k], A. Neußer [a], F. Nowacki [l], T. Otsuka [m,n], Zs. Podolyák [o], N. Saito [b], A.K. Singh [a,p], H. Weick [b], C. Wheldon [q], O. Wieland [e], M. Winkler [b], RISING Collaboration

[a] *Helmholtz-Institut für Strahlen- und Kernphysik, Universität Bonn, Germany*
[b] *Gesellschaft für Schwerionenforschung (GSI), Darmstadt, Germany*
[c] *Institut für Kernphysik, Universität zu Köln, Germany*
[d] *The Henryk Niewodniczański Institute of Nuclear Physics, PAN, Kraków, Poland*
[e] *Dipartimento di Fisica, Università di Milano, and INFN Sezione di Milano, Italy*
[f] *DAPNIA/SPhN, CEA Saclay, Gif-sur-Yvette, France*
[g] *Department of Physics, Keele University, Keele, UK*
[h] *University of Aizu, Fukushima 965-8580, Japan*
[i] *Taras Shevchenko Kiev National University, Ukraine*
[j] *Faculty of Physics, University of Sofia, Bulgaria*
[k] *Nuclear Science Centre, New Delhi, India*
[l] *IReS, Université Louis Pasteur, Strasbourg, France*
[m] *Department of Physics, University of Tokyo, Japan*
[n] *RIKEN, Hirosawa, Japan*
[o] *Department of Physics, University of Surrey, UK*
[p] *Department of Physics and Meteorology, Indian Institute of Technology Kharagpur, Kharagpur 721302, India*
[q] *SF7, Hahn-Meitner-Institut, Berlin, Germany*

Received 21 March 2005; received in revised form 3 May 2005; accepted 1 July 2005

Available online 13 July 2005

Editor: V. Metag

* Corresponding author.
E-mail address: hubel@iskp.uni-bonn.de (H. Hübel).

0370-2693/$ – see front matter
doi:10.1016/j.physletb.2005.07.004

Abstract

The first excited 2^+ states in ^{54,56,58}Cr were populated by Coulomb excitation at relativistic energies and γ rays were measured using the RISING setup at GSI. For ^{56}Cr and ^{58}Cr the $B(\mathrm{E2}, 2_1^+ \to 0^+)$ values relative to the previously known $B(\mathrm{E2})$ value for ^{54}Cr are determined as 8.7(3.0) and 14.8(4.2) W.u., respectively. The results are consistent with a subshell closure at neutron number $N = 32$ which was already indicated by the higher energy of the 2_1^+ state in ^{56}Cr. Recent large-scale shell model calculations using effective interactions reproduce the trend in the excitation energies, but fail to account for the minimum in the $B(\mathrm{E2})$ values at $N = 32$.

PACS: 27.40.+z; 25.70.De; 23.20.Ck; 21.60.Cs

Keywords: Radioactive beams; Relativistic Coulomb excitation; Transition probabilities; Shell model

Nuclei far off the valley of stability have become more accessible in recent years through the use of radioactive ion beams. The investigation of shell structures of such nuclei is a key topic of nuclear structure studies. It has become evident that shell and subshell closures may differ significantly from those of nuclei near stability, in particular for very neutron-rich nuclei [1]. However, experimental data, needed to test and refine the interactions used in the shell model calculations [2–5], are still scarce. Modifications of the shell structure have far reaching consequences for nuclear properties and also beyond nuclear structure physics, e.g. for the rapid neutron-capture process (r-process) of stellar nucleosynthesis and the resulting isotopic abundances [6].

The experimental evidence of changing shell structures for very neutron-rich nuclei along the $N = 8$, 20 and 28 isotonic sequences can be explained in terms of the monopole part of the nucleon–nucleon (NN) residual interaction. Schematically this is due to the $(\sigma\sigma)(\tau\tau)$ term in the interaction, where σ and τ denote the spin and isospin operators, respectively. This term is strongly binding in the $S = 0$ (spin–flip), $\Delta l = 0$ (spin–orbit partners) and $T = 0$ (proton–neutron) channel of the two-body interaction. It causes large monopole shifts of neutron single-particle orbitals due to their missing $S = 0$ proton partners at large neutron excess and, thus, may generate new shell gaps. The effect was first discussed for the (s, d) shell [2,3] and for the (p, f) shell [1,3]. For heavier nuclei the tensor part of the NN interaction creates a likewise strong monopole interaction between $S = 0$, $\Delta l = 1$ and $T = 0$ orbits of adjacent harmonic oscillator shells [7,8], which plays a key role in the evolution of the spin–orbit splitting. It has recently been shown, that both terms originate from the tensor force which, in a major shell with fixed parity, reduces essentially to the $(\sigma\sigma)(\tau\tau)$ term [8]. To date the investigations concentrate, in the region of neutron-rich Ca, Ni and Sn isotopes, on the most significant matrix elements, the spectroscopic factors and the magnetic moments which are sensitive indicators of their structure.

The neutron-rich Cr isotopes are located at a key point on the pathway from the $N = 40$ subshell closure via a deformed region to spherical nuclei at $N = 28$. Two large-scale shell model calculations have been performed based on different realistic effective interactions with empirically tuned monopoles [9,10]. The results await experimental proof with respect to model space and evolution of subshells and deformation. Experimentally, a possible subshell closure at $N = 32, 34$ seems to develop in the Ca isotopes beyond $N = 28$ as indicated by a rise in the 2_1^+ energies. The Cr and Ti isotopes show a maximum of those energies at $N = 32$ [4,11–14]. However, the Ni isotopes do not show such an effect. Within the $N = 34$ isotones, $E(2_1^+)$ is increasing from Fe to Cr in contrast to the expected trend towards mid-shell, which may suggest an $N = 34$ closure [4]. Besides the 2_1^+ energies, masses and $B(\mathrm{E2})$ values are an important test of the evolution of the subshell structure. A recent determination of $B(\mathrm{E2}, 0^+ \to 2_1^+)$ values in ^{52,54,56}Ti confirms the subshell closure at $N = 32$, but provides no evidence for the predicted $N = 34$ closure [15]. The measurement of $B(\mathrm{E2})$ values for the $N = 32$ and 34 isotopes of Cr, which is the subject of the present investigation, confirms the $N = 32$ subshell closure for $Z = 24$.

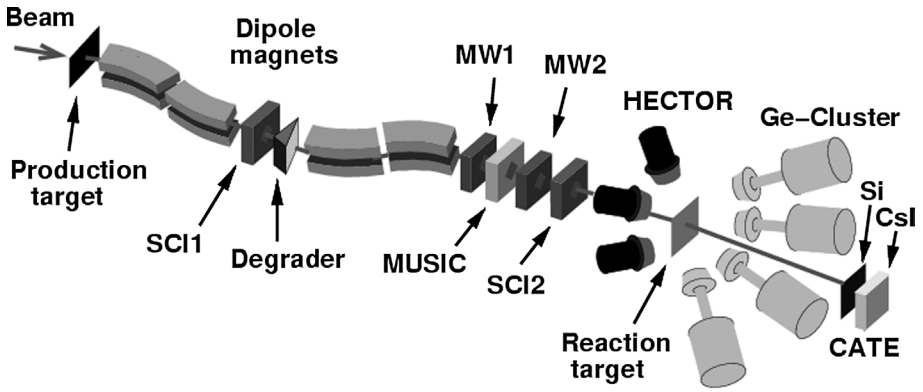

Fig. 1. Schematic illustration of the RISING setup at the fragment separator, FRS, at GSI. The BaF_2 scintillation spectrometers of the HECTOR array were used only in the setup phase. An additional degrader, which was placed between the first two dipole magnets, is not shown.

Table 1
Summary of beam times, beam intensities and compositions for the three experiments

Isotope	Beam time [h]	Intensity [s^{-1}]	^{A}Cr component [%]	Other main comp.
^{54}Cr	22	2000	45	^{55}Mn, ^{53}V
^{56}Cr	20	1400	35	^{57}Mn, ^{55}V
^{58}Cr	55	600	25	^{59}Mn, ^{57}V

Three consecutive experiments were performed to measure Coulomb excitation of high-energy ^{54}Cr, ^{56}Cr and ^{58}Cr beams using the FRS-RISING setup at GSI [16]. The setup is shown schematically in Fig. 1. Fully stripped Cr ions were produced by fragmentation of a ^{86}Kr beam on a ^{9}Be production target with a thickness of 2.5 g/cm^2 placed in front of the fragment separator FRS. The ^{86}Kr beams with energies of around 480 A MeV and an intensity of 3 to 10×10^8 ions per second were provided by the heavy-ion synchrotron SIS. The nuclei of interest were selected in the FRS by their magnetic rigidity, $B\rho$, and their specific energy loss in the degraders, ΔE. The various detectors on the way to the reaction target, see Fig. 1, were used to perform A and Z identification as well as position tracking [16]. Table 1 summarises the beam times and the intensities and compositions of the beams obtained in each of the three experiments.

The energies of the Cr beams were adjusted to around 136 A MeV before the reaction target, a 7×7 cm^2 Au foil of 1 g/cm^2 thickness, in which the ions were slowed down to 100 A MeV in all three experiments. The identification of the nuclei behind the reaction target in Z and A is performed by the array of nine Si and CsI(Tl) detectors of the calorimeter telescope CATE [17]. The Z resolution of CATE is good, but masses of neighbouring isotopes partly overlap.

Gamma rays emitted after Coulomb excitation were measured in the array of 15 Ge-Cluster detectors of the RISING setup [16]. Due to the high recoil velocities of $v/c \approx 0.43$, the Doppler broadening of the γ-ray lines is appreciable. To maintain a good energy resolution, the Ge detectors were placed at forward angles with a small opening angle of 3°. The photopeak efficiency of the Cluster array was 1.13(1)% at 1.33 MeV, measured with a ^{60}Co source. However, the solid angle transformation increases the efficiency to 2.3% for γ rays emitted from the high-energy Cr ions. To reduce background contributions, the Cluster detectors were surrounded at the sides by lead shielding of 6 mm thickness. Thinner Pb absorbers were used in front of the detectors to suppress γ rays with energies below 500 keV in the laboratory frame.

Particle-gamma coincidences were recorded requiring a γ ray in one or more of the Ge detectors, an incoming particle in scintillator SCI2 and an outgoing particle in one of the CsI detectors of CATE. To determine the number of beam particles, events without γ-ray coincidence condition were recorded. In the off-line analysis event-by-event tracking and identification of the incoming ions was performed. For the correction of Doppler shifts of the γ-ray energies, the trajectory of each incoming Cr projectile, the position

of the scattered particle measured in CATE and the position of the Ge crystal detecting a γ ray were used to determine the γ-ray emission angle with respect to the direction of the scattered projectile. The ion velocities after the target were calculated for each event from the time of flight between the two scintillation detectors, SCI1 and SCI2, taking the energy loss in the Au target into account. After Doppler correction, an energy resolution of 2% was obtained. The accepted scattering angles of the Cr fragments were limited to the range of 0.6° to 2.8° to select predominantly Coulomb-excitation events. This range of scattering angles corresponds to impact parameters between 10 fm (below which nuclear reactions prevail) and 50 fm (above which atomic background becomes dominant).

Examples of the γ-ray spectra obtained for the three Cr isotopes are displayed in Fig. 2. They were obtained after event-by-event correction for Doppler shifts and for the efficiencies of the individual Ge detectors. Isotope identification was made before and after the Au target and a prompt time gate was set to reduce the background from γ rays produced at various places along the beam line. The gate widths were varied within reasonable limits. A variation in the number of counts in the resulting spectra was taken into account in the uncertainties. Other peaks in the spectra originate from neighbouring Cr isotopes produced by transfer reactions which cannot be completely separated due to the insufficient mass resolution after the target. However, these contaminations do not influence the results as they represent a negligible fraction of the number of projectiles, N_{pro}, which is the number of projectiles within the scattering-angle range identified as Cr both before and after the target. The other ions, mainly Mn and V, present in the beam do not give rise to contaminations in the spectra since they are well separated from the gates on the Cr ions.

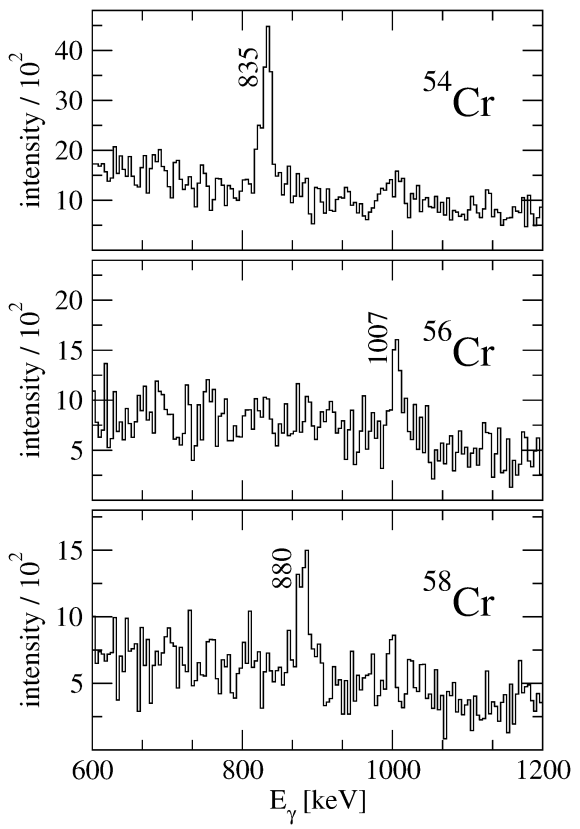

Fig. 2. Examples of Doppler- and efficiency-corrected γ-ray spectra showing the $2_1^+ \rightarrow 0^+$ transitions in ^{54,56,58}Cr.

The γ-ray transition intensities, I_γ, were obtained by integrating over the $2_1^+ \rightarrow 0^+$ peaks in the three spectra and subtracting the background. Angular distribution effects, which should be identical for the three Cr isotopes, were not taken into account. In principle, B(E2) values could be determined from the Coulomb-excitation cross sections for the three isotopes [19,20]. However, to avoid possible systematic errors, e.g. from uncertain parameters in the high-energy Coulomb excitation calculation, from possible excitations of higher-lying 2^+ states (for which we see no evidence in the spectra) or from unknown angular distribution effects, we prefer to give the B(E2) values for ^{56}Cr and ^{58}Cr relative to the previously known value of ^{54}Cr, see Table 2. The B(E2) values

Table 2
Number of projectiles identified as Cr before and after the target (N_{pro}), number of counts in the 2_1^+ peaks (N_γ), γ-ray intensities (I_γ), $B(\mathrm{E2}; 2_1^+ \rightarrow 0^+)$ values and gamma-ray energies (E_γ), for ^{54,56,58}Cr

Isotope	^{54}Cr	^{56}Cr	^{58}Cr
N_{pro} [10^6]	37	18	12
N_γ	501(64)	126(44)	148(43)
I_γ [10^2]	211(27)	61(20)	73(19)
B(E2) [W.u.]	14.6(0.6)[a]	8.7(3.0)	14.8(4.2)
$E(2_1^+)$ [keV]	835[a]	1007[a]	880[b]

[a] From Ref. [18].
[b] From Ref. [4].

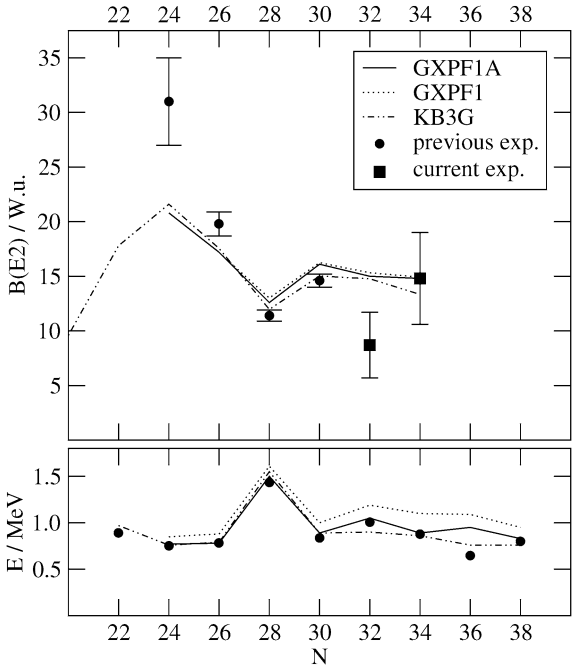

Fig. 3. Calculated (from [8–10]) and experimental energies (from [4,18]), $E(2_1^+)$, and $B(\mathrm{E2}, 2_1^+ \to 0^+)$ values (from [18] and this work) for Cr isotopes.

for ^{56,58}Cr are determined using the relation:

$$B\big(\mathrm{E2}, {}^{A}\mathrm{Cr}\big) = \frac{I_\gamma({}^{A}\mathrm{Cr})/N_{\mathrm{pro}}({}^{A}\mathrm{Cr})}{I_\gamma({}^{54}\mathrm{Cr})/N_{\mathrm{pro}}({}^{54}\mathrm{Cr})} B\big(\mathrm{E2}, {}^{54}\mathrm{Cr}\big).$$

In Fig. 3 the experimental 2_1^+ excitation energies, $E(2_1^+)$, and the $B(\mathrm{E2}, 2_1^+ \to 0^+)$ values for the Cr isotopes are displayed. The B(E2) values show that the collectivity of the 2_1^+ state in ^{56}Cr with $N = 32$ is significantly lower than that of the neighbouring isotopes, ^{54}Cr and ^{58}Cr with $N = 30$ and 34, respectively. In fact, it appears to be similar to that of ^{52}Cr with the $N = 28$ shell closure. The experimental values are compared to results of large-scale shell model calculations using two different approaches. In the calculations the effective NN interactions GXPF1 [9] and KB3G [10], respectively, were used in the (p, f) model space. The B(E2) values were calculated with equal polarisation charges for protons and neutrons, $\delta e = 0.5e$. For $N \geqslant 36$ the $\nu(\mathrm{g}_{9/2}, \mathrm{d}_{5/2})$ orbitals were included in Ref. [10] to account for the onset of deformation expected due to the upward monopole drift of the $\nu\mathrm{f}_{5/2}$ orbital which closes the $N = 40$ gap. However, up to $N = 36$ little effect is predicted as compared to the (p, f) model-space values. The GXPF1 interaction was recently modified (GXPF1A) to better account for the $E(2_1^+)$ energies in Ti and Cr isotopes, but with marginal effect for the B(E2) values (see Fig. 3) [8]. The interactions GXPF1 and KB3G differ mainly in the prediction of an $N = 34$ subshell in ^{54}Ca, which is only produced by GXPF1. The difference can be traced back to the $\nu(\mathrm{p}_{1/2})^2$ $T = 1$, $J = 0$ two-body matrix element which is not related to the tensor interaction. It is strongly binding in GXPF1A [8] and stabilises the $N = 32$ and 34 shell gaps with the $\nu\mathrm{p}_{1/2}$ subshell filled in between. The situation is analogous to the (s, d) shell for $N = 14$, 16 in ^{22,24}O and $Z = 14$, 16 in ^{34}Si, ^{36}S and to the proton (p, f) shell in the $N = 50$ isotones ^{88}Sr, ^{90}Zr at $Z = 38$, 40 [7]. Despite the variations in the $E(2_1^+)$ energies, the B(E2) values are virtually unchanged in both shell model approaches and are almost constant from $N = 30$ to 34 (see Fig. 3). The experimental value for ^{56}Cr clearly lies below the theoretical predictions. The small B(E2) value is evidence for the $N = 32$ subshell closure already indicated by the higher 2_1^+ energy. This result is in agreement with a recent measurement of B(E2) values in ^{52,54,56}Ti [15] which also show a decrease in collectivity for ^{54}Ti with $N = 32$. Further inspection of the shell model results reveals that the effective gap between the $\mathrm{p}_{3/2}$ and $\mathrm{p}_{1/2}$ neutrons stays constant at a value of about 2 MeV for both interactions when going from Ca to Cr, in agreement with the experimental B(E2) trend. The $\mathrm{f}_{5/2}$–$\mathrm{p}_{1/2}$ gap decreases from 3.5 MeV in Ca to 1.5 MeV in Cr for GXPF1A while it disappears for KB3G [8]. This explains the fact that the $N = 34$ gap has not developed in Cr and Ti, which makes Ca the crucial experimental benchmark. It also accounts for the agreement within the two theoretical approaches for Cr and Ti. The experimental trend of the B(E2) values implies that the $\mathrm{p}_{3/2}$–$\mathrm{p}_{1/2}$ gap is larger than predicted while the $\mathrm{f}_{5/2}$–$\mathrm{p}_{1/2}$ gap is smaller than inferred from the GXPF1 interactions. The B(E2) values in the $N = 32$, 34 Cr isotopes must also be seen in the light of a comparison to the shell model values for the Fe and Ni isotopes [10] which show the normal peaking in the $(\mathrm{p}, \mathrm{f}_{5/2})$ mid-shell at $N = 32$–34. A further test of the model predictions would be a study of the heavier Cr isotopes which should show a steep increase in the B(E2) values towards deformation.

Acknowledgements

The authors wish to thank the technical staff at GSI for providing the Cr beams. The work was supported by the German BMBF under grant Nos. 06BN-109, 06OK-167 and by the Polish State Committee for Scientific Research (KBN grant No. 620/E-77/SPB/GSI/P-03/DWM105/2004-2007).

References

[1] H. Grawe, Acta Phys. Pol. B 34 (2003) 2267.
[2] T. Otsuka, et al., Phys. Rev. Lett. 87 (2001) 082502.
[3] T. Otsuka, et al., Eur. Phys. J. A 13 (2002) 69.
[4] J.I. Prisciandaro, et al., Phys. Lett. B 510 (2001) 17.
[5] A.P. Zuker, Phys. Rev. Lett. 90 (2003) 042502.
[6] B. Pfeiffer, et al., Nucl. Phys. A 693 (2001) 282.
[7] H. Grawe, Lecture Notes in Physics, vol. 65, 2004, p. 33.
[8] T. Otsuka, et al., Acta Phys. Pol. B 36 (2005) 1213.
[9] M. Honma, et al., Phys. Rev. C 69 (2004) 034335.
[10] E. Caurier, et al., Eur. Phys. J. A 15 (2002) 145.
[11] R.V.F. Janssens, et al., Phys. Lett. B 546 (2002) 55.
[12] B. Fornal, et al., Phys. Rev. C 70 (2004) 064304.
[13] S.N. Liddick, et al., Phys. Rev. C 70 (2004) 064303.
[14] S.N. Liddick, et al., Phys. Rev. Lett. 92 (2004) 072502.
[15] D.-C. Dinca, et al., Phys. Rev. C 71 (2005) 041302.
[16] H. Wollersheim, et al., Nucl. Instrum. Methods A 537 (2004) 637.
[17] R. Lozeva, et al., Acta Phys. Pol. B 36 (2005) 1245.
[18] ENSDF database, http://www.nndc.bnl.gov/ensdf/.
[19] T. Glasmacher, Nucl. Phys. A 693 (2001) 90.
[20] C. Bertulani, et al., Comput. Phys. Commun. 152 (2003) 317.

Eur. Phys. J. A **25**, s01, 719–722 (2005)
DOI: 10.1140/epjad/i2005-06-170-5

EPJ A direct
electronic only

Status of the RISING project at GSI

F. Becker[1,a], A. Banu[1], T. Beck[1], P. Bednarczyk[1,2], P. Doornenbal[1], H. Geissel[1], J. Gerl[1], M. Górska[1], H. Grawe[1], J. Grebosz[1,2], M. Hellström[1], I. Kojouharov[1], N. Kurz[1], R. Lozeva[1], S. Mandal[1], S. Muralithar[1], W. Prokopowicz[1], N. Saito[1], T.R. Saito[1], H. Schaffner[1], H. Weick[1], C. Wheldon[1], M. Winkler[1], H.J. Wollersheim[1], J. Jolie[3], P. Reiter[3], N. Warr[3], A. Bürger[4], H. Hübel[4], J. Simpson[5], M.A. Bentley[6], G. Hammond[6], G. Benzoni[7], A. Bracco[7], F. Camera[7], B. Million[7], O. Wieland[7], M. Kmiecik[2], A. Maj[2], W. Meczynski[2], J. Styczeń[2], C. Fahlander[8], and D. Rudolph[8]

[1] Gesellschaft für Schwerionenforschung, Planckstr. 1, D-64291 Darmstadt, Germany
[2] IFJ PAN, ul. Radzikowskiego 152, 31-342 Krakow, Poland
[3] Institut für Kernphysik, Universität zu Köln, Zülpicherstr. 77, D-50937 Köln, Germany
[4] Helmholtz-Institut für Strahlen- und Kernphysik, Nußallee 14-16, D-53115 Bonn, Germany
[5] CCLRC Daresbury Laboratory, Daresbury Warrington, Cheshire WA44AD, UK
[6] Department of Physics, Keele University, Keele, Staffordshire ST55BG, UK
[7] INFN, Via G. Celoria, 16, I-20133 Milano, Italy
[8] IRES, B.P. 28, F-67037 Strasbourg Cedex 2, France
[9] Department of Physics, Lund University, Box 118, SE-22100 Lund, Sweden

Received: 14 January 2005 /
Published online: 2 August 2005 –

Abstract. The FRS-RISING set-up at GSI uses secondary radioactive beams at relativistic energies for nuclear structure studies. At GSI the fragmentation or fission of stable primary beams up to ^{238}U provide secondary beams with sufficient intensity to perform γ-ray spectroscopy. The RISING set-up is described and results of the first RISING campaign are presented. New experimental methods at relativistic energies are being investigated. Future experiments focus on state-of-the art nuclear structure physics covering exotic nuclei all over the nuclear chart.

PACS. 25.70.De Coulomb excitation – 25.70.Mn Projectile and target fragmentation – 29.30.-h Spectrometers and spectroscopic techniques – 29.30.Kv X- and γ-ray spectroscopy

1 Introduction

The RISING (Rare ISotope INvestigations at GSI) set-up [1] consists of the fragment separator FRS [2] and a highly efficient γ-ray spectrometer. EUROBALL Ge-Cluster detectors [3] together with BaF_2 detectors from the HECTOR array [4] form the γ-ray array which is placed at the final focus of the FRS. The SIS/FRS facility [2] provides secondary beams of unstable rare isotopes produced via fragmentation reactions or fission of relativistic heavy ions. These unique radioactive beams have sufficient intensity to perform γ-ray spectroscopy measurements. In the first campaign fast beams in the range of 100 to 400 $A \cdot$ MeV were used for relativistic Coulomb excitation and secondary fragmentation experiments.

Coulomb excitation at intermediate energies is a powerful spectroscopic method to study low-spin collective states of exotic nuclei [5]. It takes advantage of the large beam velocities and allows the use of thick secondary targets. Unwanted nuclear contributions to the excitation process are excluded by selecting events with forward scattering angles corresponding to sufficiently large impact parameters. Contrary to Coulomb excitation, fragmentation and nucleon removal reactions at the secondary target are a universal tool to produce exotic nuclei in rather high spin states [1]. Besides being an excellent tool to investigate radioactive fragments up to higher spin states, fragmentation reactions provide a selective trigger, particularly suppressing the strong background of purely atomic interaction events. For the first fast beam campaign the RISING set-up was optimized to the study of the following subjects of exotic nuclei: the shell structure of nuclei around doubly magic ^{56}Ni and ^{100}Sn, the evolution of shell structure towards extreme isospin, the investigation of shapes and shape coexistence in particular around the $N = Z$ line and the mirror symmetry, as well as collective modes and the $E1$ strength distribution in neutron-rich nuclei ($N \gg Z$).

2 Experiments

2.1 Experimental details

The SIS facility at GSI provides primary beams of all stable nuclei up to ^{238}U. For various nuclei a projectile energy up to 1 $A \cdot$ GeV and intensities up to 10^9/s are available. Radioactive beams are produced by projectile fragmentation or fission of ^{238}U. From the exotic fragments

[a] e-mail: F.Becker@gsi.de

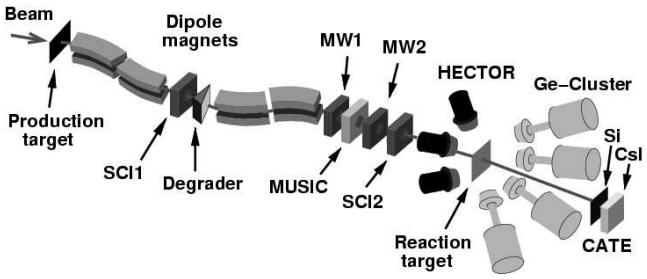

Fig. 1. Schematic sketch of the FRS-RISING set-up. Two multiwire detectors (MW1 and MW2), an ionization chamber (MUSIC), and two scintillator detectors (SCI1 and SCI2) are the beam diagnostic elements for the FRS. γ-rays produced in the reaction target at the final focus of the FRS are measured with BaF_2-HECTOR and Ge-Cluster detectors. The CATE array identifies the outgoing reaction products by mass and charge.

produced, the nuclei of interest are selected by the FRS using the combined $B\rho$-ΔE technique [2]. The RISING set-up at the FRS is shown schematically in fig. 1. For the FRS beam diagnostics, scintillator detectors (SCI), an ionization chamber (MUSIC), and multiwire detectors (MW) are employed to identify the produced ions and select the nucleus of interest. The position-sensitive SCI detectors determine the time-of-flight (TOF) and together with the MWs the position of the beam in the FRS. From the TOF and the flight path length, the velocity of the ion is determined. The MUSIC detector measures the energy loss of the ions and gives the atomic number Z. Together with the ion velocity a particle identification in Z and A/Q is achieved. At the final focal plane of the FRS, a reaction target is placed. In all Coulomb excitation experiments this was a gold target, while for the secondary fragmentation experiment a ^{9}Be target was used. To identify type and track of the particles hitting the secondary target, the two MWs placed upstream were applied. The outgoing particles were identified in charge and mass by the calorimeter telescope CATE [6,7,8], a Si-CsI array. The position-sensitive Si detectors of CATE allow tracking of the outgoing particles required for the scattering angle selection in the Coulomb excitation experiments and for the Doppler correction procedure. In order to perform γ-ray spectroscopy a highly efficient γ-ray array was placed in the view of the reaction target. It consists of EUROBALL Cluster Ge detectors [3] and BaF_2 detectors from the HECTOR array [4]. The Cluster detectors benefit from being placed under forward angles between 15 and 36 degrees, since the Lorentz boost increases the γ-ray efficiency from 1.3% measured with a ^{60}Co source at rest to 2.8% (at 100 $A\cdot$ MeV) for the in-beam studies at relativistic energies. A distance of 70 cm between the Ge detectors and the target is necessary for an energy resolution between 1–3% after Doppler correction.

2.2 Present results

In a commissioning experiment a primary ^{84}Kr beam was used. The aim was to investigate the feasibility of Coulomb excitation measurements under the present conditions. The $2^+ \rightarrow 0^+$ transition in ^{84}Kr was employed to study the impact parameter dependence at relativistic energies. From the γ-array design about 1% energy resolution is expected for a γ-ray emitted from a moving nucleus with $\beta \sim 0.4$ [1]. The commissioning with a primary ^{84}Kr beam confirms the expected energy resolution of $\sim 1.5\%$ for the Doppler-corrected $2^+ \rightarrow 0^+$ transition at 884 keV ($\beta \sim 0.4$).

Relativistic Coulomb excitation measurements with secondary beams were performed to measure for the first time $B(E2)$ values of first excited 2^+ states. Excitation of ^{54,56,58}Cr was chosen in order to investigate the shell structure of nuclei with extreme isospin. The secondary beam was produced by fragmentation of a primary ^{84}Kr beam. In another experiment fragmentation of a primary ^{124}Xe beam produced secondary ^{108,112}Sn beams. The measurement of the electromagnetic $2^+ \rightarrow 0^+$ transition probability in the neutron-deficient nucleus ^{108}Sn gives insight in the nuclear structure towards ^{100}Sn. It is a sensitive test of $E2$ correlations related to core polarization. The known $B(E2)$ value in ^{112}Sn is used for normalization.

Secondary fragmentation was used to study the mirror pair ^{53}Mn/^{53}Ni. The identification of the so far unknown first excited states in ^{53}Ni would provide information on isospin symmetry and Coulomb effects at a large proton excess as well as a rigorous test of the shell model. Secondary beams of ^{55}Ni and ^{55}Co were produced by fragmentation of a primary ^{58}Ni beam. The fragmentation of the secondary beams produced many exotic nuclei, among them the nuclei of interest ^{53}Mn and ^{53}Ni.

Compared to primary beams, secondary beams have a broader momentum distribution. In order to achieve a good energy resolution an accurate vertex reconstruction of incoming and outgoing particles is required. The analysis of the relativistic Coulomb excitation of ^{54}Cr provides an example [9]. The energy resolution of the 834 keV transition in ^{54}Cr could be improved from $\sim 4\%$ to $\sim 2\%$ without and with vertex reconstruction for the Doppler correction procedure, respectively.

Figure 2 shows the γ-ray spectra of ^{54,56,58}Cr. The intensities of the clearly visible $2^+ \rightarrow 0^+$ transitions are a measure of the $B(E2)$ strength which reveals information on the evolution of a possible $N = 32$ sub-shell closure. A detailed publication on the $B(E2)$ values can be found in references [10,11]. The relativistic Coulomb excitation study of ^{108}Sn revealed for the first time the $B(E2)$ value for the $2^+ \rightarrow 0^+$ transition [12].

Concerning the two-step fragmentation of the ^{55}Ni and ^{55}Co secondary beams, the ongoing analysis reveals so far the mirror pair ^{54}Fe and ^{54}Ni, this is presented in fig. 3. The spectra acquired from $\approx 50\%$ of the data show good statistics and complement previous experiments on ^{54}Ni obtained in a recent EUROBALL experiment [13] and intermediate-energy Coulomb excitation studies at NSCL [14]. The resolution of the γ-ray lines in fig. 3 is inferior to that of the γ-ray lines shown in fig. 2 due to the different reaction process. The goal to obtain ^{53}Mn/^{53}Ni with a factor 50–100 lower cross-section could be reachable

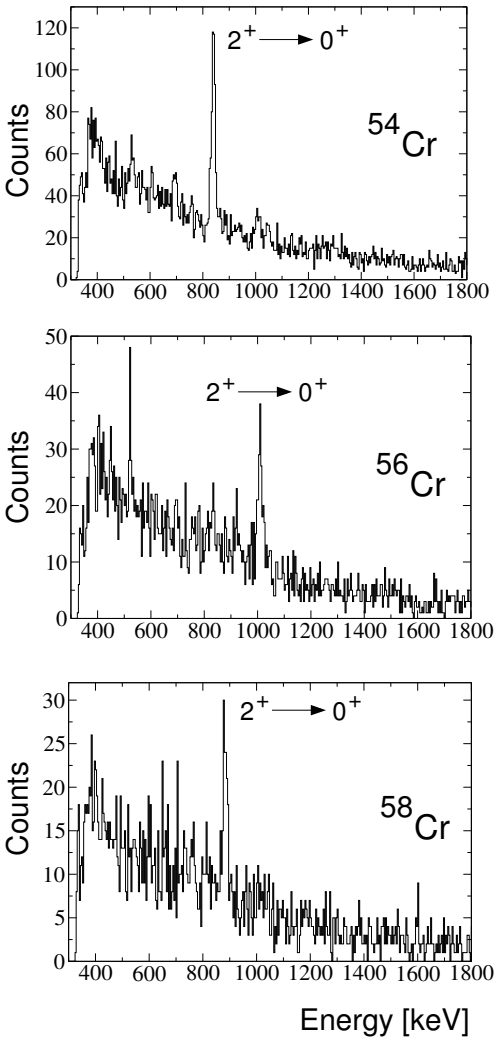

Fig. 2. Relativistic Coulomb excitation: γ-ray spectra of ^{54,56,58}Cr [10,11].

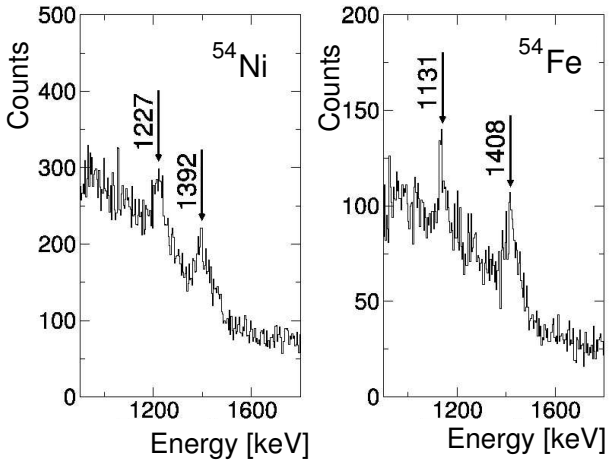

Fig. 3. Exotic nuclei produced by secondary fragmentation reactions: γ-ray spectra were obtained for ^{54}Ni (left) and ^{54}Fe (right) [15].

with an improved analysis using the full statistics, a refined tracking Doppler correction, and in particular an improved mass determination [15].

The mass resolution in the secondary fragmentation reactions is limited by the accuracy of the momentum distribution determination of the projectile fragments. According to the statistical model derived by Goldhaber [16] the mass resolution of fragments at 100 $A \cdot$ MeV amounts to 2–3% (FWHM) without a momentum or time-of-flight measurement. With the actual CATE set-up we could achieve a mass resolution of the 2–3% for fragmentation and 1–2% for Coulomb excitation reaction channels [8].

From recent experiments we have the following online results. The structure of neutron-rich Mg nuclei is being investigated by lifetime measurements. In the chain of the Mg isotopes strong prolate deformations are expected. $B(E2)$ values of excited states deduced from lifetimes will be a measure of the deformation. The experiment takes advantage of the high abundance of nuclei produced via a two-step fragmentation reaction. According to the expected lifetime a stack of three targets has to be arranged at well defined distances. This allows the extraction of the lifetimes of states in the picosecond range by analysing the specific γ-ray line shapes.

The $A \approx 130$ region shows strong evidence for the existence of stable triaxial shapes [17]. This is indicated in this transitional region by the observation of chiral doublet structures in the odd-odd $N = 75$ isotones [18]. $N = 74$ even-even nuclei ^{132}Ba, ^{134}Ce and ^{136}Nd are good candidates since they are cores of the $N = 75$ odd-odd nuclei ^{132}La, ^{134}Pr and ^{136}Pm where chiral doublet bands were observed. Relativistic Coulomb excitation of the even-even nuclei are being performed within the RISING campaign. The measurement of the $B(E2)$ values of the transitions depopulating the 2_1^+ and 2_2^+ states will provide a sensitive test for the results of the Monte Carlo shell model. The calculations predict comparable strengths for the $B(E2)$ values of the $4_1^+ \rightarrow 2_1^+$ and the $2_2^+ \rightarrow 2_1^+$ transitions as a fingerprint of the underlying triaxiality [19].

A technical upgrade is a detector behind the reaction target, an additional CATE ΔE Si detector. Compared to the vertex reconstruction achieved with the MW detectors 3 m upstream of the reaction target, the accuracy of the position determination at the target was improved from 1 cm to 3 mm (FWHM). Measuring twice the ΔE, at the target and at CATE, enhanced the measured Z resolution by a factor 1.4.

3 Perspectives

The differential Doppler shift method applied for the neutron-rich Mg isotopes can also be employed in the light Pb isotopes. The proposed investigation on ^{185,186,187}Pb would probe the scenario of the predicted triple shape coexistence by the experimental determination of the deformation parameters. The lifetime information on the first excited states could again be extracted from the γ-ray line shapes produced in a secondary fragmentation reaction.

The investigation of collective modes in nuclei far from the stability line is still in its infancy. In the neutron-rich nuclei the p-n asymmetry could influence the shell structure. Predictions by theory point to changes in the giant dipole resonance (GDR) strength distribution in exotic neutron-rich nuclei like $^{68-78}$Ni. The GDR is supposed to fragment the strength towards lower excitation energy, the so called Pygmy resonances. The RISING set-up provides besides the Ge-Cluster also BaF_2 detectors. The latter permit the measurement of γ-rays at relatively high energies making it possible to cover the entire dipole response function. The measurement of the γ-ray decay stemming from GDR is a proposed RISING experiment on ^{68}Ni.

Further it is planned to investigate the structure of neutron-rich nuclei with respect to mixed symmetry [20]. IBM-2 calculations predict mixed-symmetry states in the $N = 52$ isotones, *i.e.* non-symmetric states with respect to the p-n degree of freedom. To study the evolution of this structure at $N = 52$ below $Z = 40$ suggests an investigation of the neutron-rich nuclei ^{88}Kr and ^{90}Sr. Relativistic Coulomb excitation experiments could reveal the $B(E2)$ values for the predicted low-lying first and second excited 2^+ states. The 2_2^+ value would be a sensitive test for detailed shell model and IBM-2 calculations and would contribute to understand the evolution of mixed-symmetry configurations [21].

A possible weakening of the spin-orbit splitting resulting in a restoration of the harmonic-oscillator shell closures is predicted by theory for very neutron-rich nuclei [22]. In this scenario the harmonic-oscillator magic numbers would supersede the magic numbers based on the Woods-Saxon potential well known for nuclei close to stability. For the neutron-rich Ni and Sn isotopes the information on the most significant matrix elements, magnetic moments and spectroscopic factors are up to now not available. RISING will contribute revealing these sensitive pieces of nuclear structure information.

An investigation of the nuclear structure in the vicinity of ^{132}Sn is a good testing ground for the evolution of the spin-orbit splitting [23]. For neutron-rich nuclei far from stability this splitting is predicted to decrease or vanish [22]. The RISING set-up offers the opportunity to determine the information on the spin-orbit splitting by the measurement of the spectroscopic factors. It is proposed to measure spectroscopic factors in ^{131}Sn by a neutron removal reaction of a radioactive ^{132}Sn beam produced by fission of ^{238}U.

The structure of the unstable neutron-rich isotopes ^{132,134,136}Te is strongly influenced by the $N = 82$ shell closure and two protons outside the magic $Z = 50$ shell [24]. Measurements of g-factors performed within the RISING project would yield the information on the dominant role of protons or neutrons being involved in the configurations of the first excited states. A comparison with predictions by theory would give the information on the specific components induced by neutron and proton orbitals. The proposed measurement of perturbed γ-ray angular correlations for lifetimes in the picosecond range is at present only feasible by the technique of transient magnetic fields (TF). The future g-factor experiment will employ the relativistic Coulomb excitation of secondary ^{132,134,136}Te beams in combination with the TF technique.

Spectacular is the observation of an anomalous Coulomb energy difference behaviour in the $N = Z$ nucleus ^{70}Br [25]. Coulomb distortion of the nucleon orbitals is indicated (Thomas-Ehrman shift). This effect should increase as the drip line is approached. The RISING proposal on the supposed proton emitting nucleus ^{69}Br would allow the investigation of the heaviest mirror pair ^{69}Br/^{69}Se at the proton drip line. Moreover ^{69}Br plays an important role in the rapid-proton capture (rp) process. The odd-Z isotope ^{69}Br is considered as being a possible termination point in the rp-process when the proton capture lifetime of the ^{68}Se target is longer than competing decays and the proton flux duration. Previous experiments [26,27,28] could not attribute clear evidence for the stability of ^{69}Br due to difficulties of the flight path limit. In the proposed RISING experiment an investigation of the prompt production in a secondary fragmentation reaction would overcome this limitation. At the same time the measurement of the prompt γ-ray decay would give insight into mirror pair properties at the proton drip line.

References

1. H.-J. Wollersheim *et al.*, Nucl. Instrum. Methods A **537**, 637 (2005).
2. H. Geissel *et al.*, Nucl. Instrum. Methods B **70**, 286 (1992).
3. J. Eberth *et al.*, Nucl. Instrum. Methods A **369**, 135 (1996).
4. A. Maj *et al.*, Nucl. Phys. A **571**, 185 (1994).
5. T. Motobayashi *et al.*, Phys. Lett. B **346**, 9 (1995).
6. R. Lozeva *et al.*, Acta Phys. Pol. B **36**, 1245 (2005).
7. R. Lozeva *et al.*, Nucl. Instrum. Methods B **204**, 678 (2003).
8. R. Lozeva *et al.*, submitted to J. Phys. G.
9. P. Bednarczyk *et al.*, Acta Phys. Pol. B **36**, 1235 (2005).
10. A. Bürger *et al.*, Acta Phys. Pol. B **36**, 1249 (2005).
11. A. Bürger *et al.*, to be published in Phys. Lett. B.
12. A. Banu *et al.*, submitted to Phys. Rev. C.
13. A. Gadea *et al.*, LNL Annu. Rep. 2003, INFN (REP) 202/2004, p. 8.
14. K.L. Yurkewicz *et al.*, Phys. Rev. C **70**, 054319 (2004).
15. G. Hammond *et al.*, Acta Phys. Pol. B **36**, 1253 (2005).
16. A. Goldhaber *et al.*, Phys. Lett. B **53**, 306 (1974).
17. C.M. Petrache *et al.*, Phys. Rev. C **61**, 011305(R) (2000).
18. K. Starosta *et al.*, Phys. Rev. Lett. **86**, 971 (2001).
19. T. Otsuka, private communication; T. Saito *et al.*, RISING proposal.
20. N. Pietralla *et al.*, Phys. Rev. C **64**, 031301(R) (2001).
21. A. Lisetskiy *et al.*, Nucl. Phys. A **677**, 100 (2000).
22. J. Dobaczewski *et al.*, Phys. Rev. Lett. **72**, 981 (1994).
23. J.P. Schiffer *et al.*, Phys. Rev. Lett. **92**, 162501 (2004).
24. D.C. Radford *et al.*, Phys. Rev. Lett. **88**, 222501 (2002).
25. G. de Angelis *et al.*, Eur. J. Phys. **12**, 51 (2001).
26. M.F. Mohar *et al.*, Phys. Rev. Lett. **66**, 1571 (1991).
27. B. Blank *et al.*, Phys. Rev. Lett. **74**, 4611 (1995).
28. R. Pfaff *et al.*, Phys. Rev. C **53**, 1753 (1996).

RARE ISOTOPES INVESTIGATIONS AT GSI (RISING) USING RELATIVISTIC ION BEAMS.

J. JOLIE, G. ILIE, P. REITER, A. RICHARD, A. SCHERILLO,
T. STRIEPLING, N. WARR
Institut für Kernphysik, Univerität zu Köln, Zulpicher Str. 77, 50937 Köln, Germany
A. BANU, F. BECKER, P.BEDNARCZYK, P. DOORNENBAL, J. GERL,
H. GRAWE, M. GORSKA, R.GRZYWACZ, I. KOJUHAROV, S. MANDAL,
N. SAITOH, T. SAITOH, H.J. WOLLERSHEIM
GSI-Darmstadt, Germany
S. MALLION, G. NEYENS, K. TURZO, P. VAN DUPPEN, N. VERMEULEN
K.U. Leuven, Belgium
ZS. PODOLYAK, W. GELLETLY, P.H. REGAN, P.M. WALKER,W.N. CATFORD,
Z. LIU, S. WILLIAMS
University of Surrey, UK
A.BLAZHEV, R. LOZEVA, P. DETISTOV, L. ATANASOVA, G. DAMYANOVA
University of Sofia, Bulgaria
D. CORTINA GIL, J. BENLLIURE, T. KURTUKIAN NIETO, E. CASEREJOS
Universidad de Santiago de Compostela, Spain
J.M. DAUGAS, G. BELIER, V. MEOT, O. ROIG
CEA, Bruyères le Chatel, France
G. SIMPSON, I.S. TSEKHANOVICH
ILL Grenoble, France
I.MATEA
CENBG Bordeaux, France
R. SCHWENGNER
IKHP Rossendorf, Germany
M. HASS, B.S. NARA SINGH, S.K. CHAMOLI, G. GOLDRING, I. REGEV,
S. VAINTRAUB
The Weizmann Institute, Israel
D.L. BALABANSKI, G. LO BIANCO, K. GLADNISHKI, A. SALTARELLI, C. PETRACHE
University of Camerino, Italy
G. BENZONI, N. BLASI, A. BRACCO, F. CAMERA, B. MILLION, S. LEONI, O. WIELAND
University of Milano, Italy
A.MAJ, M. KMIECIK, J. GRĘBOSZ, P. BEDNARCZYK, J. STYCZEŃ,
M. LACH, W. MĘCZYŃSKI, K. MAZUREK
IFJ PAN Krakow, Poland
M. PFŰTZNER, A. KORGUL
Warsaw University, Poland
M. IONESCU-BUJOR, A. IORDACHESCU, V. ZAMFIR
NIPNE, Bucharest, Romania
A. JUNGCLAUS

Universidad Autonoma de Madrid, Spain
G. GEORGIEV
ISOLDE-CERN, Switzerland
:D.M. CULLEN, S.J. FREEMAN, A.G. SMITH, R. ORLANDI
Manchester University, U.K
R.M.CLARK
Lawrence Berkeley National Lab USA
M.A.BENTLEY, G. HAMMOND, R.WADSWORTH
University of York, UK
A.BUERGER, H. HÜBEL
University of Bonn, Germany
D. RUDOLPH, C.FAHLANDER
University of Lund, Schweden
J.SIMPSON
CLRC Daresbury, UK
R..D. HERZBERG **,** R.D. PAGE, P. NOLAN
University of Liverpool, UK
T. DAVIDSON, P.WOODS
University of Edinburgh, UK
A.M. BRUCE
University of Brighton, UK
T. FAESTERMANN, R. KRUECKEN
TU-Muenchen, Germany
H. MACH
Uppsala University, Schweden
A. RUBIO, A. ALGORA
IFIC Valencia, Spain

The initial experiments performed using the fast fragmentation beams and the RISING gamma-ray spectrometer are reviewed and their results discussed. Plans for the future campaigns using ions which are slowed down and stopped in a catcher will also be presented, including details of experiments which measure magnetic moments (g-factor) and β decays using an active stopper.

1. Introduction

The study of atomic nuclei and their dynamics at low excitation energy has been performed over several decades using more and more sophisticated experimental techniques. The themes of modern day nuclear structure research are changing. On one hand they are refocusing towards the study of low-spin properties and the associated complete spectroscopy; while on the other, nuclear structure research is now able to manipulate an extremely important degree of freedom, namely the neutron-to-proton ratio, with the advent of the new radioactive beam facilities. Here, not only predictions of present day nuclear models can be tested, but effects due to the underlying neutron-proton degree of freedom can be thoroughly studied. Besides this,

new properties can be revealed, such as the coupling of bound states with the continuum, dilute nuclear matter, clustering and new decay modes. With the availability of Radioactive Ion Beams (RIB), all essential degrees of freedom will become available for experimental manipulation. Such work, however, requires infrastructure that can only be afforded on a supranational scale. That said, the discovery potential is very large and new facilities, such as RIA and the GSI extension FAIR, will be built in the coming decade.

Essential for RIB and stable-beam research is the use of high-performance detector arrays to study properties of stable and exotic nuclei. Large γ-ray spectrometers such as Euroball and Gammasphere were developed for the study of high-spin physics where they have been very successful. Nowadays they are being partly converted towards lower-spin applications. The challenge is that 'low-spin' physicists need the 'high-spin' technology and high-spin physicists need the low-spin methods and theoretical approaches. The most advanced project in this direction concerns the Euroball spectrometer, which was dismantled in 2003 for this specific goal. The 15 Euroball Cluster detectors are now installed at the Fragment Recoil Separator (FRS) of GSI as part of the RISING project [1] for RIB research. It is also worth noting that the other major components of the Euroball spectrometer have been successfuly installed at the RITU spectrometer in Jyvaskyla and within the CLARA array at INFN-Legnaro for use in stable-beam induced experiments.

2. The RISING fast beam campaign.

The first RISING campaign (spokesman P. Reiter) ran from summer 2003 until spring 2005 and was aimed at γ–ray spectroscopy of exotic nuclei moving at relativistic energies. The set-up was conceived in such a way that the gamma-ray detection efficiency was maximized, with the restriction that the energy resolution was at the one percent level for each individual Euroball Cluster segment for recoil velocities of v/c = 0.43. Due to the Lorentz boost this implied a strongly asymmetric setup whereby all detectors were mounted behind the target in three rings around the 16 cm wide beam tube. With this set up, a photopeak efficiency of 2.81% (at 1.33 MeV) and an energy resolution of 1.56% was attained [1]. In part of the fast beam experiments two additional rings holding seven additional MINIBALL triple detectors were added, increasing the photopeak efficiency to 7.3%. In the backward direction, eight BaF_2 detectors from the HECTOR array were mounted. These were used to measure very high energy γ-rays and also provide a very good timing reference. After the target the Calormetric Telescope array CATE was used to identify the scattered particles and breakup products. It consisted of position sensitive ΔE-E detectors constructed from thin Si and

thick CsI(Tl) telescope detectors [2]. To analyze the data each event is tracked and reconstructed. Figure 1 shows a photograph of the complete 'Fast RISING' setup.

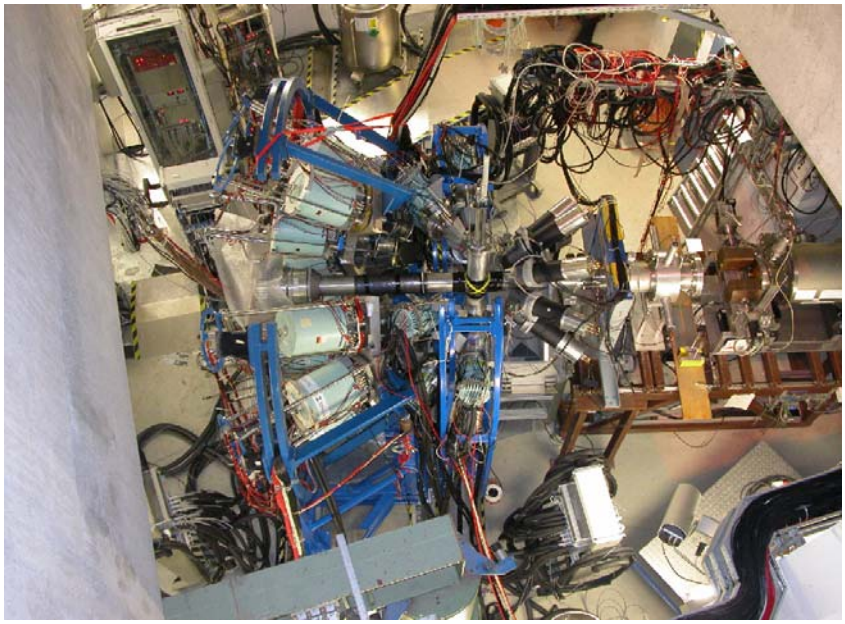

Figure 1: RISING fast beam setup. The beam enters the setup from the right. After hitting the target the ions are detected in the CATE detector. The γ rays are detected using the HECTOR array (right) the MINIBALL detectors (middle) and the EUROBALL Cluster detectors (left).

The first results of the fast campaign are now available. Relativistic Coulomb excitation was used in several experiments in order to extract absolute B(E2) values of the first excited state in a number of unstable nuclei, which provides an independent test of the collectivity of this fundamental excitation. For ^{56}Cr and ^{58}Cr, the results confirm the presence of a subshell closure at N=32, which was already indicated by the anomalous excitation energy of the 2^+ state in ^{56}Cr [3]. The result presents a challenge for large scale shell-model calculations which over predict the B(E2:$2^+ \rightarrow 0^+$) value for this nucleus. In the ^{108}Sn isotope the obtained B(E2:$2^+ \rightarrow 0^+$) value is in agreement with the theoretical calculations [4].

In order to study proton-rich unstable nuclei, two-step fragmentation reactions were used in several experiments. Preliminary results on the T=3/2 mirror nuclei in the A~50 region show the potential of this method [5]. In addition to the first results discussed above, a significant number of other new results are expected following the completion of the complex data analysis

associated with these experiments, including those performed with the addition of the MINIBALL detectors to the RISING array.

3. The g-factor campaign

Static nuclear moments (specifically magnetic dipole and electric quadrupole moments) present critical tests for the nuclear wave functions obtained within theoretical models, since only one state is involved in the calculation of the expectation values of these observables. The magnetic moment, μ, being the product of the nuclear g-factor and the spin I, is a very sensitive probe of the single-particle structure of nuclear states. High-spin isomers in the region of doubly-magic nuclei often have a rather pure single particle configuration, for which the g-factor is a very good observable to determine the valence nucleon configuration. Measurements of nuclear g-factors can also serve as stringent tests of spin and parity assignments [6]. This is particularly true in far-from-stability regions where such assignments are often based on systematics and theoretical predictions.

Starting in the Autumn of 2005, the RISING collaboration will perform a dedicated campaign of g-factor measurements (spokeswoman G. Neyens) using the Time Differential Perturbed Angular Distribution (TDPAD) method. The method of g-factor determination (or a spectroscopic quadrupole moment) for an isomer state is based on measuring the perturbation of the γ–ray anisotropy due to externally applied magnetic (or electric) interactions, following the implantation of the spin-oriented isomeric beam into a suitable stopper (i.e., a crystal or foil). This method has been used extensively over the last couple of decades for measurements of static moments of isomeric states which were produce (and spin-aligned) following in-beam fusion-evaporation reactions [6]. However, in order to investigate isomers with lifetimes in the range of 10^{-7} – 10^{-4} s in neutron-rich nuclei, the projectile fragmentation and projectile fission reactions are the most suitable (and often the *only* available) methods for producing, spin-orienting and selecting the isomers in a fast and efficient way.

To date, only a few TDPAD measurements have been made on isomers produced in fragmentation reactions at intermediate and relativistic energies of the primary beam [7,8,9]. The major difference between these and the former in-beam experiments, is that the isomers are first mass separated in-flight using dipole magnets. During the separation process, the reaction-induced spin-orientation needs to be maintained until the moment of implantation. The hyperfine interaction between the nuclear and random-oriented electron spin can cause a loss of orientation during the flight through vacuum. To avoid this hyperfine interaction, we have two possibilities: either (i) the isomer is produced without electrons (fully stripped fragments), or (ii) the isomeric beam is selected in a noble-gas-like charge state. The high

primary beam energies used in fragmentation reactions mean that most fragments can be produced fully stripped, and therefore such beams have been used until now. In a pioneering experiment, Schmidt-Ott and collaborators demonstrated that considerable alignment (~ 30%) is observed in the ^{43m}Sc isomeric ensemble selected with the FRS at GSI and produced in the fragmentation of a relativistic ^{46}Ti beam (500 MeV/u) [7].

For the planned experiments at the FRS a dedicated magnet system allowing magnetic fields up to about 1.5 T (with a gap of 5 cm between the poles) up to 1.1 T (with a gap of 10 cm) will be used. The γ decays will be detected using 8 Clusters mounted in a close geometry in the horizontal plane (see Figure 2).

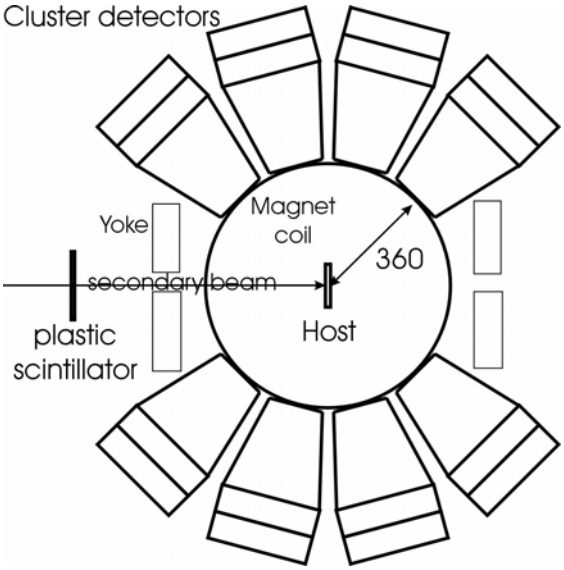

Figure 2: Schematic layout of the TDPAD set-up for measuring isomeric g-factors viewed from above. Detectors are at 36 cm from the stopper, and at relative angles of 60^{o} to each other. The total γ-ray detection efficiency is estimated at 4%.

Experiments with fully stripped fragments were limited up to now to nuclei up to mass number $A_{max} \approx 80$ using intermediate energies as provided at e.g. GANIL, RIKEN and MSU. This is because the probability of picking up electrons increases with Z for a fixed beam energy, while it decreases with the beam energy for a given Z. RISING will address mass $A \approx 100 \rightarrow 200$ nuclei. The proposed experiments can be peformed at present only at GSI, because the energy and charge of the primary beam at other facilities is not

high enough. Furthermore, the fragmentation of a relativistic ^{238}U beam (available only at GSI) offers the unique possibility of studying isomers in neutron-rich nuclei approaching ^{132}Sn. The presence of spin-alignment in fragments produced by a relativistic ^{238}U fission reaction will be demonstrated for the first time as part of the g-RISING campaign.

The proposed g-factor studies focus on nuclei in regions along shell closures (Z=50 and Z=82) and near doubly magic nuclei. Near the Z=50 shell closure, the structure of isomeric states which consist of rather pure particle and/or hole configurations with respect to the doubly-magic proton-rich ^{100}Sn and the doubly-magic neutron rich ^{132}Sn cores will be investigated. Study of the g-factors of isomers in these regions will help to pin down the suggested configurations and spin assignments, as well allowing investigation of the properties of the M1 operator and its suggested quenching at the extremes of isospin between ^{100}Sn and ^{132}Sn.

Nuclei along the Z=82 proton shell closure exhibit a variety of nuclear structures at low excitation energy. In the neutron mid-shell region, a transition from a typical shell model type structure towards more collective states seems to set in. Here the g-factors in this region are investigated to probe the onset of collectivity in the isomeric wave functions.

4. The stopped beam campaign

Following the g-factor measurement the RISING Stopped Beam Campaign (spokesman P. Regan) will start. Here the 15 EUROBALL Cluster detectors will be used to build a compact array around a passive or active stopper. They will be used to measure γ-rays following β-decay to excited states and to measure the direct decay of long lived isomers. For the study of the former process, a position sensitive silicon detector will be used as an active stopper so that the incoming heavy ion can be correlated to its subsequent β-decay. The compact set-up is expected to reach a photopeak efficiency of 11% at 1.33 MeV and 20% at 0.662 keV (see Figure 3). It can be extended with 8 BaF_2 fast scintillators for fast-timing experiments. The FRS will be used in monochromatic mode which allows the stopping of selected isotopes in a 1mm thick Si stopper at the focal plane. This allows a spreading of specific species across a wide area of the focal plane, both increasing the sensitivity of the experiments and allowing longer decay times for subsequent heavy-ion-implantation-β−decay correlation measurements to take place.

The physics aims of the Stopped RISING project are focused on obtaining spectroscopic information on nuclei with highly exotic proton-to-neutron ratios. These include specific studies of (i) isospin and seniority isomers along the N=Z line (specifically ^{54}Ni and N=Z=41→43); (ii) the use

of 'cold fragmentation reactions' to populate rather neutron-rich nuclei and in particular isomeric states arising from the maximal spin coupling of 2-particle (or hole) states in near doubly magic systems 'south' of ^{132}Sn (^{130}Cd) and ^{208}Pb (^{206}Hg, ^{204}Pt); (iii) the investigation of very neutron-rich Zr nuclei approaching the ^{110}Zr harmonic oscillator double shell closure following projectile fission reactions; (iv) and the utilization of K-isomeric states to map out collectivity and axial symmetry around the valence proton-neutron-product (Np.Nn) maximum nucleus ^{170}Dy.

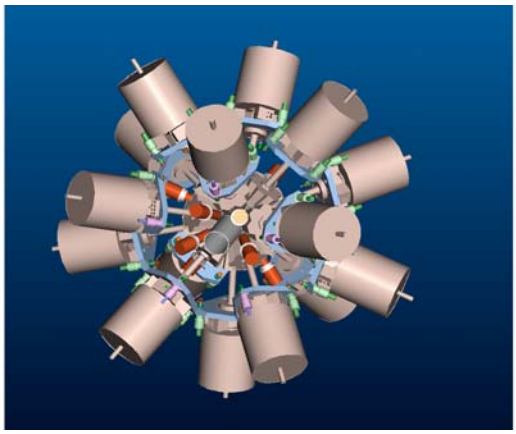

Figure 3. CAD drawing of the Stopped Beam RISING array.

5. Conclusions

The RISING project is aimed at frontier research in nuclear structure physics using relativistic RIB. It therefore has to combine the complicated FRS infrastructure with state-of-the-art γ-ray detectors. Although as expected several technical problems can arise (e.g., atomic background, operation of the FRS in new settings) the project is moving forward and the first experiments are providing new and interesting results and, more importantly perhaps, paving new experimental pathways into the unknown regions of the Segre chart. These experiments will be of vital importance for the future FAIR and RIA facilities. The first results of the fast beam campaign are now available and a new series of experiments using stopped beams will be performed in 2006-7. RISING is a major effort of the European nuclear physics community and has already demonstrated that the traditional low- and high-spin communities can merge and pursue common scientific goals in the future.

Acknowledgments

This work was supported by the BMBF under grant 06K167 and the EPSRC(UK).

References

1. H.J. Wollersheim et al. Nucl. Instr. and Meth. In Phys. Res. A **537** 637 (2005).
2. R. Lozeva et al. Nucl. Instr. and Meth. In Phys. Res. B **204** 678 (2003). R. Lozeva et al. Acta Phys. Pol. B**36** 1249 (2005).
3. A. Buerger et al. Phys. Lett B**622** 29 (2005).
4. A. Banu et al., subm. for publ. to Phys. Rev. C.
5. G. Hammond et al. Acta Physica Polonica B**36** 1249 (2005).
6. G. Neyens, Reports on Progress in Physics **66** 633 (+ 1251) (2003).
7. W.D. Schmidt-Ott et al., Z. Phys. A **350** 215 (1994).
8. G. Georgiev et al., J. Phys. G **28** 2993-3006 (2002).
9. I. Matea et al., Phys. Rev. Lett. **93**, 142503 (2004).

PHYSICAL REVIEW C **72**, 061305(R) (2005)

^{108}Sn studied with intermediate-energy Coulomb excitation

A. Banu,[1,2,*] J. Gerl,[1] C. Fahlander,[3] M. Górska,[1] H. Grawe,[1] T. R. Saito,[1] H.-J. Wollersheim,[1] E. Caurier,[4] T. Engeland,[5] A. Gniady,[4] M. Hjorth-Jensen,[5] F. Nowacki,[4] T. Beck,[1] F. Becker,[1] P. Bednarczyk,[1,6] M. A. Bentley,[7] A. Bürger,[8] F. Cristancho,[3,†] G. de Angelis,[9] Zs. Dombrádi,[10] P. Doornenbal,[1,11] H. Geissel,[1] J. Grębosz,[1,6] G. Hammond,[12,‡] M. Hellström,[1,§] J. Jolie,[11] I. Kojouharov,[1] N. Kurz,[1] R. Lozeva,[1,||] S. Mandal,[1,¶] N. Mărginean,[9] S. Muralithar,[1,**] J. Nyberg,[13] J. Pochodzalla,[2] W. Prokopowicz,[1,6] P. Reiter,[11] D. Rudolph,[3] C. Rusu,[9] N. Saito,[1] H. Schaffner,[1] D. Sohler,[10] H. Weick,[1] C. Wheldon,[1,††] and M. Winkler[1]

[1]*Gesellschaft für Schwerionenforschung (GSI), D-64291 Darmstadt, Germany*
[2]*Institut für Kernphysik, Universität Mainz, D-55099 Mainz, Germany*
[3]*Department of Physics, Lund University, S-22100 Lund, Sweden*
[4]*IReS, F-67037 Strasbourg Cedex 2, France*
[5]*Department of Physics and Center of Mathematics for Applications, University of Oslo, N-0316 Oslo, Norway*
[6]*The Henryk Niewodniczański Institute of Nuclear Physics, PAN, PL-31-342 Kraków, Poland*
[7]*Department of Physics, University of York, Heslington, York YO10 5DD, United Kingdom*
[8]*Helmholtz-Institut für Strahlen- und Kernphysik, Universität Bonn, D-53115 Bonn, Germany*
[9]*INFN Laboratori Nazionali di Legnaro, I-35020 Legnaro, Italy*
[10]*Institute of Nuclear Research of the Hungarian Academy of Sciences, H-4001 Debrecen, Hungary*
[11]*Institut für Kernphysik, Universität zu Köln, D-50937 Köln, Germany*
[12]*Department of Physics, University of Keele, Keele, Staffordshire ST5 5BG, United Kingdom*
[13]*Department of Radiation Sciences, Uppsala University, SE-75121 Uppsala, Sweden*

(Received 3 May 2005; published 29 December 2005)

The unstable neutron-deficient ^{108}Sn isotope has been studied in inverse kinematics by intermediate-energy Coulomb excitation using the RISING/FRS experimental setup at GSI. This is the highest Z nucleus studied so far with this method. Its reduced transition probability $B(E2;0^+_{\text{g.s.}} \rightarrow 2^+_1)$ has been measured for the first time. The extracted $B(E2)$ value of $0.230(57)e^2\,\text{b}^2$ has been determined relative to the known value in the stable ^{112}Sn isotope. The result is discussed in the framework of recent large-scale shell model calculations performed with realistic effective interactions. The roles of particle-hole excitations of the ^{100}Sn core and of the $Z = 50$ shell gap for the $E2$ polarization are investigated.

DOI: 10.1103/PhysRevC.72.061305 PACS number(s): 21.10.−k, 25.70.De, 23.20.Js, 21.60.Cs

The structure of nuclei far from β stability is currently a key topic of research, both experimentally and theoretically. Emphasis is put on phenomena such as shell evolution, proton-neutron interaction, and changes of collective properties. A burning question in nuclear structure physics is whether the shell closures known close to the valley of stability are preserved when approaching the limits of nuclear existence. Toward the proton drip line, because of the confinement of protons by the Coulomb barrier and/or the vicinity of the $N = Z$ line, changes in shell structure as well as collectivity are expected to be driven exclusively by the monopole drift [1–3] of single-particle states and the proton-neutron interaction between identical shell model orbitals [4]. Hence, core polarization studied in spin ($M1$, Gamow-Teller) and shape ($E2$) response, proton-neutron pairing, and isospin symmetry are appealing nuclear structure investigations. In this respect, the heaviest proton bound $N = Z$ doubly magic nucleus ^{100}Sn and its neighbors provide a principle test ground. Information on quadrupole polarization of the magic core can be inferred from the energy of the first excited 2^+ states and their $E2$ transition rates to the ground state. Experimentally, the nuclear properties of ^{100}Sn are only indirectly known [5–7], although its existence has already been confirmed [8,9].

The Sn isotopes between the $N = 50$ and 82 shell closures provide the longest chain of semi-magic nuclei accessible to nuclear structure studies, both in the neutron valence space of a full major shell and with emphasis on excitations of the $Z = 50$ core. The $B(E2;0^+_{\text{g.s.}} \rightarrow 2^+_1)$ value is most sensitive to details of shell structure and $E2$ core polarization. However, the existence of higher lying isomeric states in the tin isotopes hampers a direct measurement of the lifetime of the 2^+_1 states by standard Doppler methods (DSAM, RDM) and the very short lifetimes of the 2^+_1 states are not accessible to electronic timing methods. Therefore, a Coulomb excitation measurement is the only way to obtain this nuclear structure

*Present address: Cyclotron Institute, Texas A & M University, College Station, TX 77843, USA.
†On leave of absence from Universidad Nacional de Colombia, Bogota, Colombia.
‡Present address: Department of Physics, University of York, Heslington, York, UK.
§Present address: Department of Physics, Lund University, Lund, Sweden.
||Present address: Faculty of Physics, University of Sofia, Sofia, Bulgaria.
¶Present address: University of Delhi, New Delhi, India.
**Present address: Nuclear Science Center, New Delhi, India.
††Present address: Hahn-Meitner-Institut Berlin, Berlin, Germany.

information. Until recently only the $B(E2;0^+_{g.s.} \rightarrow 2^+_1)$ values of the stable $^{112-124}$Sn nuclei were measured in sub-barrier Coulomb excitation [10].

In the following, we report on the first intermediate-energy Coulomb excitation experiment performed on the ^{108,112}Sn isotopes using the RISING/FRS setup [11]. A primary beam of ^{124}Xe at 700 MeV/nucleon energy and an average intensity of 6×10^7 s^{-1}, delivered by the SIS accelerator at GSI, impinged on a 4 g/cm^2 ^{9}Be production target located at the entrance of the fragment separator (FRS) [12]. The Sn isotopes were produced via projectile fragmentation. Secondary beams were separated by the FRS operated in achromatic optics mode and identified on an event-by-event basis by coincidence measurements of energy loss in an ionization chamber, magnetic rigidity, and time of flight using two scintillator detectors. The trajectories of the projectiles were tracked with two multiwire proportional chambers. A wedge-shaped aluminium degrader with thickness of 4.59 g/cm^2 and 4.83 g/cm^2 for the ^{108}Sn and ^{112}Sn fragment settings, respectively, was placed at the middle focal plane of the FRS. This allowed an optimized separation of the fragments of interest, amounting in both cases to $\simeq$60% of the secondary beam cocktail. A secondary ^{197}Au target with a thickness of 386 mg/cm^2 was placed at the final focal plane of the fragment separator. The ^{108,112}Sn nuclei impinging on the gold target at 142 MeV/nucleon and 147 MeV/nucleon energies, respectively, were mainly excited by means of electromagnetic interaction. Gamma rays in coincidence with projectile residues were detected by the 15 RISING Ge-Cluster detectors [11,13]. The position-sensitive detector array CATE [14], consisting of 3 × 3 Si-CsI(Tl) modular ΔE-E telescopes, and covering an opening angle of 58 mrad, was placed 1426 mm downstream from the secondary target. It served for the reaction channel selection as well as for the scattering angle determination.

At intermediate energies, a Coulomb excitation measurement is an experimental challenge because of intense atomic background radiation and relativistic Doppler effects. Previously, the method has been applied to nuclei with $Z \leqslant 30$ only. The 15 RISING Ge-Cluster detectors were positioned at forward angles with a small opening angle of 3° (for each single crystal) to maximize the effective solid angle affected by the Lorentz boost, while at the same time minimizing the Doppler broadening. This allowed an energy resolution of 3% to be achieved for projectile residue velocities of $\cong$0.46c. To suppress the atomic background radiation, each Ge-Cluster detector was surrounded on the side by a lead sheet of 2 mm thickness, and its front face was shielded by a combination of Pb, Sn, and Al absorbers of 5 mm thickness. In the analysis, an add-back procedure (applied to all seven crystals within a Ge-Cluster) and a Doppler-shift correction were performed event by event. For technical reasons (see Ref. [15] for details) only five of the RISING Ge-Cluster detectors were suitable for the off-line data analysis. The top panel in Fig. 1 shows the Doppler-corrected energy spectrum of the excited ^{112}Sn, with the γ-ray line of interest at 1257 keV. The bottom panel shows the corresponding spectrum for ^{108}Sn with the γ-ray line at 1206 keV.

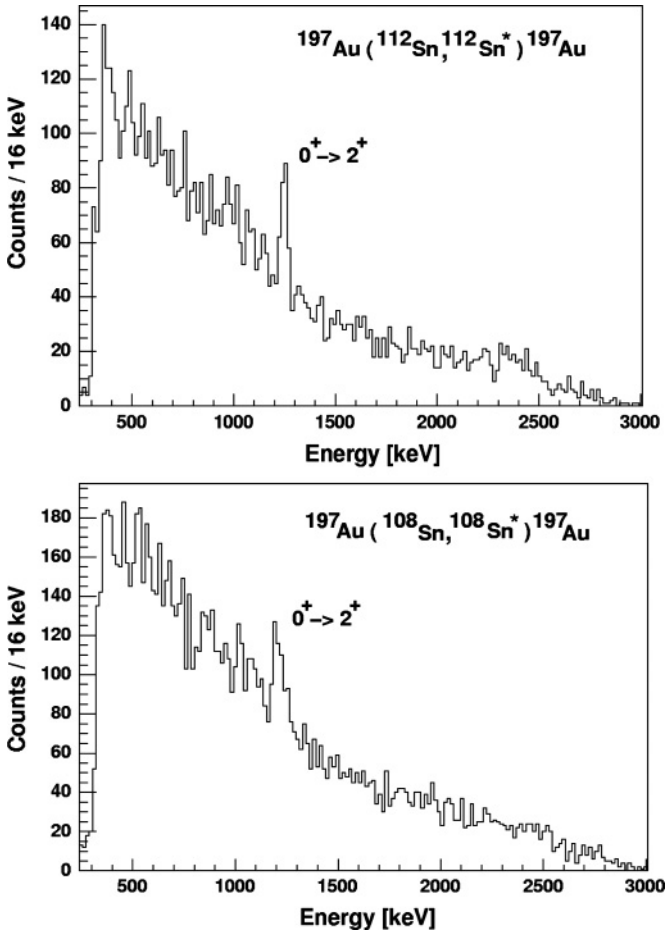

FIG. 1. De-excitation γ-ray lines following $0^+_{g.s.} \rightarrow 2^+_1$ Coulomb excitation of the ^{112,108}Sn projectiles, respectively.

The conditions applied in the data analysis to obtain the spectra in Fig. 1 are the following:

(i) fragment selection before the target with the FRS;
(ii) fragment selection after the target with CATE;
(iii) prompt γ time "window" (26 ns wide) selection;
(iv) Ge-Cluster multiplicity $M_\gamma(E_\gamma \geqslant 500\,\text{keV}) = 1$; and
(v) scattering angle selection between 1° and 2°.

Of the fragments selected in the FRS, about 80% of these events were tagged in CATE with 25% of these corresponding to Coulomb excitation and the rest to fragmentation reaction channels in the target. The intermediate-energy Coulomb excitation reaction is predominantly an *one-step process*, which implies a γ-hit multiplicity equal to one. However, it is possible that the de-excitation event is recorded in coincidence with background radiation originating from either atomic processes in the target or additional fragmentation reactions in the 1-cm-thick CATE-CsI detectors. In our case, owing to a small γ detection efficiency ($\lesssim$1%), only 3% of the recorded events correspond to a Ge-Cluster multiplicity greater than one. For an appropriate Coulomb excitation event selection, it was required in the analysis that the condition of single γ-hit cluster multiplicity is satisfied only for prompt γ rays at energies in

excess of 500 keV (in the laboratory frame), thus excluding nonsuppressed atomic radiation. The requested condition on the scattering angle (calculated in the laboratory frame) between 1° and 2° corresponds approximately to impact parameters in the range 11–22 fm [15]. Below this range one expects nuclear interactions to contribute, whereas above the elastic channel dominates with an increase in the electromagnetic radiation background. Further details on the optimization of the aforementioned conditions may be found in [15].

In spite of the strict data analysis, the spectra in Fig. 1 exhibit significant background even at energies around or above 1000 keV. This background is expected [11] to be manly created by fragmentation of the ^{108}Sn/^{112}Sn nuclei in the thick CATE-CsI detectors. The time resolution of the Ge-Clusters ($\simeq$14ns) is insufficient to disentangle it from γ rays emitted by fragments interacting with the gold target.

From the observation of the Doppler corrected γ line corresponding to the $0^+_{\text{g.s.}} \rightarrow 2^+_1$ transition in ^{108}Sn, the Coulomb excitation cross section can be extracted, which is directly proportional to the $B(E2)$ value [16]. In the analysis, effects such as particle-γ angular correlations, nuclear excitation, or excitations of higher lying 2^+ states (feeding contributions) have to be considered. These data are not available owing to limited statistics. Therefore, we present the experimental result of a relative measurement of the $B(E2; 0^+_{\text{g.s.}} \rightarrow 2^+_1)$ value in ^{108}Sn. The intermediate-energy Coulomb excitation measurement performed on ^{112}Sn with $B(E2; 0^+_{\text{g.s.}} \rightarrow 2^+_1) = 0.240(14)\ e^2\ \text{b}^2$ extracted from a subbarrier Coulomb excitation experiment [10] was used as normalization. This is justified since the two Coulomb excitation experiments were performed under very similar conditions [15]. The unknown feeding pattern is thus canceled out (assuming similar nuclear structure in both ^{108}Sn and ^{112}Sn as supported by theory), as well as the remaining nuclear contribution not removed by the scattering angle condition.

In Table I the experimental parameters needed to calculate the $B(E2)$ value in ^{108}Sn are listed. Additional information on data-taking time and the secondary beam intensity is given for both fragment settings.

The $B(E2; 0^+_{\text{g.s.}} \rightarrow 2^+_1)$ value in ^{108}Sn was determined as follows

$$B(E2\uparrow)_{108} = B(E2\uparrow)_{112} \times \frac{N_\gamma^{108}}{N_\gamma^{112}} \times \frac{N_p^{112}}{N_p^{108}} \times 0.88,$$

yielding $B(E2; 0^+_{\text{g.s.}} \rightarrow 2^+_1)_{108} = 0.230(57)\ e^2\,\text{b}^2$. The value 0.88 corresponds to the ratio of the proportionality factors between the excitation cross section and the reduced transition probability for ^{112}Sn and ^{108}Sn. The proportionality factors were calculated with the standard code DWEIKO [17] used for nuclear scattering at intermediate and high energies ($E_{\text{lab}} \geqslant 50$ MeV/nucleon), taking into account the scattering angle selection applied in the data analysis. Because the 2^+_1 excited states in ^{108,112}Sn lie close in energy, equal γ-ray efficiencies within experimental uncertainties were considered in the $B(E2)$ determination.

TABLE I. Photon yield N_γ, particle flux on target, N_p, data-taking time, and intensity (projectiles per second) for the two ^{108,112}Sn fragment settings.

Isotope	N_γ[a]	N_p[b]	Data-taking time	Intensity
^{108}Sn	174(26)	15×10^7	58 h	2480 Hz
^{112}Sn	106(20)	10×10^7	33 h	2400 Hz

[a]The photon yield was recorded with γ-particle trigger.
[b]The particle flux on target was inferred from down-scaled particle trigger (see Ref. [15]).

In the following, the measured $B(E2\uparrow)$ value in unstable ^{108}Sn is compared to the results of two large-scale shell model (LSSM) calculations. The first set of LSSM calculations was performed for the tin isotopes $^{102-130}$Sn, with a model space for neutrons consisting of the $1d_{5/2}$, $0g_{7/2}$, $1d_{3/2}$, $2s_{1/2}$, and $0h_{11/2}$ orbitals. Two sets of interactions with closed-shell cores ^{100}Sn and ^{132}Sn were considered, following the prescription outlined in Ref. [18] and using the CD-Bonn potential for the bare nucleon-nucleon interaction [19]. In the discussion here we focus however on the results obtained with the ^{100}Sn closed-shell core. A harmonic-oscillator basis was chosen for the single-particle wave functions, with an oscillator energy $\hbar\omega = 8.5$ MeV. The single-particle energies of the chosen model space orbits are $\epsilon_{1d_{5/2}} = 0.00$ MeV, $\epsilon_{0g_{7/2}} = 0.08$ MeV, $\epsilon_{1d_{3/2}} = 1.66$ MeV, $\epsilon_{2s_{1/2}} = 1.55$ MeV, and $\epsilon_{0h_{11/2}} = 3.55$ MeV. The neutron effective charge used in the calculations is $1.0e$. The results of the calculations for the energies of the 2^+_1 excited states and $B(E2; 0^+_{\text{g.s.}} \rightarrow 2^+_1)$ values are presented in columns 3 and 5 of Table II together with the experimental data measured recently for the unstable light isotope ^{108}Sn (this work), the unstable heavy isotopes ^{126,128,130}Sn [20], and the previously measured values for the stable isotopes $^{112-124}$Sn [10].

TABLE II. $I^\pi = 2^+$ energies and $E2$ strengths in $^{102-130}$Sn.

Isotope	$E_{2^+_1}$ [keV]		$B(E2\uparrow)[e^2\,\text{b}^2]$		
	Exp.[a]	SM[b]	Exp.	SM[b]	SM[c]
^{102}Sn	1472.0(2)	1647		0.043	0.044
^{104}Sn	1260.1(3)	1343		0.094	0.090
^{106}Sn	1207.7(5)	1231		0.137	0.125
^{108}Sn	1206.1(1)	1243	0.230(57)[d]	0.171	0.162
^{110}Sn	1211.9(2)	1259		0.192	0.192
^{112}Sn	1256.9(7)	1237	0.240(14)[a]	0.203	0.219
^{114}Sn	1299.9(7)	1208	0.24(5)[a]	0.209	0.235
^{116}Sn	1293.6(8)	1135	0.209(6)[a]	0.210	0.241
^{118}Sn	1229.7(2)	1068	0.209(8)[a]	0.208	0.239
^{120}Sn	1171.3(2)	1044	0.202(4)[a]	0.201	0.228
^{122}Sn	1140.6(3)	1076	0.192(4)[a]	0.184	0.206
^{124}Sn	1131.7(2)	1118	0.166(4)[a]	0.156	0.174
^{126}Sn	1141.2(4)	1214	0.10(3)[e]	0.118	0.134
^{128}Sn	1168.8(4)	1233	0.073(6)[e]	0.079	0.090
^{130}Sn	1121.3(5)	1191	0.023(5)[e]	0.042	0.047

[a]Ref. [10].
[b]LSSM in $\nu(g_{7/2}, d, s, h_{11/2})$ shell model space with ^{100}Sn closed-shell core and $e^\nu_{\text{eff}} = 1.0e$.
[c]LSSM in $\pi(g, d, s)$ and $\nu(g_{7/2}, d, s, h_{11/2})$ shell model space with ^{90}Zr closed-shell core and $e^\nu_{\text{eff}} = 0.5e$ (see text).
[d]This work.
[e]Ref. [20].

The comparison between experiment and theory shows agreement for the heavier Sn isotopes and in the case of ^{108}Sn within the error bars. However, a closer inspection of the light Sn isotopes reveals that part of the systematics seems to exceed the theoretical predictions. In the case of the interaction inferred for a ^{132}Sn core, the experimental $B(E2\uparrow)$ values are reproduced with effective charges between $0.7e$ and $0.8e$ [21]. This indicates a different character of core excitations in the $N = Z$ and $N > Z$ regions of the tin isotopic chain. Moreover, the effective charges for the lighter Sn isotopes show stronger renormalization effects, implying larger core polarization owing to particle-hole (ph) excitations.

To shed more light on the role of core-polarization effects, our second set of large-scale shell model calculations includes protons in the $0g_{9/2}$, $0g_{7/2}$, $1d_{5/2}$, $1d_{3/2}$, and $2s_{1/2}$ single-particle orbits as well, in addition to neutrons in the same model space as in the first set of calculations. The calculations allow up to 4p-4h proton core excitations (our computational limit), and the effective charges are set to the unscreened values $1.5e$ and $0.5e$ for protons and neutrons, respectively. Our closed-shell core is this time ^{90}Zr, and the effective interaction, derived along the same lines as was done previously and with the same nucleon-nucleon interaction, was, however, phenomenologically adjusted to the spectroscopy of Sn isotopes and $N = 82$ isotones; see Ref. [22] for more details. Because in this model space the *m*-scheme dimension [23] would be excessively large, the coupled code NATHAN [23] is used, which allows for a seniority truncation. Convergence was nearly obtained for seniority $v = 8$.

The experimentally observed asymmetry of the $B(E2)$ systematics, supported also by recent preliminary results on ^{110}Sn measured at REX-ISOLDE [24], suggests the importance of studying the role of proton core excitations and the evolution of the $Z = 50$ shell gap. The proton-neutron interaction, in particular the $\pi(0g_{9/2})-\nu(0g_{7/2}1d_{5/2}1d_{3/2}2s_{1/2})$ monopoles, responsible for the evolution of the spectroscopy between ^{91}Zr and ^{101}Sn, governs the evolution of the proton $Z = 50$ gap with the neutron filling. The tuning of the interaction for ^{91}Zr and ^{101}Sn is therefore sufficient to maintain the experimental $Z = 50$ shell gap as extracted from mass measurements. This is reflected in Fig. 2 for the proton effective single particle energies (ESPEs), as defined in Ref. [2], along the tin chain. Note that the ESPEs shown are not identical to the experimentally observed single-particle states that comprise configuration mixing. In particular, Fig. 2 shows the crossing for the ESPEs of the $1d_{5/2}$ and $0g_{7/2}$ orbitals owing to a strong $g_{7/2}-h_{11/2}$ proton-neutron monopole. An equally strong $g_{9/2}-h_{11/2}$ proton-neutron monopole is also needed to maintain a sufficiently closed ^{132}Sn core.

In Fig. 3 the experimental $B(E2)$ values [10,15,20] are compared to LSSM results for an increasing number $t = n$ of proton np-nh excitations. The evolutions of the $B(E2)$ systematics presented here from the pure neutron space to $t = 4$ proton excitations are very instructive: besides reflecting the number of interacting nucleons, the $t = 0$ curve shows a slight asymmetric maximum at $N = 70$, which is shifted to $N = 68$ ($t = 2$) and $N = 66$ ($t = 4$) with increasing number of ph excitations. It should be noticed that for the lightest Sn isotopes the calculations suffer from the strong assumptions

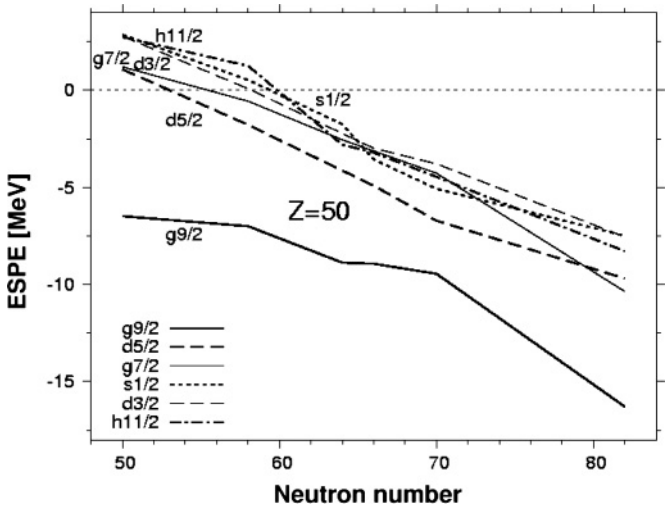

FIG. 2. Calculated evolution of the proton ESPE with the neutron number *N* along the chain of Sn isotopes.

of a $N = 50$ closure; thus the $B(E2)$ values for $^{102-106}$Sn are not fully trustworthy in our valence space. A gain of 15% in the $E2$ strength has been estimated for ^{106}Sn in the *gds* shell model space when both proton and neutron core excitations are allowed. It is also interesting to note that the untruncated 4p-4h proton core excitations ($t = 4gds$), with the corresponding $B(E2)$ values listed in the last column of Table II, show no increase but rather a small decrease in the $B(E2)$ strength for the heavy Sn isotopes in comparison to the $t = 4$ calculations truncated to the $0g_{9/2}$, $0g_{7/2}$, $1d_{5/2}$ orbitals, whereas for the light ones a substantial increase is observed. For the midshell and heavy Sn isotopes the $t = 4$ calculations seem to overestimate the $E2$ strength, which

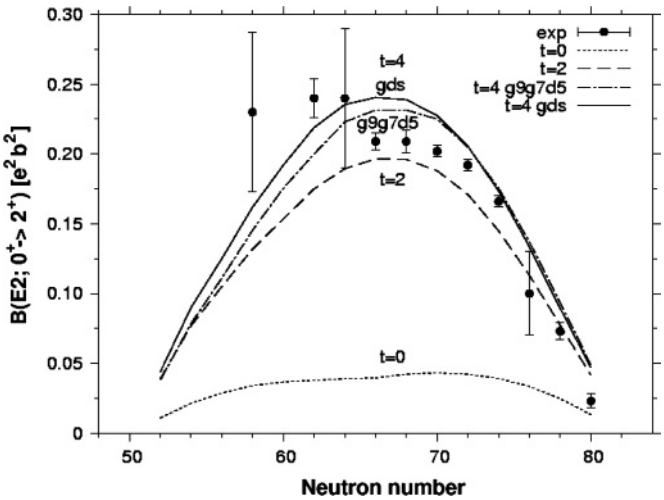

FIG. 3. Comparison of measured $B(E2\uparrow)$ values with LSSM predictions by taking into account ph core excitations. The $t = 0$ curve corresponds to calculations only for the valence neutrons as active particles. The $t = 2$ curve shows the major contribution as given by proton core excitations. The $t = 4$ curves are shown for the whole tin chain in a truncated proton model space and untruncated in the *gds* major shell.

can be ascribed to an ambiguity in the $\pi(0g_{9/2})-\nu(1h_{11/2})$ monopole owing to experimental uncertainties in the $11/2^-$ states of $N = 51$ isotones. A slight increase of the monopole contribution to the interaction would enlarge the $Z = 50$ shell gap in the heavier Sn isotopes and hence reduce the $B(E2)$ values. These calculations demonstrate the important role of core-polarization effects when one breaks the ^{100}Sn core and allows for proton excitations. Starting with the "canonical" neutron effective charge of $0.5e$, one clearly sees how the experimental $B(E2)$ values are reached when one allows for more proton ph excitations. Without these excitations and with neutrons only as degrees of freedom one would need neutron effective charges in the range of $(1-1.5)e$ to explain the experimental data. A more detailed discussion of these calculations will be presented in a forthcoming paper [22].

In conclusion, the $B(E2; 0^+_{\text{g.s.}} \rightarrow 2^+_1)$ value in the unstable ^{108}Sn isotope was measured for the first time by intermediate-energy Coulomb excitation. This is the highest Z nucleus studied with this method. The comparison with two different but complementary large-scale shell model calculations shows reasonable agreement with experiment and gives insight into the microscopic structure of the neutron $E2$ polarization charge. The evolution of proton ESPEs and the $Z = 50$ shell gap with increasing occupation of the $N = 50-82$ major shell governs the $E2$ correlations related to core polarization. The experimentally observed asymmetry can be traced back to enhanced polarization for light Sn isotopes at $t \geqslant 4$ proton ph excitations and/or to neutron core excitations across the $N = 50$ shell gap. The successful $B(E2)$ measurement on ^{108}Sn at GSI opens the research path to study with intermediate-energy Coulomb excitation the lighter Sn isotopes toward ^{100}Sn.

We thank the GSI accelerator staff for their efforts to produce a good-quality primary ^{124}Xe beam and the DVEE division at GSI for their support in data acquisition and Go4 software. This work was supported by the BMBF under Contract Nos. 06MZ176 and 06-K-167.

[1] P. Federman and S. Pittel Phys. Rev. C **20**, 820 (1979).
[2] T. Otsuka *et al*., Phys. Rev. Lett. **87**, 082502 (2001).
[3] H. Grawe, in *The Euroschool Lectures on Physics with Exotic Beams*, Vol. I, Lect. Notes Phys. **651** (Springer, Berlin Heidelberg, 2004), p. 33.
[4] A. Poves and A. P. Zuker, Phys. Rep. **70**, 235 (1981).
[5] M. Lipoglavsek *et al*., Phys. Lett. **B440**, 246 (1998).
[6] M. Górska *et al*., Phys. Rev. C **58**, 108 (1998).
[7] A. Blazhev *et al*., Phys. Rev. C **69**, 64304 (2004).
[8] M. Lewitowicz *et al*., Phys. Lett. **B332**, 20 (1994).
[9] R Schneider *et al*., Z. Phys. A **348**, 241 (1994).
[10] S. Raman, C. W. Nestor, and P. Tikkanen, At. Data Nucl. Data Tables **78**, 1 (2001).
[11] H. J. Wollersheim *et al*., Nucl. Instrum. Methods Phys. Res. A **537**, 637 (2005).
[12] H. Geissel *et al*., Nucl. Instrum. Methods Phys. Res. B **70**, 286 (1992).
[13] J. Simpson, Z. Phys. A **358**, 139 (1997).
[14] R. Lozeva *et al*., Acta Phys. Pol. B **36**, 1245 (2005).
[15] A. Banu, Ph.D. thesis, University of Mainz, 2005; http://archimed.uni-mainz.de
[16] A. Winther and K. Alder, Nucl. Phys. **A319**, 518 (1979).
[17] C. A. Bertulani, C. M. Campbell, and T. Glasmacher, Comput. Phys. Commun. **152**, 317 (2003).
[18] M. Hjorth-Jensen, T. T. S. Kuo, and E. Osnes, Phys. Rep. **261**, 125 (1995).
[19] R. Machleidt, F. Sammarruca, and Y. Song, Phys. Rev. C **53**, 1483(R) (1996).
[20] D. C. Radford *et al*., Nucl. Phys. **A746**, 83c (2004).
[21] A. Holt, T. Engeland, M. Hjorth-Jensen, and E. Osnes, Nucl. Phys. **A634**, 41 (1998).
[22] A. Gniady *et al*. (to be published).
[23] E. Caurier and G. Martínez-Pinedo, Nucl. Phys. **A704**, 60c (2002).
[24] J. Cederkäll *et al*. (to be published).

Available online at www.sciencedirect.com
SCIENCE DIRECT
Nuclear Instruments and Methods in Physics Research A 562 (2006) 298–305
NUCLEAR INSTRUMENTS & METHODS IN PHYSICS RESEARCH Section A
www.elsevier.com/locate/nima

A novel Calorimeter Telescope for identification of relativistic heavy-ion reaction channels

R. Lozeva[a,b,*], J. Gerl[b], M. Górska[b], I. Kojouharov[b], S. Mandal[b,1], H.-J. Wollersheim[b], D. Balabanski[a,c,2], F. Becker[b], J. Gręboszb[,d], A. Banu[b,3], P. Bednarczyk[b,d], P. Doornenbal[b,e], H. Schaffner[b]

[a]*Faculty of Physics, University of Sofia "St. Kl. Ohridski", Dj. Bourchier blvd. 5, 1164-Sofia, Bulgaria*
[b]*Gesellschaft für Schwerionenforschung, Planckstrasse 1, D-64291 Darmstadt, Germany*
[c]*Dipartamento di Fisica, Universitàdi Camerino, Via Madonna delle Carceri str. 9, 62032-Camerino, Italy*
[d]*The Henryk Niewodniczański Institute of Nuclear Physics, Radzikowskiego str. 152, 31342-Krakow, Poland*
[e]*Institut für Kernphysik, Universität zu Köln, Zülpicherstr. 77, D-50937, Cologne, Germany*

Received 4 October 2005; received in revised form 10 February 2006; accepted 19 February 2006
Available online 20 March 2006

Abstract

A novel Calorimeter Telescope (CATE) is employed in the fast beam Rare Isotope Investigations at GSI (RISING) γ-campaign with relativistic energies at the Fragment Separator (FRS) at GSI. CATE consists of nine modular Si−CsI(Tl) detector telescopes for position and $\Delta E - E_{res}$ measurements. It registers the scattering angle and identifies the charge (Z) and the mass (A) of exotic heavy ions produced after secondary fragmentation or Coulomb excitation.

PACS: 29.40.Gx; 29.40.Mc; 29.40.Vj

Keywords: Tracking and position sensitive detectors; Scintillation detectors; Calorimeters

1. Introduction and motivation

The FRS facility [1] at GSI provides a unique opportunity to separate a variety of relativistic heavy-ion beams which are produced at a primary target and transported to a final focus, where a secondary target is located. The FRS allows an isotope separation using the Bρ-ΔE-Bρ technique [1] and an identification using a system of tracking detectors (see Fig. 1) before the secondary reaction target.

At this position the RISING [2] spectrometer is situated, utilizing fifteen of the ex-EUROBALL [3] Ge-Cluster detectors [4]. Within the first, "fast beam" phase, the RISING experiments aimed at γ-ray spectroscopy of secondary isotopes, produced in nucleon knockout and fragmentation reactions or relativistic Coulomb excitation at the secondary target, yielding unique nuclear structure information which cannot be obtained by other techniques.

In order to obtain information about the excited residues, channel selection after the reaction target is needed. Here, the energy loss (ΔE) combined with a residual energy (E_{res}) measurement, known as $\Delta E - E_{res}$ method is favored for identification of the secondary reaction products and to measure their scattering angle (for kinematics reconstruction). Detector systems utilizing this type of energy measurement have shown a large and simple applicability in a wide range of experimental conditions in

*Corresponding author. Faculty of Physics, University of Sofia "St. Kl. Ohridski", Dj. Bourchier blvd. 5, 1164-Sofia, Bulgaria.
E-mail addresses: rady@phys.uni-sofia.bg, r.lozeva@gsi.de (R. Lozeva).
[1]Present address: University of Delhi, University Road, 110007-New Delhi, India.
[2]Present address: Institute of Nuclear Research and Nuclear Energy, Bulgarian Academy of Science, Tzarigradsko chaussee blvd. 72, 1784-Sofia, Bulgaria.
[3]Cyclotron Institute, Texas A&M University, College Station, TX 77843, MS#3366, USA.

0168-9002/$ - see front matter © 2006 Elsevier B.V. All rights reserved.
doi:10.1016/j.nima.2006.02.163

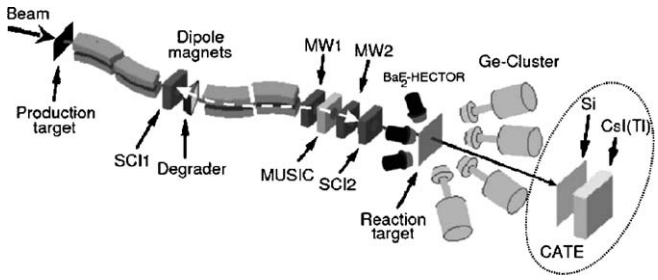

Fig. 1. Schematic layout of the RISING experimental setup for the fast beam campaign. The identification detectors consist of two Multi Wire detectors (MW1 and MW2) for position (x, y) measurement, an Ionization Chamber (MUSIC) for energy loss (respectively Z) measurement and two plastic scintillators (SCI1 and SCI2) for Time-of-Flight, ToF (respectively velocity β) measurement. The identification after the secondary target is performed with the new Calorimeter Telescope CATE.

many laboratories [5–12]. However, a $\Delta E - E_{\mathrm{res}}$ detector system has not been employed for a relativistic heavy-ion identification so far. The present paper reports on a novel calorimeter telescope constructed for this purpose. In order to design such a new system, several investigations have been performed for the selection of particle detectors for ΔE and E_{res} measurements. Based on these experimental studies, a new position sensitive $\Delta E - E_{\mathrm{res}}$ Calorimeter Telescope (CATE) [13] has been built, consisting of a Si and a CsI(Tl) detector arrays.

The position sensitive Si detector array measures the particle's (x, y) position and is used for the reconstruction of the scattering angle after the secondary target. From the energy loss, detected in the Si (ΔE) and CsI(Tl) (E_{res}) detectors, the ion charge Z and mass A are derived, respectively. The CATE detector system has been used within the RISING fast beam campaign for the detection of primary and secondary heavy ions from ^{53}V up to ^{132}Xe in the energy range between 90 and 400 A MeV (at the detectors) with instantaneous rates between 10^2 and 10^4 pps.

2. Calorimeter Telescope—CATE

CATE is a chessboard-like array of nine $\Delta E - E_{\mathrm{res}}$ telescopes. Each of them comprises a position sensitive Si-pin detector and a corresponding CsI(Tl) detector coupled to a photodiode [13]. It is placed 1.4 m downstream from the secondary target (see Fig. 1) in order to have sufficient angular coverage for impact parameter measurements in the relativistic Coulomb excitation reactions. Thus, the opening angles are $\theta \in [-3.2, 3.2]^\circ$ and $\phi \in [-180, 180]^\circ$. Taking into account the solid angle coverage of the detectors in the array (see Fig. 2(a,b)), the efficiency with respect to the incoming particles amounts to 92%.

2.1. CATE-Si array

Two types of Si-pin detectors have been used for the CATE-Si array. These are a Si-IPP type semiconductor (model: $IPP2D50x50 - 300 - SPE$) [14] and a Si-PIPS[4] type semiconductor (model: $PF50x50 - 300EB - L$) [15]. They differ slightly by their thickness, and significantly, by the resistivity of the resistive layer.

Each Si-ΔE counter has a size of $(50 \times 50)\,\mathrm{mm}^2$ and a thickness of 0.30 mm (for the Si-IPP) and 0.32 mm (for the Si-PIPS). A resistive carbon layer with a sheet resistance of $1-2\,\mathrm{k\Omega/cm}^2$ (for the Si-IPP) and $4-5\,\mathrm{k\Omega/cm}^2$ (for the Si-PIPS) serves as a front contact. This layer is used as a charge divider with four contact electrodes at the four corners. By comparing the relative pulse heights, obtained at these four electrodes, the position is calculated (see Section 3). Each corner contact has in addition a resistor of $1-1.5\,\mathrm{k\Omega}$ (for the Si-IPP) and $1.5-1.6\,\mathrm{k\Omega}$ (for the Si-PIPS) to reduce nonlinearities in the position determination as described i.e. in Refs. [16,17]. All detectors are placed in separate frames with size $(54 \times 54)\,\mathrm{mm}^2$ and altogether on a motherboard, as shown in Fig. 2(a,c).

The energy, ΔE, deposited by the incident particle, is measured by the back-side contact and the signal is proportional to the total charge created. From the energy loss in the detector (ΔE), the charge Z of the impinging particle is obtained (see Section 5.1).

An α-test measurement with a ^{241}Am source revealed the intrinsic position resolution $(\Delta x, \Delta y)$ of these detectors. It is better than $(5 \times 5)\,\mathrm{mm}^2$ for the Si-IPP detectors and better than $(3 \times 3)\,\mathrm{mm}^2$ for the Si-PIPS detectors. The intrinsic energy resolution for 5.5 MeV α-particles stopped inside the detector is better than 1.5% (FWHM) for both Si types. In-beam, the intrinsic energy resolution of both Si types, acting as transmission detectors, is found to be about 2.0% (FWHM) with primary ^{86}Kr ions with an energy of 150 A MeV and ^{58}Ni ions with an energy of 120 A MeV.

2.2. CATE-CsI(Tl) array

The CsI(Tl) array (see Fig. 2(d)) is placed about 40 mm behind the Si array in the CATE detector chamber to yield the residual energy, E_{res}, of the fragments. Each CsI(Tl) scintillator (model: $V52P25/18M - E2 - \mathrm{Cs}-X(SSX848)$) [18] has a truncated pyramidal shape (see right-bottom part of Fig. 2(d)) with a base size of $(54 \times 54)\,\mathrm{mm}^2$, a minimal height of 10 mm and a maximal height of 25 mm. In 10 mm thickness all heavy ions with $Z \geqslant 7$ and $A \geqslant 14$ with an energy of $\leqslant 100$ A MeV are fully stopped [19]. For readout a photodiode with size of $(18 \times 18)\,\mathrm{mm}^2$ is attached at the smaller base, together with an integrated appropriate preamplifier [20]. The detectors are covered by 2 μm thick Mylar,[5] to protect the crystal, and to assure good light collection. All detectors are mounted in a very close geometry and separated in front by an Al holder frame, which covers a spacing of 4 mm between each two of them, thus reproducing the geometrical efficiency of the Si array.

[4]PIPS is a Trademark of Canberra.
[5]Mylar is a Trademark of DuPont.

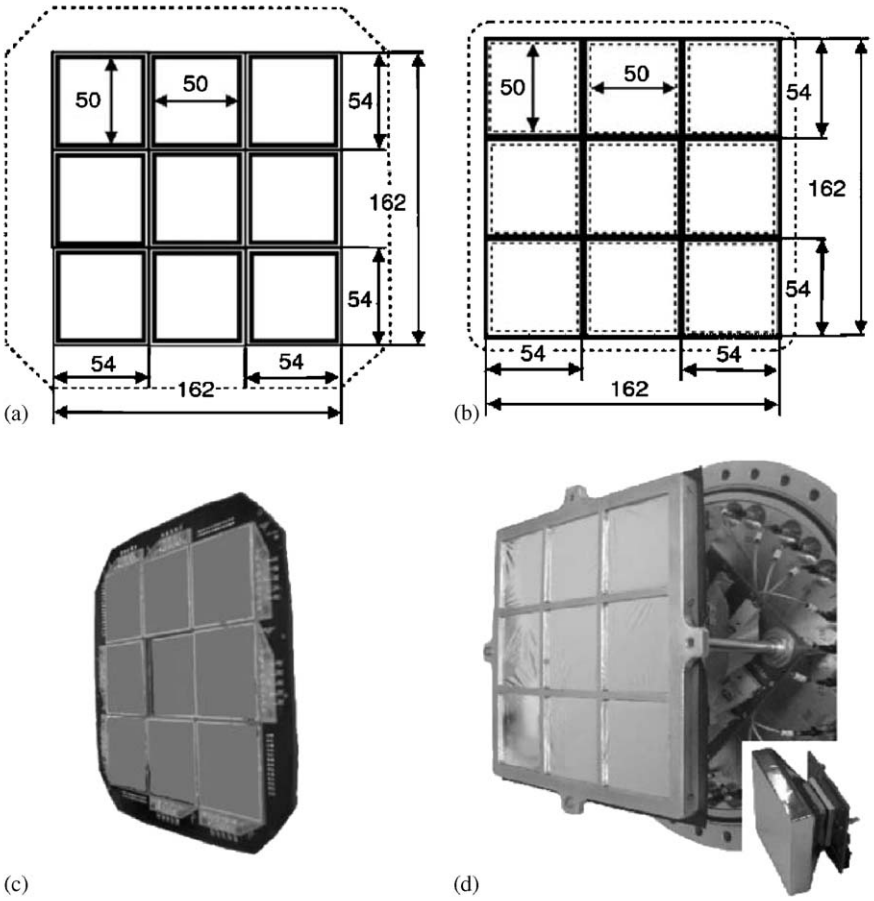

Fig. 2. Schematic representation of (a) the CATE-Si array and (b) the CATE-CsI(Tl) array; a photograph of (c) the CATE-Si array and (d) the CATE-CsI(Tl) array. A single CsI(Tl) detector is shown in the bottom-right corner.

The intrinsic energy resolution of the CsI(Tl) detectors was found to be about 0.7% (FWHM) for both a primary ^{86}Kr beam at an energy of 145 A MeV and for a ^{58}Ni beam at an energy of 113 A MeV.

3. Position sensitivity

The position, determined with the Si detectors gives a measure of the scattering angle of the particles, scattered off the RISING secondary target. The thickness of the secondary target is usually chosen to keep the angular straggling in the order of 10 mrad, corresponding to a position uncertainty at CATE of about 1 cm [2]. This value is not critical, compared to the beam spot size, and still allows suppression of the atomic background by selecting narrow forward angles.

The position in a Si detector is determined using the following algorithm:

$$x = \frac{D_x}{2}\frac{(q_B + q_C) - (q_A + q_D)}{q_A + q_B + q_C + q_D},$$
$$y = \frac{D_y}{2}\frac{(q_C + q_D) - (q_A + q_B)}{q_A + q_B + q_C + q_D} \quad (1)$$

where q_A, q_B, q_C and q_D are the charges collected in the four corners A, B, C and D in Fig. 3(a), respectively. The used geometrical algorithm assumes that the co-ordinate system center is in the center of the active area, whose dimensions are D_x and D_y.

The algorithm is applied for the calculation of the two dimensional position with both Si detector types, and does not depend on the particle type and energy. However, due to the difference in the sheet resistance of the Si-IPP and Si-PIPS detectors, their performance differs as will be illustrated in the next sections.

3.1. Performance of CATE with Si-IPP detectors

The response of the CATE-Si array on ^{58}Ni particles with an energy of about 120 A MeV is shown in Fig. 3(b). As can be seen, the position reconstruction does not follow the real geometrical shape of the detectors and the spacings between them are not as in reality. The existing non-linearity deteriorates the position measurement, and is known as pin cushion effect [16]. This distortion of the position shape [17,21,22] for Si (2D-PSD) [14] detectors strongly depends on the resistivity of the resistive sheet, the

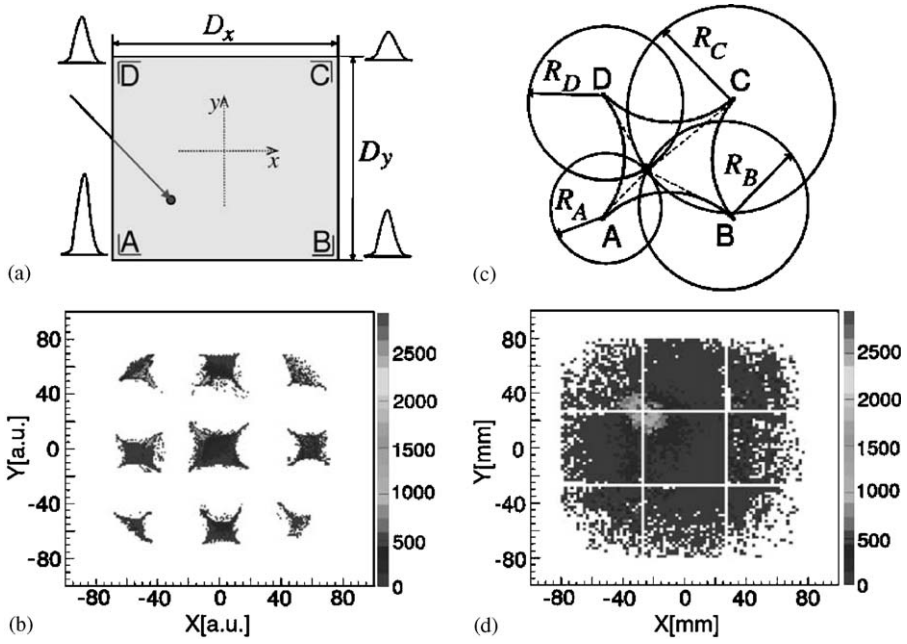

Fig. 3. Position determination (a) with a single Si-IPP detector; (b) initial position spectrum from the whole CATE Si-IPP array for ^{58}Ni particles with 120 A MeV; (c) schematic presentation of the $(1/R + \text{const})$ approximation for the position correction of a single Si-IPP detector; (d) corrected position spectrum of the whole CATE Si-IPP array, using the $(1/R + \text{const})$ approximation.

electrode termination resistors, the filter components of the preamplifier and the shaping time of the amplifier. Well developed correction methods [17,21,22] require knowledge of electronic details and separate current flow measurements not available for these detectors. Therefore, in order to correct the position response, a new linearization procedure has been developed.

3.2. Position corrections with Si-IPP detectors

To perform the position corrections, each detector is treated separately. The initial amplitude distributions of the four position signals (pins) are normalized to the back (sum) contact (A/E, B/E, C/E and D/E) in order to be able to disentangle the noise contributions from small amplitude signals due to interactions at the opposite corner. These new pin values are used for the reconstruction of the (x, y) position, calculated via Eq. (1). To symmetrize the obtained position shape, the normalized pin distributions are calibrated to each other, using a linear function, i.e. for pin A

$$A' = (A/E) \cdot \text{slope}_A + \text{offset}_A. \tag{2}$$

To normalize the symmetrized position shape to the real size of the Si-IPP detector, two new linear functions are constructed, acting in x and y directions

$$x'' = \text{blow}_x \cdot (x' + \text{offset}_x), \quad y'' = \text{blow}_y \cdot (y' + \text{offset}_y). \tag{3}$$

The $\text{blow}_{x,y}$ factors correct for the measured position squeezing and the $\text{offset}_{x,y}$ factors correct for the measured position offset. They are obtained from the projections on the x and y axes.

Further, it is assumed that all particles impinging at the same radial distance from a certain corner produce the same pulse height at that corner. This is valid for all other corners as well, and the position can be approximated with circles, whose four centers are the four corners, as demonstrated in Fig. 3(c). A simulation of the spectral response from a pin shows that the maximum radius ($R_{\max}$) achieved is equal to the size of the detector.

In this way, the position (x, y) becomes a function of the distance to each of the corners $f(R) = 1/(R + \text{const})$, namely

$$x = c_1 \cdot c_2 \times \frac{(1/R_A + c_1) + (1/R_D + c_1)}{(1/R_A + c_1) + (1/R_B + c_1) + (1/R_C + c_1) + (1/R_D + c_1)}$$
$$y = c_1 \cdot c_2 \times \frac{(1/R_B + c_1) + (1/R_C + c_1)}{(1/R_A + c_1) + (1/R_B + c_1) + (1/R_C + c_1) + (1/R_D + c_1)} \tag{4}$$

where $1/R_A$, $1/R_B$, $1/R_C$ and $1/R_D$ are the distances to the corners A, B, C and D, respectively. The values of the two constants c_1 and c_2, utilized in Eq. (4), were determined empirically. The regular intensity distribution of the corrected position matrix leads to an estimated position uncertainty of $\leqslant 2$ mm with this simple approximation.

3.3. Performance of CATE with Si-PIPS detectors

The Si-PIPS type CATE detectors display a linear behavior of the measured position shape as can be seen in Fig. 4(a) for ^{58}Cr ions with an energy of about

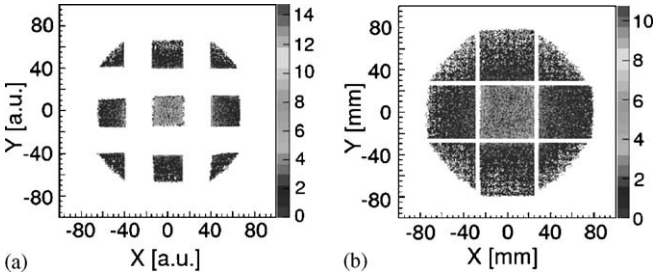

Fig. 4. (a) Raw and (b) corrected position from the CATE-Si PIPS detector array.

120 A MeV. Therefore, they do not need the correction procedure applied for the Si-IPP type. In order to expand the measured shape a simple calibration of the type presented in Eq. (3) is used. The corrected position matrix from the Si-PIPS array is plotted in Fig. 4(b).

4. The energy measurement and corrections

The energies detected in the CATE Si, ΔE, and CsI(Tl), E_{res}, detectors are used for the particle identification. Measured values are influenced by several effects: (i) the particle position, (ii) the beam velocity, (iii) the beam rate, (iv) the thickness of the secondary target, and (v) the reaction mechanism. The first effect is related to the nature of the detectors and their inhomogeneity, while the next two are effects related to the beam. The corrections can be done with well-defined primary beams and the intrinsic energy resolution of the detectors can be determined. The last two effects are typical for secondary beams. The target thickness chosen for an experiment is usually a compromise between the desired luminosity on one hand, and the still acceptable angular and energy straggling, on the other. Knock-out and fragmentation reactions are in addition associated with uncorrectable momentum spread (see Section 5.3). In general, the following corrections are applied:

(i) The effect of the particle impact position is observed as a centroid shift of the energies, determined by the CATE detectors, after applying a position condition to the Si (x, y) position matrix. This matrix is sub-divided into $(3 \times 3)\,\mathrm{mm}^2$ pixels. The correction is then done by aligning the energy for each of the pixels with respect to the central pixel. Thereby, the pixel correction factors are obtained by a calibration run using a primary beam well defined in energy, which is being swept across the active area of the detector.
(ii) The second effect, which is due to the particle momentum, is observed as a correlation between the detected energies with CATE and the velocity β, determined from the ToF, measured between the mid-section and the end of the FRS (see Fig. 1).
(iii) The high beam intensity and its distribution also influences the energy resolutions of the CATE detectors. When the particle rate at the detectors exceeds 10 kHz, an energy shift is observed in their spectral response towards low amplitudes. This effect is more strongly pronounced for the semiconductor detectors compared to the scintillators due to the time constant of their electronics.
(iv) The initial energy spread of the beam, observed by the variation of ToF, is amplified in the subsequent particle detectors and in the target. This effect is caused by the significant energy dependence of the energy loss in matter at around 100 A MeV. It can be corrected for, parametrizing this dependence as a function of β.

5. The particle identification

5.1. Charge (Z) determination

The atomic number, Z, is determined, as $\sqrt{\Delta E} \approx Z$ by measuring the energy loss ΔE in the Si detectors of CATE. It is approximated to be equal to the ion charge, q, at relativistic energies [1].

In all in-beam studies, the detector response revealed a unique Z identification. A typical example from secondary reactions of ^{55}Ni on a ^{9}Be target at 100 A MeV is depicted in Fig. 5(a). After a linearization, which is done by geometrical rotation around the main spot in the distribution and a calibration to the known incoming Z, the extracted resolution is $\Delta Z \approx 0.7$ (FWHM) (for $Z \in [18, 28]$). The typical spectrum in Z units can be seen in the insert of the figure.

Another example for the heavier system ^{112}Sn on ^{197}Au (see Fig. 5(b)), confirms the Z identification with resolution of $\Delta Z \approx 0.8$ (FWHM) (for $Z \in [30, 50]$). Thus, we conclude that the mean Z resolution from the out-coming particle cocktail is sufficient for the charge identification after the secondary target.

5.2. Mass (A) determination

The mass A of an impinging ion with a total energy, E_{tot}, can be determined using the relation $E_{\mathrm{tot}} \approx A \cdot \beta_A^2$. This holds if a constant velocity $\beta_A = \mathrm{const}$ for all ions is assumed. Combining the energy loss in the Si detectors, ΔE, with the energy, deposited in the CsI(Tl), E_{res}, the total energy of the ions $E_{\mathrm{tot}} = \Delta E + E_{\mathrm{res}}$ is obtained. After an error propagation, using the intrinsic energy resolutions of the CATE detectors the mass resolution $\Delta A/A$ is expected to be $\leqslant 1\%$. To achieve this value in the experimental data from secondary reactions corrections for all possible effects, described in Section 4, need to be done.

5.2.1. Coulomb excitation at the secondary target

The energy spread detected in CATE depends (i) on the straggling effects in the isotope production, the straggling

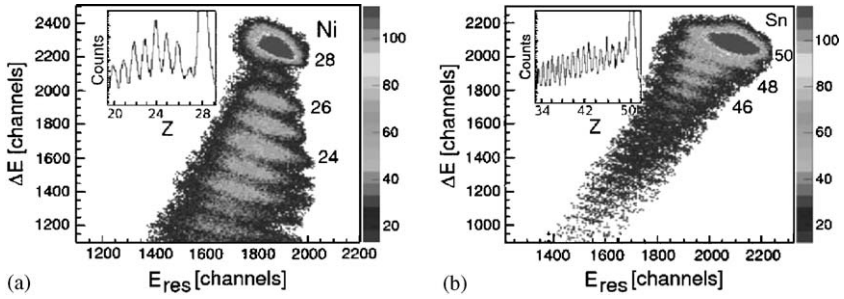

Fig. 5. $\Delta E - E_{res}$ identification by CATE for the products from the reactions (a) ^{55}Ni on ^{9}Be target and (b) ^{112}Sn on ^{197}Au target. Spectra in Z units are shown in the inserts.

in the FRS tracking detectors, the straggling in the secondary target and the intrinsic resolution of the CATE detectors themselves; and (ii) on the isotope cocktail produced by neutron knock-out/fragmentation in the secondary target. In relativistic Coulomb excitation reactions, CATE is used to detect the same outgoing particles which impinge on the secondary target. Therefore, the incoming ions of interest are selected with the FRS identification detectors and no absolute energy calibration needs to be performed for the CATE detectors.

The mass resolution can be determined from the particle singles or from particle-γ events with very small scattering angles corresponding to atomic interactions because only the above mentioned "type (i)" effects are relevant. A typical reaction at an energy of about 170 A MeV is the system ^{53}V, ^{54}Cr and ^{55}Mn on ^{197}Au target. The $\Delta E - E_{res}$ identification with CATE is similar to the one depicted in Fig. 5(b). To obtain the mass resolution in this case, a geometrical linearization by rotation of the distribution around the main spot is performed. After a Z selection from the linearized $\Delta E - E_{res}$ distribution the deposited residual energy, E_{res}, is projected. The "mass" spectra with particle-γ coincidence condition for the three isotopes ^{53}V (top), ^{54}Cr (middle) and ^{55}Mn (bottom) are plotted in Fig. 6 with solid line. The nuclear reaction channels form in this case a wide distribution. Selecting a particle trigger condition pronounces the secondary beam-like residues, as depicted in Fig. 6 with dashed line. The mass resolution of CATE corresponds then to the width of these Coulomb excitation channels which is determined to be between 2 and 3% (FWHM).

5.2.2. Fragmentation reactions at the secondary target

In secondary fragmentation reaction (i.e. of ^{55}Ni particles as shown on Fig. 5(a)) CATE is used to identify each isotope produced in the secondary (^{9}Be) target to select the associated γ-ray spectrum. Therefore, an absolute calibration of the CATE detectors is performed using primary beam with well-defined energy and a small spot size.

5.2.3. Linearization procedure

To linearize the $\Delta E - E_{res}$ distribution, following the formalism of Bethe [23], the power law method [24,25] is

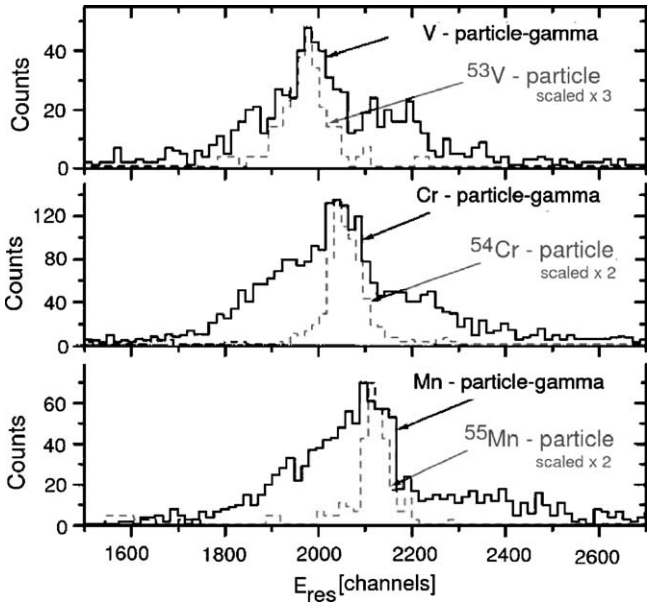

Fig. 6. Mass spectrum for the ^{53}V (top), ^{54}Cr (middle) and ^{55}Mn (bottom) isotopes with solid line for particle-gamma condition and with dashed line for particle singles.

used. Its modifications and applicability [26–28] have been limited by the approximations made to the actual energy loss of the particles involved. Recently, a new method to treat the response of a $\Delta E - E$ telescope for charge, Z, and mass, A, identification has been developed by Tassan-Got [29] for the INDRA detector array [11]. With the help of energy functionals, an interpolation or extrapolation into regions with low statistics is allowed and have shown a good accuracy for relativistic particles, in comparison to identification functionals used in the past [24,26,28]. Therefore, these functionals have been preferred for the linearization of the CATE detector energies (ΔE and E_{res}).

The mass A of the particles is calculated

$$A = \left[\frac{(\Delta E + E)^{\mu+1} - (g \cdot E)^{\mu+1}}{\lambda^{\mu+1} Z^2}\right]^{1/\mu} \quad (5)$$

where the parameter g is the electronic gain ratio which in this case is the ratio between the slope coefficients from the energy calibration of the Si and the CsI(Tl)

detectors: $g = a_{\Delta E}/a_{E_{res}}$; the parameter μ takes a typical value for the Bethe approximation of 0.7 [26,27]; the parameter λ is taken to be the absolute value of the ratio between the offsets from the energy calibration of the Si and the CsI(Tl) detectors respectively: $\lambda = |b_{\Delta E}/b_E|$.

The corresponding calculation of the mass difference ΔM is

$$\Delta M = E^p_{\text{tot}} - E^p_{\text{res}} \quad (6)$$

where the optimal parameter p for this specific data set is found to be 1.71.

A new function for the particle identification, PI_{dynamic}, is constructed, including the Z dependence of ΔM. The last is calculated for the observed charges $19 \leqslant Z \leqslant 28$ and fitted with a second order polynomial. In this way the particle identification function is calculated using

$$PI_{\text{dynamic}} = (Z(\Delta M) + w \cdot A - 2 \cdot Z(\Delta M))/k \quad (7)$$

where the optimal value of the parameter w is found to be $w = 0.4$ and k is a scaling coefficient. The identification of the different particles in terms of Z and A is then given by the correlation of the particle identification, PI_{dynamic}, as a function of the total energy, E_{tot}, deposited in the CATE detectors. The mass analysis is performed by selecting one of the parallel Z distributions from PI_{dynamic} and projecting it onto the total energy axis.

5.3. Mass resolution and comparison with simulations

One of the available ion-optical Monte Carlo simulation programs LISE [30] allows not only the calculation of the transmitted ions trough the FRS and its particle detectors but also precise energy loss calculations and realistic distributions. A comparison between a simulation using the LISE code [30] (see Fig. 7(a)) and the experimental data (see Fig. 7(b)) for the reaction ^{55}Ni on ^{9}Be target, demonstrates a good agreement. First review on this subject has been published in Ref. [31]. Contrary to the good charge identification, unique mass identification is not achieved. This is mainly caused by the reaction mechanism, leading to a broad momentum distribution which can not be corrected as the other effects described in Section 4. It has been explained by Goldhaber [32] as particle momentum widening due to the abrasion of nucleons, which leads a spread of the momentum or, respectively, the velocity of the final fragment. Therefore, the assumption of constant velocity for all secondary ion species does not hold. Consequently, without a time-of-flight measurement after the secondary target, the possible mass resolution is typically 2–3% (FWHM) at energies of about 100 A MeV.

A theoretical calculation of the single mass distributions, using the LISE code [30] was performed in order to compare and identify the experimental E_{tot} distribution, after an absolute energy calibration and linearization (see Section 5.2.3) [31]. As an illustration, the E_{tot} spectrum for $Z = 24$ isotopes is presented on Fig. 8(a) with multiple fit and deconvolution to single distributions (with reduced $\chi^2 \leqslant 15$; $\chi^2 = \chi^2/n$, where n is the number of degrees of freedom). The identification is performed by comparison of the energy centroids with the simulated single mass distributions. The experimental mass resolution is about 2–3% (FWHM).

5.4. Reaction channel selection by CATE

In Fig. 8(a) mass distributions for ^{49}Cr and ^{50}Cr are marked. In order to construct a particle-γ correlation, the particle-γ angle is calculated from particle angle after the secondary target, measured by CATE, and the γ-ray angle defined by the Ge detectors. This angle is used for the Doppler correction, applied to the measured, calibrated energy of all Ge detectors. The velocity of each isotope after the secondary target is calculated from the measured ToF and the energy losses in the experimental set-up. This velocity is normalized to the velocity, for each particular isotope, deduced after corrections from the total energy measured by the CATE detectors. Here these are the energy centroids of the mass distributions for ^{49}Cr and ^{50}Cr isotopes. The γ-spectra corresponding to these isotopes are obtained using particle tracking before and after the secondary target, from the calibrated and Doppler corrected Ge detector energies. Typically, additional conditions are applied to the time and multiplicity spectra of the Ge detectors. The channel selection by a CATE telescope is performed by selection of a single charge, Z, from the $PI_{\text{dynamic}}(E_{\text{tot}})$ identification and a single mass, A, from the projection to the E_{tot} axis (as demonstrated in the

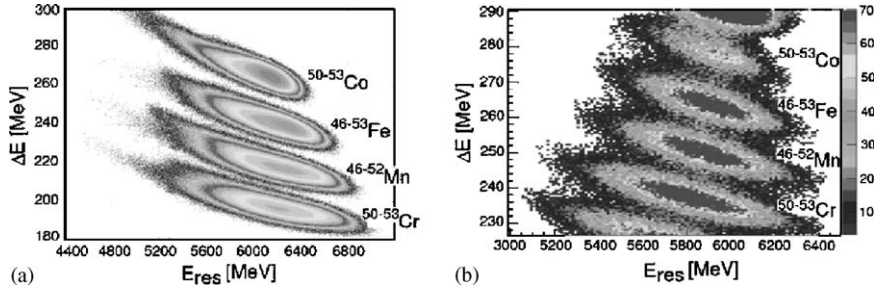

Fig. 7. Comparison between (a) a simulation and (b) the experimental data for the reaction ^{55}Ni on ^{9}Be target.

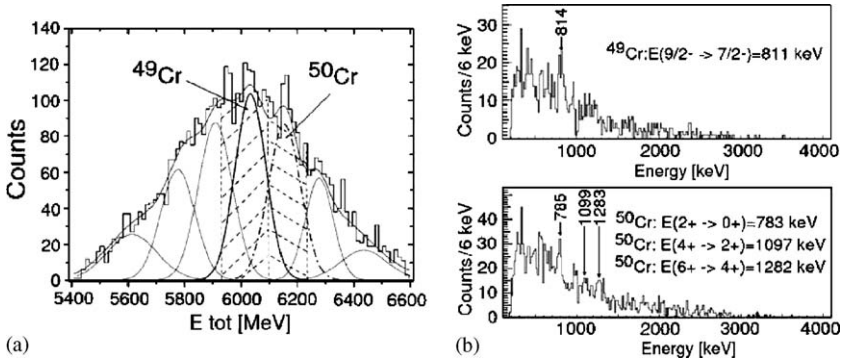

Fig. 8. Measured (a) total energy spectrum (E_{tot}) for the ^{49}Cr (thick solid line) and ^{50}Cr (dash-dotted line) isotopes, produced in the reaction ^{55}Ni on ^{9}Be target. Measured (b) γ-spectra for the ^{49}Cr (top) and ^{50}Cr (bottom) isotopes [33].

figure). This is done because, as explained in Section 5.2.3, the $PI_{\mathrm{dynamic}}(E_{\mathrm{tot}})$ distribution is constructed so that it corresponds to the identification $Z(A)$. The observed γ-lines for ^{49}Cr are shown in Fig. 8(b) (top) and for ^{50}Cr in Fig. 8(b) (bottom). The observed γ-rays correspond to known transitions in these nuclei [33]. Their energies are indicated in Fig. 8(b). These lines can not be seen when applying only Z selection from CATE, which proves the importance of both Z and A identification after the RISING secondary target. The unidentified lines in the spectra originate from higher excited states and from remaining background in the Ge detectors.

6. Summary

With the newly developed $\Delta E - E_{\mathrm{res}}$ telescope, CATE, charge and mass identification of relativistic heavy ions at energies $\geqslant 100$ A MeV can be performed. The system has a good position resolution $(\Delta x, \Delta y) \approx (3 \times 3)\,\mathrm{mm}^2$ for scattering angle reconstruction, a unique charge resolution ΔZ of 0.7 (FWHM) (for $Z \in [18, 28]$) and 0.8 (FWHM) (for $Z \in [30, 50]$) and a mass resolution of 1–3% (FWHM), limited by the target thickness for Coulomb excitation events, and 2–3% (FWHM) for fragmentation channels, further limited by the momentum broadening in the reaction. With an additional time-of-flight measurement of the outgoing particles the mass resolution for fragments could be improved to about 1% (FWHM).

References

[1] H. Geissel, et al., Nucl. Instr. and Meth. B 70 (1992) 286 ⟨www-wnt.gsi.de/frs/index.asp⟩.
[2] H.-J. Wollersheim, et al., Nucl. Instr. and Meth. A 537 (2005) 637 ⟨www-aix.gsi.de/~wolle/EB_at_GSI/rising.html⟩.
[3] J. Simpson, et al., Z. Phys. A 358 (1997) 139.
[4] J. Eberth, et al., Nucl. Instr. and Meth. A 369 (1996) 135.
[5] G. Marcazzan, et al., Nuovo Cimento 10 (1958) 155.
[6] D. Brayant, et al., IRE Trans. Nucl. Sci. NS-9 (3) (1962) 376.
[7] W. Wilcke, et al., Nucl. Instr. and Meth. 188 (1981) 293.
[8] S. Aiello, et al., Nucl. Phys. A 583 (1995) 461.
[9] F. Gramegna, et al., Nucl. Phys. A 389 (1997) 474.
[10] M. Simon, et al., Nucl. Instr. and Meth. A 452 (2000) 205.
[11] M. Parlog, etal., Nucl. Instr. and Meth. A 482 (2002) 674 and 693.
[12] S. Nageswara Rao, et al., Nucl. Instr. and Meth. B 111 (2003) 1.
[13] R. Lozeva, et al., Nucl. Instr. and Meth. B 204 (2003) 678.
[14] User's Manual for Si IPP-IPP 2D detectors, Eurisys Measures, 2001.
[15] PIPS Specification and performance sheet, Canberra Semiconductor Industries, 2004, ⟨www.canberra.com⟩, ⟨www.canberraeurisys.com⟩.
[16] T. Doke, et al., Nucl. Instr. and Meth. A 261 (1987) 605, and the references therein.
[17] R. Cowin, et al., Nucl. Instr. and Meth. A 399 (1997) 365.
[18] Scionix Co., 2004, ⟨www.scionix.nl⟩, ⟨www.scionixusa.com⟩.
[19] C. Scheidenberger, H. Geissel, Nucl. Instr. and Meth. B 135 (1998) 25 ⟨www-aix.gsi.de/~weick/atima/⟩.
[20] A. Pullia, et al., IEEE Trans. Nucl. Sci. NS-48 (3) (2001) 530.
[21] T. Yagimachi, et al., Nucl. Instr. and Meth. A 275 (1989) 307.
[22] M. Bruno, et al., Nucl. Instr. and Meth. A 311 (1992) 189.
[23] H. Bethe, Rev. Mod. Phys. 9 (1937) 69.
[24] F. Goulding, et al., Nucl. Instr. and Meth. 34 (1964) 1.
[25] F. Goulding, D. Landis, IEEE Trans. Nucl. Sci. NS-13 (1966) 514.
[26] G. Butler, et al., Nucl. Instr. and Meth. 89 (1970) 189.
[27] F. Goulding, B. Harvey, Ann. Rev. Nucl. Sci. 25 (1975) 167.
[28] T. Shimoda, et al., Nucl. Instr. and Meth. 165 (1970) 261.
[29] L. Tassan-Got, Nucl. Instr. and Meth. B 194 (2002) 503.
[30] O. Tarasov, D. Basin, Nucl Instr. and Meth. B 204 (2003) 174 ⟨dnr080.jinr.ru/lise⟩, ⟨groups.nscl.msu.edu/lise⟩.
[31] R. Lozeva, et al., Acta Phys. Pol. B 36 (2005) 1245.
[32] A. Goldhaber, et al., Phys. Lett B 53 (1974) 306.
[33] ENSDF database ⟨www.nndc.bnl.gov⟩.

International Journal of Modern Physics E
Vol. 15, No. 7 (2006) 1495–1503

World Scientific
www.worldscientific.com

SHELL STRUCTURE, COLLECTIVITY AND NUCLEAR SHAPES — RISING IN-BEAM EXPERIMENTS AT RELATIVISTIC ENERGIES

PIETER DOORNENBAL for the RISING Collaboration

Institut für Kernphysik, Universität zu Köln,
Zülpicher Straße 77, Köln, 50937, Germany
p.doornenbal@gsi.de

Received 1 October 2006

The RISING fast beam campaign aims at high resolution γ-ray spectroscopy experiments with relativistic radioactive beams at GSI. The secondary beams produced by fragmentation or fission are used for Coulomb excitation or secondary fragmentation experiments to perform studies of nuclei far off stability. The physics phenomena studied with this method include nuclear structure experiments targeting at the evolution of shell structure toward the drip lines, mirror symmetry, collectivity and electromagnetic transition strengths. Example results of this fast beam campaign are presented and compared to various shell model calculations and nuclear structure models.

1. Introduction

The RISING (Rare ISotope INvestigations at GSI) setup for in-beam experiments at relativistic energies consists of the fragment separator FRS and a highly e - cient -detector array at the nal focus of the FRS, composed of EUROBALL Ge-Cluster detectors, MINIBALL Ge-detectors and BaF_2 detectors from the HECTOR array.[1–4] The investigated nuclei are produced via fragmentation reactions or ssion of relativistic heavy ions. In the in-beam campaign fast beams in the range of 100 to 300 A MeV were used for Coulomb Excitation and two-step fragmentation experiments.

The following topics were covered in the nuclear structure experiments performed within the RISING fast beam campaign:

(i) shell structure and its modi cations in nuclei far o stability,
(ii) isospin symmetry along the $N = Z$ line,
(iii) shapes and shape coexistence,
(iv) collective modes and $E1$ strength distributions.

1.1. *Monopole driven shell structure*

The monopole part of the residual interaction controls the propagation of single particle energies with increasing occupation of a major shell.[5] It causes the change in shell structure for very neutron-rich nuclei along the $N = 8, 20$ and 28 isotonic sequences, which is due to the $(\sigma\sigma)(\tau\tau)$ term of the residual interaction, where σ and τ indicate the spin and isospin operators. This term is strongly binding for proton-neutron, spin- ip and spin-orbit partners and leads to a change of harmonic oscillator shell closures with magic numbers $N_m = 8, 20$ to $N_m - 2 \times N = 6, 16(14)$, N being the harmonic oscillator main quantum number.[6,7] For the weak $N = 40$ harmonic oscillator case it should nd its continuation in a $N = 32, 34$ subshell closure.[7] The monopole driven shell evolution far o stability is expected to be of isospin symmetric nature, which may be studied in $N = 20$ isotones and their $Z = 20$ mirror nuclei.

The RISING experiment gives access to excitation energies $E_{2_1^+}$ of $I^\pi = 2_1^+$ states and $B(E2; 2_1^+ \rightarrow 0^+)$ values and can be used as signatures for shell structure. Two type of experiments were performed: First, a Coulomb excitation experiment of the neutron rich ^{54,56,58}Cr, which are located at a key point on the pathway from the $N = 40$ subshell closure across a deformed region to spherical nuclei at $N = 28$, second, a two step fragmentation experiment to investigate the mirror energy di erence, de ned as $\Delta E_M = E_x(I, T_z = -T) - E_x(I, T_z = +T)$, between ^{36}Ca and ^{36}S.

1.2. *Deformed nuclear shapes between closed shells*

The A 130 region shows evidence of stable triaxial shapes.[8] There are also some indications in this transitional region for chiral doublet structures in odd-odd $N = 75$ isotones.[9] The $N = 74$ even-even nuclei ^{132}Ba, ^{134}Ce and ^{136}Nd are the core nuclei of ^{132}La, ^{134}Pr and ^{136}Pm and therefore the collective properties of these nuclei are of great interest and good candidates to search for signs of triaxial deformation. Relativistic Coulomb excitation experiments where performed in ^{134}Ce and ^{136}Nd.

2. Experimental Details

The SIS facility at GSI provides primary beams of all stable nuclei up to ^{238}U with a projectile energy up to 1 A GeV and intensities up to 10^9/s are available. These beams are incident upon a ^{9}Be target at the entrance of the FRS. The fragments of interest are selected with the B -ΔE-B method by placing a wedge-shaped aluminum degrader at the middle focal plane of the FRS, optimizing the secondary beam at the nal focus. The particles are identi ed in- ight on an event-by-event basis using their magnetic rigidity B , their time of ight between the two scintillation detectors SCI1 and SCI2, see Fig. 1, and their energy loss in the multi sampling ionization chamber MUSIC.

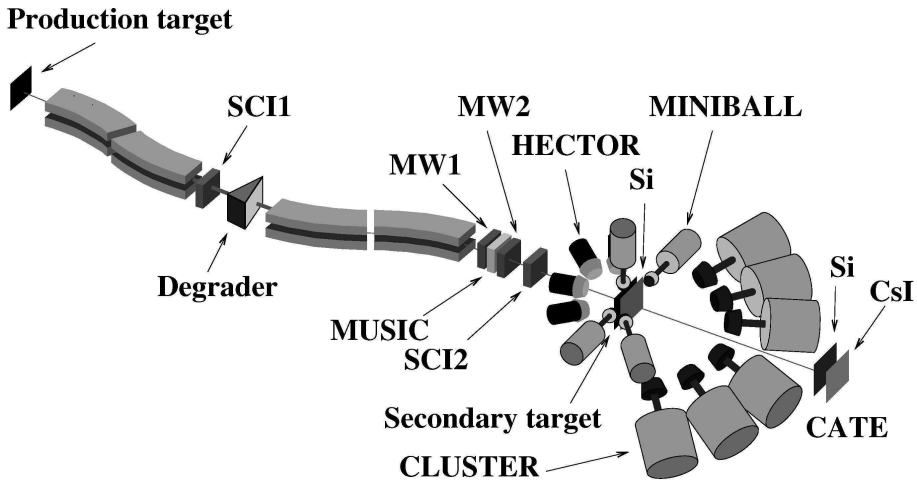

Fig. 1. Schematic layout of the RISING setup at the FRS. See text for details.

At the nal focus of the FRS, a reaction target is placed. For Coulomb excitation experiments a ^{197}Au target of 0.4 to 2.0 g/cm^2 thickness is used, while two step fragmentation experiments are carried out with a 0.7 g/cm^2 ^{9}Be target. The reaction products are selected using the calorimeter telescope array CATE, consisting of 3×3 Si-CsI(Tl) modular ΔE-E telescopes 1400 mm downstream of the target.[10] The energy loss in the Si detectors provides a good charge resolution for unambiguous Z identi cation after the secondary target. Due to the parallel momentum distribution in fragmentation processes, the total energy measurement of the fragments is insu cient to completely distinguish masses. The position sensitive CATE Si detectors and a single equal type Si detector placed directly after the target serve as tracking detectors for a proper Doppler correction. In the case of Coulomb excitation, unwanted nuclear contributions can be excluded by selecting scattering angles corresponding to su ciently large impact parameters for which the multiwire detectors MW1 and MW2 upstream the target are needed.

In order to measure -rays emitted by excited states, the target area is surrounded by numerous detectors:

(i) 15 Cluster Ge-detectors, positioned in three rings at extreme forward angles,
(ii) seven six-fold segmented MINIBALL triple Ge-detectors, arranged in two rings with central angles of 45° and 85°,
(iii) the HECTOR array, consisting of eight large volume BaF_2 detectors, situated at angles of 85° and 142°.

The fragmentation technique at relativistic beam energies allows for in-beam spectroscopy of -unstable nuclei far from stability with very thick targets, partially counterbalancing the low beam intensities. However, the beam slows down in the secondary target, which consequently causes a velocity distribution of the projectile

at the time of photon emission, depending on the target thickness and the lifetime of the excited state. Accordingly, the spread in secondary beam velocity and the opening angle of the -detectors e ect the -ray energy resolution after Doppler-correction.[1]

3. Mirror Symmetry in $A = 36$, $T = 2$ Nuclei

The new $N, Z = 14(16)$ shell stabilization and the $N = 20$ shell quenching in $^{32}\mathrm{Mg}_{20}$ are expected to be dominated by the monopole part of the two-body interaction. Moreover, the scenario is anticipated to be symmetric with respect to the isospin projection T_z and may not or little e ected by neutron binding energy di erences.[6,7] The ideal site in the Segre chart where this can be veri ed is the $N = 20$ mirror region along the light Ca ($Z = 20$) isotopes. The lightest Ca isotope with detailed spectroscopy is ^{38}Ca, while no excited states are known for the $N = 16$ isotope, thus the mirror nucleus of the doubly magic ^{36}S is of high interest.

Recently, the Coulomb energy di erence of isobaric analog states and especially the mirror energy di erence in $T_z = \pm T$ pairs of nuclei have been extensively studied.[11,12] In connection with precise large-scale shell model calculations they have proved to be a sensitive spectroscopic probe to investigate orbital radii in excited states and reduced overlap of identical proton and neutron orbitals at the driplines.[13] Experimental information can be deduced from the ΔE_M measurement between ^{36}Ca and ^{36}S.

The two step fragmentation technique of a stable ^{40}Ca and an intermediate ^{37}Ca beam was used to populate excited states in ^{36}Ca. In Fig. 2 Doppler corrected -ray spectra of ^{36}Ca are shown for the MINIBALL, Cluster and HECTOR detectors. The energy of the $2_1^+ \rightarrow 0^+$ transition has been determined to be 3015(16) keV from the two Ge-detector arrays, resulting in $\Delta E_M = -276(16)$ keV for the $A = 36$, $T = 2$ mirror pair. Surprisingly, this new value is signi cantly larger than mirror energy di erences observed in the *sd* shell for $T = 1$ states and predominantly single-j $T = 1$ valence states in the *pf* shell.[14] Other known $T = 2$ mirrors in the *sd* shell, $A = 24$ and 32, also exhibit much smaller mirror energy di erences of $-102(11)$ keV and $-117(12)$ keV, respectively.[15,16] A comparable mirror energy di erence can be found in the *p* shell for the $A = 14$, $T = 1$ nuclei with $\Delta E_M = -422(10)$ keV for their $2_1^+ \rightarrow 0^+$ transition.[14] Though in general the $T = 2$ mirror energy di erences are larger than the $T = 1$ values, which may be due to the proton-rich partner lying closer to the dripline, the unique $A = 36$ and $A = 14$ cases are obvious.

In a rst systematic attempt based on the isospin symmetric interaction USD, mirror energy di erences in the *sd* shell were calculated for astrophysical application to the *rp*-process, but do not reproduce the experimental value of the $A = 36$, $T = 2$ mirror pair by a large margin.[17,18] In a preliminary approach we have used the experimental single particle energies from the $A = 17$, $T = 1/2$ mirrors and applied on a modi ed USD interaction.[19] Monopole corrections were applied to reproduce the $Z, N = 14, 16$ shell gaps, the $I^\pi = 2_1^+$ excitation energies and the

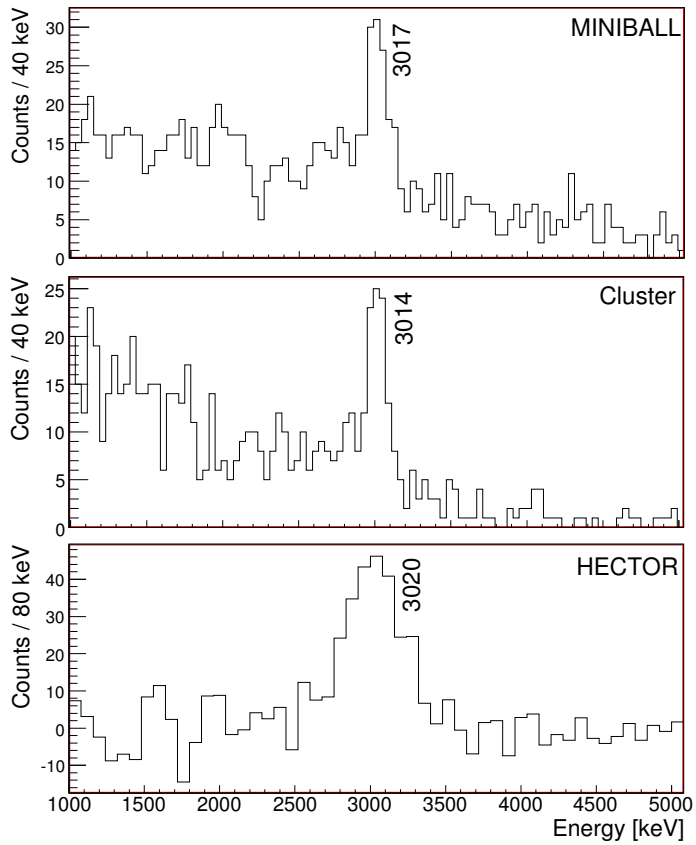

Fig. 2. Doppler corrected ^{36}Ca gated γ-ray spectra measured with the MINIBALL, Cluster and HECTOR detectors. For the HECTOR array the background was subtracted.

Table 1. Comparison of shell model calculation with experimental values for ^{36}Ca and ^{36}S.

	$E_{2_1^+}$ [keV]		π-gap [MeV]		ν-gap [MeV]	
Nucleus	Exp.[a]	SM[b]	Exp.	SM	Exp.	SM
^{36}Ca	3015(16)[c]	3290	4.55(30)		4.16(9)	3.999
^{36}S	3290.9(3)	3558	4.524(2)[d]	4.244	5.585	

[a]From Ref. 14.
[b]Shell model calculation, see text for details.
[c]This work.
[d]Coulomb Corrected.

^{40}Ca single hole energies. The results are shown in Table 1 for ^{36}Ca and ^{36}S and yield a value of $\Delta E_M = -268$ keV, in agreement with the experimental result. Isospin symmetry is preserved in the interaction two-body matrix elements but not in the single particle energies used, indicating that the experimental single

particle energies account empirically for the one-body part of Thomas-Ehrman and/or Coulomb e ects.[20,21]

4. The Subshell Closure at $N = 32, 34$ — Coulomb Excitation of ^{54,56,58}Cr

The neutron-rich Cr isotopes are located at a key point on the pathway from the $N = 40$ subshell closure via a deformed region to spherical nuclei at $N = 28$. Experimentally, possible subshell closures may develop at $N = 32, 34$ in neutron rich Ca isotopes as indicated by a rise in the 2_1^+ energy of ^{52}Ca.[22] The Ti and Cr isotopes exhibit a maximum of those energies at $N = 32$, while the Ni isotopes show constant values.[14,23,24]

Besides the 2_1^+ energies, $B(E2; 2_1^+ \rightarrow 0^+)$ values provide crucial information to test the evolution of subshell structures. Three experiments were performed to measure the Coulomb excitation of ^{54}Cr, ^{56}Cr and ^{58}Cr, where the known

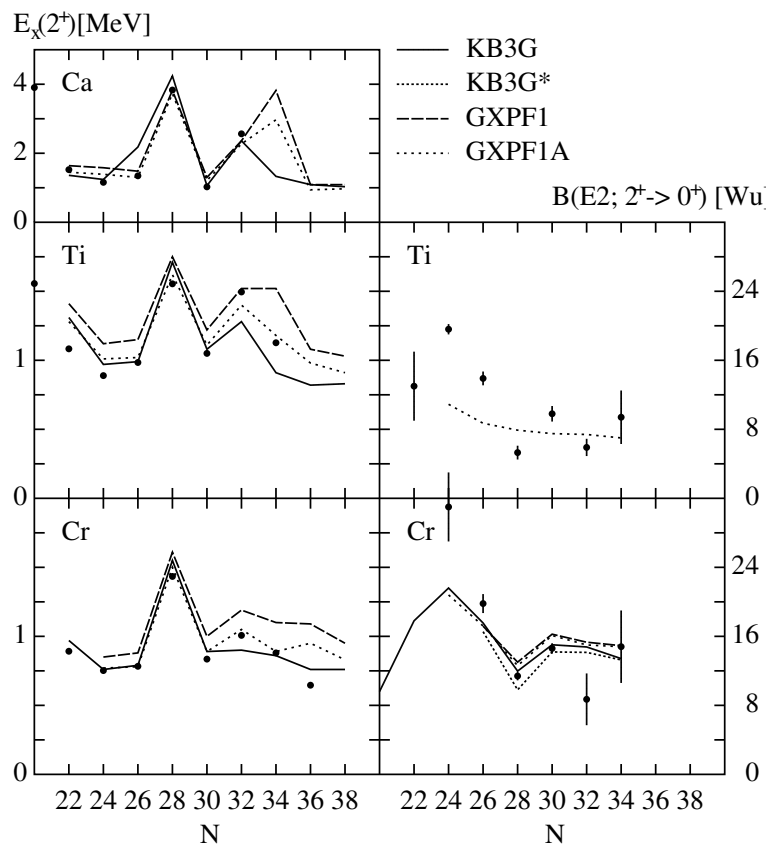

Fig. 3. Experimental $B(E2; 2_1^+ \rightarrow 0^+)$ values and 2_1^+ energies of neutron rich Ca, Ti and Cr isotopes in comparison to different shell model calculations.

$B(E2; 2_1^+ \rightarrow 0^+)$ value in ^{54}Cr served as normalization and reference for possible systematic errors in the analysis. Details of the experiment are given in the publication by A. Burger *et al.*[25] The obtained Doppler corrected Cr spectra yield values of 8.7(3.0) W.u. for ^{56}Cr and 14.8(4.2) W.u. for ^{58}C. The results of this experiment are shown in Fig. 3 together with the experimental $B(E2; 2_1^+ \rightarrow 0^+)$ and 2_1^+ systematics of the Ti and Cr isotopes in comparison to various shell model calculations (KB3G, GXPF1, GXPF1A).[25,26–28]

The local peak in the $N = 32$ 2_1^+ energies is con rmed by a minimum of the $B(E2; 2_1^+ \rightarrow 0^+)$ values in the present experiment and a recent result for Ti isotopes.[26] For $N = 34$, however, the gap is developed in Cr and Ti which leaves ^{54,56}Ca as the crucial experimental probes. The shell model calculations reproduce the variation in the 2_1^+ energies. However, the $B(E2; 2_1^+ \rightarrow 0^+)$ values are virtually unchanged in the di erent approaches and almost constant from $N = 30$ to 34.

5. Triaxiality in ^{134}Ce and ^{136}Nd

As nuclear properties are investigated from closed shells toward the mid-shell regions, a transition from spherical to deformed shapes takes place in the mass A 130 region. Since the origin of the deformation is mainly of quadrupole nature and the shape is connected with the collective motion of the nucleons, this in uences the nature of low lying 2^+ states. The properties of these 2^+ states can be related to quadrupole triaxiality. However, the shape may not be well de ned due to surface vibrations, resulting in a -soft con guration. To gain information on the nuclear shape of ^{134}Ce and ^{136}Nd, two nuclei which are candidates for being cores of chiral twin bands, relativistic Coulomb excitation experiments were performed. Here, not only the rst 2_1^+ but also the second 2_2^+ state was observed for the rst time after relativistic Coulomb excitation.

Detailed information on the experiment will be given in an upcoming paper.[29] The results of this experiment, given in Table 2 and Fig. 4, can be compared with a nuclear model, namely the asymmetric rotor model for a rigid triaxial nucleus.[30] The model can be extended to account for intrinsic vibrations of the nuclear surface, introducing an additional parameter μ which speci es the deformability of the surface in this soft asymmetric rotor model.[31] Details of this comparison are discussed by T. Saito *et al.*[29]

Table 2. $B(E2)$ values of ^{132}Ba, ^{134}Ce and ^{136}Nd depopulating the 2_1^+ and 2_2^+ states.

Transition	^{132}Ba $B(E2)$ [W.u.]	^{134}Ce $B(E2)$ [W.u.]	^{136}Nd $B(E2)$ [W.u.]
$2_1^+ \rightarrow 0^+$	42(4)[a]	52(5)[a]	80(11)
$2_2^+ \rightarrow 0^+$	3.9(4)[a]	≤ 11	11(3)
$2_2^+ \rightarrow 2_1^+$	144(14)[a]	≤ 140	182(93)

[a]From Ref. 14.

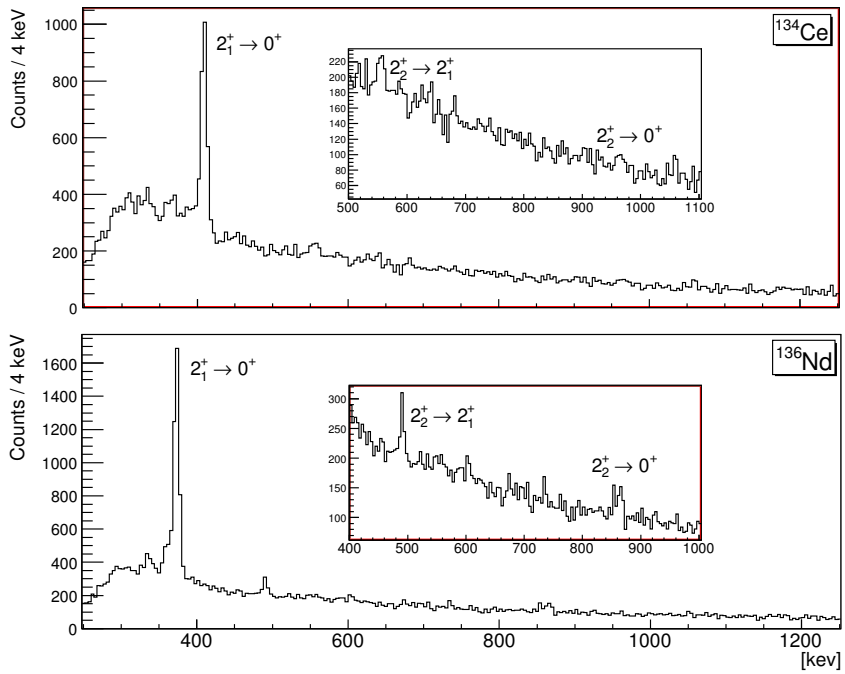

Fig. 4. Doppler corrected γ-ray spectra for ^{134}Ce and ^{136}Nd.

6. Summary

The shown results demonstrate the feasibility of high resolution -ray spectroscopy at relativistic energies utilizing the two-step fragmentation or Coulomb excitation technique with RISING. The ability of the SIS facility to accelerate all stable nuclei to several hundred MeV and the ensuing selection of fragmentation or ssion products enables the study of interesting nuclear phenomena arising in regions far away from the valley of stability.

Acknowledgments

The collaboration would like to thank the EUROBALL Owners Comittee, the MINIBALL collaboration and the HECTOR collaboration for providing their - detectors to the RISING fast-beam campaign at GSI. This work was supported by the German BMBF under grant Nos. 06BN-109, 06K-167 and by the Polish State Committee for Scienti c Research (KBN grant No. 620/E-77/SPB/GSI/P-03/DWM105/2004-2007).

References

1. H. J. Wollersheim *et al.*, *Nucl. Instr. Meth.* **A537** (2005) 637.
2. H. Geissel *et al.*, *Nucl. Instr. Meth.* **B70** (1992) 286.

3. J. Eberth *et al.*, *Nucl. Instr. Meth.* **A369** (1996) 135.
4. A. Maj *et al.*, *Nucl. Phys.* **A571** (1994) 185.
5. E. Caurier *et al.*, *Phys. Rev.***C60** (1994) 225.
6. T. Otsuka *et al.*, *Phys. Rev. Lett.* **87** (2001) 082502.
7. H. Grawe, *Act. Phys. Pol.* **B34** (2003) 2267.
8. C. M. Petrache *et al.*, *Phys. Rev.* **C61** (2000) 011305(R).
9. K. Starosta *et al.*, *Phys. Rev. Lett.* **86** (2001) 971.
10. R. Lozeva *et al.*, *Nucl. Instr. Meth.* **A562** (2005) 298.
11. S. M. Lenzi *et al.*, *Phys. Rev. Lett.* **87** (2002) 122501.
12. A. P. Zuker *et al.*, *Phys. Rev. Lett.* **87** (2002) 142502.
13. G. de Angelis *et al.*, *Eur. Phys. J.* **A12** (2001) 51.
14. ENSDF database, `http://www.nndc.bnl.gov/ensdf/`
15. S. Kanno *et al.*, *Prog. Theor. Phys.* (Kyoto), Suppl. **146** (2002) 575.
16. P. D. Cottle *et al.*, *Phys. Rev. Lett.* **88** (2002) 172502.
17. B. A. Brown and B. H. Wildenthal, *Ann. Rev. of Nucl. Part. Sci.* **38** (1988) 29.
18. H. Herndl *et al.*, *Phys. Rev.* **C52** (1995) 1078.
19. Y. Utsuno *et al.*, *Phys. Rev.* **C60** (1999) 054315.
20. R. G. Thomas, *Phys. Rev.* **88** (1952) 1109.
21. J. B. Ehrman, *Phys. Rev.* **81** (1951) 412.
22. A. Huck *et al.*, *Phys. Rev.* **C31** (1985) 2226.
23. S. N. Liddick *et al.*, *Phys. Rev. Lett.* **92** (2004) 072502.
24. P. F. Mantica *et al.*, *Phys. Rev.* **C67** (2003) 014311.
25. A. Burger *et al.*, *Phys. Lett.* **B622** (2005) 29.
26. D. C. Dinca *et al.*, *Phys. Rev.* **C71** (2005) 041302.
27. E. Caurier *et al.*, *Eur. Phys. J.* **A15** (2002) 145.
28. M. Honma *et al.*, *Phys. Rev.* **C69** (2004) 034335.
29. T. Saito *et al.*, to be published.
30. A. S. Davydov and G. F. Filippov, *Nucl. Phys.* **8** (1958) 237.
31. A. S. Davydov and A. A. Chaban, *Nucl. Phys.* **20** (1960) 499.

RISING: Gamma-ray Spectroscopy with Radioactive Beams at GSI

P. Doornenbal[a,b], A. Bürger[c], D. Rudolph[d], H. Grawe[b], H. Hübel[c], P.H. Regan[e], P. Reiter[a], A. Banu[b], T. Beck[b], F. Becker[b], P. Bednarczyk[b,f], L. Caceres[b,g], H. Geissel[b], J. Gerl[b], M. Górska[b], J. Grębosz[b,f], M. Kavatsyuk[b], O. Kavatsyuk[b], A. Kelic[b], I. Kojouharov[b], N. Kurz[b], R. Lozeva[b,h], F. Montes[b], W. Prokopowicz[b], N. Saito[b], T. Saito[b], H. Schaffner[b], S. Tashenov[b], H. Weick[b], E. Werner-Malento[b,i], M. Winkler[b], H.-J. Wollersheim[b], A. Al-Khatib[c], L.-L. Andersson[d], L. Atanasova[h], D.L. Balabanski[j], M.A. Bentley[k], G. Benzoni[l], A. Blazhev[a], A. Bracco[l], S. Brambilla[l], C. Brandau[b,e], P. Bringel[c], J.R. Brown[k], F. Camera[l], S. Chmel[c], E. Clément[m], F.C.L. Crespi[l], C. Fahlander[d], A.B. Garnsworthy[e,n], A. Görgen[m], G. Hammond[o], M. Hellström[d], R. Hoischen[d], H. Honma[p], E.K. Johansson[d], A. Jungclaus[g], M. Kmieciek[f], W. Korten[m], A. Maj[f], S. Mandal[q], W. Meczynski[f], B. Million[l], A. Neußer[c], F. Nowacki[r], T. Otsuka[s,t], M. Pfützner[i], S. Pietri[e], Zs. Podolyák[e], A. Richard[a], M. Seidlitz[a], S.J. Steer[e], T. Striepling[a], T. Utsuno[s,t], J. Walker[g], N. Warr[a], C. Wheldon[u] and O. Wieland[l]

[a]*Institut für Kernphysik, Universität zu Köln, D-50937 Köln, Germany*
[b]*Gesellschaft für Schwerionenforschung, D-64291 Darmstadt, Germany*
[c]*Helmholtz-Institut für Strahlen- und Kernphysik, Universität Bonn, D-53115 Bonn, Germany*
[d]*Department of Physics, Lund University, S-22100 Lund, Sweden*
[e]*Department of Physics, University of Surrey, Guildford, GU2 7XH, UK*
[f]*The Henryk Niewodniczański Institute of Nuclear Physics, PL-31-342 Kraków, Poland*
[g]*Departamento de Física Teórica, Universidad Autonoma de Madrid, E-28049 Madrid, Spain*
[h]*Faculty of Physics, University of Sofia, BG-1164 Sofia, Bulgaria*
[i]*Institute of Experimental Physics, Warsaw University, PL-00-681 Warsaw, Poland*
[j]*Institute for Nuclear Research and Nuclear Energy, Bulgarian Academy of Sciences, BG-1784 Sofia, Bulgaria*
[k]*Department of Physics, University of York, York, Y01 5DD, UK*
[l]*Dipartimento di Fisica, Università di Milano, and INFN sezione di Milano, I-20133 Milano, Italy*
[m]*DAPNIA/SPhN, CEA Saclay, Gif-sur-Yvette, France*
[n]*WNSL, Yale University, New Haven, CT 06520-8124, USA*
[o]*School of Chemistry and Physics, Keele University, Staffordshire, ST5 5BG, UK*
[p]*University of Aizu, Fukushima 965-8580, Japan*
[q]*Department of Physics and Astrophysics, University of Delhi, Delhi - 110 007, India*
[r]*IReS, Université Louis Pasteur, Strasbourg, France*
[s]*Department of Physics and Center for Nuclear Study, University of Tokyo, Hongo, Tokyo 113-0033, Japan*
[t]*RIKEN, Hirosawa, Wako-shi, Saitama 351-0198, Japan*
[u]*Department SF7, Hahn-Meitner-Institut, D-14109 Berlin, Germany*

Abstract. The Rare Isotope Spectroscopic INvestigation at GSI (RISING) project is a major pan-European collaboration. Its physics aims are the studies of exotic nuclear matter with abnormal proton-to-neutron ratios compared with naturally occurring isotopes. RISING combines the FRagment Separator (FRS) which allows relativistic energies and projectile fragmentation reactions with EUROBALL Ge Cluster detectors for γ spectroscopic research. The RISING setup can be used in two different configurations. Either the nuclei of interest are investigated after being stopped or the heavy ions hit a secondary target at relativistic energies and the thereby occurring excitations are studied. For the latter case, MINIBALL Ge detectors and the HECTOR array are used in addition. Example achievements of the Fast Beam setup are presented and compared to various shell model calculations, while for the Stopped Beam setup initial results are shown.

Keywords: Gamma-ray spectroscopy; nuclear structure; excitation probabilities; nuclear isomers
PACS: 21.60.Cs; 23.20.Lv; 25.70.Mn

INTRODUCTION

One of the key issues in current nuclear structure physics research is the exploration of nuclei far away from the line of β-stability. This has led to the development of different techniques that permit the study of specific radioactive nuclei. In the case of projectile fragmentation or relativistic fission heavy ion beams are accelerated to an energy of up to 1 *A* GeV and then strike a thick target. Since this produces a vast number of different nuclei, the fragments of interest must be selected using their magnetic rigidity after the target, which is done at the FRS at GSI [1]. Here, two pairs of dipoles are used in the so called Bρ-ΔE-Bρ mode by placing a wedge-shaped aluminum degrader at the central focal plane of the FRS and setting the second pair of dipoles according to the energy loss of the sought-after fragments. The ions passing from the intermediate to the final focus of the FRS are identified on an event-by-event basis using their magnetic rigidity Bρ, their time of flight between two scintillation detectors, and their energy loss in a multi sampling ionization chamber.

RISING SETUP

When the heavy ions reach the final focus of the FRS, they can hit a secondary target, which enables the study of Coulomb excitation at relativistic energies or fragmentation processes towards even more exotic nuclei. Alternatively, they are implanted into a passive stopper followed by γ ray measurements of decays of isomeric states produced by the fragmentation or fission process in the primary target. This paper reports on initial and selected results of these two major RISING setups, the former being the Fast Beam setup [2], the latter being the Stopped Beam setup [3–5].

The Fast Beam Setup

In the Fast Beam setup relativistic Coulomb excitation and two-step fragmentation experiments were performed with energies in the range of 100 to 600 *A* MeV. A ^{197}Au reaction target with thicknesses from 0.4 to 2.0 g/cm^2 was used in the case of Coulomb

excitation, while two-step fragmentation experiments were carried out with a 0.7 g/cm^2 ^{9}Be target. The resulting reaction products were identified with respect to their charge and mass with the calorimeter telescope array CATE [6], consisting of 3 $\times$ 3 Si-CsI(Tl) modular ΔE-E telescopes mounted 1400 mm downstream of the target. For the proper Doppler correction, the position sensitive CATE Si detectors and an identical Si detector placed directly after the target served as tracking detectors. In the case of Coulomb excitation, unwanted nuclear contributions could be excluded by selecting sufficiently large impact parameters. This impact parameter could be obtained by tracking the heavy ions with position sensitive multiwire detectors upstream the target and the afore mentioned Si detectors.

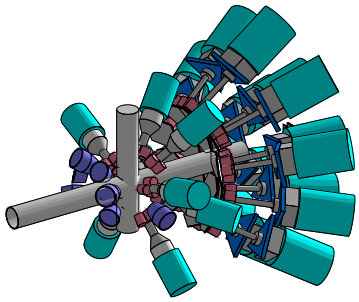

FIGURE 1. Drawing of the γ ray detector setup during the Fast Beam campaign. See text for details.

In order to measure γ rays emitted by excited states, the target area was surrounded by numerous detectors, as shown in Fig. 1: (i) 15 Cluster Ge detectors [7], positioned in three rings at extreme forward angles of 16°, 33°, and 36° at distances of 700 to 1400 mm, (ii) eight six-fold segmented MINIBALL triple Ge detectors [8] at distances of 200 to 400 mm, arranged in two rings with central angles of 51° and 85°, (iii) the HECTOR array [9, 10] at a distance of 300 mm, consisting of eight large volume BaF_2 detectors, situated at angles of 85° and 142°. In its least distance configuration, the efficiency for a γ ray of 1332 keV emitted from heavy ions at 100 A MeV was simulated to be 1.7% for the Cluster detectors, 3.8% for MINIBALL and 1.7% for HECTOR, not including add-back events.

The Stopped Beam Setup

The Stopped Beam setup can be used in two configurations to measure γ rays: Isomeric states produced in the fragmentation process are implanted into a passive stopper or heavy ions are implanted into an active β-sensitive stopper, thus enabling the search for excited states of exotic nuclei following β-decay. In contrast to the Fast Beam setup, a second degrader of variable thickness was put at the final focus of the FRS. This allowed the energy loss of the heavy ions to be tuned in such a way that the stopper could be kept at a moderate thickness.

The fifteen Ge Cluster detectors surrounding the stopper in the Stopped Beam setup are shown in Fig. 2. The Cluster detectors were placed in three rings of five detectors at angles of 51°, 90°, and 129° relative to the beam axis at a distance of approximately

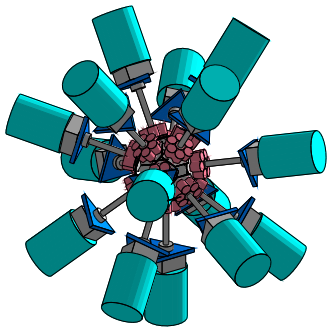

FIGURE 2. Drawing of the γ ray detector setup during the Stopped Beam campaign. See text for details.

22 cm from the center of the final focal plane of the FRS. The photopeak γ ray efficiency of the Stopped Beam Ge detector setup was measured to be 9(1)% at 1332 keV, not including add-back events [5]. Due to the high granularity of the Ge detector array of 105 crystals in total, a higher loss of efficiency was avoided after the prompt γ flash that was produced in the stopping process of the heavy ions. In order to identify the metastable states after the implantation, each γ ray was time stamped using a 40 MHz clock, which was part of the DGF4 timing and energy signal processing [11]. For both short-lived isomers and redundancy a conventional timing branch was installed in parallel and digitized with a short-range ($t \leq 1.0$ μs) and a long-range $t \leq 0.8$ ms VME TDC. This enabled the measurement of decays from isomeric states with half-lives in the region between several tens of ns up to 1 ms.

SELECTED EXPERIMENTAL RESULTS

Monopole Driven Shell Structure

During the Fast Beam campaign one of the key interests was the investigation of the monopole driven shell structure. This monopole part of the residual interaction controls the propagation of single particle energies with increasing occupation of a major shell. It causes a change of oscillator shell closures with magic numbers for very neutron rich nuclei of $N = 8, 20$ towards $N - 2 \times N_{HO} = 6, 16(14)$ [12, 13]. N_{HO} is the harmonic oscillator main quantum number . The weak $N = 40$ harmonic oscillator case should shift to a $N = 32, 34$ subshell closure, where the ambiguity for $N_{HO} > 1$ stems from the presence of j = 1/2 orbits which strongly mix with the neighboring higher-spin orbitals [13]. The monopole residual interaction is also expected to be of isospin symmetric nature, hence its effects can be studied by comparing the nuclear structure of the $N = 20$ isotones below ^{40}Ca with their $Z = 20$ mirror nuclei.

The RISING Fast Beam setup gives access to excitation energies $E_{2_1^+}$ of $I^\pi = 2_1^+$ and $B(E2; 2_1^+ \rightarrow 0^+)$ values that can both be used as signatures for shell structure. Two type of experiments were performed: A Coulomb excitation experiment of the neutron rich ^{54,56,58}Cr, which are located in between the $N = 40$ subshell closure across a deformed region to spherical nuclei at $N = 28$, second, and a two-step fragmentation

experiment to investigate the mirror energy difference, defined as $\Delta E_M = E_x(I, T_z = -T) - E_x(I, T_z = +T)$, between ^{36}Ca and ^{36}S.

The Subshell Closure at $N = 32, 34$ — Coulomb Excitation of ^{54,56,58}Cr

Experimentally, possible subshell closures may develop at $N = 32, 34$ in neutron rich Ca ($Z = 20$) isotopes as indicated by a rise in the 2_1^+ energy of ^{52}Ca [14]. The Ti and Cr ($Z = 22, 24$) isotopes exhibit a maximum of those energies at $N = 32$ [15–17].

Besides the 2_1^+ energies, $B(E2; 2_1^+ \rightarrow 0^+)$ values provide crucial information to test the evolution of subshell structures. Therefore, three experiments were performed to measure the Coulomb excitation of ^{54}Cr, ^{56}Cr and ^{58}Cr, where the known $B(E2; 2_1^+ \rightarrow 0^+)$ value in ^{54}Cr served as normalization and reference for possible systematic errors in the analysis.

A primary beam of ^{86}Kr with an energy of 480 A MeV was incident on a 2.5 g/cm^2 ^{9}Be target. Out of the fragmentation products, the Cr isotopes were selected and incident on a 1.0 g/cm^2 ^{197}Au target at energies of around 136 A MeV. More details of the experiment are given in Ref. [18]. The obtained Doppler corrected Cr spectra yield values of 8.7(30) W.u. for ^{56}Cr and 14.8(42) W.u. for ^{58}Cr. These results are shown in Fig. 3 together with the experimental $B(E2; 2_1^+ \rightarrow 0^+)$ and 2_1^+ systematics of the Ti and Cr isotopes and are compared to shell model calculations (KB3G, GXPF1, GXPF1A) [19–21].

The local peak in the $N = 32$ 2_1^+ energies is confirmed by a minimum of the $B(E2; 2_1^+ \rightarrow 0^+)$ values in the present experiment and a recent result for Ti isotopes [19]. For $N = 34$, however, the gap is not developed in Cr and Ti which leaves ^{54,56}Ca as

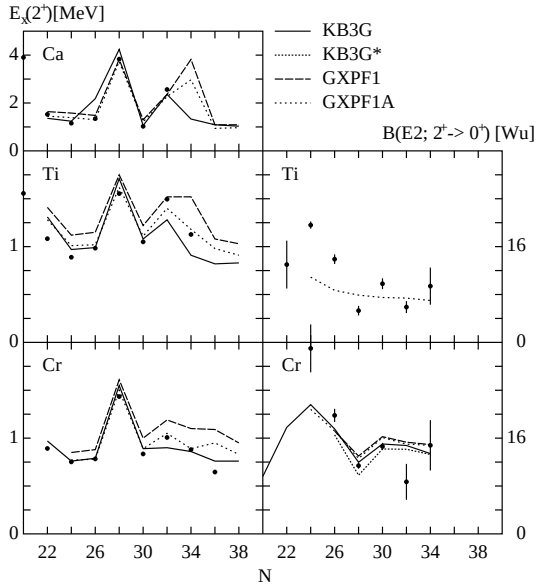

FIGURE 3. Experimental 2_1^+ energies and $B(E2; 2_1^+ \rightarrow 0^+)$ values of neutron rich Ca, Ti and Cr isotopes in comparison to different shell model calculations.

the crucial experimental probes. The shell model calculations reproduce the variation in the 2_1^+ energies but fail to reproduce the $B(E2;2_1^+ \rightarrow 0^+)$ values which stay almost unchanged in the different approaches from $N = 30$ to 34.

Mirror Symmetry in $A = 36$, $T = 2$ Nuclei

Going along the $N = 20$ isotones south of ^{40}Ca, the shell stabilization of ^{36}S, ^{34}Si and the shell quenching in ^{32}Mg are expected to be caused by the monopole part of the two-body interaction. This scenario is anticipated to be symmetric in isospin and may not or little affected by neutron binding energy differences [12, 13]. It can be verified in the $N = 20$ mirror region along the light Ca ($Z = 20$) isotopes. From the Ca isotopes, detailed spectroscopy exists only for ^{38}Ca [22], while no excited states are known for the $N = 16$ isotope, thus the mirror nucleus of ^{36}S is of high interest.

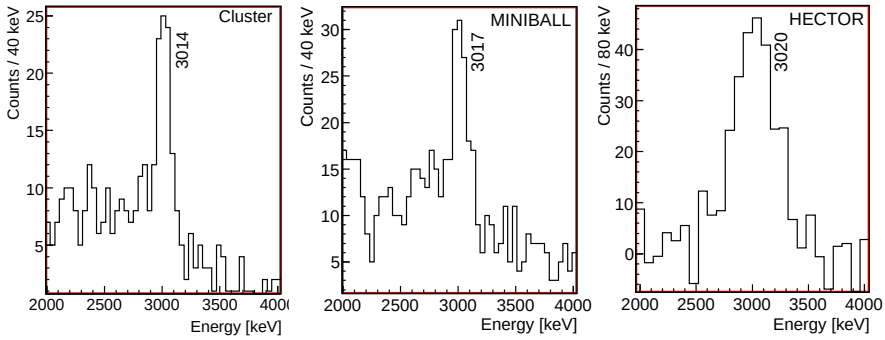

FIGURE 4. Doppler corrected ^{36}Ca gated γ ray spectra measured with the Cluster, MINIBALL and HECTOR detectors. For the HECTOR array the background was subtracted.

A beam of ^{40}Ca at an energy of 420 A MeV was bombarded on a 4.0 g/cm^2 ^{9}Be target. As a secondary beam ^{37}Ca was selected and incident on a 0.7 g/cm^2 ^{9}Be secondary target to populate excited states in ^{36}Ca. In Fig. 4 Doppler corrected γ ray spectra of ^{36}Ca are shown for the MINIBALL, Cluster and HECTOR detectors. The energy of the $2_1^+ \rightarrow 0^+$ transition was determined to 3015(16) keV, yielding a value of ΔE_M = –276(16) keV for the $A = 36$, $T = 2$ mirror pair. This value is significantly larger than mirror energy differences observed for $T = 1$ states in the *sd* and *pf* shell [15]. Other known $T = 2$ mirrors in the *sd* shell, $A = 24$ and 32, also exhibit much smaller mirror energy differences of –102(11) keV and –117(12) keV, respectively [23, 24].

In our approach to understand the large ΔE_M, we have used the experimental single-particle energies from the $A = 17$, $T = 1/2$ mirrors and applied these onto a modified isospin symmetric USD interaction [25, 26] in a shell model calculation. Monopole corrections were applied to reproduce the $Z, N = 14, 16$ shell gaps, the $I^\pi = 2_1^+$ excitation energies and the ^{40}Ca single hole energies. The results of this calculation are shown in Table 1 for ^{36}Ca and ^{36}S, yielding a value of ΔE_M = –268 keV. This is in close agreement to the experimental result and shows that the experimental single-particle energies may account empirically for the one-body part of Thomas-Ehrman and/or Coulomb effects [27, 28], since the isospin symmetry is preserved in the interactions' two-body matrix elements but not in the single-particle energies used.

TABLE 1. Comparison of shell model calculation with experimental values for ^{36}Ca and ^{36}S.

	$E_{2_1^+}$ **[keV]**		π**-gap [MeV]**		ν**-gap [MeV]**	
	Exp.*	**SM**†	**Exp.**	**SM**	**Exp.**	**SM**
^{36}Ca	3015(16)**	3290	4.55(30)		4.16(9)	3.999
^{36}S	3290.9(3)	3558	4.524(2)‡	4.244	5.585	

* From Ref. [15].
† Shell model calculation, see text for details.
** This work.
‡ Coulomb Corrected.

First Results from the Stopped Beam Setup

The Stopped Beam campaign started with the investigation of heavy odd-odd $N = Z$ nuclei along the proton drip-line [3]. It was followed by isomeric decay studies in the region of the doubly magic ^{56}Ni, ^{132}Sn and ^{208}Pb [29, 30]. We will focus on the results of ^{54}Ni, produced after the fragmentation of a ^{58}Ni primary beam, which demonstrate nicely the excellent possibilities of combining the FRS with the RISING γ ray spectrometer in its Stopped Beam configuration.

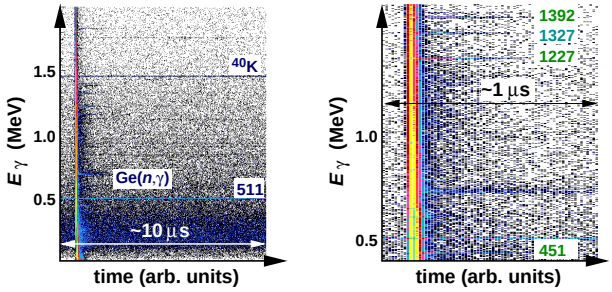

FIGURE 5. ^{54}Ni gated two-dimensional matrices of γ energy versus time after implantation.

After the identification of ^{54}Ni reaching the final focal plane with the FRS detectors, a correlation matrix between the γ energy and the time after the implantation can be generated. Two examples are shown in Fig. 5. On the left hand, a more general view provides an indication of the so-called prompt flash (vertical line), which marks the implantation time $t = 0$, as well as horizontal lines arising from, for example, room background or (n,γ) reactions in the Ge detectors. But more than that, also distinct and as a function of time fading horizontal lines are visible, indicating decays from isomeric states. Some of these are highlighted on the right hand side of Fig. 5, which zooms into the energy-time region of interest for ^{54}Ni. By setting cuts on distinct times after the implantation and comparing the intensities, information on the half-lives of the isomers can be obtained. Moreover, provided that the spectra are rich enough in statistics, $\gamma\gamma$ coincidence measurements can help to examine the level structure. This is done in Fig. 6 where in the upper background subtracted spectrum a simple projection of the two-dimensional panel is shown for the time range 0.05 μs $\leq t \leq$ 1.0 μs. In

this spectrum six discrete γ transitions at 146, 451, 1227, 1327, 1392, and 3241 keV are visible and all have a lifetime of $\tau \sim 220$ ns. In the lower panel, however, gates on the already established $6^+ \rightarrow 4^+ \rightarrow 2^+ \rightarrow 0^+$ cascade [31–33] are set at energies of 451, 1227, and 1392 keV. Since the lines observed at 146 and 3241 keV are clearly in coincidence with the cascade, they are suggested to be the $10^+ \rightarrow 8^+$ and $8^+ \rightarrow 6^+$ transitions [34], what also follows from the known mirror isomer ^{54}Fe [15]. Even a weak line at 3386 keV is visible, which can be associated to the small $10^+ \rightarrow 6^+$ $E4$ branch. The most surprising result is, however, that none of the observed γ rays comes in coincidence with the 1327 keV line, which is seen only in the singles spectrum. Since it has the same energy as the $9/2^- \rightarrow 7/2^-$ ground state transition in ^{53}Co, it is suggested that this $9/2^-$ state in ^{53}Co can be populated via a direct proton decay ($Q_p \sim 1.3$ MeV) from the isomeric state in ^{54}Ni [34].

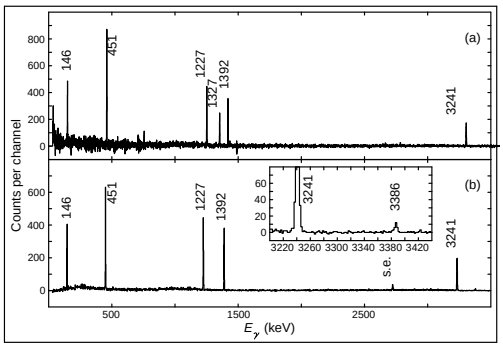

FIGURE 6. The upper panel (a) shows the background subtracted energy projection of the two-dimensional matrix of ^{54}Ni for the range $0.05\ \mu\text{s} \leq t \leq 1.0\ \mu\text{s}$. In the lower panel (b), the $\gamma\gamma$ coincidence with one of the transitions at 451, 1227, and 1392 keV demonstrates the correlation to other observed lines.

SUMMARY

The shown exemplary results demonstrate the possibilities of high resolution γ ray spectroscopy at relativistic energies utilizing the two-step fragmentation or Coulomb excitation technique with RISING, as has been shown for the results of ^{54,56,58}Cr and ^{36}Ca. A wealth of other interesting results have been obtained for example in relativistic Coulomb excitation of ^{108,112}Sn, ^{134}Ce, and ^{136}Nd [35, 36]. For the Stopped Beam campaign, a wide range of nuclei have been populated in isomeric states following fragmentation and fission: For example the long sought-after ^{82}Nb, ^{86}Tc, ^{130}Cd, and ^{204}Pt [29, 30, 37, 38]. Here, ^{54}Ni was chosen to illustrate the large capabilities of a highly efficient γ ray spectrometer used in combination with the FRS. In the future, a series of active stopper experiments is foreseen to perform β-delayed γ ray spectroscopy.

ACKNOWLEDGMENTS

The collaboration would like to thank the EUROBALL Owners Committee, the MINIBALL collaboration and the HECTOR collaboration for providing their γ detectors to

the RISING project. We also acknowledge the high beam intensities provided by the accelerator department at GSI. This permits us to study very exotic nuclei. This work is supported by the European Commission contract No. 506065 (EURONS), the German BMBF under grant Nos. 06BN-109, 06K-167, the Swedish Research Council, the Polish State Committee for Scientific Research (KBN grant No. 620/E-77/SPB/GSI/P-03/DWM105/2004-2007), the Bulgarian Science Fund under grant No. VUF06/05, and the EPRSC(UK).

REFERENCES

1. H. Geissel *et al.*, Nucl. Instr. Meth. B **70** (1992) 286.
2. H.J. Wollersheim *et al.*, Nucl. Instr. Meth. A **537** (2005) 637.
3. P.H. Regan *et al.*, Proc. of the NN06 conference, Nucl. Phys. **A**, in press.
4. S. Pietri *et al.*, Proc. of the CAARI'06 conference, to be published in Nucl. Inst. Meth. **B**.
5. S. Pietri *et al.*, Proc. of the 41st Zakopane School of Physics, to be published in Act. Phys. Pol. **B**.
6. R. Lozeva *et al.*, Nucl. Instr. Meth. A **562** (2006) 298.
7. J. Eberth *et al.*, Nucl. Inst. Meth. A **369** (1996) 135.
8. J. Eberth *et al.*, Prog. Part. Nucl. Phys. **46** (2001) 389.
9. A. Maj *et al.*, Nucl. Phys. A **571** (1994) 185.
10. F. Camera, Ph. D. Thesis, University of Milano, Italy, 1992.
11. M. Pfützner *et al.*, Nucl. Inst. Meth. A **493** (2002) 155.
12. T. Otsuka *et al.*, Phys. Rev. Lett. **87** (2001) 082502.
13. H. Grawe, Act. Phys. Pol. **B 34** (2003) 2267.
14. A. Huck *et al.*, Phys. Rev. **C 31** (1985) 2226.
15. ENSDF database, `http://www.nndc.bnl.gov/ensdf/`.
16. S.N. Liddick *et al.*, Phys. Rev. Lett. **92** (2004) 072502.
17. P.F. Mantica *et al.*, Phys. Rev. **C 67** (2003) 014311.
18. A. Bürger *et al.*, Phys. Lett. **B 622** (2005) 29.
19. D.C. Dinca *et al.*, Phys. Rev. **C 71** (2005) 041302.
20. E. Caurier *et al.*, Eur. Phys. J. **A 15** (2002) 145.
21. M. Honma *et al.*, Phys. Rev. **C 69** (2004) 034335.
22. P.D. Cottle *et al.*, Phys. Rev. **C 60** (1999) 031301.
23. S. Kanno *et al.*, Prog. Theor. Phys. (Kyoto), Suppl. **146** (2002) 575.
24. P.D. Cottle *et al.*, Phys. Rev. Lett. **88** (2002) 172502.
25. B.A. Brown, B.H. Wildenthal, Ann. Rev. of Nucl. Part. Sci. **38** (1988) 29.
26. Y. Utsuno *et al.*, Phys. Rev. **C 60** (1999) 054315.
27. R.G. Thomas, Phys. Rev. **88** (1952) 1109.
28. J.B. Ehrman, Phys. Rev. **81** (1951) 412.
29. M. Górska, A. Jungclaus, M. Pfützner *et al.*, to be published.
30. Zs. Podolyák *et al.*, Proc. of the RNB7 conference, to be published in Eur. Phys. J. **A**.
31. K.L. Yurkewicz *et al.*, Phys. Rev. C **70** (2004) 054319.
32. K. Yamada *et al.*, Eur. Phys. J. **A25** S1 (2005) 409.
33. A. Gadea *et al.*, Phys. Rev. Lett. **97** (2006) 152501.
34. D. Rudolph *et al.*, to be published.
35. A. Banu *et al.*, Phys. Rev. C **72** (2005) 061305(R).
36. T. Saito *et al.*, submitted to Phys. Rev. Lett.
37. L. Caceres *et al.*, Proc. of the 41st Zakopane School of Physics, to be published in Act. Phys. Pol. **B**.
38. A.B. Garnsworthy *et al.*, Proc. of the 41st Zakopane School of Physics, to be published in Act. Phys. Pol. **B**.

Available online at www.sciencedirect.com
ScienceDirect
Computer Physics Communications ••• (••••) •••–•••
Computer Physics Communications
www.elsevier.com/locate/cpc

The Cracow code—an interactive method of sophisticated online analysis

Jerzy Grębosz [a,b,1]

[a] *The Henryk Niewodniczański Institute of Nuclear Physics (IFJ PAN), Kraków, Poland*
[b] *Gesellschaft fuer Schwerionen Forschung (GSI), Darmstadt, Germany*

Received 3 August 2006; accepted 28 September 2006

Abstract

A crucial issue in many complex experiments is the flexibility and ease of the online data analysis. Here we present an easy-to-learn and intuitive-to-operate method of interactive online analysis for use in projectile fragmentation induced gamma-ray spectroscopy experiments at the GSI facility (the RISING experiments). With a sequence of dialogue boxes the experimenter can create a complex definition, which will produce a conditional spectrum. These definitions can be immediately applied by the online analysis, which runs in parallel as a separate program. Some problems regarding the logic of gating conditions are discussed.

PACS: 29.85.+c; 29.30.Kv

Keywords: Online analysis; Data acquisition and analysis system; Event sorting

1. Introduction

During in-beam nuclear physics experiments, which require complicated apparatus, one of the crucial issues is the quality of the online data analysis. High quality online analysis allows the right decisions to be made about possible changes to the settings of the running experiments. The RISING [1] experiments use the cluster detectors from the former EUROBALL IV germanium-detector array [2]. Although RISING is similarly a γ-ray spectroscopy apparatus, there is a fundamental difference in the online analysis used by these two instruments. In the case of EUROBALL (installed at the beam line from the VIVITRON accelerator) the experimenter was sure what kind of projectile (i.e. the 'beam') was hitting the target. This is different for the RISING experiments. RISING receives the beam from the GSI Fragment Separator FRS [3]. During typical usage the FRS separator gives rise to a 'cocktail' beam consisting of several secondary projectiles. Several types of isotope of numerous elements hit the user's final target, it is the user's responsibility to select events associated with the desired projectile. The user can do this using algorithms implemented in the online analysis program. To make this feasible, the data acquisition system (DAQ) collects not only data from the RISING germanium detectors, but also from many particle detectors in the FRS (such as: multiwire chambers, scintillators, MUSIC ionisation chamber, etc.). After using complicated algorithms, the online analysis program should finally show two-dimensional scatter plots, on which the different projectiles (isotopes) can be separated.

Unfortunately there is no single universal particle identification algorithm. Depending on the experiment there are different procedures used for selecting a desired projectile from the rest of the projectiles hitting the target/final focus. This is why experimenters need a tool which is flexible, enabling them to produce the highest resolution selection for each particular isotope.

Complicated experiments require complicated software. This implies that scientists present during the experiment are dependent on the one or few people who are able to modify the online analysis program and instantly adapt it for a specific situation.

Sometimes, when everything goes wrong during a night shift, a professor might ask: *"Could we see this spectrum—gated by time, by this isotope coming from the Fragment Sep-*

E-mail address: jerzy.grebosz@ifj.edu.pl.
[1] Present address: Institute of Nuclear Physics, Polish Academy of Sciences (IFJ PAN), ul. Radzikowskiego 152, 31-342 Cracow, Poland.

0010-4655/$ – see front matter
doi:10.1016/j.cpc.2006.09.006

arator, and by the position of fragments on this scintillator?" Very often the answer is: *"No, because the Ph.D. student, who knows how to make it, is currently sleeping"*. This sounds like an anecdote, but is not it so?...

As a technician, I always keep in my mind the following bitter saying: "The humanists are the people who know '*what*', but do not know '*how*'. The technicians...—they would know '*how'*, but they do not know '*what for*' ". There is something wrong in this attitude. Why should it not be possible to combine these two skills? Why not introduce to the online analysis an instrument that the people who have brilliant ideas can use, so that they can check their ideas by themselves, instantly; without the necessity of reading a long manual.

This was the inspiration for the work described in this paper.

2. Online analysis

RISING is an example of experiments where the data is collected using "event by event" acquisition. Its data-acquisition system DAQ (called MBS) [4] collects events and stores information on disk, but does not provide any data viewing facilities, this is the work of the online analysis program. Therefore, the basic task of the online analysis is to extract the events (i.e. unpack them from the blocks of data) and to display one-dimensional histograms (spectra) of the raw data. By watching these (typically) hundreds of individual spectra, the experimenter can monitor the operation of the experiment's detectors and their associated electronic modules.

However, in most cases, the experimenter would like to see more. Thus, the real task of the online analysis is to take the events, coming one by one, from the data acquisition system, and then analyse them using algorithms specially dedicated to that particular experiment. These algorithms are usually carefully prepared before the experiment. By monitoring these spectra, the scientist would hope to see the first signs of a successful experiment. If they cannot see the expected results of the analysis, they may wish to alter the algorithms, in particular, algorithms used to gate other online created histograms, or they may decide to change the particle separation or beam settings. For example, they may wish to see newly defined spectra and to collect them only when some specific conditions occur.

The current article describes one way of performing the online analysis which enables the experimenter the freedom to create any kind of new one or two-dimensional spectrum, gated by sophisticated conditions, which are also user defined. This program does not require the experimenter to have significant knowledge of programming, nor does it require any modification of the online analysis program. There is no need to recompile the program or to stop the running online analysis program to update the gating conditions. All that is needed is the specially prepared Graphic User Interface (GUI) program—called 'Cracow'.

Note, that the package contains two distinct programs. The first program, 'spy' is run as a "command line" program and is responsible for making the online analysis. The second program, 'Cracow', has a graphic user interface which allows the spectra produced by spy to be displayed. It also provides the methods by which the experimenter can instruct the online analysis program to create the new, sophisticated conditional spectra.

3. 'Cracow' GUI

As shown in Fig. 1, there are two programs at work, but this article concentrates only on the 'Cracow' code and, in particular, on its methods of creating the user-defined spectra and user-defined conditions.

The main goal in the design of the 'Cracow' code was to make it sufficiently experimenter friendly that the user does not need to read a manual. Using the 'Cracow' GUI, the experimenter follows sequences of dialogue boxes—called 'creators' (or 'wizards'). By asking questions and expecting straightforward answers the wizards can create any kind of spectra, gated by many different types of conditions. The products of these

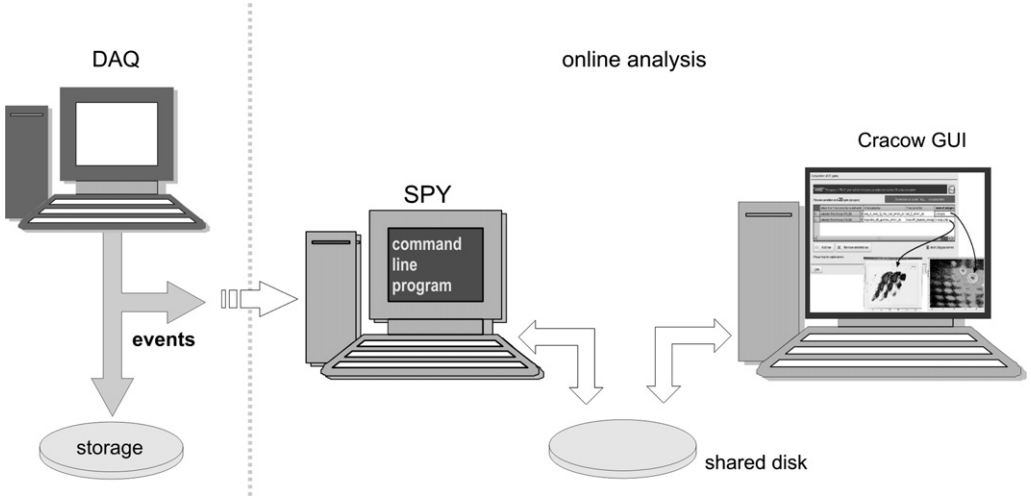

Fig. 1. Schematic of the RISING online analysis. The two separate programs 'spy' (which analyses events), and 'Cracow' (which allows on-line viewing of the spectra) communicate only by a shared disc. Using the graphic user interface of 'Cracow' it is possible to tell the 'spy' to start collecting a new kind of conditional (i.e. gated) spectrum.

Please cite this article as: J. Grębosz, The Cracow code—an interactive method of sophisticated online analysis, Computer Physics Communications (2006), doi:10.1016/j.cpc.2006.09.006

wizards, which are definitions of spectra or definitions of conditions, are stored on the disk as text files. (In this way they are 'persistent' and may be used in all future analysis.)

Once finished working with the wizard, 'Cracow' checks whether the online analysis program ('spy') is currently running. If yes, it is automatically informed about the new "wish" of the experimenter. The 'spy' program then:

- opens the definitions of the new spectra and the new conditions,
- creates the corresponding objects in the program,
- immediately starts to increment the new spectra with data coming from the experiment.

The experimenter using the same 'Cracow' program can then observe the result of their work, i.e. the new spectra collected using his/her newly introduced gating algorithm.

4. Incrementer

The key concept of the system described in this article is the so-called *incrementer*. An incrementer represents a variable in the online analysis program; a variable, which can be used to increment any given spectrum. Three types of variables from the RISING online analysis C++ 'spy' program can become incrementers: *int*, *double*, *bool*.

Of course not every variable in the program is worth being defined as an incrementer. This decision is made by the scientist who writes the online analysis program. If he decides that a variable may be useful as an incrementer, he defines a meaningful name which is then included in the list of the available incrementers. The GUI program reads the list of names and presents them on the screen. At any time, the experimenter can select the desired incrementer from such a list, when for example they need to create a histogram of a variable.

An example of an incrementer available in the RISING online analysis program is the energy of a γ-ray detected by one of the germanium detectors. The DAQ delivers the raw value of this data variable. Having this raw data, the online analysis program produces a gain-matched (calibrated) version and if required, a Doppler corrected energy. These three variables, raw, calibrated and Doppler corrected, can be chosen to be accessible as incrementers. As there are 105 such individual germanium detectors in the RISING array, by this action there would be $105 * 3 = 315$ incrementers available.

5. Some incrementers must be validated

Most of the users of the 'Cracow' GUI do not have to understand the concept of incrementers. They can simply treat them as variables in the analysis program. The user should however understand that in some events these 'variables' (incrementers) may contain undefined values.

Some incrementers always have a physically meaningful value, for instance, a variable which represents the multiplicity of germanium crystals which fired in a particular event. Since the online analysis program registers how many crystals fired in a given event, the incrementer representing this variable always contains a physically meaningful value.

However not all incrementers are of this nature. For example, in the RISING experiments there is a multiwire chamber which is used to trace the trajectory of projectile fragment ions. One expects that for any particular event both the 'left' and 'right' cathodes will deliver signals in the 'data'. These two data values are used by the online-analysis program to calculate the horizontal position of the ion in millimetres. The calculated value of this geometrical position is a useful incrementer, usually containing a value in the range $[-150, +150]$. Unfortunately sometimes only one cathode delivers the data. In this case it is impossible to calculate the position of the ion.

What, in such a case, should the contents of the incrementer representing the geometric position be? Zero? No, zero means that the geometric position of the ion is precisely centred in the axis of the beam line.

There must be another way to inform the rest of the analysis code (and the user of the incrementer) that in this particular event it was not possible to calculate the position (i.e. that this variable does not contain a meaningful value). For this purpose some incrementers are associated with another Boolean value which validates the current contents of the incrementer. In the case of the multiwire chamber this is a flag noting if the calculation of the position was successful or not.

The name of an incrementer which has a validator usually ends with the word "_when_...". For example:

mw41_x_**when**_ok

which means: Multiwire chamber named "mw41", its horizontal position x *when* its calculation was successful. This suffix "*when...*" informs the user about the nature of the incrementer. If the 'Cracow' GUI notices the use of an incrementer which is validated, the GUI may also ask us how to behave when the incrementer is not valid.

6. The user-defined spectra creator

The online analysis program of the RISING experiments produces typically more than 2000 standard spectra related to the different detectors used in the experiment. Many are defined by default, primarily because they are used the most often. If the experimenter would like to see a special spectrum, he can make it using a special instrument, a *spectra creator* (a user-defined spectra "wizard") available in 'Cracow' GUI. Now we will see the method of creating a user-defined spectrum in a "step by step" manner.

The first thing to do is to choose the name of the new spectrum. The chosen name is always preceded by the prefix "user_". This later helps to distinguish user-defined spectra from the standard spectra produced in the online analysis program by default.

The first page of the wizard is shown in Fig. 2. (As displayed in the figure, the spectrum name suggests that the histogram will define the sum of energy spectra of the 7 Germanium crystals belonging to the cluster detector named 'B'.)

Please cite this article as: J. Grębosz, The Cracow code—an interactive method of sophisticated online analysis, Computer Physics Communications (2006), doi:10.1016/j.cpc.2006.09.006

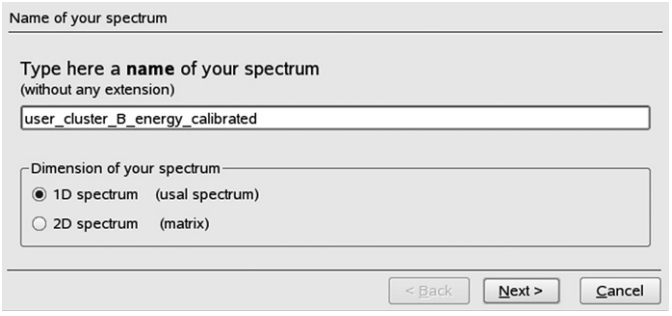

Fig. 2. The user can define a 1D or 2D spectrum. Depending what the user chooses the following pages of the wizard look differently.

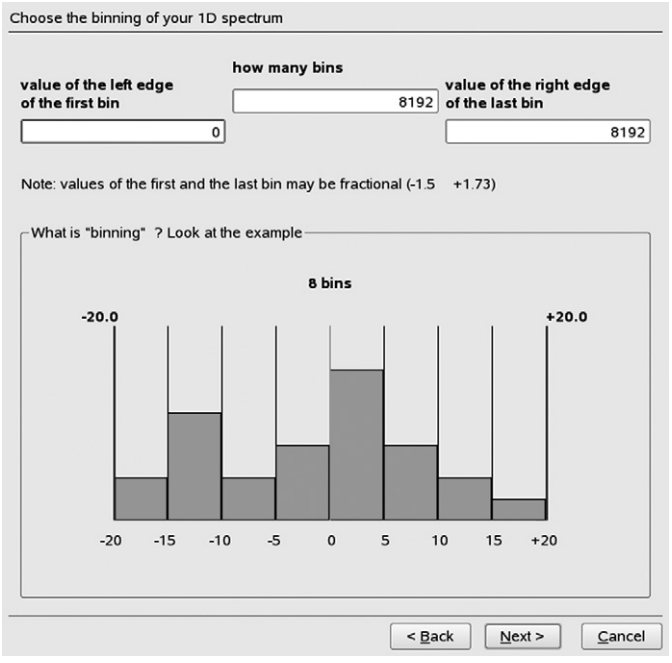

Fig. 3. Choosing the range of a 1D spectrum.

The second decision on this page of the wizard, concerns the dimension of the spectrum. The user can select a one-dimensional spectrum or a two dimensional matrix (scatter plot). If the user chooses a 1D spectrum and presses the button 'Next', then the following page of the wizard requests information about the range and binning of the spectrum. (See Fig. 3.)

Experience shows that some users mix the concepts of "bin" and "channel". In order to help clarify these concepts there follows a graph explaining the idea of binning.

On the following page of the wizard (see Fig. 4) the experimenter defines which variables from the online analysis program may increment this spectrum. There is a table in which the experimenter places the names of the chosen incrementers. During the online analysis the chosen incrementers will increment the spectrum for every event (assuming it is valid and no further condition is applied).

The table shown in Fig. 4 already contains a list of seven incrementers. They have rather long names, intended to be self-explanatory. The user does not have to type these names but rather selects them from a list. In the lower part of the dialogue

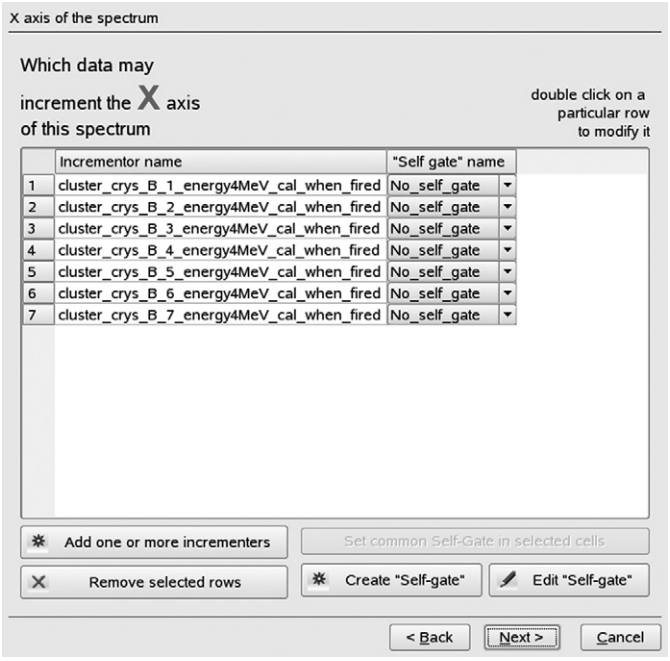

Fig. 4. A list of variables chosen by the user to 'contribute' to their spectrum. Placing more than one incrementer here creates the sum spectrum of those incrementers. Each of the (valid) incrementers will then increment the same spectrum.

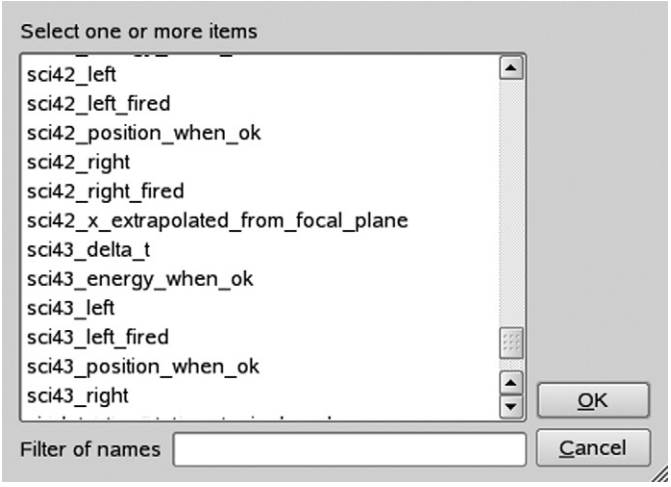

Fig. 5. A list of all incrementers offered by the 'spy' program, visible in the special dialogue box.

page there is a button called "Add one or more incrementers". This button opens a new dialogue box with the list of all the available incrementers (see Fig. 5).

There are circa 2500 available incrementers which are listed alphabetically. To ease the orientation, the names of the incrementers consist of the name of the object (detector) which the incrementer belongs to, this is then followed by the description of the meaning of a particular incrementer (such as energy, position, time, etc.).

For example, looking at Fig. 5, the last but one incrementer in this dialogue box has the name "sci43_position_when_ok". This name explains to the experimenter that the incrementer

Please cite this article as: J. Grębosz, The Cracow code—an interactive method of sophisticated online analysis, Computer Physics Communications (2006), doi:10.1016/j.cpc.2006.09.006

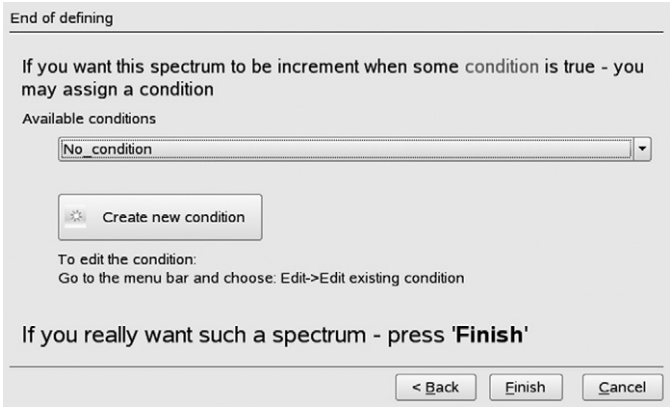

Fig. 6. The user defined spectrum may be incremented under some condition. The user can choose any condition from the list, or create a new condition.

is defined in the scintillator detector called "sci43" and it represents the position calculated by this object. The suffix "when_ok" informs the user that incrementer does not always contain a sensible value (it has a validator checking whether it was possible/impossible to calculate the position).

By knowing this naming convention the user can find the incrementer of interest from this list. There is a tool which makes such a search easier. At the bottom of the window there is a text filter, which allows the list to only include incrementers which pass a given filter.

Returning to the example, using the filter one can display only those incrementers which represent the calibrated (gain-matched) energy data of all the germanium detector crystals. In this case the experimenter is interested only in those belonging to cluster 'B', they can be selected and confirmed by pressing the *OK* button. The dialogue window disappears and the selected incrementers are automatically placed in the table shown on Fig. 4.

The 'Next' button moves us to the last page of the wizard. (See Fig. 6.)

Here the user may apply some condition, but if a condition is not needed, they can finish the work of the wizard. By this the definition of the spectrum is stored on the disk as a text file. The 'Cracow' GUI knows whether the online analysis program ('spy') is currently running, so it can command the 'spy' to read the definition prepared on the disk. The 'spy' reads the definition, and starts to collect the desired spectrum. The new spectrum can be observed immediately using the 'Cracow' GUI spectra viewer in the same way as any other standard spectra. The only difference is that the name of our spectrum starts with the prefix "user_".

Practice shows that the experimenters learn this tool very quickly. Some may think that the names of incrementers and their meaning are the most difficult things here. On the contrary, the names of the incrementers are self-explanatory for experimenters. These are just the general terms which are used while working on experiments and the algorithms of the analysis.

The experimenter can define many different user-defined spectra. At anytime they can also modify an already existing definition. If the definition of some new spectrum is going to be similar to the one which already exists, there is a time saving

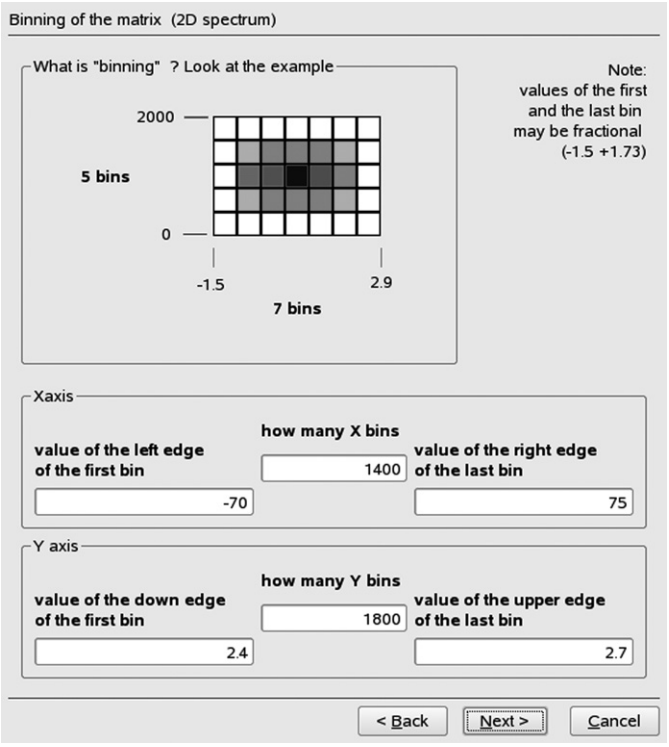

Fig. 7. If the user decided to create the definition of a 2D spectrum (matrix), the second page of the spectrum wizard looks different—it asks questions about the size of two axes instead of just one.

option available of cloning the definition and then modifying this 'clone'.

7. Two-dimensional spectra (matrices)

The wizard is a powerful tool in the GUI. It asks questions "step by step" and, depending upon the answers, adapts the following pages of the wizard to the current situation. Therefore if on the first page of the wizard the user decides that a spectrum needs to be two-dimensional, the next page will look different (see Fig. 7) to the one-dimensional option.

In the case of choosing a 2D spectrum, after the page dedicated to incrementers of the X-axis (Fig. 4), there is a new page which asks a similar question about the incrementers used for the Y-axis. For example, if the user wishes to construct a matrix of "γ-time versus γ-energy" the incrementers representing the γ-energy should be placed on the X-axis while those representing the γ-time on the Y-axis. Fig. 8 shows this example.

In one table the user can place as many incrementers, as they want. What does this actually mean for a 2D spectrum? In the case of only one incrementer for the X-axis of the matrix, and only one for the Y-axis it is clear that the user wants the spy program (during the analysis of each event) to increment the matrix at a point with the following coordinates $P(x, y)$, where

x is current value of the incrementer X and
y is current value of the incrementer Y.

But, as mentioned earlier, the user can apply more than one incrementer on a particular axis.

Please cite this article as: J. Grębosz, The Cracow code—an interactive method of sophisticated online analysis, Computer Physics Communications (2006), doi:10.1016/j.cpc.2006.09.006

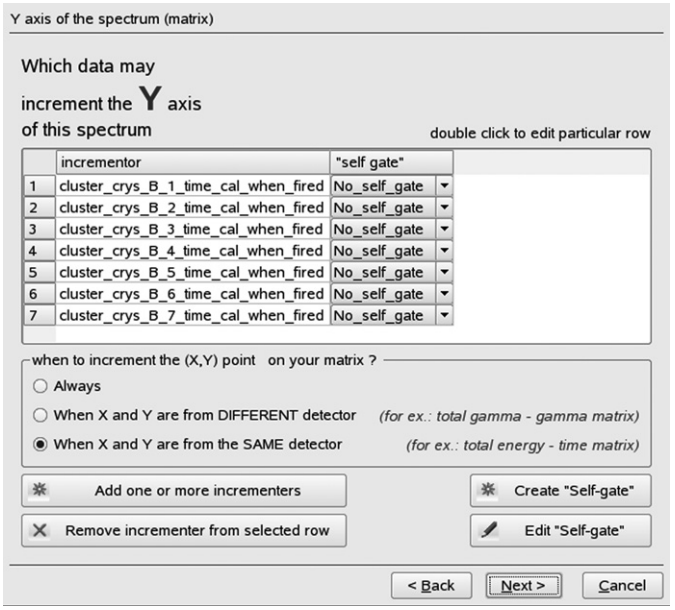

Fig. 8. The matrix must have a list of incrementers responsible for y coordinates of the incremented point $P(x, y)$. Below the list of incrementers there is set of radio buttons, which allows the choice of one of three modes of work. This is important if there is more than one item on the X or Y lists.

For example, for such a user-defined spectrum where there are 7 incrementers defined for the X-axis and also 7 defined for the Y-axis, there is a table produced as follows:

Table of X incrementers	Table of Y incrementers
x_1	y_1
x_2	y_2
x_3	y_3
x_4	y_4
x_5	y_5
x_6	y_6
x_7	y_7

How should the online analysis program interpret this during the analysis of a particular event? There are 3 sensible interpretations, they are outlined in the following sections.

7.1. All possible combinations of incrementers

The online analysis program understands that the user wants to increment points defined by every combination of the x and y incrementers for each event.

$$\begin{array}{llll} P(x_1, y_1) & P(x_1, y_2) & \dots & P(x_1, y_7) \\ P(x_2, y_1) & P(x_2, y_2) & \dots & P(x_2, y_7) \\ \dots & & & \\ P(x_7, y_1) & P(x_7, y_2) & \dots & P(x_7, y_7) \end{array}$$

This is the most general solution. If a user wants this, the 'Always' option on the set of radio buttons in Fig. 8 should be selected.

7.2. Incrementers from the same detector

In the case of the user defining the matrix "γ-energy versus γ-time"—they place the incrementers representing γ-energy in the table Y and the incrementers representing corresponding γ-times in the table X. For this type of matrix the user only wants combinations of the γ-ray energy data coming from the same detector as the γ-time data. Generally there is no physical sense in using the combination of energy data from one detector, with the time data from another, so the user is interested in the combinations

$P(x_k, y_j)$ when x_k, y_j are incrementers from the same detector (i.e. $k \equiv j$).

Note. This does not mean that the incrementer from row 3 of the X incrementer table will be used together with the incrementer from row 3 of the Y table. Such a solution would not be user friendly, because it requires that the user places his incrementers in a strictly defined order—this is a potential source of errors and time consuming.

The user friendly approach is different; the user should not think about the rows in the table, but about the meaning of the incrementers. To facilitate this, the online analysis program ('spy') does not care about the numbers of the rows. The user can place their incrementers in the tables in any order. The 'spy' program is able to recognise which two incrementers belong to the same detector, and can use them to increment the matrix.

If the user wants this interpretation, he should select the 'when X & Y are from the SAME detector' option on the set of radio buttons shown on Fig. 8.

7.3. Incrementers from different detectors

If the experimenter is defining the coincidence matrix "γ–γ energy", they place the same incrementers representing the γ-energy in both tables X and Y. Now they are interested in a different combination of listed incrementers.

If, continuing the example, it is going to be a γ–γ energy coincidence matrix of the germanium crystals belonging to the cluster called 'B' they choose 7 energy incrementers for the X-axis, and the same 7 incrementers for the Y-axis. But now the desired combinations are different. In this case, the user wants to increment their matrix only for the points:

$P(x_k, y_j)$ where x_k, y_j are incrementers from different detectors (i.e. $k \neq j$).

Again, here the k and j do not mean the row in the incrementer tables, but rather the detector which delivers this data.

In other words, in the case of coincidence matrix γ–γ energy, the user is interested in all combinations of energies of the γ quanta, except the situation where the x and y incrementer is exactly the same. (This would create on his matrix a diagonal line.)

If the user wants this interpretation—they should select the second option on the set of radio buttons shown on Fig. 8.

8. "ALL…" collective-incrementers, a list of other incrementers

Very often the user would like to create the sum spectrum of many variables/incrementers, for example, a sum spectrum of γ

Please cite this article as: J. Grębosz, The Cracow code—an interactive method of sophisticated online analysis, Computer Physics Communications (2006), doi:10.1016/j.cpc.2006.09.006

energies registered by all of the 105 germanium crystals. Such a "total" spectrum can be easily defined by placing on the list of X incrementers, the 105 incrementers representing the desired (calibrated) variables. However this can be inconvenient. To make such a task easier, there are some special, so-called, *collective-incrementers*, which are equivalent to the list (collection) of incrementers of the same kind. So, for instance, the long list of incrementers:

cluster_crys_A_1_energy_cal,
cluster_crys_A_2_energy_cal,
cluster_crys_A_3_energy_cal,
...
cluster_crys_R_7_energy_cal

can be substituted, by just one collective-incrementer called:

ALL_cluster_crys_energy_cal

The collective-incrementers (users like to call them: "ALL..." incrementers) save a lot of work when defining a spectrum. They are useful, when there are many detectors of the same kind (for example: many germanium cluster detectors, many Miniball detectors [1], many Hector BaF detectors [5]).

When using the "ALL..." collective-incrementers the definition of the γ–γ energy coincidence matrix is very simple, we just:

- place one collective-incrementer ALL_cluster_crys_energy_cal on the list of X-axis incrementers,
- place the same collective-incrementer ALL_cluster_crys_energy_cal on the list of Y-axis incrementers,
- we select the option that we are interested only in combinations where the particular incrementers (hidden inside these two "ALL..." collective-incrementers) are from different germanium crystals.

9. Manager of the user-defined spectra

The experimenter can create many user-defined spectra and all of them are on a special list handled in 'Cracow' GUI by a user-defined spectra manager. This manager allows us to modify existing definitions, remove, clone, or create brand-new. After any such change, the user has the option to immediately send his request to the currently running 'spy' (online analysis program). If 'spy' is currently not running, the changes will wait on the disk until the 'spy' has started next time.

10. User-defined conditions

The experimenter often needs to increment his user-defined spectrum only under specific condition. In the case of the RISING experiments, the most obvious condition is the selection of fragments which come out of the Fragment Separator and hit the target. The experimenter wants to increment his gamma-ray energy spectrum only when the target was hit by the desired projectile (fragment).

Of course there are also less obvious conditions, some of them are invented ad hoc just to see what is wrong with the experiment. So it is very important to give the user freedom over creating conditions. The user can define his condition swiftly online. The user-defined condition, once created by the user, is stored on the disk as a file, and can be used in all future analysis.

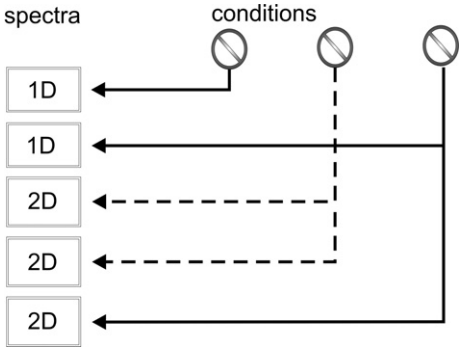

Fig. 9. User-defined spectra and user-defined conditions are separate objects in the C++ program. The user can assign any user-defined condition to affect any user-defined spectrum. The same condition can be assigned to more than one spectrum.

In the software described here, the condition is an independent object. The user creates the condition and may assign it to a user-defined spectrum. One condition can be assigned to more than one spectrum, see Fig. 9.

In this figure we see that a user-defined spectrum can have at most one condition assigned to it. (This is not a limitation, because conditions can be created, which contain a nested logic expression of other conditions.)

11. Condition wizard

The experimenter can create a new condition, or clone an existing one using the condition manager provided by 'Cracow' GUI. As conditions can have very complicated logic, the process of creating the condition is supported by a special instrument called a condition wizard. Let's look at it.

The first page of the wizard contains the simple question about the name of the object representing the condition. The user will refer to this name later when assigning the condition to spectra. To understand better the following, more difficult pages of the wizard, let's try to predict what elementary situations the user would like to test as a condition.

- Sometimes the user just wants to set a simple gate on one variable. For example, he wants to test if some energy is in the channel range 500–520. This kind of elementary condition we will call a *one-dimensional elementary condition*.
- Sometimes the user observes a matrix (created by two incrementers X and Y)—and he would like to have a condition selecting a fragment from this matrix, marked by a polygon with the shape of a banana, or a cloud. This kind of elementary condition we will call a *two-dimensional elementary condition*.

Actually, all we need are these two types of conditions. However, experience shows that the conditions the RISING experi-

Please cite this article as: J. Grębosz, The Cracow code—an interactive method of sophisticated online analysis, Computer Physics Communications (2006), doi:10.1016/j.cpc.2006.09.006

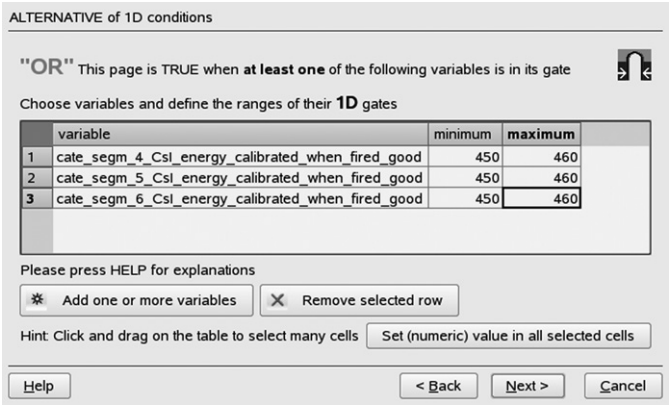

Fig. 10. A page of the condition wizard, which allows the creation of an alternative (OR) of 1D elementary conditions.

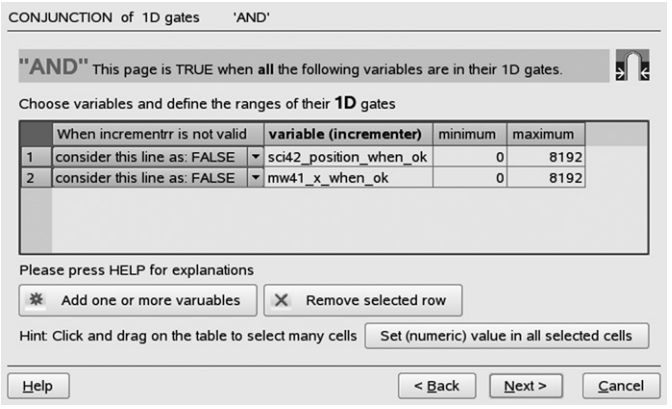

Fig. 11. If the user wants to create the conjunction of 1D elementary conditions, he should also specify how to precede if some of the incrementers do not contain the valid value. In the case of the alternative (OR) gating conditions it was not important, such a row with the elementary condition could be treated as false. With conjunction it is different; sometimes we need to treat it as true, sometimes as false.

menters need, are more complex. Every complicated condition though, can be constructed from these two elementary types, but... with a lot of clicking. So this approach would be too elementary and cumbersome. This is why the conditions available in 'Cracow' GUI are more complex. They allow more complex combinations of elementary conditions to be defined.

The conditions supplied by 'Cracow' GUI can be combinations of the following expressions:

- alternative of some 1D elementary conditions,
- conjunction of some 1D elementary conditions,
- alternative of some 2D elementary conditions,
- conjunction of some 2D elementary conditions,
- conditions of other conditions.

These five ways of defining conditions are available on the five following pages of the wizard. If the user does not need one of them—they simply leave this page empty.

11.1. "OR list" of the 1D elementary conditions

Fig. 10 shows a page of the wizard, where we can place a one-dimensional elementary condition.

To specify this part of the condition we should choose a variable and set a gate on it. It is easy: in the first row of the table there is a place for the variable name (the desired variable can be selected from a list of incrementers). Then, in the next columns, we can type two values: lower and upper limits of the gate. This is enough to create a definition of a simple condition—but very often the users need more.

If we want to have another gate on another variable, then it can be placed in the next row of this table. We can place in the rows of this table as many elementary conditions as we want. By this we create a list of elementary conditions. This list of elementary conditions has a logical value *true*, when at least one of them is *true*. More formally speaking, here the elementary conditions are creating the alternative (OR) of all of them.

$$\mathrm{row1} \vee \mathrm{row2} \vee \mathrm{row3} \cdots .$$

11.2. "AND list" of 1D elementary conditions

If the user prefers not the alternative, but the conjunction of his elementary conditions—the wizard offers this possibility on the next page, see Fig. 11.

At first glance, this page looks like the previous one, but there is an important difference. If we want to check the following conjunction

$$\mathrm{row1} \wedge \mathrm{row2} \wedge \mathrm{row3} \cdots$$

we should remember that sometimes the variable (incrementer), used in a row of this table, may not contain the meaningful value (because, for example, its detector did not fire). How should one make a conjunction of rows in such a case?

The quick answer: "let's treat this row as *false*" may not be a good solution. Imagine we want a condition telling us that all the registered γ quanta have their times in the channel range 500–600. Creating this condition we put the corresponding 105 γ-time variables (incrementers) in this table and we specify range 500–600. This would be wrong. By doing this we are creating a conjunction, which is almost never *true*, because it highly unlikely that all 105 detectors fire in the same event.

So treating a row with an incrementer from a detector which did not fire—as *false*—was not a good choice. Another possible answer: "the row with the variable (incrementer), which does not have a meaningful value, should be treated as *true*"—may also not be a good solution. Imagine, we want the conjunction of the elementary conditions related to the position of the ion as registered by the multiwire chambers.

$$\begin{aligned} &\mathrm{mw41\_x\_when\_ok} \quad \text{is in range } -5, +5 \\ &\mathrm{mw42\_x\_when\_ok} \quad \text{is in range } -5, +5 \end{aligned}$$

This condition should be *true*, when the horizontal position given by the multiwire chamber mw41 *and* the horizontal positions given by the multiwire mw42—are in a certain, small range. Unfortunately, in some events, one of these positions may be impossible to calculate (because the related multiwire

Please cite this article as: J. Grębosz, The Cracow code—an interactive method of sophisticated online analysis, Computer Physics Communications (2006), doi:10.1016/j.cpc.2006.09.006

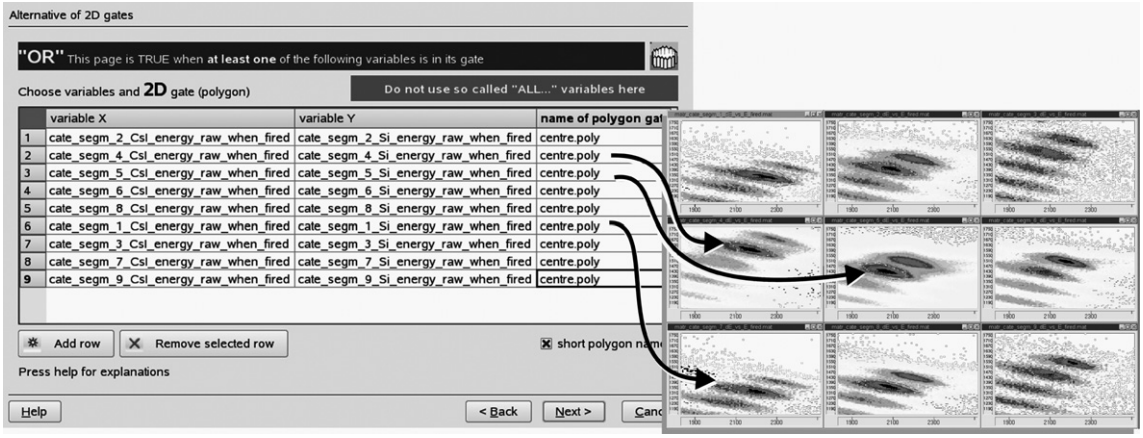

Fig. 12. The condition wizard offers also a page with an alternative (OR) of 2D elementary conditions. In the RISING experiment this was useful for the CATE detector, where the ion could hit only one of nine segments of the detector. As we see, in every row the elementary condition refers to a polygon gate called 'center'. However, there is no confusion, because the real, full name of each polygon also contains the string describing the name of the matrix where the polygon was created.

chamber did not fire in this event). So, how should one treat the row with such an elementary condition? The last example showed us that the solution "treat it as *false*" was not good. What to do? Treat it as "*true*"? No, it is obvious that if one of the multiwire chambers did not deliver the data—the elementary condition with corresponding incrementer should not be *true*. And the whole conjunction should be *false* as well.

As we see—sometimes we need one approach, sometimes the other. This is why the first column in the table contains the combo box, offering the choice.

What should we choose in a particular situation? The answer: "nobody knows this better than the experimenter himself"—is not realistic; especially in an experiment like those from RISING, where we have many new people working on each new experiment. So, to avoid confusion at this point in the condition wizard, the 'Cracow' software helps in making this choice. When the user is trying to use a variable (incrementer), which has a validator, a special wizard appears and suggests to the user what option he should (most probably) use for the incrementer in question.

11.3. Two-dimensional elementary condition on the "OR list"

The next page of the condition wizard deals with two-dimensional elementary conditions. When do we need such a condition? For instance, if the 'Cracow' GUI displays some matrix on the screen, we may draw on this matrix a polygon marking the interesting region. Such a polygon is not yet a condition; it is just a polygon defined by a set of vertices. However, we can use this polygon to create the elementary condition, just by specifying the names of two variables (x and y) and the name of the polygon.

The online analysis program during the analysis of every event will take the current values of variables x and y and check if the point $P(x, y)$ lies inside the polygon. If yes, such an elementary condition is considered as *true*.

On the corresponding page in the condition wizard of 'Cracow' GUI—we have a chance to define not just one 2D elementary condition, but the whole list of them, see Fig. 12. The logical value of the whole page is evaluated as the alternative (OR) of all the rows of this page.

In the first row of the table we can see the names of two variables, and then the name of the polygon. This example is taken from the data analysis made during the Fast Beam Campaign, where we were using the CATE detector [1]. The CATE detector is a chessboard of nine telescope detectors. The ion can hit one of these nine segments. If it does hit exactly one segment, we want to check if the values of dE and E registered by the corresponding segment are in the "banana gate" polygon, drawn on a related dE vs. E matrix.

This is why all nine elementary 2D conditions are on the list, and the logical value of this page is evaluated as the *alternative* (OR) of all elementary conditions (rows)

$$\text{row1} \vee \text{row2} \vee \text{row3} \vee \cdots \vee \text{row9}.$$

11.4. Two-dimensional elementary conditions on the "AND list"

The next page of the condition wizard is very similar to the previous one, but here all the listed elementary conditions are creating the conjunction. This is the most frequently used method of conditioning: we want some values on the X and Y variables to occur inside one polygon gate, AND we also want the current values of some other variables to occur inside another polygon related to other X and Y variables.

Fig. 13 shows the example of using the two-dimensional elementary conditions.

This page defines the condition, which is *true* when all the rows of this table containing the elementary condition are *true* (so: it is a conjunction of 2D elementary conditions)

$$(\text{row1} \wedge \text{row2} \wedge \cdots).$$

As it is a conjunction, here again arises the same problem of what to do if one of variables does not contain a meaningful value (because some detector did not fire and the calculation of some value was impossible). Should the row of the conjunction

Please cite this article as: J. Grębosz, The Cracow code—an interactive method of sophisticated online analysis, Computer Physics Communications (2006), doi:10.1016/j.cpc.2006.09.006

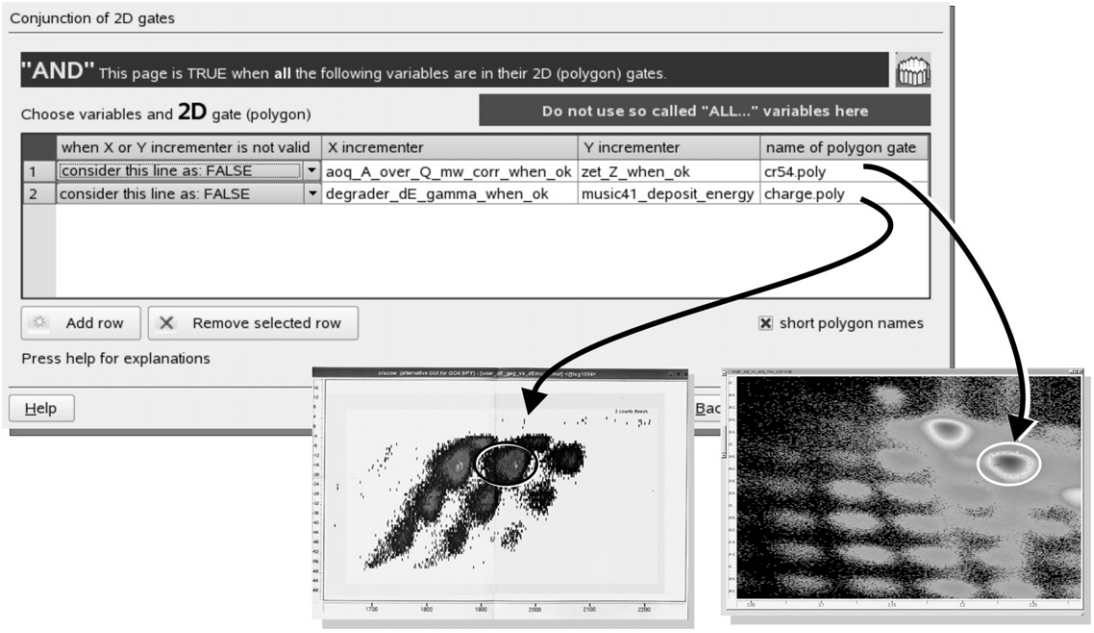

Fig. 13. The page of the condition wizard, where we can create the conjunction of 2D elementary conditions. Here, for example, this conjunction was used for better separation of the projectile coming from the fragment separator.

be in this case *false* or *true*? As there is no general answer—the user can specify case by case in the first column of the table.

11.5. Condition of conditions

The previous pages of the condition wizard can account for very sophisticated situations; with them the online analysis program was successfully used for months. However, the users demanded to have still another feature: the possibility to make logical expressions of other conditions.

When is this useful? If the user has already prepared the condition helping him to select the correct ion coming out of the fragment separator—he can use it in a more precise form, by cloning it and enriching it with additional elementary conditions. This is the correct procedure but, due to cloning, the same elementary conditions ("*is a point lying inside the polygon or not?*") will be evaluated twice for the same event, this is not efficient.

So now there is another, more economic solution. The user can say: *"I want a new condition which is true when the other condition is true, plus some extra condition. Here is this extra condition. . . "*. During the definition of his new condition—the user can also refer to the current values (*true/false*) of other conditions. This is very convenient, but is not only a matter of comfort or economy. The problem first arose when the users wanted a veto detector. There was then a need to build the condition which is *false* if some other condition is *true*.

From all these demands came the special page in the condition wizard, see Fig. 14.

On this page we can see four tables. In each of them the user can place the names of other conditions. (To be user friendly the user need only click and choose them from the list of already existing conditions.) The four tables represent the common logical operations. The first table is dedicated to the AND operator, this means that the user requires all the conditions placed here to be *true* (a conjunction of conditions). The OR table is similarly available (an alternative of conditions). For negation operations—tables with the operators NOR and NAND are provided.

We can see the four tables on this page of the wizard. We do not have to use them all. If some of them are left empty, they are considered to be non-existing. Those tables, which have some content, should be *true*. The logical value of this whole page of the wizard is a conjunction of these four tables.

11.6. Nesting of the conditions is done with care

The possibility of placing the names of other conditions is very powerful, especially as these other conditions can also refer to other existing conditions. So finally we can create a chain of conditions. The length of such a chain is not limited.

However there is a risk that some condition may appear twice in the chain, that would create an infinite loop of conditions to check. For instance: condition A refers to condition B, B refers to C, C refers to D, and D refers to B. By this, the infinite circle $B \to C \to D \to B \to \cdots$ is created. The analysis program will start analysing the first event and will spend the rest of its time jumping from condition to condition not knowing which of them should be evaluated first.

To avoid this error, during editing of the condition 'Cracow' GUI the wizard immediately checks to see whether the user has tried to create such an infinite loop. If such a loop has been created, the user is warned about the logical error.

There is no such risk if we create a brand-new condition—it is new, so no other condition can be referring to it. But if we are modifying a condition created earlier, some other conditions can already be using the now modified one on their lists. We may not remember (or know) this, so we could inadvertently

Please cite this article as: J. Grębosz, The Cracow code—an interactive method of sophisticated online analysis, Computer Physics Communications (2006), doi:10.1016/j.cpc.2006.09.006

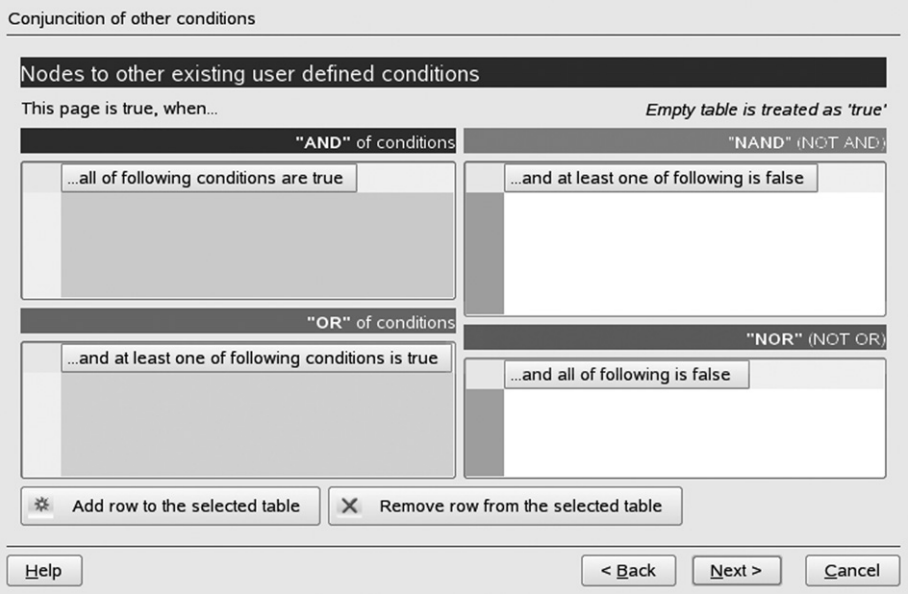

Fig. 14. Using this page of the condition wizard, the user can create any kind of logical expression from the other previously defined conditions.

created an infinite loop in our conditions. Fortunately—this error will be immediately signalled by the wizard. The wizard is even more careful here, as it checks not only the "direct" references, but also the indirect ones. An indirect reference is when we refer to a condition, which is at the beginning of a long chain and also features somewhere further along the chain.

Note that for simplicity here we speak about the 'chain', but as one condition can refer to many conditions at the same time (for example, there can be many names of conditions placed on the AND table—Fig. 14), so actually this system creates not a 'chain', but a 'tree' of conditions. This is no problem, the wizard is sophisticated enough to test all the branches of the tree. The wizard knows that the same condition can be referred to in different branches of the tree, but should never exist twice in the same branch.

This (at first glance) complicated algorithm is, of course, only a problem for the GUI programmer. The user does not have to think about the tree-structure of the condition. He will be only warned if he tries to create an invalid loop.

11.7. Veto conditions

As we have already mentioned, one of the reasons why the users demand the option to create logical expressions of conditions was for the experiments using veto detectors. The ability to implement the negation operator was very important.

If there is only one such detector in the experiment, it is not difficult for a beginner-user to prepare a veto-condition. At first he creates the condition pretending that he wants to accept events, when the veto detector not only fires, but also delivers the data in the forbidden range. Having done this, the user creates a second condition, goes directly to the last page of its wizard—condition of conditions—and here he puts the name of the first condition in the table related to the NAND, or NOR table. (If there is only one condition in the table, then it does not matter whether it is the NAND or the NOR table.) This negation is simple even for beginners.

With two veto detectors, some people have problems. This is not related to the software. Simply: many people do not remember the rules of logic. Here is an example: the user has already created two conditions specifying that his two veto detectors—det A and det B—have fired and registered forbidden situation. Now the user wants to create the condition which is *true*, when veto detector A was "not protesting", AND veto detector B was "not protesting" as well. Shortly speaking the user wants such a situation

$$(\neg \det A) \wedge (\neg \det B).$$

Unfortunately not everybody remembers De Morgan's law:

$$(\neg A) \wedge (\neg B) \equiv \neg(A \vee B).$$

This rule shows that the names of the two veto conditions should be placed on the NOR list. This list is represented by the table in the lower right corner, see Fig. 14.

Rules are rules, but we should understand that sometimes the user is creating his condition during a night shift, and is very tired. To be really user friendly, the wizard supplies the "human language" explanation on the top of the NOR table ("[true,] when all of following [conditions] are false").

11.8. Finishing the condition definition, and assigning it to a spectrum

As we have seen, the condition wizard has several pages where we can specify the lists of elementary conditions, which will be tested (by the online analysis program) every event. Very often users use only one of these pages to specify their wishes. The empty (unused) page has a logical value—*true*. The final logical value of the whole condition is a conjunction of all the 5 pages. This seems to come naturally for all users.

Please cite this article as: J. Grębosz, The Cracow code—an interactive method of sophisticated online analysis, Computer Physics Communications (2006), doi:10.1016/j.cpc.2006.09.006

When the user finishes the definition of the condition, the condition wizard saves this definition on the disk. So far the condition exists, but no spectrum uses it. Even if we apply this condition to the currently running 'spy' (online analysis program), 'spy' will not start testing this condition on the analysed events. The 'spy' knows that no spectrum (or other condition) waits for the result of such a test, so saves it time by not checking it. To be tested, the condition has to be assigned to a spectrum, or has to be used by another condition.

Assigning a condition to any user-defined spectrum is simple. We return to the definition of a spectrum, we open it using the spectrum wizard and on the wizard's last page (Fig. 6), there is a combo box with the list of all current existing conditions. By selecting one of them, we assign the chosen condition to this spectrum. From now on this is a conditional spectrum; it will be incremented only if the assigned condition is *true*.

After closing the spectra wizard, the GUI checks if the online analysis program ('spy') is currently running. If it is, the GUI asks if it should send this new definition to the 'spy'. If the definition is sent, the 'spy' opens the definitions of the spectra or conditions and then continues its normal work. The next events analysed by the 'spy', will be tested by the new condition and the new conditional spectrum incremented (or not). Once more we should underline the fact that: introducing even the most sophisticated conditional spectra can be done without the need to recompile the spy program; even without stopping it.

12. Self-gate

The user-defined spectra wizard and the user-defined conditions wizard described above—are very powerful tools. They give the experimenter the possibility to create any kind of spectrum which he needs. Unfortunately sometimes the cost is very high. In this case the cost is amount of clicking needed to create the desired conditional spectrum. If, for some chosen spectrum, we need to create (for example) 105 conditions—the solution is tedious and error prone; hence (from the logical point of view)—purely correct.

Let's take a good illustration from the everyday practice of RISING experiments: the total (sum) spectrum of all the energies registered by the germanium crystals. As these energies are gain-matched we can sum them and create the "total" spectrum. If the user wants such a spectrum all he needs to do, is to define it with a wizard. Using the wizard, on the page dedicated to the X incrementers, he needs to put

- either 105 incrementers
  cluster_crys_A_1_energy_cal
  ...
  cluster_crys_R_7_energy_cal
- or—even faster—a collective-incrementer called:
  ALL_cluster_crys_energy_cal.

After producing such a definition, the expected spectrum will be created by the online analysis. Of course, this definition is nothing special; such a total spectrum is already among the standard spectra supplied by default by the online analysis program ('spy'). The experimenter usually wants something more sophisticated; he wants this spectrum to be collected under some condition.

Let us assume that the user needs a condition where the time-of-flight value (measured by a set of scintillators) is in some particular range (of picoseconds). No problem, all the user has to do is to start the conditions wizard, which is an instrument designated to create such a condition. On the second page of the wizard, the user defines the 1D elementary condition—using variable (incrementer) called: tof_21_41_tof_in_picoseconds_when_ok. After creating such a condition and assigning it to the spectrum, the work is done. The logic of this is clear—even for a beginner.

Unfortunately some beginners tend to use the same logic in cases of some special kinds of conditions. For example: the user wants to collect the same total energy spectrum of gamma detectors, under the condition that the times registered *by the same* germanium *detectors* are in range, say, 4000–4020.

The user starts the condition manager and puts 105 incrementers related to the calibrated times of the germanium detectors in the table 1D AND. (If the user is clever, instead of 105 incrementers, he will use one collective-incrementer called "ALL_cluster_crys_time_cal" which gives the same effect.)

If the user assigns such a condition to his spectrum and starts the analysis of data, he is surprised that the spectrum remains almost empty. Seeing this, he checks the condition manager statistics list; here he can see that his condition is never *true*. No wonder, it is almost never the case that all the detectors that fire register the values of time in the same desired range. If one of them is outside, the whole condition is *false*.

The user realises his error: "*Perhaps it was nonsense to put incrementers on the AND list?*" The user opens the wizard to modify the condition, and he moves his incrementers from the page "1D AND" to the next page "1D OR".

After this modification—the conditional spectrum starts to grow quickly. It is incremented many times, but looking at this spectrum, an experienced user can easily tell that the condition does not work as it was expected. The spectrum is incremented by such γ quanta, which—for sure—were registered with times outside of desired region. So, what is wrong?

The shortest, but metaphoric answer would be: in the "logical expression" that the user creates by defining his conditional spectrum he put the parenthesises in the wrong place. Due to this error, if (in the particular event) we registered 22 γ quanta, and only one of them had a time value lying in the desired range, the condition will be *true* (because it is: OR). So the spectrum will be incremented. *Note*: it will be incremented by all of its incrementers; so by the one γ energy with "good time", and also by 21 "unwanted" γ energies, which were "out of the time range" (i.e. a total of 22 incrementers). Fig. 15 shows the scheme of such a defined conditional spectrum.

The correct way of producing such a conditional spectrum is shown on Fig. 16.

As we see here, every energy incrementer should be used to produce its own spectrum under its own, private condition (a condition, which is set on the corresponding time incre-

Please cite this article as: J. Grębosz, The Cracow code—an interactive method of sophisticated online analysis, Computer Physics Communications (2006), doi:10.1016/j.cpc.2006.09.006

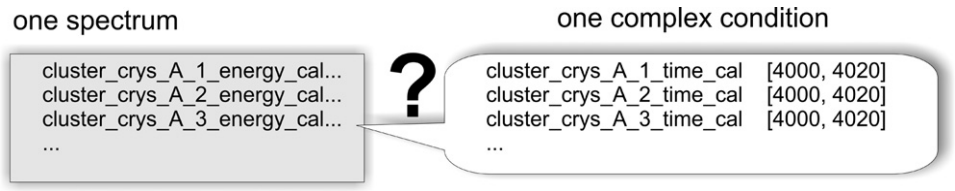

Fig. 15. A very common error, usually made by beginners during defining a conditional sum spectrum. It is not enough to create just one condition and depending of its current logical value, increment the spectrum (or not). The proper solution is shown on the next figure.

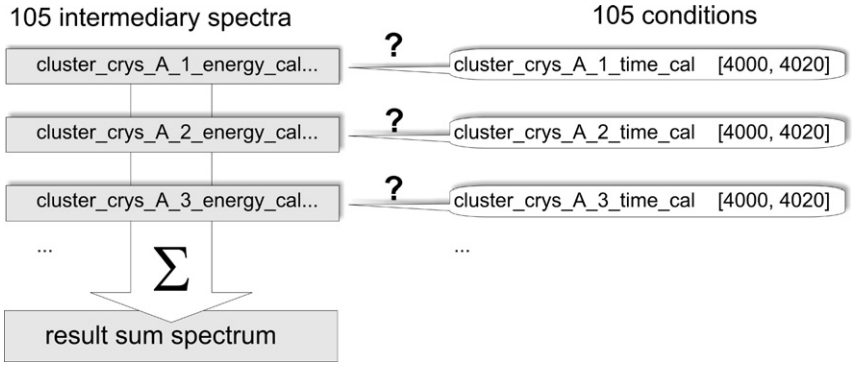

Fig. 16. The correct way of creating the conditional sum spectrum. Unfortunately this requires creating 105 intermediary conditional spectra. To avoid this—there is a better tool, called a self-gate.

menter). So, for example, we should make a definition of the energy spectrum of detector k, under the condition that the value of the time incrementer from detector k is *true*. We need 105 conditional spectra of this kind. Then, they all have to be summed to produce one 'total' spectrum. The summing of the spectra is not a problem; the 'Cracow' GUI provides this feature. The sum spectrum can be created easily and the sum in made not only once, but it is updated every 30 seconds, so the sum spectrum is automatically growing together with all the spectra which contribute to its sum.

The real problem is that the user has to create 105 spectra and 105 conditions. Even when taking advantage of the cloning option—this is a lot of clicking. This is not a user friendly solution; especially since during an experiment, such a spectrum is needed to be observed as soon as possible.

To make this task easy, a special feature has been provided. It is a small condition which we can assign to an individual incrementer placed in the spectrum definition. This specific type of condition is called a "self-gate", because *it checks other variables belonging to the same detector* to which the original incrementer belongs.

For example, if an incrementer represents the value of calibrated energy registered by the cluster crystal F4, we can assign to this incrementer a self-gate, and this self-gate will allow us to check if the calibrated time information in this same detector, F4, is in the desired range. In this case we do not have to specify that we mean the F4 detector. The self-gate looks at the incrementer to which it is assigned and recognises which detector is in question.

If the self-gate condition in a particular event is *true*, the "self-gated" incrementer is allowed to increment the spectrum. If it is *false*, the incrementer is treated (in this event) as non-existing.

The self gate has its own name, so we can apply the same self-gate to many incrementers. The self-gate can check much more than just the time value information. We can even use it to set a gate on the scattering angle or on the constant Θ and Φ angles—describing the geometric position of this detector (Fig. 17).

The self-gate is a tool which saves us from creating many conditions and many intermediate spectra, when we actually need only one. This tool is useful in cases where:

- we have many detectors of the same kind,
- each of them offers several kinds of incrementer (energy, time, scattering angle, angles of their position),
- one type of incrementer has to be summed to create a sum (total) spectrum...,
- ... only if some other variable (in the same event) of the same detector, fulfils some 1D condition.

In the case of the RISING experiments it was useful to support self-gates for:

- Germanium cluster detectors,
- Germanium detectors belonging to the Miniball array,
- BaF detectors belonging to the Hector array,
- the addback algorithm incrementers—used for all the above types of detectors (not discussed in this paper).

As we have seen, the self-gate simplifies the creation of the user-defined spectra. To prove its simplicity, let us look at an example. We need the total energy spectrum of cluster detectors under the condition that the corresponding times are in the selected channel region 4000–4020. To define such a spectrum we should:

Please cite this article as: J. Grębosz, The Cracow code—an interactive method of sophisticated online analysis, Computer Physics Communications (2006), doi:10.1016/j.cpc.2006.09.006

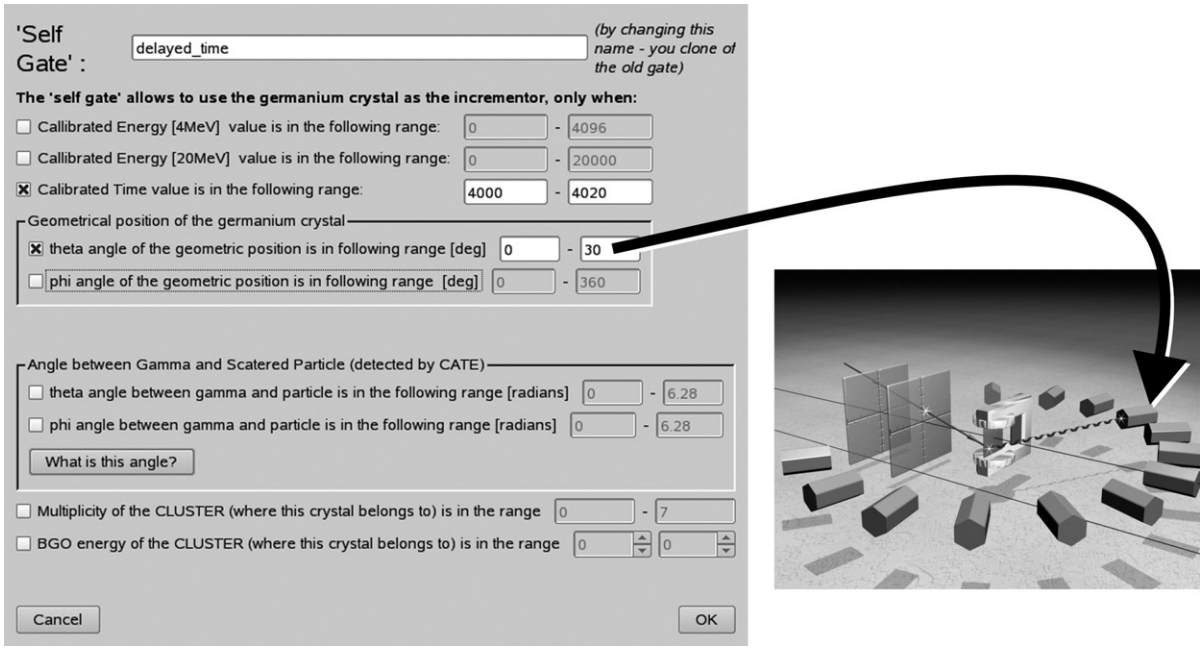

Fig. 17. A dialogue box for the definition of a self-gate used for cluster detectors (with VXI electronics). As we see, the self-gate can be set not only in the time, but also on many other variables belonging to the same germanium crystal. Here—for illustrative purposes—we can see that is was also set on the angular position of the detector.

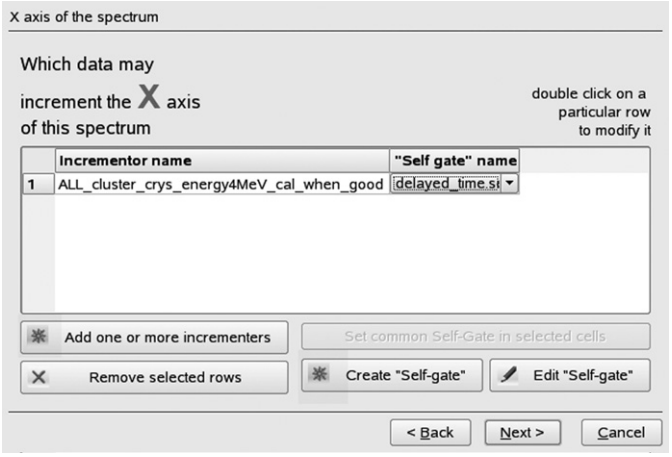

Fig. 18. Thanks to the self-gate, just on one page of the spectrum wizard we can create the conditional sum spectrum described earlier in Fig. 16.

- create the 1D user-defined spectrum, where there is one collective-incrementer ALL_cluster_crys_energy_cal_when_good,
- create a self-gate with the condition on the desired time range,
- assign this self-gate to the incrementer.

All this can be done on one page of the spectrum wizard (Fig. 18).

How does the online analysis program ('spy') proceed in the case of such a spectrum definition? For every event it will try to increment our spectrum. In the definition of this spectrum, the 'spy' sees one incrementer—the collective-incrementer (which is actually the list of 105 incrementers). The analysis program will take each of them and before using each, will go to the related detector to validate the corresponding time (checking the self-gate). Those incrementers, for whom their self-gate condition is evaluated as *true*, will be allowed to increment the spectrum.

To conclude this part, let's underline once more: from the logic the point of view, the self-gate is not necessary. All possible conditional spectra can be created by the spectra wizard and the condition wizard without self-gates. However, the self-gate allows making such definitions much simpler.

13. Online, near-line, offline analysis

The system described here makes the analysis swift enough so that it is really online. The events are coming directly from the data acquisition system in their raw form. Of course the analysis could be faster if the events were not raw, but already pre-sorted and stored on the disk in some optimised form (for example, as a so-called ROOT tree [6]). But an experiment like RISING—needs the analysis to be really online. This is especially true during the startup phase of the experiments, when the experimenter keeps one hand on a potentiometer, changing settings, while watching the expected immediate effect on the online conditional spectrum.

The 'Cracow' GUI strictly collaborates with the online analysis program 'spy' used in the RISING experiment. Here we were discussing the 'Cracow' code, but it is worth saying, that the 'spy' is based on the Go4 library [7]. Thanks to this, the events for the analysis can be obtained either online (from the DAQ system), or from the "event by event" (list mode) data file stored by the DAQ on the disk a few minutes earlier. This mode of work (a *near-line analysis)* has an advantage that 100% of events are analysed (while in the online mode—only some frac-

Please cite this article as: J. Grębosz, The Cracow code—an interactive method of sophisticated online analysis, Computer Physics Communications (2006), doi:10.1016/j.cpc.2006.09.006

tion, depending on a counting rate and complexity of the online analysis algorithms).

No matter what mode (online, near-line) of analysis the user chooses, he can use the same tools described in this paper for defining his analysis. The users like this fact, they often ask to install spy/Cracow code on their Linux laptops, because—after experiments—when they return to their home laboratories they would like to continue their analysis offline with the help of the spy/Cracow code.

Some users even ask if it would be possible to implement the Cracow code to analyse the data taken in different laboratories. Yes, it would, but—as the 'Cracow' code is strictly collaborating with the 'spy'—their local program for offline analysis (their local 'spy') should be modified, to:

- 'publish' its list of available incrementers (variables) specific to a particular experiment,
- implement the object oriented procedures responsible for handling the user defined definitions created by 'Cracow code' (spectra and conditions).

As most physicists nowadays understand that good analysis software [8] should be written using the object-oriented technique—the adaptation of such object-oriented software should not be difficult.

14. Final impressions of the author

The system of interactive creation of the user-defined spectra and user-defined conditions, was invented as a solution to make the experimenters independent (of me), by giving them a universal instrument to go through a long commissioning phase. When this phase was over, we were still profiting from this tool, so the system was constantly being improved. New users coming for the new experiments are learning this tool surprisingly quickly. Soon they forget that in their hand they have complicated software—they are now talking only about the physics seen on the screen. The physics, "extracted" by themselves—from millions of numbers.

Acknowledgements

The 'Cracow' GUI project would probably never exist without the enthusiastic experimenters and members of the RISING project. Also special thanks go to Joern Adamczewski, who patiently explained to me the mysteries of GO4 and to Steven Steer for fruitful discussions about this text.

I would like to express my gratitude to many unknown friends, the creators of the KDevelop project [9].

This work has been partly supported by the Polish Ministry of Education and Science (Grants Nr. 1 P03B 030 030 and 620/E-77/SPB/GSI/P-03/DWM105/2004-2007).

References

[1] H.J. Wollersheim, et al., Rare ISotopes INvestigation at GSI (RISING) using gamma-ray spectroscopy at relativistic energies, Nucl. Instr. Methods in Phys. Res. A 537 (2005) 637.
[2] J. Simpson, Z. Phys. A 358 (1997) 139; Achievements with the EUROBALL, in: W. Korten, S. Lunardi (Eds.), Scientific and Technical Report 1997–2003, 2003.
[3] H. Geissel, et al., Nucl. Instr. Methods B 70 (1992) 286.
[4] H. Essel, J. Hoffmann, N. Kurz, R.S. Mayer, W. Ott, D. Schall, IEEE Trans. Nucl. Sci. NS-47 (2) (2000) 337.
[5] A. Maj, et al., Nucl. Phys. A 571 (1994) 185.
[6] http://root.cern.ch/.
[7] http://www-w2k.gsi.de/go4.
[8] B. Jacobsen, Applying object-oriented software engineering at the BaBar collaboration, Nucl. Instr. Methods in Phys. Res. A 389 (1997) 1.
[9] http://www.kdevelop.org.

Please cite this article as: J. Grębosz, The Cracow code—an interactive method of sophisticated online analysis, Computer Physics Communications (2006), doi:10.1016/j.cpc.2006.09.006

Available online at www.sciencedirect.com
ScienceDirect
Physics Letters B 647 (2007) 237–242
PHYSICS LETTERS B
www.elsevier.com/locate/physletb

The $T = 2$ mirrors ^{36}Ca and ^{36}S: A test for isospin symmetry of shell gaps at the driplines

P. Doornenbal [a,b], P. Reiter [a,*], H. Grawe [b], T. Otsuka [c,d], A. Al-Khatib [e], A. Banu [b], T. Beck [b], F. Becker [b], P. Bednarczyk [b,f], G. Benzoni [g], A. Bracco [g], A. Bürger [e], L. Caceres [b,h], F. Camera [g], S. Chmel [e], F.C.L. Crespi [g], H. Geissel [b], J. Gerl [b], M. Górska [b], J. Gręboszb,f], H. Hübel [e], M. Kavatsyuk [b,i], O. Kavatsyuk [b,i], M. Kmiecik [f], I. Kojouharov [b], N. Kurz [b], R. Lozeva [b,j], A. Maj [f], S. Mandal [k], W. Meczynski [f], B. Million [g], Zs. Podolyák [l], A. Richard [a], N. Saito [b], T. Saito [b], H. Schaffner [b], M. Seidlitz [a], T. Striepling [a], Y. Utsuno [c,d], J. Walker [b], N. Warr [a], H. Weick [b], O. Wieland [g], M. Winkler [b], H.J. Wollersheim [b]

[a] *Institut für Kernphysik, Universität zu Köln, Zülpicher Straße 77, 50937 Köln, Germany*
[b] *Gesellschaft für Schwerionenforschung, Planckstraße 1, 64291 Darmstadt, Germany*
[c] *Department of Physics and Center for Nuclear Study, University of Tokyo, Hongo, Tokyo 113-0033, Japan*
[d] *RIKEN, Hirosawa, Wako-shi, Saitama 351-0198, Japan*
[e] *Helmholtz-Institut für Strahlen- und Kernphysik, Universität Bonn, Nussallee 14-16, 53115 Bonn, Germany*
[f] *The Niewodniczanski Institute of Nuclear Physics, Polish Academy of Sciences, ul. Radzikowskiego 152, 31-342 Krakow, Poland*
[g] *Dipartimento di Fisica, Università di Milano, and INFN Sezione di Milano, Via Celoria 16, 20133 Milano, Italy*
[h] *Departament de Física Tèorica, Universidad Autonoma de Madrid, E-28049 Madrid, Spain*
[i] *Taras Shevchenko Kiev National University, Ukraine*
[j] *Faculty of Physics, St. Kliment Ohridski University of Sofia, 1164 Sofia, Bulgaria*
[k] *Department of Physics and Astrophysics, University of Delhi, Delhi 110 007, India*
[l] *Department of Physics, University of Surrey, Guildford GU2 7XH, UK*

Received 18 September 2006; received in revised form 29 January 2007; accepted 1 February 2007

Available online 8 February 2007

Editor: V. Metag

Abstract

The first excited 2^+ state of ^{36}Ca has been identified by its γ-decay, exploiting the two-step fragmentation technique at the FRS-RISING setup at GSI. This is the heaviest $T_z = -2$ nucleus in the Segré chart in which a γ-decay of an excited state has been observed. A stable beam of ^{40}Ca at 420A MeV impinged on a primary ^{9}Be target. Out of the secondary beam of fragmentation products, ^{37}Ca was separated by the FRS and struck on a second ^{9}Be target at the final focus of the FRS. The energy for the 2^+_1 decay of ^{36}Ca was determined to be 3015(16) keV, which is 276 keV lower than in its $T = 2$ mirror ^{36}S. This mirror energy difference (MED) is discussed in the framework of shell model calculations using a ^{16}O core, the *sd* shell isospin symmetric interaction USD and experimental single-particle energies from ^{17}O and ^{17}F. The results show that the MED within the *sd* shell provide a sensitive test for the evolution of the $N, Z = 14, 16$ subshell gaps towards the driplines. Especially the $N, Z = 16$ gap is determined by Thomas–Ehrman shift in the $A = 17$, $T = 1/2$ isospin doublet, while Coulomb effects are found to have marginal influence.

PACS: 21.60.Cs; 23.20.Lv; 25.70.Mn

Recently, the Coulomb energy difference ΔE_C of isobaric analogue states and especially the MED in $T_z = \pm T$ pairs of nuclei have been extensively studied. In connection with pre-

* Corresponding author.
E-mail address: peter.reiter@ikp.uni-koeln.de (P. Reiter).

0370-2693/$ – see front matter
doi:10.1016/j.physletb.2007.02.001

cise large-scale shell model calculations these quantities have proved to be a sensitive spectroscopic probe to investigate orbital radii in excited states [1] and the reduced overlap of identical proton and neutron orbitals at the driplines [2]. The MED, defined as $\Delta E_M = E_x(I, T_z = -T) - E_x(I, T_z = +T)$, will be positive for increasing spin I due to alignment and therefore reduced Coulomb repulsion. This can be partly counterbalanced by a reduced orbital overlap as this quenches the two-body matrix elements. The latter effect would have a strong impact on the evolution of (sub)shell gaps. The new $N = 14(16)$ shell stabilisation in $Z = 8$ oxygen isotopes and the $N = 20$ shell quenching in $^{32}Mg_{20}$ below the $Z = 14$, 16 subshells are expected to be dominated by the monopole part of the two-body interaction. Moreover, the scenario is anticipated to be symmetric with respect to the isospin projection T_z and may only slightly be affected by decreasing neutron binding energies [3]. On the other hand, the proton-rich mirror $Z = 20$ (Ca) nuclei are situated close to the proton dripline which may destroy the T_z symmetry. Therefore, the ideal site in the Segré chart where the competing scenarios can be investigated is the $N = 20$ mirror region along the light Ca ($Z = 20$) isotopes. The lightest Ca isotope with detailed spectroscopy is ^{38}Ca, while no excited states are known for the $N = 16$ isotope, and ^{34}Ca is already particle unbound.

For the mirror pair ^{38}Ca and ^{38}Ar the MED of the first excited 2^+ state (^{38}Ca; $2_1^+ - {}^{38}$Ar; $2_1^+ = 39$ keV) is positive, which is expected for a hole configuration due to the different Coulomb repulsion in the 0^+ ground state (g.s.) and excited state. Within a fixed j^n multinucleon configuration the MED changes sign with ph conjugation [4]. A negative MED may be anticipated by approaching the proton dripline. Here the question arises whether the quenching of the two-body interaction due to a reduced orbital overlap may cause the opposite energy shift. Crucial experimental information can be deduced from a measurement of ^{36}Ca; $2_1^+ - {}^{36}$S; 2_1^+, the heaviest $T = 2$ mirror nuclei studied so far.

The FRS-RISING setup [5,6] was used to identify excited states in ^{36}Ca, especially the $2_1^+ \rightarrow 0^+_{\text{g.s.}}$ decay, employing the two step fragmentation technique. A primary beam of ^{40}Ca, provided by the heavy-ion synchrotron SIS with an energy of 420 A MeV, was incident upon a 4 g/cm^2 ^{9}Be target at the entrance of the FRS. The average beam intensity was 3×10^8 ions/s. The ^{37}Ca fragments of interest were selected and identified in-flight on an event-by-event basis using their magnetic rigidity Bρ, their time of flight between the two scintillation detectors SCI1 and SCI2, see Fig. 1, and their energy loss in the multi sampling ionization chamber MUSIC. In order to optimize the secondary ^{37}Ca beam at the final focus, a wedge-shaped aluminium degrader of 2.31 g/cm^2 was placed at the middle focal plane of the FRS, so that $\approx 85\%$ of the incoming detected ions were ^{37}Ca.

At the final focus, 2×10^3 ^{37}Ca ions/s impinged on a secondary 700 mg/cm^2 ^{9}Be target at an energy of 196 A MeV. The reaction products were selected using the calorimeter telescope array CATE [7], consisting of 3×3 Si–CsI(Tl) modular $\Delta E - E$ telescopes. The energy loss in the Si detectors provided a good charge resolution for unambiguous Z identification after the secondary target. Due to the relatively large momentum transfers in the secondary reactions, the velocities of the reaction products were spread out. Thus, the total energy spectrum did not provide for a complete mass resolution.

The γ-rays emitted by the fragmentation products were measured with 15 Cluster Ge detectors, containing 7 crystals each, and positioned in three rings at extreme forward angles of 16°, 33° and 36° with an opening angle of 3°. In addition, 7 six-fold segmented MINIBALL triple Ge detectors were arranged in two rings with central angles of 51° and 85° relative to the beam line at forward angles. The HECTOR array [8], consisting of 8 large volume BaF_2 detectors, was situated at angles of 85° and 142°. The position sensitivity of the MINIBALL detectors allowed them to be placed at a close target distance of 250 mm, while the Cluster and HECTOR detectors sat at greater distances of 700 and 300 mm, respectively.

In order to obtain the best energy resolution for the γ-rays emitted in flight ($\beta = 0.545$), an excellent tracking of the moving nuclei is mandatory. Different from the RISING setup described in [6], an additional thin position sensitive Si ΔE detector with the dimensions of 5×5 cm^2 was placed directly after the secondary target. Together with the CATE Si ΔE detectors the fragment trajectories were determined with a position resolution of 3×3 mm^2 [7].

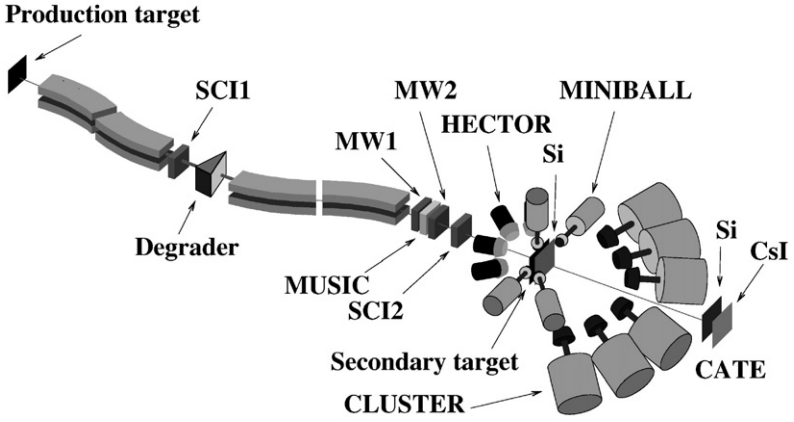

Fig. 1. Schematic layout of the RISING setup at the FRS. See text for details.

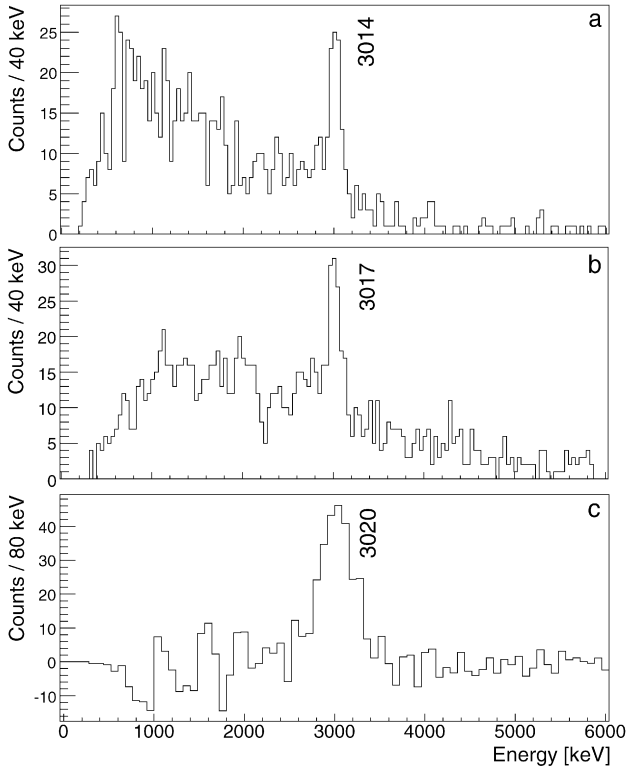

Fig. 2. Doppler corrected ^{36}Ca gated γ-ray spectra measured with the Cluster (a), MINIBALL (b) and HECTOR (c) detectors. For (c) the background was subtracted.

A precise Doppler correction has to take into account the expected lifetime of the decaying state. Since most of the decays of ^{36}Ca took place within the secondary target (the time of flight through the target was 23 ps), assuming a comparable half-life for excited states as in the mirror nucleus ^{36}S, the average β for the Doppler shift correction was given by a Monte Carlo simulation with GEANT4 [9]. The simulation included the reduced velocity due to the energy necessary to ablate nucleons [10] and the momentum distribution from the fragmentation process [11]. Deviations of this mean value, which mainly originated from the fragmentation of the primary beam, were corrected using the time of flight information from the intermediate to the final focus.

The main source of background γ-rays originated from particles identified as Ca in the CATE Si detectors that fragmented during the stopping process in the CATE CsI(Tl) detectors. These events could partially be discriminated from events that occurred in the target by imposing narrow time gates for the particle-γ conditions. Further background reduction was obtained by setting energy cuts in the CsI(Tl) detectors. The total energy deposition of the ^{37}Ca secondary beam particles in the CsI(Tl) detectors was also measured for events without γ-ray coincidence.

Another difficulty to overcome in the analysis was the high $2^+_1 \rightarrow 0^+_{\text{g.s.}}$ transition energy around 3 MeV, implying γ-ray energies of more than 5 MeV in the laboratory frame for the Cluster detectors at forward angles due to the Doppler shift. GEANT4 simulations showed, that single-hit photo peak events are then disfavoured with respect to single escape and Compton scattering events. Hence, for the Cluster detectors only add-back events which required a γ-ray multiplicity of two individual energy signals were accepted in the analysis. In the case of the MINIBALL detectors the crystal segmentation was used to determine events that scattered within the crystal. This condition also improved the peak to background ratio drastically for observed high energy γ-ray transitions in ^{36}Ca and other fragmentation products.

The obtained Doppler corrected γ-ray spectra gated on ^{36}Ca for the three different detector types are displayed in Fig. 2. An energy resolution for the $2^+_1 \rightarrow 0^+_{\text{g.s.}}$ transition of 4.3(6)% was achieved for the Cluster detectors and 4.9(10)% for the MINIBALL detectors. These values are close to the simulated values of 3.8% and 4.5%, respectively. The measured energies of γ-ray transitions from the strongest reaction channels served as consistency check for the correct energy. Known transition energies deviated less than 5 keV with respect to literature values. Differences are expected due to unresolved weak components of close lying γ-lines, Compton-edge components of higher energy transitions and unknown feeding times. The resolution of 14% for the HECTOR array forbids a comparison with known transition energies. Thus, it was excluded in the assignment of a ^{36}Ca transition energy, however the measured HECTOR energy also provided a consistent result for the interesting decay. For the Ge detectors the statistical error of the observed ^{36}Ca γ-transition energy has been determined to be 15 keV, which yields, including the previously mentioned error for known transitions of 5 keV, an assignment of the $2^+_1 \rightarrow 0^+_{\text{g.s.}}$ transition to 3015(16) keV. The spin assignment is based on a comparison to the mirror nucleus and on shell model calculations. The 3020 keV peak observed in the HECTOR array is in good agreement with this value. A recent experiment at GANIL has also detected a γ-ray transition at 3025(30) keV in ^{36}Ca [12].

Comparing with the $T = 2$ mirror nucleus ^{36}S, an experimental mirror energy difference $\Delta E_M = E(^{36}\text{Ca}) - E(^{36}\text{S}) = -276(16)$ keV is measured for the $I^\pi = 2^+_1$ states. The new value is about a factor of 5–10 larger than MED observed for $T = 1$ states in the sd shell [13] and predominantly single-j valence $T = 1$ states in the $f_{7/2}$ shell [1,4]. Surprisingly, the Coulomb energy difference for the corresponding $T = 2$ states in ^{36}Cl is only $\Delta E_C = E(^{36}\text{Cl}) - E(^{36}\text{S}) = -27(4)$ keV [14]. This is summarised in Fig. 3, where experimental MED for $I^\pi = 2^+_1$ states of the $1s0d$ shell and the adjacent $0p$ and $1p0f$ major shells are shown. Data are from this work and Refs. [4, 13,15–18]. Though in general the $T = 2$ MED are larger than the $T = 1$ values, which may be due to the proton-rich partner lying closer to the dripline, the unique $A = 36$ and $A = 14$ cases are obvious. Here the first excited $I^\pi = 2^+$ states at the proton-rich side are already unbound.

Due to the known subshell closure for $Z = 16$ in ^{36}S and the anticipated one in ^{36}Ca for $N = 16$ there is no common particle (p) and hole (h) valence space for the g.s. and excited state, but a pure pp (hh) state for the g.s. and a ph state for the $I^\pi = 2^+_1$ state. The same holds for the $A = 14$, $T = 1$ triplet with respect to the subshell closure $Z = 6$ and $N = 6$, respectively, where

a similar sign and size of the MED ($\Delta E_M = -422(10)$ keV) is observed [13]. The large MED certainly points to an effect due to shell structure and/or coupling to the continuum for the unbound state in the proton-rich partner ($S_p = 2.56(4)$ and 4.628 MeV for ^{36}Ca and ^{14}O, respectively [19]) and not to a Coulomb effect. This is corroborated by the fact that in both, the $A = 14$ and $A = 36$ mirrors, the $T_z = -T$ partner exhibits the smaller subshell and closed shell gap energies Δ, which are precisely determined by binding energy differences [19]. For example, the neutron gap energy in ^{36}Ca is 550(90) keV smaller than the proton gap energy in ^{36}S which is shown in Fig. 4.

A universal interaction USD for the *sd* model space outside an inert ^{16}O core has been determined by fitting two-body matrix elements (TBME) and single-particle energies (SPE) to experimental binding energies and excitation energies [20]. Experimental data were corrected for Coulomb shifts to warrant strict isospin symmetry of the interaction and SPE. Various shell model investigations, especially for the neutron-rich *sd* shell region close to the "island of inversion" around $^{32}_{12}$Mg$_{20}$, have been performed, which include excitations from the *sd* to the *pf* shell [21–23], preserving full isospin symmetry. To investigate the MED in the $A = 36$ mirror nuclei, the isospin symmetry has to be broken. In the hitherto first systematic attempt based on the USD, MED were calculated for application to the astrophysical *rp* process [24]. In the $T = 2$ cases $A = 24$, 32 and 36 the experimental results are largely underestimated by amounts of 70, 110 and 250 keV, respectively (see Fig. 5). The required modifications of the Thomas–Ehrman shifts in these proton-rich nuclei [25,26] may cause considerable changes in the proton capture rates entering *rp* path network calculations [24].

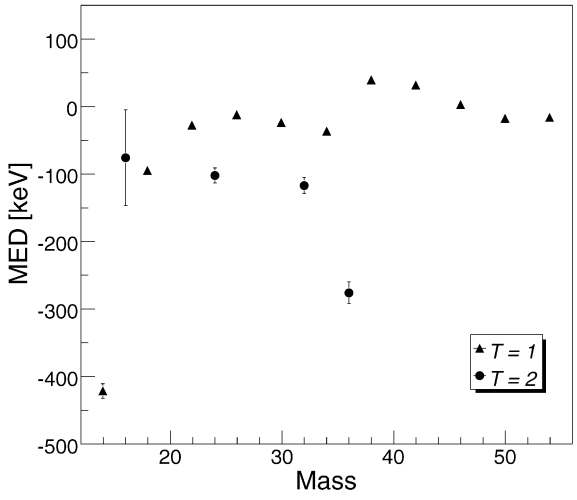

Fig. 3. Experimental mirror energy differences for the first $I^\pi = 2^+$ states of even–even $T = 1$ and $T = 2$ mirror nuclei from ^{14}C–^{14}O to ^{54}Fe–^{54}Ni (for references and details see text).

In a simpler empirical approach, hereafter referred to as USD*, we have replaced the fitted isospin symmetric SPE by the experimental values of the $A = 17$, $T = 1/2$ mirrors. This modification turns out to be the most crucial step in order to reproduce the new large MED in the ^{36}Ca–^{36}S pair. The isospin symmetry in the TBME is preserved. The configuration- and spin-dependent Coulomb corrections to the $T = 1$ proton–proton TBME have not been applied. In a second approach we have used the USD interaction as modified by Utsuno et al. [22] for use with the *pf* model space without pairing corrections. Again experimental SPE were taken from the $A = 17$, $T = 1/2$ mirrors. To get better agreement with the $N, Z = 14$ shell gaps in ^{22}O and in ^{34}Si, respectively, additional monopole corrections were applied, which modify the SPE evolution with increasing shell occupation [27]. The total monopole modifications as defined in Ref. [22] relative to USD are

$$\Delta V_{T=1,0}(d_{5/2}, d_{3/2}) = +0.20, -0.60 \text{ MeV}, \quad (1)$$

$$\Delta V_{T=1,0}(d_{5/2}, s_{1/2}) = -0.10, +0.10 \text{ MeV}. \quad (2)$$

This interaction, hereafter referred to as USD^m, reproduces the $Z, N = 14, 16$ shell gaps, the $I^\pi = 2^+_1$ excitation energies and

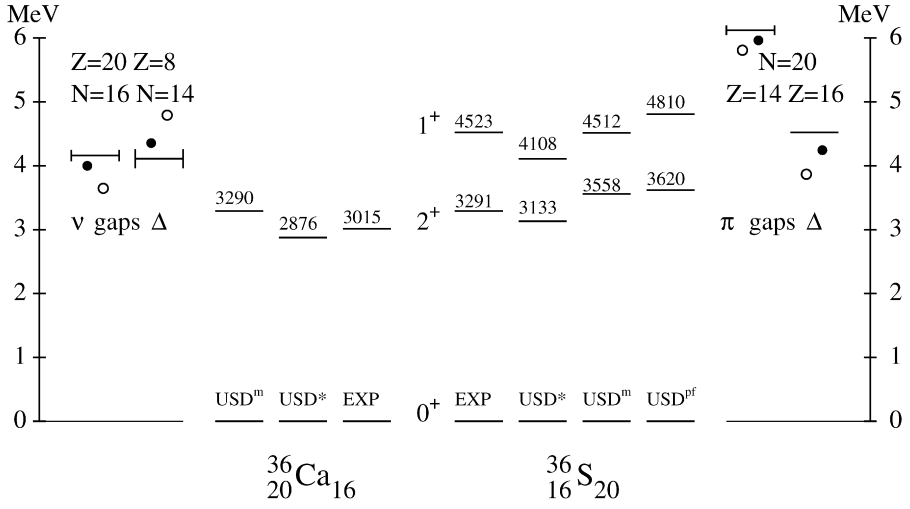

Fig. 4. Experimental ^{36}Ca and ^{36}S (partial) level schemes in comparison to shell model calculations using experimental single-particle energies and the USD interaction [20] (USD*), and a monopole modified USD based on Ref. [22] (USD^m see text). For ^{36}S the levels as calculated in the full $1s0d$–$1p0f$ space [22] (USD^{pf}) are shown, too. The $1s0d$ shell model space subshell gaps Δ for $N = 14$ (^{22}O), $N = 16$ (^{36}Ca), $Z = 14$ (^{34}Si) and $Z = 16$ (^{36}S) are shown as lines with error bars and compared to the corresponding shell model values as indicated by open (USD*) and filled (USD^m) circles.

the ^{40}Ca single-hole energies [28,29], i.e. the $Z = 8$, $N = 20$ and $Z = 20$ sd shell "fringe" nuclei, in total 13 key experimental data, with a mean level deviation [30] MLD = 275 keV. This should be compared to the USD MLD = 440 keV for the same data set. Even smaller MLD values of 224 keV (USD^m) and 207 keV (USD) are obtained for a set of 221 excitation energies in $A = 31$–39 nuclei comprising the original data [20] and new additional experimental results [13]. The results for the $I^\pi = 2^+_1$ respectively 1^+_1 states in ^{36}Ca and ^{36}S and the sd shell relevant $Z, N = 14, 16$ shell gaps are shown in Fig. 4. The calculations were performed with the code OXBASH [31].

The general agreement within the MLD is good for USD^m while the original USD* underestimates the $Z, N = 16$ gaps and correspondingly the $I^\pi = 2^+_1$ excitation energies in ^{36}Ca and ^{36}S. The striking result, however, is that independent from the interaction the use of experimental SPE, which empirically include Coulomb and Thomas–Ehrman [25,26] effects, almost fully accounts for the experimental MED. The values $\Delta E_M(\text{USD}^m) = -268$ keV and $\Delta E_M(\text{USD}^*) = -257$ keV compare well with $\Delta E_M(\text{EXP}) = -276(16)$ keV. It is therefore concluded that further Coulomb corrections beyond one-body contributions are negligible. This may be due to the ph character of the $I^\pi = 2^+_1$ states as ph conjugation changes the sign of mirror energy differences [4]. Moreover, this calculation reproduces the afore mentioned Coulomb energy difference observed in ^{36}Cl $T = 2$ states $\Delta E_C = -27(4)$ keV as -51 keV within the deviation expected from the neglect of two-body Coulomb corrections, which proves that the T_z dependence within the $T = 2$ isospin quintuplet is accounted for. Furthermore, apart from the MED and the subshell gaps at $N = 16$ in ^{36}Ca and $Z = 16$ in ^{36}S, which are robustly fixed by the $A = 17$ SPE, the evolution of shell structure for the proton-rich (^{36}Ca) and the neutron-rich (^{36}S) partners is completely determined by the isospin symmetric two-body interaction as expected for monopole driven shell structure [3,27].

The absolute values are certainly subject to change when sd–pf cross-shell excitations are included, which needs to be discussed. The USD^m $I^\pi = 2^+_1$ energies lie within the MLD but systematically about 270 keV above the experimental values. For ^{36}S a full sd–pf model space calculation within the Monte Carlo shell model (MCSM) was performed by Utsuno et al. [22], which is isospin symmetric in SPE and interaction. Excitation energies of 3620 and 4810 keV were found for the $I^\pi = 2^+$ and 1^+ states (see Fig. 4 USD^{pf}), which should be compared to 3406 and 4357 keV in the original USD [20]. The corrections due to experimental SPE as used in the present work can be estimated to first order from the difference between USD and USD* (Fig. 4) results to be about -260 keV for $I^\pi = 2^+$, 1^+, respectively, bringing the sd–pf values in good agreement to experiment. We also note that the shell gap optimised USD^m accounts well for the cross-shell excitations omitted in the present work. Their common deviation from experiment is of different origin though, namely symmetric SPE in USD^{pf} and neglect of explicit sd–pf excitation in USD^m. In the USD^{pf} approach it is found that an average of 0.74 neutrons (and 0.12 protons) are excited to the pf shell, which in the mirror nucleus ^{36}Ca should give rise to substantial coupling of the pf protons to the continuum with a large impact on the MED.

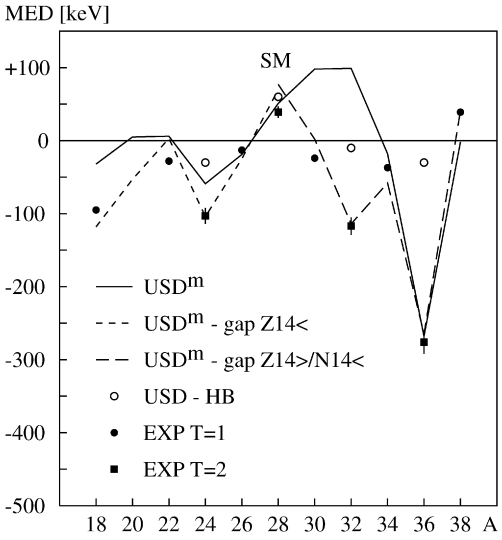

Fig. 5. Experimental mirror energy differences for the first $I^\pi = 2^+$ states of even–even $T = 1$ (filled circles) and $T = 2$ (filled squares) sd shell mirror nuclei in comparison to shell model results of Ref. [24] (open circles) and the present work (USD^m) (full line). The dashed lines correspond to a reduced $Z = 14$ gap in the lower sd shell ($A \leqslant 28$, short dashed) and a reduced $N = 14$ gap with a small increase of the corresponding mirror gap in the upper shell ($A \geqslant 28$, long dashed). For details see text.

The large value of the $A = 36$, $T = 2$ MED, the excellent agreement with the USD^m result, and the robustness against modification suggest a comparison for all experimentally known $T = 1, 2$ MED in the sd shell. This is shown in Fig. 5 by the full line. Qualitative agreement within expected deviations due to neglected Coulomb contributions is found for $A = 18$–28 and especially for $A = 34$–38. The largest deviations are found for $A = 18$ ($T = 1$), 24 ($T = 2$), 30 ($T = 1$) and 32 ($T = 2$) with even a wrong sign in the two latter cases. It is noted that the dedicated calculation of Coulomb shifts in Ref. [24] fails to reproduce the experiment except for $A = 28$ ($T = 2$). Introducing an empirical Coulomb correction to the proton $d_{5/2}$ and $d_{3/2}$, $J = 2, 4$ TBME improves agreement at the beginning and end of shell but does not cure the $A = 24$, 30, 32 discrepancy. This and the inspection of the wave functions for the corresponding mirror pairs suggest that the deviations are of structural origin, as the $Z, N = 14$ gaps are crucial in all critical cases, the $A = 30$, $T = 1$ mirrors additionally depend on the $Z, N = 16$ gaps. An isospin symmetric monopole correction obviously will not influence the MED. Moreover, due to the symmetry of the model space in protons and neutrons, any isospin asymmetric modification (which necessarily changes only the $T = 1$ TBME) that shifts a proton (neutron) SPE in the lower half of the shell will have the same effect in the upper half, however with the difference that the corresponding nuclei lie on different sides of the $N = Z$ line. Therefore, any MED improvement in the upper sd shell ($A = 30$, 32) will inevitably deteriorate the agreement in the lower shell ($A = 18$–24) and vice versa. The midshell mirror pair $A = 28$ however, which exhibits the only $T = 2$ positive MED, will remain virtually

unchanged. This value was recently measured [18] and is intriguingly well reproduced in all approaches.

To get better insight in the underlying structure, we have therefore in an empirical approach introduced different ad hoc corrections in the lower *sd* shell between the $Z = 8$, $N = 8$ and $A = 28$ isobar lines and the upper shell triangle bordered by the $Z = 20$, $N = 20$ and the $A = 28$ lines.

- In the lower mass triangle $A = 16$–28 the proton gap at $N = 8$ and $Z = 14$ (Si) was reduced by 200 keV. In addition, the proton $d_{5/2}^2$ TBME were quenched by 5% to improve the USD^m (and USD) agreement for ^{18}Ne, which introduces another reduction of the proton gap by monopole drift summing up to a total reduction in the full shell calculation of 0.32 MeV relative to its mirror neutron gap at $Z = 8$ (O) and $N = 14$.
- In the higher mass triangle $A = 28$–40 the neutron gap at $Z = 20$ (Ca), $N = 14$ was reduced by 900 keV while the $Z = 14$ (Si), $N = 20$ proton gap was increased by 300 keV to further improve the agreement shown in Fig. 4. The full calculation was done with a final reduction of 0.74 MeV of the ^{34}Ca neutron gap relative to ^{34}Si. Note that the MED are only sensitive to the gap difference.

The results are shown in Fig. 5 by short and long dashed lines for the lower and upper shell, respectively. The excellent agreement proves the sensitivity of the MED to the experimentally unknown proton gap at $Z = 14$, $N = 8$ (^{22}Si) and the neutron gap at $N = 14$, $Z = 20$ (^{34}Ca), making MED useful probes for shell structure in experimentally inaccessible regions. The substantial reduction of the $d_{5/2}$–$s_{1/2}$, $N = 14$ gap in ^{34}Ca is corroborated by the experimental evidence in its isotone ^{32}Ar of a reduced $\nu d_{5/2}$ occupation as seen in neutron knockout reactions [32]. The origin of the reduction must be sought in the approaching dripline and gradual coupling to the continuum. The assumption of a constant ad hoc shift in the upper (lower) *sd* shell is therefore only a crude approach. The effect of cross-shell excitations from the adjacent $0p$ and $1p0f$ shells would be symmetric in isospin and influences the absolute excitation energies only. The quenching of the $d_{5/2}^2$ interaction in the lower shell, needed to reproduce the MED, can be taken as first evidence for the reduced overlap of the protons involved due to coupling to the continuum. Further experimental evidence would come from a measurement of the $I^\pi = 2^+$ excitation energy in ^{20}Mg, yielding the $A = 20$ MED which is predicted to be negative in the present approach.

In conclusion, the energy for the $I^\pi = 2_1^+$ state of ^{36}Ca, the heaviest $T = 2$ nucleus with an observed γ-decay, was determined to be 3015(16) keV. The extremely large mirror energy difference relative to ^{36}S can be understood with an isospin symmetric USD based interaction using experimental proton and neutron SPE from the $A = 17$, $T = 1/2$ isospin doublet, which account empirically for the one-body part of Thomas–Ehrman and/or Coulomb effects. The results are consistent with a monopole driven shell structure scenario and the expectation that Ca isotopes below $N = 16$ develop another "island of inversion". From the systematics of $T = 1$ and $T = 2$ MED in the *sd* shell a reduction of the $Z = 14$ gap in the $N = 8$ isotones and the $N = 14$ gap in the $Z = 20$ Ca isotopes relative to their mirror gaps N, $Z = 14$ in $Z = 8$ O isotopes and $N = 20$ isotones is inferred. In view of the considerable reduction of the $Z = 20$ shell gap relative to the $N = 20$ gap in ^{36}Ca and ^{36}S, respectively, the onset of inversion may start at $N = 14$ in ^{34}Ca already.

Acknowledgements

The authors thank the accelerator department at GSI for providing the ^{40}Ca beam. This work was supported by the German BMBF under grant Nos. 06BN-109, 06K-167 and by the Polish Ministry of Education and Science (grant Nos. 1 P03B 030 30 and 620/E-77/SPB/GSI/P-03/DWM105/2004-2007).

References

[1] S.M. Lenzi, et al., Phys. Rev. Lett. 87 (2001) 122501;
A.P. Zuker, et al., Phys. Rev. Lett. 81 (2002) 142502.
[2] G. de Angelis, et al., Eur. Phys. J. A 12 (2001) 51.
[3] H. Grawe, Acta Phys. Pol. B 34 (2003) 2267;
H. Grawe, et al., Eur. Phys. J. A 25 (2005) 357.
[4] A. Gadea, et al., Phys. Rev. Lett. 97 (2006) 152501.
[5] H. Geissel, et al., Nucl. Instrum. Methods B 70 (1992) 286.
[6] H.J. Wollersheim, et al., Nucl. Instrum. Methods A 537 (2005) 637.
[7] R. Lozeva, et al., Nucl. Instrum. Methods A 562 (2006) 298.
[8] A. Maj, et al., Nucl. Phys. A 571 (1994) 185;
F. Camera, Ph.D. thesis, University of Milano, Italy, 1992.
[9] S. Agostinelli, et al., Nucl. Instrum. Methods A 506 (2003) 250.
[10] V. Borrel, et al., Z. Phys. A 314 (1983) 191.
[11] A.S. Goldhaber, Phys. Lett. B 53 (1974) 306.
[12] A. Bürger, et al., AIP Conf. Proc. 831 (2006) 418, and private communication.
[13] ENSDF database, http://www.nndc.bnl.gov/ensdf/.
[14] J. Vernotte, et al., Phys. Rev. C 13 (1976) 461.
[15] H. Schatz, et al., Phys. Rev. Lett. 79 (1997) 3845.
[16] P.D. Cottle, et al., Phys. Rev. Lett. 88 (2002) 172502.
[17] S. Kanno, et al., Prog. Theor. Phys. (Kyoto) 146 (2002) 575.
[18] K. Yoneda, et al., Phys. Rev. C 74 (2006) 021303(R).
[19] G. Audi, A.H. Wapstra, C. Thibault, Nucl. Phys. A 729 (2003) 337.
[20] B.A. Brown, B.H. Wildenthal, Annu. Rev. Nucl. Part. Sci. 38 (1988) 29.
[21] A. Poves, J. Retamosa, Phys. Lett. B 184 (1987) 311;
A. Poves, J. Retamosa, Nucl. Phys. A 571 (1994) 221.
[22] Y. Utsuno, et al., Phys. Rev. C 60 (1999) 054315.
[23] E. Caurier, et al., Phys. Rev. C 58 (1998) 2033;
E. Caurier, et al., Nucl. Phys. A 693 (2001) 374.
[24] H. Herndl, et al., Phys. Rev. C 52 (1995) 1078.
[25] R.G. Thomas, Phys. Rev. 88 (1952) 1109.
[26] J.B. Ehrman, Phys. Rev. 81 (1951) 412.
[27] H. Grawe, Springer Lecture Notes in Physics, vol. 651, 2004, p. 33.
[28] D.W. Devins, et al., Phys. Rev. C 24 (1981) 59.
[29] M. Matoba, et al., Phys. Rev. C 48 (1993) 95.
[30] R. Gross, A. Frenkel, Nucl. Phys. A 267 (1976) 85.
[31] B.A. Brown, A. Etchegoyen, W.D.M. Rae, Computer Code OXBASH, MSU-NSCL Report 524, 1988.
[32] A. Gade, et al., Phys. Rev. Lett. 93 (2004) 042501.

NUCLEAR STRUCTURE FAR OFF STABILITY — RISING CAMPAIGNS*

M. Górska[a], A. Banu[a], P. Bednarczyk[a,b], A. Bracco[c], A. Bürger[d]
F. Camera[c], E. Caurier[e], P. Doornenbal[a,f], J. Gerl[a], H. Grawe[a], M. Honma[g]
H. Hübel[d], A. Jungclaus[h], A. Maj[b], G. Neyens[i], F. Nowacki[e], T. Otsuka[j]
M. Pfützner[k], S. Pietri[l], Zs. Podolyák[l], A. Poves[h], P.H. Regan[l], P. Reiter[f]
D. Rudolph[m], H.J. Wollersheim[a]

and the RISING Collaboration

[a]Gesellschaft für Schwerionenforschung (GSI), Planckstr. 1, Darmstadt, Germany
[b]H. Niewodniczański Institute of Nuclear Physics, Kraków, Poland
[c]Dipartimento di Fisica, Universita di Milano, 20133 Milano, Italy
[d]Helmholtz-Institut für Strahlen- und Kernphysik, Universität Bonn, Germany
[e]IPHC, 67037 Strasbourg Cedex 2, France
[f]Institut für Kernphysik, Universität zu Köln, 50937 Köln, Germany
[g]University of Aizu, Fukushima 965-8580, Japan
[h]Departamento de Física Teórica, Universidad Autonoma de Madrid, Spain
[i]Katholieke Universiteit Leuven, 3001 Leuven, Belgium
[j]Department of Physics and Center for Nuclear Study, University of Tokyo, Japan
[k]Institute of Experimental Physics, Warsaw University, Poland
[l]Department of Physics, University of Surrey, Guildford, GU2 7XH, UK
[m]Department of Physics, Lund University, 22100 Lund, Sweden

(Received December 1, 2006)

Nuclear structure studies at GSI attracted recently increased interest for the results of present activities as well as for the future project FAIR. A broad range of physics phenomena can be addressed by high-resolution in-beam γ-ray spectroscopy experiments with radioactive beams offered within the Rare Isotopes Spectroscopic INvestigation at GSI (RISING) project. It combined the EUROBALL Ge-Cluster detectors, the MINIBALL Ge detectors, the HECTOR-BaF detectors, and the fragment separator FRS. The secondary beams produced at relativistic energies were used for Coulomb excitation or secondary fragmentation experiments to study projectile like nuclei by measuring de-excitation photons. The first results of the "fast beam campaign" is discussed in comparison to various shell model calculations. The discussion focuses on the $N = 32, 34$ sub-shell closure based on neutron rich Cr isotopes. Alternatively, the relativistic radioactive beams, both in their ground and isomeric states, were implanted and their decay could be investigated. The "stopped beam campaign" has started in October 2005 with a series of g-factor measurements. It continued from February 2006 with the next configuration and the main goal of identification of new isomers and angular momentum population in fragmentation reactions.

PACS numbers: 21.10.–k, 21.60.Cs, 23.20.–g, 25.60.–t

* Presented at the Zakopane Conference on Nuclear Physics, September 4–10, 2006, Zakopane, Poland.

1. Introduction

The CLUSTER [1] detector part of the EUROBALL array is presently used at GSI to explore exotic nuclei with radioactive beams. The SIS/FRS [2] facility provides secondary beams of unstable rare isotopes after fragmentation reactions or secondary fission of relativistic heavy ions with sufficient intensity for in-beam gamma-ray spectroscopy measurements. Following a workshop held in November 2000 at GSI, the RISING collaboration has been initiated to pursue this project. Secondary beams arrive to the secondary target/stopper either in the ground state or, if existing, in high spin isomeric states which are long lived enough to survive the flight path through the FRS. The beams have been used so far either *(i)* at high energies ($\geq$ 100 MeV/u) for relativistic Coulomb excitation and fragmentation reactions or *(ii)* stopped for isomeric decay studies. The letter of intent summarizing the proposed physics and the intended experimental technique of the RISING project is available [3].

The physics of experiments performed in the first RISING campaign, which is the main topic of this paper, exploit unique beams at relativistic energies in the range from 100 to 600 MeV/u [4]. Those experiments which depend on fragmentation products from heavy primary beams are only feasible at GSI. The RISING spectrometer was employed not only for relativistic Coulomb excitation but also for pioneering high-resolution γ-spectroscopy experiments after secondary nucleon removal reactions and secondary fragmentation. Several of the performed experiments focused on new methods and techniques in order to determine magnetic moments and life times of short lived states, properties of isomeric states and spectroscopic factors at relativistic energies for the first time.

2. RISING campaigns

The experimental program at RISING has been and will be performed in different campaigns requiring dedicated specifications of the experimental setup.

- In the **Fast-beam campaign** intermediate energy Coulomb excitation was used to measure the $B(E2; 0^+ \rightarrow 2^+)$ in neutron-rich $^{56-58}$Cr [5], light ^{108,112}Sn [6], and shape coexistent ^{134}Ce, ^{136}Nd [7]. In secondary fragmentation of ^{55}Ni and ^{37}Ca [8] mirror symmetry in the pf and sd shells was studied. Further experiments comprise knockout reactions in ^{132}Sn, sub-picosecond lifetime measurements following fragmentation of ^{34}Si, and collective modes in ^{68}Ni. The selected results from the fast beam campaign are further described and discussed in this paper.

- In the *g*-**RISING campaign** employing passive stoppers for implantation, running at GSI in 2005, experiments on *g*-factors of isomeric states around ^{132}Sn produced in fission as well as in fragmentation, and proton-rich ^{192}Pb were performed. Spin-alignment studies will enable to extend these experiments from fragmentation products to neutron-rich high-energy fission fragments [9].
- As a sensitive probe of shell structure changes, new isomers have been investigated within the **Stopped-beam campaign** started in 2006. The studies concentrated on $N = Z$ nuclei below ^{56}Ni where the 10^+ isomer in ^{54}Ni was identified with a proton decay branch, nuclei below ^{100}Sn where the isomers in $N = Z$ ^{82}Nb and ^{86}Tc were identified for the first time yielding information on the isospin $T = 0$ and $T = 1$ competing levels, and neutron-rich $N = 126$ isotones below ^{208}Pb where among others a (10^+) isomer in ^{204}Pt has been identified. A bulk of nuclear structure information was obtained from the fission and fragmentation studies of the $A = 132$ mass region where a number of isomeric states was found in Ag, Cd, In isotopes including an (8^+) isomer in ^{130}Cd and a core excited state in ^{131}In. More information on the performed experiments can be found in other contributions to this conference, *i.e.* [10–14] and the forthcoming papers [15, 16]. An experiment planned for December 2006 searches for X(5) symmetry candidates around $A = 110$.
- In the future stopped-beam campaign an **Active Stopper** will be used, dedicated for β-decay and μs-isomer studies of shape evolution below ^{208}Pb and K-isomers from ^{190}W to ^{170}Dy, of the Gamow–Teller resonance and isomers in ^{100}Sn and of isospin symmetry in weak and strong interactions in the $N = Z$ daughters of ^{54}Ni, ^{50}Fe and ^{46}Cr.

3. Physics interest of the fast beam campaign

The motivations to explore nuclear structure of exotic nuclei at relativistic beam energies focus on (a) shell structure of unstable doubly magic nuclei and their vicinity, (b) isospin symmetry along the $N = Z$ line and mixed symmetry states, (c) shapes and shape coexistence and (d) collective modes and E1 strength distribution.

3.1. Shell structure

Spectroscopic data on the single particle structure of unstable doubly magic nuclei and their nearest neighbours are indispensable for theoretical description of the effective interactions in large-scale shell-model calculations [17]. The studies around the $N = Z$ doubly magic nuclei ^{56}Ni and ^{100}Sn provide an excellent probe for single-particle shell structure, proton–neutron interaction and the role of correlations, normally not treated in mean

field approaches. The $B(E2; 0^+ \rightarrow 2^+)$ values in semi-magic Sn nuclei provide a sensitive test for changing (sub)shell structure, the E2 polarisability and the shape response of the magic core. For several reasons conventional techniques, employing (HI,xn) reactions, are very difficult or even impossible and the proposed Coulomb excitation measurements are the only way to obtain the information needed to investigate the evolution of shell structure close to the proton drip line. Beyond the very neutron-rich shell closures from ^{34}Si to ^{132}Sn the possible disappearance of the familiar Woods–Saxon shell closures and their reappearance as harmonic magic numbers is predicted by several mean-field calculations [18]. Moreover, ^{78}Ni and ^{132}Sn are located close to the astrophysical rapid neutron capture process path and indirect evidence for an altered shell structure and shell quenching of magic gaps at $N = 82$ and $N = 126$ is derived from recent r-process network calculations [19]. Alternatively, observed new shell structure in light and medium-heavy nuclei can be qualitatively understood in terms of monopole shifts of selected nucleon orbitals, with deviating predictions for new shell gaps and spin-orbit splitting [20, 21]. So far the investigative methods have not been able to gather information in the region of neutron-rich Ni and Sn isotopes concerning the most significant interaction matrix elements, the magnetic moments and the spectroscopic factors, which are sensitive indicators of their structure.

3.2. Symmetries

The validity of the isospin symmetry for the strong interactions is a fundamental assumption in nuclear physics. The degree to which this symmetry holds as the proton drip line is approached, remains an open question. Experimentally, the symmetry shows as nearly identical spectra in pairs of mirror nuclei obtained by interchanging protons and neutrons. A slight breakdown of the symmetry arises from the Coulomb interaction, causing small differences in excitation energies between isobaric analog states. The Coulomb energy differences between excited analog states in mirror nuclei have been studied for proton rich ($N = Z - 2$) isobars in the $A = 50$ region revealing subtle nuclear structure effects as a function of spin and energy [22].

Within the framework of the proton–neutron version of the interacting boson model (IBM-2) the existence of low-lying valence shell excitations, which are not symmetric with respect to the proton–neutron degree of freedom, are predicted. These states are called mixed-symmetry states and are *e.g.* established in all stable $N = 52$ isotones [23, 24].

3.3. Shapes

The phenomenon of shape coexistence is caused by various structure effects, which can be traced back to the polarisation by high spin intruder orbitals, which happens to occur primarily in exotic regions of the chart of

nuclides. Along semi-magic isotopic and isotonic chains, midway between shell closures ($N = 82$ and $N = 126$), $2p - 2h$ and $4p - 4h$ proton core excitations into high-spin orbitals cause coexistence of spherical, oblate and prolate shape as seen in the Pb ($Z = 82$) isotopes. States observed experimentally have no firm assignment of the specific shape so far [25]. Aided by shell gap melting, even the ground state may become deformed as in the well known $N = 20$ nucleus ^{32}Mg [26]. High-K isomers, built by multi-quasi particle configurations, due to their influence on the amount of pairing and/or collectivity left, may give rise to shape changes. Most often deformed nuclei obey axial and reflection symmetry. However, in specific nuclear regions where the Fermi level approaches pairs of close lying, opposite-parity orbitals with $\Delta j = \Delta l = 3$ reflection asymmetric shapes are predicted, *e.g.* the heavy Ba nuclei may show octupole deformed states.

3.4. Collective excitations

Collective excitations such as the giant dipole resonance (GDR), built from collections of single-particle excitations are necessarily influenced by the nuclear shell structure. In exotic nuclei like $^{68-78}$Ni the proton–neutron asymmetry may give rise to changes in the shell structure. Theoretical calculations predict a significant change in the GDR strength distribution as one progresses towards the doubly magic ^{78}Ni. The excitation function of the isovector GDR mode is expected to fragment substantially, favoring a redistribution of the strength towards lower excitation energies. Measurements of the GDR strength function provide access to the isospin dependent part of the in-medium nucleon–nucleon interaction and on dipole type vibrations of the excess neutrons. The predicted low-energy shift of the GDR strength was confirmed in neutron-rich oxygen isotopes by the LAND group at GSI by means of virtual photon absorption measurements [27]. The GDR experiment in ^{68}Ni applied a complimentary method, virtual photon scattering, which relies on real projectile γ-ray emission following the virtual excitation. In order to observe discrete γ-transitions with high resolution and γ-decay from the GDR, the RISING array was augmented by BaF scintillators. Further details on the GDR measurement in ^{68}Ni are given in Ref. [28].

4. Experimental technique

The γ-ray spectroscopy of nuclei produced from exotic beams is performed after in-flight isotope separation. The exotic beams are produced by fragmentation of a heavy stable primary beam or fission of a ^{238}U beam on a ^{9}Be or ^{208}Pb target, in front of the fragment separator, FRS.

4.1. Particle identification and tracking

The FRS was operated in a standard achromatic mode, which allows a separation of the species of interest by combining magnetic analysis with energy loss in matter. The transmission through the FRS is typically 20–70% (depending on the mass region) for fragmentation and 1–2% for fission. The separated ions are identified on an event-by-event basis with respect to mass and atomic number via combined time-of-flight, position tracking, and energy loss measurement. This is achieved with plastic detectors, multi-wire proportional chambers and a MUSIC ionisation chamber. Details on the secondary beam identification are given in Ref. [4]. After passing the identification set-up, the radioactive ions at relativistic energies are focussed onto a secondary target. Massive slits reduce the amount of unwanted species reaching the secondary target.

Behind the target the calorimeter telescope, CATE, is used for the exit channel selection. CATE consists of position sensitive Si ΔE detectors (laboratory angular range $\pm 3^\circ$) and CsI scintillators for total energy measurement. The performance of secondary fragment identification detector is described in Ref. [29].

4.2. Gamma-ray detection

For the excited fragments moving at a high velocity ($v/c = 0.43$ at the fragment energy of $100\,\mathrm{MeV}/u$) the Cluster γ-ray detectors have to be positioned at either forward or backward angles in order to minimize Doppler broadening. A photo of the γ-ray detection setup is shown in Fig. 1.

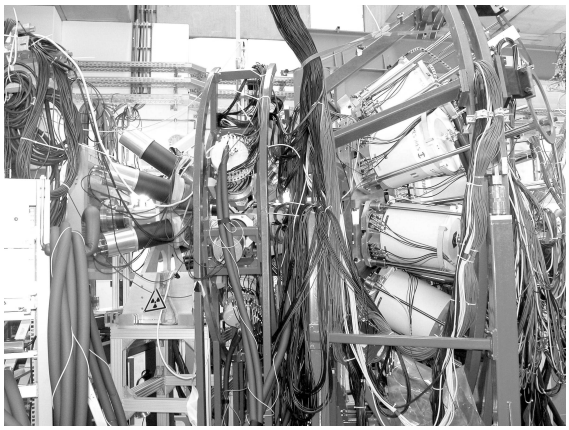

Fig. 1. The RISING fast beam set-up including Euroball-Cluster, Miniball [30] and Hector [31] detector arrays at the final focus of the FRS. The beam enters from the left.

The distance to the target depends on the required energy resolution. The best possible configuration of the 15 Cluster detectors placed in three rings available for experiments with fast beams is displayed in Fig. 2.

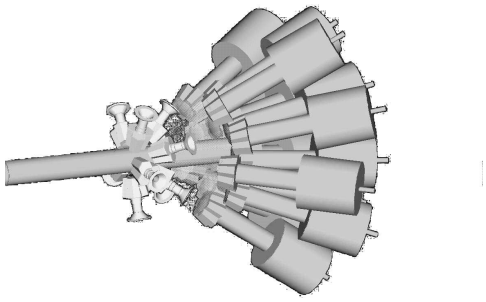

Fig. 2. Schematic picture of the Ge detector arrays used in the RISING fast beam campaign. The Miniball detectors are shown at about 90° angles (without LN_2 supply) and Cluster detectors at forward angles.

Due to the Lorentz boost the main efficiency contribution among the Cluster detectors comes from the first ring. This ring was positioned to achieve 1.5% resolution. The 5 Clusters in the 2nd and 3rd rings could be moved closer to the target position, for an increased efficiency but a lower overall resolution of 2.05% at 1.3 MeV. If both rings are placed at a minimum distance of 70 cm then the configuration reaches a total efficiency of 2.5% while the average weighted energy resolution is only slightly increased to 1.88%. The segmentation of the Miniball detectors [30] allows to place them at shorter distance and larger angles as seen in Fig. 2 not affecting the resolution significantly but contributing strongly to the total γ-ray efficiency to about 6%. The on-line analysis of the data is performed with the CRACOW software [32].

5. The $N = 32, 34$ sub-shell closure

The experimental evidence for changing shell structure along the very neutron-rich $N = 8, 20$ and 28 isotones can be explained by the monopole part of the nucleon–nucleon interaction [20, 21, 33]. It is traced back to the tensor interaction [34–36] which is strongly binding for nucleons in spin-flip configurations with $\Delta l = 0$ (spin–orbit partners) and $\Delta l = 1, 2$ in adjacent major shells in the $T = 0$ (proton–neutron) channel of the two-body interaction. It is specifically strong for optimum radial overlap, *i.e.* identical number of nodes in the radial wave function. The effect was first discussed for the p, sd and pf shells [20, 21, 33] with shell gaps changing from the HO magic neutron number $N_{\rm m} = 8, 20, 40$ to $N_{\rm m} - 2N_{\rm HO} = 6, 16(14), 34(32)$, with $N_{\rm HO}$

counting the harmonic oscillator quanta. The ambiguity for $N_{\rm HO} > 1$ is due to the presence of $j = 1/2$ orbits as *e.g.* $s_{1/2}$ or $p_{1/2}$, which have a strong $T = 1$ (pairing) monopole opening another gap when these shells are filled.

The neutron-rich Cr isotopes are located at a key point on the pathway from the $N = 40$ sub-shell closure via a deformed region to spherical $N = 28$ isotones. Experimentally a possible $N = 32$ shell develops in the 2^+ excitation energy of Ca isotopes and a maximum in this signature is also observed for Ti and Cr, while the Ni isotopes show constant 2^+ energies. Three experiments were performed to measure Coulomb excitation of high-energy ^{54}Cr, ^{56}Cr and ^{58}Cr beams with the RISING setup, where the known $B(E2; 2^+ \rightarrow 0^+)$ in ^{54}Cr served as a reference to reduce possible systematic errors. Details of the experimental results are given in Ref. [5].

The extracted $B(E2; 2^+ \rightarrow 0^+)$ and $E(2^+)$ systematics of the Ti [37] and Cr [5] isotopes has been extensively discussed in comparison to different shell model calculations KB3G [38] and GXPF1/GXPF1A [39, 40] (see *e.g.* [33]). The polarization charge used in those calculation for protons and neutrons was 0.5 e. The local peak in the experimental $N = 32$ $E(2^+)$ and a corresponding minimum in $B(E2; 2^+ \rightarrow 0^+)$, both in the Cr and Ti isotpes systematics was observed. A confirmation of these results for ^{56}Cr and ^{54}Ti was recently obtained in the plunger measurement at the Köln Tandem accelerator [41].

Closer inspection of the shell model results, which all show a rather flat behaviour with respect to shell structure, indicates that the $N = 32$ gap between $p_{1/2}$ and $p_{3/2}$ stays constant when moving from Ca to Cr into the

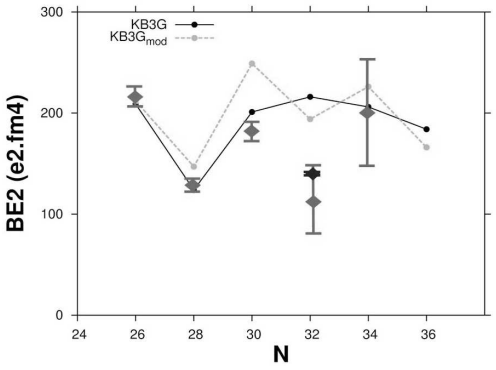

Fig. 3. Comparison of the experimental and theoretical $B(E2 : 2^+ \rightarrow 0^+)$ values for Cr isotopes. The influence of using different neutron effective charge [43] in the calculations is shown in two different curves for the KB3G (light grey) and KB3G$_{\rm mod}$ (black) interaction. The experimental points are shown in dark grey. The recent result [41] (see text) is shown in black.

proton shell while the $N = 34$ gap between $p_{3/2}$ and $f_{5/2}$ reduces strongly in the GXPF1/GXPF1A [39, 40] and disappears for KB3G [38]. Furthermore, using in the KB3G calculation the effective charges recently measured for the fp shell in the neutron deficient nuclei [42] was found to introduce staggering of the $B(E2)$ values in Ti isotopes which lowers the value for $N = 32$ almost to the experimental result [43]. The same experimental values of effective charges were used for the Cr isotopes when calculating $B(E2)$ values with KB3G. The result is shown in Fig. 3 as $\mathrm{KB3G_{mod}}$ curve. Although the staggering is observed as well, the general agreement between calculation and experiment did not improve. Nevertheless, this latest analysis proves that the indirect measurement of Cr or Ti isotopes does not give an unambiguous answer about a possible $N = 32, 34$ sub-shell closure and only studies of the respective Ca isotopes will address the problem directly.

6. Summary

The RISING project exploiting high-resolution γ-ray spectroscopy of nuclei far from stability proved to be very effective in providing new nuclear structure information in various campaigns. In particular the question of monopole driven shell structure at $N = 32, 34$ was addressed in the fast beam campaign. The final conclusion on the sub-shell closure in this region will be provided with a direct measurement of the transition probabilities in Ca isotopes. New results from Coulomb excitation were provided as well for ^{108}Sn [6] which shed light on the polarization of the ^{100}Sn core, and ^{134}Ce and ^{136}Nd [7]. The first results of the GDR measurement in ^{68}Ni are to be disclosed [28]. In the g-RISING and stopped beam campaign a wide range of nuclei was investigated yielding g-factors in neutron rich Sn isotopes [9] and newly identified isomeric states in ^{54}Ni [15], ^{82}Nb [12], ^{86}Tc [11], ^{130}Cd, ^{131}In [16], and ^{204}Pt [13]. The future campaign employing an active stopper foresees measurements of β-delayed γ rays.

This work is sponsored by the Polish Ministry of Science and Higher Education (grants 1-P03B-030-30 and 620/E-77/SPB/GSI/P-03/DWM105/ 2004–2007), the German Federal Ministry of Education and Research (grant 06KY205I) and by EURONS (European Commission contract No. 506065).

REFERENCES

[1] J. Eberth *et al., Nucl. Instrum. Methods* **A369**, 135 (1996).

[2] H. Geissel *et al., Nucl. Instrum. Methods* **B70**, 286 (1992).

[3] RISING Letter of Intent, `http://www-aix.gsi.de/~wolle/EB_at_GSI`.

[4] H.J. Wollersheim *et al., Nucl. Instrum. Methods* **A537**, 637 (2005).

[5] A. Bürger *et al., Phys. Lett.* **B622**, 29 (2005).

[6] A. Banu *et al., Phys. Rev.* **C73**, 061305(R) (2005).
[7] T. Saito *et al.*, submitted to *Phys. Rev.* **C**.
[8] P. Doornenbal *et al.*, submitted to *Phys. Lett.* **B**.
[9] G. Neyens *et al., Acta Phys. Pol. B* **38**, 1237 (2007) these proceedings.
[10] S. Pietri *et al., Acta Phys. Pol. B* **38**, 1255 (2007) these proceedings.
[11] A. Garnsworthy *et al., Acta Phys. Pol. B* **38**, 1256 (2007) these proceedings.
[12] L. Caceres *et al., Acta Phys. Pol. B* **38**, 1271 (2007) these proceedings.
[13] S. Steer *et al., Acta Phys. Pol. B* **38**, 1283 (2007) these proceedings.
[14] A. Myalski *et al., Acta Phys. Pol. B* **38**, 1277 (2007) these proceedings.
[15] D. Rudolph *et al.*, to be published.
[16] A. Jungclaus, M. Górska, M. Pfützner, *et al.*, to be published.
[17] E. Caurier *et al., Rev. Mod. Phys.* **77**, 427 (2005).
[18] J. Dobaczewski *et al., Phys. Rev. Lett.* **72**, 981 (1994).
[19] B. Pfeiffer *et al., Nucl. Phys.* **A693**, 282 (2001).
[20] T. Otsuka *et al., Phys. Rev. Lett.* **87**, 082502 (2001).
[21] H. Grawe, *Acta Phys. Pol. B* **34**, 2277 (2003).
[22] S. Lenzi *et al., Phys. Rev. Lett.* **87**, 122501 (2002).
[23] N. Pietralla *et al., Phys. Rev. Lett.* **83**, (1999) 1303.
[24] C. Fransen*et al., Phys. Lett.* **B508**, (2001) 219.
[25] A. Andreyev *et al., Nature* **405**, 430 (2000).
[26] D. Guillemaud-Mueller *et al., Nucl. Phys.* **A426**, 37 (1984).
[27] D. Cortina-Gil *et al., Phys. Rev. Lett.* **93**, 062501 (2004).
[28] A. Bracco, *Acta Phys. Pol. B* **38**, 1229 (2007) these proceedings.
[29] R. Lozeva *et al., Acta Phys. Pol. B* **36**, 1245 (2005).
[30] J. Ebert *et al., Prog. Part. Nucl. Phys.* **46**, 389 (2001)
[31] A. Maj *et al., Nucl. Phys.* **A571**, 185 (1994).
[32] J. Grębosz, *Comput. Phys. Commun.* (2006), in press.
[33] H. Grawe, *Springer Lect. Notes Phys.* **651**, 33 (2004).
[34] H. Grawe *et al., Eur. Phys. J.* **A25**, 357 (2005).
[35] H. Grawe *et al., Eur. Phys. J.* **A27**, 557 (2006).
[36] T. Otsuka *et al., Phys. Rev. Lett.* **95**, 232502 (2005).
[37] D.C. Dinca *et al., Phys. Rev.* **C71**, 041302 (2005).
[38] E. Caurier *et al., Eur. Phys. J.* **A15**, 145 (2002).
[39] M. Honma *et al., Phys. Rev.* **C69**, 034335 (2004).
[40] M. Honma *et al., Eur. Phys. J.* **A25**, 499 (2005).
[41] P. Reiter *et al.*, to be published.
[42] R. du Rietz *et al., Phys. Rev. Lett.* **93**, 222501 (2004).
[43] A. Poves *et al., Phys. Rev.* **C72**, 047302 (2005).

COULOMB EXCITATION OF ^{68}Ni AT 600 AMeV*

A. Bracco[a], G. Benzoni[a], N. Blasi[a], S. Brambilla[a], F. Camera[a]
F.C.L. Crespi[a], S. Leoni[a], B. Million[a], D. Montanari[a]
M. Pignanelli[a], O. Wieland[a], A. Maj[b], P. Bednarczyk[b,c]
J. Grębosz[b], M. Kmiecik[b], W. Męczyński[b], J. Styczeń[b]
T. Aumann[c], A. Banu[c], T. Beck[c], F. Becker[c], L. Caceres[c]
P. Doornenbal[c], H. Emling[c], J. Gerl[c], H. Geissel[c], M. Gorska[c]
O. Kavatsyuk[c], M. Kavatsyuk[c], I. Kojouharov[c], N. Kurz[c]
R. Lozeva[c], N. Saito[c], T. Saito[c], H. Shaffner[c]
H.J. Wollersheim[c], J. Jolie[d], P. Reiter[d], N. Warr[d]
G. de Angelis[e], A. Gadea[e], D. Napoli[e], S. Lenzi[f], S. Lunardi[f]
D. Balabanski[g], G. Lo Bianco[g], C. Petrache[g], A. Saltarelli[g]
M. Castoldi[h], A. Zucchiatti[h], J. Walker[i], A. Bürger[j]

and the FRS Collaboration

[a]University of Milan and INFN Section of Milan, Italy
[b]Institute of Nuclear Physics, Polish Academy of Sciences, Kraków, Poland
[c]GSI, Planckstrasse 1, 64291, Darmstadt, Germany
[d]University of Koeln, Germany
[e]National Laboratory of Legnaro, INFN, Italy
[f]University of Padova and INFN Section of Padova, Italy
[g]University of Camerino, and INFN Section of Perugia, Italy
[h]INFN Section of Genova, Italy
[i]University of Surrey, United Kingdom
[j]HISKP, University of Bonn, Nußallee 14–16, 53115 Bonn, Germany

(Received December 10, 2006)

The γ decay following the Coulomb excitation of ^{68}Ni at 600 AMeV has been measured using the RISING array at GSI. The ^{68}Ni beam has been produced from the fragmentation of ^{86}Kr at 900 AMeV from the UNILAC-SIS on a ^{9}Be target and selected using the Fragment Separator. After the selection of Coulomb excited ^{68}Ni isotopes a peak centered at approximately 10.8 MeV has been observed in all type of RISING γ detectors. Because of the reaction mechanism the measured peak is interpreted to have a dipole nature and to come from the Pygmy Dipole Resonance. The measured data are consistent with the predictions of the Relativistic Mean Field and the Random Phase Approximation approaches.

PACS numbers: 21.60, 23.20, 25.70.De, 27.50+e

* Presented at the Zakopane Conference on Nuclear Physics, September 4–10, 2006, Zakopane, Poland.

1. Introduction

The Isovector Giant Dipole Resonance (IVGDR) is one of the most important and easily accessible nuclear collective modes. A large amount of experimental data exists for nuclei in the proximity of the stability line. These data have contributed to the studies on the effective nucleon–nucleon interaction in the medium and, in general, to a deeper understanding of the structure of nuclei. At the moment, there are only very few experimental data for nuclei far from the stability line. In particular, the question on how the Giant Dipole Resonance strength evolves when going from stable to exotic, weakly bound, nuclei with extreme neutron to proton ratio is presently under discussion, both theoretically and experimentally, in connection with the existence of the so called Pygmy Resonances (PR) or soft mode [1–6].

Such topic has recently collected very high interest beyond the nuclear structure field as it could significatively change our understanding of the neutron capture process in the r-process. In fact, neutron-rich nuclei with loosely bound valence neutrons may exhibit very strong (γ, n) strength components (the so called Pygmy Resonance) near particle thresholds and thus very enhanced neutron capture rates (see for example Ref. [7,8]). This means that the Pygmy Resonance can have a striking impact on the calculated r-abundance distribution.

There are two different experimental techniques available for the measurement of the dipole strength in radioactive exotic nuclei. The first one, called virtual photon neutron breakup, consists of producing relativistic radioactive beams and have a kinematic complete measurement of the breakup products produced in the secondary target [9]. This technique does not need high intensity beams but it is limited by the fact that it cannot give any information below the particle binding energy. The second technique, named virtual photon scattering, consists of producing relativistic radioactive beams and measuring the γ-decay of the Coulomb excited projectiles. Such method, even though requires high beam intensity, produces directly the E1 strength distribution and is sensitive both below and above the particle binding energy (see for example Ref. [11–13]).

In such kind of experiments, a critical factor is the capability to disentangle dipole states from others (mainly quadrupole states) which could be excited in the Coulomb scattering reaction. Fig. 1 (taken from Ref. [9]) shows the cross section for electromagnetic excitations of different collective states as a function of beam energy in the case of a medium mass nucleus. It is clear that the dipole cross section increases with the beam energy while quadrupole states shows the opposite behavior. It is, therefore, important to have the highest possible beam energy to ensure the excitation of mainly dipole states.

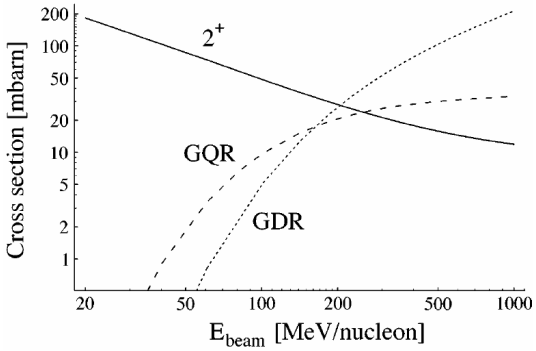

Fig. 1. The cross section for electromagnetic excitations of different collective states as a function of beam energy for a medium mass nucleus on a Au target [10].

For the ^{68}Ni isotopes recent theoretical calculations have predicted that the contribution of the low-energy region to the dipole strength distribution increases with the neutron excess [2, 3] and few percents of the Energy Weighted Sum Rule are concentrated around 10 MeV.

Recently, experiments focusing on the measurement of the dipole response of ^{68}Ni have been performed using both the virtual photon scattering (using the RISING detector array) and the virtual photon breakup technique (using the LAND array). The experiments have been performed at GSI at the Fragment Separator (FRS) facility where ^{68}Ni can be produced at relativistic energy with a sufficient high intensity (approximately 10^3–10^4 pps) for a Coulomb scattering experiment.

In this paper the preliminary results of the analysis of the data acquired with the RISING array will be presented. In Sec. 2 the experimental setup will be discussed, while in the third one, the high-energy γ-ray spectra measured in the RISING detectors will be presented.

2. The experiment

The γ-ray emission from Coulomb excited ^{68}Ni has been measured using the RISING array [14, 15] located after the FRS spectrometer. The particle identification after the target is performed by the CATE calorimeter [14, 16] which, in the present experiment, consisted of nine position sensitive Si detectors coupled to four 6 cm thick CsI arranged to equally share the intensity of the incident beam. High and low energy gamma rays have been measured using 15 HPGe clusters of the Euroball array [17, 18], 7 HPGe segmented clusters from the Miniball array [19] and 8 BaF_2 from the HECTOR array [20] located at different angles.

The ^{68}Ni beam was produced from the fragmentation of ^{86}Kr at 900 AMeV from the UNILAC-SIS with an intensity of $\sim 10^{10}$ particle per spill. The spill length was approximately 6 seconds long with a period of 10 seconds. The

primary beam was focused on a ^{9}Be target 4 g thick and the ^{68}Ni ions were selected using the Fragment Separator. The s4 scintillator, placed after the FRS and a couple of meters before the secondary Au target (3 g/cm^2), registered approximately 4×10^4 events per spill. In the beam cocktail which arrived on target the ^{68}Ni isotopes constitutes approximately 30% of the total incident isotopes as can be seen in Fig. 2.

A total of approximately 3×10^7 ^{68}Ni events was collected during 6 days of beam time.

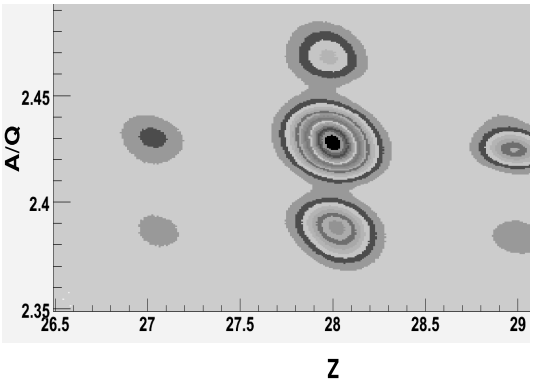

Fig. 2. The beam cocktail which arrives on the secondary target as measured after the FRS. In the x-axis the Z of the incident isotope is plotted while in the y-axis the A/Q ratio is indicated. The strongest spot in the center is relative to ^{68}Ni.

3. Results

All the beam particles were stopped in the CATE calorimeter placed approximately 1.5 meter after the target. Both the spectra from the silicon detectors and CsI scintillators were corrected, on an event by event basis, for the time drifts, the beam velocity and the position of interaction. The events with multiplicity larger than one were rejected and a consistency check between the incident direction, the interaction position and the firing detector was made. The left-upper panel of Fig. 3 shows the spectra obtained by the CATE calorimeter requiring incoming ^{68}Ni ions. In the right panels the projected spectra of the central silicon detector and one CsI are plotted. The achieved FWHM is sufficient to discriminate between different masses and charges. In the left-lower panel the Time of Flight (TOF) spectra of the BaF_2 detectors with and without the condition of a ^{68}Ni event detected in CATE is shown. It is clear that the condition eliminates completely almost all the background except for the gamma flash coming from CATE which arrives 12 ns after the prompt peak.

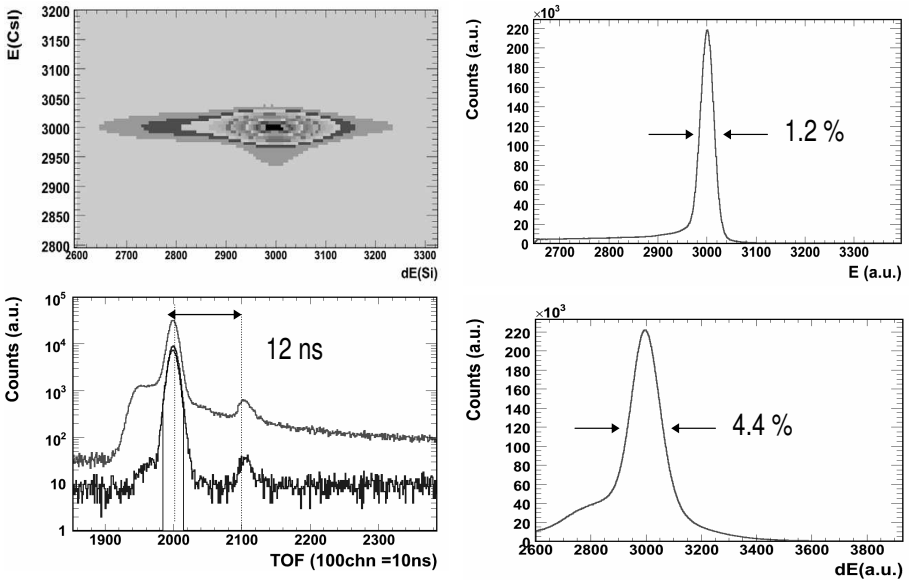

Fig. 3. The $E-\Delta E$ spectra acquired with the CATE calorimeter. In the upper-left panel the $E-\Delta E$ matrix measured in coincidence with incident ^{68}Ni isotopes is displayed. The CsI and Silicon spectra are shown in the upper-right and lower-right panels, respectively. In the left-lower panel the Time of Flight spectra of BaF_2 detectors before and after the requirement of a ^{68}Ni event in CATE calorimeter are shown.

The measured high-energy gamma-ray spectra in the three different types of γ detectors of the RISING setup are shown in Fig. 4. In the upper-left panel, the Doppler corrected BaF_2 spectra are shown. Only the ^{68}Ni events before and after the secondary target have been selected with an additional condition on the prompt time of flight peak and on the overall RISING γ multiplicity equal to one. The displayed spectra is from the detectors at 90 degrees. A peak structure centered between 10–11 MeV is evident. The line superimposed to the spectra shows the results of an accurate GEANT simulation of a monochromatic 10.8 MeV incident γ-ray. In the simulations both the Doppler broadening induced by the energy loss in the target and by the detectors subtended solid angle has been taken into account. The spectra of the BaF_2 detectors placed backwards, at 142 degrees, are dominated by background radiation. In fact, because of the very large Doppler-shift a ~ 10.8 MeV γ-ray in the center of mass is measured as a ~ 4 MeV γ-ray, where, unfortunately, the background radiation is still too intense.

A peak structure at the same energy has also been observed in the Doppler Corrected HPGe Cluster spectra and segmented HPGe Miniball spectra, as can be seen in the upper-right and lower-left panels of Fig. 4.

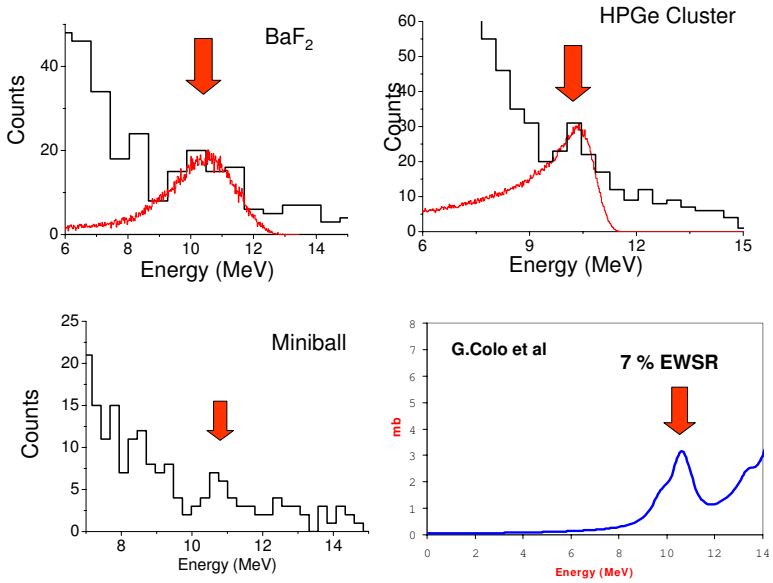

Fig. 4. The high-energy γ-ray spectra measured in the BaF_2 detector (upper-left panel), in the EUROBALL cluster detectors (upper-right panel) and in the MINIBAL HPGe segmented detectors (lower-left panel). The theoretically calculated ^{68}Ni dipole strength is displayed in the lower-right panel [21]. The continuous lines superimposed in the upper plots are the results of GEANT simulation of the peak lineshape. The arrows indicate the observed 10.8 MeV peak.

As was done for the BaF_2 detectors, only the scattered ^{68}Ni events within the TOF prompt peak and with a RISING multiplicity equal to one have been selected. In addition, in both HPGe detector types, only those events which emerged from two capsules activated in a single cryostat have been accepted. In the case of the HPGe cluster detectors, the peak line-shape corresponding to a 10.8 MeV γ-ray has been simulated using GEANT and superimposed to the spectrum.

In the right-lower panel of Fig. 4 the low energy part of the Pigmy Dipole response theoretically calculated within the RPA approach is displayed [21].

It is evident from all the plots of Fig. 4 that, even though the statistic is low and the background is high, all three detector types provide a coherent scenario, namely a peak between 10–11 MeV. The peak line-shape is consistent to GEANT simulations of the detector response and the experimental results are consistent with theoretical calculations.

It is, however, important to notice that the analysis is not complete yet. The Dipole Response of the other isotopes present in the beam cocktail needs to be analyzed and an absolute estimate of the "strength" of the measured dipole peak is still to be extracted from the available data.

4. Conclusion

In the paper we present preliminary results on the measurement, at the FRS with the RISING array, of the high energy γ-rays emitted by the Coulomb excited ^{68}Ni. A peak centered between 10–11 MeV has been observed consistently in all detector types of RISING. Its position is in the energy range theoretically predicted by RMF and RPA calculations for the Pygmy Dipole Resonance. This is the first evidence of such resonance state measured using relativistic radioactive beams and the virtual photon scattering technique and opens possibilities for a systematic study of such excited states in exotic nuclei.

The work has been supported by the Italian National Institute of Nuclear Physics (INFN), by the Polish Ministry of Science and Higher Education (grants 1-P03B-030-30 and 620/E-77/SPB/GSI/P-03/DWM105/2004-2007), by the UE under the contract N°: RII3-CT-2004-506065, by the German BMBF under grant N°: 06KY205I and 06BN-109, and by EURONS (European Commission contract number 506065).

REFERENCES

[1] H. Sagawa, T. Suzuki, *Phys. Rev.* **C59**, 3116 (1999).

[2] D. Sarchi *et al., Phys. Lett.* **B601**, 27 (2004).

[3] D. Vretnar *et al., Nucl. Phys.* **A692**, 496 (2001).

[4] P. Adrich *et al., Phys. Rev. Lett.* **95**, 132501 (2005).

[5] A. Leistenschneider *et al., Phys. Rev. Lett.* **86**, 5442 (2001).

[6] E. Tryggestad *et al., Phys. Lett.* **B541**, 52 (2002).

[7] G. Goriely, *Phys. Lett.* **B436**, 10 (1998).

[8] NuPECC Long Range Plan 2004, `www.nupecc.org/lrp02/long_range_plan_2004.pdf`

[9] T. Aumann, *Nucl. Phys.* **A752**, 289c (2005); *Eur. Phys. J.* **A26**, 441 (2005).

[10] T. Glashmaher, *Annu. Rev. Nucl. Part. Sci.* **48**, 1 (1998).

[11] F.E. Bertrand *et al., Nucl. Phys.* **A482**, 287 (1988).

[12] J.R. Beene *et al., Phys. Rev.* **C41**, 41 (1990).

[13] C.A. Bertulani *et al., Nucl. Phys.* **A458**, 725 (1986).

[14] H.J. Wollersheim *et al., Nucl. Instrum. Methods* **A537**, 637 (2005).

[15] J. Grebosz, *Comput. Phys. Commun.*, in press.

[16] R. Lozeva *et al., Nucl. Instrum. Methods* **A562**, 298 (2006).

[17] J. Simpson, *Z. Phys.* **A358**, 139 (1997).

[18] G. de Angelis, A. Bracco, D. Curien, *Eur. News* **34**, 181 (2003); W. Korten *et al.*, `http://euroball.lnl.infn.it/EBmore/EB_Final_Report.pdf`

[19] P. Reiter *et al., Nucl. Phys.* **A701**, 209c (2002); J. Eberth *et al., Nucl. Phys.* **A46**, 389 (2001).

[20] A. Maj *et al., Nucl. Phys.* A571, 185 (1994); M. Kmiecik *et al., Phys. Rev.* **C70**, 064317 (2004) and references therein.

[21] G. Colo, private communication.

Physics Letters B 669 (2008) 19–23

Contents lists available at ScienceDirect

Physics Letters B

www.elsevier.com/locate/physletb

Yrast and non-yrast 2^+ states of ^{134}Ce and ^{136}Nd populated in relativistic Coulomb excitation

T.R. Saito [a,*], N. Saito [a], K. Starosta [b], J. Beller [c], N. Pietralla [c,d,e], H.J. Wollersheim [a], D.L. Balabanski [f,h,g], A. Banu [a,1], R.A. Bark [i], T. Beck [a], F. Becker [a], P. Bednarczyk [a], K.-H. Behr [a], G. Benzoni [j], P.G. Bizzeti [k], C. Boiano [j], A. Bracco [j], S. Brambilla [j], A. Brünle [a], A. Bürger [l], L. Caceres [a,m], F. Camera [j], F.C.L. Crespi [j], P. Doornenbal [a], A.B. Garnsworthy [n], H. Geissel [a], J. Gerl [a], M. Górska [a], J. Grebosz [a,o], G. Hagemann [p], J. Jolie [d], M. Kavatsyuk [a,q], O. Kavatsyuk [a,q], T. Koike [r], I. Kojouharov [a], N. Kurz [a], J. Leske [c], G. Lo Bianco [h], A. Maj [o], S. Mallion [s], S. Mandal [t], M. Maliage [i], T. Otsuka [u,v], C.M. Petrache [h], Zs. Podolyak [n], W. Prokopowicz [a], G. Rainovski [f,e], P. Reiter [d], A. Richard [d], H. Schaffner [a], S. Schielke [l], G. Sletten [p], N.J. Thompson [n], D. Tonev [w,g], J. Walker [a,n], N. Warr [d], O. Wieland [j], Q. Zhong [w]

[a] *Gesellschaft für Schwerionenforschung (GSI), Darmstadt 64291, Germany*
[b] *Department of Physics and Astronomy and National Superconducting Cyclotron Laboratory, MSU, East Lansing, MI 48824, USA*
[c] *Institut für Kernphysik, Technische Universität Darmstadt, Schlossgartenstrasse 9, D-64289 Darmstadt, Germany*
[d] *Institut für Kernphysik, Universität zu Köln, Zülpicherstrasse 77, D-50937 Köln, Germany*
[e] *Department of Physics and Astronomy, SUNY at Stony Brook, NY 11794, USA*
[f] *Faculty of Physics, St. Kliment Ohridski University of Sofia, 1164 Sofia, Bulgaria*
[g] *The Institute for Nuclear Research and Nuclear Energy, BAS, 1784 Sofia, Bulgaria*
[h] *Dipartimento di Fisica dell'Universitá di Camerino, and INFN Sezione di Perugia, Italy*
[i] *iThemba LABS, Somerset West 7129, South Africa*
[j] *Dipartimento di Fisica, Universitá di Milano and INFN Sezione di Milano, Via Celoria 16, 20133 Milano, Italy*
[k] *Dipartimento di Fisica dell'Universitá di Firenze and INFN, Sezione di Firenze, Firenze, Italy*
[l] *Helmholtz-Institut für Strahlen- und Kernphysik, Universität Bonn, Nussallee 14-16, D-53115, Germany*
[m] *Departamento de Fisica Teorica, Universidá Autonoma de Madrid, E-28049 Madrid, Spain*
[n] *Department of Physics, University of Surrey, Guildford GU2 7XH, United Kingdom*
[o] *The Niewodniczanski Institute of Nuclear Physics, Polish Academy of Sciences, ul. Radzikowskiego 152, 31-342 Kraków, Poland*
[p] *The Niels Bohr Institute, Blegdamsvej 17, 2100 Copenhagen, Denmark*
[q] *National Taras Shevchenko University of Kyiv, 01033 Kyiv, Ukraine*
[r] *Department of Physics, Tohoku University, 980-8578 Sendai, Japan*
[s] *University of Leuven, IKS, Celestijnenlaan 200 D, 3001 Leuven, Belgium*
[t] *Department of Physics and Astrophysics, University of Delhi, New Delhi, India*
[u] *Department of Physics and Center for Nuclear Study, University of Tokyo, Hongo, Tokyo 113-0033, Japan*
[v] *RIKEN, Hirosawa, Wako-shi, Saitama 351-0198, Japan*
[w] *Laboratori Nazionali di Legnaro, Viale dell'Universitá 2, 35020 Legnaro (PD), Italy*

ARTICLE INFO

Article history:
Received 26 October 2007
Received in revised form 16 September 2008
Accepted 16 September 2008
Available online 20 September 2008
Editor: V. Metag

PACS:
23.20.En
23.20.Js
25.70.De
27.60.+j

ABSTRACT

The first 2^+ states in ^{134}Ce and ^{136}Nd and the second 2^+ state in ^{136}Nd were populated by Coulomb excitation at relativistic energies, and γ-rays were measured using the RISING setup at GSI. For ^{134}Ce an indication of the excitation to the second 2^+ state was observed. This experiment performed for the first time Coulomb excitation to second 2^+ states with rare isotope beams at relativistic energies. For ^{136}Nd the $B(E2; 2_1^+ \to 0^+)$, $B(E2; 2_2^+ \to 0^+)$, and $B(E2; 2_2^+ \to 2_1^+)$ values relative to the previously known $B(E2; 2_1^+ \to 0^+)$ value for ^{134}Ce are determined as 81(10), 11(3) and 180(92) W.u., respectively. The results are discussed in the framework of geometrical models that indicate pronounced γ-softness in these nuclei.

* Corresponding author at: GSI, Planckstrasse 1, D-64291 Darmstadt, Germany. Tel.: +49 6159 71 2032; fax: +49 6159 71 2809.
E-mail address: t.saito@gsi.de (T.R. Saito).
[1] Present address: Cyclotron Laboratory, Texas A&M University, Texas, USA.

0370-2693/$ – see front matter
doi:10.1016/j.physletb.2008.09.027

Despite the rotational invariance of the nuclear many body system, triaxial shapes originate from specific long-range correlations. They have represented an intriguing phenomenon in nuclear structure physics for five decades. Quadrupole-deformed nuclear shapes with soft-triaxiality [1,2] and with rigid triaxiality [3] have already been proposed in the 1950's. In the nuclear mass region $A \sim 130$, observed low-spin structures have been interpreted in terms of the occurrence of triaxial deformation, predominantly with a high degree of γ-softness. Corresponding nuclear spectra can be satisfactorily described [4] in terms of the corresponding O(6) dynamical symmetry [5] of the interacting boson model. The properties of the two lowest 2^+ states of even–even nuclei are particularly sensitive to a triaxial shape of the nuclear ground state and to the softness of its triaxiality. From theoretical and systematic studies [6,7], it has been suggested that the $N = 76$ nuclei are more γ-rigid than their neighbors with higher neutron number. At moderate spins, the rotation of a triaxial nucleus may give rise to pairs of identical $\Delta I = 1$ bands with the same parity—chiral twin bands [8]. In doubly-odd nuclei these structures can arise from the perpendicular coupling of the angular momenta of the valence particles and a triaxial core. The existence of self-consistent rotating mean-field solutions of chiral character has been predicted for the $N = 75$ nucleus ^{134}Pr [9], where a pair of bands with the same parity and spin close in excitation energy has already been observed [10]. In a number of nuclei in this region such bands have been observed and interpreted as chiral doublets [11–13].

The measured lifetime [14] and the analysis [15] of the band crossing of the two doublet bands in ^{134}Pr have put the chiral interpretation for this nucleus to discussion. A recent paper [16] suggests an interpretation of lifetimes and γ-ray branching ratios with theoretical calculations of the two-quasiparticle triaxial rotor and interacting boson–fermion–fermion models in terms of weak chirality dominated by shape fluctuations. In other nuclei, lifetime measurements have corroborated the chiral picture. In the odd-mass nucleus ^{135}Nd the transition probabilities for intra- and inter-band transitions confirm the chiral character and suggest that the observed behavior is associated with a transition from a chiral vibration to a chiral rotation [17]. It is interesting to study the triaxiality of the even–even nuclei, ^{134}Ce and ^{136}Nd, which are the corresponding even–even core of ^{134}Pr and the direct neighbor of ^{135}Nd, respectively, by measuring observables that are sensitive to the amount and rigidity of triaxial deformation. Therefore, relativistic Coulomb excitation experiments were performed to populate 2^+ states in ^{134}Ce and ^{136}Nd. From the decay of the first 2^+_1 and second 2^+_2 states the B(E2) values were deduced which yield information on the triaxiality parameter γ within geometrical models such as the Asymmetric Rotor Model (ARM) [2,3] or the Geometric Collective Model (GCM) by Gneuss and Greiner [18] that we will employ below.

Two consecutive experiments were performed to measure Coulomb excitation of high-energy ^{134}Ce and ^{136}Nd beams using the FRS-RISING setup at GSI [19]. A primary beam of ^{152}Sm at 750 A MeV impinged on a 4 g/cm^2 ^{9}Be production target at the entrance of the fragment separator (FRS) [20]. Fully stripped secondary beams of ^{134}Ce and ^{136}Nd were separated in the FRS by their magnetic rigidity and their specific energy loss in the degraders. The nuclei of interest were identified event-by-event by employing scintillator detectors, a multiple sampling ionization chamber (MUSIC) [21], and multi-wire proportional chambers (MWPC). Two plastic scintillators with a thickness of 3 and 0.5 mm each were mounted at the intermediate and final focal plane and served for the time of flight (TOF) measurement. From the TOF and the flight path length, the velocity of the ions was determined. The energy loss (ΔE) of each ion was provided by the MUSIC chamber and yielded the element number Z. By combining these measurements, the full in-flight identification of ions in Z and A/Q arriving at the final reaction target was achieved. The purity of the secondary ^{134}Ce and ^{136}Nd beams is almost 100% with this identification. In addition the incoming trajectories of the ions were measured by two MWPCs. The energies of ^{134}Ce and ^{136}Nd beams were around 126 A MeV before impinging on a secondary 386 mg/cm^2 gold target at the final focal plane. Projectiles and target nuclei were mainly excited by the electromagnetic interaction. The de-excitation γ-rays in coincidence with projectile residues were detected by 15 EUROBALL cluster Ge detectors [22]. The cluster Ge detectors were placed at forward angles in order to maximize the effective solid angle by the Lorentz boost and to minimize the Doppler broadening effect. They were arranged in three rings around the beam pipe, with the axis of the central detectors in each ring positioned at 16°, 33°, and 36°. A distance of 700 mm between the Ge detectors and the Au target was necessary to achieve an energy resolution of ∼3% in FWHM after Doppler correction. The identification of the nuclei behind the reaction target was performed by an array of nine position-sensitive ΔE–E calorimeter telescopes (CATE) [19] to ensure the necessary conditions for Coulomb excitations. Energy loss was measured with thin (300 μm) position-sensitive Si detectors, whereas the residual-energy detectors were made of CsI(Tl) scintillators. The CATE array covered a relevant opening angle of 58 mrad at 1426 mm from the target. For the present projectile–target combinations an angular range of about 36 mrad is important for Coulomb excitation. The position sensitivity and the information on the incoming trajectory allowed for the scattering angle determination.

In the analysis, the scattering angle between an in-coming and an out-going particle and the γ-ray emission angle with respect to the direction of the scattered projectile were calculated event-by-event and used for the Doppler correction. The ion velocity behind the target was deduced for each event from TOF taking the energy loss in the Au target into account. The accepted scattering angles in the laboratory frame were limited to the range of 0.8°–1.8° which corresponds to impact parameters in the range of 17–39 fm. At smaller impact parameters nuclear interaction interferes with Coulomb excitation and at larger impact parameters the excitation probability vanishes and the particle–γ coincidences are dominated by atomic interactions. For an optimal suppression of atomic background radiation, the analysis required single γ-hit cluster multiplicity for prompt γ-rays at energies in excess of 400 keV in the laboratory frame. Doppler shift corrected γ-ray spectra for ^{134}Ce and ^{136}Nd are displayed in Fig. 1. Gamma-rays depopulating the 2^+_1 and 2^+_2 states are indicated by solid and dashed arrows, respectively. Gamma-rays depopulating the 2^+_1 states are observed in both nuclei. The decay of the 2^+_2 is also clearly visible in ^{136}Nd, while only indications are present for the 557 keV and 966 keV transitions in ^{134}Ce. The excitation energies are already known from former investigations [24]. For the first time, the first and second 2^+ states are observed in Coulomb excitation at incident energies larger than 100 A MeV, at least for the case of ^{136}Nd.

The absolute γ-ray efficiency of the cluster Ge array was determined by a γ–γ coincidence measurement between the 1173 keV and 1333 keV transition of a ^{60}Co source taking into account all combinations of the cluster Ge detectors, combined with the relative efficiency of ^{152}Eu transitions measured as a function of γ-ray energy, and the efficiency in the rest frame was Lorentz transformed with a velocity parameter of $v/c = 0.42$ to obtain the absolute efficiency for γ-rays emitted from the moving projectiles. Besides particle–γ coincidences, beam particles were also recorded requiring an incoming particle in the last plastic scintillator. From the measured γ-ray intensities the Coulomb excitation cross sections can be determined, that are directly proportional to the reduced transition probabilities. For the analysis and especially for the $2^+_2 \rightarrow 2^+_1$ transition the γ-ray angular distribution has to be known. Since the intensity of the latter transition was

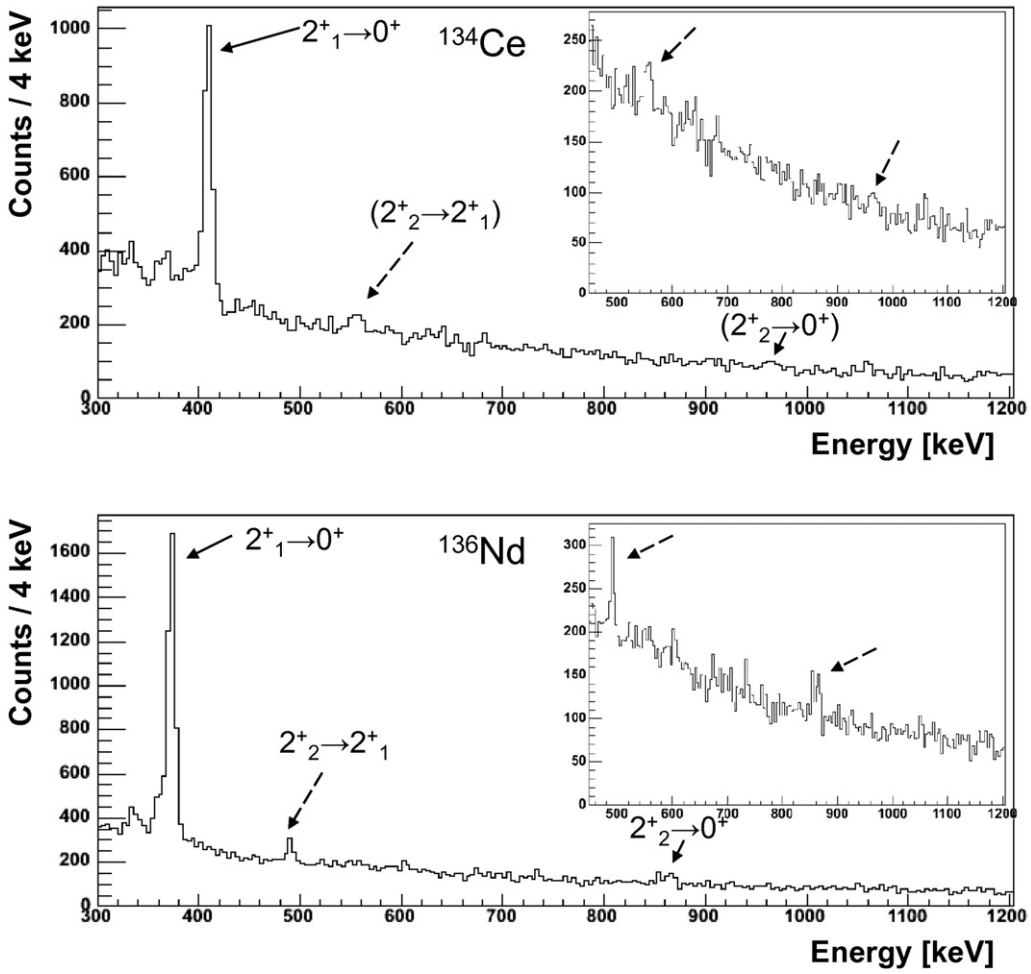

Fig. 1. Doppler shift corrected γ-ray spectra for ^{134}Ce (top panel) and ^{136}Nd (bottom panel). The insets show the regions with the weak transitions depopulating the second 2^+ state. Gamma-rays depopulating the 2^+_1 and 2^+_2 states are indicated by solid and dashed arrows, respectively.

too weak to be analyzed as a function of the γ-ray emission angle, the $2^+_1 \rightarrow 0^+$ transition in ^{134}Ce was used to extract the γ-ray angular distribution and the particle–γ angular correlation in order to obtain information on the spin alignment. Our data exhibit a flat angular distribution within statistical fluctuations. One could suppose that such a small alignment could be the result of a substantial feeding from the giant dipole resonance (GDR) states to the 2^+ states. However, a typical cross section for GDR states is expected to be on the order of 100 mb and a branching ratio for 2^+ feeding with respect to ground state decay is on the order of 1%. Therefore, the distortion of the alignment by the excitation of GDR states should be negligible. From the previous work [25] a clear angular distribution was reported for relativistic Coulomb excitations of ^{38}S and ^{40}S with a gold target. The isotropic angular distribution in the current work may be explained as a deorientation of the nuclear spin by hyperfine interactions, due to the longer lifetimes of the 2^+_1 states as compared to the sulfur nuclei and due to the presence of one or more bound electrons in the Ce and Nd ions emerging from the gold target. In fact, their velocity $v \approx 0.42c$ is very close to the classical velocity $v_0 = (Z/137)c$ of one bound electron in the first Bohr orbit of the ion, while the S ions of Ref. [25] had a velocity much larger than v_0 and were therefore fully stripped. Unfortunately, a quantitative explanation is not available. The data analysis for ^{136}Nd, hence, assumes a flat angular distribution, according to the experimental observation for ^{134}Ce.

Table 1
B(E2) and B(M1) values of transitions depopulating the 2^+_1 and 2^+_2 states in ^{132}Ba, ^{134}Ce and ^{136}Nd. The values for ^{134}Ce and ^{136}Nd are deduced in the present work

Transition	^{132}Ba B(E2) [W.u.]	^{134}Ce B(E2) [W.u.]	^{136}Nd B(E2) [W.u.]
$2^+_1 \rightarrow 0^+$	43(4)[a]	52(5)[a]	80(11)
$2^+_2 \rightarrow 0^+$	3.9(4)[a]	< 11	11(3)
$2^+_2 \rightarrow 2^+_1$	144(14)[a]	< 140	182(93)

[a] From Ref. [24].

In the present work, reduced transition probabilities, B(E2), of transitions depopulating the 2^+_1 and 2^+_2 states of ^{134}Ce and of ^{136}Nd were measured relative to the $B(\mathrm{E2}; 2^+_1 \rightarrow 0^+)$ value in ^{134}Ce which is known to be 52 ± 5 W.u. [23,24]. Following a procedure described in Refs. [26,27], the counts in the γ-ray peaks were normalized to the number of scattered projectiles taking into account the absolute efficiency of the Ge cluster detectors and the deadtime of the data acquisition system (DAQ). From the ratios of these intensities to the $2^+_1 \rightarrow 0^+$ transition in ^{134}Ce, the B(E2) values were determined. Since the relative measurements are free from the major uncertainties of the absolute efficiency calibration for the whole setup [26,27], this method was employed in the present work. The results are listed in Table 1. For the transitions depopulating the 2^+_2 state of ^{134}Ce only an upper limit of the B(E2) values could be determined. The value takes into account the known $2^+_2 \rightarrow 2^+_1/0^+_1$ γ-decay branching ratio [24]. The

decay of the 2_2^+ state proceeds via a pure E2 transition to the ground state. The $2_2^+ \to 2_1^+$ transition in ^{134}Ce is known to be of E2 character to $99.1^{+0.9}_{-1.3}$% [28]. Therefore, a pure E2 transition was assumed for the transition depopulating the 2_2^+ state in ^{134}Ce as well as in ^{136}Nd. Since Coulomb excitation of the ^{197}Au target was also observed, B(E2) values of the observed transitions in ^{134}Ce and ^{136}Nd could be deduced by normalizing to the one of the $7/2^+ \to 3/2^+$ transition of ^{197}Au by taking into account the absolute efficiency of EUROBALL cluster Ge detectors for γ-rays emitted at rest in the laboratory frame and the Coulomb excitation cross section for ^{197}Au. Deduced B(E2) values are 77(26), 97(27), 13(5) and 219(124) W.u. for transitions of $2_1^+ \to 0^+$ in ^{134}Ce, $2_1^+ \to 0^+$, $2_2^+ \to 0^+$ and $2_2^+ \to 2_1^+$ in ^{136}Nd, respectively, which are consistent within errors with the values shown in Table 1 and validate our data analysis. The E2 transition strengths of 43–80 W.u. for the $2_1^+ \to 0^+$ yrast transitions in the $N = 76$ isotones ^{132}Ba, ^{134}Ce, and ^{136}Nd suggest a comparison with a collective nuclear model. From the $B(\mathrm{E2}; 2_1^+ \to 0_1^+)$ values, the intrinsic quadrupole moments Q_0 and the axial β deformation could be estimated if one assumed applicability of the axially-symmetric rigid-rotor relations. The corresponding values would be $Q_0 = 3.0$, 3.3, 4.2 [eb] and the deformation parameters $\beta = 0.19$, 0.20, 0.24 for ^{132}Ba, ^{134}Ce, and ^{136}Nd, respectively. Deviations of the nuclear shape from axial symmetry are observed from the excitation energy ratio of the second 2_2^+ to the first excited 2_2^+ state. In the rigid asymmetric rotor model (ARM) [3] the excitation energy ratio $\mathrm{E}(2_2^+)/\mathrm{E}(2_1^+)$ is given by

$$\frac{\mathrm{E}(2_2^+)}{\mathrm{E}(2_1^+)} = \frac{3+\sqrt{9-8\cdot\sin^2(3\gamma)}}{3-\sqrt{9-8\cdot\sin^2(3\gamma)}}.$$

The γ deformation parameters for ^{132}Ba, ^{134}Ce, and ^{136}Nd derived from this relation would result in $\gamma = 26.3°$, 25.3°, and 25.7°, respectively. For these calculations, the B(E2) ratios were calculated from the intensity ratio of the two transitions depopulating the 2_2^+ state, which is given in Ref. [24]. These γ deformation parameters can be compared with the ratio of B(E2) values through the following equation

$$\frac{B(\mathrm{E2}; 2_2^+ \to 2_1^+)}{B(\mathrm{E2}; 2_2^+ \to 0^+)} = \frac{20}{7}\,\frac{\frac{\sin^2(3\gamma)}{9-8\cdot\sin^2(3\gamma)}}{1-\frac{3-2\cdot\sin^2(3\gamma)}{\sqrt{9-8\cdot\sin^2(3\gamma)}}}$$

within the ARM framework. In Fig. 2 the ratio of B(E2) values connecting the 2_2^+ decay transitions are plotted versus the energy ratio $\mathrm{E}(2_2^+)/\mathrm{E}(2_1^+)$ for ^{134}Ce and ^{136}Nd together with ^{132}Ba. The experimental data are compared with predictions of the γ-rigid [3] (dashed line) and γ-soft [2] (solid line) ARM. In a soft nucleus rotational motions are closely connected with intrinsic vibrations of the nuclear surface. Therefore, the nucleus is stretched under rotation, which leads to a change of the β and γ deformation parameters. To account for this effect Davydov developed the soft asymmetric rotor model [2] in which the additional parameter μ characterizes the deformability of the surface. For $\mu = 0$ the nucleus has a perfect rigid shape. It can be seen from Fig. 2 that only the soft ARM ($\mu \sim 0.5$, $\gamma \sim 23^0$) predicts quite satisfactorily the experimental data of ^{134}Ce and ^{136}Nd, while ^{132}Ba seems to be more γ rigid.

However, the energy staggering

$$S(I) = \frac{\mathrm{E}(I) - \mathrm{E}(I-1)}{\mathrm{E}(I+1) - \mathrm{E}(I-1)} - \frac{I}{2I+1}$$

of the quasi-γ band predicted by the ARM is opposite in phase to those observed for the $N = 76$ isotones [$S_{^{134}\mathrm{Ce}}(3_1^+) = +0.187$, $S_{^{134}\mathrm{Ce}}(4_2^+) = -0.054$, $S_{^{136}\mathrm{Nd}}(3_1^+) = +0.113$, $S_{^{136}\mathrm{Nd}}(4_2^+) = -0.063$].

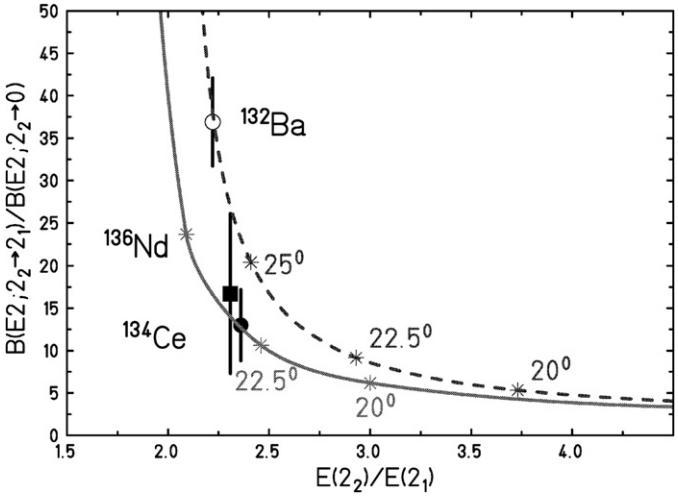

Fig. 2. Ratio of B(E2) values connecting the 2_2^+ decay transitions as a function of the energy ratio $\mathrm{E}(2_2^+)/\mathrm{E}(2_1^+)$. The data of ^{132}Ba (○), ^{134}Ce (●) and ^{136}Nd (■) are compared with predictions of the γ-rigid (dashed line) and γ-soft ($\mu = 0.5$) asymmetric rotor model [2,3]. The asterisk denote the theoretical results which are calculated in steps of 2.5^0 in γ.

The experimental staggering hints at a considerable degree of γ-softness. Complete γ-independence of the potential would result in O(5) symmetry [1,5] which yields the maximum energy staggering $S_{\mathrm{O}(5)}(3_1^+) = +0.571$ and $S_{\mathrm{O}(5)}(4_2^+) = -0.444$. These values have the right phase but are too extreme.

In order to characterize the quadrupole shape of ^{136}Nd and ^{134}Ce we have performed GCM calculations with the potential $V(\beta,\gamma) = V_0[\beta^2 + c_3\beta^3\cos(3\gamma) + c_4\beta^4 + c_6\beta^6\cos^2(3\gamma)]$. The parameters were adjusted for simultaneous description of the ground band energies, the $\mathrm{E}(2_2^+)/\mathrm{E}(2_1^+)$ energy ratio, the E2 branching ratio of the 2_2^+, and the energy staggering of the quasi-γ band.

Fig. 3 compares the low-energy level scheme of ^{136}Nd to the GCM results for potential parameters $V_0 = -2.125$ MeV; $c_3 = 0.112$; $c_4 = -9.874$ and $c_6 = -10.345$. The agreement with the experiment is satisfactory except for the moment of inertia of excited bands, as must be expected for geometrical models without intrinsic degrees of freedom. The calculated staggerings, $S_{\mathrm{GCM},^{136}\mathrm{Nd}}(3_1^+) = +0.137$ and $S_{\mathrm{GCM},^{136}\mathrm{Nd}}(4_2^+) = -0.022$ do not depend on a scaling factor for the Moments of Inertia and are close to the experimental values. Panels (c) and (d) show the potential energy as a function of the deformation variables. The potential exhibits a shallow minimum at $\beta_{\min} = 0.225$, $\gamma_{\min} = 20.6°$ with pronounced γ-softness. Our GCM fits show that a similar description holds for ^{134}Ce. We conclude that the region of γ-soft nuclei extends from the Xe, Ba-region [4,30,31] well up to ^{136}Nd at least. The even–even nuclei, ^{134}Ce and ^{136}Nd, are not sufficiently γ-rigid to serve as rigid triaxial cores of neighboring odd–odd nuclei in order to sustain chiral geometry without shape-polarizing effects from the unpaired nucleons. In turn, a possible observation of chiral structures in the particle–core coupled neighbors to ^{134}Ce or ^{136}Nd must be considered as direct evidence for these shape-polarizing effects.

In summary, the $B(\mathrm{E2}; 2_1^+ \to 0^+)$ in the ^{134}Ce and ^{136}Nd nuclei, $B(\mathrm{E2}; 2_2^+ \to 0^+)$, and $B(\mathrm{E2}; 2_2^+ \to 2_1^+)$ values in the ^{136}Nd nucleus were measured for the first time by relativistic Coulomb excitation. The comparison with the asymmetric rotor model and the Geometrical Collective Model yields information on the nuclear shape, namely the β and γ quadrupole deformation parameters. It is found that the data hint at a pronounced γ-softness of the $N = 76$ isotones even up to ^{136}Nd.

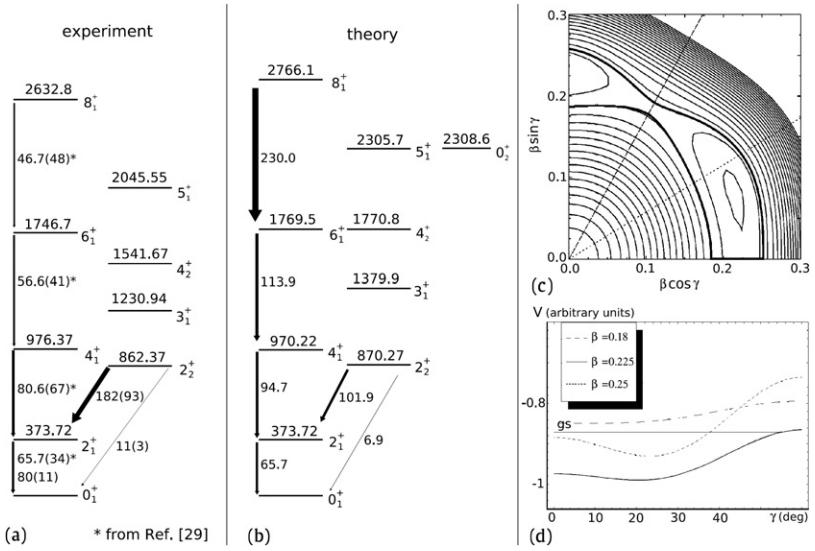

Fig. 3. Theoretical description of the low-energy level scheme of ^{136}Nd (a) with the GCM (b). Excitation energies are given in keV and E2 strengths in W.u. The experimental values indicated with "*" are taken from Ref. [29]. Panel (c) shows the potential energy surface used for the calculation as a function of the shape variables. The bold line denotes the ground state energy. Cross sections of the potential energy surface for three different values of the deformation parameter β are shown in panel (d) as a function of γ. Substantial γ-softness is obvious.

Acknowledgements

The authors would like to thank the accelerator department at GSI for their technical support during the experiment. Authors also wish to acknowledge the department of computing and experiment electronics (I.T. and E.E.) for their support on the data acquisition system and the go4 software. D.L. Balabanski was supported in part by the Bulgarian Science Fund, grant VUF05/06. J. Beller and N. Pietralla acknowledge support from the German DFG under Grant SFB 634. A. Bürger acknowledges the support by German BMBF grant No. 06BN-109. A. Maj acknowledges partial financial support by the Polish Ministry of Education and Science, Grant No. 1 P03B030 30. N. Pietralla and G. Rainovski acknowledge support by the USA DOE, Grant No. DE-FG02-04ER41334. P. Reiter was supported by German BMBF grant No. 06K-167.

References

[1] L. Wilets, M. Jean, Phys. Rev. 102 (1956) 788.
[2] A.S. Davydov, A.A. Chaban, Nucl. Phys. 20 (1960) 499.
[3] A.S. Davydov, G.F. Filippov, Nucl. Phys. 8 (1958) 237.
[4] R.F. Casten, P. von Brentano, Phys. Lett. B 152 (1985) 22.
[5] A. Arima, F. Iachello, Phys. Rev. Lett. 40 (1978) 385; A. Arima, F. Iachello, Ann. Phys. (N.Y.) 123 (1979) 468.
[6] M.O. Kortelahti, et al., Phys. Rev. C 42 (1990) 1267.
[7] B.D. Kern, et al., Phys. Rev. C 36 (1987) 1514.
[8] S. Frauendorf, J. Meng, Nucl. Phys. A 617 (1997) 131.
[9] V.I. Dimitrov, S. Frauendorf, F. Donau, Phys. Rev. Lett. 84 (2000) 5732.
[10] C.M. Petrache, et al., Nucl. Phys. A 597 (1996) 106.
[11] K. Starosta, et al., Phys. Rev. Lett. 86 (2001) 971.
[12] D.J. Hartley, et al., Phys. Rev. C 64 (2001) 031304(R).
[13] T. Koike, K. Starosta, C.J. Chiara, D.B. Fossan, D.R. LaFosse, Phys. Rev. C 67 (2003) 044319.
[14] D. Tonev, et al., Phys. Rev. Lett. 96 (2006) 052501.
[15] C.M. Petrache, G. Hagemann, I. Hamamoto, K. Starosta, Phys. Rev. Lett. 96 (2006) 112502.
[16] D. Tonev, et al., Phys. Rev. C 76 (2007) 044313.
[17] S. Mukhopadhyay, et al., Phys. Rev. Lett. 99 (2007) 172501.
[18] G. Gneuss, W. Greiner, Nucl. Phys. A 171 (1971) 449.
[19] H.J. Wollersheim, et al., Nucl. Instrum. Methods A 537 (2005) 637.
[20] H. Geissel, et al., Nucl. Instrum. Methods B 70 (1992) 286.
[21] R. Schneider, A. Stolz, Technical Manual Ionisation Chamber MUSIC80, 2000.
[22] J. Eberth, et al., Nucl. Instrum. Methods A 369 (1996) 135.
[23] D. Husar, et al., Nucl. Phys. A 292 (1977) 267.
[24] National Nuclear Data Center, http://www.nndc.bnl.gov.
[25] A.D. Davies, et al., Phys. Rev. Lett. 96 (2006) 112503.
[26] A. Bürger, et al., Phys. Lett. B 622 (2005) 29.
[27] A. Banu, et al., Phys. Rev. C 72 (2005) 061305(R).
[28] A. Gade, et al., Nucl. Phys. A 673 (2000) 45.
[29] G. Kemper, Dissertation, Univ. zu Köln, 2000, http://kups.ub.uni-koeln.de/volltexte/2003/523/.
[30] O. Vogel, et al., Phys. Rev. C 53 (1996) 1660.
[31] R.A. Meyer, et al., Phys. Rev. C 14 (1976) 2024.

Search for the Pygmy Dipole Resonance in ^{68}Ni at 600 MeV/nucleon

O. Wieland,[1] A. Bracco,[1,2] F. Camera,[1,2] G. Benzoni,[1] N. Blasi,[1] S. Brambilla,[1] F. C. L. Crespi,[1,2] S. Leoni,[1,2] B. Million,[1] R. Nicolini,[1,2] A. Maj,[3] P. Bednarczyk,[3] J. Grebosz,[3] M. Kmiecik,[3] W. Meczynski,[3] J. Styczen,[3] T. Aumann,[4] A. Banu,[4] T. Beck,[4] F. Becker,[4] L. Caceres,[4,*] P. Doornenbal,[4,†] H. Emling,[4] J. Gerl,[4] H. Geissel,[4] M. Gorska,[4] O. Kavatsyuk,[4] M. Kavatsyuk,[4] I. Kojouharov,[4] N. Kurz,[4] R. Lozeva,[4] N. Saito,[4] T. Saito,[4] H. Schaffner,[4] H. J. Wollersheim,[3] J. Jolie,[5] P. Reiter,[5] N. Warr,[5] G. deAngelis,[6] A. Gadea,[6] D. Napoli,[6] S. Lenzi,[7,8] S. Lunardi,[7,8] D. Balabanski,[9,10] G. LoBianco,[9,10] C. Petrache,[9,‡] A. Saltarelli,[9,10] M. Castoldi,[11] A. Zucchiatti,[11] J. Walker,[12] and A. Bürger[13,§]

[1]*INFN Sezione di Milano, I-20133 Milano, Italy*
[2]*Dipartimento di Fisica, Universitá di Milano, I-20133 Milano, Italy*
[3]*Institute of Nuclear Physics, Polish Academy of Sciences, 31-342 Kraków, Poland*
[4]*GSI, D-64291 Darmstadt, Germany*
[5]*Institut für Kernphysik, Universität zu Köln, D-50937 Köln, Germany*
[6]*Laboratori Nazionali di Legnaro, INFN, I-35020 Legnaro, Italy*
[7]*Dipartimento di Fisica, Universitá di Padova, I-35122 Padova, Italy*
[8]*INFN Sezione di Padova, I-35122 Padova, Italy*
[9]*Dipartimento di Fisica, Universitá di Camerino, I-62032 Camerino, Italy*
[10]*INFN Sezione di Perugia, I-06123 Perugia, Italy*
[11]*INFN Sezione di Genova, I-16146 Genova, Italy*
[12]*University of Surrey, Guildford, Surrey, GU2 7XH, United Kingdom*
[13]*HISKP, Universität Bonn, D-53115 Bonn, Germany*

(Received 19 September 2008; published 4 March 2009)

The γ decay from Coulomb excitation of ^{68}Ni at 600 MeV/nucleon on a Au target was measured using the RISING setup at the fragment separator of GSI. The ^{68}Ni beam was produced by a fragmentation reaction of ^{86}Kr at 900 MeV/nucleon on a ^{9}Be target and selected by the fragment separator. The γ rays produced at the Au target were measured with HPGe detectors at forward angles and with BaF_2 scintillators at backward angles. The measured spectra show a peak centered at approximately 11 MeV, whose intensity can be explained in terms of an enhanced strength of the dipole response function (pygmy resonance). Such pygmy structure has been predicted in this unstable neutron-rich nucleus by theory.

DOI: 10.1103/PhysRevLett.102.092502 PACS numbers: 24.30.Gd, 25.70.De, 27.50.+e

The electric dipole ($E1$) response of nuclei at energies around the particle separation energy is presently attracting a lot of attention, particularly for unstable neutron-rich nuclei produced as radioactive beams. One of the important aspects in this connection is that the dipole strength distribution affects reaction rates in astrophysical scenarios where photodisintegration reactions are important, i.e., in hot stars and stellar explosions [1]. The accumulation of $E1$ strength around the particle separation energy is commonly denoted by the pygmy dipole resonance (PDR) due to the minor size of its strength in comparison with the giant dipole resonance which dominates the $E1$ response, and exhausts the Thomas-Reiche-Kuhn (TRK) oscillator sum rule. In the case of stable nuclei extensive work has been done ([2,3] and references therein) with photon scattering experiments in different mass regions and in general it is seen that the low energy $E1$ strength (below and around the neutron binding energy) is larger than that due to the tail of the giant dipole resonance (GDR). It is also found that this low energy strength increases with the N/Z ratio. Qualitatively, this increase has been explained as due to the vibration of the neutron skin. The problem of how the $E1$ strength evolves for nuclei far from stability in the neutron-rich side is presently one of the interesting topics in nuclear structure since it provides information on the properties of the neutron skin and on the nuclear equation of state for asymmetric nuclear matter, relevant for the study of neutron stars [4]. In particular, it is presently theoretically under discussion to which extent pygmy resonances represent a collective vibration of excess neutrons against an isospin-symmetric core [5]. For nuclei far from stability the pygmy dipole resonance was investigated using the heavy-ion induced electromagnetic excitation process at high beam energies. Low-lying dipole strength in the energy region below the GDR has been observed in the oxygen isotopes $^{20-22}$O [6,7] and in several neutron-rich nuclei around ^{132}Sn [8]. The unstable nucleus ^{68}Ni represents a good case to search for pygmy structures. This nucleus is located in the middle of the long isotopic Ni chain having at the extremes the doubly magic ^{56}Ni and ^{78}Ni and is experimentally accessible with the present radioactive beam facilities. In addition, different theoretical predictions on the pygmy dipole strength are available for this mass region [9–11]. The present Letter reports on the first search of the pygmy dipole resonance in ^{68}Ni using the virtual photon scattering technique at 600 MeV/nucleon, at which the excitation of vibrations of electric dipole character is dominating over other excitation modes [12].

The ^{68}Ni beam was produced from the fragmentation of ^{86}Kr beam from SIS at GSI at 900 MeV/nucleon with an intensity of $\sim 10^{10}$ particles per 6 s spill (10 s repetition rate) and focused on a 4 g/cm^2 thick ^{9}Be target. The ^{68}Ni ions were selected together with few other ions using the fragment separator (FRS [13]). A total of approximately 3×10^7 ^{68}Ni events were collected. The upper panel of Fig. 1 displays the selected and well separated ions. The ^{68}Ni ions are the most intense component (33% of the beam cocktail) impinging on the Au target (2 g/cm^2 thick). The particle identification after the Au target was performed by a calorimeter (CATE) [14,15] placed at 0°. It consisted of nine thin position sensitive Si detectors in front of four 6 cm thick CsI detectors, arranged symmetrically with respect to the beam. The opening angle θ of CATE is $\pm 2.0°$, which is much larger than the grazing angle of 0.43°. The total energy and energy loss correlation of events measured in CATE and corresponding to ^{68}Ni ions are shown in the middle panel of Fig. 1. The FWHM of the measured total energy peak is approximately 1% and therefore the present resolution is sufficient to discriminate between different masses of the outgoing nuclei. The γ-ray emission at the target location was measured using a specific configuration of the RISING setup [14]. Gamma rays were detected at different angles, at 16°, 33°, and 36° with the 15 HPGe clusters of the RISING array [16], at 51° and 88° with 7 HPGe segmented clusters of the Miniball [17] array and at 88° and 142° with 8 BaF_2 of the HECTOR array [18]. An important requirement to obtain γ-ray spectra from the measured data is to determine the v/c of the γ emitting nuclei on an event by event basis by tracking their trajectories before and after the Au target interaction. This is particularly important for large values of v/c as in the case of this experiment having $v/c \approx 0.79$ and a thick target. In fact, the target thickness induces a spread in the v/c value of $\approx 1\%$. In addition, all the γ-ray spectra here discussed are associated to ^{68}Ni scattered at $\theta \leq 0.43°$ to select Coulomb excitation [14]. In addition, the events used for the following analysis had γ multiplicity equal to one, corresponding to one γ-ray detector firing out of the 30 available. This is to reduced high multiplicity background events. The γ-ray energy spectrum measured with the HPGe RISING cluster detectors is shown for the high-energy region in Fig. 1 (lower panel). In order to check whether or not the measured structure at around 11 MeV could be due to γ transitions in a narrow peak emitted by the projectile, a GEANT [19] simulation was made. The simulation corresponded to a γ transition of 11 MeV from a moving source and included the source and detection conditions. In particular, the angular and energy straggling of the projectile in the target and the relativistic effects depending on position and opening angle of the detector were included. The result of the simulation, shown in the bottom panel of Fig. 1 by the continuous line, reproduces rather well the measured peak structure. An additional way to confirm that the peak structure at 11 MeV is originating from the deexcitation of ^{68}Ni projectile is to verify the angular dependence of the Doppler correction of the fast moving emitting source. The spectrum measured with BaF_2 detectors at 88° and corrected for the projectile velocity (Fig. 2) clearly shows a peak at 11 MeV. The cross section values were deduced by measuring singles events, not requiring γ detection, in the CATE calorimeter and by computing the γ detection efficiency of the array taking into account the γ angular distributions as given by the Lorentz boost. Also in this BaF_2 detector spectrum a peak structure is present at around 11 MeV. The error bars reflect the statistical error and the uncertainty in the determination of the value of v/c. In the inset of the figure the peak region of the BaF_2

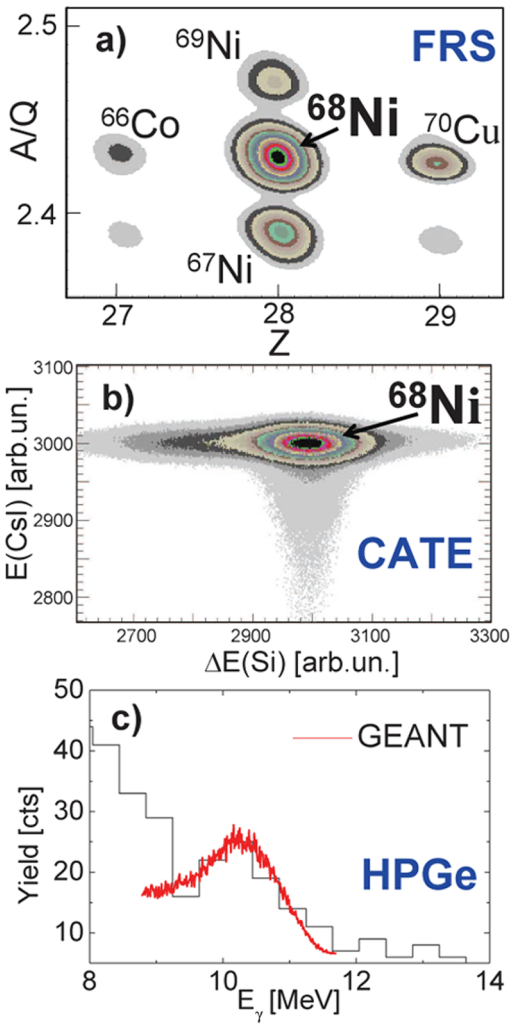

FIG. 1 (color online). In the upper panel (a) the fragments selected in the FRS are shown in a A/Q versus Z plot. The central panel (b) shows the E-ΔE spectra (from the CsI and Silicon detectors) of the outgoing beam detected after the target in the CATE calorimeter with selection of the incoming ^{68}Ni. In the lower panel (c) HPGe spectrum of the Cluster detectors after selecting incoming and outgoing ^{68}Ni and applying the Doppler correction for the projectile is shown. The continuous line is the result of a GEANT simulation for the in flight emission of a 11 MeV γ transition.

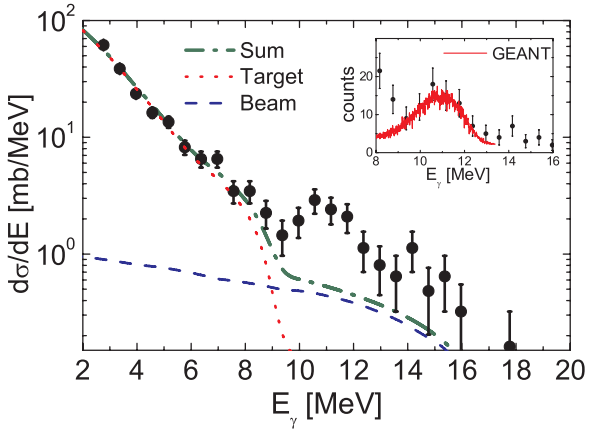

FIG. 2 (color online). The high-energy γ-ray spectrum measured with BaF_2 detectors and Doppler corrected with the velocity of the projectile. The lines are the statistical model calculations for the target (dotted line) and for the beam (dashed line) nuclei. In the inset the continuous line superimposed to the measured data is the result of a GEANT simulation for a γ-transition at 11 MeV.

detectors is shown in a linear scale together with the corresponding GEANT simulation. It is important to mention that for the HPGe detectors, being placed close to the CATE detector and having a time resolution >10 ns, the background reduction is not as good as for the BaF_2 detectors (placed backward and with a time resolution of <1 ns). For the spectra measured with BaF_2 detectors we have performed statistical model calculations [20] to interpret schematically the exponential part of the spectra. For the statistical calculation we have used the energy value given by the adiabatic cutoff energy of the Coulomb excitation process (≈ 20 MeV). The adiabatic limit of Coulomb excitation was deduced with $E_{\max} \approx \frac{\hbar c \beta \gamma}{b_{\min}}$, where $b_{\min}$ is the smallest impact parameter for which interactions involving nuclear forces are negligible. The calculated statistical emission from the target and projectile was obtained using the standard GDR strength function, by correcting the γ-ray energy for the Doppler shift due to the projectile velocity (to be consistent with the experimental data treatment) and by folding with the detector response function. The condition of detecting only one γ ray can be neglected in the statistical model calculation because both the γ-ray efficiency ($\approx 5\%$ at 1 MeV) and the γ multiplicity produced by the reaction (measured to be ≈ 1.1) are low. The statistical model predictions are shown in Fig. 2 in comparison with the data normalized at 3–5 MeV. One can note that the sum of the target and projectile statistical contributions reproduces remarkably well the exponential shape of the data and that there is an excess yield very pronounced at around 11 MeV, which can be attributed to the projectile emission on the basis of Doppler correction arguments. The data in the region of interest for searching the pygmy resonance in the electric dipole response function were obtained by subtracting from the measurements the computed statistical model contribution and some background extrapolated from the very high-energy region. The corresponding data are shown in the bottom panel of Fig. 3. The present results of the γ decay of the ^{68}Ni at 600 MeV/nucleon are characterized by a peak structure centered at 11 MeV for which it is important to understand not only the shape but also the measured value of the cross section. To describe the measured cross section for γ emission from the ^{68}Ni nucleus in the region $E_\gamma > 6$ MeV we have to evaluate the product of the excitation cross section σ^{exc} with the branching ratio for γ emission R_γ.

The γ-ray emission from the GDR is expected to be dominated by the ground state decay and the decay to the 2^+ state (due to the coupling of 1^- to 2^+) depends on the nuclear structure [21]. The latter for the pygmy, having a much smaller width (<1 MeV), is expected to be smaller. To verify this we have examined the 9–11 MeV region

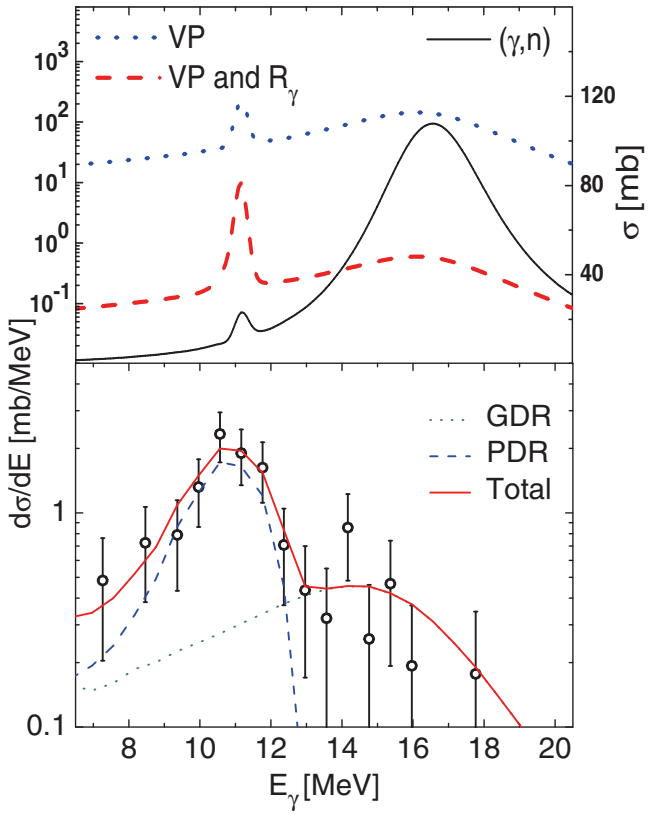

FIG. 3 (color online). In the upper part the ^{68}Ni photoabsorption cross section is shown with a full drawn line (scale on the right). The differential cross section obtained after applying the equivalent virtual photon method (VP) is shown with a dotted line (scale on the left). The dashed line (scale on the left) is obtained by including the γ branching ratio (VP and R_γ). In the bottom panel the open circles show the γ-ray cross section measured with BaF_2 detectors. The 3 lines in the bottom panel display calculations of the γ cross section (including the response function). The long dashed line is the decay of the PDR, the dotted line is the decay of the GDR and the thick line the sum of the two contributions.

when adding a possible component centered at 9 MeV (corresponding to the decay from the pygmy state to the 2^+ state at 2.033 MeV). This resulted in a worsening of the fit already with a contributions of 10%. The differential Coulomb excitation cross section for $E1$ multipolarity (integrated from a minimum impact parameter $b_{\min}$ to infinity [22]) is given by

$$\frac{d\sigma_{E1}}{dE_\gamma} = \sigma^{\mathrm{exc}} * R_\gamma = \left(\frac{1}{E_\gamma} N\sigma^{\mathrm{abs}}\right) * R_\gamma, \qquad (1)$$

where N is the equivalent virtual photon number for pure Coulomb excitation and σ^{abs} is the photonuclear cross section with multipolarity $E1$. From expression (1) one can see that indeed the γ energy and virtual photon number factors produce an excitation cross section characterized by a sizable distortion of the electric dipole response function. This point is illustrated in the top panel of Fig. 3. In this figure an electric dipole response function with a small peak at 11 MeV with 5% of the energy weighted sum rule strength (EWSR) is shown. The corresponding $\frac{1}{E_\gamma} N\sigma^{\mathrm{abs}}$ is shown in the same figure with the dotted line. The virtual photon number was evaluated by choosing as minimum impact parameter for Coulomb excited nuclei $b_{\min} = 12.85$ fm from the systematics of Benesh *et al.* [23]. The comparison of the continuous and dotted lines shows clearly how the large flux of virtual photons at the lowest energy enhances, as expected, the intensity of the electric dipole response in the pygmy region. The additional and very important effect of R_γ is displayed with dashed line curve. For the evaluation of R_γ the procedure described in Refs. [24,25] has been adopted. In particular R_γ is due to two contributions $R_\gamma = R_\gamma^{\mathrm{dir}} + R_\gamma^{\mathrm{CN}}$, where R_γ^{dir} is the direct decay contribution while R_γ^{CN} is the decay after the resonance had coupled to the compound nucleus states at the same excitation energy. This latter contribution depends on the nuclear level density. For the calculation shown with dashed line in Fig. 3 the adopted level density is based on the shell model Monte Carlo calculation [26]. Using this level density the total γ branching ratio is found to be $\approx 0.4\%$ and $\approx 4\%$ for the region of the GDR and the PDR, respectively. The present values are consistent with the total photon branch integrated over the energy interval 9.5–25 MeV of the heavier ^{208}Pb ($R_\gamma \approx 2\%$) [24]. The detector response function was folded to the dashed curve of Fig. 3 and the corresponding result is shown in the bottom panel. There is a remarkable agreement of the calculated cross section with the data both in size and shape when one assumes an electric dipole strength function with $\approx 5\%$ of EWSR strength at 11 MeV [the corresponding $B(E1)$ value being 1.2 e^2 fm^2]. In contrast, a calculation assuming a standard Lorentzian function, presented as a short dashed line in the bottom panel of Fig. 3 produces a spectral shape and size of the cross section which differs from the data by approximately 1 order of magnitude in the region below 12 MeV. Theoretical predictions are available for the pygmy resonance for neutron-rich nuclei such as Sn and Ni isotopes [9–11,27]. In particular, for the ^{68}Ni nucleus, recent calculations within the relativistic random phase approximation (RRPA) model [9] and the quasiparticle relativistic random phase (QRRPA) model [10] predict at 9–10 MeV a pygmy structure with a EWSR strength of 4% and 10%, respectively. For the analysis of the present data an assumption of 9% of the EWSR strength in the pygmy region could fit the data if the used value of the level density is a simple extrapolation from stable nuclei. The level density value from stable nuclei is a factor of ≈ 5 larger of that used in the calculation of Fig. 3 taken from more accurate calculations [26]. The interesting result here obtained on the strength of the pygmy resonance (5% to 9% of the EWSR strength) calls for experiments on level density measurements in exotic nuclei to pin down with smaller uncertainty the $E1$ strength.

In summary, we have here presented the first experimental search of a pygmy resonance in the neutron-rich ^{68}Ni nucleus using the virtual photon scattering technique. Evidence is found for the presence of sizeable strength energetically located below the GDR and centered at ≈ 11 MeV with approximately 5% of the EWSR strength. This is similar to what has been found in unstable neutron-rich ^{132}Sn [8], but is sizably larger than in stable nuclei. This result is in rather good agreement with theoretical predictions and provides relevant information which can be related to neutron skin and nuclear symmetry energy [4]. The present result for the ground state γ decay from the pygmy resonance opens interesting future perspectives with more intense radioactive beams and further improved instrumentation for γ detection at relativistic energies such as the AGATA γ-ray tracking array. In fact, it will be very interesting for the study of neutron skin in nuclei far from stability to measure more in detail and systematically the structure of the electric dipole response in an energy interval larger than that of the present experiment.

This work was partially supported by the Italian Istituto Nazionale di Fisica Nucleare and by the Polish Ministry of Science and Higher Education Grants No. 1 P03B 03030.

*Present address: Universidad Autonoma de Madrid, E-28049 Madrid, Spain.
†Present address: RIKEN, Wako, Saitama 351-0198, Japan.
‡Present address: Univerisité Paris-sud and IPN Orsay, F-91406 Orsay Cedex, France.
§Present address: University of Oslo, NO-0317 Oslo, Norway.

[1] S. Goriely, Phys. Lett. B **436**, 10 (1998); S. Goriely and E. Khan, Nucl. Phys. **A706**, 217 (2002).
[2] G. A. Bartholomew, *et al.*, Adv. Nucl. Phys. **7**, 229 (1973).
[3] T. Hartmann *et al.*, Phys. Rev. Lett. **93**, 192501 (2004).
[4] A. Klimkiewicz *et al.*, Phys. Rev. C **76**, 051603 (2007).
[5] J. Piekarewicz Phys. Rev. C **73**, 044325 (2006).

[6] A. Leistenschneider *et al.*, Phys. Rev. Lett. **86**, 5442 (2001).
[7] E. Tryggestad *et al.*, Phys. Lett. B **541**, 52 (2002).
[8] P. Adrich *et al.*, Phys. Rev. Lett. **95**, 132501 (2005).
[9] D. Vretenar *et al.*, Nucl. Phys. **A692**, 496 (2001).
[10] L. Cao and Z. Ma, Mod. Phys. Lett. A **19**, No. 38, 2845 (2004).
[11] N. Paar *et al.*, Rep. Prog. Phys. **70** 691 (2007).
[12] T. Aumann, Eur. Phys. J. A **26**, 441 (2005).
[13] H. Geissel *et al.*, Nucl. Instrum. Methods Phys. Res., Sect. B **70**, 286 (1992).
[14] H. J. Wollersheim *et al.*, Nucl. Instrum. Methods Phys. Res., Sect. A **537**, 637 (2005).
[15] R. Lozeva *et al.*, Nucl. Instrum. Methods Phys. Res., Sect. A **562**, 298 (2006).
[16] G. de Angelis, A. Bracco, and D. Curien, Europhysics News **34**, 181 (2003).
[17] J. Eberth *et al.*, Prog. Part. Nucl. Phys. **46**, 389 (2001).
[18] O. Wieland *et al.*, Phys. Rev. Lett. **97**, 012501 (2006); A. Bracco *et al.*, Mod. Phys. Lett. A**22**, No. 33, 2479 (2007).
[19] R. Brun *et al.*, CERN Report No. CERN-DD/EE/84-1.
[20] I. Dioszegi *et al.*, Phys. Rev. C **63**, 047601 (2001).
[21] V. Yu. Ponomarev and A. Krasznahorkay, Nucl. Phys. A **550**, 150 (1992).
[22] C. Bertulani and G. Baur, Phys. Rep. **163**, 299 (1988), and references therein.
[23] C. Benesh, B. Cook, and J. Vary, Phys. Rev. C **40**, 1198 (1989).
[24] J. R. Beene *et al.*, Phys. Rev. C **41**, 920 (1990).
[25] J. R. Beene, G. F. Bertsch, P. F. Bortignon, and R. A. Broglia Phys. Lett. B **164**, 19 (1985).
[26] Y. Alhassid *et al.*, Phys. Rev. Lett. **99**, 162504 (2007); C. N. Gilbreth and Y. Alhassid (private communication).
[27] D. Sarchi *et al.*, Phys. Lett. B **601**, 27 (2004).

Nuclear Instruments and Methods in Physics Research A 613 (2010) 218–225

Contents lists available at ScienceDirect

Nuclear Instruments and Methods in Physics Research A

journal homepage: www.elsevier.com/locate/nima

Lifetime effects for high-resolution gamma-ray spectroscopy at relativistic energies and their implications for the RISING spectrometer

P. Doornenbal [a,b,*], P. Reiter [a], H. Grawe [b], T. Saito [b], A. Al-Khatib [c], A. Banu [b], T. Beck [b], F. Becker [b], P. Bednarczyk [b,d], G. Benzoni [e], A. Bracco [e,f], A. Bürger [c], L. Caceres [b,g], F. Camera [e,f], S. Chmel [c,1], F.C.L. Crespi [e,f], H. Geissel [b], J. Gerl [b], M. Górska [b], J. Grębosz [b,d], H. Hübel [c], M. Kavatsyuk [b,h], O. Kavatsyuk [b,h], M. Kmiecik [d], I. Kojouharov [b], N. Kurz [b], R. Lozeva [b,i,2], A. Maj [d], S. Mandal [j], W. Meczynski [d], B. Million [e], Zs. Podolyák [k], A. Richard [a], N. Saito [b], H. Schaffner [b], M. Seidlitz [a], T. Striepling [a], J. Walker [b], N. Warr [a], H. Weick [b], O. Wieland [e], M. Winkler [b], H.J. Wollersheim [b]

[a] Institut für Kernphysik, Universität zu Köln, 50937 Köln, Germany
[b] GSI Helmholtzzentrum für Schwerionenforschung GmbH, 64291 Darmstadt, Germany
[c] Helmholtz-Institut für Strahlen- und Kernphysik, Universität Bonn, 53115 Bonn, Germany
[d] The Niewodniczanski Institute of Nuclear Physics, Polish Academy of Sciences, 31-342 Krakow, Poland
[e] INFN Sezione di Milano, 20133 Milano, Italy
[f] Dipartimento di Fisica, Università di Milano, 20133 Milano, Italy
[g] Departamento de Física Teórica, Universidad Autonoma de Madrid, 28049 Madrid, Spain
[h] Taras Shevchenko Kiev National University, 03680 Kiev, Ukraine
[i] Faculty of Physics, St. Kliment Ohridski University of Sofia, 1164 Sofia, Bulgaria
[j] Department of Physics and Astrophysics, University of Delhi, Delhi 110 007, India
[k] Department of Physics, University of Surrey, Guildford GU2 7XH, UK

ARTICLE INFO

Article history:
Received 30 October 2009
Accepted 4 November 2009
Available online 11 November 2009

Keywords:
In-beam γ−ray spectroscopy
Lifetime measurement techniques

ABSTRACT

The lineshapes and peak position of Doppler corrected γ−ray spectra from in-beam experiments at relativistic energies are investigated with respect to the intrinsic energy resolution of the employed detectors, the particles' velocities, and the photons' emission angle uncertainties at the moment of γ−ray emission. The uncertainties in velocity and photon emission angle are dependent on the lifetime of the excited state. The impact of these two observables on the lineshape and energy resolution are studied for the RISING γ−spectrometer by means of simulations and experimental results from a two-step fragmentation experiment at $\approx 200\,\mathrm{MeV}/u$. Potential use of the distinct lineshape for lifetime determination is demonstrated for measured γ−ray transitions.

1. Introduction

In recent years, the development of in-beam γ−ray spectroscopy of radioactive ion beams from in-flight facilities at relativistic energies has enabled nuclear structure investigations that were previously beyond reach. In these experiments, rare isotope facilities provide in-flight separated beams with relativistic velocities in the range of $0.3 \leq \beta \leq 0.8$ after primary fragmentation reactions, which are incident on a secondary target to induce reactions such as Coulomb excitation or knockout reactions [1,2]. A decisive advantage of this method is given by the beam's high energy. Thick secondary reaction targets can be employed due to the low energy loss at these beam energies, compensating very low secondary beam rates.

The emitted γ−rays from decaying excited states are substantially Doppler shifted in the laboratory frame, which requires a back transformation of the γ−ray energy into the nuclei's rest frame system. The achievable energy resolution after the Doppler correction depends mainly on the following factors: (i) the intrinsic detector energy resolution, (ii) the effective opening angle of the utilized γ−ray detectors, (iii) the accuracy of the position and velocity determination of the heavy ion at the moment when the γ−ray decay occurs. Position measurements of the individual beam particles are mandatory to track the heavy ions' paths in front of and behind the reaction target. Due to forward peaked small scattering angles at relativistic energies an accurate transversal position determination of the γ−ray decay

* Corresponding author. Present address: RIKEN Nishina Center for Accelerator-Based Science, 2-1 Hirosawa, Wako, Saitama 351-0198, Japan.
E-mail address: pieter@ribf.riken.jp (P. Doornenbal).
[1] Present address: Fraunhofer INT, Euskirchen, Germany.
[2] Present address: CSNSM, Universitè Paris-Sud 11, CNRS/IN2P3, F-91405 Orsay–Campus, France.

0168-9002/$ - see front matter © 2009 Elsevier B.V. All rights reserved.
doi:10.1016/j.nima.2009.11.017

point in the plane perpendicular to the beam axis is obtained. However, the longitudinal position determination along the beam axis depends on the reaction target's thickness and the lifetime of the excited state. Moreover, the velocity of the heavy ions at the γ−ray emission time is needed. Velocity measurements are also necessary before and after passing the secondary target as the secondary beam has generally a considerable momentum spread. The accuracy of the velocity determination is heavily affected by the lifetime of the excited state and the thickness of the reaction target. A considerable fraction of γ−ray decays can occur during the slowing down process within the target. As a consequence, the exact velocity at the moment of γ−ray emission stays uncertain, causing an imperfect Doppler correction, i.e., a broadening and a specific lineshape of the Doppler corrected γ−ray peaks.

To which extent the lineshape of a γ−ray peak is affected depends not only on the excited state's lifetime but is closely related to the geometry of the specific γ−ray detection array and experimental setup. In this paper, we will focus on lifetime effects for in-beam γ−ray spectroscopy with the RISING array [3], operated at the S4 focal plane of the fragment separator FRS [4] at GSI, Darmstadt. This experimental setup employs high resolution in-beam spectroscopy at the highest velocities to date. We commence with general remarks on the Doppler shift correction for in-beam γ−ray spectroscopy. Monte-Carlo simulations are performed to study and disentangle the different contributions to the line shape of the γ−ray peaks. Finally, experimental lineshapes from in-flight decay at $\approx 200\,\mathrm{MeV}/u$ kinetic energy after secondary fragmentation reactions are compared to simulations.

2. General remarks on the Doppler correction

Gamma-rays emitted from excited nuclei moving at relativistic energies are strongly Doppler shifted. The detected γ−ray energy E_γ in the laboratory frame is related to the transition energy $E_{\gamma 0}$ in the rest frame by the Doppler formula through:

$$\frac{E_\gamma}{E_{\gamma 0}} = \frac{\sqrt{1-\beta^2}}{1-\beta\cos\vartheta_\gamma}. \tag{1}$$

Here, ϑ_γ is the angle between the emitting particle and the emitted γ−ray in the laboratory frame, respectively. The resulting energy resolution after performing the Doppler correction of measured γ−ray energies E_γ is given by

$$\left(\frac{\Delta E_{\gamma 0}}{E_{\gamma 0}}\right)^2 = \left(\frac{\beta\sin\vartheta_\gamma}{1-\beta\cos\vartheta_\gamma}\right)^2 (\Delta\vartheta_\gamma)^2 + \left(\frac{\beta-\cos\vartheta_\gamma}{(1-\beta^2)(1-\beta\cos\vartheta_\gamma)}\right)^2 (\Delta\beta)^2 + \left(\frac{\Delta E_{\mathrm{intr}}}{E_\gamma}\right)^2. \tag{2}$$

Three factors determine the energy resolution after applying the Doppler shift correction: (i) angular uncertainty between particle and photon $\Delta\vartheta_\gamma$, (ii) beam velocity uncertainty $\Delta\beta$, and (iii) intrinsic energy resolution of the γ−ray detector ΔE_{intr}. The first two uncertainties in the γ−ray emission angle ϑ_γ and the beam velocity are affected by the lifetime of the decaying states.

2.1. Angular uncertainty between particle and photon $\Delta\vartheta_\gamma$

Data on three points is required to reconstruct the angle ϑ_γ. These are (i) the position of the particle at the moment of γ−ray emission, (ii) the position of the emitting particle downstream of the target, and (iii) the position of the detected γ−ray. With this information two vectors are created spanning the angle ϑ_γ.

For thin targets and short lifetimes, the finite size of the γ- ray detectors yields the major contribution to the uncertainty $\Delta\vartheta_\gamma$. To obtain the point of γ−ray decay, a suited method is to utilize a position sensitive target. Elsewise position sensitive detectors are used for tracking the individual beam particles upstream or downstream the target to reconstruct the reaction position. As the scattering angles of the particles are typically small ($\leq 4^\circ$) at relativistic energies, the position information perpendicular to the beam axis can be obtained with good accuracy. For the z-coordinate along the beam axis only the target position itself can be used as an assumption for the z-coordinate of the γ−ray decay and the reaction points. Typical target thicknesses are in range of a few hundred $\mathrm{mg/cm^2}$ up to several $\mathrm{g/cm^2}$. If low density targets such as liquid hydrogen ($\rho = 70\,\mathrm{mg/cm^3}$) are used in the experiment, the target thickness along the beam axis may even reach several cm.

As the z-coordinate of the reaction point inside the target cannot be determined, thick targets contribute to a considerable amount to the uncertainty $\Delta\vartheta_\gamma$, in particular for detectors placed at 90°. Moreover, the uncertainty in $\Delta\vartheta_\gamma$ for the Doppler shift correction is increased by the lifetime of the excited state. The particles move along the beam axis away from the target position before emitting γ−rays, thereby changing ϑ_γ. Taking into account the time t in the moving system between excitation and decay of a nuclear state and neglecting the velocity change due to energy loss inside the target, the position of the γ−ray decay along the beam axis in the laboratory system shifts by $z_\gamma = t\beta\gamma c$, which will consequently alter the angle ϑ_γ. This change in angle cannot be corrected on an event-by-event basis. For a known lifetime the mean z-coordinate of the decay position $\langle z_\gamma \rangle = T_{1/2}\beta\gamma c/\ln 2$ has to be taken into account for the Doppler correction (the target center is $z=0$). The mean decay position for three different beam velocities are shown as a function of the halflife in Fig. 1. For long halflives of more than 50 ps, which are common for $E(2_1^+)$ levels in regions of deformations in the nuclear chart, $\langle z_\gamma \rangle$ shifts by several cm. Typically, γ−ray spectrometers have distances of several tens of cm to the target. Therefore, such a shift in decay position is considerable and illustrated in Fig. 2 for three halflives of 100, 200, and 300 ps at a beam velocity of $100\,\mathrm{MeV}/u$. The decay position distribution along the z-axis cannot be accounted for in the Doppler correction and affects the obtainable energy resolution of the experiment.

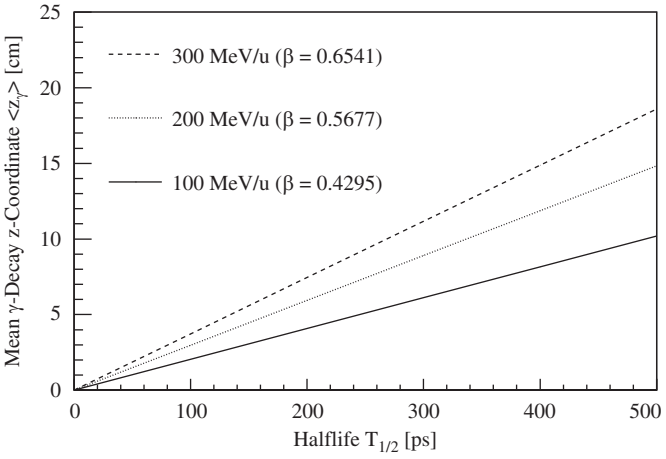

Fig. 1. Mean z-coordinate of the decay position $\langle z_\gamma \rangle$ as a function the excited state's halflife for three different secondary beam velocities. See text for details.

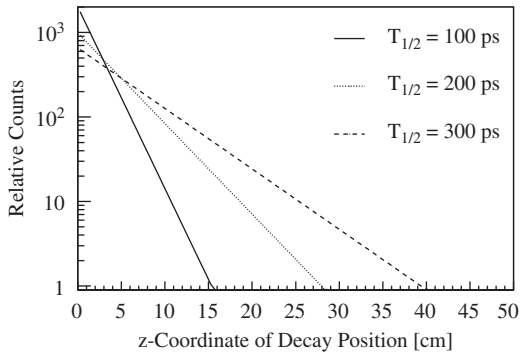

Fig. 2. z-coordinate distribution of the heavy ions' position with an energy of 100 MeV/u at the moment of γ−ray emission and halflives of an excited state of 100 (solid line), 200 (dotted line), and 300 ps (dashed line), respectively.

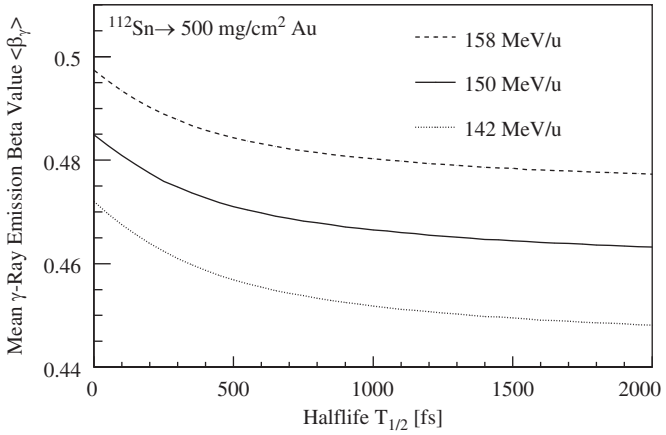

Fig. 3. Mean velocity at the moment of γ−ray emission $\langle\beta_\gamma\rangle$ as a function of the halflife of an excited state for a ^{112}Sn beam impinging on a 500 mg/cm^2 ^{197}Au target at energies of 142 (dotted line), 150 (solid line), and 158 MeV/u (dashed line), respectively. See text for details.

2.2. Beam velocity uncertainty $\Delta\beta$

While penetrating the target, the beam and its fragmentation products undergo an energy loss, which is well described by theoretical work [5]. Depending on the ratio between the lifetime of an excited state and the transmission time necessary to penetrate the target, i.e., its thickness, the γ−ray decay will occur either predominantly inside or behind the target. In the latter case, the velocity at the moment of γ−ray decay can be deduced from a velocity (time-of-flight) measurement after the target. In many cases, however, a considerable amount of decays will occur inside the target. Consequently, the exact velocity at the moment of γ−ray emission cannot be determined. In these cases, the Doppler correction must be done with an average velocity $\langle\beta_\gamma\rangle$ of the particle at the moment of γ−ray emission assuming a certain lifetime of the excited state (unless it is known). However, for a given halflife, $\langle\beta_\gamma\rangle$ depends on the incoming beam velocity. To perform an event-by-event based Doppler correction, every measured velocity before reaching (bt) or after leaving (at) the target, $\beta_{\mathrm{bt/at}}$, must be correlated with its according $\langle\beta_\gamma\rangle$ from simulation.

Because the stopping power dE/dX depends on several parameters, the impact of the velocity uncertainty for the event-by-event Doppler correction is illustrated by a typical example. For a beam of ^{112}Sn impinging on a 500 mg/cm^2 ^{197}Au target at energies of 142, 150, and 158 MeV/u Fig. 3 displays $\langle\beta_\gamma\rangle$ as a function of the halflife of an excited state. A constant excitation cross-section along the nuclei's path through the target and no momentum spread of the beam for the different energies is assumed in the simulations. The $\langle\beta_\gamma\rangle$ separation for the different lines becomes slightly larger with increasing halflife. For short halflives the change in $\langle\beta_\gamma\rangle$ is most pronounced. Excited states with halflives of $\geq$1000 fs decay predominantly after the target. For these cases, $\langle\beta_\gamma\rangle$ almost matches the velocity after the target. A different pattern is observed for low atomic number Z, low density targets, as ^{9}Be. Due to the higher stopping power of Be in units of MeV/mg/cm^2, the energy loss in a 500 mg/cm^2 ^{197}Au target for a ^{112}Sn beam at 150 MeV/u is equal to the energy loss in a 315 mg/cm^2 ^{9}Be target. Be has a much lower density ($\rho = 1.85$ g/cm^3 compared to $\rho = 19.3$ g/cm^3 for Au) and $\langle\beta_\gamma\rangle$ changes considerably up to longer halflives of several ps, as shown in Fig. 4.

For secondary beams with momentum distribution the mean velocity at the moment of γ−ray emission $\langle\langle\beta_\gamma\rangle\rangle$ corresponds to the mean velocity before or after the target, $\langle\beta_{\mathrm{bt/at}}\rangle$. The difference between $\beta_{\mathrm{bt/at}}$ to the respective mean value of the distribution, $\langle\beta_{\mathrm{bt/at}}\rangle$, can be correlated with the difference of the corresponding $\langle\beta_\gamma\rangle$ and the mean velocity at the moment of γ−ray emission, i.e., $\langle\langle\beta_\gamma\rangle\rangle$, of the distribution. In Fig. 5 this is shown for halflives of 0, 500, and 1000 fs and the ^{112}Sn beam

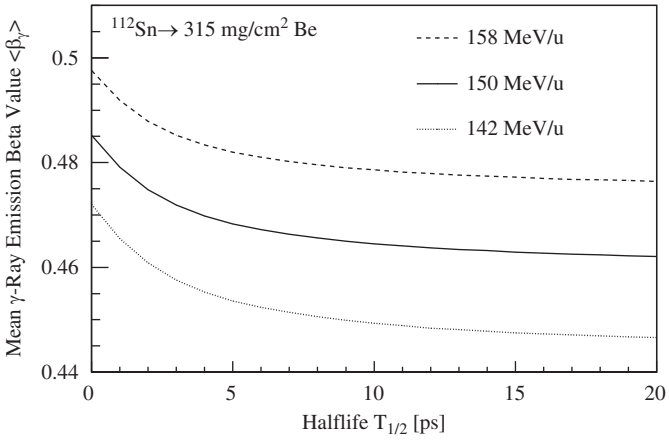

Fig. 4. Mean velocity at the moment of γ−ray emission $\langle\beta_\gamma\rangle$ as a function of the halflife of an excited state for a ^{112}Sn beam impinging on a 315 mg/cm^2 ^{9}Be target at energies of 142, 150, and 158 MeV/u, respectively. See text for details.

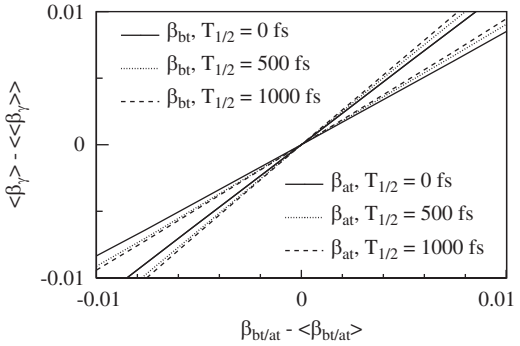

Fig. 5. Relation between the difference of the velocity before/after the secondary target β_{bt}/at and its mean value $\langle\beta_{\mathrm{bt}}/\mathrm{at}\rangle$ and the respective mean velocities at the moment of γ−ray decay, $\langle\beta_\gamma\rangle$ and $\langle\langle\beta_\gamma\rangle\rangle$. The calculations were performed for a ^{112}Sn beam with an average velocity of 150 MeV/u impinging on a 500 mg/cm^2 ^{9}Be target and halflives of 0, 500, and 1000 fs, respectively.

hitting the ^{197}Au target. The result are straight lines, their slope α increasing slightly with increasing halflife. For thin targets, i.e., only very little energy change, α is close to unity. If the velocity is measured before the target, α must be greater than one, for measurements after the target, it must be smaller than one. The slope α can be used for an event-by-event Doppler correction using the equation:

$$\beta_{Doppler} = \langle\langle\beta_\gamma\rangle\rangle + \alpha \times (\beta_{bt/at} - \langle\beta_{bt/at}\rangle). \quad (3)$$

The combined consequences of the z-coordinate and velocity uncertainty on the γ−ray energy resolution and efficiency in a real experiment will be demonstrated and discussed in the following sections. The obtained results are based on Monte-Carlo simulations and on experimental investigations performed with the RISING setup [3] at GSI, Darmstadt.

3. The RISING setup

RISING combines the fragment separator FRS [4] at GSI with a γ−ray spectrometer to observe decays from excited states of exotic nuclei. The Fast Beam setup of RISING consists of three sub-arrays: 15 Cluster High Purity Ge detectors [7], eight MINIBALL High Purity Ge detectors [8], and eight Hector BaF_2 detectors [9,10]. Details of the experimental setup and particle identification before and after passing the secondary target can be found for example in Refs. [3,4,6]. Here, it is sufficient to know that the energy spread of the heavy ions in front of the secondary target is measured by the time-of-flight between two scintillation detectors. The outgoing particle direction and the reaction point are determined via position sensitive Si detectors mounted directly after the secondary target and 1400 mm downstream.

The γ−ray detectors are mounted at different angles and distances, as shown schematically in Fig. 6. The Cluster detectors, each containing seven individually encapsulated crystals, are positioned at the most forward angles in three rings of 16°, 33°, and 36°. They can be placed at distances between 700 and 1400 mm to the secondary target. The six-fold segmented MINIBALL triple detectors are arranged in two rings of 51° and 85° and can be positioned at distances varying between 200 and 400 mm. The BaF_2 detectors are situated at angles of 85° and 142° and distances of 350 mm.

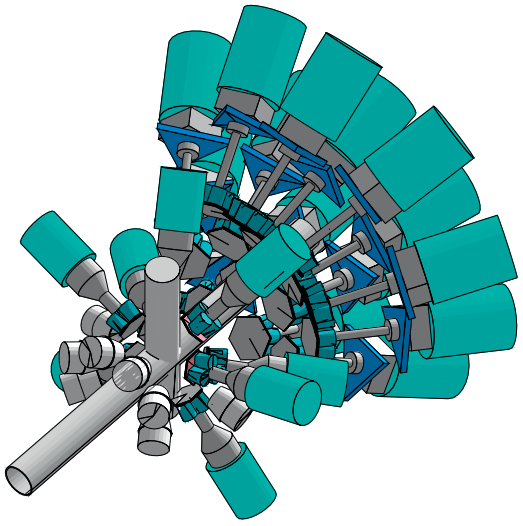

Fig. 6. (Color online) Schematic drawing of the RISING Fast Beam array. For references and details see text.

4. Lineshape simulations of the RISING setup

The lineshape and energy resolution after applying the Doppler correction are investigated via Monte-Carlo simulations for the two types of high-resolution RISING detectors, the MINIBALL and the Cluster detectors. The GEANT4 simulation package [11] is employed. As before, the lineshape caused by $\Delta\vartheta_\gamma$ and $\Delta\beta$ are discussed separately. The detectors are placed in close geometry, i.e., the distance of the Cluster detector front side to the target is 700 mm and the distance of the MINIBALL detector front side is 200 mm. The MINIBALL detectors are six fold segmented allowing a better localization and position determination for the incoming γ−ray. Only events with an interaction in solely one crystal for the Cluster detectors or solely one segment for the MINIBALL detectors are accounted for.

4.1. Lineshape due to de-excitation along the beam axis

Neglecting the energy loss in the target, the distance traveled by the particles between excitation and de-excitation depends on the velocity and on the lifetime of the excited state. In the simulations, a γ−ray of 500 keV is emitted at a beam energy of 100 MeV/u and halflives from 0 to 100 ps are assumed. Fig. 7 shows the resulting lineshapes, which are caused by the

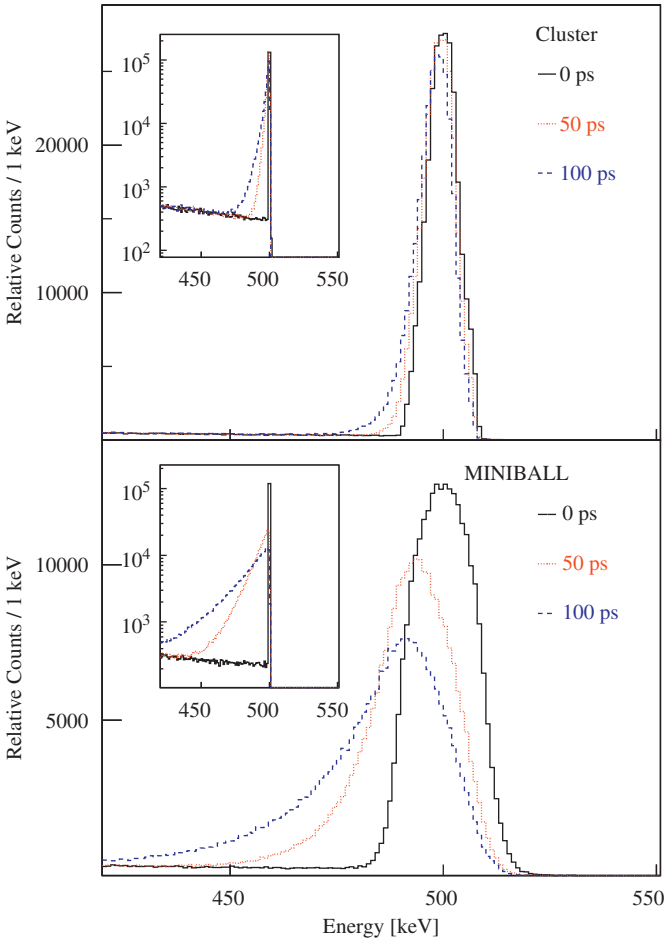

Fig. 7. Simulated Doppler corrected detector response for the Cluster (upper panel) and MINIBALL detectors (lower panel) for a γ−ray of 500 keV emitted at 100 MeV/u for three different halflife values of 0 (black solid), 50 (red dotted), and 100 ps (blue dashed). The insets show the detector response when the uncertainty of the detector's opening angles and the intrinsic resolution are disregarded in the simulation. (For interpretation of the references to the color in this figure legend, the reader is referred to the web version of this article.)

broadening due to the opening angle of the detector and the lifetime of the decaying state. For the Doppler correction, γ−ray emission at the middle of the target ($\langle z_\gamma \rangle = 0$) is assumed. For $T_{1/2} = 0$ ps the centroid of the peak distribution lies at 500 keV. As $T_{1/2}$ increases, the centroid of the distribution shifts to lower energies. This is caused by the increase in angle between the γ−ray detectors and the beam particle trajectory, leading to an exponential tail towards lower energies. The reason of this behavior can be demonstrated by neglecting the Doppler broadening due to the detectors' opening angles in the simulation, as depicted in the insets of Fig. 7. To achieve this, the simulated first interaction point of the γ−ray in the detectors' crystals is used for the Doppler correction.

The peak position shift depends on the position and distance of the γ−ray detectors. For a fixed distance to the target, the shift shows a maximum where the derivative of the square root of the first term in Eq. (2), given by

$$\frac{d}{d\vartheta_\gamma}\frac{\beta\sin\vartheta_\gamma}{1-\beta\cos\vartheta_\gamma} = \frac{\beta(\cos\vartheta_\gamma - \beta)}{(1-\beta\cos\vartheta_\gamma)^2} \tag{4}$$

is zero. This is the case for $\cos\vartheta_\gamma = \beta$, yielding values of 65°, 55°, and 49°, for energies of 100, 200, and 300 MeV/u. As the MINIBALL detectors are located in close distance to the target and all the individual segments cover ϑ−angles in the range from 41° to 101°, they are very sensitive to decays along the beam axis. On the other hand, the Cluster detectors are less affected due to the small ϑ−angles and large distances of the crystals to the target. This explains the considerable difference between the two detector groups in Fig. 7.

A linear dependence between the shift of the centroid of the peak position and the halflife of the excited state is obtained as a result. The relative energy shift, given in %, is shown in Fig. 8 as a function of the excited state's halflife for a beam energy of 100 MeV/u.

4.2. Lineshape due to γ- ray decay during the deceleration inside the target

The second major contribution to the lineshape of the γ−ray peaks is caused by the fact that γ−ray decay may occur during the emitting particles' deceleration in the target. Here the uncertainty

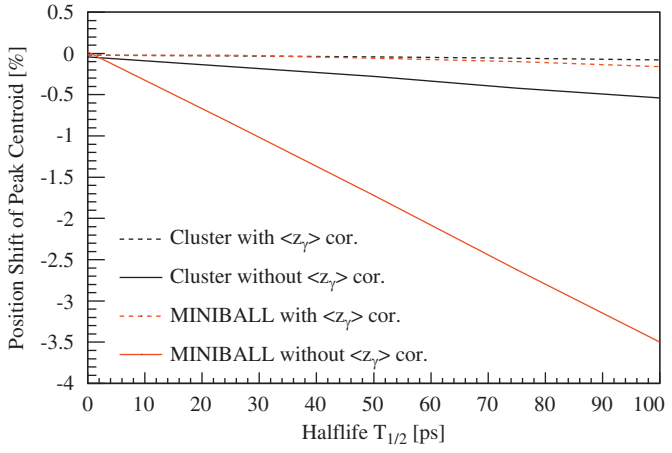

Fig. 8. Position shift of the peak centroid after applying the Doppler correction as a function of the halflife of the excited state at 100 MeV/u for the Cluster (thin black) and MINIBALL detectors (thick red). The shown Doppler corrections are applied with and without taking the centroid decay position into account. In the latter case (solid lines) $\langle z_\gamma \rangle = 0$ is assumed, while in the former the $\langle z_\gamma \rangle$ value as depicted in Fig. 1 is used. (For interpretation of the references to the color in this figure legend, the reader is referred to the web version of this article.)

$\Delta\beta$ depends on the specific combination of target, beam nuclei, beam energy, and halflife of the excited state. Lineshape effects are demonstrated quantitatively by the specific example of a ^{112}Sn beam impinging at 150 MeV/u on a 500 mg/cm^2 ^{197}Au target, like in Section 2.2. The simulated $2_1^+ \rightarrow 0_{g.s.}^+$ decay with an energy of 1256.85 keV [12] is reflecting the de-excitation process after a direct one step Coulomb excitation reaction. An accepted halflife of $T_{1/2} = 0.37(2)$ ps [12] can be used for the decay. To demonstrate lifetime effects, we vary the halflife and simulate the decay with halflives of $0.5 \cdot T_{1/2}$, $1 \cdot T_{1/2}$, and $2 \cdot T_{1/2}$, i.e., 185, 370, and 740 fs, respectively.

The velocity or β distributions at the moment of γ−ray emission are shown in Fig. 9. The number of γ−rays emitted after the target increases with increasing lifetime causing the unique value of $\beta_{at} = 0.46$ at low velocities for all three cases. In case Doppler correction is applied using the measurable β_{at}−value, energies from γ−rays decaying after the target will be shifted to the proper energy. Decays within the target are shifted to wrong energies according to the spread in velocity reflected in the second term of Eq. (2).

Generally, if $\cos\vartheta_\gamma > \beta_\gamma$, the resulting energy shift will be towards too high energies, while for $\cos\vartheta_\gamma < \beta_\gamma$ the shift will be towards too low energies. The Doppler corrected spectra of the ^{112}Sn transition for the Cluster and MINIBALL detectors are shown in Fig. 10. As the Cluster detectors occupy low ϑ_γ angles, a tail towards high energies occurs. The MINIBALL detectors are positioned around $\cos\vartheta_\gamma = \beta_\gamma$ and only a minor influence from $\Delta\beta_\gamma$ is visible. The insets of Fig. 10 illustrate again the lineshape for the case when the opening angle Doppler broadening and intrinsic energy resolution are disregarded in the simulation. As expected, the lineshape of the Cluster detectors resembles the β_γ distribution and Doppler corrected γ−ray energies are shifted up to 10% above the transition energy. For the MINIBALL detectors the effect is much smaller and almost symmetric, as shifts towards lower and higher energies are involved. The ratio of observed correct peak to tail ratio corresponds exactly to the ratio of γ−ray decays occurring after or within the target. Therefore, a precise determination of the lineshape, especially the asymmetry of the peak, enables a measure of the lifetime of an excited state.

The peak centroid deviation from the correct transition energy after applying the Doppler correction using β_{at} is shown in Fig. 11 as a function of the halflife of the excited state. For this particular projectile, beam energy, and target combination, only the Cluster detectors are affected. With measurable β_{at}−values after the target the Doppler corrected transition energy deviates from the correct value up to more than 2%. A Doppler correction using $\langle \beta_\gamma \rangle$ for 150 MeV/u from Fig. 3 shifts the energy centroid towards the proper

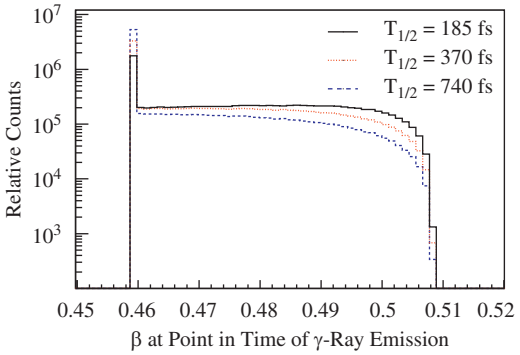

Fig. 9. β- distribution at the moment of γ−ray emission for a ^{112}Sn beam impinging at 150 MeV/u on a 500 mg/cm^2 ^{197}Au target and halflives of 185 (black solid), 370 (red dotted), and 740 fs (blue dashed), respectively. (For interpretation of the references to the color in this figure legend, the reader is referred to the web version of this article.)

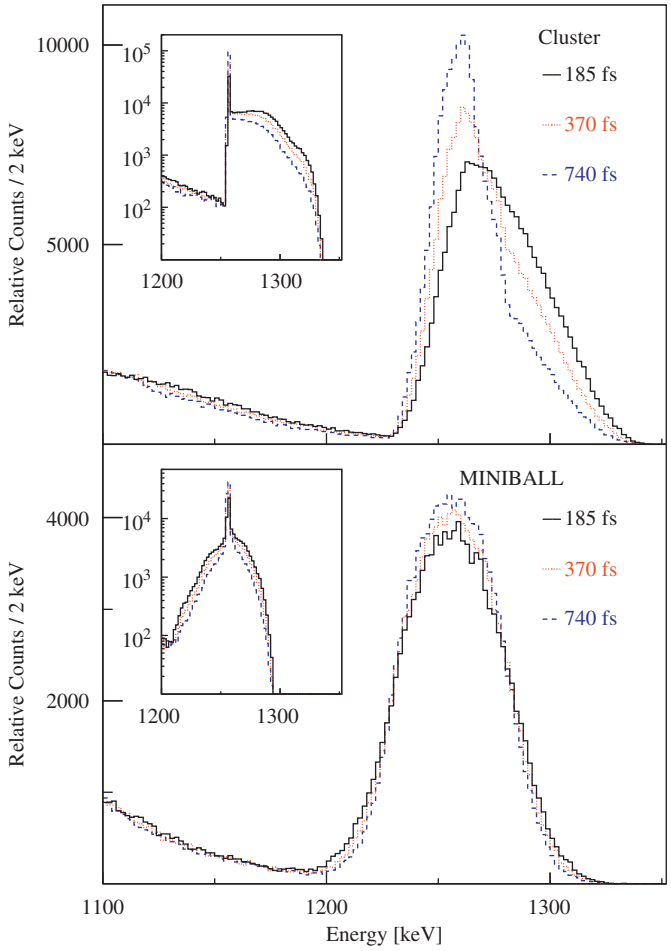

Fig. 10. Simulated Doppler corrected detector response for the Cluster (upper panel) and MINIBALL detectors (lower panel) for the $2_1^+ \rightarrow 0_{g.s.}^+$ of ^{112}Sn. The ^{112}Sn beam is impinging at 150 MeV/u on a 500 mg/cm^2 ^{197}Au target and halflives of 185 (black solid), 370 (red dotted), and 740 fs (blue dashed), respectively, are assumed. The insets show the detector response when the uncertainty of the detector's opening angles and their intrinsic resolution are "turned off". The Doppler correction is performed using β_{at}. (For interpretation of the references to the color in this figure legend, the reader is referred to the web version of this article.)

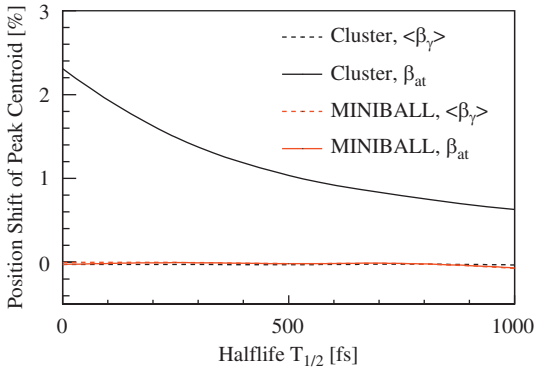

Fig. 11. Deviation of observed peak position after applying a Doppler correction using $\langle\beta_\gamma\rangle$ (dashed lines) and β_{at} (solid lines) for the Cluster (black thin) and MINIBALL (red thick) detectors. The ^{112}Sn projectile impinged at 150 MeV/u on a 500 mg/cm^2 ^{197}Au target. (For interpretation of the references to the color in this figure legend, the reader is referred to the web version of this article.)

position. Therefore, without presumption of the lifetime of the de-excitation γ−ray, the transition energy assignment is limited to a precision of $\pm 1\%$ from the Cluster detectors alone in this case.

5. Experimental results

Lineshapes of the $1_1^+ \rightarrow 0_{g.s.}^+$ decay in ^{34}Cl and the $3/2_1^+ \rightarrow 1/2_{g.s.}^+$ decay in ^{31}S were investigated experimentally, exploiting the two-step fragmentation technique. A primary beam of ^{40}Ca at an energy of 420 MeV/u was provided by the heavy ion synchrotron SIS and impinged on a ^{9}Be target with 4 g/cm^2 thickness. From the primary reaction products ^{37}Ca was selected and incident on a 700 mg/cm^2 secondary ^{9}Be target at 195.7 MeV/u to excite states in ^{34}Cl and ^{31}S after a secondary three proton and a four proton two neutron removal reaction, respectively. Details on the separation and identification of the secondary beam in this experiment can be found in Refs. [6,13]. The time-of-flight through the secondary target was ≈ 23 ps.

5.1. Lineshape of the $1_1^+ \rightarrow 0_{g.s.}^+$ decay in ^{34}Cl

The $1_1^+ \rightarrow 0_{g.s.}^+$ in ^{34}Cl has a known de-excitation energy and halflife of 461 keV and 5.2(3) ps, respectively [12]. However, in the experiment a weak $2_1^+ \rightarrow 1_1^+$ transition was observed with a strength of 12(6)% relative to the $1_1^+ \rightarrow 0_{g.s.}^+$. As the 2_1^+ state has an adopted much longer halflife of 13.7(9) ps [12], the feeding has to be accounted for, resulting in an effective halflife of 6.8(9) ps. The Doppler corrected γ−ray spectra for the Cluster and MINIBALL detectors are shown in Fig. 12. The measured spectrum is compared to simulated spectra assuming halflives of 0, 5, and 20 ps for the excited state. In both cases, experiment and simulation, the same $\langle\beta_{at}\rangle = 0.531$ values and $\langle z_\gamma\rangle = 0$ as target positions were used. The background in the simulations was adopted from the experiment by a linear fit in the region between 400 and 520 keV after subtracting the peak integral. The

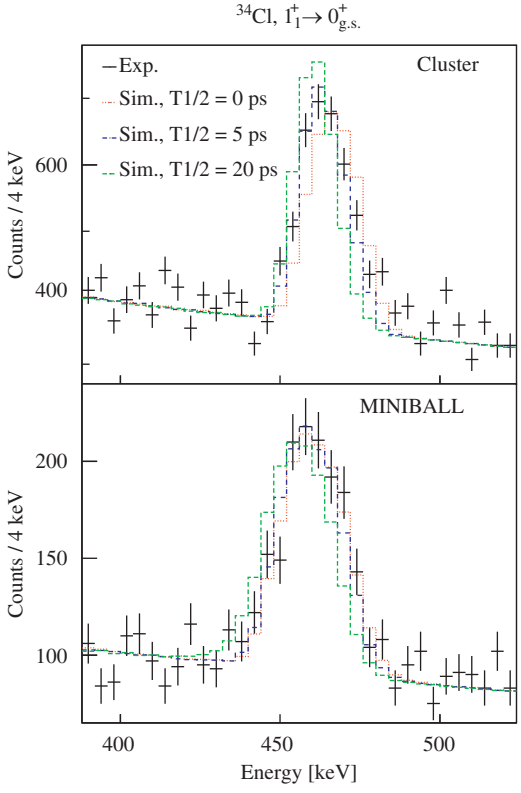

Fig. 12. Doppler corrected Cluster (upper panel) and MINIBALL (lower panel) spectra of the $1_1^+ \rightarrow 0_{g.s.}^+$ in ^{34}Cl. Also shown are the expected line shapes assuming halflives of 0 (red dotted), 5 (blue dashed), and 20 ps (green dash dotted), respectively. (For interpretation of the references to the color in this figure legend, the reader is referred to the web version of this article.)

peak integral of the simulations was normalized separately to the experimentally observed integrals in the Cluster and MINIBALL detectors.

As no attempt was made in the Doppler correction to correct for lifetime effects, the simulated peak energy position clearly shifts as a function of the halflife. A χ^2 test between experiment and simulation was performed. For the simulation the halflife value $T_{1/2}$ of the excited state was varied. Yet always the same $\langle\beta_{at}\rangle$ and $\langle z_\gamma\rangle = 0$ values were used for the Doppler correction. The χ^2 is given by

$$\chi^2 = \sum_{i=1}^{N} \frac{(I^i_{\gamma sim} - I^i_{\gamma exp})^2}{\sigma_i^2} \tag{5}$$

where N is the number of bins, $I^i_{\gamma exp}$ and $I^i_{\gamma sim}$ the number of experimental and simulated counts in the respective bin, and σ_i the statistical error of counts in the respective bin.

The results of the χ^2 test for the observed $1^+_1 \rightarrow 0^+_{g.s.}$ line in ^{34}Cl are shown in Fig. 13. The test was done for 10 energy bins of the Cluster spectrum between 440 and 480 keV and 12 energy bins of the MINIBALL spectrum between 432 and 480 keV. The experimentally observed halflife corresponds to the minimum of the χ^2 distribution. Applying a quadratic fit around the minimum, the error (σ) can be determined from the following equation (see for example Ref. [14], p. 146):

$$\frac{\partial^2\chi^2}{\partial T^2_{1/2}}(T_{1/2} = T^{min}_{1/2}) = \frac{2}{\sigma^2}. \tag{6}$$

Using Eq. (6) results in halflives of 4.0(9) ps and 2.2(20) ps for the Cluster and MINIBALL detectors, respectively, for the $1^+_1 \rightarrow 0^+_{g.s.}$ decay.

Systematic errors may arise mainly from the uncertainty of the position of the detectors relative to the target and the determination of the average β value after the target. As discussed in Sections 4.1 and 4.2, the former affects primarily the MINIBALL array while the latter influences the Cluster detectors. To investigate the systematic errors, two independent sets of simulations were performed. In the first set the target position was shifted by ± 1 mm along the beam axis relative to the γ−ray spectrometers. The resulting simulated χ^2 minimum shifted by ± 0.3 ps for the Cluster detectors and ± 3.6 ps for the MINIBALL detectors, respectively. In the second set of simulations the $\langle\beta_{at}\rangle$ value used for the Doppler correction was shifted by ± 0.001. This resulted in a shift of the χ^2 minimum of -0.7 and $+1.3$ ps for the Cluster detectors, while the shift of the χ^2 minimum for MINIBALL was negligible. The systematic error's asymmetry in the Cluster detector arises from the flat slope of $\langle\beta_{at}\rangle$ towards long halflives, as discussed in Section 2.2, which is also the cause for the asymmetry in the χ^2 distribution.

Thus, for the $1^+_1 \rightarrow 0^+_{g.s.}$ decay in ^{34}Cl values of 4.0 ± 0.9 (stat)$^{+1.3}_{-0.8}$(sys) ps and 2.2 ± 2.0(stat) ± 3.6(sys) ps were found for the Cluster and MINIBALL detectors, respectively, which is lower than the effective halflife that includes feeding contributions. It must be emphasized that the secondary beam energy and target thickness were not designed to measure lifetimes specifically. Furthermore, due to the linear correlation between energy shift and halflife of an excited state, as shown in Fig. 8, the systematic error of the MINIBALL detectors is independent of the halflife, offering an interesting tool to measure halflives ≥ 20 ps. The obtained lifetime results illustrate the additional potential use of the line shape effects at different detection angle. While the Cluster detectors are well suited to draw conclusion on the lifetime and show a distinct χ^2 minimum, the MINIBALL position

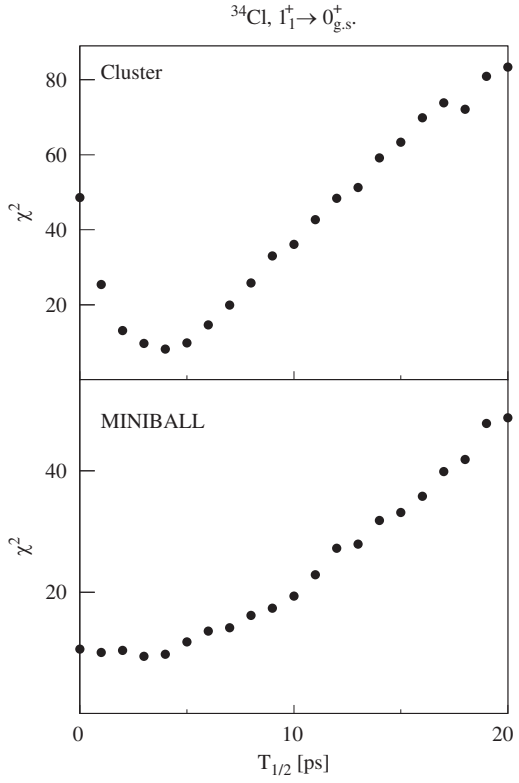

Fig. 13. χ^2 test of the observed $1^+_1 \rightarrow 0^+_{g.s.}$ decay in ^{34}Cl for the Cluster (top panel) and MINIBALL (bottom panel). In the simulations the decay's halflife was varied between 0 and 20 ps in steps of 1 ps.

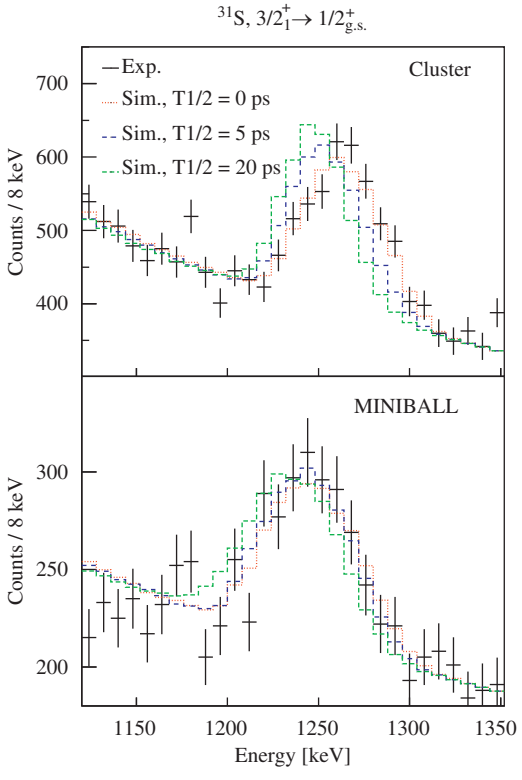

Fig. 14. Doppler corrected Cluster (upper panel) and MINIBALL (lower panel) spectra of the $3/2^+_1 \rightarrow 1/2^+_{g.s.}$ in ^{31}S. Also shown are the expected line shapes assuming halflives of 0 (red dotted), 5 (blue dashed), and 20 ps (green dash dotted), respectively. (For interpretation of the references to the color in this figure legend, the reader is referred to the web version of this article.)

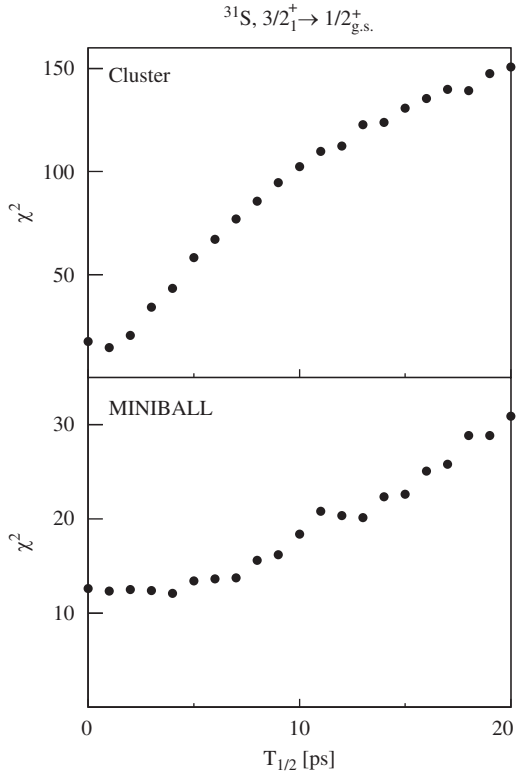

Fig. 15. χ^2 test of the observed $3/2^+_1 \rightarrow 1/2^+_{g.s.}$ decay in ^{31}S for the Cluster (top panel) and MINIBALL (bottom panel). In the simulations the decay's halflife was varied between 0 and 20 ps in steps of 1 ps.

is not sensitive to this quantity as the effective halflife is too short in this case.

5.2. Lineshape of the $3/2^+_1 \rightarrow 1/2^+_{g.s.}$ decay in ^{31}S

As second example the $3/2^+_1 \rightarrow 1/2^+_{g.s.}$ decay in ^{31}S is used to demonstrate the possibility to deduce lifetime information of observed peaks following in-beam γ–ray spectroscopy at relativistic energies. The literature values for energy and halflife are 1249 keV and 500(125) fs, respectively [12]. The Doppler corrected γ–ray spectra are shown in Fig. 14. The same procedure to find the excited state's halflife was repeated. The background was fitted by a linear function in the region in between 1150 and 1350 keV after subtracting the peak integral. The χ^2 test was applied for 13 bins in the region from 1208 to 1312 keV and for 15 bins from 1184 to 1304 keV, for the Cluster and MINIBALL detectors, respectively.

The χ^2 distributions are shown in Fig. 15. Around the χ^2 minimum a quadratic fit was applied, resulting in halflives of $0.8 \pm 0.5(\text{stat})^{+0.9}_{-0.6}(\text{sys})$ ps and $2.2 \pm 3.3(\text{stat}) \pm 3.6(\text{sys})$ ps for the Cluster and MINIBALL detectors, respectively. The systematic errors were deduced in the same way as for the $1^+_1 \rightarrow 0^+_{g.s.}$ decay in ^{34}Cl. Also this example illustrates the potential use of the detected lineshape for lifetime investigations at a much shorter time scale in case the detector positions are well located. Despite the relative error bars the applied method shows that a clear lifetime limit can be stated. A more precise result in analyzing the lineshape of halflives below 1 ps can be obtained in future experiments by employing a target with a higher stopping power per path length, i.e., higher density and atomic number.

6. Conclusions

A precise determination of transition energies in relativistic two-step fragmentation experiments with considerable thick targets needs to consider the lifetime of the γ–decaying state. Uncertainties of the energy measurement are caused by the Doppler correction and its dependence on the change of mean velocity $\langle \beta_\gamma \rangle$ and the decay position $\langle z_\gamma \rangle$ of the emitting excited nucleus. These two observables are typically not accessible in the experiment and cause variation of the energy after Doppler correction and characteristic line shape effects. Here the details of the chosen detector geometry, beam energy, projectile and target nuclei, and target thickness is crucial in order to describe the observed differences to symmetric energy peaks.

In case of a known transition energy of the de-excitation γ–ray the potential use of the described effects is a novel approach for lifetime determination. The explicit and rapid change of lineshape and peak position at different detection angles as a function of lifetime allows fitting of the measured distribution with simulations and applying a χ^2 test. For lifetimes below one ps it is favorable to use high density targets (e.g. Au or Pb) at forward ϑ–angles close to the beam axis. Low density targets as Be or plastic compounds are suitable for lifetimes up to a few tens of ps. Longer lifetimes are best deduced from detectors positioned at $\cos\vartheta_\gamma = \beta_\gamma$ and are nearly independent from the choice of target material. For unknown transition energies a two dimensional χ^2 test is necessary, varying the transition energies and halflives in the simulations.

In the RISING spectrometer the Doppler broadening due to the detectors' opening angles is generally quite large compared to lifetime effects. However, with the advent of the next generation position sensitive γ–ray spectrometers, as AGATA [15] or GRETINA [16], the opening angle will be minimized, thus becoming more sensitive to lineshapes and peak position shifts caused by the lifetimes of excited states in in-beam γ–ray spectroscopy.

Acknowledgments

The authors express their gratitude to the Accelerator Department at GSI for providing the ^{40}Ca beam. One author (P.D.) acknowledges the financial support of the Japan Society for the Promotion of Science. This work was partially supported by the German BMBF under Grant nos. 06BN-109, 06K-167, by the Polish Ministry of Science and Higher Education (Grant nos. N N202 109936 and N N202 309135), and by the Italian Istituto Nazionale di Fisica Nucleare.

References

[1] T. Glasmacher, Ann. Rev. Nucl. Part. Sci. 48 (1998) 1.
[2] F. Azaiez, et al., AIP Conf. Proc. 481 (1998) 243.
[3] H.J. Wollersheim, et al., Nucl. Instr. and Meth. A 537 (2005) 637.
[4] H. Geissel, et al., Nucl. Instr. and Meth. B 70 (1992) 286.
[5] J. Lindhard, A.H. Sørensen, Phys. Rev. A 53 (1996) 2443.
[6] P. Doornenbal, et al., Phys. Lett. B 647 (2007) 237.
[7] J. Eberth, et al., Nucl. Instr. and Meth. A 369 (1996) 135.
[8] J. Eberth, et al., Prog. Part. Nucl. Phys. 46 (2001) 389.
[9] A. Maj, et al., Nucl. Phys. Meth. A 571 (1994) 185.
[10] F. Camera, Ph.D. Thesis, University of Milano, Italy, 1992.
[11] S. Agostinelli, et al., Nucl. Instr. and Meth. A 506 (2003) 250.
[12] ENSDF Database: 〈http://www.nndc.bnl.gov/ensdf〉.
[13] P. Doornenbal, Ph.D. Thesis, University of Cologne, Germany, 2007.
[14] P.R. Bevington, D.K. Robinson, Data Reduction and Error Analysis for the Physical Sciences, second ed., McGraw-Hill, New York, 1992.
[15] J. Simpson, J. Phys. G 31 (2005) S1801.
[16] K. Vetter, et al., Nucl. Phys. Meth. A 452 (2000) 105.

IN-BEAM γ-RAY ANGULAR DISTRIBUTION AND LIFETIME MEASUREMENTS — EXPERIENCE FROM RISING AND PERSPECTIVES AT FAIR*

P. Bednarczyk, J. Grębosz, M. Kmiecik, A. Maj
W. Męczyński, S. Myalski, J. Styczeń

H. Niewodniczański Institute of Nuclear Physics PAN
Radzikowskiego 152, 31-342 Kraków, Poland

C. Domingo-Pardo, P. Doornenbal, J. Gerl
M. Górska, H.J. Wollersheim

GSI, Planckstrasse 1, 64291 Darmstadt, Germany

J. Jolie, P. Reiter

Institut für Kernphysik, Universität zu Köln
Zülpicher Strasse 77, 50937 Köln, Germany

A. Bracco, F. Camera

University of Milano and INFN, via Celoria 16, 20133 Milano, Italy

(Received January 14, 2010)

RISING experiments delivered important knowledge on difficulties in performing prompt in-beam γ-ray spectroscopy measurements, caused by the use of very fast radioactive beams. The obtained results pointed out possible ways to suppress the overwhelming γ-ray background that should be considered in setting up new facilities planned at GSI and FAIR. In the course of the RISING campaign, the spectroscopy methods: γ-ray angular distribution and lifetime measurements useful in deducing B(E2) transition rates were developed. They can be effectively applied in experiments with the new generation γ-ray detector array AGATA.

PACS numbers: 21.10.Tg, 23.20.En, 29.30.Kv, 29.38.De

* Presented at the XXXI Mazurian Lakes Conference on Physics, Piaski, Poland, August 30–September 6, 2009.

1. Introduction

In-beam nuclear structure studies by means of γ-ray spectroscopy will be the aim of HISPEC/NUSTAR Collaboration at FAIR [1]. The HISPEC forerunner experiment — PRESPEC, is currently being prepared at GSI.

At FAIR, radioactive ion beams (RIB) will be produced in fragmentation of relativistic heavy ions delivered by the SIS synchrotrons. Fragments with a sufficiently long half-life $T_{1/2} \geq 100$ ns, will be selected by the fragment separator Super-FRS and slowed down to intermediate kinetic energies of 50–150 A MeV. The radioactive projectiles impinging on a secondary reaction target placed at the Super-FRS focal plane will be used to induce nuclear reactions: multi-nucleon transfer, fragmentation or Coulomb excitation. The emitted nuclear radiation: γ-rays, particles and fragments will be registered by a complex set of detectors surrounding the experimental area. The HISPEC campaign will be a follow up of a series of successful measurements performed at GSI with the RISING setup [2]. RISING has delivered not only new and valuable nuclear structure results [3], but was an important source of unique knowledge concerning the experimental technology, as it operated at relatively high beam energies with respect to the similar facilities available worldwide. The experience gained at RISING contributed to better understanding of the origin of an excessive prompt γ-ray background and its effective reduction. It allowed for developing in-beam spectroscopy methods to be used at the newly designed setups as γ-ray angular distribution and lifetime measurements.

2. Prompt γ-ray background at intermediate RIB energies

In the RISING setup, γ-ray detectors were positioned around the secondary target in the FRS focal plane. The setup originally consisted of an array of 15 HPGe clusters of EUROBALL placed around the beam axis at forward angles and a set of 8 large volume BaF_2 HECTOR detectors mounted at backward angles. Before hitting the target, beams of radioactive fragments selected by FRS passed through a series of energy degraders, beam monitoring detectors and slits. Scattered projectiles and reaction products were identified and stopped in a position sensitive $\Delta E - E$ telescope, which for the reason of very limited space was mounted just behind the EUROBALL array. Particles and electromagnetic radiation emitted in collisions of the fast fragments with the surrounding matter caused an excessive background seen in the γ-ray detectors. Fig. 1(A) demonstrates a typical prompt γ-spectrum measured in the Ge clusters in the reaction of scattering ^{54}Cr fragments on a gold target at 100 A MeV kinetic energy. In the spectrum, on top of the dominant smooth background, one sees a group of Doppler broadened γ-lines characteristic for the inelastic scattering of fast neutrons

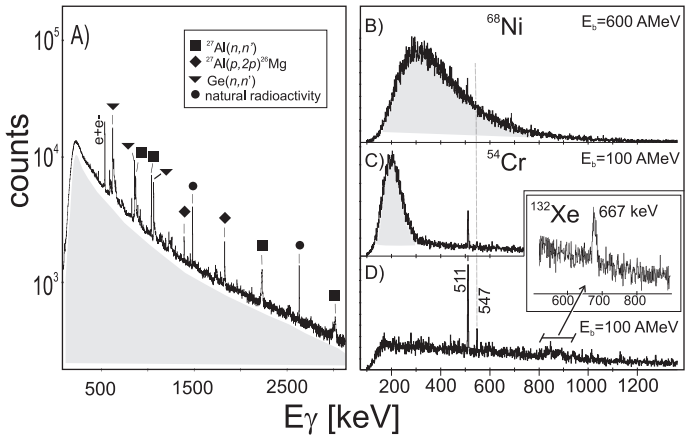

Fig. 1. (A) Prompt γ-ray spectrum measured in coincidence with RIB. There are peaks induced by fast particles (as marked) on top of the excessive background (filled area). (B), (C) Not Doppler corrected γ-ray spectra measured in coincidence with RIB scattered on a gold target. Position of the 547 keV transition from Coulomb excited ^{197}Au is indicated. The low energy atomic background is shadowed. (D) Respective γ-ray spectrum registered with the stable ^{132}Xe beam. In the inset, the 667 keV, $2^+ \rightarrow 0^+$ transition seen in the Doppler corrected spectrum.

on aluminum, the main component of the reaction chamber. Sharp ^{26}Mg transitions also visible in the spectrum, suggest occurrence of the quasi free proton scattering reaction: $^{27}\mathrm{Al}(p, 2p)^{26}\mathrm{Mg}$ induced by protons with energy $E_p > 100$ MeV, produced in the collisions. A direct interaction of particles (p, π, e) with the Ge crystals could explain a saturation of detector preamplified signals that were observed in a beam pulse, predominantly in the five clusters mounted close to the beam-line. These signals were associated with the cluster multiplicity close to the maximum fold of 7. Parallel use of digital XIA DGF cards, besides the standard analog VXI electronics, for reading out a few of the Ge detector channels allowed for filtering out these irregular signals. Inversely, the requirement of only low folds in the clusters guaranteed that properly shaped signals induced by γ-rays were accepted for the acquisition. As it was shown in [2], γ-ray measurement with HECTOR allowed to determine the origin of the registered radiation due to the very good timing properties of the BaF_2 crystals. It turned out that in addition to γ-rays from the target, strong radiation was emitted at the FRS side. On the other hand, the beam stopper was also identified as a source of huge γ-ray background. In the EUROBALL detectors, likewise in HECTOR, selection of a narrow window in the projectile-γ time spectrum, which corresponded to the target prompt γ-emission events, allowed to suppress the unwanted background radiation emitted downstream and upstream of the beam line.

At intermediate beam energies, atomic processes are the important constituents of the prompt γ-ray background. In this energy regime intense bremsstrahlung is expected to be orders of magnitude stronger than the nuclear radiation, and depending on the incident beam velocity may reach energies of several hundreds keV [2]. In Fig. 1(B), (C) and (D) are shown non Doppler corrected γ-ray spectra measured in Coulex reactions with RIB: ^{68}Ni at 600 A MeV, ^{54}Cr at 100 A MeV, and a primary ^{132}Xe beam at 100 A MeV, respectively. In all the three cases γ-rays were registered in coincidence with scattered projectiles selected by the HI detectors before and after a gold target. In the γ-spectra obtained with the fragmented beams, one notices intense low energy atomic background which in the case of the 600 A MeV ^{68}Ni beam extends to almost 1 MeV. In contrast, in the spectrum registered in the reaction with the stable ^{132}Xe projectiles such increase of the background is not observed. The excessive atomic background induced by the secondary beams may be associated with their large spatial spread that resulted in scattering on the surrounding material. Indeed, a RIB spot size was measured to be about 20 cm^2 at the target position, whereas for the stable beam it was close to 1 cm^2.

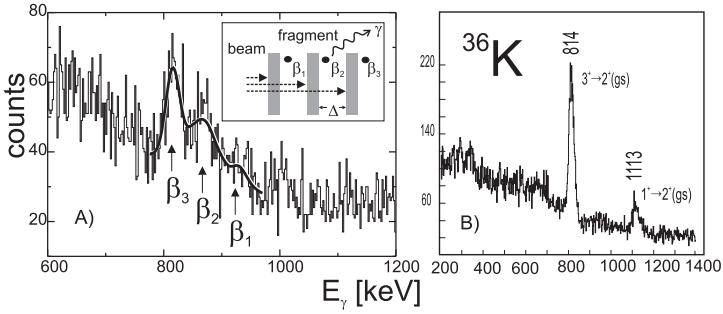

Fig. 2. (A) Splitting of the 814 keV line from ^{36}K due to γ-ray emission at the different fragment velocities: $\beta_1 = 0.53$, $\beta_2 = 0.49$ and $\beta_3 = 0.43$. The best fit to the data yielded the ^{36}K, 3^+ level lifetime of 28(6) ps. In the inset, a sketch of the plunger device. (B) The 814 keV transition in ^{36}K measured in the secondary fragmentation reaction of ^{37}Ca on a Be target.

3. Gamma-ray spectroscopy methods developed at RISING: γ-ray angular distribution and lifetime measurements

Spectroscopic investigations of exotic nuclei reveal evolution of the structure of magic nuclei. They come across new regions of nuclear deformation far from stability. Experiments performed so far at the intermediate energy RIB facilities explored these phenomena through measurements of transition energies and B(E2) rates.

Coulomb excitation is the ideal tool to study low lying levels in the unstable long-lived nuclei. However, in the intermediate energy range, Coulex cross-section measurements may suffer from not negligible contribution of nuclear reactions that can appear at small impact parameters but are not fully controlled in the experiments. The admixture of the nuclear interaction might perturb the determination of the B(E2) probabilities estimated from the Coulex theory. RISING experiments have shown that the electromagnetic interaction along with the residual nuclear forces present in the inelastic scattering reactions accounted for the measured γ-ray angular distributions $W(\theta)$. Despite the large composite detector size and their big angular overlap, the $W(\theta)$ functions were determined by grouping individual EUROBALL detector crystals in shells at four distinct angles. Comparison of the experimental $W(\theta)$ for the target and the projectile nuclei with model calculations allowed for more precise estimation of the Coulex cross-section, thus B(E2) in some cases. More details are given in Ref. [4].

Alternatively to Coulex, in promptly-decaying exotic nuclei, excited states may be populated in secondary fragmentation reactions. In such a case, the corresponding B(E2) transition rates can be deduced from the transition energies and level lifetimes τ. At RISING, a pioneering lifetime measurement making use of a simple plunger prototype was performed. The plunger consisted of three equidistant iron plates that acted as secondary targets and degraders at the same time (*cf.* the inset in Fig. 2.(A)). The distance Δ between the plates could be adjusted according to the expected range of τ. RIB selected in FRS impinging in the plunger targets yielded to fragmentation. Gamma-radiation emitted from the secondary fragments occurred at a velocity that gradually decreased as the fragment passed through consecutive degraders. The variable γ-ray Doppler shift resulted in the γ-line splitting. The transition intensity was shared between the three peaks according to τ and Δ. In Fig. 2(A) it is shown a summed γ-ray spectrum of all Cluster detectors recorded in coincidence with the ^{37}Ca projectiles of the 200 A MeV initial energy, produced in the fragmentation of ^{48}Ca. The ^{36}K secondary fragments from the most intense $1p$ removal reaction channel were simultaneously selected. The three components of the 814 keV line corresponding to the $3^+ \rightarrow 2^+$ ground state transition in ^{36}K are weak but clearly seen. For comparison, Fig. 2(B) presents the same line measured in the fragmentation of the ^{37}Ca beam on a monolithic Be target. In order to extract the lifetime of the 3^+ state in ^{36}K, so far unknown, the 814 keV line shape was compared to a calculated distribution. This solution was more appropriate than a simple intensity analysis of the three peaks, since the low statistics imposed the necessity of summing data obtained for the two distances: $\Delta = 2$ mm, $\Delta = 8$ mm and all detection angles. In the model calculations, the Lorentz boosted γ-ray $W(\theta)$ function, which strongly

depends on the radiation source velocity, and the γ-ray emission inside degraders were taken into account. The best fit to the data was obtained for $\tau = 28(6)$ ps. This value is comparable with the lifetime of the analogous 3^+ level at 788 keV in the ^{36}Cl mirror nucleus, which amounts to $\tau = 20(2)$ ps. More details on the lifetime data analysis will be given in a forthcoming publication.

4. Conclusion and perspectives

The results from the RISING in-beam measurements show that the excessive γ-ray background induced by fast RIB can be effectively reduced by minimization of the secondary beam spatial spread and application of an appropriate γ-ray detector shielding. On the other hand, in the new Ge detector setup planned at FAIR, application of fast signal reset preamplifiers and a digital readout electronics will be essential for selecting properly shaped signals. Moreover, a good time resolution of the electronics will play important role in filtering out the intense γ-radiation emitted outside the reaction target. These conditions will be fulfilled by the new generation Ge detector array AGATA. The use of the complete AGATA array at HISPEC and the AGATA demonstrator at PRESPEC will be advantageous in experiments aimed at γ-ray angular distribution measurements. The AGATA modularity will provide a flexible detector geometry that can be optimized for a particular experiment in order to cover the maximum angular range, thus increasing the array efficiency. Still, the array γ-ray tracking capability should allow for maintaining a very good angular resolution of the order of 1°, and to some extent by using imaging techniques, reproducing the γ-ray emission point. Already in the PRESPEC phase, the setup sensitivity is expected to be by more than 10 times greater, with respect to RISING. Therefore, the lifetime plunger measurements, will be feasible for reaction channels much weaker than those studied at RISING.

This work is supported by the Polish Ministry of Science and Higher Education Grants No: N N202 309135, N N202 109936 and N N202 240637.

REFERENCES

[1] Z. Podolyak, *Acta Phys. Pol. B* **41**, 493 (2010) this issue.
[2] H.J. Wollersheim *et al.*, *Nucl. Instrum. Methods* **A537**, 637 (2004).
[3] F. Camera, J. Gerl, *Nucl. Phys. News* **19**, 7 (2009).
[4] P. Bednarczyk *et al.*, *Acta. Phys. Pol. B* **40**, 835 (2009).

Nuclear Theory'25
ed. S. Dimitrova, Heron Press, Sofia, 2006

g-factor measurements at RISING: The case of ^{127}Sn

L. Atanasova[1], D. L. Balabanski[2,3], M. Hass[4], D. Bazzacco[5], F. Becker[6], P. Bednarczyk[6,7], G. Benzoni[8], N. Blasi[8], A. Blazhev[9], A. Bracco[8], C. Brandau[6,10], L. Caceres[6,11], F. Camera[8], S. K. Chamoli[4], F.C.L. Crespi[8], P. Detistov[1], P. Doornenbal[6], C. Fahlander[12], E. Farnea[5], G. Georgiev[13], J. Gerl[6], K. Gladnishki[3], M. Górska[6], H. Grawe[6], J. Grebosz[6,7], R. Hoischen[12], G. Ilie[9,14], M. Ionescu-Bujor[14], A. Iordachescu[14], A. Jungclaus[11], G. Lo Bianco[3], M. Kmiecik[7], I. Kojouharov[6], N. Kurz[6], S. Lakshmi[4], R. Lozeva[1,15], A. Maj[7], D. Montanari[8], G. Neyens[15], M. Pfützner[16], S. Pietri[10], Zs. Podolyák[10], W. Prokopowicz[6,7], D. Rudolph[12], G. Rusev[17], T. R. Saito[6], A. Saltarelli[3], H. Schaffner[6], R. Schwengner[17], G. Simpson[18], S. Tashenov[6], J. J. Valente-Dubon[19], N. Vermeulen[15], J. Walker[6,10], E. Werner-Malento[6,16], O. Wieland[8], H. J. Wollersheim[6]

[1]Faculty of Physics, University of Sofia, BG-1164 Sofia, Bulgaria
[2]INRNE, Bulgarian Academy of Sciences, BG-1784 Sofia, Bulgaria
[3]Universitti di Camerino and INFN-Perugia, 62032 Camerino, Italy
[4]Weizmann Institute of Science, Rehovot 76100, Israel
[5]Universitti di Padova and INFN-Padova, 35131 Padova, Italy
[6]GSI, Planckstrasse 1, D-64291, Darmstadt, Germany
[7]IFJ PAN, Polish Academy of Sciences, PL-31-342 Kraków, Poland
[8]Universitti di Milano and INFN-Milano, 20133 Milano, Italy
[9]IKP, Universität zu Köln, D-50937, Köln, Germany
[10]Department of Physics, University of Surrey, Guildford, GU2 7XH, UK
[11]Universidad Autonoma de Madrid, E-28049 Madrid, Spain
[12]Department of Physics, Lund University, S-22100 Lund, Sweden
[13]CSNSM, F-91405 Orsay Campus, France
[14]NIPNE, RO-077125, Bucharest, Romania
[15]IKS, K.U.Leuven, 3001 Leuven, Belgium
[16]IEP, Warsaw University, PL-00-681 Warsaw, Poland
[17]Institut für Strahlenphysik, FZ Rossendorf, D-01314, Dresden, Germany
[18]LPSC, 38026 Grenoble Cedex, France
[19]INFN - Laboratori Nazionali di Legnaro, 35020 Legnaro (Padova), Italy

Abstract.

We report a g-factor measurement of the $19/2^+$ $T_{1/2} = 4.5(3)$ μs isomer in ^{127}Sn, which was carried out within the g-RISING project at GSI, Darmstadt, Germany, utilizing the time-differential perturbed angular distribution method. Isomers in $A \approx 130$ nuclei were populated in relativistic projectile fragmentation of a ^{136}Xe beam at $E/A = 600$ MeV on a 1024 mg/cm^2 Be production target. Fully-stripped ions were separated with the fragment separator, which allowed the preservation of the orientation of the nuclear spin ensemble as obtained in the reaction. The ions were implanted in a Copper plate, which provided a perturbation-free environment for the isomeric γ decay. The nuclei of interest were tracked and identified on an event-by-event basis and ion-γ coincidences were recorded. The γ rays deexciting the isomers were detected with eight Cluster Ge detectors mounted in the horizontal plane perpendicular to a 0.12 T external magnetic field. The experiment, data analysis and preliminary results are presented.

1 Introduction

The g-RISING experimental campaign was carried out at the GSI laboratory in Darmstadt, Germany within a RISING (Rare ISotope INvestigations at GSI) project [1] and aimed at g factors studies of isomers in exotic nuclei far from stability which were populated in projectile fragmentation or fission at relativistic energies. Isomers have a rather pure single particle configuration in regions around doubly-magic nuclei. Measurements of their g factors can provide information about their wave functions and their purity. They can confirm suggested spin and parity assignments, especially in regions far from stability, where they are based on theoretical predictions or analogy with neighbouring nuclei.

Three experiments were approved for the g-RISING campaign. Two of them aimed at studies of isomeric g factors in the vicinity of the doubly-magic ^{132}Sn. The isomers of interest were populated in the fragmentation of a ^{136}Xe beam in the first case, and in relativistic fission of the ^{238}U in the second. This makes possible the direct comparison of the spin-alignment in fragmentation and fission reactions at relativistic energies and provides two independent measurements of the g factor of the $(19/2^+)$, $T_{1/2} = 4.5(3)$ μs isomer in ^{127}Sn [2]. Here we report the status of the analysis of the fragmentation experiment.

The configurations of the isomeric states in Sn isotopes below the $N = 82$ shell gap consist of neutron holes in the $d_{3/2}$, $h_{11/2}$ and $s_{1/2}$ shell model orbits. The corresponding empirical g factors of these states, which are based on measurements of states ascribed to single-particle configurations, are $g(d_{3/2}) \approx 0.50$, $g(h_{11/2}) \approx -0.24$ and $g(s_{1/2}) \approx -2.1$. For non-pure shell model states, the g factor depends also on the configuration mixing.

Microsecond $19/2^+$ isomers were observed in the odd-A Sn isotopes with masses between $A = 119$ and $A = 129$ [3]. The spin and parity assignments

for the isomer in ^{127}Sn are based on energy systematic and comparison with theoretical calculations. The excitation energies of the $19/2^+$ states are similar to those of the 5^- isomers in the neighbouring even-even Sn isotopes. Thus, it was suggested [2] that the main component of the wave function of the isomeric level is $(\nu h_{11/2}^{-1} \otimes 5^-)_{19/2+}$. The measured g-factor of the 5^- isomers is $g \approx -0.067(13)$ [4] which suggests that the major contribution in the 5^- wave function is due to the $(\nu s_{1/2}^{-1} h_{11/2}^{-1})$ configuration, which has an empirical g factor of $g(s_{1/2}h_{11/2}) \approx -0.093$.

The $19/2^+$ isomers are suggested to decay partially via strongly hindered transitions of predominantly M2 character to a $15/2^-$ state in $^{123-127}$Sn. This state, together with the $11/2^-$ and $13/2^-$ states are expected to be rather pure members of the $h_{11/2}$ multiplet. Because of L forbiddenness, this transition cannot take place between states with the $(\nu h_{11/2}^{-3})$ and $(\nu s_{1/2}^{-1} h_{11/2}^{-2})$ configurations and an admixture of $(\nu g_{7/2}^{-1} h_{11/2}^{-2})$ is suggested in the $(19/2^+)$ wave function [2]. Different g factors are expected for these two configurations: $g(s_{1/2}^{-1} h_{11/2}^{-2}) \approx -0.156$ and $g(g_{7/2}^{-1} h_{11/2}^{-2}) \approx -0.23$, so the experiment will determine whether the suggested configuration is correct and what is the amount of admixture.

For the measurement of g factors of interest we applied the Time Dependent Perturbed Angular Distribution (TDPAD) method, which is based on measuring the perturbation of the γ anisotropy of the spin-oriented nuclear ensemble due to an externally applied magnetic field. Prior to this experiment, several TDPAD measurements on isomers produced in fragmentation reactions of the primary beam at relativistic [5] and intermediate energies [6, 7] were performed. A major requirement to study the nuclear electromagnetic moments is to observe the decay of a spin-oriented ensemble. In fragmentation reactions, spin orientation of the isomers is obtained in the reaction itself and it is necessary to preserve the produced alignment to the implantation point. As the isomers are in-flight mass separated, the hyperfine interaction between the nuclear and random oriented electron spin can destroy the orientation of the nuclear ensemble. The fragments are produced fully stripped due to the high energy of the primary beam. The pick-up of electrons increases with Z of the ions for similar beam energy and decreases with the beam energy for ions with the same Z. This limits the opportunities to perform such experiments at intermediate energies of the primary beam ($E/A \sim 60 - 100$ MeV) to masses $A \leq 80$. For heavier nuclei such experiments can be done only with relativistic beams, which are available at GSI.

2 Experiment

The neutron-rich nuclei around $A \approx 130$ were produced in relativistic projectile fragmentation of a ^{136}Xe beam at $E/A = 600$ MeV on a thin 1024 mg/cm^2 Be production target. The primary beam, which had an average intensity of

$2 \cdot 10^9$ ions per 10 s spill, was provided by the GSI heavy ion synchrotron (SIS). The fully-stripped ions were separated and identified with the two-stage high resolution magnetic zero-degree FRagment Separator (FRS) [8], which was operated in the standard achromatic mode. A schematic view of the set-up is shown in Figure 1.

The longitudinal momentum distribution of the fragments was measured by the position sensitive scintillator detector *Sc21* in the second focal plane of FRS (*S2*). In front of it, slits were introduced to cut the primary beam. The time of flight, measured with scintillator detectors *Sc21* and *Sc41* (see Figure 1) together with the magnetic rigidity of the beam, $B\rho$, was used to determine the mass-to-charge ratio, A/q. The ion charge Z was determined by the energy loss in the MUlti-Sampling Ionization Chamber (*MUSIC*) at the final focus. This allows the identification of the ions which reach the final focus of the FRS as shown in Figure 2. The multiwire proportional chambers, *Mw41* and *Mw42*, together with the position information from *Sc21*, were used for the precise beam tracking of

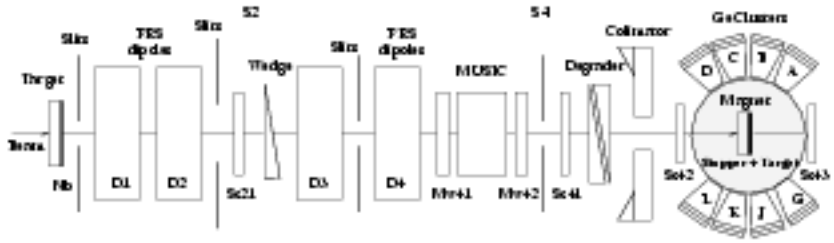

Figure 1. Schematic view of the experimental set-up consisting of the FRS, the beam-line detectors, the γ-ray detectors and an electromagnet (see text for explanations).

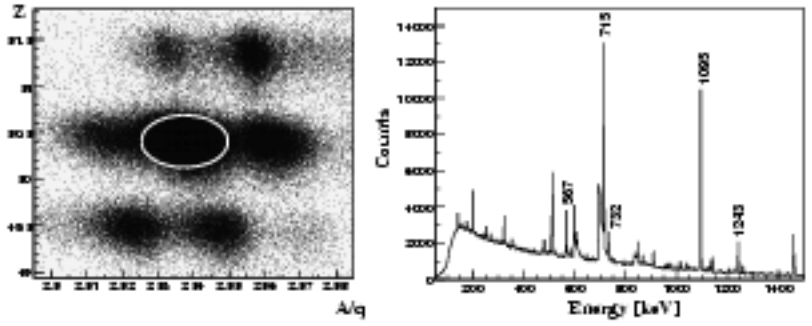

Figure 2. Left: Typical identification plot; the ellipse indicates the gate on ^{127}Sn. The spots left and right of it correspond to ^{126}Sn and ^{128}Sn, respectively, while the upper ones are for ^{129}Sb and ^{130}Sb, and the lower ones for ^{124}In and ^{125}In. Right: Energy spectrum for ^{127}Sn gated on the identification plot. The labelled transitions belong to the decay of the $19/2^+$ isomer.

each ion.

The ^{127}Sn secondary beam was transported through the FRS with an energy of 300 MeV per nucleon. At the final focal plane of FRS (*S4*) the ions were stopped by using a thick 15 mm Plexiglas degrader glued in front of a high-purity (99.998%) 2 mm annealed Copper plate which served as an implantation host. It has a cubic lattice, without electric field gradients, and provided a perturbation-free environment for the implanted ions. It was placed between the poles in the center of an electromagnet that provided a constant magnetic field B in the vertical direction. The magnet was shielded upstream with a Pb brick wall. The beam entered the magnet through a hole in the yoke with a diameter of 75 mm. Upstream a Pb collimator was built in in the Pb wall with a diameter of 70 mm. In this way, the beam spot at the secondary target position had a diameter of 70 mm. Two additional scintillator detectors, *Sc42* and *Sc43*, were placed in front and behind the catcher, which allows us to validate the implantation of the impinging ions.

The isomeric γ rays were detected with eight Cluster Ge detectors mounted in the horizontal plane perpendicular to the magnetic field. A Cluster detector consists of seven tapered hexagonal Ge crystals in a common cryostat. Each crystal can act as a separate detector. The average distance from the stopper to the front face of the detectors was approximately 43 cm. The total γ-ray efficiency was measured by placing a calibrated ^{152}Eu source at six different positions at the catcher, covering the whole implantation spot and is approximately 2% at 1000 keV. In Figure 2 (right) an isotope gated energy spectrum is presented. There are some contaminating transitions from neighbouring Sn isotopes and background lines in the spectrum.

The nuclei of interest were identified on an event-by-event basis. Coincidences between ion signals from the FRS detectors and γ rays detected with the Ge detectors were recorded within a time window of 12 μs, provided by a common time-to-amplitude converter. In addition, signals from each crystal of the Cluster detectors were sent to an individual TDC, which opened an extra 2 μs window. This allows successive isomers to be studied, as well as to time-align the individual crystals. The fast signal from *Sc41* which was generated by an impinging ion was used to start the time measurement ($t = 0$ signal). The measured time spectrum for the $19/2^+$ isomer in ^{127}Sn is presented in the top section of Figure 3.

The magnetic field $B = 0.12$ T was chosen such that with the minimal expected g factor of $g = -0.1$ at least two periods in the $R(t)$ function occur, as demonstrated in the bottom part of Figure 3. The direction of the magnetic field was switched manually up and down every four hours during the experiment.

3 Data Analysis

Within the present experiment in total $2 \cdot 10^5$ single-hit photopeak events ($2.5 \cdot 10^5$ photopeak events in add-back mode), which belong to the γ-decay of

the $19/2^+$ isomer in ^{127}Sn, were detected. In order to extract the experimental $R(t)$ function, it is necessary to apply conditions on the longitudinal momentum distribution, by selecting events which belong either to the center, or to the wing. This reduces the number of events which are used in the data analysis, as presented in Table 1. At this stage of the analysis only single-hits in each Cluster were considered.

Table 1. Number of counts for the measured γ rays belonging to the decay of the $19/2^+$ isomer in ^{127}Sn for all detectors, and for both directions of the magnetic field.

	1095 keV	732 keV	715 keV
Center	23980	8360	33590
Wing	13700	4870	19030
Total	68100	23700	94900
Total[1]	66435	6318	58998

[1] after background subtraction

3.1 The $R(t)$ functions

The constant magnetic field B induces rotation of the spins of the aligned nuclear ensemble around the magnetic field axis with a Larmor frequency $\omega_L = -\frac{g\mu_N B}{\hbar}$ which depends on the isomeric g-factor and applied magnetic field. The intensity of the γ decay, detected in the horizontal plane at an angle θ with respect to the beam axis is related to the angular distribution:

$$I(t,\theta,\omega_L) = I_0 e^{-\lambda t} W(t,\theta,\omega_L)$$
$$= I_0 e^{-\lambda t}\{1 + A_2(\gamma)B_2 P_2[(\cos(\theta - \omega_L t - \alpha))]\}. \quad (1)$$

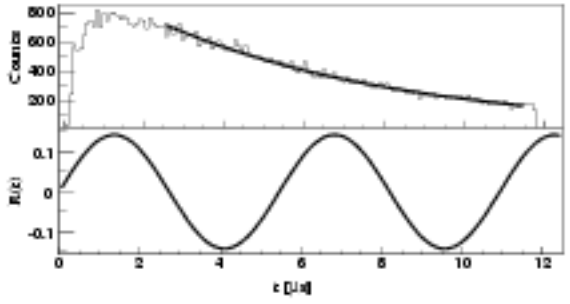

Figure 3. Top: Time spectrum for the 1095 keV line in ^{127}Sn with the half-life of 4.5(3) μs; Bottom: Calculated $R(t)$ function assuming $g = -0.1$ and a magnetic field $B = 0.12$ T.

Here $A_2(\gamma)$ is the angular distribution coefficient, depending on the details of the γ decay, B_2 is the orientation parameter, depending on the degree of alignment produced in the reaction. $P_2(\cos(\theta))$ is the 2^{nd} order Legendre Polynomial and α is the angle between the beam direction and the symmetry axis of the spin-oriented ensemble, which in this case is equal to zero, because FRS is a zero-degree fragment separator. We neglect the 4^{th} and higher order components, because they are usually about an order of magnitude smaller.

To extract the precession pattern from measured time spectra, they are combined in $R(t)$ functions for each γ transition

$$R(t,\theta,\theta',\omega_L) = \frac{I_1(t,\theta,\omega_L) - I_2(t,\theta',\omega_L)}{I_1(t,\theta,\omega_L) + I_2(t,\theta',\omega_L)}, \tag{2}$$

where I_1 stays for the time spectrum of a detector placed at an angle θ with respect to the beam, and I_2 is the time spectrum for a detector at an angle θ'. This expression does not depend on the isomeric decay constant. It has the highest amplitude for the detectors placed at 90° with respect to each other and at ±45° and ±135° with respect to the beam axis, provided that $\alpha = 0$.

$$R(t,\omega_L) = \frac{3A_2B_2}{4 + A_2B_2}\sin(2\omega_L t). \tag{3}$$

It is possible to compose an $R(t)$ using the data from the same detector but for two opposite directions of the magnetic field. For a detector placed at angle θ we obtain

$$R(t,\theta,\pm B,\omega_L) = \frac{3A_2B_2\sin(2\theta)\sin(2\omega_L t)}{4 + A_2B_2 + 3A_2B_2\cos(2\theta)\cos(2\omega_L t)}. \tag{4}$$

Using such $R(t)$ functions we eliminate some detector-related effects which can cause systematic errors.

If the specific symmetries of the set-up are considered we arrive to an expression for the $R(t)$ function identical with Eqn. (3) for the detectors at ±45° and ±135°. This means that the following detector combinations are possible (see Figure 1 for the detector labels): $I_1 = (A + L)\ |\ +(D + G)\ |$ and $I_2 = (A + L)\ |\ +(D + G)\ |$, where | and | denotes opposite directions of the applied field. Similarly another combination of detectors can be done, but the amplitude of the $R(t)$ function will be reduced and the phase will be shifted. For example, if the detectors at ±75° and ±105° with respect to the beam direction (±30° with respect to each other) are considered ($I_1 = (B + K)\ |\ +(C + J)\ |$ and $I_2 = (B + K)\ |\ +(C + J)\ |$), the $R(t)$ function will have almost the same phase as in Eqn. (3), but twice smaller amplitude

$$R(t,\omega_L) = \frac{3A_2B_2\sin(2\omega_L t)}{8 + 2A_2B_2 - 3\sqrt{3}A_2B_2\cos(2\omega_L t)}. \tag{5}$$

For the combination of detectors at $\pm 150^{\circ}$ with respect to each other, $\pm 45^{\circ}$ and $\pm 105^{\circ}$ with respect to the beam, the following time spectra can be considered: $I_1 = (A + L) \mid +(C + J) \mid$ and $I_2 = (K + B) \mid +(G + D) \mid$. The $R(t)$ function will have a phase shift and twice smaller amplitude

$$R(t,\omega_L) = \frac{3A_2B_2(\sin(2\omega_L t) + \sqrt{3}\cos(2\omega_L t))}{16 + 4A_2B_2 + 3A_2B_2(3\sin(2\omega_L t) - \sqrt{3}\cos(2\omega_L t)}. \quad (6)$$

The phase shift of the $R(t)$ function depends on the value of the g factor, while the reduction of the amplitude is fixed for each combination of detectors. This allows a simultaneous fit of all detector combinations using two fit parameters, the Larmor frequency and the amplitude of the $R(t)$ function, which is related to the orientation of the nuclear spin ensemble.

Most of the crystals of the Cluster detectors do not lie exactly in the horizontal plane, but are misaligned at a small angle ϕ. This causes an additional reduction of the amplitude. However, due to the large distance between the implantation spot and the detector faces, this effect, as well as the influence of geometric factors due to the finite dimensions of the implantation spot, can be neglected. A more elaborate analysis needs to take into consideration the implantation position of each ion, and the crystal of the first hit in a Cluster detector. Here we report results obtained only with detectors at 90° with respect to each other, at $\pm 45^{\circ}$ and $\pm 135^{\circ}$ with respect to beam axis.

3.2 Momentum Selection

In fragmentation reactions the fragments have a longitudinal momentum distribution $exp(-p^2/2\sigma^2)$, with $\sigma = \sigma_0^2 A_{fr}(A_p - A_{fr})/(A_p - 1)$, where A_p and A_{fr} are the mass numbers of the projectile and the fragment, and $\sigma_0 \approx 90$ MeV/c [9].

The alignment of the nuclear spin ensemble depends on the longitudinal momentum distribution [7]. Under alignment of the nuclear ensemble the different m substates for a given spin I, $m = -I, -I+1, ..., I$ have different population, but the $\pm m$ substates are equally populated. Positive (oblate) alignment occurs when the spin ensemble is oriented in a plane perpendicular to the beam axis, while for negative (prolate) alignment the spins are oriented perpendicularly to this plane. It is obvious that a change of the sign of the alignment will result in a change of the sign of the $R(t)$ function. Experiments at intermediate energies demonstrated that the alignment changes its magnitude and sign from the center towards the outermost wing of the momentum distribution. This effect was studied also theoretically and qualitative understanding was achieved [10]. Therefore, it is necessary to determine the position of the center and the wing to eliminate interference effects resulting from mixing of alignment. So far some measurements were done at intermediate energies and such data did not exist at relativistic energies.

The measured momentum distribution with *Sc21* is shown in the left-hand-side of Figure 4. The lower wing was cut with the *S2* slits of the FRS (see Figure 1). During the experiment the shape of the momentum distribution gradually changed to more complicate form. The reason is that beam which hits scintillator *Sc21* was close to the maximum ($2 \cdot 10^5$ ions/s) and the properties of the scintillator deteriorated. For this reason we deduced the isomeric ratio for the $19/2^+$ isomer in ^{127}Sn as a function of the momentum distribution and used it as a criterium to define the position of the center and the outermost wing (see Figure 4, right). The isomeric ratio is expected to have a minimum in the center and maximum in the wing of momentum distribution [11].

The isomeric ratio is defined as the probability that in a reaction an isomeric state is excited

$$IR = \frac{Y}{N_{imp}FG} = \frac{N_\gamma(1+\alpha_{tot})}{\epsilon_{eff} b_\gamma N_{imp} FG}, \tag{7}$$

where N_γ is the number of counts in the peak corresponding to the transition depopulating the isomer, α_{tot} is the total conversion coefficient for this transition, b_γ is its absolute branching ratio, ϵ_{eff} is the efficiency correction and N_{imp} is the number of implanted ions of the isotope of interest. F and G are the correction factors for the inflight isomer decay and the finite detection time of the γ ray, respectively. The isomeric ratio plotted in Figure 4 is the average for the most intense transitions in ^{127}Sn, without corrections which do not depend on momentum distribution. At this stage of the analysis it is enough to determine the relative, not the absolute values for the isomeric ratio.

4 Results and Discussion

The $R(t)$ functions of the 1095 keV and 715 keV γ rays and for different cuts of the longitudinal momentum distribution are presented in Figure 5. The amplitude of the $R(t)$ function, which is sorted for the sum of the time spectra of

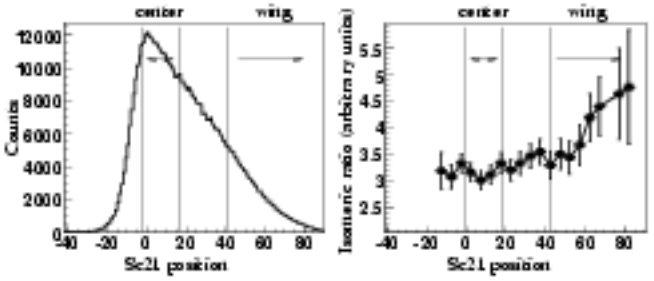

Figure 4. Left: Longitudinal momentum distribution for ^{127}Sn measured with *Sci21*; Right: The isomeric ratio for the $19/2^+$ isomer in ^{127}Sn as a function of momentum distribution. The positions of center and wing are indicated with vertical lines.

the 1095 keV E2 and 732 keV M2 transition for the center of the momentum distribution (see the middle section of Figure 5), is very small and has an opposite phase compared to the $R(t)$ function for the outermost wing (see the upper section of Figure 5). This indicates a sign change of the alignment of the nuclear spin ensemble between the center and the wing of the momentum distribution.

The $R(t)$ function for the 715 keV transition was sorted for the outmost wing of the momentum distribution (see the lower section of Figure 5). It display opposite phase, compared to the $R(t)$ function for the 1095 keV transition, which is not in agreement with the published level scheme [2]. According to the published spin and parities, the 715 keV transition should have E1 multipolarity. In such a case its angular distribution coefficient would be $A_2 = -0.4$, which is similar to the values of the coefficients for the 1095 keV E2 transition, $A_2 = -0.39$, and the 732 keV M2 transition, $A_2 = -0.37$ [12].

Fits of the $R(t)$ functions are displayed in Figure 5. The obtained absolute values of the g factor, $|g| \approx 0.16$ are in agreement with the theoretical expectations based on the empirical g factors and on large-scale shell model calculations. These results will be discussed elsewhere [13].

For the $R(t)$ function of the 715 keV transition $\sim 10^4$ photopeak events were

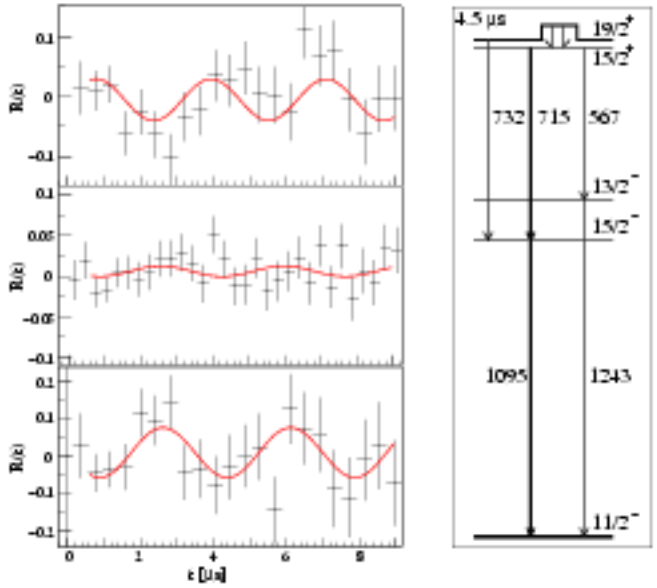

Figure 5. Left: (up) $R(t)$ function for the 1095 keV and 732 keV transitions at the wing of the momentum distribution; (middle) $R(t)$ function for 1095 keV and 732 keV transitions at the center of the momentum distribution; (down) $R(t)$ function for 715 keV transition at the wing of the momentum distribution. Right: Partial level scheme of ^{127}Sn, revealing the decay of the $19/2^+$ isomer [2].

used in the data analysis, which provides the lowest limit for such experiments.

5 Conclusions

First results from the g-RISING campaign for the g factor of the $19/2^+$ isomer in ^{127}Sn from relativistic fragmentation demonstrate that significant alignment ($\sim$10%) is observed in the outermost wing of the momentum distribution. The results indicate that a sign change of the alignment takes place between the center and the wing. The present experiment provides a benchmark (in terms of intensity of the isomer beam and number of detected γ rays) for further determinations of electromagnetic moments of isomers in nuclei yet farther away from stability

Acknowledgments

This work was supported in part by the EC EURONS RII3-CT-2004-506065 project and the Bulgarian National Science Fund grant VUF06/05.

References

[1] H.J. Wollersheim et al (2005) *Nucl. Instr. Meth. Phys. Res. A* 537 637; www-aix.gsi.de/ wolle/EB_at_GSI/FRS-WORKING/main.html
[2] J.A. Pinston et al. (2000) *Phys. Rev. C* 61 024312.
[3] J.A. Pinston and J. Genevey (2004) *J. Phys. G* 30 R57.
[4] P. Raghavan (1989) *Atomic Data and Nuclear Data Tables* 42 189.
[5] W.D. Schmidt-Ott et al. (1994) *Z. Phys. A* 350 215.
[6] G. Georgiev et al. (2002) *J. Phys. G* 28 2993-3006.
[7] I. Matea et al. (2004) *Phys. Rev. Lett.* 93 142503.
[8] H. Geissel et al. (1992) *Nucl. Instr. Meth. B* 70 286.
[9] A.S. Goldhaber (1974) *Phys Lett B* 53 306.
[10] N. Collier et al. (2001) *Phys. Rev. C* 63 054605.
[11] J.M. Dangas et al. (2001) *Phys. Rev. C* 63 064609.
[12] T. Yamazaki (1967) *Nuclear Data A* 3 1.
[13] L. Atanasova et al. (2006) in preparation.

First Results from the g-RISING campaign: The g factor of the $19/2^+$ isomer in ^{127}Sn

D. L. Balabanski[1,2], L. Atanasova[3], M. Hass[4], D. Bazzacco[5], F. Becker[6], P. Bednarczyk[6,7], G. Benzoni[8], N. Blasi[8], A. Blazhev[9], A. Bracco[8], L. Caceres[6,10], F. Camera[8], S. K. Chamoli[4], F. Crespi[8], P. Detistov[3], P. Doornenbal[6], C. Fahlander[11], E. Farnea[5], G. Georgiev[12], J. Gerl[6], K. Gladnishki[1], M. Górska[6], H. Grawe[6], J. Grebosz[6,7], R. Hoischen[11], G. Ilie[9], M. Ionescu-Bujor[13], A. Iordachescu[13], A. Jungclaus[10], G. Lo Bianco[1], M. Kmiecik[7], I. Kojouharov[6], N. Kurz[6], S. Lakshmi[4], R. Lozeva[14], A. Maj[7], D. Montanari[8], G. Neyens[14], M. Pfützner[15], S. Pietri[16], Zs. Podolyák[16], W. Prokopowicz[6,7], D. Rudolph[11], G. Rusev[17], T. R. Saito[6], A. Saltarelli[1], H. Schaffner[6], R. Schwengner[17], G. Simpson[18], S. Tachenov[6], J. J. Valente-Dubon[19], N. Vermeulen[14], J. Walker[6,16], E. Werner-Malento[6,15], O. Wieland[8], H. J. Wollersheim[6], and M. Hjorth-Jensen[20]

[1] *Dipartimento di Fisica, Universitá di Camerino and INFN, Sezione di Perugia, 62032 Camerino, Italy*
[2] *Institute for Nuclear Research and Nuclear Energy, Bulgarian Academy of Sciences, BG–1784 Sofia, Bulgaria*
[3] *Faculty of Physics, St. Kliment Ohridski University of Sofia, BG–1164 Sofia, Bulgaria*
[4] *Department of Particle Physics, Weizmann Institute of Science, Rehovot 76100, Israel*
[5] *Dipartimento di Fisica, Universitá di Padova and INFN, Sezione di Padova, 35131 Padova, Italy*
[6] *GSI, Planckstrasse 1, D-64291, Darmstadt, Germany*
[7] *The Henryk Niewodniczanski Institute of Nuclear Physics, Polish Academy of Sciences, PL–31-342 Krakow, Poland*
[8] *Dipartimento di Fisica, Universitá di Milano and INFN, Sezione di Milano, 20133 Milano, Italy*
[9] *IKP, Universität zu Köln, D-50937, Köln, Germany*
[10] *Departamento de Fisica Teórica, Universidad Autonoma de Madrid, E–28049 Madrid, Spain*
[11] *Department of Physics, Lund University, S–22100 Lund, Sweden*
[12] *Centre de Spectrometrie Nucleaire et de Spectrometrie de Masse,F–91405 Orsay Campus, France*
[13] *National Institute for Physics and Nuclear Engineering, P.O. Box MG-6, Bucharest, Romania*
[14] *Instituut voor Kern- en Stralingsfysica, K.U.Leuven, Celestijnenlaan 200D, 3001 Leuven, Belgium*
[15] *Institute of Experimental Physics, Warsaw University, PL–00-681 Warsaw, Poland*
[16] *Department of Physics, University of Surrey, Guildford, GU2 7XH, UK*
[17] *Institut für Kern- und Hadronenphysik, Forschungszentrum Rossendorf, D–01314, Dresden, Germany*
[18] *LPSC, 38026 Grenoble Cedex, France*
[19] *INFN - Laboratori Nazionali di Legnaro, 35020 Legnaro (Padova), Italy*
[20] *Department of Physics, University of Oslo, N-0316 Oslo, Norway*

First results will be reported from g-factors studies of isomers in exotic nuclei, which were carried out within the g-RISING (Rare Isotope Investigations at GSI) project. The isomeric g factors were measured using the Time-Differential Perturbed Angular Distribution (TDPAD) method. GSI is the only facility where intense beams of fully stripped heavy ions ($A \geq 80$) ions can be separated, which allows the preservation of the orientation of the nuclear spin ensemble as obtained in the fragmentation reaction. Isomers in the $A \approx 130$ nuclei were populated in relativistic projectile fragmentation of a ^{136}Xe beam at 600 MeV/u provided by the SIS synchrotron at GSI. It was impinging on a 1 g/cm^2 Beryllium production target located at the entrance of the fragment separator (FRS). The final reaction products were stopped in a Copper plate in the final focal point of the FRS, which was mounted between the poles of an electromagnet, and provided a perturbation-free environment for the implanted isomers. The nuclei of interest were identified on an event-by-event basis and ion-γ coincidences were recorded in the experiment. The isomeric γ decay was detected with eight Cluster Ge detectors (four of them with BGO shields) mounted in a ring in the horizontal plane, providing a singles γ-ray efficiency $\varepsilon \approx 3\%$ at 1.3 MeV. An overview of the experimental technique will be given, together with of the performance of the array. The presentation will focus on the results for the $19/2^+$ 4.5 μs isomer in ^{127}Sn, which will be compared to large scale shell-model (LSSM) calculations.

g FACTOR MEASUREMENTS ON RELATIVISTIC ISOMERIC BEAMS PRODUCED BY FRAGMENTATION AND U-FISSION: THE g-RISING PROJECT AT GSI*

G. Neyens[a], L. Atanasova[b], D.L. Balabanski[c,d], F. Becker[e]
P. Bednarczyk[e,f], L. Caceres[e,g], P. Doornenbal[e,h], J. Gerl[e], M. Górska[e]
J. Grębosz[e,f], M. Hass[i], G. Ilie[h,j], N. Kurz[e], I. Kojouharov[e], R. Lozeva[a,b]
A. Maj[f], M. Pfützner[k], S. Pietri[l], Zs. Podolyak[l], W. Prokopowicz[e]
T.R. Saitoh[e], H. Schaffner[e], G. Simpson[m], N. Vermeulen[a]
E. Werner-Malento[e], J. Walker[l], H.J. Wollersheim[e], D. Bazzacco[n]
G. Benzoni[o], A. Blazhev[g], N. Blasi[o], A. Bracco[o], C. Brandau[l], F. Camera[o]
S.K. Chamoli[i], S. Chmel[p], F.C.L. Crespi[o], J.M. Daugas[q], M. De Rydt[a]
P. Detistov[b], C. Fahlander[r], E. Farnea[n], G. Georgiev[s], K. Gladnishki[t]
R. Hoischen[r], M. Ionescu-Bujor[j], A. Iordachescu[j], J. Jolie[h], A. Jungclaus[g]
M. Kmiecik[f], A. Krasznahorkay[u], R. Kulessa[w], S. Lakshmi[i], G. Lo Bianco[c]
S. Mallion[a], K. Mazurek[f], W. Meczynski[f], D. Montanari[o], S. Myalsky[f]
O. Perru[q], D. Rudolph[r], G. Rusev[y], A. Saltarelli[c,t], R. Schwengner[y]
J. Styczen[f], K. Turzó[a], J.J. Valiente-Dobón [z], O. Wieland[o], M. Zieblinski[f]

[a]Katholieke Universiteit Leuven, Belgium
[b]St. Kliments Ohridsky University of Sofia, Bulgaria
[c]University of Camerino, Italy
[d]INRNE, Academy of Sciences, Sofia, Bulgaria
[e]Gesellschaft für Schwerionenforschung, Darmstadt, Germany
[f]IFJ PAN, Kraków, Poland
[g]Universidad Autonoma de Madrid, Spain
[h]IKP, Köln, Germany
[i]The Weismann Institute, Rehovot, Israel
[j]National Institute for Physics and Nuclear Engineering, Bucharest, Romania
[k]Institute of Experimental Physics, Warsaw University, Poland
[l]University of Surrey, United Kingdom
[m]Institut Laue Langevin, Grenoble, France
[n]University of Padova and INFN, Padova, Italy
[o]University of Milano and INFN, Milano, Italy
[p]ISKP University of Bonn, Germany
[q]CEA/DIF/DPTA/PN, Bruyeres le Chatel, France
[r]Department of Physics, Lund University, Sweden
[s]University Paris-Sud, CSNSM, ORSAY-Campus, France
[t]INFN, Sezione di Perugia, Italy
[u]ATOMKI, Debrecen, Hungary
[w]Jagiellonian University, Kraków, Poland
[y]Institut fuer Strahlenphysik, FZ Rossendorf, Dresden, Germany
[z]Legnaro National Laboratory, Legnaro, Italy

(Received November 11, 2006)

* Presented at the Zakopane Conference on Nuclear Physics, September 4–10, 2006, Zakopane, Poland.

Within the RISING (Rare ISotope INvestigations @ GSI) Collaboration at GSI, g factor measurements have been performed on isomeric states in neutron-rich isotopes approaching ^{132}Sn and in the neutron deficient Pb-region (the g-RISING campaign). We present the experimental technique and some typical aspects related to such studies on relativistic beams selected with the FRS fragment separator. First results are presented for the $(19/2^+)$ 4.5 μs isomeric state in ^{127}Sn, which has been produced by means of fission of a relativistic ^{238}U beam on the one hand, and by the fragmentation of a relativistic ^{136}Xe beam on the other hand. Spin-alignment has been observed in both reactions. It was the first time that spin-alignment has been established in a relativistic fission reaction.

PACS numbers: 21.10.Ky, 24.70.+s, 27.60.+j

1. Introduction

The magnetic dipole moment, $\mu = g \cdot I$, is a very sensitive probe to investigate the single-particle configuration of a nuclear state, because nucleon g factors depend strongly on their orbital and total momentum. High-spin isomers in the region of doubly-magic nuclei often have a rather pure single-particle configuration, and then the g factor is a fingerprint of the unpaired nucleon configuration [1]. Measurements of g factors can help to assign or confirm the spin and parity of a nuclear state, especially in far-from-stability regions, where such assignments are often based on systematics and theoretical predictions.

To measure the g factor of microsecond isomeric states, the Time Differential Perturbed Angular Distribution (TDPAD) method is most suited [2]. It is based on the observation of the Larmor precession of a spin-aligned ensemble of isomers implanted in a suitable stopper that is placed in a static magnetic field. Spin-aligned isomers are produced in most nuclear reactions, such as fusion-evaporation [3], projectile fragmentation [4–6] or spontaneous fission [7]. If the isomers are produced and stopped in the production target, they maintain their spin-alignment if a large enough magnetic field is applied and if the target material has suitable properties. In such case, one can investigate their g factor "in-beam" [2]. However, to study isomers in exotic isotopes, one often needs to select the isomers of interest with an in-flight fragment separator [8]. The spin-alignment in an isomeric beam is then preserved during the selection process, only if the isotopes are fully stripped [5, 6]. If electrons occur around the free nucleus, the hyperfine interaction between the nuclear spin and the randomly oriented electron spin causes a loss of the reaction-induced orientation during the flight through vacuum. In some cases the alignment can be partially maintained if a noble gas charge state is selected [9]. To obtain fully-stripped isotopes from a projectile fragmentation reaction the primary beam needs to have a sufficiently

high energy, which increases with the mass of the desired isotope. In order to avoid the pick-up of electrons in the particle identification detectors along the beam trajectory, the secondary beam energy needs to stay sufficiently high up to the point of implantation. For isotopes in the region of ^{132}Sn, the secondary beam energy should be at least 300 MeV/u along the whole trajectory. Thus the primary beam has to be relativistic, with an energy of more than 500 MeV/u. Such beams are provided at the GSI facility in Darmstadt, Germany.

We present here the goals and some preliminary results from a campaign to measure for the first time the g factors of isotopes with $A > 100$ using relativistic beams. The Cluster HPGe detectors from RISING [10] have been used for detecting the isomeric decay. Both fragmentation and fission reactions were investigated. For the latter, the present experiment serves as a proof that spin-aligned isomeric beams can be selected after a relativistic fission reaction. Results for isomers in the region of ^{132}Sn, produced by both reactions mechanisms, are presented. In the neutron-rich isotopes near ^{132}Sn, several isomers have been observed during the past decades. Different methods were used for producing the isomers: deep-inelastic reactions [11], spontaneous fission [12], thermal neutron-induced fission [13, 14], proton-induced fission followed by β-decay into the isomer [15,16], relativistic fission of a ^{238}U beam [17] and recently also fragmentation of a ^{136}Xe beam. To study the g factor of these neutron-rich isomers, spin-aligned relativistic beams as produced at the FRagment Separator FRS [18], may proof to be one of the few available methods.

2. Experimental method and set-up

2.1. Production and selection of the isomeric beams

A primary target of 1 g/cm^2 ^{9}Be (with a 221 mg/cm^2 Nb stripper foil), placed at the entrance of the FRS, is bombarded by a ^{238}U beam (750 MeV/u, average intensity 10^8 pps) to produce fission fragments or a 600 MeV/u ^{136}Xe beam (average intensity 2×10^8 pps) to produce projectile fragments, respectively. In both experiments, a cocktail of isotopes around ^{127}Sn is selected using the four dipole stages of the FRS and an Al degrader placed in its middle focus (schematic layout shown in Fig. 1) [18]. A thickness of 5 g/cm^2 Al was used to select fission fragments, while for the projectile fragments the wedge degrader was 2 g/cm^2 thick.

Ion identification is performed on an event-by-event basis using a system of tracking detectors: two multi-wire proportional counters (MW41 and MW42) for position determination, a MUltiple Sampling Ionizing Chamber (MUSIC) for Z determination and two fast scintillators (position sensitive Sc21 in the middle focus and Sc41 at the final focus) for time-of-flight (TOF) measurements [10].

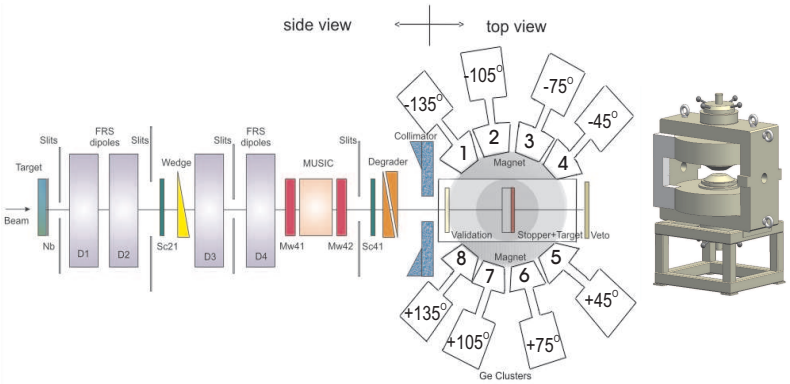

Fig. 1. Schematic layout of the FRS and g-RISING set-up (left) and drawing of the magnet (right).

Scintillator Sc41 is used also as a particle trigger for ions entering the g-RISING set-up and to give the start for the subsequent γ-decay measurement. A scintillator (validation) inside the magnet is used to validate the γ-event, and another scintillator (veto) at the end of the set-up is used to exclude events that come with an ion observed in this detector (and thus did not stop in the stopper). Figure 2 shows the selected isotopes in both experiments.

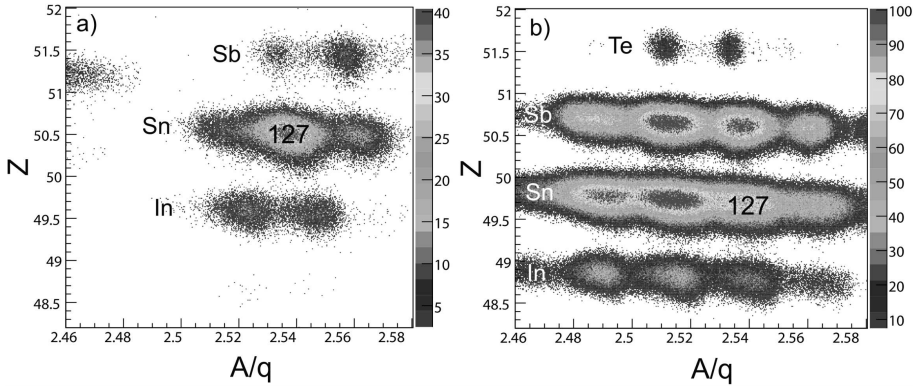

Fig. 2. Isotopes selected in case of a Xe-fragmentation reaction (a) and a U-fission reaction (b).

The particle cocktail arrives at the final FRS focus with an energy of almost 500–600 MeV/u, where all the detectors are placed with air gaps between them. Thus the probability for picking up electrons needs to be estimated according to the energy loss after each detector. Such calculations

were performed using the simulation codes GLOBAL [19] and LISE++ [20]. For the fission fragments around ^{127}Sn almost 90% of the isotopes are fully stripped after Sc41. Their energy of about 500 MeV/u is further reduced by a variable thickness Al degrader placed in front of the g-RISING set-up, in order to adjust their implantation point in the stopper. To avoid the pick-up of electrons in the air and in the validation detector behind this degrader, the energy of the fragments needs to stay above 300 MeV/u. The Al-degrader thickness was therefore limited to less then 3 g/cm^2. To protect the set-up from upstream radiation, a lead wall with a collimator of 70 mm diameter is used in front of the magnet yoke, which has a hole with diameter 75 mm through which the beam has to pass (Fig. 1).

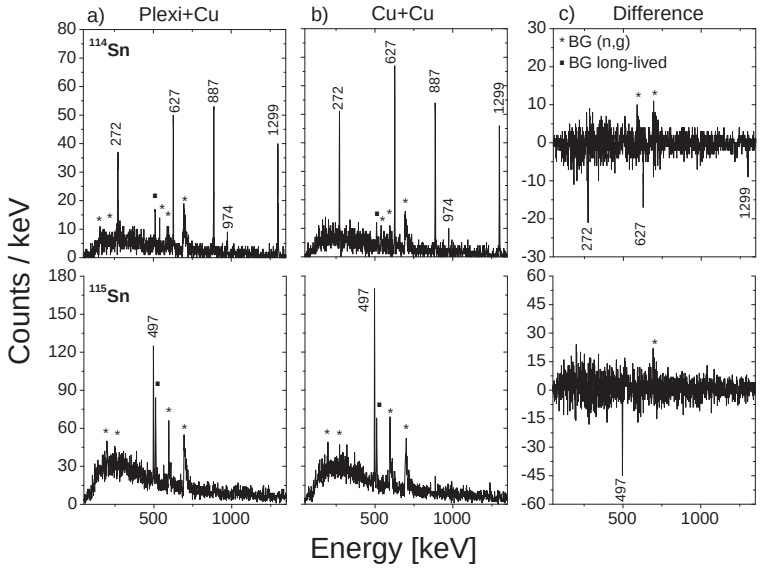

Fig. 3. γ-spectra from ^{114}Sn (upper panel) and ^{115}Sn (lower panel) isomeric decays. The isomeric transitions are shown with their energies. They are more intense for a Cu+Cu (b) than for a plexi+Cu (a) degrader/stopper combination. In (c) the difference spectra illustrate that the low-energy background radiation is similar in both spectra.

A high-purity (4N) Cu foil with a size of 80×80 mm^2 and 2 mm thickness, annealed under Ar atmosphere up to 750°C during several hours, was used as a perturbation free environment for the isomers. To stop a 300 MeV/u beam in Cu, a total thickness of 4 mm is required, which is obtained by gluing another 2 mm Cu to the stopper plate (to avoid an air gap). In [10] it was calculated that the cross section for atomic processes leading to low-energy background radiation in the γ-spectra increases with increasing Z of the

target material. Therefore, we compared isomeric γ-spectra measured with a low-Z (20 mm plexiglass) and with a high-Z (2 mm Cu) degrader fixed to the Cu stopper (Fig. 3(a) and 3(b)). For ^{114}Sn ($I^\pi = 7^-$, $t_{1/2} = 733$ ns) the γ-spectrum is recorded in a [160 ns — 3 μs] time window after the ion arrival (top row Fig. 3) and for ^{115}Sn (I^π=$11/2^-$, $t_{1/2} = 159\,\mu$s) the time window is [160 ns — 15.5 μs] (bottom row Fig. 3). The isomeric transitions are on average 27% and 36% more intense for the Cu/Cu combination. This is in agreement with calculations from the LISE++ code, which predicts 24% loss of isomers caused by the higher amount of nuclear reactions in the plexi-glass degrader. Subtracting both spectra, in Fig. 3c, shows that the low-energy background radiation in the Cu/Cu case is not significantly larger than in the plexi/Cu case. Thus using a high-Z degrader is more advantageous than using a low-Z one, contrary to what was believed before. However, in the experiments we used the plexi/Cu combination.

2.2. g-Factor measurement using RISING detectors

To study the g factor of microsecond isomers, a spin-aligned ensemble of isomers is implanted in the annealed Cu host that maintains the spin-orientation during the nuclear lifetime. By applying a static magnetic field, the isomeric spins are decoupled from possible remaining perturbing electric field gradients [21]. The spin-oriented ensemble performs a Larmor precession around this vertically oriented static field. From the measured precession frequency $\omega_{\mathrm{L}} = \frac{g\mu_N B}{\hbar}$, the nuclear g factor is deduced if the applied magnetic field is known. The γ-decay is measured as a function of time in order to observe the Larmor precession, using eight former EUROBALL cluster detectors [22] placed in the horizontal plane around the magnet at a distance of about 43 cm from the center (Fig. 1). Each cluster consists of seven encapsulated HPGe crystals. For each of the fifty-six crystals, the γ-ray energy and decay time with respect to the ion arrival time in Sc41 is recorded in a time window of almost 20 μs. The trigger was given by a delayed γ detected within 600 ns to 20 μs after the ion arrival. The particle rate in Sc41 was used as a trigger as well, but reduced by a factor 2^8. Thus the event rate in the data acquisition system was typically 5000/s, with the delayed events favored and the dead time below 40%.

In earlier projectile fragmentation reactions at intermediate [5, 6] and relativistic [23] beam energies, positive spin-alignment was observed for isomers selected in the center of their longitudinal momentum distribution and negative alignment in the wing of the distribution. In the present Xe-fragmentation experiment, the longitudinal momentum selection is not made by using the slits after the target or the wedge. Instead, the slits are fully open and the momentum selection is made off-line, using the position-sensitivity of the middle focal plane detector Sc21.

In the relativistic fission of a ^{238}U beam, spin-alignment has never been demonstrated. However, it is well-known that in spontaneous fission a strong correlation exists between the emission direction of the γ-ray and that of the fission fragment [7, 24]. We therefore expect to observe also spin-alignment in a selected ensemble of relativistic fission fragments. In a first step, no off-line momentum cut is performed, because the acceptance of the FRS ($\sim$ 2%) [18] is much smaller than the total width of the fission fragment longitudinal momentum distribution ($\approx$ 10%).

3. Results for ^{127}Sn

Prior to our study, two microsecond isomers were reported (lower part of Fig. 4). The ^{127}Sn fragments produced by thermal neutron induced fission were selected with the in-flight Lohengrin spectrometer at ILL Grenoble, where Pinston *et al.* [13] observed five γ lines with a $t_{1/2}$=4.5(3) μs. They assigned a spin/parity $19/2^+$ to this isomeric level, based on similarities with the decay schemes of the less exotic odd Sn isotopes. In the β-decay of ^{127}In to ^{127}Sn, Gausemel *et al.* [25] observed another microsecond isomer to which they assigned spin/parity $23/2^+$, with a half life of 1.26(15) μs, feeding the lower-lying $19/2^+$ state.

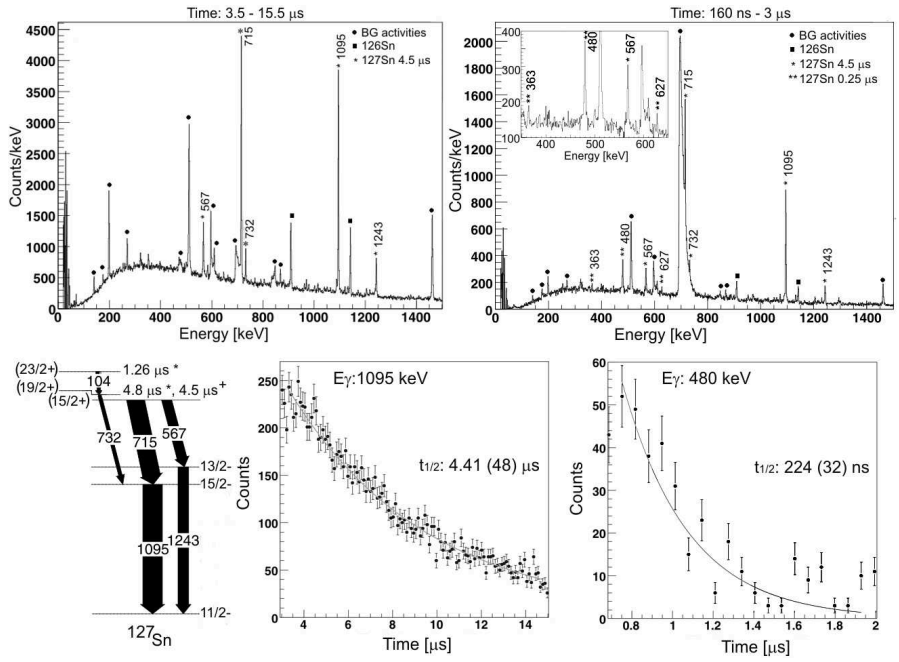

Fig. 4. Top: γ-spectra from the ^{127}Sn decay. Bottom: known isomeric levels and decay scheme (see text) and decay curves for the known and newly observed isomers.

The γ-spectrum correlated to relativistic ^{127}Sn fission fragments is shown in Fig. 4 for different time windows. In the larger time window the five isomeric transitions from the $19/2^+$ decay are marked with their energy. The low energy of the γ transition connecting the $(23/2^+)$ and the $(19/2^+)$ isomers is not in the sensitivity range of our Ge detectors, because of the shielding we added to avoid the atomic background radiation, as suggested in [10]. Therefore, the population and decay of this isomer can only be observed indirectly through the γ-branch depopulating the $(19/2^+)$ isomer. The background subtracted decay curve for the $E = 1095$ keV transition can be fitted assuming one microsecond isomer (Fig. 4), with a lifetime in agreement with previous values. We see no significant contribution from an isomer above the $(19/2^+)$. A few short-lived transitions appear if only γ's in the first 3 μs are visualized, as shown in the right panel of Fig. 4. The newly observed short-lived isomer, for which the decay curve is shown, has a half life of about $t_{1/2} \approx 0.22$ μs. This isomer is most likely the seniority three $\nu(h^{-3}_{11/2})27/2^-$ isomer, which was observed previously also in the less exotic Sn isotopes [11]. Further analysis to build a level scheme and to give more arguments for the suggested spin/parity assignment, is in progress [26].

A detailed investigation of the γ spectra correlated to each isotope produced and selected by the relativistic fission of ^{238}U (Fig. 2b), has revealed more than thirty isomers, of which six new ones. This analysis is still in progress [26].

The goal of these experiments was of course to demonstrate that spin-alignment is present in the relativistic fission of ^{238}U and to compare it to that obtained via projectile fragmentation. The spin-alignment gives rise to a non-zero amplitude of the $R(t)$ function, constructed by combining the decay curves measured for individual detectors with opposite directions of the vertically applied magnetic field. They are labeled U (up) and D (down), respectively (see [27] for more details). The decay curves from detectors positioned at 90° and 180° with respect to each other (1,5 and 4,8 in Fig. 1), can be combined such that the $R(t)$ function reduces to a simple sine function:

$$R(t) \;=\; \frac{I_{\rm U}(t) - \epsilon I_{\rm D}(t)}{I_{\rm U}(t) + \epsilon I_{\rm D}(t)} = \frac{3A_2B_2}{4 + A_2B_2}\sin(2\omega_{\rm L}t) \qquad (1)$$

with $I_{\rm U}(t) = (I_1{+}I_5)\uparrow + (I_4{+}I_8)\downarrow$ and $I_{\rm D}(t) = (I_1{+}I_5)\downarrow + (I_4{+}I_8)\uparrow$. The summed U and D spectra were normalized by a scaling factor ϵ to correct for the different total statistics in each. To include also the statistics from the inner detectors (2,3,6,7), their time-spectra have to be shifted with respect to (1,4,5,8).

The time shift depends on the unknown g factor:

$$\Delta t = \frac{\Delta \Phi}{\omega_{\mathrm{L}}} = \frac{\pm 30^{\circ}\hbar}{g\mu_N B} \tag{2}$$

and therefore an iterative procedure has to be applied.

Here we present the results from the $R(t)$ functions constructed with part of the statistics using the four detectors placed at $\pm 45^{\circ}$ and $\pm 135^{\circ}$ (following expression (1)). In the fragmentation experiment we collected $\approx 10^4$ events in the decay curve of the 715 keV transition (for four detectors and both field directions, and making a momentum cut in the wing of the momentum distribution). The applied magnetic field was chosen such that it would lead to an $R(t)$ oscillation with a period of the order of the nuclear lifetime, $B \approx 0.12$ T. The obtained result is shown in Fig. 5. In the U-fission experiment the applied magnetic field was much higher, $B \approx 0.70$ T, which leads to a very fast oscillation with respect to the isomeric decay time. Therefore, we applied an autocorrelation analysis to fold back the statistics from the total 15.5 μs observation time window into the first 3 μs. In its discrete and normalized form, the autocorrelation function $AC(n)$ is given by:

$$AC(n) = \sum_{k=k_1}^{k_2-n} \frac{R(k)R(k+n)}{k_2-k_1-n} \Big/ \sum_{k=k_1}^{k_2} \frac{R^2(k)}{k_2-k_1}, \tag{3}$$

where $R(k)$ presents the data as a function of the channel number k, (k_2-k_1) is the detection window and n runs up to a maximum N, the folding window, with $N << k_2 - k_1$. If the data $R(k)$ would describe a pure sine function without noise components or relaxation, then also $AC(n)$ will be a pure sine function with the same period and with an amplitude 1. Thus any information related to the amount of alignment is lost in such analysis. To quantify it, the analysis will have to be done on the data including statistics from all detectors and in the full observation window of 15.5 μs. Events from the 715 keV and 1095 keV transitions were added to construct the $R(k)$ function. By taking the full momentum acceptance window, a total of 2.10^4 events (sum of both field directions) is collected.

The result from the autocorrelation analysis of the fission data is compared to the $R(t)$ result from the Xe-fragmentation data in Fig. 5. The periods deduced from both experiments agree with each other, considering that the applied magnetic field was about 5.5 times larger in the fission experiment. Thus the deduced g factors are in agreement with each other (a preliminary value $|g| \approx 0.16$ is found) and also in agreement with the empirical value for a $19/2^+$ isomer dominated by a $\nu(h_{11/2}^{-1} \otimes 5^-)$ configuration [27]. However, the fact that the analysed γ-transitions are fed also via

the higher-lying isomers, will have to be considered in the analysis. Thus firm conclusions related to the nuclear structure cannot be made at this stage of analysis. A detailed analysis on the amount of spin-alignment and a comparison for both reactions is in progress.

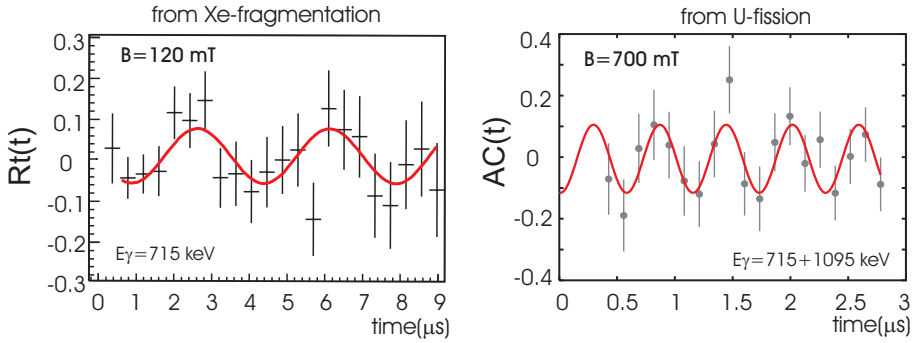

Fig. 5. Preliminary results from the $R(t)$ analysis for the $(19/2^+)$ isomer in ^{127}Sn.

4. Conclusions

The first results from two of the g-factor experiments performed within the g-RISING campaign at GSI have been presented. Isomers in ^{127}Sn have been produced by means of fission of a relativistic ^{238}U beam on one hand, and by the fragmentation of a ^{136}Xe beam on the other hand. A preliminary value for the g factor has been deduced from both data sets, leading to a preliminary consistent value $|g| \approx 0.16$. The fact that very different external field strengths were applied, gives confidence that the observed oscillations are indeed induced by the Larmor precession of a spin-aligned ensemble of isomers. A significant amount of spin-alignment has been observed for the first time in the relativistic fission of a ^{238}U beam, as well as in the fragmentation of a relativistic ^{136}Xe beam. Further analysis, including the observation of several new isomers, as well as the investigation of g factors of some other isomers, is in progress.

This work was supported in part by the FWO-Vlaanderen and the IAP project No. p5-07 of OSCT Belgium, by the Polish Ministry of Education and Science (Grants No. 1 P03B 030 30 and 620/E-77/SPB/GSI/P-03/DWM105/2004-2007), by the Israel Science Foundation and the Swedish Research Council, and by Bulgarian Science Fund (Grant VUF/06/05). The collaboration acknowledges support through the European Community FP6 Integrated Infrastructure Initiative EURONS contract No. RII3-CT-2004-506065.

REFERENCES

[1] G. Neyens, *Rep. Prog. Phys.* **66**, 633 (2003); Erratum 1251 (2003).

[2] G. Goldring, M. Hass, *Treaties on Heavy Ion Science* vol. 3, ed. D.A. Bromley, Plenum, New York 1985, p. 539.

[3] P.A. Butler, P.J. Nolan, *Nucl. Instrum. Methods* **190**, 283 (1981).

[4] K. Asahi *et al.*, *Phys. Rev.* **C43**, 456 (1991).

[5] G. Georgiev *et al.*, *J. Phys.* **G28**, 2993 (2002).

[6] I. Matea *et al.*, *Phys. Rev. Lett.* **93**, 142503 (2004).

[7] J.B. Wilhelmy *et al., Phys. Rev.* **C5**, 2041 (1972).

[8] D.J. Morrissey, B.M. Sherrill, *Lect. Notes Phys.* **651**, 113 (2004).

[9] M. Hass *et al.*, Proc. First Int. Conf. on Radioactive Beams, eds. W.D. Myers, J.M. Nitschke, E.B. Norman, World Scientific, 1990.

[10] H.J. Wollersheim *et al.*, *Nucl. Instrum. Methods Phys. Res.* **A537**, 637 (2005).

[11] R. H. Mayer *et al.*, *Phys. Lett.* **B336**, 308 (1994).

[12] C.T. Zhang *et al.*, *Phys. Rev. Lett.* **77**, 3743 (1996).

[13] J.A. Pinston *et al.*, *Phys. Rev.* **C61**, 024312 (2000).

[14] J.A. Pinston *et al.*, *J. Phys.* **G30**, R57 (2004).

[15] B. Fogelberg *et al.*, *Nucl. Phys.* **A352**, 157 (1981).

[16] L.-E. De Geer, G.B. Holm, *Phys. Rev.* **C22**, 2177 (1980).

[17] M.N. Mineva *et al.*, *Eur. Phys. J.* **A11**, 9 (2001).

[18] H. Geissel *et al.*, *Nucl. Instrum. Methods Phys. Res.* **B70**, 286 (1992).

[19] C. Scheidenberger *et al.*, *Nucl. Instrum. Methods* **B142**, 444 (1998).

[20] D. Bazin *et al.*, *Nucl. Instrum. Methods Phys. Res.* **A482**, 307 (2002).

[21] A. Wolf, E. Cheifetz, *Phys. Rev. Lett.* **36**, 1072 (1976); D. Henzlova *et al.*, *Nucl. Phys.* **A749**, 110C(2005).

[22] J. Eberth *et al.*, *Nucl. Instrum. Methods Phys. Res.* **A369**, 135 (1996).

[23] W.-D. Schmidt-Ott *et al.*, *Z. Phys.* **A50**, 215 (1994).

[24] K. Skarsvag, *Phys. Rev.* **C22**, 638 (1980).

[25] H. Gausemel *et al.*, *Phys. Rev.* **C69**, 054307 (2004); B. Fogelberg *et al.*, *Phys. Rev.* **C70** 034312 (2004).

[26] R. Lozeva *et al.*, in preparation.

[27] L. Atanasova *et al.*, Proc. 25^{th} Int. Nuclear Theory Workshop, Rila Mountains, Bulgaria, 2006, submitted.

Available online at www.sciencedirect.com
ScienceDirect
Progress in Particle and Nuclear Physics 59 (2007) 355–357
Progress in Particle and Nuclear Physics
www.elsevier.com/locate/ppnp

Review

A RISING g-factor measurement of the $19/2^+$ isomer in ^{127}Sn

L. Atanasova[a,*], D.L. Balabanski[b,c], M. Hass[d], F. Becker[e], P. Bednarczyk[e,f], S.K. Chamoli[d], P. Doornenbal[e], G. Georgiev[g], J. Gerl[e], K.A. Gladnishki[c], M. Górska[e], J. Grebosz[e,f], M. Kmiecik[f], S. Lakshmi[d], R. Lozeva[a,h], A. Maj[f], G. Neyens[h], M. Pfützner[i], G. Simpson[j], N. Vermeulen[h], H.J. Wollersheim[e] and the g-RISING Collaboration

[a] *Faculty of Physics, University of Sofia, BG-1164 Sofia, Bulgaria*
[b] *INRNE, Bulgarian Academy of Sciences, BG-1784 Sofia, Bulgaria*
[c] *Universitá di Camerino and INFN-Perugia, 62032 Camerino, Italy*
[d] *Weizmann Institute of Science, Rehovot 76100, Israel*
[e] *GSI, Planckstrasse 1, D-64291, Darmstadt, Germany*
[f] *IFJ PAN, PL-31-342 Kraków, Poland*
[g] *CSNSM, F-91405 Orsay Campus, France*
[h] *IKS, K.U. Leuven, 3001 Leuven, Belgium*
[i] *IEP, Warsaw University, PL-00-681 Warsaw, Poland*
[j] *LPSC, 38026 Grenoble Cedex, France*

Abstract

The g-factor of the $19/2^+ T_{1/2} = 4.5(3)$ μs isomer in ^{127}Sn, which was populated in relativistic projectile fragmentation, was measured within the g-RISING campaign at GSI, utilizing the time-differential perturbed angular distribution method. The deduced g-factor $|g| \approx 0.16$ is in agreement with theoretical estimates based on the empirical g-factors.

* Corresponding address: Department of Atomic Physics, Faculty of Physics, University of Sofia, 5 James Bourchier Blvd, BG-1164 Sofia, Bulgaria. Tel.: +359 2 8161 834.
E-mail address: liliya@phys.uni-sofia.bg (L. Atanasova).

0146-6410/$ - see front matter © 2007 Elsevier B.V. All rights reserved.
doi:10.1016/j.ppnp.2006.12.016

Keywords: Electromagnetic moments; Angular distribution and correlation measurements; Projectile and target fragmentation; $90 \leq A \geq 149$

The g-factor measurement of the $19/2^+$, $T_{1/2} = 4.5(3)$ μs isomer in ^{127}Sn [1,2] aims at a study of the structure of the neutron-rich nuclei in the vicinity of the doubly-magic ^{132}Sn. The experiment was done in relativistic projectile fragmentation of a ^{136}Xe beam at $E/A = 600$ MeV on a thin Be production target within the RISING (Rare ISotope INvestigations at GSI) project [3] at the GSI laboratory, Germany. The fully-stripped ions were separated, tracked and identified on an event-by-event basis. They were implanted in a high-purity Cooper plate, which provided a perturbation-free environment for the isomeric decay. Ion–γ coincidences were recorded and analyzed with the CRACOW software [4]. The experimental set-up is discussed in detail in [5].

The Time-Differential Perturbed Angular Distributions (TDPAD) method, based on the measurement of the Larmor precession of a spin-oriented nuclear ensemble in an external magnetic field B, was applied; the Larmor frequency $\omega_L = -\frac{g\mu_N B}{\hbar}$ is measured in the experiment. The magnitude and sign of alignment of the ensemble depend on the longitudinal momentum distribution [6] of the fragments. In order to preserve the orientation produced in the reaction, fully-stripped ions are separated at relativistic energies. Note that ions heavier than $A = 80$ produced and separated as fully-stripped fragments are available only at GSI.

To extract the g-factor, the γ-decay time spectra, measured at $\pm 45°$ and $\pm 135°$ with respect to the beam axis in a horizontal plane, were combined and compared with the theoretical $R(t)$ function, $R(t, \omega_L) = \frac{3a_2}{4+a_2} \sin(2\omega_L t)$, where a_2 depends on details of the γ decay and the amount of orientation. The $R(t)$ functions of the 1095 and 715 keV γ-rays for the outmost wing of the momentum distribution are presented in Fig. 1. They are out of phase, which is in disagreement with the published level scheme [1]. For the $R(t)$ function of the 715 keV transition $\sim 10^4$ photopeak events were used in the data analysis, which sets a limit for such experiments.

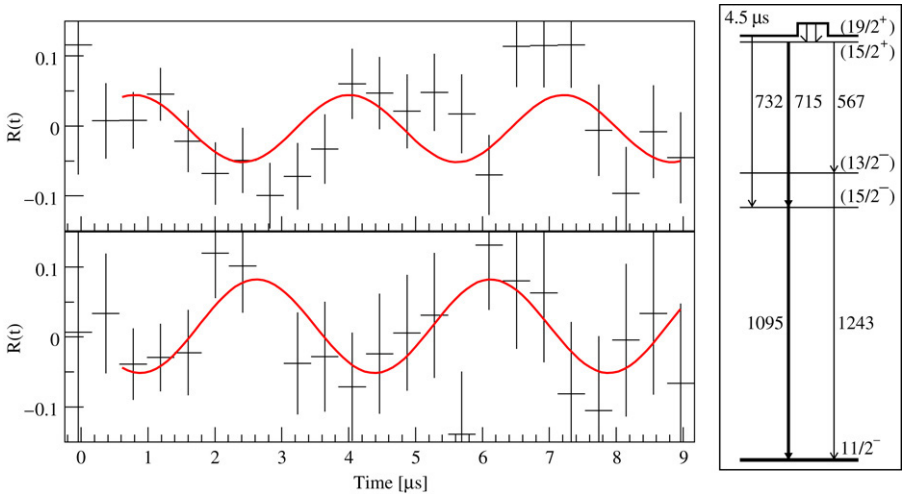

Fig. 1. Left: $R(t)$ functions for the 1095 keV transition (up) and for the 715 keV transition (down) at the wing of the momentum distribution. Right: partial level scheme of ^{127}Sn, revealing the decay of the $19/2^+$ isomer [1].

The deduced value of the g-factor, $|g| \approx 0.16$, is in agreement with theoretical expectations based on the empirical g-factors, which yield a value $g(s_{1/2}^{-1}h_{11/2}^{-2}) \approx -0.156$ for the main component of the wave function, and with large-scale shell model calculations. These results will be discussed in detail elsewhere [7].

First results from the g-RISING campaign for the g-factor of the $19/2^+$ isomer in ^{127}Sn from relativistic fragmentation demonstrate that significant alignment ($\sim$10%) is observed in the outmost wing of the momentum distribution. The present experiment provides a benchmark (in terms of intensity of the isomer beam and number of detected γ-rays) for further studies of electromagnetic moments of isomers in nuclei yet farther away from stability.

Acknowledgments

This work was supported in part by the EC EURONS RII3-CT-2004-506065 project, the Bulgarian National Science Fund grant VUF06/05 and the Polish Ministry of Science and Higher Education grants 1-P03B-030-30 and 620/E-77/SPB/GSI/P-03/DWM105/2004-2007.

References

[1] J.A. Pinston, et al., Phys. Rev. C 61 (2000) 024312.
[2] J.A. Pinston, J. Genevey, J. Phys. G 30 (2004) R57.
[3] H.J. Wollersheim, et al., Nucl. Instr. Meth. Phys. Res. A 537 (2005) 637.
[4] J. Grebosz, Comp. Phys. Communications 176 (2006) 251.
[5] G. Neyens, et al., Acta Phys. Pol. B (2006) (in press).
[6] I. Matea, et al., Phys. Rev. Lett. 93 (2004) 142503.
[7] L. Atanasova, et al., 2007 (in preparation).

New sub-μs isomers in ^{125,127,129}Sn and isomer systematics of $^{124-130}$Sn

R. L. Lozeva,[1,2,3,*] G. S. Simpson,[4,5] H. Grawe,[6] G. Neyens,[1] L. A. Atanasova,[2] D. L. Balabanski,[7,8,9] D. Bazzacco,[10] F. Becker,[6] P. Bednarczyk,[6,11] G. Benzoni,[12] N. Blasi,[12] A. Blazhev,[13] A. Bracco,[12,14] C. Brandau,[15] L. Cáceres,[6,16] F. Camera,[12,14] S. K. Chamoli,[17] F. C. L. Crespi,[12,14] J.-M. Daugas,[18] P. Detistov,[2] M. De Rydt,[1] P. Doornenbal,[6,13] C. Fahlander,[19] E. Farnea,[10] G. Georgiev,[3] J. Gerl,[6] K. A. Gladnishki,[2,8] M. Górska,[6] J. Grębosz,[6,11] M. Hass,[17] R. Hoischen,[19] G. Ilie,[13,20] M. Ionescu-Bujor,[20] A. Iordachescu,[20] J. Jolie,[13] A. Jungclaus,[16] M. Kmiecik,[11] I. Kojouharov,[6] N. Kurz,[6] S. P. Lakshmi,[17] G. Lo Bianco,[7,8] S. Mallion,[1] A. Maj,[11] D. Montanari,[12,14] O. Perru,[18] M. Pfützner,[21] S. Pietri,[15] J. A. Pinston,[4] Zs. Podolyák,[15] W. Prokopowicz,[6] D. Rudolph,[19] G. Rusev,[22] T. R. Saitoh,[6] A. Saltarelli,[7,8] H. Schaffner,[6] R. Schwengner,[22] S. Tashenov,[6] K. Turzó,[1] J. J. Valiente-Dobón,[23] N. Vermeulen,[1] J. Walker,[6,15,16] E. Werner-Malento,[6] O. Wieland,[12] and H.-J. Wollersheim[6]

[1]*Instituut voor Kern- en Stralingsfysica, Katholieke Universiteit Leuven, B-3001 Leuven, Belgium*
[2]*Faculty of Physics, University of Sofia "St. Kl. Ohridski," BG-1164 Sofia, Bulgaria*
[3]*CSNSM, Université Paris-Sud, CNRS/IN2P3, F-91400 Orsay-Campus, France*
[4]*LPSC, Université Joseph Fourier Grenoble 1, CNRS/IN2P3, Institut National Polytechnique de Grenoble, F-38026 Grenoble Cedex, France*
[5]*Institut Laue-Langevin, F-38042 Grenoble Cedex 9, France*
[6]*Gesellschaft für Schwerionenforschung, D-64291 Darmstadt, Germany*
[7]*Dipartamento di Fisica, Università degli Studi di Camerino, I-62032 Camerino, Italy*
[8]*INFN Sezione di Perugia, I-06123 Perugia, Italy*
[9]*Institute for Nuclear Research and Nuclear Energy, Bulgarian Academy of Sciences, BG-1784 Sofia, Bulgaria*
[10]*Università degli Studi di Padova and INFN, Sezione di Padova, I-35122 Padova, Italy*
[11]*Henryk Niewodniczański Institute of Nuclear Physics, Polish Academy of Sciences, PL-31342 Krakow, Poland*
[12]*INFN Sezione di Milano, I-20133 Milano, Italy*
[13]*Institut für Kernphysik, Universität zu Köln, D-50937 Köln, Germany*
[14]*Università degli Studi di Milano, I-20133 Milano, Italy*
[15]*University of Surrey, Guildford, Surrey GU2 7XH, United Kingdom*
[16]*Departamento de Física Teórica, Universidad Autónoma de Madrid, E-28049 Madrid, Spain*
[17]*Weizman Institute of Science, 76100 Rehovot, Israel*
[18]*CEA/DIF/DPTA/SPN, Bruyères le Châtel, F-91297 Arpajon Cedex, France*
[19]*Department of Physics, Lund University, S-22100 Lund, Sweden*
[20]*National Institute for Physics and Nuclear Engineering, RO-76900 Bucharest, Romania*
[21]*Institute of Experimental Physics, Warsaw University, PL-00681 Warsaw, Poland*
[22]*Institut für Strahlenphysik, Forschungszentrum Dresden-Rossendorf, D-01314 Dresden, Germany*
[23]*INFN Laboratori Nazionali di Legnaro, I-35020 Legnaro, Italy*

(Received 27 March 2008; published 17 June 2008)

New sub-μs isomers have been observed in the neutron-rich Sn isotopes. ^{125,127,129}Sn nuclei have been produced in a relativistic fission reaction of ^{238}U on a ^{9}Be target at 750 A·MeV and by the fragmentation of ^{136}Xe at 600 A·MeV populating high-spin yrast states. In addition to the already known μs isomers, three new ones with sub-μs half-lives have been observed. These yrast isomers are the high-spin members of the $\nu(d_{3/2}^{-1}h_{11/2}^{-2})$ and $\nu h_{11/2}^{-n}$, seniority $v = 3$ multiplets leading to isomeric $(23/2^+)$ and $(27/2^-)$ states, respectively. Added to the already known $19/2^+$ μs isomers in this region the current work completes the systematic information of neutron-hole excitations toward the filling of the last $h_{11/2}$ orbital at $N = 82$. The results are discussed in the framework of state-of-the-art shell-model calculations using realistic interactions.

DOI: 10.1103/PhysRevC.77.064313 PACS number(s): 21.10.Tg, 21.60.Cs, 23.20.Lv, 27.60.+j

I. INTRODUCTION

Nuclei close to double shell closures offer an ideal environment for testing realistic shell-model calculations as these nuclei have a particularly simple structure: just a few particles or holes outside an inert core. Isomeric states are abundant in Sn isotopes with a few neutron holes away from ^{132}Sn. They are typically formed by yrast spin traps and allow the observation of decay cascades in exotic nuclei. Such isomeric states exist because of the short-range, repulsive character of the nucleon-nucleon interaction for alike nucleons, which leads to small level spacings between the highest-spin states of a multiplet where the wave functions of the nucleons are not allowed to reach maximum overlap due to the Pauli principle. The unique-parity $h_{11/2}$ neutron-hole orbital, which lies close to the Fermi surface, is responsible for exactly this type of isomerism in nuclei near ^{132}Sn with $N < 82$.

To date, intermediate-spin states have been observed, in the Sn isotopes at, or a few neutrons away from, stability by using

*Radomira.Lozeva@csnsm.in2p3.fr

deep-inelastic reactions [1–4]. Further away from stability, Sn nuclei and their vicinity have been studied by using relativistic fission [5–7] and fragmentation [8,9] reactions. Intermediate-spin states were observed either directly after in-flight mass separation of μs isomeric states, produced by thermal neutron-induced fission [10–12], or by the β decay of intermediate-spin long-lived (seconds) In isomers [13,14]. The aforementioned experiments have allowed the complete $\nu h_{11/2}^{-n}$, seniority $v = 2$ multiplet to be measured for even-mass Sn isotopes in the mass range $A = 116$–130. In these nuclei the filling of the $h_{11/2}$ orbital is not isolated. The presence of, for example, the close lying $d_{3/2}$ orbital leads to a delayed filling of the $h_{11/2}$ orbital as nucleons can scatter into it. The filling of the lower half of the $h_{11/2}$ orbital could well be enhanced due to scattering from the lower lying $g_{7/2}, d_{5/2}, s_{1/2}$ orbitals, which in total leads to deviations from the symmetric $B(E2)$ trend in an isolated high-spin orbital [15,16].

In addition to the $v = 2$ states, $\nu h_{11/2}^{-n}$, $v = 3$ isomeric states were also observed by using deep-inelastic reactions for ^{119,121,123}Sn [2]. These isomers, however, were not observed in the more neutron-rich Sn isotopes using fission reactions, as β decay cannot populate such high-spin states and their predicted lifetime of $\sim$200 ns is below the observational limit of the Lohengrin mass spectrometer at the ILL, where the flight time is around 2 μs [10]. Valuable information about intermediate-spin states in the heavy odd Sn nuclei was however obtained from the decay of $\nu h_{11/2}^{-2} d_{3/2}^{-1}$ μs isomeric states [10–12]. In order to complete the systematic data for the $\nu h_{11/2}^{-n}$, $v = 3$ isomers, to see whether their $B(E2)$ values fit into the trend of the $v = 2$ isomers, and to gain more information on intermediate-spin states in these nuclei, data from a recent experimental campaign using relativistic fission or fragmentation performed at the fragment separator (FRS) at GSI [17] were examined, where the flight time of the reaction products was around 300 ns.

The new isomeric states were interpreted by using shell-model calculations performed with a realistic interaction derived from the CD-Bonn nucleon-nucleon potential [18]. A good description of the experimental data is found from using an effective neutron charge of $e_n = 0.70e$, in agreement with previous work in this region [19,20], and at variance with the larger values found in Refs. [3,12,21]. The experimental method and results are introduced in Secs. II and III, respectively, followed by an interpretation of these results in terms of probable configurations of the states involved in the decay sequence in Sec. IV.

II. EXPERIMENTAL DETAILS

Delayed γ rays from neutron-rich Sn isotopes were observed at the final focal point of the FRS [17] by using eight Cluster detectors [22] from the RISING array [23]. The experimental setup, shown schematically in Fig. 1(a), was used for the study of g factors of μs isomeric states as part of the g-RISING campaign [24].

The Sn nuclei were produced in two separate experimental runs: by relativistic projectile fission of a 750 A·MeV ^{238}U beam, with an intensity of $\sim 8 \times 10^7$ ions/s impinging on a 1023 mg/cm^2 Be primary target (with Nb backing of 221 mg/cm^2), and by the fragmentation of a ^{136}Xe beam, with an intensity of $\sim 2 \times 10^8$ ions/s impinging on the same target at 600 A·MeV [25].

The reaction products were identified by the FRS, which was set up in a standard achromatic configuration [17]. Mass identification of the ions was performed by an event-by-event measurement of the magnetic rigidity ($B\rho$) at the dispersive (middle) focal plane and the velocity, determined in a time-of-flight (ToF) measurement by using position-sensitive scintillators placed at middle (Sc1) and final (Sc2) focuses of the spectrometer. Z determination was performed by measurements of the energy loss in an ionization chamber (MUSIC), while (x, y) tracking of the ions was achieved by using two multiwire proportional counters (MW1 and MW2).

Ions entering the gap of the magnet used for g-factor studies were also detected by a scintillation detector (validation), whose signal was required for the acceptance of an ion-γ coincidence event in the analysis. The ions, after being slowed through 15 mm of Plexiglass, were stopped in a 2 mm thick Cu catcher placed at the center of the magnet's poles. A scintillator (veto) placed behind the catcher was used to reject ions passing through it. To adjust the implantation depth in the Cu foil a variable-thickness Al degrader was used at the final focus.

The Ge detector setup, where all Cluster detectors were placed in the horizontal plane shown in Fig. 1(a), had a γ-ray detection efficiency of 2.2% at 500 keV and 1.8% at 1.3 MeV. Add-back of up to three (out of seven) neighboring crystals in each Cluster was performed, chosen after a study of the best peak/background ratio. A time restriction for prompt γ rays for single crystals with Cluster multiplicity one was used in the analysis. Wider time and multiplicity restrictions were performed for the add-back energies. Half of the detectors were used with their BGO anti-Compton suppression shields [26] in place. To suppress the low-energy atomic bremsstrahlung associated with the arrival of the beam [23], all detector faces were covered by Cu and Pb absorbers, each 1 mm thick. This provided a useful γ-ray energy detection range of between $\sim$140 keV and $\sim$4 MeV, the upper limit being due to the selected ADC range of the used Euroball VXI cards. Ion-γ coincidences were accepted up to 15.4 μs after the arrival of an ion and were measured by using a common TAC, started by the first γ ray measured in any of the Ge detectors, and stopped by a delayed signal from scintillator Sc2. Times between the first γ ray, detected within the ion-γ time window, and any other coincident γ rays were measured by a TDC, which had a range of 1.2 μs. The constant fraction discriminators (CFDs) of the Ge detectors were inhibited for the first 300 ns after the arrival of an ion to avoid the TDC time window being opened by the prompt atomic bremsstrahlung from the beam. The time resolution of the Ge detectors was $\sim$20 ns.

Electronics effects such as the blocking effect of the Ge detectors' CFDs and the sharp end of the coincidence gate for particles and γ rays limit the useful range for time analysis to between 800 ns and 14.6 μs, respectively. During the suppression of the prompt background (BG) radiation in the first few hundreds of nanoseconds, when the Ge detectors' CFDs recover, a short-lived isomeric radiation can be observed more clearly and with a higher intensity. Therefore, this time range

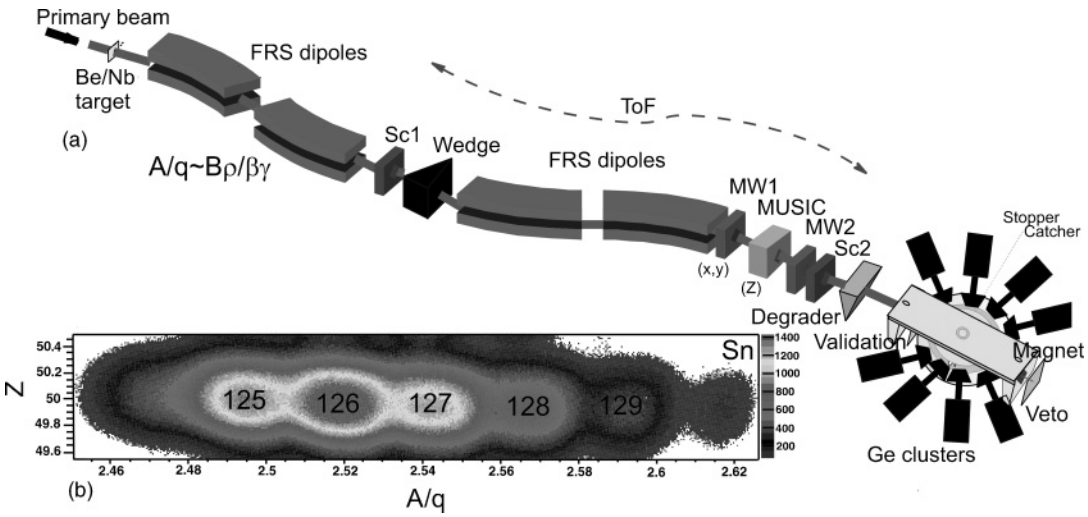

FIG. 1. (a) Experimental setup and (b) the identified Sn isotopes from ^{238}U fission.

is used only for visualization, whereas all time analysis starts 800 ns after the arrival of the ions, as will be shown in Sec. III.

III. ANALYSIS AND RESULTS

A. Notes about the background

Because of the high bombarding energies, the large amount of material close to the detectors (electromagnet), and the high ion rates (typically $\sim 5 \times 10^3$ ions/s) the nuclear BG detected in the Ge detectors is rather high. Over short time ranges the main contribution to the BG comes from (n, γ) reactions in the Ge or/and the surrounding materials (Fe and Al) including the catcher itself (Cu). Most of these contributions are prompt, however, a certain amount persists at longer times. Additionally, the photopeaks at low γ-ray energy "sit" on a continuous BG from Compton scattering of higher energy γ rays. Therefore, an accurate background subtraction is important for the analysis. The single γ-ray spectra of

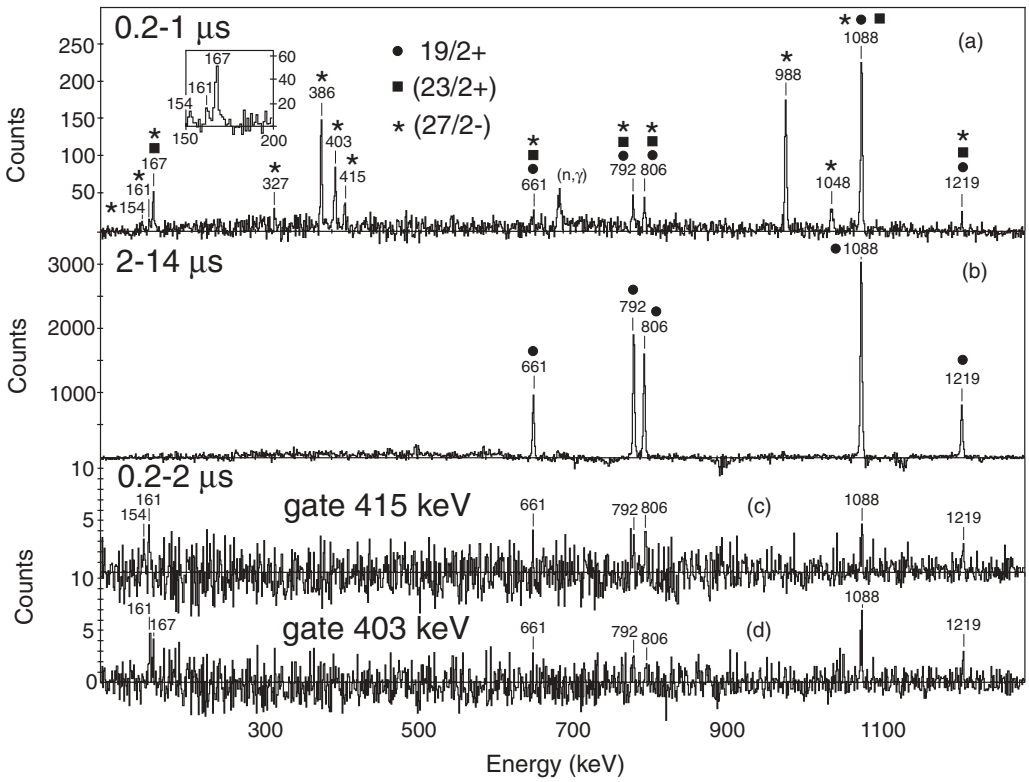

FIG. 2. BG-subtracted γ-ray spectra for time windows of (a) 0.2–1 μs and (b) 2–14 μs and coincident with (c) 415 keV and (d) 403 keV γ rays correlated with ^{125}Sn from ^{238}U fission.

odd-A nuclei [see, e.g., Figs. 2(a) and 2(b)] are cleaned of these BG contributions (present in the energy spectra of all nuclei) by subtracting a normalized portion from their even-A neighbors, whereas for the coincidence γ-ray spectra [see, e.g., Figs. 2(c) and 2(d)] a subtraction of the BG for the total energy projection is performed by using the methods described in Refs. [27,28]. The time structure of the BG is investigated over the entire energy range. Such an analysis reveals a mean half-life of 0.33(4) μs, dominated mostly by the short-lived neutron-knockout activities. Therefore, a proper BG subtraction is essential. The experimental procedure was verified for several long-lived BG activities, for example, for the 198.4 keV line in ^{71}Ge ($T_{1/2} = 20.4$ ms [29,30]) and the 1460.9 keV line in ^{40}K ($T_{1/2} = 1.25 \times 10^9$ yr [31]) and, as expected, a constant time spectrum is observed.

The data analysis was performed by using SPY/CRACOW [32], ROOT [33], and the RADWARE [34] packages.

B. Odd-mass Sn nuclei

The isotopic identification of the Sn nuclei transmitted by the FRS is depicted in Fig. 1(b), where the atomic number Z is represented as a function of the mass/charge ratio (A/q). The spectrometer was tuned to optimally select ^{126}Sn, leading to a similar but reduced production and transmission of ^{125,127}Sn as well. The ToF measurement with Sc1 [Fig. 1(a)] was influenced by the high ion rates at the middle focus of the separator, which led to slightly overlapping distributions for the neighboring isotopes. Therefore, the corresponding contaminations of the odd Sn isotopes were removed in the analysis by subtracting a normalized portion from their even neighbors.

The relativistic fission and fragmentation reactions can populate high-spin states. Their decay proceeds toward states near the yrast line, some of which can be μs isomers in the Sn region. In the following sections we confirm the μs lifetimes of known isomers in ^{125,127,129}Sn and report on a new sub-μs isomer in each of these isotopes.

1. ^{125}Sn

A new $(23/2^+)$ isomer has been observed in ^{125}Sn, along with the previously known 0.23(3) μs $(27/2^-)$ and 6.2(7) μs $19/2^+$ isomeric states reported in Refs. [1] and [10], respectively. The decay schemes of these isomers are confirmed in this work and four new transitions are added to the decay cascade out of the $(27/2^-)$ isomer. The γ-ray spectrum in Fig. 2(a) shows the observed transitions in ^{125}Sn in a time window from 200 ns to 1 μs after the arrival of the ion from the fission data set. It represents a BG-subtracted energy spectrum, taken shortly after the implantation, for which the contribution deduced from an equal time region at the end of the time range is canceled. The BG contributions are subtracted as explained in Sec. III A. As a result, the only remaining peak, not belonging to ^{125}Sn, that could not be fully removed by the BG subtraction comes from the strong short-lived 691.4 keV ^{72}Ge(n,γ) transition [35].

A BG-subtracted spectrum in a time range from 2 to 14 μs from the same data set is presented in Fig. 2(b). All γ rays in the spectrum belong to the known decay of the $19/2^+$ isomer in ^{125}Sn [10].

Half-lives of 0.23(2) and 6.2(2) μs are determined for the $(27/2^-)$ and $19/2^+$ states, respectively, by using only the strongest transitions in the cascades for the lifetime determinations.

The $(23/2^+)$ state has already been observed as an isomer in the neighboring ^{123,127,129}Sn nuclei [2,12,36]. Two previous experiments [1,10] studying ^{125}Sn at intermediate spin were unable to observe the $(23/2^+)$ isomer due to poor particle identification and a lack of statistics, respectively.

The four newly observed γ rays of energies 154, 167, 403, and 415 keV are seen in Fig. 2(a). One has to note that these transitions have not been reported in the previous work for the $(27/2^-)$ isomer in this nucleus [1], where only the direct depopulation of the $(27/2^-)$ state, through the negative-parity states, could be observed.

The γ-γ coincidence relations from the current work are shown in Figs. 2(c) and 2(d). They are performed for the first 2 μs of the time window after a BG subtraction (see Sec. III A). The coincidences with known transitions represent the corresponding feeding of the short-lived isomer and the consecutive decay of the longer lived one. By setting gates in a γ-time matrix, to extract time information about the new transitions, and also by observing the γ-γ coincidences it was possible to associate the 154, 403, and 415 keV transitions with the decay cascade out of the 0.23(2) μs $(27/2^-)$ isomer alone and the 167 keV transition with the decay out of another lower lying isomer. The 154 keV γ ray is in coincidence with the 415 keV transition [Fig. 2(c)]. If the sum of these two γ-ray energies is added to the energy of the 1894 keV $19/2^+$ isomer an energy of 2463 keV is obtained, the same as that of the $(23/2^-)$ state reported in Ref. [1]. The 154 keV transition is associated with the decay out of the $(23/2^-)$ level and the 415 keV with the decay of a $(21/2^+)$ state [see Sec. IV B1].

The newly observed 167 keV transition has a half-life of 0.6(2) μs [Fig. 3(b)], which is inconsistent with any of the known isomers in this nucleus. This transition is also in coincidence with the 403 keV γ ray [Fig. 2(d)]. The sum of these two transitions and the 1894 keV $19/2^+$ isomer also gives 2464 keV, which is the energy of $(23/2^-)$ state from Ref. [1]. The 403 keV transition is therefore postulated to be another decay out of the $(23/2^-)$ level.

The ground state (g.s.) 1088 keV transition in the fission data was fitted with three decay components [in the inset of Fig. 3(b)], consistent with the three observed isomeric decays in ^{125}Sn. It is interesting to note that the strong direct decay of the $(27/2^-)$ isomer is visible from the pronounced hump at the beginning of the spectrum. This decay branch is considerably reduced in the heavier Sn isotopes as, for example, visible from the decay curve for the 1095 keV transition in ^{127}Sn [in the inset of Fig. 3(d)] and the 1136 + 570 keV transitions in ^{129}Sn [Fig. 3(f)]. A detailed comparison of the isomeric population from both fission and fragmentation data sets will be the subject of a forthcoming article.

2. ^{127}Sn

Isomeric $19/2^+$ and $23/2^+$ states with half-lives of 4.5(3) and 1.26(15) μs, respectively, were previously reported in

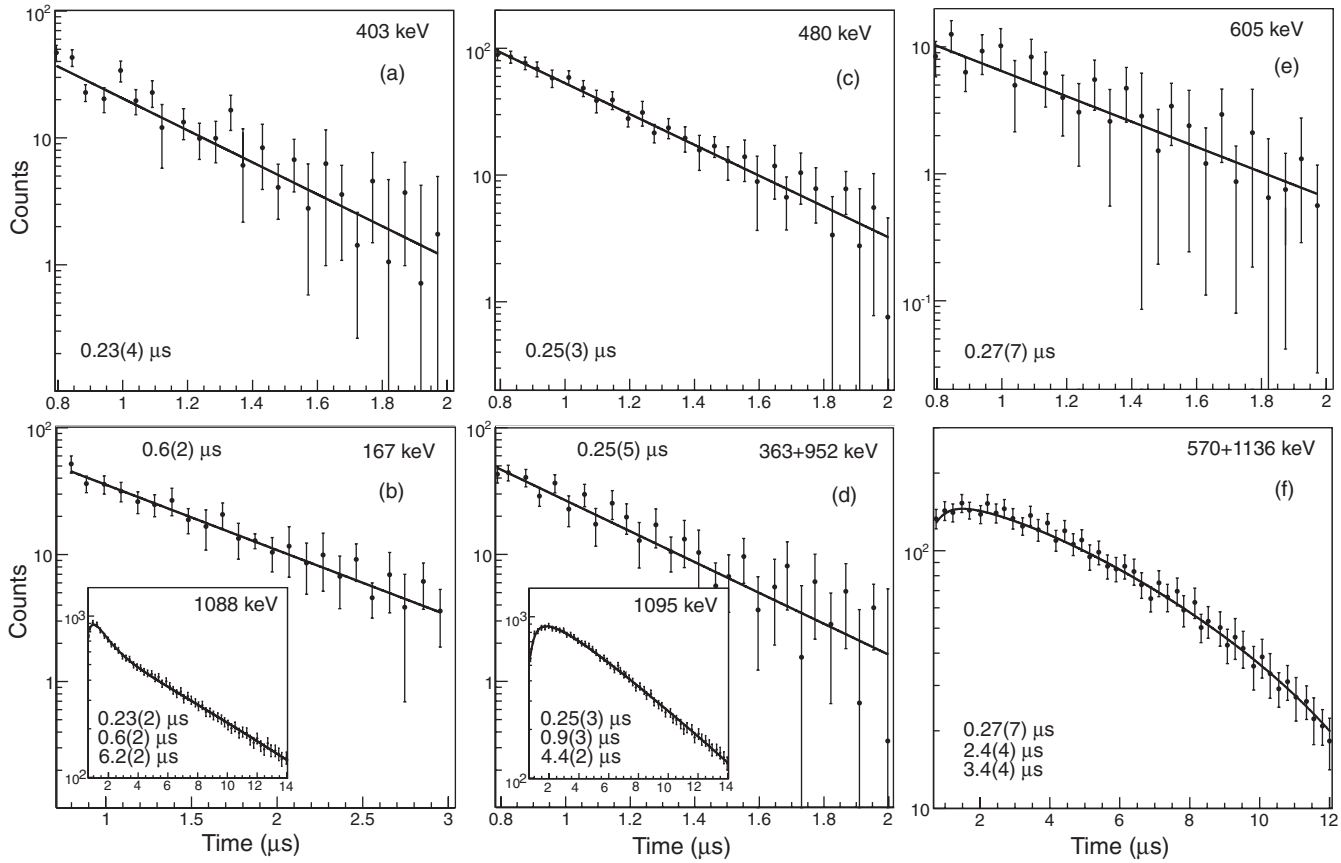

FIG. 3. Decay curves for the newly observed γ transitions in (a and b) ^{125}Sn, (c and d) ^{127}Sn, and (e) ^{129}Sn from ^{238}U fission. The decay curves of the g.s. transitions in the three nuclei are shown in the insets of (b) and (d) and in (f).

Refs. [10,36]. The decay scheme of the $19/2^+$ isomer is confirmed in this work, although the $23/2^+$ isomer decaying by a 104 keV isomeric transition was not observed due to the low efficiency of the Ge detector setup at such low γ-ray energies. In addition to these two isomers in ^{127}Sn, a new $(27/2^-)$ isomer with a half-life of 0.25(3) μs and four associated delayed γ rays at energies of 142, 363, 480, and 952 keV are seen in this work. All new transitions are present in the BG-subtracted energy spectrum, taken shortly after the implantation (similar to ^{125}Sn) in Fig. 4(a), which represents data from both ^{238}U fission and ^{136}Xe fragmentation. This isomer was not observed in previous isomer studies of this nucleus [10], due to its short half-life, and was not populated in β-decay studies [36], due to its high spin.

The four newly observed transitions can be assigned to the decay cascade of a new $(27/2^-)$ isomer by measurements of their half-lives [Figs. 3(c) and 3(d)] and observations of γ-γ coincidences [Figs. 4(c)–4(e)], which also permitted the level scheme construction. The new 2410 keV level is obtained by summing the 363, 952, and known 1095 keV transitions, which are observed in mutual coincidence. The 363 and 952 keV γ rays have similar intensities (see Table I). The sum of the 1931 keV $23/2^+$ isomeric level and the new 480 keV transition also gives a similarly consistent energy of 2411 keV. Note that a 952 keV transition was observed in β-decay studies [36] and placed in the decay scheme in a cascade with the 1095 keV transition. However, no spin-parity (I^π) suggestions for this state were made. The newly observed 142 keV transition is in coincidence with all other new transitions [Fig. 4(c)] and is very likely the isomeric $(27/2^-) \rightarrow (23/2^-)$ transition. The extended level scheme for ^{127}Sn is shown in Fig. 3(b) and is discussed in Sec. IV B2.

3. ^{129}Sn

Two new γ rays of 145 and 605 keV have been observed in the BG-subtracted energy spectrum for ^{129}Sn, taken shortly after the implantation [Fig. 5(a)], in the same way as those for ^{125}Sn and ^{127}Sn. The data from both ^{238}U fission and ^{136}Xe fragmentation experiments were added to obtain better statistics. As in ^{125}Sn, the only remaining peak, not belonging to ^{129}Sn, comes from the strong short-lived 691.4 keV line ^{72}Ge(n,γ) [35], which could not be perfectly subtracted.

The two newly observed transitions are assigned to the decay of a new 0.27(7) μs $(27/2^-)$ isomer [Fig. 3(e)]. Because of the thick absorbers and the low efficiency of the setup at energies around 140 keV the half-life of this isomer could be extracted only from the 605 keV transition after an appropriate BG subtraction. The obtained result was in addition verified by using a double exponential fit for the non-BG subtracted data to account for the exponential BG present at short times

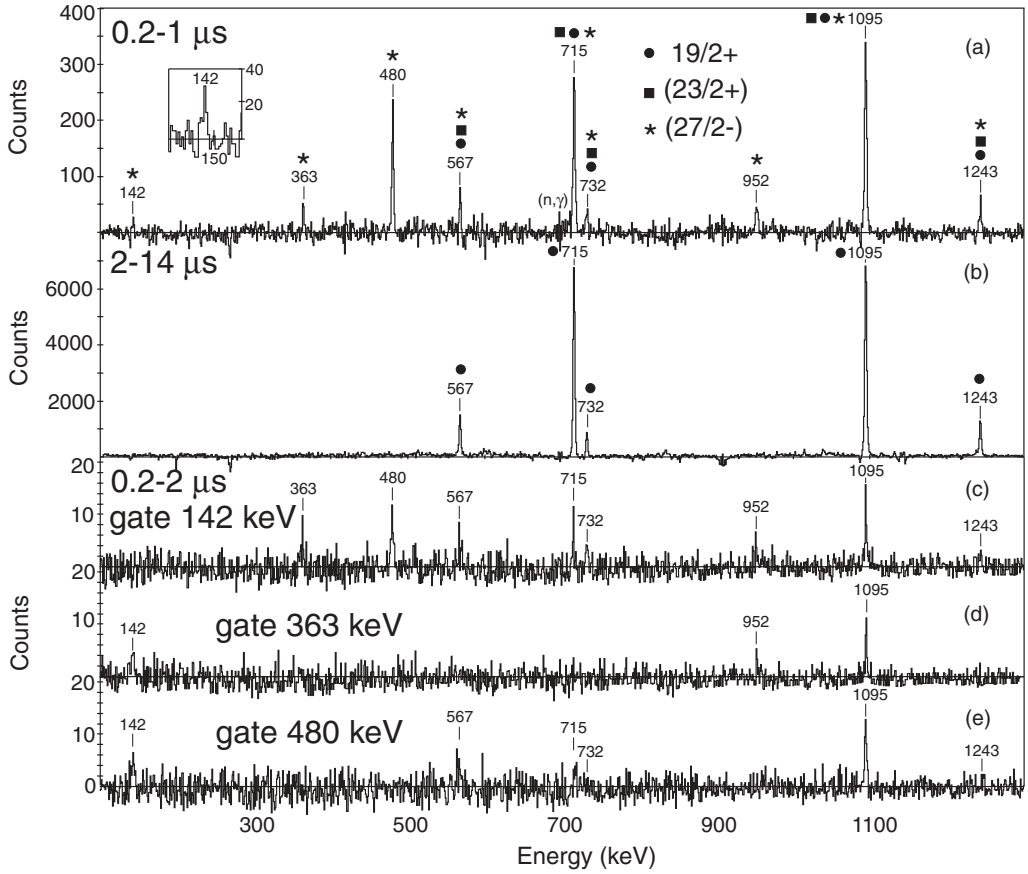

FIG. 4. BG-subtracted γ-ray spectra for time windows of (a) 0.2–1 μs and (b) 2–14 μs and coincident with (c) 142 keV, (d) 363 keV, and (e) 480 keV γ rays correlated with ^{127}Sn from ^{238}U fission and ^{136}Xe fragmentation.

from neutron activities (see Sec. III A). The given uncertainty for the half-life value includes the statistical one from such an analysis.

The previously reported level schemes of Refs. [12,36] are confirmed here, though the low-energy decays of the 3.6(2) μs $19/2^+$ isomer (19.7 keV) and the 2.4(2) μs $23/2^+$ isomer (41.0 keV) were not observed. A BG-subtracted energy spectrum from the end of the time range (as for ^{125}Sn and ^{127}Sn) is presented in Fig. 5(b). All γ rays labeled with their energy belong to the known decay of the $19/2^+$ isomer in ^{129}Sn [12].

Due to the lack of statistics for this nucleus a summed coincidence spectrum was constructed with gates on all known (and the new 605 keV) transitions [Fig. 5(c)]. In this spectrum, the 145 keV transition is clearly visible, supporting its placement as $(27/2^-) \rightarrow (23/2^-)$ in analogy to the 142 and 161 keV transitions in ^{127}Sn and ^{125}Sn, respectively.

IV. DISCUSSION

The half-lives obtained in the current data set are compared with the existing data in Table I, where one can notice a good agreement. The measured energies of all observed γ-ray transitions and their absolute intensities, normalized to the most intense one for each nucleus, are listed for each isomeric state.

Additionally, all μs isomers in the even-A ^{124,126,128,130}Sn isotopes were remeasured. The half-lives obtained for the 10^+, 7^- (in ^{124,126}Sn), and 5^- (in ^{124}Sn) isomeric states are fully in agreement with the literature values [1,3,11,13,37]. Therefore, the lifetimes in the even Sn isotopes are used only for the odd-even renormalization of the reduced transition probabilities (see Sec. IV E).

A. Shell-model calculations

Shell-model (SM) calculations are performed in a model space $p_{1/2}$, $g_{9/2}$ for protons and $g_{7/2}$, $s_{1/2}$, $d_{5/2}$, $d_{3/2}$, $h_{11/2}$ for neutrons outside an inert ^{88}Sr core. Therefore, proton-core excitations across $Z = 50$ and neutron-core excitations across $N = 82$ are not considered in this approach. The polarization by proton-core excitations for a well-tuned realistic interaction has a negligible impact on the level energies, but its effect on the γ-ray transition rates, in general, comprises the use of effective operators. For specific transitions, however, namely weak ones, major discrepancies may occur owing to the restriction to a pure neutron configuration space. Starting from the G matrix, including folded diagrams and higher order

TABLE I. Isomeric half-lives and γ-ray transitions observed in the decay of the ^{125}Sn, ^{127}Sn, and ^{129}Sn isomers ($\Delta E_\gamma \sim 0.3$ keV, $\Delta I_\gamma \sim 10\%$). The intensities of all low-energy transitions could not be obtained due to the high uncertainty in the extrapolation of the efficiency curve.

Nucleus	State	$T_{1/2}(\mu s)$ Literature	This work	Adopted	E_γ (keV) (I_γ)
^{125}Sn	$27/2^-$	0.23(3)[a]	0.23(2)	0.23(2)	154.0, 161.3, 326.7 (9), 385.9 (46), 402.9 (30), 415.3 (15), 988.4 (45), 1048.3 (9)
^{125}Sn	$23/2^+$	–	0.6(2)[e]	0.6(2)	167.0
^{125}Sn	$19/2^+$	6.2(7)[b]	6.2(2)	6.2(2)	661.5 (29), 791.6 (55), 805.5 (45), 1087.7 (100), 1219.0 (25)
^{127}Sn	$27/2^-$	–	0.25(3)[e]	0.25(3)	142.0, 363.1 (16), 952.3 (16), 479.7 (57)
^{127}Sn	$23/2^+$	1.26(15)[c]	0.9(3)	1.2(1)	–
^{127}Sn	$19/2^+$	4.5(3)[b], 4.8(3)[c]	4.4(2)	4.5(1)	567.1 (20), 715.4 (85), 731.8 (15), 1094.9 (100), 1242.6 (19)
^{129}Sn	$27/2^-$	–	0.27(7)[e]	0.27(7)	145.3, 605.0 (97)
^{129}Sn	$23/2^+$	2.0(2)[c], 2.4(2)[d]	2.4(4)	2.2(1)	–
^{129}Sn	$19/2^+$	3.7(2)[b], 3.2(2)[c], 3.6(2)[d]	3.4(4)	3.4(1)	382.1 (69), 570.3 (100), 1136.1 (88), 1324.4 (65)

[a]Taken from Ref. [1].
[b]Taken from Ref. [10].
[c]Taken from Ref. [36].
[d]Taken from Ref. [12].
[e]Newly observed isomer.

many-body corrections for this valence space, we can derive an effective interaction from the CD-BONN nucleon-nucleon (NN) potential with the method described in Ref. [38]. The evolution of the experimental single-particle energies in ^{88}Sr for proton holes and in ^{100}Sn for neutrons, as adopted from Refs. [15,39], is reproduced by applying monopole corrections. The effective interaction is found to describe very well both high-spin states and Gamow-Teller decays in the ^{100}Sn region [40]. For the ^{132}Sn region, besides $A^{-1/3}$ scaling, additional monopole corrections are applied to describe the single-hole energies in ^{132}Sn [15,39], without modifying the ^{100}Sn results. Transition strengths for $E2$, $E3$, $M1$, and $M2$ transitions were calculated with an effective charge $e_n = 0.70e$ and a quenched g factor $g_n^s = 0.7 g_{\text{free}}^s$. Calculations were performed with the code OXBASH [41]. In the following mainly levels and $E2$ strengths will be discussed. A full account of all

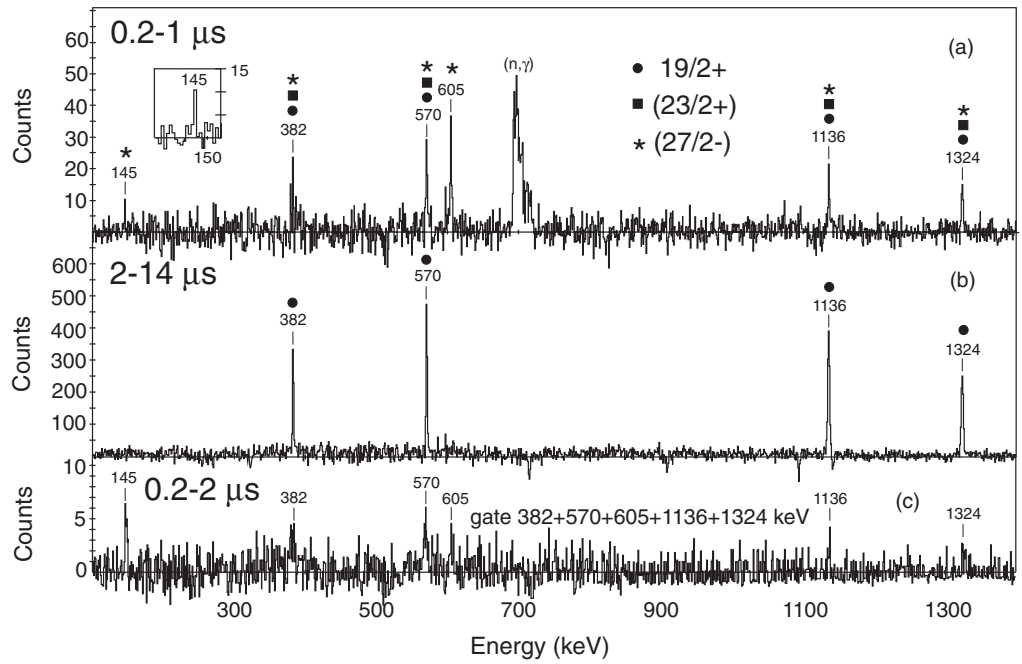

FIG. 5. BG-subtracted γ-ray spectra for time windows of (a) 0.2–1 μs and (b) 2–14 μs and coincident (summed-up) γ rays correlated with ^{129}Sn from ^{238}U fission and ^{136}Xe fragmentation.

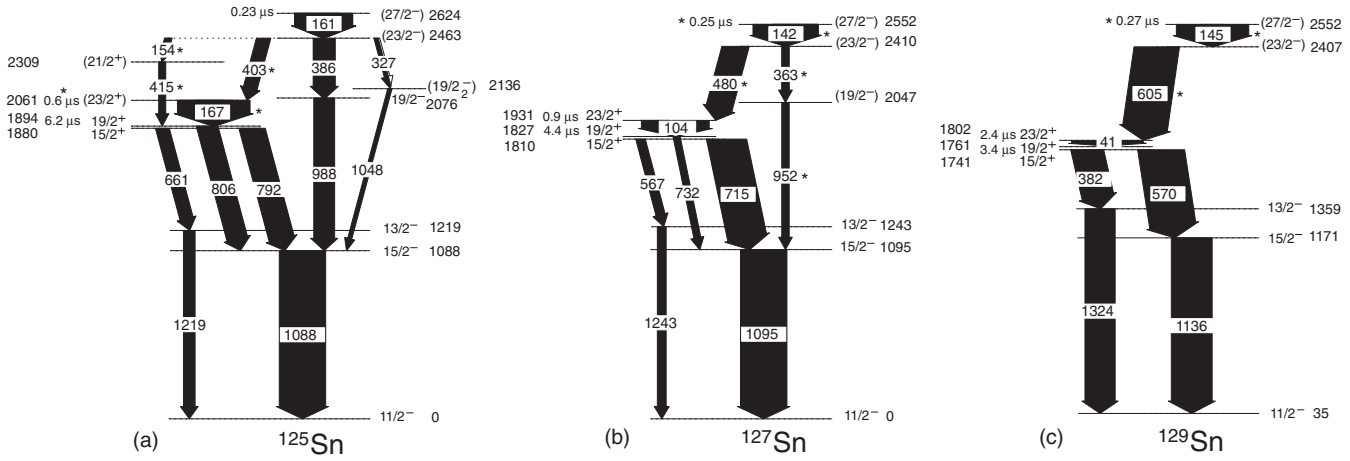

FIG. 6. Extended level schemes for (a) ^{125}Sn, (b) ^{127}Sn, and (c) ^{129}Sn. The newly observed γ lines and isomers are marked with asterisks. The intensities (represented by the arrow widths) for the low-energy transitions are estimated from balances with all other feeding/branching-transition intensities.

SM results in the ^{132}Sn region will be given in a forthcoming paper [42].

The results from the SM calculations are discussed in Sec. IV B. Level energies are compared with the experimental data in Figs. 7 and 8 and transition probabilities for selected $E2$ transitions are presented in Fig. 11 and Table II.

B. Level schemes

In Fig. 6 we present the extended level schemes, including the newly observed isomeric levels and their decay paths. Newly observed γ lines are indicated by asterisks. This is discussed further below for each case.

1. ^{125}Sn

The newly observed isomeric γ transitions of 154, 167, 403, and 415 keV in ^{125}Sn are placed in the extended level scheme, presented in Fig. 6(a), by using lifetime analysis and coincidence relations. Based on that, we suggest a new isomer of $I^{\pi} = (23/2^{+})$, thus completing the $(23/2^{+})$ systematics from ^{123}Sn [2] to ^{127,129}Sn [36]. The measured half-life is in agreement with an $E2$ decay to the $19/2^{+}$ state from Weisskopf estimates (WE) and SM considerations and we place this level at 167 keV above the $19/2^{+}$ state. The other newly observed transitions correspond to the decay of the $(27/2^{-})$ isomer toward the positive-parity states through two new intermediate states of $I^{\pi} = (21/2^{+})$ and $I^{\pi} = (23/2^{+})$. The $(19/2^{-}_{1,2})$ states, suggested in Ref. [1], are consistent with our measurement.

The proposed level scheme is in full agreement with the SM calculations (Sec. IV A). The theoretical SM states for ^{125,127,129}Sn are compared with the experimental ones in Fig. 7 for both positive and negative parities. A good agreement is visible for the three nuclei of interest. In Figs. 7(a)–7(c) one can see that three of the states are candidates for yrast spin traps: $19/2^{+}$, $23/2^{+}$, and $27/2^{-}$. The highest spin yrast trap $27/2^{-}$ is populated directly in the reaction, whereas the other isomers are populated both directly and indirectly by feeding from the top isomer, which is consistent with our lifetime measurements. As can be seen, for example, in Fig. 7(a), where the decay path is represented by full arrows, the decay from the $27/2^{-}$ trap is possible only by a low-energy $E2$ transition to the $23/2^{-}$ state with a half-life of about

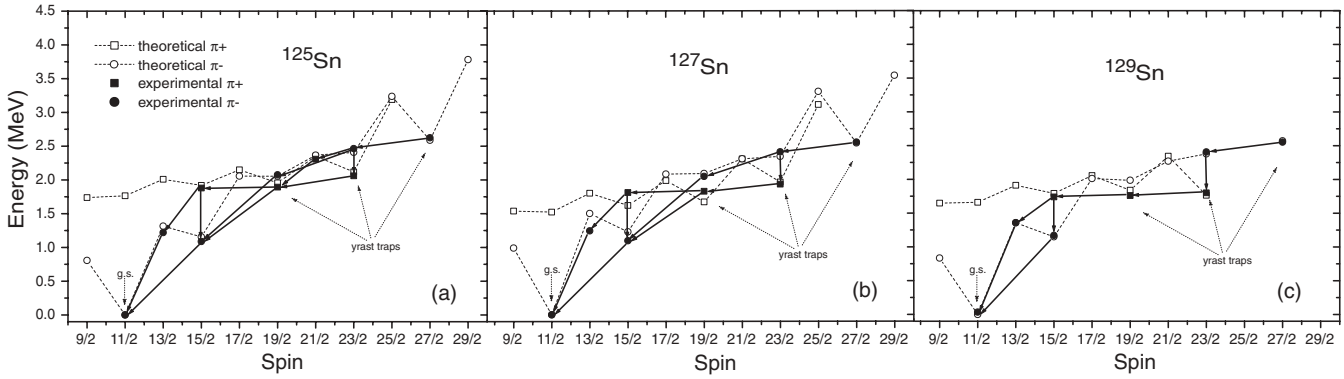

FIG. 7. Theoretical (empty symbols) and experimental (filled symbols) yrast states for (a) ^{125}Sn, (b) ^{127}Sn, and (c) ^{129}Sn for positive (squares) and negative (circles) parity. The decay path of the isomers in these nuclei is indicated with arrows.

200 ns, as indeed reported in Ref. [1] and observed in this work (see Table I). Due to the energy gap between the $23/2^-$ and the $23/2^+$ states, the isomeric decay proceeds most probably by an $E1$ branch toward the positive-parity states. The de-excitation of the $23/2^+$ state favors an $E2$ transition to the $19/2^+$ state, theoretically expected to be of 161 keV (from the SM energy level differences), which is experimentally found to be of 167 keV. The theoretically estimated half-life for this state is of the order of 500 ns, which agrees well with the experimental value of 0.6(2) μs. The decay from the $19/2^+$ state proceeds through the $15/2^+$ state as well as the low-lying $13/2^-$ and $15/2^-$ states, as already known from the literature [10].

2. ^{127}Sn

All new isomeric transitions (142, 363, 480, and 952 keV) in ^{127}Sn, presented in Fig. 6(b), have the same half-life of 0.25(3) μs, in agreement with the expected value of about 200 ns [10] for a new $(27/2^-)$ isomer in this nucleus. The 142 keV transition is coincident with all other transitions [Fig. 4(c)] and its energy is in agreement with an $E2$ decay to the $(23/2^-)$ state from WE and SM considerations. This transition was also suggested semiempirically to be of the order of 135(2) keV [10]. The cascade out of the new $(27/2^-)$ isomer is analogous to that in ^{125}Sn. The intensities of all isomeric decays however are distributed differently than those in the lighter Sn nuclei. The suggested experimental states in the proposed level scheme [Fig. 6(b)] match the theoretical SM states well, as can be seen in Fig. 7(b).

3. ^{129}Sn

The new isomeric γ transitions of 145 and 605 keV in ^{129}Sn are placed in the extended level scheme, presented in Fig. 6(c), by using lifetime analysis and coincidence relations. Thus, the new isomer of $I^\pi = (27/2^-)$ completes the systematics of known $(27/2^-)$ states from ^{119}Sn [2] to ^{129}Sn [36].

A comparison with the SM calculation (Sec. IV B) and empirical shell-model (ESM) estimates suggests that the 145 keV transition is very likely responsible for the isomerism whereas the 605 keV transition is assigned as the decay from the $(23/2^-)$ state to the $23/2^+$ state. In the ESM, if we assume pure $h^n_{11/2}$ configurations, the relative positions of the $23/2^-$ and $27/2^-$ states in ^{129}Sn can be calculated from the known 6^+ to 10^+ states in ^{130}Sn (see, e.g., Refs. [4,10,15]). The result for the $27/2^- \rightarrow 23/2^-$ transition energy is 135(2) keV (the same as for ^{127}Sn), where the systematic uncertainty is estimated from the configurational purity of the high-spin states involved in the full shell-model calculation. The 145 keV γ ray is the only candidate in that energy range seen in Fig. 5(a). This was confirmed in a follow-up experiment employing fragmentation of ^{136}Xe and a more efficient detector setup [43].

The 145 keV transition is placed at the top of the level scheme, suggesting that the new isomer of $I^\pi = (27/2^-)$ decays analogously to the ones in the lighter Sn nuclei, which is indeed expected from WE and SM predictions.

An $E2$ cascade out of the $(23/2^-)$ state can be suggested based on an ESM estimate in the spirit of Ref. [10], with the full shell-model calculation and extrapolations from systematics to be of 307 and 929 keV (with a similar uncertainty as for the predicted 135 keV transition) for the $23/2^- \rightarrow 19/2^-$ and the $19/2^- \rightarrow 15/2^-$ transitions, respectively. Following the intensity distribution of the isomeric decays in the lighter odd-A neighbors, the observation of this cascade would require better statistics. Assuming the SM $E2$ decay energy and reduced transition strengths equal to ^{127}Sn would increase the $E1$(605 keV)/$E2$(307 keV) branching by at least a factor of 5 relative to ^{127}Sn.

The suggested experimental states in the proposed level scheme [Fig. 6(c)] match the theoretical SM states quite well, as can be seen in Fig. 7(c). Thus, the decay of the $(27/2^-)$ isomer seems to be shifted toward the positive-parity states through the 605 keV transition. This is supported by the energy differences between the theoretically calculated states in Fig. 7(c), where the energy gap between the $23/2^- \rightarrow 23/2^+$ states is larger than the one between the $23/2^- \rightarrow 19/2^-$ states. The intensity of the 605 keV ($E1$) transition is also consistent with the increasing intensity of the branch toward the heavier masses, following the trend from ^{125,127}Sn.

In conclusion, the following points summarize the decay of the three μs isomers in ^{125,127,129}Sn:

(i) The $(27/2^-)$ isomers decay through $E2$ cascades toward the negative-parity states in the lighter Sn nuclei. These branches become very weak as A increases.
(ii) The decay path via $E1$ transitions from the $(23/2^-)$ to the $(23/2^+)$ levels toward the positive-parity states is enhanced, as the energy spacing between these states also increases with A.
(iii) The energies of the $E2$ transitions from the $(27/2^-)$ to the $(23/2^-)$ levels stay almost constant, reflecting similar isomeric half-lives and pure configurations, whereas the excitation energy of the $27/2^-$ isomer is lowered toward $N = 82$.
(iv) The $E2$-transition energies of the $(23/2^+) \rightarrow 19/2^+$ de-excitation decrease with increasing A, whereas the $19/2^+ \rightarrow 15/2^+$ transition energy stays nearly constant.
(v) The intensity distribution of the decays from the $19/2^+$ states differs significantly in the lower masses, where the feeding to the $15/2^-$ states is almost equally contributed to by transitions from the $19/2^+$ and $15/2^+$ states.
(vi) In the heavier odd-A Sn nuclei, de-excitations from the $15/2^+$ states only are favored as the energy for a $19/2^+ \rightarrow 15/2^-$ transition decreases.
(vii) Although in the lighter odd-A Sn isotopes the branches involving the $13/2^-$ states are weak, in the heavier A nuclei, these branches become dominant and even comparable with the branches involving the $15/2^-$ states.

C. High-spin states

1. $27/2^-$ states

A comparison between the energies of the calculated and the experimental $(27/2^-)$ and $(23/2^-)$ states is presented in

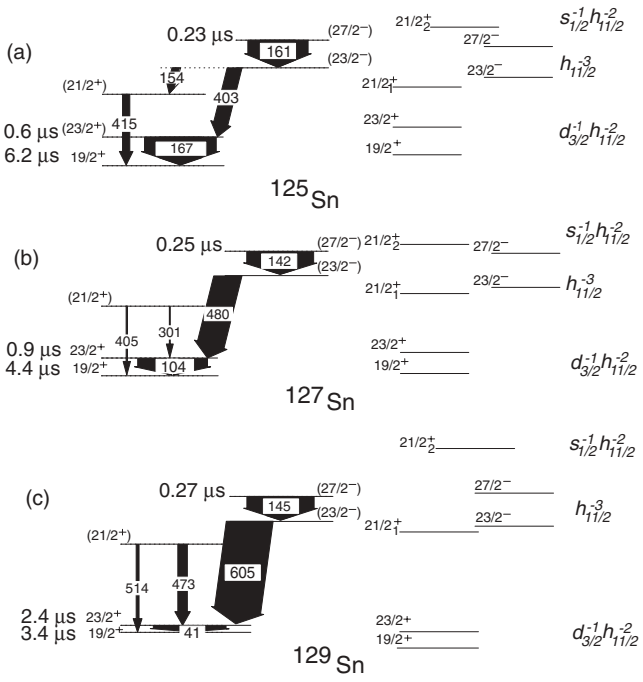

FIG. 8. Theoretical and experimental high-spin states. The transitions shown are from the current work and Ref. [36].

Fig. 8. According to the SM calculations, these states are the highest members of the $h_{11/2}^{-3}$ quasiparticle multiplet. For $A = 129$ the $h_{11/2}^{-3}$ probabilities in the wave functions are 100% and 99.5%, respectively. For the lighter isotopes the weights of the pure $h_{11/2}^{-n}$ configurations, with $n = 132 - A$, reduce to 32.4% and 28.4% for ^{127}Sn and 11.5% and 11.7% for ^{125}Sn due to pair scattering from the positive-parity g, d, s orbitals. As seniority is a good quantum number the total amount of $v = 3$ in the wave functions is more than 95%. The $23/2^-$, $19/2^-$, $15/2^-$, and $13/2^-$ excited states and the $11/2^-$ (g.s.) belong to the same multiplet. The $15/2^-$ and $13/2^-$ states have increasing admixtures of $d_{3/2}^{-1}s_{1/2}^{-1}h_{11/2}^{-1}$ and $d_{5/2}^{-1}s_{1/2}^{-1}h_{11/2}^{-1}$ quasiparticle configurations, respectively, which amount to about 30% and 15% in ^{129}Sn. This reflects the coupling of the $h_{11/2}$ particle to the 2^+ states in the neighboring even isotopes.

2. $23/2^+$ *states*

According to SM calculations, the yrast trap at spin $23/2^+$ (Fig. 7) has a dominant quasiparticle configuration of $\nu d_{3/2}^{-1}h_{11/2}^{-2}$, as discussed in Ref. [36]. In ^{125}Sn the dominant component is $\nu d_{3/2}^{-1}h_{11/2}^{-4}$ with 36.4%, while $\nu d_{3/2}^{-3}h_{11/2}^{-2}$ contributes with 22.0%. If only unpaired neutrons are considered, this is indeed the same type of quasiparticle configuration as in the heavier Sn, as discussed already in Ref. [36]. The leading quasiparticle configuration of $\nu d_{3/2}^{-1}h_{11/2}^{-2}$ in the heavier Sn, according to the calculations, has probabilities of 64.8% (^{127}Sn) and 97.0% (^{129}Sn). These numbers indicate the increasing purity of these states, as the seniority mixing decreases, toward the filling of all involved orbitals at $N = 82$.

3. $21/2^+$ *states*

In ^{125}Sn we observe a state [Fig. 8(a)] and suggest $I^\pi = (21/2^+)$ based on the observation of this state in studies of the heavier Sn [36], which is also supported by theoretical calculations. The 2232 and 2275 keV levels [Figs. 8(b) and 8(c)] were assigned with a spin of (21/2) in Ref. [36] for $A = 127$ and $A = 129$, respectively. The decay transitions to the $19/2^+$ and $23/2^+$ states, shown in Figs. 8(b) and 8(c), are taken from Ref. [36] and were not observed in the current data set due to insufficient statistics. The nonobservation of the branch from $23/2^-$ toward the $(21/2^+)$ state in ^{129}Sn is partly a consequence of the increasing energy of the $23/2^- \rightarrow 23/2^+$ transition, which is nicely reproduced by the SM calculations, while the distance between the $23/2^-$ and $21/2^+$ states stays essentially constant. This branch appeared in ^{125}Sn and transported about 15% of the total intensity from the $23/2^-$ state, compared to the 30% intensity of the $23/2^- \rightarrow 23/2^+$ branch. In the heavier mass nuclei the intensity is transported through the stronger $23/2^- \rightarrow 23/2^+$ transitions, which take about 76% (the 480 keV transition with respect to 363 keV transition) from the total intensity of the $23/2^-$ state in ^{127}Sn and 100% in ^{129}Sn (e.g., no branch other than the 605 keV transition is observed). In fact, the branches involving the $(21/2^+)$ states most probably become weaker as the mass increases and better statistics would be required to find out their exact contribution.

The $21/2_1^+$ states have a leading quasiparticle configuration of $\nu d_{3/2}^{-1}h_{11/2}^{-2}$ with a contribution of greater than 30% in ^{125}Sn [Fig. 8(a)] to above 96% in ^{129}Sn [Fig. 8(c)]. In the $21/2_2^+$ states the configuration involving the $\nu s_{1/2}$ orbital is enhanced and dominates (above 98%) in ^{129}Sn. For $A = 127$ [Fig. 8(b)], nevertheless, $\nu d_{3/2}^{-1}$ is dominant with 62.6% whereas in the lighter ^{125}Sn the $d_{3/2}$ and $s_{1/2}$ components are 20.5% and 35.1%, respectively. Note that the increased probability for hole excitation involving the $d_{3/2}$ orbital at $A = 127$ is reflected in the wave functions of all excited states [Fig. 8(b)].

D. Level systematics

The observation of three new isomers in the odd neutron-rich Sn isotopes allows a comparison with the information available on both the even and odd neutron-rich Sn nuclei. Such a plot representing the different origin of the isomeric states and the overall trend in the heavy Sn region is presented in Fig. 9(a).

Because of the closed proton shell at $Z = 50$ the decay schemes of the Sn nuclei originate mostly from neutron excitations across the subshells between the shell gaps at $N = 50$ and $N = 82$. The last $h_{11/2}$ orbital is strongly involved in single particle/hole excitations, represented by the seniority scheme [2,3]. The general features of the decays of the odd Sn (^{125,127,129}Sn) nuclei are quite similar to each other and to the lighter $^{119-121}$Sn, with the exception of ^{123}Sn ($N = 73$)-the half-filling point of the $h_{11/2}$ neutron orbital [3].

The μs isomeric states present in these nuclei originate from different configurations:

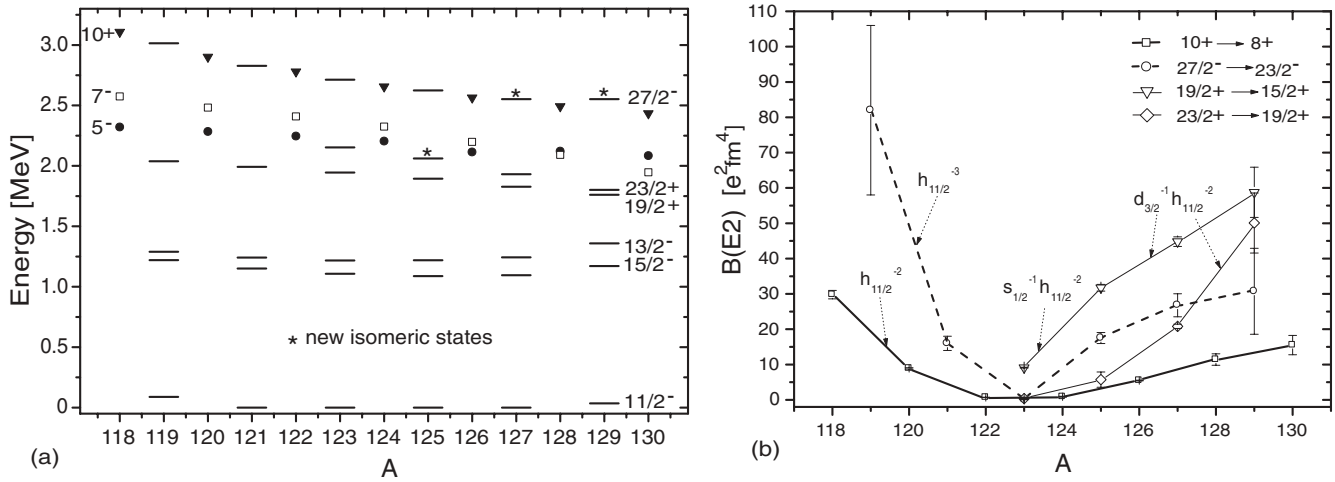

FIG. 9. (a) Systematics of the known and new (indicated by an asterisk) $19/2^+$, $23/2^+$, and $27/2^-$ isomeric states in the odd and even Sn isotopes. The first excited $15/2^-$ and $13/2^-$ states are given for comparison together with the $11/2^-$ g.s. (with exceptions for ^{119,129}Sn, where $1/2^+$ and $3/2^+$ become the g.s., respectively). (b) Experimental $B(E2)$ values for the total $h_{11/2}$ shell. All values in $A = 124$–130 are obtained from the current data set. The remaining values are taken from Refs. [2,3]. Note that in the configuration of the $19/2^+$ states above $N = 73$, $d_{3/2}$ and $s_{1/2}$ contributions are comparable. Lines in panel (b) are drawn to guide the eye.

(i) The $19/2^+$ isomeric state has been reported in the mass chain $A = 119$–129 [10,11,44] with a dominant configuration of a $h_{11/2}^{-1}$ neutron hole orbital coupled to the 5^- core of the even Sn neighbor. Note that the 5^- state in the even Sn originates from a dominant $s_{1/2}^{-1}h_{11/2}^{-1}$ quasiparticle configuration, confirmed by g-factor measurements for the ^{116,118,120}Sn isomers [45]. The 5^- states are μs isomers in ^{116}Sn [46] and ^{124}Sn [47] only, but these are ns isomers in the other even-$A^{118-122,128-130}$Sn nuclei [48–52] because they can decay by $E1$ transitions to the 4^+ states lying just below them. However, in the odd-A isotopes, the $19/2^+$ states are all isomeric in the μs range because each of them comes below the $(4^+ \otimes \nu h_{11/2})17/2^-$ and $19/2^-$ states. Therefore, the decay from these states must proceed by an $M2$ transition to the $(2^+ \otimes \nu h_{11/2})15/2^-$ state [11]. Note that $M2$ transitions in this model space can occur only between the orbitals $h_{11/2}$ and $g_{7/2}$, the latter of which lies deep below the Fermi level. According to SM calculations [42], the $\Delta I = 2$ parity changing transitions may have a comparable $E3$ width due to a $h_{11/2} \rightarrow d_{5/2}$ transition. In Ref. [10] large hindrance factors consistent with an $M2$ multipolarity are measured and a weak admixture of $h_{11/2}^{-2}g_{7/2}^{-1}$ was suggested, in agreement with SM calculations. Besides the aforementioned $s_{1/2}^{-1}h_{11/2}^{-1}$ component the SM yields a strong $d_{3/2}^{-1}h_{11/2}^{-1}$ amplitude in the $19/2^+$ that increases toward ^{129}Sn. The magnetic moment of this isomer in ^{127}Sn has been measured in this experimental campaign, and its result will shed more light on the configuration and the decay of the $19/2^+$ state in ^{127}Sn [53].

(ii) The $23/2^+$ isomeric state has been previously observed in ^{123}Sn [2] and in the heavier $^{127-129}$Sn [12,36] nuclei with a leading configuration of a neutron hole in the $h_{11/2}$ orbital coupled to the 7^- core of the even Sn neighbor. All of the 7^- states are isomeric and have mostly $d_{3/2}^{-1}h_{11/2}^{-1}$ character. These states decay by $E2$ transitions to the 5^- states in the mass range $A = 118$–126. In contrast, in ^{128}Sn and ^{130}Sn, where the 5^- is above the 7^- level, due to a reduced $s_{1/2}$ component in its wave function, the half-lives of the 7^- are well beyond the μs range. The as-yet unobserved $23/2^+$ states in the lighter Sn isotopes are expected also to follow the trend of the 7^- states of their even partners and are a subject of future measurements.

(iii) The $27/2^-$ isomeric state has been observed in the mass range $^{119-125}$Sn [1,2,4] with a pure single-particle $h_{11/2}^{-n}$, seniority $v = 3$ configuration and predicted in the heavy $^{127-129}$Sn with a sub-μs half-life [10].

The experimental energy levels from the current work for a new $(23/2^+)$ state in ^{125}Sn and new $(27/2^-)$ states in ^{127,129}Sn are added to the systematics [Fig. 9(a)]. One sees a lowering of the excited states toward the doubly magic region. The energy spacing between the different states originates most probably from an admixture in the configurations, where one or another orbital contribution becomes dominant as, for example, at $A =$ 127–128 .

E. SM and transition probabilities

The experimental reduced $E2$ transition probabilities for the 10^+ isomers in the even Sn isotopes extracted from the current data ($A \geqslant 124$) are compared to those of the $19/2^+$, $23/2^+$, and $27/2^-$ states in Fig. 9(b). The data points for $A < 124$ are taken from Refs. [2,3]. This plot shows the systematic trends of the $B(E2)$ values as the $h_{11/2}$ orbital is filled.

TABLE II. Reduced $I \rightarrow I-2$ transition probabilities for the $19/2^+$, $23/2^+$, and $27/2^-$ isomers in ^{125}Sn, ^{127}Sn, and ^{129}Sn. The conversion coefficients used are taken from Ref. [55].

Nucleus	I^π	$B(E2)(e^2\,\mathrm{fm}^4)$			
		Literature	This work	Adopted	SM
^{125}Sn	$27/2^-$	18(2)[a]	17.5(16)	17.7(12)	6.1
^{125}Sn	$23/2^+$	–	5.7(21)	5.7(21)	8.5
^{125}Sn	$19/2^+$	18(3)[b]	20.5(6)	20.4(6)	11.6
^{127}Sn	$27/2^-$	–	26.8(32)	26.8(32)	28.2
^{127}Sn	$23/2^+$	15.2(20)[c]	20.8(59)	15.8(19)	21.8
^{127}Sn	$19/2^+$	34(4)[b], 34(3)[c]	40.8(12)	39.4(11)	30.1
^{129}Sn	$27/2^-$	–	30.7(122)	30.7(122)	21.9
^{129}Sn	$23/2^+$	50(6)[c], 48(4)[d]	50.1(85)	48.8(31)	38.4
^{129}Sn	$19/2^+$	32(2)[b], 51(7)[c], 53(3)[d]	58.8(71)	40.1(16)	64.4

[a]From Ref. [1].
[b]From Ref. [10].
[c]From Ref. [36].
[d]From Ref. [12].

The $B(E2)$ dependence on $\nu h_{11/2}$ subshell occupation in even-A and odd-A Sn nuclei was discussed in Refs. [1,2], where the experimental $E2$ matrix elements as inferred from the square root of $B(E2)$, adopting a sign convention that changes in mid-shell, have been plotted as a function of the mass number A. The updated version is shown in Fig. 10, where it can be seen that the new data points for ^{127,129}Sn match up smoothly with the results for the other isotopes. These results reinforce earlier conclusions about the $\nu h_{11/2}$ subshell filling and about the enhancement of the neutron effective charge toward the middle of the $N = 50$–82 major shell [2]. The smooth systematic trend exhibited by these seniority isomers reflects the quasispin tensorial structure of the $E2$ operator as established from abundant data in other subshells and regions of the Segré chart such as $N = 50(g^n_{9/2})$, $82(h^n_{11/2})$, and 126 $(h^n_{9/2})$ isotones and Pb $(i^n_{13/2})$ isotopes. The presence of the $d_{3/2}$ shell leads to a delayed occupation of the $h_{11/2}$ shell close to ^{132}Sn.

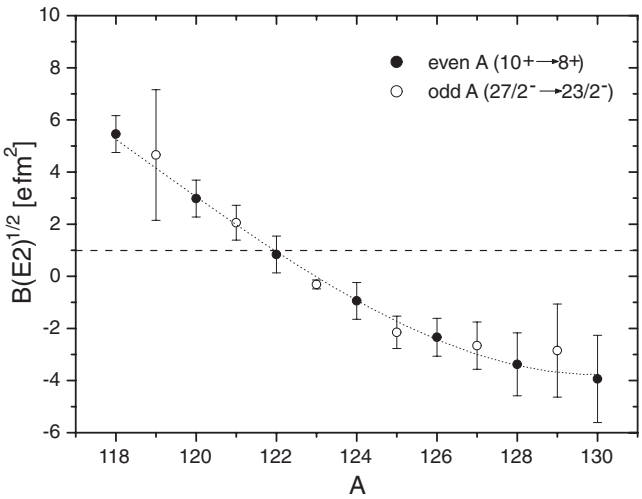

FIG. 10. Experimental $E2$ transition amplitudes for the $h^{-n}_{11/2}10^+(v=2)$ and $27/2^-(v=3)$ isomeric states in the Sn isotopes [with the odd-A values scaled by 0.514 to compensate for the different geometrical factors entering $v=2$ and $v=3$ $B(E2)$ equations]. All values in $A = 124$–130 are obtained from the current data set. The remaining values are taken from Refs. [2,3]. The dotted curve is drawn to guide the eye.

The reduced $E2$ transition probabilities of the odd-A Sn isotopes, along with the corresponding transitions in the even-A nuclei, are compared to each other and SM results in Fig. 11 and Table II. One has to note that the half-lives and $B(E2)$ values of the present work for the even Sn isotopes agree well with the literature values [1,10,12,54]. In Fig. 11(a) the experimental and SM $B(E2)$ strengths for the $h^{-n}_{11/2}$, $v=2$ configurations $10^+ \rightarrow 8^+$ (even A) and $v=3$ $27/2^- \rightarrow 23/2^-$ (odd A) are compared. The odd-A values are scaled with a factor 0.264, which accounts for the different angular momentum recoupling factors for $v=2$ and $v=3$ configurations and normalizes the odd-A $B(E2)$ values to the average of the neighboring even-A strength [56]. In this way the trend with decreasing A reflects directly the emptying of the $h_{11/2}$ orbital [1,4]. The staggering at $A = 129$ is artificial as the normalization is inadequate beyond $A = 128$. This is due to the presence of the $d_{3/2}$ shell, which is emptied first before the $h_{11/2}$ orbital. From the $A = 128$–130 values one may conclude that the choice of an effective charge of $0.70e$, as taken from the literature [57], is probably on the low side and a value of $0.85e$ would be more appropriate [13,36]. This increase, however, would not cure the discrepancy observed toward mid-shell, which clearly indicates a too fast emptying of the $h_{11/2}$ orbital. For ^{125}Sn the leading components of the $27/2^-$ and $23/2^-$ wave functions are $d^{-2}_{3/2}h^{-3}_{11/2}$ and $h^{-3}_{11/2}$ with 45% and 12%, respectively. As the $E2$ matrix elements in the lowest seniority change sign in mid-shell, which reflects the shape change from prolate to oblate, the contributions of these two configurations interfere destructively. A reduction of the minority component to half its value would bring the theoretical value close to experiment. As pointed out in Sec. IV A, the weak $B(E2)$ values in the $h_{11/2}$ mid-shell are specifically sensitive to the neglect of proton-core excitations. This was demonstrated in the $N = 50$ isotones one major

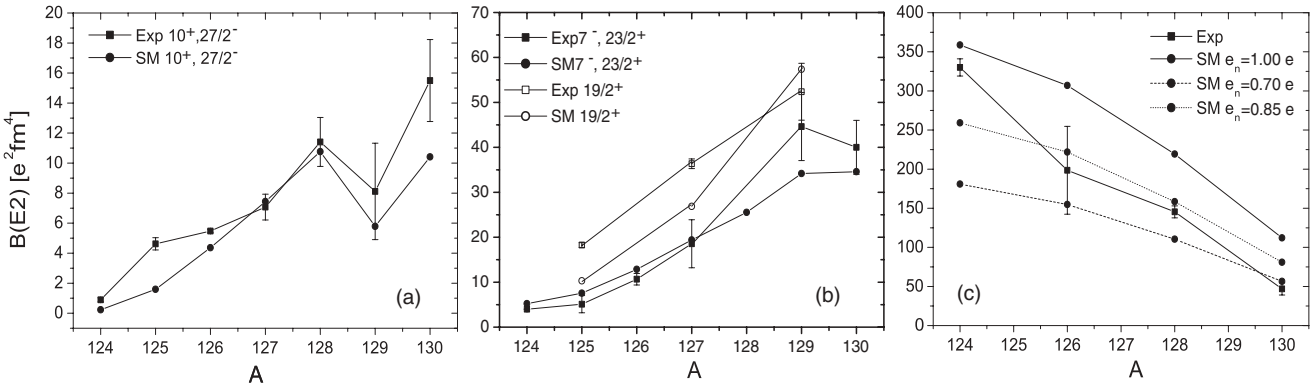

FIG. 11. Comparison between experimental and theoretical reduced transition probabilities for (a) the $h_{11/2}^{-n}10^+(v=2)$ and $27/2^-(v=3)$ isomeric states in the heavy Sn isotopes [with the odd-A values scaled by 0.264 to compensate for the different geometrical factors entering $v=2$ and $v=3$ $B(E2)$ equations] and (b) mixed $h_{11/2}^{n}(s,d)$ states. $B(E2;5^-\rightarrow 7^-)$ in ^{128,130}Sn are converted into $B(E2;7^-\rightarrow 5^-)$ for better comparison; the odd-A values are scaled by 0.891. The effective neutron charge is 0.70e. SM (squares) and experimental $B(E2;2^+\rightarrow 0^+)$ (circles) [1,21,47,51,52] are shown in (c) for effective charges $e_n=1.00e$ (solid line), 0.70e (dashed line), and 0.85e (dotted line).

shell below for $g_{9/2}$ protons [15,58]. Further SM tests of the $h_{11/2}^{-n}$ $B(E2)$ have revealed that the underestimation of the ^{125,126}Sn values can be cured by reducing the pairing two-body matrix elements (TBME) involving $h_{11/2}$, while the $B(E2)$ for the other configurations are virtually unchanged. The ^{124}Sn $10^+\rightarrow 8^+$ transition is not affected, which supports the conclusion that deviations in the decreasing $B(E2)$ toward mid-shell for all transitions shown in Fig. 11 are due to the increasing influence of proton-core excitations.

In Fig. 11(b) the $E2$ transition strengths for the positive-parity yrast traps with mixed configuration $h_{11/2}^{-n}(s,d)$, $23/2^+$ and $19/2^+$, are compared to the $7^-\rightarrow 5^-$ strengths and SM results. Because of the changing configurational character of the states involved, a simple geometrical scaling of odd-A to even-A values is not meaningful. Therefore, the odd-A values are scaled to have equal values for the two- and three-hole isotopes, ^{130,129}Sn. For ^{130}Sn the experimentally observed $5^-\rightarrow 7^-$ strength is converted to $7^-\rightarrow 5^-$. Again the values for $A=129$ and 130 indicate a too small effective charge; the trend with decreasing mass number, however, is nicely reproduced by the SM. From the smooth trend of both experimental and SM values, the unobserved branch for the $5^-\rightarrow 7^-$ transition in ^{128}Sn can be estimated to be 0.2% [Fig. 11(b)]. The $19/2^+\rightarrow 15/2^+E2$ strengths below $A=129$ seem to be systematically underestimated by the shell model. The situation for these nonstretched states resembles the 2^+ systematics [Fig. 11(c)], where the optimum effective charge changes from 0.70e to 1.00e from ^{130}Sn to ^{124}Sn in the present calculations. It seems that the value of 0.85e best describes the experimental values [21].

Proton-core excitation besides generally increasing effective charges will increase seniority mixing in configurations coupled to less than maximum spin due to the proton-neutron (pn) interaction. The $19/2^+$ and $15/2^+$ wave functions comprise of the $h_{11/2}^{\pm 4,6}$ configuration with two 6^+ and 8^+ states with $v=2,4$ within 150 keV, which will undergo increased mixing by virtue of pn interaction and, depending on the relative sign of the valence and core-excited contribution, enable constructive or destructive interference of $\Delta v=2$ contributions to the $E2$ matrix element. It should be noted that while the $\Delta v=0$ strength disappears in mid-shell, the $\Delta v=2$ transition strength peaks there (see, e.g., $2^+\rightarrow 0^+$ transitions [15,21] (Fig. 2) for the $g_{9/2}^n$ system).

V. SUMMARY

In relativistic fission and fragmentation reactions several Sn isotopes in the vicinity of ^{132}Sn have been populated and their decay in the 0.2 to 14 μs range has been studied. The data allowed the observation of three new isomeric states in ^{125}Sn, ^{127}Sn, and ^{129}Sn. The new states have been suggested to have $I^\pi=(23/2^+)$ in ^{125}Sn and $(27/2^-)$ in ^{127}Sn and ^{129}Sn, based on theoretical calculations for the yrast traps in this high-spin region. The level schemes of these nuclei have been extended and, additionally, the transition probabilities for all isomeric states have been extracted.

Shell-model calculations in an untruncated $N=50$–82 neutron space give an excellent description of the experimental level schemes and their systematics with increasing distance from the doubly-magic ^{132}Sn. The evolution of the $E2$ strengths for transitions from the stretched and pure $h_{11/2}^{-n}$ $I^\pi=27/2^-, 10^+$ seniority $v=3,2$ states toward mid-shell and from the mixed-orbital $I^\pi=23/2^+, 7^-$, and $19/2^+$ isomers is well described. Deviations in the absolute values for small $B(E2)$ and transitions involving nonstretched configurations may be ascribed to the neglect of proton excitations across $Z=50$, which can only be partly absorbed by the choice of a constant effective neutron charge of $e_n=0.70e$. A variation from 0.70e at $N=82$ to 1.00e at $N\sim 70$ might be more appropriate.

ACKNOWLEDGMENTS

The authors would like to thank M. Hjorth-Jensen for providing the original interaction two-body matrix elements. This work was supported in part by the EU, EURONS Contract

No. RII3-CT-2004-506065, the Flemish Science Foundation FWO Project No. G0446-05, the Belgian Science Policy IAP Project No. P6/23, the Bulgarian National Science Fund Grant No. VUF06/05, the Polish Ministry of Science and Higher Education Grant Nos. 1 P03B 03030 and 620/E-77/SPB/GSI/P-03/DWM105/2004-2007, BMBF Contract No. 06KY205I, the Romanian National Authority for Scientific Research Contract No. 52/07, the Swedish Research Council, and the Spanish Ministerio de Educación y Ciencia Nos. FPA2005-00696 and FPA2007-66069.

[1] C. T. Zhang, P. Bhattacharyya, P. J. Daly, Z. W. Grabowski, R. Broda, B. Fornal, and J. Blomqvist, Phys. Rev. C **62**, 057305 (2000).
[2] R. Mayer, D. Nisius, I. Bearden, E. Bhattacharyya, L. Richter, M. Sferrazza, Z. Grabowski, E. Daly, R. Broda, B. Fornal *et al.*, Phys. Lett. **B336**, 308 (1994).
[3] R. Broda, R. Mayer, I. Bearden, P. Benet, P. Daly, Z. Gabrowski, M. Carpenter, R. Janssens, T. Khoo, T. Lauritsen *et al.*, Phys. Rev. Lett. **68**, 1671 (1992).
[4] P. J. Daly, R. Mayer, D. Nisius, I. Bearden, P. Bhattacharyya, L. Richter, M. Sferrazza, Z. Gabrowski, R. Broda, B. Fornal *et al.*, Phys. Scr. **T56**, 94 (1995).
[5] M. Mineva, M. Hellström, M. Bernas, J. Gerl, H. Grawe, M. Pfützner, P. Regan, M. Rejmund, D. Rudolph, F. Becker *et al.*, Eur. Phys. J. A **11**, 9 (2001).
[6] M. Hellström, M. Mineva, A. Blazhev, H. Boardman, J. Ekman, J. Gerl, K. Gladnishki, H. Grawe, R. Page, Z. Podolyak *et al.*, in *Proceedings of the International Workshop XXXI on Cross Properties of Nuclei and Nuclear Excitations, Hirschegg, Austria*, edited by H. Feldmeier, J. Knoll, W. Nörenberg, and J. Wambach (GSI Darmstadt, 2003), p. 72.
[7] M. Hellström, M. Mineva, A. Blazhev, H. Boardman, J. Ekman, K. Gladnishki, H. Grawe, J. Gerl, R. Page, Z. Podolyak *et al.*, in *Proceedings of the Third International Conference on Fission and Properties of Neutron-Rich Nuclei*, Sanibel Island, Florida, USA, edited by J. Hamilton, A. Ramayya, and H. Carter (World Scientific, 2002), p. 22.
[8] A. Jungclaus, L. Caceres, M. Gorska, M. Pfützner, S. Pietri, E. Werner-Malento, H. Grawe, K. Langanke, G. Martinez-Pinedo, F. Nowacki *et al.*, Phys. Rev. Lett. **99**, 132501 (2007).
[9] N. Hoteling, W. Walters, B. Tomlin, P. Mantica, J. Pereira, A. Becerril, T. Fleckenstein, A. Hecht, G. Lorusso, M. Quinn *et al.*, Phys. Rev. C **76**, 044324 (2007).
[10] J. A. Pinston, C. Foin, J. Genevey, R. Beraud, E. Chabanat, H. Faust, S. Oberstedt, and B. Weiss, Phys. Rev. C **61**, 024312 (2000).
[11] J. A. Pinston and J. Genevey, J. Phys. G: Nucl. Part. Phys. **30**, R57 (2004).
[12] J. Genevey, J. A. Pinston, C. Foin, M. Rejmund, H. Faust, and B. Weiss, Phys. Rev. C **65**, 034322 (2002).
[13] B. Fogelberg, K. Heyde, and J. Sau, Nucl. Phys. **A352**, 157 (1981).
[14] L. E. DeGeer and G. B. Holm, Phys. Rev. C **22**, 2163 (1980).
[15] H. Grawe, Lect. Notes Phys. **651**, 33 (2004).
[16] R. F. Casten, *Nuclear Structure from a Simple Perspective,* 2nd ed. (Oxford Univ. Press, New York, 2000), p. 153.
[17] H. Geissel, P. Armbruster, K.-H. Behr, A. Brunle, K.-H. Burkard, M. Chen, H. Folger, B. Franczak, H. Keller, and O. Klepper, Nucl. Instrum. Methods B **70**, 286 (1992).
[18] R. Machleidt, F. Sammarruca, and Y. Song, Phys. Rev. C **53**, R1483 (1996).
[19] L. Coraggio, A. Covello, A. Gargano, and N. Itaco, Phys. Rev. C **65**, 051306(R) (2002).
[20] J. Shergur, B. Brown, V. Fedoseyev, U. Koester, K.-L. Kratz, D. Seweryniak, W. Walters, A. Woehr, D. Fedorov, M. Hannawald *et al.*, Phys. Rev. C **65**, 034313 (2002).
[21] A. Banu, J. Gerl, C. Fahlander, M. Gorska, H. Grawe, T. Saito, H.-J. Wollersheim, E. Caurier, T. Engeland, A. Gniady *et al.*, Phys. Rev. C **72**, 061305(R) (2005).
[22] J. Eberth, H. Thomas, P. von Brentano, R. Lieder, H. Jäger, H. Kämmerfing, M. Berst, D. Gutknecht, and R. Henck, Nucl. Instrum. Methods A **369**, 135 (1996).
[23] H.-J. Wollersheim, D. Appelbe, A. Banu, R. Bassini, T. Beck, F. Becker, P. Bednarczyk, K.-H. Behr, M. Bentley, G. Benzoni *et al.*, Nucl. Instrum. Methods A **537**, 637 (2005).
[24] G. Neyens, L. Atanasova, D. Balabanski, F. Becker, P. Bednarczyk, L. Caceres, P. Doornenbal, J. Gerl, M. Gorska, J. Grebosz *et al.*, Acta Phys. Pol. B **38**, 1237 (2007).
[25] L. Atanasova, D. Balabanski, M. Hass, F. Becker, P. Bednarczyk, S. Chamoli, P. Doornenbal, G. Georgiev, J. Gerl, K. Gladnishki *et al.*, Prog. Part. Nucl. Phys. **59**, 355 (2007).
[26] M. Wilhelm, J. Eberth, G. Pascovici, E. Radermacher, P. von Brentano, H. Prade, and R. Lieder, Nucl. Instrum. Methods A **381**, 462 (1996).
[27] B. Herskind, J. Phys. (Paris) Colloq. **41**, C10, 106 (1980).
[28] D. Radford, Nucl. Instrum. Methods A **361**, 306 (1995).
[29] M. Bhat, Nucl. Data Sheets **68**, 579 (1993).
[30] R. Bunting and J. Kraushaar, Nucl. Instrum. Methods **118**, 565 (1974).
[31] K. Kossert and E. Guenther, Appl. Radiat. Isot. **60**, 459 (2004).
[32] J. Grebosz, Comput. Phys. Commun. **176**, 251 (2007).
[33] ROOT, www.root.cern.ch
[34] RADWARE, radware.phy.ornl.gov
[35] W.-T. Chou and M. King, Nucl. Data Sheets **73**, 215 (1994).
[36] H. Gausemel, B. Fogelberg, T. Engeland, M. Hjorth-Jensen, P. Hoff, H. Mach, K. A. Mezilev, and J. P. Omtvedt, Phys. Rev. C **69**, 054307 (2004).
[37] B. Fogelberg and P. Carle, Nucl. Phys. **A323**, 205 (1979).
[38] M. Hjorth-Jensen, T. Kuo, and E. Osnes, Phys. Rep. **261**, 125 (1995).
[39] H. Grawe, K. Langanke, and G. Martínez-Pinedo, Rep. Prog. Phys. **70**, 1525 (2007).
[40] O. Kavatsyuk, C. Mazzocchi, Z. Janas, A. Banu, L. Batist, F. Becker, A. Blazhev, W. Brüchle, J. Döring, T. Faestermann *et al.*, Eur. Phys. J. A **31**, 319 (2007).
[41] B. Brown, A. Etchegoyen, W. R. N. Godwin, W. Richter, W. Orman, E. Warburton, J. Winfield, L. Zhao, and C. Zimmerman, OXBASH for Windows, MSU-NSCL Report No. 1289, 2004.
[42] H. Grawe *et al.* (to be published).
[43] S. Pietri *et al.* (in preparation).
[44] R. Mayer, B. Fornal, R. Broda, I. Beardcn, Z. Grabowski, S. Lunardi, T. Lauritsen, M. Carpenter, R. Janssens, T. L. Khoo *et al.*, Z. Phys. A **342**, 247 (1992).
[45] N. Stone, At. Data Nucl. Data Tables **90**, 75 (2005).

[46] J. Blachot, Nucl. Data Sheets **92**, 455 (2001).
[47] H. Iimura, J. Katakura, K. Kitao, and T. Tamura, Nucl. Data Sheets **80**, 895 (1997).
[48] K. Kitao, Nucl. Data Sheets **75**, 99 (1995).
[49] K. Kitao, Y. Tendow, and A. Hashizume, Nucl. Data Sheets **96**, 241 (2002).
[50] T. Tamura, Nucl. Data Sheets **108**, 455 (2007).
[51] M. Kanbe and K. Kitao, Nucl. Data Sheets **94**, 227 (2001).
[52] B. Singh, Nucl. Data Sheets **93**, 33 (2001).
[53] L. Atanasova *et al*. (in preparation).
[54] B. Fogelberg, H. Gausemel, K. Mezilev, P. Hoff, H. Mach, M. Sanchez-Vega, A. Lindroth, E. Ramström, J. Genevey, J. Pinston *et al*., Phys. Rev. C **70**, 034312 (2004).
[55] T. Kibedi, T. W. Burrows, M. B. Trzhaskovskaya, P. M. Davidson, and C. W. Nestor, Nucl. Instrum. Methods A **589**, 202 (2008).
[56] J. H. McNeill, J. Blomqvist, A. A. Chishti, P. J. Daly, W. Gelletly, M. A. C. Hotchkis, M. Piiparinen, B. J. Varley, and P. J. Woods, Phys. Rev. Lett. **63**, 860 (1989).
[57] A. Holt, T. Engeland, M. Hjorth-Jensen, and E. Osnes, Nucl. Phys. **A634**, 41 (1998).
[58] H. Grawe, A. Blazhev, M. Gorska, R. Grzywacz, H. Mach, and I. Mukha, Eur. Phys. J. A **27**, s01, 257 (2006).

Physics Letters B 687 (2010) 305–309

Contents lists available at ScienceDirect

Physics Letters B

www.elsevier.com/locate/physletb

g Factor of the 7^- isomer in ^{126}Sn and first observation of spin-alignment in relativistic fission

G. Ilie [a,b,*,1], G. Neyens [c], G.S. Simpson [d,e], J. Jolie [a], A. Blazhev [a], H. Grawe [f], R.L. Lozeva [c,g], N. Vermeulen [c], L. Atanasova [g], D.L. Balabanski [h,i], F. Becker [f], P. Bednarczyk [f,j], C. Brandau [f,k], L. Caceres [f,l], S.K. Chamoli [m], J.M. Daugas [n], P. Doornenbal [f], J. Gerl [f], M. Górska [f], J. Grębosz [f,j], M. Hass [m], M. Ionescu-Bujor [b], A. Jungclaus [l], M. Kmiecik [j], I. Kojouharov [f], N. Kurz [f], A. Maj [j], S. Mallion [c], O. Perru [n], M. Pfützner [o], Zs. Podolyák [k], W. Prokopowicz [f], M. De Rydt [c], T.R. Saito [f], H. Schaffner [f], K. Turzó [c], J. Walker [k], E. Werner-Malento [f], H.J. Wollersheim [f]

[a] IKP, Universität zu Köln, 50937 Köln, Germany
[b] National Institute for Physics and Nuclear Engineering, 76900 Bucharest, Romania
[c] Instituut voor Kern- en Stralingsfysica, K.U. Leuven, 3001 Leuven, Belgium
[d] ILL, 38042 Grenoble Cedex, France
[e] LPSC, Université Joseph Fourier Grenoble 1, CNRS/IN2P3, INPG, 38026 Grenoble Cedex, France
[f] GSI, 64291 Darmstadt, Germany
[g] Faculty of Physics, University of Sofia "St. Kl. Ohridski", 1164 Sofia, Bulgaria
[h] Dipartimento di Fisica, Universitá di Camerino, 62032 Camerino, Italy
[i] INRNE, Bulgarian Academy of Sciences, 1784 Sofia, Bulgaria
[j] The Henryk Niewodniczański Institute of Nuclear Physics, PAN, 31342 Kraków, Poland
[k] Department of Physics, University of Surrey, Guildford, GU2 7XH, UK
[l] Departamento de Fisica Teórica, Universidad Autonoma de Madrid, 28049 Madrid, Spain
[m] Department of Particle Physics, Weizmann Institute of Science, 76100 Rehovot, Israel
[n] CEA, DAM, DIF, 91297 Arpajon Cedex, France
[o] IEP, Warsaw University, 00681 Warsaw, Poland

ARTICLE INFO

Article history:
Received 6 October 2009
Received in revised form 17 February 2010
Accepted 9 March 2010
Available online 16 March 2010
Editor: V. Metag

Keywords:
Nuclear moments
Lifetimes
Shell model calculations
Projectile fission reactions

ABSTRACT

We report on the g factor measurement of the isomeric 7^- state ($E^* = 2219$ keV, $T_{1/2} = 5.9(8)$ μs) in the neutron-rich ^{126}Sn nucleus. The nucleus was produced by the fission of a relativistic ^{238}U beam and reaction products were selected by the FRS fragment separator at GSI. For the first time, spin-alignment was observed after relativistic fission. It was used to deduce the g factor of the 7^- isomeric state, $g(7^-) = -0.098(9)$, from the measured perturbed angular distribution of its γ decay using the RISING Cluster detectors. The observed value confirms the suggested $\nu(h_{11/2}^{-1}d_{3/2}^{-1})$ dominant configuration, which has been proposed for the 7^- isomers in neutron-rich Sn isotopes. The failure of the g factor additivity rule and the importance of core polarization evolution with increasing distance from the doubly-magic ^{132}Sn is discussed. The first observation of 18(8)% of spin-alignment produced by the relativistic fission of a ^{238}U beam paves the way to study moments of neutron-rich (sub-)microsecond isomers, which are difficult to align by other means.

The availability of beams of exotic radioactive nuclei for detailed spectroscopic studies, has allowed the observation of changes in the structure of atomic nuclei when going from stability, both to proton- and neutron-rich regions. Near the $Z = 50$ shell closure for example, the persistence of the $N = 82$ shell gap is being debated for neutron-rich isotopes below the doubly-magic ^{132}Sn [1–4]. Magnetic moments of isomeric states may serve as ideal probes to test nuclear models and effective shell-model interactions in this neutron-rich region near the r-process path. Many microsecond isomers have been observed in this region, mainly using neutron-induced fission reactions [5], β-decay [6] and more recently also using relativistic fission [4,7] and fragmentation [8]. Magnetic moments of high-spin isomeric states provide key information on the nature of their single-particle configuration, and can be directly compared to predictions with different models.

* Corresponding author.
E-mail address: gabriela.ilie@yale.edu (G. Ilie).
[1] Present address: WNSL, Yale University, New Haven, CT 06520, USA.

0370-2693/$ – see front matter
doi:10.1016/j.physletb.2010.03.033

In order to study electromagnetic moments of isomeric states, one needs spin-aligned nuclear ensembles. Through the observation of the rotation of the nuclear spin-aligned ensemble, as a time-dependent change of the γ-ray angular distribution (TDPAD) in a magnetic field, the nuclear g factor can be measured [9]. Spin-aligned isomeric nuclear states are produced in several types of nuclear reactions [10]. The difficulty is to maintain the alignment up to the implantation point in cases where in-flight selection is performed. At relativistic beam energies, the first observation of spin-alignment in isomeric beams was reported by Schmidt-Ott [11] using the projectile fragmentation reaction. For neutron-induced fission and relativistic fission reactions, alignment has not been observed yet and the reaction mechanism to produce oriented states via relativistic fission is not completely understood. However, spin-alignment is known to exist in spontaneous fission [12] and has been used to study the g factor of the 6^+ isomer in ^{134}Te [13].

The aim of the experiment reported here is to prove, for the first time, the presence of spin-alignment in projectile fission at relativistic energies. At the same time, the g factor of the 7^- isomeric state at 2219 keV in the neutron-rich isotope ^{126}Sn [6] was investigated. It is expected to be small due to the opposite sign of contributions by $d_{3/2}$ and $h_{11/2}$ neutrons in the leading $(d_{3/2}h_{11/2})_{7-}$ configuration. Therefore it provides a crucial probe for small components in the wave function and for studying core polarization evolution away from ^{132}Sn. The experiment was performed at the GSI facility, where a ^{238}U beam was accelerated up to 750 MeV/u by the SIS-18 synchrotron, with a mean intensity of 10^8 pps. The beam impinged on a 1 g/cm^2 ^{9}Be target placed at the entrance of the FRS spectrometer [14] operated in achromatic mode, allowing the selection of one charge state per element. A 221 mg/cm^2 Nb stripper foil was mounted behind the Be target in order to produce more than 99% of fully stripped fragments (as calculated with the LISE++ simulation code [15]). Fully stripped fragments are required to maintain the eventual reaction-induced spin-alignment during transport through the FRS [16].

The nuclei of interest were selected and identified in two stages. In the first part of the FRS spectrometer, a selection in the longitudinal momentum distribution was carried out, in order to select a spin-aligned ensemble of isomers. As it has been shown already in fragmentation, that the spin alignment in the selected ensemble can be understood by simple kinematical arguments, and is related to its longitudinal momentum [11,17,16,18]. Similar arguments can be used to understand how spin-alignment can be produced in a relativistic-fission reaction, considering the spin-alignment process that is known to exist in spontaneous fission [12]. In such a fission process, two fragments are emitted back to back with equal momenta in the center-of-mass system and their spins are preferentially oriented in a plane perpendicular to their emission direction. Thus if a cone of the ensemble of fragments emitted into 4π is selected, an oblate-aligned ensemble is obtained with the alignment symmetry axis along the emission direction [13]. When the fissioning nuclei have a relativistic energy, the fission fragments are emitted in a forward focussed cone, with a velocity that is spread around the beam velocity. Fragments with a lower/higher velocity correspond to fission products that were emitted anti-parallel/parallel to the beam direction. Thus by selecting the higher or lower part of the longitudinal momentum distribution of the fission fragments, an oblate spin-aligned ensemble could be obtained whereby the spins are aligned perpendicular to the beam direction. The FRS was tuned to select the higher part of this distribution on the group of fission fragments with $Z = 50$. Using the Monte Carlo simulation code MOCADI [19] the calculated kinematic properties of ^{126}Sn ions produced in the reaction are presented in Fig. 1. The longitudinal momentum distribution

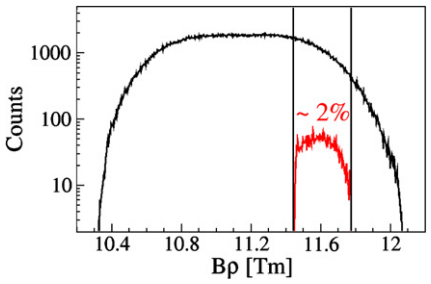

Fig. 1. MOCADI simulation of the distribution of the ^{126}Sn fragments after fission of ^{238}U at 750 MeV/nucleon. The acceptance of the FRS (red curve) is marked with a rectangular window. (For interpretation of the references to colour in this figure legend, the reader is referred to the web version of this Letter.)

of the fragments is proportional to the magnetic rigidity ($B\rho$) and was measured by a position-sensitive scintillator detector. In front of it, we keep the slits fully open. Fig. 1 simulates the total fission fragment longitudinal momentum distribution. The momentum acceptance of the FRS, which is only 2% of this total distribution, is indicated around the selected window. Fig. 1 illustrates the limitation of the spectrometer and the difficulty in selecting fission fragments. Based on previous studies a cut was made in the longitudinal momentum close to the maximum value of the magnetic rigidity ($B\rho$).

Once this momentum selection was performed, a further selection was accomplished using an achromatic Al wedge shaped degrader of 5 mg/cm^2 at the intermediate focal plane (more than 90% of the ions remained fully stripped after they passed this degrader). The identification of the reaction products in A/q and Z was performed in the second half of the FRS using the various detectors in the beam line, see [20] for details. The settings of the FRS allowed to select only fully stripped ions at the final focal point. The probability for electron pick-up in this final part of the beam line has been limited to less than 10% [21] by limiting the thickness of the final energy degrader just in front of the experimental set-up. After this degrader and before entering the set-up the beam intensity was 2.2×10^4 ions/s and the energy about 300 MeV/u. We expect a value for the isomeric ratio, around 10%, similar to the one obtained in [22]. In order to sufficiently reduce the beam energy prior to implantation in the Cu host, a 20 mm plexi-glass degrader has been fixed to the Cu stopper [16]. An air gap between the plexi-glass degrader and the stopper was avoided by putting a thin layer of grease between them. Thus the randomly oriented electron spins were decoupled from the nuclear spins as soon as the isomers reached the plexi-glass degrader and up to the implantation point in the Cu host, allowing to maintain the nuclear spin-alignment. Because the FRS is a zero-degree fragment separator, the spin-alignment symmetry axis is parallel to the beam axis at the implantation point [16]. The spin-aligned beam was implanted into an annealed high-purity 2 mm thick Cu foil (cubic lattice structure), placed between the poles of an electromagnet providing a vertical magnetic field of $B = 7000(10)G$, whose direction was periodically switched. A plastic scintillator at the focal plane of the FRS, placed upstream of the magnet, was used to provide the $t = 0$ signal for the γ-decay measurement, based on an event-by-event ion–gamma correlation [16]. The isomeric γ decays were measured during a 16 µs time window by the RISING array composed of eight former EUROBALL Cluster detectors [23], each containing seven encapsulated HPGe crystals. Each crystal had a relative efficiency of $\sim 60\%$ and an energy resolution of ~ 2 keV at 1332 keV. The detectors were placed in the horizontal plane at ± 45, ± 75, ± 105 and ± 135 degrees relative to the beam direction. The prompt atomic background radiation was eliminated from the γ-spectra by placing a hardware gate of 600 ns, thus making

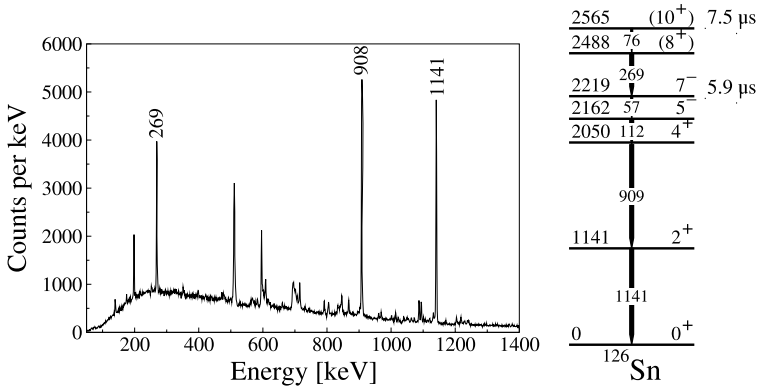

Fig. 2. The measured γ rays emitted after the decay of the isomeric states in ^{126}Sn (left) and the partial level scheme (right).

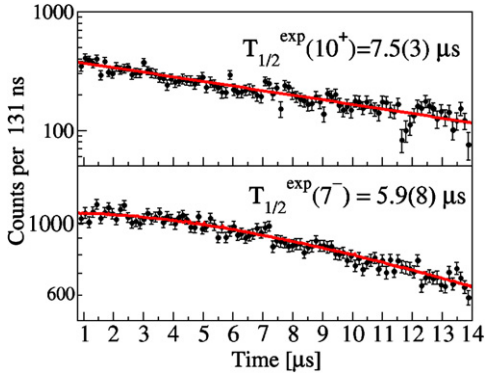

Fig. 3. (Color online.) Time distribution of the γ rays deexciting the isomeric levels in ^{126}Sn. Top: For the 269 keV line. Bottom: For the sum of γ rays with energies 909 keV and 1141 keV.

time analysis prior to this time impossible. More details on the experimental set-up and measuring procedure can be found in [21], while information of the data taking and analysis procedures are described in [20]. Data was analyzed using the Spy/Cracow software [24].

Two previously known microsecond isomeric states in ^{126}Sn have been populated (Fig. 2) [6,25]. Decay curves are obtained from the γ-time matrix by subtracting from each peak-decay curve a time spectrum produced in a background region near the peak. For the 269 keV decay from the 10^+ isomer a half-life $T_{1/2}(10^+) = 7.5(3)$ μs (Fig. 3 top) is found, in good agreement with the earlier reported value of 7.7(5) μs [25,26]. The decay curve of the 7^- isomeric level consists of two components: the direct decay from 7^- isomers implanted at $t = 0$ and the growth-decay curve originating from 10^+ isomers decaying into the lower one after implantation. The two component fit of the time spectrum of the 909 keV + 1141 keV, performed by keeping the half-life of the upper 10^+ isomer fixed, allowed the half-life of $T_{1/2}(7^-) = 5.9(8)$ μs (Fig. 3 bottom) and the ratio of the direct isomer population $N_7/N_{10} = 0.9(2)$ to be determined. The deduced half-life is in good agreement with the previously reported value 6.6(1.4) μs [6].

For the g factor determination the time-differential perturbed angular distribution (TDPAD) method [9] has been used. The background-corrected and normalized time spectra measured for the two field directions (up and down), are combined to produce the experimental $R(t)$ spectrum:

$$R_{exp}(t) = \frac{Y(t, B_{up}) - Y(t, B_{down})}{Y(t, B_{up}) + Y(t, B_{down})} \quad (1)$$

Time spectra gated on the 909 keV and 1141 keV transitions registered at the angles $\theta = \pm 45$ and $\theta = \pm 135$, with respect to the beam direction have been used to create an $R(t)$ spectrum with maximum amplitude (see [21] for details). The oscillation amplitude of the $R(t)$ spectrum created with the detectors placed at $\theta = \pm 75$ and $\theta = \pm 105$ is reduced by a factor of two compared to that of the $R(t)$ created with detectors in the geometry $\theta = \pm 45$ and $\theta = \pm 135$. In the present experimental conditions, characterized by a rather low degree of the nuclear alignment (see below), the $R(t)$ spectrum corresponding to the detectors placed at $\theta = \pm 75$ and $\theta = \pm 105$ did not evidence any oscillation, and therefore these data were not included in the analyses.

In the present case two cascade decaying isomeric levels with comparable half-lives are simultaneously populated in the nuclear reaction. The modulation ratio corresponding to γ rays that depopulated the upper 10^+ isomeric state could not be fitted due to the low statistics for the 269 keV γ ray. The g factor of the 10^+ state has been assumed to be $g(10^+) = -0.243$ (the average value measured for the $11/2^-$ states in the neigbouring odd isotopes [27] with a similar $(\nu h_{11/2})$ hole configuration). The g factors for the 10^+ state have been measured in ^{116}Sn and ^{118}Sn, with values of $-0.2326(15)$ and $-0.2447(7)$, respectively, and they agree within 7% with the g factors of the $11/2^-$ states in neighbouring odd-mass Sn [27]. A shell-model calculation [20,29] predicts $g_{SM}(10^+) = -0.238$, agreeing well with this estimated value. The $R(t)$ ratio for the 269 keV γ ray, constructed with a time calibration appropriate to observe the fast Larmor oscillations corresponding to the expected g factor, has large statistical errors, about 0.15 (three times larger than the errors of the $R(t)$ for 909 + 1141 keV, see Fig. 4 below). These large errors prevented the observation of low amplitude oscillations corresponding to the small alignment degree of this experiment (see below).

The experimental $R(t)$ spectrum for the sum of 909 and 1141 keV γ rays de-exciting the lower lying 7^- isomer is illustrated in Fig. 4a. In this case the modulated intensity is composed of two contributions: the cascade component coming from the 10^+ state and the direct component coming from the reaction. The calculated modulation ratio, depending on the Larmor frequencies ω_{10} and ω_7 that are describing the precession in the states 10^+ and 7^-, respectively, has the form (see Ref. [28]):

$$R(t) = \frac{b_2}{1 + A(t)} \cos 2(\theta - \omega_7 t) + \frac{A(t)}{1 + A(t)} R_{casc}(t, \omega_7, \omega_{10}) \quad (2)$$

where

$$R_{casc}(t, \omega_7, \omega_{10}) = b_2 \cos\alpha \left[\cos\left[2(\theta - \omega_{10} t) - \alpha\right)\right] + 2\left(1 - e^{\Delta\lambda t}\right)^{-1} \sin\left[2\theta - (\omega_7 + \omega_{10})t - \alpha\right] \sin \Delta\omega t \quad (3)$$

and

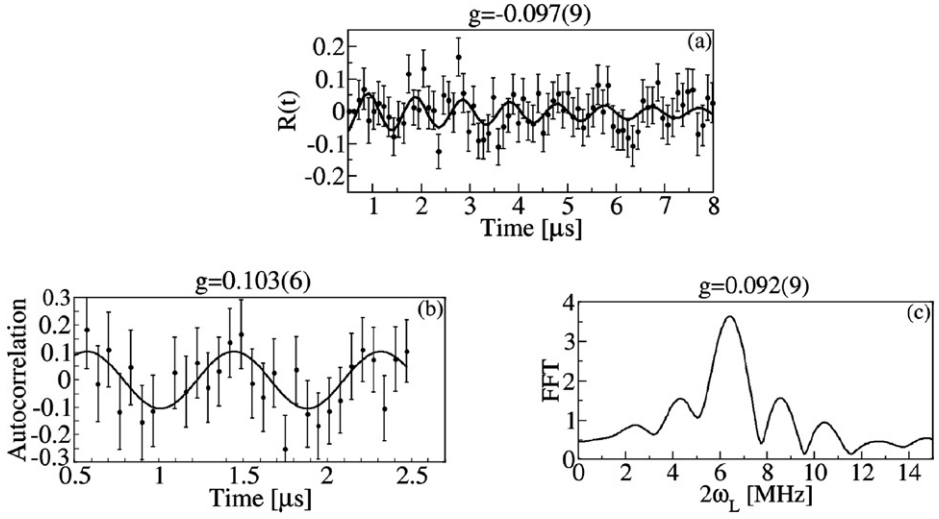

Fig. 4. The direct fit of the $R(t)$ function for $(909 + 1141)$ keV transitions in ^{126}Sn (a), autocorrelation analysis (b) and Fast Fourier Transform result (c).

$$A(t) = \frac{N_{10}}{N_7}\frac{\lambda_{10}}{\Delta\lambda}\left(e^{\Delta\lambda t} - 1\right)$$

$$\Delta\lambda = \lambda_7 - \lambda_{10}, \quad \text{with} \quad \lambda_i = \frac{\ln 2}{T_{1/2}}$$

$$\Delta\omega = \omega_7 - \omega_{10}$$

$$\alpha = \arctan(2\Delta\omega/\Delta\lambda)$$

The values for the decay constants λ_{10} and λ_7 and the ratio N_7/N_{10} of the population of the two isomeric levels have been extracted from the lifetime analysis. The amplitude of the oscillation b_2 is given by $b_2 = \frac{3}{4}A_2$, where A_2 is the angular distribution coefficient dependent on the transition type and on the degree of spin alignment. The same coefficients b_2 were assigned to the direct and cascade decays, assuming identical alignments for the two isomers.

The contribution of the term R_{casc} was dramatically reduced in our case on account of the $\cos\alpha$ factor, which for the large applied magnetic field of 7 kG took a value of 0.0008. Therefore for fitting the experimental $R(t)$ only the first term in expression (2) was used, with the amplitude b_2 and the Larmor frequency $\omega_7 = \frac{g(7^-)B\mu_n}{\hbar}$ as free parameters. As seen in Fig. 4a, the observed damping is well accounted for by the time-dependent amplitude $\frac{1}{1+A(t)}$. From the least-squares analysis of the modulation curve, the g factor of the 7^- isomer $g(7^-) = -0.097(9)$, and the amplitude $b_2 = 0.07(3)$, have been derived.

Since the period of the Larmor precession (~ 1 μs, see Fig. 4a) is shorter than the lifetime of the isomer (5.9(8) μs), an autocorrelation analysis was performed [16]. The calculated autocorrelation function ($ACF(n)$) has the form:

$$ACF(n) = \sum_{k=k_1}^{k_2-n} \frac{f(k)f(k+n)}{k_2-k_1-n} \Bigg/ \sum_{k=k_1}^{k_2} \frac{f^2(k)}{k_2-k_1} \tag{4}$$

where $f(k)$ represents the experimental data as a function of the channel number k, $k_2 - k_1$ is the observation window and n is the folding back window ($n \ll k_2 - k_1$). The information from a 7 μs window have been folded back into a 2 μs time window (see Fig. 4b). In the present experimental conditions and due to the smearing out of the oscillation pattern after 8 μs only data up to 7 μs have been included in the autocorrelation analysis to obtain the optimal amplitude. If data from later times are included the amplitude of the autocorrelation function is reduced. Fitting the autocorrelation data leads to a g-factor value of 0.103(6), which is in good agreement with the value obtained from fitting the raw $R(t)$, see Fig. 4b. Note that in this case phase and amplitude have no longer a physical meaning.

As a last step, we have performed a Fast Fourier analysis (FFT), which reveals a peak at $2\omega_L = 6.2(6)$ MHz (Fig. 4c), corresponding to a g factor of 0.092(9), in agreement with the values deduced by the other analysis procedures.

As a final value, we adopt the mean from the different analysis procedures, resulting in $g(7^-) = -0.098(9)$.

Table 1
Experimental g factor for the 7^- isomer in even mass Sn isotopes compared to shell-model calculations.

Isotope	E_x (keV)	$T_{1/2}$	g_{exp}	g_{free}	g_{eff}[1]	g_{cp}[2]
^{114}Sn	3088	765 ns	−0.0806(5)[3]			
^{118}Sn	2575	217 ns	−0.0978(6)[3]			
^{126}Sn	2219	5.9 μs	−0.098(9)	−0.081	−0.057	−0.082
^{128}Sn	2092	6.5 s		−0.076	−0.054	−0.070
^{130}Sn	1947	1.7 m	−0.0544(4)[4]	−0.067	−0.048	−0.048

[1] SM $g_s(\nu) = -2.513$ and $g_l(\nu) = -0.0039$.
[2] SM corrected for A dependence of core polarization.
[3] Ref. [33].
[4] Ref. [34].

In Table 1 this value has been compared to the g factors of other 7^- states in even-Sn isotopes with main quasi-particle configuration $(h_{11/2}^{-1}d_{3/2}^{-1})$. The Schmidt value for this configuration is $g_{schmidt} = -0.11$, which is close to the observed experimental values and confirms that this is the leading configuration of these isomers. The extreme sensitivity of $g(7^-)$ to small components in the wave function due to the partial cancellation of the $d_{3/2}$ and $h_{11/2}$ contributions of opposite sign allows a more detailed discussion. Extended untruncated shell-model calculations in the full $N = 50$–82 neutron space $(g_{7/2}, d_{5/2}, d_{3/2}, s_{1/2}, h_{11/2})$, were recently performed for the whole Sn region down to ^{124}Sn, using a realistic two-body interaction based on the CD-Bonn interaction and ^{88}Sr as a core [20,29]. The obtained g factors using free and effective single nucleon values are given in Table 1. Effective neutron g factors $g_s = -2.513$ and $g_l = -0.0039$ were adjusted to the experimental single hole values for $d_{3/2}$ and $h_{11/2}$ in ^{131}Sn. Fair agreement with experiment is observed from ^{130}Sn to ^{126}Sn, but the increase of $|g|$ with increasing distance from ^{132}Sn is only qualitatively reproduced. Note that for ^{126}Sn a slightly better agreement is observed if free g factors are used, which will be further discussed. Moreover, additivity of g factors is consider-

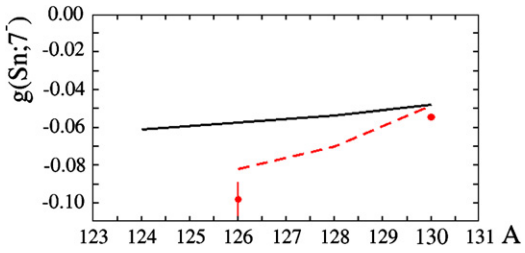

Fig. 5. g Factors for $I^\pi = 7^-$ states in even Sn isotopes. The full line represent g_{eff} and the dashed g_{cp} from Table 1. Directly measured values (red circles) are compared to SM results. The error on the g factor in ^{130}Sn is smaller than the symbol size. (For interpretation of the references to colour in this figure legend, the reader is referred to the web version of this Letter.)

ably violated for ^{130}Sn and ^{126}Sn, yielding values of $-0.0756(10)$ and $-0.0826(10)$, respectively, as calculated from the experimental $g(3/2^+)$ and $g(11/2^-)$ in the neighboring odd-A isotopes. These values are nicely reproduced using shell-model values for the $3/2^+$ and $11/2^-$ states, yielding additivity values of -0.076 and -0.077 for ^{130}Sn and ^{126}Sn. These values, however, are quite different from the calculated $g(7^-)$ (see Table 1), indicating that admixtures of different origin appear in the $I^\pi = 7^-$ and the $I^\pi = 3/2^+$, $11/2^-$ wave functions. The respective components amount to less than 2% of the wave function, yet they have a strong influence on the calculated moments.

The too weak A dependence of the shell model $g(7^-)$ values may be due to the fact that a common effective operator cannot account for partial blocking of core polarization with increasing distance from ^{132}Sn as this is not covered by the present valence space. The main core polarization configurations for the M1 operator in this region are the neutron $\nu(h^{-1}_{11/2}h_{9/2})$ and the proton $\pi(g^{-1}_{9/2}g_{7/2})$ $N = 82$ and $Z = 50$ cross-shell excitations [30] besides the $\nu(d^{-1}_{5/2}d_{3/2})$ which is included in the shell-model valence space. Corrections due to the A dependence (blocking and mixing) of core-excited configurations were calculated with an interaction and valence space used recently for core excited states in ^{132}Sn and ^{131}In [4]. Free nucleon g factors were used which account for the experimental $\nu d_{3/2}$ and $\nu h_{11/2}$ g factors in ^{131}Sn. The results are shown in the last column of Table 1 and account very well for the experimental g factor trend (Fig. 5). Core polarization amounts to 4.8% (^{130}Sn) to 2.5% (^{126}Sn) of the wave function, confirming the increased blocking as one moves away from ^{132}Sn. The corrections should be regarded as a trend estimate, as they were obtained in a different model space with a different interaction. We note that this approach also reproduces the absolute values and A dependence of the $d_{3/2}$ and $h_{11/2}$ quasi-particle states in $^{125-131}$Sn. All shell model results in the present work were performed with the code OXBASH [31].

Apart from extracting the g factor for this isomeric state, another goal of this work was to establish whether and how much alignment can be produced in a relativistic fission reaction. The amplitude of the experimental $R(t)$ curve (Fig. 4a) is indeed related to the amount of alignment that is present in the implanted ensemble of isomers [18]. From the experimental amplitude $b_2 = 0.07(3)$, and considering the angular distribution coefficient for total alignment $A_2^{\max} = 0.51$ [32] for the stretched E2 cascade $(4 \to 2 \to 0)$, we find an alignment $A = 18(8)\%$. Herewith, we have proven for the first time that isomers produced in a relativistic fission reaction and subsequently selected as fully-stripped ions through a fragment separator, are aligned and can maintain their alignment during the in-flight selection process. The observed amount is similar to that observed for fragments produced in an intermediate- or high-energy projectile fragmentation reaction (order of 10–20%).

In conclusion, for the first time a spin-aligned isomeric ensemble was observed in a relativistic-fission reaction. A comparison with the shell-model calculation for the g factor of the 7^- state in ^{126}Sn supports the assigned configuration and reveals details on small admixtures in the wave functions both from inside and outside the pure neutron model space. The amount of spin alignment deduced from this experiment and the fact that it can be maintained during the in-flight selection process, opens the possibility for further investigations on electromagnetic moments of exotic nuclei produced in relativistic fission.

Acknowledgements

This work was performed using the grant 06KY205I of the BMBF (Germany), IAP contract P6/23 of BELSPO (Belgium) and GO446-05 of FWO Vlaanderen, the Polish Ministry of Science and Higher Education (Grant 1-P03B-030-30), the Romanian National Authority for Scientific Research contract IDEI 52/07, the Bulgarian National Science Fund grant No. VUF06/05 and by the European Commision Contract No. RII3-CT-2004-506065. We acknowledge the technical support received from the GSI accelerator facility.

References

[1] J. Dobaczewski, et al., Phys. Rev. C 53 (1996) 2809.
[2] T. Kautzsch, et al., Eur. Phys. J. A 9 (2000) 201.
[3] A. Jungclaus, et al., Phys. Rev. Lett. 99 (2007) 132501.
[4] M. Górska, et al., Phys. Lett. B 672 (2009).
[5] J. Pinston, J. Genevey, J. Phys.: Nucl. Part. Phys. 30 (2004) R57.
[6] B. Fogelberg, et al., Nucl. Phys. A 323 (1979) 205.
[7] M. Mineva, et al., Eur. Phys. J. A 11 (2001) 9.
[8] Z. Podolyak, et al., Phys. Lett. B 632 (2006) 203.
[9] K. Alder, R.M. Steffen, Annu. Rev. Nucl. Sci. 14 (1964) 403.
[10] G. Neyens, Rep. Prog. Phys. 66 (2003) 633.
[11] W.-D. Schmidt-Ott, et al., Z. Phys. A 350 (1994) 215.
[12] J.B. Wilhelmy, et al., Phys. Rev. C 5 (1972) 2041.
[13] A. Wolf, et al., Phys. Rev. Lett. 36 (1976) 1072.
[14] H. Geissel, et al., Nucl. Instrum. Methods Phys. Res. B 70 (1992) 286.
[15] O.B. Tarasov, D. Bazin, Nucl. Instrum. Methods B 266 (2008) 4657.
[16] G. Georgiev, et al., J. Phys. G 28 (2002) 2993.
[17] K. Asahi, et al., Phys. Rev. C 43 (1991) 456.
[18] I. Matea, et al., Phys. Rev. Lett. 93 (2004) 142503.
[19] Th. Schwab, GSI report 91-10, 1991.
[20] R. Lozeva, et al., Phys. Rev. C 77 (2008) 064313.
[21] G. Neyens, et al., Acta Phys. Pol. 38 (2007) 1237.
[22] M. Mineva, PhD thesis, University of Lund, 2004.
[23] J. Eberth, et al., Nucl. Instrum. Methods Phys. Res. A 369 (1996) 135.
[24] J. Grębosz, Comput. Phys. Commun. 251 (2007) 176.
[25] J. Genevey, et al., in: B.M. Sherill, D.L. Morrissey, C.N. Davids (Eds.), Exotic Nuclei and Atomic Masses, AIP, New York, 1998, p. 694.
[26] C.T. Zhang, et al., Phys. Rev. C 62 (2000) 057305.
[27] N.J. Stone, Atomic Data and Nuclear Data Tables 90 (2005) 75.
[28] M. Ionescu-Bujor, et al., Nucl. Phys. A 272 (1976) 1.
[29] H. Grawe, in press, 2010.
[30] B.A. Brown, et al., Phys. Rev. C 71 (2005) 044317.
[31] B.A. Brown, et al., Oxbash for windows, MSU-NSCL report 1289, 2004.
[32] T. Yamazaki, Nucl. Data A 3 (1967) 1.
[33] M. Ishihara, et al., in: J. de Boer, H.J. Mang (Eds.), Proccedings of the International Conference on Nuclear Physics, vol. 1, North-Holland, Amsterdam, 1973, p. 256.
[34] F. le Blanc, et al., Phys. Rev. C 72 (2005) 034305.

EPJ A
Hadrons and Nuclei

EPJ.org
your physics journal

Eur. Phys. J. A **45**, 153–158 (2010) DOI: 10.1140/epja/i2010-11003-4

Spin-alignment and g-factor measurement of the $I^{\pi} = 12^{+}$ isomer in ^{192}Pb produced in the relativistic-energy fragmentation of a ^{238}U beam

M. Kmiecik *et al.*

EDP SCIENCES Società Italiana di Fisica Springer

Eur. Phys. J. A **45**, 153–158 (2010)
DOI 10.1140/epja/i2010-11003-4

THE EUROPEAN PHYSICAL JOURNAL A

Regular Article – Experimental Physics

Spin-alignment and g-factor measurement of the $I^\pi = 12^+$ isomer in ^{192}Pb produced in the relativistic-energy fragmentation of a ^{238}U beam

M. Kmiecik[1,a], A. Maj[1], J. Gerl[2], G. Neyens[3], L. Atanasova[4], D.L. Balabanski[5,6], F. Becker[2], P. Bednarczyk[1,2], G. Benzoni[7], N. Blasi[7], A. Bracco[7,8], S. Brambilla[7], L. Caceres[2], F. Camera[7,8], M. Ciemała[1], F.C.L. Crespi[7,8], S.K. Chamoli[9], S. Chmel[10], J.M. Daugas[11], P. Detistov[4], P. Doornenbal[2], G. Georgiev[12], K. Gladnishki[4,5], M. Górska[2], H. Grawe[2], J. Gręboszl[1], M. Hass[9], R. Hoischen[13], G. Ilie[14,15], M. Ionescu-Bujor[15], J. Jolie[14], I. Kojuharov[2], A. Krasznahorkay[16], R. Kulessa[17], M. Lach[1†], S. Lakshmi[9], S. Leoni[7,8], G. Lo Bianco[5], R. Lozeva[3,4,12], K.H. Maier[1], S. Mallion[3], K. Mazurek[1], W. Męczyński[1], B. Million[7], D. Montanari[7,8], S. Myalski[1], C. Petrache[5], M. Pfützner[18], S. Pietri[19], Zs. Podolyák[19], W. Prokopowicz[2], D. Rudolph[13], N. Saito[2], T.R. Saito[2], A. Saltarelli[5], G.S. Simpson[20], J. Styczeń[1], N. Vermeulen[3], E. Werner-Malento[2,21], O. Wieland[7], H.J. Wollersheim[2], and M. Zięblińskil[1]

[1] H. Niewodniczański Institute of Nuclear Physics PAN, ul. Radzikowskiego 152, 31-342 Kraków, Poland
[2] GSI, Planckstrasse 1, D-64291 Darmstadt, Germany
[3] K.U. Leuven, Instituut voor Kern- en Stralingsfysica B-3001 Leuven, Belgium
[4] Faculty of Physics, University of Sofia "St. Kl. Ohridski", BG-1164 Sofia, Bulgaria
[5] Dipartamento di Fisica, Università degli Studi di Camerino and INFN sez. Perugia, I-62032 Camerino, Italy
[6] Institute for Nuclear Research and Nuclear Energy, Bulgarian Academy of Sciences, BG-1784 Sofia, Bulgaria
[7] INFN Sez. di Milano, Via Celoria 16, 20133 Milano, Italy
[8] Università degli Studi di Milano, I-20133 Milano, Italy
[9] Weizman Institute of Science, 76100 Rehovot, Israel
[10] Fraunhofer INT, D 53879 Euskirchen, Germany
[11] CEA, DAM, DIF, F-91297 Arpajon Cedex, France
[12] CSNSM, Université Paris-Sud 11, CNRS/IN2P3, F-91405 Orsay-Campus, France
[13] Department of Physics, Lund University, S-22100 Lund, Sweden
[14] Institut für Kernphysik, Universität zu Köln, D-50937 Köln, Germany
[15] National Institute for Physics and Nuclear Engineering, RO-76900 Bucharest, Romania
[16] Institute of Nuclear Research of the Hungarian Academy of Sciences (ATOMKI), Debrecen, Hungary
[17] Jagiellonian University, Kraków, Poland
[18] University of Warsaw, PL-00681 Warsaw, Poland
[19] Department of Physics, University of Surrey, Guildford, GU2 7XH, UK
[20] Institut Laue Langevin, Grenoble, France
[21] Institute of Physics PAN, Warsaw, Poland

Received: 30 December 2009 / Revised: 27 April 2010
Published online: 8 July 2010

Communicated by C. Signorini

Abstract. The feasibility of measuring g-factors using the TDPAD method applied to high-energy, heavy fragmentation products is explored. The 2623 keV $I^\pi = 12^+$ isomer in ^{192}Pb with $\tau = 1.57\,\mu$s has been produced using the fragmentation of a 1 A GeV ^{238}U beam. The results presented demonstrate for the first time that such heavy nuclei produced in a fragmentation reaction with a relativistic beam are sufficiently well spin-aligned. Moreover, the rather large value of the alignment, 28(10)% of the maximum possible, is preserved during the separation process allowing the determination of magnetic moments. The measured values of the lifetime, $\tau = 1.54(9)\,\mu$s, and the g-factor, $g = -0.175(20)$, agree with the results of previous investigations using fusion-evaporation reactions.

1 Introduction

g-factors are sensitive probes of the nuclear wave function which allow detailed tests of model predictions. They can provide reliable information on the single-particle structure of nuclear levels, help to assign spin and parity to the nuclear state, and in favorable cases details of its wave function can be deduced.

[a] e-mail: maria.kmiecik@ifj.edu.pl
[†] Deceased.

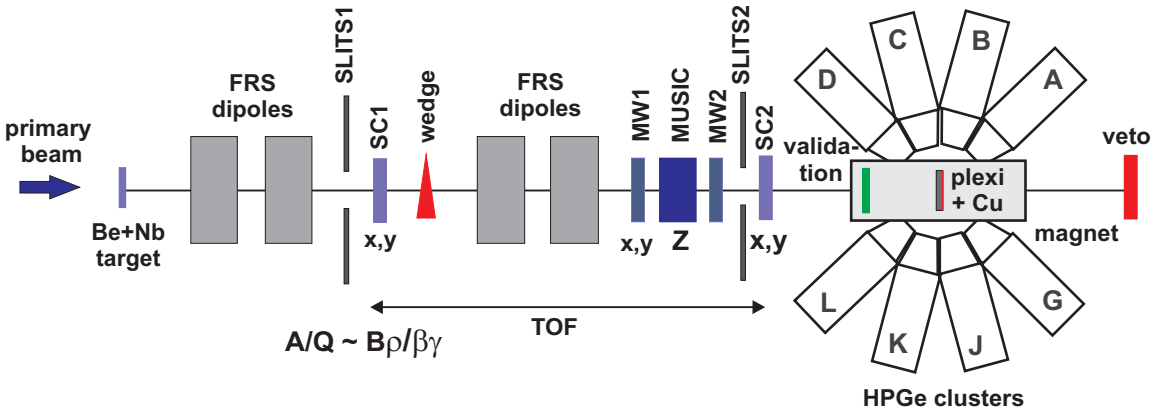

Fig. 1. The experimental set-up: the FRS with the detectors for the isotope selection, the stopper in the center of the magnet, the Ge array and ancillary detectors (validation and veto).

Therefore, the feasibility of the g-factor measurements is important, particularly for nuclei far from stability (see *e.g.* [1–4] and references therein) where nuclear structure often does not follow a systematic behavior and experimental observables providing details about the nuclear structure are of great importance. Fragmentation reactions can populate a wide range of exotic nuclei simultaneously, and sophisticated analyzing systems can uniquely separate, select or identify a specific nucleus on an ion-by-ion basis. These nuclei can be implanted into a stopper and, if they have a suitable lifetime (ns to μs), their γ decay can be measured and correlated with the ions implantation time. If the spin orientation induced in an ensemble of nuclei by reaction is not isotropic, but spins are oriented preferentially along or perpendicular to the beam direction ("spin-aligned") also their Larmor precession in an applied magnetic field can be measured and the g-factor determined.

Fragmentation reactions have been employed rather in few experiments for investigations of electromagnetic moments in isomeric states in light and medium mass nuclei [1,2,5–7]. The mechanism by which the nuclear spin-alignment or polarization is produced in such processes is only partly understood [5,6,8,9]. The spin orientation of nuclei produced in the reaction can be reduced or even lost due to the hyperfine interaction with its randomly oriented electron spin during the flight path through the mass separator. By producing fully stripped nuclei and maintaining them fully stripped all the time when passing through the analyzing system —with magnets, particle detectors and absorbers— the nuclear spin orientation can be preserved [1,2,5,6].

To conserve a high fraction of the spin-alignment, the beam impinging on the stopper has to be of very high energy. As hyperfine interactions posses Z^3-dependence [10], their effect on destroying the spin-alignment will be much more severe for heavy nuclei. For isotopes of $A \approx 200$ this requires production of fragments with an energy higher than $\approx 250\,A$ MeV up to the last piece of solid material before the perturbation free stopper (*e.g.* made from copper material). In consequence, a high fraction of fully stripped ions is preserved, since the probability for picking-up electrons is inversely proportional to the fragments velocity.

In addition, even for not fully stripped ions, in the present case the effect of static hyperfine interactions is limited. As discussed by Nordhagen *et al.* [11], in the absence of external fields, the total spin $\boldsymbol{F}$, which couples the nuclear spin $\boldsymbol{I}$ with the atomic spin $\boldsymbol{J}$, is conserved. For a high-spin isomer, $\boldsymbol{I} \gg \boldsymbol{J}$ so $\boldsymbol{I}$ is kept almost parallel to the total spin $\boldsymbol{F}$ when the external field acts on $\boldsymbol{J}$.

So far, successful measurements of magnetic moments with the fragmentation reactions have only been performed for nuclei around Ni and some lighter nuclei. Only very recently, we have undertaken such experiments within the gRISING campaign at GSI, for the measurement of the g-factor in ^{127}Sn [3] and, presently, for ^{192}Pb. Such fragmentation reactions may become an essential tool to investigate heavy nuclei far off the stability line.

The latter case, presented in this paper, is to stress upon the feasibility test for such measurements in the Pb region using U-fragmentation. To obtain information on alignment preserved in this type of experiment, the g-factor of the 12^+ isomer at 2623 keV in ^{192}Pb has been measured with the fragmentation of a 1 A GeV ^{238}U beam and compared to the known value determined before in a fusion-evaporation reaction [12,13].

2 Experiment

The experiment was performed at the SIS/FRS facility in GSI. A ^{238}U primary beam at an energy of 1 A GeV bombarded an 1.023 g/cm^2 ^{9}Be production target backed by a 0.221 g/cm^2 Nb stripper foil to increase the fraction of fully stripped ions. The target thickness was chosen not to influence significantly the momentum spread. Pb isotopes were produced via fragmentation and separated using the FRagment Separator (FRS) [14] presented schematically together with the associated detectors in fig. 1. The beam intensity was ca. 10^8 pps, and the rate of the ions implanted into the catcher reached in average about 60 pps per Pb isotope. (The time for the measurement was about 47 hours excluding the time for setting up the apparatus and calibrations.) The ions were identified event-by-event using several detectors to determine position (multiwire counters —MW1 and MW2), atomic number Z (MUSIC

—ionization chamber) and time of flight (fast scintillators —SC1 and SC2— measuring also the position) [15]. Mass identification was performed by measuring both the magnetic rigidity ($B\rho$) and the velocity obtained from time of flight. The scintillators were placed at the middle and the final focal planes of the spectrometer. The measured position of ions *versus* A/Q, in both foci (see fig. 3 for the final focus SC2), enabled the fragments to be identified and allowed the selection of the isotopes of interest ion-by-ion. For more details about the identification procedure see, for example, ref. [16].

In the present experiment, the primary beam energy of 1 A GeV was high enough to produce Pb ions with a remaining energy of ≈ 290 A MeV just before the stopper. As a result 90% of the ^{192}Pb ions was fully stripped at the final focal plane, reducing the chance of a substantial loss of alignment by hyperfine interactions.

The spin-alignment of ions produced in fragmentation reactions is correlated with the momentum of the products [5]. Nuclei with lower (or higher) momentum than the mean of the momentum distribution correspond to fragments to which the linear momentum has been transferred either parallel or antiparallel to the beam direction. The angular momentum of the outgoing nucleus, calculated empirically as the vector product of the impact parameter and transferred momentum, is about perpendicular to the beam as in fusion-evaporation reactions, so the low values of magnetic substate $|m|$ prevail. This constraint does not apply to the nuclei with momentum around the mean value, consequently substates with higher values of $|m|$ can be populated. Gamma angular distributions generated by nuclei with different selection of momentum may then have, in an extreme case, even opposite concavity. Those two types of alignment may lead, if not separated, to a cancellation of the measured anisotropy of the γ-radiation. So, in order to increase the effect of the spin-alignment of the selected ^{192}Pb nuclei, a cut was imposed on the momentum distribution. This was done by closing the slits (denoted SLITS1 in fig. 1) asymmetrically (to the positions 0 and -20 mm) to select the low momentum tail of the distribution, *i.e.* ions possessing spins about perpendicular to the beam direction. Such measurement condition was required also to reduce the counting rate for the detector SC1. The momentum distribution calculated with the LISE++ code [17,18] for open and closed slits is presented in fig. 2.

The incoming ions were slowed down in a 2 cm Plexiglas ($(C_5O_2H_8)_n$) plate which was glued to a 2 mm Cu foil that served as a perturbation-free host for the stopped nuclei (see [1,2]). The copper stopper had been annealed prior to the experiment. The stopper was placed in the center of the magnet providing a vertically oriented external magnetic field $B = 0.160(1)$ T (measured by the Hall probe). The polarization of the magnetic field was alternated up and down every three hours. The stopper was surrounded by 8 HPGe detectors from the RISING set-up [15], placed at $\pm 45°$, $\pm 75°$, $\pm 105°$ and $\pm 135°$, to measure delayed γ-rays from the isomeric decay. An additional scintillator was placed at the entry to the magnet (validation detector) to select only the ions incoming

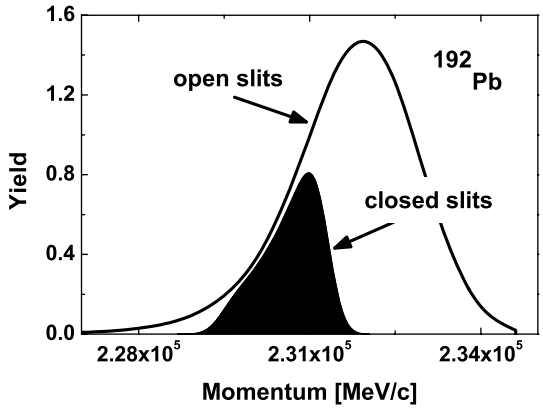

Fig. 2. The momentum distribution of ^{192}Pb calculated using the LISE++ code at the SC1 position for open (line) and closed (black area) SLITS1. The beam energy was ≈ 590 A MeV at this point.

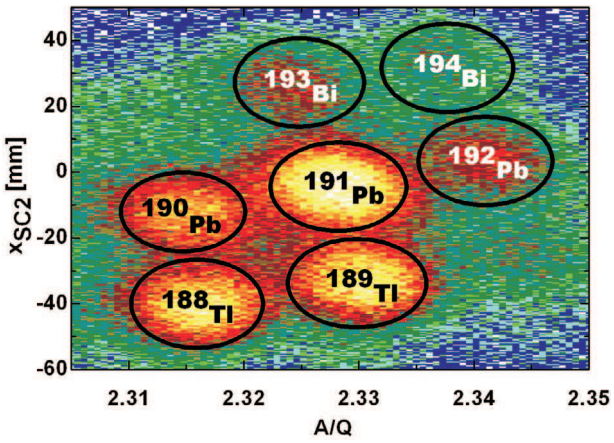

Fig. 3. The isotopes produced in ^{238}U beam fragmentation reaction selected at the final focus of the FRS.

to the magnet. A veto detector placed after the magnet served to monitor nuclei that had not been stopped and reject the coincident γ-rays.

The data analysis of the separated isotopes was performed with the use of the SPY/CRACOW software [19]. The result of the selection obtained at the final focus plane of the FRS (SC2) is shown in fig. 3. Since the FRS was set up to choose only the lowest part of the momentum distribution of the ^{192}Pb ions, the observation of other nuclides —mainly ^{191}Pb— is relatively enhanced. To analyze the γ-rays associated with ^{192}Pb, the appropriate two-dimensional gate on the SC2 position *vs.* A/Q was set. N.B.: with the time settings used in our experiment no significant isomeric γ transitions were present for gates set on other than ^{192}Pb isotopes visible in fig. 3.

3 Analysis

The Larmor precession frequency of the isomeric spins is $\omega_L = g\mu_N B/\hbar$, where g is the nuclear gyromagnetic factor, μ_N is the nuclear magneton, and B is the strength of the external magnetic field. For a state with a μs isomeric

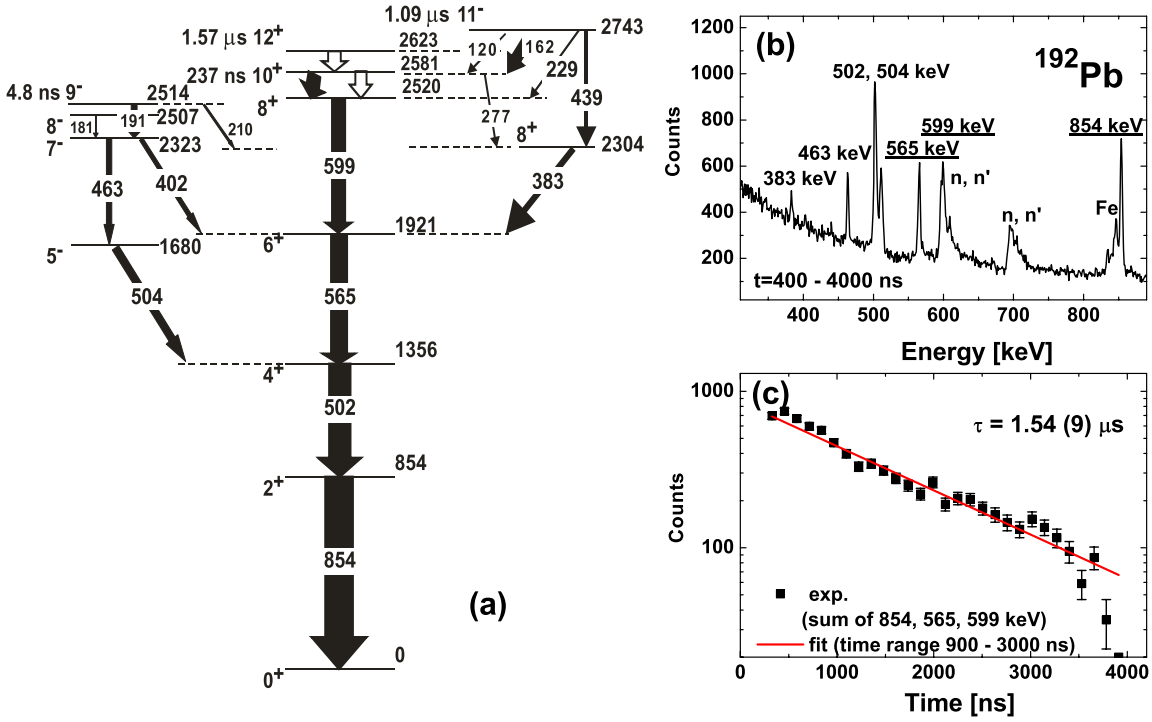

Fig. 4. (a) Partial level scheme of ^{192}Pb and intensities taken from ref. [21]. (b) The delayed γ-ray energy spectrum associated to the 12^+ isomeric state decay in ^{192}Pb. (c) The time spectrum obtained by gating on $E2$ γ transitions 599, 565 and 854 keV with the fit determining the lifetime.

lifetime, such as the $I^\pi = 12^+$ isomer in ^{192}Pb, the ω_L can be measured by the Time Differential Perturbed Angular Distribution (TDPAD) method [20,1] since it is most suitable for investigation of g-factors of isomeric states with lifetimes in the $\tau = 10\,\text{ns}$–$100\,\mu\text{s}$ range. In this method, the Larmor frequency is observed as a modulation of the time spectra of the isomeric decay. The known field B and ω_L evaluated from the time spectra provide the g-factor.

As a result of the experiment described in sect. 2, the time spectra of decaying nuclei measured in coincidence with the appropriate γ-ray energies were obtained. The delayed (for a time of $400\,\text{ns} < t < 4\,\mu\text{s}$) γ-ray energy spectrum with the indicated energies of γ-rays from the decay of ^{192}Pb is shown in fig. 4b. At shorter delay times the spectrum was not analyzed as it was affected by the atomic bremsstrahlung [15] caused by the stopping of the high-energy ($\approx 290\,A\,\text{MeV}$) ions in the Plexiglas plate. The time spectra for the g-factor evaluation were obtained gating on the 599, 565 and 854 keV stretched $E2$ transitions (cf. the partial level scheme in fig. 4a). The statistics from the individual detectors was too small to determine the g-factor. Therefore we choose four detectors which could be used to obtain $R(t)$ according the formula given in the next section. Summed time spectra for the aforementioned transitions were obtained for the detectors (denoted A, L, D, and G in fig. 1) at $\pm 45°$ and $\pm 135°$ and both field directions. One common background spectrum was generated as the total projection on the time axis of the γ energy *versus* the γ time matrix. This spectrum was subtracted from the individual time spectra associated with each considered γ transition after normalizing its intensity to the background under the respective γ line in the energy spectrum.

The sum of the background-subtracted time spectra (fig. 4c) was fitted by an exponential function giving a lifetime of $\tau = 1.54(9)\,\mu\text{s}$ for the $I^\pi = 12^+$ isomer in ^{192}Pb in agreement with the value measured in fusion-evaporation reactions ($1.57(6)\,\mu\text{s}$ [21,22]).

4 Results and discussion

From the time spectra measured with the detectors denoted A, L, D, and G (see fig. 1), and the two opposite directions of the magnetic field, the two combined spectra were obtained: a = A↑ + L↑ + D↓ + G↓, b = A↓ + L↓ + D↑ + G↑ (see [23] for more details). In this notation, letters mean spectra taken with given HPGe detectors while arrows show the directions of the magnetic field, *e.g.* A↑ is the time spectrum measured with detector A (at 45°) with the field vector pointing upwards.

From these spectra the experimental ratio $R(t)$ defined as $R(t) = \frac{a-b}{a+b}$ was created which for the chosen detector angles ($90° \pm 45°$) is described by the function $R(t)_{th} = \frac{3A_2B_2}{4+A_2B_2}\sin(2\omega_L t)$ that contains only the angular-distribution coefficients A_2B_2 and the Larmor frequency. The A_4B_4 term of the angular distribution was neglected.

The experimental $R(t)$ data were fitted by $R_{fit} = A\sin(2\omega_L t - \phi)$ using the χ^2 minimization procedure. The

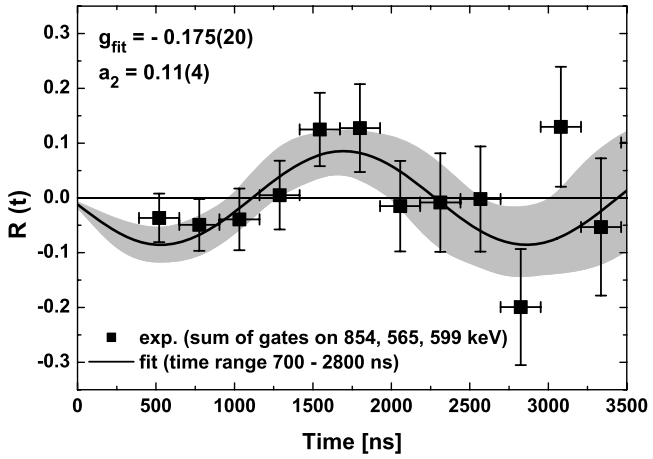

Fig. 5. The experimental $R(t)$-function (filled squares) and the result of the fit (solid line) (see the text for explanation). The quality of the fit is shown by the uncertainty depicted as a shaded area around the fitting function. This region represents all possible $R_{fit}(t)$-functions calculated for parameters ω_L, A and ϕ within the error limit obtained from the fit.

fit function $R_{fit}(t)$ included a phase ϕ which should be zero if one uses a zero-degree spectrometer (such as the FRS) and if only a single isomer is involved. In the ^{192}Pb case the γ cascade from the 12^+ state passes through the also isomeric 10^+ state with $\tau = 237$ ns. However, as the dominant wave function configuration of both the 12^+ and 10^+ isomers is the neutron $i^{-2}_{13/2}$ [12,13], both states have very similar g-factors, and consequently the nuclei in both isomeric states precess with the same frequency. Therefore no phase shift in the $R(t)$-function is expected.

The experimental $R(t)$-function is presented in fig. 5 together with the best fit curve. The amplitude, frequency and phase obtained from the fit to the experimental data are $A = 0.087(30)$, $\omega_L = 0.00135(16)\,\mathrm{ns}^{-1}$ and $\phi = 0.14(50)^\circ$, respectively.

From the ω_L value for $B = 0.16$ T, the g-factor, $g_{fit} = -0.175(20)$, was deduced. The negative sign of the g-factor comes from the negative value of the $R(t)$-function for the first half-period of the oscillation (see fig. 5) and from the $A_2 > 0$ values of the stretched $E2$ transitions chosen to obtain $R(t)$. The deduced g-factor is in agreement with the value $-0.173(2)$ measured in fusion-evaporation reactions [12,13]. Also the fitted phase is zero within the error bars ($0.1(5)^\circ$) as it is expected.

The possible influence of the higher-lying 11^- isomer on the perturbed $R(t)$ pattern, and on the deduced g-factor value, is negligible. The most intense 162 keV transition as well as the 439 keV γ-ray which directly feeds the 8^+ level at 2304 keV excitation energy (see fig. 4a), are not observed. The presence of the 383 keV transition de-exciting the 8^+ state can be understood as arising from the population of this state through the 12^+ decay.

The main result of the present work is the value of the amplitude, A, of the fit function $R_{fit}(t)$, which gives the amount of preserved alignment after the implantation [24]. It contains information on the coefficient $a_2 = A_2 B_2$, where A_2 is the angular-distribution coefficient (which depends on the multipolarity of the transition) while B_2 is the orientation parameter (depending on the orientation mechanism and the spin of the nuclear state). The obtained $a_2 = 0.11(4)$, calculated from the measured $A = \frac{3a_2}{4+a_2}$, can be compared to the value corresponding to the maximum possible angular-distribution coefficient in a stretched $E2$-cascade, *i.e.* for full alignment of the 12^+ isomer. This value, taken from Yamazaki [25], is $a_{2max} = 0.40$. Comparing them one can say that the alignment remaining after production, transportation, selection and implantation is around $28\% \pm 10\%$ of the maximum. It is sufficiently large, as can be judged from fig. 5, to apply the TDPAD method for determining a g-factor.

5 Summary

We have presented the results of the g-factor measurement with the TDPAD method for the 12^+ state in the ^{192}Pb nucleus produced in a fragmentation reaction using a relativistic beam. The obtained values of the lifetime and g-factor of this state are in satisfactory agreement with the previous results of measurements using fusion-evaporation reactions [12,13,21,22]. This was the first g-factor measurement for such heavy mass nucleus produced in fragmentation reaction. Up to now similar measurement was done for the much lighter ^{127}Sn [3], but without deriving information on the alignment. The main aim of the present experiment was to check if for very heavy nuclei produced in fragmentation reactions of the relativistic beam a sufficient alignment can be produced and preserved until the ions are stopped. This has clearly been proven.

The obtained value of the coefficient $a_2 = 0.11(4)$, containing information on alignment, might be compared with the result $a_2 = 0.30$ for the fusion-evaporation reaction [12,13] and the maximum possible value $a_2 = 0.40$ for stretched $E2$ transitions and complete alignment [25]. The achieved value can be also related to the alignment measured for medium mass nuclei produced in the fragmentation of intermediate projectile energy [2,6] and found to be around 15%.

The alignment obtained in the present work for ^{192}Pb proves the feasibility of the g-factor measurement for very heavy nuclei, using fragmentations of relativistic beams. It shows that such reactions can indeed be used as a key tool in investigations of electromagnetic moments of heavy nuclei far from the stability line, probably also for nuclei with extreme neutron-to-proton ratios. Very low cross-sections for the reaction channels to reach those exotic nuclei can be overcome by increasing the intensity of the primary beam (what will be possible at FAIR facility) and the use of the more efficient detector arrays.

This work was supported in part by the EURONS contract No. RII3-CT-2004-506065, the Polish Ministry of Science and Higher Education (Grants No. N N202 309135 and N N202 240637) and by the Hungarian OTKA Foundation No. K72566.

References

1. G. Georgiev *et al.*, J. Phys. G **28**, 2993 (2002).
2. I. Matea *et al.*, Phys. Rev. Lett. **93**, 142503 (2004).
3. L. Atanasova *et al.*, Prog. Part. Nucl. Phys. **59**, 355 (2007).
4. G. Ilie *et al.*, Phys. Lett. B **687**, 305 (2010).
5. K. Asahi *et al.*, Phys. Rev. C **43**, 456 (1991).
6. W.-D. Schmidt-Ott *et al.*, Z. Phys. A **350**, 215 (1994).
7. N. Vermeulen *et al.*, Phys. Rev. C **75**, 051302(R) (2007).
8. D. Borremans *et al.*, Phys. Rev. C **66**, 054601 (2002).
9. D.E. Groh *et al.*, Phys. Rev. C **76**, 054608 (2007).
10. P. Seelig *et al.*, Phys. Rev. Lett. **81**, 4824 (1998).
11. R. Nordhagen *et al.*, Nucl. Phys. A **142**, 577 (1970).
12. Ch. Stenzel *et al.*, Hyperfine Interact. **15/16**, 97 (1983).
13. Ch. Stenzel *et al.*, Nucl. Phys. A **411**, 248 (1983).
14. H. Geissel *et al.*, Nucl. Instrum. Methods Phys. Res. B **70**, 286 (1992).
15. H.J. Wollersheim *et al.*, Nucl. Instrum. Methods Phys. Res. A **537**, 637 (2005).
16. R. Lozeva *et al.*, Phys. Rev. C **77**, 064313 (2008).
17. D. Bazin *et al.*, Nucl. Instrum. Methods Phys. Res. A **482**, 307 (2002).
18. O. Tarasov *et al.*, Nucl. Instrum. Methods Phys. Res. B **266**, 4657 (2008).
19. J. Gręsbosz, Comput. Phys. Commun. **176**, 251 (2007).
20. G. Goldring, M. Hass, *Treaties on Heavy Ion Science*, edited by D. Allan Bromley, Vol. **3** (Plenum, New York, 1985) p. 539.
21. M. Ionescu-Bujor *et al.*, Phys. Lett. B **650**, 141 (2007).
22. C.M. Baglin, Nucl. Data Sheets **84**, 717 (1998).
23. G. Neyens *et al.*, Acta Phys. Pol. B **38**, 1237 (2007).
24. G. Neyens, Rep. Prog. Phys. **66**, 633 (2003).
25. T. Yamazaki, Nucl. Data A **3**, 1 (1967).

A LETTERS JOURNAL EXPLORING THE FRONTIERS OF PHYSICS

OFFPRINT

g-factor measurements at RISING: The cases of ^{127}Sn and ^{128}Sn

L. Atanasova, D. L. Balabanski, S. K. Chamoli, M. Hass, G. S. Simpson, D. Bazzacco, F. Becker, P. Bednarczyk, G. Benzoni, N. Blasi, A. Blazhev, A. Bracco, C. Brandau, L. Caceres, F. Camera, F. C. L. Crespi, P. Detistov, P. Doornenbal, C. Fahlander, E. Farnea, G. Georgiev, J. Gerl, K. A. Gladnishki, M. Górska, J. Grebosz, R. Hoischen, G. Ilie, M. Ionescu-Bujor, A. Iordachescu, A. Jungclaus, G. Lo Bianco, M. Kmiecik, I. Kojouharov, N. Kurz, S. Lakshmi, R. Lozeva, A. Maj, D. Montanari, G. Neyens, M. Pfützner, S. Pietri, Zs. Podolyák, W. Prokopowicz, D. Rudolph, G. Rusev, T. R. Saito, A. Saltarelli, H. Schaffner, R. Schwengner, S. Tashenov, J. J. Valiente-Dobón, N. Vermeulen, J. Walker, E. Werner-Malento, O. Wieland, H. J. Wollersheim, H. Grawe and M. Hjorth-Jensen

EPL, **91** (2010) 42001

A Letters Journal Exploring the Frontiers of Physics

August 2010

EPL, **91** (2010) 42001 www.epljournal.org
doi: 10.1209/0295-5075/91/42001

g-factor measurements at RISING: The cases of ^{127}Sn and ^{128}Sn

L. Atanasova[1(a)], D. L. Balabanski[1,2], S. K. Chamoli[3], M. Hass[3], G. S. Simpson[4], D. Bazzacco[5], F. Becker[6], P. Bednarczyk[6,7], G. Benzoni[8], N. Blasi[8], A. Blazhev[9], A. Bracco[8], C. Brandau[6,10], L. Caceres[6], F. Camera[8], F. C. L. Crespi[8], P. Detistov[1], P. Doornenbal[6], C. Fahlander[11], E. Farnea[5], G. Georgiev[12], J. Gerl[6], K. A. Gladnishki[2,13], M. Górska[6], J. Grebosz[6,7], R. Hoischen[11], G. Ilie[9,14], M. Ionescu-Bujor[14], A. Iordachescu[14], A. Jungclaus[15], G. Lo Bianco[2], M. Kmiecik[7], I. Kojouharov[6], N. Kurz[6], S. Lakshmi[3], R. Lozeva[13,16], A. Maj[7], D. Montanari[8], G. Neyens[16], M. Pfützner[17], S. Pietri[10], Zs. Podolyák[10], W. Prokopowicz[6,7], D. Rudolph[11], G. Rusev[18], T. R. Saito[6], A. Saltarelli[2], H. Schaffner[6], R. Schwengner[18], S. Tashenov[6], J. J. Valiente-Dobón[19], N. Vermeulen[16], J. Walker[6,10], E. Werner-Malento[6,17], O. Wieland[8], H. J. Wollersheim[6], H. Grawe[6] and M. Hjorth-Jensen[20]

[1] *Institute for Nuclear Research and Nuclear Energy, Bulgarian Academy of Sciences - BG-1784 Sofia, Bulgaria, EU*
[2] *Physics Division, School of Science and Technology, Università di Camerino and INFN, Sezione di Perugia I-62032 Camerino (Macerata), Italy, EU*
[3] *Weizmann Institute of Science - Rehovot 76100, Israel*
[4] *LPSC, Université Joseph Fourier Grenoble 1, CNRS/IN2P3, Institut National Polytechnique de Grenoble F-38026 Grenoble Cedex, France, EU*
[5] *Dipartimento di Fisica, Università di Padova and INFN, Sezione di Padova - I-35131 Padova, Italy, EU*
[6] *GSI Helmholtzzentrum für Schwerionenforschung GmbH - Planckstr. 1, D-64291 Darmstadt, Germany, EU*
[7] *The Henryk Niewodniczański Institute of Nuclear Physics, PAN - PL-31342 Kraków, Poland, EU*
[8] *Dipartimento di Fisica, Università degli Studi di Milano and INFN, Sezione di Milano - I-20133 Milano, Italy, EU*
[9] *IKP, Universität zu Köln - D-50937, Köln, Germany, EU*
[10] *Department of Physics, University of Surrey - Guildford, GU2 7XH, UK, EU*
[11] *Department of Physics, Lund University - S-22100 Lund, Sweden, EU*
[12] *CSNSM, Université Paris-Sud 11, CNRS/IN2P3 - F-91405 Orsay-Campus, France, EU*
[13] *Faculty of Physics, St. Kliment Ohridski University of Sofia - BG-1164 Sofia, Bulgaria, EU*
[14] *Horia Hulubei National Institute of Physics and Nuclear Engineering - R-077125, Bucharest, Romania, EU*
[15] *Instituto de Estructura de la Materia, CSIC - E-28006 Madrid, Spain, EU*
[16] *Instituut voor Kern- en Stralingsfysica, K.U. Leuven - Celestijnenlaan 200D, B-3001 Leuven, Belgium, EU*
[17] *IEP, Warsaw University - PL-00681 Warsaw, Poland, EU*
[18] *Institut für Strahlenphysik, FZ Dresden-Rossendorf - D-01314, Dresden, Germany, EU*
[19] *INFN - Laboratori Nazionali di Legnaro - I-35020 Legnaro (Padova), Italy, EU*
[20] *Department of Physics and Centre of Mathematics for Applications, University of Oslo - N-0316 Oslo, Norway*

received 6 June 2010; accepted in final form 10 August 2010
published online 3 September 2010

PACS 21.10.Ky – Electromagnetic moments
PACS 21.60.Cs – Shell model
PACS 25.70.Mn – Projectile and target fragmentation

Abstract – We report on g-factor measurements of the $19/2^+$ $T_{1/2} = 4.5(3)\,\mu$s isomer in ^{127}Sn and the 10^+ $T_{1/2} = 2.69(23)\,\mu$s isomer in ^{128}Sn. These isomers were produced and spin-aligned in relativistic heavy-ion fragmentation at GSI and were selected and separated by the GSI fragment separator (FRS). The γ-rays of the isomeric decay were detected by the RISING γ-ray spectrometer. The method of time-differential perturbed angular distributions was utilized. The measured g-factors, $g(19/2^+;\ ^{127}\mathrm{Sn}) = -0.17(2)$ and $g(10^+;\ ^{128}\mathrm{Sn}) = -0.20(4)$, are compared with shell model calculations. The measured g-factors confirm the predominantly $\nu h_{11/2}^{-2}$ and $\nu(s_{1/2}^{-1}h_{11/2}^{-2})$ character of the 10^+ and $19/2^-$ isomers in ^{128}Sn and ^{127}Sn, respectively. The results demonstrate the feasibility of the method for similar measurements in exotic neutron-rich nuclei.

(a) E-mail: liliya@inrne.bas.bg

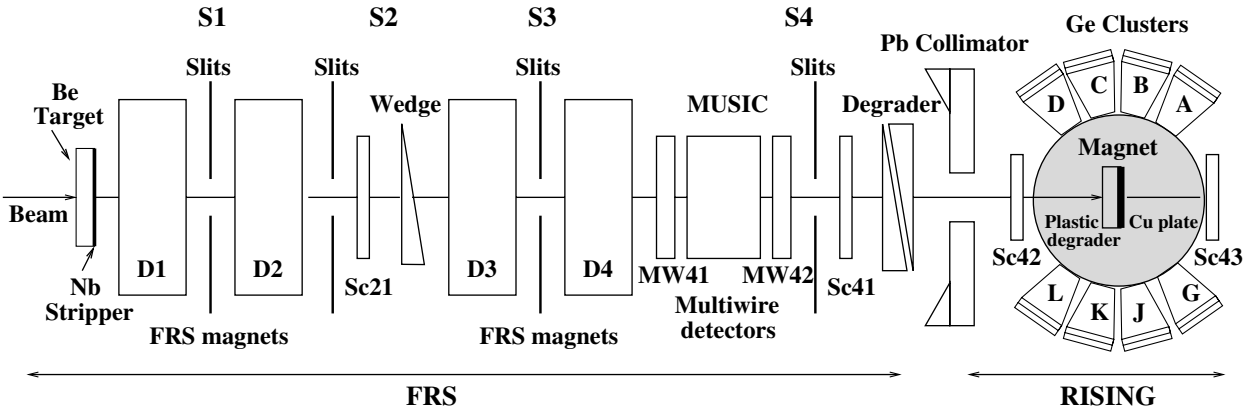

Fig. 1: Schematic view of the experimental set-up (see text): the fragment separator (FRS) with the beam-tracking detectors, the RISING γ-ray detectors (A–D) and (G–L), the electromagnet and the implantation detectors.

Introduction. – Nuclei in the vicinity of closed proton and neutron shells exhibit simple single-particle excitation spectra, with rather pure wave functions. This is due to the fact that there are only few levels close to the Fermi surface and configuration mixing effects, resulting from particle-hole excitations across the shell gaps, are suppressed to a great extent [1]. However, the nuclear shell model traditionally was established and critically tested for nuclei close to the region of stability. It is, therefore, important for a further understanding of the nuclear shell structure to study nuclei in the vicinity of closed proton and neutron shells away from the valley of β-stability, such as $^{132}_{50}\mathrm{Sn}_{82}$ or $^{78}_{28}\mathrm{Ni}_{50}$.

Nuclear g-factors play a special role in such a quest since they provide information about the configuration of the states of interest. In particular, in the vicinity of doubly magic nuclei, they shed light on the purity of the nuclear wave function, reflecting the stability of nuclear shells.

A possibility to investigate neutron-rich nuclei is provided by projectile fragmentation. So far, such reactions were utilized for studies of isomeric moments in nuclei with $A \leqslant 70$ [2–7]. The spin-orientation of the isomeric ensemble is produced in the reaction itself. To preserve as much alignment as possible only fully stripped nuclei are selected during the flight through a separator. In such a way perturbation effects, due to the hyperfine interaction with the randomly oriented electron spin, are avoided. Within the RISING (Rare ISotope INvestigations @ GSI) γ array project [8] g-factor measurements of heavier nuclei were performed [9], taking advantage of the relativistic beams at GSI.

The cases under study are microsecond isomers in the neutron-rich Sn isotopes, which have a magic number of protons $Z = 50$. The structure of Sn isotopes in the vicinity of ^{132}Sn with neutron numbers $N < 82$ is governed by neutron hole configurations in the negative-parity $1h_{11/2}$ and the positive-parity $2d_{3/2}$ and $3s_{1/2}$ orbitals. Microsecond isomers are known in the spectra of the even-A and odd-A Sn isotopes with $N < 82$, correspondingly [10]. The 10^+ microsecond isomers with a leading configuration of $\nu 1h^{-2}_{11/2}$ and seniority $\nu = 2$ are observed experimentally in the Sn isotopes in the mass range $A = 116$–130 [10]. Three quasiparticle $19/2^+$ isomers were observed for the odd-A Sn nuclei with masses between $A = 119$ and $A = 129$ [10]. The $\nu(3s^{-1}_{1/2}1h^{-2}_{11/2})_{19/2^+}$ configuration was assigned to them [11].

This paper reports a measurement of the g-factors of the $19/2^+$ isomer with $T_{1/2} = 4.5(3)\,\mu$s in ^{127}Sn [11] and the 10^+ isomer with $T_{1/2} = 2.69(23)\,\mu$s in ^{128}Sn [12] and addresses the ensuing shell model interpretation. Preliminary results for ^{127}Sn were published in conference proceedings [13,14].

Experimental technique and results. – Neutron-rich nuclei around $A \approx 130$ were produced and spin-oriented in relativistic projectile fragmentation of a ^{136}Xe beam at $E/A = 600\,\mathrm{MeV}/A$ on a $1024\,\mathrm{mg/cm^2}$ Be production target. The primary beam was provided by the GSI heavy-ion synchrotron (SIS) with an average intensity of about 10^8 ions/s ($2 \cdot 10^9$ ions per 10 s spill with a 18 s repetition period). The fully stripped ions were separated and identified with the two-stage high-resolution magnetic zero-degree FRagment Separator (FRS) [15], which was operated in the standard achromatic mode.

A schematic view of the experimental set-up is shown in fig. 1. The fragment selection was optimized for ^{127}Sn. The nuclei of interest were tracked and identified on an event-by-event basis. The mass-to-charge ratio, A/q, was determined by measuring the time of flight with scintillator detectors Sc21 and Sc41 (see fig. 1) and the magnetic rigidity of the beam, $B\rho$. Since the Sn isotopes of interest have A/q values rather close to the primary beam, it was necessary to introduce slits at the S2 position of the FRS in order to cut the primary beam and to optimize the load of the position-sensitive scintillator Sc21, limiting its rate to below 10^6 ions/s. The ionic charge, Z, was determined by the energy loss in the MUlti-Sampling Ionization Chamber (MUSIC) at the final focus, S4. A typical identification plot of the ions which reach the final focus of the FRS, in the present experiment, is shown in fig. 2(a).

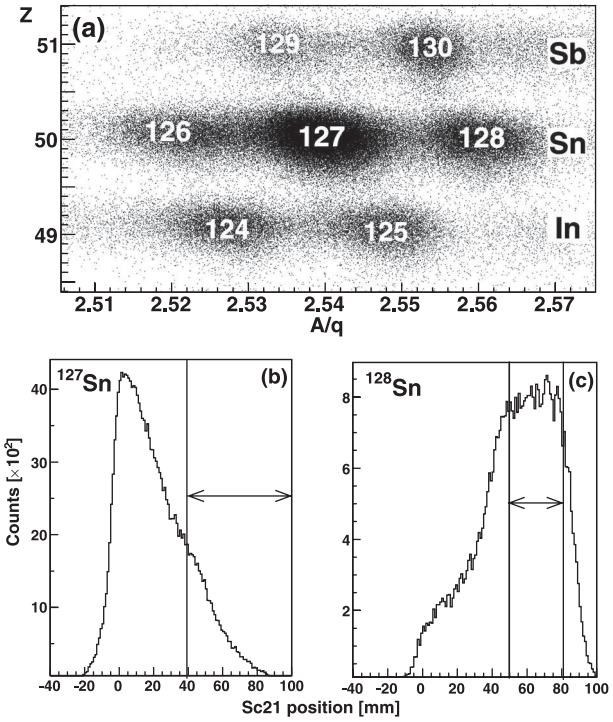

Fig. 2: (a) Ion identification plot. The spots corresponding to different isotopes are labelled with the isotope notation; (b) longitudinal momentum distribution for ^{127}Sn; (c) longitudinal momentum distribution for ^{128}Sn. The momentum distribution is measured with Sc21. The vertical lines in (b) and (c) indicate the momentum selection, which was used in the data analysis.

The isomeric ensemble produced in the projectile fragmentation reaction is spin-oriented, provided that only a specific part of the longitudinal momentum distribution is selected, with prolate alignment at the center and oblate alignment at the wing [2]. The momentum distribution of the fragments was measured by the position-sensitive scintillator detector Sc21 at the second focal plane of FRS (see fig. 1). The momentum distributions for ^{127,128}Sn, which were measured with the FRS setting of the experiment, are presented in fig. 2(b), (c). An asymmetric S2 slit was used in order to suppress the primary beam. It cuts also parts of the momentum distribution for ^{127}Sn (the left wing and part of the center) and ^{128}Sn (the leftmost wing and the right wing).

The selected ions were implanted in a high-purity (99.998%) 2 mm annealed copper plate, fixed to a thick plastic degrader to guarantee that the ions of interest are stopped in the Cu [9]. The Sc42 and Sc43 detectors were used for control of the implantation. The isomeric γ-rays were measured with eight cluster Ge detectors, mounted in the horizontal plane. They were placed at angles of $\pm 45°$, $\pm 75°$, $\pm 105°$ and $\pm 135°$ with respect to the beam direction. Each cluster detector consists of seven tapered Ge crystals, mounted in a common cryostat [16]. The total γ-ray efficiency of the set-up is about 2% at 1 MeV. Ion-γ coincidences between the ions identified with the FRS

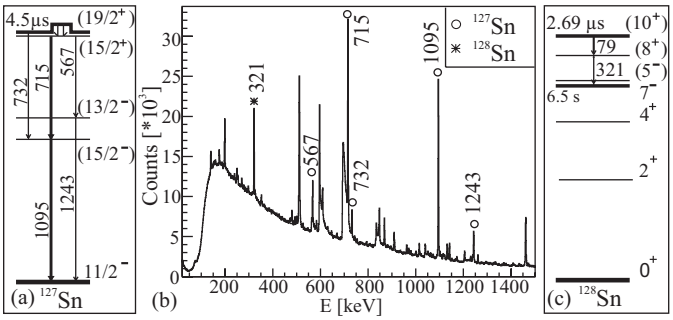

Fig. 3: (a) Partial level scheme of ^{127}Sn showing the decay of $19/2^+$ isomer. (b) Energy spectrum for ^{127}Sn and ^{128}Sn gated on the identification plot. The labelled transitions belong to the decay of the $19/2^+$ isomer in ^{127}Sn and 10^+ isomer in ^{128}Sn. Unlabled transitions are due to different interactions of the beam with the set-up materials and natural radioactivity. (c) Partial level scheme of ^{128}Sn showing the decay of 10^+ isomer.

beam-tracking detectors and the isomeric γ-rays were used as trigger of the data acquisition system in the experiment. The data analysis was done with the SPY/CRACOW [17] and ROOT [18] software. Transitions belonging to the isomeric decay of ^{127,128}Sn can be clearly identified in the γ-ray spectrum in fig. 3. The rapid drop of intensity below 150 keV is due to absorbers that were mounted in front of the Ge detectors in order to suppress the prompt bremsstrahlung flash. Partial level schemes, revealing the isomeric decay of ^{127,128}Sn, are presented in fig. 3(a), (c). Note that the spin-parity assignments in ^{127}Sn are based on the similarity with the level schemes for the lighter Sn isotopes and theoretical calculations [11].

The method of the time-differential perturbed angular distribution (TDPAD) [4,19] was used for the determination of the g-factors of the isomers in ^{127,128}Sn. The spin-oriented isomeric ensemble was implanted in a Cu cubic lattice host. It was placed between the poles of an electromagnet that generated a constant magnetic field $\vec{B}$ in a vertical direction, $B = 0.1200(3)$ T. As a result, the isomeric spin ensemble precesses around the magnetic field with a Larmor frequency $\omega_L = -gB\mu_N/\hbar$, which depends on the value of the magnetic-field strength, B, and the isomeric g-factor.

The intensity of the isomeric transitions was recorded as a function of time. The $t = 0$ signal was generated by an ion impinging on the plastic scintillator Sc41. The frequency of the Larmor precession was extracted from the measured time spectra by sorting experimental $R(t)$ functions for each γ transition, using detectors positioned at symmetric angles, θ and $\theta + \pi$, with respect to the beam line. The $R(t)$-function is defined as

$$R(t,\theta,\omega_L) = \frac{I(t,\theta,\omega_L) - \epsilon I(t,\theta+\pi/2,\omega_L)}{I(t,\theta,\omega_L) + \epsilon I(t,\theta+\pi/2,\omega_L)} = \frac{3A_2B_2}{4+A_2B_2}\sin(2\omega_L t), \quad (1)$$

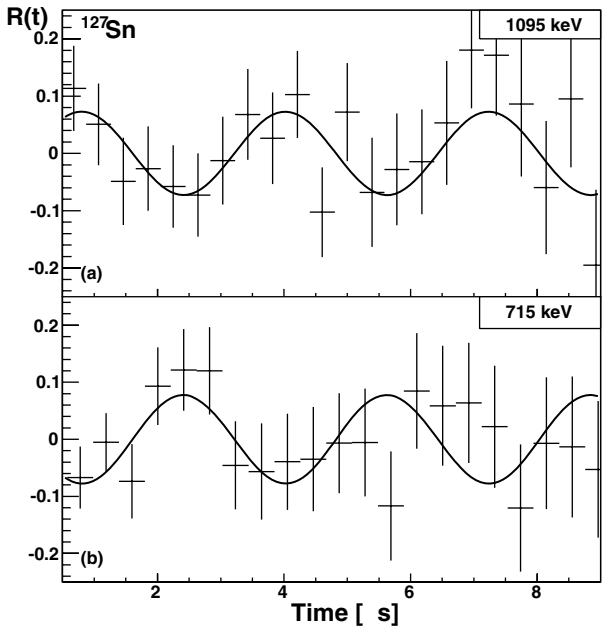

Fig. 4: $R(t)$-function of ^{127}Sn for the 1095 keV (a) and the 715 keV (b) transition at the wing of the momentum distribution.

where $A_2(\gamma)$ is the angular-distribution coefficient, depending on the spin and multipolarity of the γ-rays, B_2 is the orientation parameter, depending on the degree of alignment produced in the reaction and ϵ is a normalization coefficient. The 4th and higher-order terms were neglected, because their contribution is about one order of magnitude smaller. The amplitude of the $R(t)$-function depends on the magnitude of the spin alignment of the isomeric ensemble through the orientation parameter B_2.

To reduce systematic errors, it is customary to compose $R(t)$-functions using data from the same detector for two opposite directions of the magnetic field [20]. The following detector combinations were used (see fig. 1 for the detector labels): $I_1 = (\mathrm{A}+\mathrm{L})\uparrow + (\mathrm{D}+\mathrm{G})\downarrow$ and $I_2 = (\mathrm{A}+\mathrm{L})\downarrow + (\mathrm{D}+\mathrm{G})\uparrow$, where $\uparrow$ and $\downarrow$ denotes opposite (up and down) directions of the applied field. In addition, γ-rays detected by detectors B, C and J, K, which are placed at less sensitive angles, were used in the analysis [13]. $R(t)$-functions for isomeric decay γ-rays of ^{127,128}Sn are presented in fig. 4(a), (b) and fig. 5, respectively. After introducing the momentum selection, about 10^4 ion-γ coincidence events were used in the analysis of each of the transitions presented in figs. 4 and 5. Useful data could be obtained only for relatively long times, typically few hundred ns after the prompt event, due to the atomic bremsstrahlung caused by the stopping of the high-energy (300 MeV/A) ions in the stopper. Even though the TDPAD method is generally applicable to isomeric states with lifetimes in the $\tau = 10$ ns–10 μs range, this "prompt flash" and the detector response effectively limit the applicability range to about 1 μs and longer when working with relativistic ions under similar conditions.

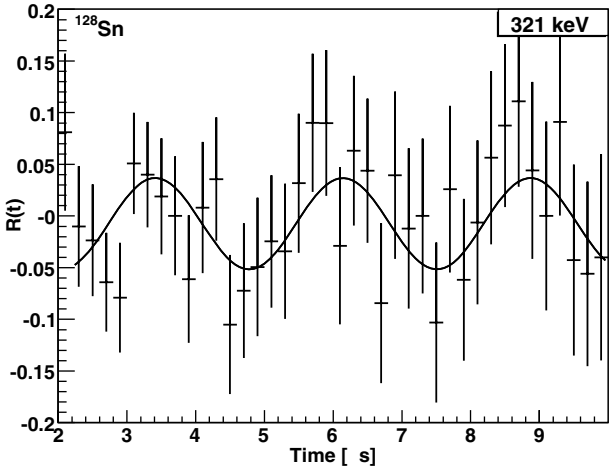

Fig. 5: $R(t)$-function for the 321 keV transition of ^{128}Sn.

Table 1: Experimental g-factors for single-particle (s.p.) states in the Sn isotopes and empirical g-factors for the $19/2^+$ state.

s.p. config.	g_{exp}	$19/2^+$ config.	g_{emp}
$\nu(1h^{-1}_{11/2})$	$-0.242(1)$ [21]		
$\nu(3s^{-1}_{1/2})$	-2.05 [22]	$\nu(3s^{-1}_{1/2}1h^{-2}_{11/2})$	-0.156
$\nu(2d^{-1}_{3/2})$	$+0.505(3)$ [21]	$\nu(2d^{-1}_{3/2}1h^{-2}_{11/2})$	-0.266
$\nu(2d^{-1}_{5/2})$	$-0.432(2)$ [23]	$\nu(2d^{-1}_{5/2}1h^{-2}_{11/2})$	-0.241
$\nu(1g^{-1}_{7/2})$	$+0.195(3)$ [22]	$\nu(1g^{-1}_{7/2}1h^{-2}_{11/2})$	-0.230

The phase of the $R(t)$-function for the 1095 keV, $(15/2^-) \to (11/2^-)$, stretched, $E2$ transition in ^{127}Sn corresponds to a negative sign of the g-factor. The sign has been deduced from the known direction of the magnetic field, assuming negative alignment in the wing of the momentum distribution, which is in line with the measured values [5] and the predictions of the kinematical fragmentation model [2,24]. The 715 keV transition in ^{127}Sn is a mixed $E1/M2$ transition suggested to connect levels with different parities, $(15/2^+) \to (15/2^-)$ and displays an opposite phase compared to the 1095 keV transition. The phase of the $R(t)$-function for the 321 keV $8^+ \to 7^-$ stretched $E1$ transition in ^{128}Sn, which is measured in the centre of the momentum distribution, also corresponds to a negative sign of the g-factor.

The fit of the $R(t)$-functions yields $g(19/2^+;\ ^{127}\mathrm{Sn}) = -0.17(2)$ and $g(10^+;\ ^{128}\mathrm{Sn}) = -0.20(4)$. The relatively large uncertainties are due to the fact that the number of isomeric γ-rays used in the analysis, $\sim 10^4$, is rather low. However, the present results provide a feasibility proof for such experiments. Future improvements in beam intensity and rate-hardened plastic scintillators can result in more accurate results in even farther-from-stability nuclei.

The amplitude of the $R(t)$-function

$$a = \frac{3A_2B_2}{4 + A_2B_2} \qquad (2)$$

Table 2: Experimental and calculated isomeric g-factors for the Sn isotopes.

	I^π	g_{exp}	SM I		SM II	
			g_{free}	g_{eff}	g_{free}	g_{eff}
^{125}Sn	$19/2^+$		-0.214	-0.150	-0.190	-0.133
^{127}Sn	$3/2^+$	$+0.505(3)$ [21]	$+0.933$	$+0.653$	$+0.737$	$+0.516$
	$11/2^-$	$-0.242(1)$ [21]	-0.371	-0.260	-0.342	-0.239
	$19/2^+$	$-0.17(2)^a$	-0.212	-0.148	-0.178	-0.125
^{129}Sn	$19/2^+$		-0.184	-0.129	-0.166	-0.116
^{124}Sn	10^+		-0.349	-0.246	-0.337	-0.236
^{126}Sn	10^+		-0.355	-0.249	-0.340	-0.238
^{128}Sn	8^+		-0.361	-0.253	-0.343	-0.240
	10^+	$-0.20(4)^a$	-0.359	-0.251	-0.344	-0.241
^{130}Sn	10^+		-0.364	-0.255	-0.348	-0.244

[a] Present work.

was deduced as $a = 0.060(15)$ in the case of the 1095 keV transition in ^{127}Sn, which is assumed as a stretched quadrupole transition. This results in an alignment of $-19(5)\%$ in the wing of the momentum distribution, compared to a fully oblate-aligned spin ensemble. The amplitude of the $R(t)$-function of the 312 keV $8^- \to 7^-$ transition in ^{128}Sn (stretched $E1$) is $a = 0.044(16)$, which corresponds to an alignment of $+12(4)\%$ in the centre of the momentum distribution, compared to a fully prolate-aligned spin ensemble.

Discussion. –

^{127}Sn. The excitation energies of the $19/2^+$ isomers in the Sn isotopes display a similar trend to those of the 5^- states in the neighbouring even-even Sn isotopes [10]. The wave function of the 5^- isomers is suggested as an admixture of $\nu(3s^{-1}_{1/2}1h^{-1}_{11/2})$ and $\nu(2d^{-1}_{3/2}1h^{-1}_{11/2})$ terms, the former being the dominant one, as confirmed by g-factor measurements for ^{116,118,120}Sn, $g(5^-, \mathrm{Sn}) \approx -0.066$ [22]. Similarly, the main component of the wave function of the $19/2^+$ isomers is accepted as $\nu(3s^{-1}_{1/2}1h^{-2}_{11/2})$ with an admixture of $\nu(2d^{-1}_{3/2}1h^{-2}_{11/2})$ [11]. In addition, a $\nu(1g^{-1}_{7/2}1h^{-2}_{11/2})$ admixture was suggested in the $19/2^+$ wave function [11], for the explanation of the existence of the 15% 732 keV, $(19/2^+) \to (15/2^-)$, stretched, $M2$ transition (fig. 3(a)). Because of the L-forbiddenness, this transition cannot take place between states with the $\nu(3s^{-1}_{1/2}1h^{-2}_{11/2})$ or $\nu(2d^{-1}_{3/2}1h^{-2}_{11/2})$ and the $\nu 1h^{-3}_{11/2}$ configurations. It can have $M2/E3$ multipolarity, which in turn will involve a $\nu(2d^{-1}_{5/2}1h^{-2}_{11/2})$ admixture in the $19/2^+$ wave function.

The empirical g-factors for these configurations, calculated using the experimental g-factors for one-quasiparticle states in the Sn isotopes, are presented in table 1. The g-factor values for the $\nu 3s^{-1}_{1/2}$, $\nu 2d^{-1}_{5/2}$ and the $\nu 1g^{-1}_{7/2}$ states are known for lighter Sn isotopes.

The measured g-factor $g(19/2^+, ^{127}Sn) = -0.17(2)$ is in good agreement with the suggested main component of the wave function. Within the experimental uncertainty, some configuration mixing might be expected.

^{128}Sn. The 10^+ isomers in the Sn nuclei are suggested to have the $\nu 1h^{-2}_{11/2}$ configuration. The 10^+ microsecond isomer in ^{128}Sn decays to the 8^+ state with a stretched $E2$ transition, which in turn decays via a stretched $E1$ transition to the 7^- isomer ($T_{1/2} = 6.5$ s) [12].

The main configuration of the 7^- states in the even-mass Sn nuclei is $\nu(2d^{-1}_{3/2}1h^{-1}_{11/2})$. A detailed study of the g-factor of this isomer revealed the necessity to consider core-polarization configurations for the $M1$ operator in this region, originating from excitations across the $N = 82$ and $Z = 50$ shells [25].

The 10^+ and 8^+ states are part of $\nu 1h^{-2}_{11/2}$, seniority $\nu = 2$ multiplet. As there are two neutrons on the same orbital, the g-factor of such a configuration is independent of the total spin to which they are coupled and $g_{emp}(\nu 1h^{-2}_{11/2}) = g_{exp}(\nu 1h^{-1}_{11/2}; Sn) = -0.24$ is expected. This value is an average of the measured g-factors in the neighbouring odd-A Sn isotopes. An average value of $g(10^+; Sn) \approx -0.24$ [22] was measured for the 10^+ states in ^{116,118}Sn. The g-factor, $g(10^+, ^{128}Sn) = -0.20(4)$, measured in this experiment is in agreement with these values, but within the observed experimental uncertainty some admixtures originating from core-polarizing excitations might be present in this case, too.

Shell model calculations. Shell model analysis was done starting from two different closed cores. The first model (SM I) assumes ^{132}Sn as a closed core and uses a model space for neutron holes in $3s_{1/2}, 2d_{3/2}, 2d_{5/2}$ and $1g_{7/2}$ from the $N = 4$ shell plus the intruder $1h_{11/2}$ from the $N = 5$ shell. The realistic nucleon-nucleon potential derived from modern meson exchange models was renormalized taking into account the specific nuclear medium to produce the nuclear reaction G-matrix, which was the starting point for a perturbative many-body scheme for deriving shell model interactions [26]. The calculations were done using the CENS software [27]. The experimental

single-hole energies for the orbitals are taken from ^{131}Sn. Calculations of the low-lying levels of ^{127}Sn and ^{129}Sn with the same effective interaction were presented in ref. [28] and the results are in a good agreement with the experimental data.

The second model assumes ^{88}Sr as an inert core and uses the model space for protons $2p_{1/2}, 1g_{9/2}$ and for neutrons $1g_{7/2}, 3s_{1/2}, 2d_{5/2}, 2d_{3/2}, 1h_{11/2}$ [29], *i.e.* the Sn valence space is the same as in SM I. Non-truncated shell model calculations (SM II) were recently performed for the whole Sn region down to ^{124}Sn, using a realistic two-body CD-Bonn interaction according to the method described in ref. [28]. Effective $M1$ operators as described above were used, and calculations were performed with the OXBASH code [30]. The interaction was monopole tuned to reproduce the ^{131}Sn single-hole energies. The calculations of the levels of odd Sn isotopes with the same effective interaction were presented in ref. [31].

Results with both models for g-factors of single-particle states in ^{127}Sn, $19/2^+$ isomers in the odd-A ^{125,127,129}Sn isotopes and 10^+ isomers in even-even ^{124,126,128}Sn isotopes, together with the experimental values, are shown in table 2. Values denoted as g_{free} are calculated with the g-factors for free nucleons, the g_{eff} values are calculated with the effective nucleon g-factors $g_s = 0.7 \cdot g_s^{free}$.

Based on the occupation numbers, the shell model analysis supports the suggested main component of the wave function of the $19/2^+$ isomer. In general, the calculated effective g-factors within both approaches are in agreement with the experimental values. The small differences between the calculated values are mainly due to the different cores, and perhaps to the fact that SM II uses monopole modified interactions.

The calculated g-factors for the 10^+ isomer in ^{128}Sn within both approaches are in a good agreement with the experimental value. The calculations demonstrate an amazing stability for the g-factor value of this state for the $^{124-130}$Sn isotopes. Both approaches reproduce well the g-factors of the $\nu 2d_{3/2}$ and $\nu 1h_{11/2}$ states, but somewhat underestimate the measured g-factor for the $19/2^+$ isomer in ^{127}Sn, when the effective nucleon g-factors are used. This can be due to a $\nu 2d_{5/2}$ admixture in the wave function, 4.7% and 3.5% for SM I and SM II, respectively. It allows a large non-diagonal $\nu 2d_{5/2} \rightarrow \nu 2d_{3/2}$ spin-flip matrix element, a core-polarization contribution that should already be accounted for in the adopted g_s quenching.

Summary. – The measured experimental values for the g-factors of the $19/2^+$ and the 10^+ isomers in ^{127}Sn and ^{128}Sn, respectively, confirm the shell model picture for these nuclei. The experiment provides evidence that the wave functions of these nuclei, which lie close to the doubly magic $^{132}_{50}$Sn$_{82}$, are rather pure. The success of the present technique using relativistic fragments paves the way to measurements of nuclei farther from stability in this mass region.

* * *

This work was supported in part by the EC EURONS RII3-CT-2004-506065, the Bulgarian NSF DID02/16 and DRNF02/5, the Belgian IAP P6-23, the German BMBF 06KY205I, the Spanish Ministerio de Ciencias e Innovación FPA2007-66069 projects and the UK EPSRC.

REFERENCES

[1] Talmi I., *Simple Models of Complex Nuclei, The Shell Model and the Interacting Boson Model* (Harwood Academic Publishers, New York) 1993.
[2] Asahi K. *et al.*, *Phys. Rev. C*, **43** (1991) 456.
[3] Schmidt-Ott W. D. *et al.*, *Z. Phys. A*, **350** (1994) 215.
[4] Georgiev G. *et al.*, *J. Phys. G*, **28** (2002) 2993.
[5] Matea I. *et al.*, *Phys. Rev. Lett.*, **93** (2004) 142503.
[6] Vermeulen N. *et al.*, *Phys. Rev. C*, **75** (2007) 051302(R).
[7] Gaudefroy L. *et al.*, *Phys. Rev. Lett.*, **102** (2009) 092501.
[8] Wollersheim H. J. *et al.*, *Nucl. Instrum. Methods A*, **537** (2005) 637.
[9] Neyens G. *et al.*, *Acta Phys. Pol. B*, **40** (2007) 1237.
[10] Pinston J. A. and Genevey J., *J. Phys. G*, **30** (2004) R57.
[11] Pinston J. A. *et al.*, *Phys. Rev. C*, **61** (2000) 024312.
[12] Fogelberg B. *et al.*, *Nucl. Phys. A*, **352** (1981) 157.
[13] Atanasova L. *et al.*, in *Proceedings of the XXV International Nuclear Theory Workshop, Rila Mountains, Bulgaria*, edited by Dimitrova S. (Diomira, Sofia) 2006, p. 161.
[14] Atanasova L. *et al.*, *Prog. Part. Nucl. Phys.*, **59** (2007) 355.
[15] Geissel H. *et al.*, *Nucl. Instrum. Methods B*, **70** (1992) 286.
[16] Eberth J. *et al.*, *Nucl. Instrum. Methods A*, **369** (1996) 135.
[17] Grebosz J., *Comput. Phys. Commun.*, **176** (2007) 251.
[18] `http://root.cern.ch/drupal/`.
[19] Goldring G. and Hass M., in *Treatise on Heavy Ion Science,* Vol. **3**, edited by Bromley D. Allan (Plenum, New York) 1985, p. 539.
[20] Georgiev G. *et al.*, *Eur. Phys. J. A*, **30** (2006) 351.
[21] Le Blanc F. *et al.*, *Phys. Rev. C*, **72** (2005) 034305.
[22] Stone N. J., *At. Data Nucl. Data Tables*, **90** (2005) 75.
[23] Eberz J. *et al.*, *Z. Phys. A*, **326** (1987) 121.
[24] Daugas J. M. *et al.*, *Phys. Rev. C*, **63** (2001) 064609.
[25] Ilie G. *et al.*, *Phys. Lett. B*, **687** (2010) 305.
[26] Hjorth-Jensen M. *et al.*, *Phys. Rep.*, **261** (1995) 125; Dean D. J. *et al.*, *Prog. Part. Nucl. Phys.*, **53** (2004) 419.
[27] Engeland T. *et al.*, *The CENS Software, a Computational Environment for Nuclear Structure*, `http://www.fys.uio.no/compphys/cp/software.html`.
[28] Gausemel H. *et al.*, *Phys. Rev. C*, **69** (2004) 054307.
[29] Grawe H., in preparation (2010).
[30] Brown B. A. *et al.*, Oxbash for Windows, MSU-NSCL report No. 1289, 2004.
[31] Lozeva R. *et al.*, *Phys. Rev. C*, **77** (2008) 064313.

Eur. Phys. J. Special Topics **150**, 165–168 (2007)

DOI: 10.1140/epjst/e2007-00294-4

THE EUROPEAN PHYSICAL JOURNAL SPECIAL TOPICS

Isomeric decay studies around ^{204}Pt and ^{148}Tb

Zs. Podolyák[1], S.J. Steer[1], S. Pietri[1], E. Werner-Malento[2,3], P.H. Regan[1], D. Rudolph[4], A.B. Garnsworthy[1], R. Hoischen[4], M. Górska[2], J. Gerl[2], H.J. Wollersheim[2], T. Kurtukian-Nieto[5], G. Benzoni[6], F. Becker[2], P. Bednarczyk[2,7], L. Caceres[2,8], P. Doornenbal[2], H. Geissel[2], J. Grębosz[2,7], A. Kelic[2], I. Kojouharov[2], N. Kurz[2], F. Montes[2], W. Prokopowicz[2,5], T. Saito[2], H. Schaffner[2], S. Tashenov[2], A. Heinz[9], M. Pfützner[3], M. Hellström[4], A. Jungclaus[8], L.-L. Andersson[4], L. Atanasova[10], D.L. Balabanski[11], M.A. Bentley[12], B. Blank[13], A. Blazhev[14], C. Brandau[1,2], J. Brown[12], A.M. Bruce[15], F. Camera[6], W.N. Catford[1], I.J. Cullen[1], Zs. Dombrádi[16], E. Estevez[5], C. Fahlander[4], W. Gelletly[1], G. Ilie[14], E.K. Johansson[4], J. Jolie[14], G.A. Jones[1], M. Kmiecik[7], F.G. Kondev[17], S. Lalkovski[10,15], Z. Liu[1], A Maj[7], S. Myalski[7], T. Shizuma[1,18], A.J. Simons[1], S. Schwertel[19], P.M. Walker[1], O. Wieland[6], and B.A. Brown[20]

[1] Department of Physics, University of Surrey, Guildford, GU2 7XH, UK
[2] GSI, Planckstrasse 1, 64291 Darmstadt, Germany
[3] IEP, Warsaw University, Hoża 69, 00681 Warsaw, Poland
[4] Department of Physics, Lund University, 22100 Lund, Sweden
[5] Universidad de Santiago de Compostela, 15706 Santiago de Compostela, Spain
[6] INFN, Universitá degli Studi di Milano, 20133 Milano, Italy
[7] The Henryk Niewodniczański Institute of Nuclear Physics, 31342 Kraków, Poland
[8] Departamento de Fisica Teórica, Universidad Autonoma de Madrid, 28049 Madrid, Spain
[9] WNSL, Yale University, New Haven, CT 06520-8124, USA
[10] Faculty of Physics, University of Sofia, 1164 Sofia, Bulgaria
[11] Inst. for Nucl. Research and Nucl. Energy, Bulgarian Academy of Sciences, 1784 Sofia, Bulgaria
[12] Dept. of Physics, University of York, Heslington, York, Y01 5DD, UK
[13] CENBG, Le Haut Vigneau, BP. 120, 33175 Gradignan Cedex, France
[14] IKP, Universität zu Köln, 50937 Köln, Germany
[15] School of Engineering, University of Brighton, Brighton, BN2 4GJ, UK
[16] Institute for Nuclear Research, ATOMKI, 4001 Debrecen, Hungary
[17] Nuclear Engineering Division, Argonne National Laboratory, Argonne, IL 60439, USA
[18] Japan Atomic Energy Agency, Kyoto 619-0215, Japan
[19] Physik Department E12, Technische Universität München, Garching, Germany
[20] Department of Physics and Astronomy, Michigan State University, East Lansing, MI 48824, USA

Received: January 31, 2007

Abstract. Relativistic energy projectile fragmentation of ^{208}Pb has been used to produce a range of exotic nuclei. The nuclei of interest were studied by detecting delayed gamma rays following the decay of isomeric states. Experimental information on the excited states of the neutron-rich N = 126 nucleus, ^{204}Pt, following internal decay of two isomeric states, was obtained for the first time. In addition, decays from the previously reported isomeric $I = 27\hbar$ and $I = (49/2)\hbar$ states in ^{148}Tb and ^{147}Gd, respectively, have been observed. These isomeric decays represent the highest spin discrete states observed to date following a projectile fragmentation reaction, and opens further the possibility of doing 'high-spin physics' using this technique.

PACS. 25.70.Mn Projectile and target fragmentation – 29.30.Kv X- and gamma-ray spectroscopy

1 Introduction

First results from a major new initiative of experiments focusing on the study of the internal structure of nuclei at the extremes of N/Z ratio using isomer spectroscopy are reported. These experiments represent the first of the Stopped Beam section of the *Rare Isotopes Investigations at GSI* (RISING) project. Exotic nuclei were synthesized using relativistic projectile fragmentation of E/A = 500–1000 MeV beams of ^{58}Ni, ^{107}Ag, ^{208}Pb.

The present paper presents selected highlightss of the initial experimental results from this highly successful campaign, with the focus on heavy systems populated in the fragmentation of the ^{208}Pb projectile. Some results obtained on the N $\sim$ Z nuclei are discussed in [1].

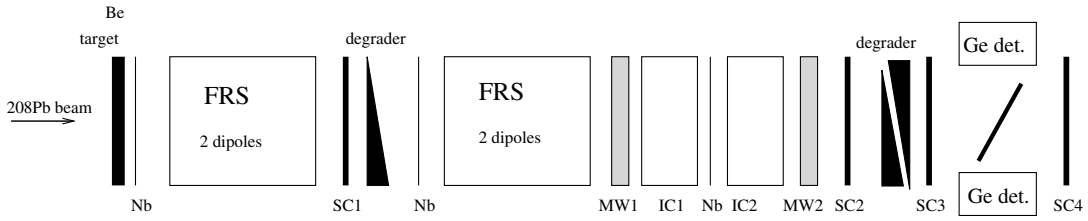

Fig. 1. Schematic view of the experimental setup. For details see the text.

2 Experimental details

Fragmentation has proven to be an efficient tool to produce exotic nuclear species. When projectile fragmentation is combined with high sensitivity gamma detection arrays, structure information can be gained for otherwise inaccessible nuclei. The highest sensitivity is achieved with the so-called isomer decay spectroscopy. In this technique the delayed gamma rays are correlated with the individually identified ions, therefore there is a minimum of background radiation. Information on the excited states populated in this way can be obtained with only some 1000 nuclei produced. Heavy nuclear species were populated in relativistic energy projectile fragmentation. A beryllium target of thickness 2.5 g/cm^2 was bombarded with an E/A = 1 GeV ^{208}Pb beam provided by the SIS accelerator at GSI, Darmstadt, Germany. The nuclei of interest were separated and identified using the FRagment Separator (FRS) [2] operated in standard achromatic mode. The setup is shown in figure 1. The achromatic wedge-shaped aluminum degrader in the intermediate focal plane of the separator had an average thickness of 4900 mg/cm^2. Niobium foils of thicknesses 221 mg/cm^2 and 108 mg/cm^2 were placed after the target and the degrader, respectively, in order to maximise the electron stripping.

The mass-to-charge ratio of the ions, A/q, was determined from the performed time of flight (measured between two scintillator detectors SC1 and SC2) and magnetic rigidity measurements in the second part of the FRS (the ions were tracked using position information from SC1 and the multiwire detectors MW1 and MW2). The energy deposition of the fragments was measured as they passed through two gas ionisation chambers (IC1 and IC2) separated by a 221 mg/cm^2 Nb foil. Following this, they were slowed down in a variable thickness aluminum degrader and finally stopped in a ∼7–9 mm thick plastic catcher. Scintillator detectors were placed both in front of and behind the catcher (SC3 and SC4), allowing the offline suppression of those fragments destroyed in the slowing down process or those which were not stopped in the catcher. The identification of the fragments is based on the determined A/q, the energy loss in the ionisation chambers (≈Z), and the longitudinal position of the nuclei at the intermediate and final focal planes of the FRS. For more details about the identification procedure see [3].

The plastic catcher was surrounded by the high-efficiency, high granularity Stopped RISING γ-ray spectrometer [4]. It consists of 15 Euroball cluster Ge-detectors, and in the present configurations has nearly 4π geometry. Time-correlated gamma decays upto a delay time of 400 μs from individually identified nuclear species have been measured, allowing the clean identification of isomeric decays in a wide range of exotic nuclei. In this simple form (using a passive stopper) the technique is sensitive to isomeric decays with lifetimes between 100 ns and 1 ms. The lower limit arrises form the flightime through the fragment separator (≈300 ns); the upper limit is from the necessity to correlate the delayed gamma rays with the implanted ion. Longer correlation times can be obtained by using active stoppers.

3 Along the N = 126 line

Information on the neutron-rich N = 126 nuclei is very scarce. The lack of information is due to the difficulties in populating these nuclei. Below the doubly magic ^{208}Pb nucleus there is experimental information on only three isotones: ^{207}Tl, ^{206}Hg and ^{205}Au. While in both ^{207}Tl [5] and ^{206}Hg [6] excited states have been observed (including isomeric states, see figure 2), in ^{205}Au only the ground state is known ($I^\pi = (3/2^+)$ [7]).

3.1 ^{206}Hg

The yrast states of ^{206}Hg have been previously studied using deep-inelastic reactions [6]. The partial level scheme together with the dominant shell model configurations is shown in figure 2.

The present observation of isomeric states in ^{206}Hg is important for reaction studies. The delayed gamma-ray spectrum is shown in figure 3. Population of the 10^+ and 5^- isomeric states relative to the ground state, the so called isomeric ratio, will be determined.

^{206}Hg was populated by removing two protons from the ^{208}Pb beam. Non-direct population of ^{206}Hg states, by one proton removal to excites states in ^{207}Tl followed by proton evaporation, involves intermediate states above the neutron evaporation threshold and it is expected to be small [8]. Therefore ^{206}Hg is synthesized in a direct two-proton knockout (also called cold fragmentation) reaction.

Two proton removal cross sections, from E/A = 1 GeV ^{208}Pb on a ^{9}Be target, were calculated by Tostevin [8]. The two-protons were assumed to be uncorrelated and both the stripping and the diffraction mechanisms were considered. The direct population of the individual states 10^+ (configuration $\pi h_{11/2}^{-2}$), 8^+ ($\pi h_{11/2}^{-2}$), 7^- ($\pi h_{11/2}^{-1} d_{3/2}^{-1}$) and

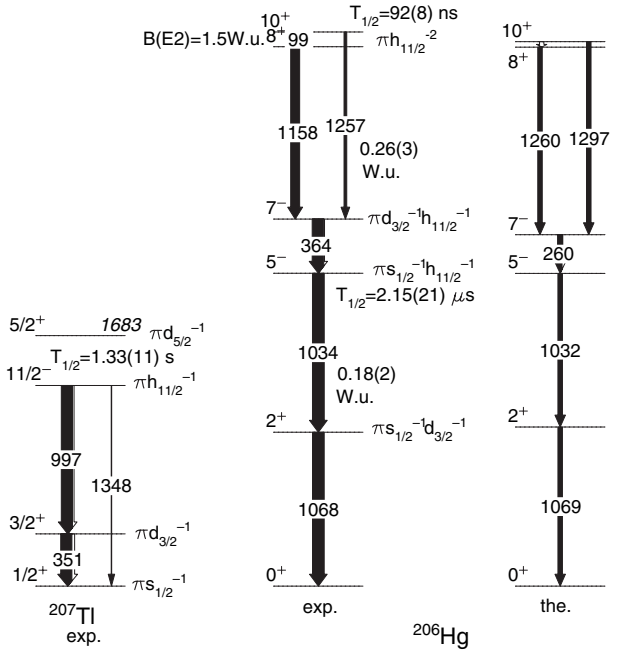

Fig. 2. Partial level schemes of ^{207}Tl [5] and ^{206}Hg [6]. The result of the shell model calculation for ^{206}Hg is shown on the right hand side of the figure.

5^- $(\pi h_{11/2}^{-1} s_{1/2}^{-1})$ has been estimated. The calculated cross sections result in a predicted ratio of isomeric ratios of the 10^+ and 5^- isomers of 21:83 [8]. This value, and the individual isomeric ratios, will be compared with those extracted from the present experiment. Note that the 5^- isomer has been previously observed in a former fragmentation experiment, and an upper limit of the isomeric ratio has been determined [9].

3.2 ^{204}Pt

^{204}Pt has four protons less than the doubly magic ^{208}Pb nucleus. Its yrast structure is expected to be dominated by the proton-hole orbitals $\pi d_{3/2}$, $\pi s_{1/2}$, $\pi h_{11/2}$ and possible $\pi d_{5/2}$ (see level scheme of ^{207}Tl in figure 2.). Its level scheme is expected to be similar to that of ^{206}Hg.

Gamma-ray spectra associated with ^{204}Pt are shown in figure 4. Two isomeric decays have been observed, with a longer lifetime associated to the 872 keV and 1123 keV transitions, and a shorter to the 1061 keV, 1158 keV and 96 keV gamma-lines. Shell-model calculations are being performed using the OXBASH code [10], and results on ^{206}Hg are shown in figure 2. The empirical interaction matrix elements are from [11] and are based on those of Kuo and Herling [12]. The experimental proton-hole energies were taken from the experimental level scheme of ^{207}Tl, as shown in figure 2. There is a rather good agreement between theory and experiment for ^{206}Hg (note that the interaction matrix elements were obtained by fitting on a range of nuclei, including the 2^+ and 5^- states of ^{206}Hg [11]). For ^{204}Pt the interpretation of the results and comparison with shell-model calculations are in progress.

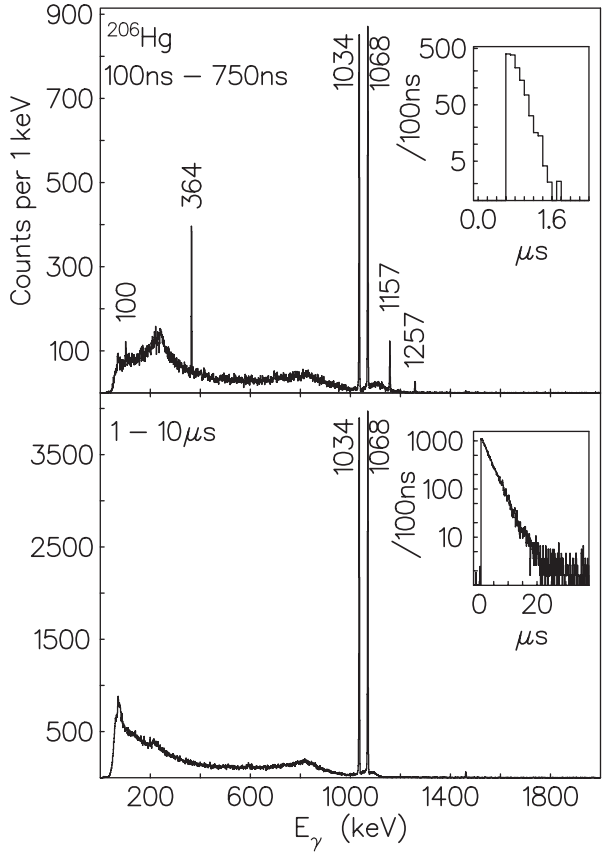

Fig. 3. Delayed gamma-ray spectra associated with ^{206}Hg. Note that the shape of the background around ∼300 keV is unphysical, and it is due to used data analysis method.

4 Population of high-spin states

The fragmentation process can be described by the abrasion-ablation model rather successfully [13]. A key aspect of this fragmentation model is the estimation of the excitation energy and angular momentum of the prefragments. Such information can be obtained by studying the population of long lived states. Experimentally we cannot determine the population of a single state with a given angular momentum, but only the total population of all the states decaying into the level of interest. Therefore, the study of the population at high angular momentum from the tail of the distribution, provides a much more stringent test of the theory than populations at lower angular momenta. Previous studies showed that in order to understand the population of high-spin states two sources of angular momenta have to be considered: from the single-particles knocked out in the abrasion phase of the fragmentation, and a collective angular momentum related to 'friction' (and eventually to the binding energy of the knocked out nucleons) [14].

In order to study the population of isomeric states with high angular momenta a measurement with the magnetic rigidity setting of the FRS centred on ^{147}Gd was performed. Several previously known isomeric states were observed, including the high-spin isomers $I = 27\hbar$ in

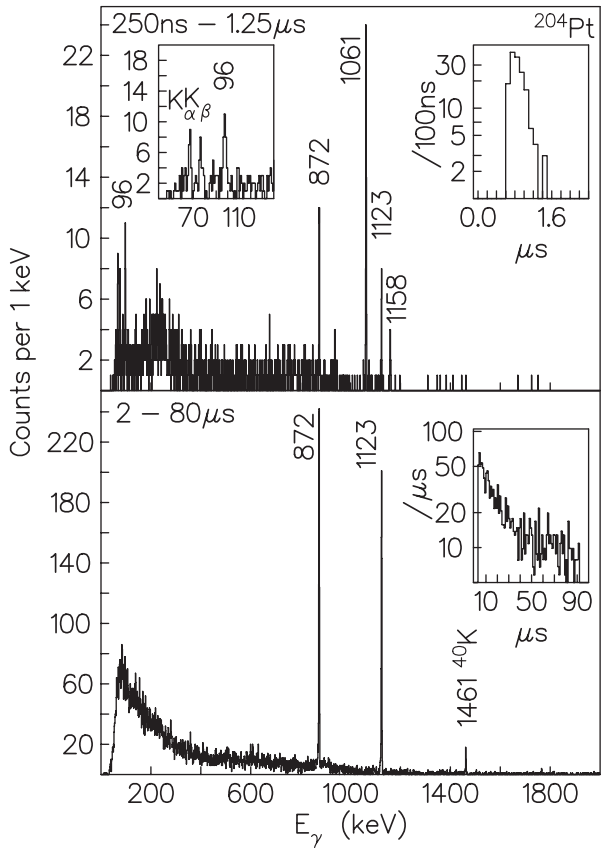

Fig. 4. Delayed gamma-ray spectra associated with ^{204}Pt. Note that the shape of the background around ∼300 keV is unphysical, and it is due to used data analysis method.

^{148}Tb [15] and $I = (49/2)\hbar$ in ^{147}Gd [16] (see figure 5). These are the highest spin discrete states observed to date following a projectile fragmentation reaction. The isomeric ratios will be determined and compared with predictions of different fragmentation models.

5 Conclusions

A wide range of nuclei have been populated in fragmentation of relativistic energy ^{208}Pb. The experiment has been performed at the FRS-RISING setup at GSI and was devoted to both nuclear structure and fragmentation reaction studies. Preliminary results have been presented, with the highlights on: (i) nuclei along the N = 126 line, especially the first information on excited states in the four proton-hole nucleus ^{204}Pt, and (ii) high angular momentum states populated in the region around ^{148}Tb.

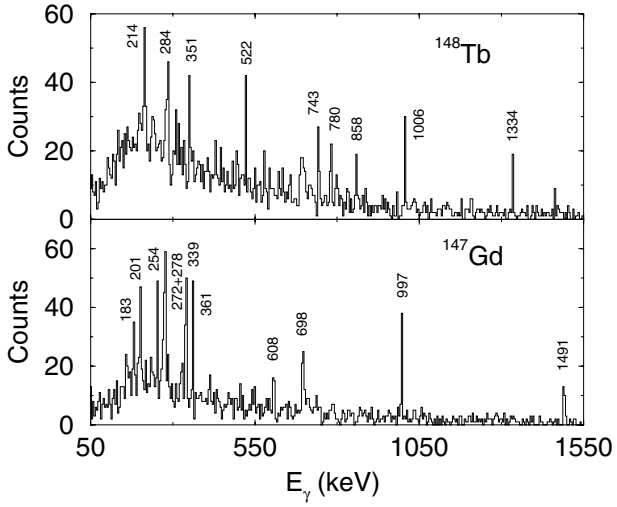

Fig. 5. Delayed gamma-ray spectra associated with ^{148}Tb and ^{147}Gd. The transitions labelled with their energies in keV originate from the decay of the high spin isomers $I = 27\hbar$ in ^{148}Tb [15] and $I = 49/2\hbar$ in ^{147}Gd [16], respectively.

This work is supported by EURONS European Commission contract No. 506065, EPRSC(UK), the Swedish Research Council, the Polish Ministry of Science and Higher Education, the Bulgarian Science Fund and the US Department of Energy.

References

1. D. Rudolph et al. (this conference)
2. H. Geissel et al., Nucl. Instrum. Meth. Phys. Res. Sect. B **70**, 286 (1992)
3. K. Gladnishki et al., Phys. Rev. C **69**, 024617 (2004)
4. S. Pietri et al. (this conference)
5. D. Eccleshall, M.J.L.Yates, Phys. Lett. **19**, 301 (1965)
6. B. Fornal et al., Phys. Rev. Lett. **87**, 212501 (2001)
7. Ch. Wennemann et al., Z. Phys. A **347**, 185 (1994); F.G. Kondev, Nucl. Data Sheets **101**, 521 (2004)
8. J. Tostevin, in AIP Conf. Proc., **819**, 523 (2006)
9. M. Pfützner et al., Phys. Rev. C **65**, 064604 (2002)
10. B.A. Brown, A. Etchegoyen, W.D.M. Rae, Computer code OXBASH, MSU-NSCL, Report No. 524 (1986)
11. L. Rydström et al., Nucl. Phys. A **512**, 217 (1990)
12. T.T.S. Kuo, G.H. Herling, Naval Research Laboratory, Report No. 2259 (Washington, DC, 1971)
13. J.-J. Gaimard, K.-H. Schmidt, Nucl. Phys. A **531**, 709 (1991)
14. Zs. Podolyák et al., Phys. Lett. B **632**, 203 (2006)
15. E. Ideguchi et al., Z. Phys. A **352**, 363 (1995)
16. R. Broda et al., Z. Phys. A **285**, 423 (1978); Z. Phys. A **305**, 281 (1982)

Eur. Phys. J. Special Topics **150**, 173–176 (2007)

DOI: 10.1140/epjst/e2007-00296-2

THE EUROPEAN PHYSICAL JOURNAL SPECIAL TOPICS

Exciting isomers from the first stopped-beam RISING campaign

D. Rudolph[1], S. Pietri[2], Zs. Podolyák[2], P.H. Regan[2], A.B. Garnsworthy[2,3], R. Hoischen[1], S.J. Steer[2], F. Becker[4], P. Bednarczyk[4,5], L. Caceres[4,6], P. Doornenbal[4], H. Geissel[4], J. Gerl[4], M. Górska[4], J. Grębosz[5,4], A. Kelic[4], I. Kojouharov[4], N. Kurz[4], F. Montes[4], W. Prokopowicz[4,5], T. Saito[4], H. Schaffner[4], S. Tashenov[4], E. Werner-Malento[4,7], H.J. Wollersheim[4], L.-L. Andersson[1], L. Atanasova[8], D.L. Balabanski[9], M.A. Bentley[10], G. Benzoni[11], B. Blank[12], A. Blazhev[13], C. Brandau[2,4], J.R. Brown[10], A.M. Bruce[14], F. Camera[11], W.N. Catford[2], I.J. Cullen[2], Zs. Dombrádi[15], E. Estevez[16], C. Fahlander[1], W. Gelletly[2], A. Heinz[3], M. Hellström[1], G. Ilie[13], E.K. Johansson[1], J. Jolie[13], G.A. Jones[2], A. Jungclaus[6], M. Kmiecik[5], F.G. Kondev[17], T. Kurtukian-Nieto[16], S. Lalkovski[8], Z. Liu[2], A. Maj[5], S. Myalski[5], M. Pfützner[7], T. Shizuma[2,18], A.J. Simons[2], S. Schwertel[19], P.M. Walker[2], and O. Wieland[11]

[1] Department of Physics, Lund University, 22100 Lund, Sweden
[2] Department of Physics, University of Surrey, Guildford, GU2 7XH, UK
[3] WNSL, Yale University, New Haven, CT 06520-8124, USA
[4] Gesellschaft für Schwerionenforschung mbH, 64291 Darmstadt, Germany
[5] The Henryk Niewodniczański Institute of Nuclear Physics (IFJ PAN), 31342 Kraków, Poland
[6] Departamento de Fisica Teórica, Universidad Autonoma de Madrid, 28049 Madrid, Spain
[7] Institute of Experimental Physics, Warsaw University, 00681 Warsaw, Poland
[8] Faculty of Physics, University of Sofia, 1164 Sofia, Bulgaria
[9] Institute for Nuclear Research and Nuclear Energy, Bulgarian Academy of Sciences, 1784 Sofia, Bulgaria
[10] Department of Physics, University of York, York, Y01 5DD, UK
[11] INFN, Universitá degli Studi di Milano, 20133 Milano, Italy
[12] CEN Bordeaux-Gradignan, 33175 Gradignan Cedex, France
[13] Institut für Kernphysik, Universität zu Köln, 50937 Köln, Germany
[14] School of Engineering, University of Brighton, Brighton, BN2 4GJ, UK
[15] Institute for Nuclear Research, Debrecen, 4001 Debrecen, Hungary
[16] Universidad de Santiago de Compostela, 15706 Santiago de Compostela, Spain
[17] Nuclear Engineering Division, Argonne National Laboratory, Argonne, IL 60439, USA
[18] Japan Atomic Energy Agency, Kyoto 619-0215, Japan
[19] Physik Department E12, Technische Universität München, 85748 Garching, Germany

Received: January 31, 2007

Abstract. First results are reported from a major new initiative of experiments, which focus on nuclear structure studies at extreme isospin values by means of isomer spectroscopy. The experiments represent the first part of the so-called stopped-beam campaign within the Rare ISotope INvestigations at GSI (RISING) project. Time-correlated γ decays from individually identified nuclear species have been measured, allowing the clean identification of isomeric decays in a wide range of exotic nuclei both at the proton drip-line and in heavy, neutron-rich systems. An overview of the experimental technique will be given, together with the performance of the new germanium detector array and future research plans for the collaboration.

PACS. 23.20.-g – 23.50.+z – 25.70.Mn – 27.40.+z – 27.50.+e

1 Introduction

A central topic in contemporary nuclear structure physics is the investigation of exotic nuclear matter far from the line of β stability. An important tool in these studies is γ-ray spectroscopy, providing valuable fingerprints of these exotic nuclei and, subsequently, revealing information on their internal structure. *Rare ISotope INvestigations at GSI* (RISING) combine the existing *FRagment Separator* (FRS) [1] – to discriminate radioactive nuclear beam species – with primarily fifteen high-efficiency CLUSTER germanium detectors [2] for γ-ray detection.

RISING started in 2003 with the so-called fast-beam campaign, within which exotic nuclei were studied by means of relativistic Coulomb excitation, secondary fragmentation, or knock-out reactions [3,4]. In late 2005 these experiments were followed by the g-RISING campaign aiming at the measurement of magnetic moments of isomeric states populated by either fragmentation reactions or relativistic fission of heavy primary beam particles. In the

Table 1. Summary of the main characteristics of the experiments performed within the passive-stopper part of the stopped-beam RISING campaign.

Focus	Aim	Primary Beam	Spokesperson	Date
^{86}Tc	$T = 0 - T = 1$ competition in heavy odd-odd $N = Z$ nuclei	^{107}Ag at 750 AMeV	P.H. Regan	02/06
^{204}Pt	Shell-structure south of ^{208}Pb	^{208}Pb at 1000 AMeV	Zs. Podolyák	02/06
^{54}Ni	Isospin symmetry and effective charges near ^{56}Ni	^{58}Ni at 550 AMeV	D. Rudolph	03/06
^{130}Cd	Search for the 8^+ $\pi(g_{9/2})^{-2}$ isomer in $N = 82$ ^{130}Cd	^{136}Xe at 700 AMeV	A. Jungclaus	06/06
^{130}Cd	Evolution of shell structure near ^{132}Sn	^{238}U at 650 AMeV	M. Górska & M. Pfützner	07/06
^{110}Zr	Dynamical symmetries in neutron-rich Zr isotopes	^{238}U at 750 AMeV	A.M. Bruce	12/06

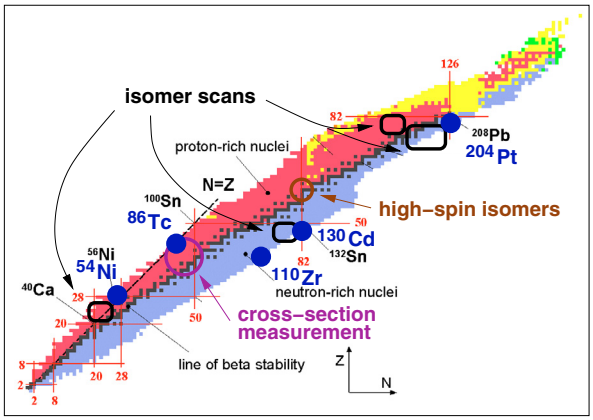

Fig. 1. Overview of the main aims and additional studies (to be) performed within the passive-stopper part of the stopped-beam RISING campaign. See also Table 1.

beginning of 2006 RISING was reconfigured once more to enable the so-called stopped-beam campaign. This campaign has two major incentives, namely (i) to identify and study electromagnetic decays of metastable, excited nuclear states, and (ii) measure γ rays following β decays to excited states into the daughter nuclei. In both cases, the nuclei are implanted and stopped in the center of the RISING array; either in a passive stopper material, such as metal or plastic plates, or in the future in an active stopper material in form of segmented silicon detectors.

This contribution focuses on a summary and some first results of the first passive-stopper, stopped-beam RISING campaign. More information is provided in [5,6].

2 Experiments

An overview of the topics and main characteristics of the RISING experiments within the passive-stopper, stopped-beam campaign is presented in Table 1 and figure 1. All six experiments aim at nuclei located at the present border of knowledge and yield for γ-ray spectroscopy. The two experiments on the neutron-deficient side of the nuclidic chart shall reveal information on isospin symmetry aspects of the effective nuclear force, while the four experiments on the neutron-rich side intend to probe the evolution of shell structure far from stability. These topics are mainly investigated by means of nuclei, which have few nucleon holes with respect to "classical", doubly-magic nuclei such as ^{56}Ni, ^{132}Sn, and ^{208}Pb.

The experiments performed so far have all been very succesful for the primary goals outlined above: The predicted isomeric states could be identified in ^{54}Ni, ^{86}Tc, ^{130}Cd, and ^{204}Pt. Furthermore, each experiment was able to allocate time for a number of secondary goals, which are also indicated in figure 1. For example, several surveys for new isomers were performed as well as cross-section measurements and quests for high-spin states populated in fragmentation reactions (cf. [5,6]).

The nuclei of interest were produced by either fragmentation reactions or relativistic fission of primary beams (cf. Table 1) provided by the SIS accelerator at GSI, Darmstadt, Germany. These beams hit beryllium targets of varying thicknesses between 1.0 and 4.0 g/cm^2. Subsequently, the reaction products were selected by means of a $B\rho - \Delta E - B\rho$ technique in the FRS [1]. The identification in terms of mass A and proton number Z of each transmitted ion is performed with a suite of detector elements placed at the intermediate S2 and final S4 focus of the FRS (cf. [6] for one specific example).

A photograph of the S4 set-up taken at the end of the first part of the campaign is provided in figure 2. It shows the respective detector elements as well as the RISING Ge-array. The secondary beam including the nuclear species of interest enters the picture at the bottom right. It first passes two multiwire chambers (MW41 and MW42) and two ionization chambers (MUSIC41 and MUSIC42). The multiwire chambers yield position and incident angle of the individual ions, while their differential energy loss in the ionization chambers provides their proton number, Z. The following scintillator SC41 provides both the trigger signal for the data acquisition, the start signal for the γ-ray timing, and the logic start signal of the time-of-flight measurement between S2 and S4, from which the mass-to-charge ratio A/Q of the ions can be derived. Note that $Q = Z$ for most of the experiments. The ions are then slowed down in an aluminum degrader with variable thickness to achieve proper implantion in a plastic, beryllium, or copper stopper "foil" (catcher). These have thicknesses of a few millimeters and are optimized for the respective experiment. The catcher is hidden in the center of the encircled RISING Ge-array in figure 2. Scintillation detectors SC42 and SC43 are placed before

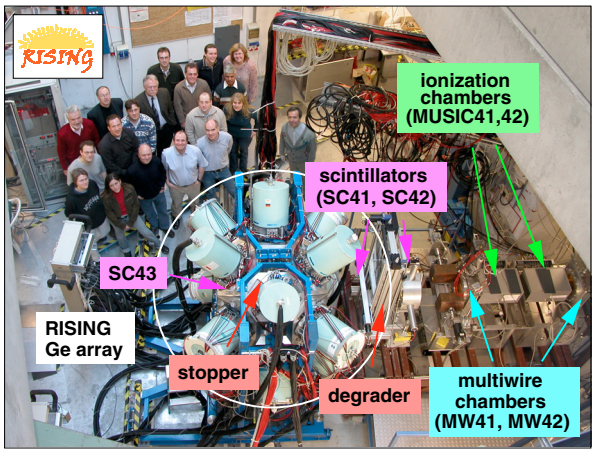

Fig. 2. Focal-plane set-up of the stopped-beam RISING campaign. See text for details.

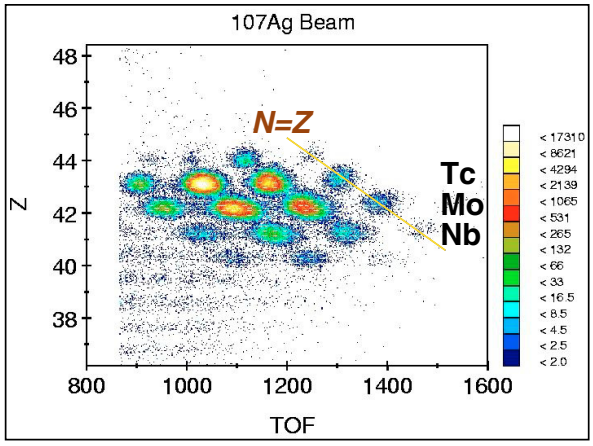

Fig. 3. Identification of isotopes reaching the S4 focal plane of the FRS for the ^{86}Tc setting.

and behind the catcher to allow for suppression of ions having been destroyed during the slowing down process or passing through the catcher, respectively, in the offline analysis.

The RISING Ge-array comprises fifteen CLUSTER germanium detectors [2], i.e., a total of 105 Ge crystals. In the stopped-beam configuration the CLUSTER detectors are arranged in three rings of five detectors at central angles of 51°, 90°, and 129° with respect to the secondary beam direction. The distance of the crystals from the center of the S4 focal plane amounts to ∼21 cm. Hence, the array combines high efficiency with high granularity. Notably, the latter proved to be extremely important for dealing with the so-called "prompt flash", which is radiation emitted while the residues slow down in the catcher. Depending on reaction and secondary beam energy, only five to ten crystals were affected in a given event, and could thus not be used to detect isomeric γ-rays.

Another major step is the digital processing of energy and timing signals of the 105 Ge crystals using thirty 4-channel XIA Digital Gamma Finder (DGF) modules, i.e., two per CLUSTER. These modules include an

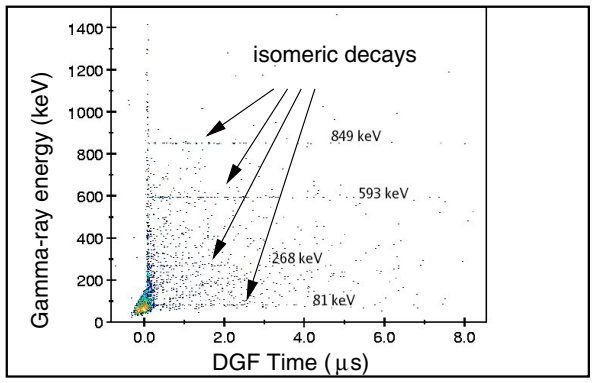

Fig. 4. Correlation matrix between γ-ray energies and times following implantations of ^{86}Tc in the stopper. Time zero of the implantation is given by the intense, vertical line at channel number ≈ 1008. Delayed γ-ray transition are seen as horizontal lines fading out towards longer and longer times.

internal 40 MHz clock, which allows for time stamping of the γ-ray events in steps of 25 ns. For time $t = 0$ reference, the SC41 trigger signal was also processed in three DGF channels. For both short-lived isomers and redundancy, a conventional timing branch is installed in parallel and digitized with a short-range ($t \leq 1$ μs) and a long-range ($t \leq 0.8$ ms) VME TDC. If the isomer survives the 150–200 ns flight time through the FRS, the γ-ray set-up was sensitive to isomeric decays in the range of about 10 ns to 1 ms. See [5] for more information on these issues.

3 First results

The first step in the analysis aims at event-by-event isotope identification of the secondary beam particles. Figure 3 provides a typical example, taken from the very first experiment within the campaign. A number of Nb, Mo, and Tc isotopes can be discriminated in a scatter plot of Z determined from the ionization chambers vs. time-of-flight (TOF) between the S2 and S4 areas. Here, the focus lies on the odd-odd $N = Z$ nuclei ^{86}Tc [7] and ^{82}Nb.

For a selected isotope, the next step implies the construction of a correlation matrix between γ-ray energy and (delayed) time of its observation relative to the implantation of the ions in the catcher. This is illustrated in figure 4 for the case of ^{86}Tc. The vertical line on the left hand side marks the "prompt flash", i.e., implantation time $t = 0$, while fading, horizontal lines (here: E_γ = 81, 268, 593, and 849 keV) indicate decays from isomeric states.

The preliminary results for ^{82}Nb and ^{86}Tc include good candidates for the 2^+ $T = 1$ isobaric analogue states of ^{82}Zr and ^{86}Mo, respectively, while the observed isomeric states most likely have negative parity, which is in line with available Nilsson orbitals close to the Fermi surface [8,9]. The final results will thus probe fundamental isospin $T = 0$ and $T = 1$ competition (cf. [10–12]).

Starting from isotope selected γ-ray energy-time correlations as displayed in figure 4, time spectra can be produced for selected γ rays, which are then used to derive the

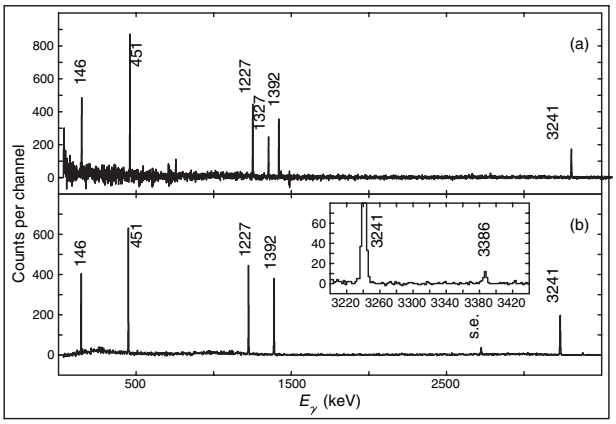

Fig. 5. Panel (a) provides a γ-ray singles spectrum in the time range 0.05 μs $\leq t \leq$ 1.0 μs following the implantation of ^{54}Ni ions in the stopper. Panel (b) is a $\gamma\gamma$ correlation spectrum in coincidence with one of the 451, 1227, or 1392 keV transitions in ^{54}Ni. The same timing conditions as for panel (a) were applied, but the FRS gates were less restrictive.

half-lives of the isomers. In turn, clean γ-ray energy spectra and, provided there is sufficient statistics, $\gamma\gamma$ correlation matrices can be produced by choosing proper timing windows. This is illustrated in the case of ^{54}Ni in figure 5. The top spectrum reveals six delayed γ-ray transitions at 146, 451, 1227, 1327, 1392, and 3241 keV, all having the same lifetime of $\tau \sim 220$ ns. Note that the 451, 1227, and 1392 keV lines are known to belong to ^{54}Ni, representing the $6^+ \rightarrow 4^+ \rightarrow 2^+ \rightarrow 0^+$ cascade in that nucleus [13–15]. The 146 and 3241 keV lines are suggested to be the $10^+ \rightarrow 8^+$ and $8^+ \rightarrow 6^+$ transitions, at first based on mirror symmetry to ^{54}Fe, which has a well established isomeric 10^+ state with $\tau = 525(10)$ ns [16]. More reliably, they are found in coincidence with the known cascade, which is proven by figure 5(b). Here, another weak but distinct line can be discriminated at 3386 keV, which marks the $10^+ \rightarrow 6^+$ $E4$ branch of the isomeric decay in ^{54}Ni.

Interestingly, the 1327 keV line seen clearly in figure 5(a) is absent in figure 5(b). Since it exhibits (within uncertainties) the same half-life as the other transitions and because it fits in energy, we associate it with the $9/2^- \rightarrow 7/2^-$ ground-state transition in ^{53}Co. The $9/2^-$ state in ^{53}Co can be populated with a direct proton decay of 1.28 MeV from the 10^+ isomer in ^{54}Ni. This would be the first (indirect) evidence for proton emission following a fragmentation reaction and bring the associated research field back to its roots, since direct proton decay was first observed in ^{53m}Co in 1970 [17].

4 Summary and outlook

To summarize, the first part of the RISING stopped-beam campaign was highly succesful by discriminating in part long-sought isomeric states in ^{54}Ni, ^{82}Nb, ^{86}Tc, ^{130}Cd, and ^{204}Pt. As an unexpected highlight, the first proton-emitting state following fragmentation reactions could be established in ^{54}Ni. In addition, the data comprise isomeric states in numerous neutron-deficient and neutron-rich nuclei, which will allow for detailed and systematic investigations of the fragmentation and relativistic fission processes, mainly by means of isomeric ratios (cf. [18] and Refs. therein). Here, the observation of an isomeric 27^+ state in ^{148}Tb sets a new high-spin world record for fragmentation reactions (cf. [6]).

At present (August 2006), the passive-stopper part is envisaged to be followed by a series of active-stopper experiments in 2007. These include isospin symmetry tests by means of comparing Gamow-Teller strengths derived from β decay and charge-exchange reactions, related proton-neutron pairing effects on β decay beyond $N = Z$, studies of the evolution of collectivity south of ^{208}Pb, and, last but not least, a revisit of the ^{100}Sn region.

The authors gratefully acknowledge the outstanding work of the GSI accelerator and ion-source crews in providing the experiments with the envisaged high beam intensities. This work is supported by the European Commission contract No. 506065 (EURONS), the Swedish Research Council, EPSRC (United Kingdom), the German BMBF, the Polish Ministry of Science and Higher Education, the Bulgarian Science Fund, the Spanish, Italian, and French science councils, and the US Department of Energy.

References

1. H. Geissel et al., Nucl. Instrum. Meth. B **70**, 286 (1992)
2. J. Eberth et al., Nucl. Instrum. Meth. A **369**, 135 (1996)
3. H.J. Wollersheim et al., Nucl. Instrum. Meth. A **537**, 637 (2005)
4. J. Gerl et al. (this conference)
5. S. Pietri et al. (this conference)
6. Zs. Podolyák et al. (this conference)
7. C. Chandler et al., Phys. Rev. C **61**, 044309 (2000)
8. A.B. Garnsworthy et al., Acta Phys. Pol. **38**, 1265 (2007) (submitted to Phys. Rev. Lett.)
9. L.S. Cáceres et al., Acta Phys. Pol. **38**, 1271 (2007)
10. J. Jänecke, T.W. O'Donnell, Phys. Lett. B **605**, 87 (2005)
11. B.S. Nara Singh et al. (this conference)
12. P. van Isacker (this conference)
13. K.L. Yurkewicz et al., Phys. Rev. C **70**, 054319 (2004)
14. K. Yamada et al., Eur. Phys. J. A **25**, 409 (2005)
15. A. Gadea et al., Phys. Rev. Lett. **97**, 152501 (2006)
16. J. Huo et al., Nucl. Data Sheets **68**, 887 (1993)
17. K.P. Jackson et al., Phys. Lett. B **33**, 281 (1970); J. Cerny et al., Phys. Lett. B **33**, 284 (1970)
18. Zs. Podolyák et al., Phys. Lett. B **632**, 203 (2006)

Eur. Phys. J. Special Topics **150**, 319–320 (2007)

DOI: 10.1140/epjst/e2007-00336-y

THE EUROPEAN PHYSICAL JOURNAL SPECIAL TOPICS

Experimental details of the Stopped Beam RISING campaign

S. Pietri[1], P.H. Rega[1], Zs. Podolyák[1], A. Jungclaus[2], M. Pfützner[3], D. Rudolph[4], A.B. Garnsworthy[1,5], S.J. Steer[1], R. Hoischen[4], M. Górska[6], J. Gerl[6], H.J. Wollersheim[6], I. Kojouharov[6], H. Schaffner[6], J. Gręboszˇ[6,7], F. Becker[6], P. Bednarczyk[6,7], L. Caceres[2,6], P. Doornenbal[6], H. Geissel[6], A. Kelic[6], N. Kurz[6], F. Montes[6], W. Prokopowicz[6,8], T. Saito[6], S. Tashenov[6], E. Werner-Malento[6,7], and W. Gelletly[1], for the Stopped Beam RISING Collaboration

[1] Department of Physics, University of Surrey, Guildford, GU2 7XH, UK
[2] Departamento de Fisica Teórica, Universidad Autonoma de Madrid, 28049 Madrid, Spain
[3] IEP, Warsaw University, Hoża 69, 00681 Poland
[4] Department of Physics, Lund University, 22100 Lund, Sweden
[5] WNSL, Yale University, New Haven, CT 06520-8124, USA
[6] GSI, Planckstrasse 1, 64291 Darmstadt, Germany
[7] The Henryk Niewodniczański Institute of Nuclear Physics, 31342 Kraków, Poland
[8] Jagelonian University, 31342 Kraców, Poland

Received: January 31, 2007

Abstract. The RISING (Rare ISotope INvestigations at GSI) project constitutes a major pan-european initiative to study nuclear structure in exotic nuclei. A brief outline of the technical details specific to studies of isomeric decays following relativistic projectile fragmentation reactions is presented.

1 Introduction

The motivation behind the RISING collaboration is to utilise relativistic energy stable beams produced by the SIS synchrotron at GSI to synthesise exotic nuclei via projectile fragmentation which can then be studied via gamma-ray spectroscopic techniques. The GSI Fragment Separator (FRS) [1] allows the identification of the exotic secondary species of interest. A previous configuration of the RISING germanium detector array has been used to study in-beam γ-ray spectroscopy at relativistic energies [2]. In February 2006 the RISING detectors were moved to the Stopped Beam configuration which is the focus of this brief report. In this configuration, the RISING array consists of fifteen, seven-element, Euroball IV germanium 'cluster' detectors, mounted in a high-efficiency, close packed geometry around the final focal point of the FRS. The nuclei of interest were implanted in a series of passive stoppers made from either perspex, copper or berylium placed in the centre of the array. Gamma-ray transitions depopulating isomeric states could then be observed using the technique outlined in [3–5]. Reports of the first physics results obtained in the 2006 Stopped Beam campaign can be found in [6,7]. A brief outline of the technical details and performance characteristics of the RISING array are presented below.

2 Technical details

2.1 Production, selection and identification of exotic nuclei

Exotic secondary beams were produced using the projectile fragmentation of high-energy stable beams from the SIS synchrotron at GSI on thick ($\sim$g/cm^2) ^{9}Be targets. The FRagment Separator (FRS) [1] was used in achromatic mode for the selection and identification of the reaction products using standard time of flight and energy loss techniques. Particle identification was achieved by the use of plastic scintillators at the middle and final focal points to define the magnetic rigidities and velocities of the secondary ions. MUlti Sampling Ionization Chambers (MUSIC) at the end of the FRS provided energy loss signals from which the atomic number of the incoming ion could be deduced. Details of the particle identification procedure can be found in [6].

2.2 The germanium array geometry and electronics

In its Stopped Beam configuration the RISING array ([7]) comprises fifteen, seven-element germanium cluster detectors [8]. The detectors are placed in three angular rings of five detectors at 51, 90 and 129 degrees to the primary

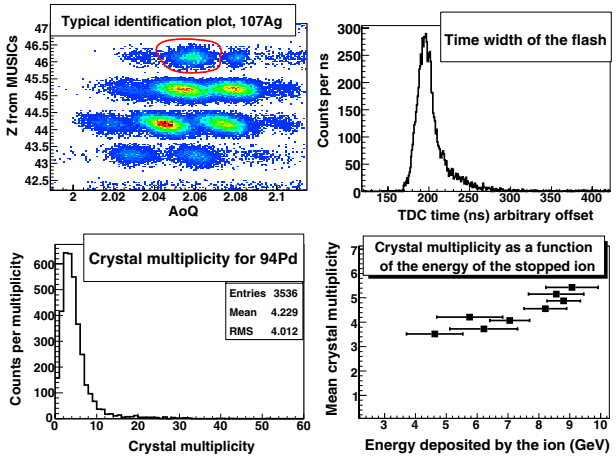

Fig. 1. (Upper left) Particle identification spectrum showing production of ^{94}Pd (highlighted ion) following the fragmentation of ^{107}Ag ions. (Upper right) Width of the prompt flash in time. (Lower left) Measured prompt crystal multiplicity in RISING Array for the ^{94}Pd. (Lower right) Mean crystal multiplicity of the prompt flash as a function of the energy they deposit in the stopper, see text for details.

beam axis. The average distance of the detectors to the centre of the array was approximately 22 cm. The photopeak efficiency of the array as measured using a standard ^{137}Cs source placed at the stopper was approximately 15% at 661 keV. Each individual germanium detector had two parallel pre-amplifier energy outputs which were sent to two separate branches of the electronics. One was used in the fully 'digital' branch and provided the input signal for 105 Digital Gamma Finder(DGF-4C) modules [9]. Three parallel CAMAC crates, each holding ten, quad-input modules were used for this part of the electronics. The individual DGF channel triggers were validated by a master trigger signal generated from a fast plastic scintilator detector at the FRS focal point. This signal was also sent to a DGF channel in each crate in order to provide an internal check of the synchronisation of the DGF clocks and also to provide a time-difference measurement between the arrival of an ion in the plastic scintillator and the measurement of a delayed gamma-ray via the DGF gamma time signal. The clock frequency of the DGF was 40 MHz (i.e., 25 ns time steps). The second output from the germanium preamplifier was sent to an analogue timing branch which was composed of a standard TFA-CFD-TDC timing circuit. The output of the CFD was sent to two seperate TDC modules, one 'short-range' (1 μs full range and 0.31 ns/channel step) and the other 'long range' (up to 800 μs and a 0.73 ns/channel step). The analogue branch allowed a precise definition of shorter-lived ($\sim$10 ns) isomers.

3 Array performance

Stopping ions with energies of several GeV in front of a high-efficiency germanium array such as RISING has a problem due to the production of atomic radiation (the so-called 'prompt flash'). This can cause multiple germanium detectors to fire with the prompt arrival of the ion and thus significantly reduces the effective efficiency for the measurement of delayed isomeric decays in the same event. This was a major concern in the previous fragmentation isomer campaign at GSI (see [4]) causing losses of up to 80% of the effective gamma-ray efficiency. The high granularity of the 105 element RISING array was intended to help to improve this problem. As in the previous campaign the current data show that the multiplicity of the prompt flash (i.e. number of detector elements which fire) is dependent on the energy of the ions as they implant in the stopper (see figure 1). Note that the values are small with respect to the number of detectors (typically about 5%). Figure 1 shows the particle identificaton plot form the fragmentation of a ^{107}Ag primary beam of energy 750 MeV/u on a 4 g/cm ^{9}Be target with the ions of the ^{94}Pd isotope outlined. This isotope has a known [10] 14^{+} isomer we use for in-beam efficiency callibration. The flash width in time and mean flash multiplicity are also shown. The lower right figure shows the flash mean crystal multiplicity for the species in the identification plot, the energy deposition has been evaluated from a simulation of the FRS [11]. The stopper present for this setting was a 7 mm thick perspex foil.

4 Conclusion and outlook

The RISING Stopped Beam setup will continue with the development of a position sensitive silicon detector for use as an 'active' stopper. This will allow the correlation of implanted ions with subsequent beta-decays in the 100ms $\rightarrow$ 10s range, enabling beta-delayed gamma-ray spectroscopy of exotic, neutron-rich nuclei using the RISING array (see [12] for proof of principle of particle-β delayed correlation). The first experiments using this new setup are planned for mid-2007.

This work is supported by the EPSRC(UK) and EU-FP6 Contract (EURONS) RII3-CT-2004-506065.

References

1. H. Geisel et al., Nucl. Instrum. Meth. B **70**, 286 (1992)
2. H.J. Wollersheim et al., Nucl. Instrum. Meth. A **537**, 637 (2005)
3. R. Grzywacz et al., Phys. Rev. C **55**, 1126 (1997)
4. Zs. Podolyak et al., Nucl. Phys. A **722**, 273c (2003)
5. Zs. Podolyak et al., Phys. Lett. B **632**, 203 (2006)
6. Zs. Podolyak et al. (this conference)
7. D. Rudolph et al. (this conference)
8. M. Wilhem et al., Nucl. Instrum. Meth. A **381**, 462 (1996)
9. http://www.xia.com/DGF-4C_Download.html
10. M. Gorska et al., Z. Phys. A **353**, 233 (1995)
11. D. Bazin et al., Nucl. Instrum. Meth. A **482**, 307 (2002)
12. T. Kurtukian-Nieto et al., AIP Conf. Proc. **80**, 73 (2005)

Eur. Phys. J. Special Topics **150**, 353–356 (2007)

DOI: 10.1140/epjst/e2007-00344-y

THE EUROPEAN PHYSICAL JOURNAL SPECIAL TOPICS

Gamma spectroscopy with RIBs from RISING to AGATA

J. Gerl[a]

GSI, 64291 Darmstadt, Germany

Received: January 31, 2007

Abstract. Nuclear spectroscopy using radioactive isotope beams requires dedicated set-ups. State-of-the-art Ge arrays recently started to provide valuable γ spectroscopic data. At the SIS/FRS facility at GSI exotic beams at relativistic energies were employed for Coulomb excitation and secondary fragmentation experiments with the fast beam RISING set-up. Shell evolution far off stability, pn-pairing, symmetries and nuclear shapes were studied in nuclei ranging from ^{36}Ca to ^{136}Nd. The observation of a I = 27 $\hbar$ state demonstrated that high spin states can be reached in massive fragmentation reactions. This and the large sensitivity of relativistic in-beam experiments opens a rich ground for advanced nuclear structure studies. Combining RISING with AGATA γ-tracking detectors and improved particle detection is planned for future experimental investigations.

PACS. 23.20.-g – 23.50.+z – 25.70.Mn – 27.40.+z – 27.50.+e

1 Introduction

Key subjects of contemporary and future nuclear structure research include:

- shell structure of known and predicted doubly magic nuclei and nuclei in their vicinity far off stability,
- isospin symmetry along the N = Z line and mixed symmetry states,
- deformed shapes and shape coexistence,
- collective modes of nuclear excitation and E1 strength distribution,
- nuclear moments.

Rare isotope beams (RIB) from both ISOL and fragmentation accelerator facilities together with high resolution γ-ray spectroscopy provide the means for experimental studies in this field. This contribution focuses on the current spectroscopy activities at GSI, i.e. the RISING [1] project at the SIS/FRS fragmentation facility, and discusses future perspectives with FAIR/NUSTAR [2] and AGATA [3].

2 The RISING experiment

The RISING project started in 2003 with a series of in-beam experiments employing RIBs at relativistic energies. In fall 2005 the set-up was modified to enable g-factor experiments with stopped beams. Since early 2006 decay experiments are being pursued.

The RISING γ spectroscopy set-up uses rare isotope beams from the SIS/FRS facility. Primary heavy ion beams provided by the heavy ion synchrotron SIS with a typical energy of 400–900 A$\cdot$ MeV impinge on a production target at the entrance of the fragment separator FRS. Fragments of interest are selected and identified in-flight on an event-by-event basis using their magnetic rigidity Bρ, their time of flight between the two scintillation detectors SCI1 and SCI2, see figure 1, and their energy loss in the multi sampling ionization chamber MUSIC. In order to optimize the secondary beam at the final focus, a wedge-shaped aluminium degrader is placed at the middle focal plane of the FRS. The multiwire detectors MW1 and MW2 serve to determine the position and direction of the beam particles in order to obtain the interaction point at the secondary target. Be or Au targets of several 100 mg/cm^2 thickness are used at the final focus for secondary fragmentation reactions and Coulomb excitation respectively. The reaction products are selected using the calorimeter telescope array CATE [4], consisting of an array of 3 × 3 Si-CsI(Tl) ΔE-E telescopes. The energy loss in the Si detectors provides unambiguous Z identification after the secondary target. Due to the parallel momentum distribution in fragmentation processes, the total energy measurement of the fragments is however insufficient to completely distinguish masses. Position sensitivity of the Si detectors enables scattering angle determination. Since 2005 an additional thin position sensitive Si ΔE detector with a size of 5 × 5 cm^2 was placed directly after the secondary target. Together with the CATE Si ΔE detectors the fragment trajectories were determined with a position resolution of 3 mm in x and y.

The γ-rays emitted by the reaction products were measured in the in-flight experiments with 15 Cluster Ge detectors, containing 7 crystals each, positioned in three

[a] for the RISING and AGATA Collaboration

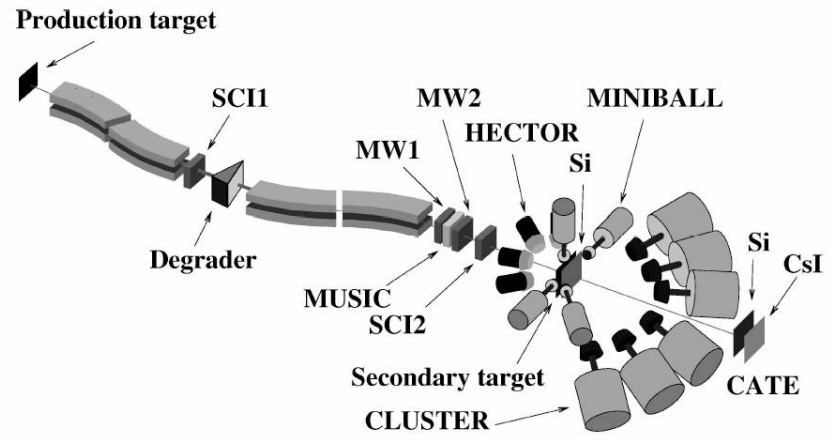

Fig. 1. Schematic of the RISING in-flight set-up.

rings at extreme forward angles of 16°, 33° and 36°. For some experiments up to 8 six-fold segmented MINIBALL triple Ge detectors were arranged in two rings with central angles of 45° and 85° relative to the beam line at forward angles. The full energy efficiency of this arrangement amounts to 3% for 1.3 MeV γ rays emitted at v/c = 0.5. In addition the HECTOR array [5], consisting of 8 large volume BaF2 detectors, was situated at angles of 85° and 142°. The position sensitivity of the MINIBALL detectors allowed them to be placed at a close target distance of 250 mm, while the Cluster and HECTOR detectors sat at larger distances of 700 mm and 300 mm, respectively. In order to obtain the best energy resolution for the γ-rays emitted in flight at velocities of v/c $\approx$ 0.5, excellent tracking of the moving nuclei is mandatory. Employing sophisticated analysis algorithms an energy resolution of $\leq$1.5% was achieved.

Relativistic Coulomb excitation was used in several experiments in order to extract absolute B(E2) values of the first excited state in unstable nuclei. In the isotopes ^{56}Cr and ^{58}Cr the results confirm the subshell closure at $N = 32$ which was already indicated by the excitation energy of the 2^+ state in ^{56}Cr [6]. The result presents a challenge for large scale shell model calculations which predict a much larger B(E2) value. In the ^{108}Sn isotope the obtained B(E2) value is in agreement with the theoretical calculations [7]. Secondary fragmentation reactions were used in several experiments to study proton rich unstable nuclei. Preliminary results on T = 3/2 mirror nuclei in the A $\sim$ 50 region show the potential power of this method [8].

The secondary 1n knock-out reaction was used to measure the energy of the first excited 2^+ state in ^{36}Ca which is the mirror nucleus of ^{36}S [9]. The excitation energy was found to be 276 keV lower than in the T = 2 mirror nucleus ^{36}S, indicating that a major part of the Coulomb energy difference is due to the Thomas-Ehrmann shift.

Besides the Coulomb excitation of the first excited 2^+ state, relativistic Coulomb excitation of ^{136}Nd at RISING allowed to populate also the second excited 2^+ state and to deduce three B(E2) values. Figure 2 shows the corresponding γ spectrum, demonstrating the high quality which can be achieved by optimal background reduction and Doppler correction in the analysis. The results confirm that this nucleus is indeed triaxial.

The decay spectroscopy programme of the RISING project is discussed in another contribution to this issue [10]. One finding of this on-going campaign opens an important perspective for in-beam experiments. By massive fragmentation of a ^{208}Pb beam on a Be target a 27^+ isomer was populated in the isotope ^{148}Tb [11]. The population of medium spin metastable states produced in relativistic-energy fragmentation of a ^{238}U beam has been observed previously already [12]. For states with angular momentum $\leq 20\hbar$, a much higher population than expected has been found. By introducing a collective component to the generation of angular momentum the experimental data can be understood. The new data support this interpretation and demonstrate convincingly that the high angular momentum part of the spin distribution in massive transfer can reach several percent. Therefore fragmentation reactions may be used for in-flight high spin spectroscopy, complementing classical fusion evaporation reactions which are not suited for neutron rich nuclei.

3 The AGATA Demonstrator

To fully exploit the exotic beams, lasting problems in detection efficiency have to be solved. They result from limited beam intensity, particularly for the most exotic nuclei, a wide range of beam velocities (from stopped to v/c $\sim$ 0.5), high γ ray and particle background and γ ray multiplicities up to M = 30, which are typical characteristics of the reactions. A 4π γ-ray array with highest efficiency, selectivity and energy resolution is required which is capable of high event rates. These features can only be achieved with a close packed arrangement of detectors. The individual interaction points of the γ quanta have to be determined by pulse shape analysis and disentangled by tracking algorithms. The Advanced GAmma Tracking Array, AGATA [3], will provide 25% to 40% full energy

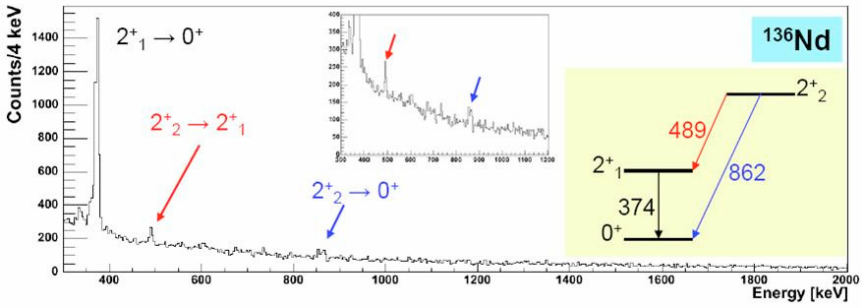

Fig. 2. Doppler corrected γ spectrum of ^{136}Nd after Coulomb excitation on Au.

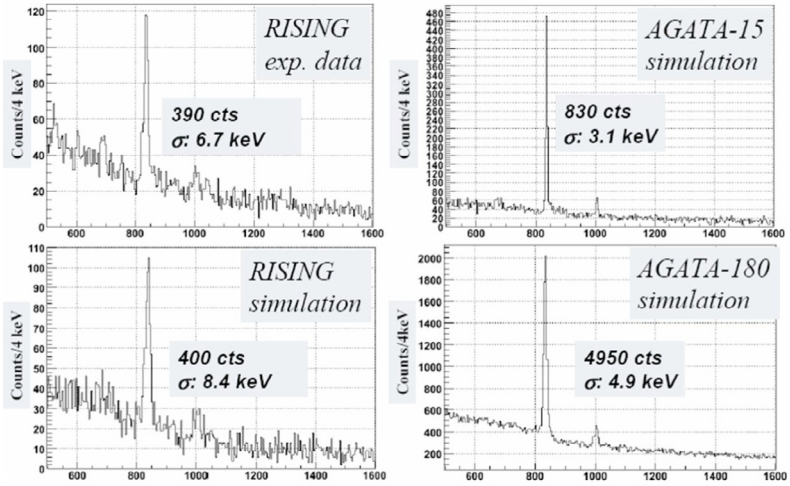

Fig. 3. Comparison of spectrum quality with RISING (left) and AGATA (right) (courtesy A. Bürger [13]).

efficiency depending on the γ multiplicity. The position resolution is sufficient for an energy resolution of 0.4% at a beam velocity of v/c = 0.5. The first AGATA detector unit even surpassed its design qualities in an in-beam experiment. Therefore planning of experimental campaigns employing AGATA detectors has started in accord with the advent of future RIB facilities.

For future γ ray detection at the SIS/FRS facility the AGATA Demonstrator array is proposed in conjunction with the Cluster Ge detectors used in RISING. The 15 detector elements of the AGATA sub-array placed at a distance of ca. 15 cm at forward angles already provide about 8% efficiency at 100 MeV/u. The position resolution of <5 mm ensures an energy resolution after Doppler correction of ≈0.4% at 100 MeV/u. Figure 3 shows the improvement of spectrum quality inferred from simulation calculations [13]. The 15 Cluster detectors are proposed to cover intermediate and backward angles. In a compact arrangement they will add 16% efficiency at a moderate 4% energy resolution. Combining both systems enables highly selective $\gamma\gamma$-coincidences to be measured in fragmentation reactions.

For the proposed campaign novel detectors emerging from FAIR/NUSTAR developments should become available. In particular it is planned to replace the MUSIC detector and one of the multi-wire chambers by Si strip detectors to increase the count rate capability at the final focal plane and reduce the energy straggling.

Experience from RISING plus CATE experiments shows that high-quality beam tracking and higher granularity at central angles is crucial to achieve optimal mass resolution. The inclusion of flight-time measurement is also essential, because the velocity uncertainty due to reaction mechanisms and slowing down processes in the secondary target prevent a clean mass identification solely based on ΔE/E information. Therefore, E_{tot}-ToF will be employed with a position sensitive ΔE/E calorimeter and fast scintillators. The set of detectors behind the target will be renewed completely within the LYCCA (Lund-York-Cologne CAlorimeter) project, initiated to upgrade RISING.

The efficiency as well as the energy resolution of the AGATA part of the proposed layout is almost three times higher then what is achieved with the current RISING set-up. The total efficiency including the Cluster detectors is even 24%! Keeping in mind the low to moderate multiplicities expected the gain in sensitivity and selectivity is substantial. Combining both systems enables e.g. for the first time highly selective $\gamma\gamma$-coincidences to be measured in fragmentation reactions. In addition, a suite of ancillary

detectors which will be developed within FAIR/NUSTAR, may be used to further enhance the sensitivity and selectivity of the set-up.

References

1. H.J. Wollersheim et al., Nucl. Instrum. Meth. A **537**, 637 (2005)
2. NUSTAR Technical Proposal (GSI Darmstadt, 2005)
3. AGATA Technical Proposal, edited by J. Gerl, W. Korten (GSI Darmstadt, 2001)
4. R. Lozeva et al., Nucl. Instrum. Meth. A **562**, 298 (2006)
5. A. Maj et al., Nucl. Phys. A **571**, 185 (1994); F.Camera, Ph.D. thesis, University of Milano, Italy, 1992
6. A. Bürger et al., Phys. Lett. B **622**, 29 (2005)
7. A. Banu et al., Phys. Rev. C **72**, 061305 (2005)
8. G. Hammond et al., Acta Phys. Pol. B **36**, 1253 (2005)
9. P. Doornenbal et al. (private communication); Phys. Lett. B (submitted)
10. D. Rudolph et al. (this conference)
11. Zs. Podolyák et al. (this conference)
12. Zs. Podolyák et al., Phys. Lett. B **632**, 203 (2006)
13. A. Bürger, W. Korten (private communication)

First Results from the Stopped RISING Campaign at GSI: The Mapping of Isomeric Decays in Highly Exotic Nuclei

P.H.Regan[1], A.B.Garnsworthy[1,2], S.J.Steer[1], S.Pietri[1], Zs.Podolyák[1], D.Rudolph[3], M.Górska[4], L.Caceres[4,5], E.Werner-Malento[4,6], J.Gerl[4], H.J.Wollersheim[4], F.Becker[4], P.Bednarczyk[4], P.D.Doornenbal[4], H.Geissel[4], H. Grawe[4], J.Gręboszˆ[4,7], R.Hoischen[3], A.Kelic[4], I.Kojouharov[4], N.Kurz[4], F.Montes[4], W.Prokopowicz[4], T.Saito[4], H.Schaffner[4], S.Tashenov[4], A.Heinz[2], M.Pfützner[6], T.Kurtukian-Nieto[8], G.Benzoni[9], M.Hellström[2], A.Jungclaus[5], L.-L.Andersson[3], L.Atanasova[10], D.L.Balabanski[11], M.A.Bentley[12], B.Blank[13], A.Blazhev[14], C.Brandau[1,4], J.Brown[12], A.M.Bruce[15], F.Camera[9], W.N.Catford[1], I.J.Cullen[1], Zs.Dombradi[16], E.Estevez[8], C.Fahlander[3], W.Gelletly[1], G.Ilie[14], E.K.Johansson[3], J.Jolie[14], G.A.Jones[1], M.Kmiecik[6], F.G.Kondev[17], S. Lalkovski[10,15], Z.Liu[1], A.Maj[7], S.Myalski[7], S.Schwertel[18], T.Shizuma[1,19], A.J.Simons[1], P.M.Walker[1], O. Wieland[9]

[1]Dept. of Physics, University of Surrey, Guildford, GU2 7XH, UK
[2]WNSL, Yale University, New Haven, CT 06520-8124, USA
[3]Department of Physics, Lund University, S-22100 Lund, Sweden
[4]GSI, Planckstrasse 1, D-64291, Darmstadt, Germany
[5]Departamento de Fisica Teórica, Universidad Autonoma de Madrid, E-28049, Madrid, Spain
[6]IEP Warsaw University, Hoża 69, PL-00-681
[7]The Henryk Niewodniczański Institute of NuclearPhysics, PL-31-342, Kraków, Poland
[8]Universidad de Santiago de Compostela, E-15706, Santiago de Compostela, Spain
[9]INFN, Universitá degli Studi di Milano, I-20133, Milano, Italy
[10]Faculty of Physics, University of Sofia, BG-1164, Bulgaria & The Institute for Nuclear Research, Bulgarian Academy of Science, BG-1784, Sofia, Bulgaria
[11]Dipartimento di Fisica, Universit ´a di Camerino, I-62032, Italy
[12]Dept. of Physics, University of York, Heslington, York, Y01 5DD, UK
[13]CENBG, le Haut Vigneau, F-33175, Gradignan Cedex, France
[14]IKP, Universit¨at zu K¨oln, D-50937, K¨oln, Germany
[15]School of Engineering, University of Brighton, Brighton, BN2 4GJ, UK
[16]Institute for Nuclear Research, Debrecen, H-4001, Hungary
[17]Nuclear Engineering Division, Argonne National Laboratory, Argonne IL-60439, USA
[18]Physik Department E12, Technische Universität München, Garching, Germany
[19]Japan Atomic Energy Agency, Kyoto, 619-0215, Japan

Abstract. The first results from the Stopped Beam RISING experimental campaign performed at the GSI laboratory in Darmstadt, Germany, are presented. RISING (*Rare ISotope INvestigations at GSI*) constitutes a major new experimental program in European nuclear structure physics research aimed at using relativistic-energy, projectile-fragmentation reactions to study nuclei with exotic proton-to-neutron ratios. This paper introduces the physics aims of the Stopped RISING collaboration and presents some technical details and initial results from experiments using the RISING array to study decays from metastable nuclear states in both proton and neutron-rich nuclei.

Keywords: Gamma-ray spectroscopy; nuclear isomers; nuclear structure; nuclear level lifetimes.
PACS: 21.10.-k ; 23.20.Lv ; 25.70.Mn

INTRODUCTION

The study of the internal structure of atomic nuclei with exotic proton to neutron ratios has become a main thrust of nuclear physics research worldwide [1]. This interest has led to the development of radioactive beam facilities which allow the production and study of nuclei species of specific elements as radioactive beams of nuclei [2]. Two main techniques are used for such work, namely (i) Isotope Separation On Line and (ii) Projectile Fragmentation/Fission. In the latter, fast beams traveling at speeds greater than the Fermi velocity (i.e. typically with energies greater than 50 MeV per nucleon) are used to induce reactions on thick stationary targets. Large magnetic separators such as the GSI Fragment Separator (FRS) [3,4] can then be used to both select and identify the exotic secondary species of interest using magnetic rigidity, time of flight and energy loss measurements. Such high-energy collisions produce a plethora of residual nuclei following a two step process of abrasion (i.e., the initial removal of nucleons from the beam nucleus) and a ablation (i.e. the evaporation of subsequent light particles as the hot initial fragment cools down) [5]. This paper reports on the first results of the Stopped RISING collaboration, aimed at investigating the structure of exotic nuclei following their production in projectile fragmentation reactions at GSI.

THE RISING PROJECT

RISING is the acronym for 'Rare Isotope INvestigations at GSI' and involves the use of high-efficiency germanium CLUSTER detectors [6] for nuclear spectroscopy studies using projectile fragmentation beams.

The Stopped Beam RISING Project

The Stopped Beam RISING project is aimed at utilizing the combined power of a highly modular γ-ray spectrometer with the selection power of the FRS to identify decays from (i) metastable states in and/or (ii) following the β-decay of the exotic nuclei. The use of projectile fragmentation reactions to study decays from metastable states was pioneered in experiments at the GANIL laboratory using intermediate energy beams [8-10]. Subsequent work using higher energy beams approaching 1 GeV per nucleon has been carried at GSI using heavy beams such as ^{208}Pb [11-15] and ^{238}U [16-18]. A significant part of the Stopped Beam RISING Campaign is aimed at building on these previous experiments in order investigate the limits of nuclear isomer spectroscopy.

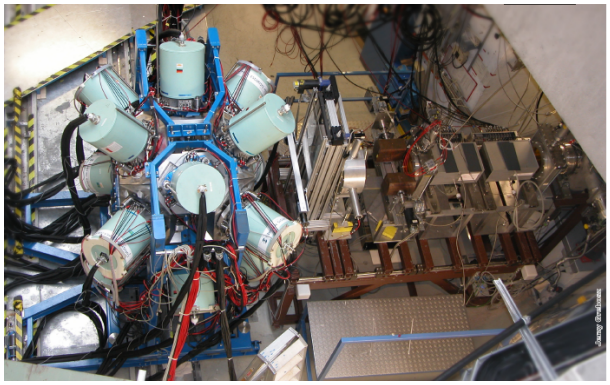

FIGURE 1. Photograph of the RISING array in its Stopped Beam configuration. To the right of the array are the variable thickness aluminum degrader together with various scintillators and ionization chambers used to provide the time of flight, position and energy loss information to identify the fragmentation residues event-by-event.

Figure 1 shows a photograph of the RISING array in its Stopped Beam configuration. The beam-line elements directly to the right of the array include a variable width aluminum energy degrader (which allows the experimenters to vary the energy of the incoming secondary ions such that they can be tuned to stop in the passive stopper placed in the center of the RISING array. In its Stopped RISING configuration RISING consists of fifteen, seven-element germanium cluster detectors [6], placed in three rings of five detectors centered at 51°, 90° and 129° to the secondary beam axis. The detectors are placed approximately 22 cm from the center of the final focal plane of the GSI Fragment Separator. The photopeak γ-ray efficiency measured in the center of a 7 mm thick plastic passive stopper placed in the focal plane was measured to be 14(1)% at 661 keV and 9(1)% at 1332 keV for 102 working crystals (note these values are without Compton add-back between neighboring detectors).

One of the major innovations utilized in the initial Stopped Beam RISING experiments was the use of digital electronics to process both the energy and timing signals from the germanium detectors. These were instrumented using 4-fold DGF ('Digital Gamma Finder') modules similar to those described in [19]. These modules incorporate a free running internal clock with an intrinsic 25ns timing stamp associated with each γ-ray event. This enables excellent correlation to be determined between specific ions implanted in the passive stopper placed in the center of the FRS final focal plane and any subsequent decay from isomeric states with half-lives in the 10ns to 1ms range.

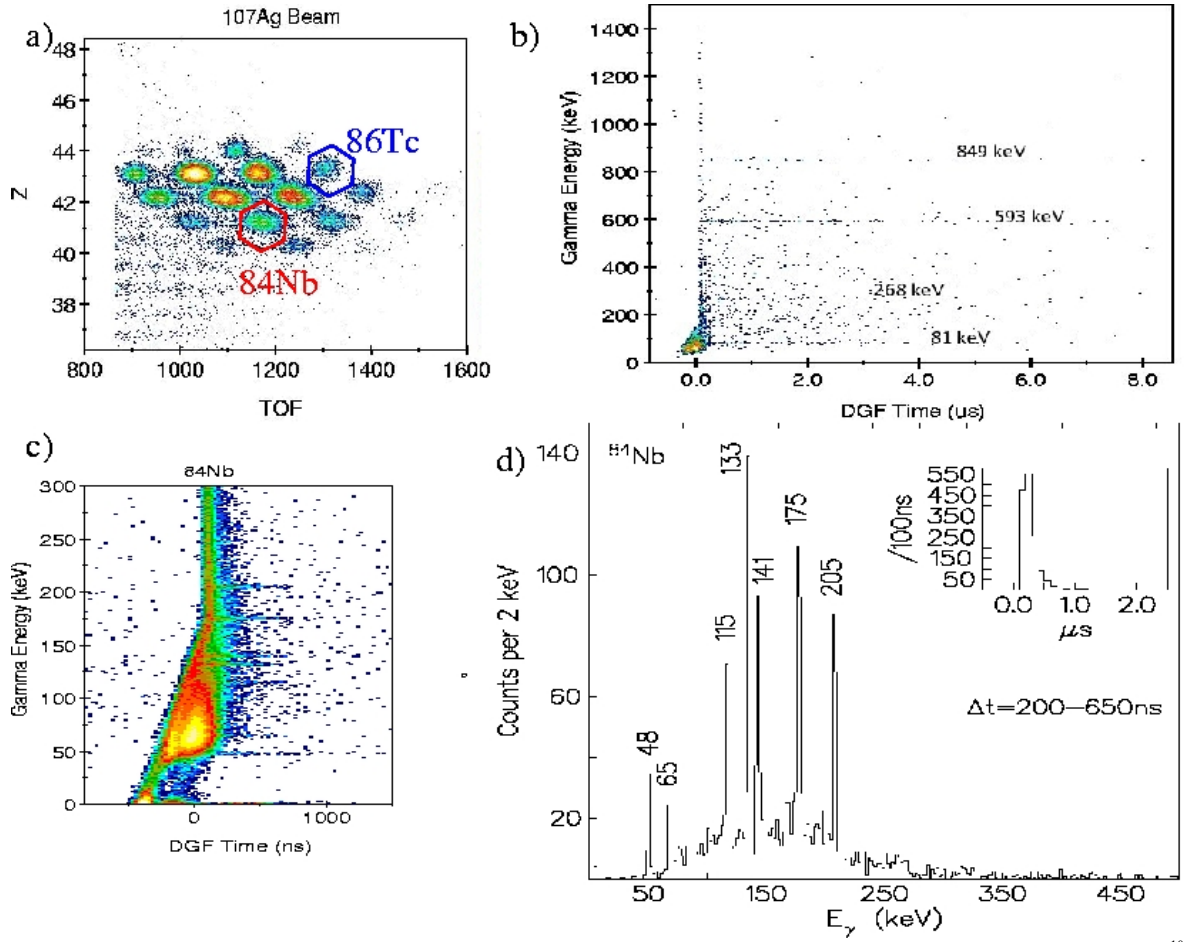

FIGURE 2. Selection of results associated with the Stopped RISING experiment using the projectile fragmentation of a ^{107}Ag primary beam to study isomeric states in N~Z nuclei. (a) Particle identification plot showing Z (deduced from the particle energy loss) and time of flight through the FRS. Those ions identified with ^{86}Tc and ^{84}Nb are highlighted using the hexagons. (b) 2-D matrix of measured γ-ray energy in the RISING detectors versus time of detection after ion implantation in the stopper as measured using the digital clock on the DGF modules. (c) Same as (b) but gated on ^{84}Nb ions. (d) transitions below the previously reported isomer in ^{84}Nb [20] from γ-ray and time projections of cuts on the matrix in figure (c)

Experimental Examples

The first two initial experiments performed as part of the Stopped RISING campaign were studies using the projectile fragmentation of: (i) a 750 MeV/*u* ^{107}Ag and (ii) 1 GeV/*u* ^{208}Pb beam to study (i) isospin symmetry and proton-neutron pairing effects and (ii) the role of proton-hole excitations in the doubly magic ^{208}Pb core and the robustness of the N=126 shell closure in neutron-rich nuclei respectively. Figure 2 shows examples of the raw particle identification spectra produced in the study of the N=Z=43 nucleus, ^{86}Tc using the ^{107}Ag primary beam. By selecting specific species, previously reported isomeric decays associated with neighboring nuclei such as ^{84}Nb [20] can be selected. Two-dimensional matrices of γ-ray energy versus decay time after implantation can then be created for each individual nuclear species.

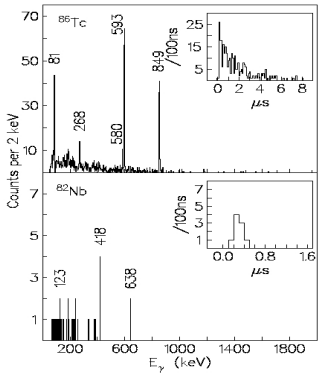

FIGURE 3. Delayed γ-ray energy and time spectra associated with isomers in the N=Z nuclei ^{86}Tc (upper) and ^{82}Nb (lower) following the fragmentation of a ^{107}Ag beam.

By making cuts on these 2-D arrays, energy and time spectra can be cleanly resolved. The low-energy

response of the array in the Stopped RISING configuration is demonstrated by the observation of the 48 and 65keV lines in ^{84}Nb (see figs 2c and 2d). Figure 3 confirms the previously reported isomer in ^{86}Tc [10] and an isomer is identified for the first time in the N=Z=41 system, ^{82}Nb. Figure 4 shows the previously reported isomers in the N=126 nucleus ^{206}Hg [21] associated with a low-lying $I^{\pi}=5^{-}$, two-proton hole excitation and a higher-lying maximally aligned $I^{\pi}=10^{+}$ $(\pi h_{11/2})^{-2}$ configuration. Similar decays are observed in the N=126 isotone ^{204}Pt for the first time in this work. The enhanced population of high-*j* seniority states in 'knockout' reactions has recently been proposed as a potential mechanism for the study of even more exotic neutron-rich systems [22].

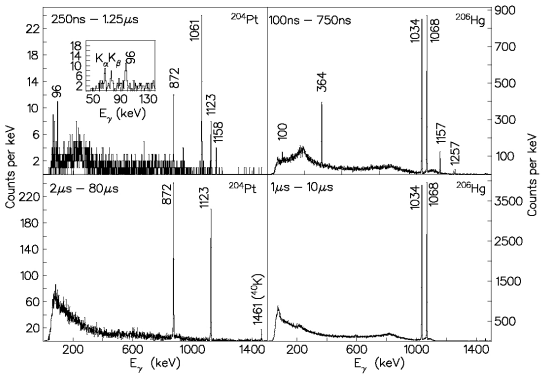

FIGURE 4. Delayed γ-ray spectra associated with isomeric decays in the N=126 isotones ^{204}Pt and ^{206}Hg [21].

Figure 5 shows the previously reported isomers in ^{147}Gd [23] and ^{148}Tb [24] populated following the fragmentation of the ^{208}Pb beam. The isomer in ^{148}Tb represents the highest discrete spin (27ħ) observed to date using projectile fragmentation reactions. This demonstrates the prospects for future high-spin studies with this method, particularly in neutron-rich nuclides inaccessible with stable beam/target fusion reactions.

Future Plans and Related Work

RISING Isomer experiments have also been performed using ^{58}Ni, ^{136}Xe and ^{238}U primary beams. Highlights include the identification of core breaking isomers in the ^{54}Fe/^{54}Ni mirror pair and new shell model isomers close to the ^{132}Sn doubly magic core. Future plans include the use of fission fragments for studies of neutron-rich A~110-130 nuclei and the implementation of a segmented silicon 'active stopper' for β-delayed spectroscopy. Initial experiments to measure β-decay half-lives have provided promising results for this future stage of the project [25].

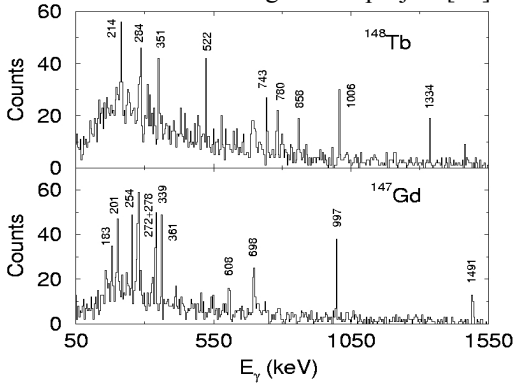

FIGURE 5. Delayed γ-ray spectra associated with the high-spin isomers in ^{148}Tb and ^{147}Gd from the ^{208}Pb experiment.

ACKNOWLEDGMENTS

This work is supported by EPRSC(UK), The Swedish Research Council, The Polish Ministry of Science and Higher Education under grants 1-P03B-030-30 & 620/E-77/SPB/GSI/P-03/ DWM105/2004-2007, The Bulgarian Science Fund VUF06/05, The US Department of Energy under grants W-31-109-ENG-38 & DE-FG02-91ER40609 and E*URONS (European Commission contract no. 506065)*

REFERENCES

1. R.F.Casten & B.M.Sherrill, *Prog.Part. Nucl. Phys.* **45**, S171 (2000).
2. H.Geissel, G.Munzenberg & K.Riisager, *Ann. Rev. Nucl. Part. Sci.* **45**, 163 (1995).
3. H.Geissel et al., *Nuc. Inst. Meth.* **B70**, 286 (1992).
4. B.Voss et al., *Nucl. Inst..Meth.* **A364**, 150 (1995).
5. M.deJong et al., *Nucl. Phys*. **A613**, 435 (1997).
6. M.Wilhelm et al., *Nucl. Inst. Meth*.. **A381**, 462 (1996).
7. H.J.Wollersheim et al., *Nucl. Inst. Meth.***A537**, 637 (2005).
8. R.Grzywacz et al*., Phys. Lett.* **355B**. 439 (1995).
9. R.Grzywacz et al., *Phys. Rev.* **C55**, 1126 (1997).
10. C.Chandler et al., *Phys. Rev.* **C61**, 044309 (2000).
11. Zs.Podolyák et al., *Phys. Lett*. **491B**, 225 (2000).
12. M.Caamano et al., *Nucl. Phys*. **A682**, 223c (2001)
13. M.Pfützner et al., *Phys. Rev.* **C65**, 064604 (2002).
14. Zs.Podolyák et al., *Nucl. Phys*. **A722**, 273c (2003).
15. M.Caamano et al., *Eur.Phys. J.* **A23**, 201 (2005).
16. M.Pfützner et al., *Phys. Lett.* **444**B, 32 (1998).
17. K.A.Gladnishki et al., *Phys. Rev.* **C69**, 024617 (2004).
18. Zs.Podolyák et al., *Phys. Lett.* **632B**, 203 (2006).
19. M.Pfützner et al., *Nucl. Inst. Meth*. **A493**, 155 (2002).
20. N. Marginean et al., *Eur. Phys. J.* **A4**, 311 (1999).
21. B.Fornal et al., *Phys. Rev. Lett*. **87**, 212501 (2001).
22. J.A.Tostevin, AIP *Conf. Procs.* **819**, 523 (2006).
23. R.Broda et al., *Z.Phys.* **A305**, 281 (1982).
24. E.Ideguchi et al., *Z.Phys*. **A352**, 363 (1995).
25. T.Kurtukian-Nieto et al., *AIP Conf. Proc.* **80**, 73 (2005).

Available online at www.sciencedirect.com
ScienceDirect
ELSEVIER
Nuclear Physics A 787 (2007) 491c–498c
NUCLEAR PHYSICS A

Isomer Spectroscopy Using Relativistic Projectile Fragmentation at the N=Z Line for A∼80→90.*

P.H. Regan[a] A.B. Garnsworthy[ab] S. Pietri[a], L. Caceres[c d], M. Górska[c], D. Rudolph[e], Zs. Podolyák[a], S.J. Steer[a], R. Hoischen[e], J. Gerl[c], H.J. Wollersheim[c], J.Grebosz[cf], H.Schaffner[c], W.Prokopwicz[c], I. Kojouharov[c], F. Becker[c], P.Bednarczyk[c] P.Doornenball[c], H. Geissel[c], H. Grawe[c], A. Kelic[c], N. Kurz[c], F. Montes[c], T. Saito[c], S. Tashenov[c], E. Werner-Malento[cg], A. Heinz[b], L. Atanasova[h], D. Balabanski[h], G. Benzoni[i] B. Blank[j], A. Blazhev[k], C. Brandau[ac], A.M. Bruce[l], W.N. Catford[a], F. Camera[i], I.J. Cullen[a], M.E. Estevez[m] C. Fahlander[e], W. Gelletly[a], G. Ilie[kn], A.Jungclaus[d], J. Jolie[k], T. Kurtukian-Nieto[m], Z. Liu[a], M. Kmiecik[f], A. Maj[f], S. Myalski[f], S. Schwertel[o], T. Shizuma[ap], A.J. Simons[aq], P.M. Walker[a], O. Wieland[i]

[a]Department of Physics, University of Surrey, Guildford, GU2 7XH, UK

[b]WNSL, Yale University, New Haven, CT 06520-8124, USA

[c]GSI, Planckstrasse 1, D-64291, Darmstadt, Germany

[d]Dept. de Fisica Teórica, Universidad Autonoma de Madrid, E-28049, Madrid, Spain

[e]Department of Physics, Lund University, S-22100 Lund, Sweden

[f]The Henryk Niewodniczański Institute of Nuclear Physics, PL-31-342, Kraków, Poland

[g]IEP, Warsaw University, Hoża 69, PL-00-681, Poland

[h]Faculty of Physics, University of Sofia, BG-1164, Sofia, Bulgaria

[i]INFN Universitá degli Studi di Milano, I-20133, Milano, Italy

[j]CENBG, le Haut Vigneau, F-33175, Gradignan Cedex, France

[k]IKP, Universität zu Köln, D-50937, Köln, Germany

[l]School of Engineering, University of Brighton, Brighton, BN2 4GJ, UK

[m]Universidad de Santiago de Compostela, E-175706, Santiago de Compostela, Spain

[n]National Institute for Physics and Nuclear Engineering, Bucharest, Romania

[o]Physics Department E12, Technische Universität München, Garching, Germany

[p]Japan Atomic Energy Agency, Kyoto, 619-0215, Japan

[q]AWE Plc, Adlermaston, Reading, RG7 4PR, UK

doi:10.1016/j.nuclphysa.2006.12.073

The preliminary results from the RISING Stopped Beam Isomer Campaign are presented, with specific focus on results of the initial experiment to investigate isomeric decays along the N=Z line around A∼80-90 following the projectile fragmentation of a ^{107}Ag primary beam at an energy of 750 MeV per nucleon. A description of the technical aspects behind the design of the RISING array is presented, together with evidence for previously unreported isomeric decays in ^{87,88}Tc and the N=Z nuclei $^{82}_{41}$Nb and $^{86}_{43}$Tc.

1. INTRODUCTION

The use of projectile fragmentation reactions as a tool to populate and study the structural properties of nuclei with exotic proton-to-neutron ratios has become widespread over the last decade. Specifically, isomeric decays from states with lifetimes ranging from tens of nanoseconds to milliseconds have been studied using the fragmentation process at both intermediate (see e.g. [1–5]) and relativistic (e.g., [6–13]) energies. RISING is the acronym for 'Rare ISotope INvestigations at GSI' and constitutes a major experimental programme in European nuclear structure physics research, aimed at using relativistic energy (typically 500→1000 MeV per nucleon) projectile fragmentation reactions to populate nuclei with highly exotic proton-to-neutron ratios compared to those on the line of beta stability. RISING consists of fifteen, seven element 'cluster' germanium detectors [14], which were formerly part of the EUROBALL gamma-ray array. The RISING array can be coupled to the Fragment Separator (FRS) [15] at GSI in order to observe decays from excited states in exotic nuclei formed following projectile fragmentation and fission at relativistic energies.

This paper describes results from the subsequent 'Stopped Beam' campaign using the RISING detectors to study decays from isomeric states. (Details of the 'in-beam' phase of the RISING project, the so-called 'Fast-Beam' campaign, can be found in reference [16].) In its high-efficiency Stopped Beam configuration, the RISING gamma-ray spectrometer consists of 105 individual, large volume germanium crystals that view a focal plane in which the exotic nuclei are brought to rest (i.e. 'stopped'). Here, decays from metastable excited states with half-lives in the nano-to milliseconds range can be observed, often providing the first spectroscopic information on these exotic nuclear species. This paper introduces the physics aims of the Stopped RISING collaboration and presents some technical details on the RISING detector array. Results from one of the initial commissioning experiments are also shown and details of the planned future experimental program are given.

2. Experimental Details and Particle Identification Techniques.

The RISING array in its Stopped Beam configuration comprises 15, seven-element germanium cluster detectors in a high-efficiency configuration (see figure 1). The detectors were placed in three angular rings at 51, 90 and 129 degrees to the secondary beam axis,

*This work is sponsored by EPSRC(UK), The Swedish Research Council, The Polish Ministry of Science and Higher Education (grants 1-P03B-030-30 and 620/E-77/SPB/GSI/P-03/DWM105/2004-2007), The Bulgarian Science Fund VUF06/05, The US Department of Energy (grant W-31-109-ENG-38 and DE-FG02-91ER40609), The German Federal Ministry of Education and Research under grant 06KY205I and EURONS (European Commission contract number 506065).

each containing 5 cluster detectors. The average distance from the front face of the detectors to the centre of the passive stopper at the final focal plane was approximately 22 cm. The measured photopeak γ-ray efficiency for the array in this geometry for sources placed in the centre of the focal plane was approximately 15% at 661 keV.

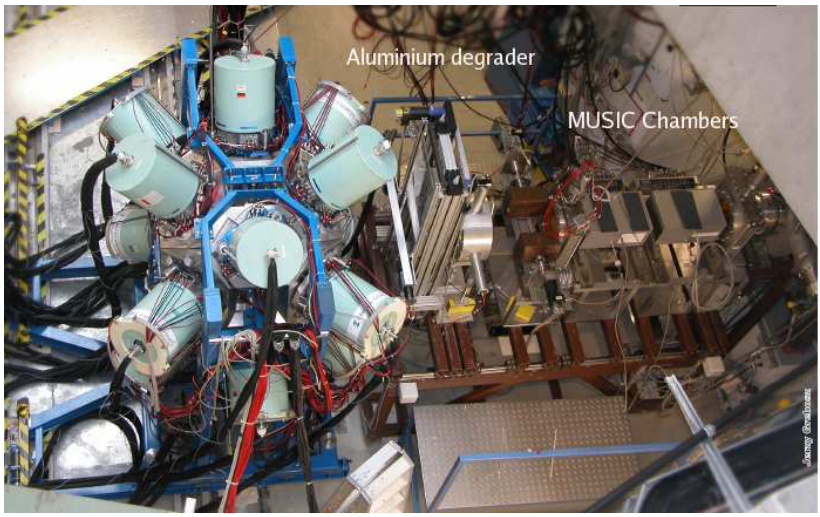

Figure 1. Photograph of the RISING gamma-ray array in its Stopped Beam configuration showing the aluiminium degrader and MUSIC energy loss detectors. The secondary beam enters from the right hand side of this picture.

The first experiment using the RISING array in its stopped beam configuration was aimed at the investigation of nuclear structure along the N=Z line approaching ^{100}Sn. Specifically, the aim was to use decays from isomeric states to populate and study the internal decays in the N=Z nuclei ^{82}Nb and ^{86}Tc in order to shed light on the competing roles of T=1 and T=0 proton-neutron pairing in atomic nuclei [17].

The nuclei of interest in the first commissioning experiment were populated following the projectile fragmentation of a ^{107}Ag primary beam at an energy of 750 MeV per nucleon. The beam impinged on a 4 g/cm^2 beryllium production target with a typical intensity of $1\rightarrow3\times10^9$ particles per extraction spill. The SIS extraction spill lengths used for the ^{86}Tc production runs were typically $5\rightarrow6$ seconds over a total cycle time of 10 seconds. Standard time of flight, position and energy loss parameters were used to provide unambiguous particle identification through the FRS. At the end of the FRS, the ions passed through a variable thickness aluminium degrader (as shown directly to the right of the gamma-ray array in figure 1) such that the ions of interest came to rest in a passive stopper placed in the centre of the RISING array. In this experiment, the stopper was made from a multi-layered perspex block of total thickness 7 mm. Delayed gamma-rays were then detected using the RISING array. Each detected gamma-ray was time-stamped

using a 40MHz clock as part of the DGF4 timing and energy signal processing [18]. More detail of the electronics and signal processing for the Stopped RISING array can be found in reference [19].

3. Experimental Results

Figure 2 shows the calibrated particle identification spectrum centred on ^{86}Tc ions following the ^{107}Ag projectile fragmentation. Figure 3 shows a two-dimensional calibrated matrix of delayed gamma-ray energy versus time after implantation in the perspex stopper, gated on the condition that clean, ^{86}Tc ions were identified in the event.

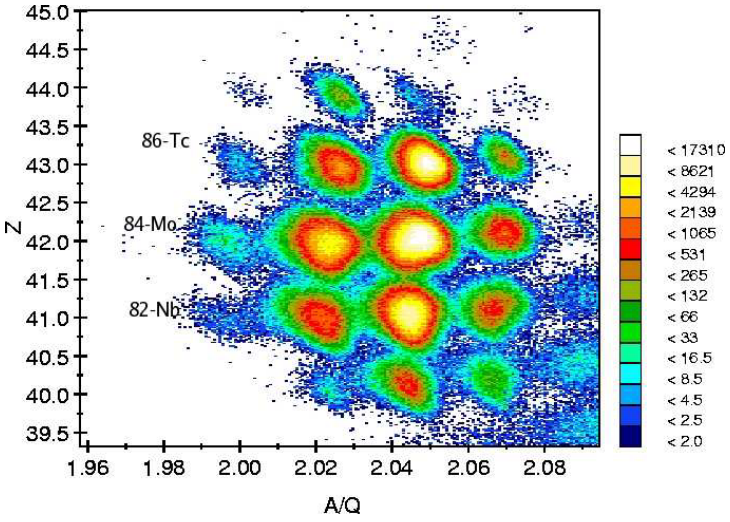

Figure 2. Calibrated particle identification spectrum centred on the N=Z line following the fragmentation of a ^{107}Ag beam. The atomic number and $\frac{A}{Q}$ parameters were derived event-by-event using time of flight, position, magnetic rigidity and energy loss parameters for the ions as they passed through the GSI Fragment Separator.

Figure 4 shows a projection of the ^{86}Tc gamma-ray energy versus time matrix shown in figure 3 and clearly identifies transitions associated with internal, isomeric decays in this N=Z=43 nucleus. The transitions at 593 keV and 849 keV are consistent with the lines assigned to this nucleus in our previous work [2,3]. The gamma rays at 593 keV, 849 keV and 81 keV are also shown to be in mutual coincidence following a gamma-gamma coincidence analysis on the current data when gated on ^{86}Tc ions. The ability to perform gamma-gamma coincidence analyses in such exotic nuclei provides a striking example of the resolving power provided by the high efficiency, high-granularity RISING array in its Stopped Beam configuration. Figure 4 also shows previously unreported transitions following isomeric decays in ^{87,88}Tc. (The published data to date on these nuclei come from

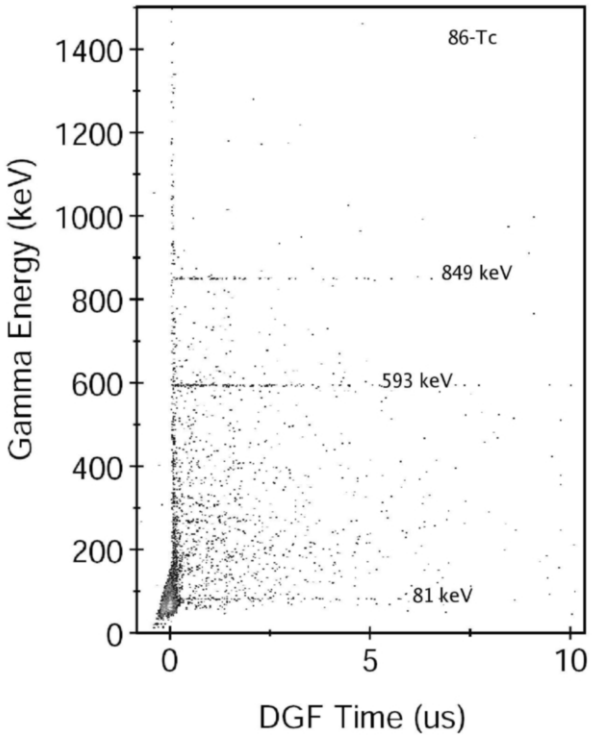

Figure 3. Two dimensional matrix of gamma-ray energy versus time after implantation (as measured using the DGF timing), gated on ^{86}Tc ions produced following the fragmentation of a ^{107}Ag beam at an energy of 750 MeV/u.

in-beam studies using the recoil-separator technique [23] and as such, were not sensitive to decays from isomeric states in the 100ns to few μs regime.)

In addition to the Tc isotopes, figure 4 shows delayed gamma-ray spectra associated with decays from isomeric states in the niobium isotopes ^{82,84}Nb. The isomer in ^{84}Nb has previously been reported [3,24]; its observation in the current work highlights the excellent low-energy efficiency response of the Stopped RISING array using the DGF timing electronics [18,19]. The transitions associated with the N=Z=41 nucleus ^{82}Nb are reported for the first time following this experiment. (Extended details of the analysis on this isotope can be found in reference [25].) We note that our previous work on this nucleus reported evidence for an isomer with a half-life in the hundred nanoseconds regime but could not confirm any discrete lines [3]. As in the case of ^{86}Tc, ^{82}Nb is the most neutron-deficient particle-bound isotope of this element [20] and is therefore located right at the proton drip line. The similarity of the transition energies at 418 and 638 keV to those decaying from the first two excited states reported in the $T_z = +1$ isobar, $^{82}_{40}$Zr at 407 keV and 634 keV [26], strongly suggest that the transitions observed in ^{82}Nb are

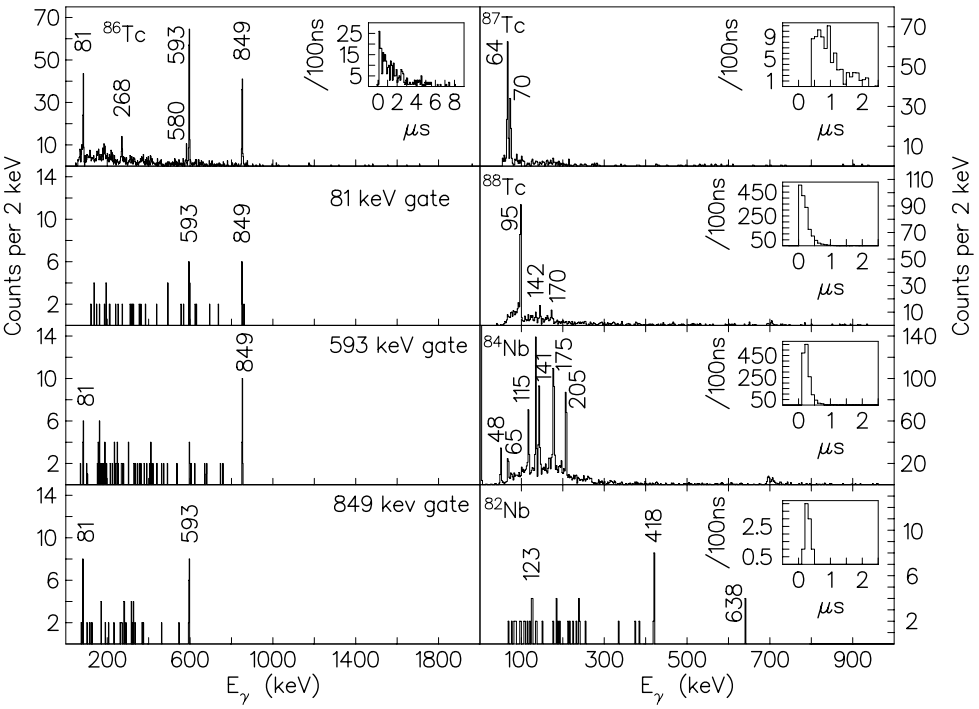

Figure 4. Gamma-ray and DGF time spectra associated with decays from isomeric states populated following the projectile fragmentation of ^{107}Ag at an energy of 750 MeV/u. (Left) Singles and $\gamma - \gamma$ coincidence spectra associated with the microsecond isomeric decay in ^{86}Tc as observed in the current work. (Right) Singles spectra showing the gamma-ray transitions and associated decay curves for isomeric decays in ^{87,88}Tc and ^{82,84}Nb as observed in the current work. See text for details.

decays from states built on the T=1, I^{π}=0^{+} ground-state structure [21,22] in ^{82}Nb.

Figure 5 shows the excitation energies of the first $I^{\pi} = 2^{+}$, T=1 states in N=Z nuclei between $^{58}_{29}$Cu and $^{88}_{44}$Ru. The data points associated with $^{82}_{41}$Nb and $^{86}_{43}$Tc as observed in the current work appear to fit the systematics of these energies. The low-energy nature of the $I^{\pi} = 2^{+}$ excitation energy associated with the newly observed 418 keV transition in ^{82}Nb suggests a large deformation for this nucleus [28].

4. Other Stopped Beam RISING Experiments and Future Prospects

In addition to the preliminary analysis presented in the current paper, RISING isomer studies have also been performed using ^{58}Ni, ^{136}Xe, ^{208}Pb and ^{238}U primary beams. Highlights from these experiments include the identification of core breaking isomers in

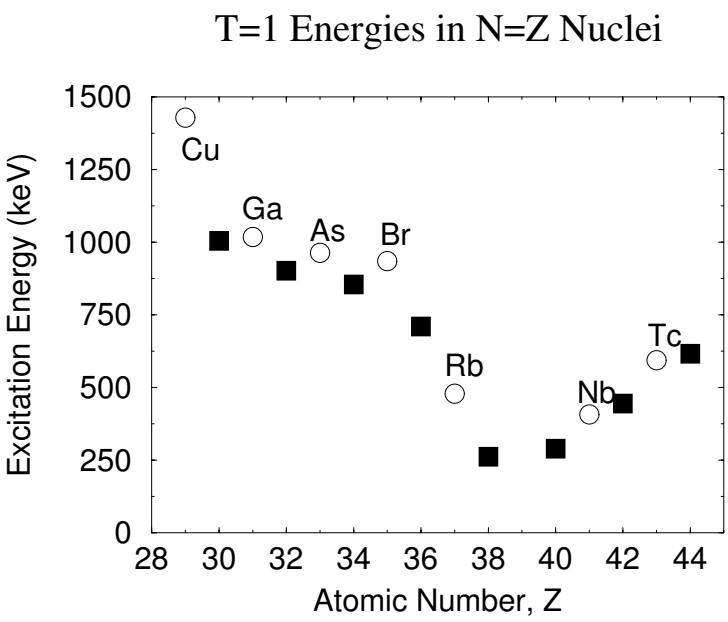

Figure 5. Excitation energy of the lowest T=1, $I^{\pi} = 2^{+}$ states in N=Z nuclei between Cu (Z=29) and Ru (Z=44). Data are taken from [32–41]. The data corresponding to even-even N=Z nuclei are represented by the filled squares with the empty circles representing the odd-odd N=Z systems.

the ^{54}Fe/^{54}Ni mirror pair [29] plus new shell model isomers corresponding to proton hole excitations in the ^{132}Sn [30] and ^{208}Pb [31] doubly magic cores. Future plans include the use of fission fragments for studies of neutron-rich A≈110→130 nuclei following production via projectile fission reactions and the implementation of a segmented silicon active stopper for β-delayed spectroscopy. Initial experiments to measure β-decay half-lives have provided promising results for this future stage of the project [42].

REFERENCES

1. R. Grzywacz et al., Phys. Lett. 335B (1995) 439; Phys. Rev. C55 (1997) 1126; Phys. Lett. 429B (1998) 247.
2. P.H. Regan et al. Acta Phys. Pol. B28 (1997) 431.
3. C. Chandler et al., Phys. Rev. C61 (2000) 044309; Phys. Rev. C56 (1997) R2924.
4. J.M.Daugas et al., Phys. Lett. 476B (2000) 213.
5. G. Georgiev et al., J. Phys. G28 (2002) 2993.
6. M. Pfützner et al., Phys. Lett. 444B (1998) 32.
7. Zs. Podolyak et al., Phys. Lett. 491B (2000) 225.
8. M. Caamano et al., Nucl. Phys. A682 (2001) 223c.
9. M. Pfützner et al., Phys. Rev. C65 (2002) 064604.

10. Zs. Podolyak et al., Nucl. Phys. A722 (2003) 273c.
11. K. Gladnishki et al., Phys. Rev. C69 (2004) 024617.
12. M. Caamano et al., Eur. Phys. J. A23 (2005) 201.
13. Zs. Podolyák et al., Phys. Lett. 632B (2006) 203.
14. M. Wilhelm et al., Nucl. Inst. Meth. Phys. Res. A381 (1996) 462.
15. H. Geissel et al., Nucl. Inst. Meth. Phys. Res. B70 (1992) 286 ; H. Geissel, G. Muzenberg and K. Riisager, Ann. Rev. Nucl. Part. Sci. 45 (1995) 163.
16. H.J. Wollersheim et al., Nucl. Instr. Meth. Phys. Res. A537 (2005) 637.
17. J. Janecke and T.W.O'Donnell Phys. Lett. 605B (2005) 87; E. Baldini-Neto, C.L. Lima and P. Van Isacker Phys. Rev. C65 (2002) 064303;W. Satula and R. Wyss Phys. Rev. Lett. 87 (2001) 052504.
18. M. Pfützner et al., Nucl. Inst. Meth. Phys. Res. A493 (2002) 155.
19. S. Pietri et al., Proceedings of the CAARI'06 conference, in press, Nucl. Inst. Meth. Phys. Res. B.
20. Z. Janas et al., Phys. Rev. Lett. 82 (1999) 295.
21. J. Garces Narro et al., Phys. Rev. C63 (2001) 044307; C. Longour et al., Phys. Rev. Lett. 81 (1998) 3337.
22. T. Faestermann et al., Eur. Phys. J. A15 (2002) 185.
23. D. Rudolph et al., J. Phys. G17 (1991) L113.
24. N. Marginean et al., Eur. Phys. J. A4 (1999) 311.
25. L. Caceres, M. Górska et al., Proceedings of the 41^{st} Zakopane School, Trends in Nuclear Physics, to be published in Acta Physica Polonica B
26. J.K. Tuli, Nucl. Data Sheet 98 (2003) 209; D. Rudolph et al., Phys. Rev. C56 (1997) 98.
27. B. Singh, Nucl. Data Sheets 94 (2001) 1; D. Rudolph et al., Phys. Rev. C54 (1996) 117; C.J. Gross et al., Phys. Rev. C44 (1991) R2253.
28. L. Grodzins, Phys. Lett. 2 (1962) 88; S. Raman et al., At. Data. Nucl. Data Tabs. 78 (2001) 1.
29. D. Rudolph et al., Proceedings of the RNB7 Conference, to be published in Eur. Phys. J. A.
30. A. Jungclaus, M. Górska, M. Pfützner et al., private communication.
31. Zs. Podolyák et al., these proceedings.
32. A.F. Lisetkiy et al., Phys. Rev. C68 (2003) 034316.
33. D. Rudolph et al., Phys. Rev. C69 (2004) 034309.
34. R. Grzywacz et al., Nucl. Phys. A682 (2001) 41c.
35. D.G. Jenkins et al., Phys. Rev. 65 (2002) 064307.
36. C.D. O'Leary et al., Phys. Rev. C67 (2003) 021301; D. Rudolph et al., Phys. Rev. Lett. 76 (1996) 376.
37. J.K. Tuli Nucl. Data Sheets 100 (2003) 347.
38. C.J. Lister et al., Phys. Rev. C42 (1990) R1191
39. S.M. Fischer et al., Phys. Rev. Lett. 87 (2001) 132501;
40. N. Marginean et al., Phys. Rev. C65 (2002) 051303; W. Gelletly et al., Phys. Lett. 253B (1991) 287.
41. N. Marginean et al., Phys. Rev. C63 (2001) 031303.
42. T. Kurtukian-Nieto et al., AIP Conference Proceedings 80 (2005) 73.

Along the N=126 closed shell: $^{204}Pt^{*}$

Zs. Podolyák[a], S.J. Steer[a], S. Pietri[a], E. Werner-Malento[b c], P.H. Regan[a], D. Rudolph[d], A.B. Garnsworthy[a], R. Hoischen[d], M. Górska[b], J. Gerl[b], H.J. Wollersheim[b], T. Kurtukian-Nieto[e], G. Benzoni[f], F. Becker[b], P. Bednarczyk[bg], L. Caceres[bh], P. Doornenbal[b], H. Geissel[b], J. Grębosz[bg], A. Kelic[b], I. Kojouharov[b], N. Kurz[b], F. Montes[b], W. Prokopowicz[be], T. Saito[b], H. Schaffner[b], S. Tashenov[b], A. Heinz[i], M. Pfützner[c], M. Hellström[d], A. Jungclaus[h], L.-L. Andersson[d], L. Atanasova[j], D.L. Balabanski[k], M.A. Bentley[l], B. Blank[m], A. Blazhev[n], C. Brandau[ab], J. Brown[l], A.M. Bruce[o], F. Camera[f], W.N. Catford[a], I.J. Cullen[a], Zs. Dombrádi[p], E. Estevez[e], C. Fahlander[d], W. Gelletly[a], G. Ilie[n], E.K. Johansson[d], J. Jolie[n], G.A. Jones[a], M. Kmiecik[g], F.G. Kondev[q], S. Lalkovski[jo], Z. Liu[a], A. Maj[g], S. Myalski[g], S. Schwertel[r], T. Shizuma[as], A.J. Simons[a], P.M. Walker[a], O. Wieland[f], B.A. Brown[t]

[a]Department of Physics, University of Surrey, Guildford, GU2 7XH, UK

[b]GSI, Planckstrasse 1, D-64291, Darmstadt, Germany

[c]IEP, Warsaw University, Hoża 69, PL-00-681, Warsaw, Poland

[d]Department of Physics, Lund University, S-22100 Lund, Sweden

[e]Universidad de Santiago de Compostela, E-15706, Santiago de Compostela, Spain

[f]INFN, Universitá degli Studi di Milano, I-20133, Milano, Italy

[g]The Henryk Niewodniczański Institute of Nuclear Physics, PL-31-342, Kraków, Poland

[h]Departamento de Fisica Teórica, Universidad Autonoma de Madrid, E-28049, Madrid, Spain

[i]WNSL, Yale University, New Haven, CT 06520-8124, USA

[j]Faculty of Physics, University of Sofia, Sofia, BG-1164, Bulgaria

[k]Inst. for Nucl. Research, Nucl. Energy, Bulgarian Academy of Sciences, BG-1784 Sofia, Bulgaria

[l]Dept. of Physics, University of York, Heslington, York, Y01 5DD, UK

[m]CENBG, le Haut Vigneau, F-33175, Gradignan Cedex, France

[n]IKP, Universität zu Köln, D-50937, Köln, Germany

[o]School of Engineering, University of Brighton, Brighton, BN2 4GJ, UK

[p]Institute for Nuclear Research, ATOMKI, Debrecen, H-4001, Hungary

[q]Nuclear Engineering Division, Argonne National Laboratory, Argonne IL-60439, USA

[r]Physik Department E12, Technische Universität München, Garching, Germany

[s]Japan Atomic Energy Agency, Kyoto, 619-0215, Japan

[t]Department of Physics and Astronomy, Michigan State University, East Lansing, Michigan 48824, USA

Relativistic energy projectile fragmentation of ^{208}Pb has been used to produce neutron-rich nuclei with N≈126. The nuclei of interest were studied by detecting delayed gamma rays following the decay of isomeric states. Experimental information on the excited states of the neutron-rich ^{204}Pt N=126 nucleus, following internal decay of two isomeric states, was obtained for the first time. Raw experiemtnal data and shell-model calculations are presented.

1. INTRODUCTION

First results from a new initiative of experiments focusing on the study of the internal structure of nuclei at the extremes of N/Z ratio using isomer spectroscopy are reported. These experiments represent the first of the Stopped Beam section of the *Rare Isotopes Investigations at GSI* (RISING) project. Exotic nuclei were synthesised using relativistic projectile fragmentation of E/A=500–1000 MeV beams of ^{58}Ni [1], ^{107}Ag [2] and ^{208}Pb.

The present paper presents selected highlights of the experimental results, with the focus on N=126 systems populated in the fragmentation of the ^{208}Pb projectile. Studies of semi-magic nuclei are of special importance since they allow direct test of the purity of the model wave functions. Information on the single-particle energies and two nucleon residual interactions can be derived from the experimental observables such as energies of the excited states and transition probabilities.

2. EXPERIMENTAL DETAILS

Heavy nuclear species were populated in relativistic energy projectile fragmentation. A beryllium target of thickness 2.5 g/cm^2 was bombarded with an E/A=1 GeV ^{208}Pb beam provided by the SIS accelerator at GSI, Darmstadt, Germany. The nuclei of interest were separated and identified using the FRagment Separator (FRS) [3] operated in standard achromatic mode. The setup is shown in fig. 1. The identification of the fragments (see fig. 2) is based on the determined A/q (∼TOF), the energy loss in the ionisation chambers ($\approx Z$), and the longitudinal position of the nuclei at the intermediate (S2) and final (S4) focal planes of the FRS. For more details about the setup used in the present experiment see ref. [5].

*This work is supported by EURONS European Commission contract no. 506065, EPRSC(UK), the Swedish Research Council, the Polish Ministry of Science and Higher Education, under grants 1-P03B-030-30 & 620E-77SPBGSIP-03 DWM1052004-2007, the Bulgarian Science Fund and VUF06/05, the US Department of Energy. under grants W-31-109-ENG-38 & DE-FG02-91ER40609.

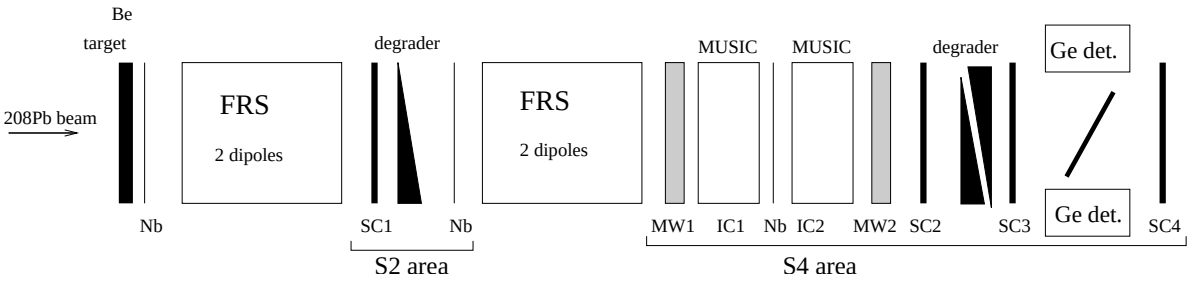

Figure 1. Schematic view of the experimental setup.

The transmitted nuclei were stopped in a cacther surrounded by the high-efficiency, high granularity Stopped RISING γ-ray spectrometer [4]. Time-correlated gamma de-

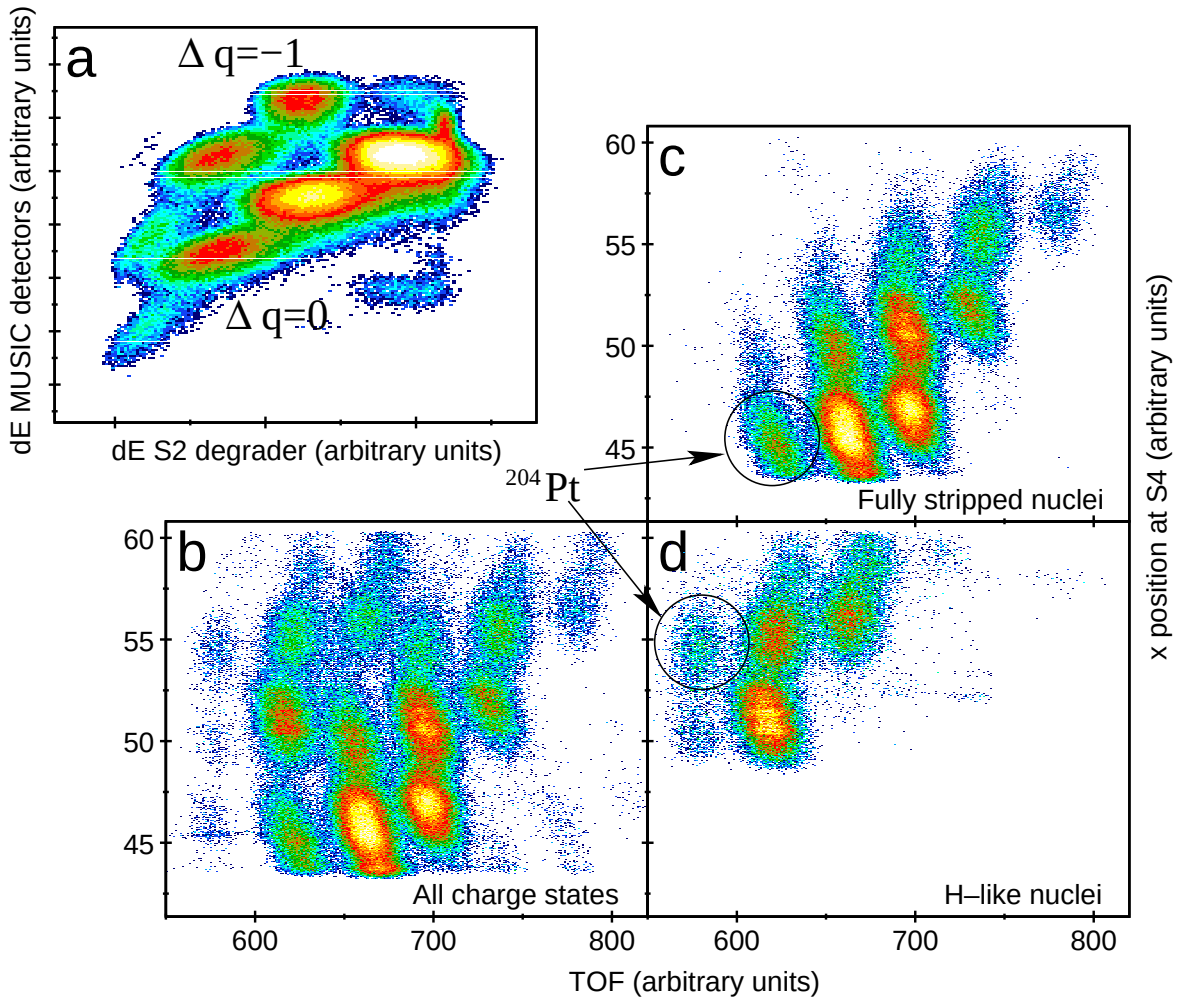

Figure 2. Identification of the fragmentation products. (a) Energy loss at the final focal plane vs. energy loss at the middle focal plane. It distinguishes between nuclei which don't change charge state at S2 from those which do. (b,c,d) energy loss vs. time-of-flight matrices without charge state condition (b), selecting fully-stripped nuclei (c) and H-like nuclei (d), respectively. The circless in (c) and (d) indicate the ^{204}Pt nuclei.

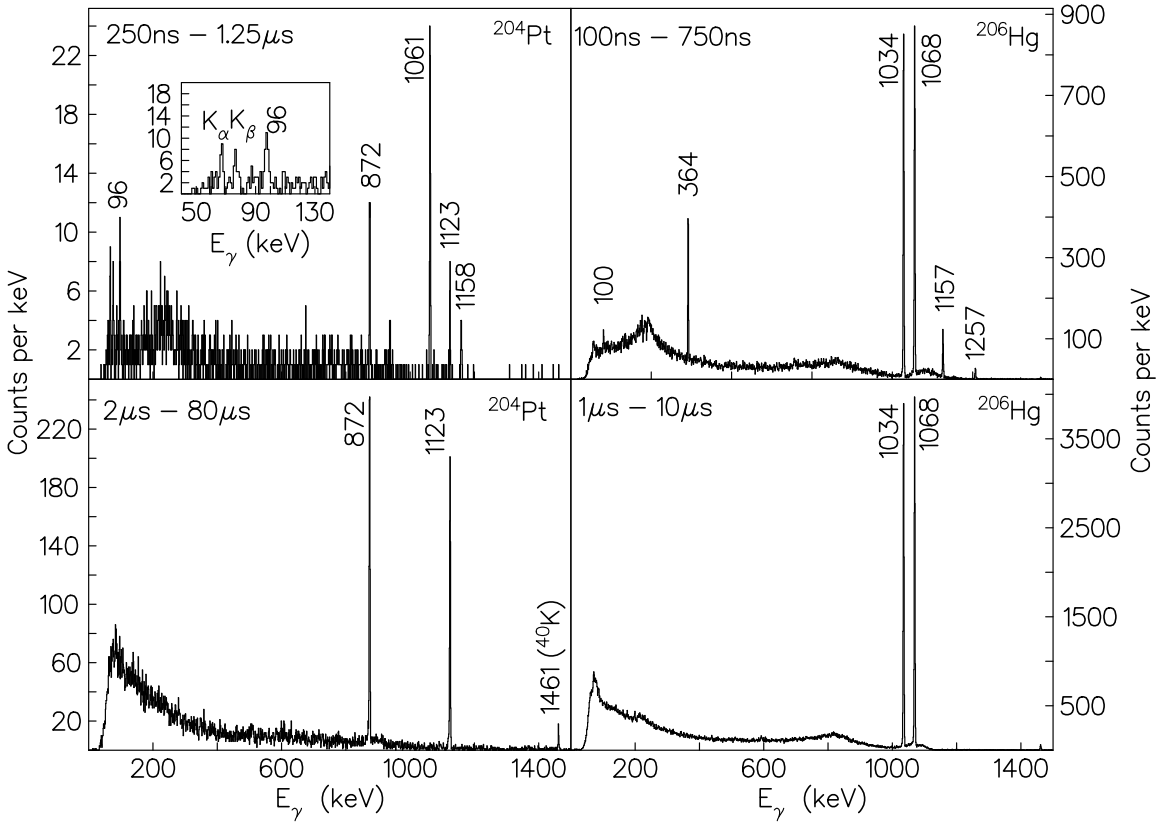

Figure 3. Delayed gamma-ray spectra associated with ^{206}Hg and ^{204}Pt. Note that in the upper panels the shape of the background around ∼300 keV is unphysical, and it is due to used data analysis method.

cays from individually identified nuclear species have been measured, allowing the clean identification of isomeric decays.

3. RESULTS AND DISCUSSION

Information on the neutron-rich N=126 nuclei is scarce. The lack of information is due to the difficulties in populating these nuclei. Below the doubly magic ^{208}Pb nucleus there is experimental information on only three isotones: ^{207}Tl, ^{206}Hg and ^{205}Au. While in both ^{207}Tl [6] and ^{206}Hg [7] excited states have been observed, in ^{205}Au only the ground state is known (I^{π}=(3/2^{+}) [8]).

^{204}Pt has four protons less than the doubly magic ^{208}Pb nucleus. Its yrast structure should be dominated by the proton-hole orbitals $\pi d_{3/2}$, $\pi s_{1/2}$, $\pi h_{11/2}$ and possible $\pi d_{5/2}$. Its level scheme is expected to be similar to that of ^{206}Hg.

Gamma-ray spectra associated with ^{204}Pt and ^{206}Hg are presented in fig.3. In ^{204}Pt two new isomeric decays have been observed, with a longer lifetime associated to the 872 keV and 1123 keV transitions, and a shorter to the 1061 keV, 1158 keV and 96 keV gamma-lines.

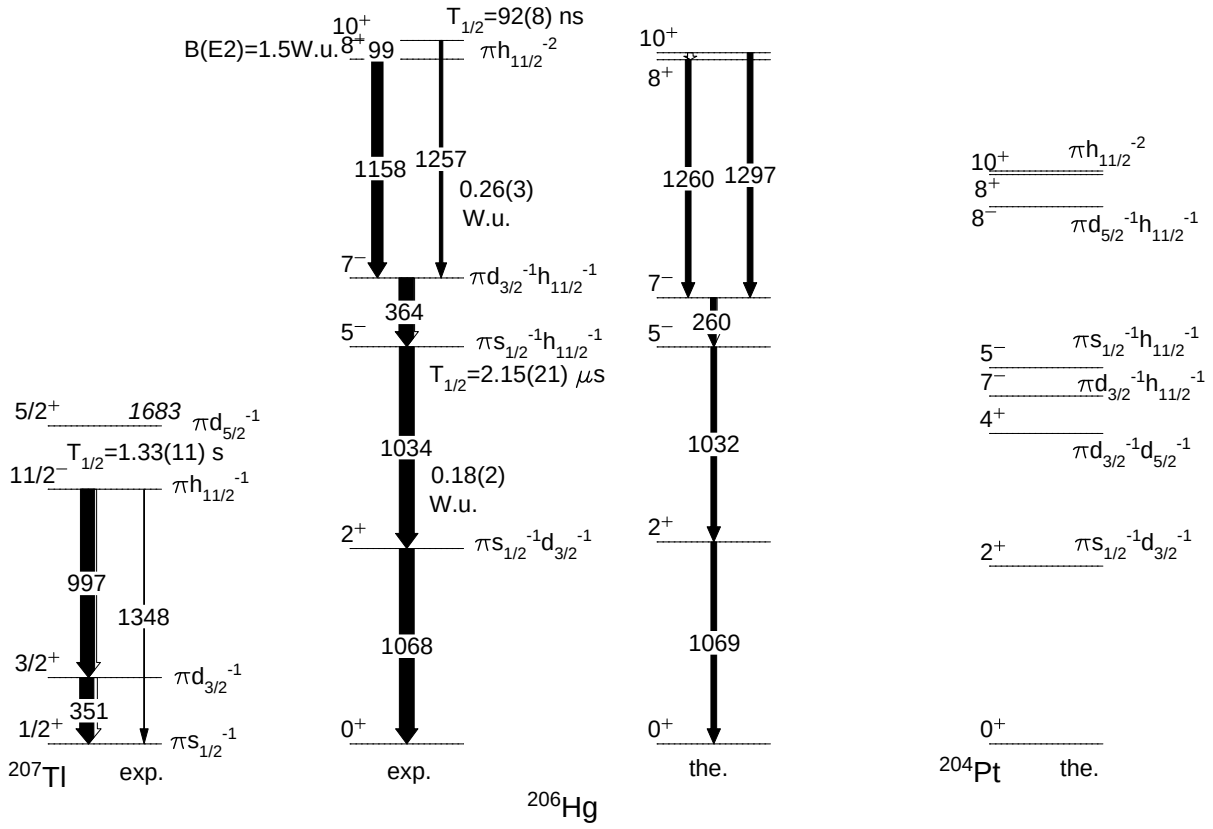

Figure 4. Partial level schemes of ^{207}Tl [6] and ^{206}Hg [7]. The results of the shell model calculation for ^{206}Hg and ^{204}Pt are shown on the right hand side.

Shell-model calculations are being performed using the OXBASH code [9]. The empirical interaction matrix elements are from [10] and are based on those of Kuo and Herling [11]. The experimental proton-hole energies were taken from the experimental level scheme of ^{207}Tl. The results of the calculations for ^{206}Hg and ^{204}Pt are presented in fig. 4. There is a rather good agreement between theory and experiment for ^{206}Hg (note that the interaction matrix elements were obtained by fitting on a range of nuclei, including the 2^+ and 5^- states of ^{206}Hg [10]). In ^{204}Pt, these calculations predict a 4^+ state at rather low energy, below both the 5^- and 7^- states, with a dominant configuration of $\pi d_{5/2}^{-1} d_{3/2}^{-1}$. The existence of a 4^+ state below the 5^- and 7^- states is in contradiction with the experimental findings: none of these states would be isomeric with microseconds lifetime. Since in the configuration of the 4^+ state a $d_{5/2}$ proton-hole is involved, further calculations were performed for nuclei where such states are known experimentally. The comparison between the OXBASH calculation and experiment for ^{203}Au are shown in figure 5. Here spectroscopic factor measurements [12] indicate that the second $5/2^+$ state

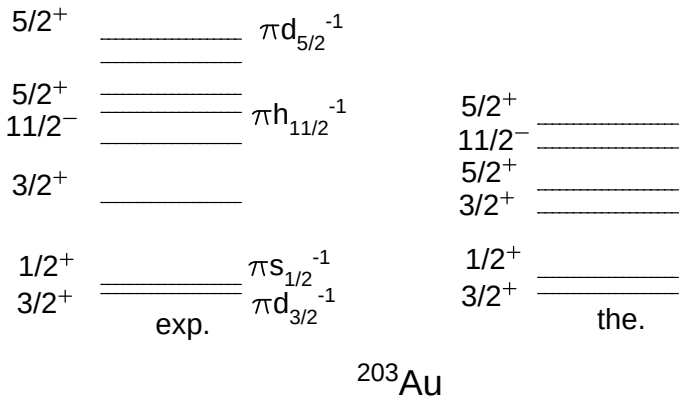

Figure 5. Comparison between experiments [12] and shell model calculation for ^{203}Au.

has the largest $\pi d_{5/2}^{-1}$ component. The calculations foresee this state at much lower energy. This might indicate that states involving the $\pi d_{5/2}^{-1}$ proton-hole lie at considerably higher energies that the present calculations predict. The interpretation of the experimental results for ^{204}Pt is in progress.

REFERENCES

1. D. Rudolph *et al.*, Eur. Phys. J. A (in press) (Proc. of the RNB7 conf, 2006, Cortina d'Ampezzo, Italy).
2. P.H. Regan *et al.*, these proceedings.
3. H. Geissel *et al.*, Nucl. Instrum. Methods Phys. Res. Sect. B70 (1992) 286.
4. Zs. Podolyák *et al.*, Eur. Phys. J. A (in press) (Proc. of the RNB7 conf, 2006, Cortina d'Ampezzo, Italy).
5. S. Pietri *et al.*,Nucl. Instrum. Methods Phys. Res. Sect.B (in press) (Proc. of the CAARI'05 conf., 2006, Dallas, USA).
6. D. Eccleshall, M.J.L.Yates, Phys. Lett. 19 (1965) 301.
7. B. Fornal *et al.*, Phys. Rev. Lett. 87 (2001) 212501.
8. Ch. Wennemann *et al.*, Z.Phys. A347 (1994) 185; F.G. Kondev, Nucl. Data Sheets 101 (2004) 521.
9. B.A. Brown A. Etchegoyen, W.D.M. Rae, The computer code OXBASH, MSU-NSCL report number 524.
10. L. Rydström *et al.*, Nucl. Phys. A512 (1990) 217.
11. T.T.S. Kuo and G.H. Herling, Naval Research Laboratory Report 2259 (Washington, DC, 1971).
12. F.G. Kondev, Nucl. Data Sheets 105 (2005) 1; P. Grabmayr *et al.*, Phys. Rev. C49 (1994) 2971.

FIRST RESULTS FROM THE STOPPED BEAM ISOMER RISING CAMPAIGN AT GSI*

S. Pietri[a], P.H. Regan[a], Zs. Podolyák[a], D. Rudolph[b], M. Górska[c]
A. Jungclaus[d], M. Pfützner[e], A.B. Garnsworthy[a,f], S.J. Steer[a]
L. Cáceres[c,d], E. Werner-Malento[c,e], R. Hoischen[b], J. Gerl[c]
I. Kojouharov[c], H. Schaffner[c], H.J. Wollersheim[c], F. Becker[c]
P. Bednarczyk[c,g], P. Doornenbal[c], H. Geissel[c], J. Grębosz[c,g], A. Kelic[c]
N. Kurz[c], F. Montes[c], W. Prokopowicz[c,h], T. Saito[c], S. Tashenov[c], A. Heinz[f]
T. Kurtukian-Nieto[i], G. Benzoni[j], M. Hellström[b], L.-L. Andersson[b]
L. Atanasova[k], D.L. Balabanski[l,m], M.A. Bentley[n], B. Blank[o], A. Blazhev[p]
C. Brandau[a,c], J.R. Brown[n], A.M. Bruce[q], F. Camera[j], W.N. Catford[a]
I.J. Cullen[a], Zs. Dombrádi[r], E. Estevez[i], C. Fahlander[b], W. Gelletly[a]
G. Ilie[p,s], E.K. Johansson[b], J. Jolie[p], G.A. Jones[a], M. Kmiecik[g]
F.G. Kondev[t], S. Lalkovski[k], Z. Liu[a], A. Maj[g], S. Myalski[g], T. Shizuma[a,u]
A.J. Simons[a], S. Schwertel[w], P.M. Walker[a], O. Wieland[j]

[a]Department of Physics, University of Surrey, Guildford, GU2 7XH, UK
[b]Department of Physics, Lund University, S-22100 Lund, Sweden
[c]GSI, Planckstrasse 1, D-64291 Darmstadt, Germany
[d]Departamento de Fisica Teórica, Universidad Autonoma de Madrid, Spain
[e]IEP, Warsaw University, Hoża 69, PL-00-681 Poland
[f]WNSL, Yale University, New Haven CT 06520-8124, USA
[g]The H. Niewodniczański Institute of Nuclear Physics PAN, Kraków, Poland
[h]Institute of Physics, Jagiellonian University, PL-31342 Kraków, Poland
[i]Universidad de Santiago de Compostela, Santiago de Compostela, Spain
[j]INFN, Universitá degli Studi di Milano, I-20133 Milano, Italy
[k]Faculty of Physics, University of Sofia, BG-1184, Bulgaria
[l]Dipartimento di Fisica, Universitá di Camerino I-62032, Italy
[m]INRNE, Bulgarian Academy of Sciences, BG-1784 Sofia, Bulgaria
[n]Department of Physics, University of York, Heslington York, Y01 5DD, UK
[o]CENBG, le Haut Vigneau, F-33175, Gradignan Cedex France
[p]IKP, Universität zu Köln, D-50937 Köln, Germany
[q]School of Engineering, University of Brighton, Brighton BN2 4GJ, UK
[r]Institute for Nuclear Research, Debrecen H-4001, Hungary
[s]National Institute of Physics and Nuclear Engineering, Bucharest, Romania
[t]Nuclear Engineering Division, Argonne National Laboratory, IL-60439, USA
[u]Japan Atomic Energy Agency, Kyoto 619-0215, Japan
[w]Physik Department E12, Technische Universität München, Garching, Germany

(Received November 19, 2006)

* Presented at the Zakopane Conference on Nuclear Physics, September 4–10, 2006, Zakopane, Poland.

The first results from a series of experiments focused on the study of the internal structure of nuclei at the extremes of N:Z ratio using isomer spectroscopy are reported. These experiments represent the first of the Stopped Beam section of the *Rare Isotopes Investigations at GSI* (RISING) project. Exotic nuclei were synthesized using relativistic projectile fragmentation of $\sim 500 \rightarrow 1000$ MeV/u beams of ^{107}Ag, ^{208}Pb, ^{136}Xe and ^{58}Ni, or fission of 750 MeV/u ^{238}U provided by the SIS synchrotron at GSI. A detailed description of the RISING stopped beam set up is given, together with a report of the performance of the associated gamma-ray spectrometer array. Selected results of the first experimental campaign are presented together with a discussion on the use of isomeric spectroscopy to study GeV range nuclear fragmentation. Details on future research plans of this collaboration are also outlined.

PACS numbers: 21.10.Tg, 23.20.–g, 25.70.Mn, 29.30.Kv

1. Introduction

The aim of the RISING (Rare ISotope INvestigations at GSI) collaboration is to use GeV range beams from the GSI/SIS synchrotron to study exotic nuclei produced through fragmentation. This production technique, coupled to a powerful germanium array from the decommissioned Euroball IV setup, plus the use of the FRS fragment separator for the selection and identification of the produced ions makes a powerful tool for the study of such nuclei. To date, two types of experiments have been conducted, the first campaign used the RISING fast beam setup [1] aimed at two-step fragmentation and/or relativistic Coulomb excitation studies. A review of these experiments can be found in [2]. The two other RISING setups used "stopped beam", either for isomer delayed γ-ray spectroscopy, which is the subject of this paper or for g-factor measurements [3]. The RISING setup moved to the Stopped Beam isomer spectroscopy configuration for the first time in February 2006. In this configuration the 105 germanium crystals of the RISING array (Fig. 1) are placed in a compact configuration around the final focal point of the FRS where they surround a passive stopper made of either perpex, copper or beryllium [4, 5]. Gamma-ray transitions depopulating isomeric states can then be observed using the fragmentation isomer spectroscopy technique as outlined in references [6–10]. Two experimental campaigns have been performed to date, aimed at studying specific physics including *(i)* evolution of shell closures around doubly magic nuclei and *(ii)* $N = Z$ symmetries. The current paper presents a description of the technical aspects of this setup as well as examples of the experimental performance of the γ-ray array. The use of microsecond isomer spectroscopy as a general tool to study the nuclear fragmentation process is also discussed.

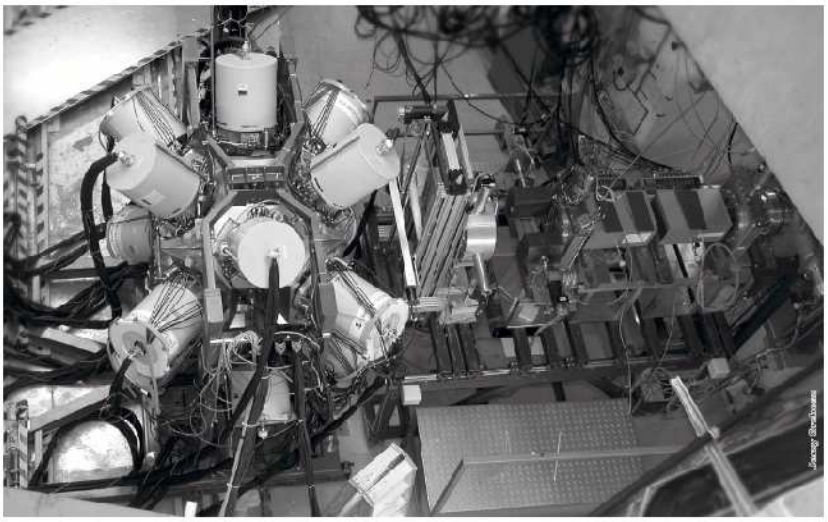

Fig. 1. Photograph of the RISING Stopped Beam γ-ray spectrometer.

2. Technical details

2.1. Production and identification of the exotic nuclei

Exotic secondary beams were produced using the projectile fragmentation of high-energy primary beams from the SIS synchrotron at GSI, incident on $1 \rightarrow 4$ g/cm^2 thick ^{9}Be production targets. The FRagment Separator (FRS) [11] was used in achromatic mode for the selection and identification of the reaction products using a standard time of flight and energy loss techniques [12]. Particle identification was achieved by the use of position-sensitive plastic scintillators at the middle and final focal points of the FRS to define the magnetic rigidities and velocities of the secondary ions. MUlti Sampling Ionization Chambers (MUSIC) before the final focus of the FRS provided energy loss signals from which the electric charge of the incoming ion could be deduced. Further details of the particle identification procedure can be found in [10]. An example from the RISING stopped beam experiment with ^{107}Ag primary beam is shown in Fig. 2. It should be noted that the achromatic degrader at the central focal point of the FRS was also used as a passive energy-loss device for charge state separation. The difference in magnetic rigidity between the first and second stage of the fragment separator can be used to estimate the energy loss of the ion through the achromatic degrader. This information together with the energy loss of the ions as measured at the final focal point using MUSIC detectors allows a unambiguous charge state discrimination. This technique is of particular interest in case of heavy, neutron-rich nuclei (see reference [13] for more details). As noted

in reference [14], for high-Z nuclei this method of charge state selection can only be achieved for high-Z nuclei with energies greater than 300 MeV per nucleon. Thus the RISING setup at GSI is ideal for spectroscopic studies in such heavy, neutron-rich systems produced following relativistic projectile fragmentation reactions.

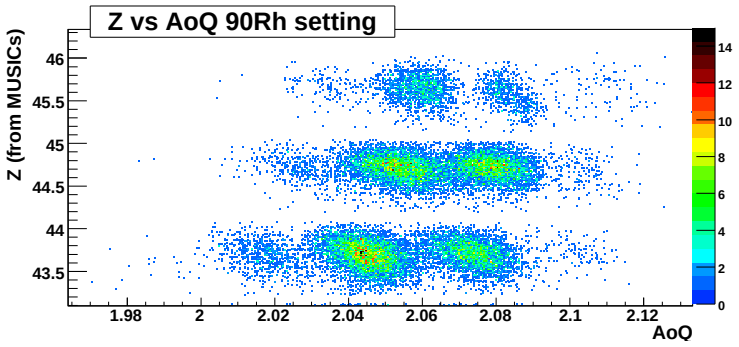

Fig. 2. Typical identification plot from the ^{107}Ag primary beam experiment. This setting was centered on the transmission of fully stripped $^{90}_{45}$Rh ions.

2.2. The stopped RISING germanium array, geometry and electronics

In its Stopped Beam configuration the RISING array comprises fifteen, seven-element germanium cluster detectors [15] from the former Euroball IV array. The detectors were placed in three angular rings of five detectors at 51°, 90° and 129° to the primary beam axis at an average distance from the centre of the array of approximately 22 cm. Each individual germanium detector had two parallel pre-amplifier outputs which were sent to two separate branches of the data acquisition. One was a fully 'digital' branch and provided the input signal for 105 channels within 30 Digital Gamma Finder (DGF-4C) modules [16]. Three parallel CAMAC crates, each holding ten, quad-input modules were used for this part of the electronics. The individual DGF channel triggers were validated by a master trigger signal generated from a fast plastic scintillator detector at the final FRS focal point. This signal was sent to a DGF channel in each crate in order to provide an internal check of the synchronization of the DGF clocks and also to provide a time-difference measurement between the arrival of an ion in the plastic scintillator and the measurement of a delayed γ ray via the DGF γ-time signal. The clock frequency of the DGF modules was 40 MHz, corresponding to a 25 ns time step. The maximum coincidence gate that could be achieved using the DGF modules was 400 μs.

The second output from the germanium preamplifier was sent to an analogue timing branch composed of a standard TFA-CFD-TDC timing circuit. The output of the CFD was sent to two separate TDC modules, one 'short-range' (1 μs full range with a 0.31 ns/channel step) and the other 'long range' (up to 800 μs with a 0.73 ns/channel step). The analogue branch allows a precise definition of shorter-lived ($\sim$ 10 ns) isomers.

2.3. Array performance: Efficiency and addback

The array performance was measured using radioactive sources both before and following the experimental beam time. The experimental conditions were found to produce an energy resolution of less than 3 keV at 1.3 MeV. The photopeak γ-ray efficiency was measured with several low intensity sources. To avoid dead time problems a pulser was used to emulate the plastic scintillator (which was used as the actual trigger during the experiments). Since the interval between the trigger pulses is longer than the acquisition dead time, the calibration is effectively dead time free. The efficiency is then, for each crystal, the number of γ rays observed divided by the number emitted during the live time of the acquisition. The former value is the number of triggers multiplied by the width of the time gates of the electronics.

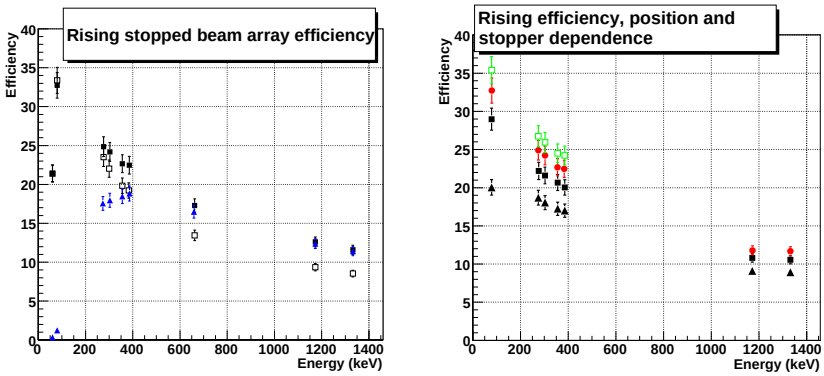

Fig. 3. Efficiency of the RISING array in its Stopped Beam configuration. Left: Comparison of sum (open squares), addback (full squares) and analog timing (triangles). Right: Efficiency for different stopper and positions. (Full circles) 7 mm perpex stopper, (empty squares) same stopper but source positioned 8 cm on the left, (full squares) 12 mm perpex stopper, (triangles) 6 mm copper stopper.

Fig. 3 shows an efficiency curve for a mixture of standard γ-ray sources placed in the middle of the Stopped Beam RISING array. During the experiments several stoppers were used depending the ultimate physics aim.

The attenuation of gamma rays following implantation in a given stopper depends on the stopper composition and on position and depth of the ion implantation. Fig. 3 shows the variation of the photopeak efficiency for several stoppers and as a function of the position of the γ-ray source. A GEANT4 simulation of the array is ongoing [17]. The preliminary results of this simulation reproduce our experimental data shown here. An "inter cluster" addback routine (*i.e.*, inclusion of Compton events scattered between crystals in *neighbouring* cluster detectors) is also being developed to increase further the absolute efficiency for low multiplicity events [18]. The full squares in Fig. 3 represent the efficiency with a Cluster Compton 'addback' routine allowing γ-ray multiplicities upto 4 per cluster such that the events are registered within 400 ns of each other. The triangle symbols represent the efficiency when requiring information in the timing (*i.e.*, TDC) branch of the acquisition. The difference in low energy efficiency arises due to the different discriminator types and settings, the leading edge type of the DGF having a sharper cutoff than the CFD of the analog timing branch. Note that the high efficiency below 100 keV arises from the absence of absorbers in front of the germanium cluster detectors.

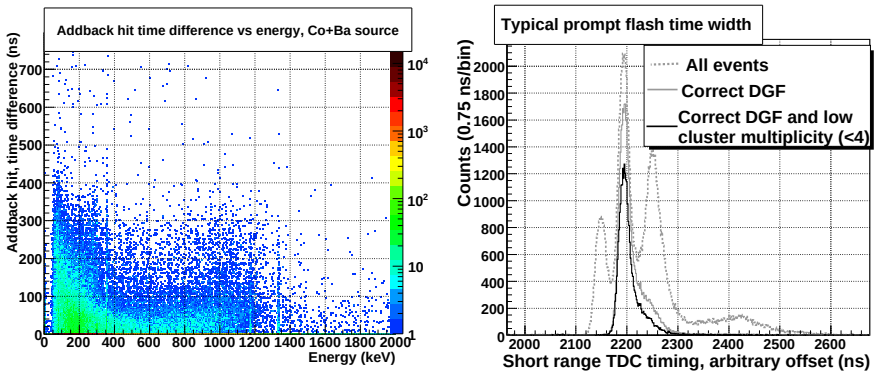

Fig. 4. Left: Time difference between hits in the addback *versus* summed γ-ray energy in the cluster detectors. Right: Time width of the prompt flash (see text for details).

Fig. 4 shows a two dimensional matrix of γ-ray summed energy versus time difference between γ-ray events used in that addback event. One can observe a significant increase in counts in that matrix for time difference less than 400 ns. The time width profile (*i.e.*, wider at lower energies) arises due to the fact that low energy γ rays typically interact in the outer most part of the crystal giving rise to the well known 'time walk' effect.

2.4. Experimental performance of the stopped beam array

Stopping ions with energies of several GeV in view of a high-efficiency γ-ray spectrometer such as RISING can be problematic due to the atomic radiation produced, the so-called 'prompt flash' [19]. This can cause multiple germanium detectors to fire with the prompt arrival of the ion and thus significantly reduces the effective efficiency for the measurement of delayed isomeric decays in the same event. This was a major concern in the previous fragmentation isomer campaign at GSI (see Ref. [8]) causing losses of up to 80% of the effective γ-ray efficiency. The high granularity of the 105 element RISING array is intended to overcome this problem. It was found that the flash multiplicity (*i.e.* number of crystal that fire during the ion implantation) depends on the energy of the implanted ion in the stopper [20]. A more systematic study, taking into account the stopper material and implantation position and depth is underway. Typical mean flash multiplicities range between 5 out of the total 105 individual detectors for the lighter ions (such as those in the ^{90}Rh setting) to 15 for the heavy nuclei (*e.g.*, ^{204}Pt). In the determination of the minimum isomeric lifetime that can be measured, the time width of this prompt flash component is of significance. Fig. 4 shows a typical prompt flash time profile. The dotted grey line is the time profile of the flash in the absence of any further software selection, while the full line represents events of multiplicity lower than 4 in any cluster and valid γ-ray energy in the DGF. The full grey line is with the proper energy in the DGF condition only. The width of the prompt flash is typically $\sim$ 30 ns. The triple peak structure apparent here has been observed in the RISING fast beam campaigns [21] and is believed to be caused by fast,light particles produced either in the stopper or in the final focal plane degrader.

The typical flight time in the FRS being a few 100 ns and the maximum gate achievable with the DGF being of 400 μs, the setup is highly sensitive to γ-ray decays from isomers with lifetimes in the range 100 ns $\rightarrow$ 1 ms. Decays with large internal conversion coefficients are hindered in their decays in flight since they are typically fully stripped of electronic electrons. In such cases, the width of the prompt flash can become a limiting factor for the observation of short-lived ($\sim$10 ns) isomers such as reported in reference [9].

3. Initial nuclear structure and reaction mechanism studies

Two RISING Stopped Beam experimental campaign have been performed to date. The first campaign begun with an experiment using a ^{107}Ag beam with the aim of producing nuclei on and around the $N = Z$ line [5]. Odd–odd $N = Z$ nucleus are of particular interest since they allow the mapping of the $T = 1$ and $T = 0$ components of the nucleon–nucleon interaction. The experiment showed evidence for isomeric decays in the $N = Z$ nuclei

$^{82}_{41}$Nb and $^{86}_{43}$Tc, the results of which are presented elsewhere in these proceedings [22, 23]. In the next experiment a ^{208}Pb 1 GeV/A beam was used to produce nuclei along and 'west' of the $N = 126$ shell closure. The initial results from this study experiments are presented in [13] and [24,25]. Finally in the first phase of experiments, a beam of ^{58}Ni was used to produce $^{54}_{28}$Ni and $^{54}_{26}$Fe to study mirror symmetries in those two $T = 1$ mirror nuclei, the initial results of this work can be found in [26].

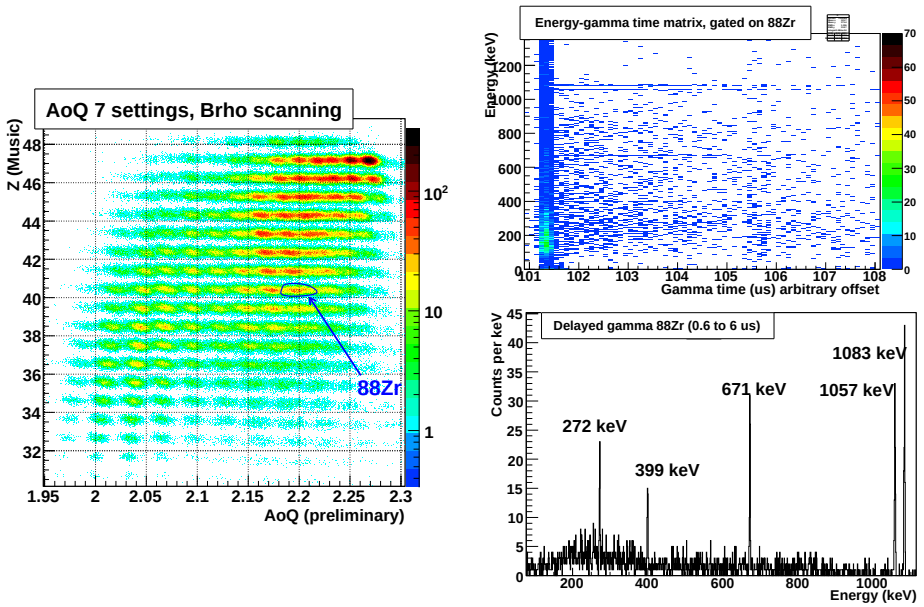

Fig. 5. Left: Sum identification plot for 6 of the 7 settings we made in Bρ scanning on the product of the ^{107}Ag 750 MeV/u beam. Right: Energy time matrix gatted on $^{88}_{40}$Zr [32] from left, and energy spectra projected for a time range after the prompt flash (600 ns to 6 μs).

During July 2007 a second Stopped RISING experimental campaign took place with the same setup, with the specific aim of studying nuclei in and close the $N = 82$ shell closure. The exotic nuclei were produced using by through fragmentation of an ^{136}Xe beam and following the relativistic projectile fission of an ^{238}U beam. The data analysis for both of these experiments is currently in progress [27].

Part of the beam time was used to pursue nuclear reaction studies with the aim of using isomeric states as a probe to test how much spin is involved in a fragmentation reaction (as in reference [28]). Indeed, for a given isomer an estimate can be made of the isomeric ratio *i.e.*, the proportion of times a given nucleus populates this isomer compared to the total number

of times the nucleus is created in the reaction. These type of studies are of particular interest for high-spin isomers such as those in ^{148}Tb or ^{147}Gd that were produced in the Stopped RISING experiment using the ^{208}Pb primary beam [25]. In such reaction studies having access of several types of observables in the same experiment allows a stringent test on the modelling of the physical reaction population and decay processes [29]. To this end, part of the ^{107}Ag primary beam time was used to perform Bρ scanning over a wide region of proton-rich nuclei in order to make measurements of nuclear production cross section and isomeric ratios (see Fig. 5). The modelling of the spin input in nuclear projectile fragmentation reactions follows the same formalism to that of the transfered linear momentum. Experimental access to the former is available through the position in the central focal point of the FRS. Thus it should be possible to make angular momentum population studies with respect to the transfered momentum for a wide range of final products using the ^{107}Ag. This analysis is currently in progress.

4. Summary and conclusions

Technical details of the RISING Stopped Beam setup have been presented together with an overview of the experiments carried out to date with this device. The setup will be upgraded with the addition of an active stopper which will allow the detection of the β decays from the implanted ions. This will allow β delayed γ-spectroscopy to be performed for heavy, exotic nuclei using a technique similar to that outlined in reference [30]. A proof of principle of this correlation can be found in [31].

This work is sponsored by the EPSRC (UK), the Swedish Research Council, the Polish Ministry of Science and Higher Education (grants 1-P03B-030-30 and 620/E-77/SPB/GSI/P-03/DWM105/2004-2007), the Spanish (Ministry of Education and Science (Minesterio de Education y Ciencias) under project number FPA2005-00696, the Bulgarian Science Fund VUF06/05, The US Department of Energy (grants DE-FG02-91ER-40609, W-31-109-ENG-38 and DE-AC02-06CH11357), the German Federal Ministry of Education and Research under grant 06KY205I and EURONS (European Commission contract number 506065). A.B.G. would also like to acknowledge financial support from the Nexia Solutions Ltd.

REFERENCES

[1] H.J. Wollersheim *et al.*, *Nucl. Instrum. Methods Phys. Res.* **A537**, 637 (2005).

[2] M. Górska *et al.*, *Acta Phys. Pol. B* **38**, 1219 (2007) these proceedings.

[3] G. Neyens *et al.*, *Acta Phys. Pol. B* **38**, 1237 (2007) these proceedings.

[4] S. Pietri *et al.*, Proc. of the 19th International Conference on the Application of Accelerators in Research and Industry, CAARI'06 Fort Worth, USA (2006), to be published in *Nucl. Instrum. Methods Phys. Res.* **B**.

[5] P.H. Regan *et al.*, Proc. of the IX$^{\text{th}}$ International Conference on Nucleus–Nucleus Collisions, Rio De Janeiro (2006), to be published in *Nucl. Phys.* **A**.

[6] R. Grzywacz *et al.*, *Phys. Rev.* **C55**, 1126 (1997).

[7] C. Chandler *et al.*, *Phys. Rev.* **C61**, 044309 (2000).

[8] Zs. Podolyák *et al.*, *Nucl. Phys.* **A722**, 273c (2003).

[9] M. Caamano *et al.*, *Eur. Phys. J.* **A23**, 201 (2005).

[10] Zs. Podolyák *et al.*, *Phys. Lett.* **B633**, 203 (2006).

[11] H. Geissel *et al.*, *Nucl. Instrum. Methods Phys. Res.* **B70**, 286 (1992).

[12] B. Voos *et al.*, *Nucl. Instrum. Methods Phys. Res.* **A364**, 150 (1995).

[13] S. Steer *et al.*, *Acta Phys. Pol. B* **38**, 1283 (2007), these proceedings.

[14] L. Audouin *et al.*, *Nucl. Instrum. Methods Phys. Res.* **A548**, 517 (2005).

[15] M. Wilhelm *et al.*, *Nucl. Instrum. Methods Phys. Res.* **A381**, 462 (1996).

[16] `http://www.xia.com/DGF-4C_Download.html`

[17] P. Doornenbal, private communication.

[18] A. Garnsworthy, private communication.

[19] P. Detistov *et al.*, *Acta Phys. Pol. B* **38**, 1287 (2007), these proceedings.

[20] S. Pietri *et al.*, Proc. of the RNB7 Conference, *Eur. Phys. J.* **A**, in press.

[21] P. Bednarczyk *et al.*, private communication.

[22] L. Caceres *et al.*, *Acta Phys. Pol. B* **38**, 1271 (2007), these proceedings.

[23] A. Garnsworthy *et al.*, *Acta Phys. Pol. B* **38**, 1265 (2007), these proceedings.

[24] Zs. Podolyak *et al.*, Proc. of the IX$^{\text{th}}$ International Conference on Nucleus–Nucleus Collisions, Rio De Janeiro (2006), to be published in **A**.

[25] Zs. Podolyák *et al.*, Proc. of the RNB7 Conference, to be published in *Eur. Phys. J.* **A**.

[26] D. Rudolph *et al.*, Proc. of the RNB7 Conference, to be published in *Eur. Phys. J.* **A**.

[27] M. Górska, A. Jungclaus, M. Pfützner *et al.*, private communication.

[28] M.Pützner *et al.*, *Phys. Rev.* **C65**, 064604 (2002).

[29] S. Pietri *et al.*, *AIP Conf. Proc.* **831**, 535 (2005); E. Le Gentil *et al.*, *Nucl. Instrum. Methods Phys. Res.* **A562**, 743 (2006).

[30] S. Grevy *et al.*, *Nucl. Phys.* **A746**, 145c (2004).

[31] T. Kurtukian-Nieto *et al.*, *AIP Conf. Proc.* **80**, 73 (2005).

[32] O. Hausser *et al.*, *Hyperfine Interact.* **4**, 196 (1978).

ISOMERIC STATES IN THE LIGHT Tc ISOTOPES*

A.B. Garnsworthy[a,b], P.H. Regan[a], S. Pietri[a], D. Rudolph[c]
L. Cáceres[d,e], M. Górska[d], Zs. Podolyák[a], S.J. Steer[a]
A. Heinz[b], F. Becker[d], P. Bednarczyk[d,g], P. Doornenbal[d]
H. Geissel[d], J. Gerl[d], H. Grawe[d], J. Grębosz[g,d], A. Kelic[d]
I. Kojouharov[d], N. Kurz[d], F. Montes[d], W. Prokopwicz[d]
T. Saito[d], H. Schaffner[d], S. Tachenov[d], E. Werner-Malento[d,f]
H.J. Wollersheim[d], G. Benzoni[h], B. Blank[i], C. Brandau[a]
A.M. Bruce[j], F. Camera[h], W.N. Catford[a], I.J. Cullen[a]
Zs. Dombrádi[k], E. Estevez[l], W. Gelletly[a], R. Hoischen[c]
G. Ilie[m,n], J. Jolie[m], G.A. Jones[a], A. Jungclaus[e], M. Kmiecik[g]
F.G. Kondev[o], T. Kurtukian-Nieto[l], S. Lalkovski[p], Z. Liu[a]
A. Maj[g], S. Myalski[g], M. Pfützner[f], T. Shizuma[a,r], A.J. Simons[a]
S. Schwertel[s], P.M. Walker[a], O. Wieland[h]

[a]Department of Physics, University of Surrey, Guildford, GU2 7XH, UK
[b]WNSL, Yale University, 272 Whitney Avenue, New Haven, CT, 06520, USA
[c]Department of Physics, Lund University, 22100 Lund, Sweden
[d]GSI, Planckstrasse 1, 64291 Darmstadt, Germany
[e]Departmento di Teórica, Universidad Autonoma de Madrid, Madrid, Spain
[f]IEP, Warsaw University, Hoża 69, 00-681 Warszawa, Poland
[g]The Institute of Nuclear Physics, 31-342 Kraków, Poland
[h]Universitá degli Studi di Milano and INFN Milano, 20133 Milano, Italy
[i]CENBG, le Haut Vigneau, 33175 Gradignan Cedex, France
[j]School of Engineering, University of Brighton, Brighton, BN2 4GJ, UK
[k]Institute for Nuclear Research, 4001 Debrecen, Hungary
[l]Universidad de Santiago de Compostela, Santiago de Campostela, Spain
[m]IKP, Universität zu Köln, 50937 Köln, Germany
[n]National Institute of Physics and Nuclear Engineering, Bucharest, Romania
[o]Nuclear Engineering Division, Argonne National Laboratory, IL-60439, USA
[p]Faculty of Physics, University of Sofia "St. Kliment Ohridsk" Sofia, Bulgaria
[r]Japan Atomic Energy Research Institute, Kyoto, 619-0215, Japan
[s]Physik Department E12, Technische Universität München, Garching, Germany

(Received November 1, 2006)

* Presented at the Zakopane Conference on Nuclear Physics, September 4–10, 2006, Zakopane, Poland.

Preliminary results from the first experiment of the Stopped Beam RISING campaign are presented. The relativistic projectile fragmentation of a 750 MeV/u beam of ^{107}Ag populated isomeric states in very neutron deficient nuclei at the proton dripline around mass 80–90. Nuclei were unambiguously identified using the FRagment Separator (FRS) and its ancillary detectors located at GSI. The ions produced were slowed down from relativistic energies by means of an Al degrader and implanted in the centre of the high-efficiency Stopped RISING array. This allowed the identification of new excited states in the $N = Z = 43$ nucleus, ^{86}Tc, populated following the de-excitation of a microsecond isomer. Preliminary results of this analysis, as well as previously unobserved isomeric states in ^{87,88}Tc, are reported.

PACS numbers: 29.30.Kv, 23.20.Lv

1. Introduction

The Rare ISotope INversigation at GSI (RISING) project utilises relativistic projectile fragmentation reactions to investigate the nuclear structure properties of highly exotic nuclei. Primary beams of energies ranging between 500 and 1000 MeV per nucleon are provided by the SIS-18 synchrotron and following fragmentation (or fission) the reaction products are separated and identified by the FRagment Separator (FRS) [1]. The FRS has a range of ancillary detectors used in the unambiguous identification of each ion on an event-by-event basis. The detector set-up at the focus of the FRS incorporates fifteen Germanium Cluster detectors, each with seven large volume crystals, in various configurations designed to meet the requirements of investigating the physics involved in each experiment [2,3]. Experiments have recently been performed as part of the collaboration's 'Stopped Beam' campaign. Here the ions are slowed down by a variable thickness aluminium degrader and brought to rest in the centre of the RISING Germanium array, arranged in a high efficiency configuration, to observe γ rays emitted in the decay of nano-to-millisecond isomeric states in exotic nuclei. Details of the earlier 'Fast-Beam' campaign which identified radiation emitted in the prompt decay of highly exotic nuclei can be found in ref [4]. Results from the first experiment of the 'Stopped Beam' campaign are presented here and further details can be found in [2,3,5].

2. Experimental details and results

A beam of ^{107}Ag was accelerated to 750 MeV/u by the SIS-18 Synchrotron and impinged on a 4 g/cm^2 Be target. The spill structure of the beam was $1\rightarrow3\times10^9$ ions over $5\rightarrow6$ secs in a total cycle time of 10 secs. The

reaction products were transported to the focal plane of the FRS and identified by A/q and Z using measurements of magnetic rigidity, time-of-flight, position and energy loss. Details of the particle identification can be found in [2, 3]. The ions were brought to rest in a perspex block of 7 mm thickness at the centre of the Stopped RISING array after being slowed down in a 2 g/cm^2 Al degrader. Gamma rays emitted from isomeric states were detected in the array and correlated with the arrival of the associated ion.

This experiment confirmed the isomer in ^{86}Tc, previously reported by Chandler *et al.* [6] and enabled the identification of previously unreported decays in ^{87,88}Tc. Figure 1 shows projections of Z for nuclei of $T_z = 0$, $\frac{1}{2}$ and 1 for which delayed γ rays were detected in various timing regimes. The uppermost panel shows the Z projection with no additional timing condition. The central panel is gated on γ rays observed between 0.5 and 5 μs after implantation to identify isomers with μs half-lives, and the lower panel shows nuclei gated between 150 and 500 ns to indicate short-lived isomers. Evidence for isomeric states in ^{86,87,88}Tc can be seen in these plots as well as the previously reported isomer in ^{84}Nb [6]. Details of the short-lived isomeric state in the $T_z = 0$ nucleus, ^{82}Nb can be found in [5].

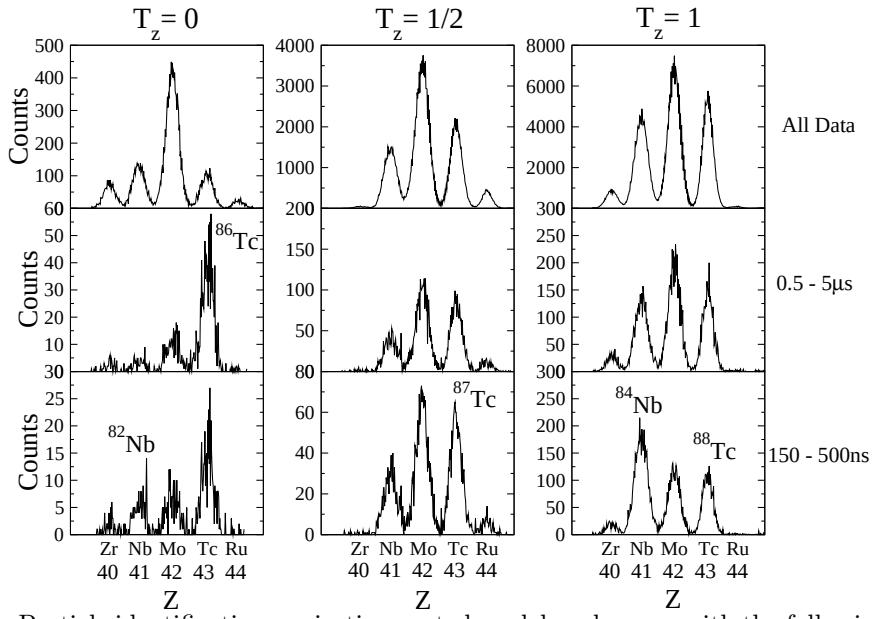

Fig. 1. Particle identification projections gated on delayed γ rays with the following time conditions: (Upper) No timing condition; (Centre) 0.5→5 μs; and (Lower) 150→500 ns after the time of implantation.

Figure 2 shows the delayed γ singles data collected for ions identified as ^{86}Tc. In this experiment we identify for the first time γ decay from isomeric states in these nuclei. Figure 2 also shows the delayed singles spectra for ions identified as ^{87}Tc and ^{88}Tc respectively. Previous work on the ^{87,88}Tc isotopes identified prompt transitions [7] but were not sensitive to the decay of isomeric states of the nano-to few microsecond range.

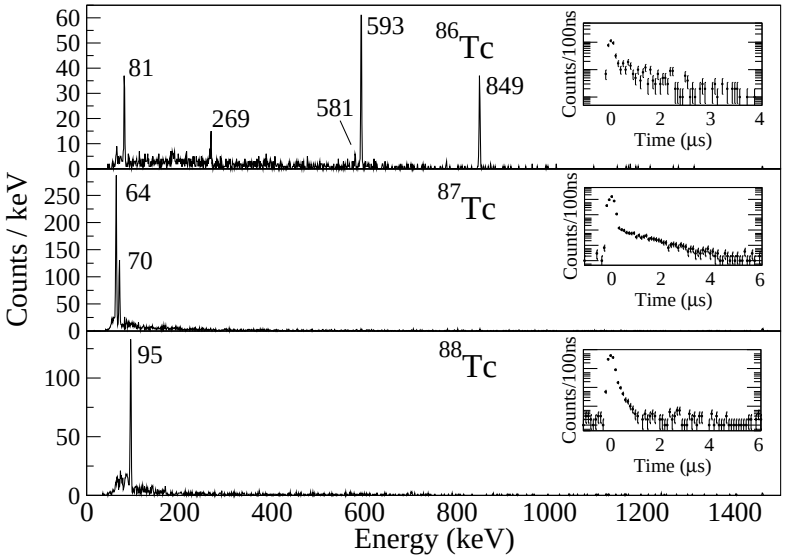

Fig. 2. Singles γ-ray spectra associated with ions identified as upper: ^{86}Tc, centre: ^{87}Tc, lower: ^{88}Tc. The insets show the time spectra produced by the signal from the DGF timing modules for each γ-ray event.

This work is sponsored by the EPSRC (UK), The Swedish Research Council, The Polish Ministry of Science and Higher Education (grants 1-P03B-030-30 and 620/E-77/SPB/GSI/P-03/DWM105/2004-2007), The Bulgarian Science Fund VUF06/05, The US Department of Energy (grants DE-FG02-91ER-40609, DE-AC02-06CH11357 and W-31-109-ENG-38), The Spanish Ministerio de Educación y Ciencia (Project number FPA2005-00696), The German Federal Ministry of Education and Research under grant 06KY205I and EURONS (European Commision contract number 506065). ABG would also like to thank Nexia Solutions Ltd for financial support.

REFERENCES

[1] H. Geissel, *Nucl. Instrum. Methods Phys. Res.* **B70**, 286 (1992).

[2] S. Pietri, accepted for *Nucl. Instrum. Methods Phys. Res.* **B**; *Acta Phys. Pol. B* **38**, 1255 (2007) these proceedings.

[3] P.H. Regan, *et al.*, *Nucl. Phys.* **A** in press.

[4] H.J. Wollersheim, *et al.*, *Nucl. Instrum. Methods Phys. Res.* **A537**, 637 (2005).

[5] L. Cáceres, *Acta Phys. Pol. B* **38**, 1271 (2007) these proceedings.

[6] C. Chandler *et al.*, *Phys. Rev.* **C61**, 044309 (2000).

[7] D. Rudolph, *et al.*, *J. Phys. G: Nucl. Part. Phys.* **17**, L113 (1991).

IDENTIFICATION OF EXCITED STATES IN THE $N = Z$ NUCLEUS ^{82}Nb*

L.S. Cáceres[a,b], M. Górska[a], A. Jungclaus[b], P.H. Regan[c] A.B. Garnsworthy[c,n], S. Pietri[c], Zs. Podolyák[c], D. Rudolph[d] S.J. Steer[c], H. Grawe[a], D.L. Balabanski[e,f], F. Becker[a] P. Bednarczyk[a,g], G. Benzoni[h], B. Blank[i], C. Brandau[a,c] A.M. Bruce[j], F. Camera[h], W.N. Catford[c], I.J. Cullen[c] Zs. Dombradi[k], P. Doornenbal[a,l], E. Estevez[m], H. Geissel[a] W. Gelletly[c], J. Gerl[a], J. Grębosz[g,a], A. Heinz[n], R. Hoischen[d] G. Ilie[l,p], J. Jolie[l], G.A. Jones[c], M. Kmiecik[g], I. Kojouharov[a] F.G. Kondev[o], T. Kurtukian-Nieto[m], N. Kurz[a], S. Lalkowski[j,s] L. Liu[c], A. Maj[g], S. Myalski[g], F. Montes[a], M. Pfützner[t] W. Prokopowicz[a,r], T. Saito[a], H. Schaffner[a], S. Schwertel[v] T. Shizuma[c,w], A.J. Simons[c], S. Tashenov[a], P.M. Walker[c] E. Werner-Malento[a,t], O. Wieland[h], H.J. Wollersheim[a]

[a]GSI, Planckstraβe 1, D-64291, Darmstadt, Germany
[b]Departamento de Física Teórica, Universidad Autónoma de Madrid, Spain
[c]Departament of Physics, University of Surrey, Guildford, UK
[d]Departament of Physics, Lund University, Sweden
[e]Dipartimento di Fisica, Universitá di Camerino, Italy
[f]Bulgarian Academy of Sciences, Sofia, Bulgaria
[g]The H. Niewodniczański Institute of Nuclear Physics, Kraków, Poland
[h]Università degli Studi di Milano and INFN Sez. di Milano, Italy
[i]CENBG, le Haut Vigneau, Bordeaux-Gradignan, France
[j]School of Engineering, University of Brighton, Brighton, UK
[k]Institute for Nuclear Research, Debrecen, Hungary
[l]IKP, Universität zu Köln, Köln, Germany
[m]Universidad de Santiago de Compostela, Santiago de Compostela, Spain
[n]Wright Nuclear Structure Laboratory, Yale University, New Haven, USA
[o]Nuclear Engineering Division, Argonne National Laboratory, USA
[p]National Institute of Physics and Nuclear Engineering, Bucharest, Romania
[r]Institute of Physics, Jagiellonian University, Kraków, Poland
[s]Faculty of Physics, University of Sofia, Sofia, Bulgaria
[t]Institute of Experimental Physics, Warsaw University, Warsaw, Poland
[v]Physik Departament E12, Technische Universität München, Garching, Germany
[w]Japan Atomic Energy Research Institute, Kyoto, Japan

(Received November 11, 2006)

* Presented at the Zakopane Conference on Nuclear Physics, September 4–10, 2006, Zakopane, Poland.

Information on the first excited states in the $N = Z = 41$ nucleus ^{82}Nb sheds light on the competition of isospin $T = 0$ and $T = 1$ states in the $A \sim 80$ region. The measurement was performed at the GSI laboratory using fragmentation of a ^{107}Ag primary beam at 750 MeV/u on a 4 g/cm^2 ^{9}Be target. The fragments were separated and identified unambiguously in the FRagment Separator. Three excited states were observed and the half-life estimate for the isomeric state was extracted. A tentative spin assignment based on the isobaric analogue states systematics in the $T_z = 1$ nucleus ^{82}Zr, and transition probabilities indicate $T = 1$ character of the first two excited states, and $T = 0$ for the isomeric state.

PACS numbers: 29.30.Kv, 23.20.Lv

1. Introduction

The low lying excited states in $N = Z$ nuclei at $A \sim 80$ have attracted many recent experimental studies. Most of them aim in the investigation of the competition between isospin $T = 0$ and $T = 1$ configuration expected in odd–odd $N = Z$ isotopes from $A = 76$ to $A = 96$ (see *e.g.* [1] for a recent review). Investigations of $^{62}_{31}$Ga [2], $^{66}_{33}$As [3] and $^{74}_{37}$Rb [4] have identified the ground state configuration with $I^\pi = 0^+$, $T = 1$ is crossed at low excitation energy by a higher spin, $T = 0$ configuration. The small density of the Nilsson single-particle levels in this region of nuclei leads to an abrupt change in the deformation by adding a few nucleons, or with the excitation energy as observed in *e.g.* ^{66}As [3], ^{70}Br [5], ^{78}Sr [6] and ^{82}Zr [6, 7]. Therefore, studies of excited states in heavier $N = Z$ isotopes will shed light on the isospin inversion and the shape evolution toward the doubly magic ^{100}Sn.

2. Experimental details, data analysis and results

The experiment performed at Gesellschaft für Schwerionenforschung (GSI) was part of the Stopped Beam Campaign using the Rare ISotope INvestigation at GSI (RISING) setup [8]. A primary beam of ^{107}Ag at 750 AMeV impinged on a 4007 mg/cm^2 ^{9}Be target. The projectile fragments were separated using the GSI FRagment Separator (FRS) [9] and identified unambiguously in terms of A and Z [10]. The $B\rho - \Delta E - B\rho$ method, used for the particle separation and identification, employed a variable wedge degrader in the middle focal place of the FRS.

At the final focal plane the ions passed through a second variable thickness degrader which slowed them down appropriately for further implantation in a perspex layer of 7 mm thickness.

γ rays were detected by the RISING Ge array consisting of 15 Euroball cluster detectors [11] placed around the stopper. Only delayed γ rays emitted after stopping of the ions were measured. The γ rays time and energy signals

were processed by XIA DGF4 [12] digital electronics (25 ns/ch). Additional analog electronic timing branches were used for short ($\leq 0.8\mu$s) and long ($\leq 100\mu$s) isomeric decay correlation times. Further experimental details can be found in Ref. [8].

The identification of ^{82}Nb ions was achieved on two-dimensional spectra analysis of atomic number Z versus A/q ratio. Complementary information was obtained from the position and energy loss of the fragments in the second focal plane of the FRS. For the selected isotope of interest, the delayed γ radiation from the de-excitation of an isomeric state was correlated in matrices of γ-ray energy versus time. The analysis was performed with the CRACOW software [13]. A time window of 25-1800 ns and 12-350 ns with respect to the ion implantation was applied to the DGF4 and short range TDCs, respectively. Three delayed transitions at energies of 123, 418 and 638 keV were associated to the isomer decay in ^{82}Nb. The effective energy threshold of the DGF4 electronic branch was lower (Fig. 1).

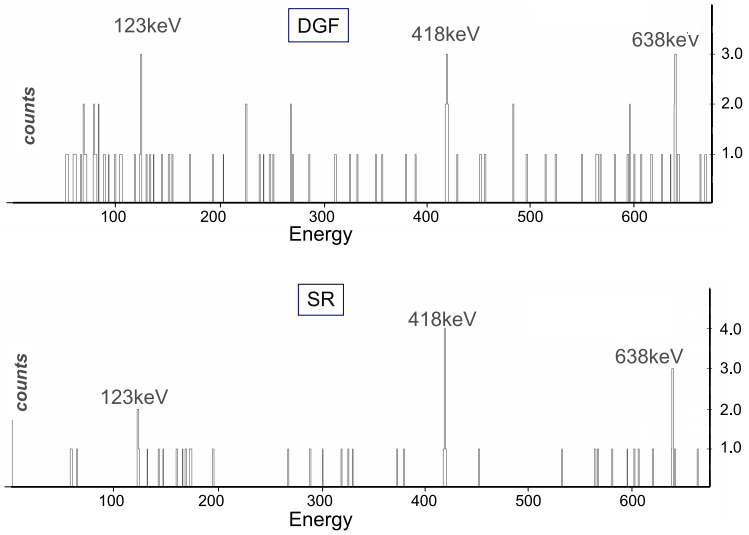

Fig. 1. Gamma ray energy spectrum of ^{82}Nb correlated with the DGF4 (DGF, upper panel) and short range (SR, lower panel) time branches.

The preliminary value of the isomeric half-life in ^{82}Nb was extracted by a fit of a single exponent to the summed time distributions of the 418 and 638 keV γ transitions away from the prompt response. The fit yielding values of 80(50) ns and 75(40) ns for the DGF4 and short range time branches, respectively, used the Maximum Likelihood method for the error bar treatment (Fig. 2).

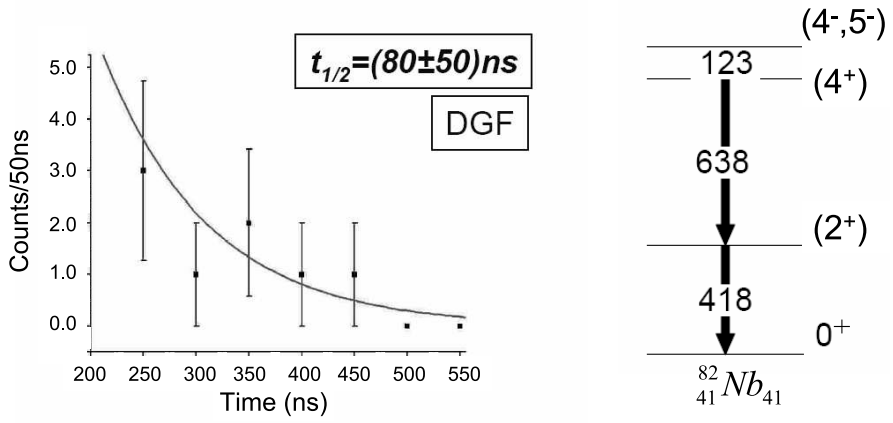

Fig. 2. Left: Isomeric decay curve fit for the DGF4 time branch. Right: Level scheme of ^{82}Nb deduced from this work.

3. Discussion

The ground state spin of ^{82}Nb was deduced *a priori* from the observation of super-allowed Fermi decay and assigned to be $I^\pi = 0^+$ and $T = 1$ [14]. The existence of short-lived isomeric state in this region of the chart of nuclei was indicated in Ref. [15]. As the ordering of transitions in the level scheme could not be deduced from the present experiment, the systematics was used for this purpose. The average $2^+ \to 0^+$ and $4^+ \to 2^+$ transition energy differences between $N = Z$ isotopes and their isobaric $T_z = 1$ analogue states amount to 20 keV and 44 keV, respectively, (^{86}Tc [16], ^{86}Mo [17]), (^{74}Rb [4], ^{74}Kr [6]), (^{70}Br [5], ^{70}Se [18]). Based on the comparison to the known transitions in ^{82}Zr the 418 keV and 638 keV were assigned to the $(2^+) \to 0^+$ decay and $(4^+) \to (2^+)$ decay respectively. The spin of the isomeric state was tentatively deduced from the transition probability analysis to $I^\pi = (4^-, 5^-)$. The low statistics did not allow for an unambiguous determination of the conversion coefficient for the 123 keV transition. This assignment implies an isospin change between the isomeric state and the (4^+) state. An E1 is the most likely assignment from both lifetime and intensity considerations, but at this stage of the analysis an M1 or mixed M1/E2 can not be ruled out completely for the 123 keV transition. Details of the interpretation will be given in a forthcoming paper.

This work is sponsored by the EPSRC (UK), the Swedish Research Council, the Polish Ministry of Science and Higher Education (grants 1-P03B-030-30 and 620/E-77/SPB/GSI/P-03/DWM105/2004-2007), the Spanish Ministry of Education and Science (project FPA2005-00696), the Bulgarian Science Fund VUF06/05, the US Department of Energy (grants DE-FG02-91ER-40609 and W-31-109-ENG-38), the German Federal Ministry of Education and Research under grant 06KY205I and EURONS (European Commission contract number 506065). ABG would also like to acknowledge financial support from Nexia Solutions Ltd.

REFERENCES

[1] J. Jänecke *et al.*, *Phys. Lett.* **B605**, 87 (2005).
[2] S.M. Vincent *et al.*, *Phys. Lett.* **B437**, 264 (1998).
[3] R. Grzywacz *et al.*, *Nucl. Phys.* **A682**, 41c (2001).
[4] D. Rudolph *et al.*, *Phys. Rev. Lett.* **76**, 376 (1996).
[5] D.G. Jenkins *et al.*, *Phys. Rev.* **C65**, 064307 (2002).
[6] D. Rudolph *et al.*, *Phys. Rev.* **C56**, 98 (1997).
[7] S.D. Paul, H.C. Jain, J.A. Sheikh, *Phys. Rev.* **C55**, 1563 (1997).
[8] S. Pietri *et al.*, accepted for *Nucl. Phys. Res. B*; *Acta Phys. Pol. B* **38**, 1255 (2007), these proceedings.
[9] H. Geissel *et al.*, *Nucl. Instrum. Methods* **B70**, 286 (1992).
[10] G. Münzenberg, *Nucl. Instrum. Methods* **B70**, 265 (1992).
[11] M. Wilhelm *et al.*, *Nucl. Instrum. Methods* **A381**, 462 (1996).
[12] `http://www.xia.com/DGF-4C_Download.html`
[13] J. Grębosz, *Comput. Phys. Commun.* (2006), in press.
[14] C. Longour *et al.*, *Phys. Rev. Lett.* **81**, 3337 (1998).
[15] C. Chandler *et al.*, *Phys. Rev.* **C61**, 044309 (2000).
[16] A. Garnsworthy *et al.*, *Acta Phys. Pol B* **38**, 1265 (2007), these proceedings.
[17] D. Rudolph *et al.*, *Phys. Rev.* **C54**, 117 (1996).
[18] T. Mylaeus *et al.*, *J. Phys. G: Nucl. Part. Phys.* **15**, L135 (1989).

ISOMERIC RATIO FOR THE $I^\pi = 8^+$ YRAST STATE IN ^{96}Pd PRODUCED IN THE RELATIVISTIC FRAGMENTATION OF ^{107}Ag*

S. Myalski[a], M. Kmiecik[a], A. Maj[a], P.H. Regan[b], A.B. Garnsworthy[b,c]
S. Pietri[b], D. Rudolph[d], Zs. Podolyák[b], S.J. Steer[b], F. Becker[e]
P. Bednarczyk[e,a], J. Gerl[e], M. Górska[e], H. Grawe[e], I. Kojouharov[e]
H. Schaffner[e], H.J. Wollersheim[e], W. Prokopowicz[e,f], J. Grębosz[a,e]
G. Benzoni[g], B. Blank[h], C. Brandau[b], A.M. Bruce[i], L. Cáceres[e,j]
F. Camera[g], W.N. Catford[b], I.J. Cullen[b], Zs. Dombradi[k]
P. Doornenbal[e], E. Estevez[l], H. Geissel[e], W. Gelletly[b]
A. Heinz[m], R. Hoischen[d], G. Ilie[m,n], G.A. Jones[b], A. Jungclaus[j]
A. Kelic[e], F.G. Kondev[o], T. Kurtukian-Nieto[l], N. Kurz[e]
S. Lalkovski[p], Z. Liu[b], F. Montes[e], M. Pfützner[r], T. Saito[e]
T. Shizuma[b,s], A.J. Simons[b], S. Schwertel[t], S. Tachenov[e]
P.M. Walker[b], E. Werner-Malento[e,r], O. Wieland[g]

[a]H. Niewodniczański Institute of Nuclear Physics, Polish Academy of Sciences
31-342, Kraków, Poland
[b]Department of Physics, University of Surrey, Guildford, GU2 7XH, UK
[c]WNSL, Yale University, 272 Whitney Avenue, New Haven, CT, 06520, USA
[d]Department of Physics, Lund University, 22100, Lund, Sweden
[e]GSI, Planckstrasse 1, 64291, Darmstadt, Germany
[f]M. Smoluchowski Institute of Physics, Jagiellonian University
30-059 Kraków, Poland
[g]Universitá degli Studi di Milano and INFN sez. Milano, 20133 Milano, Italy
[h]CENBG, le Haut Vigneau, 33175, Gradignan Cedex, France
[i]School of Engineering, University of Brighton, Brighton, BN2 4GJ, UK
[j]Departamento de Fisica Teorica, Universidad Autonoma de Madrid, Spain
[k]Institute for Nuclear Research, 4001, Debrecen, Hungary
[l]Universidad de Santiago de Compostella, Santiago de Compostella, Spain
[m]IKP, Universität zu Köln, 50937, Köln, Germany
[n]National Institute of Physics and Nuclear Engineering, Bucharest, Romania
[o]Nuclear Engineering Division, ANL, Argonne, IL 60439, USA
[p]Faculty of Physics, University of Sofia "St. Kliment Ohridsk" Sofia, Bulgaria
[r]Inst. of Experimental Physics, Warsaw University, Hoża 69, Warsaw, Poland
[s]Japan Atomic Energy Research Institute, Kyoto, 619-0215, Japan
[t]Physik Department E12, Technische Universität München, Garching, Germany

(Received November 11, 2006)

* Presented at the Zakopane Conference on Nuclear Physics, September 4–10, 2006, Zakopane, Poland.

We report on the preliminary results from a study of the decay of the $I^{\pi} = 8^{+}$ $T_{\frac{1}{2}} = 2\mu$s isomer in ^{96}Pd performed as part of the Stopped-Beam RISING campaign within the Rare Isotope Investigation at GSI (RISING). The ^{96}Pd ions were produced following the projectile fragmentation of a 750 MeV per nucleon ^{107}Ag primary beam. The reaction products were separated and identified by the in-flight method using the GSI Fragment Separator. The residues of interest were stopped in a perspex stopper surrounded by an array of 15, seven-element germanium Cluster detectors. One of the goals of the current work is to investigate the population of high-spin states produced projectile fragmentation reactions using isomeric ratio measurements to infer information on the angular momentum population distribution. In this short contribution the method and results of determining the isomeric ratio for the $I^{\pi} = 8^{+}$ microsecond isomer in ^{96}Pd nucleus are presented.

PACS numbers: 23.20.Lv, 29.30.Kv

1. Introduction and experimental details

The production of exotic nuclei following projectile fragmentation reactions has opened up the possibility for isomer-delayed spectroscopy with beams at both intermediate (*e.g.*, [1–6]) and relativistic (*e.g.*, [7–12]) energies. One area of specific interest for future studies involves the angular momentum population in such reactions which can be investigated by measurements of the isomeric ratio of specific spin/parity states. Studies compared with the 'sharp cut off model' for heavy nuclei following the relativistic fragmentation of ^{208}Pb and ^{238}U beams [7, 11] have highlighted significant isomeric ratios associated with medium-to-high spin near-yrast states. In the current work, we investigate a similar population mechanism, but specifically for *proton*-rich nuclei. The determination of the final isomeric ratio requires corrections to account for effects such as the finite in-flight-separation time of the species of interest, relativistic time dilation, internal conversion, decay branching ratios, feeding from higher-lying isomeric states and γ-ray detection efficiency (see references [9, 11, 14] for details).

This short contribution focusses on the determination of the isomeric ratio for the proton-rich nucleus ^{96}Pd which decays by a cascade of four stretched E2 transitions from the $I^{\pi} = 8^{+}$ isomer [13].

The isomeric state in the exotic nucleus of interest was produced following projectile fragmentation reactions between a primary beam of ^{107}Ag and a 4 g/cm^2 thick ^{9}Be target. The ^{107}Ag primary beam energy was 750 MeV/u and was produced in 4 second wide time spills each containing about 1.6×10^{7} ions. The different species were identified and separated through the FRS separator as described in Refs. [11, 14, 16]. At the final focus of the FRS

was the RISING γ-ray array [14–16] which detects the γ-rays depopulating the states of interest. Further experimental details can be found in Refs. [14, 17, 18].

2. Data analysis and determination of the isomeric ratio

The analysis was performed with the CRACOW software [19]. From the experimental FRS observables, namely the time-of-flight (TOF) between the intermediate and final focal plane and energy loss at the final focal plane, a 2-dimensional particle identification histogram of A/Q *vs* Z can be created, enabling the selection of the nucleus of interest. Figure 1 shows the particle identification spectrum with the γ-ray energy and time spectra for the decay of the 8^{+} isomer in the ^{96}Pd nucleus [13].

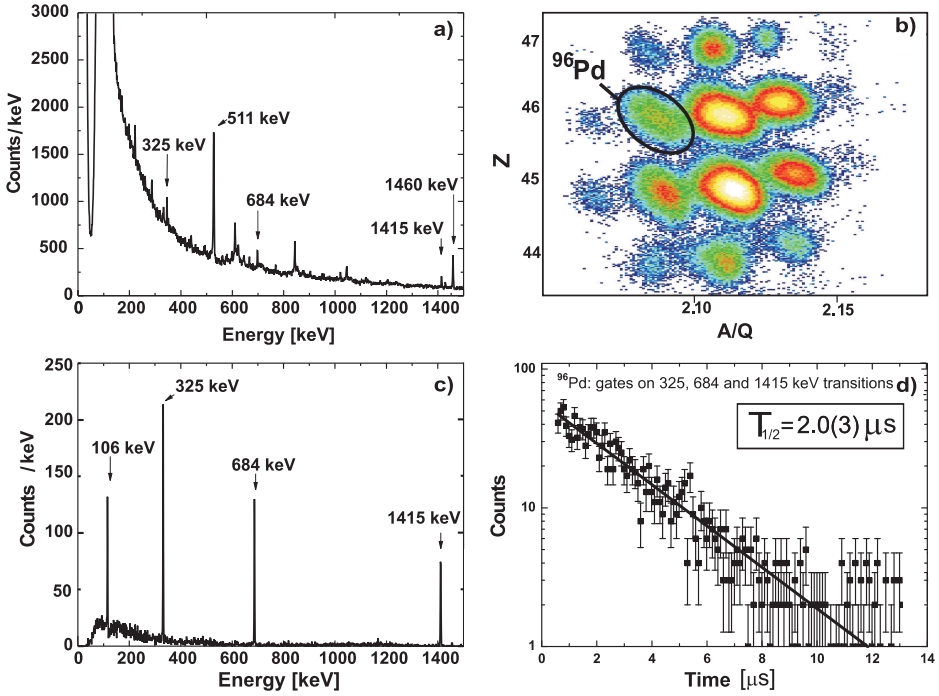

Fig. 1. (a) Ungated γ-ray spectrum; (b) Z *vs* A/Q particle-identfication spectrum showing region of fully-stripped ^{96}Pd ions; (c) ^{96}Pd ion-gated γ-ray spectrum between 150 ns and 14.7 μs following implantation in the perspex stopper; (d) Time decay spectra associated with the ^{96}Pd ions gated on the γ-ray transitions at 325, 684 and 1415 keV.

The isomeric ratio (R) is defined as the probability that in a reaction a given nucleus is produced in an given isomeric state [11]:

$$R = \frac{Y}{N_{\mathrm{imp}} F G}\,, \tag{1}$$

where N_{imp} is number of implanted heavy ions, Y is the yield, F is a correction factor for isomer losses and G is correction for finite detection time. N_{imp} is measured directly from the number of ions which are detected at the final focus of the FRS. On the other hand the yield, (Y) needs to be calculated from the intensity of γ-rays associated with the isomeric decay and corrected for in-flight losses, detection efficiency *etc.* In general, for ions which do not change charge state in flight,

$$Y = \frac{N_\gamma (1+\alpha)}{\varepsilon_{\mathrm{eff}} b_\gamma}\,, \tag{2}$$

where N_γ is intensity of gamma line at the specific energy, $\varepsilon_{\mathrm{eff}}$ is detector efficiency for that energy, α is internal conversion coefficient, and b_γ is the branching ratio. In the case of ^{96}Pd the decay follows only one branch (the 105, 325, 684 and 1415 keV transitions are all in a mutually coincident, 100% fed cascade [13]). If the ion is fully stripped of atomic electrons and the isomeric decay has a significant electron conversion branch, the decay can be significantly hindered and the effective 'in-flight' lifetime increased (*e.g.* [12]). Therefore we need also to calculate the factor F (in-flight correction for isomer losses) defined as

$$F = \exp\left[-\left(\lambda^{q_1}\frac{\mathrm{TOF}_1}{\gamma_1} + \lambda^{q_2}\frac{\mathrm{TOF}_2}{\gamma_2}\right)\right]\,, \tag{3}$$

where TOF_1 is flight time through the first part of separator, TOF_2 is flight time through the second part of separator, and accordingly γ_1 is the Lorentz factor in the first part and γ_2 corresponds to the second part. λ^{q_1} and λ^{q_2} are decay constants for the charge states in the first and the second half of separator. In the current work the ion is fully stripped during whole flight so $\lambda^{q_1} = \lambda^{q_2} = \lambda^0 = \lambda/(1+\alpha)$, with α being the conversion coefficient for the transition directly depopulating the isomer. For the first part, the flight time was estimated using the ion-optical code MOCADI [20] to be 149 ns. The second part can be measured directly comparing the timing signals from the two scintillators at the intermediate and final focal plane and was determined to be 177 ns. An internal conversion coefficient of $\alpha(\mathrm{E2}) = 1.13$ was used in the analysis for the 105 keV transition which directly depopulates the 8^+ isomer in ^{96}Pd.

Another important factor is the correction for finite detection time, (G) defined as

$$G = \exp(-\lambda t_{\rm start}) - \exp(-\lambda t_{\rm stop})\,, \tag{4}$$

where $t_{\rm start}$ is time of beginning of detection range, and $t_{\rm stop}$ is time of its end. For the spectra shown in Fig. 1, the delayed γ-ray detection range in the long-range TDCs [14] was from 150 ns to 14.7 μs following the ion implantation in the passive stopper.

To calculate the isomeric ratio, values of the half-life of the isomeric state must be known, which we measured in the current work to be 2.0(3) μs (see Fig. 1(d)). This half-life values was obtained by taking the sum of delayed γ-ray time projections in the long-range TDCs for the three strong lines at 325, 684 and 1415 keV associated with the decay cascade of the $I^\pi = 8^+$ isomer in ^{96}Pd [13]. The half-life deduced in the current work is consistent with the literature values for this isomer of 2.2(3) μs [13] and 1.7(1) μs [4]. Note also that the effective in-flight half-life for the fully-stripped ^{96}Pd ion in this experiment was calculated to be 4.3(6) μs due to the lack of any internal conversion decay branch in-flight.

We took into account the loss during the slowing down-implantation process due to nuclear reaction in the variable degrader mounted before stopper foil, which in this case corresponds to 10% of the nuclei.

Making these corrections and using the measured efficiency of the RISING array as discussed in reference [14], the value for the isomeric ratio of the yrast 8^+ state in ^{96}Pd was calculated.

Table I shows the calculated isomeric ratio values obtained using the 105 325, 684 and 1415 keV lines in the current analysis. Taking the weighted mean of these results, we obtain a value for the isomeric ratio of the $I^\pi = 8^+$ isomer in ^{96}Pd of $R = 20.5(10)\%$.

TABLE I

Data for transitions used in analysis.
The number of implanted ^{96}Pd ions was $N_{\rm imp} = 1.63\text{x}10^4$.

Energy [keV]	Counts	$\varepsilon_{\rm eff}$	α	R [%]
105	276	0.17(6)	$1.3\text{x}10^{0}$	23.4(40)
325	549	0.19(2)	$2.26\text{x}10^{-2}$	20.0(20)
684	351	0.13(1)	$2.54\text{x}10^{-3}$	18.6(15)
1415	250	0.08(1)	$4.82\text{x}10^{-4}$	20.1(15)

This value of isomeric ratio is of similar scale to the one obtained in Ref. [3], 39(6)%, although we note the two experiments were carried out in very different primary energy regimes and with different primary beams.

This work is sponsored by EPSRC (UK), the Swedish Research Council, the Polish Ministry of Science and Higher Education (grants 1-P03B-030-30 and 620/E-77/SPB/GSI/P-03/DWM105/2004-2007), the Bulgarian Science Fund VUF06/05, the US Department of Energy (grants DE-AC02-06CH11357 and DE-FG02-91ER40609), the German Federal Ministry of Education and Research under grant 06KY205I and EURONS (European Commission contract number 506065), the Spanish Ministry of Education and Science (project FPA2005-00696).

REFERENCES

[1] C. Chandler *et al.*, *Phys. Rev.* **C61**, 044309 (2000).
[2] P.H. Regan *et al.*, *Acta Phys. Pol. B* **28**, 431 (1997).
[3] R. Grzywacz *et al.*, *Phys. Lett.* **B355**, 439 (1995).
[4] R. Grzywacz *et al.*, *Phys. Rev.* **C55**, 1126 (1997).
[5] R. Grzywacz *et al.*, *Phys. Rev. Lett.* **81**, 766 (1998).
[6] J.M. Daugas *et al.*, *Phys. Lett.* **B476**, 213 (2000).
[7] Zs. Podolyák *et al.*, *Phys. Lett.* **B632**, 203 (2006).
[8] Zs. Podolyák *et al.*, *Phys. Lett.* **B491**, 225 (2000).
[9] K.A. Gladnishki *et al.*, *Phys. Rev.* **C69**, 024617 (2004).
[10] M. Pfützner *et al.*, *Phys. Lett.* **B444**, 32 (1998).
[11] M. Pfützner *et al.*, *Phys. Rev.* **65**, 064604 (2002).
[12] M. Caamano *et al.*, *Eur. Phys. J.* **A23**, 201 (2005).
[13] H. Grawe, H. Haas, *Phys. Lett.* **B120**, 63 (1983); W.F. Piel Jr *et al.*, *Phys. Rev.* **C28**, 209 (1983).
[14] S. Pietri *et al.*, *Acta Phys. Pol. B* **38**, 1255 (2007), these proceedings.
[15] P.H. Regan *et al.*, Proceedings of the IXth International Conference on Nucleus–Nucleus Collisions, Rio De Janeiro, 2006, *Nucl. Phys.* **A**, in press.
[16] S. Pietri *et al.*, Proceedings of the 19$^{\text{th}}$ International Conference on the Application of Accelerators in Research and Industry, CAARI'06, Fort Worth, USA, 2006, *Nucl. Instrum. Methods* **B**, in press.
[17] A. Garnsworthy *et al.*, *Acta Phys. Pol. B* **38**, 1265 (2007), these proceedings.
[18] L. Cáceres-Monllor *et al.*, *Acta Phys. Pol. B* **38** (2007), these proceedings.
[19] J. Grębosz, *Comput. Phys. Commun.* (2006), in press, doi:10.1016/j.cpc.2006.09.006.
[20] N. Iwasa *et al.*, *Nucl. Instrum. Methods Phys. Res.* **B126**, 284 (1997).

IDENTIFICATION OF ISOMERIC STATES 'SOUTH' OF ^{208}Pb VIA PROJECTILE FRAGMENTATION*

S.J. Steer[a], Zs. Podolyák[a], S. Pietri[a], P.H. Regan[a]
D. Rudolph[b], E. Werner-Malento[c,d], A.B. Garnsworthy[a,e]
R. Hoischen[b], M. Górska[c], J. Gerl[c], H.J. Wollersheim[c]
F. Becker[c], P. Bednarczyk[c,f], L. Cáceres[c,g], P. Doornenbal[c]
H. Geissel[c], J. Grębosz[c,f], A. Kelic[c], N. Kurz[c]
F. Montes[c], W. Prokopowicz[c,f], T. Saito[c], H. Schaffner[c]
S. Tachenov[c], A. Heinz[e], M. Pfützner[d], T. Kurtukian-Nieto[h]
G. Benzoni[i], A. Jungclaus[g], D.L. Balabanski[j,k], C. Brandau[a,c]
A.M. Bruce[l], W.N. Catford[a], I.J. Cullen[a], Zs. Dombradi[m]
E. Estevez[h], W. Gelletly[a], G. Ilie[o,p], J. Jolie[n], G.A. Jones[a]
M. Kmiecik[f], F.G. Kondev[p], S. Lalkovski[g,l], Z. Liu[a], A. Maj[f]
S. Myalski[f], T. Shizuma[a,s], S. Schwertel[t], P.M. Walker[a]
O. Wieland[i]

[a]Department of Physics, University of Surrey, Guildford, GU2 7XH, UK
[b]Department of Physics, Lund University, S-22100 Lund, Sweden
[c]GSI, Planckstrasse 1, D-64291, Darmstadt, Germany
[d]Institute of Experimental Physics, Warsaw University, Poland
[e]WNSL, Yale University, New Haven, CT, USA
[f]The Institute of Nuclear Physics PAN, Kraków, Poland
[g]Dept. di Fisica Teórica, Universidad Autonoma de Madrid, Madrid, Spain
[h]Universidad de Santiago de Compostela, Santiago de Campostela, Spain
[i]INFN, and Universitá degli Studi di Milano, Italy
[j]INRNE, Bulgarian Academy of Sciences, Sofia, Bulgaria
[k]Dipartimento di Fisica, Universitá di Camerino, Italy
[l]School of Engineering, University of Brighton, Brighton, BN2 4GJ, UK
[m]Institute of Nuclear Research, Debrecen, Hungary
[n]IKP, Universität zu Köln, Germany
[o]National Institute of Physics and Nuclear Engineering, Bucharest, Romania
[p]NED, Argonne National Laboratory, Argonne, USA
[r]Faculty of Physics, University of Sofia, Sofia, Bulgaria
[s]Japan Atomic Energy Agency, Kyoto, Japan
[t]Physik Department E12, Technische Universität München, Garching, Germany

(Received November 3, 2006)

* Presented at the Zakopane Conference on Nuclear Physics, September 4–10, 2006, Zakopane, Poland.

Relativistic fragmentation of ^{208}Pb has been used to produce excited states in neutron-rich nuclei with $N \approx 126$. Spectroscopic information for a range of nuclei has been obtained through observing delayed γ-ray emissions from isomeric states. Preliminary results for ^{203,204}Pt nuclei are presented. For the first time, excited states have been observed in ^{203}Pt and ^{204}Pt. The yrast structure of ^{204}Pt up to spin-parity, $I^{\pi} = (10^{+})$ has been tentatively inferred from the internal decay of two isomeric states.

PACS numbers: 21.10.–k, 23.20.–g, 25.70.Mn, 27.80.+w

1. Introduction

The Rare Isotopes Investigations at GSI (RISING) project has begun the Stopped Beam phase of experiments [1]; reported here are the first results from one of these measurements. Rare, exotic, neutron-rich nuclei in the vicinity of $N = 126$ were produced in the relativistic projectile fragmentation of a ^{208}Pb beam.

A number of $N \approx 126$ nuclei were produced during the fragmentation process. These present an ideal testing ground for the shell model, because of the limited number of valence nucleons involved in forming the low lying, yrast and near yrast excited states in these nuclei. The analysis of such states permits the extraction of information on the single-particle energies and residual shell-model interactions in this region.

2. Experimental details and results

The 1 GeV/nucleon ^{208}Pb beam, provided by the SIS-18 accelerator at GSI, was fragmented on a beryllium target (thickness 2.5 g/cm^2). The FRagment Separator (FRS) [2], operated in standard achromatic mode, was used to separate and identify the desired nuclei (see Fig 1). Once identified, nuclei were brought to a halt in a 7 mm plastic stopper. The delayed γ rays were detected over a 100 μs time range after implantation using the high efficiency RISING array [1], which, in its Stopped Beam configuration, surrounded the implantation target.

Delayed γ-ray spectra associated with ^{202,203,204}Pt are shown in Fig. 2. The observation of the previously identified isomeric state in ^{202}Pt [3] confirms the particle identification. Gamma rays belonging to ^{203}Pt and ^{204}Pt have been seen for the first time in this experiment. The ground state of ^{203}Pt was previously identified in projectile fragmentation at GSI [5], but the isomer in ^{203}Pt represents the first spectroscopic information on this $N = 125$ nucleus. Similarly, this is the first observation of excited states in ^{204}Pt; transitions from two isomeric states have been observed, with three γ rays (96, 1061, 1158 keV) originating from a shorter lived metastable state and two γ rays (872, 1123 keV) originating from a lower-lying, longer-lived isomer.

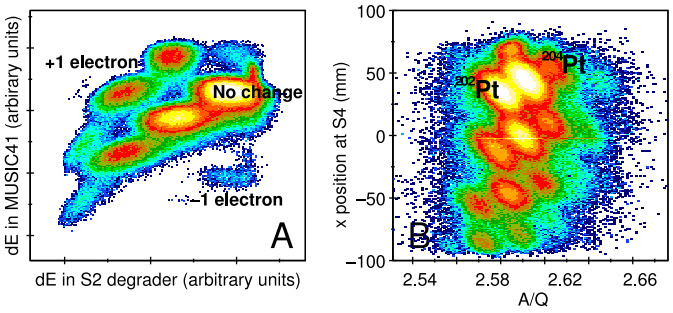

Fig. 1. Fragment identification. (A) Energy loss at the middle focal plane *versus* energy loss at the final focal plane. Charge state changes are distinguished here, allowing selection between nuclei that undergo no change, the loss of or gaining of an electron in the S2 achromatic degrader. (B) A/Q *versus* S4 position tangential to the beam direction. Only $\Delta Q = 0$ nuclei are plotted. Locations of the previously observed ^{202}Pt [3] and the newly identified ^{204}Pt nuclei are highlighted.

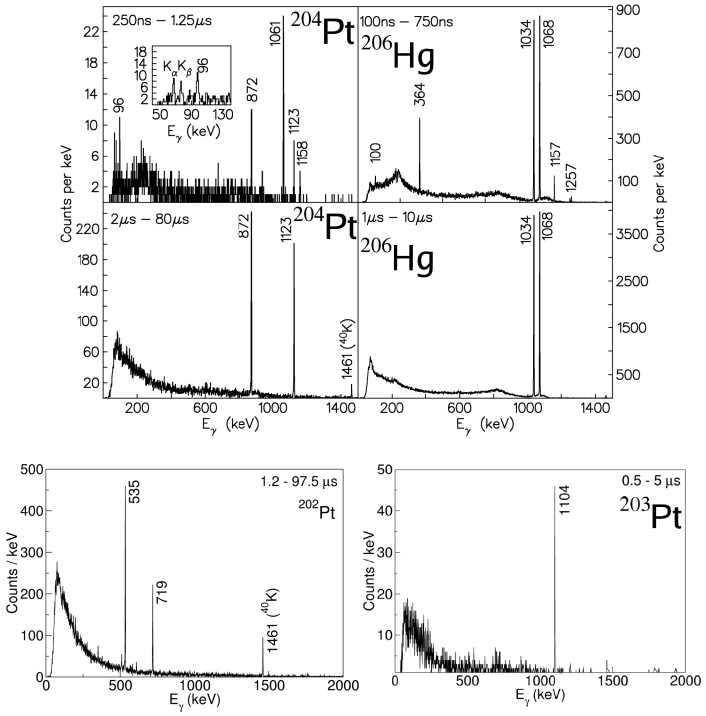

Fig. 2. Delayed γ-ray spectra associated with ^{202,203,204}Pt and ^{206}Hg. Note that the non-physical background suppression of low energy γ rays (up to ∼300 keV) is a result of data analysis techniques. Similar γ-ray spectra are observed for ^{206}Hg and ^{204}Pt, which exhibit 2-proton hole and 4-proton hole structures, respectively.

In producing ^{204}Pt four protons are removed from doubly closed shell ^{208}Pb. Like ^{206}Hg, ^{204}Pt has two isomeric states (see Fig. 2). The higher lying isomer in both cases is expected to be of a $(\pi_{h_{\frac{11}{2}}})^{-2}_{10^+}$ character [4]. This structure is associated with seniority two proton–hole states in the $Z = 82$ shell closure. A more detailed interpretation will be the subject of a future publication.

In conclusion, new spectroscopic information has been obtained on a range of heavy, neutron-rich nuclei, populated in relativistic energy projectile fragmentation. For the first time, excited states in $N = 125$ ^{203}Pt and the $N = 126$ ^{204}Pt have been presented, including the identification of three isomeric states.

This work is sponsored by the EPSRC (UK), the Swedish Research Council, the Polish Ministry of Science and Higher Education (grants 1-P03B-030-30 and 620/E-77/SPB/GSI/P-03/DWM105/2004-2007), the Bulgarian Science Fund VUF06/05, the US Department of Energy (grants DE-FG02-91ER-40609 and W-31-109-ENG-38), the German Federal Ministry of Education and Research under grant 06KY205I and EURONS (European Commision contract number 506065. ABG would like to acknowledge financial support from Nexia Solutions Ltd, FGK acknowledges the support of the US DOE, Office of Nuclear Physics, under Contract No. DE-AC02-06CH11357 and AJ acknowledges the spanish Ministerio de Educacion y Ciencia under project number FPA2005-00696.

REFERENCES

[1] S. Pietri, *et al.*, *Acta Phys. Pol. B* **38**, 1255 (2007) these proceedings.

[2] H. Geissel, *Nucl. Instrum. Methods Phys. Res.* **B70**, 286 (1992).

[3] M. Caamaño, *et al.*, *Eur. Phys. J.* **A23**, 201 (2005); Zs. Podolyák, *et al.*, *Nucl. Phys.* **A722**, 273c (2003).

[4] B. Fornal, *et al.*, *Phys. Rev. Lett.* **87**, 215201 (2001); A.R. Poletti, *et al.*, *Nucl. Phys.* **A580**, 64 (1994).

[5] T. Kurtukian-Nieto, *et al.*, *AIP Conf. Proc.* **802**, 73 (2005).

SIMULATION OF THE ELECTROMAGNETIC BACKGROUND RADIATION FOR THE RISING EXPERIMENTAL SET-UP*

P. Detistov

Faculty of Physics, St. Kliment Ohridski University of Sofia
1164 Sofia, Bulgaria

D.L. Balabanski

INRNE, Bulgarian Academy of Sciences
1784 Sofia, Bulgaria

Zs. Podolyák

Department of Physics, University of Surrey
Guildford, Surrey, GU2 7XH, UK

(Received October 29, 2006)

High level of electromagnetic radiation is produced in the interaction of relativistic ions with matter. A model to simulate it within GEANT4 has been developed in order to evaluate these sources of background and their influence on the experimental spectra. New classes have been added to the standard GEANT4 program libraries, describing the radiative electron capture, primary bremsstrahlung and secondary bremsstrahlung processes. Simulations of experiments within the RISING stopped beam campaign and comparison with the experimental results are presented.

PACS numbers: 25.75.–q, 25.70.–z, 25.70.Pq

1. Introduction

Utilization of secondary beams for spectroscopic experiments at relativistic energies is a major tool in studying exotic nuclei. Experiments with this technique are carried out at GSI, Darmstadt within the RISING (Rare

* Presented at the Zakopane Conference on Nuclear Physics, September 4–10, 2006, Zakopane, Poland.

ISotope INvestigations at GSI) project [1]. Here we report on a study of the background bremsstrahlung radiation in such experiments. The importance of the problem is related to the high production cross sections, high multiplicity and high end–point energy of the bremsstrahlung photons due to interaction of the relativistic ions with matter. As a result, the detector response is influenced to a large extent by the emitted bremsstrahlung. Detailed knowledge of the origin of the background and the way it influences the detection system is needed in order to be able reliably to determine reaction γ-rays of interest. Thus, the main motivation of this work is to create a reliable simulation tool for the background radiation processes in spectroscopic experiments with relativistic ions.

The model uses the GEANT4 [2] Monte Carlo simulation tool. In its standard distribution (up to version GEANT4.8.1) electron capture and bremsstrahlung processes for relativistic ions are not implemented. In order to introduce the bremsstrahlung emission in cases like this, two approaches are possible: *(i)* to consider the dynamics of the individual electrons involved in the stopping process of the ions and consequently track them, or *(ii)* create directly photons using theoretical cross sections for bremsstrahlung emission. The advantage of the first approach is that all particles involved in the bremsstrahlung process are tracked down one by one and proper picture of the angular distributions could be obtained. Disadvantage in this case is that the model is very time and resource consuming. The second approach takes advantage of the well defined relations describing the processes, which can be compared to experiment. A major disadvantage is the assumption that the born electrons never leave the target, reducing the applicability of this processes to thick targets. In the present study the second approach is used.

2. Bremsstrahlung of relativistic ions

The most important processes resulting in emission of electromagnetic radiation in heavy-ion atom collisions are: the K and L X-ray radiation from ionized target (or projectile) atoms, radiative electron capture (REC) — a process of capture of target electrons in a bound atomic state of the projectile, primary bremsstrahlung (PB) — a process of capturing a target electron into an atomic continuum state of the projectile, and secondary bremsstrahlung (SEB) which is emitted during the slowing down of the fast moving electrons produced in a collision with the projectile [3]. Although the X-rays originating from ionized target atoms have the highest intensity, they have very low energies in the case of light materials. In the experiments considered here they do not reach the detectors, and therefore, are not considered. REC and PB are one–step processes. REC results in dis-

crete lines, because the electron is captured in a well defined atomic state of the projectile. In the second case, due to the interaction with the continuum, the spectrum is continuous. The SEB process is a two–step process and the bremsstrahlung results from the interaction between the emitted electrons and matter, and involves the following steps: *(i)* interaction of the heavy ion with a target atom and emission of a relativistic electron and *(ii)* interaction of this electron with matter and emission of photons. In the accepted approach the electrons do not appear in the simulation process. We also assume that scattered electrons do not leave the target. The latter assumption is justified for thick targets. The properties of the three processes (energy spectra, cross sections and angular distributions) are described in details in Refs. [3, 4]. The theoretical cross sections are implemented in the simulations.

The GEANT4 cross sections for the REC process calculated within this model are compared in Fig. 1(a) with numerical calculations using different approximate models [3]. The simulations yield the proper order of magnitude of the cross section. In Fig. 1(b) the experimental data for 60 keV bremsstrahlung photons emitted in the stopping of 197 AMeV in different target materials [3] are compared with calculated PB and SEB cross sections integrated over the angle. In the low Z region the PB process has a larger contribution than SEB process, while for higher Z targets the situation is reverse. In the model the different processes are implemented in GEANT4 as separate classes (K and L REC are considered separately).

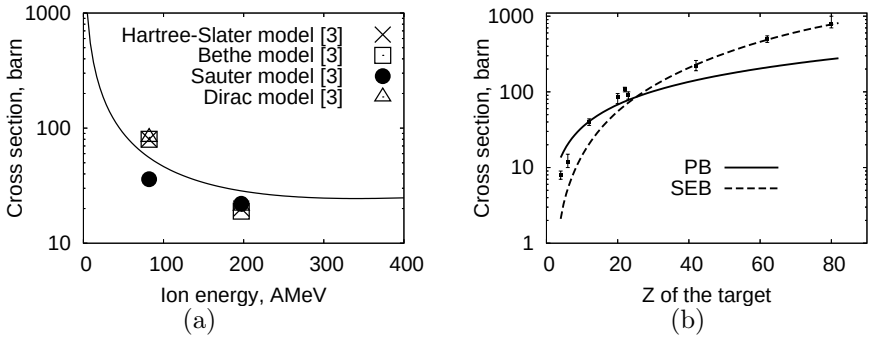

Fig. 1. (a) Comparison of GEANT4 calculations (solid line) with analytical model calculations for the REC cross section. (b) Experimental cross section for 60 keV bremsstrahlung photons as a function of the atomic number Z (dots) [3] *vs* calculations for the PB and SEB cross sections.

3. Bremsstrahlung in RISING stopped beam experiments

The RISING stopped beam set–up [7] consists of 15 Euroball Cluster detectors in 4π geometry, divided in 3 rings — at 55°, 90° and 125°. The secondary beam, which is selected by the Fragment Separator (FRS) passes in its last section through two multi-wire chambers, an ionization chamber and a time-of-flight scintillator, then it is slowed down with an Al degrader and stops in a target catcher, a 7 mm plastic in this case [8]. In the simulation the RISING detector array, the plastic target and the Al degrader, as the major source of bremsstrahlung, are considered.

An example is provided for the decay of the (7^-), $T_{1/2} = 280$ μs isomer in ^{202}Pt [5]. It decays by a cascade of three γ-rays, a doublet of 535 keV and a 719 keV γ-ray. The first 535 keV transition populates the 4_1^+ state, which decays via two consequential E2 transitions. The measured isomeric ratio is $\sim$ 15%. An event simulator for isomeric decays has been implemented which takes into consideration the orientation of the emitted γ-rays. The energy of the ions before the Al degrader is 422 AMeV, according to the MOCADI [6] (simulation program to calculate the transport of primary beams) calculations. As a result of the slow extraction of the ions from the primary target they are considered to arrive in an average interval of about 1 ms. In this way the detector response to the arrival of a single ion can be studied. The event simulator takes into consideration whether the impinging ion is an isomer and sets the time of emission of the γ-rays.

In Fig. 2 the experimental data are compared to simulated spectra for the forward and backward detectors. The simulated spectra are shifted downwards by an order of magnitude. The ratio of the experimental to the simulated spectra is shown in the lower part of the figure. There is a good agreement with the data at lower energies for forward angles. At back-

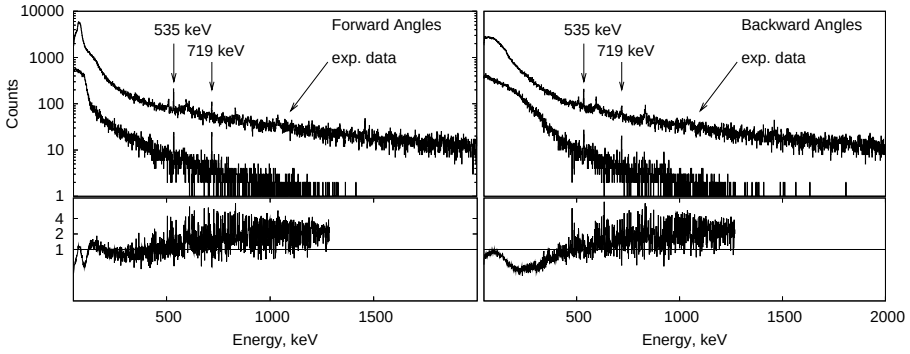

Fig. 2. Simulated *vs* experimental spectra of the ^{202}Pt isomeric decay for the forward (left) and backward (right) detectors (see details in the text).

ward angles at lower energies the agreement is worse and the simulation overestimates the bremsstrahlung flash. These photons originated from the Al degrader. At present, the simulations do not consider all construction materials, *e.g.* the supporting frame, which results in a larger number of low energy photons reaching these detectors. The model fails to reproduce also the high energy tail that is observed in the experiment. Note that this tail is much more pronounced at backward angles, while the bremsstrahlung flash is localized at forward angles. The reason for the high energy tail are relativistic electrons or light particles which come with the beam and hit directly the detectors. Such processes are not considered in the simulations. The spectra of the forward detectors are reproduced reasonably well because, due to the geometry of the experiment, these detectors see predominantly the bremsstrahlung flash. The decay γ–rays of ^{202}Pt are presented in Fig. 3. The intensities of 535 and 719 keV transitions, although overestimated, are reproduced reasonably well. For the 535 keV γ-rays the difference is about 30% and increases towards higher energies because, as mentioned, high energetic particles and other processes, resulting in low energy γ-rays radiation, are not taken into account.

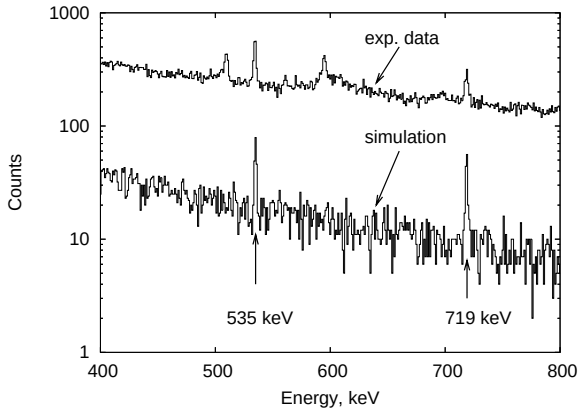

Fig. 3. The ^{202} Pt isomeric decay spectra. The upper line is experimental spectrum and the lower — the simulated spectrum which is shifted downwards by an order of magnitude.

In conclusion, the developed tool allows the bremsstrahlung emitted in stopping of relativistic heavy ions to be simulated with GEANT4. The provided example for the isomeric decay of ^{202}Pt, which was measured within the stopped beam RISING campaign [8], demonstrates the applicability of the simulation tool. In the future the developed model will be used in simulations of different experiments utilizing relativistic ions beams.

This work was supported in part by the EC EURONS RII3-CT-2004-506065 projects, the Bulgarian National Science Fund under grant VUF06/05 and by EPSRC (UK).

REFERENCES

[1] H.J. Wollersheim *et al.*, *Nucl. Instrum. Methods* **A537**, 637 (2005).
[2] `http://geant4.cern.ch`
[3] R. Anholt *et al.*, *Phys. Rev.* **A33**, 2270 (1986).
[4] R. Anholt *et al.*, *Phys. Rev. Lett.* **53**, 234 (1984).
[5] M. Caamaño *et al.*, *Eur. Phys. J.* **A23**, 201 (2005).
[6] N. Iwasa *et al.*, *Nucl. Instrum. Methods* **B126**, 284 (1997).
[7] S. Pietri *et al.*, *Eur. Phys. J.* **A**, in press.
[8] Zs. Podolyák *et al.*, *Eur. Phys. J.* **A**, in press.

Available online at www.sciencedirect.com
ScienceDirect
Nuclear Instruments and Methods in Physics Research B 261 (2007) 1079–1083
NIM B
Beam Interactions with Materials & Atoms
www.elsevier.com/locate/nimb

Recent results in fragmentation isomer spectroscopy with rising

S. Pietri [a,*], P.H. Regan [a], Zs. Podolyák [a], D. Rudolph [b], S. Steer [a], A.B. Garnsworthy [a,c], E. Werner-Malento [d,e], R. Hoischen [b], M. Górska [d], J. Gerl [d], H.J. Wollersheim [d], I. Kojouharov [d], H. Schaffner [d], F. Becker [d], P. Bednarczyk [d,f], L. Caceres [d,g], P. Doornenbal [d], H. Geissel [d], J. Grębosz [d,f], A. Kelic [d], N. Kurz [d], F. Montes [d], W. Prokopowicz [d,h], T. Saito [d], S. Tashenov [d], A. Heinz [c], M. Pfützner [e], T. Kurtukian-Nieto [i], G. Benzoni [j], M. Hellström [b], A. Jungclaus [g], J. Simpson [k], L.-L. Andersson [b], L. Atanasova [l], D. Balabanski [l,m], M.A. Bentley [n], B. Blank [o], A. Blazhev [p], C. Brandau [a,d], J.R. Brown [n], A.M. Bruce [q], F. Camera [j], W.N. Catford [a], I.J. Cullen [a], Zs. Dombrádi [r], E. Estevez [i], C. Fahlander [b], W. Gelletly [a], G. Ilie [p], E.K. Johansson [b], J. Jolie [p], G.A. Jones [a], M. Kmiecik [f], F.G. Kondev [s], S. Lalkovski [l], Z. Liu [a], A. Maj [f], S. Myalski [f], T. Shizuma [a,t], A.J. Simons [a], S. Schwertel [u], P.M. Walker [a], O. Wieland [j]

[a] *Department of Physics, University of Surrey, Guildford GU2 7XH, UK*
[b] *Department of Physics, Lund University, S-22100, Lund, Sweden*
[c] *WNSL, Yale University, New Haven, CT 06520-8124, USA*
[d] *GSI, Planckstrasse 1, D-64291 Darmstadt, Germany*
[e] *IEP, Warsaw University, Hoża 69, PL-00-681, Poland*
[f] *The Henryk Niewodniczański Institute of Nuclear Physics, PL-31-342, Kraków, Poland*
[g] *Departamento de Fisica Teórica, Universidad Autonoma de Madrid, E-28049 Madrid, Spain*
[h] *Jagellonian University, PL-31-342 Kraków, Poland*
[i] *Universidad de Santiago de Compostela, E-15706 Santiago de Compostela, Spain*
[j] *INFN, Universitá degli Studi di Milano, I-20133 Milano, Italy*
[k] *CCLRC Daresbury Laboratory, Daresbury Warrington, Cheshire WA4 4AD, United Kingdom*
[l] *Faculty of Physics, University of Sofia, BG-1164, Bulgaria*
[m] *Dipartimento di Fisica, Universitá di Camerino, I-62032, Italy*
[n] *Department of Physics, University of York, Heslington, York Y01 5DD, UK*
[o] *CENBG, le Haut Vigneau, F-33175 Gradignan Cedex, France*
[p] *IKP, Universität zu Köln, D-50937 Köln, Germany*
[q] *School of Engineering, University of Brighton, Brighton BN2 4GJ, UK*
[r] *Institute for Nuclear Research, Debrecen H-4001, Hungary*
[s] *Nuclear Engineering Division, Argonne National Laboratory, Argonne IL-60439, USA*
[t] *Japan Atomic Energy Agency, Kyoto 619-0215, Japan*
[u] *Physik Department E12, Technische Universität München, Garching, Germany*

Available online 25 April 2007

Abstract

The first results from the stopped beam RISING experimental campaign performed at the GSI laboratory in Darmstadt, Germany, are presented. RISING (Rare ISotope Investigations at GSI) constitutes a major new experimental program in European nuclear

* Corresponding author. Tel.: +44 1483 682730; fax: +44 1483 686781.
E-mail address: s.pietri@surrey.ac.uk (S. Pietri).

0168-583X/$ - see front matter
doi:10.1016/j.nimb.2007.04.219

structure physics research aimed at using relativistic energy (typically around 1 GeV per nucleon) projectile fragmentation reactions to populate nuclei with highly exotic proton-to-neutron ratios compared to the line of beta stability. In its high-efficiency 'stopped beam' configuration, the RISING γ-ray spectrometer consists of 105 individual, large volume germanium crystals which view a focal plane in which the exotic nuclei are brought to rest (i.e. 'stopped'). Here, decays from metastable or 'isomeric' states with half-lives in the nano to milliseconds range can be observed, often providing the first spectroscopic information on these exotic nuclear species. This paper introduces the physics aims of the stopped RISING collaboration and presents some technical details on the RISING detector array. Results of initial commissioning experiments are also shown and details of the planned future experimental program are given.

PACS: 21.10.Tg; 23.20.−g; 25.70.Mn; 29.30.Kv

Keywords: γ-Ray spectroscopy; Nuclear isomers; Nuclear structure

1. Introduction

The aim of the RISING collaboration is to study exotic nuclei through beam fragmentation or projectile fission at energies provided by the SIS synchrotron at GSI of a few hundreds of MeV per nucleon. Previous experimental campaigns have used these detectors for studies of 'in-beam' γ-ray spectroscopy at relativistic energies [1]. RISING was moved to its stopped beam configuration for the first time in February 2006 (Fig. 1). Two subsequent experimental campaigns have now been performed aimed at the study of nuclear structure using the isomer-delayed γ-ray spectroscopy technique as outlined in [2–4]. Some brief technical details of a selection of these experiments and the performance characteristics of the RISING array in this configuration are presented below.

2. Technichal details

2.1. Basic isotope production, selection and identification

The production of exotic beams is done by the fragmentation of a stable beam from SIS on a thick (typically a few g/cm^2) ^{9}Be target. The two-stage FRagment Separator (FRS) [5,6] is used in achromatic mode for the selection and identification of the reaction products using time of flight (ToF) and energy loss measurements. Through position determination as measured with plastic scintillators at the first and second focal plane of the FRS, the magnetic rigidity of the individual ions can be accurately determined. The time of flight information provided by these fast plastic scintillators allows the determination of the particle velocity, from which a mass over charge (A/Q) ratio can be

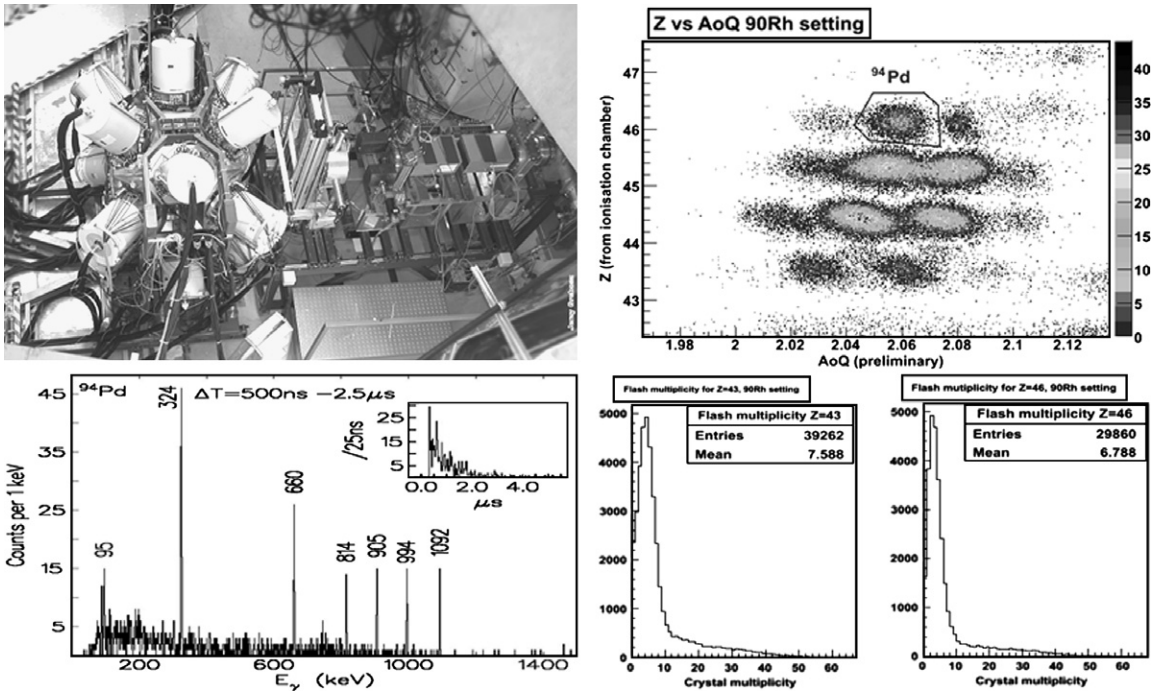

Fig. 1. Up left: the RISING stopped beam set-up, see text for details. Up right example of particle identification spectra obtained following the projectile fragmentation of the ^{107}Ag beam. The ^{94}Pd ions are selected and used to gate the delayed γ-ray energies observed between 500 ns and 2.5 μs following the ion implantation in the passive (perspex) stopper. These conditions produce the spectrum in the bottom left portion of the figure which shows gamma cascade associated with the $I^{\pi} = 14^{+}$ isomer in ^{94}Pd [2,9]. Bottom right: measured multiplicity of crystals which fired associated with the particle identification spectrum shown in Fig. 2-up for two different elements.

derived when the magnetic rigidity ($B\rho$) is known. Finally the charge is determined by two MUlti Sampling Ionization Chambers (MUSIC) at the end of the FRS (see Fig. 1) which measure the energy loss of the individual ions. A variable thickness aluminum degrader at the second focal point is used to slow down the ions such that they can be implanted in a passive stopper at the center of the germanium array. In the initial stopped RISING experiments, passive stoppers made from perspex, copper and beryllium were used. To minimize the transmission of hydrogen and higher charge states, niobium stripper foils were placed after the production target and the achromatic degrader.

2.2. The 'stopped beam' rising array

2.2.1. Technical data

The RISING array in its stopped beam configuration comprises 15 seven-element germanium cluster detectors [7] in a high-efficiency configuration (see Fig. 1). The detector were in three angular rings at 51°, 90° and 129° to the primary beam axis, each containing five cluster detectors. The average distance from the front face of the detectors to the centre of the passive stopped at the final focal place was approximately 22 cm. The measured photopeak γ-ray efficiency for the array in this geometry for sources placed in the center of the focal plane was approximately 15% at 661 keV.

2.2.2. Electronics

The two outputs from the Euroball pre-ampliers of the germanium detectors were sent to two separate electronics branch. The energy signal is processed by full digital electronic using DGF-4C modules from XIA [8]. This gives an energy resolution of less than 3 keV at 1.3 MeV under experimental conditions. Those modules have an internal clock with a 25 ns step which is used for the germanium timing signal. The fast plastic signal from the particle detector at the final focus of the FRS was also sent to each DGF crate to check the synchronization of the DGF crates. A second germanium preamplifier signal was sent to a conventional timing branch (TFA/CFD/TDC) with the TDC timing measured between the delayed gamma as a start signal and uses in 'common-stop' using the signal from the plastic in the second focal point. Two ranges of TDC were used, one with a short range of approximately 1.2 μs to give a good definition for short-lived (~10 ns) isomers and the CAEN 767 TDC with a range up to 800 μs. The total range for timing correlations between implanted ions and delayed γ-rays was determined by the maximum width of the DGF max coincidence window (400 μs).

3. Selected experimental results

During Feburary–March 2006 three experiments were performed using the stopped beam RISING set-up using beams of ^{58}Ni, ^{107}Ag and ^{208}Pb on Be production targets. The main physics aims of these studies were (i) the study of isospin symmetry $N = Z$ nuclei and (ii) the study of shell-model states in neutron-rich nuclei around the $N = 126$ shell gap. In addition, these experiments provided significant new information on the nuclear reaction mechanism associated with the population different angular momentum states in projectile fragmentation reactions.

Fig. 1 shows an example particle identification and delayed γ-ray spectra from the ^{107}Ag beam experiment using the DGF timing branch. The clean separation of the previously reported $I^{\pi} = 14^{+}$ isomer in ^{94}Pd [2,9] is readily apparent.

One of the major problems with previous fragmentation isomer studies has been a loss of γ-ray detection efficiency under the experimental conditions due to the so-called 'prompt flash' associated with light particles and bremsstrahlung during the slowing down process in the passive stopper which are observed by the germanium detectors [3]. One of the main drivers behind the design of the stopped beam array was its increased granularity over previously used set-ups [3,4]. Fig. 1 shows the measured prompt γ-ray multiplicity for Tc and Pd residues observed using the ^{107}Ag primary beam stopped in 7 mm of perspex in the center of the stopped RISING array. These results suggest that in this experiment only ~5% of the individual detectors were 'blinded' by this prompt radiation compared to values of ~80% in the closer geometry set-up [4]. The extra granularity of the RISING set-up thus clearly provides a major increase in the experimental efficiency for such studies.

3.1. Charge state separation and internal conversion suppression

In the majority of cases, the projectile fragmentation and fission products are transmitted through the FRS fully stripped of their atomic electrons (i.e. $Q = Z$), however, a fraction of the ions can be transmitted in other charge states, particularly hydrogen-like ions (i.e. $Q = Z - 1$). This can cause charge state anomalies and misidentification of ions unless accounted for. The technique outlined in [10] was used to discriminate between ions which do not change charge states between the first and second halves of the FRS (which are predominantly fully stripped ions) and those which pickup a electron (and thus change their charge by $-1e$) in the second portion of the FRS. This "$\Delta B\rho$, ΔE" technique [10] enhances the selection of fully stripped bare ions. Fig. 2 shows a particle identification plot for neutron-rich Pt and Au nuclei produced following the projectile fragmentation of a ^{208}Pb beam at 1 GeV per nucleon. The γ-ray spectra gated on fully stripped and hydrogen-like ^{204}Pt ($N = 126$ isotones of the beam) shown on the right side of Fig. 2 shows the effect the ionic charge state of the transmitted nuclei have on isomeric measurements. The transitions from isomeric decays in ^{204}Pt were observed for the first time in the February 2006 ^{208}Pb primary beam experiment. Two distinct isomers were

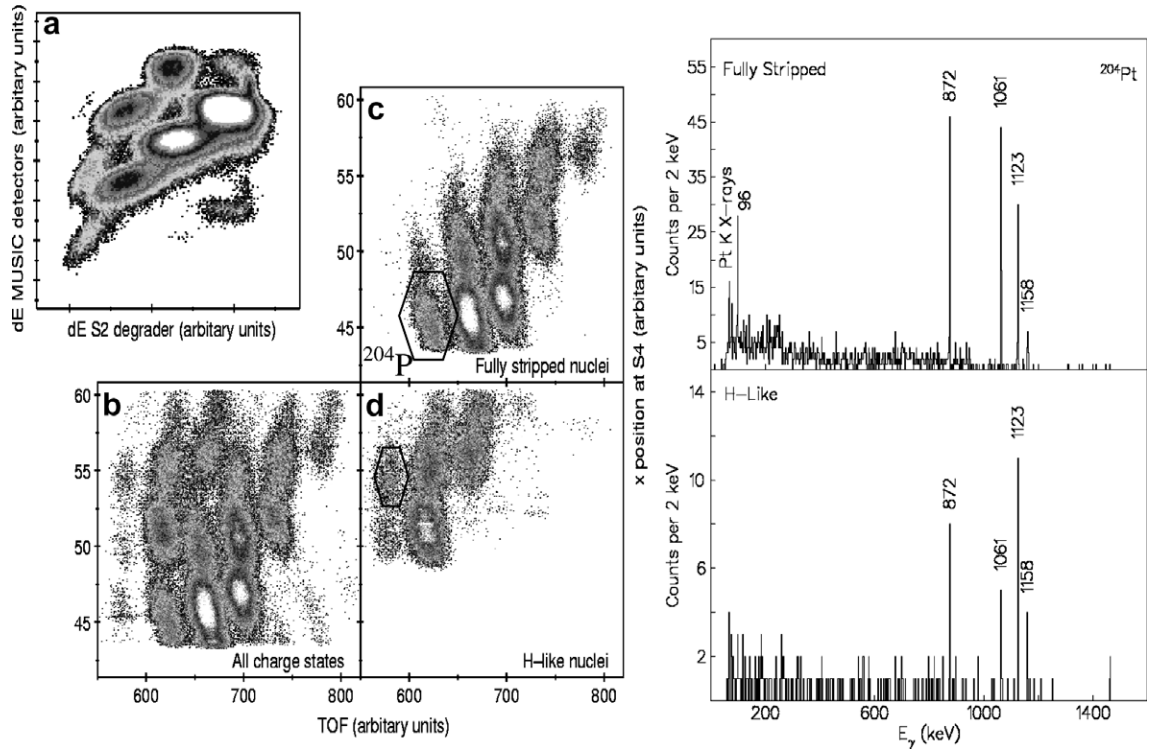

Fig. 2. (left) The charge state separation can be demonstrated using the deduced energy loss in the S2 degrader plotted against the energy loss of the ions in the MUSIC chambers. This can then be used to separate $Q = Z$ (fully stripped) and $Q = Z - 1$ (hydrogen-like) ions. (right) Transitions identified for the first time following isomeric decays in the $N = 126$ isotone ^{204}Pt for the first time following the fragmentation of a ^{208}Pb beam. The effect of fully stripping the ions of electrons and thus 'switching off' the internal conversion decay branches in flight is clearly demonstrated by the reduced observation of the 96, 1061 and 1158 keV transitions in the hydrogen-like spectrum (lower) compared to the fully stripped one (upper).

observed in this nucleus; with the higher-lying having a significant decay branch associated with a highly-converted, low-energy transition (96 keV). This internal conversion decay branch is 'switched off' for fully stripped ions and thus more of this decay survives through the few hundred nanosecond flight-time through the FRS. This is not the case for the same nucleus in the hydrogen-like state, where the decay can occur, thus explaining the difference between the relative intensities of the transitions shown in the upper and lower γ-ray spectra shown in Fig. 2.

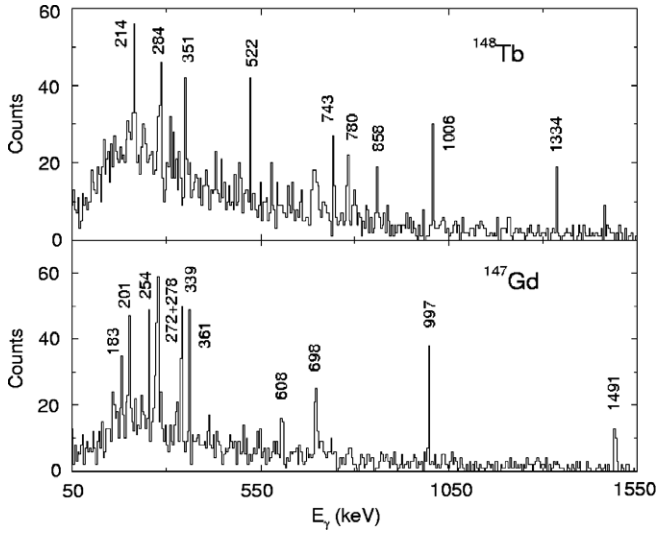

Fig. 3. γ-Ray spectra associated with the decays of the high-spin isomers in ^{147}Gd[11] and ^{148}Tb [12] as observed following the projectile of the ^{208}Pb beam. These decays represent the highest discrete spins observed to date in projectile fragmentation reactions.

3.2. High spin population in fragmentation

Fig. 3 shows the spectra associated with the previously reported isomers in ^{147}Gd [11] and ^{148}Tb [12] as observed in the current work following projectile fragmentation with the ^{208}Pb beam. The isomer in ^{148}Tb has an angular momentum of 27 h, which corresponds to the highest discrete angular momentum observed to date in projectile fragmentation reactions. The population and observation of such decay augurs well for future studies of high-spin states in exotic nuclei, particularly for neutron-rich species inaccessible with standard stable-beam/target fusion evaporation reactions.

4. Summary and conclusion

In addition to the brief results presented here from the ^{107}Ag and ^{208}Pb induced experiments, additional studies have now been performed using the stopped RISING set-up with ^{58}Ni, ^{136}Xe and ^{238}U primary beams. Highlights

from these studies include the identification of core breaking isomers in the ^{54}Fe/^{54}Ni mirror pair and the identification of new shell-model isomers close to the ^{132}Sn doubly magic core. Future plans include the use of fission fragments for studies of neutron-rich $A \sim 110$–130 nuclei and the implementation of a segmented silicon 'active stopper' placed in the centre of the RISING for β-delayed spectroscopy.

Acknowledgements

This work is supported by EPRSC(UK), The Swedish Research Council, The Polish Ministry of Science and Higher Education under grants 1-P03B-030-30 & 620/E-77/SPB/GSI/P-03/ DWM105/2004-2007, The Bulgarian Science Fund VUF06/05, The US Department of Energy under Grants W-31-109-ENG-38 & DE-FG02-91ER40609 and E*URONS (European Commission Contract No. 506065), the* German Federal Ministry of Education and Research under Grant 06KY205I.

References

[1] H.J. Wollersheim et al., Nucl. Instr. and Meth. A 537 (2005) 637.
[2] R. Grzywacz et al., Phys. Rev. C 55 (1997) 1126.
[3] Zs. Podolyak et al., Nucl. Phys. A 722 (2003) 273c.
[4] Zs. Podolyak et al., Phys. Lett. B 632 (2006) 203.
[5] H. Geissel, G. Munzenberg, K. Riisager, Ann. Rev. Nucl. Part. Sci. 45 (1995) 163.
[6] H. Geissel et al., Nucl. Instr. and Meth. B 70 (1992) 286.
[7] M. Wilhelm et al., Nucl. Instr. and Meth. A 381 (1996) 462.
[8] M. Pfützner et al., Nucl. Inst. and Meth. A 493 (2002) 155.
[9] N. Marginean et al., Phys. Rev. C 67 (2003) 061301.
[10] J. Benlliure et al., Nucl. Phys. A 660 (1999) 87.
[11] R. Broda et al., Z. Phys. A 305 (1982) 281.
[12] E. Ideguchi et al., Z. Phys. A 352 (1995) 363.

Observation of Isomeric Decays in the *r*-Process Waiting-Point Nucleus $^{130}Cd_{82}$

A. Jungclaus,[1] L. Cáceres,[1,2] M. Górska,[2] M. Pfützner,[3] S. Pietri,[4] E. Werner-Malento,[3] H. Grawe,[2] K. Langanke,[2] G. Martínez-Pinedo,[2] F. Nowacki,[5] A. Poves,[1] J. J. Cuenca-García,[2] D. Rudolph,[6] Z. Podolyak,[4] P. H. Regan,[4] P. Detistov,[7] S. Lalkovski,[8,7] V. Modamio,[1] J. Walker,[1] P. Bednarczyk,[2,9] P. Doornenbal,[2] H. Geissel,[2] J. Gerl,[2] J. Grebosz,[2,9] I. Kojouharov,[2] N. Kurz,[2] W. Prokopowicz,[2] H. Schaffner,[2] H. J. Wollersheim,[2] K. Andgren,[10] J. Benlliure,[11] G. Benzoni,[12] A. M. Bruce,[8] E. Casarejos,[11] B. Cederwall,[10] F. C. L. Crespi,[12] B. Hadinia,[10] M. Hellström,[6] R. Hoischen,[6,2] G. Ilie,[13,14] J. Jolie,[13] A. Khaplanov,[10] M. Kmiecik,[9] R. Kumar,[15] A. Maj,[9] S. Mandal,[16] F. Montes,[2] S. Myalski,[9] G. S. Simpson,[17] S. J. Steer,[4] S. Tashenov,[2] and O. Wieland[12]

[1]*Departamento de Física Teórica, Universidad Autónoma de Madrid, E-28049 Madrid, Spain*
[2]*Gesellschaft für Schwerionenforschung (GSI), D-64291 Darmstadt, Germany*
[3]*IEP, Warsaw University, PL-00681 Warsaw, Poland*
[4]*Department of Physics, University of Surrey, Guildford, GU2 7XH, United Kingdom*
[5]*IReS, IN2P3-CNRS/Université Louis Pasteur, F-67037 Strasbourg, France*
[6]*Department of Physics, Lund University, S-22100 Lund, Sweden*
[7]*Faculty of Physics, University of Sofia, BG-1164 Sofia, Bulgaria*
[8]*School of Engineering, University of Brighton, Brighton, BN2 4GJ, United Kingdom*
[9]*The Henryk Niewodniczański Institute of Nuclear Physics, PL-31342 Cracow, Poland*
[10]*KTH Stockholm, S-10691 Stockholm, Sweden*
[11]*Universidad de Santiago de Compostela, E-175706 Santiago de Compostela, Spain*
[12]*INFN, Universitádegli Studi di Milano and INFN Sezione di Milano, I-20133 Milano, Italy*
[13]*Institut für Kernphysik, Universität zu Köln, D-50937 Köln, Germany*
[14]*Institute of Physics and Nuclear Engineering, Bucharest, Romania*
[15]*Inter University Accelerator Centre, New Delhi, India*
[16]*University of Delhi, New Delhi, India*
[17]*LPSC, Université Joseph Fourier Grenoble 1, CNRS/IN2P3, Institut National Polytechnique de Grenoble, F-38026 Grenoble Cedex, France*

(Received 29 June 2007; published 24 September 2007)

The γ decay of excited states in the waiting-point nucleus $^{130}Cd_{82}$ has been observed for the first time. An 8^+ two-quasiparticle isomer has been populated both in the fragmentation of a ^{136}Xe beam as well as in projectile fission of ^{238}U, making ^{130}Cd the most neutron-rich $N = 82$ isotone for which information about excited states is available. The results, interpreted using state-of-the-art nuclear shell-model calculations, show no evidence of an $N = 82$ shell quenching at $Z = 48$. They allow us to follow nuclear isomerism throughout a full major neutron shell from $^{98}Cd_{50}$ to $^{130}Cd_{82}$ and reveal, in comparison with $^{76}Ni_{48}$ one major proton shell below, an apparently abnormal scaling of nuclear two-body interactions.

DOI: 10.1103/PhysRevLett.99.132501 PACS numbers: 21.60.Cs, 23.20.Lv, 26.30.+k, 27.60.+j

The pioneering work of Goeppert-Mayer [1] and Haxel, Jensen, and Suess [2] in realizing that the experimental evidence for nuclear magic numbers could be explained by assuming a strong spin-orbit interaction constituted a major milestone in our understanding of the internal structure of the atomic nucleus. However, it has been recognized for more than 20 years that the single-particle ordering which underlies the shell structure (and with it the magic numbers) may change for nuclei approaching the neutron dripline. It has been argued that the neutron excess causes the central potential to become diffuse, leading to a modification of the single-particle spectrum of neutron-dripline nuclei [3,4]. In addition, a strong interaction between the energetically bound orbitals and the continuum also affects the level ordering. The consequence of these modifications can be a shell quenching; i.e., the shell gaps at magic neutron numbers are less pronounced in very neutron-rich nuclei than in nuclei closer to stability. At the extreme, these gaps may even disappear. Alternatively, the tensor part of the nuclear force has been shown to cause shell reordering for very asymmetric proton and neutron numbers [5,6].

The $N = 82$ isotones below the doubly magic nucleus ^{132}Sn are crucial for stellar nucleosynthesis due to the close relation between the $N = 82$ shell closure and the $A \approx 130$ peak of the solar *r*-process abundance distribution. Based on the mass models available at that time, it was shown in the 1990s that the assumption of a quenching of the $N = 82$ neutron shell closure leads to a considerable improvement in the global abundance fit in *r*-process calculations [7,8], in particular, a filling of the troughs around $A \approx 120$ and 140. On the other hand, recently, alternative descriptions of the phenomenon have been given without invoking shell quenching at all [9,10]. Unfortunately, the very

neutron-rich $N = 82$ waiting-point nuclei are still out of reach experimentally. However, recent spectroscopic observations in nuclei close to ^{132}Sn have been interpreted as the first experimental evidence of a quenching of the $N = 82$ shell closure in ^{130}Cd [11,12], much closer to ^{132}Sn than predicted by any calculation. One such observation concerns the low excitation energy of 957 keV tentatively proposed for the 2^+ state of this nucleus [11].

In this Letter, we present the identification of an isomeric decay in ^{130}Cd, representing the most neutron-rich $N = 82$ waiting-point nucleus in which γ-ray transitions have been observed to date. The results present the most direct information with respect to any possible modification of the $N = 82$ shell gap close to ^{132}Sn.

Isomer spectroscopy was performed to search for an $I^\pi = 8^+$ isomer in ^{130}Cd. Such an isomeric state, based on a maximally aligned pair of proton holes in the $g_{9/2}$ orbit, was expected to exist in this nucleus in analogy to the 8^+ isomer observed in the valence analog Cd isotope ^{98}Cd$_{50}$ [13]. The experiment was performed at the Gesellschaft für Schwerionenforschung (GSI), Darmstadt, Germany. In the first part, ^{130}Cd was produced via 6-proton knockout from a ^{136}Xe projectile accelerated to 750 MeV/u by the SIS-18 synchrotron and impinging on a 4 g/cm^2 Be target. In the second part of the experiment, ^{130}Cd ions were produced using projectile fission of a ^{238}U beam at an energy of 650 MeV/u and a 1 g/cm^2 Be target. They were separated from other reaction products and identified ion by ion in the GSI fragment separator (FRS) [14] via the measurement of the energy loss, the magnetic rigidity, the positions in the intermediate and the final focal plane, and the time of flight in the second half of the FRS. Figure 1 illustrates the identification of the different Cd isotopes.

The fraction of the nuclei implanted in an excited isomeric state in a passive stopper at the spectrometer focal point was 10%–20% of the total population. These isomeric states then decay to the ground state by γ-ray emission. These γ rays were detected by 15 large volume Ge cluster detectors [15] from the former EUROBALL [16] spectrometer arranged in close geometry around the stopper. With the requirement of a delayed coincidence relationship between the implanted ion and the detected γ ray, the radiation can be unequivocally assigned to the decay of an isomeric state of a particular isotope. It should be stressed that only the unprecedented high gamma detection efficiency and granularity of the Ge array [17] available within the rare isotope spectroscopic investigation at GSI experimental campaign, in conjunction with the clean identification after fragmentation reactions at relativistic energies, allowed for the first time observation of isomeric decays in ^{130}Cd despite its very low production cross section.

The data for ^{130}Cd obtained from the two parts of the experiment have been combined. Figure 2 (top row) shows the spectrum of γ rays observed in delayed coincidence with a total of about 6300 identified and implanted ^{130}Cd ions. In this spectrum, four transitions are clearly observed with energies of 128, 138, 539, and 1325 keV, respectively.

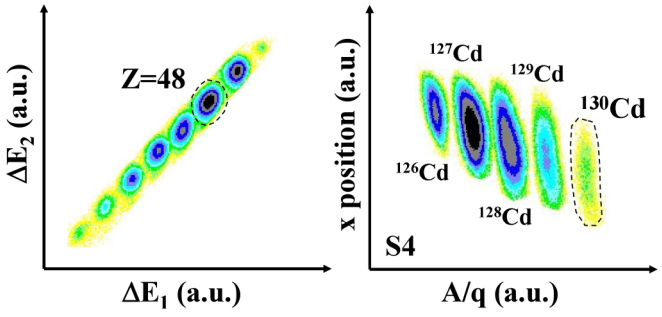

FIG. 1 (color online). Example of particle identification plots from the fragmentation of ^{136}Xe. Left: Z identification from the energy losses measured in two multiple sampling ionization chamber ionization chambers. Right: Isotope identification from the positions of the Cd ions in the final focal plane S4 of the FRS shown as a function of A/Q.

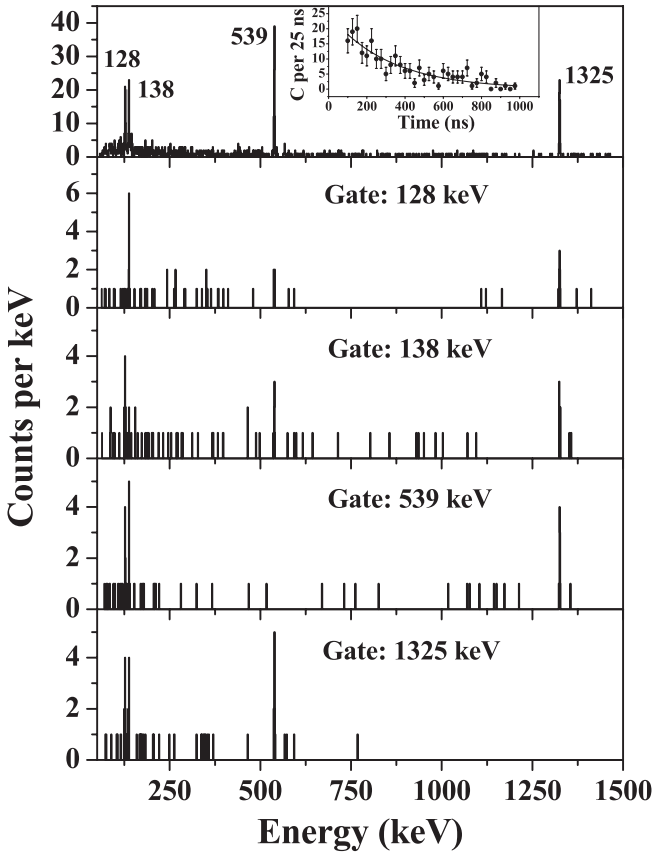

FIG. 2. Delayed γ-ray spectrum (75 ns–1 μs) in coincidence with identified ^{130}Cd ions implanted in the stopper. The inset shows the time distribution between the ion implantation and the detection of one of the four γ rays. The lower panels show the γ spectra observed in coincidence with the 128, 138, 539, and 1325 keV transitions, respectively.

TABLE I. Energy, half-life, relative intensity, and experimental and theoretical conversion coefficient for the transitions observed in delayed coincidence with implanted ^{130}Cd ions.

E_γ (keV)	$T_{1/2}$ (ns)	I_{rel}	α_{exp}	α_{theo} $E1$	α_{theo} $M1$	α_{theo} $E2$
128	216(48)	2.06(26)	0.63(26)	0.08	0.23	0.62
138	216(48)	2.16(27)	0.56(25)	0.07	0.19	0.48
539	214(33)	3.21(43)	...	...	...	...
1325	186(29)	3.62(56)	...	...	...	...

Since all of these transitions are observed in mutual coincidence as evidenced by the coincidence spectra included in Fig. 2, we may assume that they form a single cascade from one isomeric state to the ground state. Assuming that the transitions within the cascade have identical intensities, the missing gamma yield for the two low-energy transitions can be attributed to internal conversion. In Table I, we summarize the observed relative intensities of the four transitions and compare the experimental conversion coefficients for the 128 and 138 keV transitions with the theoretical ones for $E1$, $M1$, and $E2$ multipolarity. From this comparison, we conclude that $E2$ character is the most probable assignment for the two low-energy transitions.

In the $N = 50$ isotope $^{98}Cd_{50}$ [13], the transition energies in the $E2$ cascade from the maximally aligned 8^+ isomeric state to the antialigned 0^+ ground state are 147, 198, 688, and 1395 keV. We therefore assign the 1325 keV transition as the ground state transition and the 539 keV line as the $4^+ \rightarrow 2^+$ transition. The 128 and 138 keV γ rays form the $8^+ \rightarrow 6^+ \rightarrow 4^+$ sequence. Their order cannot be firmly established because their energies are so similar. The time distributions of the four transitions have been fitted separately with a single exponential decay. The resulting half-life values agree within their statistical uncertainties (see Table I). Assuming pure $\pi(g_{9/2})^{-2}$ configurations for the 2^+ to 8^+ states, the 6^+ state is expected to be an isomer with a nanosecond half-life, too. Unfortunately, the low statistics of the observed time distributions do not allow an independent determination of $T_{1/2}(6^+)$. We therefore deduced a single decay time of $T_{1/2} = 220(30)$ ns by performing a least-squares fit to the summed time spectra of all four transitions shown in the inset in Fig. 2. In ^{98}Cd, a 12^+ isomeric state has been observed feeding the 8^+ isomer [18]. We cannot exclude the existence of such a second, higher-lying isomer in ^{130}Cd.

Our experimental results are not consistent with the previous tentative assignment [11] of a 2^+ state at 957 keV in ^{130}Cd. In Fig. 3, the new level scheme for ^{130}Cd is compared to two different nuclear shell-model (SM) calculations based on a $^{88}Sr_{50}$ core and G-matrix realistic interactions derived for different model spaces from a CD-Bonn nucleon-nucleon potential [19] following the method outlined in Ref. [20]. The first, called SM-I in

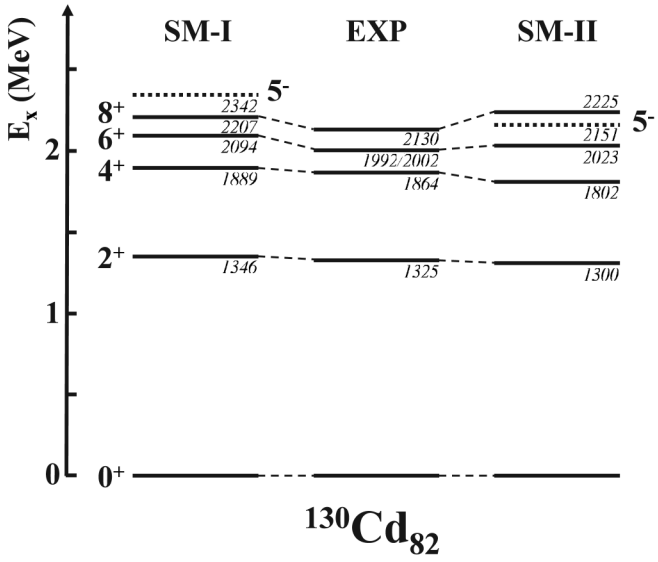

FIG. 3. Proposed level scheme of ^{130}Cd compared to two different shell-model calculations (see text for details). The isomeric 8^+ state [$T_{1/2} = 220(30)$ ns] at an excitation energy of 2130 keV is connected to the ground state via a cascade of four $E2$ transitions.

the following, uses a model space $p_{1/2}$, s, d, g for protons and $g_{7/2}$, s, d, $h_{11/2}$ for neutrons. This implies that excitations across the closed $Z = 50$ proton shell are included, whereas neutron excitations across the $N = 82$ shell closure are not. The effective interaction was monopole tuned to experimental data between $N = 50$ and 82 to reproduce single-particle and hole energies in ^{132}Sn [21]. It was first successfully applied to the study of the effects of ^{100}Sn core excitations in the $A = 102$–130 tin isotopes [22] and to β decay half-life predictions for $N = 82$ isotones [23]. Further details on the single-particle energies and effective operators used are given in Refs. [22–24]. The calculations were performed with the code ANTOINE [25]. The second shell-model calculation, SM-II, uses a model space $p_{1/2}$, $g_{9/2}$ for protons and, as in SM-I, $g_{7/2}$, s, d, $h_{11/2}$ for neutrons. Therefore, proton core excitations across $Z = 50$ and neutron core excitations across $N = 82$ are not considered in this approach. Starting from the G matrix for this valence space, an effective interaction was derived by applying monopole corrections to describe the evolution of experimental single-particle energies for ^{88}Sr to proton hole and neutron particle energies in ^{100}Sn as adopted from Refs. [9,26]. The interaction was found to describe both high-spin states and Gamow-Teller decay in the ^{100}Sn region very well [27]. For the ^{132}Sn region, besides $A^{-1/3}$ scaling, additional monopole corrections were applied to describe the single hole energies [9,26] in ^{132}Sn without modifying the ^{100}Sn results. For ^{130}Cd, proton and neutron effective charges of 1.5 e and 0.5 e, respectively, were used to calculate $E2$ transition strengths. Further details about these calculations, which were performed

with the shell-model code OXBASH [28], are given in Ref. [27]. The calculated $B(E2)$ transition strength for the $8^+ \rightarrow 6^+$ transition, $B(E2)^{\text{SM-I}} = 1.5$ W.u. and $B(E2)^{\text{SM-II}} = 1.2$ W.u., compare well with the experimental values of 1.7(2) and 1.3(2) W.u., respectively, obtained assuming either the 128 or the 138 keV γ ray to be the $8^+ \rightarrow 6^+$ transition. Note that these values are also in good agreement with the corresponding experimental value of 1.3(4) W.u. in ^{98}Cd [18]. Since both shell-model calculations employing modern interactions describe the level sequence and the decay properties of the 8^+ isomeric state, we conclude that our new experimental results on ^{130}Cd provide no evidence for a quenching of the $N = 82$ shell closure.

We close this Letter with a stunning observation. In an empirical shell-model approach [26], the $I = 2^+ - 8^+$ levels are pure $(g_{9/2})^{-2}$ states, while the 0^+ ground state is mixed with the $(p_{1/2})^{-2}$ configuration. Our new results on ^{130}Cd, in comparison with ^{98}Cd and ^{76}Ni$_{48}$ [29], therefore allow one for the first time to extract an empirical j^2 two-body interaction, namely, for $g_{9/2}$ protons and neutrons, over a wide range of atomic mass A. Apparently, the $2^+ - 8^+$ energy spread scales with A^{-1} (as indicated by solid arrows in Fig. 4), which seems to be at variance with the common assumption [25,30] of a scaling with the harmonic oscillator quantum $\hbar\omega_0 = 41A^{-1/3}$ (indicated by dashed arrows in Fig. 4). This result should not be affected by Coulomb effects as, for $I \neq 0$, Coulomb shifts are essentially constant in this model space [31]. However, this $g_{9/2}^{-2}$ interpretation of the $2^+ - 8^+$ energy difference could be altered when extended model spaces are considered. In the first approximation, the $2^+ - 8^+$ spreading can be estimated by considering only the quadrupole part of the effective interaction for which a scaling law $E_q \sim m^2/(D \cdot A^{1/3})$ has been derived that warrants shell structure and saturation [25]. Here m and D denote the number of particles at the Fermi level and the shell degeneracy. For both $T = 1$ excitations from the lower pf shell and across the $Z, N = 50$ magic shell closure to the sdg shell (proton excitations in the case of Cd, neutron excitations in the case of Ni), for which m and D are identical for all three isotopes, the familiar $A^{-1/3}$ scaling is preserved. However, for core excitations of the $Z = 28$ (^{76}Ni), $N = 50$ (^{98}Cd) and 82 (^{130}Cd) *closed shells* which involve strong proton-neutron ($T = 0$) interactions, an additional downscaling occurs with increasing major shell and D leading to the observed deviation from the $A^{-1/3}$ scaling.

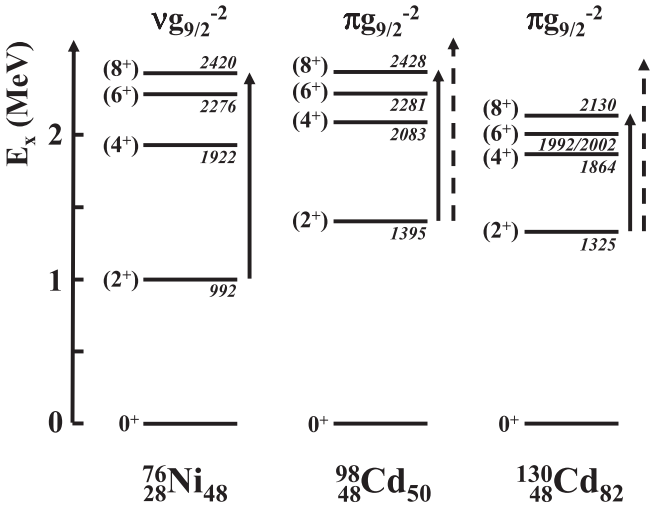

FIG. 4. Proposed level scheme of ^{130}Cd compared to the known level schemes of ^{76}Ni [29] and ^{98}Cd [13]. The solid arrows indicate the observed A^{-1} scaling, whereas the dashed arrows correspond to an $A^{-1/3}$ scaling of the $2^+ - 8^+$ energy spread.

In conclusion, the question of whether and how far below ^{132}Sn an erosion of the $N = 82$ shell closure occurs will be answered only when lighter $N = 82$ waiting-point nuclei become accessible for both mass measurements and spectroscopic investigations at future radioactive beam facilities. The new results on the level scheme of ^{130}Cd, however, give no evidence for $N = 82$ shell quenching in this nucleus.

A. J. acknowledges financial support from the Spanish Ministerio de Educación y Ciencia under Contract No. FPA2005-00696 and within the programa Ramón y Cajal. This work is further supported by the European Commission Contract No. 506065 (EURONS), the Swedish VR, EPSRC (United Kingdom), the German BMBF (No. 06KY205I), the Polish Ministry of Science and Higher Education (Grants No. 1-P03B-030-30 and No. 620/E-77/SPB/GSI/P-03/DWM105/2004-2007), and the Bulgarian Science Fund. J. L. Egido and W. Gelletly are thanked for valuable discussions and advice during the preparation of this manuscript. We acknowledge the effort of the GSI accelerator team to provide high quality beams.

[1] M. Goeppert-Mayer, Phys. Rev. **74**, 235 (1948); **75**, 1969 (1949); **78**, 16 (1950).
[2] O. Haxel, J. H. D. Jensen, and H. E. Suess, Phys. Rev. **75**, 1766 (1949).
[3] J. Dobaczewski, I. Hamamoto, W. Nazarewicz, and J. A. Sheikh, Phys. Rev. Lett. **72**, 981 (1994).
[4] M. M. Sharma and A. R. Farhan, Phys. Rev. C **65**, 044301 (2002).
[5] H. Grawe, Acta Phys. Pol. B **34**, 2267 (2003); Eur. Phys. J. A **25**, 357 (2005).
[6] T. Otsuka *et al.*, Phys. Rev. Lett. **87**, 082502 (2001); T. Otsuka, T. Suzuki, R. Fujimoto, H. Grawe, and Y. Akaishi, Phys. Rev. Lett. **95**, 232502 (2005).
[7] B. Chen *et al.*, Phys. Lett. B **355**, 37 (1995).
[8] B. Pfeiffer, K.-L. Kratz, and F.-K. Thielemann, Z. Phys. A **357**, 235 (1997).
[9] H. Grawe, K. Langanke, and G. Martínez-Pinedo, Rep. Prog. Phys. **70**, 1525 (2007).

[10] Y. Z. Qian, Nucl. Phys. **A752**, 550c (2005).
[11] T. Kautzsch *et al.*, Eur. Phys. J. A **9**, 201 (2000).
[12] I. Dillmann *et al.*, Phys. Rev. Lett. **91**, 162503 (2003).
[13] M. Górska *et al.*, Phys. Rev. Lett. **79**, 2415 (1997).
[14] H. Geissel *et al.*, Nucl. Instrum. Methods Phys. Res., Sect. B **70**, 286 (1992).
[15] J. Eberth *et al.*, Nucl. Instrum. Methods Phys. Res., Sect. A **369**, 135 (1996).
[16] J. Simpson, Z. Phys. A **358**, 139 (1997).
[17] S. Pietri *et al.*, Acta Phys. Pol. B **38**, 1255 (2007); S. Pietri *et al.*, Nucl. Instrum. Methods Phys. Res., Sect. A **261**, 1079 (2007).
[18] A. Blazhev *et al.*, Phys. Rev. C **69**, 064304 (2004).
[19] R. Machleidt, F. Sammarruca, and Y. Song, Phys. Rev. C **53**, R1483 (1996).
[20] M. Hjorth-Jensen, T. T. S. Kuo, and E. Osnes, Phys. Rep. **261**, 125 (1995).
[21] A. Gniady *et al.* (to be published).
[22] A. Banu *et al.*, Phys. Rev. C **72**, 061305(R) (2005).
[23] G. Martinez-Pinedo and K. Langanke, Phys. Rev. Lett. **83**, 4502 (1999); J. J. Cuenca-García *et al.* (to be published).
[24] K. Langanke and G. Martínez-Pinedo, Rev. Mod. Phys. **75**, 819 (2003).
[25] E. Caurier, G. Martínez-Pinedo, F. Nowacki, A. Poves, and A. P. Zuker, Rev. Mod. Phys. **77**, 427 (2005).
[26] H. Grawe, Lect. Notes Phys. **651**, 33 (2004).
[27] O. Kavatsyuk *et al.*, Eur. Phys. J. A **31**, 319 (2007).
[28] B. A. Brown *et al.*, MSU-NSCL Report No. 1289 (2004).
[29] C. Mazzocchi *et al.*, Phys. Lett. B **622**, 45 (2005).
[30] B. A. Brown, Prog. Part. Nucl. Phys. **47**, 517 (2001).
[31] R. Gross and A. Frenkel, Nucl. Phys. **A267**, 85 (1976).

Available online at www.sciencedirect.com
ScienceDirect
Physics Letters B 660 (2008) 326–330
PHYSICS LETTERS B
www.elsevier.com/locate/physletb

Neutron–proton pairing competition in $N = Z$ nuclei: Metastable state decays in the proton dripline nuclei $^{82}_{41}$Nb and $^{86}_{43}$Tc

A.B. Garnsworthy [a,b,*], P.H. Regan [a], L. Cáceres [c,d], S. Pietri [a], Y. Sun [e,f], D. Rudolph [g], M. Górska [c], Zs. Podolyák [a], S.J. Steer [a], R. Hoischen [c,g], A. Heinz [b], F. Becker [c], P. Bednarczyk [c,h], P. Doornenbal [c], H. Geissel [c], J. Gerl [c], H. Grawe [c], J. Grębosz [c,h], A. Kelic [c], I. Kojouharov [c], N. Kurz [c], F. Montes [c], W. Prokopowicz [c], T. Saito [c], H. Schaffner [c], S. Tachenov [c], E. Werner-Malento [c,i], H.J. Wollersheim [c], G. Benzoni [j], B.B. Blank [k], C. Brandau [a,c], A.M. Bruce [l], F. Camera [j], W.N. Catford [a], I.J. Cullen [a], Zs. Dombrádi [m], E. Estevez [n], W. Gelletly [a], G. Ilie [o,p], J. Jolie [o], G.A. Jones [a], A. Jungclaus [d], M. Kmiecik [h], F.G. Kondev [q], T. Kurtukian-Nieto [k,n], S. Lalkovski [l,r], Z. Liu [a], A. Maj [h], S. Myalski [h], M. Pfützner [i], S. Schwertel [s], T. Shizuma [a,t], A.J. Simons [a,u], P.M. Walker [a], O. Wieland [j], F.R. Xu [v]

[a] *Department of Physics, University of Surrey, Guildford, Surrey, GU2 7XH, UK*
[b] *WNSL, Yale University, 272 Whitney Avenue, New Haven, CT 06520, USA*
[c] *GSI, Planckstrasse 1, D-64291 Darmstadt, Germany*
[d] *Departmento di Teórica, Universidad Autonoma de Madrid, Madrid, Spain*
[e] *Department of Physics and Joint Institute for Nuclear Astrophysics, University of Notre Dame, Notre Dame, IN 46556, USA*
[f] *Department of Physics, Shanghai Jiao Tong University, Shanghai 200240, People's Republic of China*
[g] *Department of Physics, Lund University, S-22100 Lund, Sweden*
[h] *The Institute of Nuclear Physics, PL-31-342 Kraków, Poland*
[i] *IEP, Warsaw University, Hoża 69, PL-00-681, Poland*
[j] *Universitá degli Studi di Milano and INFN Milano, I-20133 Milano, Italy*
[k] *CENBG, le Haut Vigneau, F-33175, Gradignan Cedex, France*
[l] *School of Engineering, University of Brighton, Brighton, BN2 4GJ, UK*
[m] *Institute for Nuclear Research, H-4001 Debrecen, Hungary*
[n] *Universidad de Santiago de Compostela, Santiago de Campostela, Spain*
[o] *IKP, Universität zu Köln, D-50937 Köln, Germany*
[p] *National Institute of Physics and Nuclear Engineering, Bucharest, Romania*
[q] *Nuclear Engineering Division, Argonne National Laboratory, Argonne, IL 60439, USA*
[r] *Faculty of Physics, University of Sofia "St. Kliment Ohridski", Sofia, Bulgaria*
[s] *Physik Department E12, Technische Universität München, Garching, Germany*
[t] *Japan Atomic Energy Agency, Kyoto 619-0215, Japan*
[u] *AWE plc., Aldermaston, Berkshire, RG7 4PR, UK*
[v] *Department of Technical Physics, Peking University, Beijing 100871, People's Republic of China*

Received 11 October 2007; received in revised form 6 December 2007; accepted 8 January 2008

Available online 18 January 2008

Editor: V. Metag

Abstract

The low-lying structures of the self-conjugate ($N = Z$) nuclei $^{82}_{41}Nb_{41}$ and $^{86}_{43}Tc_{43}$ have been investigated using isomeric-decay spectroscopy following the projectile fragmentation of a ^{107}Ag beam. These represent the heaviest odd–odd $N = Z$ nuclei in which internal decays have been

* Corresponding author at: Department of Physics, University of Surrey, Guildford, Surrey, GU2 7XH, UK.
E-mail address: a.garnsworthy@surrey.ac.uk (A.B. Garnsworthy).

0370-2693/$ – see front matter
doi:10.1016/j.physletb.2008.01.017

identified to date. The resulting level schemes shed light on the shape evolution along the $N = Z$ line between the doubly-magic systems $^{56}_{28}$Ni and $^{100}_{50}$Sn and support a preference for $T = 1$ states in $T_z = 0$ odd–odd nuclei at low excitation energies associated with a $T = 1$ neutron–proton pairing gap. Comparison with Projected Shell Model calculations suggests that the decay in ^{82}Nb may be interpreted as an isospin-changing K isomer.

PACS: 29.30.Kv; 23.20.Lv

Pairing correlations are a fundamental aspect in describing many areas of physical structure, for example BCS pairs in superconducting metals [1]. The nucleus is a unique system in this respect as three pairing modes are present; neutron–neutron (nn), proton–proton (pp) and neutron–proton (np). The np pairing mode represents a two-fluid system in which the components can be coupled (or "paired") together in two ways, (i) with the intrinsic spins, s, parallel ($T = 0$), or (ii) anti-parallel ($T = 1$), where T is the isospin quantum number [2].

Structurally related states appear in nuclei of the same mass number, A (but different numbers of protons, Z, and neutrons, N), when an np pair is exchanged with an nn or pp pair. The appearance of these isospin multiplets is a manifestation of the charge independence of the strong nuclear force, a cornerstone of our current understanding of nuclear structure. States with the same isospin quantum number form analogous spectral patterns in these isobaric chains, with individual nuclear species characterised by their isospin projection quantum number $T_z = \frac{N-Z}{2}$. In most nuclei the states with the lowest energy have isospin values $T = T_z$. However this pattern can be modified in nuclei with equal numbers of protons and neutrons. It is only in $N \approx Z$ nuclei where the proton and neutron states at the Fermi surfaces have a sufficient spatial overlap that protons and neutrons in equivalent orbitals can couple (i.e., np pairs) to form both $T = 1$ and $T = 0$ states of similar energies [3]. There has been longstanding interest in the structure of medium mass even–even $N = Z$ nuclei with the aim of determining the magnitude of the $T = 1$, np pairing strength through the observation of 'delayed alignments' at higher spins in such systems [4,5]. Self-conjugate nuclei represent a unique laboratory in which the direct competition between the $T = 1$ and $T = 0$ neutron–proton pairing mode can be investigated.

The ground state β-decay half lives of all odd–odd $N = Z$ nuclei up to $^{98}_{49}$In have been reported [6,7]. All those between $^{34}_{17}$Cl and $^{98}_{49}$In, except $^{58}_{29}$Cu, are consistent with superallowed Fermi β-decay, indicating $T = 1$ ground states with spin/parity, $I^\pi = 0^+$. Excited states in odd–odd $N = Z$, fpg shell nuclei up to $^{78}_{39}$Y have also been identified using heavy-ion fusion-evaporation reactions and charged-particle detectors [8–15]. In each case excited states have been identified and assigned as Isobaric Analogue States of the $T = 1$, $I^\pi = 2^+$ and 4^+ states in the $T_z = 1$ isobar providing evidence for a $T = 1$, np pairing condensate. Odd-spin states at low excitation energy have also been observed and interpreted as $T = 0$ states.

Deformation plays a key role in the structure of self-conjugate nuclei due to the coinciding low level densities in both the proton and neutron nuclear potential. Stable ground-state deformation has been shown to exist along the $N = Z$ line with the maximum at $^{76}_{38}$Sr$_{38}$ [16]. A swift change from this deformed nuclear potential to a near-spherical shape is predicted to lie just above the $Z = 40$ shell gap. The $Z = 41$ nuclei are suggested to represent this boundary [17] and therefore it is expected that heavier systems will have softer, less-deformed shapes.

With the exception of ^{78}Y (^{76,77}Y are particle bound), the odd–odd $N = Z$ nuclei with $A \geqslant 70$ also lie on the proton dripline [18–20] i.e. they are the lightest particle-bound isotopes of their respective element. The low proton (compared to neutron) separation energies of these nuclei make the production cross-sections of these nuclei in fusion-evaporation reactions extremely low ($\sim$ μb) compared to the total fusion cross-section ($\sim$ 1 b). Projectile fragmentation provides an alternative mechanism to populate such nuclei, where the existence of isomers allows the identification of excited states [21].

Here we report on new results for the self-conjugate proton drip-line nuclei, $^{82}_{41}$Nb and $^{86}_{43}$Tc. These are the heaviest odd–odd $N = Z$ nuclei in which γ-ray transitions have been observed and support a dominance of the $T = 1$ pairing interaction over its $T = 0$ counterpart. The isomer in ^{86}Tc has been reported previously, and two transitions tentatively assigned [21]. In the same work evidence for a short-lived isomer was reported in ^{82}Nb but no discrete γ-rays observed. Some preliminary analyses of the current work have been reported in conference proceedings [22,23].

The current experiment was performed at the Gesellschaft für Schwerionenforschung (GSI) where a ^{107}Ag primary beam was accelerated to 750 MeV per nucleon by the SIS-18 synchrotron and made to impinge on a 4 g/cm^2 Be target. The typical primary beam current was 2×10^9 ions per beam spill over an extraction time of 5 s. The reaction products were transported to the focal plane of the FRagment Separator (FRS) [25] and identified using values of A/q and Z calculated from measurements of magnetic rigidity, time-of-flight, position and energy loss. The fully-stripped nature (i.e. $Z = q$) of the ions enabled an unambiguous particle identification [25,26]. The ions were stopped in a 7 mm thick perspex block at the centre of the Stopped RISING gamma-ray array [26,27]. In this configuration the array consisted of 105 Ge crystals grouped into 15, 7 element clusters with a measured photo-peak efficiency of $\sim$ 15% at 662 keV. Gamma-rays emitted in the decay of isomeric states were detected in the array and correlated with the arrival time of the associated ion.

During the experiment, the FRS was tuned to maximise the transmission of ^{82}Nb ($\sim$ 5 hours primary beam time) and ^{86}Tc

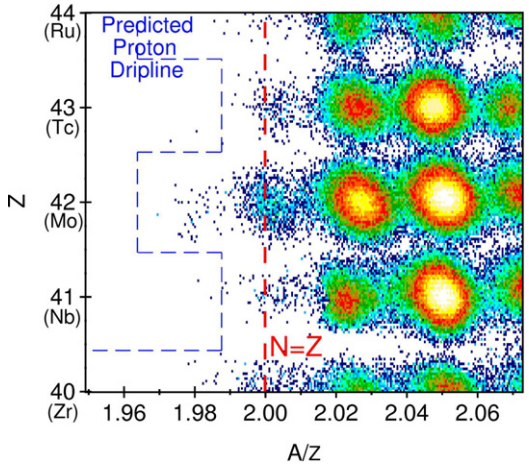

Fig. 1. Particle identification plot for combined data of the current work and the location of the predicted proton dripline as calculated from Ref. [24].

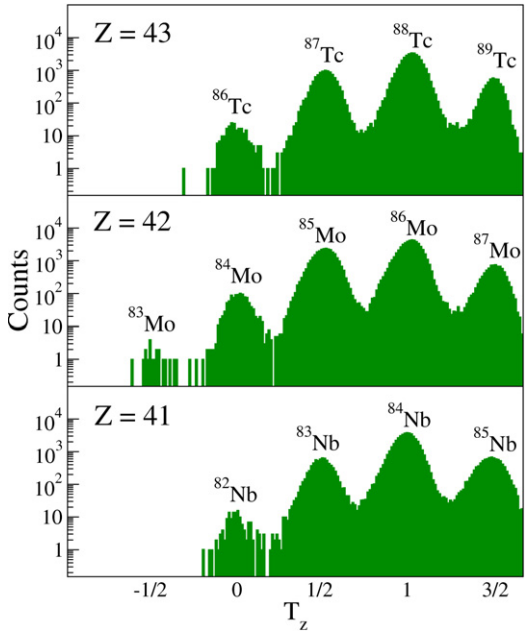

Fig. 2. Projections of the 2D spectrum in Fig. 1 for Technetium, Molybdenum and Niobium isotopes from the combined data of the current work.

(∼ 90 hours) in two separate settings. In the ^{86}Tc setting, ^{82}Nb ions were also transmitted to the focal plane and in the final analysis the data from both settings were combined. Figs. 1 and 2 show example particle identification plots from the current work. The $T_z = 0$ nuclides ^{82}Nb and ^{86}Tc, lie on the proton dripline, but the even-Z, $T_z = -\frac{1}{2}$ ^{83}Mo is also particle bound, consistent with previous findings [19,20]. Fig. 3 shows the delayed γ-ray spectra associated with isomeric decays in ^{82}Nb and ^{86}Tc. These spectra were produced from the implantation of ∼ 4500 and ∼ 7700 ions of ^{82}Nb and ^{86}Tc respectively.

Three discrete γ-ray transitions (124, 418 and 638 keV) are associated with the decay of a $T_{1/2} = 133(25)$ ns isomer in ^{82}Nb and are demonstrated to be in mutual coincidence (see Fig. 3). The half-life measurement was made by performing a least-squares fit to the summed time spectra associated with the

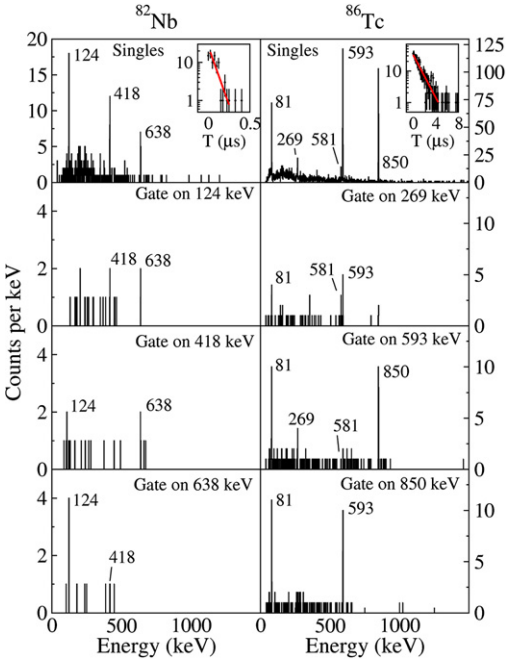

Fig. 3. Singles and coincident energy spectra of delayed γ-ray events associated with ^{82}Nb (left) and ^{86}Tc (right). The upper panels show singles data for ^{82}Nb gated between 150 → 500 ns and ^{86}Tc between 150 ns → 5 μs after implantation. The fitted half lives are 133(25) ns and 1.59(20) μs respectively.

418 and 638 keV transitions (see inset of Fig. 3). The two higher energy transitions are notably similar in energy to the $2^+ \rightarrow 0^+$ (407 keV) and $4^+ \rightarrow 2^+$ (634 keV) in the $T_z = +1$ isobar, ^{82}Zr [28] suggesting these are decays from $T = 1$ isobaric analogue states in ^{82}Nb. On this basis they are assigned as the first two transitions of the ^{82}Nb, $T = 1$ ground-state band.

The γ-ray intensity balance around the (4^+) state has been used to infer the internal conversion coefficient, α_{tot}, of the 124 keV transition to be 0.3(3). This is consistent with M1, E1 or E2 multipolarity (see Table 1 [29]), but does not allow a clear discrimination between the possibilities. The deduced value for the isomeric ratio [30] depends on the value of the internal conversion coefficient of the direct decay. Although the statistical uncertainties are significant, an E2 multipolarity for the 124 keV transition would result in an unphysically large isomeric ratio greater than 100%. E1 or M1 assignments yield more physically realistic values less than 100%. Using these arguments, plausible spin/parity assignments are restricted to $I^\pi = 5^-$ and 5^+.

Five γ-ray transitions are identified following the decay of a $T_{1/2} = 1.59(20)$ μs isomer in ^{86}Tc (Fig. 3). These data show the 81, 593 and 850 keV γ-rays to be in mutual coincidence. The latter two are assumed to be decays from the $T = 1$ isobaric analogue states of the $T_z = +1$ isobar, ^{86}Mo ($2^+ \rightarrow 0^+ =$ 567 keV and $4^+ \rightarrow 2^+ = 761$ keV [31]). The 269 and 581 keV γ-ray energies sum to 850 keV indicating a competing decay branch to the $(4^+) \rightarrow (2^+)$ transition. Although the ordering cannot be unambiguously determined here, the cascade can be confirmed by the 269 and 850 keV coincidence gates. (We note that some counts at 850 keV are observed in the 269 keV gate

Table 1
Weisskopf single-particle half life estimates (neglecting internal conversion) and total conversion coefficients for transitions in ^{82}Nb and ^{86}Tc [29]

	^{82}Nb, 124 keV		^{86}Tc, 81 keV	
	$T_{1/2}$ (s)	α_{tot}	$T_{1/2}$ (s)	α_{tot}
E1	1.87×10^{-13}	0.065	6.50×10^{-13}	0.245
M1	1.46×10^{-12}	0.131	3.41×10^{-12}	0.514
E2	8.97×10^{-7}	0.534	7.08×10^{-6}	2.690
M2	5.64×10^{-5}	1.120	4.59×10^{-4}	6.420

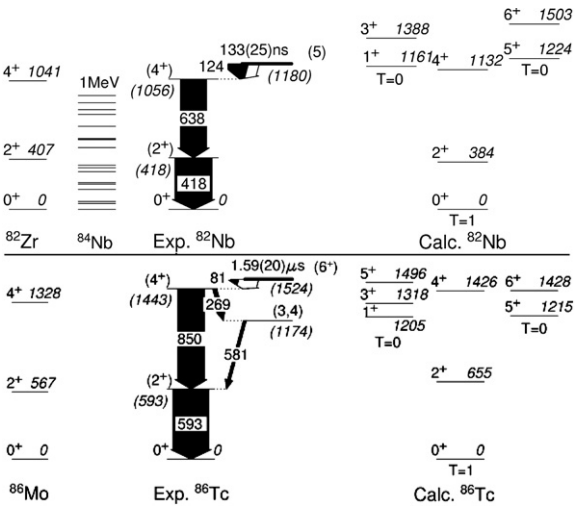

Fig. 4. The experimental and theoretical (projected shell model) level schemes of ^{82}Nb and ^{86}Tc. Partial level schemes of ^{82}Zr, ^{84}Nb and ^{86}Mo are also shown for comparison [31–33].

due to components of the Compton background associated with the 593 keV transition.)

Using intensity balance arguments the internal conversion coefficient for the 81 keV γ-ray is inferred to be $\alpha_{tot} = 3.5(8)$. A comparison with calculated values (Table 1) indicates this transition to be a stretched E2, leading to a spin/parity assignment of (6^+) for the isomeric state. While such a conversion coefficient could in principle arise from a highly mixed E1/M2 transition such an assignment is unlikely on the basis of the expected partial half-lives for such competing multipoles (see Table 1). The measured half life is also consistent with a single-particle 81 keV E2 transition rate.

Level schemes for ^{82}Nb and ^{86}Tc are presented in Fig. 4. The low level-density observed following the isomeric decay is consistent with the reduced level density reported in other odd–odd $N = Z$ systems. Only one excited state is observed below 1 MeV in ^{82}Nb compared to 17 excited states reported in ^{84}Nb [33]. We suggest this is further evidence for a $T = 1$ np pair gap specific to $N = Z$ nuclei [11,12].

The Projected Shell Model (PSM) [34] including np interactions [35] reproduces the observed ground state structures in the even–even $N = Z$ nuclei with $A = 68 \rightarrow 88$. PSM calculations have now been performed for ^{82}Nb and ^{86}Tc. The results for the positive parity states are shown in Fig. 4. For both nuclei, the calculation shows a low-lying $I^\pi = 5^+$ 2-quasiparticle state with a Nilsson configuration of $\nu[422]5/2^+ \times \pi[422]5/2^+$. In

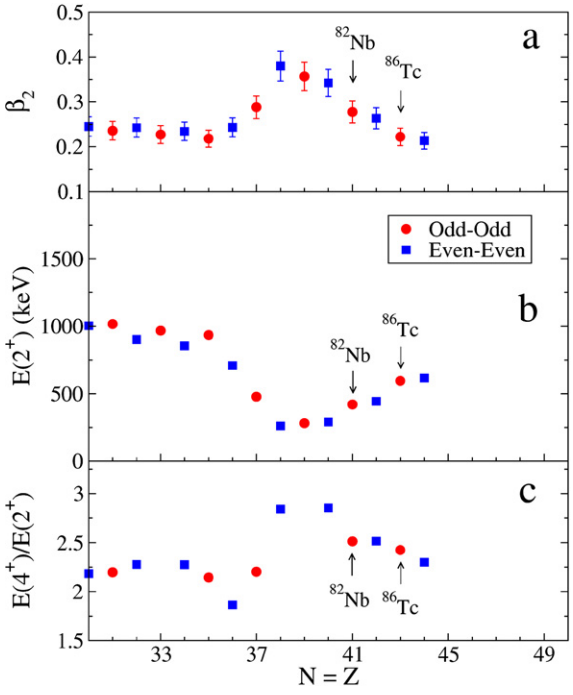

Fig. 5. Structural evolution of the $N = Z$ nuclei across the fpg shell. (a) Deformation calculated using the empirical relationship described in Ref. [38], (b) excitation energy of the first $I^\pi = 2^+$ state, and (c) $E(4^+)/E(2^+)$ ratio.

^{82}Nb this $I^\pi = 5^+$ configuration is predicted to lie just above the $T = 1$, 4^+ state. The population of a $T = 0$ state with this configuration is consistent with the low-lying band structures in the $T_z = +\frac{1}{2}$ neighbours ^{81}Zr [36] and ^{83}Nb [17,37]. The calculations also predict two low-lying $K = 4^-$ states at approximately 1.3 MeV in ^{82}Nb and negative parity states of mixed $K = 5, 6$ at ≈ 1.2 MeV in ^{86}Tc. A $I^\pi = K^\pi = 6^+$ state can be formed in ^{86}Tc by a coupling of the $[422]5/2^+$ and $[413]7/2^+$ Nilsson orbitals but appears at a significantly higher excitation energy in the calculation.

Fig. 5 shows energy systematics for $N = Z$ nuclei from $A = 60 \rightarrow 88$ including the current data. Using an empirical relationship between the energy of the first 2^+ energy and quadrupole deformation (β_2) [38] an estimate of the ground-state deformation can be made for both even–even ($T = 0$) and odd–odd ($T = 1$) structures.

One mechanism by which nuclear half lives can be prolonged in axially deformed nuclei is that of K hindrance [39]. The quantum number K, is the projection of the total angular momentum along the nuclear axis of symmetry. If there is a significant mismatch between the K values of initial and final states in electromagnetic decay, such that $\Delta K \geqslant \lambda$ where λ is the multipole order of the decaying transition, then the transition is expected to be 'K hindered'. A 124 keV M1 decay from an $I^\pi = K^\pi = 5^+$ to an $I^\pi = 4^+$, $K = 0$ state has $\Delta K = 5$, $\nu = 4$, where $\nu = \Delta K - \lambda$. The reduced hindrance for K-isomeric decays is defined by $f_\nu = (T_{1/2}/T^W_{1/2})^{1/\nu}$ [39]. An assumption of a pure M1 isomeric decay in ^{82}Nb gives $f_\nu \approx 18$, a substantial value intermediate between the accepted values of $f_\nu \sim 100$ for the best case axially-symmetric K isomers and ~ 1 for unhindered decays.

It is noteworthy that the isomeric state in ^{86}Tc lies in the vicinity of the predicted proton separation energy of 1393 (409) keV [24] thus allowing the possibility of direct proton emission from the isomer competing with internal electromagnetic decay. Such a competing (proton) decay branch would speed up the total mean lifetime of the isomeric state and could explain the apparent absence of any K-hindrance in this nucleus. This possibility cannot be confirmed in the current experiment. (The proton separation energy for ^{82}Nb is calculated to be 1775 (341) keV [24].)

In even–even nuclei, the ratio of excitation energies of the yrast 4^+ and 2^+ states ($R = \frac{E(4^+)}{E(2^+)}$) is used as a signature for nuclear shapes with an idealised quadrupole vibrational nucleus having $R = 2.0$ and a perfect axially symmetric rotor having $R = 3.33$. Fig. 5 shows such a plot for $N = Z$ nuclei between $^{60}_{30}$Zn and $^{88}_{44}$Ru. The value of $R = 2.53$ for ^{82}Nb is consistent with some axial asymmetry and/or γ-softness, which could explain the inferred reduced hindrance for an M1 transition. We note that any proposed K-hindrance is not apparent for the (likely) E2 isomeric decay in ^{86}Tc. This could be qualitatively understood by a reduction in the deformation and associated increase in γ-softness compared to ^{82}Nb or by competition from an unobserved proton decay branch.

In summary, we have identified low-lying structures in ^{82}Nb and ^{86}Tc, the heaviest odd–odd $N = Z$ systems for which internal decays have been measured to date. The data suggest a dominance of the $T = 1$ pairing interaction over its $T = 0$ counterpart throughout the fpg shell. Plausible evidence for an isospin changing K isomer along the $N = Z$ line is also presented.

Acknowledgements

Prof. J.A. Tostevin is thanked for insightful discussions on this manuscript. This work is supported by the EPSRC and AWE plc. (UK), The Swedish Research Council, The Polish Ministry of Science and Higher Education (1-P03B-030-30 and 620/E-77/SPB/GSI/P-03/DWM105/2004-2007), The Bulgarian Science Fund VUF06/05, The US Department of Energy (DE-FG02-91ER-40609 and DE-AC02-06CH11357), The Spanish Ministerio de Educación y Ciencia (FPA2005-00696), The German Federal Ministry of Education and Research (06KY205I), EURONS (EU contract number 506065), The Hungarian Science Foundation (OTKA K-68801) and the Italian INFN. A.B.G. acknowledges Nexia Solutions Ltd, a subsidiary of BNFL.

References

[1] J. Bardeen, L.N. Cooper, J.R. Schrieffer, Phys. Rev. 108 (1957) 1175.
[2] D.D. Warner, M.A. Bentley, P. Van Isacker, Nature Phys. 2 (2006) 311.
[3] A.L. Goodman, Adv. Nucl. Phys. 11 (1979) 263.
[4] S.M. Fischer, et al., Phys. Rev. Lett. 87 (2001) 132501.
[5] N. Mărginean, et al., Phys. Rev. C 65 (2002) 051303(R).
[6] C. Longour, et al., Phys. Rev. Lett. 81 (1998) 3337.
[7] T. Faestermann, et al., Eur. Phys. J. A 15 (2002) 185.
[8] S.M. Vincent, et al., Phys. Lett. B 437 (1998) 264.
[9] D. Rudolph, et al., Phys. Rev. C 69 (2004) 034309.
[10] R. Grzywacz, et al., Nucl. Phys. A 682 (2001) 41c.
[11] D.G. Jenkins, et al., Phys. Rev. C 65 (2002) 064307.
[12] D. Rudolph, et al., Phys. Rev. Lett. 76 (1996) 376.
[13] C.D. O'Leary, et al., Phys. Rev. C 67 (2003) 021301(R).
[14] J. Uusitalo, et al., Phys. Rev. C 57 (1998) 2259.
[15] B.S. Nara Singh, et al., Phys. Rev. C 75 (2007) 061301.
[16] C.J. Lister, et al., Phys. Rev. C 42 (1990) R1191.
[17] S.M. Fischer, et al., Phys. Rev. C 75 (2007) 064310.
[18] R. Pfaff, et al., Phys. Rev. C 53 (1996) 1753.
[19] A. Stolz, et al., Phys. Rev. C 65 (2002) 064603.
[20] Z. Janas, et al., Phys. Rev. Lett. 82 (1999) 295.
[21] C. Chandler, et al., Phys. Rev. C 61 (2000) 044309.
[22] L.S. Cáceres, et al., Acta Phys. Pol. B 38 (2007) 1271.
[23] A.B. Garnsworthy, et al., Acta Phys. Pol. B 38 (2007) 1265.
[24] A.H. Wapstra, G. Audi, C. Thibault, Nucl. Phys. A 729 (2003) 129.
[25] H. Geissel, Nucl. Instrum. Methods B 70 (1992) 286.
[26] S. Pietri, et al., Acta Phys. Pol. B 38 (2007) 1255.
[27] S. Pietri, et al., Nucl. Instrum. Methods B 261 (2007) 1079.
[28] S.D. Paul, et al., Phys. Rev. C 55 (1997) 1563.
[29] F. Rösel, et al., At. Data Nucl. Data Tables 21 (1978) 291.
[30] M. Pfützner, et al., Phys. Rev. C 65 (2002) 064604.
[31] D. Rudolph, et al., Phys. Rev. C 54 (1996) 117.
[32] D. Rudolph, et al., Phys. Rev. C 56 (1997) 98.
[33] N. Mărginean, et al., Eur. Phys. J. A 4 (1999) 311.
[34] Y. Sun, Eur. Phys. J. A 20 (2004) 133.
[35] Y. Sun, J.A. Sheikh, Phys. Rev. C 64 (2001) 031302(R).
[36] N. Mărginean, et al., Phys. Rev. C 69 (2004) 054301.
[37] C.J. Gross, et al., Phys. Rev. C 43 (1991) R5.
[38] S. Raman, C.W. Nestor Jr., P. Tikkanen, At. Data Nucl. Data Tables 78 (2001) 1.
[39] K.E.G. Löbner, Phys. Lett. B 26 (1968) 369;
P.M. Walker, G. Dracoulis, Nature 399 (1999) 35.

Physics Letters B 668 (2008) 460

Contents lists available at ScienceDirect

Physics Letters B

www.elsevier.com/locate/physletb

Erratum

Erratum to: "Neutron–proton pairing competition in $N = Z$ nuclei: Metastable state decays in the proton dripline nuclei $^{82}_{41}$Nb and $^{86}_{43}$Tc" [Phys. Lett. B 660 (2008) 326]

A.B. Garnsworthy [a,b,*], P.H. Regan [a], L. Cáceres [c,d], S. Pietri [a], Y. Sun [e,f], D. Rudolph [g], M. Górska [c], Zs. Podolyák [a], S.J. Steer [a], R. Hoischen [g,c], A. Heinz [b], F. Becker [c], P. Bednarczyk [c,h], P. Doornenbal [c], H. Geissel [c], J. Gerl [c], H. Grawe [c], J. Grębosz [h,c], A. Kelic [c], I. Kojouharov [c], N. Kurz [c], F. Montes [c], W. Prokopowicz [c], T. Saito [c], H. Schaffner [c], S. Tachenov [c], E. Werner-Malento [c,i], H.J. Wollersheim [c], G. Benzoni [j], B.B. Blank [k], C. Brandau [a,c], A.M. Bruce [l], F. Camera [j], W.N. Catford [a], I.J. Cullen [a], Zs. Dombrádi [m], E. Estevez [n], W. Gelletly [a], G. Ilie [o,p], J. Jolie [o], G.A. Jones [a], A. Jungclaus [d], M. Kmiecik [h], F.G. Kondev [q], T. Kurtukian-Nieto [n,k], S. Lalkovski [l,r], Z. Liu [a], A. Maj [h], S. Myalski [h], M. Pfützner [i], S. Schwertel [s], T. Shizuma [a,t], A.J. Simons [u,a], P.M. Walker [a], O. Wieland [j], F.R. Xu [v]

[a] *Department of Physics, University of Surrey, Guildford, Surrey, GU2 7XH, UK*
[b] *WNSL, Yale University, 272 Whitney Avenue, New Haven, CT 06520, USA*
[c] *GSI, Planckstrasse 1, D-64291 Darmstadt, Germany*
[d] *Departmento di Teórica, Universidad Autonoma de Madrid, Madrid, Spain*
[e] *Department of Physics and Joint Institute for Nuclear Astrophysics, University of Notre Dame, Notre Dame, IN 46556, USA*
[f] *Department of Physics, Shanghai Jiao Tong University, Shanghai 200240, People's Republic of China*
[g] *Department of Physics, Lund University, S-22100 Lund, Sweden*
[h] *The Institute of Nuclear Physics, PL-31-342 Kraków, Poland*
[i] *IEP, Warsaw University, Hoża 69, PL-00-681, Poland*
[j] *Universitá degli Studi di Milano and INFN Milano, I-20133 Milano, Italy*
[k] *CENBG, le Haut Vigneau, F-33175, Gradignan Cedex, France*
[l] *School of Engineering, University of Brighton, Brighton, BN2 4GJ, UK*
[m] *Institute for Nuclear Research, H-4001 Debrecen, Hungary*
[n] *Universidad de Santiago de Compostela, Santiago de Campostela, Spain*
[o] *IKP, Universität zu Köln, D-50937 Köln, Germany*
[p] *National Institute of Physics and Nuclear Engineering, Bucharest, Romania*
[q] *Nuclear Engineering Division, Argonne National Laboratory, Argonne, IL 60439, USA*
[r] *Faculty of Physics, University of Sofia "St. Kliment Ohridski" Sofia, Bulgaria*
[s] *Physik Department E12, Technische Universität München, Garching, Germany*
[t] *Japan Atomic Energy Agency, Kyoto 619-0215, Japan*
[u] *AWE plc., Aldermaston, Berkshire, RG7 4PR, UK*
[v] *Department of Technical Physics, Peking University, Beijing 100871, People's Republic of China*

ARTICLE INFO

Article history:
Received 27 August 2008
Available online 18 September 2008

The quoted values for the half-lives of the isomeric states in ^{82}Nb and ^{86}Tc are the values of the mean lifetimes of these states. The correct half-lives are $T_{1/2} = 93(17)$ ns for the (1180) keV state in ^{82}Nb and $T_{1/2} = 1.10(14)$ μs for the (1524) keV state in ^{86}Tc. All other values quoted or discussed in the article were calculated correctly and are not affected by this typographical error.

DOI of original article: 10.1016/j.physletb.2008.01.017.
* Corresponding author at: Department of Physics, University of Surrey, Guildford, Surrey, GU2 7XH, UK.
E-mail address: a.garnsworthy@surrey.ac.uk (A.B. Garnsworthy).

0370-2693/$ – see front matter
doi:10.1016/j.physletb.2008.09.020

Available online at www.sciencedirect.com
ScienceDirect
Nuclear Instruments and Methods in Physics Research B 266 (2008) 4589–4594
NIM B
Beam Interactions with Materials & Atoms
www.elsevier.com/locate/nimb

From RISING to HISPEC/DESPEC

Zsolt Podolyák, for the HISPEC/DESPEC collaboration

Department of Physics, University of Surrey, Guildford, GU2 7XH, United Kingdom

Available online 7 June 2008

Abstract

The Rare ISotopes INvestigations at GSI (RISING) project is aimed at nuclear structure and reaction studies using high-resolution gamma-ray spectroscopy as its main tool. At the future FAIR facility, these tools will be employed by the High-resolution In-flight SPECtroscopy (HISPEC) and DECay SPECtroscopy (DESPEC) projects. The improvements in the experimental setups, together with the opportunities to be opened, are discussed.

PACS: 29.30.−h; 29.40.−n; 28.38.−c

Keywords: Spectroscopy; Fragmentation; Nuclear structure

1. Introduction

The next generation European fragmentation-based radioactive beam facility is part of the Facility for Antiproton and Ion Research (FAIR) project [1]. The new facility will provide beams of radioactive ions with unprecedented intensities with the aim of studying the atomic nucleus. The High-resolution In-flight SPECtroscopy (HISPEC) and DESPEC (DEcay SPECtroscopy) projects address nuclear physics questions using radioactive beams at energies of $E/A < 200$ MeV. The projects focus on those aspects of nuclear investigations with rare isotope beams which require high-resolution γ-spectroscopy setups.

At present, the GSI facility provides radioactive ion beams produced in fragmentation and in-flight fission. The Rare ISotopes INvestigations at GSI (RISING) project exploits these beams, with experiments performed at two energy regimes so far, $E/A = 0$ (at rest) and $E/A \approx 100$ MeV.

The planned technical improvements as we move from RISING to HISPEC/DESPEC are discussed in the present paper. The resulting much increased efficiency will allow for both the study of nuclei further away form the stability and the application of new techniques. The schematic layout of the FAIR facility, including the existing GSI, with the location of the projects discussed, is shown in Fig. 1.

2. From GSI to FAIR

The Facility for Antiproton and Ion Research [1,2] (FAIR) will be built in an international collaboration at the site of the present GSI laboratory in Darmstadt, Germany. The primary beam will be accelerated by the existing linear accelerator (UNILAC) and synchrotron (SIS), and the new synchrotron (SIS100/300). The primary beam intensity will be increased by about a factor of ≈100 compared to the existing GSI facility. This increase is due to two main factors (i) a higher number of nuclei circulating in the ring, achieved by having ions in a lower charge state thus overcoming the present limitations due to the space-charge limit, and (ii) shorter acceleration times, achieved by using fast ramping magnets in the synchrotrons. The FAIR facility will be able to produce intense, high brilliance primary beams of all stable chemical elements up to uranium with energies in the range E/A 1–30 GeV and also anti-protons. Beams of short-lived radioactive species

E-mail address: Z.Podolyak@surrey.ac.uk

0168-583X/$ - see front matter © 2008 Elsevier B.V. All rights reserved.
doi:10.1016/j.nimb.2008.05.106

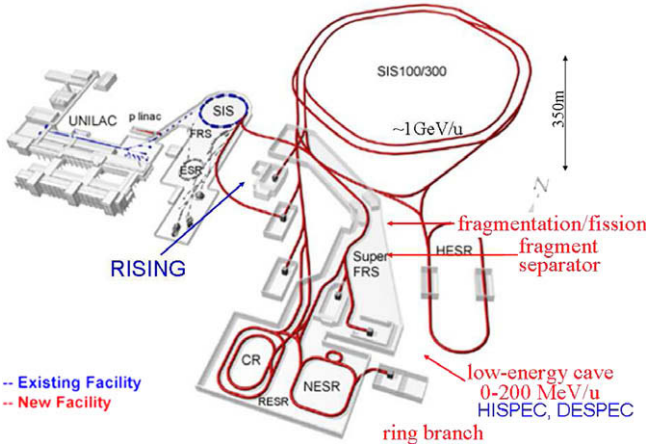

Fig. 1. Schematic view of the FAIR facility. The location of RISING at the present GSI facility, and the location of HISPEC and DESPEC at the future FAIR facility are indicated.

will be generated in fragmentation/spallation and fission reactions. The Super FRagment Separator (SuperFRS) [3] will be used to identify and separate the species of interest. The SuperFRS, compared to the existing Fragment Separator [4] will provide (i)'cleaner' beams (due to its six dipole magnets as opposed to four) and (ii) higher transmission (due to the higher apertures of its magnets), especially for fission products.

Such a fragmentation facility is complementary to the Isotope-Separation-On-Line facilities, such as ISOLDE and SPIRAL2. It has the advantages of being able to provide any isotope independently of the chemical properties of the element and the process is fast, resulting in beams of the shortest-lived, and hence most exotic nuclei (albeit at lower optical quality than those at ISOL facilities). FAIR will be unique among the fragmentation facilities in several ways: (i) experiments can be carried out at high energies up to $E/A \approx 2$ GeV; (ii) cleanest radioactive beams for heavy nuclei and (iii) the existence of storage rings (see Fig. 1).

Both HISPEC and DESPEC will be located on the low energy branch of the SuperFRS, and they will profit from the unique beam properties, such as: (i) isotopes of all elements between uranium and hydrogen can be uniquely prepared as beams with energies from about $E/A = 0$ (stopped beam) MeV to $E/A = 200$ MeV and with intensities appropriate for in-flight spectroscopy; (ii) ions with very short lifetimes (a few 100 ns) can be studied; (iii) beams composed of several isotopes, mono-isotopic beams and beams in high spin isomeric states will be available; (iv) the beam quality enables high-resolution γ-spectroscopy, including angular correlations, polarisation, g-factor and lifetime measurements and (v) for energies around the Coulomb barrier employing the New Experimental Storage Ring even high-resolution particle spectroscopy becomes possible.

The physics case for the HISPEC/DESPEC experiments [5,6] is part of the overall NUSTAR physics programme [7] and shares the common goals of attempting to understand nuclear structure and nuclear reactions and related questions in nuclear astrophysics. The collaboration will concentrate on those aspects of nuclear structure, reactions and astrophysics investigations which can be exclusively addressed with the proposed high-resolution spectroscopy set-up using the beams unique to the FAIR facility. The technical proposal of HISPEC/DESPEC can be found at [8].

3. From RISING to HISPEC

Within the HISPEC project the nuclei of interest will be populated in-flight, using nuclear and Coulomb excitation reactions. Detailed spectroscopic information will be deduced by γ-ray, charged-particle and neutron spectroscopy. The experimental techniques to be used can be grouped together in relation to two different energy regimes. Secondary fragmentation and single step Coulomb excitation will be used at intermediate, $E/A \approx 100$ MeV, energies. Thick targets, of the order of several 100 mg/cm^2, can be used. Such experiments have been already performed at RISING [9] (see Fig. 2). For example: Coulomb excitation of ^{54,56,58}Cr nuclei [10], providing $B(E2; 2^+ \rightarrow 0^+)$ transition strengths, gave information about the shell evolution around $N = 34$; secondary fragmentation reactions were used to test isospin symmetry at the drip line, by measuring the 2^+ excited state in ^{36}Ca [11].

At Coulomb barrier energies thinner targets will be used, and consequently higher beam intensities will re required. Such experiments have not been performed at RISING yet. The main difficulties arise from the need of tracking of such low-energy beam particles. Tests were already performed, and more planned, with the aim to gain experience on tracking low-energy, high-emittance beams [12].

The schematic view of the HISPEC setup is shown in Fig. 3. HISPEC will comprise beam tracking and identification detectors placed before [13] and behind the secondary target, the AGATA Ge array, charged-particle detectors, plungers, a magnetic spectrometer and other ancillary detectors.

3.1. The AGATA spectrometer

The HISPEC set-up has at its core AGATA [14], the next generation gamma-ray tracking array, with a resolving power hugely exceeding the presently available Ge-arrays. Advanced GAmma Tracking Array (AGATA) is designed to be a 4π detector consisting of 180 germanium detectors. Each detector crystal will be segmented 36 ways. Within each detector pulse shape analysis will be used to determine the interaction positions of the gamma rays to an accuracy of 2 mm. Tracking algorithms will be employed to reconstruct the paths of gamma rays passing through the detectors.

The effect of ancillary detectors (charged particle arrays, plunger) to be used in conjunction with AGATA has been simulated. Special emphasis was given to the uncertainties in energy, position and angle of the γ-ray emitting particles.

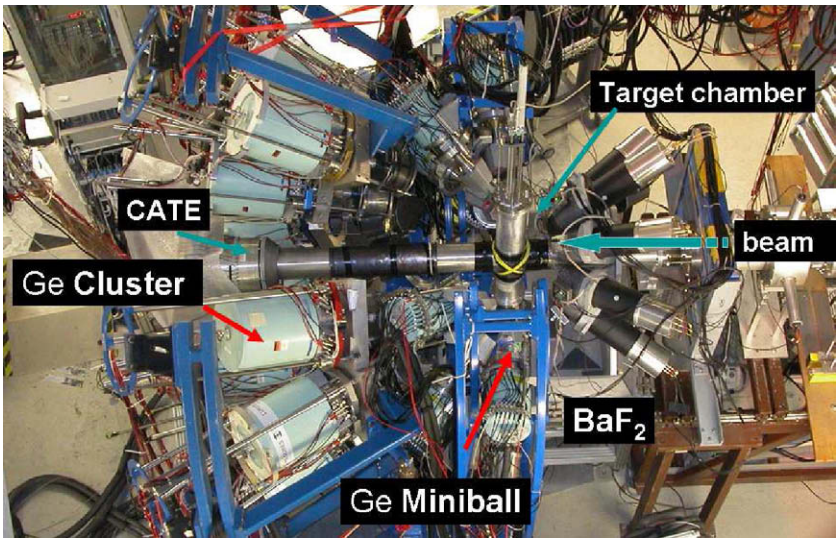

Fig. 2. Photograph of the RISING array in its configuration used for fast beam experiments.

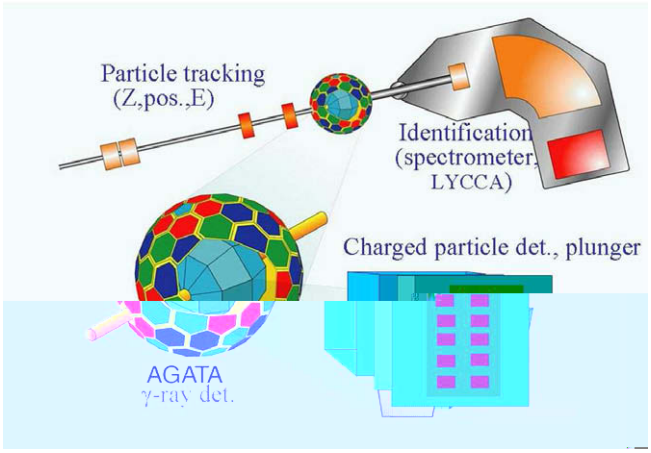

Fig. 3. Schematic illustration of the HISPEC experimental setup.

The requirements with respect to the beam tracking detectors have been determined [15,5], and this performance can, in principle, be reached with existing technologies.

The AGATA demonstrator, consisting of five triple cluster modules (15 Ge crystals) will start to operate in Legnaro National Laboratories, Italy, in 2008. It is envisaged that AGATA will be moved to the SIS-FRS facility in around 2011 for an early implementation physics programme within the HISPEC project. It is expected that 45 detectors, covering a solid angle of 1π will be available at that time. They will be placed at a distance of $\approx$15 cm at forward angles. The calculations predict a photopeak efficiency for this 1π array of $\approx$15% for $E/A = 100$ MeV ($\beta = 0.43$), and an energy resolution better than 1%. In contrast, the full peak efficiency of the 15 cluster detectors of the RISING array in its fast beam configuration [9] is 2.8% for a 1.3 MeV gamma ray emitted in-flight at $E/A = 100$ MeV.

The energy resolution is $\Delta E/E < 2\%$. This represents an increase of a factor of $\approx$6 in efficiency compared with RISING in singles and even higher for coincidence spectroscopy. It will enable highly selective $\gamma\gamma$-coincidences to be measured in fragmentation reactions. The collaboration will investigate if the 15 Cluster detectors should also be used for specific experiments. These could be located at backward angles to increase the efficiency, or mounted in a stand alone frame downstream of the target.

3.2. Identification after the secondary target

For the identification of isotopes following different types of reactions in the secondary target, versatile charged-particle detector arrays with different geometries must be constructed, including the potential of coupling them with a magnetic spectrometer. The LYCCA array will consist of ΔE–E telescopes and in addition it will measure the time-of-flight between the reaction target and the array. For TOF measurement three options are considered and these are being tested, using: polycrystalline diamond, ultra fast scintillators and Si detectors with fast electronics. According to simulations, this system will allow the identification of ions up to a mass of $A \approx 100$. In contrast, the present CATE array [16] is based on ΔE–E measurements only. It allows for element determination through the ΔE measurement. However, the mass of the ions cannot be uniquely determined due to the uncertainties in the velocity of the ions. These uncertainties arose from energy straggling in the target and from the reaction mechanism itself. The TOF measurement of LYCCA will overcome this problem.

For heavier ions ($A > 100$) an additional momentum dispersion $\Delta p/p$ provided by a magnetic device is necessary to achieve the desired mass resolution. The ionic charge state distribution has also to be determined. The ultimate solution is the combination of an ion-optic device providing A/q separation and possibly magnetic focusing in combination with the LYCCA array comprising tracking- and

$\Delta E/E$ detectors. The first part of the energy buncher [17,18] will serve as high-resolution magnetic spectrometer.

3.3. Other HISPEC detectors

Several other detectors will be available to be used in conjunction with AGATA. Plunger devices can be used for lifetime measurements. The usual stopper foil will be replaced by degrader foils to enable the detection of the nuclei of interest downstream of the degrader foils in order to clean the spectra of the strong background radiation. Other possible detectors include novel scintillator detectors, such as $LaCl_3$(Ce) and $LaBr_3$(Ce) for gamma-ray detection, as well as Si detectors for prompt charged particle emission. For nuclear reaction studies at relatively low energies ($E/A = 10$–50 MeV) the 4π HYbrid DEtector array (HYDE) [19] is being developed for the detection of charged particles.

4. From RISING to DESPEC

The radioactive ion beams can be stopped and their consequent decay measured. These radioactive decays (α, β, γ, proton and neutron) will be measured and position-correlated with implants. Key physics information such as particle decay branching ratios, half-lives, first excited states and isomeric decays will be obtained. The technique is very sensitive, the needed beam intensities are in the order of $10^{-5} - 10^{3}$ ion/s.

Decay measurements have been performed with the present RISING, with the detectors surrounding the target in spherical symmetry (see Fig. 4). Both isomeric decay experiments using passive stoppers (including magnetic moment measurements [20]), and beta-decay experiments using active Si stopper have been performed. The photopeak efficiency of the RISING array in its stopped beam configuration [21] is 10% at 1.3 MeV. Highlights include the study of the structure of the r-process pass nucleus ^{130}Cd by internal isomeric decay [22] and conversion electron spectroscopy in the $N = 126$ ^{205}Au nucleus [23].

The DESPEC setup [6] will comprise a Si based implantation and decay detector, a compact Ge array, neutron detectors, total absorption spectrometer, scintillation detectors (BaF_2, $LaCl_3$(Ce), $LaBr_3$(Ce)) and equipment for moment measurements of long-lived states. A schematic view of DESPEC setup is shown in Fig. 5.

The implantation and decay detector based on Si DSSD technology will measure both the very high energies (GeV) deposited by the radioactive ions as they stop in the DSSD stack, and the subsequent decay events with MeV energies for protons and alpha particles and an energy loss (ΔE) of a few hundred keV in the case of β particles. This represents an extremely large dynamic range and demands a very low energy threshold, of the order of a few tens of keV. The low threshold is particulary important in the case of internal decay studies, through conversion electron detection. The detector system will consist up to a maximum of eight 1 mm layers of Si, covering an area of 8 cm $\times$ 24 cm. Each detector of size 8 cm $\times$ 24 cm will have 128 vertical and 128 horizontal strips. The high segmentation of the DSSDs minimises the effects of random correlations between successive implants and decays, and between implants and the decay of long-lived activities.

High-resolution γ-ray detectors will be positioned around the implantation detector. A highly flexible and modular γ-ray detection array consisting of 24 stacks of planar pixelated (or double-sided strip) Ge detectors is proposed [24]. These modules can be arranged in different

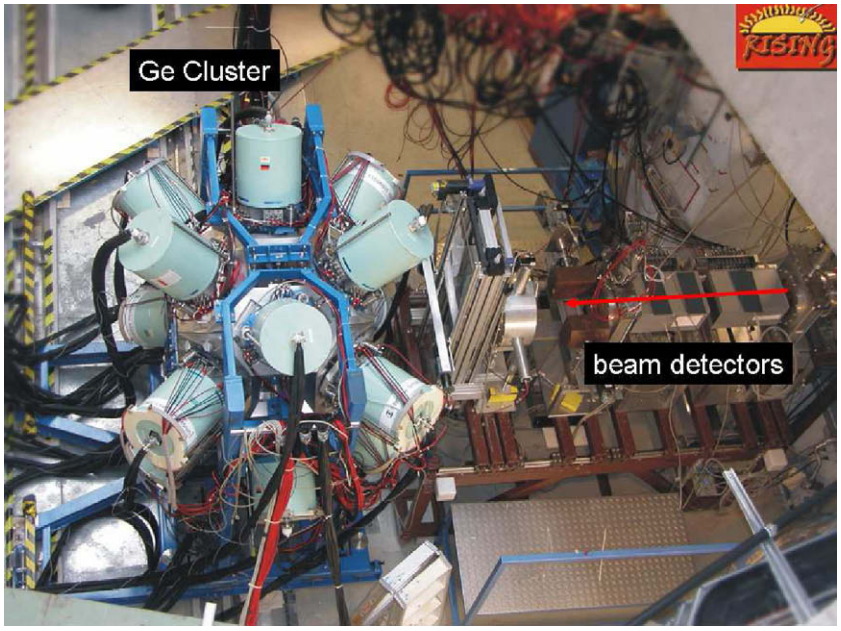

Fig. 4. Photograph of the RISING array in its configuration used for stopped beam experiments.

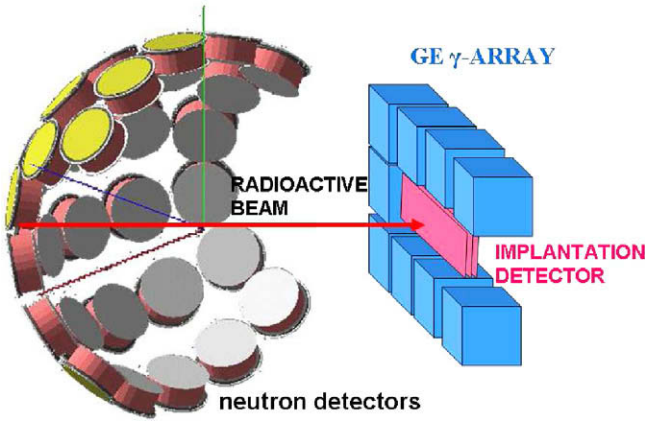

Fig. 5. Schematic illustration of the DESPEC experimental setup.

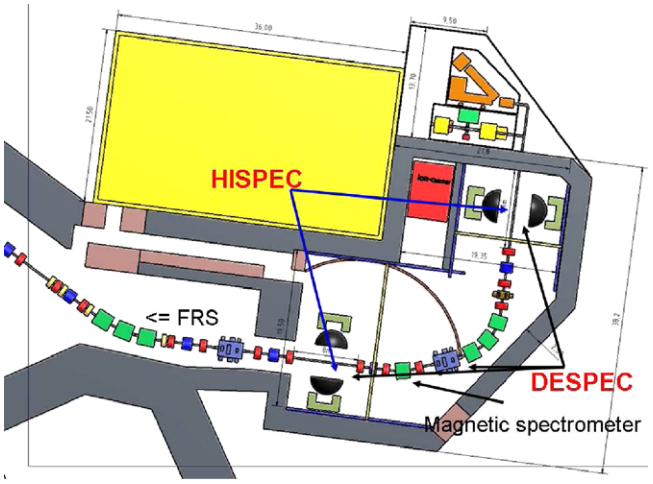

Fig. 6. Schematic view showing the possible positions of the HISPEC and DESPEC experimental setups in the low energy cave.

geometries optimised to the different types of experiments envisaged at DESPEC. The high granularity of the Ge detectors is important in order to assure high efficiency of the array during the "prompt flash" of radiation associated with the implantation of high energy ions into the focal plane catcher and thus to allow the study of decays with very short lifetimes. In addition the granularity, combined with tracking, might allows us to track the origin of the detected γ-ray [25]. This tracking allows us to associate an implanted ion with its decay γ-rays (excluding random coincidences with background radiation produced upstream) and, hence, enables long decay times to be studied at high implantation rates. In addition the position information can be used to measure angular correlations and polarizations.

Other detectors to be used within the DESPEC setup include neutron detectors, a total absorbtion spectrometer and fast scintillator detectors for lifetime measurements. Neutron detectors are particularly important, considering the research interest in the structure of nuclei with high neutron excess. They are designed with the main aim to detect β-delayed neutrons. The variety of the detectors to be available in conjunction with the implantation/decay and the γ-ray detectors is a particular strength of the DESPEC setup.

5. The low energy branch and HISPEC and DESPEC coupled together

The HISPEC and DESPEC setups will operate in the low energy branch of the SuperFRS. A sketch of the layout of the low energy cave is shown in Fig. 6. The layout is dominated, due its size, by the energy buncher [17,18]. The energy buncher, consisting of four dipole magnets, a mono-energetic degrader and focussing elements, will be used to deliver relatively mono-energetic beams [26]. These beams have the disadvantage of worse beam quality, manifesting itself in higher angular and position spread. The main applications of the mono-energetic beams are in experiments where stopping them in a thin layer of matter, such as a gas catcher, is vital. More importantly for HISPEC and DESPEC the first part of the energy buncher, with one dipole magnet, can serve as a high-resolution magnetic spectrometer.

Recoil decay tagging is a powerful technique to study the nuclear structure. It requires the detection of both the prompt radiation at the reaction target and the delayed decay at the final focal plane of the magnetic spectrometer. Therefore, the HISPEC and DESPEC setups have to be able to work together.

The HIPSEC setup can be positioned in two different places (as shown in Fig. 6): (i) before the energy buncher to receive beam directly from the SuperFRS; and (ii) after the energy buncher, receiving mono-energetic beams. DESPEC can be positioned in three different places: (i) before the energy buncher; (ii) after the energy buncher; and (iii) after the magnetic spectrometer for recoil decay tagging experiments.

Acknowledgement

HISPEC/DESPEC is a collaboration involving more than 150 scientists from about 50 institutions throughout the world. The full list of participants can be found in [8]. The contributions made by all participants is acknowledged.

References

[1] <www.gsi.de/fair>.
[2] R. Krücken, J. Phys. G: Nucl. Part. Phys. 31 (2005) S1807.
[3] H. Geissel et al., Nucl. Instr. and Meth. Phys. Res. B204 (2003) 71.
[4] H. Geissel et al., Nucl. Instr. and Meth. Phys. Res. B70 (1992) 286.
[5] Zs. Podolyák, Int. J. Mod. Phys. E15 (2006) 1967.
[6] B. Rubio, Int. J. Mod. Phys. E15 (2006) 1979.
[7] Nuclear Structure, Astrophysics and Reactions (NUSTAR), <www.gsi.de/nustar>.;
B. Rubio, T. Nilsson, Nucl. Phys. News 16 (3) (2006) 9.
[8] HISPEC/DESPEC Technical Proposal, <http://www.gsi.de/fair/experiments/NUSTAR/Proposals.html>.

[9] H.-J. Wollersheim et al., Nucl. Instr. and Meth. Phys. Res. A537 (2005) 637.
[10] A. Bürger et al., Phys. Lett. B622 (2005) 29.
[11] P. Doornenbal et al., Phys. Lett. B647 (2007) 237.
[12] P. Boutachkov, et al., private communication.
[13] J. Gerl, J. Jolie, W. Korten, Zs. Podolyák, GSI Scientific Report 2005, GSI Report 2006-1, p.37.
[14] AGATA, Technical proposal, in: J Gerl, W. Korten (Ed.), GSI Darmstadt, 2001.;
J. Simpson, J. Phys. G: Nucl. Phys. 31 (2005) S1801.
[15] E. Farnea, et al., LNL-INFN 202/2004, p. 158.;
F. Recchia, LNL-INFN 202/2004, p. 160.
[16] R. Lozeva et al., Nucl. Instr. and Meth. Phys. Res. B204 (2003) 678;
R. Lozeva et al., Acta Phys. Pol. B36 (2005) 1245.
[17] H. Geissel et al., Nucl. Instr. and Meth. Phys. Res. A282 (1989) 247.
[18] C. Brandau et al., Eur. Phys. J. Special Top. 150 (2007) 25.
[19] J.M. Andujar, R. Berjillos, J. Duenas, J.L. Flores, I. Martel, D. Rodriguez, P. Salmeron, GSI Scientific Report 2006, GSI Report 2007-1, p. 30.
[20] G. Neyens et al., Acta Phys. Pol. B38 (2007) 1237.
[21] S. Pietri et al., Nucl.Instr. and Meth. Phys. Res. Sect. B261 (2007) 1079;
P.H. Regan et al., Nucl. Phys. A787 (2007) 491c.
[22] A. Jungclaus et al., Phys. Rev. Lett. 99 (2007) 132501.
[23] Zs. Podolyák, et al., in: Proc. of the Int. Symposium on the Phys. of Unstable Nuclei, ISPUN07, World Scientific, 2008, p.48.
[24] A. Algora, B. Rubio, S. Tashenov, J. Gerl, B. Quintana, M. Doncel, F. Lorenzo, A. Jungclaus, Scientific Report 2006, GSI Report 2007-1, p. 31.
[25] S. Tashenov, J. Gerl, GSI Scientific Report 2006, GSI Report 2007-1, p. 29.
[26] C. Scheindenberger et al., Nucl. Instr. and Meth. Phys. Res. B204 (2003) 119.

Eur. Phys. J. A **36**, 131–138 (2008)
DOI 10.1140/epja/i2008-10587-4

THE EUROPEAN PHYSICAL JOURNAL A

Regular Article – Experimental Physics

Evidence for an isomeric $3/2^-$ state in ^{53}Co

D. Rudolph[1,a], R. Hoischen[1,2], M. Hellström[1], S. Pietri[3], Zs. Podolyák[3], P.H. Regan[3], A.B. Garnsworthy[3,4], S.J. Steer[3], F. Becker[2,b], P. Bednarczyk[2,5], L. Cáceres[2,6], P. Doornenbal[2,7,c], J. Gerl[2], M. Górska[2], J. Grębosz[5,2], I. Kojouharov[2], N. Kurz[2], W. Prokopowicz[2,5], H. Schaffner[2], H.J. Wollersheim[2], L.-L. Andersson[1], L. Atanasova[8], D.L. Balabanski[8,9], M.A. Bentley[10], A. Blazhev[7], C. Brandau[2,3], J.R. Brown[10], C. Fahlander[1], E.K. Johansson[1], and A. Jungclaus[6]

[1] Department of Physics, Lund University, S-221 00 Lund, Sweden
[2] Gesellschaft für Schwerionenforschung mbH, D-64291 Darmstadt, Germany
[3] Department of Physics, University of Surrey, Guildford, GU2 7XH, United Kingdom
[4] Wright Nuclear Structure Laboratory, Yale University, New Haven, CT 06520-8124, USA
[5] The Henryk Niewodniczański Institute of Nuclear Physics (IFJ PAN), PL-31342 Kraków, Poland
[6] Departamento de Física Teórica, Universidad Autónoma de Madrid, E-28049 Madrid, Spain
[7] Institut für Kernphysik, Universität zu Köln, D-50937 Köln, Germany
[8] Faculty of Physics, University of Sofia, BG-1164 Sofia, Bulgaria
[9] Institute for Nuclear Research and Nuclear Energy, Bulgarian Academy of Sciences, BG-1784 Sofia, Bulgaria
[10] Department of Physics, University of York, York, YO10 5DD, UK

Received: 4 March 2008 / Revised: 28 April 2008
Published online: 21 May 2008 –
Communicated by R. Krücken

Abstract. The fragmentation of a 550 MeV/u primary beam of ^{58}Ni on a ^{9}Be target has been used to measure time- and energy-correlated γ decays following the implantation of event-by-event discriminated secondary fragments into a ^{9}Be stopper plate. A new isomeric γ decay with $T_{1/2} = 14(^{6}_{4})$ ns and $E_\gamma = 646.2(2)$ keV is observed and attributed to the decay of the yrast $3/2^-$ state in $^{53}_{27}$Co$_{26}$. This short-lived isomeric state has been populated by means of nuclear reactions during the stopping process of the secondary fragments. The experimental findings are discussed in the framework of large-scale spherical shell model calculations in conjunction with isospin symmetry-breaking residual interactions for the $A = 53$, $T_z = \pm 1/2$ mirror nuclei ^{53}Co and ^{53}Fe.

PACS. 21.60.Cs Shell model – 23.20.-g Electromagnetic transitions – 25.70.Mn Projectile and target fragmentation – 27.40.+z $39 \leq A \leq 58$

1 Introduction

Metastable or isomeric states have a long-standing history in nuclear-structure research [1]. In fact, recent experimental developments have reached a level of detection sensitivity to radiation associated with the decay from such quantum levels which requires the production of less than thousand nuclei of a certain isotope. Thereby, often the first valuable fingerprints become visible for exotic nuclei far from the line of β-stability [2–6].

Of particular interest are isomeric states near doubly magic nuclei, because they efficiently probe the nuclear interaction active at these cornerstones of the spherical shell model —not only by means of precise excitation energies of specific states but more importantly via dynamic and static electromagnetic moments. The situation becomes even more substantial when it is possible to compare and relate the decay characteristics of isobaric analogue states near self-conjugate doubly magic nuclei such as ^{40}Ca or ^{56}Ni. In this mass region, isospin symmetry-breaking effects can be investigated in great detail [7]. This is largely owing to the confinement of the $\mathcal{N} = 3$, "fp shell", combined with the option of reliable large-scale shell model calculations in a spherical harmonic-oscillator basis including well-established residual interactions [8–13].

First steps beyond basic studies of so-called mirror energy differences (MED), which refer to the difference of excitation energies of isobaric analogue states as a function of the angular momentum, have been undertaken. For example, lifetime measurements of specific $I^\pi = 27/2^-$ states in the $A = 51$, $T_z = \pm 1/2$ nuclei $^{51}_{26}$Fe$_{25}$ and $^{51}_{25}$Mn$_{26}$

[a] e-mail: Dirk.Rudolph@nuclear.lu.se
[b] *Present address:* FZ Karlsruhe, D-76344 Eggenstein-Leopoldshafen, Germany.
[c] *Present address:* RIKEN, Saitama 351-0198, Japan.

established on an experimental basis isoscalar and isovector polarization charges near ^{56}Ni by means of absolute and relative $E2$ transition strenghts [14]. These results have recently been confirmed in a study of 10^+ "mirror isomers" in the $T_z = \pm 1$ system $^{54}_{28}\mathrm{Ni}_{26}$ —$^{54}_{26}\mathrm{Fe}_{28}$ [15], while an attempt using the more complex 2^+ states of these two nuclei proved less significant [16].

In the present study we show another test case, namely $3/2^-$ states in the $A = 53$, $T_z = \pm 1/2$ system comprising $^{53}_{27}\mathrm{Co}_{26}$ and $^{53}_{26}\mathrm{Fe}_{27}$ [17]. While the less exotic nuclide ^{53}Fe has been studied rather extensively by light ion transfer and heavy-ion fusion-evaporation reactions [17,18], information on ^{53}Co is rather scarce. The mainly β-decaying $19/2^-$ spin-gap isomer at $E_x = 3190$ keV excitation energy marks the first reported state with a direct proton decay branch [19], but it took more than 30 years for an in-beam γ-ray study to follow. And even so, only the yrast cascade between the $7/2^-$ ground state and an excited $17/2^-$ state at 4.1 MeV could be established. Nevertheless, this allowed for a profound MED study of the $A = 53$, $T_z = \pm 1/2$ mirror pair [20].

The experimental approach is outlined in the next section, followed by a presentation of the experimental results in sect. 3. The shell model calculations and the comparison with the experimental data are the subject of sect. 4.

2 Experimental method

Rare isotopes can be efficiently produced by nuclear fragmentation of a stable heavy-ion beam at relativistic energies on relatively thick targets. Within the *Rare Isotope Spectroscopic INvestigations at GSI* (RISING) campaign [5,6], the nuclei of interest were produced by fragmentation of a ^{58}Ni primary beam at 550 MeV/u on a 1 g/cm^2 Be target. The beam was provided by the UNILAC-SIS accelerator complex at the Gesellschaft für Schwerionenforschung mbH (GSI), Darmstadt, Germany. Due to the high kinetic energy all atomic electrons are fully stripped off the primary beam ions, *i.e.* the charge state $Q = Z = 28$ is being used. The reaction products then enter the approximately 70 m long *FRagment Separator* (FRS) [21] with energies of some 515 MeV/u. A sketch of the FRS and its detector set-up is provided in fig. 1. The fragments, alike the beam particles, start with the charge state $Q = Z$. Because of the relatively low proton number of the fragments in the present case, this maximum charge state is held throughout the passage through the FRS with a probability of essentially 100%.

The fragments pass a first magnetic dipole separation stage of magnetic rigidity $B\rho_1$ and arrive dispersed in momentum at the intermediate focus in an achromatic setting of the FRS. The momentum spread is compensated for by inducing differently matched energy losses, ΔE, in the wedge degrader (cf. fig. 1). In addition, scintillator SC1 provides energy loss signals and position information in the dispersive plane, as well as a timing signal for a time-of-flight measurement for all ions reaching the final focal plane. In the second $B\rho_2$ stage of the FRS the fragments have kinetic energies of 300 to 320 MeV/u, and the

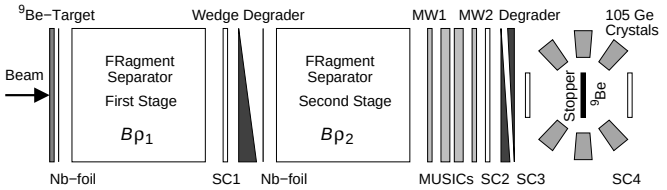

Fig. 1. Schematic drawing of the experimental set-up including the various materials and detectors placed along the beamline. See text and refs. [21,23,24] for details.

typical flight time through the second half of the FRS is approximately 190 ns. Scintillator SC2 provides not only the second signal for the time-of-flight measurement and energy loss and position information, but it also gives the start signal for the RISING Ge-detector array to await prompt and delayed γ radiation coming from those fragments, which are implanted in a 4 mm thick Be plate in the center of the array.

Before finally coming to rest, the fragments i) have passed through multiwire tracking detectors, MW1 and MW2; ii) have given rise to a total of sixteen energy loss signals in two multi-sampling ionisation chambers, MUSIC1 and MUSIC2; iii) have been slowed-down to some 70 MeV/u in an aluminum degrader (to reduce disturbing Bremsstrahlung produced in the stopper); and iv) have been cross-checked for non-destruction via an energy loss measurement in scintillator SC3. The last scintillator SC4 serves as implantation veto.

Invoking the *complete* and thus unequivocal identification scheme of the FRS and its associated detector systems, a total of 8.2 million implanted $A \sim 50$ nuclei have been clearly discriminated by mass, A, and proton number, Z, during about 60 hours of beam time. The implanted beam cocktail comprised ^{51,52}Fe (together 0.4%), ^{52,53}Co (15.5 and 21.3%), and ^{53,54,55}Ni (1.4, 58.6, and 2.8%).

The RISING germanium array itself consists of fifteen high-efficiency CLUSTER germanium detectors [22], providing up front 105 germanium crystals for γ-ray detection, while four crystals were malfunctioning during the experiment. Additionally, on average less than four of the crystals were blinded for delayed nuclear radiation due to the prompt Bremsstrahlung caused by the incoming fragments. The 105 Ge-detector electronics channels were split into two branches, one of which was read out by digital electronics. This branch provided γ-ray energy and γ-ray time in steps of 25 ns with respect to the SC2 trigger signal. The second branch saw a conventional timing sequence of fast signal amplification, constant fraction discrimination, and time-to-digital converters. Here, the timing resolution was down to less than 1 ns per digitized spectrum channel. The data acquisition system was set to wait for about 20 μs after the SC2 trigger signal, then reset itself in waiting position for the next incoming ion. The events were stored in listmode type on computer hard disks, comprising the encoded information of the FRS detectors and time and energy of the correlated, prompt and delayed γ rays. More information on the experiment and the respective RISING set-up can be found in refs. [23–25].

3 Experimental results

The present experimental setting was in principle sensitive only to isomeric states in one of the seven implanted $N < Z$ nuclides mentioned in the previous section and half-lives in the range of $\sim 100\,\mathrm{ns} < T_{1/2} < 50\,\mu\mathrm{s}$. The upper half-life limit was chosen by the experimenters for optimizing the set-up towards the main goal, namely spectroscopy of the 10^+ isomer in ^{54}Ni [15]. The lower limit, however, is an estimate and depends on the number of nuclei produced in the isomeric state of interest with respect to the flight time and, hence, the time period for isomeric decay already *inside* the FRS. Another important quantity, which can reduce the lower limit even further, is the ratio with which the isomer decays by internal conversion —since the fragments are bare nuclei, this decay mode is turned off during the passage through the separator. Good examples for this effect are isomeric states in ^{72}Kr [0_2^+ at 671(2) keV, $T_{1/2} = 26(2)$ ns] [26], ^{74}Kr [0_2^+ at 509(1) keV, $T_{1/2} = 13(7)$ ns] [27,28,26], and ^{200}Pt [7^- and 12^+ states, $T_{1/2} < 15$ ns] [29].

There is yet another possibility for the study of (short-lived) isomeric states, namely via the production by nuclear reactions of the incoming primary fragments along the slowing-down path in the stopper material. For the present experiment this implies a secondary ^{9}Be stopper "target" being subject to mainly ^{52,53}Co and ^{54}Ni secondary beams of some 50 MeV/u down to essentially zero energy, which is reached at some 2–3 mm depth depending on the ion species. Assuming a generic nuclear-reaction cross-section of 1 barn, this gives rise to some

$$8.2 \cdot 10^6 \cdot \frac{0.25\,\mathrm{cm} \cdot 1.85\,\mathrm{g/cm^3}}{9\,\mathrm{g/mol}} \cdot \frac{6 \cdot 10^{23}}{\mathrm{mol}} \cdot 1\,\mathrm{barn} \sim 250000 \quad (1)$$

potential nuclear reactions and, consequently, nuclear-reaction products. Compared with as little as about a thousand implanted ions being necessary for isomeric γ decay detection at RISING (see, *e.g.*, refs. [2,4]), 250000 is clearly a substantial number. However, the observation of such *in situ* populated isomeric states should likely be limited to i) less exotic nuclides (since nuclear-reaction channels with relatively large cross-sections take the nuclear system towards the line of stability), and ii) products close to the incoming fragments, because too violent nuclear processes including the emission of possibly several light particles or fragments could easily trigger the SC4 veto detector and, hence, be disregarded in the offline analysis.

Figure 2 provides three delayed γ-ray spectra correlated with heavy ions implanted in the ^{9}Be stopper. Note the logarithmic scale. The top spectrum and the middle spectrum were taken in the time range from 0.1 μs to 1.0 μs after implantation of ^{54}Ni and combined ^{52,53}Co fragments, respectively. For reference, the bottom spectrum represents the radiation from long-lived background sources. The latter is dominated by the positron annihilation peak at 511 keV, the ^{40}K peak at 1461 keV, and shows several weaker peaks originating from natural thorium and uranium decay chains. In addition, there is one

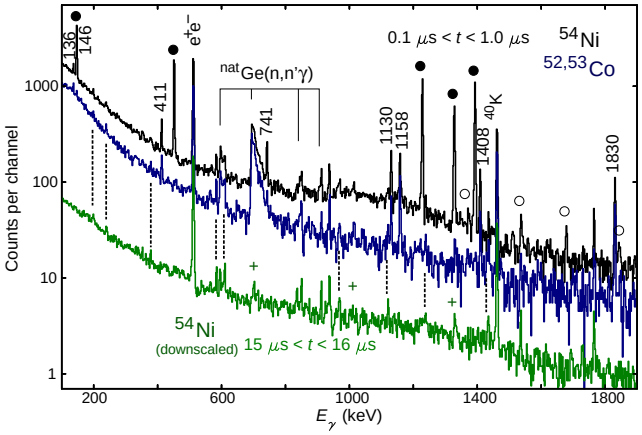

Fig. 2. (Color online) Gamma-ray spectra correlated with implanted ^{54}Ni (top and bottom) and ^{52,53}Co ions (middle). The top and middle spectra were taken between 0.1 and 1.0 μs after implantation, the bottom spectrum between 15 and 16 μs after implantation. The latter is downscaled by a factor of ten for better visibility. Several peaks are marked with their energy in keV, others with their source. Filled circles represent peaks associated with the decay of the 10^+ isomer in ^{54}Ni [15] and open circles denote pile-up of two of the ^{54}Ni transitions in the same or neighbouring Ge crystals. Plus signs label experiment specific long-lived background activity, namely the decay of the $19/2^-$ spin gap isomer in ^{53}Fe [17].

experiment specific long-lived background source, namely the $19/2^-$ spin-gap isomer in ^{53}Fe, which signs responsible for the peaks at 701, 1010, and 1328 keV, marked with "+" in fig. 2. These peaks are also visible in the other two spectra, unless they are covered by lines of different origin with about the same γ-ray energy.

Next to the radiation due to neutron capture reactions in the Ge crystals of the RISING spectrometer, the top spectrum is, of course, dominated by the peaks associated with the decay of the 10^+ isomer in ^{54}Ni [15] —these have energies of 146, 451, 1227, 1327, and 1392 keV, and they are marked with filled circles. The peaks marked with open circles are also related to the ^{54}Ni isomer; they refer to the pile-up of two γ-rays hitting the same or neighbouring Ge crystals, the signals of which were added together if occuring within 50 ns.

Disregarding all peaks in fig. 2 related to (natural) background or the ^{54}Ni isomer, there are several peaks left in *both* the ^{54}Ni *and* the ^{52,53}Co correlated spectrum, namely at 136, (146), 411, 741, 1130, 1158, 1408, and 1830 keV. (Another peak at 3432 keV is out of the range of fig. 2.) Interestingly, all these peaks relate to known isomers in the mass region: the peaks at 136, 1158, and 1830 keV originate from the $19/2^-$ isomer at 3123 keV excitation energy in ^{43}Sc [$T_{1/2} = 470(4)$ ns] [30], the peaks at 146 (doublet with ^{54}Ni), 411, 1130, 1408, and 3432 keV originate from the 10^+ isomer at 6527 keV in ^{54}Fe [$T_{1/2} = 364(7)$ ns] [31], and the peak at 741 keV originates from the $3/2^-$ state at 741 keV in ^{53}Fe [$T_{1/2} = 63.5(14)$ ns] [17]. Note that the three ^{43}Sc related peaks have comparable yields in the two spectra. On the contrary, the peaks

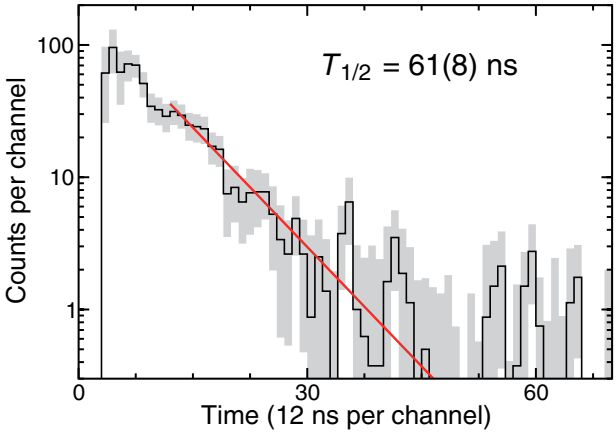

Fig. 3. (Color online) Decay curve of the 741 keV γ-ray (^{53}Fe) following the implantation of ^{54}Ni fragments in the stopper. The data is histogrammed in bins of 12 ns per channel with the grey area providing the experimental uncertainties. The straight line represents a least-squares fit to the data.

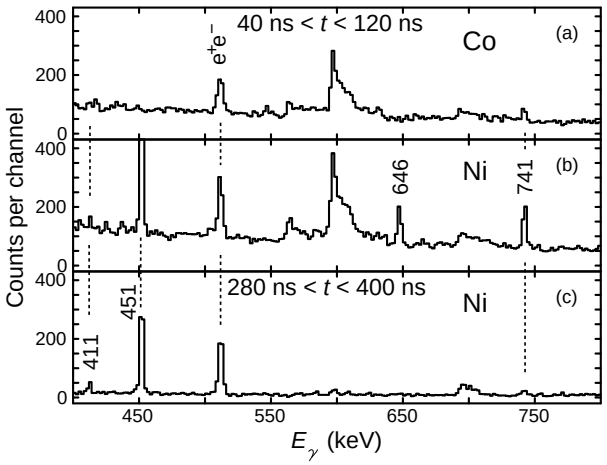

Fig. 4. Gamma-ray spectra correlated with implanted ^{54}Ni (panels (b) and (c)) and ^{52,53}Co ions (panel (a)). The top and middle spectra were taken between 40 and 120 ns after implantation, the bottom spectrum between 280 and 400 ns after implantation. Severeal peaks are marked with their energy in keV. The peak at 511 keV relates to positron annihilation (e^+e^-), and the broad structures between 550 and 630 keV and at about 700 keV are due to radiation from neutron capture reactions in the Ge crystals.

from the ^{54}Fe transitions are somewhat less intense and the ^{53}Fe 741 keV peak is much less intense in the middle, cobalt-correlated spectrum compared with the top, nickel-correlated spectrum. This points towards different nuclear production types in the beryllium stopper for the Sc and Fe isomers, respectively.

The above association of peaks in fig. 2 with isomers in ^{43}Sc and ^{53,54}Fe can, of course, be cross-checked with the time behaviour of the respective decay. As an example, the decay curve of the 741 keV transition is shown in fig. 3. It invokes the conventional RISING time branch (cf. sect. 2), and the data is binned to 12 ns per channel. A least-squares fitting procedure gives $T_{1/2} = 61(8)$ ns for this sample, which is in agreement with the above-mentioned literature value. The peaks suggested to arise from ^{43}Sc and ^{54}Fe can be proven to belong to these two isotopes in a corresponding fashion.

It is also clear that the ^{53}Fe isomer must have been populated in the beryllium stopper, because neither can missing atomic electrons prolong the lifetime, nor can any significant amount of ^{53}Fe produced in the primary target reach the stopper with such a short isomeric half-life —not to mention that the setting of the FRS prohibited transmission of ^{53}Fe (and ^{54}Fe as well as ^{43}Sc) in the first place, and that energy loss correlations in the MUSICs and SC2 and SC3 (cf. fig. 1) ensure implantation of nickel ions.

Figure 4 focuses on short-lived decays by providing γ-ray spectra correlated with ^{52,53}Co (panel (a)) and ^{54}Ni (panels (b) and (c)). While the spectra in figs. 4(a) and (b) were taken between 40 ns and 120 ns after implantation, panel (c) shows a spectrum measured during a somewhat later time window. The broad structures between γ-ray energies of 550 to 630 keV and at about 700 keV again relate to radiation from neutron capture reactions in the Ge crystals. All spectra also reveal once more the positron annihilation peak, and panels (b) and (c) comprise the 451 keV peak from the $6^+ \rightarrow 4^+$ decay in ^{54}Ni. The 411 keV peak from the $6^+ \rightarrow 4^+$ decay in ^{54}Fe becomes more apparent at later times (fig. 4(c)), while the 741 keV $3/2^- \rightarrow 7/2^-$ decay in ^{53}Fe is very pronounced in fig. 4(b), simply because of the earlier time period compared with the top spectrum in fig. 2. Some late remainders of the 741 keV peak are present in fig. 4(c), while it becomes obvious that the $3/2^-$ isomer in ^{53}Fe is produced significantly less efficient with the cobalt ions than with the ^{54}Ni fragments by comparing figs. 4(a) and (b).

Most interestingly, however, there is one additional peak visible at 646 keV in fig. 4(b). It has a similar yield as the 741 keV line, and it is completely absent in both the spectrum correlated with cobalt fragments as well as in the one taken at slightly later times. The latter is an indication for a rather short-lived isomer, while the former observation limits the isotopic origin to either Ni or Co isotopes with $N \sim Z$, *i.e.* most likely to ^{55,56}Ni or ^{53,54,55}Co. Any lighter residue with $Z \leq 26$ would have left a significant signal at 646 keV in fig. 4(a), too. The massive production of exotic $N < Z$ isotopes with $Z \geq 27$ is highly unlikely because of the small reaction cross-sections involved. A data base search [32] for a delayed γ-ray of 646(1) keV in isotopes with $20 \leq N, Z \leq 32$ turned out negative.

^{55}Co has been studied extensively by means of several different experimental approaches [33,34]. So far, no isomeric state has been observed in that nuclide, and due to the shell gap at particle number $N = Z = 28$, excited states in $^{55}_{27}$Co are expected and observed first beyond 2 MeV excitation energy. No signs of the respective ground-state transitions are seen in the present data. Therefore, we exclude ^{55}Co from the list of candidates. Likewise, its mirror nucleus ^{55}Ni is disregarded based on isospin symmetry considerations. The low- to medium-spin regimes of ^{54}Co [31,34,35] and ^{56}Ni [34,36–38] are

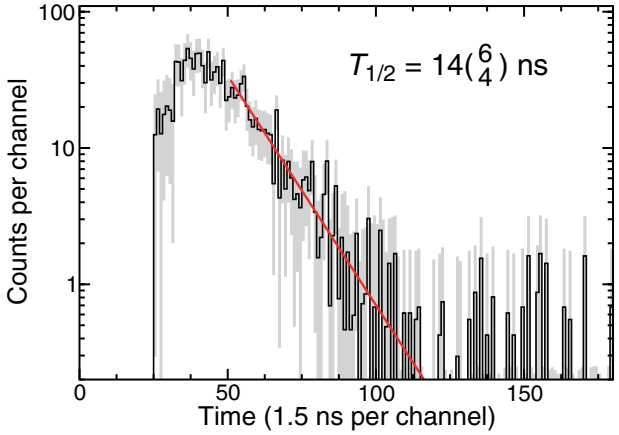

Fig. 5. (Color online) Background-subtracted decay curve of the previously unobserved 646 keV γ-ray following the implantation of ^{54}Ni fragments in the ^{9}Be stopper. The data is histogrammed in bins of 1.5 ns per channel with the grey area providing the experimental uncertainties. The straight line represents a least-squares fit to the data starting some 30 ns after the nominal position of the prompt timing distribution.

also well known, and for reasons similar to the above, also these two nuclei can be disregarded. Thus, the only obvious candidate left is an isomeric state in $^{53}_{27}$Co$_{26}$. Indeed, the mirror nucleus $^{53}_{26}$Fe$_{27}$ does have an isomeric state at comparable excitation energy and half-life, namely the $3/2^-$ state at 741 keV, which is readily observed in figs. 2 and 4, and which has been discussed above.

The decay curve of the 646 keV γ-ray is shown in fig. 5. Due to its short half-life and hence close proximity to the prompt timing peak, the half-life result contains a rather large uncertainty (the least-squares fitting procedure displayed in fig. 5 starts some 30 ns beyond the position of the prompt timing distribution). In conclusion, we attribute the peak at 646.2(2) keV in fig. 4(b) to the decay of an isomeric $I^\pi = 3/2^-$ state in ^{53}Co, situated at 646.2(2) keV excitation energy and with a half-life of $T_{1/2} = 14(^{6}_{4})$ ns. These experimental characteristics are close to the ones of the isobaric analogue state in ^{53}Fe [17].

4 Shell model calculations and discussion

Spherical large-scale shell model calculations were performed with the code ANTOINE [39]. The full fp space is considered including the $1f_{7/2}$ shell below and the $2p_{3/2}$, $1f_{5/2}$, and $2p_{1/2}$ shells above the $N = Z = 28$ shell closure. Nevertheless, the model space has to be truncated allowing a certain number, t, of particles (protons or neutrons) to be excited across the shell closure. Here, a maximum $t = 7$ is chosen to compromise between available computing power and sufficient convergence of the calculated numbers. Both the KB3G [11] and GXPF1A [12, 13] effective interactions have been employed, the predictions of which are generally very reliable for mass $A \sim 50$ nuclei [8–10, 40].

The evolution of the predicted excitation energies of a number of $A = 53$, $T_z = \pm 1/2$ low- to medium-spin

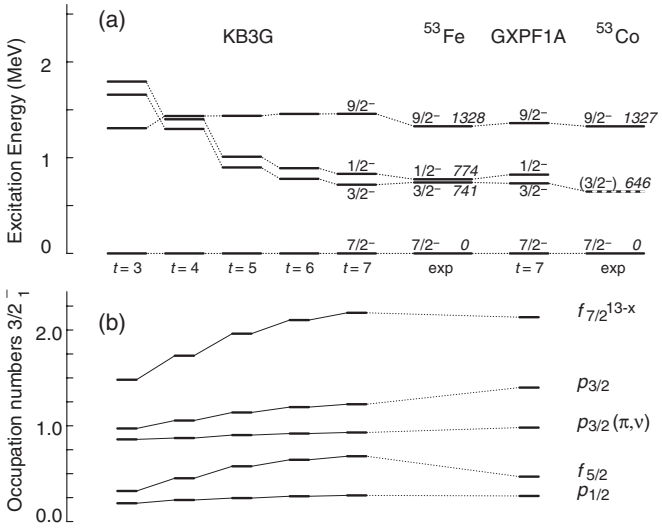

Fig. 6. Results of shell-model calculations for low-spin states in the mass $A = 53$ nuclei ^{53}Co and ^{53}Fe. The left-hand side of panel (a) illustrates the evolution of excitation energies as a function of the number of particles allowed in the upper fp shell, t, for the KB3G [11] fp shell effective interaction. The $t = 7$ predictions using the alternative GXPF1A interaction [13] are included on the right-hand side, surrounded by the respective experimentally known states of the two isobars [17, 20]. Panel (b) illustrates the occupation numbers of the $3/2^-$ yrast state. The plot for the $f_{7/2}$ shell concerns the number of particles *missing* with respect to the originally thirteen particles relative to ^{40}Ca. The plot denoted by $p_{3/2}$ (π, ν) represents the occupation number of only the respective unpaired proton (^{53}Co) or unpaired neutron (^{53}Fe).

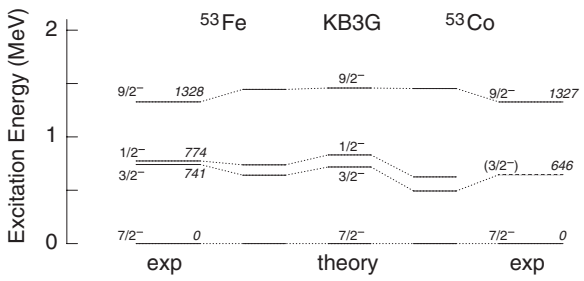

Fig. 7. Comparison of the excitation energies of experimental low-spin states in the mass $A = 53$ nuclei ^{53}Co and ^{53}Fe with predictions from isospin-dependent shell model calculations ($t = 7$) based on the KB3G effective interaction.

states as a function of t is illustrated on the left-hand side of fig. 6(a). An increased t induces in general more correlation energy, but the strongly downsloping excitation energies of the predicted $1/2^-$ and $3/2^-$ low-spin states are apparently much more affected compared with the $9/2^- \rightarrow 7/2^-$ yrast cascade, because the relative energy between these two states remains essentially constant. The $9/2^-$ state, which has been discussed in earlier mass $A = 53$ investigations [18, 20], is included in figs. 6 and 7 as reference.

The enhanced correlations as a function of t find their counterpart in the reduced single-particle character of the

predicted wave functions of the yrast $3/2^-$ ($2p_{3/2}$) state: the $2p_{3/2}$ single-particle partition to the wave function of the $3/2^-$ state drops from 54% ($t = 3$) to 34% ($t = 7$) using KB3G. Figure 6(b) provides the average occupation numbers of the $3/2^-$ state. In line with the above, increasing t increases the average number of proton and neutron holes in the $1f_{7/2}$ shell as well as the average number of protons and neutrons in the $2p_{3/2}$ and $1f_{5/2}$ shells —the latter even more pronounced. The $2p_{1/2}$ shell occupancy does not see any significant change. It is worth mentioning that the occupation number of the unpaired proton (^{53}Co) or unpaired neutron (^{53}Fe), which is denoted $p_{3/2}(\pi, \nu)$ in fig. 6(b), remains essentially constant at about unity. This implies that the correlations are inferred by excitations across the shell gap at $N, Z = 28$ into the $1f_{5/2}$ shell or excitations of the respective other nuclear fluid into the $2p_{3/2}$ shell, *i.e.*, the neutrons in case of ^{53}Co and the protons in case of ^{53}Fe.

Towards the right-hand side of fig. 6 the predictions of a $t = 7$ calculation using the GXPF1A interaction are shown, and in general the results are similar to the predictions based on the KB3G interaction, in particular the calculated energies of the low-spin states. One peculiarity, however, is that the wave function of the yrast $3/2^-$ state predicted by GXPF1A has only about half the $1f_{5/2}$ occupation of the prediction using the KB3G interaction, which is balanced by an on average increased $2p_{3/2}$ occupancy and a slightly reduced number of holes in the $1f_{7/2}$ shell. Moreover, the predicted excitation energy of the yrare $3/2^-_2$ state ($E_x = 1852\,\mathrm{keV}$) differs significantly from the $t = 7$ prediction of the KB3G interaction ($E_x = 2446\,\mathrm{keV}$), while the experimentally known state in ^{53}Fe is situated roughly in between ($E_x = 2043\,\mathrm{keV}$). Such details appear interesting, but they are difficult to trace back to individual two-body matrix-elements or the slightly different single-particle energies of the two effective interactions. Hence, a more thorough theoretical investigation is required.

To study the mirror symmetry of isobaric analogue states in ^{53}Fe and ^{53}Co in more detail, isospin-breaking terms have been incorporated along the notations of refs. [7,9,10]. Multipole harmonic-oscillator Coulomb matrix elements, V_{CM}, the monopole electromagnetic spin-orbit interaction, V_{Cls}, and monopole radial effects have been added to both the bare GXPF1A and KB3G interactions following the prescription of ref. [10]. The matrix element of the effective interaction for two protons in the $1f_{7/2}$ orbital coupled to $J = 2$ has been increased by 100 keV. This isospin-breaking term, usually denoted V_{BM}, has been deduced by Zuker *et al.* [7] from the MED in mass $A = 42$. It showed to be essential to successfully reproduce the MED of several mirror pairs in the mass region [7,9,15,20,41]. To describe the electromagnetic decay properties, effective charges of $e_{eff,p} = 1.15$ and $e_{eff,n} = 0.80$ taken from ref. [14] are used and related to predictions with the standard plain isoscalar values $e_{eff,p} = 1.5$ and $e_{eff,n} = 0.5$ [8]. Magnetic properties are described with free gyromagnetic factors.

Table 1. Mirror energy differences, $E_x(^{53}\mathrm{Co}) - E_x(^{53}\mathrm{Fe})$, for the excited yrast $3/2^-$ and $9/2^-$ states. The calculated numbers are based on the given interactions but involve isospin-breaking components. See text for details.

	Level, I^π	$3/2^-$	$9/2^-$
Experiment	present [20]	−95 keV	−1 keV
Theory	KB3G [11]	−147 keV	8 keV
	GXPF1A [13]	−130 keV	1 keV

The results of the isospin-dependent $t = 7$ calculations based on the KB3G interaction are illustrated in fig. 7. Tables 1 and 2 provide a summary for both the KB3G and GXPF1A interactions. The left-hand side of fig. 7 depicts the comparison of observed and predicted energy levels for ^{53}Fe, while the right-hand side shows the results for ^{53}Co. For reference, the results based on the bare interaction (cf. fig. 6) are repeated in the central part of the figure.

In the case of the yrast $9/2^-$ state the net effect of including isospin-breaking components in the interaction is close to zero; the predicted excitation energies change very little, and the related MED values, *i.e.*, $E_x(^{53}\mathrm{Co}) - E_x(^{53}\mathrm{Fe})$, are small and in nearly perfect agreement with experiment and in line with the discussions in ref. [20]. The actual numbers are summarized in the rightmost column of table 1, and the fact that the MED are small points towards a similar overall structure of the $7/2^-$ ground state and the excited $9/2^-$ state. A closer look at the calculated wave functions of these two states reveals that on average about the same number of protons and neutrons are predicted to be excited across the shell gap for both $A = 53$ nuclei.

The situation is at variance for the $3/2^-$ low-spin yrast state. Here, the wave functions are predicted to comprise distinctively different amounts of protons and neutrons in the $\ell = 1$ p-orbits of the upper fp shell (cf. fig. 6(b)). These protons are less bound and thus easier to excite, and the related energy differences of these excitations lead to large negative MED values for in particular the $3/2^-$ states. The large negative MED prediction is in good agreement with the rather large experimental MED = −95 keV for the $3/2^-$ yrast states. However, including the isospin-breaking components in the shell model calculations, the agreement between experiment and theory on the absolute excitation energy scale is worsened for the presumed single-particle–like $3/2^-$ yrast states (cf. fig. 7). For example, the predicted energy of the $3/2^-$ yrast state for the isospin-symmetric calculation, $E_x = 718\,\mathrm{keV}$ is in line with both the $3/2^-$ state in ^{53}Fe ($E_x = 741\,\mathrm{keV}$, $\Delta E = |E_{x,th} - E_{x,exp}| = 23\,\mathrm{keV}$) and ^{53}Co ($E_x = 646\,\mathrm{keV}$, $\Delta E = 72\,\mathrm{keV}$). However, including the isospin-breaking terms as described above, the predicted excitation energies drop to $E_x = 640\,\mathrm{keV}$ ($\Delta E = 101\,\mathrm{keV}$) for ^{53}Fe and $E_x = 493\,\mathrm{keV}$ for ^{53}Co ($\Delta E = 153\,\mathrm{keV}$), respectively.

The predicted and measured half-lives of some observed low- to medium-spin states in the $A = 53$ nuclei are summarized in table 2. A very good quantitative agreement is achieved for the $11/2^- \to 9/2^- \to 7/2^-$ yrast cascades, and the half-life predictions turn out to be rather

Table 2. Experimental half-lives of experimentally observed states compared to predictions from isospin-dependent fp shell model calculations and using the experimental transition energies for the $A = 53$, $T_z = \pm 1/2$ mirror pair.

	^{53}Fe					^{53}Co				
	Exp [17]	KB3G		GXPF1A		Exp	KB3G		GXPF1A	
State		C1[a]	C2[b]	C1	C2		C1	C2	C1	C2
$1/2^-$	2.0(2) ns	1.8 ns	1.8 ns	4.3 ns	4.3 ns					
$3/2^-$	63.5(14) ns	7.8 ns	13 ns	11 ns	25 ns	$14(^{6}_{4})$ ns	7.6 ns	5.1 ns	7.9 ns	5.0 ns
$5/2^-$	2.8(7) ps	6.0 ps	6.1 ps	4.7 ps	4.8 ps					
$7/2^-_2$	$1.4(^{21}_{7})$	1.6 ps	1.6 ps	1.7 ps	1.6 ps					
$9/2^-$	17(7) fs	24 fs	23 fs	28 fs	27 fs		22 fs	23 fs	25 fs	25 fs
$11/2^-$	53(12) fs	29 fs	28 fs	40 fs	39 fs		27 fs	27 fs	30 fs	31 fs

[a] C1 uses effective charges of $e_{eff,p} = 1.15$ and $e_{eff,n} = 0.80$ [14].
[b] C2 uses effective charges of $e_{eff,p} = 1.5$ and $e_{eff,n} = 0.5$ [8].

independent of the effective charges and effective interaction used. For the yrast $1/2^-$ and $5/2^-$ as well as the yrare $7/2^-_2$ states in ^{53}Fe the agreement is still good.

The crux, however, lies in the predicted half-lives of the yrast $3/2^-$ states. Despite their presumed simplicity of being dominated by $2p_{3/2}$ single-particle components, their half-lives are predicted a factor of 3–8 (^{53}Fe) and 2–3 (^{53}Co) too *short*, *i.e.*, the calculated transition rates are too *fast*. Typically, transition rates are calculated too low because of the lack of the correlations across shell gaps, but in the present case the opposite holds true. Therefore, going to larger values of $t > 7$ or a full fp calculation will not solve the problem. Moreover, the predictions using the effective charges of ref. [14] are worse than the ones neglecting isovector contributions, at variance to other mirror systems in the mass region. This discrepancy becomes most apparent when looking at the comparison of the ratio of the experimental half-lives, which ranges from $R[T_{1/2}(^{53}\mathrm{Fe})/T_{1/2}(^{53}\mathrm{Co})] \sim 3.1$–$6.5$, to the ratio of predicted half-lives, which is close to unity for the calculations with $e_{eff,p} = 1.15$ and $e_{eff,n} = 0.80$. It is only the calculation using the GXPF1A interaction and plain isoscalar effective charges, for which the ratio $R = 5.0$ falls into the experimental ballpark —nevertheless, it is off by almost a factor of three on the absolute scale for both mirror partners. Therefore, a local adjustment of effective charges does not seem to solve the puzzle either, and the answer is considered to rather lie in the nature of the predicted wave functions.

For example, both proton and neutron single-particle energies may be lowered to potentially achieve purer $3/2^-$ states, or a detailed modification of the interaction may be necessary on some decisive two-body matrix elements. While this is considered a purely theoretical prescription beyond the scope of the present work, it should be pointed out that this discrepancy of the decay properties of *both* $3/2^-$ yrast states in the $A = 53$, $T_z = \pm 1/2$ mirror pair is highly unusual considering the overall excellent agreement of large-scale shell model calculations achieved in this mass regime —with or without invoking isospin-breaking terms.

5 Summary

To summarize, short-lived isomeric states have been observed following secondary nuclear reactions of neutron-deficient radioactive $A \sim 50$ fragment beams in a ^{9}Be stopper plate positioned inside the RISING γ-ray spectrometer. A previously unreported delayed γ-ray of 646.2(2) keV with an associated half-life of $T_{1/2} = 14(^{6}_{4})$ ns was observed and attributed to the decay of the $3/2^-$ yrast state of ^{53}Co. Isospin-dependent large-scale shell model calculations agree well with the relative energies of the reported and new isobaric analogue states of the $A = 53$, $T_z = \pm 1/2$ mirror pair. While this type of predictions is commonly in excellent agreement with experimental observations in the upper half of the $1f_{7/2}$ shell, both the calculated absolute energies and, more importantly, the decay strengths of the yrast $3/2^-$ states in ^{53}Co *and* ^{53}Fe deviate considerably from the experimental values. Given the presumed simplicity of this state, this comes as a surprise. On the theoretical side, this calls for a more detailed tracing of the residual interactions and single-particle energies, while experiment may aim at a better definition of the $3/2^-$ states in both the $A = 53$ and $A = 55$ mirror pairs.

The authors gratefully acknowledge the outstanding work of the GSI accelerator and ion source crews in providing the experiment with the envisaged high beam intensities. DR would also like to thank F. Nowacki and G. Kalus for patient support with the new ANTOINE installation. This work is supported by the European Commission contract no. 506065 (EURONS), the Swedish Research Council, EPSRC (UK), the German BMBF under grant 06KY205I, the Polish Ministry of Science and Higher Education under grant 1-P03B-030-30 the Bulgarian Science Fund, grant No. VUF06/05, the Spanish Ministerio de Educación y Ciencia (FPA2005-00696), and the U.S. Department of Energy grants DE-FG02-91ER-40609 and W-31-109-ENG-38.

References

1. P. Walker, G. Dracoulis, Nature **399**, 35 (1999).
2. A. Jungclaus *et al.*, Phys. Rev. Lett. **99**, 132501 (2007).

3. C. Chandler *et al.*, Phys. Rev. C **61**, 044309 (2000).
4. A.B. Garnsworthy *et al.*, Phys. Lett. B **660**, 32 (2008).
5. P.H. Regan *et al.*, Nucl. Phys. A **787**, 491c (2007).
6. D. Rudolph *et al.*, Eur. Phys. J. ST **150**, 173 (2007).
7. A.P. Zuker, S.M. Lenzi, G. Martinez-Pinedo, A. Poves, Phys. Rev. Lett. **89**, 142502 (2002).
8. E. Caurier, G. Martinez-Pinedo, F. Nowacki, A. Poves, A.P. Zuker, Rev. Mod. Phys. **77**, 427 (2005).
9. M.A. Bentley, S.M. Lenzi, Prog. Part. Nucl. Phys. **59**, 497 (2007).
10. J. Ekman, C. Fahlander, D. Rudolph, Mod. Phys. Lett. A **20**, 2977 (2005).
11. A. Poves, J. Sanchez-Solano, E. Caurier, F. Nowacki, Nucl. Phys. A **694**, 157 (2001).
12. M. Honma, B.A. Brown, T. Mizusaki, T. Otsuka, Phys. Rev. C **65**, 061301(R) (2002).
13. M. Honma, B.A. Brown, T. Mizusaki, T. Otsuka, Phys. Rev. C **69**, 034335 (2004); Eur. Phys. J. A **25**, s01, 499 (2005).
14. R. du Rietz *et al.*, Phys. Rev. Lett. **93**, 222501 (2004).
15. D. Rudolph *et al.*, submitted to Phys. Rev. Lett.
16. K.L. Yurkewicz *et al.*, Phys. Rev. C **70**, 054319 (2004).
17. H. Junde, Nucl. Data Sheets **87**, 507 (1999).
18. R. du Rietz *et al.*, Phys. Rev. C **72**, 014307 (2005).
19. K.P. Jackson, C.U. Cardinal, H.C. Evans, N.A. Jelley, J. Cerny, Phys. Lett. B **33**, 281 (1970); J. Cerny, J.E. Esterl, R.A. Gough, R.G. Sextro, Phys. Lett. B **33**, 284 (1970).
20. S.J. Williams *et al.*, Phys. Rev. C **68**, 011301(R) (2003).
21. H. Geissel *et al.*, Nucl. Instrum. Methods B **70**, 286 (1992).
22. J. Eberth, H.G. Thomas, P. von Brentano, R.M. Lieder, H.M. Jäger, H. Kämmerling, M. Berst, D. Gutknecht, R. Henck, Nucl. Instrum. Methods A **369**, 135 (1996).
23. R. Hoischen, Master thesis, Lund University, unpublished, `http://wwwnsg.nuclear.lu.se/projects.asp`.
24. S. Pietri *et al.*, Acta Phys. Pol. **38**, 1255 (2007).
25. S. Pietri *et al.*, Nucl. Instrum. Methods B **261**, 1079 (2007).
26. E. Bouchez *et al.*, Phys. Rev. Lett. **90**, 082502 (2003).
27. C. Chandler *et al.*, Phys. Rev. C **56**, R2924 (1997).
28. F. Becker *et al.*, Eur. Phys. J. A **4**, 103 (1999).
29. M. Caamaño *et al.*, Eur. Phys. J. A **23**, 201 (2005).
30. J.A. Cameron, B. Singh, Nucl. Data Sheets **92**, 783 (2001).
31. H. Junde, H. Su, Nucl. Data Sheets **107**, 1393 (2006).
32. Nuclear Structure and Decay Data base, NuDat 2.4, `http://www.nndc.bnl.gov/nudat2`.
33. H. Junde, Nucl. Data Sheets **64**, 723 (1991) and ENSDF updates.
34. D. Rudolph, C. Baktash, M.J. Brinkman, M. Devlin, H.-Q. Jin, D.R. LaFosse, L.L. Riedinger, D.G. Sarantites, C.-H. Yu, Eur. Phys. J. A **4**, 115 (1999).
35. I. Schneider, A.F. Lisetskiy, C. Frießner, R.V. Jolos, N. Pietralla, A. Schmidt, D. Weisshaar, P. von Brentano, Phys. Rev. C **61**, 044312 (2000).
36. E.K. Johansson *et al.*, Eur. Phys. J. A **27**, 157 (2006).
37. N. Pietralla, private communication.
38. H. Junde, Nucl. Data Sheets **86**, 315 (1999).
39. E. Caurier, shell model code ANTOINE, IReS Strasbourg 1989, 2002; E. Caurier, F. Nowacki, Acta Phys. Pol. **30**, 705 (1999).
40. M. Horoi, B.A. Brown, T. Otsuka, M. Honma, T. Mizusaki, Phys. Rev. C **73**, 061305(R) (2006).
41. A. Gadea *et al.*, Phys. Rev. Lett. **97**, 152501 (2006).

PHYSICAL REVIEW C **78**, 021301(R) (2008)

Isospin symmetry and proton decay: Identification of the 10^+ isomer in ^{54}Ni

D. Rudolph,[1] R. Hoischen,[1,2] M. Hellström,[1] S. Pietri,[3] Zs. Podolyák,[3] P. H. Regan,[3] A. B. Garnsworthy,[3,4] S. J. Steer,[3] F. Becker,[2,*] P. Bednarczyk,[2,5] L. Cáceres,[2,6] P. Doornenbal,[2,7,†] J. Gerl,[2] M. Górska,[2] J. Grębosz,[2,5] I. Kojouharov,[2] N. Kurz,[2] W. Prokopowicz,[2,5] H. Schaffner,[2] H. J. Wollersheim,[2] L.-L. Andersson,[1] L. Atanasova,[8] D. L. Balabanski,[8,9] M. A. Bentley,[10] A. Blazhev,[7] C. Brandau,[2,3] J. R. Brown,[10] C. Fahlander,[1] E. K. Johansson,[1] A. Jungclaus,[6] and S. M. Lenzi[11]

[1]*Department of Physics, Lund University, S-22100 Lund, Sweden*
[2]*Gesellschaft für Schwerionenforschung mbH, D-64291 Darmstadt, Germany*
[3]*Department of Physics, University of Surrey, Guildford, GU2 7XH, United Kingdom*
[4]*Wright Nuclear Structure Laboratory, Yale University, New Haven, Connecticut 06520-8124, USA*
[5]*The Henryk Niewodniczaski Institute of Nuclear Physics (IFJ PAN), PL-31342 Kraków, Poland*
[6]*Departamento de Fisica Teórica, Universidad Autonoma de Madrid, E-28049 Madrid, Spain*
[7]*Institut für Kernphysik, Universität zu Köln, D-50937 Köln, Germany*
[8]*Faculty of Physics, University of Sofia, BG-1164 Sofia, Bulgaria*
[9]*Bulgarian Academy of Sciences, BG-1784 Sofia, Bulgaria*
[10]*Department of Physics, University of York, York, YO10 5DD, United Kingdom,*
[11]*Dipartimento di Fisica dell'Università and INFN, Sezione di Padova, I-35131 Padova, Italy*

(Received 7 February 2008; published 6 August 2008)

The γ decays from an isomeric 10^+ state at 6457 keV in the nucleus $^{54}_{28}Ni_{26}$ have been identified using the GSI fragment separator in conjunction with the RISING Ge-detector array. The state is interpreted as the isobaric analog of the 6527-keV 10^+ isomer in $^{54}_{26}Fe_{28}$. The results are discussed in terms of isospin-dependent shell-model calculations. Clear evidence is presented for a discrete $\ell = 5$ proton decay branch into the first excited $9/2^-$ state of the daughter ^{53}Co. This decay is the first of its kind observed following projectile fragmentation reactions.

DOI: 10.1103/PhysRevC.78.021301 PACS number(s): 23.20.−g, 23.50.+z, 25.70.Mn, 27.40.+z

A central topic in contemporary nuclear structure physics is the investigation of exotic nuclear matter far from the line of β stability. Long-standing questions are "Where are the proton and neutron drip lines situated?" and "How does the nuclear force depend on varying proton-to-neutron ratios?" [1]. These issues can be addressed by investigating long isotopic chains: The magic $Z = 28$ nickel chain covers four potentially doubly-magic nuclides, namely, with $N = 20$, $N = 28$, $N = 40$, and $N = 50$. Indeed, ^{48}Ni is found to denote the proton dripline [2], while measurements on ^{78}Ni provide crucial information on the astrophysical rapid neutron capture process [3]. As with ^{68}Ni [4], the self-conjugate $N = Z$ nucleus ^{56}Ni shows distinct features of a soft doubly-magic core, becoming strongly deformed at modest excitation energies and angular momenta. Furthermore, a rotational state at ∼10 MeV excitation energy in ^{56}Ni revealed a fast, discrete proton decay branch [5,6].

Another evergreen of nuclear structure studies along the $N = Z$ line is isospin symmetry or, more precisely, the breaking of isospin symmetry due to the Coulomb force as well as, possibly, some components of the strong nucleon-nucleon interaction [7]. Here, the so-called "$J = 2$ anomaly" must be mentioned: It relates to unusual mirror energy differences (MED) in excited states, the wave functions of which are thought to be dominated by spin $J = 2$, isospin $T = 1$ couplings [7–9]. During the past decade, the prime region for such investigations has been the rather well-confined $\mathcal{N} = 3$, "fp shell" reaching from ^{40}Ca toward ^{80}Zr while passing ^{56}Ni. Related work has been summarized recently [10–12].

This rapid communication provides new experimental results on the $T_z = -1$ nucleus ^{54}Ni, hence addressing both the dripline and the isospin symmetry breaking aspects indicated above. The existence of an isomeric 10^+ state in ^{54}Fe has been known for decades [13], and thus an isobaric analog state is expected to exist in ^{54}Ni. Besides basic studies of MED, its observation bears the potential of isospin symmetry studies of electromagnetic moments and decay properties, for example, an independent check on the recently established isoscalar and isovector polarization charges near ^{56}Ni [14] and a possible extension to $E4$ transitions. Previous knowledge on ^{54}Ni includes the yrast $6^+ \rightarrow 4^+ \rightarrow 2^+ \rightarrow 0^+$ ground-state cascade established via in-beam γ-ray spectroscopy [9] and measurements of $B(E2; 2^+ \rightarrow 0^+) = 122(24)\ e^2\text{fm}^4$ by relativistic Coulomb excitation experiments [15,16].

Within the *Rare Isotope Spectroscopic INvestigations at GSI* (RISING) campaign, the nuclei of interest were produced by fragmentation of a ^{58}Ni primary beam at 550 MeV/u on a 1 g/cm^2 ^{9}Be target. Subsequently, the reaction products were selected by means of a $B\rho - \Delta E - B\rho$ technique in the *FRagment Separator* (FRS) [17]. The ion-by-ion identification in terms of mass, A, and proton number, Z, of each transmitted ion is performed uniquely with a suite of scintillator and ionization detectors placed at the intermediate and final focus of the FRS. The identified secondary ions, namely, ^{51,52}Fe (0.4%), ^{52,53}Co (15.5 and 21.3%), and ^{53,54,55}Ni (1.4, 58.6, and 2.8%), finally came to rest in a 4 mm thick Be plate after some 350 ns flight time through the FRS. The Be plate was

[*]Present address: FZ Karlsruhe
[†]Present address: RIKEN

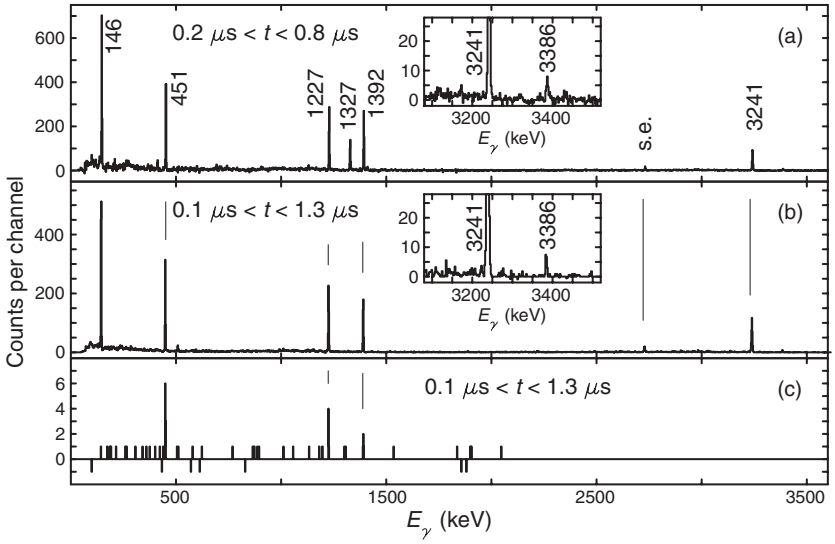

FIG. 1. γ-ray spectra associated with implanted ^{54}Ni ions. Part (a) shows a spectrum requiring a complete ion identification. It was taken between 0.2 and 0.8 μs after implantation. Implantation-correlated background radiation is removed with correspondingly selected spectra of other implanted ions, namely, ^{53,55}Ni and ^{52,53}Co, which do not show any delayed γ rays in this time range. Room and long-lived β-decay background is subtracted with a spectrum taken between 19.0 and 19.6 μs after implantation. Parts (b) and (c) provide spectra in coincidence with the known yrast cascade [9] in ^{54}Ni and the new 3386-keV, $10^+ \rightarrow 6^+$ $E4$ transition.

surrounded by fifteen high-efficiency CLUSTER Ge detectors [18] for γ-ray detection. Each ion arriving at the final focus started a clock and subsequent γ decays from isomeric states were recorded for 20 μs before the data acquisition system reset itself. More details on the experiment and the RISING setup can be found in Refs. [19,20].

During 60 h of beam time and employing a very restrictive and stringent heavy-ion identification procedure on the FRS data, some 4.8 million implanted ^{54}Ni nuclei have been identified. Figure 1(a) provides the associated time-correlated and background subtracted γ-ray spectrum. It reveals seven delayed γ-ray transitions at 146.1(2), 451.0(3), 1227.4(4), 1327.3(4), 1392.3(4), 3240.7(7), and 3386.2(9) keV. The latter is highlighted in the inset, and the single-escape line of the 3241 keV transition is also present. The 451-, 1227-, and 1392-keV lines are known to belong to ^{54}Ni [9]. The 146- and 3241-keV transitions are very similar in energy to the $10^+ \rightarrow 8^+ \rightarrow 6^+$ sequence in the mirror nucleus ^{54}Fe, and the 3386-keV line represents a parallel 5.1(11)% $10^+ \rightarrow 6^+ E4$ branch. The branching ratio is corrected for possible pileup of the 146- and 3241-keV transitions in the same Ge detector. This scheme is underpinned by the γ-ray spectra in Figs. 1(b) and 1(c), which are based on delayed $\gamma\gamma$ coincidences. Both the time range and the FRS identification scheme are somewhat relaxed to allow for increased statistics. The spectrum in Fig. 1(b) is taken in prompt coincidence with the known ground-state cascade and confirms the placement of the 146-, 3241-, and 3386-keV transitions on top of it. Figure 1(c) is the coincidence spectrum of the weak 3386-keV line, proving that it lies parallel to the 146- to 3241-keV cascade.

The peak at 1327 keV, which is clearly seen in Fig. 1(a), is absent in both Figs. 1(b) and 1(c); i.e., it is *not* in coincidence with any other γ-ray transition associated with the decay of the presumed 10^+ isomer in ^{54}Ni. Nevertheless, within uncertainties the 1327-keV line exhibits the same half-life as the ^{54}Ni transitions. This is shown in Fig. 2, which provides three scaled decay curves of the previously reported transitions in ^{54}Ni (top), the new high-energetic ones (middle), and the 1327-keV line (bottom). The conclusion is that the single γ ray at 1327 keV must have the same isomeric origin as the other six transitions. Because 1327 keV matches exactly the prompt $9/2^- \rightarrow 7/2^-$ ground-state γ transition in ^{53}Co [8], a discrete 1.28(5)-MeV, $\ell = 5$ proton decay from the isomeric 10^+ state in ^{54}Ni into the excited $9/2^-$ state in the daughter ^{53}Co is inferred. This marks the first evidence for discrete proton emission competing with γ radiation following a projectile fragmentation reaction. The evidence is indirect, because both the present setup and the implantation depth of ^{54}Ni ions in the stopper together with the short half-life prevent a direct measurement of the protons. Historically, this observation takes proton decay studies back to its roots, as the first reported proton decay ever was observed from the long-lived $19/2^-$ high-spin state in ^{53}Co [21,22]. The existence of the present type of discrete proton decay opens a plethora of subsequent, unprecedented investigations: isospin aspects of static moments and, ultimately, proton angular distributions from an aligned state with known quadrupole moment.

The lifetime of the 10^+ state in ^{54}Ni averages to $T_{1/2} = 152(4)$ ns. The experimental information is summarized in Table I and illustrated in Fig. 3.

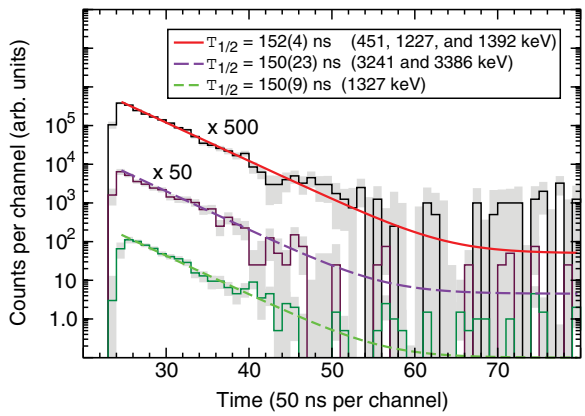

FIG. 2. (Color online) Decay curves of different combinations of γ-ray transitions associated with the isomeric 10^+ state in ^{54}Ni. The lines represent the least-squares fits to the data.

TABLE I. Experimental results and theoretical predictions from isospin-dependent fp shell-model calculations. The experimental numbers of ^{54}Ni are corrected for the measured 36(2)% proton branch. $B(E2)$ and $B(E4)$ values are in W.u.

Observable	^{54}Fe		^{54}Ni		
	exp [13]	KB3G	exp	KB3G	exp'[a]
$B(E2; 6^+ \rightarrow 4^+)$	3.25(5)	2.85	–	2.29	–
$B(E2; 10^+ \rightarrow 8^+)$[b]	1.69(4)	2.03	2.48(7)	2.06	1.98(6)
$B(E4; 10^+ \rightarrow 6^+)$	0.79(8)	1.30	5.7(13)	4.66	4.6(10)
$\mathrm{br}_{\gamma+e^-}(10^+ \rightarrow 6^+)$	1.8(2)	2.4	5.1(11)	5.0	5.1(11)
$T_{1/2}(10^+)_{\gamma+e^-}$ (ns)	364(7)	303	237(6)	286	296(8)
$Q(10^+)$ ($e$fm^2)	52(8)[c]	55.6	–	58.5	–
$\mu(10^+)(\mu_N{}^2)$	7.281(10)	6.82	–	4.24	–

[a]Assuming an additional proton-decay branch, br_{p2}, into the ground state of ^{53}Co with $\mathrm{br}_{\gamma+e^-} : \mathrm{br}_{p1} : \mathrm{br}_{p2} = 64(2) : 36(2) : 25$.
[b]Including conversion coefficients of $\alpha_{\mathrm{tot}} = 0.115(4)$ and $\alpha_{\mathrm{tot}} = 0.135(4)$ for ^{54}Fe and ^{54}Ni, respectively [23].
[c]Using the revised $Q(3/2^-)$ of ^{57}Fe as outlined in Ref. [24].

Spherical large-scale shell-model calculations were performed with the code ANTOINE [25,26]. They employ the full fp space, but the model space needs to be truncated to allow for excitations of up to $t = 6$ particles across the shell closure at $N = Z = 28$. This is a compromise between available computing power and sufficient convergence of the calculated numbers for near-spherical yrast states in the mass region [10–12,27]. The KB3G [28] and GXPF1A [29] interactions are studied, and for the main body of predictions isospin breaking terms are included.

Following the notations of Refs. [7,10,11], multipole harmonic-oscillator Coulomb matrix elements, V_{CM}, and the monopole electromagnetic spin-orbit effect, V_{Cls}, are readily included. To account for other monopole related shifts of single-particle energy levels the prescription of Ref. [11] (V_{Cr}) is followed. Finally, charge-asymmetric components of the strong nucleon-nucleon interaction are included. A repulsive 100-keV term, V_{BM-2}, was introduced for the $1f_{7/2}{}^2$, $J = 2$ two-proton matrix element by Zuker *et al.* [6] to account for an anomalous MED value of the 2^+ states in the $A = 42$ mirror pair. The use of V_{BM-2} has been shown to improve the MED description of nuclei throughout the entire $1f_{7/2}$ shell [8–10]. Electromagnetic decay properties are calculated with the $E2$ effective charges of $e^p_{\mathrm{eff}} = 1.15$ and $e^n_{\mathrm{eff}} = 0.80$ derived in Ref. [14], while for $B(E4)$ strengths the values [12] $e^p_{\mathrm{eff}} = 1.5$ and $e^n_{\mathrm{eff}} = 0.5$ are used as a starting point [30].

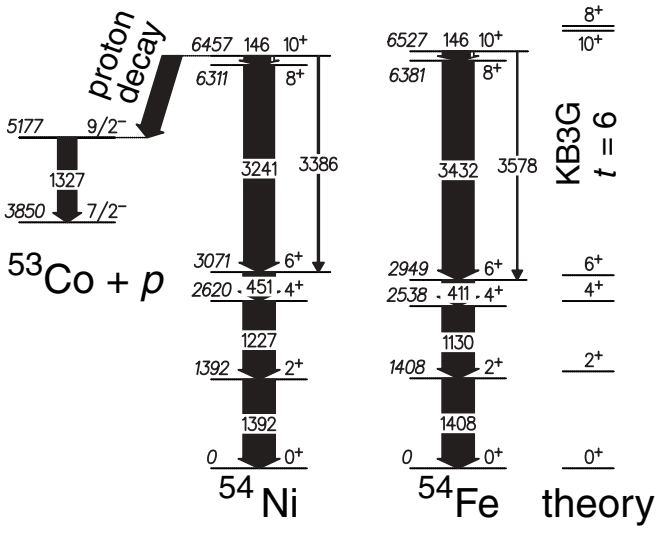

FIG. 3. Decay scheme of the 10^+ isomer in ^{54}Ni deduced from the present work. The relevant decays of the mirror nucleus ^{54}Fe [13] are shown for comparison. On the right-hand side, level energies from isospin-symmetric $A = 54$, $T = 1$ shell-model calculations are shown. See text for details.

Figure 3 compares the energy levels of the KB3G interaction with the experimental cascade in ^{54}Ni (and ^{54}Fe). The known $1f_{7/2}{}^{-2}$ dominated 0^+, 2^+, 4^+, 6^+ yrast cascade [9] is well described. However, some deficiencies of the interaction become apparent for the core-excited 8^+ and 10^+ states: the energy gap is predicted somewhat too large, and the two states are inverted, though still within the typical predictive power for level energies [10,12].

Figure 4 provides the experimental MED diagram for the $T_z = \pm 1$, $A = 54$ system (black dots) and the predictions using the KB3G interaction. Though differing in details, predictions using the GXPF1A interaction do yield essentially the same picture. The calculations *without* any nuclear isospin breaking component (dotted line) fail to reproduce the MED of the 2^+ states. While this is expected [7,9], also the MED values of the 8^+ and 10^+ states are being missed. In turn, the MED predictions including V_{BM-2} (solid black line) are in nearly perfect agreement with the experimental values; i.e., they account for the above-mentioned MED discrepancies at *both* spin $I = 2$ and spins $I = 8$ and $I = 10$. A similar effect on MED values might be achieved by instead using an attractive 100-keV term, V_{BM-0}, for the $1f_{7/2}{}^2$, $J = 0$ two-proton matrix element. In fact, the calculation using the V_{BM-0} term (solid grey line) also improves on the MED of the 2^+, 8^+, and 10^+ states. However, the predictions for the intermediate spin $I = 4$

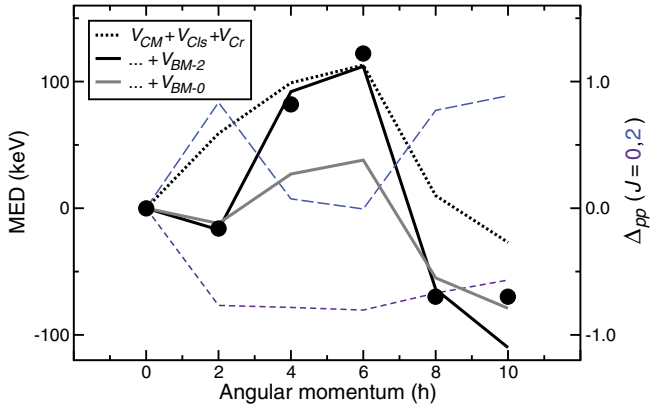

FIG. 4. (Color online) Mirror energy difference, $E_x(^{54}\mathrm{Ni}) - E_x(^{54}\mathrm{Fe})$, as a function of spin. Solid circles denote the experimental values. The dotted line accounts only for Coulomb related isospin breaking terms [11], while the solid black and grey lines include the V_{BM-2} [7] and V_{BM-0} terms, based on the KB3G interaction. The long- and short-dashed lines provide the difference between ^{54}Fe and ^{54}Ni of $T = 1$ proton pairs, Δ_{pp}, coupled to either $J = 2$ or $J = 0$, respectively.

and $I = 6$ states are significantly worsened; i.e., V_{BM-0} seems to be able to improve the MED predictions locally, while V_{BM-2} appears to act globally.

To study the influence of these two nuclear isospin breaking terms in some more detail, Fig. 4 provides also the difference of the number of two-proton $J = 0$ pairs [thin dashed lines, $\Delta_{pp}(J = 0)$] and $J = 2$ pairs [thin long-dashed lines, $\Delta_{pp}(J = 2)$] between ^{54}Fe and ^{54}Ni as a function of angular momentum. In the case of $\Delta_{pp}(J = 0)$, the curve trivially drops exactly once between $I = 0$ and $I = 2$, but then remains essentially constant. On the contrary, $\Delta_{pp}(J = 2)$ peaks at $I = 2$ and once more at $I = 8$ and $I = 10$, which is nicely correlated with the respective global reproduction of the experimental MED with shell-model calculations accounting for the V_{BM-2} term. This presents the first clear evidence that the non-Coulomb isospin-breaking component has its origin in the $J = 2$ coupling, rather than $J = 0$, of $1f_{7/2}$ particles.

Experimental and predicted electromagnetic decay properties are compared in Table I. Excellent agreement is achieved, with two exceptions: the $B(E4)$ strength in ^{54}Fe and its related $E4$ branch, and the lifetime of the isomer itself in ^{54}Ni. The latter discrepancy becomes more obvious when comparing the ratios of the lifetime predictions, $R = 1.06$, with the experimental values, $R = 1.53(5)$. This rather significant mismatch could be cured by an additional ∼25% proton branch into the ground state of ^{53}Co, to which the present experiment is insensitive. The right-most column of Table I includes this correction. Indeed, simple WKB estimates provide similar tunneling probabilities for a 1.28-MeV, $\ell = 5$ proton into the $9/2^-$ state in ^{53}Co and a 2.61-MeV, $\ell = 7$ proton into the ground state of ^{53}Co [31]; the structural hindrance factors are on the order of 10^6, which remain to be explained by tiny $1h_{11/2}$ or $1j_{13/2}$ proton partitions in the wave function of the 10^+ state in ^{54}Ni.

The possible existence of a second proton branch prevents a dedicated analysis of $E4$ polarization charges along the scheme developed in Ref. [14], because an absolute number for the $10^+ \rightarrow 6^+$ transition in ^{54}Ni is missing. Nevertheless, using the extremes the ratio of the $B(E4)$ values in ^{54}Fe and ^{54}Ni is limited to $R \sim 0.10$–0.25, which requires negative isovector $E4$ polarization charges. The best agreement for the (corrected) experimental data is achieved with $e_{\mathrm{eff,p}}(E4) \sim 1.35$ and $e_{\mathrm{eff,n}}(E4) \sim 0.25$.

In summary, the 10^+ mirror isomer in ^{54}Ni has been identified. Its electromagnetic decay characteristics provide new constraints on large-scale fp shell-model calculations in conjunction with isospin symmetry. It is shown that the MED values for the 2^+, 8^+, and 10^+ states can be associated with the isospin symmetry breaking $J = 2$, $T = 1$ interaction. Evidence is presented for a distinct direct proton decay branch into the excited $9/2^-$ state in ^{53}Co, and a significant discrepancy of the experimental and predicted half-life of the isomer points to an additional proton branch into the ground state of ^{53}Co.

The authors gratefully acknowledge the outstanding work of the GSI accelerator and ion-source crews in providing the experiment with the envisaged high beam intensities. This work is supported by the European Commission (Contract 506065) (EURONS), the Swedish Research Council, the EPSRC (United Kingdom), the German BMBF, the Polish Ministry of Science and Higher Education, the Bulgarian Science Fund, the Spanish Ministerio de Educación y Ciencia, and the U.S. Department of Energy.

[1] *NuPECC Long Range Plan 2004*, edited by M. Harakeh *et al.*, www.nupecc.org, (2004).
[2] C. Dossat *et al.*, Phys. Rev. C **72**, 054315 (2005).
[3] P. T. Hosmer *et al.*, Phys. Rev. Lett. **94**, 112501 (2005).
[4] O. Sorlin *et al.*, Phys. Rev. Lett. **88**, 092501 (2002).
[5] D. Rudolph *et al.*, Phys. Rev. Lett. **82**, 3763 (1999).
[6] E. K. Johansson *et al.*, Phys. Rev. C **77**, 064316 (2008).
[7] A. P. Zuker, S. M. Lenzi, G. Martinez-Pinedo, and A. Poves, Phys. Rev. Lett. **89**, 142502 (2002).
[8] S. J. Williams *et al.*, Phys. Rev. C **68**, 011301(R) (2003).
[9] A. Gadea *et al.*, Phys. Rev. Lett. **97**, 152501 (2006).
[10] M. A. Bentley and S. M. Lenzi, Prog. Part. Nucl. Phys. **59**, 497 (2007).
[11] J. Ekman, C. Fahlander, and D. Rudolph, Mod. Phys. Lett. A **20**, 2977 (2005).
[12] E. Caurier *et al.*, Rev. Mod. Phys. **77**, 427 (2005).
[13] H. Junde and H. Su, Nucl. Data Sheets **107**, 1393 (2006).
[14] R. du Rietz *et al.*, Phys. Rev. Lett. **93**, 222501 (2004).
[15] K. L. Yurkewicz *et al.*, Phys. Rev. C **70**, 054319 (2004).
[16] K. Yamada *et al.*, Eur. Phys. J. A **25** S1, 409 (2005).
[17] H. Geissel *et al.*, Nucl. Instrum. Methods B **70**, 286 (1992).
[18] J. Eberth *et al.*, Nucl. Instrum. Methods A **369**, 135 (1996).
[19] S. Pietri *et al.*, Acta Phys. Pol. **38**, 1255 (2007); Nucl. Instrum. Methods B **261**, 1079 (2007).

[20] D. Rudolph *et al*., Eur. Phys. J. A **36**, 131 (2008).
[21] K. P. Jackson *et al*., Phys. Lett. **B33**, 281 (1970).
[22] J. Cerny *et al*., Phys. Lett. **B33**, 284 (1970).
[23] T. Kibédi *et al*., AIP Conf. Proc. **769**, 268 (2005).
[24] G. Martínez-Pinedo *et al*., Phys. Rev. Lett. **87**, 062701 (2001).
[25] E. Caurier, shell model code ANTOINE, IReS Strasbourg 1989, 2002.
[26] E. Caurier and F. Nowacki, Acta Phys. Pol. **30**, 705 (1999).
[27] M. Horoi, B. A. Brown, T. Otsuka, M. Honma, and T. Mizusaki, Phys. Rev. C **73**, 061305(R) (2006).
[28] A. Poves *et al*., Nucl. Phys. **A694**, 157 (2001).
[29] M. Honma, T. Otsuka, B. A. Brown, and T. Mizusaki, Phys. Rev. C **65**, 061301(R) (2002); **69**, 034335 (2004); Eur. Phys. J. A **25**, s01, 499 (2005).
[30] A. Gadea *et al*., Phys. Lett. **B619**, 88 (2005).
[31] S. Hofmann (private communication).

PHYSICAL REVIEW C **78**, 061302(R) (2008)

Single-particle behavior at $N = 126$: Isomeric decays in neutron-rich ^{204}Pt

S. J. Steer,[1,*] Zs. Podolyák,[1] S. Pietri,[1] M. Górska,[2] P. H. Regan,[1] D. Rudolph,[3] E. Werner-Malento,[2] A. B. Garnsworthy,[1,4] R. Hoischen,[3] J. Gerl,[2] H. J. Wollersheim,[2] K. H. Maier,[5,6] H. Grawe,[2] F. Becker,[2] P. Bednarczyk,[2,6] L. Cáceres,[2,7] P. Doornenbal,[2,8] H. Geissel,[2] J. Grębosz,[2,6] A. Kelic,[2] I. Kojouharov,[2] N. Kurz,[2] F. Montes,[2] W. Prokopowicz,[2] T. Saito,[2] H. Schaffner,[2] S. Tashenov,[2] A. Heinz,[4] M. Pfützner,[9] T. Kurtukian-Nieto,[10] G. Benzoni,[11] A. Jungclaus,[7] D. L. Balabanski,[12,13] C. Brandau,[1] B. A. Brown,[1,14] A. M. Bruce,[15] W. N. Catford,[1] I. J. Cullen,[1] Zs. Dombrádi,[16] M. E. Estevez,[17] W. Gelletly,[1] G. Ilie,[8,18] J. Jolie,[8] G. A. Jones,[1] M. Kmiecik,[6] F. G. Kondev,[19] R. Krücken,[20] S. Lalkovski,[15,21] Z. Liu,[1] A. Maj,[6] S. Myalski,[6] S. Schwertel,[20] T. Shizuma,[1,22] P. M. Walker,[1] and O. Wieland[11]

[1]*University of Surrey, Guildford, Surrey GU2 7XH, United Kingdom*
[2]*GSI, Planckstrasse 1, D-64291 Darmstadt, Germany*
[3]*Department of Physics, Lund University, S-22100 Lund, Sweden*
[4]*WNSL, Yale University, 272 Whitney Avenue, New Haven, Connecticut 06520, USA*
[5]*University of West of Scotland, Paisley PA1 2BE, United Kingdom*
[6]*The Institute of Nuclear Physics, PL-31-342 Kraków, Poland*
[7]*Departmento de Fisica Teórica, Universidad Autonoma de Madrid, Madrid, Spain*
[8]*IKP, Universität zu Köln, D-50937 Köln, Germany*
[9]*IEP, Warsaw University, Hoża 69, PL-00-681, Poland*
[10]*Universidad de Santiago de Compostela, Santiago de Campostela, Spain*
[11]*INFN sezione di Milano, I-20133 Milano, Italy*
[12]*INRNE, Bulgarian Academy of Sciences, BG-1784 Sofia, Bulgaria*
[13]*Dipartimento di Fisica, Università di Camerino, I-62032 Camerino, Italy*
[14]*NSCL, Michigan State University, East Lansing, Michigan 48824-1321, USA*
[15]*School of Engineering, University of Brighton, Brighton BN2 4GJ, United Kingdom*
[16]*Institute for Nuclear Research, H-4001 Debrecen, Hungary*
[17]*Instituto de Fisica Corpuscular, Valencia, Spain*
[18]*National Institute of Physics and Nuclear Engineering, Bucharest, Romania*
[19]*Nuclear Engineering Division, Argonne National Laboratory, Argonne, Illinois 60439, USA*
[20]*Physik Department E12, Technische Universität München, Garching, Germany*
[21]*Faculty of Physics, University of Sofia "St. Kliment Ohridski," Sofia, Bulgaria*
[22]*Japan Atomic Energy Research Institute, Kyoto 619-0215, Japan*

(Received 31 March 2008; published 18 December 2008)

The four proton-hole nucleus ^{204}Pt was populated in the fragmentation of an $E/A = 1$ GeV ^{208}Pb beam. The yrast structure of ^{204}Pt has been observed up to angular momentum $I = 10\hbar$ by detecting delayed γ-ray transitions originating from metastable states. These long-lived excited states have been identified to have spin-parities of $I^{\pi} = (10^{+})$, (7^{-}), and (5^{-}) and half-lives of $T_{1/2} = 146(14)$ ns, 55(3) μs, and 5.5(7) μs, respectively. The structure of the magic $N = 126$ ^{204}Pt nucleus is discussed and understood in terms of the spherical shell model. The data suggest a revision of the two-body interaction for $N = 126$, $Z < 82$, which determines the evolution of nuclear structure toward the r-process waiting point nuclei.

DOI: 10.1103/PhysRevC.78.061302 PACS number(s): 23.20.Lv, 21.10.Pc, 27.80.+w, 29.30.Kv

The evolution of the properties of atomic nuclei with respect to neutron and proton numbers is a key question of nuclear physics. The study of unstable, neutron-rich nuclei represents one of the foremost pursuits of modern nuclear physics. Over the coming decade new radioactive ion beam facilities are being built with the main objectives being to probe neutron-rich nuclei. Within recent years surprising phenomena have been observed in neutron-rich nuclei such as neutron skins, halos, and dramatic changes in the ordering and spacing of energy levels [1].

While the stability of the $N = 82$ shell gap is an active topic of research [2,3], an open question is whether or not there is a quenching of the $N = 126$ shell gap as protons are removed from doubly magic ^{208}Pb. The proton dripline has been experimentally reached up to heavy elements [4], our present knowledge of the neutron dripline is limited to light species. The part of the nuclear chart with the least information on neutron-rich nuclei is the $_{76}$Os to $_{82}$Pb region, with experimental knowledge on only a few isotopes. This mass region is, however, an ideal testing ground of nuclear theories. With the removal of just a few protons and neutrons the landscape evolves from spherical to elongated prolate through disk-shaped oblate and triaxial forms [5]. Consequently the information gained on neutron-rich, $N = 126$ nuclei is essential for the understanding of nuclear structure in heavy nuclei. From a longer-term perspective, experiments in this region pave the way toward the proposed

*s.steer@surrey.ac.uk

nuclear-astrophysical r-process waiting point nuclei along the $N = 126$ shell closure [6,7]. Studies of magic nuclei are of fundamental importance in our understanding of nuclear structure because they allow direct tests of the purity of shell model wave functions. Information on the single particle energies and two-body residual interactions can be derived from the experimental observables such as energies of the excited states and transition probabilities.

Experimental information on the neutron-rich, $N = 126$ nuclei is very scarce. Information has been obtained on excited states for only two isotones with $Z < 82$: ^{207}Tl [8] and ^{206}Hg [9–11]. In the case of ^{205}Au only the ground state is known [12]. The lack of information on nuclei "below" ^{208}Pb is due to difficulties in populating these neutron-rich nuclei. Fragmentation has proven to be an efficient tool in producing exotic nuclear species. When projectile fragmentation is combined with high-sensitivity γ-detection arrays, structural information can be gained for otherwise inaccessible nuclei. The highest sensitivity is achieved with both isomeric and β-delayed γ-ray spectroscopy techniques; delayed γ rays are time-correlated with individually identified ions, thereby minimizing the associated background radiation. Information on the excited states populated in this way can be obtained when producing only a few hundred nuclei of interest [13,14].

In this Rapid Communication the first spectroscopic information on the structure of the four proton-hole nucleus ^{204}Pt is presented. Preliminary results were published in conference proceedings [15,16].

The SIS-18 accelerator at GSI provided a ^{208}Pb beam at $E/A = 1$ GeV. The average beam intensity was $\sim 4 \times 10^8$ ion/s and the total operating time was $\sim$105 h. The ^{208}Pb ions impinged on a target of ^{9}Be of thickness 2.5 g/cm^2. The nuclei of interest were selected and identified in flight by the FRagment Separator (FRS) [17]. The FRS was operated in standard achromatic mode using an Al wedge-shaped degrader of thickness 4.9 g/cm^2, positioned at the intermediate focal plane. To maximize the number of fully stripped ($q = Z$) nuclei passing through the FRS, niobium foils of 221 and 108 mg/cm^2 thicknesses were, respectively, placed after both the target and the intermediate focal plane degrader. According to the charge state calculations (using the GLOBAL code [18]), 93.7% of the ^{204}Pt ions were fully stripped exiting the target and 76.6% were stripped after the intermediate focal plane. The identified ions were slowed in an Al degrader and halted in a 7-mm-thick plastic stopper, positioned at the final focal plane of the FRS. Scintillation detectors placed before and after this Al degrader allowed suppression of events where the fragments of interest were destroyed in the slowing down process ($\approx$18%) and in cases where they did not implant in the stopper ($\approx$0.2%). The stopper was surrounded by the RISING array in the "Stopped Beam" configuration [19,20], consisting of 15 former EUROBALL HPGe cluster detectors [21]. The photopeak efficiency of this array was measured to be 15% at 661 keV [22]. These detectors recorded the delayed γ-ray transitions associated with the implanted nuclei.

The identification of the fragments is demonstrated in Fig. 1. The calibration of the particle identification is confirmed by the detection of previously identified γ rays that follow

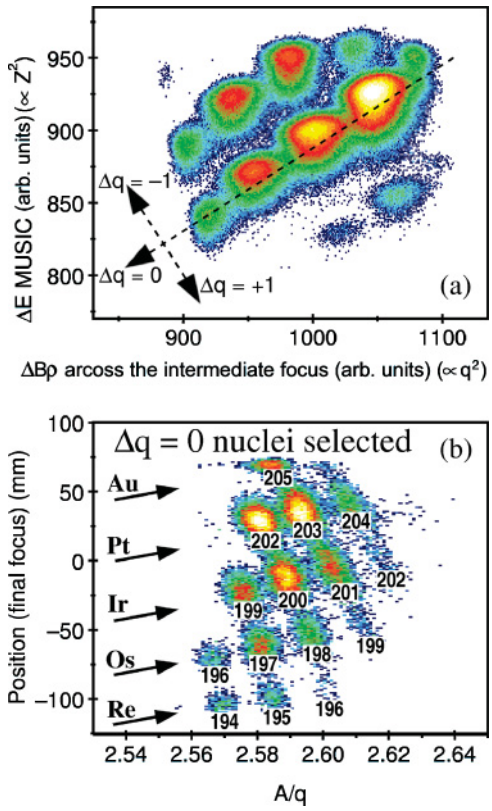

FIG. 1. (Color online) Identification of the fragmentation products in the FRS setting optimized for ^{203}Ir transmission. (**a**) Energy loss at the final focal plane vs change in magnetic rigidity, $\Delta B\rho (\propto q^2)$, at the intermediate focal plane. This distinguishes which nuclei change charge state in the middle of the FRS (approximately all $\Delta q = 0$ correspond to $q = Z$ for the entire FRS flight time). (**b**) Position in the final focal plane versus A/q for fully stripped ($\Delta q = 0$) nuclei.

the deexcitation of the $I^\pi = 7^-$ isomer in ^{202}Pt [23,24]. The identification process is described in more detail in Ref. [25].

The results for ^{204}Pt were obtained from four different magnetic rigidity settings of the FRS. A total of 9.3×10^4 ^{204}Pt ions was implanted in the stopper. Most of the data, $\sim$70% (in 24 h), were recorded in a setting optimized for the transmission of ^{203}Ir. In this setting the delayed γ rays were measured over a range of $0 \rightarrow 80$ μs following implantation. In the other settings, the γ rays were detected over a range of $0 \rightarrow 380$ μs.

Delayed γ rays associated with ^{204}Pt nuclei are shown in Fig. 2. In the sub-microsecond regime three γ-ray transitions with energies of 97, 1061, and 1158 keV, together with characteristic platinum x rays have been identified, all showing similar decay characteristics. The measured half-life is $T_{1/2} =$ 146(14) ns; see inset to Fig. 2 (top). Two additional γ rays with energies 872 and 1123 keV have been observed over a longer time range, see Fig. 2 (middle). However, their decay curve cannot be fitted with a single decay component. Two components must be considered, resulting in one half-life of $T_{1/2} = 5.5(7)$ μs, populated by a higher lying isomer with a longer half-life of $T_{1/2} = 55(3)$ μs.

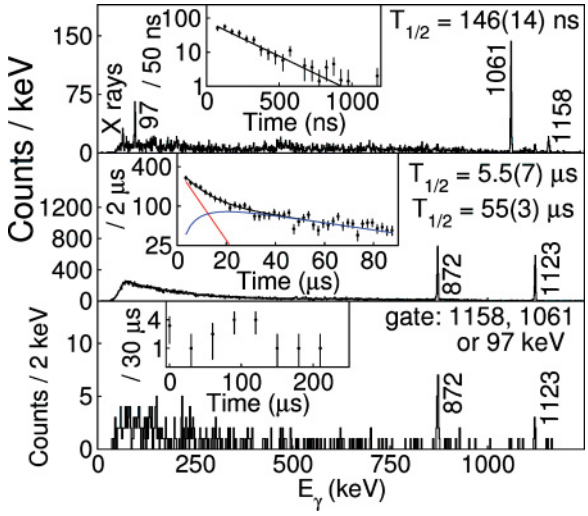

FIG. 2. (Color online) γ-ray spectra associated with ^{204}Pt. (Top) γ rays detected between 50 and 850 ns after implantation. (Inset) Decay curve of 1061 and 1158 keV γ rays. (Middle) γ rays observed between 2.5 and 80 μs after implantation. (Inset) Decay curve of the 872 and 1123 keV γ rays. (Bottom) Time-differentiated $\gamma\gamma$ coincidence. Shown are γ rays detected from 2.5 to 380 μs following implantation, after a $T_{1/2} = 146$ ns associated γ ray (97, 1061, 1158 keV) has been observed over the range 50 to 850 ns. (Inset) Time difference between detection of $T_{1/2} = 146$ ns associated γ rays and the later observed 872 and 1123 keV transitions.

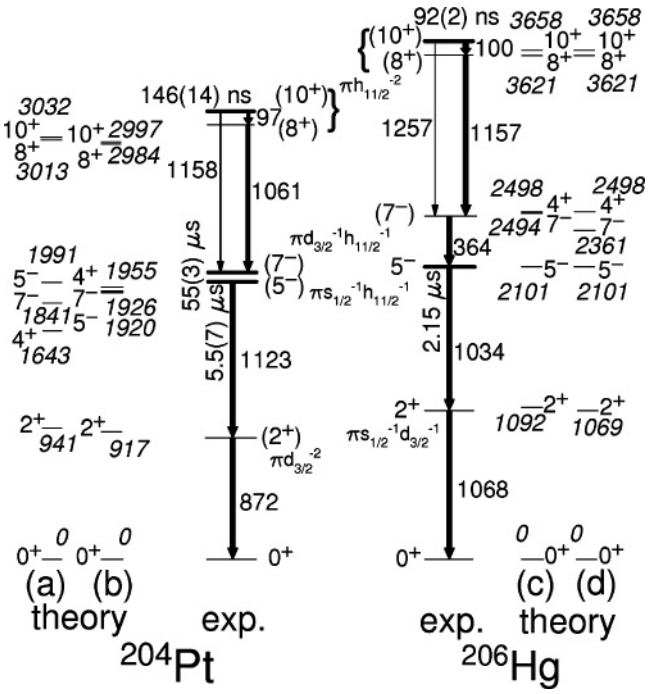

FIG. 3. Experimental and calculated partial level schemes of the $N = 126$ ^{204}Pt and ^{206}Hg [9] nuclei. Arrow widths denote relative intensities of parallel decay branches. The dominant state configurations are indicated. (a) and (d) are calculations using the Rydsrtöm matrix elements, while (b) and (c) are with the modified ones, as described in the text.

The sum energy of the 97 and 1061 keV transitions is equal to that of the third transition (1158 keV). Therefore it is likely that they form a parallel branch. Considering that the 97 and 1061 keV transitions should have identical intensity after allowing for electron conversion of the transition branches, we conclude that the 97 keV transition is of $E2$ or $M1$ character. The 872 and 1123 keV γ-ray peaks have equal intensities within experimental uncertainties. The data allow the extraction of coincidence relationships. The 97 and 1061 keV transitions, as well the 872 and 1123 keV pair, are in mutual coincidence. The spectrum in Fig. 2 (bottom) shows the transitions following the decay out of the short-lived isomer (gating on 97, 1061, and 1158 keV), together with the time difference between the transitions associated with the shorter lived and longer lived isomeric states. This demonstrates that the shorter lived ($T_{1/2} = 146$ ns) isomer decays into both of the longer lived ones. This is in agreement with the extracted relative population at the time of implantation of the isomeric states: 1:4.5:1.4 for $T_{1/2} = 146$ ns, 55 μs, and 5.5 μs, respectively. The implantation rate of ^{204}Pt nuclei is 0.4 nuclei/s; thus the number of chance coincidences in Fig. 2 (bottom) is negligible.

Based on these experimental data the level scheme has been constructed and has been compared with the two proton-hole $N = 126$ isotone ^{206}Hg in Fig. 3. It is established from experiment, except the tentative spin assignments and also the sequence of the 97, 1061 keV and the 872, 1123 keV pairs of transitions, which are respectively taken from comparison with ^{206}Hg and theoretical considerations.

Shell model calculations have been performed in the $s_{1/2}, d_{3/2}, h_{11/2}, d_{5/2}, g_{7/2}$ ^{208}Pb proton-hole space with the OXBASH code using single particle energies from ^{207}Tl and two-body matrix elements (TBME) from Ref. [26]. These are based on the Kuo-Herling interaction including core polarization, but the decisive elements for the then known 2^+ and 5^- states of ^{206}Hg had been adjusted. The resulting states and their main configurations are included in Fig. 3. The 2^+ and 5^- states in ^{206}Hg are trivially well reproduced, but also the 8^+ and 10^+ fit well, while the 7^- is off by 100 keV.

In ^{204}Pt the highest lying 146 ns isomer is without any doubt assigned to the calculated $(h_{11/2})^{-2}10^+$ level and also the 8^+ and 7^- states populated in its decay are certain. The two other lifetimes measured in ^{204}Pt give the proposed spin sequence (moving upward) of 5^-, 7^-, and an unobserved 4^+, while the calculations give 7^- below 5^- and a 4^+ state below both, incompatible with experiment. By this proposal the 7^- to 5^- $E2$ transition has the astonishingly large $T_{1/2} = 55$ μs, and the 5.5 μs is ascribed to the 5^- to 2^+ $E3$. If the 4^+ is below the 5^- the possible $E1$ decay would destroy the isomerism and if the 7^- is below the 5^- it could only decay by a much slower low-energy $E3$ to 4^+ or by $E5$ to 2^+. The $B(E2, 10^+ \rightarrow 8^+)$ and $B(E3, 10^+ \rightarrow 7^-)$ agree within errors with those measured in ^{206}Hg [9].

The 872 and 1123 keV γ rays are assigned as the decays from the 5^- isomeric state. It is expected that the 2^+ energy of ^{204}Pt, with a predominantly $(d_{3/2})^{-2}$ orbital configuration, is smaller than that of ^{206}Hg, with a mainly $(d_{3/2})^{-1}(s_{1/2})^{-1}$

TABLE I. Transition strengths for experiment, the Rydström [26] shell model (SM), and the new TBMEs (SM_{mod}) (see text) in ^{204}Pt. Effective charges of 1.5 and 2.0 e for $E2$ and $E3$, respectively, were assumed, which were chosen to reproduce the ^{206}Hg $10^+ \rightarrow 8^+ E2$ and $10^+ \rightarrow 7^- E3$ transitions [9].

Transition	EL	$B(EL)$ (W.u.)		
		Exp.	SM	SM_{mod}
$10^+ \rightarrow 8^+$	$E2$	0.80(8)	2.64	1.22
$10^+ \rightarrow 7^-$	$E3$	0.19(3)	0.21	0.22
$7^- \rightarrow 5^-$	$E2$	$0.017 \rightarrow 0.0034$[a]	1.21	0.0037
$5^- \rightarrow 2^+$	$E3$	0.039(5)	0.713	0.612

[a]Assuming a transition energy between $10 \rightarrow 78$ keV.

configuration. It is lower by about 200 keV, taking into account differences in single particle ($(s_{1/2})^{-1}$ vs $(d_{3/2})^{-1}$) and interaction ($(d_{3/2})^{-2}$ vs $(s_{1/2})^{-1}(d_{3/2})^{-1}$) energies. This suggests that the energy of the first excited state is 872 keV. The $E3$ $5^- \rightarrow 2^+$ transition proceeds mainly from the dominant $(s_{1/2})^{-1}(h_{11/2})^{-1}$ component of the 5^- state to the weak admixture of the $(s_{1/2})^{-1}(d_{5/2})^{-1}$ configuration in the predominantly $(d_{3/2})^{-2}$ state. The experimental $E3$ transition strength is weak (see Table I).

The transition linking the proposed 7^- and 5^- isomeric states was not observed in the present experiment. The lack of K x rays associated with the long-lived decay suggests a transition energy below the binding energy of the K electron (78.4 keV).

In light of the new ^{204}Pt and updated ^{206}Hg data [9] the Rydström interaction [26] was modified in three points: (i) the $(d_{3/2}h_{11/2})_{7^-}$ TBME was increased by +135 keV as requested by ^{206}Hg; (ii) the $(s_{1/2}d_{5/2})$ monopole was increased by +250 keV, which accounts for the 4^+ level energy and the increased blocking of the $h_{11/2} \otimes 3^-$ coupling lowering the effective $d_{5/2}$ single hole energy; (iii) following a systematic search of the influence of nondiagonal TBME on the $E2$ strength evolution from ^{206}Hg to ^{204}Pt the $(s_{1/2}h_{11/2}; d_{3/2}h_{11/2})_{6^-}$ TBME was changed to +160 keV, close to the value for the responding 5^- TBME. With these minor modifications, the observed excited states within both ^{206}Hg and ^{204}Pt are well reproduced, including the ordering of the $5^-, 7^-$, and 4^+ states (see Fig. 3). The calculated $E2$ and $E3$ strengths with the exception of the $5^- \rightarrow 2^+ E3$ agree with experiment (see Table I). The latter discrepancy is common to both ^{206}Hg and ^{204}Pt and most likely due to the 2^+ wave function, which in a pure proton model space is poorly described. Note that $E3$ transitions are mediated by the $h_{11/2} \rightarrow d_{5/2}$ conversion, i.e., the weak $d_{5/2}$ content in the wave functions, and any further components such as, e.g., $N = 126$ cross shell excitations, will reduce this contribution in low-spin states. These revised shell model calculations reproduce the measured magnetic and quadrupole moments of the 5^- isomer in ^{206}Hg: $\mu(5^-)_{the} = 5.24\ \mu_N$ with $g_s = 0.7 g_{free}$, $\mu(5^-)_{exp} = 5.45(5)\ \mu_N$ [11], $Q(5^-)_{the} = 0.57$ eb, $Q(5^-)_{exp} = 0.65(13)$ eb [10].

It is thus found that small modifications to the two-body interaction, though not unambiguous, significantly improve the description of levels and γ transition rates in ^{204}Pt. Recently new approaches to infer realistic nucleon-nucleon interactions were made, based on the renormalized G matrix [27,28] and the V_{low-k} potential [29]. Further investigations, both experimental and theoretical, are needed to understand the nuclear structure evolution of the $N \sim 126$ region toward the anticipated r-process waiting nuclei at $Z \leqslant 72$.

In summary, we have identified excited states in the four proton-hole nucleus ^{204}Pt. The yrast sequence has been established up to spin-parity $I^\pi = (10^+)$, through the observation of decays from three isomers. The character of the excited states can be understood in terms of the shell model, although to get a consistent description of the experimental level scheme the accepted set of matrix elements has been modified to account for the changing intrinsic shell structure affecting the isomer configuration. The persistence of the isomeric structure, the related transition strengths, and their reproduction in a pure proton space strongly support an unquenched $N = 126$ gap. Due to the crucial role of the $\pi h_{11/2}$ orbit in both allowed and first forbidden β decay of $\nu h_{9/2}$ and $\nu i_{13/2}$ neutrons, respectively [7,30], this study paves the way for examining nuclear structure as both the anticipated pathways for the astrophysical r-process and candidate nuclei for shell quenching are approached.

The excellent work of the GSI accelerator staff is acknowledged. This work is supported by the EPSRC (UK) and AWE plc. (UK), the EU Access to Large Scale Facilities Programme (EURONS, EU Contract 506065), The Swedish Research Council, The Polish Ministry of Science and Higher Education, The Bulgarian Science Fund, The US Department of Energy, The Spanish Ministeriode Educacion y Ciencia, The German BMBF, The Hungarian Science Foundation, and the Italian INFN.

[1] A. Klimkiewicz *et al.*, Phys. Rev. C **76**, 051603(R) (2007).
[2] A. Jungclaus *et al.*, Phys. Rev. Lett. **99**, 132501 (2007).
[3] I. Dillmann *et al.*, Phys. Rev. Lett. **91**, 162503 (2003).
[4] P. J. Woods and C. N. Davids, Annu. Rev. Nucl. Part. Sci. **47**, 541 (1997).
[5] P. D. Bond, R. F. Casten, D. D. Warner, and D. Horn, Phys. Lett. **B130**, 167 (1983).
[6] Y.-Z. Qian, Prog. Part. Nucl. Phys. **50**, 153 (2003).
[7] H. Grawe, K. Langanke, and G. Martínez-Pinedo, Rep. Prog. Phys. **70**, 1525 (2007).
[8] D. Eccleshall and M. J. L. Yates, Phys. Lett. **19**, 301 (1965).
[9] B. Fornal *et al.*, Phys. Rev. Lett. **87**, 212501 (2001).
[10] K. H. Maier *et al.*, Phys. Rev. C **30**, 1702 (1984).
[11] J. A. Becker *et al.*, Phys. Rev. C **26**, 914 (1982).
[12] C. Wennemann *et al.*, Z. Phys. A **347**, 185 (1994).
[13] M. Pfützner *et al.*, Phys. Lett. **B444**, 32 (1998).
[14] Z. Podolyák *et al.*, Phys. Lett. **B491**, 225 (2000).
[15] S. J. Steer *et al.*, Acta Phys. Pol. B **38**, 1283 (2007).
[16] Z. Podolyák *et al.*, Eur. Phys. J. Spec. Top. **150**, 165 (2007).
[17] H. Geissel *et al.*, Nucl. Instrum. Methods B **70**, 286 (1992).
[18] C. Scheidenberger *et al.*, Nucl. Instrum. Methods B **142**, 441 (1998).

[19] S. Pietri *et al*., Nucl. Instrum. Methods B **261**, 1079 (2007).
[20] P. H. Regan *et al*., Nucl. Phys. **A787**, 491c (2007).
[21] P. J. Nolan, F. A. Beck, and D. B. Fossan, Annu. Rev. Nucl. Part. Sci. **44**, 561 (1994).
[22] S. Pietri *et al*., Acta Phys. Pol. B **38**, 1255 (2007).
[23] M. Caamaño *et al*., Eur. Phys. J. A **23**, 201 (2005).
[24] Z. Podolyák *et al*., Prog. Theor. Phys. **146**, 467 (2002).
[25] J. Benlliure *et al*., Nucl. Phys. **A660**, 87 (1999).
[26] L. Rydström *et al*., Nucl. Phys. **A512**, 217 (1990).
[27] M. Hjorth-Jensen, T. T. S. Kuo, and E. Osnes, Phys. Rep. **261**, 125 (1995).
[28] B. A. Brown (private communication, 2008).
[29] L. Coraggio, A. Covello, A. Gargano, N. Itaco, and T. T. S. Kuo, Phys. Rev. C **60**, 064306 (1999).
[30] I. M. Borzov, Nucl. Phys. **A777**, 645 (2006).

International Journal of Modern Physics E
Vol. 17, Supplement (2008) 8–20

World Scientific
www.worldscientific.com

FIRST RESULTS WITH THE RISING ACTIVE STOPPER*

P. H. REGAN†, N. ALKHOMASHI, N. AL-DAHAN, Zs. PODOLYÁK, S. B. PIETRI‡, S. J. STEER, A. B. GARNSWORTHY§, E. B. SUCKLING, P. D. STEVENSON, G. FARRELLY, I. J. CULLEN, W. GELLETLY and P. M. WALKER

Department of Physics, University of Surrey, Guildford, GU2 7XH, UK
†*p.regan@surrey.ac.uk*

J. BENLLIURE, A. I. MORALES, E. CASAJEROS and M. E. ESTEVEZ

Universidad de Santiago de Compostela, E-15706, Santiago de Compostela, Spain

J. GERL, M. GÓRSKA, H. J. WOLLERSHEIM, P. BOUTACHKOV, S. TASHENOV, I. KOJOUHAROV, H. SCHAFFNER, N. KURZ and R. KUMAR¶

GSI, Planckstrasse 1, D-64291, Darmstadt, Germany

B. RUBIO, A. ALGORA‖ and F. MOLINA

Instituto de Fisica Corpuscular, Universidad de Valencia, E-46071, Spain

J. GREBOSZ

The Henryk Niewodniczanski Institute of Nuclear Physics, PL-31-342, Krakow, Poland

G. BENZONI

INFN, Universitá degli Studi di Milano, I-20133, Milano, Italy

D. MÜCHER

IKP, Universität zu Köln, D-50937, Köln, Germany

A. M. BRUCE, A. M. DENIS BACELAR and S. LALKOVSKI

School of Environment and Technology, University of Brighton, Brighton, BN2 4GJ, UK

*This work is supported by the EPSRC and STFC(UK), the EU Access to Large Scale Facilities Programme (EURONS, EU contract 506065), The Spanish Ministerio de Educacion y Ciencia and The German BMBF.
†Corresponding author.
‡Present address, GSI, Planckstrasse 1, D-64291, Darmstadt, Germany.
§Current address, TRIUMF, 4004 Wesbrook Mall, Vancouver, BC V6T 2A3, Canada.
¶On leave from Inter University Accelerator Centre, New Delhi, India.
‖On leave from MTA ATOMKI, Debrecen, Hungary.

Y. FUJITA
Department of Physics, Osaka University Toyonaka, Osaka 560–0043, Japan

A. TAMII
Reseach Center for Nuclear Physics, Osaka University, Ibaraki, Osaka 567-0047, Japan

R. HOISCHEN
Department of Physics, Lund University, Lund, S-22100 Lund, Sweden

Z. LIU and P. J. WOODS
Department of Physics and Astronomy, University of Edinburgh, Edinburgh, UK

C. MIHAI
National Institute for Physics and Nuclear Engineering, RO-077125, Bucharest, Romania

J. J. VALIENTE-DOBÓN
INFN-Laboratori Nazionali di Legnaro, Italy

This paper outlines some of the physics opportunities available with the GSI RISING active stopper and presents preliminary results from an experiment aimed at performing beta-delayed gamma-ray spectroscopic studies in heavy-neutron-rich nuclei produced following the projectile fragmentation of a 1 GeV per nucleon ^{208}Pb primary beam. The energy response of the silicon active stopping detector for both heavy secondary fragments and beta-particles is demonstrated and preliminary results on the decays of neutron-rich Tantalum (Ta) to Tungsten (W) isotopes are presented as examples of the potential of this technique to allow new structural studies in hitherto experimentally unreachable heavy, neutron-rich nuclei. The resulting spectral information inferred from excited states in the tungsten daughter nuclei are compared with results from axially symmetric Hartree–Fock calculations of the nuclear shape and suggest a change in ground state structure for the N = 116 isotone ^{190}W compared to the lighter isotopes of this element.

1. Introduction

The structure of nuclei with exotic proton-to-neutron ratios is at the forefront of current nuclear physics research. In particular, the use of high-energy beams of radioactive nuclei produced following relativistic projectile fragmentation and/or fission reactions allows the production and synthesis of hitherto unreachable nuclei in the outer regions of the Segré chart.[1]

By utilizing magnetic separators such as the Fragment Separator (FRS) at GSI,[2] specific nuclei of interest can be distinguished from the vast plethora of other secondary products from such reactions and cleanly transmitted to a final focus, where spectral studies may be performed. Such studies using gamma-ray spectroscopy include decays from isomeric states in exotic nuclei[3–13] and/or (b) decay studies following alpha and/or beta-decay of the exotic nucleus.

This paper focusses on the first results using the Stopped RISING Active Stopper which allows correlations to be made between the exotic heavy-ions produced by

relativistic fragmentation/fission reactions and their subsequent beta-decays. This in turn allows beta-delayed spectroscopy to be performed in the daughter nucleus, representing, in some cases, the first spectral information in such systems.

2. The Stopped RISING Gamma-Ray Setup

The RISING gamma-ray array[14] consists of fifteen, high efficiency seven-element germanium cluster detectors. These detectors can be placed in a number of different geometries to allow inter-alia studies of "fast" fragmentation beams[15] and decay studies[16,17] using a close, compact set-up. The latter represents the "Stopped RISING" set-up[10,11,13,16,17] which is the focus of the current paper. In the Stopped-Beam configuration, the RISING detectors are placed in three rings of 5 cluster-detectors, providing a photo-peak efficiency for decay studies using fragmentation beams of ∼15% at 662 keV.[16,17]

2.1. *The RISING active stopper*

Figure 1 shows a schematic of the experimental set-up for the active stopper measurements using the RISING gamma-ray array.

The RISING Active Stopper consists of a series of Double Sided Silicon Strip Detectors (DSSSDs) and is made up of (up to) 6 DSSSDs, each with 16 horizontal and vertical strips respectively, giving 256 pixels per DSSSD. Each DSSSD was 5 cm by 5 cm in overall dimension and 1 mm thick. The DSSSDs were used to determine both the energy and position of the (a) implanted secondary fragment of interest directly from the projectile fragmentation reaction and (b) beta-particle(s) following the subsequent radioactive decay(s) of the often highly exotic nucleus of interest

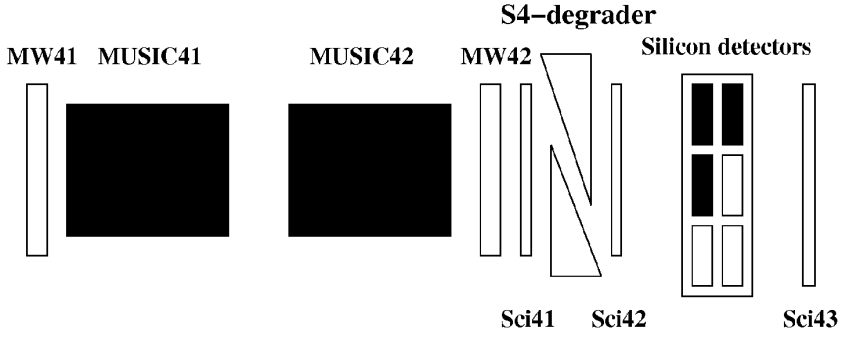

Fig. 1. Schematic of the detector configuration at the final focus of the GSI Fragment Separator for the current work. Note that only three of the possible six positions (black boxes) in the active stopper were occupied by DSSSDs in this particular experiment. MW = MultiWire position detectors; Sci=plastic scintillator detectors. The number "4" corresponds to the detectors being placed at the final focus, (i.e. after the 4th dipole magnet) GSI Fragments Separator. The secondary beam would be moving products from left to right on this schematic.

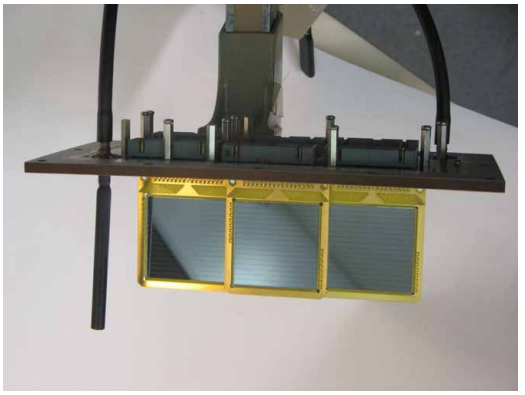

Fig. 2. Photograph of the bare DSSSDs used in the RISING active stopper in their holder with the light-tight outer box removed. (Note this was not the final geometry used for the three DSSSDs in the current work.)

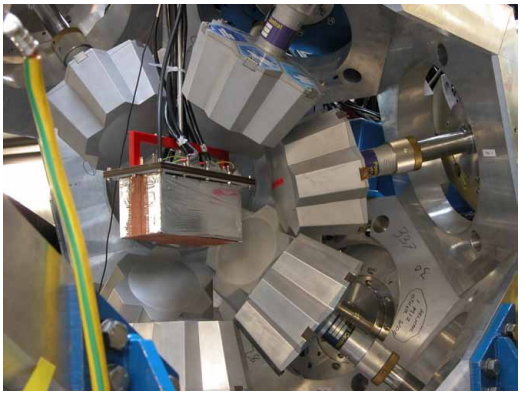

Fig. 3. Photograph of the DSSSDs in-situ at the centre of the RISING array in its Stopped Beam configuration. The active stopper is housed in the light tight box in the middle of the opened array.

and its daughter decays. The ultimate aim of the device is to correlate beta-decay events with specific exotic radioactive mother nuclei on an event-by-event basis. Figures 2 and 3 show photographs of the bare DSSSDs and their position within a light-tight box placed in the middle of the RISING array.

The technical difficulty with such measurements is that the dynamic range for the measurement of secondary reaction products and β-particles are orders-of-magnitude apart (i.e. $\sim$many GeV for the implanted fragment kinetic energies and $\sim$200 keV $\rightarrow$ a few MeV for the β-particles. This issue was addressed in the current work by the utilization of a pre-amplifier for the DSSSD energy signals, which was linear in the low-energy response range, followed by a logarithmic response at

higher gains. Semi-logarithmic preamplifiers were used, providing linear amplification up to 10 MeV and logarithmic amplification for the 10 MeV $\rightarrow$ 3 GeV range. The linear part allowed for both measurements of β (and in principle also, the spectroscopy of the charged particle decay) and was calibrated using an open, internal conversion electron ^{207}Bi source, yielding an energy resolution of FWHM = 20 keV and a minimum detection threshold of approximately 200 keV. The logarithmic part of the DSSSD output range allowed for the determination of the implantation position in an individual pixel (i.e. the pixel with maximum energy output compared to its neighbors) and was calibrated for energy response using a pulser. Scintillation detectors were placed both in front of and behind the catcher, allowing the off-line suppression of the majority of fragments which were destroyed in the slowing down process. Further details on the response of the semi-logarithmic pre-amplifier can be found in a forthcoming paper.[18]

3. Experimental Details, Data Analysis and Results

The experiment used to commission the RISING Active Stopper used a ^{208}Pb primary beam accelerated using the SIS-18 synchrotron at GSI to an energy of 1 GeV per nucleon and impinging on a 2.5 g/cm^2 thick Be target. The secondary products of interest were transmitted through the FRS and particle identification made on an event-by-event basis using the standard magnetic rigidity, time-of-flight, energy loss and position measurements (details of the particle identification procedure can be found in Refs. 5, 13, 19). A number of FRS settings were selected to maximize the transmission of a range of nuclei and the FRS was operated in achromatic mode in order to spread out the area of implantation of ions at the final focus thus reducing the ion-implantation rate per DSSSD pixel. This paper shows results from 2 settings, one centered on ^{188}Ta and the other on ^{190}Ta. Typical primary beam currents were 10^8 and 10^9 particles per beam spill for the ^{188}Ta and ^{190}Ta settings respectively. The typical beam spill length was approximately 1 second with a period of approximately 15 $\rightarrow$ 20 seconds.

3.1. *Particle identification procedure*

The nuclei of specific interest in this experiment were the neutron-rich Hf $\rightarrow$ Os nuclei with A$\sim$190. The study of heavy and exotic neutron-rich species can be hindered in such experiments by the presence of non-fully stripped ions (i.e., $Q \neq Z$) which are transmitted through the FRS in parallel with fully stripped ions. A prescription to (largely) eliminate this so-called $\frac{A}{Q}$ anomaly is outlined in Ref. 19 and uses the effective energy loss in the passive energy degrader placed at the central focus of the FRS to determine *changes* in charge state for ions as they pass through the first and second halves of the GSI fragment separator. Figure 4 shows the effect of plotting the energy loss of the ions as measured through a pair of Multi-Sampling Ionization Chambers (or "MUSIC") at the final focus of the FRS (see Fig. 1) versus the derived energy loss of the ions from their difference in magnetic rigidity through

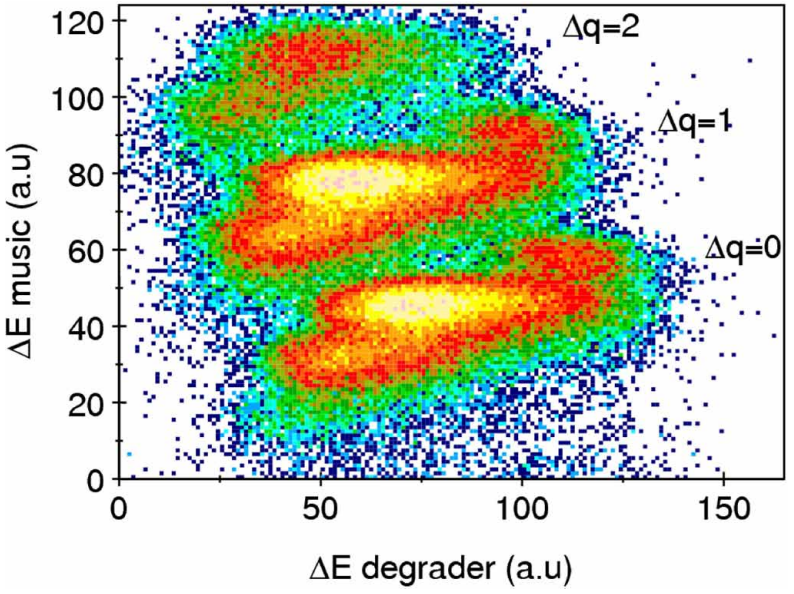

Fig. 4. Plot of ionic energy loss in the MUSIC detectors versus the derived energy loss in the passive degrader in the middle of the FRS for ions in the current experiment. Note the ions are separated into three distinct loci related to the *change* in charge state through the FRS. By far the most likely scenario for no change in charge state are those ions which are fully stripped (i.e. $Q = Z$) through both sections of the FRS.

the first and second halves of the FRS. This energy loss can be inferred from the measured time-of-flight of the ions in the second half of the FRS and the calculated time-of-flight of the ions in the first half of the separator.

Once the procedure outlined above had been applied to the events and (predominantly) fully-stripped ions with ionic charge, Q equal to Ze (where Z is the atomic number and e is the fundamental electronic charge) selected, a final, particle identification could be made for each ion on an event-by-event basis. This was made essentially using the measured time-of-flight of the ions as they passed through the second part of the FRS and known magnetic rigidity ($B\rho$) of the FRS dipole magnets, to calculate a value of mass over charge ($\frac{A}{Q=Z}$) for each ion. This quantity could then be correlated with the ion's energy loss (ΔE) as the ion passed through the MUSIC detectors, which is dependent on the atomic number Z. The responses of the detectors to specific values of $\frac{A}{Q}$ and Z for given velocities was determined following pre-experiment calibrations using the ^{208}Pb primary beam and could thus be applied to the final experimental data to provide calibrated measurements of the $\frac{A}{Q=Z}$ and Z values for each transmitted ion on an event-by-event basis by measuring their times-of-flight and energy losses respectively. Figure 5 shows a particle identification matrix from the current experimental work with a sum of two settings focussed on ions of ^{188}Ta and ^{190}Ta.

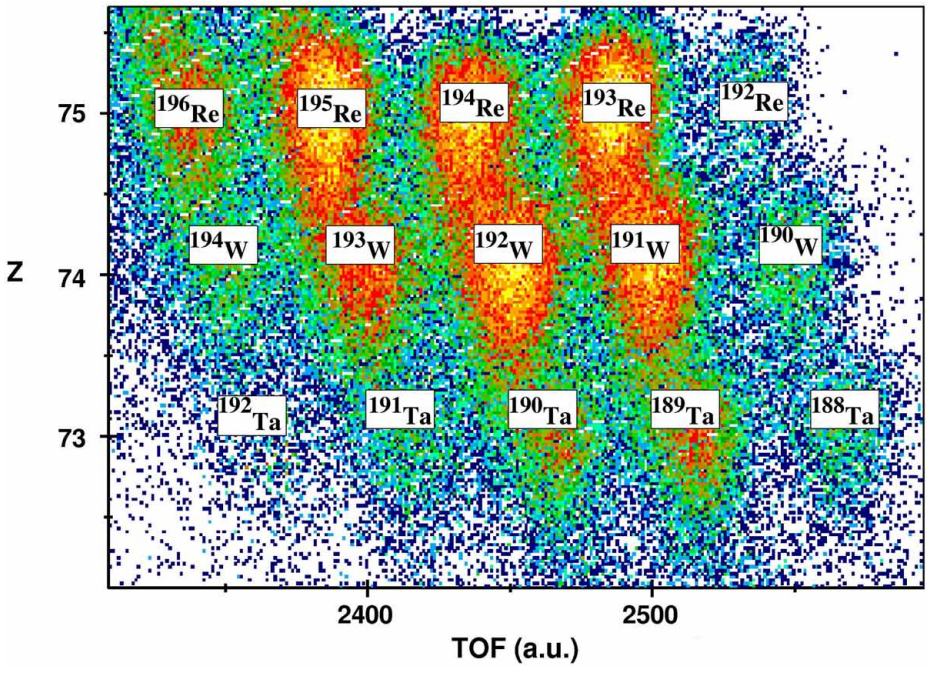

Fig. 5. Final particle identification plot for fully-stripped (i.e., $\Delta Q = 0$) ions following the fragmentation of a 1 GeV per nucleon ^{208}Pb beam. The data shown here are the sum of two FRS magnet settings centered on the transmission of ions of ^{188}Ta and ^{190}Ta respectively.

3.2. *Decays from isomeric states*

Decays from isomeric states in secondary beam particles which were transmitted through the FRS were observed in the RISING gamma-ray array. Since the gamma-ray transition energies and their decay lifetimes are characteristic of specific nuclei, these decays can be correlated with specific ions and used as an internal check and calibration of the particle identification procedure. Figure 6 shows gamma-ray spectra and their associated decay time profiles for previously reported[7] isomeric states in ^{188}Ta, ^{190}W and ^{192,193}Re which were observed in the current work. (Aside: We note in passing the apparent lack of evidence for the previously reported[4,7] 591 keV transition in the isomeric decay of ^{190}W. This is discussed further elsewhere[20,21]).

3.3. *Beta-delayed spectroscopy of secondary fragments*

Figure 7 shows the energy spectrum of ions and beta-particles taken from the sum of silicon strips in the three DSSSDs in the current work. Note that the use of the Mesytec 'semi-logarithmic' preamplifier allows the responses for both the heavy-ion implantation (i.e., the high energy *implant*) and beta-particle (low-energy *decay*) to be made using the same electronic channel. This allowed a clean identification pixel by pixel of the position of the implanted ion of interest which could then be

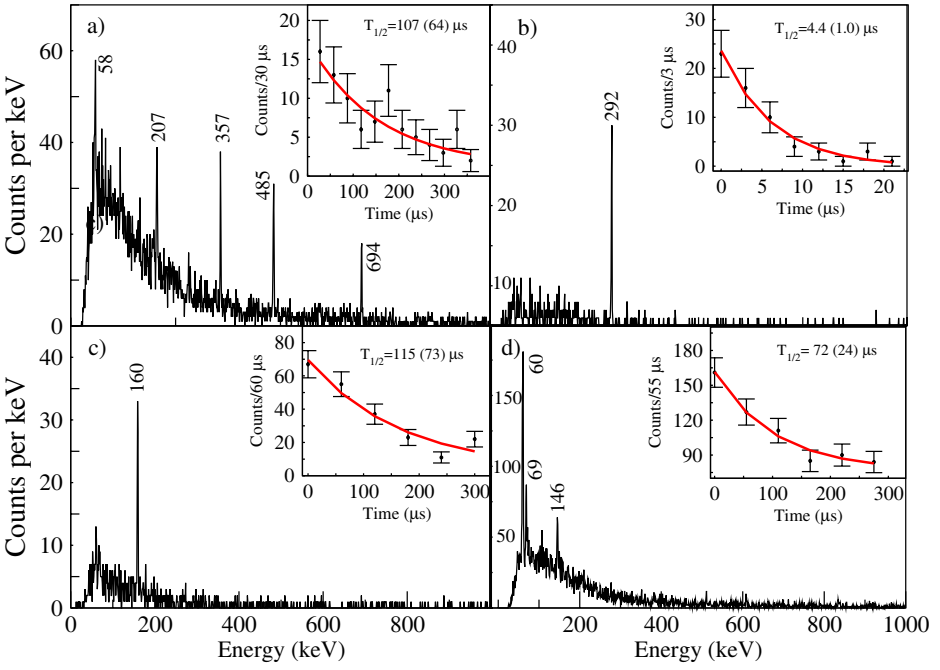

Fig. 6. Decays from previously reported[7] isomeric states in (a) ^{190}W, (b) ^{188}Ta, (c) ^{192}Re and (d) ^{193}Re observed in the current work and used to validate the particle identification procedure.

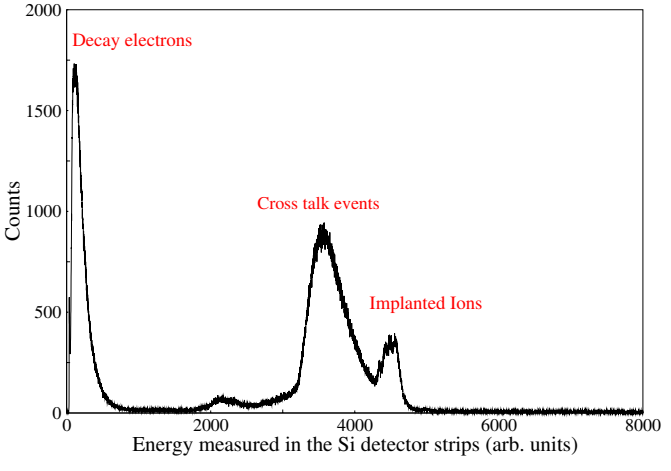

Fig. 7. Energy response spectrum (on a mixed linear and logarithmic scale) for the sum of each of the strips in the three DSSSDs used in the current work. The energy response of the detector is determined by the use of the Mesytec "semi-logarithmic pre-amplifier" which allows both β particles (energies ∼200 keV → a few MeV) and implanted secondary projectile fragments (energies ∼GeV to be measured in the same electronics channel. For more details see Ref. 18.

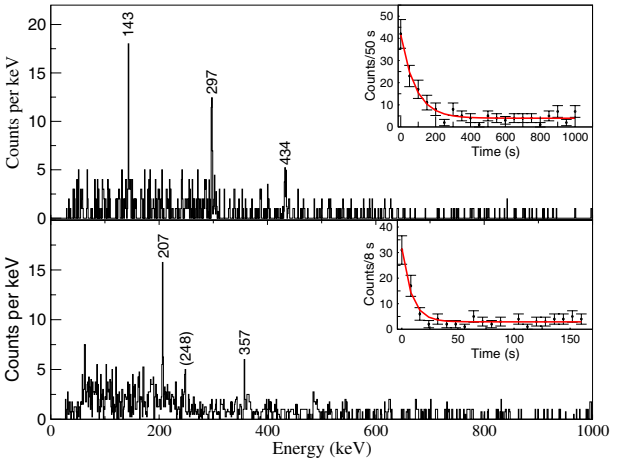

Fig. 8. Beta-delayed gamma-ray spectra from the current work showing transitions in ^{188}W and ^{190}W following the correlated β^- decay of ^{188}Ta and ^{190}Ta ions respectively. The insets show the measured time difference spectra between the radioactive tantalum implants and their subsequent β^- decays in the same or directly neighboring pixel in the DSSSDs.

correlated with subsequent β^- decay events (i.e., low-energy events measured in the DSSSDs) in the same and directly neighboring pixels. By investigating temporally-correlated $\beta^- - \gamma$ events with prompt gamma-ray coincidences between the β^- particle and γ rays measured in the Stopped RISING array, nuclide specific, β^--delayed gamma-ray spectra could be obtained providing spectral information on the daughter nuclei of the primary radioactive implants.

Figure 8 shows the gamma-ray spectra in coincidence with β^- particles following decays from the ^{188}Ta and ^{190}Ta mother nuclei (i.e., gamma-ray transitions in the daughter ^{188}W and ^{190}W respectively). The spectra showing the gamma rays correlated with the $^{188}\text{Ta} \rightarrow {}^{188}\text{W}$ decays clearly identify transitions at energies of 143, 297 and 434 keV respectively. These transitions have been previously reported as decays from the yrast states in ^{188}W with spin/parities of 2^+, 4^+ and 6^+ respectively as observed from in-beam studies using deep-inelastic[22] and two-neutron transfer reactions.[23] Transitions from states with spins greater than $6\hbar$ reported in Ref. 23 are not observed in the present work which is populated following β^- decay.

Similarly, the β^--correlated decays of transitions in ^{190}W in the current work show the previously reported[4,7] transitions at 207 and 357 keV. Note that the same transitions are also observed in the isomeric population of this nucleus in the current work (see Fig. 6(a)), however the 485 and 694 keV transitions identified in the isomeric decay are not observed in the β^--delayed feeding of this nucleus in the present work. On this basis and their relative intensities, the 207 and 357 keV transitions are thus established as the decays from the yrast 2^+ and 4^+ states in ^{190}W respectively.

4. Discussion of Preliminary Results

The energy systematics of the low-lying excited states in heavy nuclei can be used as a first insight into the structural properties of such nuclei. In cases such as the present work when the nuclei of interest are at the limits of experimental accessibility, it is often only the energy systematics which can be measured and used to obtain and extend global systematics of nuclear structure over long chains of proton and neutron number. Figure 9 shows the energy systematics of a wide chain of W and Os isotopes including the data from the current work on ^{190}W. Both the increasing energy of the yrast 2^+ energy and the parallel reduction in the energy ratio between the yrast 4^+ and 2^+ states is indicative of a reduction in collectivity as the neutron number of these elements approaches the N=126 closed shell.

The ratio of the 4^+ to 2^+ energies in ^{190}W has been the subject of some discussion in the literature with Os and W nuclei around A$\sim$190 $\rightarrow$ 194 being proposed as possible candidates for weakly-deformed *oblate* shapes.[4,24–27] Possible evidence for such a sudden change from well-deformed, prolate ground-state shapes to weakly-deformed oblate shapes might be evidenced by discontinuities in the energy systematics of such nuclei. Such spectral information can be obtained using the β^--delayed spectroscopic technique outlined above.

Figure 10 shows Hartree–Fock calculations assuming axial symmetry for neutron-rich W and Os nuclei around A$\sim$190. The prolate-oblate minima are pre-

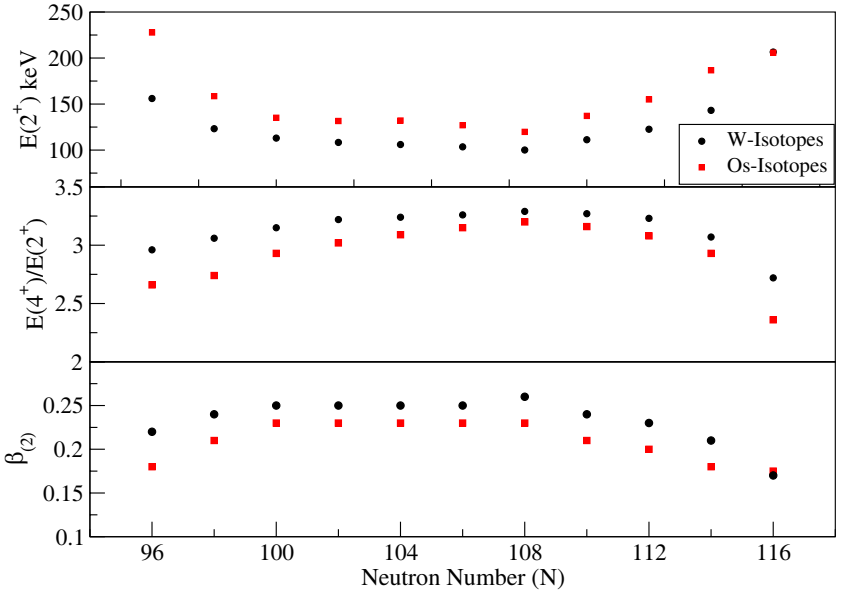

Fig. 9. Low-lying energy systematics of even-even W and Os isotopes, including data from the current work. The deformation parameter, β_2 is inferred from the empirical relation proposed by Raman.[28]

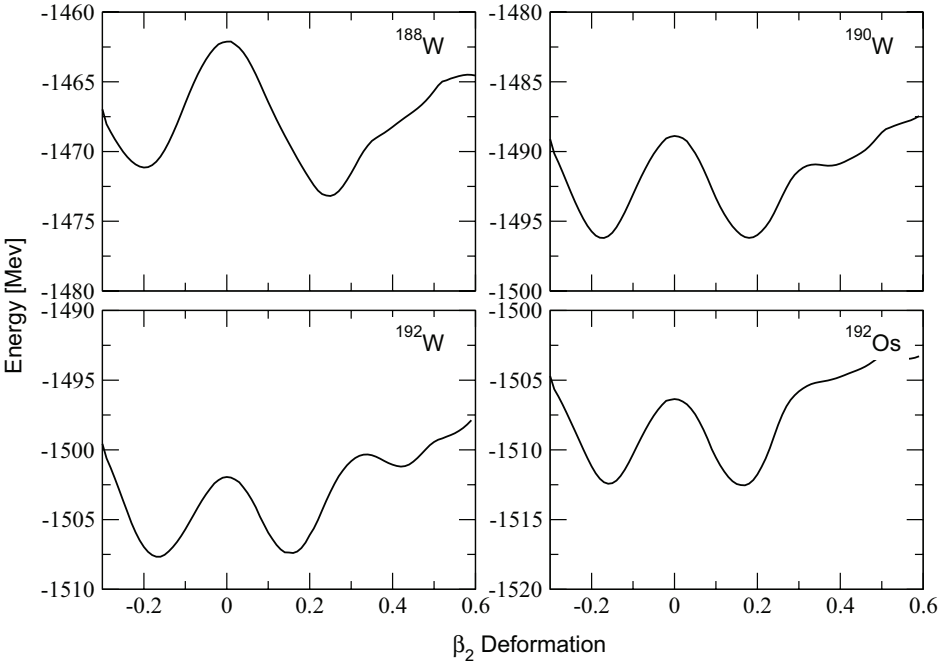

Fig. 10. Hartree–Fock calculations (assuming axially symmetry) of the ground state energy of ^{188,190,192}W and ^{192}Os a function of quadrupole deformation, β_2. For more details, see Ref. 24.

dicted to be competitive in this region with them being almost equal in energy for ^{190}W with the calculations suggesting that the oblate minimum becomes favored for the N = 118 isotone ^{192}W. The estimate for the quadrupole deformation, β_2, inferred from the empirically derived relation with the energy of the first 2^+ state by Raman *et al.*,[28] is consistent with the magnitude of the deformation predicted for the preferred minimum in the calculations shown in Fig. 10.

5. Summary and Future Work

In summary, the RISING active stopper has been used for gamma-ray spectroscopic measurements following the correlated beta-decays of heavy neutron-rich nuclei in the Hf → Os region for the first time. The measurements demonstrate the power of the decay spectroscopy techniques when applied to the projectile fragmentation mechanism for the production and selection of nuclear species with very exotic proton-to-neutron ratios. The first data allowing correlated gamma-ray spectroscopic measurements following the beta-decay of the neutron-rich ^{188,190}Ta isotopes into their W daughter nuclei highlights the effectiveness of the RISING "Active stopper" in such studies. Similar measurements have been made from the same data set on previously reported[29,30] decays from ^{192}Re and ^{198}Ir and the

current data have also been used to establish the beta-decay of ^{194}Re for the first time,[31] with the expected gamma-ray transitions in the ^{194}Os daughter nucleus[32] have been clearly identified. The spin/parities populated in the daughter nuclei can then be used with the measured lifetime of the decay to deduce the $F\tau$ value for that particular β^- decay. This can be used with the standard β^- decay selection rules to infer the spin/parity of the mother nucleus which can also be used to infer information on the shape (i.e. prolate or oblate) of the mother nucleus.[33]

The active stopper can also be used to measure decays from long-lived ($T_{\frac{1}{2}}$ ∼seconds) states which decay with significant internal conversion branches. Discrete-line internal conversion energy data have been observed in the same experiment[34] discussed in this paper from the internal decay between the proposed $\frac{11}{2}^-$ and $\frac{3}{2}^+$ states in the N = 126 isotone ^{205}Au with the particle identification of this nucleus confirmed using the observation of the previously reported[35] γ rays observed in the daughter nucleus following the β^- decay of the ^{205}Au ground state. Other subsequent measurements using the active stopper for beta-delayed measurements of fragmentation products of ^{238}U primary beams have also been carried out. Together with the present work this technique expands the regime of nuclei available for spectral study and is of particular significance for heavy neutron-rich nuclei approaching the rapid-neutron process paths around N∼126.

References

1. A. Gade and T. Glasmacher *Prog. Part. Nucl. Phys.* **60** (2008) 161; R. F. Casten and B. M. Sherrill *Prog. Part. Nucl. Phys.* **45** (2000) S171.
2. H. Geissel, *Nucl. Instr. Meth. Phys. Res. B* **261** (2007) 1079.
3. M. Pfützner *et al.*, *Phys. Lett. B* **444** (1998) 32.
4. Zs. Podolyák *et al.*, *Phys. Lett. B* **491** (2000) 225.
5. M. Pfützner *et al.*, *Phys. Rev. C* **65** (2002) 064604.
6. Zs. Podolyák *et al.*, *Nucl. Phys. Phys. A* **722** (2003) 273c.
7. M. Caamano *et al.*, *Eur. Phys. J. A* **23** (2005) 201.
8. K. A. Gladnishki *et al.*, *Phys. Rev. C* **69** (2004) 024617
9. Zs. Podolyák *et al.*, *Phys. Lett. B* **632** (2006) 203.
10. P. H. Regan *et al.*, *Nucl. Phys. A* **787** (2007) 491c.
11. A. Jungclaus *et al.*, *Phys. Rev. Lett.* **99** (2007) 132501.
12. A. B. Garnsworthy Ph.D. Thesis, Univ. of Surrey, UK (2007).
13. A. B. Garnsworthy *et al.*, *Phys. Lett. B* **660** (2008) 326.
14. M. Górska *et al.*, *Acta. Phys. Pol. B* **28** (2007) 1219.
15. H. J. Wollersheim *et al.*, *Nucl. Inst. Meth. Phys. Res. A* **537** (2005) 637.
16. S. Pietri *et al.*, *Acta Phys. Pol. B* **38** (2007) 1255.
17. S. Pietri *et al.*, *Nucl. Inst. Meth. Phys. Res. B* **261** (2007) 1079.
18. R. Kumar *et al.*, *submitted to Nucl. Inst. Meth. Phys. Res. A.*
19. J. Benlliure *et al.*, *Nucl. Phys. A* **660** (1997) 87; erratum *Nucl. Phys. A* **674** (2000) 578.
20. G. Farrelly, Zs. Podolyák *et al.*, private communication.
21. G. J. Lane *et al.*, contribution to the Nuclear Structure NS08 Conference, Michigan State University (2008).
22. Zs. Podolyak *et al.*, *Int. J. Mod. Phys. E* **13** (2004) 123.

23. T. Shizuma *et al.*, *Eur. Phys. J. A* **30** (2006) 391.
24. P. D. Stevenson *et al.*, *Phys. Rev. C* **72** (2005) 047303.
25. P. Finelli *et al.*, *Nucl. Phys. A* **770** (2006) 1.
26. P. Sarriguren *et al.*, *Phys. Rev. C* **77** (2008) 064322.
27. J. Jolie and A. Linnemann *Phys. Rev. C* **68** (2003) 031301.
28. S. Raman *et al.*, *At. Data Nucl. Data Tables* **78** (2001) 1.
29. C. M. Baglin *Nuc. Data Sheets* **84** (1998) 717.
30. Z. Chunmei, *Nucl. Data. Sheets* **95** (2002) 59; A. Szalay and S. Uray, *Radiochim. Radioanal. Lett.* **14** (1973) 135.
31. P. H. Regan and N. Al-Dahan *et al.*, in the Proceedings of the 13th Conference on Capture Gamma Spectrosocopy and Related Topics, Köln, Germany (2008), to be published in AIP Conference Proceedings.
32. C. Wheldon *et al.*, *Phys. Rev. C* **63** (2001) 011304.
33. P. M. Walker and F. R. Xu *Phys. Rev. C* **74** (2006) 067303.
34. Zs. Podolyák, G. Farrelly and P. H. Regan *et al.*, *submitted to Phys. Lett. B.*
35. F. G. Kondev *Nucl. Data Sheets* **101** (2004) 521; Ch. Wennemann *et al.*, *Z. Phys. A* **347** (1994) 185.

Nuclear Instruments and Methods in Physics Research A 598 (2009) 754–758

Contents lists available at ScienceDirect

Nuclear Instruments and Methods in Physics Research A

journal homepage: www.elsevier.com/locate/nima

Testing of a DSSSD detector for the stopped RISING project

R. Kumar [a,b,*], F.G. Molina [c], S. Pietri [d], E. Casarejos [f], A. Algora [c,g], J. Benlliure [f], P. Doornenbal [e,b], J. Gerl [b], M. Gorska [b], I. Kojouharov [b], Zs. Podolyák [d], W. Prokopowicz [b], P.H. Regan [d], B. Rubio [c], H. Schaffner [b], S. Tashenov [b], H.-J. Wollersheim [b]

[a] Inter University Accelerator Centre, New Delhi 110067, India
[b] Gesellschaft für Schwerionenforchung (GSI), D-64291 Darmstadt, Germany
[c] Instituto de Física Corpuscular, CSIC-Univ. Valencia, E 46071 Valencia, Spain
[d] Department of Physics, University of Surrey, Guildford GU2 7XH, UK
[e] Institut für Kernphysik, Universität zu Köln, D-50937 Köln, Germany
[f] Departimento de Física de particulas, Universidad de Santiago de Compostela, E-15782 Santiago de Compostela, Spain
[g] Institute of Nuclear Research of the Hungarian Academy of Sciences, POB 51, 4001 Debrecen, Hungary

ARTICLE INFO

Article history:
Received 3 June 2008
Received in revised form
18 August 2008
Accepted 20 August 2008
Available online 1 November 2008

Keywords:
β-decay
HI implantation
Silicon detectors

ABSTRACT

An active stopper for the RISING project at GSI has been developed for β-decay studies and conversion electron spectroscopy following projectile fragmentation/fission reactions. This system employs six double-sided silicon strip detectors in the final focal plane of the GSI FRagment Separator (FRS) to detect both the fragment implantations and their subsequent charged-particle (α, β, p) decays. The wide range of energy response required (150 keV up to several GeVs) was covered by the use of a logarithmic preamplifier. Measurements with a ^{207}Bi conversion electron source yielded an energy resolution of 20 keV at electron energies of ~1 MeV and a detection threshold of 150 keV. The response to the implantation of 400 AMeV ^{136}Xe ions in the active stopper is also discussed in the present paper.

1. Introduction

A new beta counting system has been developed for the RISING (Rare Isotope Spectroscopic INvestigation at GSI) project [1] to study the β-decay of exotic nuclei produced by projectile fragmentation and in-flight fission. The system employs up to six Micron Semiconductor Ltd. [2] Model W1(DS)-1000 DC coupled double-sided silicon strip detectors (DSSSD) with thickness of 1 mm to detect both fragment implantations and their subsequent β-decays. While this detector thickness provides an efficient implantation of heavy ions, the range of the β-particles emitted by the nuclear decays is usually significantly larger than 1 mm of silicon. This fact results in the probable escape of the particles from the DSSSD before they deposit their full kinetic energy. The deposited energy depends on the path of the electron in the silicon and therefore on the implantation depth. Fig. 1 (left) shows the simulated energy spectrum of the electrons emitted by the β-decay and detected by the DSSSD. A Fermi–Curie initial electron energy distribution with $Q_\beta = 5$ MeV was assumed. For different Q_β-values the simulated energy distribution only changes on the high-energetic side. The Monte-Carlo simulations were performed using the GEANT4 simulation toolkit [3] with the 'GEANT4 Low Energy Electromagnetic Physics' package [4]. Two cases of the implantation were considered: uniformly distributed and exact central implantation. In the later case the minimum distance to the surface is 0.5 mm, which corresponds to the minimum energy of 0.1 MeV that the electrons deposit in the crystal. This fact highlights the importance of achieving the low-energy threshold at 0.1 MeV as well as the importance of the accurate central implantation. Fig. 1 (right) shows the efficiency to detect β-particles in the 1 mm thick DSSSD as a function of the low-energy threshold for the two considered implantation scenarios. The efficiency is clearly high for a low detection threshold.

The array of six DSSSDs can be used in different configurations. The most common is to use three detectors positioned in two rows, one behind the other, at the final focal plane of the FRagment Separator (FRS) [5] which is used for the selection and identification of the radioactive nuclei. Each detector consists of 16 front strips and 16 back strips, each of width 3 mm, thus providing 256 3×3 mm^2 pixels on a 5×5 cm^2 detector to encode x–y positions. A variable thickness aluminium degrader is used just in front of the DSSSD array to slow down the ions such that they are implanted in the active stopper at the centre of the stopped RISING germanium array [1]. Implantation and β-decay

*Corresponding author at: Inter University Accelerator Centre, New Delhi 110067, India. Tel.: +91 9868207046.
E-mail address: rakuiuac@gmail.com (R. Kumar).

0168-9002/$ - see front matter © 2008 Elsevier B.V. All rights reserved.
doi:10.1016/j.nima.2008.08.155

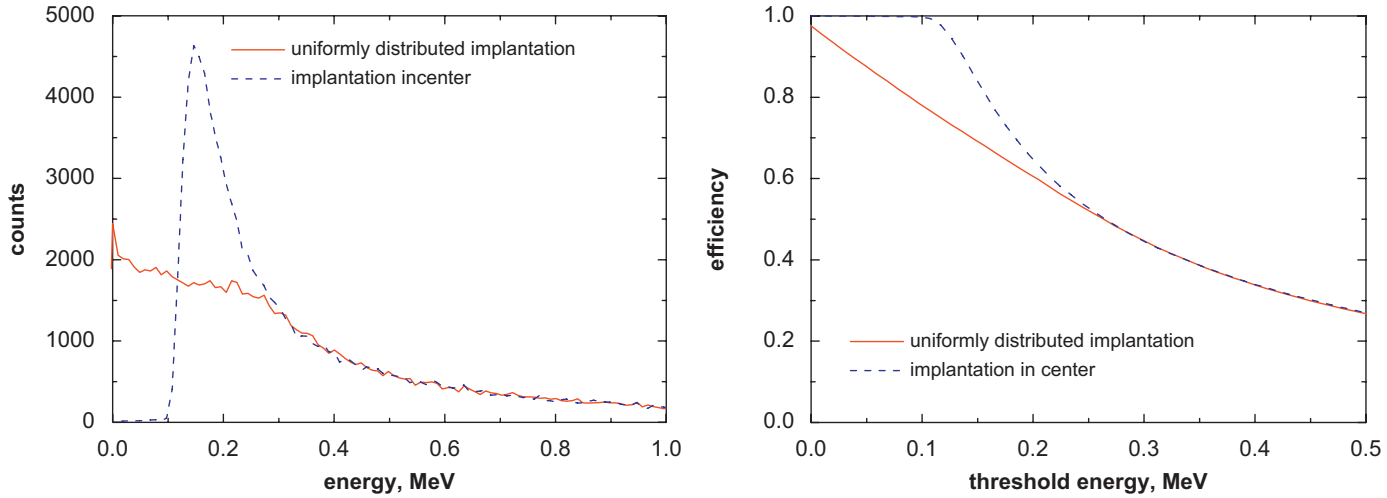

Fig. 1. Simulated energy spectrum of β-particles emitted from fragments implanted uniformly (solid line) and exactly in the centre (dashed line) of a DSSSD (left). The simulation assumes a Q_β-value of 5 MeV and a Fermi–Curie distribution for β-particles. The right figure shows the calculated β-detection efficiency as a function of the DSSSD threshold for the two considered implantation scenarios discussed in the text.

events are directly correlated within each pixel of the detector, which requires accurate knowledge of the implantation position. The half-life of the nucleus is deduced from the time correlation between the implantation time of the identified fragments in the active catcher and the subsequent β-decay. The time correlation is measured with a time stamping system providing a resolution of 25 ns.

One of the challenges in designing the electronics for the beta counting system is the range of charged particle energies that must be measured. A fast fragment implantation will deposit more than 1 GeV total energy when it is stopped in the centre of the DSSSD, while an emitted β-particle will deposit less than 1 MeV. Measurements with *Mesytec* [6] electronics are described in Section 2. The experimental results with a ^{207}Bi β-source are compared with the data taken with *Multi Channel Systems* [7] electronics in Section 3. Finally, a measurement with ^{136}Xe ions was performed in order to investigate the heavy-ion implantation response in the DSSSD. These results are presented in Section 4.

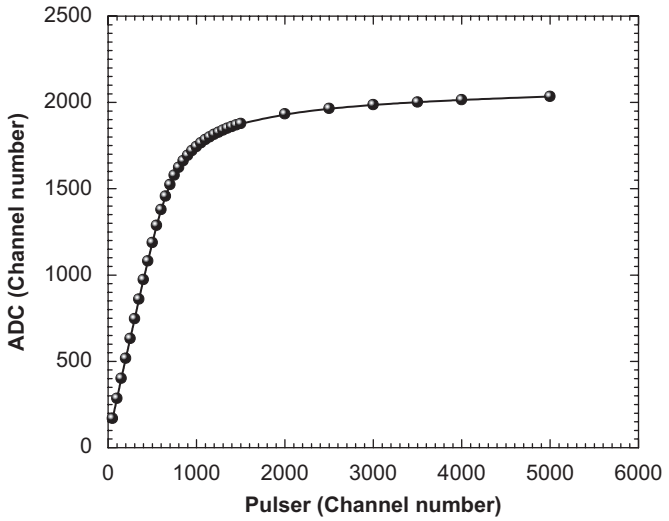

Fig. 2. The characteristics of the logarithmic MPR-32 preamplifier was measured with a 10 MeV linear range setting and STM-16 spectroscopy amplifiers.

2. Measurements with *Mesytec* electronics

The *Mesytec* MPR-32 preamplifier is a 32-channel input preamplifier which was used for the 16 front and 16 back strips of a single DSSSD. It can accept positive or negative input polarities. The *Mesytec* MPR-32 multi-channel preamplifier is available in a linear or logarithmic mode. For the linear MPR-32 preamplifier an amplification range of 5 or 25 MeV can be chosen. For the 978 keV line seen from the ^{207}Bi conversion electron source the MPR-32 output signal has a pulse height of approximately 200 mV and its signal-to-noise ratio is 10:1 (5 MeV range). The logarithmic MPR-32 preamplifier provides a linear range of 2.5 or 10 MeV, which covers 70% of the total range. The last 30% covers the energy range from 10 MeV up to 3 GeV. Both MPR-32 units have a full voltage range of preamplifier output of 4 V. Fig. 2 shows the characteristics of the logarithmic MPR-32 preamplifier which was measured with a research pulser. It is worth mentioning that the pulse height cannot be directly related to the implantation energy because of the pulse height defect in solid state detectors.

The MPR-32 was combined with two *Mesytec* STM-16 shaping-/timing filter/discriminator modules when the differential input version is used. The STM-16 is a NIM-powered device which has 16 input channels allowing parallel processing. The gain was adjusted individually in 16 steps with a maximum gain of 30. A shaping time of 1 or 2.5 μs (FWHM) was chosen. For the following measurements a shaping time of 1 μs (FWHM) was selected as this would be needed for higher count rate experiments.

The STM-16 was controlled by a NIM-module MRC-1 which works as a bus master. One *Mesytec* MRC-1 can control 32 various *Mesytec* modules (not only STM-16). It is prepared for the remote control of (i) individual discriminator thresholds (0–40% of maximum range, 4 V) and (ii) gains (in 16 steps) for pairs of channels. Communication with a control PC is done via RS-232 serial interface. Each analogue signal was fed directly to a CAEN V785AF VME-ADC which has a maximum input voltage of 8 V. The trigger signal of STM-16 is a logical OR of the 16 discriminator channels and was used to produce the ADC gate. In Fig. 3 semi-logarithmic energy spectra of a ^{207}Bi β-source are shown for different discriminator thresholds of the *Mesytec* STM-16 module. As can be seen, the detection limit for electron measurements using this system was set as low as 150 keV with the present electronics and the detectors/electronics working at room

temperature. This limit was defined at 50% of the logarithmic spectral curvature caused by the discriminator threshold.

3. Energy resolution measured with electrons of a ^{207}Bi source

First, a standard ^{241}Am source was used to verify the performance of the DSSSD and to measure the resolution of the system. The alpha source was placed 5 cm from the detector's surface in a vacuum vessel. Individual strips displayed energy resolutions of 0.48–0.52% (front) and 0.51–0.64% (back) FWHM for the 5.5 MeV peak. Then a ^{207}Bi source, which emits mono-energetic conversion electrons, was used to calibrate the DSSSD. The ^{207}Bi source was covered with 70 μg/cm^2 polypropylene foil and positioned at 5 cm from the front face of the detector. The measured electron spectrum for a front strip is shown in Fig. 4 (left). Four peaks (482, 555, 976 and 1049 keV) are clearly observed, due to K and L + M + N conversion electrons of the 570 keV (E2) and 1060 keV (M4) transition in ^{207}Pb. The energy resolution of the 976 keV line is 14.4 keV (FWHM) for this strip. Fig. 4 (right) shows an overview of the energy resolution as a function of the strip number. The front junction side of the detector has clearly got better resolution compared to the rear ohmic side. A comparison between the linear and logarithmic MPR-32 preamplifier reveals a slightly poorer energy resolution in the logarithmic one, 19.7 keV compared to 15.3 keV for a selected front strip of the DSSSD-2243-5. However, the logarithmic MPR-32 has the advantage of being able to measure both the heavy-ion implantation as well as the β-particle. All the data discussed so far were obtained for detector tests performed in vacuum. DSSSD tests were also carried out in dry nitrogen. The energy resolutions measured in vacuum and dry nitrogen were the same within the experimental uncertainties. Therefore, the RISING experiments with an active stopper can be performed in dry nitrogen, allowing the use of a detector vessel with thin walls, thereby minimizing the absorption of the emitted γ-rays.

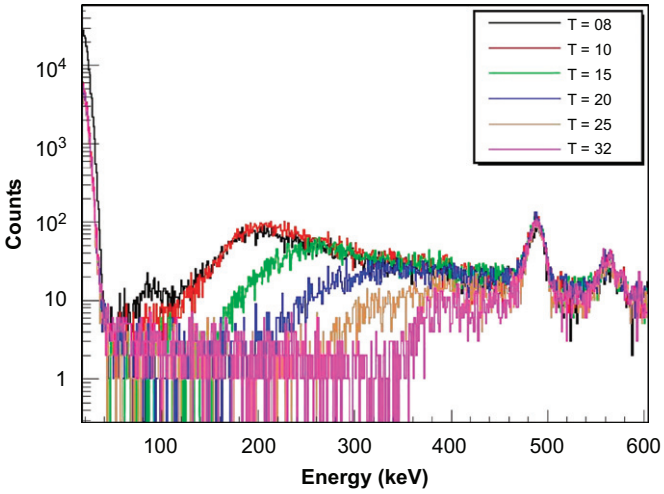

Fig. 3. Energy spectra of a ^{207}Bi β-source measured for different discriminator thresholds labelled $T = 8-32$ of the *Mesytec* STM-16 module.

At the National Superconducting Cyclotron Laboratory (NSCL) at Michigan State University (MSU), a beta counting system [8] has been developed with different electronics which yields reliable energy information for both implants and decays. The DSSSD signals are first processed by two 16-channel charge sensitive preamplifier modules CPA-16 supplied by *Multi Channel Systems* [7]. These modules contain precision pre- and shaping amplifier electronics and provide both high gain (2 V/pC) and low gain (0.1 V/pC) analogue outputs. They have a full voltage range of preamplifier output of 5 V. The high gain signals carry information from low-energy β-decay events, and they require further amplification. This is accomplished at MSU using *Pico Systems* [9] 16-channel shaper/discriminator modules in CAMAC. The shaper output of the Pico Systems module is sent directly to an ADC. For the present DSSSD tests two 16-channel charge sensitive preamplifier modules CPA-16 were also tested at GSI. For a ^{207}Bi β-source the CPA-16 output signals have a pulse height of approximately 200 mV and a signal-to-noise ratio of 7:1. At GSI *ORTEC* 572 and 16-channel *CAEN* N568BC amplifiers were used for

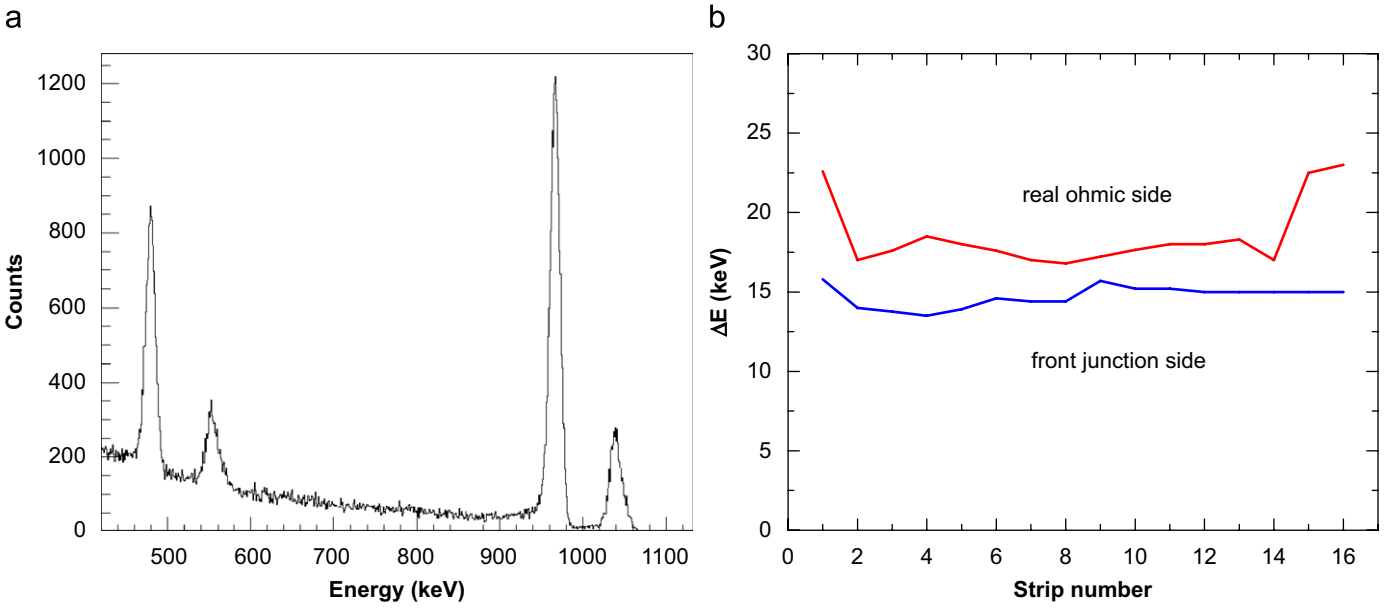

Fig. 4. The conversion electron spectrum of ^{207}Bi measured with a linear MPR-32 preamplifier for a front strip of DSSSD-2512-17. The four peaks at 482, 555, 976 and 1049 keV result from mono-energetic electrons—see text for details (left). The energy resolution for the front junction and the rear ohmic side versus the strip number is plotted on the right side.

shaping the high gain CPA-16 output signals. Three different measurements were performed: (i) the high gain output signal of the CPA-16 preamplifier was sent directly to the CAEN V785AF VME-ADC, (ii) it was additionally amplified using an *ORTEC* 572 amplifier with shaping times of 0.5, 1.0 and 2.0 μs, respectively, and (iii) using a *CAEN* N568BC module with a shaping time 2.0 μs before sending it to the same ADC. Fig. 5 shows the conversion electron spectrum of ^{207}Bi without further amplification. Only two peaks (482 and 976 keV) were clearly seen in the energy spectrum, due to K conversion electrons of the 570 and 1060 keV transitions in ^{207}Pb. The energy resolution of the 976 keV line varied between 100 and 120 keV depending on the different measurements. The detection limit for electrons was found to be approximately 300 keV.

In summary, with a ^{207}Bi source an energy resolution of 15–20 keV and an energy threshold of 150 keV were obtained for the *Mesytec* electronic, compared to a FWHM of 100 keV and a threshold of 300 keV for *Multi Channel Systems* electronics. Since conversion electron spectroscopy studies are also part of the RISING stopped beam campaign the *Mesytec* electronic was selected for the readout of the DSSSDs.

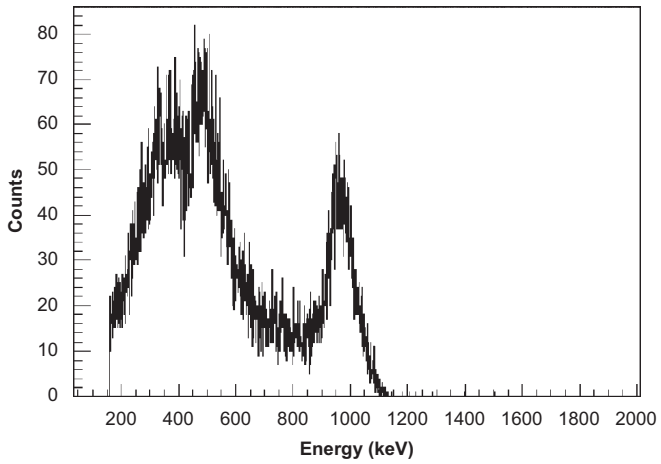

Fig. 5. The conversion electron spectrum of ^{207}Bi measured with the multi-channels electronics for the same strip of DSSSD-2243-5. The two peaks at 482 and 976 keV result from mono-energetic electrons.

4. Implantation measurement with a ^{136}Xe beam

A test measurement has been performed with the RISING set-up to investigate the heavy-ion implantation in the DSSSD. A primary beam of ^{136}Xe with an initial energy of 400 AMeV was slowed down in the aluminium degrader and implanted in the Si-detector. The active stopper vessel for the DSSSD was made out of Pertinax (phenolic–formaldehyde cellulose-paper PF CP 2061) with an entrance and exit window covered by a thin black Pocalon C foil of thickness 20 μm. The Pertinax wall was 2 mm thick, corresponding to an aluminium equivalent for γ-transmission of 0.7 mm.

Two measurements, triggered by a scintillation detector for beam particles in the FRS, were carried out with the linear and logarithmic MPR-32 preamplifiers. The linear MPR-32 preamplifier is well suited for the electron measurement (MeV range), however, for the implantation of heavy ions (GeV range) the output signals saturate. The energy spectra (see e.g. Fig. 7) show the low-energetic part of the implantation caused by light charged particles and atomic X-rays. In most cases all the strips of the DSSSD fire (see Fig. 6, left), since no condition is set on the implantation of the heavy ions. If only the overflow data of the energy spectra (>10 MeV) are considered (see Fig. 6, right), the multiplicity spectrum is localized at small values, which is expected for the implantation. For multiplicity one on each side of the DSSSD the position is uniquely determined, while for higher multiplicities the centroid has to be determined. When using the linear MPR-32 preamplifier each saturated strip has the same weight for this calculation, since the individual strip energies above 10 MeV are not measured. Therefore, the overflow data of the DSSSD only allow a zero order position determination of the heavy-ion implantation. Based on the multiplicity distribution (Fig. 6, right) one obtains an average shift of 2.3 mm (0.75*strip width) for each event.

The logarithmic MPR-32 preamplifier is well suited for both electron measurement (MeV range) and heavy-ion implantation (GeV range). The measured energy spectrum (10 MeV range

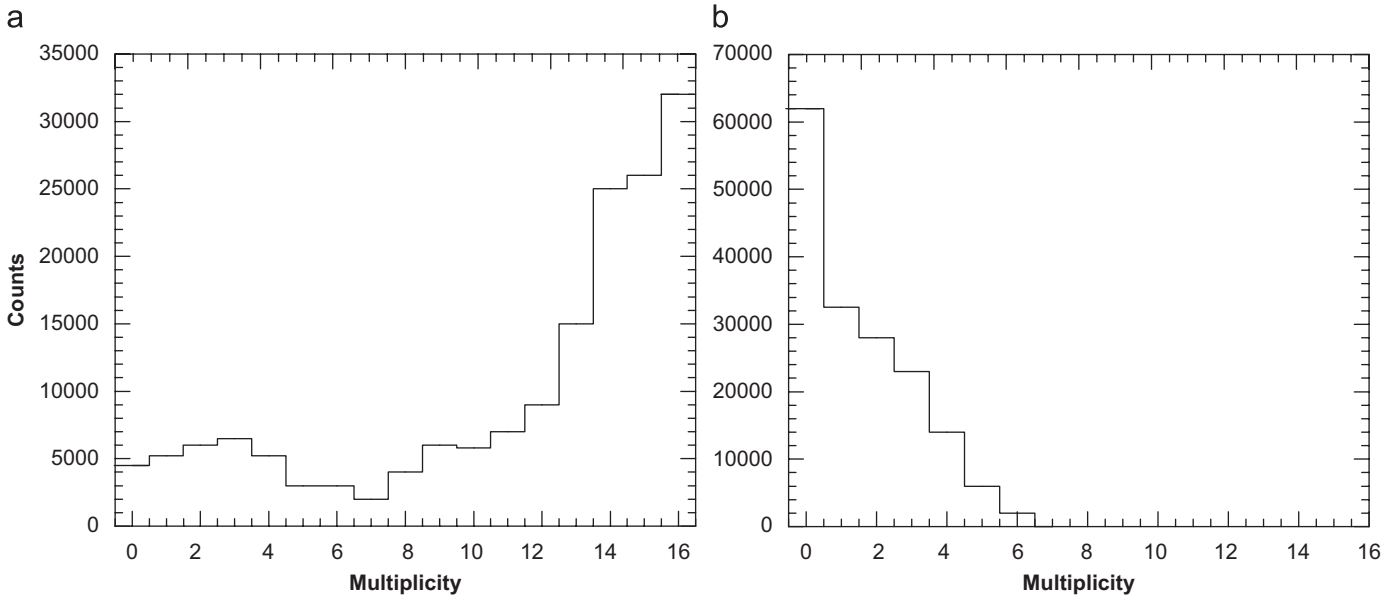

Fig. 6. Multiplicity distributions measured by x-strips for different energy thresholds. For a very low-energy threshold almost all x-strips are firing (left), while for the overflow (>10 MeV) data the hit probability is very low (right), as expected for the implantation of ^{136}Xe ions.

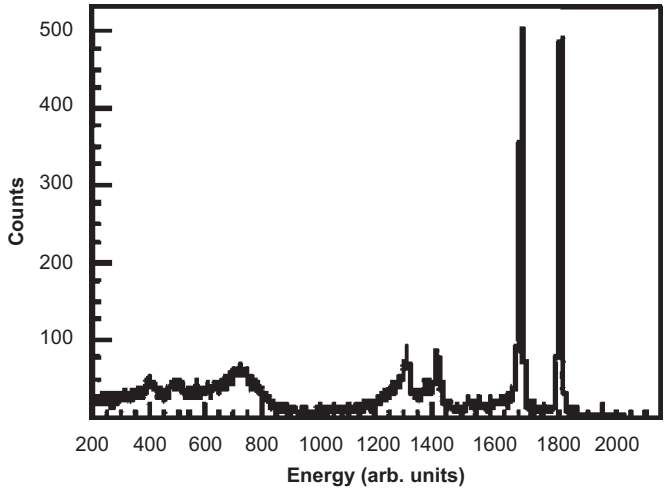

Fig. 7. Measured energy spectrum (10 MeV range for the linear part of the logarithmic MPR-32 preamplifier) obtained by a x-strip (front junction) for the implantation of ^{136}Xe ions. The double hump structure around 1600 and 1800 is related to the stopping of the heavy ions.

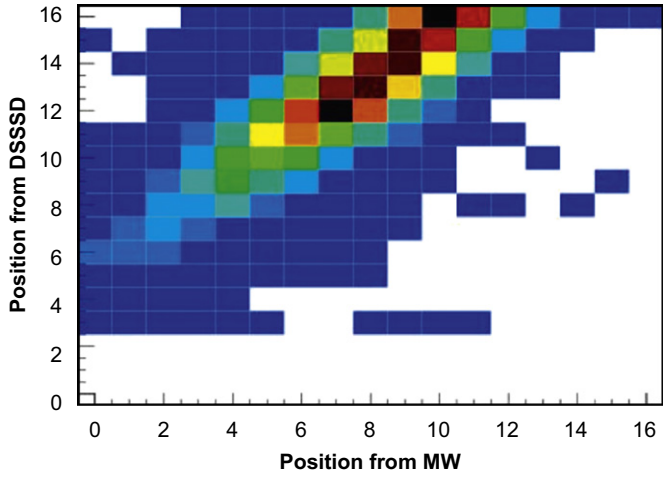

Fig. 8. Position correlation in *x* direction between the DSSSD and the multi-wire (MW) detector of the FRS. For the DSSSD the position of the implanted ^{136}Xe ion was determined from the mean of highest energy peaks, when a logarithmic MPR-32 preamplifier was used. The position of the MW was projected on the strip number of the DSSSD.

setting for the linear part of the logarithmic preamplifier) obtained from a x-strip (front junction) is shown in Fig. 7 for the implantation of ^{136}Xe ions. It shows a similar distribution to that obtained from the linear MPR-32, and a pronounced double hump structure in the logarithmic part of the spectrum. The double hump structure (see Fig. 7) is related to the implantation of the ^{136}Xe ions. A detailed analysis of the implantation events showed that in most cases only one (88%) or two (11%) strips on the *x*- and *y*-side of DSSSD were activated, which is quite different to the result with the linear MPR-32 (see Fig. 6, right) The highest energy peak could always be related to the implantation, while the second highest peak is due to the cross talk with the neighbouring strip. In 90% of all multiplicity two events the second highest peak was observed in the neighbouring strip. For the logarithmic MPR-32 preamplifier the mean of the highest peak of the double hump structure was used for the position determination. In summary, the measurement with the logarithmic preamplifier yields in 98% of all events an implantation within one strip, while the analysis with linear preamplifier determines, on average, a false shift of the implantation by 2.3 mm. Since no decay electrons were measured in this part of the study (^{136}Xe is a β-stable beam), a position correlation in *x*-direction between the DSSSD and a multi-wire (MW) detector of the FRS (in front of the active stopper) was determined. This is displayed in Fig. 8. It shows a strong correlation but also an offset since the DSSSD was not accurately centred in the frame of the FRS.

In conclusion, the logarithmic MPR-32 preamplifier is well suited for the active stopper of the RISING project. It covers a large energy range from fragment implantation down to β-decay. After the implantation of the exotic nuclei, the β-particles will be measured with high efficiency due to the low detection threshold of 150 keV. Since the DSSSDs are operated in dry nitrogen, a detector vessel with thin walls can be used to minimize the absorption of the emitted γ-rays. The excellent energy resolution of 20 keV also allows conversion electron spectroscopy to be performed as part of the stopped beam RISING campaign. Such an electron conversion measurement on ^{205}Au [10] was successfully performed with the present setup.

Acknowledgements

This work is supported by EPRSC (UK) and EURONS (EU Contract number 506065). Work partially supported by Spanish MEC, Grants FPA2005-03993 and FPA2005-00732. A.A. recognizes partial support of the Ramon y Cajal program.

References

[1] S. Pietri, et al., Nucl. Instr. and Meth. B 261 (2007) 1079.
[2] Micron Semiconductor Ltd., Marlborough Road, Lancing Sussex, England ⟨www.micronsemiconductor.co.uk⟩.
[3] S. Agostinelli, et al., Nucl. Instr. and Meth. A 506 (2003) 250.
[4] S. Chauvie, et al., in: Nuclear Science Symposium Conference Record, vol. 3, IEEE, New York, 2004, p. 1881.
[5] H. Geissel, et al., Nucl. Instr. and Meth. B 70 (1992) 286.
[6] Mesytec GmBH, Werner Von Braun Str. 1, D-85640 Putzbrunn, Germany ⟨www.mesytec.com⟩.
[7] Multi Channel Systems, Aspenhaustrasse 21, D-72770 Rutlingen, Germany ⟨www.multichannelsystems.com⟩.
[8] J.I. Prisciandaro, et al., Nucl. Instr. and Meth. A 505 (2003) 140.
[9] J. Elson, Pico Systems, 543 Lindeman Rd., Kirkwood, MO ⟨elson@pico-systems.compico-systems.com/shapdisc.html⟩.
[10] Zs. Podolyak, et al., in: Proceedings of the International Symposium on Physics of Unstable Nuclei (ISPUN07), World Scientific, Singapore, 2008, pp. 48–55 and Phys. Lett. B, submitted for publication.

PHYSICAL REVIEW C **79**, 011301(R) (2009)

Spherical proton-neutron structure of isomeric states in ^{128}Cd

L. Cáceres,[1,2,*] M. Górska,[1] A. Jungclaus,[2,3] M. Pfützner,[4] H. Grawe,[1] F. Nowacki,[5] K. Sieja,[1] S. Pietri,[6,†] D. Rudolph,[7] Zs. Podolyák,[6] P. H. Regan,[6] E. Werner-Malento,[4,‡] P. Detistov,[8,§] S. Lalkovski,[8,9] V. Modamio,[2] J. Walker,[2] K. Andgren,[10] P. Bednarczyk,[1,11] J. Benlliure,[12] G. Benzoni,[13] A. M. Bruce,[9] E. Casarejos,[12] B. Cederwall,[10] F. C. L. Crespi,[13] P. Doornenbal,[1,14,‖] H. Geissel,[1] J. Gerl,[1] J. Gręboszz,[1,11] B. Hadinia,[10] M. Hellström,[7] R. Hoischen,[1,7] G. Ilie,[14,15] A. Khaplanov,[10] M. Kmiecik,[11] I. Kojouharov,[1] R. Kumar,[16] N. Kurz,[1] A. Maj,[11] S. Mandal,[17] F. Montes,[1,¶] G. Martínez-Pinedo,[1] S. Myalski,[11] W. Prokopowicz,[1] H. Schaffner,[1] G. S. Simpson,[18] S. J. Steer,[6] S. Tashenov,[1] O. Wieland,[13] and H. J. Wollersheim[1]

[1]*Gesellschaft für Schwerionenforschung (GSI), D-64291 Darmstadt, Germany*
[2]*Departamento de Física Teórica, Universidad Autónoma de Madrid, E-28049 Madrid, Spain*
[3]*Instituto de Estructura de la Materia, CSIC, Serrano 113 bis, E-28006 Madrid, Spain*
[4]*IEP, Warsaw University, PL-00681 Warsaw, Poland*
[5]*IReS, IN2P3-CNRS/University Louis Pasteur, F-67037, Strasbourg, France*
[6]*Department of Physics, University of Surrey, Guildford GU2 7XH, United Kingdom*
[7]*Department of Physics, Lund University, S-22100 Lund, Sweden*
[8]*Faculty of Physics, University of Sofia, BG-1164 Sofia, Bulgaria*
[9]*School of Engineering, University of Brighton, Brighton BN2 4GJ, United Kingdom*
[10]*KTH Stockholm, S-10691 Stockholm, Sweden*
[11]*The Henryk Niewodniczański Institute of Nuclear Physics, PAN, PL-31342 Kraków, Poland*
[12]*Universidade de Santiago de Compostela, E-15782 Santiago de Compostela, Spain*
[13]*INFN, Universitádegli Studi di Milano and INFN sezione di Milano, I-20133 Milano, Italy*
[14]*Institut für Kernphysik, Universität zu Köln, D-50937 Köln, Germany*
[15]*National Institute of Physics and Nuclear Engineering, Bucharest 76900, Romania*
[16]*Inter University Accelerator Centre, New Delhi, India*
[17]*University of Delhi, New Delhi, India*
[18]*LPSC, Université Joseph Fourier Grenoble 1, CNRS/IN2P3, Institut National Polytechnique de Grenoble, F-38026 Grenoble Cedex, France*

(Received 24 September 2008; published 7 January 2009)

The γ-ray decay of isomeric states in the even-even nucleus ^{128}Cd has been observed. The nucleus of interest was produced both by the fragmentation of ^{136}Xe and the fission of ^{238}U primary beams. The level scheme was unambiguously constructed based on $\gamma\gamma$ coincidence relations in conjunction with detailed lifetime analysis employed for the first time on this nucleus. Large-scale shell-model calculations, without consideration of excitations across the $N = 82$ shell closure, were performed and provide a consistent description of the experimental level scheme. The structure of the isomeric states and their decays exhibit coexistence of proton, neutron, and strongly mixed configurations due to $\pi\nu$ interaction in overlapping orbitals for both proton and neutron holes.

DOI: 10.1103/PhysRevC.79.011301 PACS number(s): 21.60.Cs, 23.20.Lv, 23.35.+g, 27.60.+j

The development of the first generation radioactive beam facilities over the last decade has allowed access to experimentally very exotic nuclei with extreme proton-to-neutron ratios. Neutron-rich nuclei close to the doubly magic nucleus $^{132}_{50}$Sn$_{50}$ are relevant both for nuclear structure studies and for their implication for r-process nucleosynthesis. Hartree-Fock-Bogoliubov (HFB) calculations with the Skyrme force predict a reduction of the size of the $N = 82$ neutron shell gap when approaching $Z = 40$ [1]. This effect has been attributed to a reduction of the spin-orbit coupling strength caused by the strong interaction between bound orbitals and low-j continuum states. This is due to a large diffuseness of the outer neutron distribution and its influence on the central potential in exotic nuclei with large neutron excess. Dillmann *et al.* [2] pointed out that the experimental Q_β value of ^{130}Cd, only two proton-holes below ^{132}Sn, was better reproduced by those mass models that included "shell quenching" at $N = 82$ [3,4]. Moreover, the flattening of the Cd yrast 2^+ systematics from ^{126}Cd to ^{128}Cd, two-proton holes and four- and two-neutron holes with respect to ^{132}Sn, respectively, and the indication of a low lying 2^+ state in ^{130}Cd [5] have been interpreted as indirect evidence of the reduction of the $N = 82$ neutron shell gap

*L.Caceres@gsi.de
†Present address: Gesellschaft für Schwerionenforschung (GSI), D-64291 Darmstadt, Germany.
‡Present address: IF PAN, Warsaw, Poland.
§Present address: Universidad de Salamanca, E-37008 Salamanca, Spain.
‖Present address: RIKEN, Japan.
¶Present address: University of Michigan, MSU, USA.

already at $Z = 48$. In the same work it has been suggested that some collectivity persists in those very neutron-rich Cd nuclei approaching the neutron shell closure. The recently reported isomeric γ decay in ^{130}Cd [6] that unambiguously established the 2^+ excitation energy at 1325 keV concluded that there is no evidence for shell quenching at that atomic number. This conclusion is confirmed in a forthcoming publication where the measurement of a core excited isomeric state in ^{131}In [7] is reported. However, the low value of the 2^+ excitation energy in ^{128}Cd is still an open question. Beyond-mean-field calculations [8] attribute the anomalous behavior of the $E(2^+)$ in the Cd chain to the presence of quadrupole collectivity close to the $N = 82$ shell gap as suggested in Refs. [5,9,10]. To shed light on the structural aspects of the nucleus discussed above, a study of high-spin isomers and their decay has been performed. Recently, based on a similar experimental approach, however without any time correlations, a level scheme for the near-yrast states of ^{128}Cd has been proposed [11].

Because high-spin isomeric states in the ^{132}Sn region can be populated in fragmentation and/or fission reactions, the ^{128}Cd nuclei in this experiment were produced both in fragmentation of a ^{136}Xe primary beam at 750 MeV/u and average intensity $\sim 7.4 \times 10^8$ ions/s and in fission of a ^{238}U primary beam at 650 MeV/u and average intensity $\sim 2.7 \times 10^8$ ions/s delivered by the SIS accelerator complex of GSI Darmstadt, Germany. The Xe and U primary beams impinged on ^{9}Be targets of 4 g/cm^2 and 1 g/cm^2 thickness, respectively. The reaction products were separated by means of the $B\rho$-ΔE-$B\rho$ method in the FRagment Separator (FRS) at GSI [12] operated in achromatic mode. The identification was performed on an event-by-event basis by measuring the time of flight between two scintillator detectors placed in the intermediate and the final focal planes of the FRS, the energy loss in two ionization chambers, and the magnetic rigidity of the ions. Figure 1 shows an example identification plot for the nuclei produced in the fragmentation reaction with the FRS set to optimize the transmission of ^{130}Cd ions. In total 3.29×10^5 ^{128}Cd nuclei were identified. The ions were slowed down in an Al degrader and stopped in a plastic stopper positioned at the final focal plane of the FRS. The isomeric states populated

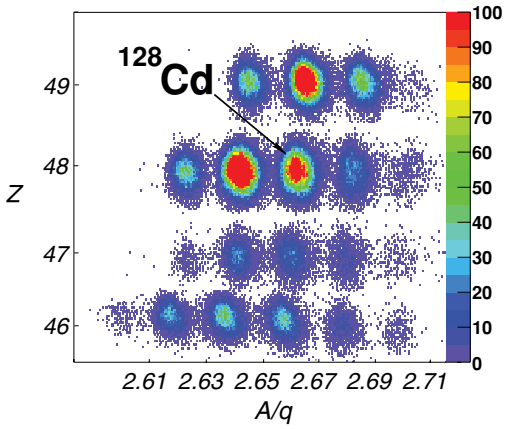

FIG. 1. (Color online) Particle identification plot of the ion production of 25% of the data from the fragmentation of a ^{136}Xe beam.

in these reactions with a half-life long enough to survive the flight through the FRS (≈300 ns) come to rest in the stopper and can be identified by their characteristic γ-ray emissions. The RISING Ge array placed in close geometry around the stopper was used to measure the γ radiation from the isomeric decays. The array consists of 15 Ge cluster detectors [13] from the former EUROBALL [14] spectrometer. By requiring a coincidence between the identified ion and the detected γ radiation over a range from 0 to 23 μs after implantation, the detected γ rays can be unambiguously assigned to the isomeric decay of one particular isotope. The time was measured in two independent electronic circuits: An analog branch with a time increment/scale of 0.7 ns/ch and a digital branch with 25 ns/ch. The γ-ray energy measurement ranged from 30 keV to 6 MeV. The high efficiency [15] and granularity of this Ge array in combination with the particle identification of the FRS makes this setup a unique tool for γ-ray spectroscopy studies. The delayed γ-ray singles spectrum measured following the implantation of ^{128}Cd is shown in Fig. 2(a). All previously reported transitions [5,11] are visible and in addition two strong lines at 69 and 1224 keV are observed for the first time. The level scheme proposed in Ref. [11] will not be considered further in view of the analysis presented in this work which includes $\gamma\gamma$ coincidences (Fig. 2) and half-life analysis (Figs. 3 and 4). Based on these results the inferred level scheme shown in Fig. 5 is discussed. The γ-ray energies, their relative intensities normalized to the most intense 646 keV transition, and the half-lives of the isomeric states observed in ^{128}Cd in this experiment are summarized in Table I.

In the $\gamma\gamma$ coincidence analysis with an open time condition ($\Delta t = 23.254$ μs) it was found that all strong γ rays seen in Fig. 2(a) belong to the main cascade with the exception of the 1224 keV transition, which is not observed in coincidence with the 440 and 785 keV lines. The coincidence spectrum gated on the latter is shown in Fig. 2(b). The 785 and 646 keV transitions were assigned from β-decay studies in Ref. [5] to form the $4^+ \rightarrow 2^+ \rightarrow 0^+$ cascade. The ordering of these two transitions is now unambiguously confirmed by the new $\gamma\gamma$ coincidence information. The 440 keV line was placed feeding the 4^+ state and decaying from the 1871 keV level. Furthermore, a $\gamma\gamma$ matrix was constructed requiring the time difference between the two coincident γ rays to be less than 125 ns. The spectrum obtained from this matrix by gating on the 238 keV transition shows a strong reduction in the intensity of the 646, 785, 440, and 1224 keV γ rays when compared to the 538 keV γ peak as visible in Fig 2(c). Corresponding coincidence relations were found by gating on the 538 and 69 keV peaks, with respect to the 238 keV intensity, and the other lines. This observation indicates the existence of at least two isomeric states with different lifetimes in ^{128}Cd. The time distributions of the γ rays below the 1871 keV level show indeed two decay components while the 69, 238, and 538 keV transitions decaying from the state at 2714 keV show only a single exponential decay, resulting in an isomeric half-life of 3.56(6) μs for this state (Fig. 3). The half-life of the state at 1871 keV was extracted from the γ versus relative γ-ray time difference matrix between the 238 keV transition and the γ lines below that state. Under this condition, the time distributions of the 648, 785, 1220, and 440 keV γ rays show

TABLE I. Experimental results and deduced spin and parity assignments for the excited states in ^{128}Cd. The γ intensities are normalized to the 646 keV transition.

E_i (keV)	$T_{1/2}$ (μs)	$I_i^\pi \rightarrow I_f^\pi$	E_γ (keV)	I_γ (%)	$\alpha_{\rm exp}$
646		$2^+ \rightarrow 0^+$	645.8(2)	100(5)	
1430		$4^+ \rightarrow 2^+$	784.6(1)	90(5)	
1871	0.270(7)	$(5^-) \rightarrow (4^+)$	440.0(3)	84(4)	
		$(5^-) \rightarrow (2^+)$	1224.0(6)	11(1)	
2108	0.012(2)[a]	$(7^-) \rightarrow (5^-)$	237.9(5)	39(2)	
2195		$(6^+) \rightarrow (4^+)$	765.0(3)	1.2(2)	
2646		$(8^+) \rightarrow (7^-)$	537.6(2)	47(3)	
		$(8^+) \rightarrow (6^+)$	450.4(3)	1.8(3)	
2714	3.56(6)	$(10^+) \rightarrow (8^+)$	68.7(1)	5.2(5)	6.38(86)[b]

[a]Extracted from the energy versus relative time matrix gated on the 538 keV transition.
[b]Extracted from the $\gamma\gamma$ matrix gating on the 238 keV transition.

a single exponential decay yielding a half-life of 270(7) ns for the isomeric state. This type of analysis also allowed us to determine the ordering of the 538 and 238 keV transitions. The time distribution of the 238 keV line with respect to the 538 keV transition exhibits a Gaussian shape with an exponential tail. The centroid shift method [16] and the least squares fit of the exponential component result in a half-life of 12(2) ns for the level at 2108 keV as shown in Fig. 4.

In addition to the strong γ rays mentioned above, two more weak transitions at 450 and 765 keV [Fig. 2(d)] are observed in coincidence with the 646 and 785 keV lines and are not present in the 538 keV γ-ray gate. The 450 keV transition was placed as preceding the one with 765 keV based on the weak coincidence relations of the 450 keV γ peak with the 238 and 440 keV transitions. These two γ rays are not in coincidence with the 765 keV transition. The 450 and 765 keV transitions form a parallel branch with an intermediate level at 2195 keV feeding the 4^+ state at 1430 keV. Their time distributions corroborate a one component fit to the decay of the 2714 keV level. The sum energy of the 538, 238, and 440 keV transitions is equal to that of 450 and 765 keV lines forming a state at 2646 keV.

The spin and parity assignment to the excited states is based on the electromagnetic transitions probabilities, relative intensity balance, and inferred conversion coefficients. The isomeric state at 1871 keV decays mainly by a 440 keV $E1\,\gamma$ ray to the 4^+ level with $B(E1;(5^-) \rightarrow 4^+) = 9.74(61) \times 10^{-9}$ W.u. and a parallel branch to the 2^+ by the

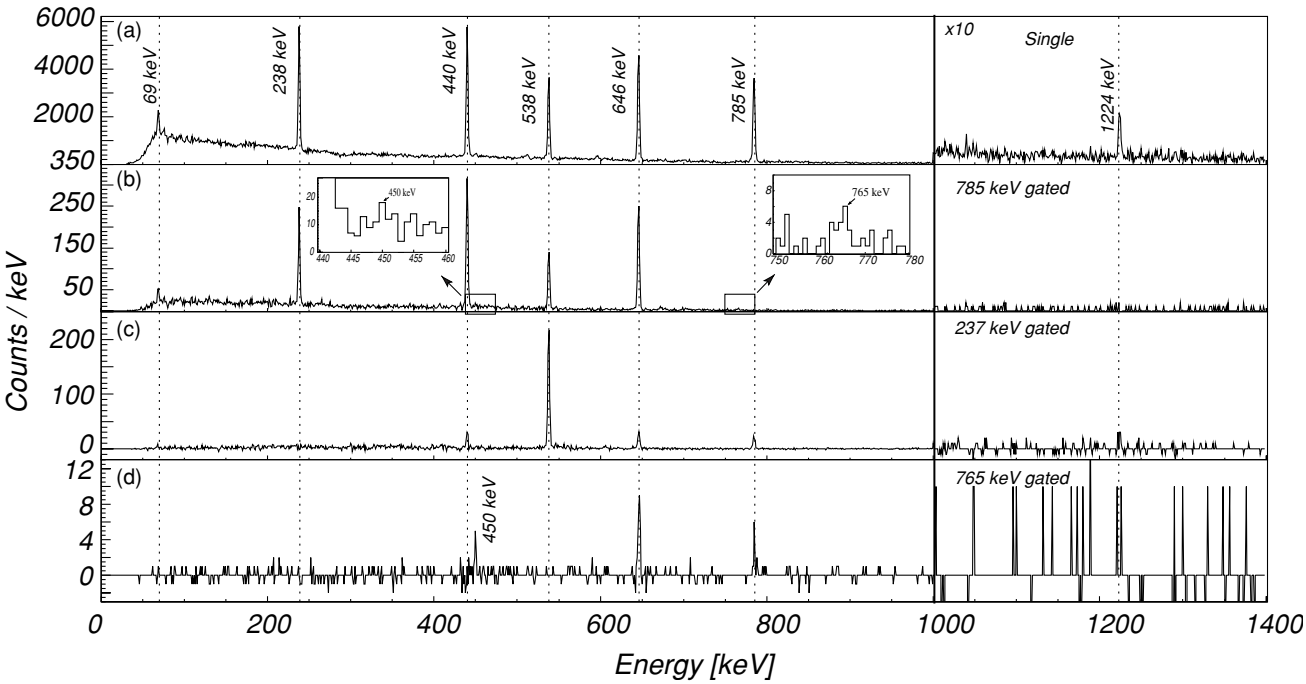

FIG. 2. (a) Singles γ-ray spectrum in coincidence with implanted ^{128}Cd ions. (b) Spectrum from the $\gamma\gamma$ matrix gated by the 785 keV transition with an open time condition applied ($\Delta t = 23.25$ μs). (c, d) Spectra obtained from the $\gamma\gamma$ matrix gated by the 238 and 765 keV transitions with the condition that the time difference between coincident γ rays is less than 125 ns, respectively.

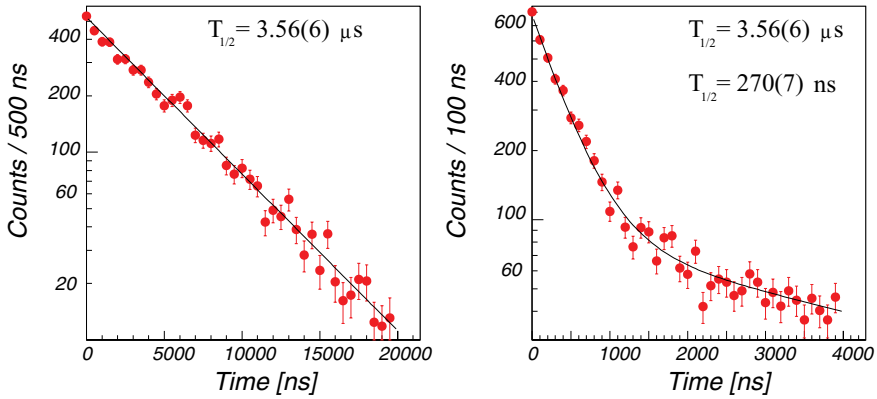

FIG. 3. (Color online) Time distribution relative to the ion implantation of the 238 keV (left) and 646 keV (right) γ transitions.

1224 keV $E3\,\gamma$ line with $B(E3;(5^-)\rightarrow 2^+) = 0.125(13)$ W.u. This $E3$ strength is comparable to the value $B(E3;7^-\rightarrow 4^+) = 0.133$ W.u. in ^{128}Sn [17] four-neutron holes in the doubly magic ^{132}Sn. An $E4$ character for the 1224 keV transition would not account for the experimental half-life; therefore, $I^\pi = (5^-)$ is assigned to the 1871 keV level. The multipolarity assignments for the 238, 450, 538, and 765 keV transitions are based on the following arguments. The 2108 keV isomeric state decays by the 238 keV transition with $B(E2;(7^-)\rightarrow(5^-)) = 1.5(3)$ W.u. strength, a value comparable with the $E2$ strength of a corresponding transition in the isotone ^{130}Sn [18]. The 2646 keV level decays by the emission of a 538 keV γ ray to the 2108 keV level and via a weak 450 keV transition to the 2195 keV state. The $B(E1;8^+\rightarrow 7^-) > 3.5\times 10^{-6}$ W.u. strength in ^{130}Sn [18] would correspond to a half-life of $<$0.5 ns for the 2646 keV state that cannot be excluded from our data. Within the experimental sensitivity the 538 keV transition is emitted promptly after the 69 keV γ ray. Because the spin difference between the 1430 and 2646 keV levels is $4\hbar$, both the 450 and 765 keV γ rays must be $E2$ transitions. The assignment of a higher multipolarity to any of those transitions would lead to a half-life longer than 50 μs for the 2195 or 2646 keV states. The latter is therefore assigned to $I^\pi = (8^+)$. The exchange of the spin and parity for the 2108 and 2195 keV levels would be at variance with the nonobservation of a 325 keV transition feeding the 1871 keV state. Therefore $I^\pi = (7^-)$ is assigned to the 2108 keV level and $I^\pi = (6^+)$ to the excited state at 2195 keV. The isomeric state at 2714 keV excitation energy was attributed spin and parity (10^+). It decays by a 69 keV $E2$ transition of 0.39(1) W.u. strength to the 2646 keV level. The experimental conversion coefficient for this γ ray was extracted by intensity balance arguments to be 6.38(86) in agreement with the theoretical value of $\alpha_{\rm tot}(E2) = 5.9$, thus corroborating this assignment.

The experimental data were compared to the results of large-scale shell-model (LSSM) calculations performed in a model space based on a ^{78}Ni core, comprising the proton $\pi(p_{3/2}, p_{1/2}, f_{5/2}, g_{9/2})$ and neutron $\nu(g_{7/2}, s_{1/2}, d_{5/2}, d_{3/2}, h_{11/2})$ orbitals. The effective interaction was derived from the CD-Bonn nucleon-nucleon potential [19] using G-matrix theory and adapted to the model space using many-body perturbation techniques [20]. Monopole corrections were applied to reproduce correctly the excitation energies of the neutron-rich nuclei below ^{132}Sn [21]. In particular, the evolution of the $1/2^-$ and $9/2^+$ proton doublet along the

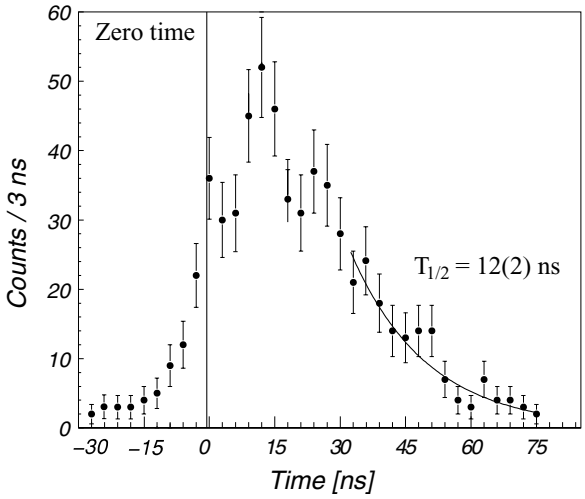

FIG. 4. Time distribution of the 238 keV line with respect to the 538 keV transition. The curve represents the result of the single exponential fit.

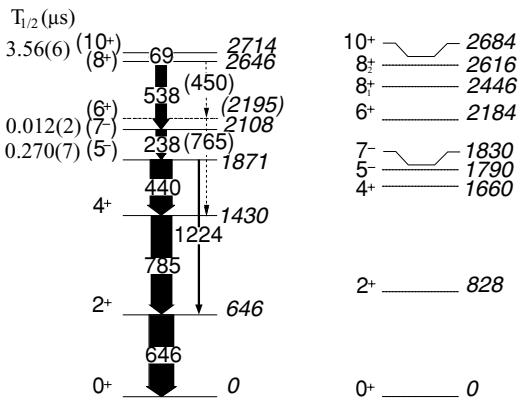

FIG. 5. Comparison of the deduced experimental level scheme for the isomeric deexcitation of ^{128}Cd (left) with shell model calculations (right).

indium chain and the neutron level schemes along the tin chain were reproduced. Because the adjustment of the monopole component of the interaction is part of a general shell model interaction study of the ^{78}Ni to ^{132}Sn model space [22], no further modifications specific for ^{128}Cd were applied. The calculations were performed with the codes ANTOINE and NATHAN [23]. Electromagnetic transition rates were calculated with a standard common polarization charge of 0.5 e for both protons and neutrons.

In Fig. 5 the experimental level scheme is compared to the LSSM calculations. The overall agreement between theory and experiment is satisfying in view of the fact that the spectrum is *a priori* rather complex with the coexistence of proton and neutron states. In particular, the high lying 8_2^+ and 10^+ states have predominant $h_{11/2}^{-2}$ neutron character (cf. ^{130}Sn) and are correctly located with respect to the $0^+ - 8_1^+ g_{9/2}^{-2}$ and $4^-, 5^-, g_{9/2}^{-1} p_{1/2}^{-1}$ proton multiplets (cf. ^{130}Cd). The shift in the excitation energies of the 2^+ and 4^+ states reveals the ground-state sensitivity to the mixing between the $\pi g_{9/2}$ and $\pi p_{1/2}$ proton configuration. An additional binding energy added to the $p_{1/2}$ single particle orbital would reduce the mixing and bring the results in agreement for the 2^+ and 4^+ states, however, at the cost of spoiling the location of the 5^- level. The latter with a predominant $\pi g_{9/2}^{-1} p_{1/2}^{-1}$ proton configuration (70%) is well reproduced in the calculation, whereas a slight discrepancy concerns the 7^- level dominated by the $(d_{3/2})^{-1}(h_{11/2})^{-1}$ neutron configuration that can be possibly traced back to the $\pi g_{9/2} \nu d_{3/2}$ monopole. The 6^+ has a mixed configuration proton-neutron wave function, which explains why it is populated from the neutron 8_2^+ and lies well below the proton 8_1^+ state, which is not seen in experiment (see below). Excellent agreement is, however, found for the energy of the isomeric 10^+ state. It appears to be formed mainly (86%) by the two maximum aligned neutron holes in the $h_{11/2}$ orbital and decays by an $E2$ transition to the 8_2^+ state dominated as well by the two-neutron hole configuration. The calculated 8_1^+ state at energy of 2446 keV is found to have a pronounced (64%) proton component that explains why it is not populated in the isomeric decay of the neutron 10^+. The $E2$ theoretical transition rates of $B(E2; 10^+ \rightarrow 8_2^+) = 0.59$ W.u. and $B(E2; 7^- \rightarrow 5^-) = 0.83$ W.u. agree well with the experimental values 0.39(1) W.u. and 1.5(3) W.u., respectively. The $B(E2; 10^+ \rightarrow 8_1^+) = 0.15$ W.u., though smaller by a factor of four compared to the transition to the 8_2^+, matches nonobservation only if the two 8^+ states are experimentally close in energy.

Summarizing, three isomeric states have been identified with the RISING Ge array in combination with the event-by-event particle identification by the FRS. The $\gamma\gamma$ coincidence and lifetime analysis allowed the construction of the level scheme populated following decays from isomeric states in ^{128}Cd. The experimental data indicate that the isomeric decay pattern is selective to the structure of the populated states and their leading π or ν configuration. This conclusion is further supported by comparison to LSSM calculations that yield an overall good agreement and additionally strengthen the spin and parity assignments. The deviations in level energies between experiment and shell model at intermediate spins reveal the need for a further adjustment of the interaction that could be achieved by minor monopole corrections in those multiplets that are experimentally not well determined in the benchmark nuclei used so far. Theoretical work in the framework of a general shell model study of the ^{78}Ni to ^{132}Sn model space is in progress [22].

This work is supported by the Spanish Ministerio de Educación y Ciencia under Contracts FPA2005-00696 and FPA2007-66069, the European Commission Contract 506065 (EURONS), the Swedish VR, EPSRC, and STFC (United Kingdom), the German BMBF, the Polish Ministry of Science and Higher Education (Grants 1-P03B-030-30 and 620/E-77/SPB/GSI/P-03/DWM105/2004-2007), and the Bulgarian Science Fund.

[1] J. Dobaczewski, I. Hamamoto, W. Nazarewicz, and J. A. Sheikh, Phys. Rev. Lett. **72**, 981 (1994).
[2] I. Dillmann *et al.*, Phys. Rev. Lett. **91**, 162503 (2003).
[3] J. Dobaczewski *et al.*, Phys. Rev. C **53**, 2809 (1996).
[4] J. M. Pearson *et al.*, Phys. Lett. **B387**, 455 (1996).
[5] T. Kautzsch *et al.*, Eur. Phys. J. A **9**, 201 (2000).
[6] A. Jungclaus *et al.*, Phys. Rev. Lett. **99**, 132501 (2007).
[7] M. Górska *et al.* (submitted for publication).
[8] T. Rodríguez, J. L. Egido, and A. Jungclaus, Phys. Lett. **B668**, 410 (2008).
[9] J. K. Hwang, A. V. Ramayya, and J. H. Hamilton, J. Phys. G **35**, 055102 (2008).
[10] A. Scherillo *et al.*, Phys. Rev. C **70**, 054318 (2004).
[11] N. Hoteling *et al.*, Phys. Rev. C **76**, 044324 (2007).
[12] H. Geissel *et al.*, Nucl. Instrum. Methods Phys. Res. B **70**, 286 (1992).
[13] J. Eberth *et al.*, Nucl. Instrum. Methods Phys. Res. A **369**, 135 (1996).
[14] J. Simpson, Z. Phys. A **358**, 139 (1997).
[15] S. Pietri *et al.*, Nucl. Instrum. Methods Phys. Res. B **261**, 1079 (2007).
[16] W. Andrejtscheff *et al.*, Nucl. Instrum. Methods **204**, 123 (1982).
[17] B. Fogelberg and P. Carlé, Nucl. Phys. **A323**, 205 (1979).
[18] B. Fogelberg, K. Heyde, and J. Sau, Nucl. Phys. **A352**, 157 (1981).
[19] R. Machleidt, Phys. Rev. C **63**, 024001 (2001).
[20] M. Hjorth-Jensen, T. T. S. Kuo, and E. Osnes, Phys. Rep. **261** (3&4), 125 (1995).
[21] ENSDF database (28/10/2008), http://www.nndc.bnl.gov/ensdf/.
[22] K. Sieja *et al.* (unpublished).
[23] E. Caurier, G. Martínez-Pinedo, F. Nowacki, A. Poves, and A. P. Zuker, Rev. Mod. Phys. **77**, 427 (2005).

Physics Letters B 672 (2009) 116–119

Contents lists available at ScienceDirect

Physics Letters B

www.elsevier.com/locate/physletb

Proton–hole excitation in the closed shell nucleus ^{205}Au

Zs. Podolyák [a,*], G.F. Farrelly [a], P.H. Regan [a], A.B. Garnsworthy [a], S.J. Steer [a], M. Górska [b], J. Benlliure [c], E. Casarejos [c], S. Pietri [a], J. Gerl [b], H.J. Wollersheim [b], R. Kumar [d], F. Molina [e], A. Algora [e,f], N. Alkhomashi [a], G. Benzoni [g], A. Blazhev [h], P. Boutachkov [b], A.M. Bruce [i], L. Caceres [b,j], I.J. Cullen [a], A.M. Denis Bacelar [i], P. Doornenbal [b], M.E. Estevez [c], Y. Fujita [k], W. Gelletly [a], H. Geissel [b], H. Grawe [b], J. Grębosz [b,l], R. Hoischen [m,b], I. Kojouharov [b], S. Lalkovski [i], Z. Liu [a], K.H. Maier [n,l], C. Mihai [o], D. Mücher [h], B. Rubio [e], H. Schaffner [b], A. Tamii [k], S. Tashenov [b], J.J. Valiente-Dobón [p], P.M. Walker [a], P.J. Woods [q]

[a] *Department of Physics, University of Surrey, Guildford GU2 7XH, UK*
[b] *GSI, Planckstrasse 1, D-64291 Darmstadt, Germany*
[c] *Universidad de Santiago de Compostela, E-15706, Santiago de Compostela, Spain*
[d] *Inter University Accelerator Centre, New Delhi, India*
[e] *Instituto de Fisica Corpuscular, Universidad de Valencia, E-46071, Spain*
[f] *Institute for Nuclear Research, H-4001 Debrecen, Hungary*
[g] *INFN, Universitá degli Studi di Milano, I-20133 Milano, Italy*
[h] *IKP, Universität zu Köln, D-50937 Köln, Germany*
[i] *School of Environment and Technology, University of Brighton, Brighton BN2 4GJ, UK*
[j] *Departamento de Fisica Teórica, Universidad Autonoma de Madrid, E-28049 Madrid, Spain*
[k] *Department of Physics, Osaka University, Toyonaka, Osaka 560-0043, Japan*
[l] *The Henryk Niewodniczański Institute of Nuclear Physics, PL-31-342 Kraków, Poland*
[m] *Department of Physics, Lund University, S-22100 Lund, Sweden*
[n] *Department of Physics, University of West of Scotland, Paisley PA1 2BE, UK*
[o] *"Horea Hulubei" National Institute for Physics and Nuclear Engineering, RO-077125 Bucharest, Romania*
[p] *INFN-Laboratori Nazionali di Legnaro, Italy*
[q] *Department of Physics and Astronomy, University of Edinburgh, UK*

ARTICLE INFO

Article history:
Received 7 July 2008
Received in revised form 26 November 2008
Accepted 7 January 2009
Available online 10 January 2009
Editor: V. Metag

PACS:
25.70.Mn
27.80.+w

ABSTRACT

The neutron-rich $N = 126$ nucleus ^{205}Au has been populated following the relativistic energy projectile fragmentation of $E/A = 1$ GeV ^{208}Pb, and studied via charged-particle decay spectroscopy. An internal decay with a transition energy of 907(5) keV and a half-life of $T_{1/2} = 6(2)$ s has been identified through the observation of the corresponding K and L internal conversion electron lines. The 907 keV energy level corresponds to the $\pi h_{11/2}^{-1}$ proton–hole state and decays both internally into the $\pi d_{3/2}^{-1}$ ground-state and via β decay into ^{205}Hg. The obtained data provides information on the evolution of single-proton hole energies which are vital inputs of shell model descriptions for nuclei around the $^{208}_{82}$Pb$_{126}$ doubly magic core.

Studies of magic nuclei are of fundamental importance in our understanding of nuclear structure since they allow direct tests of the purity of shell model wave functions. Information on the single-particle energies can be derived from the experimental observables such as energies of the excited states and transition probabilities.

The doubly magic ^{208}Pb nucleus, with 82 protons and 126 neutrons, provides the heaviest classic shell model core. Current experimental information on the neutron-rich $N = 126$ nuclei is very scarce. The data on the excited states of proton–hole $N = 126$ isotones is restricted to three nuclei, namely: $^{207}_{81}$Tl [1], $^{206}_{80}$Hg [2] and $^{204}_{78}$Pt [3]. In the case of $^{205}_{79}$Au, only a tentative spin-parity of the groundstate is known [4,5]. The experimental information on the structure of these nuclei can be used as building blocks for calculating more complex configurations. More information is available, more robust predictions can be made on the properties of more neutron-rich species. These are of particular importance as the r-process path nuclei, experimentally unreachable in this mass region so far, are approached [6].

The lack of information on proton–hole nuclei compared to the ^{208}Pb core arises from difficulties in populating such neutron-rich nuclei. Projectile fragmentation has proved to be an efficient tool to produce exotic nuclear species. When projectile fragmentation is combined with high sensitivity gamma detection arrays, struc-

* Corresponding author.
E-mail address: z.podolyak@surrey.ac.uk (Zs. Podolyák).

0370-2693/$ – see front matter
doi:10.1016/j.physletb.2009.01.007

ture information can be gained for otherwise inaccessible nuclei (e.g. ^{204}Pt [3]). The highest sensitivity is achieved with decay spectroscopy. In this technique the delayed gamma rays are correlated with the individually identified ion, therefore minimising the associated background radiation [7–9]. Here we employed a different version of the technique. Conversion electron spectroscopy following relativistic energy fragmentation was performed (according to our knowledge) for the first time.

In this Letter results on the $N = 126$ nucleus ^{205}Au are reported. A beryllium target of thickness 2.5 g/cm^2 was bombarded with an $E/A = 1$ GeV ^{208}Pb beam provided by the SIS accelerator at GSI, Darmstadt, Germany. The nuclei of interest, populated in relativistic energy projectile fragmentation, were separated and identified using the FRagment Separator (FRS) [10] operated in *monochromatic* mode with a wedge-shaped aluminium degrader in the intermediate focal plane of the separator. Niobium foils were placed after both the target and the degrader in order to maximise the electron stripping.

The mass-to-charge ratio of the ions, A/q, was determined from their time of flight and magnetic rigidity measurements in the second part of the FRS. The measured change of the magnetic rigidity of ions before and after they passed through this degrader was used to obtain unambiguous charge identification. The energy deposition of the identified fragments, which gives information on Z, was measured as they passed through two gas ionisation chambers. By determining A/q, the charge state and Z, an unambiguous event-by-event identification has been obtained. The transmitted (and identified) ions were slowed down in a variable thickness aluminium degrader and finally stopped in an active catcher.

The catcher consisted of three 1 mm thick 5×5 cm^2 double sided silicon strip detectors. Each Si had 16 X-strips and 16 Y-strips. The catcher allowed for the detection of both the implanted ion and the subsequent charged particle decay. A charged-particle decay observed in a given pixel was correlated with the previous implant detected in the very same pixel. Due to the large number of pixels, correlation between the implanted ion and the subsequent charged particle decay could be obtained over periods longer than seconds. Semilogarithmic preamplifiers were used, providing linear amplification up to 10 MeV and logarithmic for the 10 MeV–3 GeV range. The linear part allowed for the spectroscopy of the charged particle decay and was calibrated using an open internal conversion electron ^{207}Bi source, yielding an energy resolution of FWHM = 20 keV and a minimum detection threshold of 150 keV [11]. The logarithmic part allowed for the determination of the implantation position and was calibrated with a pulser. For details on the Si catcher and its electronics see Ref. [11]. Scintillation detectors were placed both in front of and behind the catcher, allowing the offline suppression of the majority of fragments destroyed in the slowing down process.

The catcher was surrounded by the high-efficiency, high granularity RISING γ-ray spectrometer in the "Stopped Beam" configuration [12]. The array consists of 15 former Euroball cluster Ge detectors and has a full peak efficiency of 15% at 662 keV [12]. Time-correlated γ decays following both internal-decay and β-decay have been recorded. The experiment was monitored using the Cracow analysis software [13].

A dedicated fragment separator setting was used to study the neutron-rich ^{205}Au nucleus. After the production target the magnetic rigidity of the fully stripped ^{205}Au nuclei is close to those of the intense He-like primary ^{208}Pb beam. In order to avoid this contamination, the first half of the fragment separator was set to transmit the H-like ^{205}Au ions. Although only an estimated 6.5% of the ions of interest were in their H-like charged state [14], the high production cross section in the order of 10^{-2} mbarn [15] ensures sufficient statistics for the current measurement. In the second part of the fragment separator, after the monochromatic degrader, ^{205}Au was transmitted in its fully stripped charged state. This setting provided a beam consisting predominantly ($\sim 55\%$) of ^{205}Au nuclei, as shown in Fig. 1.

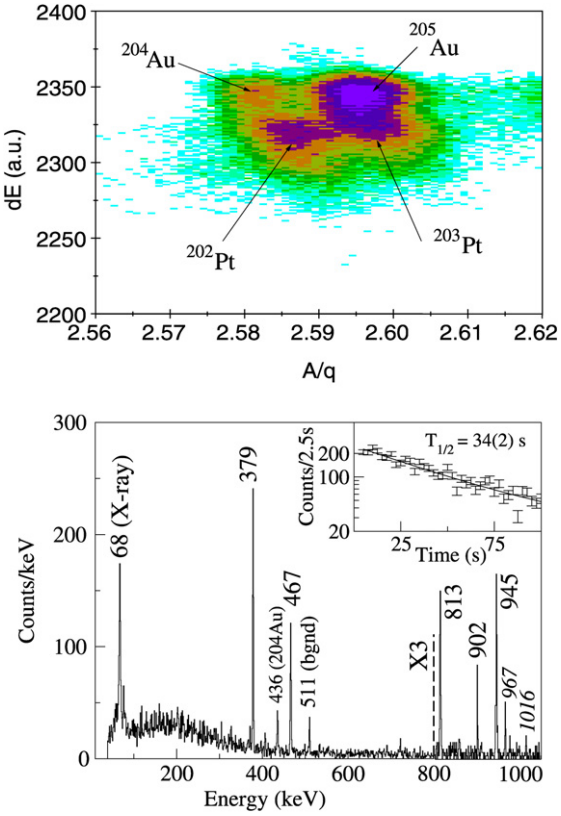

Fig. 1. (Top) Identification plot of the fragments of interest. (Bottom) γ-ray spectrum associated to the β decay of the ^{205}Au ions using a maximum implantation-decay correlation time of 5 s. The labelled peaks, unless stated otherwise, belong to ^{205}Hg [5] and confirm the identification. The peaks labelled in normal letters originate from the previously studied β decay of the ^{205}Au groundstate [4], with the inset showing the corresponding decay curve. The peaks labelled in *italic* are associated with the β decay of the isomeric state of ^{205}Au observed in the present work. For details see the text.

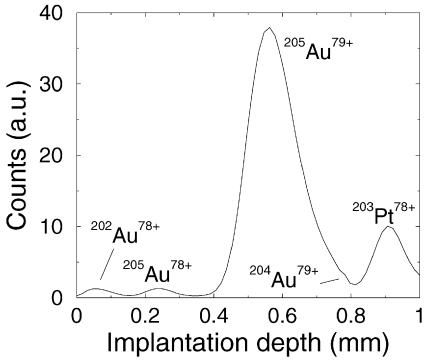

Fig. 2. Simulated implantation profile in the 1 mm thick Si detector.

The primary ^{208}Pb beam intensity was 7×10^8 ion/spill, with the spill consisting of 1 s beam-on period followed by 10 s beam-off. The average implantation yield was ~ 30 ^{205}Au ion/spill, corresponding to a total of 76×10^3 collected ions. The observation of the previously identified γ-ray transitions in ^{205}Hg in coincidence with the β-decay of the ground-state ^{205}Au [4] confirmed the identification (see Fig. 1).

The use of the fragment separator in monochromatic mode allowed for the implantation of ^{205}Au in a thin layer of Si, maximising the efficiency of the charged particle detection. Fig. 2 shows the

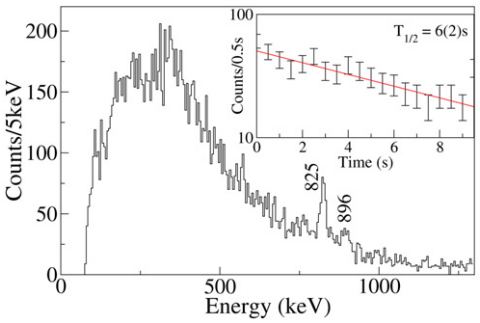

Fig. 3. Delayed charged particle spectrum associated to ^{205}Au. In addition to the continuous energy of the β decay, two peaks are observed. These are interpreted as K and L internal conversion electron peaks corresponding to a 907(5) keV transition.

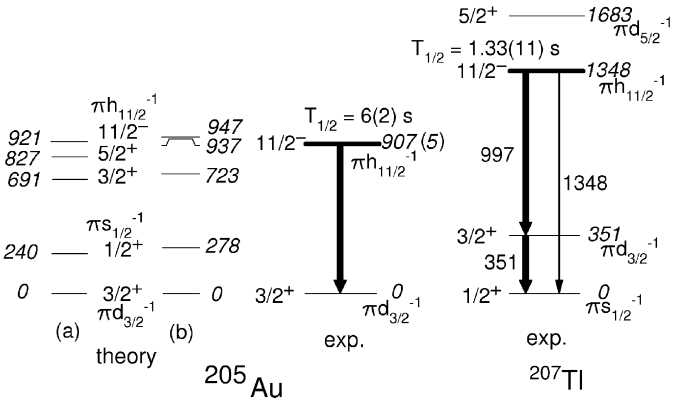

Fig. 4. Calculated and experimental level schemes of ^{205}Au. Calculations have been performed using both the standard set of matrix elements of Ref. [18] (labelled (a)) and a modified set optimised for the description of ^{204}Pt [3] (labelled (b)). For comparison the partial level scheme of ^{207}Tl is also given [1].

simulated range distribution within the 1 mm thick silicon detector. According to these simulations, performed with the LISE code [16], 70% of the implanted ions were ^{205}Au. The delayed charged particle spectrum measured in the Si detector and correlated to the implanted ^{205}Au ions is presented in Fig. 3. In addition to the continuous energy spectrum of the β electron from the ^{205}Au decay, two discrete peaks can be observed. These are interpreted as the K and L internal conversion electrons associated to a γ-ray transition with an energy of 907(5) keV. (Note that the L line contains contribution from the weak and unresolved $M, N, \ldots$ lines.) The energy difference between the K and L lines, as well as the intensity ratio of the two peaks supports this interpretation. The measured lifetime of the decay is $T_{1/2} = 6(2)$ s. This lifetime suggests a transition with M4 or E4 character (considering a transition strength between 10^{-4} and 10^{+3} W.u.).

The γ-ray spectrum associated to the β decay of ^{205}Au is shown in Fig. 1. When compared with that of the previous study of Ch. Wennemann et al. [4], one notices that the spectrum contains two additional transitions with energies of 967 and 1016 keV. These γ lines are clearly visible when a maximum implantation-decay correlation time in the order of seconds is used (5 s in Fig. 1), and they disappear in the background if a much longer maximum correlation time is chosen. These γ lines were previously identified in ^{205}Hg (but not from β decay) and they deexcite states with spin-parities $7/2^-$ and $9/2^-$, respectively [5]. These spins are high when compared to that of the $3/2^+$ groundstate of ^{205}Au, therefore it is unlikely that these γ-ray transitions originate from the β decay of the ^{205}Au groundstate. The lifetimes associated to these two γ-ray transitions are consistent with the 6 s half-life of the conversion electron, and in the case of the stronger 967 keV transition inconsistent with the much longer lifetime of the groundstate β decay. All these experimental findings suggest the identification of an isomeric state in ^{205}Au, and that this state decays both internally and via β decay. The branching ratio between these decays cannot be determined due to poor knowledge of the full peak conversion electron detection efficiency.

The proton–hole orbitals below the $Z = 82$ closed proton shell are $s_{1/2}$, $d_{3/2}$, $h_{11/2}$, $d_{5/2}$ and $g_{7/2}$. The experimental level scheme of the $Z = 81$, $N = 126$ single-hole ^{207}Tl nucleus gives a clear graphical demonstration of this, as shown in Fig. 4. ^{205}Au is a three proton–hole nucleus, with an expected groundstate configuration of $\pi d_{3/2}^{-1}$ (with the $s_{1/2}$ being empty) and spin-parity $I^\pi = 3/2^+$. The $\pi h_{11/2}$ excited state should be long lived since it can decay only through high multipolarity transitions, similarly like in ^{207}Tl. Accordingly, the transition observed in the present experiment should originate from the decay of the $11/2^-$ isomeric state. The experimentally identified 907(5) keV transition corresponds to the $11/2^- \rightarrow 3/2^+$ transition of M4 character and a theoretical internal conversion coefficient [21] of $\alpha = 0.18$. The relatively high electron conversion coefficient together with the high energy of the transition, a rare combination, made possible the identification of this transition with the present method.

In order to obtain a quantitative understanding of the underlying single-particle structure of the excited states of ^{205}Au, shell-model calculations have been performed employing the OXBASH code [17]. The standard interaction two-body matrix elements (TBMEs) were used as taken from Ref. [18]. They are based on the Kuo–Brown interaction including core polarisation [19,20], with slight modifications introduced to obtain an improved description of the experimental data available at the time. The proton–hole energies were taken from the experimental level scheme of ^{207}Tl [1]. This parameterisation gives a good description of the reported excited states in the two proton–hole ^{206}Hg [2] and reasonable description for the four proton–hole nucleus ^{204}Pt [3]. In order to get a good description for all available information on the $N = 126$ isotones below lead, both on excitation energies and transition strengths, small modifications of the standard TBMEs were required [3]. Calculations with these modified matrix elements were also performed. The results of the calculations for ^{205}Au, using both sets of TBMEs, are compared with the experimental level schemes in Fig. 4. The dominant configurations are also indicated.

The measured energy of the isomeric state with the proposed $11/2^-$ spin-parity is in good agreement with the shell model calculations. The calculations also predict a $5/2^+$ state to lie below the $11/2^-$ isomer, therefore the isomer could decay into it via an E3 transition. The Weisskopf estimate for the partial lifetime of this transition is in the order of 0.1 s. This transition, even if it exists, could not be observed in the present experiment: the energy of the corresponding conversion electron is low and could not be discerned from the background; the γ branch could have not been correlated with the ^{205}Au ions due to the long lifetime of the isomer. As a consequence, the M4/E3 branching ratio could not be ascertained in the current work. Since the $11/2^-$ isomeric state β decays and possibly decays internally through an E3 branch, only an upper limit for the B(M4) transition strength was determined, $B(\mathrm{M4}) \leqslant 1.7(7)$ W.u. This limit is somewhat lower than that of the equivalent M4 transition strength, 3.2(3) W.u. [1], in ^{207}Tl, and similar to those determined in lighter gold isotopes: 2.4(8) W.u. in ^{197}Au [22] and 2.2(3) W.u. in ^{195}Au [23]. This suggests that the E3 branching might be missing altogether, possible because the $5/2^+$ state lies above the $11/2^-$ isomer.

In conclusion, an excited state in the neutron-rich $N = 126$ ^{205}Au nucleus has been identified through conversion electron spectroscopy. It has an excitation energy of 907(5) keV and a half-life of $T_{1/2} = 6(2)$ s. It corresponds to the $\pi h_{11/2}^{-1}$ single proton–

hole excitation and decays both internally into the $\pi d_{3/2}^{-1}$ ground-state and via β decay into excited states of ^{205}Hg. The energy of the isomeric state is in good agreement with the shell-model calculations.

Acknowledgements

The excellent work of the GSI accelerator staff is acknowledged. This work is supported by the EPSRC (UK), STFC (UK), the EU Access to Large Scale Facilities Programme (EURONS, EU contract 506065), The Spanish Ministerio de Educacion y Ciencia and The German BMBF.

References

[1] D. Eccleshall, M.J.L. Yates, Phys. Lett. 19 (1965) 301; M.J. Martin, Nucl. Data Sheets 70 (1993) 315.
[2] B. Fornal, et al., Phys. Rev. Lett. 87 (2001) 212501.
[3] S. Steer, et al., Phys. Rev. C 78 (2008) 061302(R).
[4] Ch. Wennemann, et al., Z. Phys. A 347 (1994) 185.
[5] F.G. Kondev, Nucl. Data Sheets 101 (2004) 521.
[6] H. Grawe, K. Langanke, G. Martinez-Pinedo, Rep. Prog. Phys. 70 (2007) 1525.
[7] R. Grzywacz, et al., Phys. Lett. B 335 (1995) 439.
[8] M. Pfützner, et al., Phys. Lett. B 444 (1998) 32.
[9] Zs. Podolyák, et al., Phys. Lett. B 491 (2000) 225.
[10] H. Geissel, et al., Nucl. Instrum. Methods Phys. Res. Sect. B 70 (1992) 286.
[11] R. Kumar, et al., Nucl. Instrum. Methods A 598 (2009) 754.
[12] S. Pietri, et al., Nucl. Instrum. Methods B 261 (2007) 1079; P.H. Regan, et al., Nucl. Phys. A 787 (2007) 491c.
[13] J. Grebosz, Comput. Phys. 176 (2007) 251.
[14] C. Scheidenberger, et al., Nucl. Instrum. Methods B 142 (1998) 441.
[15] L. Audouin, et al., Nucl. Phys. A 768 (2006) 1.
[16] D. Bazin, O. Tarasov, M. Lewitowicz, O. Sorlin, Nucl. Instrum. Methods A 482 (2002) 307.
[17] B.A. Brown, A. Etchegoyen, W.D.M. Rae, The computer code OXBASH, MSU-NSCL report number 524.
[18] L. Rydström, et al., Nucl. Phys. A 512 (1990) 217.
[19] T.T.S. Kuo, G.H. Herling, Naval Research Laboratory Report 2259 (Washington, DC, 1971).
[20] G.H. Herling, T.T.S. Kuo, Nucl. Phys. A 181 (1972) 113.
[21] T. Kibédi, T.W. Burrows, M.B. Trzhaskovskaya, C.W. Nestor Jr., AIP Conf. Proc. 769 (2005) 268.
[22] X. Huang, C. Zhou, Nucl. Data Sheets 104 (2005) 283.
[23] C. Zhou, Nucl. Data Sheets 86 (1999) 645.

Physics Letters B 672 (2009) 313–316

Contents lists available at ScienceDirect

Physics Letters B

www.elsevier.com/locate/physletb

Evolution of the $N = 82$ shell gap below ^{132}Sn inferred from core excited states in ^{131}In

M. Górska [a,*], L. Cáceres [a,b], H. Grawe [a], M. Pfützner [c], A. Jungclaus [b,d], S. Pietri [e,1], E. Werner-Malento [c,2], Z. Podolyák [e], P.H. Regan [e], D. Rudolph [f], P. Detistov [g], S. Lalkovski [g,h], V. Modamio [b], J. Walker [b], T. Beck [a], P. Bednarczyk [a,i], P. Doornenbal [a,j,3], H. Geissel [a], J. Gerl [a], J. Grębosz [a,i], R. Hoischen [f,a], I. Kojouharov [a], N. Kurz [a], W. Prokopowicz [a,i], H. Schaffner [a], H. Weick [a], H.-J. Wollersheim [a], K. Andgren [k], J. Benlliure [l], G. Benzoni [m], A.M. Bruce [h], E. Casarejos [l], B. Cederwall [k], F.C. L. Crespi [m], B. Hadinia [f], M. Hellström [f], G. Ilie [j,n], A. Khaplanov [k], M. Kmiecik [i], R. Kumar [o], A. Maj [i], S. Mandal [p], F. Montes [a], S. Myalski [i], G.S. Simpson [q], S.J. Steer [e], S. Tashenov [a], O. Wieland [m], Zs. Dombrádi [r], P. Reiter [j], D. Sohler [r]

[a] *Gesellschaft für Schwerionenforschung (GSI), D-64291 Darmstadt, Germany*
[b] *Departamento de Física Teórica, Universidad Autónoma de Madrid, E-28049 Madrid, Spain*
[c] *IEP, University of Warsaw, PL-00681 Warsaw, Poland*
[d] *Instituto de Estructuras de la Materia, CSIC, Serrano113bis, E-28006 Madrid, Spain*
[e] *Department of Physics, University of Surrey, Guildford, GU2 7XH, UK*
[f] *Department of Physics, Lund University, S-22100 Lund, Sweden*
[g] *Faculty of Physics, University of Sofia, BG-1164 Sofia, Bulgaria*
[h] *School of Enviroment and Technology, University of Brighton, Brighton, BN2 4GJ, UK*
[i] *The Henryk Niewodniczański Institute of Nuclear Physics, PAN, PL-31342 Kraków, Poland*
[j] *Institut für Kernphysik, Universität zu Köln, D-50937 Köln, Germany*
[k] *Department of Physics, The Royal Insitute of Technology, SE-106 91 Stockholm, Sweden*
[l] *Universidade de Santiago de Compostela, E-15782 Santiago de Compostela, Spain*
[m] *INFN, Universitá degli Studi di Milano and INFN sezione di Milano, I-20133 Milano, Italy*
[n] *National Intitute of Physics and Nuclear Engineering, Bucharest, Romania*
[o] *Inter University Accelerator Centre, New Delhi, India*
[p] *University of Delhi, New Delhi, India*
[q] *LPSC, Université Joseph Fourier Grenoble 1, CNRS/IN2P3, Institute National Polytechnique de Grenoble, F-38026 Grenoble Cedex, France*
[r] *Institute of Nuclear Research of the Hungarian Academy of Sciences, H-4001 Debrecen, Hungary*

ARTICLE INFO

Article history:
Received 13 August 2008
Received in revised form 28 November 2008
Accepted 15 January 2009
Available online 21 January 2009
Editor: V. Metag

PACS:
21.10.-k
21.10.Pc
21.10.Tg
21.60.Cs
23.20.Lv

ABSTRACT

The γ-ray decay of an excited state in ^{131}In, the one proton hole neighbor of the doubly magic ^{132}Sn has been measured. A high-spin, core-excited isomer with $T_{1/2} = 630(60)$ ns was identified following production by both relativistic fragmentation of a ^{136}Xe beam and fission of a ^{238}U beam. This state deexcites by a single γ-ray branch of 3782(2) keV from which direct evidence for the size of the $N = 82$ shell gap is inferred. The results are discussed in comparison to a shell-model calculation including configurations across the closed shells at $N = 82$ and $Z = 50$.

Shell evolution in nuclei has been an outstanding subject in nuclear structure physics of the last decade. Two main mechanisms are predicted to drive the possible shell evolution phenomena: the so-called monopole migration [1] acting for proton-rich nuclei as well as those with neutron excess, and the second, shell quenching due to a softening of the potential shape by excessive neutrons, especially pronounced in very neutron-rich nuclei [2]. These mech-

* Corresponding author.
E-mail address: m.gorska@gsi.de (M. Górska).
[1] Present address: GSI Darmstadt, Germany.
[2] Present address: IF PAN, Warsaw, Poland.
[3] Present address: RIKEN, Japan.

0370-2693/$ – see front matter
doi:10.1016/j.physletb.2009.01.027

anisms modify the known magic numbers as a consequence of shifting effective single-particle levels when going towards either the proton or the neutron drip lines. In medium-heavy nuclei the effort to establish shell evolution concentrates around the ^{100}Sn [3] and ^{132}Sn [4,5] doubly magic nuclei. The Sn isotopes form the longest isotopic chain in the nuclear chart accessible to current experimental study and thus provide a stringent testing ground for nuclear structure models. A remarkable similarity was found between the decay of 8^+ isomers in ^{98}Cd$_{50}$ [6] and ^{130}Cd$_{82}$ [5] which both have a pure $g_{9/2}^{-2}$ proton-hole configuration. However, the analogue of the known core excited isomer in ^{98}Cd [7] was not observed in ^{130}Cd within experimental sensitivity underlining the differences in the underlying neutron single particle structure. The understanding of analogies in the structure of both regions of nuclei and the evolution of the $N = 82$ shell gap below ^{132}Sn is of importance in predicting the path of the rapid-neutron capture r-process which partially drives the production of elements heavier than Fe in nature. Only in one $N = 82$ r-process waiting point nucleus, namely ^{130}Cd [5], have excited states been identified to date. In that case the persistence of the 8^+ isomer and the decay halflife suggested that no substantial shell gap reduction was present.

The expectation that magic numbers may be altered in nuclei far from the valley of stability has provided significant motivation for experiments with rare isotope beams coupled to the most efficient detector setups. At GSI Darmstadt the power of the FRagment Separator (FRS) spectrometer [8] in separating and selecting secondary radioactive beams has been combined with a highly efficient Ge array to form the RISING project [9,10]. The identification of a core excited state in ^{131}In (i.e., the single proton hole neighbour of ^{132}Sn) using the RISING setup, is presented in the current work. The excitation energy of this state provides a more direct measure of the size of the $N = 82$ shell energy gap than the qualitative conclusion drawn from ^{130}Cd isomerism [5]. To date only two β-emitting isomers have been identified above the $(9/2^+)$ ground state in ^{131}In with proposed spin-parity $(1/2^-)$ and $(21/2^+)$ and excitation energies inferred from Q_β measurements [11].

The experiment to identify the γ decay of excited states in ^{131}In was performed using primary beams of ^{136}Xe at 750 MeV/u and ^{238}U at 650 MeV/u to populate ^{131}In following projectile fragmentation and fission reactions on Be targets of 4 g/cm^2 and 1 g/cm^2 thickness, respectively. The secondary beams were separated and identified event-by-event with respect to their nuclear charge (Z) and mass (A) using the FRS [8], and implanted at the final focal plane in a passive stopper made of plastic to reduce the rate of electromagnetic atomic radiation produced during the implantation process. Gamma rays emitted in the isomeric decay process were measured in an array of 15 Cluster detectors [12] from the former Euroball spectrometer [13], which surrounded the stopper in a compact geometry, such that high detection efficiency could be achieved with high granularity. The photo-peak efficiency for the RISING array in the configuration used in the current work covered a range from 3.0(3)% at 45 keV, passing a maximum of 25(1)% at $\sim$ 65 keV and falling to 5.1(2)% for a 3.8 MeV gamma ray. More details on the Ge array are given in Ref. [10]. Directly after the ion implantion, γ rays were registered within a 50 µs time window.

An identification plot obtained from the fission experiment is shown in Fig. 1 where the A/Z distribution in a gate on implanted $Z = 49$ ions is indicated. A total sum of 175,000 ^{131}In ions were identified in the fission and fragmentation experiments. The γ-ray spectrum in delayed coincidence with fully stripped ^{131}In ions is shown in Fig. 2. Only one γ ray transition at 3782(2) keV energy is clearly visible. Additional counts of this γ ray were registered at 3271(2) keV from the single escape peak. The halflife of the

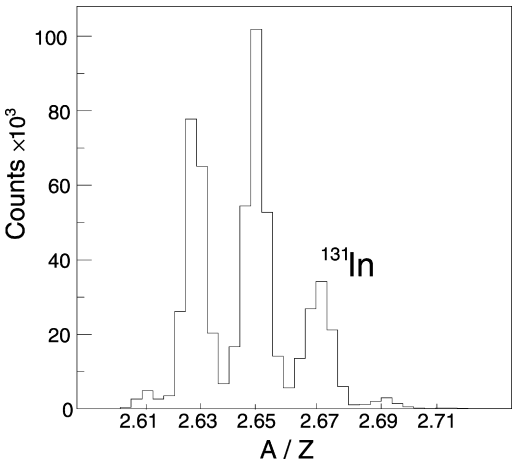

Fig. 1. The experimental spectrum of the A/Z value for In isotopes obtained in the fission experiment.

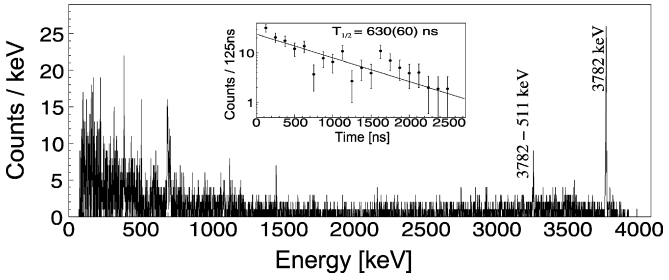

Fig. 2. Gamma ray energy spectrum of the isomeric decay in ^{131}In. Inset: Time distribution of the 3782 keV transition with a single component exponential fit.

isomeric state was extracted based on a least-squares fit of the time distribution of the 3782 keV transition to a single exponential decay curve, resulting in a value of $T_{1/2} = 630(60)$ ns as shown in the inset of Fig. 2. No other transitions associated with ^{131}In were observed within the sensitivity range i.e., from 55 keV to 6 MeV. For any transition with lower than the observed energy the efficiency would be significantly higher unless such transitions were highly converted. Low-energy transitions of different possible multipolarities are distinguished by their decay modes (conversion electron vs. γ-ray emission) and γ detection sensitivity. Assuming the same total intensity for a low-energy transition as for the 3782 keV line, the lower γ-ray observational limits of 52, 59, and 77 keV for E1, M1, and E2 transitions, respectively, were extracted based on the experimental data.

If the isomer decays by a 100% branch of a non-observed primary transition with an energy between the observational limit and the indium L-binding energy, the following limits for transition probabilities are derived from the measured half life: 1.3×10^{-6} W.u. $\leqslant B(\mathrm{E1}) \leqslant 3.0 \times 10^{-5}$ W.u., 1.5 W.u. $\leqslant B(\mathrm{E2}) \leqslant 9.2$ W.u., and 0.38×10^{-4} W.u. $\leqslant B(\mathrm{M1}) \leqslant 6.4 \times 10^{-4}$ W.u., respectively. The possibility of an $M1$ transition can be ruled out as values of 10^{-4} W.u. correspond to a retardation an order of magnitude larger than has been observed for M1 transitions between core excited states in ^{132}Sn [14]. The required E2 strength is rather large in comparison to the strengths of less than the 0.6 W.u. observed between core excited states in ^{132}Sn [14] but cannot be firmly excluded. Allowing E1 or E2 multipolarity for a possible non-observed transition in cascade with a $\Delta I = 0 - 3$ fast 3782 keV γ ray to the $(9/2^+)$ ground state would require a competing, high energy crossover transition of multipolarity E3, M3, E4 which would be well within the detection sensitivity. A lower multipolarity cross-over transition would destroy the isomerism while higher multipolarity transitions such as M4, M5, E5 would have too

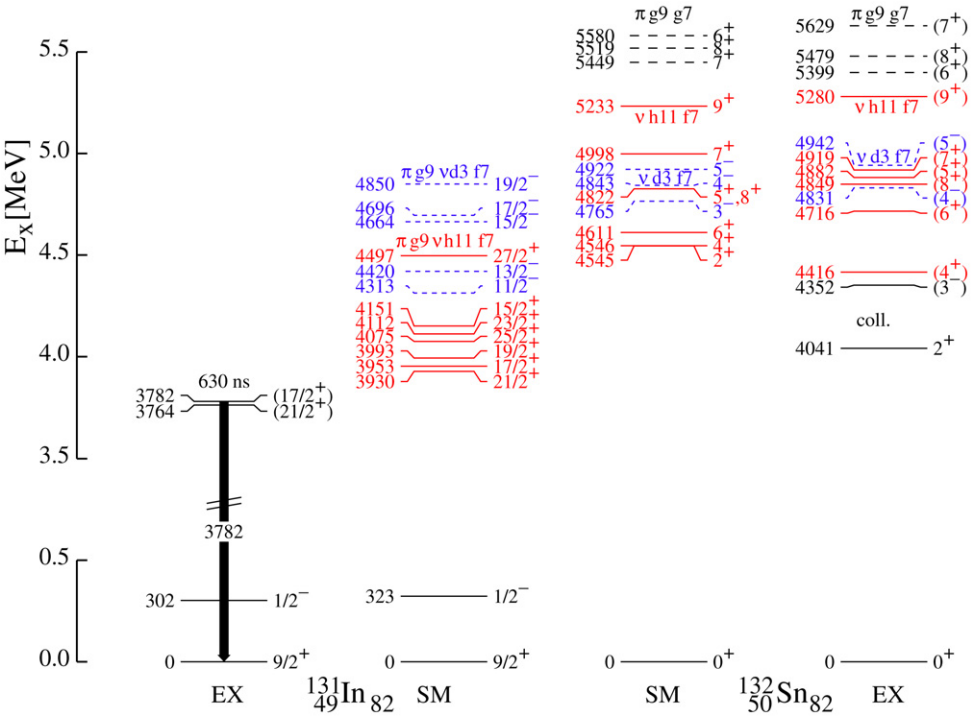

Fig. 3. Experimental level scheme in comparison to shell model calculation for ^{131}In and ^{132}Sn (colored in electronic version). The core excited states are labelled according to their leading configuration $\nu h^{-1}_{11/2} f_{7/2}$ (red—full line), $\nu d^{-1}_{3/2} f_{7/2}$ (blue—short-dashed) and $\pi g^{-1}_{9/2} g_{7/2}$ (black—long dashed). (For interpretation of the references to color in this figure legend, the reader is referred to the web version of this Letter.)

small partial width to compete. This leaves possible spin-parity assignments of $17/2^{\pm}$ and $19/2^{-}$for the isomer in this scenario as $19/2^{+}$ would allow an $M1$ to the $21/2^{+}$ isomer at variance with the observed half life (see above). Odd-parity assignments are unlikely as the corresponding odd-parity $(4,5)^{-}$ core states in ^{132}Sn needed to couple the proton $g_{9/2}$ hole to the required spin lie 400–500 keV above the 4^{+} state which can be coupled to $17/2^{+}$ (see Fig. 3).

A 3782 keV primary transition is compatible with E4 multipolarity, resulting in a $(17/2^{+})$ assignment for the isomer with decay strength of $B(\mathrm{E4}) = 1.48(14)$ W.u., similar to those reported in ^{132}Sn [14] and ^{98}Cd [7]. Any single γ ray or cascade feeding the $(1/2^{-})$ isomer can be excluded due to fast competing branches from the isomer to the ground state or the $(1/2^{-})$ state. On this basis, we assigned the observed 3782 keV transition to the direct decay from a $I^{\pi} = (17/2^{+})$ isomer to the ground state.

The isomeric ratio, defined as the ratio of nuclei in excited states to the total number of nuclei amounts to 4.0(4)% averaged from fission and fragmentation data and is consistent with a relatively high spin and/or non yrast isomeric state [15,16], consistent with the proposed $(17/2^{+})$ assignment.

The ground state of ^{131}In is reported from beta decay measurements to be $(9/2^{+})$ [11] and is understood as one proton hole in the $g_{9/2}$ orbital. The first excited state at 302 keV energy [17] is the isomeric $(1/2^{-})$ state [11] formed when a proton from the $p_{1/2}$ orbit is excited, thereby filling the $g_{9/2}$ orbital. In the same work a high-spin beta-decaying isomer at 3764(88) keV excitation energy was also observed and interpreted as a $(21/2^{+})$ state based on its feeding to the $19/2^{+}$, $19/2^{-}$ and the $(23/2^{-})$ states in the daughter ^{131}Sn. In this earlier work [11] a neutron core excitation $\pi g^{-1}_{9/2} \nu h^{-1}_{11/2} f_{7/2}$ configuration was suggested for this isomer based on the fact that no proton-hole state configuration could explain the existence of that high-spin state. In the present work, due to the finite time correlation window, no beta decaying states were associated with γ rays and only the direct γ decay from isomeric states was registered. The proposed $(17/2^{+})$ state established at an excitation energy of 3782 keV must therefore lie above the $(21/2^{+})$ isomer at 3764(88) keV [11,14]. A possible highly converted, low energy E2 branch to this state makes the measured E4 strength an upper limit and explains the small isomeric ratio.

We have performed shell-model calculations in the proton $\pi(p_{1/2}, g_{9/2}, g_{7/2}, d_{5/2})$ and neutron $\nu(s_{1/2}, h_{11/2}, d_{3/2}, f_{7/2}, h_{9/2})$ model space using a ^{132}Sn core and experimental single-particle (hole) energies [14,18]. The two-body matrix elements (TBME) of the residual interaction were inferred from a realistic interaction for ^{208}Pb [19], one harmonic oscillator shell higher, replacing single-particle orbits (n, l, j) by $(n, l-1, j-1)$, which maintains the proper radial wave functions following the prescription given in Ref. [20]. The interaction strength was scaled up by $(208/132)^{1/3}$, and for intermediate spins in a multiplet interpolated according to their angular orbital overlap [21]. Calculations were performed using the code OXBASH [22]. Only $1p1h$ excitations were allowed for each valence orbit. The ph TBME for the 4^{+}, 6^{+} and 9^{+} states of the $\nu h^{-1}_{11/2} f_{7/2}$ configuration, and the 3^{-} state of the $\nu d^{-1}_{3/2} f_{7/2}$ were changed by -200, -200, $+200$, and -250 keV, respectively, to improve the relative level positions in the benchmark nucleus ^{132}Sn. In addition the monopoles for the $\nu h^{-1}_{11/2} f_{7/2}$, $\nu d^{-1}_{3/2} f_{7/2}$ and $\pi g^{-1}_{9/2} g_{7/2}$ multiplets were tuned to reproduce the corresponding unambiguously identified members of the multiplets in ^{132}Sn. These modifications compensate partly for the truncation which affects low-spin states in the multiplets stronger than the stretched coupled states. E2 and E4 transition strengths were calculated with effective charges of 1.5 e [5] and 0.7 e [23] for protons and neutrons, respectively. The results for levels in ^{132}Sn and ^{131}In are compared to experiment in Fig. 3. For ^{132}Sn a one-to-one correspondence between the experimental and shell model sequences of states is found with neutron core excitations being energetically favoured. The low-spin states $I^{\pi} = 2^{+}, (4^{+}), (3^{-})$ of collective character cannot be expected to be reproduced quantitatively in a $1p1h$ calculation. The high-spin states such as $I^{\pi} = 9^{+}$ agree well with experiment. Deviations are therefore ascribed to the trunca-

tion and the interaction is considered to be reliable. For ^{131}In the shell-model level sequence supports the spin-parity assignments of the isomers in the present and previous work. The predicted E4 strength of the $(17/2^+) \rightarrow (9/2^+)$ transition in ^{131}In is calculated to be 2.4 W.u., which compares well with the experimental upper limit of 1.6 W.u. which takes into account a possible non-observed E2 branch to the $(21/2^+)$ isomer. The reduction of the strength relative to the $4^+ \rightarrow 0^+$ transition in ^{132}Sn is due to the fact that the $17/2^+$ wave function besides the $g_{9/2}^{-1} \times 4^+$ components contains also couplings to the higher spin $(5\text{–}9)^+$ states which do not contribute to the E4 transition. With the shell model prediction of $B(\mathrm{E2}; 17/2^+) \rightarrow (21/2^+) = 0.29$ W.u. a total branch of $\leqslant 17\%$, which includes electron conversion and γ decay, is calculated for transition energies below the observational limit of 77 keV.

The extraction of a shell gap from the excitation energies of the $I^\pi = (21/2^+)$ and $(17/2^+)$ isomers in ^{131}In requires a careful assessment of the residual interaction. The standard procedure to extract a shell gap Δ for an even-even core nucleus involves the ground state binding energies (BE) of its odd–even neighbours according to $\Delta(Z,N) = 2\mathrm{BE}(Z,N) - \mathrm{BE}(Z,N+1) - \mathrm{BE}(Z,N-1)$ for neutrons and for protons accordingly [24]. This is equivalent within a few tens of keV to the spin-multiplicity weighted average of the excitation energies of a complete multiplet which can be verified for ^{132}Sn (Fig. 3) even if the low-spin $I^\pi = 2^+$ (collective) and 3^+ (not known) states are omitted. This method, however, is not applicable to an odd–even core nucleus like ^{131}In as the BE of the odd–odd neighbours is strongly determined by the residual interaction which is binding in the hole-hole neighbour ^{130}In while it is repulsive in the particle-hole case of ^{132}In. The $Z = 50$ shell gaps in the Sn isotopic chain provide a textbook example for this effect. The effect is evident in the SM results of Fig. 3, where the centroids of the $\nu h_{11/2}^{-1} f_{7/2}$ multiplet in ^{132}Sn and the respective $\pi g_{9/2} \nu h_{11/2}^{-1} f_{7/2}$ states in ^{131}In are shifted by about 910 keV which would indicate an apparently dramatic but erroneous shell gap reduction. The overall good agreement for core excited states in ^{132}Sn and ^{131}In in both sequence and maximum spin states, suggests that the interaction for the respective *ph* multiplets is well accounted for in the shell model calculation, which therefore can be used to infer consistently with ^{132}Sn a shell gap Δ for the even-even core ^{130}Cd from the calculated ground state binding energies of $^{129\text{–}131}$Cd. The result is a considerable decrease of the ^{132}Sn neutron gap of 4.89(8) MeV [14] by 610(100) keV which, however, is in the range of e.g. the reduction of the $Z = 50$ gap from $N = 82$ to 80 [25] of 680 keV. The uncertainty of the reduction due to interaction and truncation is estimated from the mean level deviation [21] within the $\nu h_{11/2}^{-1} f_{7/2}$ multiplet in ^{132}Sn and includes the experimental error in the $N = 82$ gap in the core nucleus. It is therefore concluded that the shell-gap reduction does not need any quenching mechanism due to excessive neutrons but can be explained by classical monopole-driven shell evolution. We note in passing that the interaction used does not predict a $1p1h$ isomer in ^{130}Cd.

In conclusion, a core-excited γ-decaying isomer has been identified in ^{131}In using the RISING-FRS setup. The data on energies and transition strengths are well reproduced by shell model calculations including $1p1h$ configurations. Based on the calculations, the shell gap in ^{130}Cd is inferred and interpreted as monopole driven.

Acknowledgements

We would like to thank Prof. B.A. Brown from MSU for valuable discussions. This work is supported by the EU Access to Large Scale Facilities Programme (EURONS, EU contract 506065), the Polish Ministry of Science and Higher Education (1-P03B-030-30 and 620/E-77/SPB/GSI/P-03/DWM105/2004-2007), the Spanish Ministerio de Educacion y Ciencia (FPA2005-00696, FPA2005-00732 and FPA2007-66069), EPSRC/STFC (UK), The Swedish Research Council, The Bulgarian Science Fund VUF06/05, The US Dept. of Energy (DE-FG02-91ER-40609 and DE-AC02-06CH11357), The German Federal Ministry of Education and Research (06KY205I), The Hungarian Science Foundation (OTKA K-68801) and the Italian INFN.

References

[1] T. Otsuka, et al., Phys. Rev. Lett. 95 (2005) 232502.
[2] J. Dobaczewski, I. Hamamoto, W. Nazarewicz, J.A. Sheik, Phys. Rev. Lett. 72 (1994) 981.
[3] H. Grawe, et al., Eur. Phys. J. 27 (2006) 257.
[4] A. Shergur, et al., Eur. Phys. J. A 25 (2005) 121.
[5] A. Jungclaus, et al., Phys. Rev. Lett. 99 (2007) 132501.
[6] M. Górska, et al., Phys. Rev. Lett. 79 (1997) 2415.
[7] A. Blazhev, et al., Phys. Rev. C 69 (2004) 064304.
[8] H. Geissel, et al., Nucl. Instrum. Methods Phys. Res. B 70 (1992) 286.
[9] H.-J. Wollersheim, et al., Nucl. Instrum. Methods Phys. Res. A 537 (2006) 637.
[10] S. Pietri, et al., Nucl. Instrum. Methods Phys. Res. B 261 (2007) 1079.
[11] B. Fogelberg, J. Blomqvist, Nucl. Phys. A 429 (1984) 205.
[12] J. Eberth, et al., Nucl. Instrum. Methods Phys. Res. A 369 (1996) 135.
[13] J. Simpson, Z. Phys. A 358 (1997) 139.
[14] ENSDF database, http://www.nndc.bnl.gov/ensdf/.
[15] M. Pfützner, et al., Phys. Rev. C 65 (2002) 064604.
[16] Zs. Podolyak, et al., Phys. Lett. B 632 (2006) 203.
[17] B. Fogelberg, et al., Phys. Rev. C 70 (2004) 034312.
[18] H. Grawe, K. Langanke, G. Martínez-Pinedo, Rep. Prog. Phys. 70 (2007) 1525.
[19] E.K. Warburton, Phys. Rev. C 44 (1991) 233.
[20] J. Blomqvist, CERN Report No. 81-09, CERN, Geneva, 1981, p. 535.
[21] H. Grawe, Springer Lect. Notes Phys. 651 (2004) 33.
[22] B.A. Brown et al., Oxbash for windows, MSU-NSCL report 1289, 2004.
[23] R. Lozeva, et al., Phys. Rev. C 77 (2008) 064313.
[24] B.A. Brown, Rep. Progr. Phys. 47 (2001) 517.
[25] A.H. Wapstra, G. Audi, C. Thibault, Nucl. Phys. A 729 (2003) 337.

PHYSICAL REVIEW C **79**, 031305(R) (2009)

Weakly deformed oblate structures in $^{198}_{76}Os_{122}$

Zs. Podolyák,[1,*] S. J. Steer,[1] S. Pietri,[1] F. R. Xu,[2] H. L. Liu,[2] P. H. Regan,[1] D. Rudolph,[3] A. B. Garnsworthy,[1,4] R. Hoischen,[3,5] M. Górska,[5] J. Gerl,[5] H. J. Wollersheim,[5] T. Kurtukian-Nieto,[6] G. Benzoni,[7] T. Shizuma,[1,8] F. Becker,[5] P. Bednarczyk,[5,9] L. Caceres,[5,10] P. Doornenbal,[5] H. Geissel,[5] J. Gręboszz,[5,9] A. Kelic,[5] I. Kojouharov,[5] N. Kurz,[5] F. Montes,[5] W. Prokopowicz,[5,9] T. Saito,[5] H. Schaffner,[5] S. Tashenov,[5] A. Heinz,[4] M. Pfützner,[11] A. Jungclaus,[10] D. L. Balabanski,[12] C. Brandau,[1] A. M. Bruce,[13] W. N. Catford,[1] I. J. Cullen,[1] Zs. Dombrádi,[14] E. Estevez,[6] W. Gelletly,[1] G. Ilie,[15] J. Jolie,[15] G. A. Jones,[1] M. Kmiecik,[9] F. G. Kondev,[16] R. Krücken,[17] S. Lalkovski,[13] Z. Liu,[1] A. Maj,[9] S. Myalski,[9] S. Schwertel,[17] P. M. Walker,[1] E. Werner-Malento,[5,18] and O. Wieland[7]

[1]*Department of Physics, University of Surrey, Guildford GU2 7XH, United Kingdom*
[2]*Department of Technical Physics, Peking University, Beijing 100871, People's Republic of China*
[3]*Department of Physics, Lund University, S-22100 Lund, Sweden*
[4]*WNSL, Yale University, New Haven, Connecticut 06520-8124, USA*
[5]*GSI, Planckstrasse 1, D-64291 Darmstadt, Germany*
[6]*Universidad de Santiago de Compostela, E-15706 Santiago de Compostela, Spain*
[7]*INFN, Universitá degli Studi di Milano, I-20133 Milano, Italy*
[8]*Japan Atomic Energy Agency, Kyoto 619-0215, Japan*
[9]*The Henryk Niewodniczański Institute of Nuclear Physics, PL-31-342 Kraków, Poland*
[10]*Departamento de Fisica Teórica, Universidad Autonoma de Madrid, E-28049 Madrid, Spain*
[11]*IEP, Warsaw University, Hoża 69, PL-00-681 Warsaw, Poland*
[12]*Institute for Nuclear Research and Nuclear Energy, Bulgarian Academy of Sciences, BG-1784 Sofia, Bulgaria*
[13]*School of Engineering, University of Brighton, Brighton BN2 4GJ, United Kingdom*
[14]*Institute for Nuclear Research, ATOMKI, H-4001 Debrecen, Hungary*
[15]*IKP, Universität zu Köln, D-50937 Köln, Germany*
[16]*Nuclear Engineering Division, Argonne National Laboratory, Argonne, Illinois 60439, USA*
[17]*Physik Department E12, Technische Universität München, Garching, Germany*
[18]*Institute of Physics PAS, Al. Lotnikow 32/46, PL-02-668 Warsaw, Poland*

(Received 23 January 2009; published 16 March 2009)

Gamma rays de-exciting isomeric states in the neutron-rich nucleus $^{198}_{76}Os_{122}$ have been observed following relativistic projectile fragmentation of a 1 GeV per nucleon ^{208}Pb beam. The ground-state band has properties compatible with oblate deformation. The evolution of the structure of Os isotopes characterized by sudden prolate-oblate shape change is discussed and contrasted with the smooth change known in the Pt chain.

DOI: 10.1103/PhysRevC.79.031305 PACS number(s): 25.70.Mn, 21.10.Re, 27.80.+w

The neutron-rich W-Os-Pt region is characterized by the presence of nuclei with different shapes in their ground states, such as prolate, oblate, triaxial, and spherical. Shape transitional nuclei are difficult to treat theoretically; consequently, this region is considered to be a crucial testing ground for nuclear models. The lighter isotopes are prolate deformed, and by adding more and more neutrons the shape becomes oblate [1,2]. As the $N = 126$ closed shell is approached the nuclei become spherical [3,4]. In the prolate-oblate transition region the nuclei can be described by a potential with similar energy minima corresponding to prolate and oblate shapes. For the tungsten ($Z = 74$) nuclei a sudden prolate-to-oblate shape change is predicted to happen at around mass 190–192 [1,2], with some experimental evidence for shape coexistence in $^{190}W_{114}$ [5,6]. The transitional region in the case of the platinum ($Z = 78$) nuclei starts at around mass $A = 192$ and persists till $A \approx 200$ [7]. These nuclei are understood to have axially asymmetric shapes and they are considered to present the best examples of γ-softness throughout the whole nuclide chart [8]. In the case of osmium nuclei ($Z = 76$) the prolate-oblate shape change is predicted to be a sudden one [7,9]. The exact place where this change occurs for the ground state of the osmium isotopes is not clear. Experimental information suggests that up to mass $A = 194$ the osmium isotopes are prolate [10], but the γ degree of freedom is also important [11]. In $^{196}Os_{116}$ the available experimental information is too scarce to draw a definite conclusion, as only two excited states were observed [7].

Despite the intense theoretical interest in the shape transitional W-Pt region, this is the part of the nuclide chart with the least information on neutron-rich nuclei. The high sensitivity achievable in the isomeric decay experiments and the recent increase in relativistic energy primary beam intensities have opened up new possibilities. Here we present the first experimental information on $^{198}_{76}Os_{122}$.

Heavy nuclear species were populated in relativistic energy projectile fragmentation. A beryllium target of thickness 2.5 g/cm^2 was bombarded with an $E/A = 1$ GeV, ^{208}Pb beam provided by the SIS accelerator at GSI, Darmstadt, Germany. The typical, on-target beam intensity was (0.5–1.0) $\times 10^9$ lead

*Corresponding author: Z.Podolyak@surrey.ac.uk

ions per ≈8-s long spill. The spills were separated by ≈18-s periods without beam. The nuclei of interest were separated and identified by using the FRagment Separator (FRS) [12] operated in standard achromatic mode with a wedge-shaped aluminium degrader in the intermediate focal plane. The transmitted ions were slowed in a variable thickness aluminium degrader and finally stopped in a 9-mm-thick plastic (perspex) catcher. The catcher was surrounded by the high-efficiency, high-granularity stopped RISING γ-ray spectrometer [13], which has a full-energy peak efficiency of 15% at 662 keV. Time-correlated γ decays from individually identified ions have been measured, allowing unambiguous identification of isomeric decays. For details of the identification procedure and the setup used in the present experiment see Refs. [4,14].

The results for ^{198}Os were obtained from two different magnetic rigidity settings. Approximately half of the data comes from a setting optimized to select fully stripped ions centered on the maximal transmission of ^{199}Os; the other half comes from a setting centered on ^{203}Ir.

A total of 7.8×10^4 ^{198}Os ions were implanted in the catcher. The detection of the previously identified γ rays following the de-excitation of isomeric states in ^{200}Pt [15], ^{201,202}Pt, ^{193}Re, ^{195}Os, and ^{198}Ir [16] were used to confirm the calibration of the particle identification.

The total γ-ray spectrum observed in delayed coincidence with ^{198}Os ions is shown in Fig. 1. The high efficiency of the RISING array and the large number of identified ^{198}Os nuclei allowed the determination of the coincidence relationships between the observed γ rays (see the bottom part of Fig. 1). Based on the γ-ray intensities and the coincidence relations the level scheme shown in Fig. 2 has been built. All the γ rays placed in the level scheme of Fig. 2 show a similar time behavior, suggesting that they are fed from the depopulation of the same isomeric state. The extracted half-life of the isomer is $T_{1/2} = 16(1)$ ns (see inset of Fig. 1). This lifetime is much shorter than the flight time between the production target and

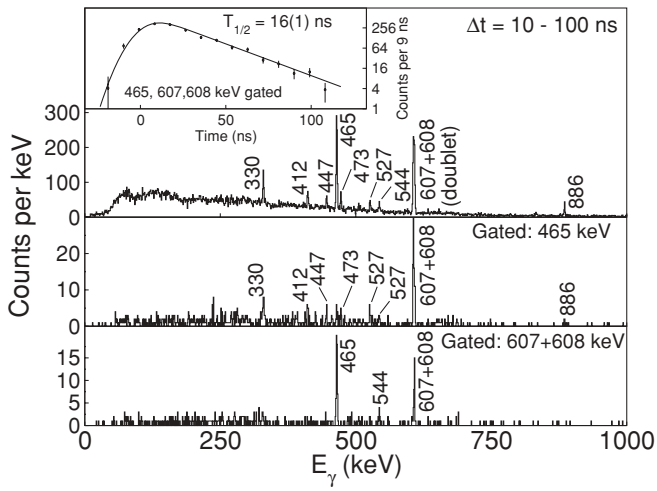

FIG. 1. Delayed γ-ray spectra associated with ^{198}Os. (Top) Singles spectrum taken within 100 ns after implantation. The inset shows the time spectrum associated with the strongest γ-ray transitions. (Bottom) Coincidence spectra obtained by gating on the 465-keV and (607 + 608)-keV transitions.

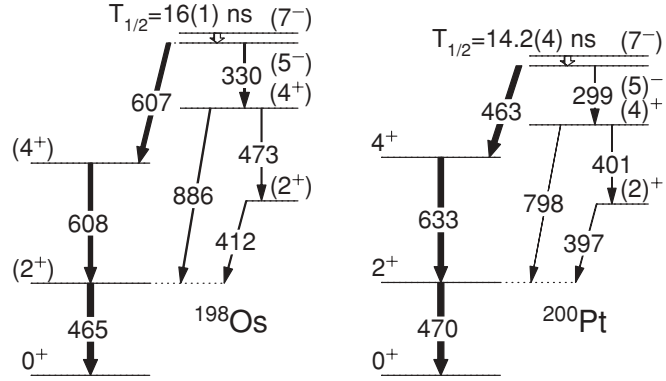

FIG. 2. Proposed level scheme of ^{198}Os. For comparison the partial level scheme of the $N = 122$ isotone ^{200}Pt is also shown [15–17]. The unobserved $(7^-) \rightarrow (5^-)$ transitions are estimated to have energies of <90 keV.

the detection position (≈230 ns). The survival of the nucleus in its isomeric state indicates that the decay-out transition has a large electron conversion coefficient and is therefore of low energy. This unobserved transition is estimated to have an energy of less than 90 keV. The spin-parity values of the excited states are tentative and are based on both systematics and theoretical considerations. For comparison, the partial level scheme of the $N = 122$ isotone ^{200}Pt [15–17] is also shown in Fig. 2. The low-intensity 447-, 527-, and 544-keV transitions shown in Fig. 1 are in tentative coincidence relationships with each other and all the other γ rays placed in the level scheme of Fig. 2. They must originate from a higher lying isomer, with an extracted half-life of $T_{1/2} = 18(3)$ ns.

We note that during the present experiment the ^{196}Os nucleus was also produced and implanted in the catcher. Despite of the large statistics (121×10^3 implanted ^{196}Os nuclei compared to 78×10^3 of ^{198}Os), no evidence of isomeric decay was found. This suggests that in ^{196}Os the 7^- state lies at least 100 keV higher in energy than the 5^- state, and it decays during the flight time within the fragment separator. The other possible scenario, that the 7^- is below the 5^-, would result in a 7^- isomer with a half-life of hundreds of microseconds (as is in the case of ^{202}Pt [16]) and it should be observable with the present setup.

Isomeric states with $I^\pi = 7^-$ have been reported in the even $A = 196$–202 platinum isotopes [15,16,18,19]. They were interpreted as having a mixed two-proton $\pi h_{11/2} d_{3/2}$ and two-neutron $\nu i_{13/2} p_{1/2}$ character. Whereas in ^{196}Pt the two-neutron component is stronger [18], in the heavier platinum nuclei the two protons are dominant [16,19]. In ^{196,198,200}Pt the 7^- isomers decay into the yrast $\pi h_{11/2} s_{1/2} 5^-$ state by a low-energy transition with $E2$ character. The half-lives are in the range of nanoseconds, and the $B(E2 : 7^- \rightarrow 5^-)$ transition strengths in the region of 15–25 W.u., decreasing with mass. Based on the similarities between the level structure of the $^{196-200}$Pt isotopes and the ^{198}Os nucleus we suggest that in ^{198}Os the isomeric state has $\pi h_{11/2} d_{3/2}$ character and $I^\pi = 7^-$, and it decays via a low-energy transition into the 5^- state with $\pi h_{11/2} s_{1/2}$ configuration. The determined transition strength is $B(E2; 7^- \rightarrow 5^-) = 15(5)$ W.u. We note that there is a lack

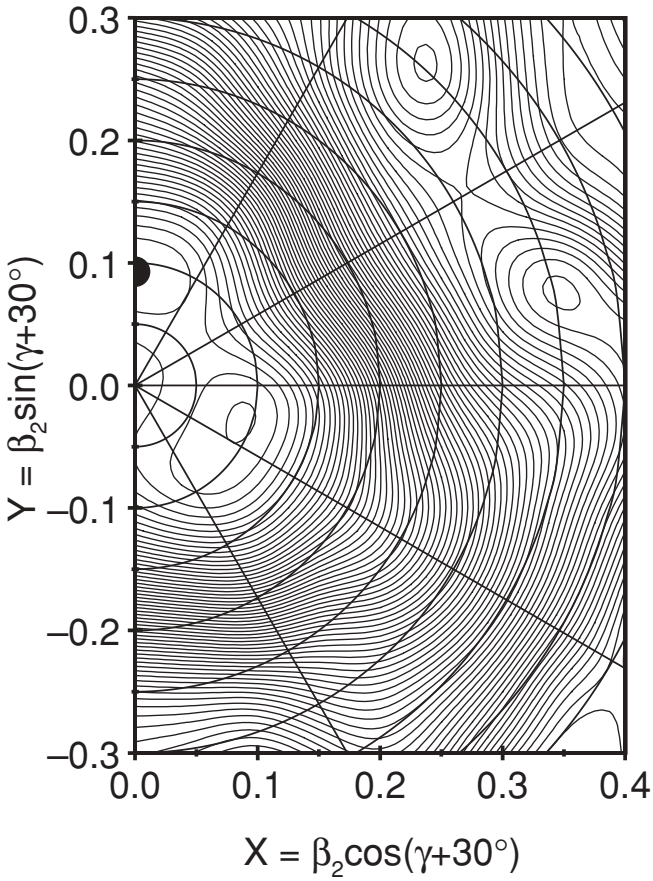

FIG. 3. Potential energy surface calculations for the ground state of ^{198}Os. The energy difference between two successive contour lines is 200 keV. The calculations indicate a shape with deformation parameters $\beta_2 = 0.093$, $\beta_4 = -0.028$, and $\gamma = 60^\circ$ (black dot).

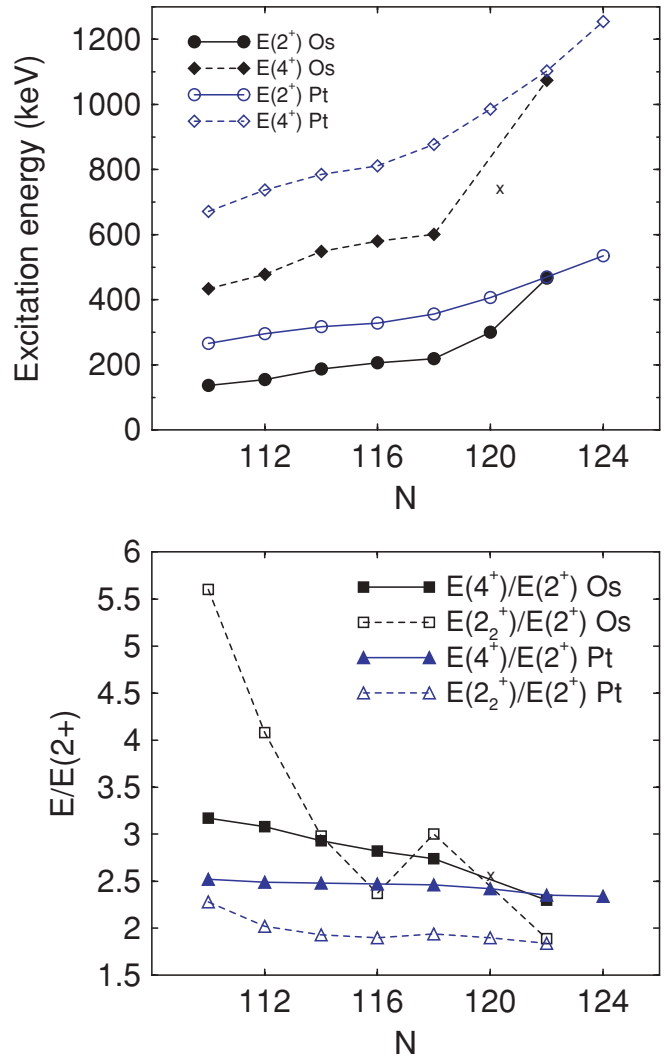

FIG. 4. (Color online) Systematics of the $E(2^+)$ and $E(4^+)$ energies and the $E(4^+)/E(2^+)$ and $E(2_2^+)/E(2^+)$ energy ratios in the even mass $A = 188$–202 osmium and platinum isotopes. The values corresponding to the second excited state in ^{196}Os, which is either the yrast 4^+ or the second 2^+ state, are indicated with the symbol x.

of sensitivity of the transition strength to the transition energy owing to the large effect of the electron conversion. The higher lying isomer in ^{198}Os observed here is very similar in its decay pattern and half-life to that observed in ^{200}Pt [16] and it probably has fully aligned $\nu i^2_{13/2}$ character with $I^\pi = 12^+$. Excited states with this structure were identified in less neutron rich platinum and mercury isotopes [20,21] as well.

The oblate-prolate shape transition in the Hf-Pt region has been theoretically studied with several approaches. Mean-field calculations have been performed with different interactions. For example, self-consistent axially deformed Hartree-Fock calculations with a separable monopole interaction predict prolate shape for osmium isotopes with $A \leqslant 190$ and oblate shape for $^{192-198}$Os [2]. However, mean-field calculations performed by Sarriguren *et al.* [1], Ansari [9], and Naik *et al.* [22] using a range of approximations predict that the lightest oblate isotope is ^{194}Os, ^{196}Os, or ^{198}Os, depending on the approach employed.

The interacting boson model (IBM) is often employed to describe the properties of transitional nuclei. It is considered that the platinum nuclei are close to the O(6) limit, which corresponds to a γ unstable shape, with ^{196}Pt being the best example of this symmetry [23]. Recently, Jolie and Linnemann [24] successfully described a range of nuclear properties in the Hf-Hg region, including the quadrupole moments that are directly related to the shape. It was shown that there is a prolate-oblate SU(3)–$\overline{\text{SU(3)}}$ *phase* transition predicted in this region.

Here, Woods-Saxon-Strutinsky calculations have been performed, as described in Ref. [25]. This type of calculation has been extensively employed and has proved successful in this mass region [5,10]. The potential energy minimization has been done in the three-dimensional deformation space of β_2, β_4, and γ. Axially symmetric prolate shapes correspond to $\gamma = 0^\circ$, whereas noncollective oblate shapes correspond to $\gamma = 60^\circ$. For ^{198}Os the calculations indicate a very soft system in both γ and β degrees of freedom, with a minimum corresponding to weak oblate deformation with parameters $\beta_2 = 0.093$, $\beta_4 = -0.028$, and $\gamma = 60^\circ$ (see Fig. 3). The same type of calculation performed for lighter osmium isotopes indicates a prolate shape for ^{190,192,194}Os, with decreasing

quadrupole deformation for increasing mass, and an oblate shape with $\beta_2 = 0.12$ for ^{196}Os [10].

The yrast structures of ^{190,192,194}Os nuclei were observed up to at least spin-parity 10^+. They are well understood by considering a prolate shape. The prolate character of ^{194}Os is consistent with the nonobservation of back-bending before 10^+ [10]. ^{196}Os is the heaviest osmium isotope where excited states were previously observed [7]. It was populated in the ^{198}Pt(^{14}C,^{16}O) reaction and excited states with energies of 300(20) and 760(20) keV were observed. Although the first excited state is almost certainly the yrast 2^+, the other observed state could be either the second 2^+ or the yrast 4^+ state. It was inferred from the high $E(2^+)$ energy that this nucleus is significantly less deformed than the lighter prolate isotopes.

The energies of the lowest excited states can be used to infer information about the character of the nuclei. Systematics related to the yrast 2^+ and 4^+ states as well the second 2^+ state (2_2^+) are presented in Fig. 4. In ^{198}Os, the ordering of the coincident 412- and 473-keV transitions cannot be determined from the present experiment. Here we considered the ordering shown in Fig. 2, resulting in an $E(2_2^+)/E(2^+)$ energy ratio of 1.89. By changing the order of the transitions the ratio is slightly modified to 2.02. This assumption does not have any consequences on the discussion that follows. As shown in Fig. 4, the platinum energies change slowly with atomic mass. The yrast $E(2^+)$ and $E(4^+)$ energies increase smoothly, and the $E(4^+)/E(2^+)$ energy ratio remains constant at about 2.5, the ratio expected for perfect O(6) γ-soft nuclei. The $E(2_2^+)/E(2^+)$ energy ratio is smoothly decreasing and has a value of around $\sim$2. In contrast to the platinum nuclei, in the osmium isotopes there is a sudden change at around $A = 196$. The large $E(4^+)/E(2^+)$ energy ratio and the smooth change of the yrast $E(2^+)$ and $E(4^+)$ energies in the case of the $A = 188$–194 osmium nuclei indicate that these isotopes are deformed. At $A = 196$ there is an abrupt increase in the energy of the 2^+ state. This is even more obvious in the case of ^{198}Os, where both the $E(4^+)$ and $E(2^+)$ energies are much higher than in the lighter Os nuclei. Similarly, the $E(4^+)/E(2^+)$ and $E(2_2^+)/E(2^+)$ energy ratios drop to the lowest values for the osmium isotopes in the region. The low $E(4)/E(2)$ ratio is consistent with a low deformation and is less than the predicted 2.5 for γ-soft O(6) nuclei, whereas the low $E(2_2^+)/E(2^+)$ ratio also indicates the γ-softness of the system.

In conclusion, excited states in the neutron-rich ^{198}Os nucleus have been identified following internal decays of isomeric states populated in relativistic energy fragmentation reactions. The energies of the yrast 2^+ and 4^+ states suggest a weakly deformed character, and the low energy of the second 2^+ state is consistent with the γ-softness characteristic to this mass region. This interpretation is compatible with the theoretical calculations predicting ^{198}Os to be a weakly deformed oblate nucleus. The sudden drop in $E(2_2^+)/E(2^+)$ for $A > 194$ osmium isotopes might be a signature of a prolate-to-oblate shape change, but more detailed theoretical calculations are needed to clarify this surprising feature.

The excellent work of the GSI accelerator staff is acknowledged. This work is supported by the STFC/EPSRC (UK) and AWE plc. (UK), the EU Access to Large Scale Facilities Programme (EURONS, EU Contract No. 506065), the Swedish Research Council, the Polish Ministry of Science and Higher Education (Grant Nos. 1 P03B 030 30 and N N202 309135), the Bulgarian Science Fund, the US DOE (Grant No. DE-FG02-91ER-40609), the Spanish Ministerio de Educacion y Ciencia, the German BMBF, the Hungarian Science Foundation, and the Italian INFN.

[1] P. Sarriguren, R. Rodriguez-Guzmán, and L. M. Robledo, Phys. Rev. C **77**, 064322 (2008).
[2] P. D. Stevenson, M. P. Brine, Zs. Podolyák, P. H. Regan, P. M. Walker, and J. R. Stone, Phys. Rev. C **72**, 047303 (2005).
[3] K. H. Maier *et al.*, Phys. Rev. C **30**, 1702 (1984).
[4] S. Steer *et al.*, Phys. Rev. C **78**, 061302 (2008).
[5] Zs. Podolyák *et al.*, Phys. Lett. **B491**, 225 (2000).
[6] P. M. Walker and F. R. Xu, Phys. Lett. **B635**, 285 (2006).
[7] P. D. Bond, R. F. Casten, D. D. Warner, and D. Horn, Phys. Lett. **B130**, 167 (1983).
[8] R. F. Casten, *Nuclear Structure from a Simple Perspective* (Oxford University Press, New York, 1990); 2nd Ed. (Oxford University Press, 2000), p. 463.
[9] A. Ansari, Phys. Rev. C **33**, 321 (1986).
[10] C. Wheldon *et al.*, Phys. Rev. C **63**, 011304(R) (2000).
[11] C. Y. Wu and D. Cline, Nucl. Phys. **A607**, 178 (1996).
[12] H. Geissel *et al.*, Nucl. Instrum. Methods Phys. Res. B **70**, 286 (1992).
[13] S. Pietri *et al.*, Nucl. Instrum. Methods B **261**, 1079 (2007); P. H. Regan *et al.*, Nucl. Phys. **A787**, 491c (2007).
[14] Zs. Podolyák *et al.*, Eur. Phys. J. Spec. Top. **150**, 165 (2007).
[15] S. Yates *et al.*, Phys. Rev. C **37**, 1889 (1988).
[16] M. Caamano *et al.*, Eur. Phys. J. A **23**, 201 (2005).
[17] F. G. Kondev and S. Lalkovski, Nucl. Data Sheets **108**, 1471 (2007).
[18] X. Huang, Nucl. Data Sheets **108**, 1093 (2007).
[19] C. Zhou, Nucl. Data Sheets **95**, 59 (2002); P. Schuler *et al.*, Z. Phys. A **317**, 313 (1984).
[20] J. J. Valiente-Dobón *et al.*, Phys. Rev. C **69**, 024316 (2004).
[21] C. Günther *et al.*, Phys. Rev. C **15**, 1298 (1977).
[22] Z. Naik *et al.*, Pramana J. Phys. **62**, 827 (2004).
[23] J. A. Cizewski *et al.*, Phys. Rev. Lett. **40**, 167 (1978).
[24] J. Jolie and A. Linnemann, Phys. Rev. C **68**, 031301(R) (2003).
[25] W. Nazarewicz *et al.*, Nucl. Phys. **A435**, 397 (1985).

Nuclear Instruments and Methods in Physics Research A 606 (2009) 589–597

Contents lists available at ScienceDirect

Nuclear Instruments and Methods in Physics Research A

journal homepage: www.elsevier.com/locate/nima

A new simulation package to model detector systems with fragmentation reactions and ion separators: Application to the LYCCA-0 system

M.J. Taylor [a,*], M.A. Bentley [a], D. Rudolph [b], C. Fahlander [b], P. Golubev [b], R. Hoischen [b], P. Reiter [c], J. Gerl [d], M. Górska [d]

[a] Department of Physics, University of York, Heslington, York YO10 5DD, UK
[b] Department of Physics, Lund University, 22100 Lund, Sweden
[c] Institut für Kernphysik, Universität zu Köln, 50937 Köln, Germany
[d] Gesellschaft für Schwerionenforschung (GSI), Planckstrasse 1, 64291 Darmstadt, Germany

ARTICLE INFO

Article history:
Received 27 November 2008
Received in revised form
1 May 2009
Accepted 3 May 2009
Available online 13 May 2009

Keywords:
Monte-Carlo
Geant4
Mocadi
Simulation
Fragmentation
LYCCA

ABSTRACT

A Monte-Carlo simulation package has been developed to model the response of a detector system for ion identification used in conjunction with ion separators following nuclear reactions. The simulation is written predominantly using the GEANT4 framework but utilises the ion transport code MOCADI for accurate separator and reaction modelling. A novel MOCADI–GEANT4 interface has been developed to utilise the parameter file output option of MOCADI as an event generator for the GEANT4 detector simulation. Test simulation results have been compared with experimental data and excellent agreement was observed. The simulation has successfully been used to model a new particle detection system prototype (Lund-York-Cologne CAlorimeter (LYCCA)-0) and validate a method of ion identification using energy and time-of-flight with this system.

1. Introduction

As experimental nuclear structure studies extend away from stable nuclei and towards the proton and neutron drip-lines, accessing more exotic isotopes becomes extremely difficult with stable beams and targets. Therefore the future of nuclear structure physics will need radioactive ion beams (RIBs) to produce the nuclei of interest. One method of RIB production is projectile fragmentation which is currently used by many accelerator facilities worldwide with new facilities and upgrades at existing laboratories planned to extend the range and quality of RIBs. The nuclei to be studied will often be produced with small cross-sections, thus the clean identification of all (non-light particle) reaction products is essential. Spectroscopic studies in particular will require accurate ion identification in order to ascertain the origin of detected nuclear de-excitation radiation. Many techniques and devices are currently employed to determine the charge and mass of reaction products including electromagnetic spectrometers and solid state detector telescopes. New systems to identify and select low cross-section reaction channels are becoming increasingly complex, hence it is desirable to not only be able to simulate the detector system to be utilised but also the whole measurement environment including the reaction process. Moreover, the added complexity and cost of new systems means that simulating detector response becomes a crucial stage in their design.

Various software packages and codes exist to simulate nuclear reactions such as projectile fragmentation, transfer and Coulomb excitation as well as the passage of ions through magnetic separators. For example, reaction codes such as ABRABLA [1] and EPAX2 [2] can calculate cross-sections and yields for fragmentation reactions and GOSIA [3] and CLX [4] calculate similar quantities for Coulomb excitation. MOCADI [5] and LISE++ [6,7] incorporate EPAX2 to not only model the reaction process but also the passage of the produced ions through a magnetic separator. There also exists software to model particle detector geometries and their response to ion implantation and radiation. Software frameworks such as GEANT4 [8] and MCNP [9] allow the user to define and model detector systems by tracking particles and radiation through sensitive detectors. Although all of these software packages are state-of-the-art and have been rigorously tested and improved, some over many years, there does not exist a software package to completely simulate detector response, nuclear reactions at relativistic energies and magnetic separators to produce simulated data in a format analogous to that collected during a real experiment. Ideally, one would utilise some of these

* Corresponding author. Tel.: +44 1904 432245; fax: +44 1904 432214.
E-mail address: mjt502@york.ac.uk (M.J. Taylor).

0168-9002/$ - see front matter © 2009 Elsevier B.V. All rights reserved.
doi:10.1016/j.nima.2009.05.003

tried and tested programs to build a complete experimental simulation package but difficulties arise at the interfaces between the codes. A new simulation package has therefore been created which incorporates some of the aforementioned programs along with newly developed interfaces and modules.

2. Simulation overview

Fig. 1 shows a basic block diagram of the complete simulation package which can be considered to consist of three main stages with interfaces between each stage. The first stage is primarily concerned with the generation of RIBs via projectile fragmentation reactions. The reaction between a stable beam and target is modelled and the resulting reaction products enter a device to separate and select a particular fragment. The final part of stage 1 is to model a secondary reaction involving the newly produced RIB to produce and/or excite the nuclei to be studied.

The second stage of the simulation is concerned with the tracking of the nuclei from stage 1 onto and through a virtual particle detector system. Physics processes are invoked to determine the results of interactions between the nuclei and the sensitive detector material. The third and final stage takes the simulated detector signals, digitises and stores them in a suitable format for later analysis. Simple algorithms can also be applied at this stage, the results of which can be histogrammed along with the raw detector signals.

3. Software choices

The Monte-Carlo simulation framework GEANT4 was chosen to model the particle detector elements for stage 2. GEANT4 has been used extensively by the high energy physics community for detector simulations but its capabilities are now being realised by nuclear physicists. A GEANT4 user application can not only model the response of particle detectors but also model a number of nuclear reactions and has the ability to track the passage of charged particles through magnetic fields. Using GEANT4 to simulate an ion separation device or nuclear reactions (in stage 1) is not a trivial task and is also rather unnecessary as many such tried and tested applications already exist (see Section 1). Therefore, to simulate the passage of ions through an ion separator in stage 1 the program MOCADI was chosen.

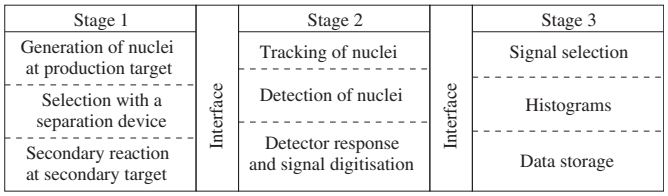

Fig. 1. A basic schematic diagram detailing the three main stages that comprise the complete simulation package.

MOCADI allows the user to simulate a range of separators by defining the corresponding magnets, collimators, slits and tracking detector materials. Fragmentation reactions incorporating the Goldhaber momentum distribution [10] can also be modelled with MOCADI with an option to output parameters describing the ions at certain points in the separator setup to a text file.

The data analysis package ROOT [11] is the software chosen with which to analyse the simulation results for stage 3. The ROOT package contains a powerful data compression feature for the storage of large correlated data sets. ROOT is written in C++, as is the GEANT4 framework and therefore can easily be linked with a GEANT4 application negating the need for an interface between stages 2 and 3 (Fig. 1). All of this makes ROOT an ideal choice for the histogramming, storage and analysis of the simulated data.

Fig. 2 shows a more detailed schematic diagram of the simulation package highlighting the three stages involved and the need for only a single interface (between stages 1 and 2) due to the outlined software choices.

4. Stage 1: MOCADI simulations

One advantage of using an external program such as MOCADI to model a nuclear reaction and produce a file parameterising the reaction products is that the file can be used repeatedly for different detector geometries. This maintains a level of consistency when optimising or investigating different detector configurations and also reduces the simulation running time as new reaction products need not be generated after each detector modification. MOCADI is used to simulate both the primary and the secondary reactions, that is, the RIB production and the production/excitation of the nuclei of interest. A MOCADI input file is produced which describes all of the magnet elements, collimating slits and tracking detector materials for the ion separator being simulated as well as any reaction targets to be used. A primary beam with, energy, spatial distribution and divergence parameters is defined along with the number of primary beam particles to be generated. After the primary

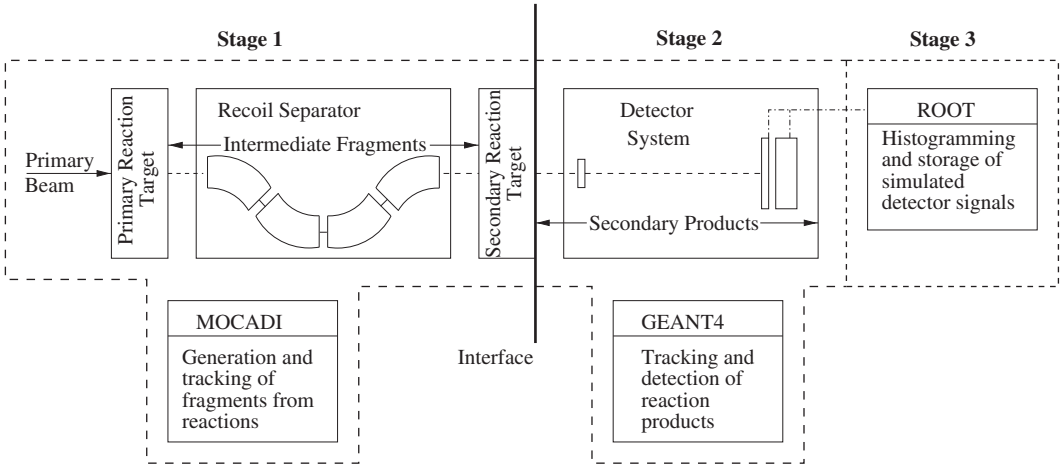

Fig. 2. A detailed schematic diagram of the simulation package highlighting the software choices and their roles for each stage of the process.

reaction between the beam and the first reaction target, the ion optics are optimised for a particular intermediate fragment (see Fig. 2). The intermediate fragments that emerge from the separator can then impinge on a second reaction target. To produce a range of secondary reaction products, MOCADI needs to be run multiple times, once for each required ion type. For each generated primary beam particle, the parameters describing each intermediate and/or secondary ion are written to a file at every user defined 'save point' that the ion successfully reaches in the virtual separator setup. These save points can be used to evaluate quantities such as position and energy loss in the separator tracking detectors. After stage 1 of the simulation, the generated parameter files need to be collated and modified in order to be used in stage 2.

5. MOCADI–GEANT4 interface

The parameter files produced by MOCADI (stage 1) are used to generate the ions in the GEANT4 application (stage 2) that will interact with the detector system. As MOCADI was never developed with this goal in mind, some modifications to the parameter files need to be performed to produce files suitable for stage 2. This is the interface stage shown in Fig. 2 and is a multi-step process utilising scripts and programs developed using Perl and C++. Perl is a powerful scripting language with many file manipulation commands and C++ is a multipurpose, high-level object-oriented programming language in which GEANT4 is written, making them both the languages of choice.

As mentioned in Section 4, MOCADI has to be run multiple times if a range of nuclei are to be produced in the secondary reaction. This is performed with a Perl script which substitutes new A and Z values in the input file, from a pre-determined list, for each required secondary reaction product. After each substitution, the script executes MOCADI and appends an integer to each outputted text file. Once all of the parameter files have been generated another Perl script is used to separate the data into two files, one containing all of the parameters describing the intermediate fragments at each save point and another for the secondary reaction products. This step is required as only the secondary products are tracked by the GEANT4 application. As MOCADI outputs the parameters for every surviving ion, production cross-sections need to be applied to reflect the relative yields. The EPAX2 production cross-sections are listed for each ion in the corresponding output files. These are automatically retrieved and then applied to the secondary products listed in the parameter file by a C++ program. During the cross-section application process the correlations between the intermediate and secondary ions are preserved; any intermediate fragments that do not reach the second reaction target are discarded. Once all of the modifications have been applied, two parameter files exist describing the correlated intermediate and secondary ions, which are then used as input files for the next stage of the simulation.

6. Stage 2: GEANT4 application

Stage two of the simulation package consists of an application written predominantly using the GEANT4 framework. Within the code, each detector geometry is defined as well as the physics processes that govern the ion interactions with the sensitive detector regions. A new C++ class has been developed, *ReadMocadiEvent*, to read the parameter files and pass the values to the GEANT4 application event-by-event. For each event, the application uses the GEANT4 *particleGun* class to create an ion, at a particular spatial position, with mass, charge, energy and trajectory, all defined by the read parameters. After creation, the ion is tracked onto and through the complete detection system geometry until it either leaves the specified 'world volume' or comes to rest inside a detector medium. A *Digitisation* module, for signal processing, is defined in the application for each detector type. The module outputs digitised detector signals, for example, deposited energy, position and time. The *Digitisation* method also applies a Gaussian distribution, of specified width, to each signal in order to simulate the time and/or energy resolution of the detector and associated electronics. The application has a graphical interface which allows the user to change the detection system position and various detector resolution widths interactively without the need to recompile the code.

7. Stage 3: ROOT analysis

The third and final stage of the simulation is the analysis, histogramming and storage of the simulated detector signals. ROOT histogram creation methods are called directly by the GEANT4 application and the histograms are filled on an event-by-event basis. The *Analysis* module can also be used to perform basic signal analysis, for example, a time-of-flight calculation from the difference between detector time signals. All of the user calculated quantities and raw detector signals are stored in a ROOT Tree object for post-simulation data analysis.

8. Simulation test case

8.1. Detector: LYCCA-0

LYCCA-0 is the first prototype of LYCCA (Lund-York-Cologne CAlorimeter) [12], a device to identify nuclei following reactions involving exotic radioactive beams. LYCCA will be used in the HISPEC (High resolution In-flight SPECtroscopy) [13] programme as part of the NuStAR (Nuclear Structure Astrophysics and Reactions) [14] collaboration at the international facility FAIR (Facility for Anti-proton and Ion Research) [15]. The system will consist of separate detector modules which can be positioned in a variety of geometries and will use an energy loss (ΔE), residual energy (E_r) and time-of-flight (TOF) method to identify nuclei following the secondary reaction. Each LYCCA-0 module has a $6 \times 6\,\mathrm{cm}^2$, 300 μm thick, position sensitive DSSSD (Doubled-Sided Silicon-Strip Detector) for accurate particle tracking and charge identification through energy loss; 5 mm behind each DSSSD resides one or more CsI(Tl) scintillation detectors to record the residual energy as the particles come to rest. Two types of CsI detector will be used, $5.4 \times 5.4\,\mathrm{cm}^2$, 1 cm thick and $19 \times 19\,\mathrm{mm}^2$, 11 mm thick. The $19 \times 19\,\mathrm{mm}^2$ square detectors will be arranged in a 3×3 array to obtain a similar active area as one of the $5.4 \times 5.4\,\mathrm{cm}^2$ detectors. For the TOF measurement the start timing detector will be a 3×3 array of $19 \times 19\,\mathrm{mm}^2$, 200 μm thick CVD (Chemical Vapour Deposition) polycrystalline Diamond detectors positioned 1 cm behind the secondary reaction target. Three different detector options are being considered for the stop timing measurement at the position of the LYCCA modules; a large area fast plastic scintillator, Diamond detectors or the DSSSD themselves.

8.2. Reaction: two-step fragmentation

One of the methods of radioactive ion beam production at HISPEC will be projectile fragmentation. Intermediate fragments will be separated using the FAIR/NuStAR fragment separator Super-FRS (Superconducting FRagment Separator) [16]. Although

the primary reaction before the Super-FRS may be of fragmentation type the second reaction to populate excited states in the nuclei of interest can take many forms including a second fragmentation reaction. The use of fragmentation reactions with RIBs poses many challenges, in particular the identification of the reaction products with broad energy and momentum distributions. The simulation is an ideal tool to investigate ion identification techniques with LYCCA-0 following two-step fragmentation reactions.

The sequence of reactions $^{58}\mathrm{Ni} + {}^{9}\mathrm{Be} \rightarrow {}^{55}\mathrm{Ni}$, $^{55}\mathrm{Ni} + {}^{9}\mathrm{Be} \rightarrow {}^{53}\mathrm{Ni}$ was chosen for the test case as real experimental data exist against which the simulation results can be compared. The data are from an experiment that was performed during the first RISING (Rare Isotope Spectroscopic INvestigation at GSI) [17] fast beam campaign to study the $T_z = -\frac{3}{2}$ nucleus ^{53}Ni [18–20]. A 600 MeV/u ^{58}Ni beam was incident on a 4 g/cm^2 ^{9}Be target and ^{55}Ni reaction products were tracked and separated by the existing GSI fragment separator FRS [21]. A range of intermediate fragments resulted from the primary reaction; however, for the simulated reaction an assumption has been made that in the analysis of real experimental data from fragment separator devices there would be unique identification of the intermediate fragments on an event-by-event basis. This was indeed achieved for the RISING experiment and thus the need to simulate reaction products other than ^{55}Ni was deemed unnecessary. The selected ^{55}Ni ions were then incident on another ^{9}Be target of thickness 700 mg/cm^2 where a second fragmentation reaction occurred. Again a large range of nuclei were produced following the secondary reaction along with the ^{53}Ni nuclei of interest. These secondary reaction products were identified using a combination of energy loss (Z) and total implantation energy (A) by the CATE (CAlorimeter TElescope) detector [22]. CATE measured fragment energy loss using an array of Si (ΔE) detectors and residual energy using an array of CsI (E_r) detectors located directly behind the Si. The intermediate fragment energy range for which the simulation package is applicable is dictated by the separating device being simulated. The FRS can analyse all ion beams of hydrogen through to uranium spanning energy ranges of 0.8–4.5 and 0.2–1.3 GeV/u, respectively [21].

Fig. 3a shows the ΔE versus E_t spectrum created from the CATE detector signals where $E_t = \Delta E + E_r$. Fig. 3a highlights the large range of secondary fragments produced and thus the need for good ion identification. Fig. 3a also shows that fragments with differing charge are fairly distinguishable. Fig. 3b shows the Fe gated projection of Fig. 3a onto the total energy (x) axis. As the total fragment energy is mass dependent, it was originally envisaged that the selection of a particular isotope, for prompt γ-ray correlations, would be possible from the measured total energy. However, Fig. 3b clearly shows that for this type of reaction and mass region, this was not possible with the CATE detector system. From this reaction the isotopes of Fe with the largest production cross-sections (calculated with EPAX2) are ^{52}Fe ($\sigma = 31.1$ mb) and ^{53}Fe ($\sigma = 52.8$ mb) which cannot be resolved in Fig. 3b. This is just one of the reasons behind the development of LYCCA: to achieve complete fragment identification in Z and A in order to produce clean γ-ray spectra for specific nuclei.

8.3. LYCCA-0 simulation

Fig. 4 shows the positions and geometries of the LYCCA-0 detector elements as defined in GEANT4. This version of the simulation incorporates the three different stop timing detector options, fast plastic, Diamond and Si and the LYCCA-0 modules are located such that the nominal secondary target-Si detector distance is 3.4 m.

The CsI detectors located behind the Si detectors are also shown. Only the active areas of the detectorsdefined in the simulation, surrounding dead material such as PCB, wire bonds

nuclear physics solid state detector materials except for the Diamond detectors which have an increased carbon density of $3.5\,g/cm^3$, as per real CVD Diamond. The default resolutions imposed on the simulation detectors are summarised in Table 1 although these values can be modified interactively between each simulation run along with the target-detector module distance.

The definition of a 'good' event, within the simulation, is one that produces a start timing signal in the target position Diamond detectors, a stop timing signal in any one of the three stop timing detectors and ΔE, E_r signals in the Si and CsI detectors, respectively. This imposes a range of secondary fragment energies for which the simulation is applicable as the physics to be addressed requires the ions being studied to not only reach and deposit energy in the CsI detectors but also stop and not punch through. For the LYCCA-0 setup this energy range was determined for ^{12}C and ^{208}Pb fragments to be 20–105 and 55–445 MeV/u, respectively. If an event fulfils the 'good' event criteria the application reads in the corresponding intermediate fragment parameters and digitised FRS tracking detector signals are produced. All of the detector signals for 'good' events are passed to the *Analysis* module for storage and histogramming.

Table 1
Default full-width half-maximum (FWHM) values and units for the LYCCA-0 detector resolutions along with the acceptable ranges for the interactively changeable values.

Detector	Signal	Units	Range	Default value
Diamond	Energy	%	–[a]	1.0
	Time	ns	0–1000	0.05
Plastic	Energy	%	0–100	2.0
	Time	ns	0–1000	0.1
Si	Energy	%	0–100	1.0
	Time	ns	0–1000	0.2
CsI	Energy	%	0–100	0.5

[a] Not changed interactively.

9. Simulation results

This section will present some of the results from various investigations utilising the new simulation package for the reactions defined in Section 8.2 and the detector system defined in Section 8.1. For brevity the results shown use only the Diamond detectors for timing information and therefore the fast plastic detector was removed from the setup and the number of LYCCA-0 module Diamond detectors was increased to cover the same active area as the Si. Also, the final incarnation of the LYCCA detector system will incorporate only one type of timing detector and therefore the results presented here would have extra significance if Diamond was chosen.

9.1. $A \approx 50$

To truly validate simulation results, a comparison must be made with real experimental data. Fig. 5a shows, for comparison, the same CATE ΔE (Si) versus E_t (Si + CsI) plot as shown in Fig. 3a, along side Fig. 5b which is a similar plot created using the simulated LYCCA-0 Si and CsI detector signals. Unlike the simulated data the experimental data required a particle-γ coincidence condition which accounts for the difference in the relative fragment yields between the two plots. Also the Rutherford scattered ^{55}Ni intermediate fragments are not simulated but could be if required. The $A \approx 50$ event files were created using $\approx 1.1 \times 10^6$ primary beam particles which was the maximum number allowed for this reaction without exceeding the 2 GB file size limit. This resulted in $\approx 9.7 \times 10^5$ secondary events for a total of 91 fragment species with production

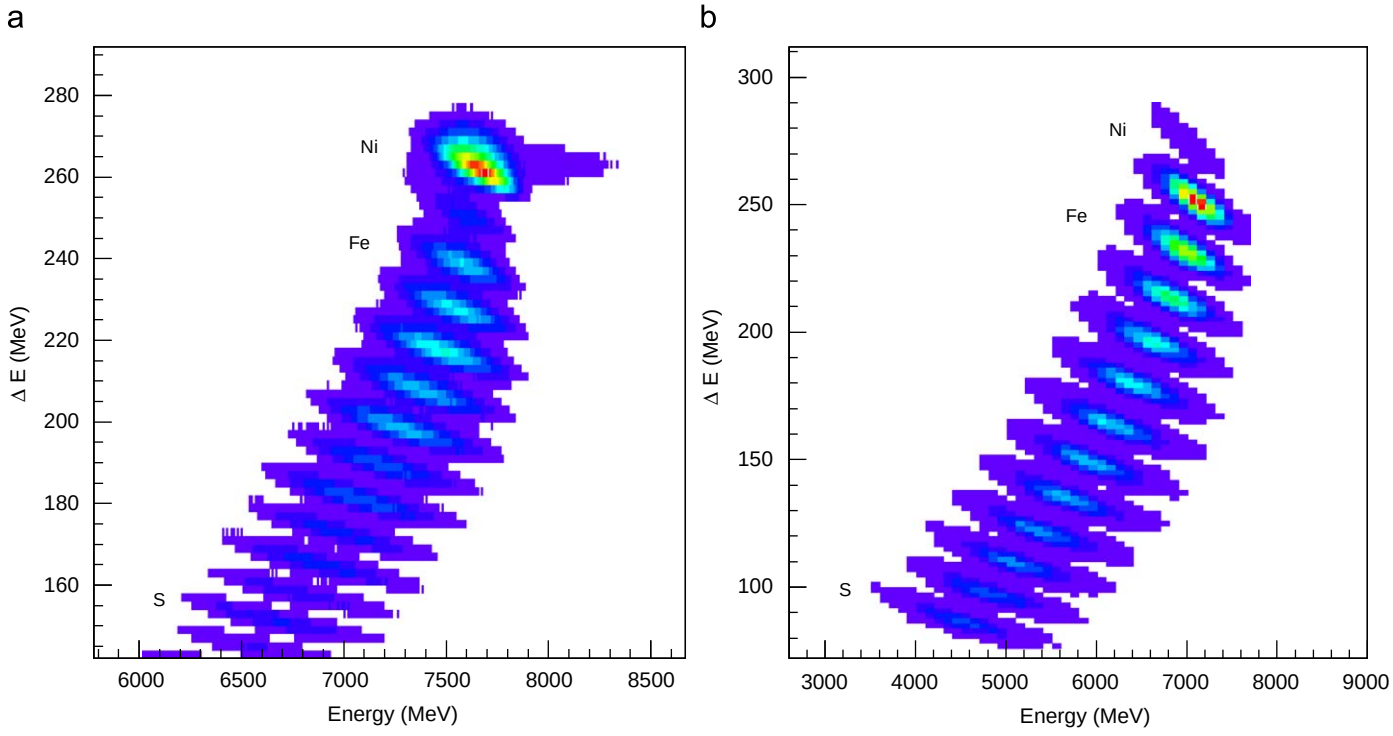

Fig. 5. (a) (same as in Fig. 3a) CATE ΔE versus E_t spectrum created with real experimental (particle-γ coincidence) data taken during the RISING ^{53}Ni experiment. (b) Simulated data, no particle-γ requirement and no Rutherford scattered ^{55}Ni fragments are simulated. The isotopes $^{53,54}Ni$, $^{49-53}Fe$ and $^{30-38}S$ were simulated for the labelled fragment species.

cross-sections $>1\,\mu b$. This yielded isotopes of ^{53,54}Ni, $^{49-53}$Fe and $^{30-38}$S for the fragment species labelled in Fig. 5. The simulation *system* runtime for these events was 45 s using a laptop PC with an Intel Pentium Centrino 2 GHz processor.

The primary purpose of the simulation of LYCCA-0 is to investigate fragment identification from energy and TOF measurements. Selecting $Z = 26$ (Fe) fragments a TOF versus energy (E_t) spectrum was produced using the start and stop timing signals from the CVD Diamond detectors. Fig. 6a shows the result of this analysis for a target-Si detector distance of 2 m (actual TOF path 1.98 m) and Fig. 6b for a distance of 3.4 m, the distance planned for LYCCA-0. Isotopic separation is clearly improved for the longer TOF path due to the fixed timing resolution (50 ps FWHM) of the Diamond detectors and four distinct regions can clearly be seen corresponding to the isotopes $^{50-53}$Fe. Figs. 6c and d show the same analysis but for sulphur isotopes. The isotopic separation is already very good at 2 m for the sulphur isotopes and becomes excellent when the distance is increased to 3.4 m. The separation improvement for low mass fragments over higher masses is predominantly due to the Si and CsI detector energy resolutions (1.0% and 0.5% FWHM, respectively) being a percentage of the measured energy. Hence the resolution decreases as the fragment mass increases.

An advantage of simulating detector systems is that acceptable detector properties, such as time resolution, can be investigated before any physical detectors are purchased. The simulation was used to determine the minimum acceptable resolution of the timing detectors for which clean fragment identification was possible using the proposed technique. Fig. 7a shows an Fe ($Z = 26$) gated, TOF versus E_t plot for a target-Si distance of 3.4 m but with a Diamond detector time resolution of 100 ps FWHM and Fig. 7b for 150 ps FWHM. Fe isotopic separation is just visible for the 100 ps case and disappears completely for 150 ps resolution. This analysis shows that a timing detector resolution of much less than 100 ps is required for $A \approx 50$ fragment identification using the TOF-ΔE–E_t technique with the Si, CsI energy resolutions unchanged.

9.2. Intermediate-secondary fragment correlations

The secondary fragment identification technique, as outlined in Section 8.1, requires the measurement of the fragment energy and TOF. Fig. 6 showed that isotopic separation (i.e. mass 'resolution') became less pronounced as the fragment mass increased and the TOF path decreased, also Fig. 7 showed a deterioration as the timing detector resolution decreased. To address these technique limitations, an investigation into the possibility of mass resolution improvement through correlations with the intermediate fragments was performed. The simulation allows the user to investigate correlations between the LYCCA-0 and the FRS tracking detector signals. As the intermediate fragments pass through the FRS, (x, y) position information from multiwire proportional counters, timing from scintillation detec-

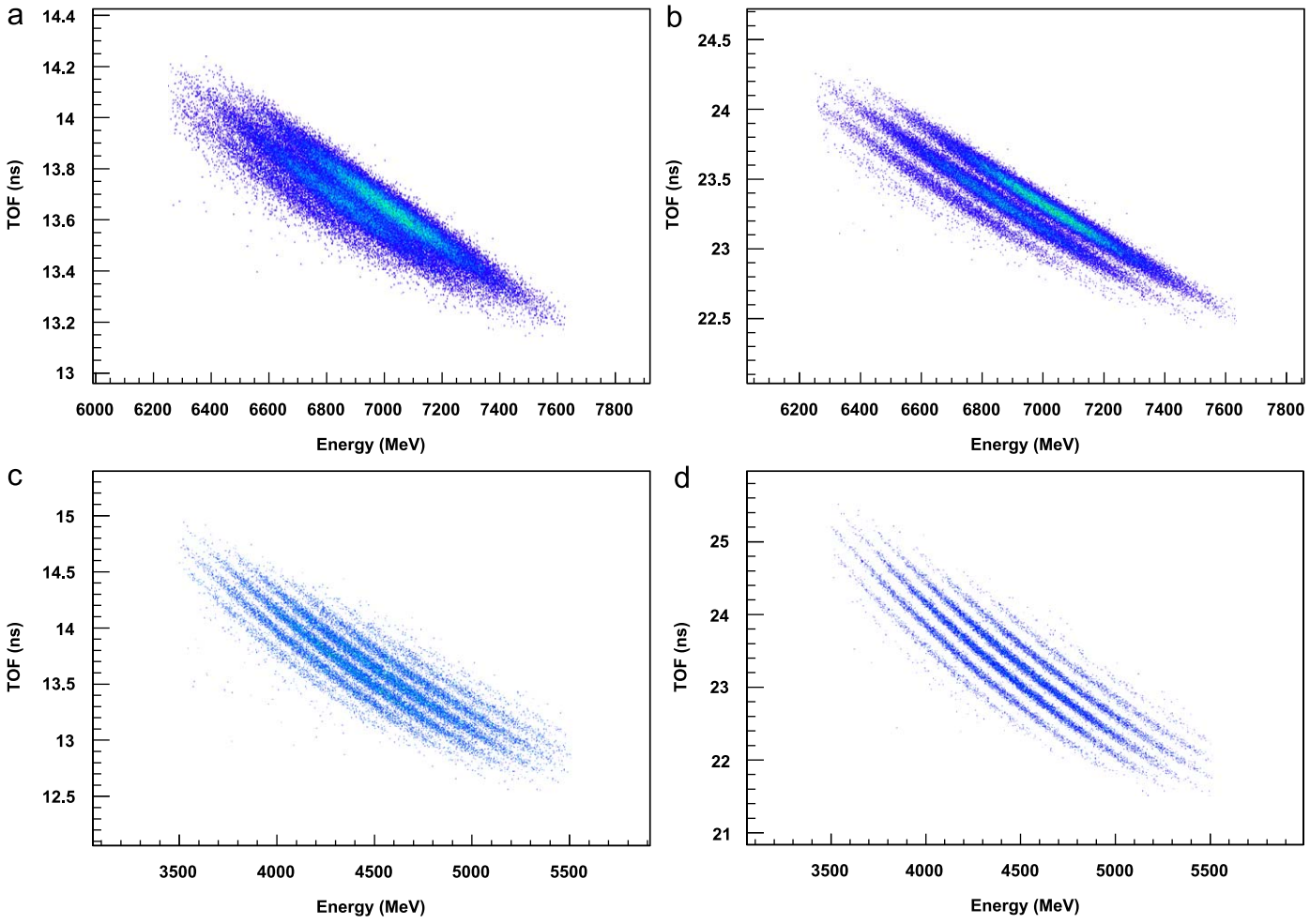

Fig. 6. Simulation results: TOF versus energy (E_t) spectra for two fragment types and two target-Si detector distances. (a) Fe and 2 m, (b) Fe and 3.4 m, (c) S and 2 m and (d) S and 3.4 m.

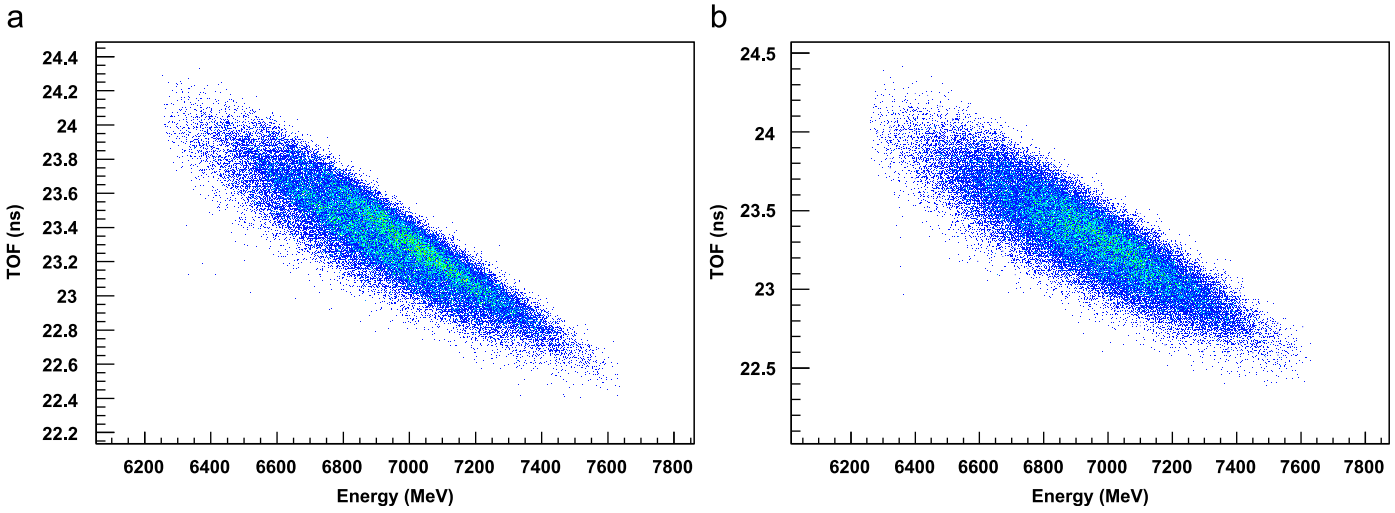

Fig. 7. TOF versus E_t spectra for $^{49-53}$Fe fragments with Diamond timing detector resolutions of (a) 100 ps and (b) 150 ps.

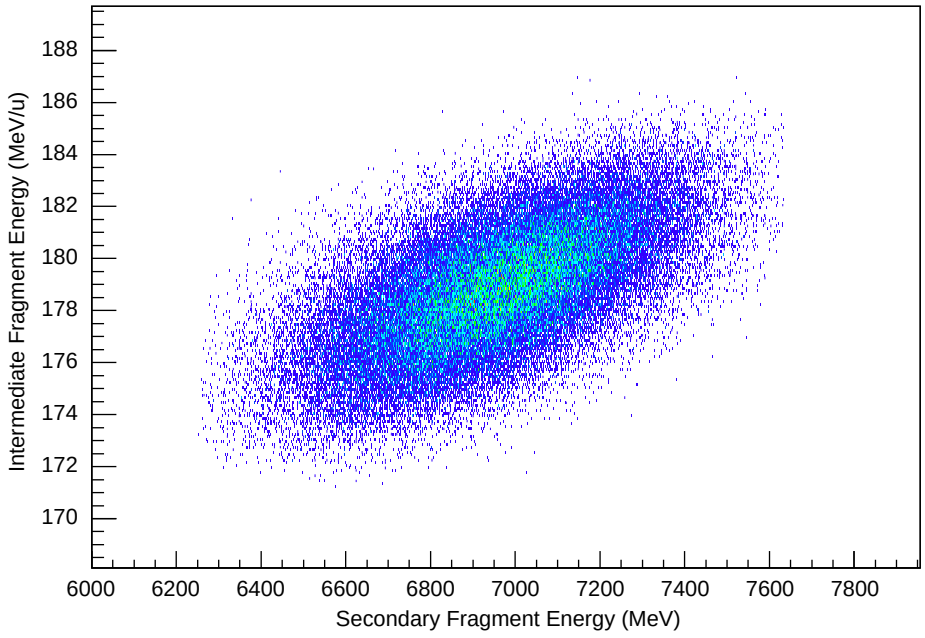

Fig. 8. Intermediate fragment energy just before the second reaction target plotted against the secondary fragment energy (E_t), as measured by the LYCCA-0 Si and CsI detectors, for Fe secondary fragments. As the energy of the fragment is used to determine its mass, this correlation gives another observable to aid fragment identification.

tors and energy loss from an ionisation chamber are all recorded. Within the simulation, the user can also access particle characteristics at any position in the experimental setup without the need for a virtual detector at that position. For example, the energy of a ^{55}Ni intermediate fragment can be accessed immediately before the second reaction target.

Firstly, the intermediate fragment energies were plotted against E_t for Fe secondary fragments to ascertain whether a correlation exists. The result of this analysis is shown in Fig. 8 where a definite correlation between the two quantities can be seen.

Fig. 9a shows the intermediate fragment energy, taken directly before the second reaction target, plotted against the Fe secondary fragments mass which is calculated from energy and TOF as measured by the LYCCA-0 CsI and Diamond detectors, respectively. Fig. 9b shows a projection of 9a onto the mass (x) axis. Although distinct peaks relating to the different Fe fragment masses can be seen in Fig. 9b, Fig. 9a shows that this spectrum could clearly be improved if the semi-major axes of the distributions were all vertical. It is also important to note that the calculated fragment mass numbers (A) are incorrect as the largest distribution should result from ^{53}Fe fragments. The observed correlation and incorrect mass numbers in Fig. 9 are due to the exclusion of the energy lost in the timing and Si detectors situated in the fragments flight path. For the best possible fragment mass identification, using only information gained from the LYCCA-0 detectors, an accurate measurement of the fragments total energy is required. In reality the energy resolution of the Diamond and Si detectors may be significantly different from that estimated for such high energy fragments. If this is the case, the measured energy loss in these detectors, when included in the mass calculation for Fig. 9, may not result in any significant improvement in mass separation. Also, the final LYCCA-0 detectors will be chosen and tailored for specific measurements. For example, the TOF detectors will be chosen purely on the basis of timing characteristics, not energy resolution, and therefore only

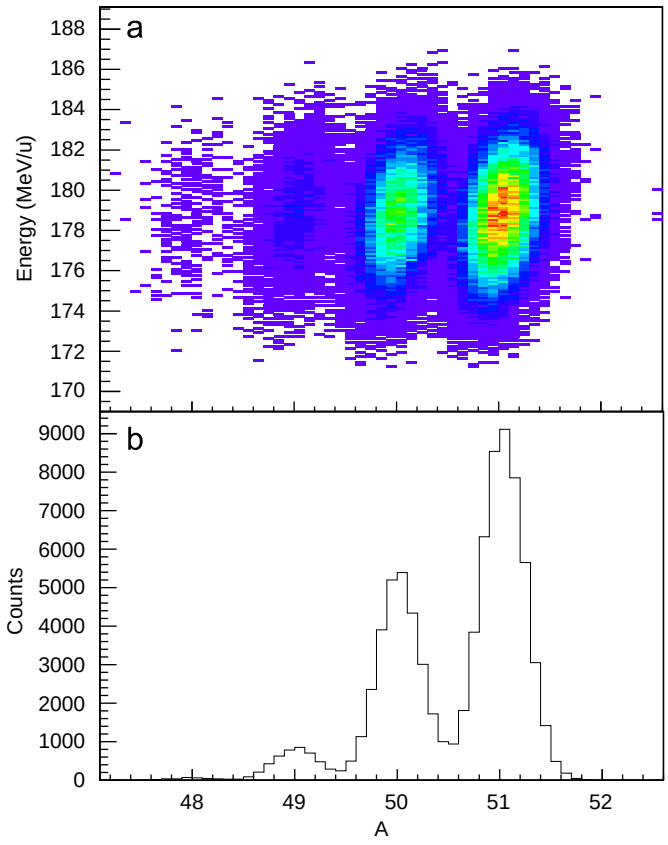

Fig. 9. (a) Intermediate fragment energy immediately before the second reaction target plotted against the secondary fragment mass calculated from the fragments TOF and energy as measured by the Diamond and CsI detectors, respectively. (b) Total projection of (a) onto the mass (x) axis.

timing signals may be collected from these detectors. In fact, it may be that calculating the energy loss in the timing and Si detectors yields far less uncertainty than actual measurement. It may be possible to improve Fig. 9b with the incorporation of the calculated energy loss in each detector determined by the fragments flight path. The fragment trajectory would be deduced from the segmentation and position sensitivity of the detectors. These calculations and analysis are beyond the scope of this article, but they demonstrate effectively how the simulation may be used to determine the optimum experimental configuration and analysis methodology. Fig. 9 ultimately shows that fragment mass resolution could be improved with the accurate knowledge of either the intermediate or the secondary fragment energy along with the measured TOF across the LYCCA-0 detectors.

9.3. $A \approx 100$

Experiments performed at HISPEC would not be limited to nuclei with $A \approx 50$ or less and therefore determining the validity of the identification technique for higher mass fragments is crucial. The simulation is ideally suited for this and can help to establish any limitations by simulating a variety of experiments with the nuclei of interest covering a large mass and energy range. A two-step fragmentation reaction was simulated to produce nuclei in the $A \approx 100$ region. A primary beam of ^{112}Sn at 635 MeV was used to produce ^{110}Sn intermediate fragments which were then used to produce $^{104-107}$Cd secondary fragments. The reaction targets, FRS tracking detectors and LYCCA-0 detector system remained unchanged from the Ni reaction.

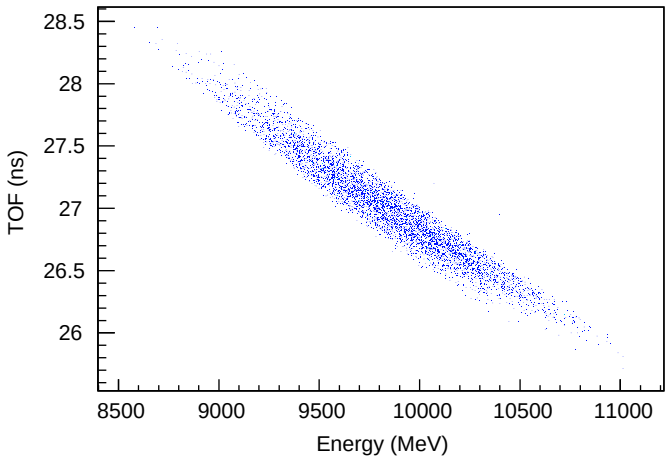

Fig. 10. TOF versus E_t spectrum for Cd fragments, produced in the simulated ^{112}Sn → ^{110}Sn → $^{104-107}$Cd reaction, with a target-Si detector distance of 3.4 m.

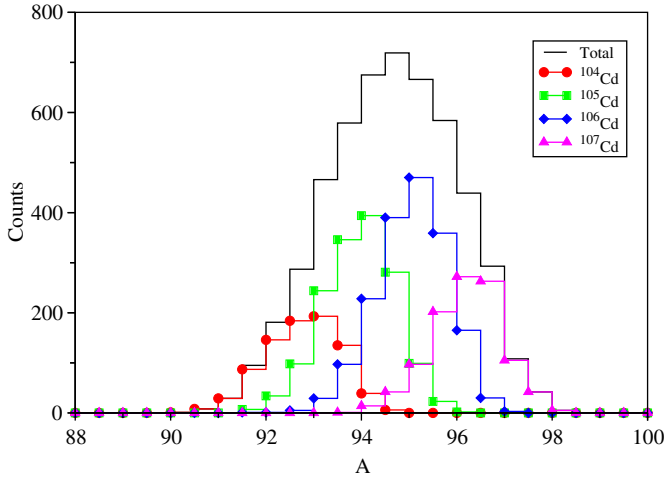

Fig. 11. Calculated mass distributions from TOF and energy (E_r) measurements for the $^{104-107}$Cd fragments along with their summation.

Fig. 10 shows the result of plotting the TOF versus E_t for the Cd reaction, for a target-Si detector distance of 3.4 m. The detector resolutions imposed for this analysis are as per Table 1 and the plot does not show clear isotopic separation for the Cd isotopes.

Fig. 11 shows the calculated mass distributions for the Cd isotopes from TOF (Diamond) and energy (CsI only) measurements. Although the centroids of the individual mass distributions are separated the resolution is of the order of three mass units and therefore the clean selection of a particular isotope would be extremely difficult without contamination from neighbouring isotopes. This analysis starts to highlight the limitations of the fragment identification technique with the described setup for experiments involving $A \approx 100$ fragments and indicates that for this mass region, additional selection devices are likely to be required.

10. Summary

A new simulation package has been developed which utilises the ion transport code MOCADI to generate parameters describing realistic ions following a fragmentation reaction which are tracked through a separator device. The output from MOCADI is modified into a format which can then be read by the next stage of the simulation which is an application written using the GEANT4 framework. The secondary fragments are tracked through the virtual

detector system and parameters such as energy loss, interaction position and time are digitised and passed to an analysis module. The simulation uses the data analysis software ROOT to histogram and store the digitised detector signals. This allows the user to perform data analysis on the simulated data in much the same way as one would with real experimental data. The simulation has been used to successfully model a new detector system prototype, LYCCA-0, which in the first instance will be used to identify reaction products following two-step fragmentation reactions. The results from this have been used to validate an ion identification technique which uses fragment time-of-flight and energy as measured by LYCCA-0 modules. The simulation package can presently be downloaded via the LYCCA web page: http://www.nsg.nuclear.lu.se/lycca/.

Acknowledgements

The authors wish to thank Helmut Weick for his help with certain aspects of MOCADI and the RISING collaboration for their contribution during the collection of the ^{53}Ni data. MJT and MAB would also like to acknowledge financial support for this work from the Engineering and Physical Sciences Research Council (EPSRC) and the Science and Technology Facilities Council (STFC).

References

[1] J.J. Gaimard, K-H. Schmidt, Nucl. Phys. A 531 (1991) 709.
[2] K. Sümmerer, B. Blank, Phys. Rev. C 61 (2000) 034607.
[3] T. Czosnyka, et al., Nucl. Phys. A 458 (1986) 123.
[4] H. Ower, Computer Program CLX.
[5] N. Iwasa, et al., Nucl. Instr. and Meth. B 126 (1997) 284.
[6] D. Bazin, et al., Nucl. Instr. and Meth. A 482 (2002) 307.
[7] O. Tarasov, D. Bazin, Nucl. Phys. A 746 (2004) 411.
[8] Geant4 Collaboration, Nucl. Instr. and Meth. A 506 (2003) 250.
[9] X-5 Monte Carlo Team, Los Alamos National Laboratory, Los Alamos, USA, April 2003.
[10] A.S. Goldhaber, Phys. Lett. B 53 (1974) 306.
[11] R. Brun, F. Rademakers, Nucl. Instr. and Meth. A 389 (1997) 81 (see also ⟨http://root.cern.ch/⟩).
[12] LYCCA Homepage, ⟨http://www.nsg.nuclear.lu.se/lycca/⟩.
[13] HISPEC Homepage, ⟨http://www.gsi.de/fair/experiments/NUSTAR/hispec_e.html⟩.
[14] NuStAR Collaboration Homepage, ⟨http://www.gsi.de/fair/experiments/NUSTAR/index_e.html⟩.
[15] FAIR Facility Homepage, ⟨http://www.gsi.de/fair/index_e.html⟩.
[16] H. Geissel, et al., Nucl. Instr. and Meth. B 204 (2003) 71.
[17] H.J. Wollersheim, et al., Nucl. Instr. and Meth. A 537 (2005) 637.
[18] M.J. Taylor, et al., J. Phys. G Nucl. Part. Phys. 31 (2005) S1527.
[19] G. Hammond, et al., Acta Phys. Pol. B 36 (2005) 1253.
[20] G. Hammond, Ph.D. Thesis, University of Keele, 2008.
[21] H. Geissel, et al., Nucl. Instr. and Meth. B 70 (1992) 286.
[22] R. Lozeva, et al., Nucl. Instr. and Meth. A 562 (2006) 298.

PHYSICAL REVIEW C **80**, 061302(R) (2009)

Nuclear structure "southeast" of ^{208}Pb: Isomeric states in ^{208}Hg and ^{209}Tl

N. Al-Dahan,[1,2] Zs. Podolyák,[1,*] P. H. Regan,[1] M. Górska,[3] H. Grawe,[3] K. H. Maier,[4] J. Gerl,[3] S. B. Pietri,[3] H. J. Wollersheim,[3] N. Alkhomashi,[1] A. Y. Deo,[1] A. M. Denis Bacelar,[5] G. Farrelly,[1] S. J. Steer,[1] A. M. Bruce,[5] P. Boutachkov,[3] C. Domingo-Pardo,[3] A. Algora,[6,7] J. Benlliure,[8] A. Bracco,[9] E. Calore,[10] E. Casarejos,[8] I. J. Cullen,[1] P. Detistov,[11] Zs. Dombrádi,[7] M. Doncel,[12] F. Farinon,[3] W. Gelletly,[1] H. Geissel,[3] N. Goel,[3] J. Grebosz,[4] R. Hoischen,[3,13] I. Kojouharov,[3] N. Kurz,[3] S. Lalkovski,[5] S. Leoni,[14] F. Molina,[6] D. Montanari,[9] A. I. Morales,[8] A. Musumarra,[3,15] D. R. Napoli,[10] R. Nicolini,[9] C. Nociforo,[3] A. Prochazka,[3] W. Prokopowicz,[3] B. Rubio,[6] D. Rudolph,[3,13] H. Schaffner,[3] P. Strmen,[16] I. Szarka,[16] T. Swan,[1] J. S. Thomas,[1] J. J. Valiente-Dobón,[10] S. Verma,[8] P. M. Walker,[1] and H. Weick[3]

[1]*Department of Physics, University of Surrey, Guildford GU2 7XH, United Kingdom*
[2]*Department of Physics, University of Kerbala, Kerbala, Iraq*
[3]*GSI, D-64291 Darmstadt, Germany*
[4]*The Henryk Niewodniczànski Institute of Nuclear Physics, PL-31-342 Kraków, Poland*
[5]*School of Environment and Technology, University of Brighton, Brighton BN2 4GJ, United Kingdom*
[6]*IFIC, CSIC—Universidad de Valencia, E-46071 Valencia, Spain*
[7]*Institute of Nuclear Research of the Hungarian Academy of Sciences, Debrecen H-4001, Hungary*
[8]*Universidad de Santiago de Compostela, E-15705 Santiago de Compostela, Spain*
[9]*Dipartmento di Fisica, Università di Milano and INFN sez. Milano, I-20133 Milano, Italy*
[10]*INFN—Laboratori Nazionali di Legnaro, I-35020 Legnaro, Italy*
[11]*St. Kliment Ohridsky University of Sofia, BG-1164 Sofia, Bulgaria*
[12]*Laboratorio de Radiaciones Ionizantes, Universidad de Salamanca, E-37008 Salamanca, Spain*
[13]*Department of Physics, Lund University, S-22100 Lund, Sweden*
[14]*Dipartmento di Fisica, Università di Milano, I-20133 Milano, Italy*
[15]*INFN—Laboratori Nazionali del Sud, I-95125 Catania, Italy*
[16]*Faculty of Mathematics and Physics, Comenius University, SK-84215 Bratislava, Slovak Republic*

(Received 1 October 2009; published 15 December 2009)

The nuclear structure of neutron-rich $N > 126$ nuclei has been investigated following their production via relativistic projectile fragmentation of a $E/A = 1$ GeV ^{238}U beam. Metastable states in the $N = 128$ isotones ^{208}Hg and ^{209}Tl have been identified. Delayed γ-ray transitions are interpreted as arising from the decay of $I^{\pi} = (8^{+})$ and $(17/2^{+})$ isomers, respectively. The data allow for the so far most comprehensive verification of the shell-model approach in the region determined by magic numbers $Z < 82$ and $N > 126$.

DOI: 10.1103/PhysRevC.80.061302 PACS number(s): 25.70.Mn, 23.35.+g, 27.80.+w, 29.30.Kv

The understanding of how shell structure arises and develops is a major goal in contemporary nuclear physics. To this end, it is of particular importance to measure the properties of nuclei in the vicinity of closed shells. Information on the single-particle energies, proton-neutron interactions, and two-body residual interactions can be derived from experimental observables such as masses, energies of excited states, and transition probabilities [1].

Furthermore, information on the global behavior of nuclei can be obtained from the energy spacing of the lowest lying states in even-even systems. Recently, it was shown that there is direct empirical correlation between the *p-n* interaction strength and the growth of collectivity determined from the energies of the first 2^{+} and 4^{+} excitations [2]. The *p-n* interaction [2–4], especially among valence nucleons, is an important factor in controlling the onset and development of collectivity and deformation in nuclei and in determining the structure of nuclear transition regions. However, there is no double-magic nucleus (above mass 48), around which spectroscopic data are available in all four quadrants beyond the one- and two-particle neighbors.

Although many nuclei in the ^{208}Pb region have been studied, we have no information on the excited states of even-even nuclei in the "southeast" quadrant defined by $Z < 82$ and $N > 126$. Yet, such nuclei, representing the particle-hole sector surrounding ^{208}Pb, are critical for understanding the effects of seniority, the onset of proton-neutron configuration mixing that drives collectivity and nuclear deformation. This study provides the first spectroscopic data on an even-even nucleus in this region, namely ^{208}Hg, and it allows the first detailed verification of the shell-model approach and nucleon-nucleon interaction in this region away from the semi-magic nuclei and the particle-hole neighbor ^{208}Tl [5]. Recently, the mass of ^{208}Hg was measured [4], allowing the extraction of the average *p-n* interaction for ^{210}Pb, the first value in the proton-hole-neutron-particle quadrant. The combination of mass and spectroscopic data is essential in understanding the evolution of structure near doubly magic nuclei. Indeed, it has recently been shown that the link between masses and structure is stronger and more sensitive than hitherto thought [6]. Furthermore, because the newly accessible region near ^{132}Sn [7] shares many similarities with the Pb region, studies

*Corresponding author: Z.Podolyak@surrey.ac.uk

in the latter may have broader implications for the former and for other doubly magic regions in exotic nuclei.

To date, our knowledge of the properties of heavy neutron-rich nuclei at or near the $N = 126$ shell is very limited. In the case of nuclei with $Z < 82$ and $N > 126$, excited states were reported only in ^{208}Tl [8] and ^{209}Tl [9,10]. The lack of information on nuclei in this region is mainly from the difficulties in creating and populating excited states in these neutron-rich nuclei. Fragmentation has proven to be an efficient tool for producing exotic nuclear species, and when combined with high sensitivity γ-detection arrays, structural information can be gained for otherwise inaccessible nuclei. The highest sensitivity is achieved with both isomeric and β-delayed γ-ray spectroscopy techniques; delayed γ rays are time-correlated with individually identified ions, thereby minimizing the associated background radiation [11–13]. Information on the excited states populated in this way can be obtained when producing only a few hundred nuclei of interest [12]. In this rapid communication, results on the structure of heavy neutron-rich nuclei with $N > 126$ are reported. Isomeric states in the $N = 128$ isotones ^{208}Hg and ^{209}Tl have been identified for the first time. Preliminary experimental results have been reported in conference proceedings [14,15].

Heavy neutron-rich nuclei were populated in relativistic energy projectile fragmentation. The primary ^{238}U beam at an energy of $E/A = 1$ GeV was provided by the SIS-18 accelerator at GSI, Darmstadt, Germany. The maximum primary beam intensity was $\sim 10^9$ ions/spill. The $\simeq$2 s spills were separated by $\simeq$2 s periods without beam. The ^{238}U ions impinged on a target composed of 2.5 g/cm^2 ^{9}Be + 223 mg/cm^2 Nb, where the Nb foil serves for electron stripping of the reaction products. The nuclides of interest were selected and identified in flight on an event-by-event basis by the Fragment Separator (FRS) [16]. The FRS was optimized for the transmission of ^{205}Pt ions. Details of the experiment and particle identification technique are given in Refs. [14], [15], and [17–19]. The transmitted (and identified) ions were slowed down in a variable-thickness aluminium degrader and finally implanted in an active stopper. The total number of implants included $\sim$700 ^{208}Hg and $\sim$620 ^{209}Tl nuclei.

The stopper covered an area of 15×5 cm^2 and had a thickness of 2 mm. It consisted of six double-sided silicon detectors, each of size 5×5 cm^2 and 1 mm thickness [20]. It was surrounded by the Rare Isotope Investigations at GSI (RISING) germanium array in the "Stopped Beam" configuration. The array consists of 15 Euroball cluster germanium detectors and has a photopeak efficiency of $\sim$15% at 661 keV [18].

Correlated with the implanted ions, γ decays following both internal decay and β decay have been recorded. The particle identification is confirmed by the observation of the previously reported isomeric decays in ^{204}Au [21], ^{205}Au [21,22], and ^{206}Hg [23]. The γ-ray spectrum as well as the decay curve associated with ^{206}Hg are shown in Fig. 1(a). The half-life of the $I^\pi = 10^+$ isomeric state obtained in our work, $T_{1/2} =$ 96(15) ns, is in good agreement with the previously measured value of $T_{1/2} = 92(8)$ ns [23].

Evidence of decays from isomeric states in the $N =$ 128 isotones ^{208}Hg and ^{209}Tl is observed. Delayed γ rays associated with ^{208}Hg nuclei are shown in Fig. 1(b). Three γ-ray transitions with energies 203, 425, and 669 keV, together with characteristic Hg K_α X rays are identified. The three γ-ray transitions are in mutual coincidence, and they have similar half-lives within experimental uncertainties. The measured half-life is $T_{1/2} = 99(14)$ ns [see inset to Fig. 1(b)]. The measured relative γ-ray intensities are $I_\gamma(669.0) = 100(16)$, $I_\gamma(424.9) = 107(16)$, and $I_\gamma(203.0) = 77(11)$. Assuming that the three γ-ray transitions form a single cascade, the total transition intensities have to be equal, and the conversion coefficient of the 203 keV transition can be determined

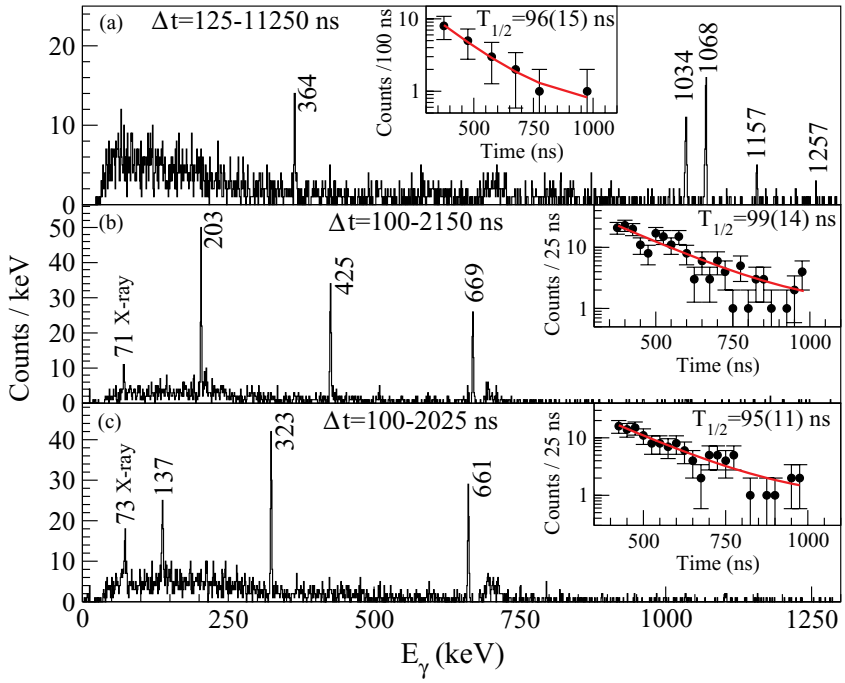

FIG. 1. (Color online) Delayed γ-ray spectra and decay curves associated with (a) $^{206}_{80}$Hg [23], (b) $^{208}_{80}$Hg, and (c) $^{209}_{81}$Tl.

TABLE I. Comparison between experimental and shell-model $B(E2)$ transition strengths. Values are given in Weisskopf units. Effective charges of 1.5 e for protons and 1.0 e for neutrons were assumed.

Nucleus	Transition	$B(E2)_{\rm exp}$	$B(E2)_{\rm calc}$
^{210}Pb	$8^+ \rightarrow 6^+$	0.64(7) [28,29]	0.69
^{206}Hg	$(10^+) \rightarrow (8^+)$	0.99(18) [23,30]	0.87
^{208}Hg	$(8^+) \rightarrow (6^+)$	1.95(39)–1.58(22)[a]	1.22
^{209}Tl	$(17/2^+) \rightarrow (13/2^+)$	1.87(22)–1.51(18)[a]	0.96

[a]Assuming a transition energy between 20 and 80 keV.

(the other transitions are considered to have $E2$ character): $\alpha = 0.36(6)$. This suggests that the 203 keV transition has $E2$ ($\alpha_{\rm the} = 0.37$) character. The amount of K_α X rays following the conversion electron emission is in agreement with the observed intensity.

In ^{209}Tl, an isomeric decay in a similar time range is in evidence. γ rays with energies of 137, 323, and 661 keV, together with the characteristic Tl K_α X ray are identified [see Fig. 1(c)]. The 137, 323, and 661 keV transitions are in mutual coincidence, and their half-lives agree within errors. Therefore, they form a cascade. No parallel branches are observed. From the γ-ray intensities, $I_\gamma(323.1) = 100(15)$, $I_\gamma(661.2) = 96(19)$, and $I_\gamma(136.8) = 41(10)$, the conversion coefficient of the 137 keV transition can be determined: $\alpha = 1.5(4)$, suggesting that it is an $E2$ ($\alpha_{\rm the} = 1.60$). The amount of K_α X rays following the conversion electron emission is in agreement with the observed intensity. The measured half-life is $T_{1/2} = 95(11)$ ns [see inset to Fig. 1(c)].

To obtain a quantitative understanding of the underlying single-particle structure of the excited states in the $N = 128$ nuclei ^{208}Hg and ^{209}Tl, shell-model calculations have been performed. The OXBASH code [24] was employed. The model space considered consisted of the proton orbitals $2d_{5/2}$, $2d_{3/2}$, $3s_{1/2}$, and $1h_{11/2}$ below the $Z = 82$ closed shell and the neutron orbitals $2g_{9/2}$, $1i_{11/2}$, and $1j_{15/2}$ above the closed $N = 126$ shell. Therefore, no core excitations across the ^{208}Pb double-shell closure are allowed. The single proton-hole and neutron-particle energies are taken from the experimental spectra of ^{207}Tl and ^{209}Pb, respectively. The two-body interaction matrix elements (TBMEs) are from Ref. [25]. These are based on the Kuo-Herling realistic interaction [26] for proton-proton and neutron-neutron TBMEs derived from a free nucleon-nucleon potential with core polarization renormalization needed due to the finite model space. The proton-neutron interaction is the bare H7B G matrix [27] without core polarization as justified in Ref. [25]. The only additional correction made in this work is a shift of +40 keV to the $(\nu g_{9/2})^2_{8+}$ TBME to get the correct ordering of the 6^+ and 8^+ sequence in ^{208}Hg. The interaction reproduces very well binding energies, excited states, and $B(E2)$ transition strengths (see Table I) in the two-proton-hole and two-neutron-particle nuclei ^{206}Hg and ^{210}Pb.

The ^{208}Hg nucleus has two-proton holes and two-neutron particles outside the doubly magic $^{208}_{82}$Pb$_{126}$ core. The results of the shell-model calculations are shown in Fig. 2. The comparison with the experimental information suggests an 8^+ assignment for the observed isomer. The three observed transitions at 669, 425, and 203 keV correspond to the $6^+ \rightarrow 4^+ \rightarrow 2^+ \rightarrow 0^+$ sequence. The $8^+ \rightarrow 6^+$ transition is not observed because of the high conversion coefficient at low energies. All these states are of predominantly $\nu g^2_{9/2}$ character. The low intensity of the observed K_α X ray indicates that the energy of this missing transition is below the binding energy of the K electron (i.e., below 83.1 keV). The transition strength extracted from the experiment is slightly larger than the calculated value of $B(E2) = 1.22$ W.u. (see Table I). The ground-state mass [4] is well reproduced by the calculations.

The ^{209}Tl nucleus has one-proton-hole and two-neutron-hole particles outside the doubly magic $^{208}_{82}$Pb$_{126}$ core. The calculation (see Fig. 2) suggests a $17/2^+$ isomeric state that

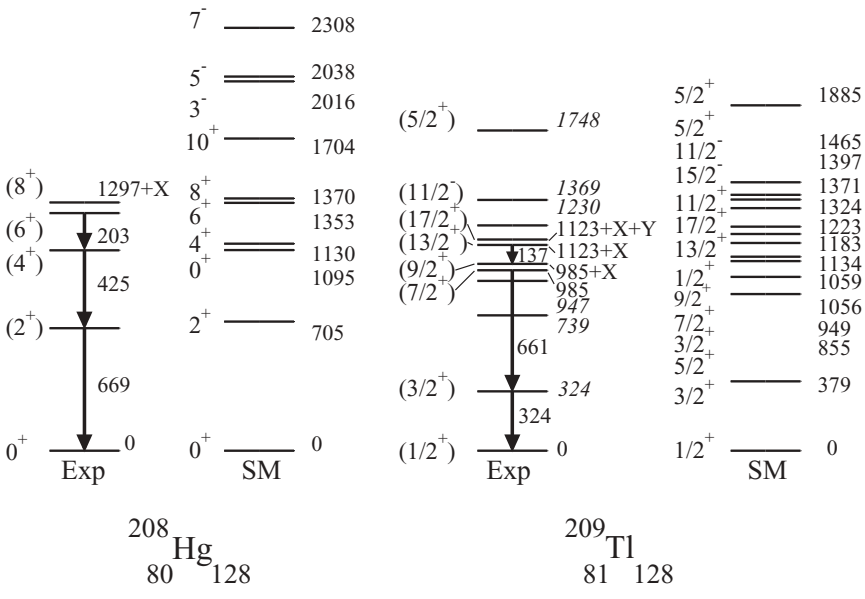

FIG. 2. Experimental and calculated partial level schemes of the $N = 128$ ^{208}Hg and ^{209}Tl nuclei. The excited states labeled in italics in ^{209}Tl were already known [9,10].

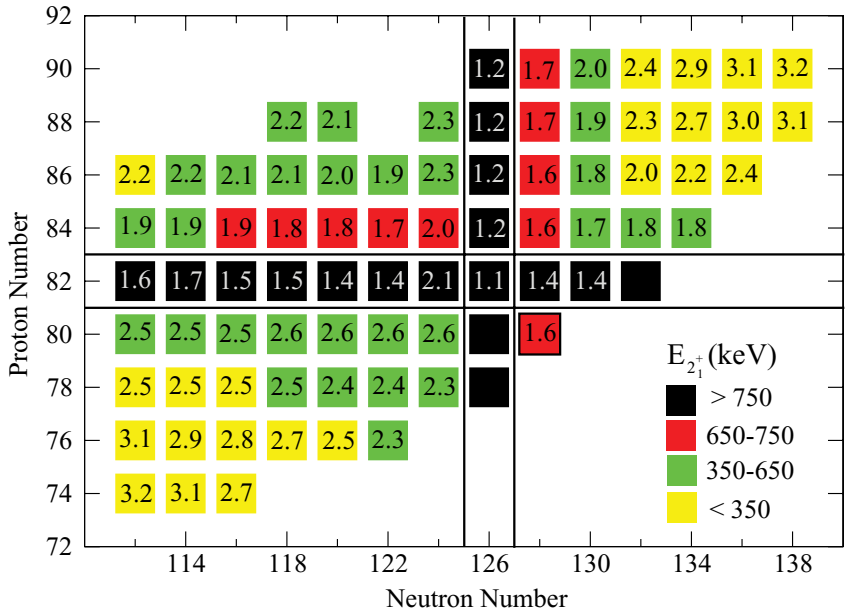

FIG. 3. (Color online) Systematics of the $E(2^+)$ energies and the $E(4^+)/E(2^+)$ energy ratios for even-even nuclei around ^{208}Pb. The red box with a black square is from the current work on ^{208}Hg.

would decay via the $17/2^+ \rightarrow 13/2^+ \rightarrow 9/2^+ \rightarrow 7/2^+ \rightarrow 3/2^+ \rightarrow 1/2^+$ sequence. The isomer has predominantly a $\nu(g_{9/2})^2_{8+}\pi s_{1/2}$ character and decays via an unobserved low-energy $E2$ transition into the mainly $\nu(g_{9/2})^2_{6+}\pi s_{1/2}$ $13/2^+$ state. The 137 and 661 keV lines are interpreted as the $13/2^+ \rightarrow 9/2^+$ and $7/2^+ \rightarrow 3/2^+$ transitions, respectively. The low-energy $9/2^+ \rightarrow 7/2^+$ allowed $M1$-transition connecting states with a $(\nu g_{9/2})^2_{4+}\pi s^{-1}_{1/2}$ configuration is not observed. The low intensity of the observed K_α line indicates that the energies of both unobserved transitions are below the binding energy of the K electron (i.e., below 85.5 keV). The γ-decay scenario is a consequence of the $(^{210}\mathrm{Pb}; I) \times s_{1/2}$ weak-coupling structure of ^{209}Tl, which forbids $\Delta I = 2$ $M1$ transitions as reflected in the shell-model wave functions.

The region around the doubly magic nucleus ^{208}Pb presents a unique testing ground of basic nuclear physics concepts. With the new results on ^{208}Hg, this is the only region of the nuclide chart above ^{48}Ca where information is available on excited states on all four neighboring even-even nuclei (see Fig. 3). The general trend is that with an increasing number of valence protons and neutrons, the yrast $E(2^+)$ energy decreases and the $E(4^+)/E(2^+)$ ratio increases toward 3.3. By concentrating on two-proton, two-neutron nuclei outside the closed shell, one observes that the 2^+ energies are similar, ~700 keV, for three of these nuclei (^{208}Hg, ^{212}Po, and ^{206}Po) but much lower for ^{204}Hg. Likewise, the $E(4^+)/E(2^+)$ ratio is around 1.6–2.0 for the former three and much larger for ^{204}Hg. This is understood by considering the individual proton and neutron orbitals around the closed shell. For example, in ^{208}Hg, the predominant character of the observed yrast states is $(\nu g_{9/2})^2_{8+}$. Therefore, their energies can be directly compared with the corresponding states in the two-neutron nucleus ^{210}Pb. The energies of the 4^+, 6^+, and 8^+ states are very similar, indicating that the proton admixture into these states in ^{208}Hg is small. However, the 2^+ state in ^{208}Hg is 130 keV lower than in ^{210}Pb. The lowering is primarily caused by mixing the $\pi s_{1/2}d_{3/2}$ configuration (which is predominant in the 2^+ state of ^{206}Hg) with the $(\nu g_{9/2})^2_{2+}$ partition. A similar constellation preserves the dominant $\pi g^2_{9/2}$ configuration in $^{208,210,212}_{84}$Po. In contrast, ^{204}Hg is governed by $j = 1/2$–$5/2$ low-spin orbitals resembling the classical deformation driving the SU(3) structure in the sd shell and the $f_{5/2}, p$ shell above ^{56}Ni.

From mass measurement, it was shown [4] that the general rule that the average p-n interaction is large if both protons and neutrons are above or below the shell closure, and small if one of them is above and the other below such a closure, applies for the nuclei around ^{208}Pb [4]. However, as we see in Fig. 3, this symmetry does not apply if we look into energies of the simplest excitations. To understand the excitation spectrum of nuclei, configuration-specific information about the nucleon-nucleon interaction is needed [31]. The information on the excited states of ^{208}Hg and ^{209}Tl obtained in our work tests this configuration-specific nucleon-nucleon interaction.

In summary, we have identified metastable states in the $N = 128$ isotones, ^{208}Hg and ^{209}Tl. The data provide the first comprehensive experimental test of shell-model calculations and residual interactions for the model space $Z < 82$, $N > 126$. Our results and those of Ref. [4] represent the beginnings of nuclear structure studies in this entire, hitherto unknown, major shell quadrant to the "southeast"of ^{208}Pb. Other experiments, extending this information further into the quadrant in the direction toward increasing the neutron number and/or decreasing the proton number, although very challenging, would be highly valuable.

The excellent work of the GSI accelerator staff is acknowledged. We thank R. F. Casten for fruitful discussions. This work is supported by the EPSRC(UK), STFC(UK), the Iraqi Ministry of Higher Eduction and Scientific Research, the University of Kerbala, AWE plc, the Hungarian OTKA K68801, the Italian INFN, the Spanish Ministerio de Educacion y Ciencia, and the German BMBF.

[1] B. A. Brown, Prog. Part. Nucl. Phys. **47**, 517 (2001).
[2] R. B. Cakirli and R. F. Casten, Phys. Rev. Lett. **96**, 132501 (2006).
[3] D. S. Brenner, R. B. Cakirli, and R. F. Casten, Phys. Rev. C **73**, 034315 (2006).
[4] L. Chen *et al.*, Phys. Rev. Lett. **102**, 122503 (2009).
[5] M. Rejmund *et al.*, Eur. Phys. J. A **8**, 161 (2000).
[6] R. B. Cakirli, R. F. Casten, R. Winkler, K. Blaum, and M. Kowalska, Phys. Rev. Lett. **102**, 082501 (2009).
[7] A. Jungclaus *et al.*, Phys. Rev. Lett. **99**, 132501 (2007).
[8] M. J. Martin, Nucl. Data Sheets **108**, 1583 (2007).
[9] C. Ellegaard, P. D. Barnes, and E. R. Flynn, Nucl. Phys. **A259**, 435 (1976).
[10] M. J. Martin, Nucl. Data Sheets **63**, 723 (1991).
[11] R. Grzywacz *et al.*, Phys. Lett. **B355**, 439 (1995).
[12] M. Pfützner *et al.*, Phys. Lett. **B444**, 32 (1998).
[13] Zs. Podolyák *et al.*, Phys. Lett. **B491**, 225 (2000).
[14] N. Al-Dahan *et al.*, Acta Phys. Pol. B **40**, 871 (2009).
[15] N. Al-Dahan *et al.*, AIP Conf. Proc. **1090**, 145 (2009).
[16] H. Geissel *et al.*, Nucl. Instrum. Methods B **70**, 286 (1992).
[17] S. J. Steer *et al.*, Phys. Rev. C **78**, 061302 (2008).
[18] S. Pietri *et al.*, Nucl. Instrum. Methods B **261**, 1079 (2007); P. H. Regan *et al.*, Nucl. Phys. **A787**, 491c (2007).
[19] Zs. Podolyák *et al.*, Phys. Lett. **B672**, 116 (2009).
[20] R. Kumar *et al.*, Nucl. Instrum. Methods A **598**, 754 (2009); P. H. Regan *et al.*, Int. J. Mod. Phys. E **17**, 8 (2008).
[21] S. J. Steer *et al.*, Int. J. Mod. Phys. E **18**, 1002 (2009).
[22] Zs. Podolyák *et al.*, Eur. Phys. J. A **42**, 489 (2009).
[23] B. Fornal *et al.*, Phys. Rev. Lett. **87**, 212501 (2001).
[24] B. A. Brown *et al.*, OXBASH for Windows, MSU-NSCL Report No. 1289, 2004.
[25] E. K. Warburton, Phys. Rev. C **44**, 233 (1991).
[26] T. T. S. Kuo and G. H. Herling, U.S. Naval Research Laboratory Report No. 2258, 1971 (unpublished).
[27] A. Hosaka, K.-I. Kubo, and H. Toki, Nucl. Phys. **A444**, 76 (1985).
[28] E. Browne, Nucl. Data Sheets **99**, 649 (2003).
[29] D. J. Decman *et al.*, Phys. Rev. C **28**, 1060 (1983).
[30] F. G. Kondev, Nucl. Data Sheets **109**, 1527 (2008).
[31] K. H. Maier and M. Rejmund, Eur. Phys. J. A **14**, 349 (2002).

Isomeric states in neutron-deficient $A \sim 80$–90 nuclei populated in the fragmentation of ^{107}Ag

A. B. Garnsworthy,[1,2,*] P. H. Regan,[1] S. Pietri,[1] Y. Sun,[3] F. R. Xu,[4] D. Rudolph,[5] M. Górska,[6] L. Cáceres,[6,7] Zs. Podolyák,[1] S. J. Steer,[1] R. Hoischen,[5,6] A. Heinz,[2] F. Becker,[6] P. Bednarczyk,[6,8] P. Doornenbal,[6] H. Geissel,[6] J. Gerl,[6] H. Grawe,[6] J. Gręboszz,[6,8] A. Kelic,[6] I. Kojouharov,[6] N. Kurz,[6] F. Montes,[6] W. Prokopwicz,[6] T. Saito,[6] H. Schaffner,[6] S. Tachenov,[6] E. Werner-Malento,[9,†] H. J. Wollersheim,[6] G. Benzoni,[10] B. Blank,[11] C. Brandau,[1] A. M. Bruce,[12] F. Camera,[10] W. N. Catford,[1] I. J. Cullen,[1] Zs. Dombrádi,[13] E. Estevez,[14] W. Gelletly,[1] G. Ilie,[15,16] J. Jolie,[15] G. A. Jones,[1] A. Jungclaus,[7,17] M. Kmiecik,[8] F. G. Kondev,[18] T. Kurtukian-Nieto,[14] S. Lalkovski,[12,19] Z. Liu,[1] A. Maj,[8] S. Myalski,[8] M. Pfützner,[9] S. Schwertel,[20] T. Shizuma,[1,21] A. J. Simons,[1,22] P. M. Walker,[1] and O. Wieland[10]

[1]*Department of Physics, University of Surrey, Guildford, Surrey GU2 7XH, United Kingdom*
[2]*WNSL, Yale University, New Haven, Connecticut 06520, USA*
[3]*Department of Physics, Shanghai Jiao Tong University, Shanghai 200240, People's Republic of China*
[4]*Department of Technical Physics, Peking University, Beijing 100871, People's Republic of China*
[5]*Department of Physics, Lund University, S-22100 Lund, Sweden*
[6]*GSI, D-64291 Darmstadt, Germany*
[7]*Departmento di Teórica, Universidad Autonoma de Madrid, E-28050 Madrid, Spain*
[8]*The Institute of Nuclear Physics, PL-31-342 Kraków, Poland*
[9]*IEP, Warsaw University, PL-00-681 Warsaw, Poland*
[10]*Universitá degli Studi di Milano and INFN Milano, I-20133 Milano, Italy*
[11]*CENBG, F-33175 Gradignan Cedex, France*
[12]*School of Environment and Technology, University of Brighton, Brighton BN2 4GJ, United Kingdom*
[13]*Institute of Nuclear Research, H-4001 Debrecen, Hungary*
[14]*Universidad de Santiago de Compostela, E-15705 Santiago de Campostela, Spain*
[15]*IKP, Universität zu Köln, D-50937 Köln, Germany*
[16]*National Institute of Physics and Nuclear Engineering, Bucharest, Romania*
[17]*Instituto de Estructura de la Materia, CSIC, Serrano, E-28006 Madrid, Spain*
[18]*Nuclear Engineering Division, Argonne National Laboratory, Argonne, Illinois 60439, USA*
[19]*Faculty of Physics, University of Sofia "St. Kliment Ohridsk" Sofia, Bulgaria*
[20]*Physik Department E12, Technische Universität München, D-80290 München, Germany*
[21]*Japan Atomic Energy Agency, Kyoto 619-0215, Japan*
[22]*Atomic Weapons Establishment, Aldermaston, Berkshire RG7 4PR, United Kingdom*

(Received 3 July 2009; published 7 December 2009)

The relativistic projectile fragmentation of a 750 MeV per nucleon beam of ^{107}Ag was used to populate isomeric states in neutron-deficient nuclei around $A = 80$–90. Reaction products were separated and unambiguously identified using the GSI FRagment Separator (FRS) and its ancillary detectors. At the final focal plane, the fragments were slowed from relativistic energies by means of an aluminium degrader and implanted in a passive stopper in the center of the high-efficiency, high-granularity Stopped Rare Isotope Spectroscopic INvestigation at GSI (RISING) germanium array. This allowed the identification of excited states in the $N = Z$ nuclei $^{86}_{43}$Tc and, for the first time, $^{82}_{41}$Nb. Isomeric states have also been identified for the first time in ^{87,88}Tc, and a previously unreported isomer was observed in ^{84}Nb. Experimental results are presented along with a discussion on the structure of these nuclei based on interpretations provided by several theoretical models.

DOI: 10.1103/PhysRevC.80.064303 PACS number(s): 29.30.Kv, 23.20.Lv, 23.35.+g, 27.50.+e

I. INTRODUCTION

The region of nuclei close to the $N = Z$ line between ^{56}Ni and ^{100}Sn is a region containing a diverse mixture of nuclear structure features. A low density of single-particle energy levels between the spherical magic numbers 28 and 50 leads to the appearance of prominent shell gaps at oblate ($N, Z = 34, 36$), spherical (40), and prolate (34, 38) shapes [1]. In nuclei close to $N = Z$, neutrons and protons occupy the same single-particle levels. This feature reinforces the tendency for the nucleus to assume a deformed shape and leads to dramatic shape changes with the addition of only a few nucleons [2] or a few hundred keV of excitation [3]. This situation produces several opportunities for excited nuclear states to become long-lived. Shape isomers are possible in this region [3], and the presence of both low-j ($2p_{1/2}$, $2p_{3/2}$) and high-j ($f_{5/2}$, $g_{9/2}$) orbitals can lead to spin-trap isomeric states [4,5]. Toward the top of the shell, nuclear shapes become softer and the $N = Z$ line moves through a transitional region. The proximity now to the N and $Z = 50$ shell closures also

*Present address: TRIUMF, 4004 Wesbrook Mall, Vancouver, BC, Canada V6T 2A3; garns@triumf.ca
†Present address: Institute of Physics Polish Academy of Science, Al. Lotników 32/46, PL-02-668 Warsaw, Poland.

makes seniority isomers an important consideration [6]. The identification and interpretation of isomeric states in this region can lead to important insights into the wide variety of nuclear structure features at play.

The study of $N \sim Z$ nuclei also has important implications in the understanding of explosive nucleosynthesis in nuclear astrophysics. It has been suggested that in x-ray emitting binary systems, nuclei are synthesized via the rapid proton capture process (rp-process) [7] in which a sequence of proton captures and β decays is responsible for the burning of hydrogen into heavier elements. The rp-process proceeds through the exotic mass region with $N \sim Z$ above ^{56}Ni close to the proton dripline. Modern reaction network calculations [8] have suggested that the rp-process can extend up to the heavy Sn-Te mass region, involving nuclei of interest in the current study. Because the detailed reaction rates depend sensitively on the nuclear structure, any information on the low-energy levels of relevant nuclei is potentially of significant importance for such calculations [9].

Projectile fragmentation provides a viable mechanism with which to populate nuclei far from the valley of stability. Long-lived nuclear states present the opportunity to study excited states and structure in exotic nuclei. Several studies involving the fragmentation of heavy ion beams of ^{92}Mo [10], ^{106}Cd [11,12], and ^{112}Sn [13,14] have been carried out to study $N \approx Z$ nuclei between $A = 80 \rightarrow 100$. This article presents experimental results of isomer spectroscopy performed on nuclei populated after the fragmentation of ^{107}Ag projectiles. The structure of the excited states observed in these nuclei is discussed in the framework of the shell model, projected shell-model (PSM), and configuration-constrained total Routhian surface (TRS) calculations.

II. EXPERIMENTAL DETAILS

The experiment was performed as part of the Rare Isotope Spectroscopic INvestigation at GSI (RISING) project [15], an international collaboration using relativistic projectile fragmentation (or fission) reactions to study many aspects of nuclear structure. In the current experiment, the first of the "Stopped beam" campaign, a primary beam of ^{107}Ag ions with 750 MeV per nucleon was provided by the SIS-18 Synchrotron located at Gesellschaft für Schwerionenforschung (GSI). The beam was incident on a 4-g/cm^2 Be production target. The products from projectile fragmentation reactions were transported to the focal plane of the GSI FRagment Separator (FRS) [16], which was operated in achromatic mode. Each transmitted ion was unambiguously identified by measurements of time-of-flight (TOF), position, and energy loss (ΔE) in a series of beamline detectors whose relative positions are shown schematically in Fig. 1. These parameters, when combined with the magnetic rigidity of the dipole magnets, are used to extract the mass-to-charge ratio, A/q, and Z of the transmitted ions on a particle-by-particle basis. In this $B\rho - \Delta E - B\rho$ identification method (where $B\rho$ means magnetic rigidity), a 3.7 g/cm^2 degrader was used at the central focal plane of the FRS (S2 degrader). Further details of the particle identification analysis can be found in Refs. [16] and [17].

After separation and identification, the ions were slowed in a variable-thickness aluminium degrader (S4 degrader) and brought to rest in a multilayer perspex stopper with a total thickness of 7 mm. This passive stopper is located at the central focus of the Stopped RISING germanium array [17,18]. This high-efficiency, high-granularity array consists of 105 hyper-pure germanium detectors arranged in 15 clusters of seven crystals each. The clusters are arranged in three rings at 51°, 90°, and 129° to the secondary beam axis. Gamma rays emitted in the decay of isomeric states are detected in the array and correlated with the arrival of the associated ion. The array has a singles full photopeak efficiency of 11% at 1.3 MeV [18] without add back, and because of the passive stopper being located in air, the absence of a beam pipe between the decaying nucleus and the detectors leads to a γ-ray singles photopeak efficiency of ~34% at 80 keV (with a perspex stopper).

The XIA digital pulse processors (digital gamma finder) DGF4 are used to process the signals recorded by the germanium detectors [17]. The DGF4 module produces an energy and an absolute time-stamp signal with a time resolution of

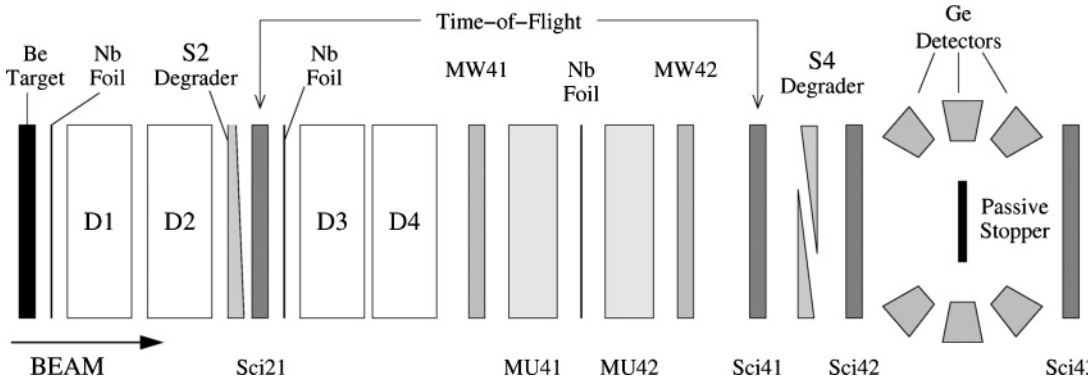

FIG. 1. Schematic outline of the GSI FRS and the suite of beamline detectors used for event-by-event particle identification in the current work. The fragmentation products traverse four dipole magnets (D1–4), two aluminium degraders (S2 and S4), two multiwire proportional counters (MW41,42), two MUSIC (MU41,42), and three scintillators (Sci21,41,42) before coming to rest in a perspex passive stopper at the center of the RISING Stopped Ge array. An additional scintillator (Sci43) is also present after the stopper to veto any ions that do not come to rest there.

TABLE I. Spill structures of the various FRS settings.

Nucleus of central transmission	^{107}Ag ions per spill	Extraction length (s)	Total spill time (s)	Measuring period (h)
^{96}Pd	4×10^6	10	30	16
^{90}Rh	$2–3 \times 10^9$	6	25	5
^{86}Tc	$1–3 \times 10^9$	5–6	25	90
^{82}Nb	2×10^9	5	25	5

25 ns. Two additional analog timing signals are produced by short-range (SR) and long-range (LR) TDCs. These TDCs have 0.293-ns resolution in a total recording period of 850 ns and 0.76-ns resolution in a total recording period of 140 μs, respectively. The start signal for each timing signal comes from a scintillator (Sci41) located immediately before the S4 degrader and before the stopper. The stop signal is provided by the associated Ge crystal.

The magnetic field strength of the dipole magnets of the FRS can be tuned to maximize the transmission of a specific nuclear species. During this experiment, different settings, focused on the fully stripped species of $^{96}_{46}$Pd, $^{90}_{45}$Rh, $^{86}_{43}$Tc, and $^{82}_{41}$Nb, were used. Table I shows the spill structure and measuring period of each setting. The magnetic field strength and S4 degrader thicknesses are shown in Table II. Several nuclear species were transmitted to the focal plane in multiple settings, and in the final analysis, the data from different settings were combined where appropriate.

A. Particle identification and methods of background reduction

The standard particle identification variables are the atomic number, Z, calculated from the energy loss in multisampling ionization chambers (MUSIC) [19], and the mass-to-charge ratio, A/q, determined from measurements of magnetic rigidity and the TOF between Sci21 and Sci41 (Fig. 1). These variables were calibrated using measurements of the primary beam, in this case, ^{107}Ag. Figure 2 shows the identification plot determined by these variables for the combined ^{90}Rh, ^{86}Tc, and ^{82}Nb settings. Gamma-ray spectra associated with delayed events in individual nuclear species can be produced using software coincidence gates on these, and other, particle identification parameters.

Isomeric states that have been previously identified and reported have provided a confirmation of the particle identification and an additional internal calibration of the γ-ray energies, intensities, and timing. Previously reported isomeric decays in ^{94,96}Pd and ^{93}Ru were observed in the current work, and the data obtained are shown in Fig. 3. The half-lives measured for ^{94}Pd and ^{96}Pd in the current work using the digital timing are consistent with those reported in Refs. [20–22].

TABLE II. Magnetic field settings of the dipole magnets of the FRS and the S4 degrader thicknesses used in different settings.

Nucleus of central transmission	D1 (T)	D2 (T)	D3 (T)	D4 (T)	S4 degrader, Al thickness (mg/cm^2)
^{96}Pd	0.73085	0.73284	0.54660	0.54910	1900
^{90}Rh	0.70210	0.70420	0.51880	0.52090	1500
^{86}Tc	0.70015	0.70214	0.52920	0.53150	1900
^{82}Nb	0.70240	0.70460	0.54170	0.54400	2400

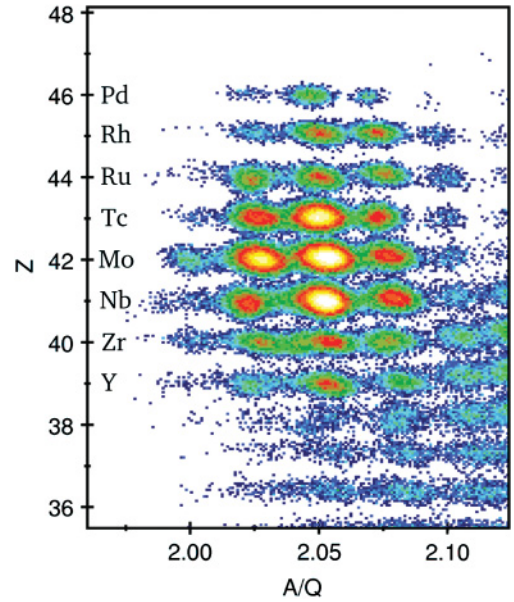

FIG. 2. (Color online) Final, calibrated Z vs. A/q identification plot from the combined ^{90}Rh, ^{86}Tc, and ^{82}Nb settings.

It is worth emphasizing that, with the exception of those for ^{84}Nb, no γ-ray background subtraction has been performed on any of the spectra shown here. The low background in the gamma-ray spectra is achieved by using this event-by-event method of particle identification that provides very sensitive selection of individual nuclear species. The use of appropriate temporal gating highlights specific isomeric decays in the (typically) 100-ns to 100-μs range. The shortest measurable half-lives are limited by the flight time through the separator and by the large background from bremsstrahlung radiation associated with the implantation of the reaction product in the stopper. The longest measurable half-lives are limited by the length of the hardware coincidence window and the time period between implanted ions. The particle identification for γ-ray spectra is improved through additional software gates on combinations of experimental variables to veto events in which fragments undergo subsequent interactions with materials in the beamline. For example, a comparison of the energy loss in the first and second MUSIC chambers can be used to identify and exclude from the analysis ions that undergo reactions in the gas of the MUSIC chambers or the Nb foil between them (upper panel of Fig. 4). Also, fragments that are destroyed in the S4 degrader can be removed by gating on the energy loss in the first MUSIC chamber (MU41) and the energy loss in scintillator 42, which is located immediately after the S4 degrader (lower panel of Fig. 4). A scintillator is also placed after the RISING Stopped array (Sci43) to identify and veto ions that do not come to rest in, or undergo nuclear reactions in, the final stopper.

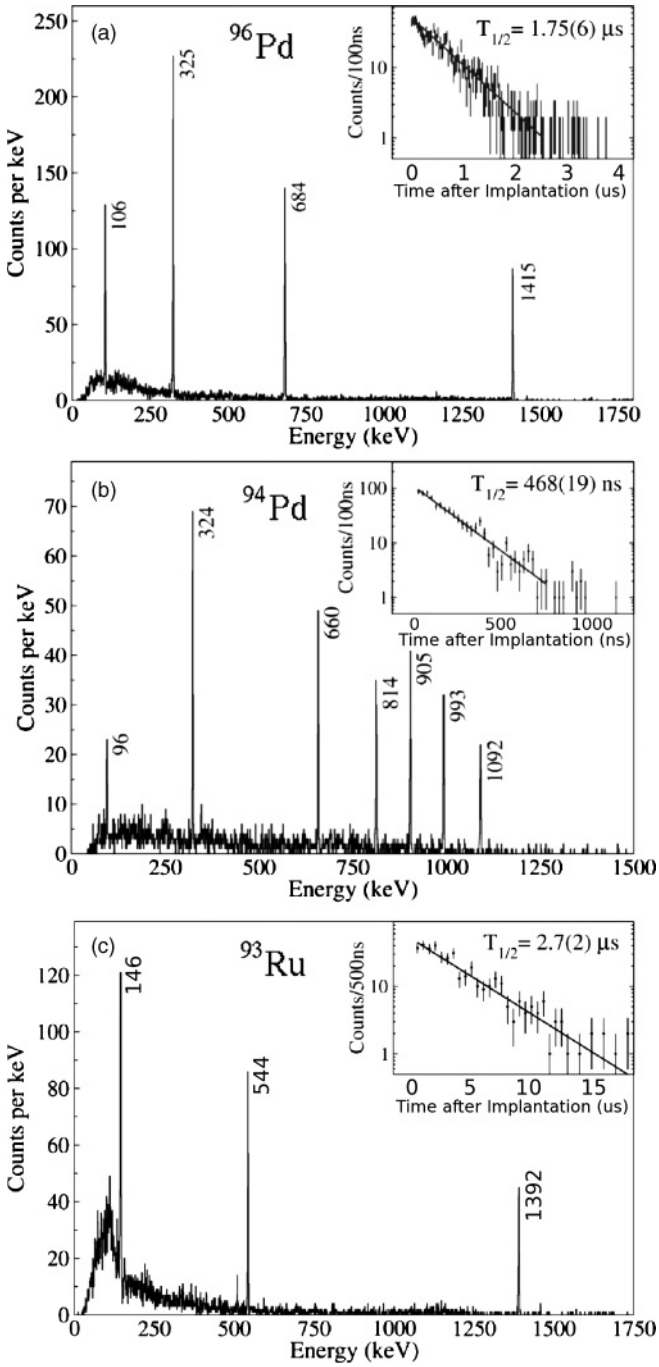

FIG. 3. γ-ray spectra of delayed events associated with ions identified as (a) ^{96}Pd, (b) ^{94}Pd, and (c) ^{93}Ru. The spectra are gated between 150 ns and 5 μs after the time of implantation. The insets show the associated decay curves using a least-squares fit to the DGF timing data.

III. EXPERIMENTAL RESULTS AND DISCUSSION

The primary motivation for the current work was to investigate the low-lying structures in the odd-odd self-conjugate nuclei, ^{82}Nb and ^{86}Tc. Results for these nuclei related to neutron-proton pairing have already been presented in Ref. [23]. Other preliminary results from this work have been presented in a series of conference proceedings [18,24–29].

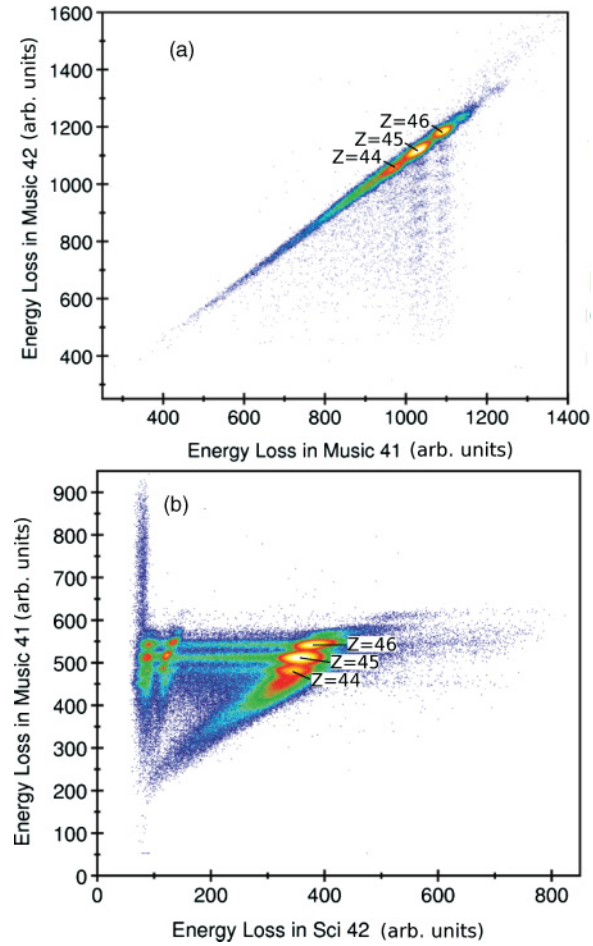

FIG. 4. (Color online) (a) Energy loss in the second MUSIC chamber plotted against energy loss in the first. (b) Energy loss in the first MUSIC chamber plotted against the energy loss in scintillator 42 located immediately after the S4 degrader. Both plots show data collected during the setting focused on ^{96}Pd.

This article reports results from the analysis of the complete data set.

A. Isomeric ratio measurements

The reaction mechanism of projectile fragmentation has been found to populate preferentially the near-yrast states in the product nuclei [30–32]. An isomeric ratio can be defined as the ratio between the number of times a nucleus is populated in that isomeric state and the total number of times that nucleus is produced. Measurements of isomeric ratios can provide insight into both the reaction process and the nature of the observed isomeric states (i.e., an yrast or a nonyrast state). In the current work, the isomeric ratio, R, is defined as in Ref [32] by the expression

$$R = \frac{N_{\text{isomer}}}{N_{\text{ions}} F G}, \tag{1}$$

where N_{isomer} is the number of ions observed in the isomeric state, N_{ions} is the total number of ions of that nuclear species produced, and F and G are correction factors for in-flight losses and for a finite measuring period, respectively. The

number of ions observed in the isomeric state is equal to

$$N_{\text{isomer}} = \sum_i \frac{N_{\gamma_i}}{\epsilon_i} \frac{(1+\alpha_i)}{b_{\gamma_i}}, \tag{2}$$

where N_{γ_i} is the number of γ rays observed in the decay of the ith decay branch depopulating the isomeric state, ϵ_i is the absolute photopeak efficiency of the germanium detectors at that energy, b_γ is the branching ratio of the γ-ray transition, and α_i is the internal conversion coefficient of that γ-ray transition. The correction for in-flight losses is

$$F = \exp\left[-\left(\lambda_{q1}\frac{\text{TOF}_1}{\gamma_1} + \lambda_{q2}\frac{\text{TOF}_2}{\gamma_2}\right)\right], \tag{3}$$

where λ_{qn} is the decay constant for the nucleus in charge state q_n in the first ($n = 1$) and second ($n = 2$) halves of the separator. TOF_1 is the time-of-flight from the production target to the scintillator (Sci21) positioned immediately after the S2 degrader, and TOF_2 is the time-of-flight from Sci21 to Sci41 located immediately before the S4 degrader. γ_n is the corresponding Lorentz factor ($\gamma = \frac{1}{\sqrt{1-(\frac{v}{c})^2}}$). In the mass region of interest here, $A \sim 80$–90, the ions are fully stripped through the full length of the separator so $q_1 = q_2 = Z$. The finite γ-ray measuring time period is accounted for by

$$G = e^{(-\lambda t_i)} - e^{(-\lambda t_f)}, \tag{4}$$

where t_i and t_f are the initial and final measuring times between which the observed isomeric yield is determined. The times are defined with respect to the time of ion implantation in the stopper. Unmeasured losses caused by reaction products being destroyed in the slowing process in the stopper are also taken into account in determining isomeric ratio uncertainties. The isomeric ratios measured in the current experiment are shown in Table III. Also shown are previously reported half-life measurements for comparison that are taken from Refs. [10,21,22,33].

B. $^{82}_{41}\text{Nb}_{41}$

In the work of Chandler *et al.* [10], a short-lived isomeric state was tentatively identified in ^{82}Nb. Low statistics for this nuclide in that experiment prevented the identification of any discrete γ rays or a half-life measurement. The singles spectrum gated on ^{82}Nb ions from the current work is shown in Fig. 5. Three γ rays are now assigned to originate from the decay of this $T_{1/2} = 93(20)$ ns isomeric state [34], and a γ-γ energy coincidence analysis finds all three γ rays to be in mutual coincidence. The level scheme constructed from these data is shown in Fig. 6.

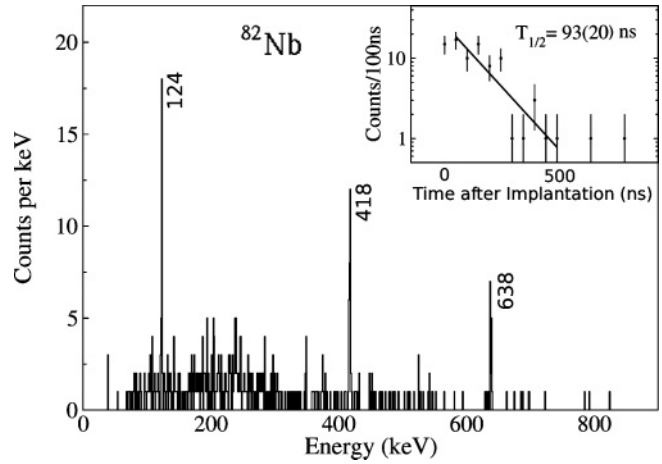

FIG. 5. Singles γ-ray spectrum of delayed events associated with ions identified as ^{82}Nb. The data are gated between 150 and 500 ns after the time of implantation.

The two γ rays at 418 and 638 keV lie close in energy to the $2^+ \rightarrow 0^+$ (407 keV) and $4^+ \rightarrow 2^+$ (634 keV) isobaric analog transitions in ^{82}Zr [35,36]. On this basis, these γ rays are assigned as the first two transitions of the ground-state band in ^{82}Nb. The isomeric state that decays into this band is suggested to have $I = (5)$ based on internal conversion coefficient and transition rate arguments described in detail in Ref. [23].

TRS calculations can be used to predict the deformation and single-particle structure in the vicinity of the Fermi surface in a given nucleus. The configuration-constrained potential-energy-surface calculations developed by Xu *et al.* [37] can predict the deformation for a specific multi-quasiparticle configuration while including the γ degree of freedom. Figure 7 shows a TRS calculation for the ground state of

TABLE III. Isomeric ratios, R, measured in the current experiment. E and J^π refer to the excitation energy, spin, and parity of the isomeric state. The half-lives ($T_{1/2}$) measured in the current work were used to calculate the isomeric ratio quoted. Also shown are previously reported half-life measurements.

Nucleus	E (keV)	J^π	$T_{1/2}$ (this work)	$T_{1/2}$ (other)	R (%)	Number of ions
^{94}Pd	4884	(14^+)	468(19) ns	530(10) ns [21]	28(5)	12721
^{96}Pd	2531	8^+	1.75(6) μs	2.2(3) μs [22]	17(3)	13375
^{93}Ru	2083	$(21/2^+)$	2.7(2) μs	2.20(17) μs [33]	7(1)	44628
^{86}Tc	(1524)	(6^+)	1.10(14) μs	1.11(21) μs [10]	41(7)	7650
^{87}Tc	$71 + x$	$(7/2^+)$	647(24) ns		11(5)	44127
^{88}Tc	95	(4^+)	146(12) ns		6(5)	119298
^{82}Nb	(1180)	(5^+)	93(20) ns		78(77)	4455
^{84}Nb	(48)	(3^+)	176(46) ns		5(2)	240615
^{84}Nb	(305)	(5^+)	50(8) ns		0.5(4)	240615
^{84}Nb	(337)	5^-	92(5) ns	102(19) ns [10]	16(7)	240615

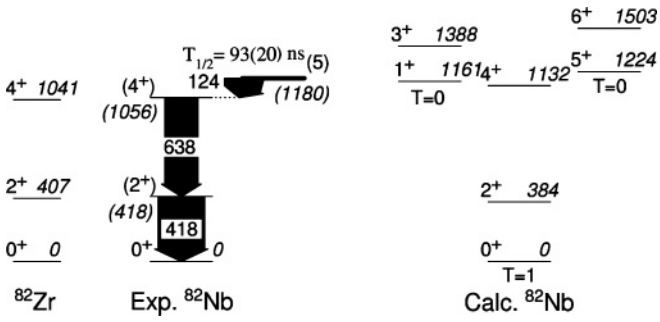

FIG. 6. Experimental level scheme of ^{82}Nb constructed from the current data and results of a PSM calculation. The isobaric analog states in ^{82}Zr are also shown for comparison.

^{82}Nb. The calculation predicts a large stable prolate deformation with $\beta_2 = 0.430$. This compares well with the value of $\beta_2 = 0.41(7)$ in the isobaric analog, ^{82}Zr, which was deduced from the $B(E2 : 2^+ \rightarrow 0^+)$ value and assuming axial symmetry [35,36].

The PSM [38], including neutron-proton (np) interactions [39], has been successful in describing the observed ground-state structures in the even-even $N = Z$ nuclei with $A = 68$ to 88. It was also shown to reproduce well the excited structure in the odd-Z nucleus, ^{83}Nb [40]. In the current work, the PSM has been used to suggest possible configurations for the isomeric state observed in ^{82}Nb. The calculation, for which the positive-parity results are shown in Fig. 6, predicts an $I^\pi = 5^+$ two-quasiparticle state with a Nilsson configuration of $\nu[422]5/2^+ \times \pi[422]5/2^+$ at an excitation energy of 1224 keV. This state is predicted to lie just above the $T = 1$, $I^\pi = 4^+$ state and is a plausible candidate for the configuration of the isomer. The population of a $T = 0$ state with this configuration is consistent with the low-lying

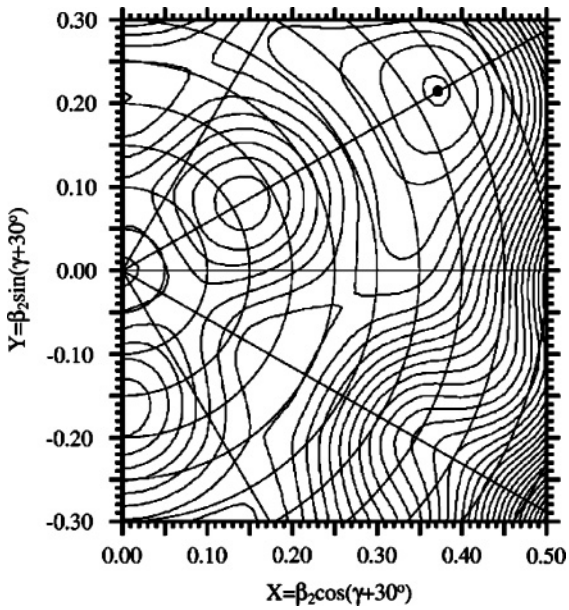

FIG. 7. TRS calculation for the ground state of ^{82}Nb. The minimum is located at $\beta_2 = 0.430$, $\gamma = 0.1^\circ$, and $\beta_4 = -0.023$. The spacing between the contour lines corresponds to 200 keV.

TABLE IV. Calculated partial half-lives derived from the single-particle Weisskopf estimates ($T^W_{1/2}$) [43] and total conversion coefficients [43] of a 124-keV transition in ^{82}Nb.

	124 keV		
	$T^W_{1/2}$ (s)	$\alpha_{\rm tot}$	$T^\gamma_{1/2}$ (s)
$E1$	1.87×10^{-13}	0.065	9.90×10^{-8}
$M1$	1.46×10^{-12}	0.131	1.05×10^{-7}
$E2$	8.97×10^{-7}	0.534	1.43×10^{-7}
$M2$	5.64×10^{-5}	1.120	1.97×10^{-7}

band structures observed in the $T_z = +\frac{1}{2}$ neighbors ^{81}Zr [41] and ^{83}Nb [40,42]. The calculations also predict two low-lying $K^\pi = 4^-$ states at approximately 1.3 MeV (not shown in Fig. 6).

Assuming a dipole transition from the isomeric state, the measured half-life is much greater than the calculated partial half-life shown in Table IV [43]. As discussed in Ref. [23], we attribute this to K hindrance [44], the well-known mechanism by which nuclear half-lives are prolonged in axially well-deformed nuclei. In this particular case of a 124-keV $M1$ $\Delta K = 5$, $\nu = 4$ decay, a reduced hindrance of $f_\nu = (T^\gamma_{1/2}/T^W_{1/2})^{1/\nu} \approx 16$ is intermediate between the accepted f_ν values for the best-case axially symmetric K isomers ($\sim$100) and that of unhindered decays ($\sim$1). An intermediate value is consistent with some degree of K mixing associated with γ-softness, which is supported by predictions from the TRS calculation shown in Fig. 7 and ^{82}Zr [35].

C. $^{84}_{41}$Nb$_{43}$

The first γ-ray transitions assigned to ^{84}Nb were identified by Gross *et al.* [42], where two band structures were observed but were not fitted into a joint level scheme. A further in-beam study by Mărginean *et al.* [45] enabled the construction of a comprehensive level scheme at low excitation energy. In the Mărginean *et al.* study, several rotational bands were identified (including those suggested by Gross *et al.*) and connected to the low-lying structure. The authors noted the confirmation of a previously reported isomeric state, but within their experimental setup, they were unable to measure the half-life or to identify other long-lived states. The isomer reported had been observed in the fragmentation of a ^{92}Mo beam. Preliminary results from the fragmentation study were published in Ref. [46] prior to the work of Mărginean *et al.* The final analysis was published later by Chandler *et al.* [10], where two decay paths depopulating an isomeric state at an excitation energy of 338 keV were reported with a mean lifetime of 148(28) ns. That paper also suggested that a state at 48 keV may have an additional lifetime associated with its decay, but low statistics prevented this from being confirmed.

Our work is in agreement with the findings of Chandler *et al.* [10] and has made it possible to measure the mean lifetime of the 48-keV state. In addition, our work finds that a state at 305 keV reported by Mărginean *et al.* [45] is isomeric. Delayed γ-ray spectra produced from gating on ions

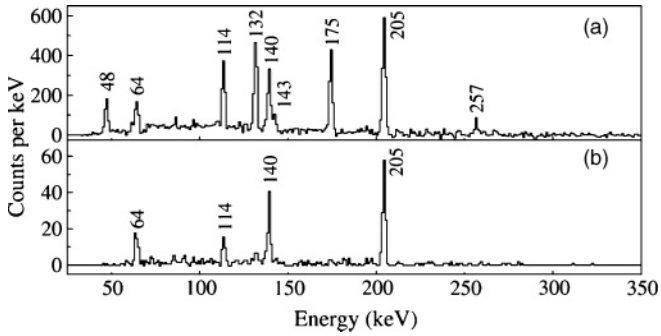

FIG. 8. (a) Singles γ-ray spectra gated on ions identified as ^{84}Nb and a time gate between 200 ns and 1.75 μs. (b) Sum of coincidence energy gates on 132- and 175-keV transitions to highlight the previously observed isomeric decay. Spectrum (b) has the same ion identification and timing conditions as (a).

identified as ^{84}Nb are shown in Fig. 8. Relative intensities of the observed γ rays are shown in Table V along with calculated internal conversion coefficients and single-particle Weisskopf estimates [43]. Because of the short half-life of the isomeric states and the low energy of the transitions in this nucleus, the intensity measured for each γ ray in this case is especially sensitive to the chosen start channel of the time gate. The quoted uncertainty takes this into consideration.

The upper panel of Fig. 8 demonstrates a singles spectrum that in addition to previously reported isomeric transitions shows delayed γ rays at 143 and 257 keV. As our is only sensitive to delayed transitions, these γ rays must decay from a previously unreported isomeric state in ^{84}Nb. These transitions were not observed by Chandler *et al.* [10] but are included in the level scheme reported in the in-beam study [45]. A sum of energy coincidence gates on the 132- and 175-keV direct decays from the previously reported isomeric state is shown in the lower panel and indicates the previously reported decay paths. The 143- and 257-keV transitions, which are shown in the singles spectrum, are too weak to appear in coincidence gating but were identified in Ref. [45] to be depopulating a level at 305-keV excitation energy. The transitions and relative intensities observed in the current work are shown in the level

TABLE V. Relative transition intensities of delayed transitions associated with ^{84}Nb. The intensities have been normalized to the intensity of the 114-keV transition. Also shown are calculated internal conversion coefficients [43] and the single-particle Weisskopf estimate of the assigned multipolarity [43].

E_γ (keV)	$\alpha(M1)$	$\alpha(E1)$	$\alpha(E2)$	$I_{\rm tot}$		$T^W_{1/2}$ (s)
47.9	1.97	1.06	18.0	605(28)	$E2$	1.11×10^{-4}
63.8	0.85	0.46	6.10	98(30)	$E2$	2.57×10^{-5}
114.0	0.16	0.08	0.72	100(19)	$E2$	1.32×10^{-6}
132.4	0.11	0.05	0.42	162(29)	$E2$	6.36×10^{-7}
140.3	0.09	0.04	0.34	89(17)	$E1$	1.28×10^{-13}
143.2	0.09	0.04	0.32	24(4)	$M1$	1.10×10^{-12}
174.8	0.05	0.02	0.15	104(15)	$E1$	6.55×10^{-14}
205.1	0.03	0.02	0.09	156(23)	$E2$	7.04×10^{-8}
257.2	0.02	<0.01	0.04	23(8)	$E2$	2.27×10^{-8}

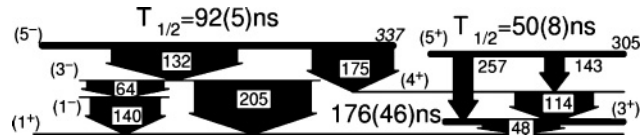

FIG. 9. Proposed level scheme for ^{84}Nb observed in the current work. The widths of the arrows indicate the relative intensities of the transitions.

scheme of Fig. 9. The ground-state spin and parity is taken as 1^+ based on compelling evidence provided in a recent β-decay study of the ^{84}Mo parent [47]. The spin and parity assignment of the 337-keV state is from Ref. [45].

The ordering of the 64- and 140-keV transitions presented in this work is reversed with respect to that in previous publications. This follows the necessary multipolarity assignments made in the current work to satisfy the intensity balance. The original ordering would have resulted in the intermediate state having the same spin/parity as the ground state, and the coexistence of two such states is not justified.

Least-squares fits to the associated decay curves have been made to determine the half-lives of the three isomeric states observed in ^{84}Nb. The fits are shown in Fig. 10. The upper panel is the DGF time spectrum associated with the 132- and 175-keV transitions. The deduced half-life in the current work of 92(5) ns is consistent with the previous measurement by Chandler *et al.* [10] of 102(19) ns.

The 48-keV transition seems to have a longer half-life than the other transitions, which indicates that the 48-keV state is also isomeric. Figure 11 shows the time-difference spectra between the 64- and 140-keV transitions and the 48- and 114-keV transitions. Despite the low coincidence statistics, a significant number of counts appear to the right of the centroid in the lower panel that are absent in the upper. This is an indication that the 48-keV state has a half-life associated with it. Feeding from the 92(5)-ns isomeric state at 337 keV must be taken into account so a two-component least-squares fit has

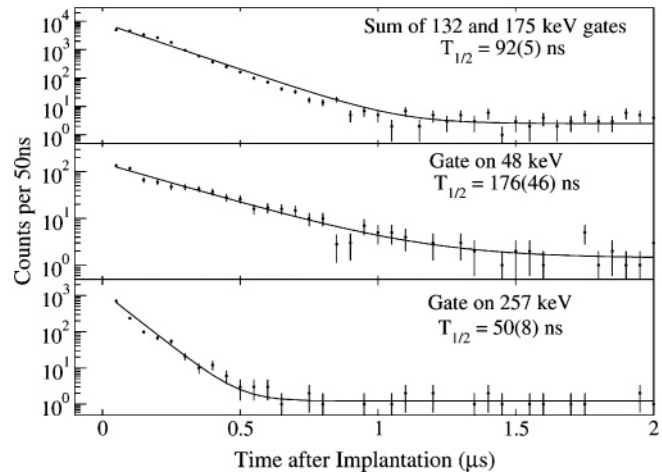

FIG. 10. Half-life measurements from least-squares fits to the DGF timing signal of γ rays associated with the decay of the isomeric states in ^{84}Nb. The decay from the 48-keV isomeric state has been fitted using a two-component least-squares fit assuming feeding from the higher lying, $T_{1/2} = 92(5)$ ns isomeric state.

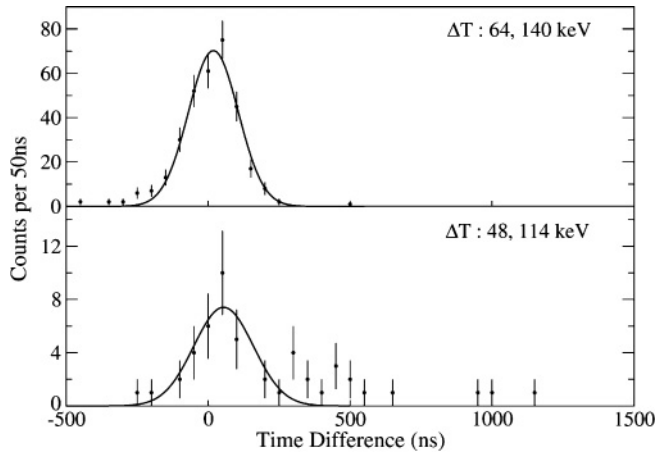

FIG. 11. Time-difference spectra between the 64- and 140-keV transitions (upper panel) and the 48- and 114-keV transitions (lower panel) in ^{84}Nb. The fit assumes no lifetime, so it reflects the time resolution of the setup at these energies. The counts that appear with a large time difference indicate the 48-keV state is isomeric.

been used in this case. The half-life of the 305-keV state has been obtained by a least-squares fit to the 257-keV transition and is found to be 50(8) ns.

D. $^{86}_{43}$Tc$_{43}$

A microsecond isomer in ^{86}Tc was previously reported, and two γ rays tentatively assigned, by Chandler *et al.* [10].

The current work finds five γ rays to be emitted in the decay of a $T_{1/2} = 1.10(14)$ μs isomeric state [34] in ^{86}Tc, as shown in Fig. 12. The measurement of the half-life of this state was made by performing a least-squares fit to the summed time spectra associated with the 593- and 850-keV transitions (inset of Fig. 12). A γ-γ energy coincidence analysis finds the 81-, 593-, and 850-keV γ rays to be in mutual coincidence. These latter two γ rays lie notably close in energy to the $2^+ \rightarrow 0^+$ (567 keV) and $4^+ \rightarrow 2^+$ (761 keV) isobaric analog transitions

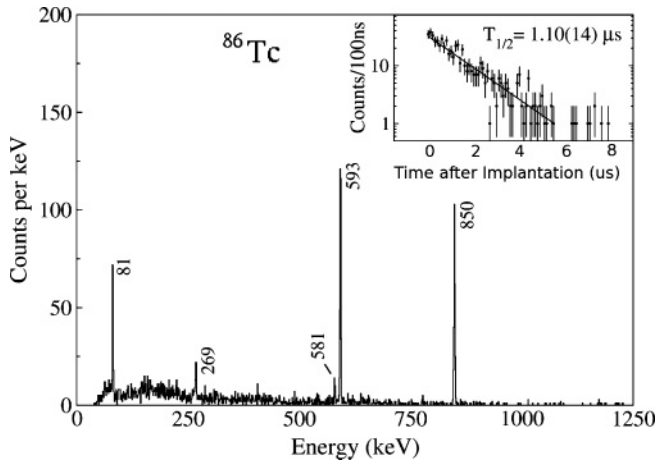

FIG. 12. γ-ray spectra of delayed events associated with ions identified as ^{86}Tc. The data are gated between 150 ns and 5 μs after the time the associated ion arrived in the stopper.

TABLE VI. Calculated γ-ray partial half-lives derived from the single-particle Weisskopf estimates [43] and total conversion coefficients [43] of an 81-keV transition in ^{86}Tc.

	81 keV	
	$T^W_{1/2}$ (s)	$\alpha_{\rm tot}$
$E1$	6.50×10^{-13}	0.245
$E2$	7.08×10^{-6}	2.690
$M1$	3.41×10^{-12}	0.514
$M2$	4.59×10^{-4}	6.420

in $^{86}_{42}$Mo$_{44}$ [48]. On this basis, they are assigned to be the first two transitions of the $T = 1$ ground-state band in ^{86}Tc.

The 269- and 581-keV γ-ray energies sum to 850 keV, which suggests a competing decay branch to the $(4^+) \rightarrow (2^+)$ transition, and this is confirmed in a γ-γ coincidence analysis. The spin and parity of this state is most likely 3^+ or 4^+ when γ-ray selection rules and Weisskopf estimates of the transitions are considered.

An intensity balance around the (4^+) state has been used to infer the conversion coefficient, $\alpha_{\rm tot}$, of the 81-keV γ ray to be 3.49(80). Calculated values of total conversion coefficients for this transition are displayed in Table VI. Good agreement in the current analysis was found for the conversion coefficient of the 96-keV, $14^+ \rightarrow 12^+$, transition in ^{94}Pd, previously reported in Ref. [21]. In our work, this is inferred to be 1.6(3) compared with the previously measured value of 1.9(4) [21] and a theoretical value of 1.61 [43]. On this basis, the 81-keV transition in ^{86}Tc is assigned to be of a stretched-$E2$ multipolarity, leading to a spin/parity assignment of (6^+) for the isomeric state.

The $I^\pi = 6^+$ member of the ground-state band in ^{86}Mo lies at 2260 keV, 932 keV above the 4^+ state. Considering the similarity in energy of the (2^+) and (4^+) members, the $T = 1$, $I^\pi = 6^+$ state in ^{86}Tc would therefore be expected to have an excitation energy of around 2.5 MeV. The isomeric 6^+ state appears at an excitation energy of 1524 keV creating an yrast-trap isomeric state. The fact that this 6^+ state appears only 81 keV above the yrast 4^+ state would explain the somewhat large isomeric ratio (Table III).

The results of a configuration-constrained potential-energy-surface calculation for the ground state in ^{86}Tc are shown in Fig. 13. The minimum for a rotational frequency of $\omega = 0.0$ MeV/$\hbar$ is at $\beta_2 = 0.004$, $\gamma = 0^\circ$. However, if the system is allowed to rotate, then the minimum quickly moves to the triaxially soft, oblate minimum focused around $\beta_2 \approx 0.2$, which is also prominent in Fig. 13. This soft triaxial shape suggests that $N = Z = 43$ represents the boundary along the $N = Z$ line of the transitional region as the doubly magic ^{100}Sn is approached. These findings are in agreement with recent results described by Fischer *et al.* [40].

The positive-parity states in ^{86}Tc predicted by the PSM are shown in Fig. 14. Negative parity states with $K = 5, 6$ are also predicted at $\approx$1.2 MeV. The ground-state band is shown to be well reproduced in the calculation. The $I^\pi = 6^+$ state predicted at 1428 keV is the first excited member of a rotational band built on the $I^\pi = 5^+$ 2-quasiparticle

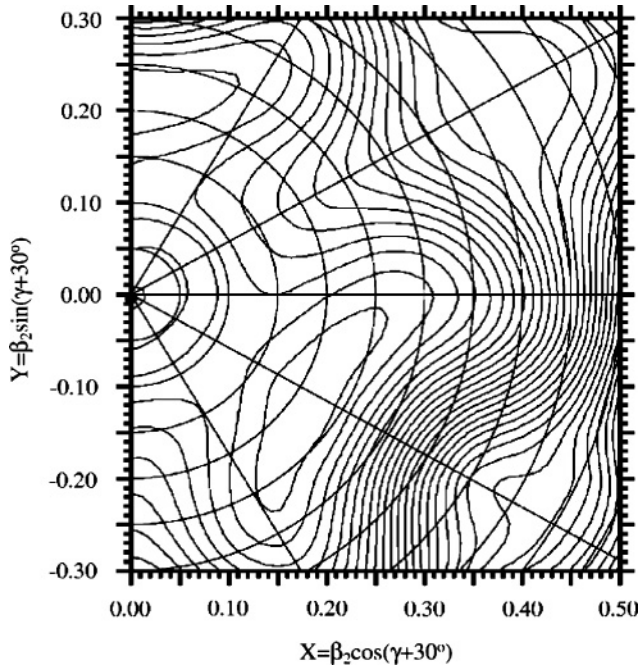

FIG. 13. A configuration-constrained potential-energy-surface calculation for the ground state of ^{86}Tc. The minimum is at $\beta_2 = 0.004$, $\gamma = 0^\circ$ with a shallow oblate minimum around $\beta_2 \approx 0.2$, $\gamma = -60^\circ$, which becomes favored for $\omega > 0$ MeV/$\hbar$. The spacing between the contour lines corresponds to 200 keV.

band head ($\nu[422]5/2^+ \times \pi[422]5/2^+$) and therefore seems unlikely to be isomeric unless rotational alignment brings the 6^+ below the 5^+ state. A more probable configuration for an $I^\pi = 6^+$ isomeric state would be a coupling of the $[413]7/2^+ \times [422]5/2^+$ Nilsson orbitals. Both of these orbitals lie close to the Fermi surface, but the calculation places this state at a significantly higher excitation energy.

It is worth acknowledging an alternative situation in which the isomeric state has $I^\pi = 5^-$ and decays by a mixed $E1/M2$ transition to the (4^+) state. A mixed transition of this type could result in a measured internal conversion coefficient of a similar magnitude to that observed. A mixing ratio of $\delta(E1/M2) = 1.07$ is required for $\alpha_{\rm tot} = 3.49(18)$ matching the measured value or $\delta(E1/M2) = 0.76$, $\alpha_{\rm tot} = 2.47(13)$, to match the calculated pure $E2$ value [49].

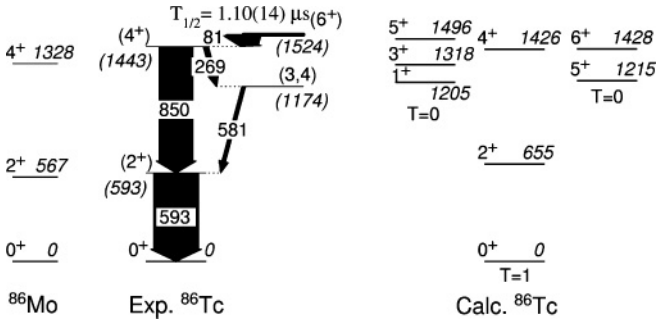

FIG. 14. Experimental and theoretical (PSM) level schemes of ^{86}Tc. The ground-state band of ^{86}Mo is also shown for comparison.

It is also noteworthy that the isomeric state in ^{86}Tc lies in the vicinity of the proton separation energy of 1393(409) keV [50], thus raising the possibility of direct proton emission from the isomer competing with internal γ-ray decay. However, the experimental arrangement used here does not allow us to observe this possible decay mode.

E. $^{87}_{43}$Tc$_{44}$

Two γ rays, likely to form a deformed band built on a proton $g_{9/2}$ state, have been observed in this nucleus previously [51] but no linking transitions to the ground state were identified. The nuclei were produced in fusion-evaporation reactions and studied using prompt spectroscopy. The experimental setup used was only sensitive to γ rays between 0.1 and 2.4 MeV, which were emitted in the first 0.5 ns after production.

Our work identifies two delayed γ rays associated with ^{87}Tc. They can be seen in the singles γ-ray spectrum in Fig. 15. The two transitions of 64 and 71 keV are found to not be in

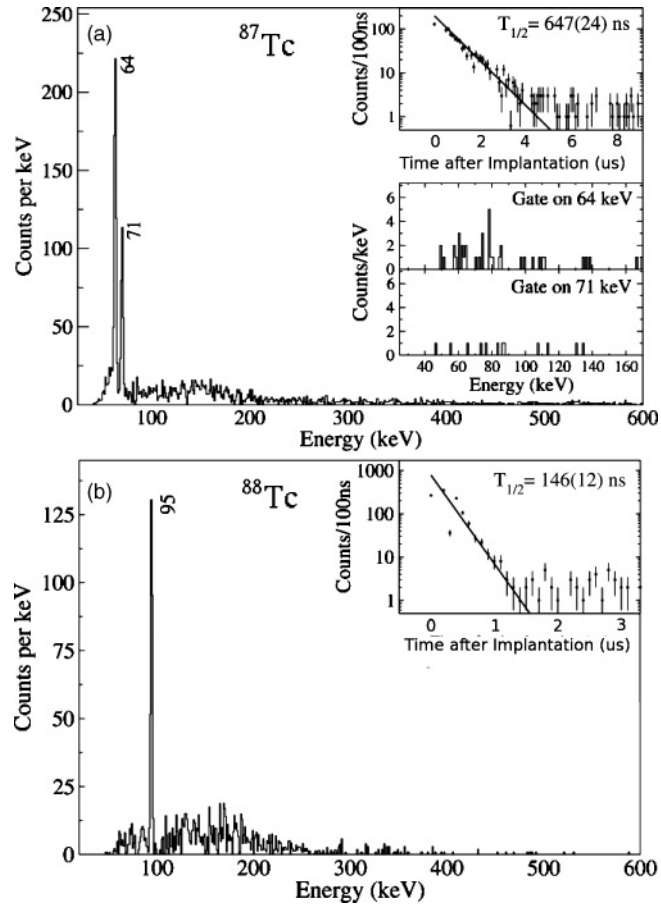

FIG. 15. γ-ray spectra of delayed events associated with ions identified as (a) ^{87}Tc and (b) ^{88}Tc. The spectra are gated from 150 ns to 3.4 μs and from 150 ns to 1.5 μs after implantation, respectively. The insets show the associated decay curves from the DGF timing, and in the case of ^{87}Tc, this is the sum of gates on both the 64- and 71-keV γ rays. The second inset of the upper panel shows energy coincidence gates on the two transitions that are shown to not be in mutual coincidence.

TABLE VII. Calculated partial half-lives for transitions in ^{87}Tc of various multipolarities derived from the single-particle-unit Weisskopf estimates [43]. The units are in seconds.

	7 keV	64 keV	71 keV
$E1$	6.69×10^{-10}	1.31×10^{-12}	9.18×10^{-13}
$E2$	7.42×10^{-1}	2.26×10^{-5}	1.26×10^{-5}
$M1$	3.50×10^{-10}	5.47×10^{-12}	4.32×10^{-12}
$M2$	$4.85 \times 10^{+1}$	1.48×10^{-3}	8.21×10^{-4}

mutual coincidence with each other (inset of Fig. 15). This either constitutes separate decay paths from a single isomeric state or represents the decay of two separate isomeric states in ^{87}Tc. Least-squares fits to the decay curves associated with the individual γ rays finds their half-lives to be the same within experimental uncertainties: 597(33) ns for the 64-keV transition and 680(57) for the 71-keV γ ray. The most likely scenario is therefore a single isomeric state with competing decay paths. A single component half-life fit to the summed decay curve (inset of Fig. 15) gives a half-life measurement of 647(24) ns.

An inspection of the calculated partial half-lives (Table VII) of these observed γ rays indicates that only hindered $E1$ or $M1$ multipolarity can likely result in the observed half-life of the isomeric state. Other multipolarities would result in a much longer lived isomer. $E1$ and $M1$ transitions still require a large degree of hindrance that could be a result of shape hindrance in the decay of an oblate $7/2^+$ ([413]7/2) state to prolate states of $5/2^+$ ([422]5/2) and $5/2^-$ ([303]5/2). All of these single-particle levels lie at the Fermi surface, and similar low-lying structures built on these states have been observed in $N = 43$ isotones [53,54].

F. $^{88}_{43}$Tc$_{45}$

Two β-decaying states with half-lives of 6.4 and 5.8 s have been previously reported in this nucleus [55]. In addition, a quasirotational band was identified during an in-beam study [51] and a partial decay scheme was constructed. It is not clear which β-decaying state, if either, is the ground state of this nucleus or into which state the quasirotational band decays. The new experimental data from our work, combined with theoretical interpretation of these levels, leads to a consistent picture for the low-lying structure of this nucleus.

TABLE VIII. Calculated γ-ray partial half-lives derived from the single-particle Weisskopf estimates and total conversion coefficients of a 95-keV transition in ^{88}Tc [43].

	95 keV	
	$T^W_{1/2}$ (s)	$\alpha_{\rm tot}$
$E1$	3.97×10^{-13}	0.155
$E2$	3.09×10^{-6}	1.520
$M1$	2.48×10^{-12}	0.327
$M2$	2.04×10^{-4}	3.550

In our work, a $T_{1/2} = 146(12)$ ns isomeric state is found to decay via a single 95-keV γ ray as shown in Fig. 15. An inspection of the Weisskopf estimates (Table VIII) suggest either a hindered dipole or an enhanced $E2$ transition.

The results of a shell-model calculation using the Gross-Frenkel interaction [56] in a $1g_{9/2}$-$2p_{1/2}$ model space are shown to the right of Fig. 16. This shell-model space has been shown to consistently perform well for the low-spin, near-spherical states in nuclei with $Z = 40$–45 and $N = 46$–50 [57].

The calculation suggests that the two β-decaying states observed by Odahara *et al.* [55] have spin 2^+ and 6^+ because a low-energy $E4$ transition between these two states is highly unlikely to compete with β decay. In addition, a comparison between the predicted yrast states and the experimental decay scheme strongly suggests $I = 8$ for the X+312 level shown on the left-hand side of Fig. 16. Not only the energy pattern but moreover predicted decay strengths yield a pattern very similar to the observed one (i.e., the 312-keV transition is associated with an $8^+ \rightarrow 6^+$ transition). This implies that the tentative 291-keV transition would be falsely positioned in the experimental decay scheme.

Thus, one is left with two possibilities for a low-energy isomeric transition: either the $4^+ \rightarrow 6^+$ or the $4^+ \rightarrow 2^+$ transition, which means in principle *two* parallel electromagnetic transitions from a possibly isomeric 4^+ level, only one of which is observed in this study. Both the lowest negative-parity states, which are predicted at some 700-keV excitation energy, and odd-spin positive-parity states shown on the right-hand side of

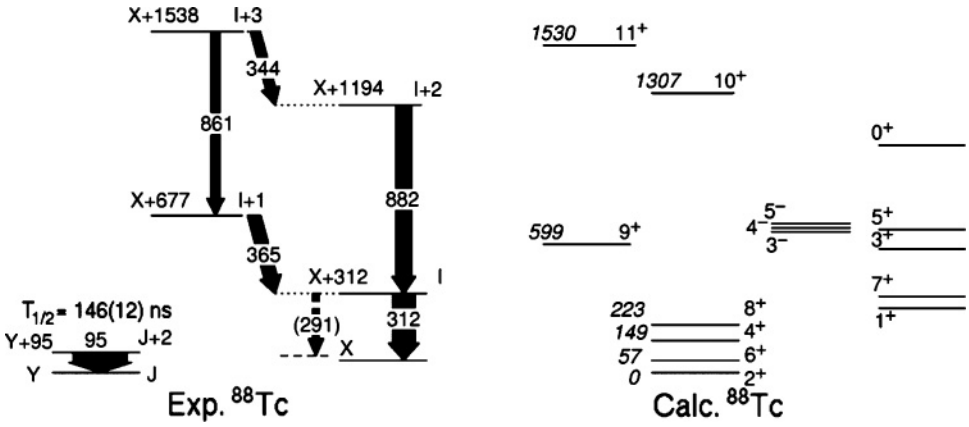

FIG. 16. Experimental and calculated low-spin excitation schemes of ^{88}Tc. The experimental scheme is constructed from the current work (95-keV transition only) and Refs. [55] and [51]. The widths of the arrows indicate relative intensities of the γ rays; the energy labels are in keV, and tentative transitions and levels are dashed. The predictions are based on shell-model calculations in a $1g_{9/2}$-$2p_{1/2}$ model space.

Fig. 16 have open $E1$, $M1$, or $E2$ γ-decay branches of several hundred keV, which precludes these to be isomeric beyond the nanosecond scale.

Assuming the $E2$ character for the observed 95-keV transition, one obtains

$$B(E2)_{\rm exp} = br \times \frac{1}{1+\alpha_{\rm tot}} \times \frac{0.566}{T_{1/2}E_\gamma^5} \sim 200\ e^2\ {\rm fm}^4 \qquad (5)$$

with an experimental branching, $br = 1.0$, $\alpha_{\rm tot} = 1.52(7)$, $T_{1/2} = 146(12)$ ns, and $E_\gamma = 0.095(1)$ MeV. This can be compared with the predictions of $B(E2;4^+ \rightarrow 2^+) = 320\ e^2\ {\rm fm}^4$ and $B(E2;4^+ \rightarrow 6^+) = 7.9\ e^2\ {\rm fm}^4$, respectively, using the effective charges provided for the Gross-Frenkel shell-model interaction [57]. Compared with the experimental number, this clearly points toward matching the observed 95-keV transition with the predicted $4^+ \rightarrow 2^+$ decay, in terms of both excitation energies and, moreover, decay strengths, which would imply $I = 2$ and, most likely, $Y = 0$ keV and $X \sim Y$, on the left-hand side of Fig. 16. This scenario also provides an explanation as to why the $4^+ \rightarrow 6^+$ transition is not seen in the current work and only one isomeric γ-ray transition is observed.

IV. CONCLUSIONS

Experimental results from the first experiment of the RISING "Stopped beam" campaign are reported with a discussion on the structure of these nuclei based on interpretations provided by several theoretical models. These data have allowed the identification of previously unobserved excited states in the self-conjugate odd-odd nuclei ^{82}Nb and ^{86}Tc. The low-lying structures of both systems are dominated by $T = 1$, np pairing effects that have already been observed in the other odd-odd $N = Z$ nuclei above $^{42}_{21}$Sc. The current data suggest that the $T = 1$, rather than the $T = 0$, pairing interaction is the dominant feature throughout the fpg shell [23]. In addition, previously unreported isomeric states have been identified in ^{87}Tc and ^{88}Tc with half-lives of 647(24) ns and 146(12) ns, respectively. These states are interpreted as a shape isomer in ^{87}Tc, and comparison with shell-model calculations finds the (4^+) member of the ground-state band in ^{88}Tc to be isomeric. A previously reported isomeric state in ^{84}Nb has been observed in this data, and another previously identified excited state in this nucleus has now been assigned as isomeric with a half-life of 155(24) ns.

ACKNOWLEDGMENTS

The excellent work of the GSI accelerator and ion source technical staff is gratefully acknowledged. This work was sponsored by the EPSRC (UK) and STFC (UK), The Swedish Research Council, The Polish Ministry of Science and Higher Education (Grant Nos. P03B03030 and N N202 309135), the Bulgarian Science Fund VUF06/05, the US Department of Energy (Grant Nos. DE-FG02-91ER-40609 and DE-AC02-06CH11357), the Spanish Ministerio de Educación y Ciencia (Project Nos. FPA2005-00696 and FPA2007-66069), the German Federal Ministry of Education, the Hungarian Scientific Research Fund (Contract No. K68801), research under Grant No. 06KY205I, and EURONS (European Commision Contract No. 506065). Y.S. acknowledges funding from the Chinese Major State Basic Development Program through Grant No. 2007CB815005 and the Natural Science Foundation of China under Contract No. 10875077. P.M.W. acknowledges funding from the AWE plc. A.B.G. would also like to thank Nexia Solutions Ltd, a subsidiary of BNFL, for financial support.

[1] W. Nazarewicz, J. Dudek, R. Bengtsson, T. Bengtsson, and I. Ragnarsson, Nucl. Phys. **A435**, 397 (1985).
[2] S. Raman, C. W. Nestor Jr., and P. Tikkanen, At. Data Nucl. Data Tables **78**, 1 (2001).
[3] E. Clément *et al.*, Phys. Rev. C **75**, 054313 (2007).
[4] J. Uusitalo, D. Seweryniak, P. F. Mantica, J. Rikovska, D. S. Brenner, M. Huhta, J. Greene, J. J. Ressler, B. Tomlin, C. N. Davids, C. J. Lister, and W. B. Walters, Phys. Rev. C **57**, 2259 (1998).
[5] M. Karny, L. Batist, D. Jenkins, M. Kavatsyuk, O. Kavatsyuk, R. Kirchner, A. Korgul, E. Roeckl, and J. Zylicz, Phys. Rev. C **70**, 014310 (2004).
[6] J. J. Ressler *et al.*, Phys. Rev. C **69**, 034317 (2004).
[7] H. Schatz *et al.*, Phys. Rep. **294**, 167 (1998).
[8] H. Schatz, A. Aprahamian, V. Barnard, L. Bildsten, A. Cumming, M. Ouellette, T. Rauscher, F.-K. Thielemann, and M. Wiescher, Phys. Rev. Lett. **86**, 3471 (2001); H. Grawe, K. Langanke, and G. Martinez-Pinedo, Rep. Prog. Phys. **70**, 1525 (2007).
[9] A. Aprahamian and Y. Sun, Nature Phys. **1**, 81 (2005).
[10] C. Chandler *et al.*, Phys. Rev. C **61**, 044309 (2000).
[11] M. Hencheck *et al.*, Phys. Rev. C **50**, 2219 (1994).
[12] D. J. Morrissey (A1200 Group), Nucl. Phys. **A588**, c203 (1995).
[13] R. Grzywacz *et al.*, Phys. Rev. C **55**, 1126 (1997).
[14] A. Stolz *et al.*, Phys. Rev. C **65**, 064603 (2002).
[15] M. Górska *et al.*, Acta Phys. Pol. B **38**, 1219 (2007).
[16] H. Geissel *et al.*, Nucl. Instrum. Methods Phys. Res. B **70**, 286 (1992).
[17] S. Pietri *et al.*, Nucl. Instrum. Methods Phys. Res. B **261**, 1079 (2007).
[18] S. Pietri *et al.*, Acta Phys. Pol. B **38**, 1255 (2007).
[19] M. Pfützner, H. Geissel, G. Münzenberg, F. Nickel, Ch. Scheidenberger, K.-H. Schmidt, K. Sümmerer, T. Brohm, B. Voss, and H. Bichsel, Nucl. Instrum. Methods Phys. Res. B **86**, 213 (1994).
[20] M. Górska *et al.*, Z. Phys. A **353**, 233 (1995).
[21] R. Grzywacz, in *Proceedings of ENAM, 1998* [AIP Conf. Proc. **455**, 430 (1998)].
[22] H. Grawe and H. Haas, Phys. Lett. **B120**, 63 (1983).
[23] A. B. Garnsworthy *et al.*, Phys. Lett. **B660**, 326 (2008); [Erratum-*ibid.* **B668**, 460 (2008)].
[24] A. B. Garnsworthy *et al.*, Acta Phys. Pol. B **38**, 1265 (2007).
[25] S. Myalski *et al.*, Acta Phys. Pol. B **38**, 1277 (2007).
[26] P. H. Regan *et al.*, Nucl. Phys. **A787**, 491c (2007).
[27] P. H. Regan *et al.*, AIP Conf. Proc. **899**, 19 (2007).
[28] D. Rudolph *et al.*, Eur. Phys. J. Special Topics **150**, 173 (2007).

[29] L. S. Cáceres *et al.*, Acta Phys. Pol. B **38**, 1271 (2007).
[30] Zs. Podolyák *et al.*, Phys. Lett. **B632**, 203 (2006).
[31] K. A. Gladnishki *et al.*, Phys. Rev. C **69**, 024617 (2004).
[32] M. Pfützner *et al.*, Phys. Rev. C **65**, 064604 (2002).
[33] C. M. Baglin, Nucl. Data Sheets **80**, 1 (1997).
[34] The published value for the half-life of this state in Ref. [23] is in fact the value of the mean lifetime. The correct half-life is the one quoted here. All other values quoted or discussed in Ref. [23] were calculated correctly and are not affected by this error.
[35] D. Rudolph *et al.*, Phys. Rev. C **56**, 98 (1997).
[36] S. D. Paul, H. C. Jain, and J. A. Sheikh, Phys. Rev. C **55**, 1563 (1997).
[37] F. R. Xu, P. M. Walker, J. A. Sheikh, and R. Wyss, Phys. Lett. **B435**, 257 (1998).
[38] Y. Sun, Eur. Phys. J. A **20**, 133 (2004).
[39] Y. Sun and J. A. Sheikh, Phys. Rev. C **64**, 031302(R) (2001).
[40] S. M. Fischer *et al.*, Phys. Rev. C **75**, 064310 (2007).
[41] N. Mărginean *et al.*, Phys. Rev. C **69**, 054301 (2004).
[42] C. J. Gross, W. Gelletly, M. A. Bentley, H. G. Price, J. Simpson, B. J. Varley, J. L. Durell, Ö. Skeppstedt, and S. Rastikerdar, Phys. Rev. C **43**, R5 (1991).
[43] F. Rösel, H. M. Friess, K. Alder, and H. C. Pauli, At. Data Nucl. Data Tables **21**, 291 (1978).
[44] K. E. G. Löbner, Phys. Lett. **B26**, 369 (1968); P. M. Walker and G. Dracoulis, Nature (London) **399**, 35 (1999).
[45] N. Mărginean *et al.*, Eur. Phys. J. A **4**, 311 (1999).
[46] P. H. Regan *et al.*, Acta Phys. Pol. B **28**, 431 (1997).
[47] J. B. Stoker *et al.*, Phys. Rev. C **79**, 015803 (2009).
[48] D. Rudolph *et al.*, Phys. Rev. C **54**, 117 (1996).
[49] T. Kibédi, T. W. Burrows, M. B. Trzhaskovskaya, P. M. Davidson, and C. W. Nestor Jr., Nucl. Instrum. Methods Phys. Res. A **589**, 202 (2008).
[50] A. H. Wapstra, G. Audi, and C. Thibault, Nucl. Phys. **A729**, 129 (2003).
[51] D. Rudolph *et al.*, J. Phys. G **17**, L113 (1991).
[52] P. M. Endt, At. Data Nucl. Data Tables **23**, 547 (1979).
[53] N. Mărginean *et al.*, Phys. Rev. C **65**, 034315 (2002).
[54] U. J. Hüttmeier, C. J. Gross, D. M. Headly, E. F. Moore, S. L. Tabor, T. M. Cormier, P. M. Stwertka, and W. Nazarewicz, Phys. Rev. C **37**, 118 (1988).
[55] A. Odahara *et al.*, Z. Phys **354**, 231 (1996).
[56] R. Gross and A. Frenkel, Nucl. Phys. **A267**, 85 (1976).
[57] D. Rudolph, K. P. Lieb, and H. Grawe, Nucl. Phys. **A597**, 298 (1996).

β^--delayed spectroscopy of neutron-rich tantalum nuclei: Shape evolution in neutron-rich tungsten isotopes

N. Alkhomashi,[1,*] P. H. Regan,[1] Zs. Podolyák,[1] S. Pietri,[1] A. B. Garnsworthy,[1] S. J. Steer,[1] J. Benlliure,[2] E. Caserejos,[2] R. F. Casten,[3] J. Gerl,[4] H. J. Wollersheim,[4] J. Grebosz,[5] G. Farrelly,[1] M. Górska,[4] I. Kojouharov,[4] H. Schaffner,[4] A. Algora,[6,7] G. Benzoni,[8] A. Blazhev,[9] P. Boutachkov,[4] A. M. Bruce,[10] A. M. Denis Bacelar,[10] I. J. Cullen,[1] L. Cáceres,[4] P. Doornenbal,[4] M. E. Estevez,[2] Y. Fujita,[11] W. Gelletly,[1] R. Hoischen,[4,12] R. Kumar,[13] N. Kurz,[4] S. Lalkovski,[10] Z. Liu,[14] C. Mihai,[15] F. Molina,[6] A. I. Morales,[2] D. Mücher,[9] W. Prokopowicz,[4] B. Rubio,[6] Y. Shi,[16] A. Tamii,[17] S. Tashenov,[4] J. J. Valiente-Dobón,[18] P. M. Walker,[1] P. J. Woods,[14] and F. R. Xu[16]

[1]*Department of Physics, University of Surrey, Guildford GU2 7XH, United Kingdom*
[2]*Universidad de Santiago de Compostela, E-15706 Santiago de Compostela, Spain*
[3]*WNSL, Yale University, New Haven, Connecticut 06520, USA*
[4]*GSI, Plankstrasse 1, D-64291 Darmstadt, Germany*
[5]*The Henryk Niewodniczànski Institute of Nuclear Physics, PL-31-342 Kraków, Poland*
[6]*IFIC, CSIC-Universidad de Valencia, E-46071 Valencia, Spain*
[7]*Institute of Nuclear Research of the Hungarian Academy of Sciences, Debrecen H-4001, Hungary*
[8]*INFN, Università degli Studi di Milano, I-20133 Milano, Italy*
[9]*IKP, University of Cologne, D-50937 Cologne, Germany*
[10]*School of Environment and Technology, University of Brighton, Brighton BN2 4GJ, United Kingdom*
[11]*Department of Physics, Osaka University, Osaka, Japan*
[12]*Department of Physics, Lund University, S-22100 Lund, Sweden*
[13]*IUAC, New Delhi, India*
[14]*School of Physics and Astronomy, University of Edinburgh, Edinburgh EH9 3JZ, United Kingdom*
[15]*Horia Hulubei National Institute of Physics and Nuclear Engineering, R-76900 Bucharest, Romania*
[16]*Department of Technical Physics, Peking University, Beijing 100871, People's Republic of China*
[17]*Research Center for Nuclear Physics, Osaka University, Osaka, Japan*
[18]*INFN-Laboratori Nazionali di Legnaro, I-35020 Legnaro, Italy*

(Received 18 September 2009; published 8 December 2009)

The low-lying structure of ^{188,190,192}W has been studied following β decays of the neutron-rich mother nuclei ^{188,190,192}Ta produced following the projectile fragmentation of a 1-GeV-per-nucleon ^{208}Pb primary beam on a natural beryllium target at the GSI Fragment Separator. The β-decay half-lives of ^{188}Ta, ^{190}Ta, and ^{192}Ta have been measured, with γ-ray decays of low-lying states in their respective W daughter nuclei, using heavy-ion β-γ correlations and a position-sensitive silicon detector setup. The data provide information on the low-lying excited states in ^{188}W, ^{190}W, and ^{192}W, which highlight a change in nuclear shape at ^{190}W compared with that of lighter W isotopes. This evolution of ground-state structure along the W isotopic chain is discussed as evidence for a possible proton subshell effect for the $A \sim 190$ region and is consistent with maximization of the γ-softness of the nuclear potential around $N \sim 116$.

DOI: 10.1103/PhysRevC.80.064308 PACS number(s): 21.10.−k, 23.40.−s, 27.80.+w, 29.38.Db

I. INTRODUCTION

Nuclei with $A \sim 190$ for the elements between Hf ($Z = 72$) and Pt ($Z = 78$) exhibit a wide variation of nuclear structural properties, including well-deformed prolate shapes with rotational band structures [1], K-isomeric states associated with axial symmetry in a deformed nuclear potential [2], and shape transitions across isotopic and isotonic chains [3,4]. The evolution from axially symmetric deformed prolate shapes around the valence maximum nucleus at ^{170}Dy [5] toward spherical, single-particle–like excitations close to the doubly magic nucleus ^{208}Pb is predicted to pass through a region of triaxial γ-soft and oblate nuclei [6–8]. Nuclei that are predicted to lie on the boundary between regions of prolate and oblate deformation have been described by Jolie and Linneman as prolate-oblate phase-transitional systems [9]. The phase-transitional region between axially symmetric, deformed prolate and oblate shapes is also relevant to the limits of geometric symmetry within the interacting boson model (IBM) [10–13]. Platinum isotopes with $N = 116$ and 118 represent the best cases thus far for the experimental realization of the O(6) symmetry limit of the IBM, which can be associated with a nuclear potential that is flat in the triaxial degree of freedom [14–16].

Evidence of increased γ-softness in the nuclear potential can be inferred from a number of simple experimental signatures. These signatures include a decrease in the excitation energy of the second $I^\pi = 2^+$ state [17] relative to the yrast $I^\pi = 2^+$ state and a reduction in the ratio of the excitation

*n.alkhomashi@surrey.ac.uk

TABLE I. Experimental parameters for the two FRS settings studied in the current work.

Setting	Magnetic rigidity $B\rho_1$ (Tm)	Magnetic rigidity $B\rho_2$ (Tm)	S2 degrader thickness (mg/cm^2)	S4 degrader thickness (mg/cm^2)	Beam current (p/spill)	Spill repetition (s)	Total collection time (h)
^{190}Ta	13.0805	9.5915	5050	3320	10^8	20	62
^{192}Ta	13.2285	9.7479	5050	3450	10^9	15	66

energies of the yrast $I^\pi = 4^+$ and 2^+ states, $R(4/2)$, compared to the perfect axial rotor limit of 3.33. Evidence for such behavior has been reported in a number of nuclei in this region, including ^{192}Os [18] and ^{194,196}Pt [15,19].

One focus of the current work is to extend the spectral knowledge of heavy, neutron-rich nuclei, with the specific aim of studying the predicted evolution from prolate-deformed, through γ-soft, to oblate-deformed shapes in neutron-rich tungsten ($Z = 74$) isotopes [7].

The heaviest stable tungsten isotope is $^{186}W_{112}$. Experimental information on the neutron-rich isotopes of tungsten with $N \geqslant 116$ is sparse because of the neutron-rich nature of these systems. To investigate the change of structure with increasing neutron number and the expected evolution toward a more γ-soft and possibly oblate shape, the nuclei of interest must be studied by either deep-inelastic collisions [20–22] or projectile fragmentation reactions. Prior to this work, the heaviest even-N tungsten isotopes for which even the most rudimentary spectral information had been reported were ^{188}W and ^{190}W. In-beam spectroscopy of $^{188}W_{114}$ was studied previously using deep-inelastic [22] and two-nucleon transfer reactions [23], which provided information on the structure of the yrast sequence up to a spin of $8\hbar$. Transitions populating the ground-state band of $^{190}W_{116}$ were identified via isomer-delayed γ-ray spectroscopy following relativistic projectile fragmentation of a ^{208}Pb beam [24–26]. The inferred $R(4/2)$ value for ^{190}W showed a sudden decrease in value compared to the systematics in the region [24].

The present work primarily investigates the low-lying nuclear structure of ^{188}W, ^{190}W, and ^{192}W following β-delayed spectroscopy of their mother nuclei, ^{188}Ta, ^{190}Ta, and ^{192}Ta, respectively. The data confirm the previously reported $R(4/2)$ value in ^{190}W and also provide evidence for the observation of the second 2^+ state in this nucleus. The excitation energy of the yrast 2^+ state in ^{192}W is also reported for the first time in the current work. Preliminary results from this study have been reported in a series of conference papers [27–29]; this article provides the complete analysis of this work.

II. EXPERIMENTAL DETAILS

The nuclei of interest were produced following projectile fragmentation reactions between a primary beam of ^{208}Pb impinging on a natural beryllium target of thickness 2446 mg/cm^2. The 1 GeV/nucleon beam was provided by the SIS-18 heavy-ion synchrotron at GSI, Germany, with primary beam intensities of up to 10^9 ions/spill. The duration of each primary beam spill was approximately 1 s with a typical repetition period of 15–20 s. The secondary fragmentation reaction residues were separated and identified event-by-event using the GSI Fragment Separator (FRS) [30], operated in monochromatic mode with an aluminum wedge-shaped degrader positioned in the intermediate focal plane. Two specific FRS settings were used in the current work, one centered on fully stripped (i.e., $Q = Z$) ions of ^{190}Ta and the second centered on fully stripped ^{192}Ta ions. Table I gives a summary of the experimental parameters for the FRS in these two settings.

A. Detector configuration at the FRS focal plane

A schematic of the experimental configuration used in the current work is shown in Fig. 1. The secondary ions were implanted into the RISING active stopper, which consisted of a series of double-sided silicon strip detectors (DSSSDs; see Refs. [28,31] for details). In the current work, the stopper configuration was positioned as shown in Fig. 1 and consisted of three 5 cm × 5 cm × 1 mm DSSSDs [32], each with 16 individual 3-mm-width strips on the front and back faces. The DSSSDs were used to determine the position of the implanted ion and to correlate it with its subsequent β^- decay detected in the same or neighboring pixels of the DSSSD.

The correlation of low-energy (typically hundreds of keV) β particles with significantly higher energy (typically a few GeV) implanted ions was afforded by the use of Mesytec semilogarithmic preamplifiers applied to the energy outputs of the DSSSDs [31]. These preamplifiers allowed a linear

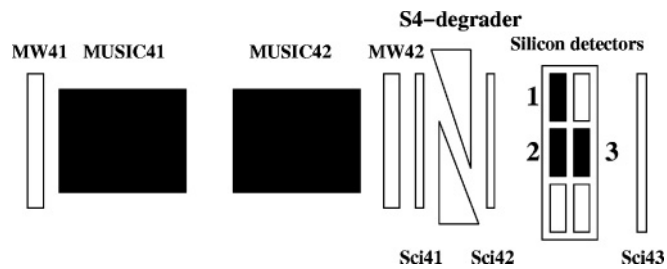

FIG. 1. Schematic of the detector configuration at the final focus of the GSI FRS for the current work. Three of the possible six positions (black boxes) in the active stopper were occupied by DSSSDs in this particular experiment. MW = multiwire position detectors; Sci = plastic scintillator detectors; MUSIC = multiple sampling ionization chamber detectors. The number 4 corresponds to the detectors being placed at the final focus (i.e., after the fourth dipole magnet) of the GSI FRS. The secondary ions are transmitted from left to right on this schematic.

amplification of the DSSSD signal for energies of up to 10 MeV, whereas a logarithmic amplification range was used for implantation energies of between 10 MeV and 3 GeV. The linear region of the preamplifier response was calibrated using the monoenergetic internal conversion electrons emitted using a standard ^{207}Bi calibration source, which yielded a measured energy full width at half maximum (FWHM) of 20 keV at 980 keV and a minimum detection threshold of approximately 150 keV. This level of electron energy resolution was used to select delayed internal conversion electron lines following decays that were observed in other FRS settings from the same experiment (for example, in the internal conversion decay of a long-lived isomer in ^{205}Au [33]). For the logarithmic portion of the preamplifier energy response, simulated signals from a pulser were used for the initial energy calibration, which was then checked by comparing the experimental data to simulations from the LISE3 code [34,35].

The active stopper was viewed by the stopped RISING γ-ray spectrometer array, which consists of 15 seven-element germanium cluster detectors with a measured total photopeak efficiency of ∼15% at 662 keV [36,37]. Previously, the RISING array has been used to detect γ-ray transitions emitted following the decay of isomeric states in secondary fragments produced by projectile fragmentation and fission, using the techniques described in Refs. [24,25,38–42]. This experiment represents the first time that the RISING array was also used to correlate γ-ray transitions arising from the decays of states populated following the β decay of secondary fragmentation products.

B. Data reduction and particle identification process

The identification of the projectile fragments was based on the time-of-flight (TOF) position and energy loss techniques described in Ref. [43]. The TOF in the second stage of the FRS was determined by measuring the time difference between the ions passing between two plastic scintillators mounted (i) before the degrader at the intermediate focal plane (after region S2) and (ii) at the final focal plane (after region S4). Two multiwire proportional chambers and two multiple sampling ionization chambers (MUSICs) provided position determination and energy loss information of the fragments at the final focal plane, respectively. The secondary ions of interest were then slowed down in a variable-thickness aluminum degrader (see Table I) before coming to rest in the RISING active stopper. Two plastic scintillators were placed before and after the active stopper to act as veto detectors for reactions in the final degrader and to remove events that produced light particles from nuclear reactions in the final degrader.

1. Charge-state selection of secondary ions

Charge-state anomalies in the transmitted secondary ions can cause problems with particle identification and the subsequent tagging of a β decay from specific neutron-rich isotopes. In particular, hydrogen-like (i.e., $q = Z - 1$) ions of a given element can have a similar mass-to-charge ratio, A/q, as fully stripped ($q = Z$) ions. Thus, heavier neutron-rich isotopes of the same element can cause problems in the selection process. Such so-called A/q anomalies can be partially resolved using the technique described in Ref. [43]. The difference in the magnetic rigidity of the ions, $B\rho$, before and after the intermediate focal plane degrader can be used to estimate the energy loss of the transmitted ions. This value can be correlated with the measured energy loss of the same ions in the two MUSICs at the final focus of the FRS to give loci of ions associated with different *changes* in charge state through the first and second halves of the FRS [30,37]. Niobium foils were placed after the target and the intermediate degrader to improve the atomic electron stripping efficiency. The ions transmitted through the FRS degrader were distributed into three main charge-state groups: (i) The group in which $\Delta q = 0$ is assumed to include predominantly ions that are fully stripped in both halves of the FRS. We note that there is a finite probability that the $\Delta q = 0$ condition could be satisfied by ions that are hydrogen-like in both halves of the FRS. However, the expected charge-state distributions for the ions using the GLOBAL code [44] suggest that the transmission of such events is highly suppressed compared to the fully stripped species. (ii) The group $\Delta q = +1$ is assumed to include predominantly ions that are fully stripped in the first part of the FRS and hydrogen-like ions (i.e., with one attached electron) in the second half of the FRS (i.e., after the intermediate focal plane degrader). (iii) The group $\Delta q = +2$ involves predominantly helium-like ions (two electrons) in the second half of the FRS and fully stripped in the first half. The GLOBAL code [44] gives a prediction that 96.7% of the ^{190}Ta ions were fully stripped in the first half of FRS and 81.7% in the second half. Figure 2 shows the charge-state change groups of the transmitted ions by plotting the energy loss in a MUSIC detector versus energy loss in the intermediate degrader.

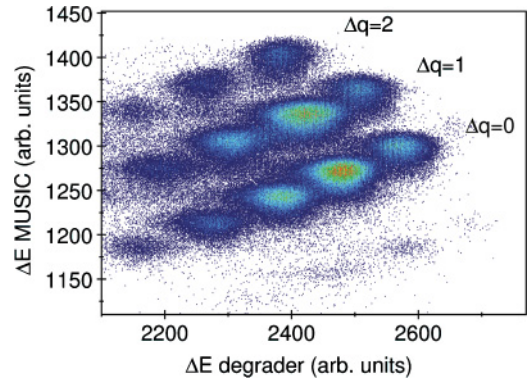

FIG. 2. (Color online) The identification of the three charge-state change groups determined using the energy loss in the intermediate degrader and the MUSIC detector at the final focal plane of the FRS. These data are taken from both the ^{190}Ta- and ^{192}Ta-centered settings. The lower group of $\Delta q = 0$ corresponds predominantly to the fully stripped charge-state transmitted through the FRS (i.e., fully stripped ions in both the first and second halves of the FRS).

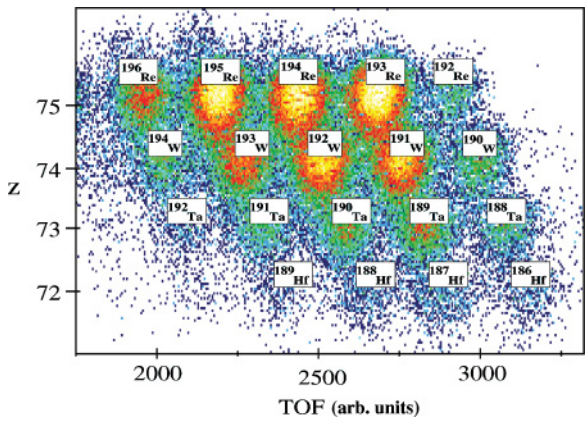

FIG. 3. (Color online) Two-dimensional particle identification plot associated with $\Delta q = 0$ (i.e., fully stripped) ions from both ^{190}Ta- and ^{192}Ta-centered settings.

2. *Particle identification*

The particle identification procedure was based on selecting the ions with $\Delta q = 0$, as illustrated in Fig. 2. Figure 3 shows the particle identification plot for $\Delta q = 0$ ions in terms of the atomic number, Z, as derived from the measured energy loss of the fragments in the MUSIC detector, versus the measured TOF in the second half of the FRS, which is related via the magnetic rigidity to the mass-over-charge ratio of the transmitted ions.

A two-dimensional matrix of detected γ-ray energies, as measured by the RISING array, versus their detection time relative to the signal from the heavy ion passing through the scintillation detector (Sci41) was created for all identified species in Fig. 3. The germanium γ-ray timing signal was recorded using the XIA DGF modules for each germanium channel, which gave an absolute time measurement with a resolution of 25 ns (see Refs. [37–41] for details). γ-rays from decays of previously reported isomeric states were used as internal checks on the particle identification procedure and to provide an independent validation of the γ-ray energy and timing measurement calibrations. Figure 4 shows selected γ-ray energy spectra and associated decay curves corresponding to γ-ray decays from isomeric states identified in the current work. Decays from the previously reported isomers in ^{188}Ta, ^{190}W,[1] ^{192}Re, and ^{193}Re [25] are all clearly identified.

The current data also show evidence for isomeric states in ^{187}Hf, ^{189,190}Ta, and ^{191}W. Evidence for the decays in ^{189}Ta and ^{191}W was previously reported in a conference proceeding from our Collaboration [45] following a survey of the region using the projectile fragmentation of a ^{208}Pb beam with RISING and a passive stopper. The current data confirm these observations. In addition, previously unreported isomeric decays in ^{187}Hf

[1]We note that the data from the current work on the isomeric decay in ^{190}W do not show any clear evidence for the 591 keV transition reported in Refs. [24,25]. This is discussed further in Ref. [26].

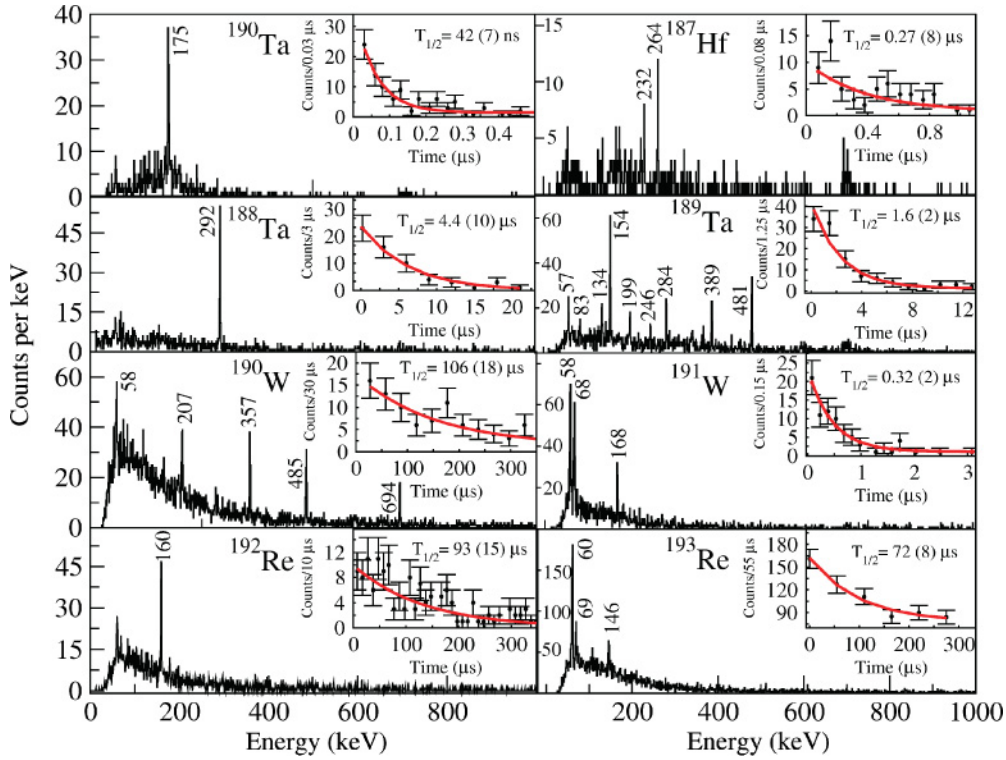

FIG. 4. (Color online) γ-ray energy and decay-time spectra of delayed events associated with isomeric states identified in ^{188,189,190}Ta (Δt = 0.2 → 22, 0.2 → 12, and 0.03→ 0.55 μs, respectively), ^{190,191}W (Δt = 2 → 395 and 0.08→ 3 μs, respectively), ^{192,193}Re (Δt = 3 → 350 and 2 → 350 μs, respectively), and ^{187}Hf (Δt = 0.08 → 1.1 μs).

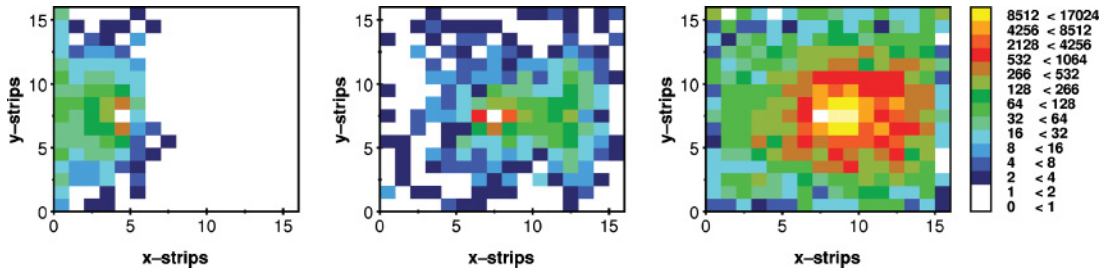

FIG. 5. (Color online) The implantion event maps for ^{188}Ta (left), ^{190}W (center), and ^{192}Re (right) as measured in the front central DSSSD from the ^{190}Ta setting.

and ^{190}Ta have been identified for the first time in the current work.

C. Implant-decay correlation technique

The technique of correlating the implanted ions with their subsequent β decay is based on the identification of the implantation position in the active stopper and the time of correlation between the implanted ion and subsequent β particle in the same or neighboring pixels of the DSSSD. The FRS was operated in monochromatic mode [46] in this experiment, which had the effect of distributing the implanted ions across a relatively wide area on the active stopper silicon detectors. This approach was required so that the probability of having multiple implantations of nuclei in the same pixel within a typical correlation time would be minimized. The use of the monochromatic mode also had the advantage of minimizing the range distribution of ions of a given species within the active stopper; thus, in general, selected isotopes of interest were stopped in a single layer of a given DSSSD. The radioactive ions were implanted in the DSSSD, with the implantation strip positions determined and an absolute measurement of the implantation time made via a digital, absolute time stamp. A valid implanted event was selected with the criterion that it produced a high-energy signal in the active stopper (>10 MeV) using the logarithmic region of the preamplifier response. Figure 5 shows two-dimensional position histograms of the implantations within one of the DSSSDs for ^{188}Ta, ^{190}W, and ^{192}Re from the ^{190}Ta setting.

The strip position, energy deposited, and time stamp for β^--decay signals in the DSSSD were correlated with the most recent implantation signal in the same or near-neighboring pixel. Figure 6 shows the energy spectrum of ions and β particles taken from the sum of energies deposited in DSSSD 1 and 2 (see Fig. 1). For each secondary ion of interest implanted in a well-defined DSSSD pixel, any energy above the threshold identified in that or neighboring pixels was considered a candidate for β^- events from the implanted mother nucleus. The time differences between the implanted events and their correlated β particle were then used to generate the β-decay time curves.

III. RESULTS

A total of 4132, 8579, and 1722 implantation events were identified for ^{188}Ta, ^{190}Ta, and ^{192}Ta ions, respectively. The β-delayed γ rays associated with these events are shown in Fig. 7, which provides spectral information on the daughter nuclei, ^{188}W, ^{190}W, and ^{192}W. Implant-β time differences of up to 100, 30, and 15 s for ^{188}Ta, ^{190}Ta, and ^{192}Ta, respectively, were used in this analysis. These γ-ray spectra have all had random, normalized γ-ray spectra subtracted from them, with the random spectra generated from long correlation times after the implantation and normalized to the time range of the original time gate. The insets of Fig. 7 show the time spectra associated with β decays of ^{188}Ta, ^{190}Ta, and ^{192}Ta, gated on discrete γ-ray lines identified in the tungsten daughter nuclei. The quoted decay half-lives were determined using a single-component exponential decay with a least-squares-fit minimization method and assuming a constant background level. A summary of the results from this γ-ray analysis for the decays identified in ^{188}W, ^{190}W, and ^{192}W in the present work is given in Table II.

A. Decay of ^{188}Ta to ^{188}W

Figure 7(a) shows discrete transitions at γ-ray energies of 143, 297, and 434 keV following the β decay of ^{188}Ta to excited states in ^{188}W. A half-life of 19.6(20) s for this β^--decaying

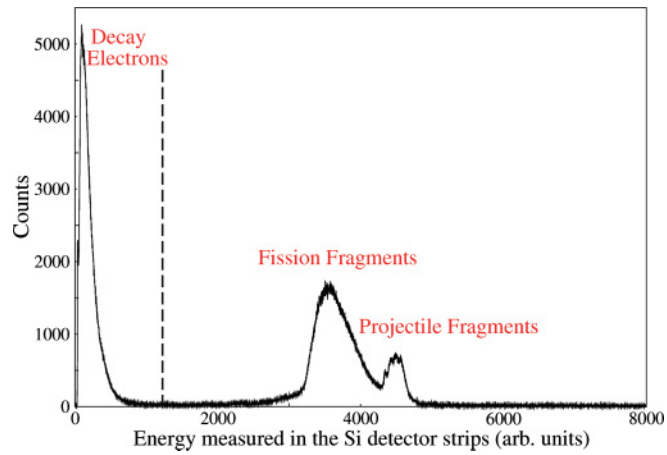

FIG. 6. (Color online) Total energy implanted by the nuclei within the silicon active stopper detector for the ^{190}Ta and ^{192}Ta settings. The double-peaked structure represents the energy deposited from both the direct implantations and for fission fragments, which are also transmitted through the FRS and pass through the active stopper. The deposited energies of β particles is shown on the left-hand side of the figure.

TABLE II. Energies, relative intensities, total internal conversion coefficient (α_{tot}), β intensities, and deduced log *ft* values associated with the γ-ray transitions observed in the β decay of ^{188,190,192}Ta.

Nucleus	E_{level} (keV)	E_γ (keV)	I_γ	α_{tot} [47]	I_{tot}[a]	$I_i \rightarrow I_f$	I_β (%)	log *ft*
^{188}Ta $\rightarrow$ ^{188}W	143	143	100(22)	1.03	203(44)	$2^+ \rightarrow 0^+$	–	–
$Q_\beta = 4854(196)$ keV	440	297	123(31)	0.09	134(35)	$4^+ \rightarrow 2^+$	–	–
	874	434	80(26)	0.04	83(26)	$6^+ \rightarrow 4^+$	53(20)	5.82(20)
	207	207	100(19)	0.29	129(24)	$2^+ \rightarrow 0^+$	$17(^{+21}_{-17})$	$6.3(^{+\infty}_{-0.4})$
^{190}Ta $\rightarrow$ ^{190}W	454	247	60(14)	0.16[a]	69(16)	$2^+_2 \rightarrow 2^+$	61(19)	5.65(24)
$Q_\beta = 5634(466)$ keV	454	454	24(10)	0.03	25(11)	$2^+_2 \rightarrow 0^+$	61(19)	5.65(24)
	564	357	30(12)	0.05	32(13)	$4^+ \rightarrow 2^+$	22(8)	6.08(23)
^{192}Ta $\rightarrow$ ^{192}W	219	219	100(26)	0.23	123(32)	$2^+ \rightarrow 0^+$	100	5.40
$Q_\beta = 6501$ keV[b]								

[a]Calculated assuming the extremum of a pure $E2$ multipolarity for the $2^+_2 \rightarrow 2^+_1$ decay.
[b]Extrapolated value, taken from Ref. [48].

state in ^{188}Ta was deduced in the current work [see the inset in Fig. 7(a)].[2]

These γ-ray energies correspond to previously observed decays from the first three excited states in the ground-state band of ^{188}W, reported following in-beam studies using both deep-inelastic reactions [22] and two-neutron transfer reactions [23]. By contrast, the transition from the yrast 8^+ state in ^{188}W ($E_\gamma = 554$ keV) as reported in Ref. [23] is not apparent in this spectrum. γ-ray energy peaks at 184, 204, and 401 keV are also identified in the β-delayed spectrum. These transitions were reported by Lane *et al.* [49] following the decay of an isomeric state in ^{188}W, with a lifetime in the 100-ns regime. The current work does not have sufficient statistics for a γ-γ coincidence analysis of the decays from this isomer.

The log *ft* values were calculated assuming ground-state mass values taken from Ref. [50]. For the ^{188}Ta decay, the log *ft* value was estimated assuming a direct β^--feeding branch to the yrast $I^\pi = 6^+$ in ^{188}W. It should be noted, however, that the observation of discrete transitions associated with the isomer decay branch reported by Lane *et al.* suggests some degree of competition in the direct feeding through a parallel branch in ^{188}W. From the observed γ-ray intensities in Fig. 7(a), an estimate of the direct β feeding to the yrast $I^\pi = 6^+$ state has been made, which in turn has been used to extract a value for log *ft* for the decay of ^{188}Ta to the yrast 6^+ state in ^{188}W, given in Table II.[3] There is no evidence

[2]Note that this discussion assumes that a single β-decaying state is observed in the present work. The presence of two parallel, low-lying, β-decaying states in ^{188}Ta with similar half-lives cannot be ruled out in the current work.

[3]Because the complete feeding intensity into the tungsten daughter is not established in the current work, we note that the log *ft* values given in Table II should be regarded as lower limits rather than precise values.

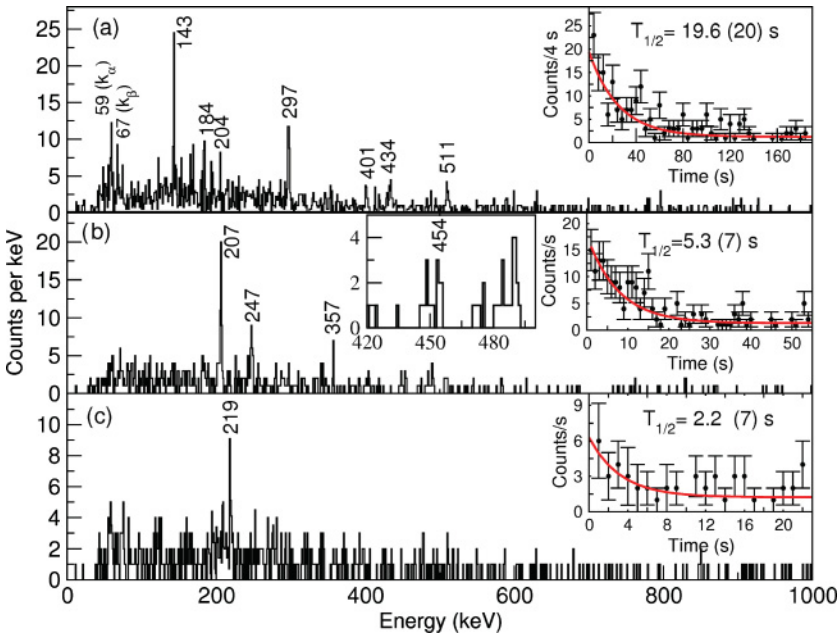

FIG. 7. (Color online) β-delayed γ-ray spectra to populate excited states in (a) ^{188}W ($\Delta t_{implant-\beta} = 100$ s); (b) ^{190}W ($\Delta t_{implant-\beta} = 30$ s), with the insert showing the enlargement of the 420→500 keV region; and (c) ^{192}W ($\Delta t_{implant-\beta} = 15$ s). A normalized random background has been subtracted from each γ-ray spectrum.

in the current work that the decays from the reported isomer feed the $I^\pi = 6^+$ yrast state in ^{188}W. Accordingly, we assume that the β^--decay feeding from the decay of ^{188}Ta leads to two parallel cascades of γ rays with 53% of direct feeding to the yrast $I^\pi = 6^+$ state and the remainder feeding to the isomeric state. Under these assumptions, it is possible to derive a lower limit for the log ft value of 5.82(20) from the direct β^--decay transition to the $I^\pi = 6^+$ state from the measured half-life of ^{188}Ta of 19.6(20) s.

B. Decay of ^{190}Ta to ^{190}W

The β-delayed γ-ray spectrum for transitions in ^{190}W is shown in Fig. 7(b). The previously reported isomeric state in ^{190}W [24–26] was also directly populated via projectile fragmentation in the current work, as shown in Fig. 4. Following population by the β^- decay of ^{190}Ta, two discrete γ-ray lines at energies of 207 and 357 keV are observed, establishing these as the decays from the yrast states with $I^\pi = 2^+$ and 4^+, respectively, in ^{190}W. A γ-γ coincidence analysis was also performed with the data from this experiment on the isomer-delayed transitions in ^{190}W, which confirmed the mutually coincident nature of the 207- and 357-keV transitions (see Fig. 8).

In addition to these previously reported transitions in ^{190}W, a transition at 247 keV is also observed in the β-delayed coincidence spectra following the decay of ^{190}Ta. This transition is interpreted as arising from the decay of the 2_2^+ state in ^{190}W, which feeds directly into the yrast $I^\pi = 2^+$ state. The limited statistics in the current β-delayed data preclude a γ-γ coincidence analysis to prove the direct feeding of the 247-keV line into the yrast $I^\pi = 2^+$ state; however, this interpretation is made on the following basis: (i) There are no other γ-ray transitions of similar intensity present in the ^{190}Ta correlated, β-delayed spectrum shown in Fig. 7(b); (ii) The 485-keV transition (which is assumed to decay from the $I^\pi = 6^+$ member of the ^{190}W ground-state band [24–26]) is not apparent in the β-decay data. (Note that the population of the yrast 6^+ state in ^{190}W is observed following the isomeric decay of the same nucleus in the current work; see Fig. 8.) Thus, it is suggested that $I^\pi = 2^+$ is the most likely spin-parity assignment for this level. (iii) An $I^\pi = 4^+$ assignment would make the 454-keV state yrast, in which case it would have been expected to have been populated in the decay of the isomeric state previously reported in ^{190}W, which it is not. An $I^\pi = 3^+$ assignment would imply that it is a collective state and built on the $I^\pi = 2^+$ bandhead of the γ-band, which can be ruled out on the basis of a lack of observation of a candidate for the required $3_\gamma^+ \rightarrow 2_2^+$ transition. (iv) Assignments of either 1^+ or 1^- at this energy in an even-even nucleus are inherently unlikely. The assumption of a 2_2^+ assignment for this state is further strengthened by the observation of a weak transition at 454 keV energy in the β-delayed spectrum for transitions in ^{190}W [see inset in Fig. 7(b)], which would represent the direct transition from the 2_2^+ state to the 0^+ ground state in ^{190}W.

The preceding arguments, together with the measured intensities (see Table II) for the observed decays from the 4^+ and 2^+ yrast states at 564 and 207 keV, respectively, in Fig. 7(b) imply a spin of $3\hbar$ for the β-decaying state in ^{190}Ta. The assumption of a spin of $3\hbar$ for the β-decaying state in ^{190}Ta is consistent (assuming direct population) with the previously discussed $I^\pi = 2^+$ assignment for the 454-keV level.

Figure 9 shows the systematics of the low-lying states in even-even tungsten isotopes with $A = 180 \rightarrow 192$ including the proposed 2_2^+ state in ^{190}W. Such states in deformed nuclei usually are associated with the bandhead of the $K^\pi = 2^+\gamma$-vibrational band. We note that the assumption of the second 2^+ state in ^{190}W at an excitation energy of 454 keV is in line with the trend expected for this region, with the ongoing, systematic decrease in the energy of the 2_2^+ state relative to the yrast 4^+ states in this isotopic chain approaching the $N = 116$ isotone, ^{190}W.

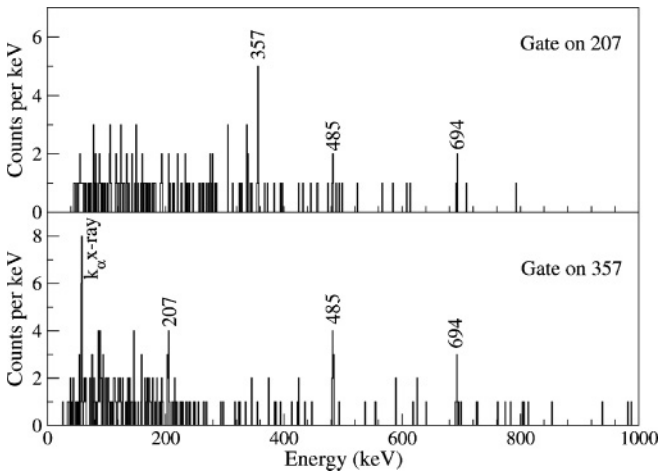

FIG. 8. Isomer-delayed γ-γ coincidence gate on (upper panel) the 207-keV transition in ^{190}W and (lower panel) the 357-keV transition in ^{190}W. The time gate condition was selected from $2\rightarrow$ 395 μs following the ion implantation in the active stopper.

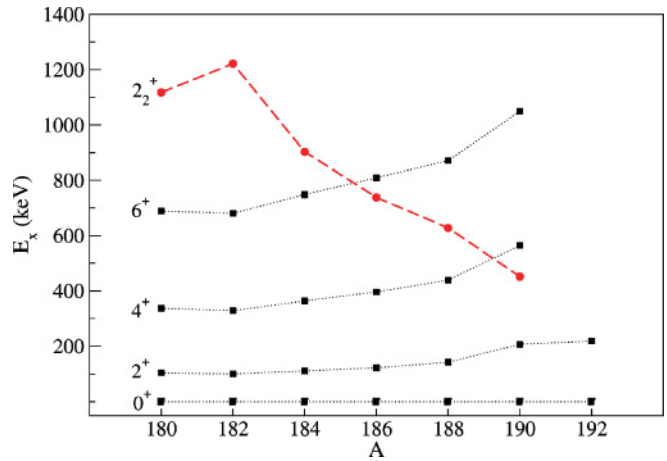

FIG. 9. (Color online) Systematic behavior of the low-lying states of even-A tungsten isotopes with $A = 180 \rightarrow 192$. The dashed lines correspond to the second $I^\pi = 2^+$ states. The data are taken from Ref. [51] and the current work.

If it is assumed that the β^- decay of the ^{190}Ta ground state feeds only the 207, 454 and 564 keV levels, then the logft values for the β^- feeding of these levels given in Table II can be derived using the half-life measured in the present work and a Q_{β^-} value of 5.634 MeV [50].

C. Decay of ^{192}Ta to ^{192}W

The β-delayed γ-ray spectrum showing transitions in ^{192}W following the decay of ^{192}Ta is shown in Fig. 7(c). A single γ-ray line at an energy of 219 keV is evident and is interpreted as arising from the yrast $2^+ \rightarrow 0^+$ transition in ^{192}W. The decay half-life measurement for ^{192}Ta gated on the 219-keV γ-ray photopeak is 2.2 ± 0.7 s. We note that 219 keV is almost the same energy as the $2^+ \rightarrow 0^+$ transition in the $N = 118$ isotone, ^{194}Os [$E(2^+) = 218$ keV], and indeed the same, near-isospectral behavior is also evident for the $N = 116$ isotonic doublet ^{190}W and ^{192}Os [$E(2^+) \approx 207$ keV]. The possibility that the 219-keV transition observed in the present work is the result of a misassignment of the β decay of ^{194}Re into ^{194}Os can be discounted as this specific decay has also been studied in the same data set, with multiple other transitions observed resulting from decays from higher spin states in ^{194}Os [27].

The likely spin of the decaying state in the ^{192}Ta parent nucleus can be restricted to $1\hbar$ or $2\hbar$ on the basis of the expected β^--decay selection rules and the lack of any apparent line associated with the $4^+ \rightarrow 2^+$ transition in ^{192}W. However, it should be noted that, on the basis of the statistics in the current work as shown in Fig. 7(c), the possible population of higher spin states in the yrast cascade in ^{192}W and thus a higher spin for the β-decaying state cannot be ruled out. From a comparison of the number of implants and associated β^--γ-ray coincident event, there is no strong evidence of direct feeding from the β^- decay of ^{192}Ta to the ground state of ^{192}W, although such a branch cannot be exclusively ruled out in the current work. The lower limit for the logft value for this decay given in Table II assumes 100% feeding in the β^- decay to the proposed yrast $I^\pi = 2^+$ state in ^{192}W.

IV. DISCUSSION

A. Subshell closure for the $A \sim 190$ region?

The systematics of the energy ratio $R(4/2) = E(4^+)/E(2^+)$ is arguably the best indicator of changes in low-lying nuclear structure [17]. However, for the most exotic nuclei, often only the energy of the first 2^+ state is known. In general, the energy of the first 2^+ state has been shown to decrease as the number of the valence nucleons (and related quadrupole collectivity) increases [52]. This general trend is opposite to the magnitude of the energy ratio and, thus, the $1/E(2_1^+)$ systematics should follow behavior similar to that for the $R(4/2)$ ratio. Cakirli and Casten [53] have recently used these empirically derived observables to demonstrate evidence for subshell closures in different regions of the nuclear chart. They also noted that the behavior of the $R(4/2)$ and $1/E(2_1^+)$ observables appear to scale with each other in regions of shape evolution and that evidence of subshell closures can be seen

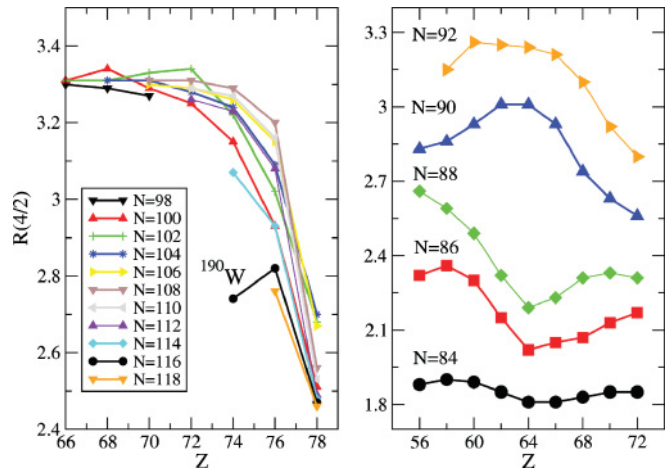

FIG. 10. (Color online) Experimental ratio of the excitation energies of the yrast $I^\pi = 4^+$ and 2^+ states [$R(4/2)$] for the even-even nuclei with (left) $Z = 66 \rightarrow 78$ and for $N > 98$ and (right) similar plot for $Z = 56 \rightarrow 72$ and for $N = 84 \rightarrow 92$, showing the effect of the subshell closure in this region. These data are taken from Ref. [51] and the present work.

in the appearance of a "bubble" in the evolution of such plots as a function of proton or neutron number.

The energy ratios in Fig. 10 show a gradual, systematic decrease in the value of $R(4/2)$ with neutron number from $^{182}W_{108}$ [$R(4/2) = 3.29$] to $^{188}W_{114}$ [$R(4/2) = 3.07$]. This is followed by a very dramatic decrease at the $N = 116$ isotone, ^{190}W, for which the ratio drops to a value of $R(4/2) = 2.7$, approaching the triaxial-rotor limit of $R(4/2) = 2.5$. This gives rise to what appears to be the onset of the bubble effect described by Cakirli and Casten. With the data point for ^{192}W from the current work, this behavior is even more dramatically demonstrated by the behavior of the $1/E(2_1^+)$ observable, as shown in Fig. 11, which shows the beginning of a gap/bubble pattern for the $A \sim 190$ region. Evidence for such a subshell effect or dramatic shape evolution with the addition or removal of two nucleons can also be seen from the *difference*

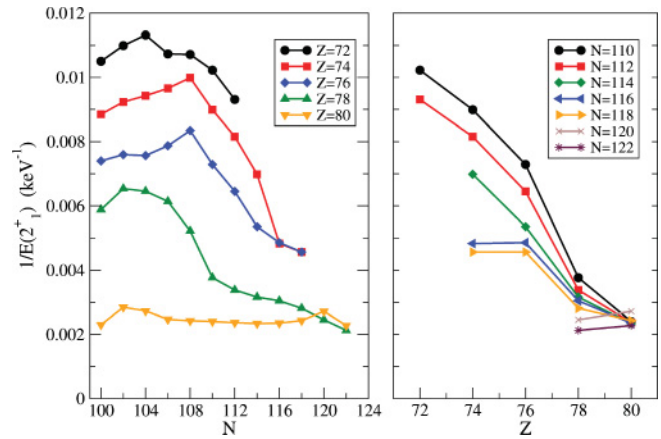

FIG. 11. (Color online) The empirical $1/E(2_1^+)$ values plotted (left) against the proton number for the $A \sim 190$ region and (right) as a function of neutron number, N, between 100 and 122. These data are taken from Ref. [51] and the present work.

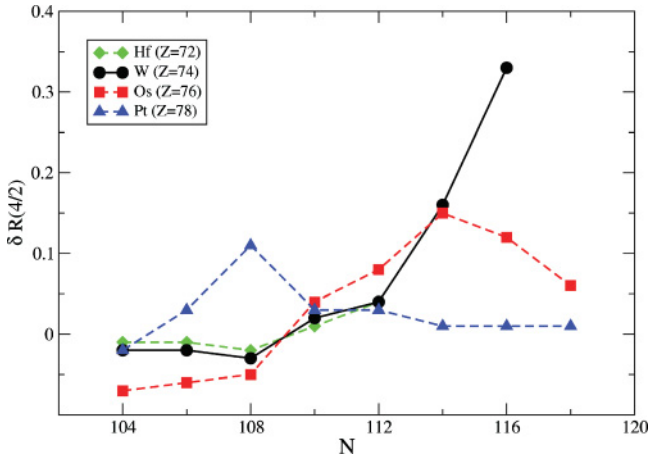

FIG. 12. (Color online) Systematics of the difference in the excitation energy ratio, $\delta R(4/2)$, for heavy even-even neutron-rich nuclei with $N = 104 \rightarrow 118$. These data are taken from Ref. [51] and the present work.

in $R(4/2)$ between neighboring even-even isotopes; that is, $\delta R(4/2) = R(4/2)_{Z,N} - R(4/2)_{Z,N-2}$ [54]. Figure 12 shows this quantity for the Hf, W, Os, and Pt isotopes with neutron numbers ranging from the midshell at $N = 104$ up to $N = 118$. The value for $\delta R(4/2)$ of greater than 0.3 between ^{188}W and ^{190}W represents one of the largest $\delta R(4/2)$ differences in the entire Segré chart. This provides compelling evidence for a dramatic change in the ground-state structure for W isotopes in going from $N = 114$ to $N = 116$.

B. Triaxial softness around $N = 116$

Evidence for triaxial (or γ-soft) collective behavior in nuclei can be obtained by using a number of basic experimental observables. These include (i) $R(2_2/2_1)$, the excitation energy ratio between the second and first spin-parity 2^+ states; (ii) the $R(4/2)$ ratio; and (iii) the ratio of the reduced matrix probabilities between the second and the first 2^+ states and from the second 2^+ state to the ground state, $R_2 = \frac{B(E2:2_2^+ \rightarrow 2_1^+)}{B(E2:2_2^+ \rightarrow 0_1^+)}$ [17]. The $E(2_1^+)$ energy is expected to increase with increasing neutron number as the $N = 126$ shell closure is approached. This increase seems to be continued for the heavier tungsten isotopes using the data for the 2_1^+ energy in the $N = 118$ isotone, ^{192}W, from the current work. This general behavior of a reduction in the energy ratio $R(4/2)$ and parallel increase in the energy of the first 2^+ state in these isotopes is indicative of the expected reduction in quadrupole collectivity as the neutron number approaches the $N = 126$ closed shell.

The $R(4/2)$ value in ^{190}W can be explained as a general feature of a γ-soft potential. Jolie and Linnemann [9] suggested that the region of nuclei between ^{180}Hf and ^{200}Hg exhibits prolate-oblate deformations and phase-shape transitions between these two shapes. There have also been theoretical predictions of a ground-state/low-lying shape transition from prolate to oblate shapes in this mass region using a variety of mean-field models (see Ref. [7] and references therein). This phase transition occurs at the O(6) symmetry in the interacting boson approximation (IBA) [10–13]. It is useful to apply the IBA model to ^{190}W, because it allows one to investigate the γ dependence of the potential appropriate for this nucleus. To study ^{190}W, we used a simple, two-parameter IBA-1 Hamiltonian suitable for most collective nuclei. This Hamiltonian can be written as [55,56]

$$H(\zeta) = c\left[(1-\zeta)\hat{n}_d - \frac{\zeta}{4N}\hat{Q}^\chi \cdot \hat{Q}^\chi\right], \qquad (1)$$

where N is the number of valence bosons, $\hat{n}_d = d^\dagger \cdot \tilde{d}$, and $\hat{Q}^\chi = (s^\dagger \tilde{d} + d^\dagger s) + \chi(d^\dagger \tilde{d})$.

This Hamiltonian has two parameters, ζ and χ, with an overall scaling factor. In this Hamiltonian, $\zeta = 0$ gives a U(5) or a quadrupole vibrator spectrum (the $\hat{n}_d$ term) while $\zeta = 1$ gives a rotor (the $\hat{Q} \cdot \hat{Q}$ term). In this latter case, one has an axial rotor for $\chi = -\frac{\sqrt{7}}{2} = -1.32$ and a γ-soft [O(6)] for $\chi = 0$. Intermediate values of ζ and χ allow one to span a wide range of collective structures.

To use Eq. (1), a technique was used based on the orthogonal cross-contour method [57]. In this approach, one can place a nucleus in the symmetry triangle for the IBA by using a contour of constant values of a pair of observables. With the data available, we used $R(4/2)$ and $E(2_2^+)$. In the O(6) limit, $E(2_2^+) = E(4_1^+)$ due to their common membership in the $\tau = 2$, O(5) multiplet. For any other situation, the IBA-1 Hamiltonian [55,56] of Eq. (1) gives $E(2_2^+) > E(4_1^+)$. Therefore, it is impossible to obtain a precise fit for the ^{190}W data, because the experimental values have $E(2_2^+) < E(4_1^+)$.

Experimentally, $R(4/2) = 2.72$ for ^{190}W. The contour for this value for $N = 9$ is shown in the inset of Fig. 13. To investigate the structure further, another observable is required, and so the $E(2_2^+)$ values are calculated along the $R(4/2) = 2.72$ contour. The results for $E(2_2^+)$ are compared with experimental value, as shown in Fig. 13.

The experimental value of $R(4/2)$ is consistent with a γ-soft [$R(4/2) \approx 2.5$] structure but does not establish it because a

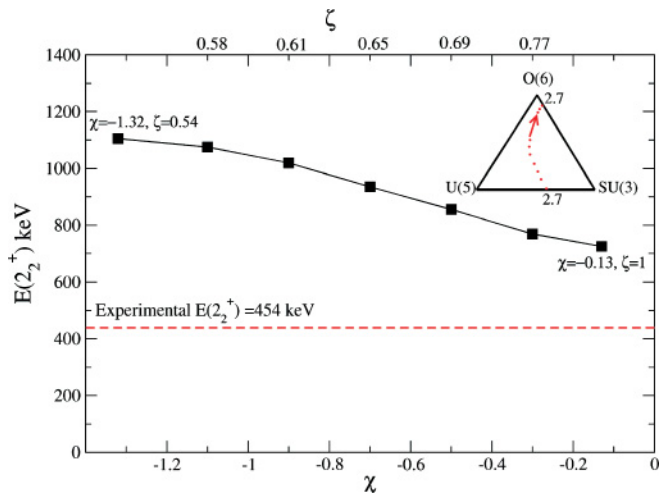

FIG. 13. (Color online) IBA-1 calculations for $E(2_2^+)$ ^{190}W along the contour in the IBA-1 symmetry triangle (dotted-line contour in the triangle) corresponding to $R(4/2) = 2.72$. The closest calculated result to the experimental $E(2_2^+)$ value is the one near the O(6) geometrically limit.

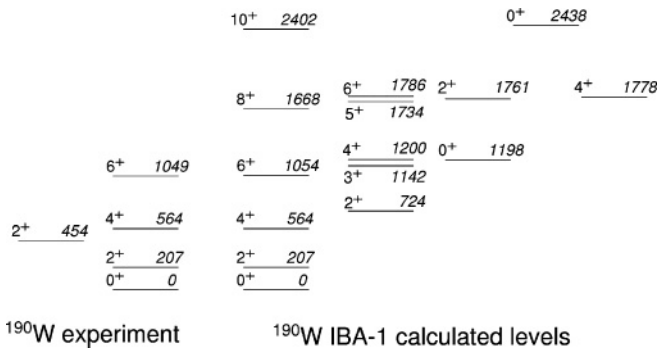

FIG. 14. Results of IBA-1 calculations for ^{190}W and comparison with the experimentally measured low-lying energy levels for this nucleus.

value of 2.7 can also be obtained for an axially symmetric quasirotor, as seen the inset of Fig. 13. Because the two parameters of the IBA-1 Hamiltonian of Eq. (1) cannot fit a 2_2^+ energy as low as observed experimentally, the best fit is obtained for a γ-soft structure very close to O(6). The theoretical-level scheme obtained from this procedure is compared with the experimental data in Fig. 14.

From a consideration of O(6) and also of the IBA calculations on the right-hand side of Fig. 14, one characteristic feature is a staggering in the γ-band energies, and in particular a near degeneracy of the 3_γ^+ and 4_γ^+ levels. Experimentally identifying these levels would provide a good future test of these ideas.

The identification of a weakly populated peak at 454 keV energy in ^{190}W suggests a direct transition from the 2_2^+ state to the ground state 0^+ in ^{190}W. In the pure, idealized O(6) limit, such a transition is forbidden [10–13]; however, in realistic, finite nuclear systems, such hindered transitions have been observed. The statistics in the current work preclude an angular distribution analysis to establish the $M1/E2$ mixing ratio of the proposed, unstretched $(2_2^+) \rightarrow 2_1^+$ transition in ^{190}W ($E_\gamma =$ 247 keV).

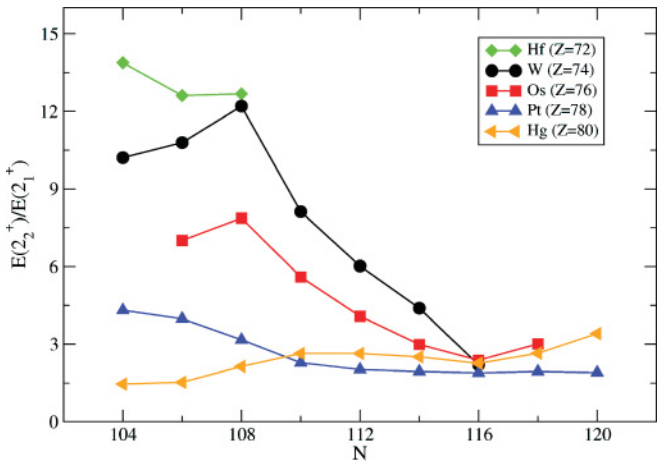

FIG. 15. (Color online) The ratio of the excitation energies of the $I^\pi = 2_2^+$ and $I^\pi = 2_1^+$ states for heavy even-even neutron-rich nuclei with $N = 104 \rightarrow 120$. These data are taken from Ref. [51] and the current work for ^{190}W.

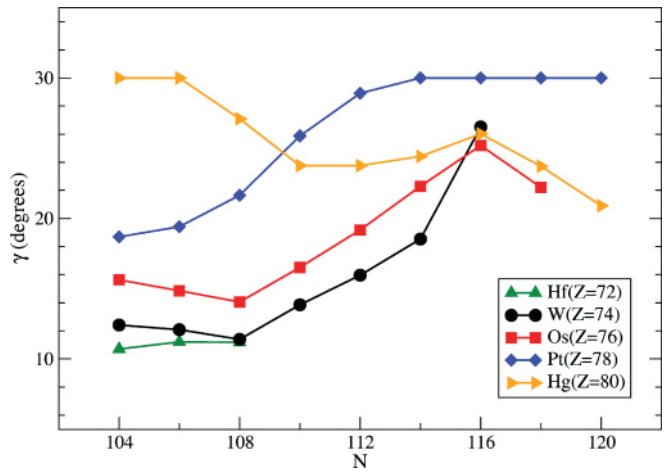

FIG. 16. (Color online) Empirically deduced γ values for heavy Hf $\rightarrow$ Hg even-even neutron-rich nuclei with $N = 104 \rightarrow 120$ using Eqs. (2) and (3) of the Davydov model (see text for details).

Another empirical quantity, which has been used to infer the prolate-oblate shape-transition regions, is the energy ratio $E(2_2^+)/E(2_1^+)$ [58]. Figure 15 shows a systematic of this ratio versus the neutron number of even-even Hf $\rightarrow$ Hg ($Z = 72 \rightarrow$ 80) isotopes $N = 104 \rightarrow 120$. The figure shows an apparent maximization of the γ softness for Os, Pt, and Hg at neutron number $N = 116$ in which the new data point for ^{190}W from the current work is consistent with this trend.

An estimate of the value of the static or average triaxial deformation parameter, γ, can be extracted from the Davydov model [59] using the energy ratio $E(2_2^+)/E(2_1^+)$. Although the Davydov model represents an asymmetric nucleus with a rigid shape, this parameter can provide a simple prediction of a static γ value that can be compared with the average γ value associated with γ-soft potentials. The expression described in

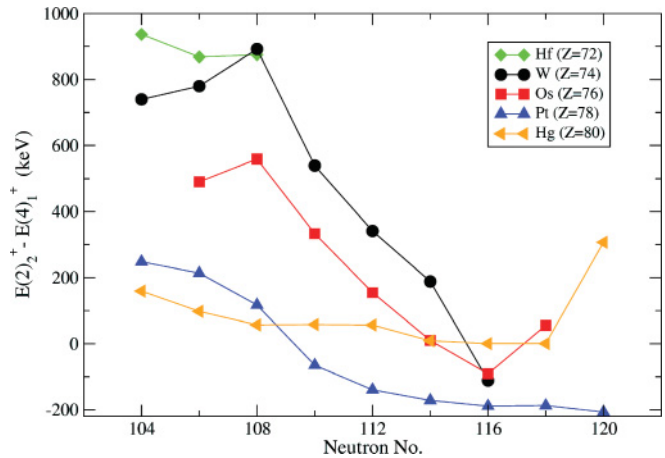

FIG. 17. (Color online) Systematics of the excitation energy difference between the $I^\pi = 2_2^+$ and $I^\pi = 4^+$ states for the even-even Hf $\rightarrow$ Hg nuclei as a function of the neutron numbers for $N = 104 \rightarrow$ 120. These data are taken from Ref. [51] and the present work.

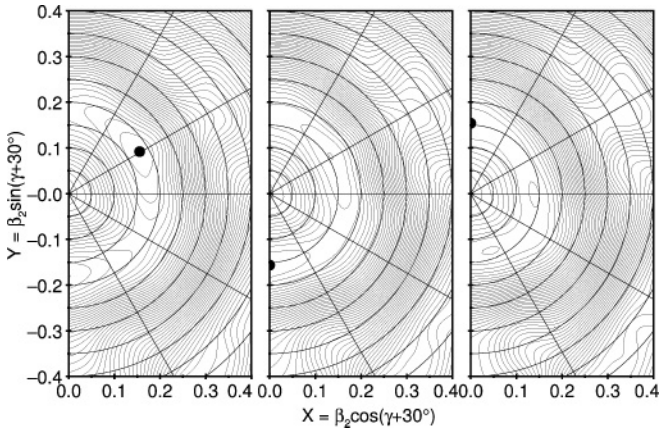

FIG. 18. (Color online) TRS calculations for the ground-state configurations of (left) ^{188}W with $\beta_2 = 0.178$ and $\gamma = 1.3°$, (middle) ^{190}W with $\beta_2 = 0.158$ and $\gamma = -120.0°$, and (right) ^{192}W with $\beta_2 = 0.136$ and $\gamma = -24.1°$. The energy contours in this figure are separated by 200 keV.

Ref. [17] is used to extract the γ value as follows:

$$\frac{E(2_2^+)}{E(2_1^+)} = \frac{[1+X]}{[1-X]}, \tag{2}$$

where

$$X = \sqrt{1 - \frac{8}{9}\sin^2(3\gamma)}. \tag{3}$$

Therefore, when $X = 1$ (i.e., for $\gamma = 0°$), the energy ratio $E(2_2^+)/E(2_1^+) \to \infty$, whereas for $X = 1/3$, $\gamma = 30°$. For ^{190}W the ratio of $E(2_2^+)/E(2_1^+)$ is equal to 2.19, leading to a value of $\gamma \approx 27°$. Figure 16 shows the γ values extracted for the even-even Hf $\to$ Hg isotopes with $N = 104 \to 120$ using Eqs. (2) and (3). The maximum γ-value appears to be reached at $N = 116$ for W, Os, and Hg.

A second quantity used to infer prolate-oblate shape-transition regions is the energy difference between the $E(2_2^+)$ and $E(4^+)$ levels [58]. According to Kumar [60], a negative value of $E(2_2^+) - E(4^+)$ (i.e., the second 2^+ state lying lower in energy than the yrast 4^+ state) is a good indicator of a region of prolate-oblate phase transition. Figure 17 shows this energy difference versus the neutron number for the region of interest. These systematics display similar characteristics to the $E(2_2^+)/E(2_1^+)$ systematics shown in Fig. 15. The neutron number $N = 116$ again appears to be associated with maximum γ softness for the low-lying states in the Os, Hg, and possibly W isotopic chains.

In their recent theoretical studies of this region using a Skyrme Hartree-Fock plus BCS pairing approach, Sarriguren *et al.* [7,61] predicted that ^{190}W lies on the near-critical point between prolate and oblate shapes in this region, with a prediction of a very shallow triaxial minimum for the ground-state shape with a predicted $\gamma = 25°$. These authors also point out that neutron number $N = 116$ appears to be a "saddle point" for the Yb, Hf, W, and Os isotopes with respect to maximum γ softness at the transition between axially symmetric prolate and oblate ground states for $N \leqslant 114$ and $N \geqslant 118$, respectively.

Total Routhian surface (TRS) calculations using the prescription described in Ref. [62] for the ground-state configurations of ^{188,190,192}W have been performed as shown in Fig. 18. The calculations predict an evolution from a prolate (albeit) γ-soft potential in ^{188}W to a very γ-soft potential for ^{190}W and ^{192}W. Indeed, the very flat energy change associated with the γ degree of freedom for $\beta_2 \approx 0.15$ can be linked to a clear predicted region of prolate/oblate shape coexistence associated with an O(6)-like potential.

V. CONCLUSIONS

The low-lying states of ^{188}W, ^{190}W, and ^{192}W have been investigated following the β^- decay of their tantalum mother nuclei populated in relativistic projectile fragmentation reactions. The results support the previously reported assignments for the first 2^+ and 4^+ states in ^{190}W and provide candidates for decays from the second 2^+ state in this nucleus and the first 2^+ state in ^{192}W. The results are consistent with the fact that $N = 116$ represents a maximum value of γ softness in this region at the intersection between prolate and oblate deformations for lighter and heavier isotopes, respectively. A direct link between the emergence of a localized proton subshell closure at $Z \leqslant 74$ for $N \geqslant 116$ and the apparent maximum values of γ softness around $N \sim 116$ is not clear at the present time.

ACKNOWLEDGMENTS

The excellent work of the GSI accelerator staff is acknowledged. This work is supported by the EPSRC/STFC (UK), King Abdulaziz City for Science and Technology (Saudi Arabia), AWE plc. (UK), the EU Access to Large Scale Facilities Programme (EURONS, EU Contract No. 506065), the Swedish Research Council, the Polish Ministry of Science and Higher Education, the Bulgarian Science Fund, the US Department of Energy under Grant No. DE-FG02-91ER-40609, the Spanish Ministerio de Educación y Ciencia, the German BMBF under Grant No. 06KY205I, the Hungarian Science Foundation, the Italian INFN, and CNCSIS under Contract No. ID-180.

[1] R. F. Casten, Nucl. Phys. **A443**, 1 (1985).
[2] P. M. Walker and G. Dracoulis, Nature (London) **399**, 35 (1999).
[3] C. Y. Wu *et al.*, Nucl. Phys. **A607**, 178 (1996).
[4] C. Wheldon, J. Garcés Narro, C. J. Pearson, P. H. Regan, Zs. Podolyák, D. D. Warner, P. Fallon, A. O. Macchiavelli, and M. Cromaz, Phys. Rev. C **63**, 011304 (2000).
[5] P. H. Regan, F. R. Xu, P. M. Walker, M. Oi, A. K. Rath, P. D. Stevenson *et al.*, Phys. Rev. C **65**, 037302 (2002).
[6] P. D. Stevenson, M. P. Brine, Zs. Podolyák, P. H. Regan, P. M. Walker, and J. R. Stone, Phys. Rev. C **72**, 047303 (2005).
[7] P. Sarriguren, R. Rodríguez-Guzmán, and L. M. Robledo, Phys. Rev. C **77**, 064322 (2008).

[8] Zs. Podolyák *et al.*, Phys. Rev. C **79**, 031305(R) (2009).
[9] J. Jolie and A. Linnemann, Phys. Rev. C **68**, 031301(R) (2003).
[10] F. Iachello and A. Arima, *The Interacting Boson Model* (Cambridge University Press, Cambridge, 1987).
[11] F. lachello and A. Arima, Phys. Lett. **B53**, 309 (1974).
[12] A. Arima and F. Iachello, Phys. Rev. Lett. **40**, 385 (1978).
[13] A. Arima and F. lachello, Phys. Rev. Lett. **35**, 1069 (1975).
[14] R. F. Casten and J. A. Cizewski, Phys. Lett. **B185**, 293 (1987).
[15] J. A. Cizewski, R. F. Casten, G. J. Smith, M. L. Stelts, W. R. Kane, H. G. Borner, and W. F. Davidson, Phys. Rev. Lett. **40**, 167 (1978).
[16] N. V. Zamfir, W.-T. Chou, and R. F. Casten, Phys. Rev. C **57**, 427 (1998).
[17] R. F. Casten, *Nuclear Structure from Simple Perspective* (Oxford University Press, Oxford, 2000), pp. 240–252.
[18] R. F. Casten, H. G. Borner, J. A. Pinston, and W. F. Davidson, Nucl. Phys. **A309**, 206 (1978).
[19] G. Berrier-Ronsin, M. Vergnes, G. Rotbard, J. Kalifa, J. Vernotte, and R. Seltz, Phys. Rev. C **23**, 2425 (1981).
[20] R. D'Alarcao *et al.*, Phys. Rev. C **59**, R1227 (1999).
[21] C. Wheldon, J. Garcés Narro, C. J. Pearson, P. H. Regan, Zs. Podolyák, D. D. Warner, P. Fallon, A. O. Macchiavelli, and M. Cromaz, Phys. Rev. C **63**, 011304(R) (2000).
[22] Zs. Podolyák *et al.*, Int. J. Mod. Phys. E **13**, 123 (2004).
[23] T. Shizuma *et al.*, Eur. Phys. J. A **30**, 391 (2006).
[24] Zs. Podolyák *et al.*, Phys. Lett. **B491**, 225 (2000).
[25] M. Caamano *et al.*, Eur. Phys. J. A **23**, 201 (2005).
[26] G. F. Farrelly *et al.*, Acta Phys. Pol. B **40**, 885 (2009).
[27] P. H. Regan *et al.*, AIP Conf. Proc. **1090**, 122 (2008).
[28] P. H. Regan *et al.*, Int. J. Mod. Phys. E **17**, 8 (2008).
[29] N. Alkhomashi *et al.*, Acta Phys. Pol. B **40**, 875 (2009).
[30] H. Geissel *et al.*, Nucl. Instrum. Methods Phys. Res. B **70**, 286 (1992).
[31] R. Kumar *et al.*, Nucl. Instrum. Methods Phys. Res. A **598**, 754 (2009).
[32] Micron Semiconductor Ltd, Marlborough Road, Lancing Sussex, England, http://www.micronsemiconductor.co.uk (2009).
[33] Zs. Podolyák *et al.*, Phys. Lett. **B672**, 116 (2009).
[34] D. Bazin, O. Tarasov, M. Lewitowicz, and O. Sorlin, Nucl. Instrum. Methods Phys. Res. A **482**, 307 (2002).
[35] O. B. Tarasov and D. Bazin, Nucl. Phys. **A746**, 411 (2004).
[36] S. Pietri *et al.*, Nucl. Instrum. Methods Phys. Res. B **261**, 1079 (2007).
[37] S. Pietri *et al.*, Acta Phys. Pol. B **38**, 1255 (2007).
[38] A. B. Garnsworthy *et al.*, Phys. Lett. **B660**, 326 (2008).
[39] S. J. Steer *et al.*, Phys. Rev. C **78**, 061302(R) (2008).
[40] D. Rudolph *et al.*, Phys. Rev. C **78**, 021301(R) (2008).
[41] M. Gorska *et al.*, Acta Phys. Pol. B **38**, 1219 (2007).
[42] L. Caceres *et al.*, Phys. Rev. C **79**, 011301(R) (2009).
[43] J. Benlliure, K.-H. Schmidt, D. Cortina-Gil, T. Enqvist, F. Farget, A. Heinz, A. R. Junghans, J. Pereira, and J. Taieb, Nucl. Phys. **A660**, 87 (1997).
[44] C. Scheidenberger, Th. Stöhlker, W. E. Meyerhof, H. Geissel, P. H. Mokler, and B. Blank, Nucl. Instrum. Methods Phys. Res. B **142**, 441 (1998).
[45] S. J. Steer *et al.*, Int. J. Mod. Phys. E **18**, 1002 (2009).
[46] G. Münzenberg, Nucl. Instrum. Methods Phys. Res. B **70**, 265 (1992).
[47] T. Kibédi, T. W. Burrows, M. B. Trzhaskovskaya, P. M. Davidson, and C. W. Nestor Jr., Nucl. Instrum. Methods Phys. Res. A **589**, 202 (2008).
[48] P. Möller, J. R. Nix, W. D. Myers, and W. J. Swiatecki, At. Data Nucl. Data Tables **59**, 185 (1995).
[49] G. Lane *et al.* (private communication, 2009).
[50] G. Audi, A. H. Wapstra, and C. Thibault, Nucl. Phys. **A729**, 337 (2003).
[51] Evaluated Nuclear Structure Data File, ENSDF, online database, National Nuclear Data Center, 2008.
[52] R. F. Casten and N. V. Zamfir, Phys. Rev. Lett. **70**, 402 (1993).
[53] R. B. Cakirli and R. F. Casten, Phys. Rev. C **78**, 041301(R) (2008).
[54] R. B. Cakirli and R. F. Casten (private communication, 2009).
[55] V. Werner, N. Pietralla, P. von Brentano, R. F. Casten, and R. V. Jolos, Phys. Rev. C **61**, 021301(R) (2000).
[56] P. O. Lipas, P. Toivonen, and D. D. Warner, Phys. Lett. **B155**, 295 (1985).
[57] E. A. McCutchan and R. F. Casten, Phys. Rev. C **74**, 057302 (2006).
[58] R. F. Casten, A. I. Namenson, W. F. Davidson, D. D. Warner, and H. G. Borner, Phys. Lett. **B76**, 280 (1978).
[59] A. S. Davydov and G. F. Filippov, Nucl. Phys. **8**, 237 (1958).
[60] K. Kumar, Phys. Rev. C **1**, 369 (1970).
[61] L. M. Robledo, R. Rodríguez-Guzmán, and P. Sarriguren, J. Phys. G: Nucl. Part. Phys. **36**, 115104 (2009).
[62] F. R. Xu, Phys. Lett. **B435**, 257 (1998).

Eur. Phys. J. A **42**, 489–493 (2009)
DOI 10.1140/epja/i2009-10794-5

THE EUROPEAN PHYSICAL JOURNAL A

Regular Article – Experimental Physics

Structure of neutron-rich nuclei around the N = 126 closed shell; the yrast structure of $^{205}Au_{126}$ up to spin-parity $I^{\pi} = (19/2^{+})$

Zs. Podolyák[1,a], S.J. Steer[1], S. Pietri[1], M. Górska[2], P.H. Regan[1], D. Rudolph[3], A.B. Garnsworthy[1,4], R. Hoischen[3], J. Gerl[2], H.J. Wollersheim[2], H. Grawe[2], K.H. Maier[5,6], F. Becker[2], P. Bednarczyk[2,5], L. Cáceres[2,7], P. Doornenbal[2,8], H. Geissel[2], J. Grębosz[2,5], A. Kelic[2], I. Kojouharov[2], N. Kurz[2], F. Montes[2], W. Prokopowicz[2], T. Saito[2], H. Schaffner[2], S. Tashenov[2], A. Heinz[4], T. Kurtukian-Nieto[9], G. Benzoni[10], M. Pfützner[11], A. Jungclaus[7], D.L. Balabanski[12], C. Brandau[1], B.A. Brown[13,1], A.M. Bruce[14], W.N. Catford[1], I.J. Cullen[1], Zs. Dombrádi[15], M.E. Estevez[16], W. Gelletly[1], G. Ilie[8], J. Jolie[8], G.A. Jones[1], M. Kmiecik[5], F.G. Kondev[17], R. Krücken[18], S. Lalkovski[14], Z. Liu[1], A. Maj[5], S. Myalski[5], S. Schwertel[18], T. Shizuma[1,19], P.M. Walker[1], E. Werner-Malento[2], and O. Wieland[10]

[1] Department of Physics, University of Surrey, Guildford, GU2 7XH, UK
[2] GSI, Planckstrasse 1, D-64291, Darmstadt, Germany
[3] Department of Physics, Lund University, S-22100, Lund, Sweden
[4] WNSL, Yale University, 272 Whitney Avenue, New Haven, CT, 06520, USA
[5] The Institute of Nuclear Physics, PL-31-342, Kraków, Poland
[6] Department of Physics, University of the West of Scotland, Paisley, PA1 2BE, Scotland
[7] Departmento de Fisica Teórica, Universidad Autonoma de Madrid, Madrid, Spain
[8] IKP, Universität zu Köln, D-50937, Köln, Germany
[9] Universidad de Santiago de Compostela, Santiago de Campostela, Spain
[10] INFN, Università degli Studi di Milano, I-20133, Milano, Italy
[11] IEP, Warsaw University, Hoża 69, PL-00-681, Poland
[12] INRNE, Bulgarian Academy of Sciences, BG-1784 Sofia, Bulgaria
[13] NSCL, Michigan State University, East Lansing, MI 48824-1321, USA
[14] School of Environment and Technology, University of Brighton, Brighton, BN2 4GJ, UK
[15] Institute for Nuclear Research, H-4001, Debrecen, Hungary
[16] Instituto de Fisica Corpuscular, Valencia, Spain
[17] Nuclear Engineering Division, Argonne National Laboratory, Argonne, IL-60439, USA
[18] Physik Department E12, Technische Universität München, Garching, Germany
[19] Japan Atomic Energy Agency, Kyoto 619-0215, Japan

Received: 31 December 2008 / Revised: 1 April 2009
Published online: 17 May 2009 –
Communicated by J. Äystö

Abstract. Heavy neutron-rich nuclei have been populated through the relativistic fragmentation of a $^{208}_{82}$Pb beam at $E/A = 1$ GeV on a 2.5 g/cm^2 thick Be target. The synthesised nuclei were selected and identified in-flight using the fragment separator at GSI. Approximately 300 ns after production, the selected nuclei were implanted in an ~ 8 mm thick perspex stopper, positioned at the centre of the RISING γ-ray detector spectrometer array. A previously unreported isomer with a half-life $T_{1/2} = 163(5)$ ns has been observed in the $N = 126$ closed-shell nucleus $^{205}_{79}$Au. Through γ-ray singles and γ-γ coincidence analysis a level scheme was established. The comparison with a shell model calculation tentatively identifies the spin-parity of the excited states, including the isomer itself, which is found to be $I^{\pi} = (19/2^{+})$.

PACS. 29.30.Kv X- and γ-ray spectroscopy – 25.70.Mn Projectile and target fragmentation – 23.35.+g Isomer decay

1 Introduction

Experimental information on the neutron-rich $N \approx 126$ nuclei is scarce. It is particularly difficult to access these nuclei experimentally. They are inaccessible with stable beam/target fusion-evaporation reactions and are too heavy to be populated in fission. Although deep inelastic reactions have been used to access relatively high-spin states in nuclei with a few neutrons more than the most

[a] e-mail: Z.Podolyak@surrey.ac.uk

neutron-rich stable isotopes [1], this technique is limited by a general difficulty in channel selection. Projectile fragmentation at intermediate and relativistic energies has proved to be an efficient and selective way of populating states in nuclei far from the valley of stability [2,3] and is an ideal tool for the study of metastable states in heavy neutron-rich nuclei [3]. The highest sensitivity is achieved with decay (both internal isomeric decay and beta decay) spectroscopy. In this technique the delayed gamma rays are correlated with the individually identified ion, thereby minimising the associated background radiation. Information on the excited states populated in this way can be obtained with only $\sim$ 1000 nuclei produced. In its simplest form the technique is sensitive to isomeric decays with lifetimes between 100 ns and 1 ms. The lower limit comes from the flight-time through the fragment separator, the upper limit is determined by the necessity of correlating delayed gamma rays with the implanted ion. However, shorter lifetimes could also be detected if the decay branch by electron conversion was hindered for specific charge states of the ion [4]. In the case of beta-decay, with the use of an active stopper, the delayed gammas and beta can be correlated with the implantation of the incoming ion over more than 10 s.

The first pioneering isomeric decay experiment following the population of heavy nuclei in fragmentation reaction was performed more than a decade ago [3], with further experiments following [5]. More recently, a set of experiments have been performed at GSI aimed at the study of neutron-rich $N \approx 126$ nuclei.

Studies of magic nuclei are of fundamental importance in our understanding of the nuclear structure since they allow direct tests of the purity of shell model wave functions. Information on the single-particle energies can be derived from the experimental observables such as the energies of the excited states and transition probabilities. The experimental information on the structure of these nuclei can be used as building blocks for calculating more complex configurations. The more information that is available, the more robust are the predictions that can be made on the properties of more neutron-rich species. These are of particular importance as the r-process path nuclei, experimentally unreachable in this mass region so far, are approached [6].

In this contribution new experimental information obtained on the closed $N = 126$ neutron shell nucleus ^{205}Au is presented. The same experiment provided a vast amount of information on a large number of nuclei with $N \leq 126$ [7–10], most notably the yrast structure of the four-proton hole nucleus $^{204}_{78}$Pt was observed up to spin-parity 10^+ [10].

2 Experimental details

Heavy neutron-rich nuclear species were synthesised through the relativistic fragmentation of a ^{208}Pb beam at $E/A = 1$ GeV on a 2.526 g/cm^2 thick Be target. The beam was accelerated using the GSI UNILAC and SIS-18 accelerators; the primary beam intensity was of 9×10^8 particles per spill, with the period between the start of each spill being 25 seconds and the spills lasting for 8 seconds. After exiting the target, the "cocktail" of secondary beam fragments was selected and identified using the GSI FRagment Separator (FRS) [11]. The FRS was operated in achromatic mode with a wedge-shaped degrader in the intermediate focal plane. The identified ions were stopped in an $\sim$ 8 mm thick perspex passive stopper, positioned at the final focal plane of the FRS. The stopper was surrounded by the RISING array in the "Stopped Beam" configuration [12,13]. The details of the experimental setup employed in the present experiment as well as the identification procedure are described in refs. [10,14].

In total nine different magnetic rigidity settings of the FRS were used during the experiment [7,9]; three of these, optimised for the maximum transmission of ^{192}W, ^{199}Os and ^{203}Ir, transmitted ^{205}Au nuclei. The total number of ^{205}Au nuclei implanted in the stopper was $\sim 340 \times 10^3$, with $\sim 240 \times 10^3$ of these ($\sim$ 70%) produced in the setting centred on ^{199}Os.

The identification spectra for the data collected in the ^{199}Os setting are given in fig. 1. The charge state of the ions can be obtained from the energy loss at the final focal plane *vs.* change in magnetic rigidity, $\Delta B\rho$ ($\propto q^2$), at the intermediate focal plane matrix (fig. 1 (top)). To a large extent the ions labelled with $\Delta q = 0$ (those that do not change charge state when passing through the wedge placed in the middle focal point of the FRS) are fully stripped during the whole flight-path from target to stopper. The nuclei labelled with $\Delta q = -1$ are those which pick up an electron in the middle of the FRS, therefore the majority of them are fully stripped in the first part of the separator and H-like in the second half of it. The nuclei labelled with $\Delta q = +1$ are those which lose an electron in the middle of the FRS, therefore they are most likely to be H-like in the first part of the separator. The final identification is given by the matrix of position in the final focal plane *vs.* A/q (fig. 1 (bottom)). The mass-over-charge ratio (A/q) is determined from the measured time of flight in the second part of the FRS and from the tracking of the ions [9,10,15].

3 Results and discussion

The γ-ray data associated with ^{205}Au from all three of the FRS settings mentioned above has been combined. The singles γ-ray spectrum is presented in fig. 2 and details of the transition energies and intensities are given in table 1. Seven transitions are observed, with energies of 243, 737, 928, 946, 962, 980 and 1172 keV. Individual measurements of the decay curves associated with each of the observed transitions have been performed. In all cases the measured half-lives are observed to be identical, within experimental uncertainties. This indicates that all of the transitions are emitted following the decay of a single isomer. The final measured half-life of that isomer is determined by combining the statistics from all of the transitions, with the exception of the 243 keV transition (which is excluded

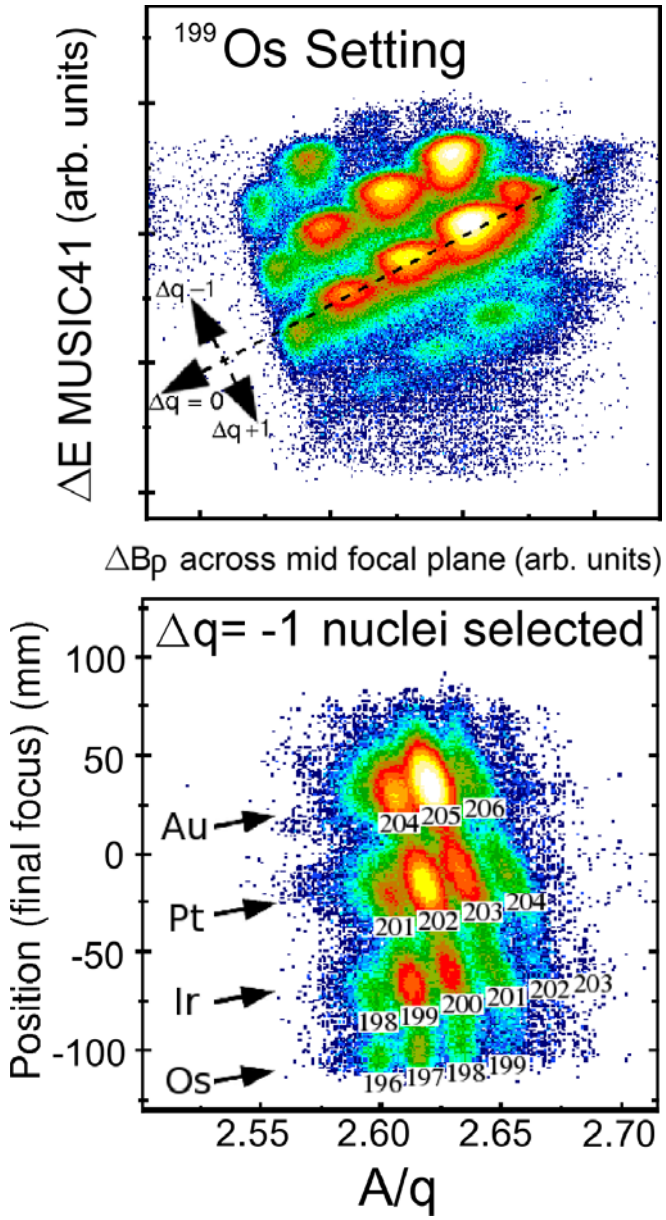

Fig. 1. Identification of the fragmentation products in the FRS setting optimised for ^{199}Os transmission. Top: energy loss at the final focal plane *vs.* change in magnetic rigidity at the intermediate focal plane. This distinguishes between nuclei with different charge states, see text. Bottom: position at the final focal plane *vs.* A/q in the second stage of the FRS for H-like ($\Delta q = -1$) nuclei.

due to its low intensity on a relatively high background). The half-life is found to be $T_{1/2} = 163(5)$ ns.

The statistics obtained allows γ-γ coincidence analysis to be performed. A γ-γ coincidence matrix was built with the conditions that both photons are detected in the time window $\Delta t = 25 \rightarrow 700$ ns following the implantation, and that they are observed within 100 ns from each other. In fig. 3 the relevant gated coincidence spectra are presented.

The energies of the identified γ-ray energies suggest the existence of three parallel decay branches. The 737 + 1172,

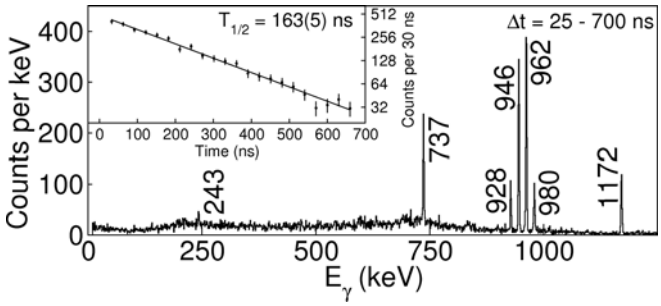

Fig. 2. Singles γ-ray spectrum observed in the time range $\Delta t = 25 \rightarrow 700$ ns following the implantation of nuclei identified as ^{205}Au. Inset: background-subtracted decay curve from the combined statistics of all identified transitions, with the exception of the 243 keV transition; the fit to the data was performed by the least-square method to a single exponential decay.

Table 1. Measured ^{205}Au transition energies and γ-ray intensities. The uncertainty on γ-ray energies is 0.3 keV, except for the 243 keV transition which has an uncertainty of 0.5 keV.

E_γ (keV)	I_γ (arb. units)
243.4	4(2)
736.9	39(2)
928.3	23(2)
946.1	94(4)
962.5	100(5)
962.5	11(4)
980.2	24(2)
1171.5	32(2)

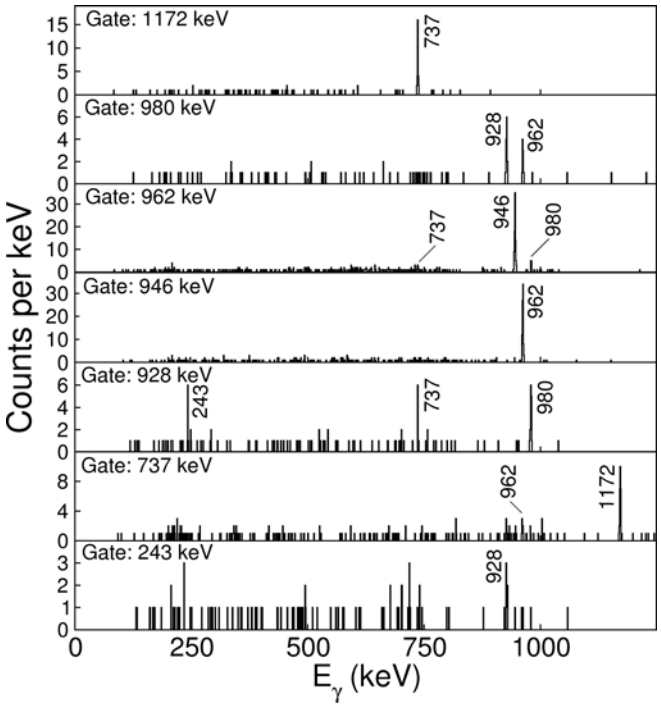

Fig. 3. γ-γ coincidence spectra associated with ^{205}Au. The γ-rays were detected in the time range $\Delta t = 25 \rightarrow 700$ ns following the implantation of the nucleus, with the time difference between the γ-rays being ≤ 100 ns.

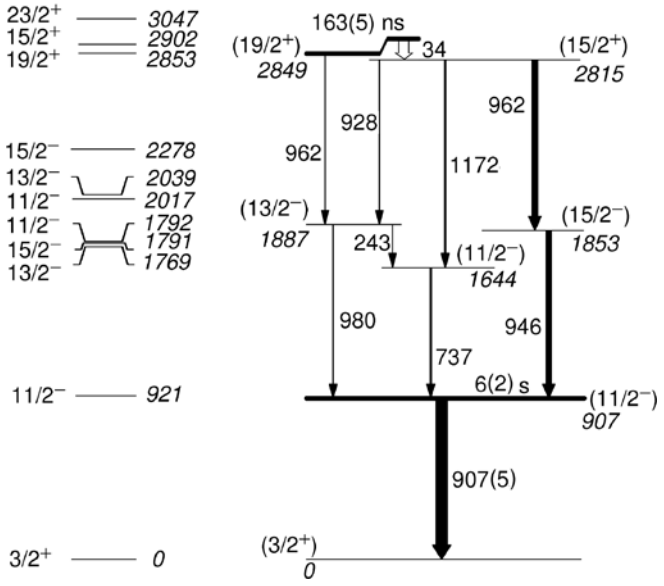

Fig. 4. Left: yrast and near-yrast predicted excited states in ^{205}Au for excitation energies of up to ~ 3 MeV, for details of the shell model calculation, see text. Right: the experimental level scheme obtained in the current work. The energy and the half-life of the first-excited state are from [21]. The spin and parity assignments were obtained from comparison with the shell model calculations.

928 + 980 and the 946 + 962 keV pairs all add up to 1908 keV to within 0.2 keV from one another (see table 1). Also, it is likely that the 243 keV γ-ray connects two of these parallel decay routes, since 980 − 737 = 243. The coincidence analysis supports these conclusions. In addition, it turned out that the 962 keV line is a doublet. It is in coincidence not only with its expected partner 946 keV transition, but also with the 980 keV line. The level scheme constructed is shown in fig. 4. The existence of an unobserved highly converted 34 keV transition had to be inferred from the data.

Shell model calculations for ^{205}Au have been performed in the $s_{1/2}$, $d_{3/2}$, $h_{11/2}$, $d_{5/2}$, $g_{7/2}$ ^{208}Pb proton-hole space with the OXBASH code [16] using single-particle energies obtained from the experimental level scheme of ^{207}Tl [17] and two-body matrix elements (TBME) from ref. [18]. These are based on the Kuo-Brown interaction including core polarisation [19,20], with slight modifications introduced to obtain an improved description of the experimental data available at the time. This parametrisation proved to describe the excited states of ^{206}Hg [1] and ^{204}Pt [10] quite well. The resulting yrast and near-yrast states in ^{205}Au are presented in fig. 4 for excitation energies up to ~ 3 MeV.

^{205}Au is a three proton-hole nucleus, with an expected ground-state configuration of $\pi d_{3/2}^{-1}$ (with the $s_{1/2}$ being empty) and spin-parity $I^\pi = 3/2^+$. The yrast $11/2^-$ state, predicted at 921 keV by the shell model calculations, has $\pi h_{11/2}$ character and it should be long lived since it can decay only through high multipolarity transitions, like in ^{207}Tl [17]. This isomeric state in ^{205}Au was identified in a recent RISING experiment. The K and L conversion electron lines associated to the $11/2^- \rightarrow 3/2^+$ M4 transition were observed. It was found that the $11/2^-$ state has an energy of 907(5) keV and a half-life of 6(2) s [21]. This half-life is much too long to be observed in the present experiment.

Table 2. Measured transition strengths in ^{205}Au compared with those of corresponding transitions in ^{206}Hg [1] and ^{204}Pt [10].

$B(EL)$ (W.u.)	^{205}Au	^{206}Hg	^{204}Pt
$B(E3\colon 19/2^+ \rightarrow 11/2^-)$	0.3(1)		
$B(E3\colon 10^+ \rightarrow 7^-)$		0.25(3)	0.19(3)
$B(E2\colon 19/2^+ \rightarrow 15/2^+)$	1.2(2)		
$B(E2\colon 10^+ \rightarrow 8^-)$		0.94(15)	0.80(8)

The isomeric state observed in the present experiment most probably decays into the $11/2^-$ yrast state. The comparison between the experimental and theoretical level schemes suggests that the isomer has a spin-parity $19/2^+$. Its main decay is via a low energy, 34 keV, $E2$ transition into the yrast $15/2^+$ level. The experimentally deduced transition strength (using the intensities of table 1) is $B(E2) = 1.2(2)$ W.u. We note that our calculations predict the yrast $19/2^+$ and $15/2^+$ states very close in energy, but with the inverse ordering. These states then decay via ~ 1 MeV transitions into the triplet of predicted states at around 1800 keV excitation energy, with spin-parities of $11/2^-$, $13/2^-$ and $15/2^-$. In addition to the low-energy branch, the isomer also has a weaker decay branch, populating the yrast $13/2^-$ state directly via the 962 keV $E3$ transition, with an experimental transition strength of $B(E3) = 0.3(1)$ W.u.

The measured transitions strengths can be compared with those of the corresponding transitions in the neighbouring $N = 126$ nuclei ^{206}Hg and ^{204}Pt (see table 2). The predominant configurations of the $19/2^+$ and $15/2^+$ states in ^{205}Au are $\pi(h^2_{11/2})_{10^+}s_{1/2}$ and $\pi(h^2_{11/2})_{8^+}s_{1/2}$, respectively. The $E2$ transition strength has similar value to those of the analoguos $B(E2\colon \pi(h^2_{11/2})_{10^+} \rightarrow \pi(h^2_{11/2})_{8^+})$ strengths in both ^{206}Hg and ^{204}Pt. The $E3$ transition in ^{205}Au connects the states with main configurations $\pi(h^2_{11/2})_{10^+}s_{1/2}$ and $\pi(h_{11/2}d_{3/2}s_{1/2})$. The corresponding $B(E3)$ transition strengths in both ^{206}Hg and ^{204}Pt are close, although in this case a strict similarity cannot be expected as in ^{205}Au the situation is complicated by the coupling of the $s_{1/2}$ and $d_{3/2}$ protons to 1^+ and 2^+. The measured transition strengths support our interpretation.

4 Conclusions and outlook

Projectile fragmentation when combined with decay spectroscopy is a powerful tool in the study of the structure of exotic nuclei. Several such experiments with the aim of the study of the structure of neutron-rich $N \sim 126$ nuclei

have been performed during the last decade. Here, new experimental information on the closed neutron shell nucleus ^{205}Au was presented. Gamma-ray transitions following the decay of an isomeric state with half-life $T_{1/2} = 163(5)$ ns have been observed and a level scheme was obtained. The spin-parity assignment was performed by comparing the experimental level scheme with shell model calculations.

During recent years a lot of progress has been made in obtaining information on the structure of the heavy neutron-rich nuclei. Recently, measurements using the same technique as presented here, but employing an active Si stopper [22], were performed and information on the β-decay of several nuclei has been obtained [23–25]. Furthermore, nuclei with $N > 126$ and $Z < 82$ were populated in the fragmentation of a ^{238}U beam [26]. The first results from these experiments have just started to emerge. By combining all the experimental information to be obtained from these studies, a much better understanding of this mass region will be achieved.

The excellent work of the GSI accelerator staff is acknowledged. This work is supported by the STFC/EPSRC(UK) and AWE plc. (UK), the EU Access to Large Scale Facilities Programme (EURONS, EU contract 506065), the Swedish Research Council, the Polish Ministry of Science and Higher Education (Grants No. 1 P03B 030 30 and N N202 309135), the Bulgarian Science Fund, the U.S. DOE (Grant No. DE-FG02-91ER-40609), the Spanish Ministerio de Educacion y Ciencia, the German BMBF, the Hungarian Science Foundation and the Italian INFN.

References

1. B. Fornal *et al.*, Phys. Rev. Lett. **87**, 212501 (2001).
2. R. Grzywacz *et al.*, Phys. Lett. B **355**, 439 (1995).
3. M. Pfützner *et al.*, Phys. Lett. B **444**, 32 (1998).
4. M. Caamano *et al.*, Eur. Phys. J. A **23**, 201 (2005).
5. Zs. Podolyák *et al.*, Phys. Lett. B **491**, 225 (2000).
6. H. Grawe, K. Langanke, G. Martinez-Pinedo, Rep. Prog. Phys. **70**, 1525 (2007).
7. S.J. Steer *et al.*, to be published in Int. J. Mod. Phys. E.
8. S.J. Steer *et al.*, in preparation.
9. S.J. Steer, PhD Thesis, University of Surrey, 2008, unpublished.
10. S.J. Steer *et al.*, Phys. Rev. C **78**, 061302(R) (2008).
11. H. Geissel *et al.*, Nucl. Instrum. Methods B **70**, 286 (1992).
12. S. Pietri *et al.*, Nucl. Instrum. Methods B **261**, 1079 (2007).
13. P.H. Regan *et al.*, Nucl. Phys. A **787**, 491c (2007).
14. Zs. Podolyák *et al.*, Eur. Phys. J. ST **150**, 165 (2007).
15. M. Pfützner *et al.*, Phys. Rev. C **65**, 064604 (2002).
16. B.A. Brown, A. Etchegoyen, W.D.M. Rae, The computer code OXBASH, MSU-NSCL report no. 524.
17. D. Eccleshall, M.J.L. Yates, Phys. Lett. **19**, 301 (1965); M.J. Martin, Nucl. Data Sheets **70**, 315 (1993).
18. L. Rydström *et al.*, Nucl. Phys. A **512**, 217 (1990).
19. T.T.S. Kuo, G.H. Herling, Naval Research Laboratory Report 2259 (Washington, DC, 1971).
20. G.H. Herling, T.T.S. Kuo, Nucl. Phys. A **181**, 113 (1972).
21. Zs. Podolyák *et al.*, Phys. Lett. B **672**, 116 (2009).
22. R. Kumar *et al.*, Nucl. Instrum. Methods A **598**, 754 (2009).
23. N. Alkhomashi *et al.*, Acta Phys. Pol. B **40**, 875 (2009).
24. P.H. Regan *et al.*, Int. J. Mod. Phys. E Suppl. **17**, 8 (2008).
25. A.I. Morales *et al.*, Acta Phys. Pol. B **40**, 867 (2009).
26. N. Al-Dahan *et al.*, Acta Phys. Pol. B **40**, 871 (2009).

ISOMERIC RATIOS FOR NUCLEI WITH Z =62–67 AND A =142–152 PRODUCED IN THE RELATIVISTIC FRAGMENTATION OF ^{208}Pb* **

S. Myalski[a], A. Maj[a], Zs. Podolyák[b]
F. Becker[c], P. Bednarczyk[a,c], G. Benzoni[d], B. Blank[e], C. Brandau[b]
A.M. Bruce[f], L. Cáceres[c,g], F. Camera[d], W.N. Catford[b], I.J. Cullen[b]
Zs. Dombradi[h], P. Doornenbal[c], E. Estevez[i], A.B. Garnsworthy[b,j]
H. Geissel[c], W. Gelletly[b], J. Gerl[c], M. Górska[c], H. Grawe[c], J. Grębosz[a,c]
A. Heinz[k], R. Hoischen[l], G. Ilie[k,m], G.A. Jones[b], A. Jungclaus[g], A. Kelic[c]
M. Kmiecik[a], I. Kojouharov[c], F.G. Kondev[n], T. Kurtukian-Nieto[i], N. Kurz[c]
S. Lalkovski[f,o], Z. Liu[b], F. Montes[c], M. Pfützner[p], S. Pietri[b]
W. Prokopowicz[c,r], P.H. Regan[b], D. Rudolph[l], T. Saito[c], H. Schaffner[c]
S. Schwertel[s], T. Shizuma[e,t], A.J. Simons[b], S.J. Steer[b], S. Tashenov[c]
P.M. Walker[b], E. Werner-Malento[u], O. Wieland[d], H.J. Wollersheim[c]

[a]Instytut Fizyki Jądrowej PAN, Kraków, Poland
[b]Department of Physics, University of Surrey, Guildford, UK
[c]GSI, Darmstadt, Germany
[d]Università degli Studi di Milano and INFN sez. Milano, Milano, Italy
[e]CENBG, le Haut Vigneau, Gradignan Cedex, France
[f]School of Engineering, University of Brighton, Brighton, UK
[g]Departamento de Fisica Teorica, Universidad Autonoma de Madrid, Spain
[h]Atommagkutató Intézete, Debrecen, Hungary
[i]Universidad de Santiago de Compostela, Santiago de Campostela, Spain
[j]WNSL, Yale University, New Haven, CT, USA
[k]IKP, Universitat zu Köln, Köln, Germany
[l]Fysiska Institutionen, Lund University, Lund, Sweden
[m]IFIN HH, Bucharest, Romania
[n]Nuclear Engineering Division, ANL, Argonne, USA
[o]Faculty of Physics, University of Sofia "St. Kliment Ohridsk" Sofia, Bulgaria
[p]Instytut Fizyki Doświadczalnej, Uniwersytet Warszawski, Poland
[r]Instytut Fizyki, Uniwersytet Jagielloński, Kraków, Poland
[s]Institut für Experimentalphysik, Technische Universität München, Germany
[t]Japan Atomic Energy Research Institute, Kyoto, Japan
[u]Instytut Fizyki PAN, Warszawa, Poland

(Received November 7, 2008; revised version received December 4, 2008)

* Presented at the Zakopane Conference on Nuclear Physics, September 1–7, 2008, Zakopane, Poland.

** This work is supported by the EURONS (EU contract number 506065) and by the Polish Ministry of Science and Higher Education (Grant No 1 P03B 030 30 and N N202 309135).

Isomeric states in nuclei with $Z = 62$–67 and $A = 142$–152 produced in the fragmentation of the relativistic (1 GeV/nucleon) ^{208}Pb beam were investigated. Isomeric ratios were determined for 10 isomeric states. Significant differences between theoretical and experimental values were observed.

PACS numbers: 25.70.Mn, 29.30.Kv, 23.35.+g, 23.20.Lv

1. Introduction

We have investigated isomeric states in a number of nuclei with $Z = 62$–67 and $A = 142$–152. They were produced in the fragmentation of the relativistic (1 GeV/nucleon) ^{208}Pb beam from the SIS-18 synchrotron of the GSI facility on a ^{9}Be target, and selected by the FRagment Separator (FRS). The selected nuclei of interest were implanted into a 7 mm thick plastic stopper. The gamma-rays from the decay of isomeric states in the implanted nuclei were measured using the high purity germanium array, RISING [1]. Details of the experiment are described in Ref. [2, 3].

2. Data analysis

In total 22 nuclides were detected, isomeric states were observed in 9 of them (see Table I and Fig. 1). Of special interest is the $I^{\pi} = 27^{+}$ state in ^{148}Tb, as this is the highest spin that has been populated via the fragmentation reaction until now. The aim of this work was the extraction of experimental isomeric ratios (R) for these isomeric states. The ratio R is the number of ions populated in a given isomeric state compared to the total number of ions populated for the selected nuclide. The value of R

TABLE I

Theoretical and experimental isomeric ratios obtained in this work. Half-lifes taken from given references.

Nucleus	Spin	$T_{1/2}$ [μs]	R_{th} [%]	R_{exp} [%]
^{152}Ho	19^{-}	8.4(3) [7]	15.7	6.4(18)
^{153}Ho	$31/2^{+}$	0.25(2) [8]	24.5	16.9(42)
^{148}Tb	27^{+}	1.31(1) [9]	2.1	1.9(3)
^{144}Gd	10^{+}	0.15(3) [10]	59.0	10.3(46)
^{147}Gd	$49/2^{+}$	0.76(4) [11]	4.4	1.1(3)
^{143}Eu	$11/2^{-}$	50.(1) [12]	88.9	12.8(17)
^{144}Eu	8^{-}	1.0(1) [13]	76.4	17.1(20)
^{145}Eu	$11/2^{-}$	0.49(3) [14]	88.7	21.7(28)
^{142}Sm	10^{+}	0.48(6) [15]	59.8	2.0(7)
^{142}Sm	7^{-}	0.17(2) [16]	88.2	21.5(46)

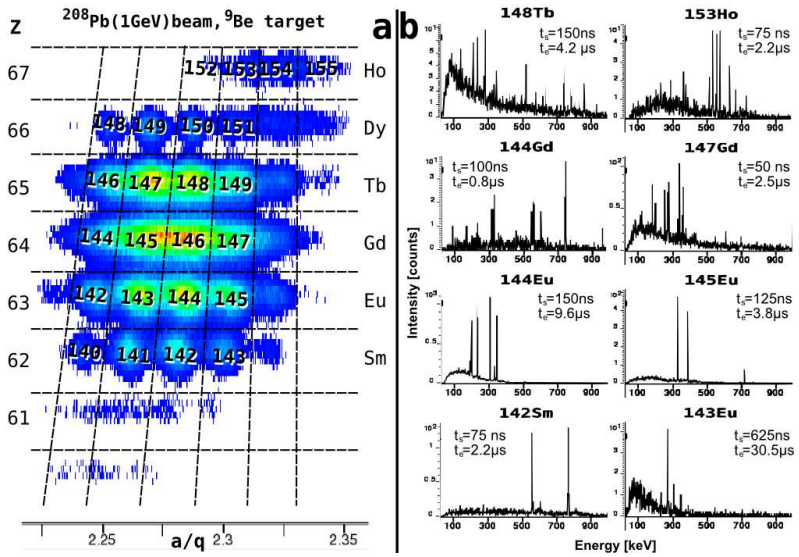

Fig. 1. Panel (a): An identification plot for the nuclei studied. Panel (b): Gamma spectra for selected nuclei measured within the indicated time intervals (t_s, t_e) after implantation in the stopper.

can provide information about the production reaction and nuclear structure. It was evaluated based on time-of-flight, half-life, in-flight losses and by considering the finite measurement time (see Refs. [5, 6] for details).

3. Theoretical predictions

Theoretical isomeric ratios, $R_{\rm th}$, were determined for a series of nuclei, using a formula based on the abrasion–ablation model [4] to predict the energies and spins of nuclei populated in fragmentation reactions. In the sharp cutoff approximation all nuclei of spin higher than that selected decay to that level. Therefore the isomeric ratio of the selected isomer is the integral of the spin distribution (P_I) for spins higher than that of the isomer (I_m):

$$R_{\rm th} = \int_{I_m}^{\infty} P_I dI = \exp\left[-\frac{I_m(I_m+1)}{2\sigma_f^2}\right], \tag{1}$$

$$\sigma_f^2 = 0.16 A_p^{2/3} \frac{(A_p - A_f)(\overline{\nu} A_p + A_f)}{(\overline{\nu}+1)^2 (A_p - 1)}, \qquad \overline{\nu} \approx \frac{N_n}{N_s} \approx \frac{E_n^*}{E_s}, \tag{2}$$

where $\overline{\nu}$ is the ratio of energy transferred during the abrasion of one nucleon (E_n^*) and the energy needed to evaporate one nucleon (E_s).

4. Results and conclusions

The experimental results obtained were compared to theoretical predictions [4] (see Fig. 2a and Sec. 2). Significant differences between experiment and theoretical predictions were observed, just as in Refs. [17,18]. In general, there is relatively good agreement with the analytical formula for high spins (above the spin cut-off parameter σ_f). However, for lower spins (below σ_f) there is no agreement at all. Very analogous behaviour has been observed in similar measurements on nuclei in the $A \approx 85$ mass region [19] (see Fig. 2b).

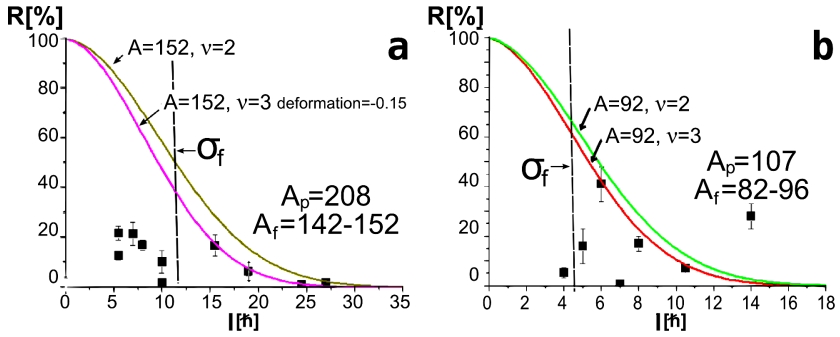

Fig. 2. Comparison between theoretical predictions and experimental results for the present data (panel (a)) and nuclei in $A \approx 85$ mass region [6, 19] (panel (b)).

This puzzle will be further investigated, both experimentally and theoretically. There are numerous effects which can contribute to such behaviour. Among them are transitions which bypass the isomeric state or spin loss due to particle evaporation during de-excitation. One can also speculate that in the case of several nucleons removed from the projectile, the reaction mechanism may be more complicated than a simple pure fragmentation process [20, 21].

REFERENCES

[1] S. Pietri *et al.*, *Nuc. Instrum. Methods* **B261**, 1079 (2007).
[2] S.J. Steer *et al.*, submitted to *Phys. Rev.* **C**.
[3] P.H. Regan *et al.*, *Nucl. Phys.* **A787**, 491c (2007).
[4] M. de Jong *et al.*, *Nucl. Phys.* **A613**, 435 (1997).
[5] M. Pfützner *et al.*, *Phys. Rev.* **C65**, 064604 (2002).
[6] S. Myalski *et al.*, *Acta Phys. Pol. B* **38**, 1277 (2007).
[7] A. Piepke *et al.*, *Nucl. Phys.* **A486**, 335 (1988).

[8] J. Borggreen *et al.*, *Z. Phys.* **A294**, 113 (1980).
[9] E. Ideguchi *et al.*, *Z. Phys.* **A352**, 363 (1995).
[10] H. Beuscher *et al.*, *Nucl. Phys.* **A311**, 395 (1978).
[11] D. Ward *et al.*, *Nucl. Phys.* **A362**, 254 (1981).
[12] R.B. Firestone *et. al.*, *Phys. Rev.* **C17**, 2 (1978).
[13] I. Funke *et al.*, *Nucl. Phys.* **A274**, 61 (1976).
[14] W.D. Fromm *et al.*, *Phys. Scr.* **12**, 91 (1975).
[15] M. Lach *et al.*, *Z. Phys.* **A319**, 235 (1984).
[16] G.G. Kennedy *et al.*, *Phys. Rev.* **C12**, 2 (1975).
[17] K.A. Gladnishki *et al.*, *Phys. Rev.* **C69**, 024617 (2004).
[18] Zs. Podolyak *et al.*, *Phys. Lett.* **B632**, 203 (2006).
[19] A.B. Garnsworthy *et al.*, *Phys. Lett.* **B660**, 326 (2008).
[20] D.E. Groh *et al.*, *Phys. Rev.* **C76**, 054608 (2007).
[21] P.F. Mantica, private communication.
[22] S. Pal, R. Palit, *Phys. Lett.* **B665**, 164 (2008).

International Journal of Modern Physics E
Vol. 18, No. 4 (2009) 1002–1007

World Scientific
www.worldscientific.com

ISOMERIC DECAY STUDIES IN NEUTRON-RICH N≈126 NUCLEI

S.J. STEER[1], ZS. PODOLYÁK[1], S. PIETRI[1], M. GÓRSKA[2], G.F. FARRELLY[1], P.H. REGAN[1], D. RUDOLPH[3], A.B. GARNSWORTHY[1,4], R. HOISCHEN[3], J. GERL[2], H.J. WOLLERSHEIM[2], H. GRAWE[2], K.H. MAIER[5,6], F. BECKER[2], P. BEDNARCZYK[2,5], L. CÁCERES[2,7], P. DOORNENBAL[2,8], H. GEISSEL[2], J. GRĘBOSZ[2,5], A. KELIC[2], I. KOJOUHAROV[2], N. KURZ[2], F. MONTES[2], W. PROKOPOWICZ[2], T. SAITO[2], H. SCHAFFNER[2], S. TASHENOV[2], A. HEINZ[4], T. KURTUKIAN-NIETO[9], G. BENZONI[10], M. PFÜTZNER[11], A. JUNGCLAUS[7], D.L. BALABANSKI[12], C. BRANDAU[1], A. BROWN[13,1], A.M. BRUCE[14], W.N. CATFORD[1], I.J. CULLEN[1], ZS. DOMBRÁDI[15], M.E. ESTEVEZ[16], W. GELLETLY[1], G. ILIE[8], J. JOLIE[8], G.A. JONES[1], M. KMIECIK[5], F.G. KONDEV[17], R. KRÜCKEN[18], S. LALKOVSKI[14], Z. LIU[1], A. MAJ[5], S. MYALSKI[5], S. SCHWERTEL[18], T. SHIZUMA[1], P.M. WALKER[1], E. WERNER-MALENTO[2], O. WIELAND[10]

[1] *Department of Physics, University of Surrey, Guildford, GU2 7XH, UK*
[2] *GSI, Planckstrasse 1, D-64291, Darmstadt, Germany*
[3] *Department of Physics, Lund University, S-22100, Lund, Sweden*
[4] *WNSL, Yale University, 272 Whitney Avenue, New Haven, CT, 06520, USA*
[5] *The Institute of Nuclear Physics, PL-31-342, Kraków, Poland*
[6] *Department of Physics, University of the West of Scotland, Paisley, PA1 2BE, Scotland*
[7] *Departmento de Fisica Teórica, Universidad Autonoma de Madrid, Madrid, Spain*
[8] *IKP, Universität zu Köln, D-50937, Köln, Germany*
[9] *Universidad de Santiago de Compostela, Santiago de Campostela, Spain*
[10] *INFN, Università degli Studi di Milano, I-20133, Milano, Italy*
[11] *IEP, Warsaw University, Hoża 69, PL-00-681, Poland*
[12] *INRNE, Bulgarian Academy of Sciences, BG-1784 Sofia, Bulgaria*
[13] *NSCL, Michigan State University, East Lansing, MI 48824-1321, USA*
[14] *School of Environment and Technology, University of Brighton, Brighton, BN2 4GJ, UK*
[15] *Institute for Nuclear Research, H-4001, Debrecen, Hungary*
[16] *Instituto de Fisica Corpuscular, Valencia, Spain*
[17] *Nuclear Engineering Division, Argonne National Laboratory, Argonne, IL-60439, USA*
[18] *Physik Department E12, Technische Universität München, Garching, Germany*

Received October 31, 2008
Revised November 25, 2008

Heavy neutron-rich nuclei were populated via relativistic energy fragmentation of a E/A=1 GeV ^{208}Pb beam. The nuclei of interest were selected and identified by a fragment separator and then implanted in a passive plastic stopper. Delayed γ rays following internal isomeric decays were detected by the RISING array. Experimental information was obtained on a number of nuclei with Z=73-80 (Ta-Hg), providing new information both on the prolate-oblate transitional region as well as on the N=126 closed shell nuclei.

1. Introduction

The evolution of the properties of atomic nuclei with respect to neutron and proton numbers is a key question of nuclear physics. The study of unstable, neutron-rich nuclei represents one of the foremost pursuits of modern nuclear physics. Over the coming decade new radioactive ion beam facilities are being constructed with one of the main objectives being to probe the structure of neutron-rich nuclei. The part of the nuclear chart with the least information on neutron-rich nuclei is the $_{76}$Os to $_{82}$Pb region. This mass region is however an ideal testing ground of nuclear theories. With the removal of just a few nucleons the landscape evolves from spherical[1–3] to elongated prolate through disk shaped oblate and triaxial formss.[4–6]

2. Experimental Details

The SIS-18 accelerator at GSI provided a ^{208}Pb beam at $E/A = 1$ GeV. The ^{208}Pb ions impinged on a target of ^{9}Be of thickness 2.5 g/cm^2. The nuclei of interest

Table 1. Approximate number, in thousands, of nuclei implanted in the plastic stopper at the end of the GSI fragment separator. All six settings as well as all charge states are considered.

Nucleus	No. (in 10^3)	Nucleus	No. (in 10^3)	Nucleus	No. (in 10^3)
^{206}Tl	86	^{202}Hg	12	^{203}Hg	142
^{204}Hg	52	^{205}Hg	417	^{206}Hg	1718
^{200}Au	2.1	^{201}Au	2.7	^{202}Au	61
^{203}Au	402	^{204}Au	133	^{205}Au	337
^{206}Au	12	^{197}Pt	7.4	^{198}Pt	24
^{199}Pt	8.8	^{200}Pt	65	^{201}Pt	68
^{202}Pt	388	^{203}Pt	319	^{204}Pt	92
^{205}Pt	1.4	^{194}Ir	1.7	^{195}Ir	8.0
^{196}Ir	3.1	^{198}Ir	51	^{199}Ir	358
^{200}Ir	354	^{201}Ir	165	^{202}Ir	36
^{203}Ir	8.0	^{191}Os	0.43	^{192}Os	2.3
^{193}Os	2.1	^{194}Os	1.1	^{195}Os	22
^{196}Os	121	^{197}Os	159	^{198}Os	78
^{199}Os	29	^{200}Os	6.3	^{201}Os	1.4
^{202}Os	0.02	^{191}Re	2.4	^{192}Re	23
^{193}Re	90	^{194}Re	101	^{195}Re	61
^{196}Re	14	^{197}Re	5.5	^{198}Re	0.71
^{188}W	3.7	^{189}W	11	^{190}W	30
^{191}W	37	^{192}W	21	^{193}W	9.4
^{194}W	2.9	^{185}Ta	1.1	^{186}Ta	3.6
^{187}Ta	11	^{188}Ta	14	^{189}Ta	9.1
^{190}Ta	3.9	^{191}Ta	0.26	^{182}Hf	0.49
^{183}Hf	3.0	^{184}Hf	5.4	^{185}Hf	7.1
^{186}Hf	5.2	^{187}Hf	2.9	^{188}Hf	1.2
^{181}Lu	0.43	^{182}Lu	1.3	^{183}Lu	1.2
^{184}Lu	0.66	^{185}Lu	0.29	^{179}Yb	0.58
^{180}Yb	0.66	^{181}Yb	0.33	^{176}Tm	0.10
^{177}Tm	0.17	^{178}Tm	0.14		

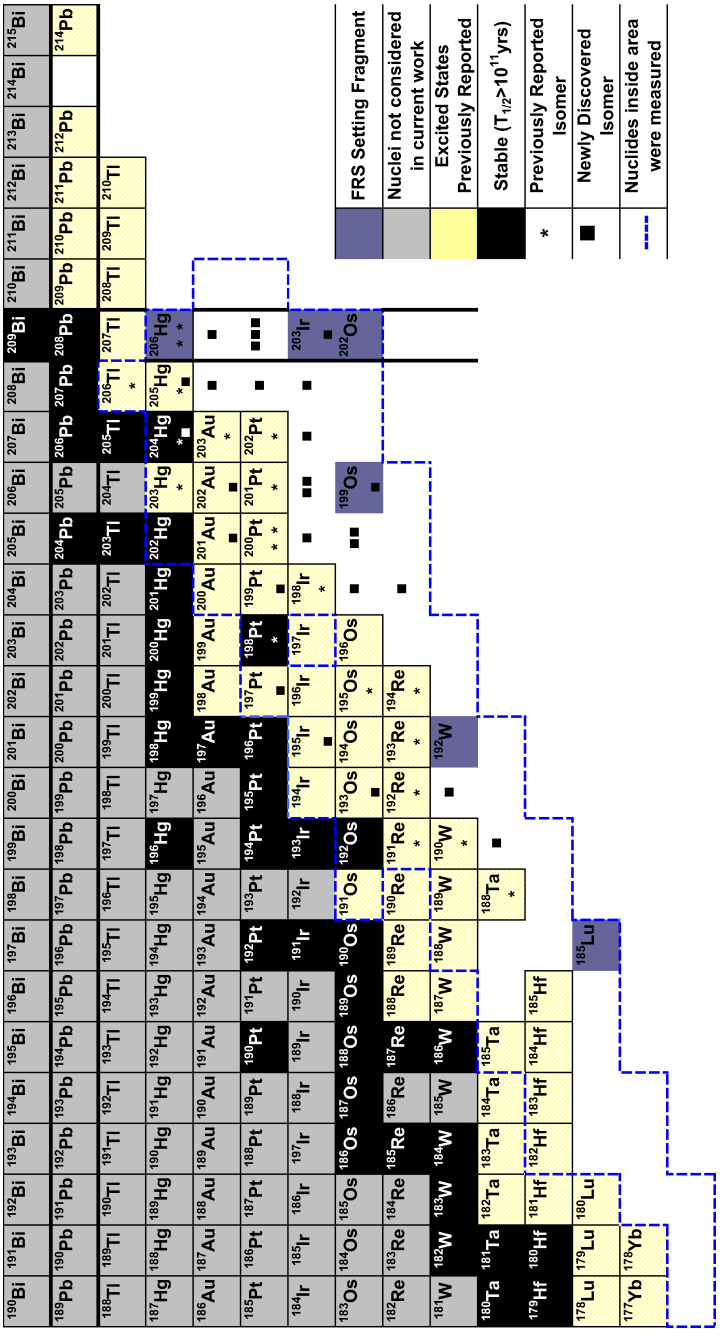

Fig. 1. Section of the nuclear chart indicating the nuclei studied in the present experiment.

were selected and identified in flight by the FRagment Separator (FRS)[7] used in achromatic mode. The identified ions were stopped in a passive stopper, positioned at the final focal plane of the FRS. The stopper was surrounded by the RISING array in the "Stopped Beam" configuration.[9,10] These detectors recorded the delayed γ-ray transitions associated with the implanted nuclei. For details on the experimental setup, identification procedure and analysis see.[2,8]

3. Results

Six different fragment separator settings were used: the magnetic rigidities were set to transmit fully stripped ions of ^{206}Hg, ^{203}Ir, ^{202}Os, ^{199}Os, ^{192}W and ^{185}Lu. An average of 20 hours of beam time was dedicated to each setting, with a primary beam intensity of $\sim 10^9$ ions/22 s spill. The number of the implanted nuclei for individual nuclides are given in Table 1.

The nuclei on which spectroscopic information was obtained in the current experiment are summarised in Fig. 1. The experiment had as its main aim the study of neutron-rich N=126 isotones. New experimental information was obtained on three of these, namely ^{205}Au, ^{204}Pt[2] and ^{203}Ir. The delayed gamma-ray spectra are shown in Fig. 2. In addition, previously unobserved isomeric decays have been identified for a wide range of nuclei with N<126 (see Fig. 3).

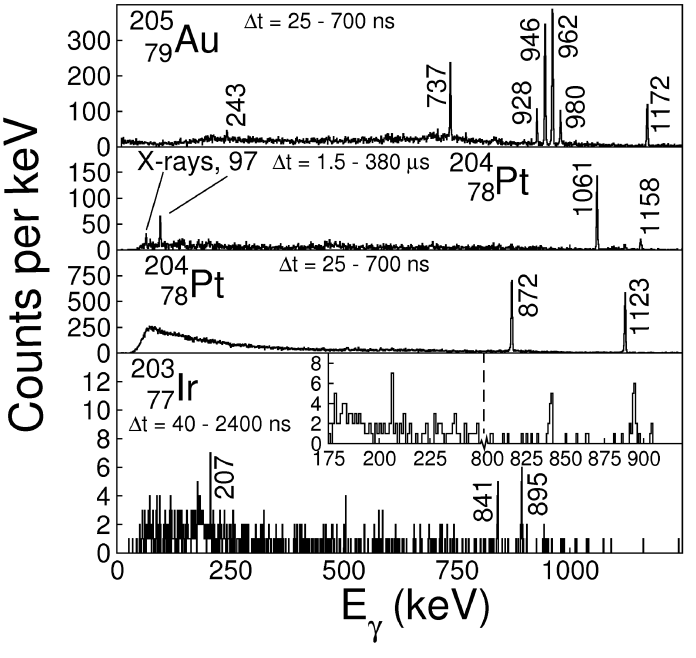

Fig. 2. Delayed γ-ray spectra obtained for the N=126 isotones ^{205}Au, ^{204}Pt[2] and ^{203}Ir.

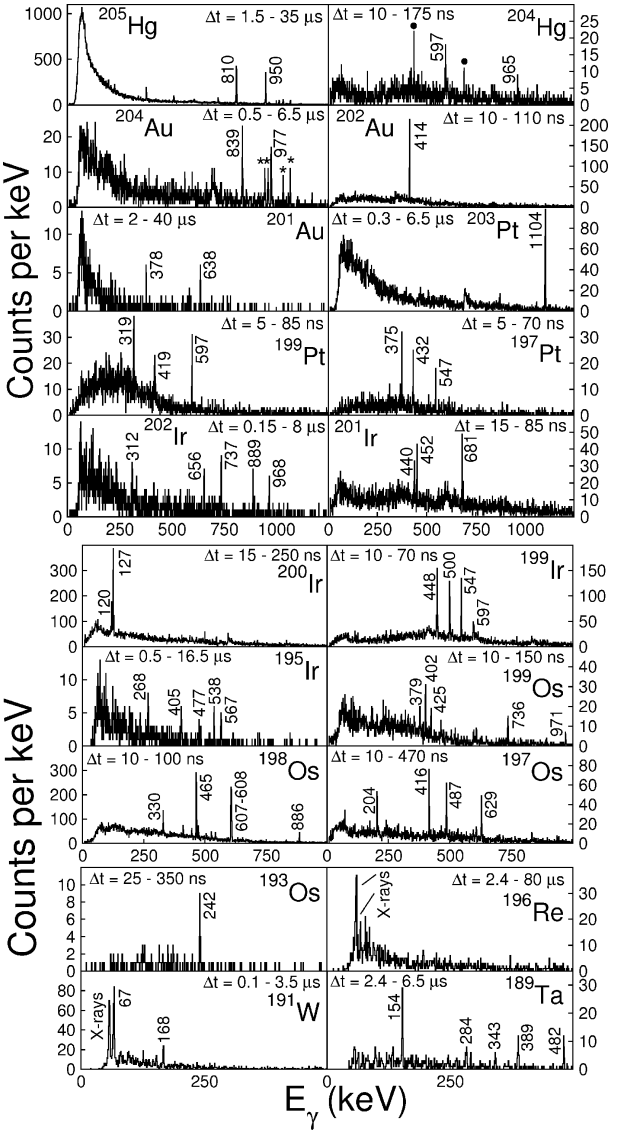

Fig. 3. Examples of delayed γ-ray spectra. The labelled transitions originate from previously unobserved isomeric decays. γ-ray transitions from previously observed isomers are labelled with •, contaminations from other nuclei with *.

4. Conclusions and Outlook

Projectile fragmentation when combined with decay spectroscopy is a powerful tool in the study of the structure of exotic nuclei. Experimental results on the heavy neutron-rich nuclei have been presented. The interpretation of the data is in progress.

More recently, further experiments have been performed aimed at the study of neutron-rich N≈126 nuclei. Measurements using the same technique as presented here, but employing an active Si stopper,[11] were performed and information on the β decay of several nuclei has been obtained.[12,13] Furthermore, nuclei with N>126 and Z< 82 were populated in the fragmentation of a ^{238}U beam.[14] By combining all the experimental information to be obtained from these studies, a much better understanding of this mass region will be achieved.

Acknowledgments

The excellent work of the GSI accelerator staff is acknowledged. This work is supported by the STFC/EPSRC(UK) and AWE plc.(UK), the EU Access to Large Scale Facilities Programme (EURONS, EU contract 506065), The Swedish Research Council, The Polish Ministry of Science and Higher Education, The Bulgarian Science Fund, The US Dept. of Energy, The Spanish Ministeriode Educacion y Ciencia, The German BMBF, The Hungarian Science Foundation and the Italian INFN.

References

1. K. H. Maier *et al.*, *Phys. Rev. C* **30** (1984) 1702.
2. S. J. Steer *et al.*, submitted to *Phys. Rev. C*.
3. Zs. Podolyák *et al.*, submitted to *Phys. Lett. B*.
4. P. D. Bond, R. F. Casten, D. D. Warner and D. Horn, *Phys. Lett. B* **130** (1983) 167.
5. C. Y. Wu *et al.*, *Nucl. Phys. A* **607** (1996) 178.
6. Zs. Podolyák *et al.*, *Phys. Lett. B* **491** (2000) 225.
7. H. Geissel *et al.*, *Nucl. Inst. and Meth. B* **70** (1992) 286.
8. Zs. Podolyák *et al.*, *Eur. Phys. J. Spec. Topics* **150** (2007) 165.
9. S. Pietri *et al.*, *Nucl. Inst. and Meth. B* **261** (2007) 1079.
10. P. H. Regan *et al.*, *Nucl. Phys. A* **787** (2007) 491c.
11. R. Kumar *et al.*, *Nucl. Inst. and Meth. A*, in press.
12. N. Alkhomashi *et al.*, *Acta Phys. Pol. B*, in press.
13. P. H. Regan *et al.*, *Int. J. of Mod. Phys. E*, in press.
14. N. Al-Dahan *et al.*, *Acta Phys. Pol. B*, in press.

Isomer spectroscopy of ^{127}Cd

F. Naqvi,[1,2,*] M. Górska,[2] L. Cáceres,[2,3,†] A. Jungclaus,[4] M. Pfützner,[5] H. Grawe,[2] F. Nowacki,[6] K. Sieja,[6] S. Pietri,[7,‡] E. Werner-Malento,[5,§] P. H. Regan,[7] D. Rudolf,[8] Z. Podolyák,[7] J. Jolie,[1] K. Andgren,[9] T. Beck,[2] P. Bednarczyk,[2,10] J. Benlliure,[11] G. Benzoni,[12] A. M. Bruce,[13] E. Casarejos,[11,‖] B. Cederwall,[9] F. C. L. Crespi,[12,14] P. Detistov,[15,¶] Zs. Dombrádi,[16] P. Doornenbal,[2,**] H. Geissel,[2] J. Gerl,[2] J. Gręboszz,[2,10] B. Hadinia,[9] M. Hellström,[8] R. Hoischen,[2,8] G. Ilie,[1,††] A. Khaplanov,[9] I. Kojouharov,[2] M. Kmiecik,[10] N. Kurz,[2] S. Lalkovski,[13,15] A. Maj,[10] S. Mandal,[17] V. Modamio,[3] F. Montes,[2,‡‡] S. Myalski,[10] W. Prokopowicz,[2] P. Reiter,[1] H. Schaffner,[2] G. Simpson,[18] D. Sohler,[19] S. J. Steer,[7] S. Tashenov,[2] J. Walker,[3] O. Wieland,[12] and H. J. Wollersheim[2]

[1]*Institut für Kernphysik, Universität zu Köln, D-50937 Köln, Germany*
[2]*Helmholtzzentrum für Schwerionenforschung (GSI), D-64291 Darmstadt, Germany*
[3]*Departmento de Física Teórica, Universidad Autónoma de Madrid, E-28049 Madrid, Spain*
[4]*Instituto de Estructura de la Materia, CSIC, E-28006 Madrid, Spain*
[5]*Faculty of Physics, University of Warsaw, PL-00681 Warsaw, Poland*
[6]*IPHC, IN2P3-CNRS/Université Louis Pasteur, F-67037, Strasbourg, France*
[7]*Department of Physics, University of Surrey, Guildford, GU2 7XH, United Kingdom*
[8]*Department of Physics, Lund University, S-22100 Lund, Sweden*
[9]*KTH Stockholm, S-10691 Stockholm, Sweden*
[10]*The Henryk Niewodniczański Institute of Nuclear Physics, PL-31342 Kraków, Poland*
[11]*Universidad de Santiago de Compostela, E-175706 Santiago de Compostela, Spain*
[12]*INFN Sezione di Milano, I-20133 Milano, Italy*
[13]*School of Engineering, University of Brighton, Brighton, BN2 4GJ, United Kingdom*
[14]*Universitá degli Studi di Milano, I-20133 Milano, Italy*
[15]*Faculty of Physics, University of Sofia, BG-1164, Sofia, Bulgaria*
[16]*Institute National Polytechnique de Grenoble, F-98026 Grenoble Cedex, France*
[17]*University of Delhi, New Delhi, India*
[18]*Institut Laue-Langevin, F-38042 Grenoble, France*
[19]*Institute of Nuclear Research, Pf. 51, H-4001 Debrecen, Hungary*

(Received 5 July 2010; published 24 September 2010)

The spin and configurational structure of excited states of ^{127}Cd, the two-proton and three-neutron hole neighbor of ^{132}Sn, has been studied. An isomeric state with a half-life of 17.5(3) μs was populated in the fragmentation of a ^{136}Xe beam on a ^{9}Be target at a beam energy of 750 MeV/u. Time distributions of the delayed γ transitions and $\gamma\gamma$ coincidence relations were exploited to construct a decay scheme. The observed yrast $(19/2)^+$ isomer is proposed to have dominant configurations of $\nu(h_{11/2}^{-3})\pi(g_{9/2}^{-1}, p_{1/2}^{-1})$, $\nu(h_{11/2}^{-2}d_{3/2}^{-1})\pi(g_{9/2}^{-2})$, and $\nu(h_{11/2}^{-2}, s_{1/2}^{-1})\pi(g_{9/2}^{-2})$ and to decay by two competing stretched $M2$ and $E3$ transitions. Experimental results are compared with the isotone ^{129}Sn. The new information provides input for the proton-neutron interaction and the evolution of neutron hole energies in nuclei around the doubly magic ^{132}Sn core.

DOI: 10.1103/PhysRevC.82.034323 PACS number(s): 21.10.Tg, 23.20.Lv, 23.35.+g, 27.60.+j

I. INTRODUCTION

The region around doubly magic ^{132}Sn has been a subject of intense research because of its several interesting features. Few valence particles and holes outside the inert core make these nuclei key points in studying the shell structure and nucleon-nucleon interaction in a neutron-rich environment. The astrophysical rapid-neutron capture process, responsible for the synthesis of heavy neutron-rich nuclei in nature, follows a path along the $N = 82$ line up to $Z = 48$. To test the theoretical models describing this process in the region around $A = 130$, the availability of experimental data on the evolution of the $N = 82$ shell gap is crucial. The predicted reduction of this gap [1,2] led to the recent investigations on the structure of ^{130}Cd [3] and ^{131}In [4]. The energy of the first excited 2^+ state in ^{130}Cd indirectly points toward a robust shell closure at $N = 82$, which was confirmed by a direct measure of the shell gap in Ref. [4]. Missing evidence for a shell quenching in all these cases calls for a need to modify the mass model [5] explaining the abundances of $A = 130$ nuclei in nature. Furthermore, information on the structure of excited states in ^{126}Cd and ^{128}Cd [6,7] indicates an enhanced quadrupole collectivity, which has also been

*F.Naqvi@gsi.de
†Present address: GANIL Caen, France.
‡Present address: GSI Darmstadt, Germany.
§Present address: IF PAN, Warsaw, Poland.
‖Present address: University of Vigo, Spain.
¶Present address: Universidad de Salamanca, Spain.
**Present address: RIKEN, Japan.
††Present address: Yale University, USA.
‡‡Present address: University of Michigan, USA.

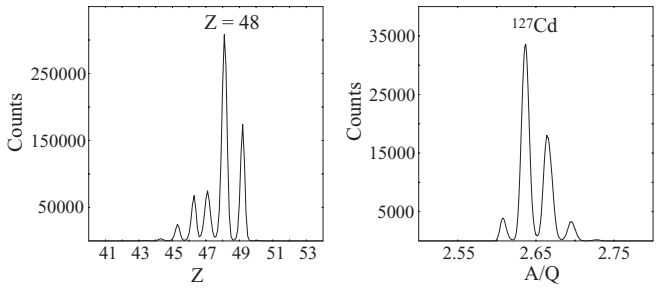

FIG. 1. Left: Z information provided by the two ionization chambers. Right: A/Q selection for Cd isotopes.

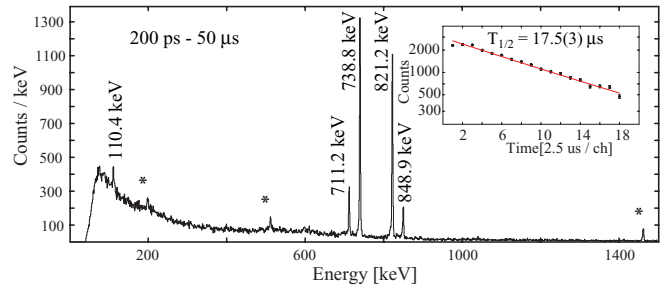

FIG. 2. (Color online) Singles γ-ray energy spectrum of ^{127}Cd. Background lines are marked with *. Inset: The sum of time distributions of the 711-, 739-, 821-, and 849-keV transitions with a single exponential decay fit.

revealed in theoretical studies [8]. To gain more insight on this issue and to extend the study of structure evolution in the Cd chain to the odd isotopes, a detailed examination of the data from an experimental campaign performed at the FRagment Separator (FRS) [9] at GSI was done. A level scheme for ^{127}Cd supported by the detailed experimental information including coincidence relations and isomeric half-life has been constructed for the first time in the present work.

II. EXPERIMENTAL TECHNIQUE

Isomeric decays of ^{127}Cd were observed following the relativistic fragmentation reaction of ^{136}Xe beam at an energy of 750 MeV/u on a ^{9}Be target of 4g/cm^2 thickness. The neutron-rich Cd isotopes were produced in two different settings of the FRS, one optimized for the maximum transmission of ^{130}Cd and the other one tuned to predominantly transmit ^{126}Cd. To select the ions of interest from the reaction products the standard $B\rho$-ΔE-$B\rho$ method was employed and the FRS was operated in its achromatic mode. Event-by-event identification of the particles in terms of their mass (A) and charge (Z) was done by measuring the time of flight between two scintillator detectors separated by a distance of 35 m and the magnetic rigidities providing the A/Q ratio. Energy loss information in two ionization chambers served to determine the atomic number Z. Corresponding plots of Z and A/Q identification are shown in Fig. 1. Isomers populated in the reaction, having lifetimes long enough to be able to reach the final focal plane, were implanted in a plastic catcher, surrounded by 15 Ge cluster detectors from the RISING array, arranged in close geometry [10]. Coincidence between the implanted ^{127}Cd ions and the detected γ rays within a time range of 50 μs ensured an unambiguous assignment of the detected radiations to the decay of the isomeric states of the ions. Stringent conditions imposed on the selection procedure of the FRS along with a clean identification of the particles enabled the observation of 7.2×10^5 ^{127}Cd ions in total from the two settings.

III. EXPERIMENTAL RESULTS

A singles γ-ray spectrum containing five γ transitions assigned to the decay of the isomer in ^{127}Cd is shown in Fig. 2. So far γ transitions in ^{127}Cd were identified in two previous experiments. Hellström *et al.* [11] assigned four γ transitions at energies of 710, 738, 820, and 342 keV to the isomeric decay. In the work of Hoteling *et al.* [12], apart from the two previously observed 738- and 820-keV γ rays, two new γ transitions at energies of 770.9 and 908.0 keV were identified. Though a level scheme for ^{127}Cd was constructed only in the latter paper, it was merely based on the systematics of known neighboring odd-mass Cd isotopes owing to low statistics and lack of lifetime information. In our experiment the previously reported γ transitions at energies of 739, 821, and 711 keV were affirmed and two new γ rays at energies of 110 and 849 keV were identified. However, the 771- and 909-keV transitions reported in Ref. [12] and the 342-keV transition reported in Ref. [11] could not be confirmed in the present work. The newly observed $\gamma\gamma$ coincidence relations of the five transitions associated with the isomeric decay in ^{127}Cd are shown in Fig. 3. Coincidences were investigated for two different coincidence time windows of 100 ns and 50 μs.

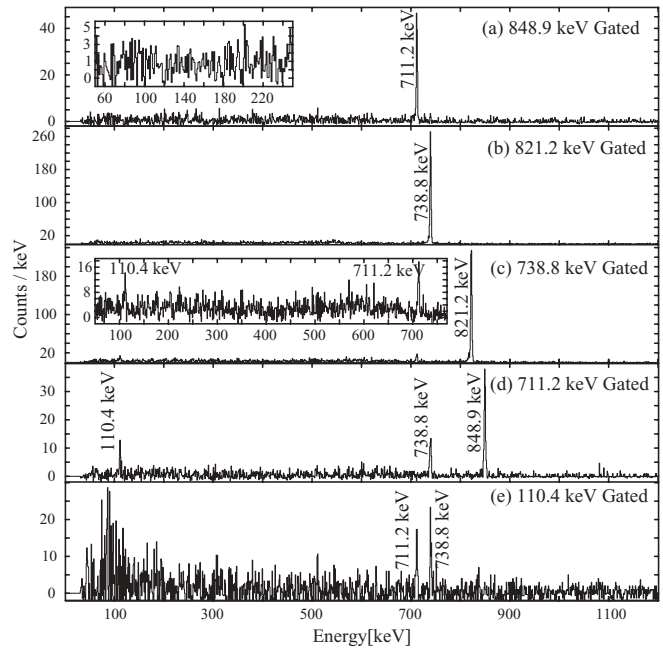

FIG. 3. $\gamma\gamma$ coincidence spectra with a coincidence window of 100 ns. Inset: Zoomed-in region of the respective weak coincidences.

TABLE I. Summary of the measured half-lives and spin and parity assignments of the levels in ^{127}Cd. Energy of the states are with respect to the $(11/2^-)$ β^- decaying isomer. The γ intensities are normalized to the 739-keV transition.

$E_i + x$ (keV)	$T_{1/2}$ (μs)	Transition $J \rightarrow I$	E_γ (keV)	$T_{1/2}$ (μs)	I_γ (%)
711		$(13/2^-) \rightarrow (11/2^-)$	711.2(2)	17.1(8)[b]	23.0(9)
821		$(15/2^-) \rightarrow (11/2^-)$	821.2(2)	17.7(4)[b]	91.8(30)
		$(15/2^-) \rightarrow (13/2^-)$	110.4(2)	17.5(12)[b]	6.2(6)
1560	17.5(3)[a]	$(19/2^+) \rightarrow (15/2^-)$	738.8(2)	17.6(4)[b]	100.0(31)
		$(19/2^+) \rightarrow (13/2^-)$	848.9(2)	17.9(6)[b]	17.3(7)

[a]Extracted from the fitting of the sum of time distributions of the 711-, 739-, 821-, and 849-keV transitions with a single exponential decay function.
[b]Extracted from the fitting of the time distribution of corresponding individual γ transition with a single exponential decay function.

Comparable relative intensities of all the γ transitions in the aforementioned conditions established the presence of only one isomer in the decay.

The proposed level scheme for ^{127}Cd is based on the following arguments. The two most intense γ transitions of 739 and 821 keV most likely form a single cascade, which is confirmed by their mutual coincidence shown in Fig. 3(b). The 711- and 849-keV lines have similar intensities and are in coincidence [see Fig. 3(a)], which points toward the existence of a second cascade in the decay. The sum of energies of the 739- and 821-keV lines is equal to that of the 849- and 711-keV lines. Also, the absence of coincidence between these two cascades confirms that they are parallel competing branches. Observation of a 110-keV transition coinciding with the differences in energies of the 849- and 739-keV lines and the 711- and 821-keV lines suggests that an intermediate level is present, fed by the 110-keV transition. Coincidence between 110-keV and 711- or 739-keV lines supports the argument of an intermediate level connecting the two cascades via the 110-keV transition. The lifetime analysis based on the single exponential decay fit of the summed time distributions of the 711-, 739-, 821-, and 849-keV transitions is shown in the inset of Fig. 2. A half-life of 17.5(3) μs was obtained for the decaying isomer. The fit of the time distributions of individual γ lines with the same function as described here was also performed and the results are listed in Table I. Because the 110-keV transition has a relative intensity of only 6%, the presence of a 115-keV background line in its vicinity made the background subtraction difficult. This resulted in a comparatively larger error in the measured value.

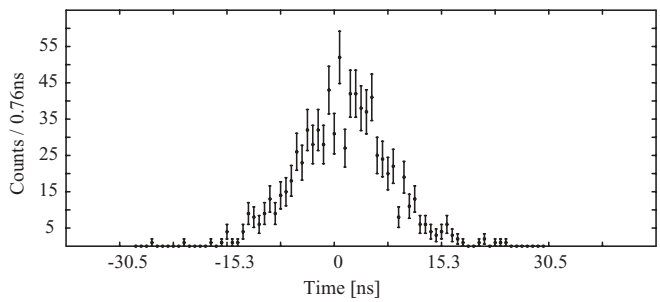

FIG. 4. Relative time distribution of the 739-keV transition with respect to the 821-keV transition. The spectrum shows a symmetric distribution.

From the half-life information and the inferred reduced transition probabilities, the multipolarity of the γ transitions is determined. Owing to similar energies and same half-lives of 711-, 739-, 821-, and 849-keV lines, all four of them qualify to be either $M2$ or $E3$, if one assumes that the isomerism is caused by any of them. Hence the ordering of these transitions could not be determined based on the experimental data. The relative time between the 739- and 821-keV transitions shows a symmetric distribution (see Fig. 4) within an electronic resolution of 0.7 ns. This implies that the state depopulated by the 110-keV line in competition with the 821- or 739-keV transitions has a half-life of less than 10 ns since a longer lifetime would lead to clear asymmetries as observed in the case of ^{128}Cd [7]. Only an $M1$ character of the 110 keV transition would be compatible with this upper half-life limit.

IV. DISCUSSION

Spins and parities were assigned to the excited states in ^{127}Cd on the basis of intensity balances, reduced transition probabilities, and the experimental information on the level scheme of the ^{129}Sn isotone [13]. According to the β^- decay studies of ^{127}Cd, $(3/2^+)$ is assigned to the β^- decaying ground state [14] with pure $\nu d_{3/2}$ neutron character. The systematics of odd-mass Cd and Sn isotopes [12,13] confirms that the γ-decaying isomer is built on a $(11/2^-)$ state. Owing to the large spin difference and long partial lifetime, γ transition between the $(11/2^-)$ and $(3/2^+)$ states is not observed and thus the former decays by a β^- emission. From the existing experimental evidence it cannot be firmly established whether the $(3/2^+)$ or the $(11/2^-)$ state is the ground state. ^{129}Sn having the same number of neutron holes in the ^{132}Sn core as ^{127}Cd provides the best case for comparison. Since in ^{129}Sn isomerism is mainly caused by $E2$ transitions of very low energies or a hindered $M2$ $(19/2^+) \rightarrow (15/2^-)$ transition, a similar explanation was assumed to be the reason of isomer formation in ^{127}Cd by Hellström *et al.* [11].

In ^{127}Cd a $(19/2^+) \rightarrow (15/2^+)$ $E2$ spin trap analogous to the one observed in ^{129}Sn given the half-life of $T_{1/2} = 17.5$ μs would require a nonobserved transition of ~30 keV and the observation of two competing $E1$ transitions, $(15/2^+) \rightarrow (15/2^-)$ and $(15/2^+) \rightarrow (13/2^-)$, with similar intensities. But the encountered branching ratios of 849 keV with respect to 739 keV and of 711 keV with respect to 821 keV rules out this possibility. Alternatively, if a $15/2^+$ state happens to lie above the $19/2^+$ state causing an isomer, the fast $15/2^+ \rightarrow 15/2^-$ and $15/2^+ \rightarrow 13/2^-$ transitions would not let the corresponding state be isomeric with a half-life of 17.5 μs. Hence we can conclude that an $M2$ transition from $(19/2^+)$ to $(15/2^-)$ in competition with an $E3$ transition from $(19/2^+)$ to $(13/2^-)$ is responsible for the measured half-life of the isomer. This argument allowed us to assign a spin of $(19/2^+)$ to the decaying isomeric state. The decay of the intermediate state is governed by a competition between the 110- and 821- or 849-keV transitions. The experimental branching ratios for the 110-keV γ line in the two cases are ~6% and 26%, respectively, while the expected value from the energy scaling of two such $M1$ transitions of equal reduced strength is ~0.5%. Therefore, this intermediate state was assigned to have spin-parity $(15/2^-)$, depopulated by a competition of a 110-keV $M1$ transition and a 821- or 849-keV $E2$ transition. Owing to the uncertainty in the ordering of γ rays just discussed the intermediate states at 711 and 821 keV shown in the level scheme in Fig. 5 (EXP) could lie at 739 and 849 keV instead with respect to the $(11/2^-)$ state. So two possibilities for the experimental level scheme of ^{127}Cd are proposed, one shown in Fig. 5 and the other with reversed ordering of the 739- and 849-keV transitions and the 821- and 711-keV transitions.

A. Shell-model interpretation

Two theoretical shell-model approaches employing different model spaces and interactions were used to investigate the nuclear structure evidence of the experimental data. In the first one a model space $\pi(p_{1/2}, g_{9/2})\nu(d_{5/2}, g_{7/2}, s_{1/2}, d_{3/2}, h_{11/2})$ outside a ^{88}Sr core was chosen (i.e., core excitations across the $Z = 50$ and $N = 82$ shells are not considered). The residual interaction is based on a G matrix derived from the CD-Bonn nucleon-nucleon potential [15] and core polarization corrections for a ^{88}Sr inert core following the many-body approach outlined in Ref. [16]. Monopole tuning following $A^{-1/3}$ scaling of the two-body matrix elements (TBME) was performed to reproduce the single hole energies (SHE) in ^{132}Sn as described in Refs. [3,13]. For the open proton-neutron $(\pi\nu)$ space two modifications were introduced. First the underbound $\pi g_{9/2}\nu h_{11/2}$, I^π=1$^-$,10$^-$ TBME were increased by -500 and -600 keV, respectively, keeping the multiplet monopole constant. This is necessary to reproduce the ground and isomeric states in ^{130}In [14]. Second, to increase the collectivity in the $(\pi\nu)$ shells, the dominating binding (negative) diagonal $\pi\nu$ TBME $\pi g_{9/2}\nu h_{11/2}$ and $\pi p_{1/2}\nu h_{11/2}$ were enhanced by a monopole shift of -100 keV. To maintain the SHE for ^{132}Sn, the experimentally unknown $\nu h_{11/2}$ SPE in ^{88}Sr was increased by $+1.2$ MeV. Further the $(\nu h_{11/2})^2_{2+}$ TBME was reduced by -150 keV, keeping the monopole of the multiplet constant, to improve the agreement in the even Sn isotopes. With these modifications, referred to as SM, the agreement with experiment in ^{128}Cd [17] and ^{127}Cd is greatly improved, though the $(13/2^-) - (15/2^-)$ sequence in the latter is not fully reproduced (Fig. 5). Further details will be given in a forthcoming paper [17]. Effective charges $e_\pi = 1.5e$ and $e_\nu = 0.7e$ for protons and neutrons and a spin g factor of $g_s = 0.7g_s^{\text{free}}$ for magnetic transitions were used [3,13]. Calculations were performed with the code OXBASH [18]. In the second approach an extended model space $\pi(p_{3/2}, p_{1/2}, f_{5/2}, g_{9/2})$ $\nu(d_{5/2}, g_{7/2}, s_{1/2}, d_{3/2}, h_{11/2})$ outside ^{78}Ni was chosen with an interaction derived from the CD-Bonn nucleon-nucleon potential using the same method as just described, but for an inert ^{78}Ni core [7]. Monopole tuning was performed to reproduce the experimental SHE for ^{132}Sn and levels in neighboring Sn isotopes, the $N = 82$ isotone ^{130}Cd, and the $\pi^{-1}\nu^{-1}$ neighbor ^{130}In. Effective charges of $1.5e$ for protons and $0.5e$ for neutrons were used for electric transitions and an effective spin g factor of $g_s = 0.75g_s^{\text{free}}$ for magnetic transitions. In addition orbital g factors of $g_l(p) = 1.1$ and $g_l(n) = -0.1$ for protons and neutrons, respectively were used. Calculations were performed with the large-scale shell-model (LSSM) codes ANTOINE and NATHAN [19] and the results are denoted by LSSM in Fig. 5.

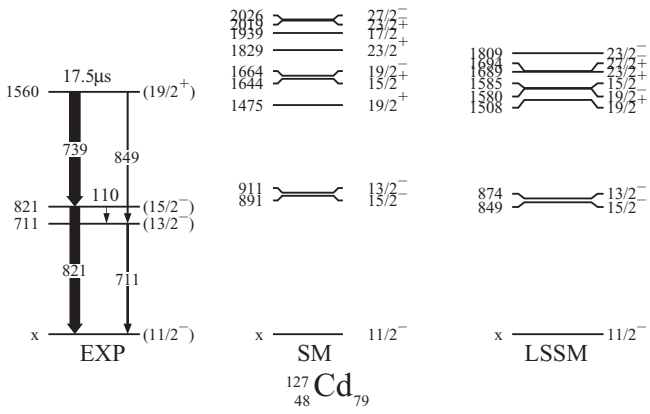

FIG. 5. The proposed level scheme for ^{127}Cd and the theoretically calculated excited levels by SM and LSSM.

From the good agreement of the shell-model approaches SM and LSSM for the experimentally known levels it can be concluded that the increased $\pi\nu$ interaction in SM to a large extent accounts for the neglect of the $\pi(p_{3/2}, f_{5/2})$ orbitals in the model space used. The 2^+ excitation energy in ^{128}Cd is still high by ~150 keV. This discrepancy is carried over into the energy of $(13/2^-)$ state in ^{127}Cd, which has leading configuration of a $\nu h_{11/2}$ hole coupled to the 2^+_1 state in ^{128}Cd. These remaining deficiencies, with the high-spin isomers being well reproduced, indicate a lack of collectivity in the low-spin states. Lifting the $\pi(p_{3/2}, f_{5/2})$ orbitals closer to the Fermi surface would create a pseudo-SU(3) hh space comprising the $\pi(p, f_{5/2})$ and $\nu(s, d)$ orbitals. This would further increase collectivity as observed one major shell higher for the Hg isotopes in the ^{208}Pb hh space as in the well studied (s, d) and (p, f) pp cases (see, e.g., [20]). Reduced transition probabilities in the two experimental scenarios

TABLE II. Transition strengths and γ branching ratios for experiment and shell model. Separate values are given for the two alternative experimental level schemes EXP[a] and EXP[b] of ^{127}Cd.

Transition	σL $J \to I$	$B(\sigma\mathrm{L})$ (W.u)			
		EXP[a]	EXP[b]	SM	LSSM
$(19/2^+) \to (13/2^-)$	$E3$[c]	$3.40(18)\times10^{-2}$	$2.30(30)\times10^{-1}$	6.19×10^{-3}	3.04×10^{-3}
$(19/2^+) \to (15/2^-)$	$M2$[c]	$2.71(14)\times10^{-4}$	$7.71(16)\times10^{-5}$	1.98×10^{-3}	5.75×10^{-3}
$(15/2^-) \to (13/2^-)$	$M1$[d]	6.3(6)%	26(3)%	5.8%	7.5%
$(15/2^-) \to (11/2^-)$	$E2$[d]	93.7(31)%	74(3)%	94.2%	92.5%

[a]Adopted order of cascades.
[b]Reversed order of cascades.
[c]Pure multipolarity assumed.
[d]Only γ branching ratio known.

are compared to SM and LSSM results in Table II. The retarded $B[E3;(19/2^+) \to (13/2^-)]$ and $B[M2;(19/2^+) \to (15/2^-)]$ are, respectively, under- and overestimated for both experimental scenarios. In the model space these transitions are $\nu h_{11/2} \to d_{5/2}$ and $\nu h_{11/2} \to g_{7/2}$, which include small components in the wave function that may be distorted by configurations from outside the model space. Moreover, the effective charges and g factors for $E3$ and $M2$ operators may be different from those for $E2$ and $M1$, respectively. A good correspondence between experimental and theoretical branching ratio is observed for the $(15/2^-) \to (11/2^-)$ 821-keV $E2$ and the $(15/2^-) \to (13/2^-)$ 110-keV $M1$ transitions in the scenario shown in Fig. 5. It should be noted that the SM and LSSM values agree as well. The drastic discrepancy for this branching in the alternative cascade assignment and slightly better agreement for the $M2$ and $E3$ transitions (see Table II) establishes a preference for the adopted order.

V. SUMMARY AND CONCLUSIONS

In conclusion, a microsecond isomer has been identified in ^{127}Cd. Based on $\gamma\gamma$ coincidence and lifetime analysis a level scheme on top of a $\nu h_{11/2}^{-1}$ isomer or ground state was constructed for this nucleus. In contrast to the odd-mass heavy Sn isotopes the isomerism in ^{127}Cd is attributed to competing hindered $E3$ and $M2$ transitions from a $(19/2^+)$ state, formed by mixed proton-neutron configurations. The sequence of the intermediate $(13/2^-)$ and $(15/2^-)$ states serves as a benchmark for shell-model calculations performed with two different interactions in a small (SM) and an extended (LSSM) model space. Since the theoretical models reproduce the energies of the low-lying pure proton and pure neutron excited levels in ^{130}Cd and ^{130}Sn, respectively, an enhanced proton-neutron interaction is attributed to be the origin of increased collectivity in the low-spin yrast region of ^{127}Cd.

ACKNOWLEDGMENTS

The authors would like to acknowledge the support of German Federal Ministry of Education and Research (06KY205I), the EU Access to Large Scale Facilities Programme (EURONS, EU Contract No. 506065), the Polish Ministry of Science and Higher Education (1-P03B-030-30 and 620/E-77/SPB/GSI/P-03/DWM105/2004-2007), the Spanish Ministerio de Ciencia e Innovación (FPA2007-66069 and FPA2009-13377-C02-02), EPSRC/STFC (UK), the Swedish Research Council, the Bulgarian Science Fund VUF06/05, the US Department of Energy (DE-FG02-91ER-40609 and DE-AC02-06CH11357), the Hungarian Science Foundation (OTKA K-68801), and the Italian INFN.

[1] J. Dobaczewski, I. Hamamoto, W. Nazarewicz, and J. A. Sheikh, Phys. Rev. Lett. **72**, 981 (1994).
[2] I. Dillmann *et al.*, Phys. Rev. Lett. **91**, 162503 (2003).
[3] A. Jungclaus *et al.*, Phys. Rev. Lett. **99**, 132501 (2007).
[4] M. Górska *et al.*, Phys. Lett. B **672**, 313 (2009).
[5] B. Chen *et al.*, Phys. Lett. B **355**, 37 (1995).
[6] T. Kautzsch *et al.*, Eur. Phys. J. A **9**, 201 (2000).
[7] L. Cáceres *et al.*, Phys. Rev. C **79**, 011301(R) (2009).
[8] T. R. Rodríguez, J. L. Egido, and A. Jungclaus, Phys. Lett. B **668**, 410 (2008).
[9] H. Geissel *et al.*, Nucl. Instrum. Methods Phys. Res. B **70**, 286 (1992).
[10] S. Pietri *et al.*, Nucl. Instrum. Methods Phys. Res. B **261**, 1079 (2007).
[11] M. Hellström *et al.*, GSI 2003-1, 2003, p. 5 (unpublished).
[12] N. Hoteling *et al.*, Phys. Rev. C **76**, 044324 (2007).
[13] R. Lozeva *et al.*, Phys. Rev. C **77**, 064313 (2008).
[14] ENSDF database, [http://www.nndc.bnl.gov/ensdf/].
[15] R. Machleidt, Phys. Rev. C **63**, 024001 (2001).
[16] M. Hjorth-Jensen, T. T. S. Kuo, and E. Osnes, Phys. Rep. **261**, 125 (1995).
[17] H. Grawe *et al.* (to be published).
[18] B. A. Brown *et al.*, OXBASH for Windows, MSU-NSCL Report 1289, 2004.
[19] E. Caurier, G. Martínez-Pinedo, F. Nowacki, A. Poves and A. P. Zuker, Rev. Mod. Phys. **77**, 427 (2005).
[20] R. F. Casten *et al.*, *Algebraic Approaches to Nuclear Structure:Interacting Boson and Fermion Model* (Harwood Academic Publishers, 1993).

Shape coexistence and isomeric states in neutron-rich ^{112}Tc and ^{113}Tc

A. M. Bruce,[1] S. Lalkovski,[1,*] A. M. Denis Bacelar,[1] M. Górska,[2] S. Pietri,[2,3] Zs. Podolyák,[3] Y. Shi,[4] P. M. Walker,[3] F. R. Xu,[4] P. Bednarczyk,[2] L. Cáceres,[2] E. Casarejos,[5] I. J. Cullen,[3] P. Doornenbal,[2,6] G. F. Farrelly,[3] A. B. Garnsworthy,[3] H. Geissel,[2] W. Gelletly,[3] J. Gerl,[2] J. Grębosz,[2,7] C. Hinke,[8] G. Ilie,[6] G. Jaworski,[9,10] I. Kojouharov,[2] N. Kurz,[2] S. Myalski,[7] M. Palacz,[9] W. Prokopowicz,[2] P. H. Regan,[3] H. Schaffner,[2] S. Steer,[3] S. Tashenov,[2] and H. J. Wollersheim[2]

[1]*School of Computing, Engineering and Mathematics, University of Brighton, Brighton BN2 4GJ, United Kingdom*

[2]*Gesellschaft für Schwerionenforschung mbH, Planckstrasse 1, D-64291 Darmstadt, Germany*

[3]*Department of Physics, University of Surrey, Guildford GU2 7XH, United Kingdom*

[4]*Department of Technical Physics, Peking University, Beijing 100871, China*

[5]*Facultad de Física, Universidad de Vigo, E-36310 Vigo, Spain*

[6]*Institut für Kernphysik, Universität zu Köln, Zülpicher Straße 77, D-50937 Köln, Germany*

[7]*Niewodniczański Institute of Nuclear Physics, Polish Academy of Science, ulica Radzikowskiego 152, Krakow 31-342, Poland*

[8]*Physik-Department E12, Technische Universität München, D-85748 Garching, Germany*

[9]*Heavy Ion Laboratory, Warsaw University, ulica Pasteura 5A, 02-093 Warszawa, Poland*

[10]*Faculty of Physics, Warsaw University of Technology, Koszykowa 75, 00-662 Warszawa, Poland*

(Received 9 September 2010; published 14 October 2010)

Isomeric states in ^{112}Tc and ^{113}Tc, with half-lives of 150(17) ns and 500(100) ns, respectively, have been observed following the relativistic fission of ^{238}U. The fission fragments have been separated in a fragment separator and identified by means of energy-loss and time-of-flight techniques. In both nuclei, the ground-state configuration is calculated to have an oblate shape and the isomerism is proposed to arise due to transitions from a triaxial excited state to a low-lying oblate state.

DOI: 10.1103/PhysRevC.82.044312 PACS number(s): 21.10.Tg, 23.20.Lv, 23.35.+g, 27.60.+j

I. INTRODUCTION

The shapes of neutron-rich nuclei with $A \approx 110$ have been the subject of intensive discussion in the last decade since large scale Finite-Range Liquid Drop Model (FRLDM) calculations [1] showed that the neutron-rich nuclei in all of the isotopic chains with $Z = 40$–48 undergo a prolate-to-oblate shape transition when approaching $N = 80$. This was reinforced by Skalski *et al.* [2], who used both the liquid drop and the FRLDM for the macroscopic energy and both BCS and the particle number projection method for the pairing energy. ^{112,113}Tc have $Z = 43$ and $N = 69,70$, respectively, and, for the neighboring $Z = 42$ (Mo) nuclei, calculations [2] indicate a ground-state shape which is prolate for $N \leqslant 66$ and oblate for $N \geqslant 68$. For $Z = 44$ (Ru), the prolate-oblate shape change in the ground state is predicted to occur between $N = 64$ and 66. Moreover, relativistic mean-field calculations [3] predict an oblate ground state at $N = 64$, ^{106}Mo and, more recently, cranked and configuration-constrained shell-model calculations have predicted the appearance of oblate multiquasiparticle states in $N = 66$ isotones with prolate ground states [4]. Clearly, this is predicted to be a region of rapidly changing shapes.

Although the nuclei which are predicted [1] to have oblate ground states in neutron-rich Zr, Nb, and Mo are not yet accessible experimentally, those in neutron-rich Tc, Ru, Rh, Pd, and Ag isotopes can be reached by "conventional" studies of fission products. Among the first experimental articles reporting on such nuclei was a study of the neutron-rich Pd isotopes [5], produced in induced fission reactions, in which the oblate shape of the ^{111}Pd ground state predicted by the FRLDM [1] was ruled out. Indeed, more recent experimental work has led to the prolate interpretation being extended to the heavier Pd isotopes with Hua *et al.* [6], suggesting that a prolate-to-oblate shape transition occurs only at ^{116}Pd. In the ruthenium isotopic chain this transition was assumed to take place at ^{111}Ru [6] but, more recently, ^{113}Ru has been interpreted to have a significant degree of triaxiality [7]. The development of techniques for fission fragment γ-ray spectroscopy has also made it possible to cross the (50,82) neutron mid shell in the Tc isotopic chain, reaching ^{111}Tc ($N = 68$) [8]. In this work the authors conclude, mainly on the basis of systematics, that the ground state corresponds to the $5/2^+[422]$ proton excitation in a prolate-deformed potential. Intriguingly, however, they do state that "there are excitations seen in ^{111}Tc which suggest that the deformation above $N = 68$ may be oblate." Thus the question of where the prolate-oblate transition occurs in the technetium isotopic chain remains open. In this context, the structures of ^{112}Tc and ^{113}Tc, which are the subject of this paper, are of particular interest.

II. EXPERIMENTAL DETAILS

The nuclei of interest were studied as part of the RISING "stopped beam" campaign [9] at Gesellschaft für Schwerionenforschung (GSI), Darmstadt. They were produced in the relativistic fission of a ^{238}U beam accelerated in the GSI LINAC to 11.4 A MeV and then to 750 A MeV in the GSI SIS18 synchrotron. The typical beam intensity was

*Current address: Department of Physics, University of Sofia, 1164 Sofia, Bulgaria.

10^9 particles per second for a 1-s beam spill, with a repetition period of 10–15 s. The beam impinged on a ^{9}Be target with a thickness of 1.0 g/cm^2. Fully stripped fission fragments were separated in the GSI FRagment Separator (FRS) [10], using the $(B\rho)_1 - \Delta E - (B\rho)_2$ technique, and identified by means of time-of-flight and energy-loss techniques. The Time of Flight (ToF) is measured between two scintillation detectors at the intermediate and final focal planes of the FRS and the energy loss is measured in an eight-anode ionization chamber (MUSIC). These detectors were calibrated using the primary ^{238}U beam. The data set presented in this paper was collected with the FRS tuned to ^{110}Nb.

At the end of the separator, the fragments were slowed by an Al degrader with a thickness of 3.7 g/cm^2 and implanted in a 5-mm-thick copper stopper. γ rays emitted by the implanted nuclei were measured in the RISING γ-ray array, comprising 15 cluster detectors, which has an efficiency of ∼15% for the 662-keV transition in ^{137}Cs [11]. The signals from each Ge detector have been processed via XIA Digital Gamma Finder modules for energy and time analysis. The time stamp of the modules was 25 ns. A detailed description of the RISING performance in its stopped beam configuration is given in [11,12]. The acquisition system was triggered by the arrival of a fragment and remained "open" for a time window of 100 μs. Fragments which did not implant triggered a scintillation detector behind the copper stopper which provided a veto.

III. EXPERIMENTAL ANALYSIS AND RESULTS

The atomic number of the fragment (Z) was calculated from the energy loss in the MUSIC detector, corrected for particle velocity and trajectory. The mass-to-charge ratio (A/q) was calculated from the magnetic rigidity of the particles and the ToF. Figure 1 shows the relevant particle identification plot where the locations of ^{106}Nb and ^{113}Tc ions are indicated. ^{106}Nb contains a known isomer with a half-life of 845(35) ns [13] which served to confirm the particle identification. In addition to the veto detector mentioned above, other

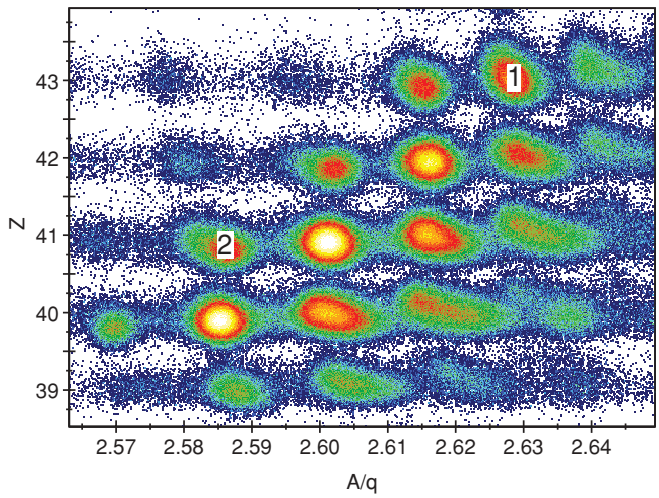

FIG. 1. (Color online) Particle identification plot with the location of the ^{113}Tc (1) and ^{106}Nb (2) ions indicated.

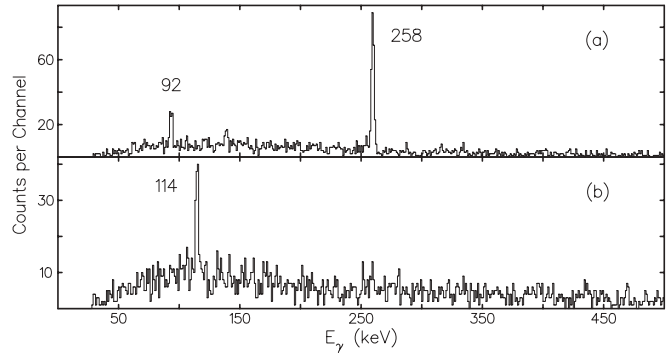

FIG. 2. γ-ray energy spectra obtained in coincidence with ^{112}Tc ions (a) and ^{113}Tc ions (b) and with a time gate of width 1.25 μs starting 300 ns after implantation (to reduce the bremsstrahlung background).

cleaning conditions imposed in the off-line analysis included the exclusion of events where the fragment changed its charge state during transmission through the separator and events where the fragment interacts with the degrader. Following identification of the fragments, two-dimensional spectra of the energies of γ rays measured in the RISING array and their emission time (relative to fragment deposition) were constructed for each isotope identified.

^{112}Tc. Figure 2(a) shows two γ rays which are associated with ^{112}Tc fragments. The relative intensities of the two transitions are $I_\gamma^{92} = 100 \pm 22\%$ and $I_\gamma^{258} = 91 \pm 9\%$. Analysis of the background fluctuations in the spectrum gives an upper limit of 10% of I_γ^{92} for a 166-keV γ ray which corresponds to the energy difference between the 92- and 258-keV transitions. There is no evidence of any transition at 340 keV, which is the sum of 258 and 92. Figure 3 shows coincidence spectra gated on (a) the 92-keV transition and (b) the 258-keV transition. These spectra have not had any background subtracted but, although the statistics are low, they do provide good evidence that the 92- and 258-keV transitions are in mutual coincidence. Figure 4(a) shows the time distribution of the 258-keV transition and a fit to this decay curve gives a half-life of 150(17) ns. The 92-keV transition is in a region with much background and a fit to its decay curve gives a half-life of 162(100) ns. Therefore it is concluded that there is one isomeric state in ^{112}Tc which has a

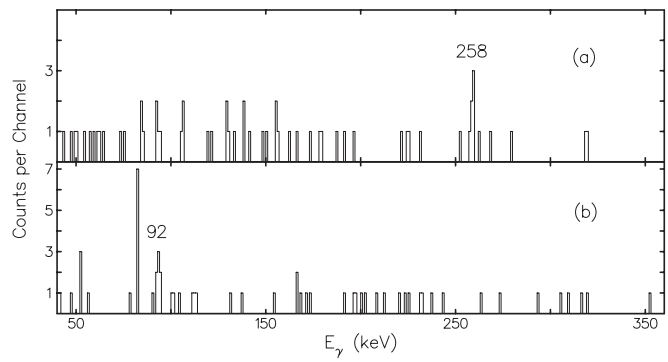

FIG. 3. γ-ray energy spectra obtained in coincidence with ^{112}Tc ions and (a) the 92-keV transition, (b) the 258-keV transition.

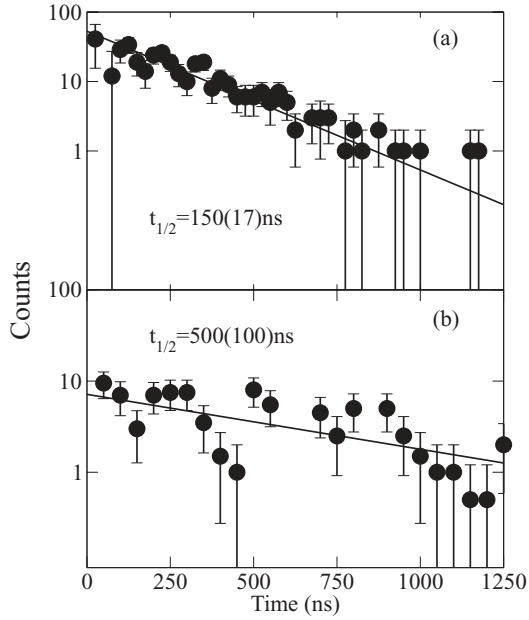

FIG. 4. Background-subtracted time distributions of (a) the 258-keV transition in ^{112}Tc and (b) the 114-keV transition in ^{113}Tc, along with associated fits.

half-life of the weighted average value of 150(17) ns. This is consistent with the recent findings of Folden *et al.* [14], who observed only the 258-keV transition and proposed that there is an isomeric state with a half-life of less than 500 ns.

^{113}Tc. Figure 2(b) shows a 114-keV γ ray which is associated with ^{113}Tc fragments. The transition is very weak but its time distribution is shown in Fig. 4(b). The associated fit indicates a half-life of the parent level of 500(100) ns. Examination of the coincidence spectrum associated with the 114-keV transition shows no evidence of coincident γ rays.

IV. INTERPRETATION AND DISCUSSION

^{112}Tc. Figure 5 shows the results of Potential-Energy Surface (PES) calculations [4] carried out separately for the positive- and negative-parity states in ^{112}Tc. The calculations indicate a negative-parity ground state [shown in Fig. 5(a)] with an oblate deformation of $\beta_2 = 0.23$ and $\beta_4 = -0.05$ formed from the $7/2^-[523]$ neutron $\otimes 5/2^+[422]$ proton coupling. This shape is in good agreement with that calculated by Möller *et al.* [1] (oblate with $\epsilon_2 = 0.25$ and $\epsilon_4 = +0.09$) and by Skalski *et al.* [2] for neighboring even-even Mo ($Z = 42$) and Ru ($Z = 44$) isotopes (oblate with $\beta_2 = 0.25$ and $\beta_4 = -0.09$). The Gallagher-Moszkowski rule indicates that the $K^\pi = 6^-$ coupling should be the lowest with the $K^\pi = 1^-$ coupling expected at an excitation energy of about 200 keV [15]. Figures 5(b) and 5(c) indicate the shapes for the two possible positive-parity states. In Fig. 5(b) the shape of the $+\nu,+\pi$ configuration with lowest energy is shown as $\beta_2 = 0.24$, $\beta_4 = -0.03$, and $\gamma = 44^\circ$ and in Fig. 5(c), the shape of the $-\nu,-\pi$ configuration with lowest energy is shown as $\beta_2 = 0.29$, $\beta_4 = -0.01$, and $\gamma = 31^\circ$. Both of these

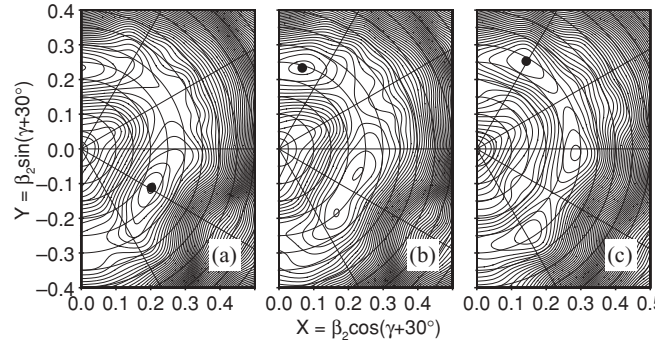

FIG. 5. Potential-Energy Surface (PES) calculations for ^{112}Tc for a negative-parity neutron and a positive-parity proton $(-\nu, +\pi)$ (a), $+\nu, +\pi$ (b), and $-\nu, -\pi$ (c). Isolines are placed at intervals of 200 keV and the energies of the minima in (b) and (c) are 411 and 474 keV relative to the $-\nu, +\pi$ ground state. The $+\nu, -\pi$ configuration is also calculated to be triaxial but at an even higher excitation energy.

configurations are calculated to have $J = 3$ and excitation energies ~450 keV.

Figure 6 shows the energy spectrum for these states and includes "in-band" oblate states calculated assuming a moment-of-inertia one-half of that of a rigid body. Comparison of the measured half-life of the observed isomeric state [150(17) ns] with calculations of Weisskopf single-particle estimates indicates that a transition with $\lambda > 2$ is unphysical. It is therefore unlikely that the observed transitions correspond to the decay from either of the $J^\pi = 3^+$ triaxial states directly to the ground state. On this basis, it is proposed that the 258-keV transition is from one of the triaxial $J^\pi = 3^+$ states to a $J^\pi = 2^-$ state built on the $J^\pi = 1^-$ state from the unfavored $7/2^-[523]$ neutron $\otimes 5/2^+[422]$ proton coupling. The measured half-life indicates that the $E1$ transition is hindered by a factor of $\sim 10^7$ compared to the Weisskopf single-particle estimate, corrected for electron conversion [16]. $E1$ transitions are known, however [17], to be hindered, typically by factors $\sim 10^5$, and a transition from a triaxial $J^\pi = 3^+$ state to an oblate $J^\pi = 2^-$ state would be expected to exhibit additional hindrance due to the shape change. In

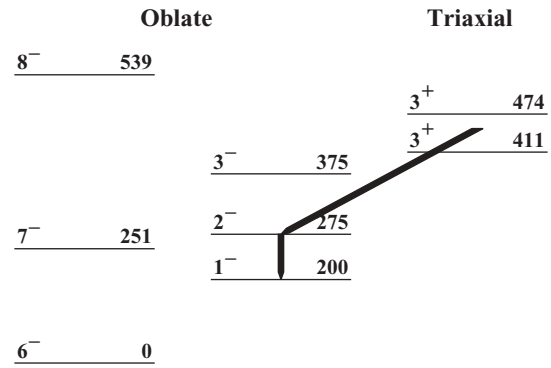

FIG. 6. The calculated energy spectrum for ^{112}Tc. The in-band oblate states assume a moment of inertia one-half of that of a rigid body. The triaxial states correspond to the configurations in Figs. 5(b) and 5(c).

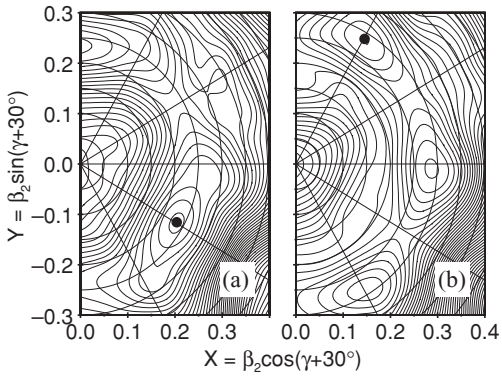

FIG. 7. PES calculations for the lowest-energy positive-parity (a) and negative-parity (b) states in ^{113}Tc. Iso-lines are placed at intervals of 200 keV.

this scenario, which is not inconsistent with the observed γ-ray intensities, the 92-keV transition then corresponds to the in-band transition from the $J^\pi = 2^-$ state to the $J^\pi = 1^-$ state. The $M5$ decay from the $J^\pi = 1^-$ to the $J^\pi = 6^-$ ground state would not be expected to be observed since the Weisskopf single-particle half-life estimate, corrected for electron conversion [16], for a level decaying by such a transition is ∼120 000 years and the level might be expected to preferentially decay by β emission.

^{113}Tc. The results of PES calculations carried out separately for the positive- and negative-parity states in ^{113}Tc are shown in Fig. 7. Figure 7(a) shows the results for the positive-parity configuration, indicating a shallow oblate minimum at $\beta_2 = 0.24$, $\beta_2 = -0.05$, $\gamma = 60^\circ$ corresponding to the $5/2^+[422]$ Nilsson orbit. The results for the negative-parity configuration in Fig. 7(b) show a deep triaxial minimum at $\beta_2 = 0.29$, $\beta_2 = -0.02$, and $\gamma = 29.8^\circ$ with $J^\pi = 5/2^-$. This state is calculated to lie above the positive-parity minimum and therefore the ground state of ^{113}Tc is assigned as $J^\pi = 5/2^+$. Under the assumption that there is no unobserved low-energy transition, it is proposed that the 114-keV transition connects the two different configurations. The Weisskopf single-particle half-life estimate, adjusted for electron conversion [16], for a 114-keV $E1$ transition is 1.8×10^{-4} ns, which, when compared with the measured value of 500(100) ns indicates a hindrance of 2.8×10^6. Given the typical $E1$ hindrance [17] discussed in the preceding section, and the additional hindrance expected due to the shape change, it is again proposed that the isomerism is due to an $E1$ transition between states of triaxial and oblate shape.

V. CONCLUSIONS

Isomeric states with half-lives of 150(17) and 500(100) ns, respectively, have been observed in ^{112}Tc and ^{113}Tc. Comparison with the results of PES calculations suggest that both nuclei have oblate ground states. The isomerism in both nuclei is interpreted as being associated with a shape change from triaxial excited states to low-lying oblate structures. The location of these isomeric levels may prove extremely useful as experimental tags in future in-beam measurements.

ACKNOWLEDGMENTS

This work is supported by the STFC(UK), AWE plc, the Bulgarian National Science Fund (Grant No. DMU02/1-06.01.2010), the Polish Ministry of Science and Higher Education (Grants No. 1-P03B-030-30 and No. 620/E-77/SPB/GSI/P-03/DWM105/2004-2007), the Spanish Ministerio de Educación y Ciencia (Grant No. FPA2005-00696), the German Federal Ministry of Education and Research (Grant No. 06KY205I), and EURONS (EU Contract No. 506065).

[1] P. Möller, J. R. Nix, W. D. Myers, and W. J. Swiatecki, At. Data Nucl. Data Tables **59**, 185 (1995).
[2] J. Skalski, S. Mizutori, and W. Nazarewicz, Nucl. Phys. A **617**, 282 (1997).
[3] G. A. Lalazissis, S. Raman, and P. Ring, At. Data Nucl. Data Tables **71**, 1 (1999).
[4] F. R. Xu, P. M. Walker, and R. Wyss, Phys. Rev. C **65**, 021303(R) (2002).
[5] T. Kutsarova *et al.*, Phys. Rev. C **58**, 1966 (1998).
[6] H. Hua *et al.*, Phys. Lett. B **562**, 201 (2003).
[7] J. Kurpeta *et al.*, Eur. Phys. J. A **33**, 307 (2007).
[8] W. Urban *et al.*, Eur. Phys. J. A **24**, 161 (2005).
[9] M. Górska *et al.*, Acta Phys. Pol. B **38**, 1219 (2007).
[10] H. Geissel, Nucl. Instrum. Methods Phys. Res. B **70**, 286 (1992).
[11] S. Pietri *et al.*, Nucl. Instrum. Methods Phys. Res. B **261**, 1079 (2007); Acta Phys. Pol. B **38**, 1255 (2007).
[12] P. Regan *et al.*, AIP Conf. Proc. **899**, 19 (2007).
[13] J. Genevey, F. Ibrahim, J. A. Pinston, H. Faust, T. Friedrichs, M. Gross, and S. Oberstedt, Phys. Rev. C **59**, 82 (1999).
[14] C. M. Folden III *et al.*, Phys. Rev. C **79**, 064318 (2009).
[15] C. J. Gallagher, Jr. and S. A. Moszkowski, Phys. Rev. **111**, 1282 (1958).
[16] T. Kibédi *et al.*, Nucl. Instrum. Methods A **589**, 202 (2008).
[17] K. E. G. Löbner, Phys. Lett. B **26**, 369 (1968).

PHYSICAL REVIEW C **82**, 061309(R) (2010)

Observation of a new high-spin isomer in ^{94}Pd

T. S. Brock,[1] B. S. Nara Singh,[1] P. Boutachkov,[2] N. Braun,[3] A. Blazhev,[3] Z. Liu,[4] R. Wadsworth,[1] M. Górska,[2] H. Grawe,[2] S. Pietri,[2] C. Domingo-Pardo,[2] D. Rudolph,[5] S. J. Steer,[6] A. Ataç,[7] L. Bettermann,[3] L. Cáceres,[2] T. Engert,[2] K. Eppinger,[8] T. Faestermann,[8] F. Farinon,[2] F. Finke,[3] K. Geibel,[3] J. Gerl,[2] R. Gernhäuser,[8] N. Goel,[2] A. Gottardo,[4] J. Grębosz,[9] C. Hinke,[8] R. Hoischen,[2,5] G. Ilie,[3] H. Iwasaki,[3] J. Jolie,[3] A. Kaşkaş,[7] I. Kojuharov,[2] R. Krücken,[8] N. Kurz,[2] E. Merchán,[10] C. Nociforo,[2] J. Nyberg,[11] M. Pfützner,[12] A. Prochazka,[2] Zs. Podolyák,[6] P. H. Regan,[6] P. Reiter,[3] S. Rinta-Antila,[13] H. Schaffner,[2] C. Scholl,[3] P.-A. Söderström,[11] N. Warr,[3] H. Weick,[2] H.-J. Wollersheim,[14] and P. J. Woods[4]

(RISING Collaboration)

[1]*Department of Physics, University of York, York YO10 5DD, United Kingdom*

[2]*GSI, D-64291 Darmstadt, Germany*

[3]*IKP, Universität zu Köln, D-50937 Köln, Germany*

[4]*School of Physics and Astronomy, University of Edinburgh, Edinburgh, United Kingdom*

[5]*Department of Physics, Lund University, S-22100 Lund, Sweden*

[6]*Department of Physics, University of Surrey, Guildford, Surrey GU2 7XH, United Kingdom*

[7]*Department of Physics, Ankara University, 06100 Tandoğan, Ankara, Turkey*

[8]*Physik Department E12, Technische Universität München, D-85748 Garching, Germany*

[9]*The Institute of Nuclear Physics PAN, Kraków, Poland*

[10]*Departamento de Física, Universidad Nacional de Colombia, Bogotá, Colombia*

[11]*Department of Physics and Astronomy, Uppsala University, SE-75120 Uppsala, Sweden*

[12]*IEP, Warsaw University, PL-00-681 Warsaw, Poland*

[13]*Department of Physics, Oliver Lodge Laboratory, University of Liverpool, Liverpool L69 7ZE, United Kingdom*

[14]*GGSI, D-64291 Darmstadt, Germany*

(Received 26 October 2010; published 30 December 2010)

A second γ-decaying high-spin isomeric state, with a half-life of 197(22)ns, has been identified in the $N = Z + 2$ nuclide ^{94}Pd as part of a stopped-beam Rare Isotope Spectroscopic INvestigation at GSI (RISING) experiment. Weisskopf estimates were used to establish a tentative spin/parity of 19^-, corresponding to the maximum possible spin of a negative parity state in the restricted ($p_{1/2}$, $g_{9/2}$) model space of empirical shell model calculations. The reproduction of the $E3$ decay properties of the isomer required an extension of the model space to include the $f_{5/2}$ and $p_{3/2}$ orbitals using the CD-Bonn potential. This is the first time that such an extension has been required for a high-spin isomer in the vicinity of ^{100}Sn and reveals the importance of such orbits for understanding the decay properties of high-spin isomers in this region. However, despite the need for the extended model space for the $E3$ decay, the dominant configuration for the 19^- state remains $(\pi p_{1/2}^{-1} g_{9/2}^{-3})_{11} \otimes (\nu g_{9/2}^{-2})_8$. The half-life of the known, 14^+, isomer was remeasured and yielded a value of 499(13) ns.

DOI: 10.1103/PhysRevC.82.061309 PACS number(s): 23.35.+g, 23.20.Lv, 21.10.Tg, 27.60.+j

The $N \approx Z$ nuclei just below ^{100}Sn are of particular interest in contemporary nuclear structure studies. As well as lying on the pathway for rp-process nucleosynthesis in x-ray burster scenarios [1], these nuclei also provide significant information in relation to shell structure close to the last doubly magic $N = Z$ nuclide [2] and constitute a key region for testing the reliability of the shell model (SM) and SM interactions [3]. The region is generally well described by the SM in a minimum space comprising $p_{1/2}$ and $g_{9/2}$ protons and neutrons [3–5]. Exploration of the limits of this approach with respect to inclusion of the $p_{3/2}$ and $f_{5/2}$ orbitals and excitations across the $N = Z = 50$ shell closure is a challenge both to the SM and experimental techniques.

This region is also remarkable for an abundance of isomeric states [6]. Particularly interesting is the occurrence of high-spin isomers which can provide an ideal testing ground for the study of neutron-proton interactions near the $N = Z$ line [6]. One of the most striking cases is the (21^+) level in ^{94}Ag, with recent papers reporting evidence for a variety of particle decay channels: β [7,8], βp [9], p [10], and $2p$ [11]. The latter of these is the subject of much debate in the literature [12–16].

The $T_z = 1$ nuclide ^{94}Pd has been studied in a number of experiments [7,8,17–21] and has a known 14^+ isomer that decays through γ decay and internal conversion (IC). The half-life of this state has been measured previously, yielding values of 800(200) [17], 600(100) [18], 530(10) [19], and 468(19) [21] ns. A cascade of transitions above the 14^+ isomer has been tentatively placed from β-decay studies of the (21^+) isomer in ^{94}Ag [7,8]. The current work presents data from a Rare Isotope Spectroscopic INvestigation at GSI (RISING) experiment showing clear evidence of a second isomeric state that feeds the 14^+ level through some of these transitions. The reproduction of the decay properties of this isomer in shell-model calculations requires the inclusion of the negative-parity $p_{3/2}$ and $f_{5/2}$ orbitals.

^{94}Pd and other nuclei of interest were produced by the fragmentation of an 850 MeV/nucleon ^{124}Xe beam, provided by the SIS synchrotron at GSI, on a 4 g/cm^2 ^{9}Be target.

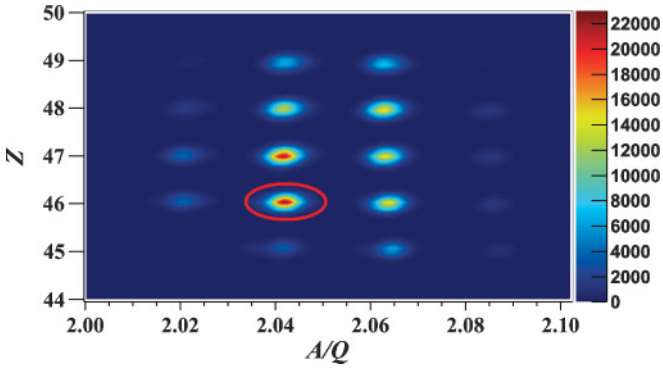

FIG. 1. (Color online) Fragment identification plot. The ^{94}Pd ions are ringed. The intensity color scale is given to the right.

Fragments were separated by the FRagment Separator (FRS) (see Ref. [22] and Fig. 1 of Ref [21]) and detectors at the central, "S2," and final, "S4," foci were used to uniquely identify each ion on an event-by-event basis as described in Refs. [21,23] with the addition of time projection chambers at each focal plane for more precise position measurements. Figure 1 shows a Z versus A/Q identification plot using the data from the FRS detectors. Due to the high energies involved, in virtually all cases the ions are fully stripped, i.e., $Q = Z$.

At the S4 focal plane the transported fragments were slowed down in an aluminum degrader, passed through a further scintillator, allowing for rejection of ions that underwent nuclear reactions in the degrader, and implanted in an active stopper. The stopper consisted of nine double-sided silicon strip detectors (DSSSD) arranged in three layers of three detectors, with each layer facing normal to the beam axis. A description of the properties of a similar, six DSSSD, stopper is given in Ref. [24]. The stopper was surrounded by the RISING

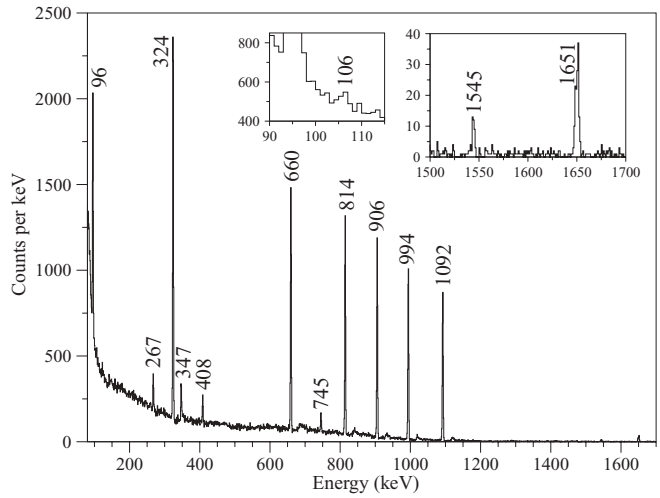

FIG. 2. Energy spectrum gated on ^{94}Pd ions. The seven largest peaks correspond to the yrast transitions from the 14^+ isomer to the ground state. The peaks at 347 and 745 keV are also from below the 14^+ isomer, but the peaks at 267 and 408 keV emanate from levels above it. The right inset shows peaks at 1545 and 1651 keV, while the left inset shows weak evidence of a 106 keV transition.

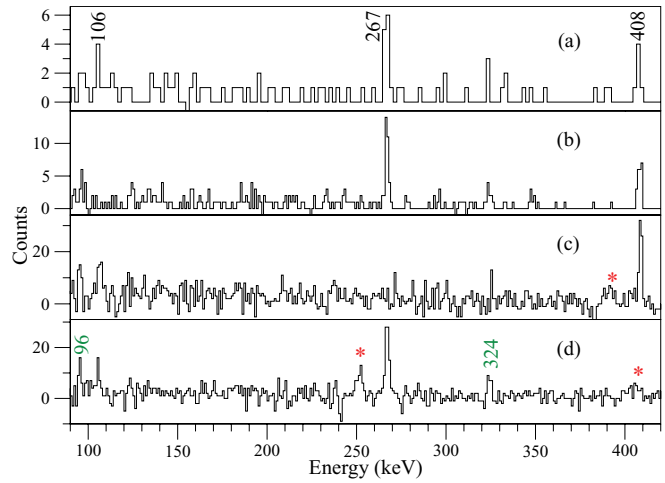

FIG. 3. (Color online) Prompt coincidences for the (a) 1545, (b) 1651, (c) 267, and (d) 408 keV transitions. (a) is 2 keV per bin and (b)–(d) are 1 keV per bin. Peaks corresponding to transitions below the 14^+ isomer can be seen due to the 250 ns width of the coincidence window. Peaks marked with "*" sum with the gating energy to 660 or 814 keV and are thus attributed to Compton scattering.

array of 105 germanium (Ge) detectors in its stopped beam configuration [23]. Using the information from the S2 and S4 detectors and the energy and timing information from the Ge detectors, time-walk corrected γ-time and γ-γ matrices were constructed for each implanted nuclide. The data were analyzed in ROOT [25] and RADWARE [26], and half-lives were determined using the ROOT implementation of MINUIT [27].

The S4 degrader has a detrimental effect on isomer spectroscopy due to bremsstrahlung radiation associated with the slowing down of the ions as they pass through [28]. This leads to spurious counts in the γ-ray spectra: the "prompt flash." Spectroscopic studies of low-energy transitions from short-lived isomers are particularly badly affected due to the (orders of magnitude) larger contribution the flash makes at lower energies (especially below ~150 keV in the present case) and the poorer time resolution at such energies which smears the flash out over a number of time bins.

Figure 2 shows a projection to the energy axis of the γ-time matrix associated with ^{94}Pd implantation events. Defining $t = 0$ as the time at which the prompt flash peaks, the time range of the projection corresponds to $t = 175$ to $t = 1025$ ns. The yrast transitions from 14^+ to 0^+ [7] are evident as are the previously identified $10_1^+ \rightarrow (8_2^+)$ and $(8_2^+) \rightarrow 6_1^+$ transitions [20] at 745 and 347 keV, respectively. The efficiency corrected ratio for the intensity of the 660, 814, 906, and 994 keV transitions compared to the 96 keV transition is 2.7(1) giving an IC coefficient for the 96 keV transition of 1.7(1), in excellent agreement with both previous measurements [20,21] and the theoretical prediction for an $E2$ transition of 1.62(7) obtained using the program BRICC [29]. The γ-ray branching ratio of the 10^+ state to the nonyrast (8^+) state was found to be 9(1)% by comparing the mean intensity of the 347 and 745 keV peaks to that of the 1092 keV peak.

Figure 2 clearly shows peaks at 267 and 408 keV. These transitions have been seen before [7,8] and tentatively assigned

as the $(16^+)\rightarrow(15^+)$ and $(15^+)\rightarrow 14^+$ transitions, respectively. The right inset of Fig. 2 indicates the presence of two further transitions. The weaker 1545 keV peak was identified in the ^{94}Ag β-decay studies and provisionally assigned as the $(18^+)\rightarrow(16^+)$ decay, but the more intense 1651 keV transition was not seen. The left inset of Fig. 2 shows evidence of a small peak at 106 keV. The agreement between the summed intensity of the 1545 and 1651 keV transitions and the individual intensities of the 267 and 408 keV transitions is excellent once detector efficiency has been accounted for. The final transition previously identified above the 14^+ state had an energy of 597 keV [7,8]. This is not seen in the present data.

Figures 3(a) and 3(b) show the low-energy part of the coincidence spectra for the 1545 and 1651 keV transitions. The coincidence gate used to produce the γ-γ matrix required that γ rays were seen between $t = 100$ and $t = 800$ ns. In both cases the 267 and 408 keV peaks can be seen. However, the 1545 coincident spectrum has a further peak at 106 keV. The same peak is seen in coincidence with the 267 and 408 keV transitions [Figs. 3(c) and 3(d)].

From the above, and the lack of any other clear transitions seen in singles or coincidence, we conclude that ^{94}Pd has a second isomer at 7212 keV that can decay through two channels, a 1651 keV transition to the (16^+) state or a 106 keV transition to the (18^+) state, as shown in the left part of Fig. 4. The experimental results for the isomers are summarized in Table I. The data unambiguously places the 1545 keV transition above the 408 and 267 keV transitions and below the 597 keV transition in the ^{94}Pd level scheme, an assignment that was previously based only on shell-model calculations and comparison with the $N = 48$ isotones [8]. However, the ordering of the 267 and 408 keV transitions still remains uncertain.

The size of the Compton background makes isomer half-life measurements using the low-energy γ rays at 267 and 408 keV difficult. Conversely, the background under the 1545 and 1651 keV peaks can have no direct contribution from Compton scattering of photons from the transitions below the 14^+ isomer; the prompt flash is also small and well constrained due to optimal time resolution at these energies. For the 1545 keV transition it is the low statistics which does not allow for a reliable half-life measurement. However, it was possible to implement a background-subtracted, weighted-least-squares exponential fit to the time distribution of counts in the 1651 keV peak, as shown in the bottom left corner of Fig. 5. This gave a value of 197(22) ns.

For the transitions below the 14^+ isomer in ^{94}Pd, the statistics are much higher. The top of Fig. 5 shows the time distribution for this isomer derived from the present work. Here the only events considered were those in which at least two γ rays are seen with energies corresponding to transitions in the yrast cascade from $12^+ \rightarrow 0^+$ (the 96 keV transition is omitted due to the poor time resolution at this energy). The time spectrum was then incremented with the time of the highest energy γ ray seen from the cascade if all the transitions seen from the cascade fell within a coincidence window of 250 ns. The line shown in the figure is a single-component exponential fit with no background subtraction, using only

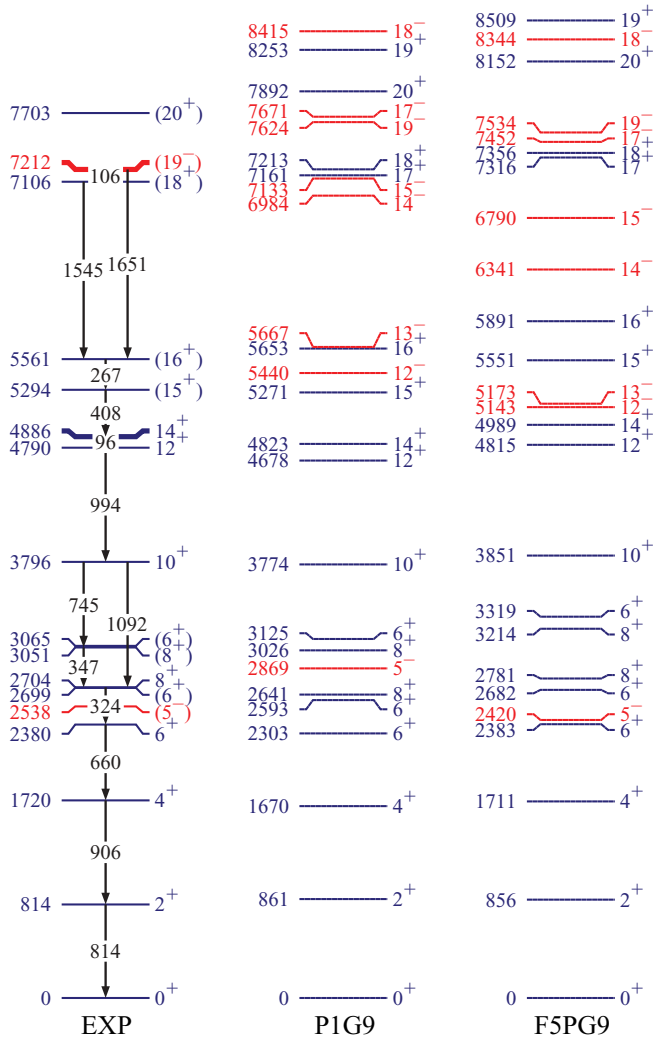

FIG. 4. (Color online) Experimental (left) and calculated energy levels (see text for details) of ^{94}Pd. The tentative spin and parity assignment for the new isomer at 7212 keV is based on the current work. Assignments for other states are based on prior results [7,8,17,20]. Only transitions observed in the current work are shown.

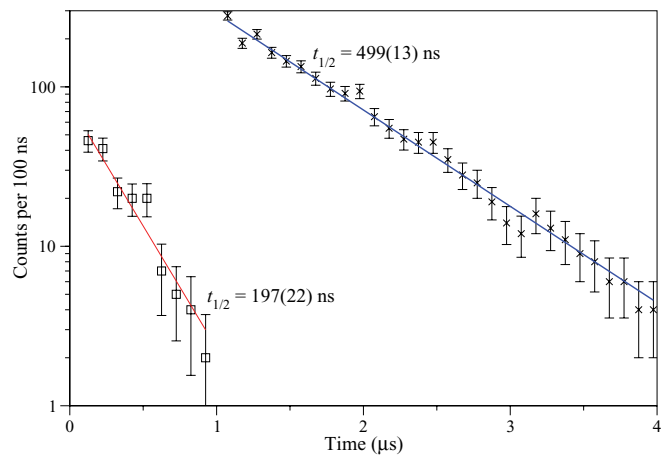

FIG. 5. (Color online) Decay curve for the 1651 keV transition (open squares) and for transitions below the 14^+ isomer (crosses) (see text).

TABLE I. Experimental decay energies, half lives, branching ratios (BR) and transition rates for the assigned electric multipoles of order L (EL) together with F5PG9 calculations of transition rates for the isomers in ^{94}Pd. "F5PG9-a" uses effective charges of 1.72/1.44e for protons/neutrons while "F5PG9-b" uses 1.5/0.5e.

						B (EL) (W.u.)		
E_{level} (keV)	Half-life (ns)	E_γ (keV)	BR (%)	$I^\pi_{\text{initial}} \rightarrow I^\pi_{\text{final}}$	EL	Expt.	F5PG9-a	F5PG9-b
7212	197(22)	1651	80(4)	$(19^-) \rightarrow (16^+)$	$E3$	0.28(4)	0.18	0.10
		106	20(4)[a]	$(19^-) \rightarrow (18^+)$	$E1$	$3(1)\times10^{-7}$		
				$19^- \rightarrow 17^-$	$E2$		9.74	5.52
4886	499(13)	96	100[a]	$14^+ \rightarrow 12^+$	$E2$	2.1(1)[b]	5.49	2.69

[a]Including internal conversion.

[b]Assuming a γ-ray energy of exactly 96 keV and IC coefficient of 1.62.

data with $t > 1$ μs. Given the measured half-life of the new isomer and its relatively low population, this fit should be characteristic of only the 14^+ isomer. From this we infer a value of 499(13) ns for this state, which is intermediate between the values of Grzywacz [530(10) ns [19]] and Garnsworthy *et al.* [468(19) ns [21]]. The reliability of the assumption of vanishing background in this analysis is confirmed by the excellent agreement with fits to the time spectra resulting from gates on individual peaks *with* background subtraction.

Assuming the prior spin/parity assignments of the state at 5561 keV to be correct (see below), Weisskopf estimates would seem to give only one reasonable option for the spin of the state of the new isomer, namely, 19. A lower spin would open the possibility of fast quadrupole decays; with a higher spin, one should expect a millisecond (or longer) half-life for a 1651 keV γ decay to a 16^+ state. Assigning the above spin, the reduced $E3$ and $M3$ transition strengths are 0.28 and 12 W.u., respectively. The latter exceeds the recommended upper limit for such a transition given in Ref. [30] by 20%. The corresponding $E1$ and $M1$ Weisskopf strengths for a 106 keV transition are 0.3 and 10 μW.u., respectively. Again the data would appear to support a transition of electric character, with retarded $E1$ transitions as low as 10^{-7} W.u. being fairly common, while $M1$ transitions with strengths of 10^{-5} W.u. are less so [30]. Hence we tentatively assign a spin and parity of 19^- to the new isomer.

In order to compare results with theoretical expectations, two different SM calculations were carried out using the code OXBASH [31]. The first—henceforth known as P1G9 and illustrated in the center of Fig. 4—used only the empirical shell-model interaction of Gross and Frenkel [4] (GF) in the $\pi\nu(p_{1/2}, g_{9/2})$ model space. This is a fit to experimental level schemes and binding energies and extrapolates proton and neutron single-hole energies (SHE) to ^{100}Sn. This is the same calculation as found in Fig. 5(b) of Ref. [7] but here we include several additional states. The second—referred to as F5PG9 and shown at the right of Fig. 4—is based on the same interaction for the $\pi\nu(p_{1/2}, g_{9/2})$ model space but was augmented by the $\pi\nu(f_{5/2}, p_{3/2})$ model space using an interaction derived from the CD-Bonn nucleon-nucleon potential [32]. Core polarization has been corrected for following the many-body approach outlined in Ref. [33] assuming a ^{56}Ni core, with the two-body matrix elements (TBME) scaled down by $(\frac{56}{100})^{1/3}$. This interaction was tuned to reproduce the experimental $p_{3/2}$ and $f_{5/2}$ SHE in ^{88}Sr and the extrapolated SHE for all valence orbits in ^{100}Sn [34]. As the GF interaction was empirically fitted to the restricted model space, it has to be corrected for the extended space to avoid "double counting" of interaction strength which is most severe in the $T = 1$ pairing channel. Therefore, all $I^\pi = 0^+$ GF TBME were reduced by 540 keV, keeping the multiplet monopole unchanged. Moreover, all nondiagonal TBME in the GF space were reduced to 50%. Transition rates were calculated using typical effective charges for the GF space of 1.72e and 1.44e [5] and alternatively 1.5e and 0.5e for protons and neutrons, respectively. For $E2$ transitions, the latter might be more appropriate for the extended F5PG9 model space which allows $E3$ and $M2$ transitions, while $E1$ is still excluded.

In both calculations the yrast states up to the 14^+ isomer are well reproduced. Above this isomer, the first question relates to the ordering and spin-parities of the states decaying via the 267 and 408 keV γ rays. In both cases the 15^+ and 16^+ states are the only states that seem reasonable with gaps in excess of 1500 keV between the 16^+ state and the next positive-parity state, while the negative-parity states are nonyrast by several hundred kilo-electron-volts. In the F5PG9 model space, the gap between the 15^+ and 16^+ states has decreased, while the 14^+ to 15^+ gap has increased, which matches the adopted order of the 408 and 267 keV transitions better than the P1G9 calculation. It is, however, the original P1G9 calculations that better match experiment for the absolute excitation energy of the proposed 16^+ state. It should be noted here that the P1G9 calculations reproduce the evolution of the $N = 48$ yrast states very well with the exception of the (16^+) in ^{92}Ru, where the (16^+_2) state seems to better fit the systematics (see Ref. [8], and references therein).

The most notable difference between the two models is the lowering of the negative-parity states with the inclusion of np-nh excitations from the negative-parity $f_{5/2}$ and $p_{3/2}$ orbitals. This yields better agreement for the excitation energy of the lowest 5^- state compared to the original P1G9 calculation though the reduction in energy is slightly too large. The sequence of high-spin states of both parities is generally well reproduced in both approaches, the key exception being the reversed order of the 17^- and 19^- states in the F5PG9 calculation, the former of which is lower in energy by about 80 keV. This is within the uncertainty of the shell-model prediction and possibly due to insufficient correction of the "double counting" of interaction strength and/or the lack of

inclusion of excitations across the $N = 50$ shell gap. The latter was seen to be important in reproducing the isomerism of the (21^+) state in ^{94}Ag [8,13]. In the P1G9 calculation, the 19^- state has a pure $(\pi p_{1/2}^{-1} g_{9/2}^{-3})_{11} \otimes (\nu g_{9/2}^{-2})_8$ configuration and corresponds to the maximum-spin negative-parity state allowed in the space; in the F5PG9 calculation this remains the dominant configuration (89.5%) but is supplemented by small admixtures of $(\pi p_{3/2}^{-1} g_{9/2}^{-3}) \otimes (\nu g_{9/2}^{-2})$ (6.3%) and $(\pi f_{5/2}^{-1} g_{9/2}^{-3}) \otimes (\nu g_{9/2}^{-2})$ (4.0%).

An alternative interpretation for the isomerism—that the state at 7212 is actually a 17^- state that is fed by an unseen, isomeric, low-energy, highly converted transition from a higher lying 19^- state—cannot be firmly ruled out from the data. However, the comparable branching ratios for the transitions from the state at 7212 keV to the states at 5561 and 7106 keV seems improbable for transitions that are of the same multipolarity but differ by an order of magnitude in energy. Since this argument would apply even if the state at 7106 were the 17^+ state and both calculations support the assignment of 16^+ for the state at 5561 keV, we discount this possibility.

SM-reduced transition strengths for observed and predicted (but not observed) transitions are listed in Table I for the two choices of effective charges. It appears that the $14^+ \rightarrow 12^+$ strength is better reproduced by the smaller polarization charge which is partly due to the extended model space. The $19^- \rightarrow 16^+$ $E3$ transition is mainly a proton $g_{9/2} \rightarrow p_{3/2}$ stretched $\Delta I = \Delta l = 3$ transition which is better reproduced by a larger effective charge. A similar feature has been observed in higher major shells above ^{132}Sn and ^{208}Pb for ^{134}Te and ^{210}Po for corresponding $h_{11/2} \rightarrow d_{5/2}$ and $i_{13/2} \rightarrow f_{7/2}$ transitions [35].

In summary, a new high-spin isomeric state with a half-life of 197(22) ns has been discovered in the $N = Z + 2$ nuclide ^{94}Pd. We tentatively assign it as a (19^-) state with dominant configuration $(\pi p_{1/2}^{-1} g_{9/2}^{-3})_{11} \otimes (\nu g_{9/2}^{-2})_8$ and both $E1$ and $E3$ decay branches. The present results reveal the importance of including the well-bound $f_{5/2}$ and $p_{3/2}$ orbits for understanding the decay properties of high-spin isomers in the vicinity of ^{100}Sn. Such isomers and their decay properties provide an excellent testing ground for empirical interactions and model spaces and form an important step in the development and understanding of proton-neutron interactions in nuclei.

The authors would like to thank the European Gammapool. This work has been supported by the UK STFC, the German BMBF under Contracts No. 06KY205I, No. 06KY9136I, and No. 06MT9156, the Swedish Research Council, and the DFG cluster of excellence *Origin and Structure of the Universe*.

[1] H. Schatz *et al.*, Phys Rep. **294**, 167 (1998).
[2] H. Grawe and M. Lewitowicz, Nucl. Phys. A **693**, 116 (2001).
[3] H. Grawe, in *Euroschool Lectures on Physics with Exotic Beams*, edited by J. Al-Khalili and E. Roeckl, Springer Lecture Notes in Physics, Vol. 1 (Springer, Berlin, 2004), p. 33.
[4] R. Gross and A. Frenkel, Nucl. Phys. A **267**, 85 (1976).
[5] D. Rudolph, K. Lieb, and H. Grawe, Nucl. Phys. A **597**, 298 (1996).
[6] H. Grawe, A. Blazhev, M. Górska, R. Grzywacz, H. Mach, and I. Mukha, Eur. Phys. J. A **27**, SO1, 257 (2006).
[7] M. La Commara *et al.*, Nucl. Phys. A **708**, 167 (2002).
[8] C. Plettner *et al.*, Nucl. Phys. A **733**, 20 (2004).
[9] I. Mukha *et al.*, Phys. Rev. C **70**, 044311 (2004).
[10] I. Mukha *et al.*, Phys. Rev. Lett. **95**, 022501 (2005).
[11] I. Mukha *et al.*, Nature (London) **439**, 298 (2006).
[12] O. L. Pechenaya *et al.*, Phys. Rev. C **76**, 011304(R) (2007).
[13] K. Kaneko, Y. Sun, M. Hasegawa, and T. Mizusaki, Phys. Rev. C **77**, 064304 (2008).
[14] A. Kankainen *et al.*, Phys. Rev. Lett. **101**, 142503 (2008).
[15] J. Cerny, D. M. Moltz, D. W. Lee, K. Peräjärvi, B. R. Barquest, L. E. Grossman, W. Jeong, and C. C. Jewett, Phys. Rev. Lett. **103**, 152502 (2009).
[16] D. G. Jenkins, Phys. Rev. C **80**, 054303 (2009).
[17] M. Górska *et al.*, Z. Phys. A **353**, 233 (1995).
[18] R. Grzywacz *et al.*, Phys. Rev. C **55**, 1126 (1997).
[19] R. Grzywacz, in ENAM 98, *Exotic Nuclei and Atomic Masses*, edited by B. M. Sherill, D. J. Morrissey, and C. N. Davids (AIP, Woodbury, NY, 1998), p. 430.
[20] N. Mărginean *et al.*, Phys. Rev. C **67**, 061301(R) (2003).
[21] A. B. Garnsworthy *et al.*, Phys. Rev. C **80**, 064303 (2009).
[22] H. Geissel *et al.*, Nucl. Instrum. Methods Phys. Res. A **70**, 286 (1992).
[23] S. Pietri *et al.*, Nucl. Instrum. Methods Phys. Res. A **261**, 1079 (2007).
[24] R. Kumar *et al.*, Nucl. Instrum. Methods Phys. Res. **598**, 754 (2009).
[25] R. Brun and F. Rademakers, ROOT — An Object Orientated Data Analysis Framework, Proceedings AIHENP'96 Workshop, Lausanne, Sep. 1996, Nucl. Instrum. Methods Phys. Res. A **389**, 81 (1997), See also [http://root.cern.ch/].
[26] D. Radford, Nucl. Instrum. Methods Phys. Res. A **361**, 297 (1995).
[27] F. James, MINUIT: Function Minimization and Error Analysis Reference Manual, CERN, CERN Geneva, Switzerland, version 94.1 ed. (2000), CERN Program Library Long Writeup D506.
[28] Zs. Podolyák *et al.*, Nucl. Phys. A **722**, C273 (2003).
[29] T. Kibédi, T. Burrows, M. Trzhaskovskaya, P. Davidson, and C. W. Nestor Jr., Nucl. Instrum. Methods Phys. Res. A **589**, 202 (2008).
[30] P. Endt, At. Data Nucl. Data Tables **26**, 47 (1981).
[31] B. Brown, A. Etchegoyen, N. Godwin, W. Rae, W. Richter, W. Ormand, E. Warburton, J. Winfield, L. Zhao, and C. Zimmerman, OXBASH for Windows, MSU-NSCL Report No. 1289, 2004.
[32] R. Machleidt, Phys. Rev. C **63**, 024001 (2001).
[33] M. Hjorth-Jensen, T. Kuo, and E. Osnes, Phys. Rep. **261**, 125 (1995).
[34] H. Grawe, K. Langanke, and G. Martínez-Pinedo, Rep. Progr. Phys. **70**, 1525 (2007); H. Grawe, R. Schubart, K. H. Maier, D. Seweryniak, and OSIRIS/NORDBALL Collaborations, Phys. Scr. T **56**, 71 (1995).
[35] J. P. Omtvedt, H. Mach, B. Fogelberg, D. Jerrestam, M. Hellström, L. Spanier, K. I. Erokhina, and V. I. Isakov, Phys. Rev. Lett. **75**, 3090 (1995).

PROTON-RICH NUCLEI STUDIED WITH RISING*

D. Rudolph

on behalf of the Stopped-Beam RISING Collaboration

Department of Physics, Lund University, 22100 Lund, Sweden

(Received February 7, 2011)

During the years 2006 to 2009, Rare Isotope Spectroscopic INvestigations at GSI (RISING) have focused on high-resolution γ-ray spectroscopy of exotic nuclear species at rest: following unambiguous discrimination and identification by the FRagment Separator (FRS) and its suite of detectors, the nuclei of interest were implanted in either a passive stopper or a stack of silicon detectors to allow for measurements of delayed ion–$\gamma(\gamma)$ or ion–β–$\gamma(\gamma)$ correlations. Results concerning experiments along the $N \sim Z$ line are summarised.

DOI:10.5506/APhysPolB.42.567
PACS numbers: 21.60.Cs, 23.20.–g, 25.70.Mn, 27.40.+z

1. Introduction

The relevance of isomeric or metastable states is an undisputed facet of nuclear structure investigations. Simply their existence but even more their decay modes continue to be valuable sources and constraints on contemporary models of the atomic nucleus. In fact, the combination of isotope-selective devices, high-resolution γ-ray spectroscopy, and pixellated charged-particle detection devices allows one to tag isomers and determine their often unusual and sometimes unexpected decay modes, which in turn reveals the first concise information on nuclei far from the line β stability — based upon samples of fewer than a thousand nuclei.

The isospin degree of freedom opens up, as soon as such investigations are directed at nuclei at or beyond the $N = Z$ line, thereby passing the doubly-magic fixed points ^{40}Ca and ^{56}Ni on the road to ^{100}Sn. Here, β-delayed

* Presented at the Zakopane Conference on Nuclear Physics "Extremes of the Nuclear Landscape", August 30–September 5, 2010, Zakopane, Poland.

γ rays are of specific interest as they delineate weak but often decisive decay paths relevant for the description of isospin symmetry and, more importantly, isospin-symmetry breaking [1]. Figure 1 highlights the various physics topics of the RISING Stopped-Beam campaign.

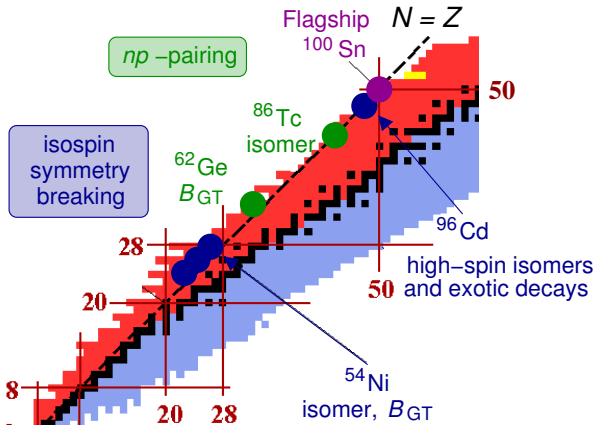

Fig. 1. Sketch of the chart of nuclides with the main isotopes of the $N \sim Z$ experiments within the RISING Stopped Beam Campaign marked.

2. Experiments and methods

The experiments discussed here have all been performed at the GSI Helmholtzzentrum für Schwerionenforschung GmbH at Darmstadt, Germany. Primary beams with intensities up to $\sim 10^9$ particles per second and energies of typically 0.5–1.0 GeV per nucleon are provided by the SIS18 and impinge on fragmentation targets at the entrance of the FRS. The latter transports and separates the isotopes of interest, with event-by-event identification of mass, A, and proton number, Z, ensured by its standard suite of detectors [2]. At the final focus of the FRS, the nuclei are implanted into either a passive piece of plastic or metal or stacks of double-sided silicon strip detectors [3], which are surrounded by 15 former EUROBALL CLUSTER detectors [4], *i.e.* a total of 105 large-volume germanium crystals. In conjunction with digital electronics, this set-up provides a world-unique combination of isotope selectivity and sensitivity for high-resolution γ-ray spectroscopy in the range 50 keV $\leq E_\gamma \leq$ 6 MeV [5]. A typical example, namely the γ decay of two isomers in ^{43}Ti, is depicted in Fig. 2.

More experimental details can also be found in Refs. [6, 7] and the respective physics papers referred to in the following sections.

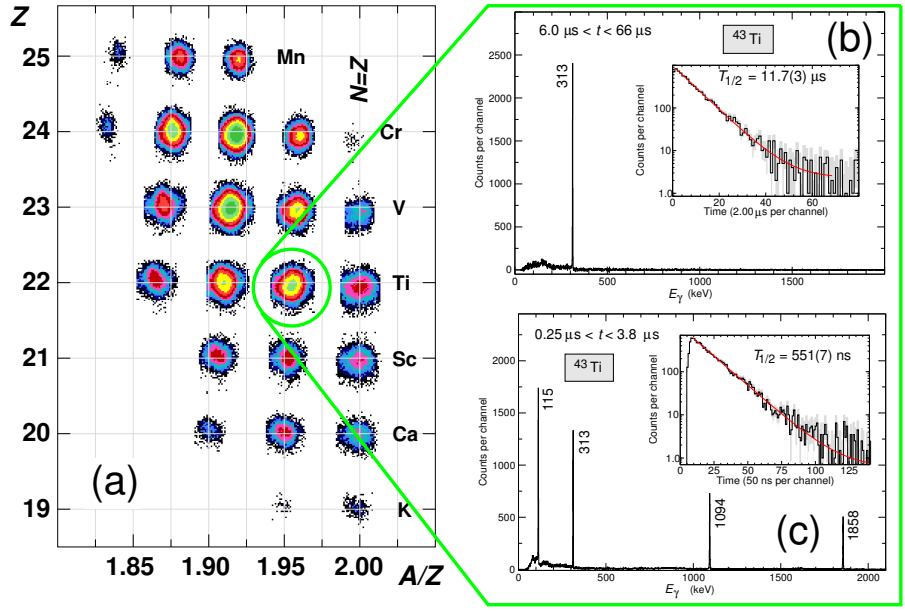

Fig. 2. (a) Example for an isotope-selective identification plot following the fragmentation of a 550-MeV/u ^{58}Ni beam. The γ-ray spectra (parts (b) and (c)) are correlated with at time $t = t_0$ implanted ^{43}Ti nuclei within different periods $[t_1, t_2]$. The insets provide the respective decay curves of the transitions depopulating the two isomeric states in ^{43}Ti.

3. Results and discussion

3.1. Mirror isomers near ^{56}Ni

The microscopic understanding of so-called mirror-energy differences (MED), *i.e.* differences in excitation energies of analogue states in mirror nuclei, has increased significantly throughout the last decade [1, 8]. The most reliable testing ground has been the *fp*-shell, and in particular nuclei located between ^{40}Ca and ^{56}Ni, where MED values call for an isospin-symmetry breaking part originating from the strong force, especially in the $T = 1$, $J = 2$ channel [9]. This proposal could be extended by the identification of a core-excited 10^+ isomer in ^{54}Ni, which mirrors a well-known 10^+ isomer in ^{54}Fe [10]. Moreover, this high-spin isomer revealed a rather intense discrete-energy $\ell = 5$ proton decay branch into the first excited $I^\pi = 9/2^-$ state of ^{53}Co, thereby taking this decay mode home to its origins [11, 12]. The high-statistics experiment on ^{54}Ni allowed also the discrimination of a short-lived $3/2^-$ mirror isomer in ^{53}Co itself: This is due to an *in situ* production inside the passive beryllium stopper by means of secondary fragmentation [13].

Another facet of this region of the chart of nuclides is the possibility to do theoretical 'shell-model spectroscopy', *i.e.* a number of reliable and profound shell-model interactions allow for detailed studies of the fp-shell nuclei. Focusing on states with rather pure configurations predicted by *all* such interactions allows us, for example, to examine effective charges in greater detail. Figure 3 provides the present status, which strongly hints at an orbital dependency [14, 15, 16, 17].

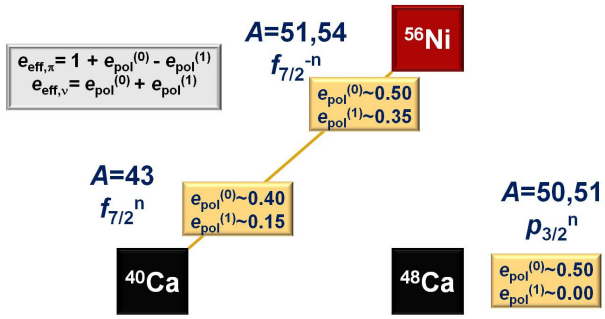

Fig. 3. Effective charges needed to reproduce decay strengths of specific states in the fp shell-model space. See text and Refs. [14, 15, 16] for details.

3.2. Gamow–Teller strength and charge exchange reactions

A fascinating way to probe isospin symmetry is to compare and relate Gamow–Teller (GT) strengths in β decay with those measured via charge-exchange reactions. Assuming a set of isobaric analogue states, GT decays between parent mirror nuclei (*e.g.*, ^{54}Ni and ^{54}Fe) and a common daughter nucleus (here: ^{54}Co) should reveal identical strength — in the absence of isospin mixing. Recent high-resolution (^{3}He,t) charge exchange reactions have been performed at RCNP Osaka [18, 19] on a series of $T = 1$ fp-shell target nuclei, and the corresponding $\beta\gamma$ coincidence decay measurements on ^{42}Ca, ^{46}Cr, ^{50}Fe, and ^{54}Ni have been performed within the RISING Active-Stopper campaign in 2008. Preliminary results are summarised in Ref. [20] and show, amongst others, the experimental RISING power by allowing the clean observation of weak γ-ray transitions with energies $E_\gamma > 5$ MeV.

3.3. Neutron–proton pairing in mass $A = 62$

The search for enhanced proton–neutron pair correlations in $N \sim Z$ nuclei continues to be of interest. Within the RISING Active-Stopper campaign, the β decay of the $N = Z - 2$ nucleus ^{62}Ge was studied, with the focus lying on GT branches into excited 1^+ states in the odd–odd $N = Z$ daughter ^{62}Ga [21] next the dominant $0^+ \rightarrow 0^+$ superallowed Fermi decay.

The idea is visualised in Fig. 4: In light nuclei, considerable GT strength can by explained by the Wigner SU(4) symmetry, which is broken by the spin-orbit splitting in heavier nuclei. This tends to lead to a fragmentation of GT strength but might be restored by a proton–neutron condensate. Arising from an IBM-4 concept [22,23], a survival of such significant proton–neutron pair correlations in medium-mass nuclei may result in enhanced GT transitions into the low(est) lying $T = 0$, $I^{\pi} = 1^{+}$ states. This is due to a predicted low-lying collective 1^{+} neutron–proton state in the odd–odd $N = Z$ nucleus, which is fed by a collective, superallowed GT transition when changing either a $T = 1$ *pp*-boson into a $T = 0$ *pn* boson, or a $T = 0$ *pn*-boson into a $T = 1$ *nn* boson.

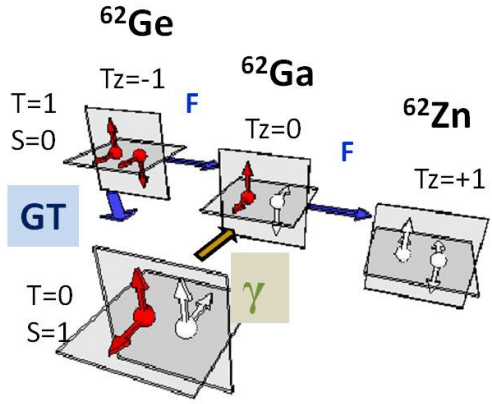

Fig. 4. Scheme of the decay path of the 0^{+} ground state of the even–even $T_z = -1$ nucleus ^{62}Ge: Either via a superallowed Fermi decay into the ground state of ^{62}Ga, or a Gamow–Teller 'bypass' followed by β-delayed $1^{+} \rightarrow 0^{+}$ γ-ray transitions [24].

In the experiment, about 16000 ^{62}Ge nuclei were implanted into the RISING Active Stopper [3]. Previous half-life measurements are nicely confirmed by correlations with subsequent β decays of ^{62}Ga. A number of γ rays are observed in coincidence with the β decays of ^{62}Ge as well, but there is no apparent preference in feeding the lowest known 1^{+} state in ^{62}Ga [24].

3.4. Isomers in odd–odd $N = Z$ nuclei

Using the fragmentation of a primary ^{107}Ag beam, the low-lying structures of a number of $N \sim Z$ nuclei in the mass $A = 80$–90 regime have been determined. The main focus lies on the competition of isospin $T = 0$ and $T = 1$ states in the hitherto heaviest odd–odd $N = Z$ nuclei with known excited states: ^{82}Nb and ^{86}Tc [25,26,27].

As shown in Fig. 5 (a), γ-ray transitions at 124, 418, and 638 keV are associated with the decay of an isomeric state in ^{82}Nb. They closely resemble the $4^+ \rightarrow 2^+ \rightarrow 0^+$ cascade in the $T_z = 1$ neighbour ^{82}Zr [28], when starting from an $I = 5$ state depopulated by the 124-keV low-energy transition. This interpretation is supported by, for instance, Total Routhian Surface calculations, which predict rather soft triaxial shapes for both ^{82}Nb and ^{82}Zr. Though similar, the spin and parity of the isomeric state in ^{86}Tc is somewhat less well defined, *i.e.* there are possible solutions for both a 6^+ (K-isomer) or 5^- scenario [27, 29]. Nevertheless, also in the case of ^{86}Tc the $T = 1$ states are clearly favoured in energy, providing a consistent picture for a series of odd–odd $N = Z$ nuclei in the $f_{5/2}pg_{9/2}$ shell.

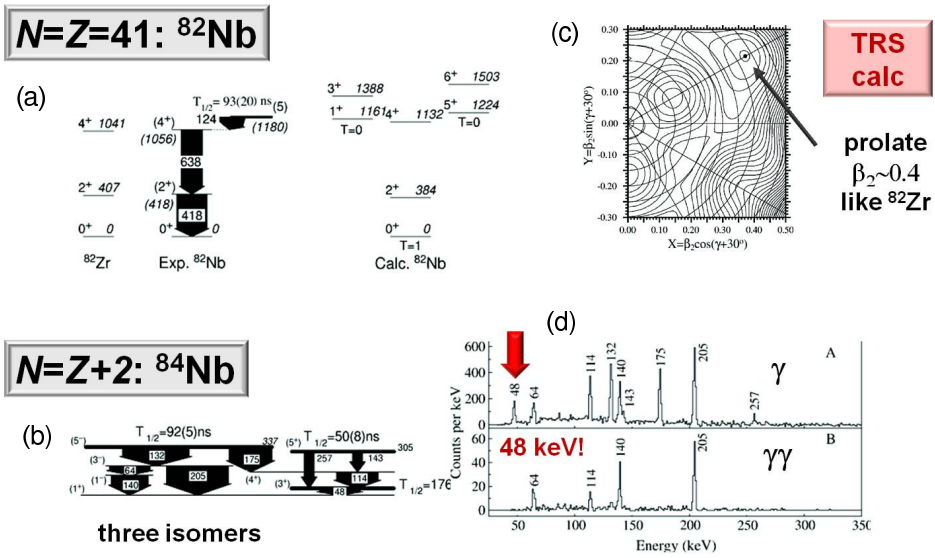

Fig. 5. Isomeric decay schemes of $N = Z = 41$ ^{82}Nb (a) and its $N = Z + 2 = 43$ odd–odd neighbour ^{84}Nb (b). Part (c) illustrates a shape prediction of a total Routhian surface (TRS) calculation for ^{82}Nb. ^{84}Nb-ion correlated, delayed γ-ray and $\gamma\gamma$-coincidence spectra are displayed in part (d). Taken from Ref. [29].

In addition to the two $N = Z$ nuclei, a number of isomeric states are detected in neighbouring nuclei such as ^{84}Nb and ^{87,88}Tc [29]. In combination with existing information from fusion-evaporation reaction studies [30, 31, 32] further light is shed on their low-lying structure: Shape hindrance is thought responsible for the isomerism in ^{87}Tc, while shell-model calculations propose a low-lying isomeric 4^+ state consistent with the observations in ^{88}Tc. The low-lying decay scheme of ^{84}Nb comprises three isomeric states and is shown in Fig. 5 (b). Compared to $N = Z$ ^{82}Nb, the striking but

expected difference is the missing *np*-pairing gap. Secondly, the γ-ray spectra on the right stress the RISING experimental access to low-energy γ-rays and $\gamma\gamma$-coincidences [29].

3.5. High-spin isomers south–west of ^{100}Sn

High-spin isomers in $N \sim Z$, mass $A \geq 90$ nuclei are a rich source of information for the shell structure at and near ^{100}Sn. Due to the strong neutron–proton pairing interaction matrix elements, the underlying origins of these isomers are aligned configurations of the type $\nu(g_{9/2})^{-n} \times \pi(g_{9/2})^{-m}$. The most prominent example is the anticipated 21^+ state in ^{94}Ag with $n = m = 3$, which is revealed to have a half-life of $T_{1/2} \sim 0.4$ s and various decay modes [33, 34, 35]. Negative-parity isomers typically involve an odd particle or hole in the $p_{1/2}$ orbital as observed in, for example, ^{94}Pd [36, 37].

Another set of isomers, which are subject to core-excited states, has also been found in the course of the recent RISING campaign. Examples are anticipated 12^+ and 19^+ states in ^{98}Cd [38, 39] and ^{96}Ag [40], respectively. Their origin is similar to the 10^+ states in ^{54}Ni and ^{54}Fe discussed in Sec. 3.1. This is illustrated in Fig. 6 (a). Not only do the energies of the core-excited states tell us about the size of the magic shell gaps at particle numbers 28 and 50, respectively, but the competition between $E2$ and $E4$ branches provides access to the details of the wave functions hence shell-model interactions. Last but not least, the RISING efficiency for high-energy γ-rays is vital for the observation, as can be seen from the delayed γ-ray spectrum attributed to ^{96}Ag in Fig. 6 (b).

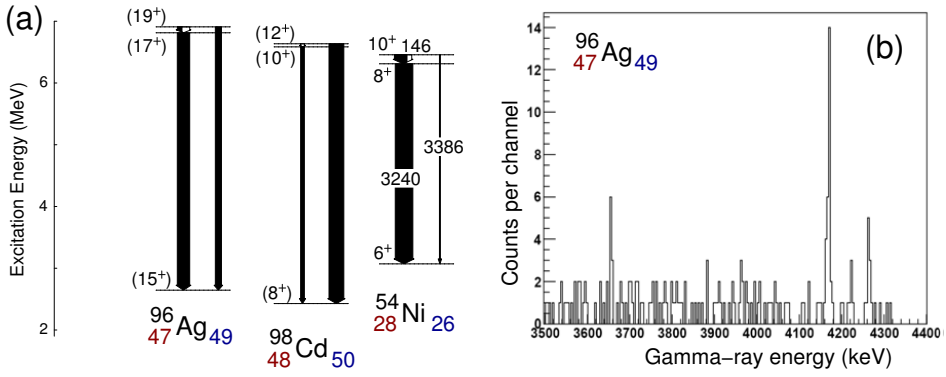

Fig. 6. (a) Comparison of core excited states in ^{96}Ag [40], ^{98}Cd [38, 39], and ^{54}Ni [10]. (b) High-energy portion of the γ-ray spectrum in delayed coincidence with implanted ^{96}Ag nuclei illustrating the respective $(17^+) \rightarrow (15^+)$ $E2$ and $(19^+) \rightarrow (15^+)$ $E4$ transitions in ^{96}Ag.

3.6. Flagging ^{100}Sn

A flagship endeavour was undertaken in 2008 to collect the hitherto most comprehensive knowledge on the decay of the $N = Z = 50$ nucleus ^{100}Sn. Led by the group at TU Munich, the collaboration combined the RISING γ-ray spectrometer with the Silicon IMplantation detector and Beta Absorber (SIMBA) [41]. Compared to all previous experimental investigations [42,43,44], a rate increase in the production of ^{100}Sn from about 1/day to roughly 1/hour was achieved, and a production cross-section of 5–10 pb derived. Due to the significantly increased primary ^{124}Xe beam intensities at GSI, the decay of more than 250 ^{100}Sn nuclei can be detailed [45].

Being the heaviest, stable, self-conjugate doubly-magic nucleus, information on ^{100}Sn is important not just for conventional shell-model approaches: the β^+ decay of ^{100}Sn surely resembles the most pure Gamow–Teller spin-flip transition on the chart of nuclei, namely an almost exclusive branch into a single low-lying $\pi(g_{9/2})^{-1} \times \nu(g_{7/2})^1$ 1^+ state in the daughter ^{100}In, which moreover lies inside the β-decay energy window.

Preliminary results provide a more precise value of the half-life, $T_{1/2}$, which is consistent with earlier numbers [42, 44]. For the first time, a β spectrum is derived, which gives rise to a world-record value of $\log ft < 3$ and, hence, a high B_{GT} strength. Five γ-ray transitions are observed in correlation with the ^{100}Sn β decays, the energies of which call for at least two parallel γ-ray cascades in ^{100}In. The possibility of an isomeric $I^\pi = 6^+$ state in ^{100}Sn has been investigated as well, though unfortunately without obvious success. Eventually, the anticipated isomer decays by direct proton emission as seen in the case of ^{54}Ni [10].

4. Summary and outlook

Undoubtedly, the RISING Stopped Beam campaign has and will significantly advance the understanding of nuclear structure along the $N = Z$ line. Particularly isospin symmetry breaking, *np*-pairing, and extended shell-model studies near doubly-magic ^{56}Ni and ^{100}Sn have been at the focus, and some of the results for the heavier nuclei relate to aspects of nuclear astrophysics. Investigations of the fragmentation reaction process itself have been and will be undertaken as well with the existing $N \sim Z$ data sets [46,47], but cannot be detailed any further here. The same is true for the majority of physics issues, which could only be touched upon briefly in this summary. Details can be found in the respective published or soon to be published manuscripts and PhD theses.

In conclusion, the basis of the great success of this RISING campaign lies in the unprecedented and unique capabilities of combining high-intensity, relativistic primary beams with an event-by-event 'isotope-identifier' followed by a highly efficient, high-resolution spectroscopy set-up with decent granularity.

While the RISING project came to an end in 2009, its successor PRESPEC is in place at the moment, which has two main aims: to prepare the nuclear structure community for the opportunities at FAIR in the mid-term future, while using existing and optimising new equipment to tackle more of the unknowns on the chart of nuclei — the physics of the PRESPEC Decay Campaign opened with a workshop as early as January 2011 in Brighton [48].

This paper is presented on behalf of the Stopped Beam RISING Collaboration. Special thanks go to my colleagues A. Blazhev, P. Boutachkov, T. Faestermann, A. Gadea, A. Garnsworthy, B. Rubio, and R. Wadsworth for providing figures and letting me use previously unpublished data and results, and W. Gelletly for the fine tuning of the manuscript. This work was partially supported by the Swedish Science Council and the European Commission (Contract 506065) (EURONS). Finally, I would like to thank the Organisers of the conference for their fantastic arrangements.

REFERENCES

[1] M.A. Bentley, S.M. Lenzi, *Prog. Part. Nucl. Phys.* **59**, 497 (2007).
[2] H. Geissel *et al.*, *Nucl. Instrum. Methods* **B70**, 286 (1992).
[3] R. Kumar *et al.*, *Nucl. Instrum. Methods* **A598**, 754 (2009).
[4] J. Eberth *et al.*, *Nucl. Instrum. Methods* **A369**, 135 (1996).
[5] S. Pietri *et al.*, *Nucl. Instrum. Methods* **B261**, 1079 (2007); *Acta Phys. Pol. B* **38**, 1255 (2007).
[6] P.H. Regan *et al.*, *Nucl. Phys.* **A787**, 491c (2007).
[7] D. Rudolph *et al.*, *Eur. Phys. J. Special Topic* **150**, 173 (2007).
[8] J. Ekman, C. Fahlander, D. Rudolph, *Mod. Phys. Lett.* **A20**, 2977 (2005).
[9] A.P. Zuker *et al.*, *Phys. Rev. Lett.* **89**, 142502 (2002).
[10] D. Rudolph *et al.*, *Phys. Rev.* **C78**, 021301(R) (2008).
[11] K.P. Jackson *et al.*, *Phys. Lett.* **B33**, 281 (1970).
[12] J. Cerny *et al.*, *Phys. Lett.* **B33**, 284 (1970).
[13] D. Rudolph *et al.*, *Eur. Phys. J.* **A36**, 131 (2008).
[14] R. Hoischen *et al.*, *J. Phys. G* **38**, 035104 (2011).
[15] R. du Rietz *et al.*, *Phys. Rev. Lett.* **93**, 222501 (2004).

[16] J.J. Valiente Dobón *et al.*, *Phys. Rev. Lett.* **102**, 242502 (2009).
[17] H.L. Ma *et al.*, *Phys. Rev.* **C80**, 014316 (2009).
[18] T. Adachi *et al.*, *Nucl. Phys.* **A788**, 70c (2007).
[19] Y. Fujita *et al.*, *J. Phys. G* **35**, 014041 (2008).
[20] F. Molina *et al.*, *AIP Conf. Proc.* **1265**, 49 (2010).
[21] D. Rudolph *et al.*, *Phys. Rev.* **C69**, 034309 (2004).
[22] F. Iachello, Proc. Int. Conf. Perspectives for the IBM, Padova, Italy, 1994.
[23] P. van Isacker, *J. Phys. Conf. Series* **20**, 131 (2005).
[24] A. Gadea *et al.*, to be published.
[25] A.B. Garnsworthy *et al.*, *Acta Phys. Pol. B* **38**, 1265 (2007).
[26] L. Cáceres *et al.*, *Acta Phys. Pol. B* **38**, 1271 (2007).
[27] A.B. Garnsworthy *et al.*, *Phys. Lett.* **B660**, 326 (2008); *Erratum-ibid.* **B668**, 460 (2008).
[28] D. Rudolph *et al.*, *Phys. Rev.* **C56**, 98 (1997).
[29] A.B. Garnsworthy *et al.*, *Phys. Rev.* **C80**, 064303 (2009).
[30] C.J. Gross *et al.*, *Phys. Rev.* **C43**, R5 (1991).
[31] N. Mărginean *et al.*, *Eur. Phys. J.* **A4**, 311 (1999).
[32] D. Rudolph *et al.*, *J. Phys. G* **17**, L113 (1991).
[33] M. La Commara *et al.*, *Nucl. Phys.* **A708**, 167 (2002).
[34] C. Plettner *et al.*, *Nucl. Phys.* **A733**, 20 (2004).
[35] I. Mukha *et al.*, *Phys. Rev. Lett.* **95**, 022501 (2005).
[36] R. Wadsworth *et al.*, *Acta Phys. Pol. B* **40**, 611 (2009).
[37] T. Brock *et al.*, *Phys. Rev.* **C82**, 061309 (R).
[38] A. Blazhev *et al.*, *J. Phys. Conf. Series* **205**, 012035 (2010).
[39] N. Braun *et al.*, to be published.
[40] P. Boutachkov *et al.*, to be published.
[41] Ch. Hinke, GSI Dissertation, 2010-15.
[42] R. Schneider *et al.*, *Z. Phys.* **A348**, 241 (1994).
[43] M. Lewitowicz *et al.*, *Phys. Lett.* **B332**, 20 (1994).
[44] D. Bazin *et al.*, *Phys. Rev. Lett.* **101**, 252501 (2008).
[45] Ch. Hinke *et al.*, to be published.
[46] S. Myalski *et al.*, *Acta Phys. Pol. B* **38**, 1277 (2007).
[47] R. Hoischen *et al.*, to be published.
[48] `http://npg.dl.ac.uk/PRESPEC-11`

First observation of the decay of a 15^- seniority $v = 4$ isomer in ^{128}Sn

S. Pietri,[1] A. Jungclaus,[2,*] M. Górska,[1] H. Grawe,[1] M. Pfützner,[3] L. Cáceres,[1,4,†] P. Detistov,[5] S. Lalkovski,[5] V. Modamio,[2,4] Z. Podolyák,[6] P. H. Regan,[6] D. Rudolph,[7] J. Walker,[2,4] E. Werner-Malento,[3] P. Bednarczyk,[8] P. Doornenbal,[1,‡] H. Geissel,[1] J. Gerl,[1] J. Grebosz,[8] I. Kojouharov,[1] N. Kurz,[1] W. Prokopowicz,[1] H. Schaffner,[1] H. J. Wollersheim,[1] K. Andgren,[9] J. Benlliure,[10] G. Benzoni,[11] A. M. Bruce,[12] E. Casarejos,[10,§] B. Cederwall,[9] F. C. L. Crespi,[11] B. Hadinia,[9] M. Hellström,[7] R. Hoischen,[1,7] G. Ilie,[13,‖] A. Khaplanov,[9] M. Kmiecik,[8] R. Kumar,[14] A. Maj,[8] S. Mandal,[15] F. Montes,[1] S. Myalski,[8] G. Simpson,[16] S. J. Steer,[6] S. Tashenov,[1] and O. Wieland[11]

[1]*Gesellschaft für Schwerionenforschung (GSI), D-64291 Darmstadt, Germany*
[2]*Instituto de Estructura de la Materia, CSIC, E-28006 Madrid, Spain*
[3]*Faculty of Physics, University of Warsaw, PL-00681 Warsaw, Poland*
[4]*Departamento de Física Teórica, Universidad Autónoma de Madrid, E-28049 Madrid, Spain*
[5]*Faculty of Physics, University of Sofia, BG-1164 Sofia, Bulgaria*
[6]*Department of Physics, University of Surrey, Guildford, GU2 7XH, United Kingdom*
[7]*Department of Physics, Lund University, S-22100 Lund, Sweden*
[8]*The Henryk Niewodniczaski Institute of Nuclear Physics, PL-31342 Cracow, Poland*
[9]*KTH Stockholm, S-10691 Stockholm, Sweden*
[10]*Universidad de Santiago de Compostela, E-175706 Santiago de Compostela, Spain*
[11]*INFN sezione di Milano, I-20133 Milano, Italy*
[12]*School of Engineering, University of Brighton, Brighton, BN2 4GJ, United Kingdom*
[13]*Institut für Kernphysik, Universität zu Köln, D-50937 Köln, Germany*
[14]*Inter University Accelerator Centre, New Delhi, India*
[15]*University of Delhi, New Delhi, India*
[16]*Institut Laue-Langevin, F-38042 Grenoble, France*

(Received 5 November 2010; published 29 April 2011)

Isomeric states in the semimagic $^{128-130}$Sn isotopes were populated in the fragmentation of a ^{136}Xe beam on a ^{9}Be target at an energy of 750 A·MeV. The decay of an isomeric state in ^{128}Sn at an excitation energy of 4098 keV has been observed. Its half live has been determined to be $T_{1/2} = 220(30)$ ns from the time distributions of the delayed γ rays emitted in its decay. $\gamma\gamma$ coincidence relations were analyzed in order to establish the decay pattern of the newly established state toward the known (7^-) and (10^+) isomers at excitation energies of 2092 and 2492 keV, respectively. Based on a comparison with results of state-of-the-art shell-model calculations the new isomeric state is proposed to have the $\nu h_{11/2}^{-3} d_{3/2}^{-1}$ configuration with the four neutron holes in ^{132}Sn maximally aligned to a total spin of $I^\pi = 15^-$.

DOI: 10.1103/PhysRevC.83.044328 PACS number(s): 21.10.Tg, 21.10.Ky, 21.60.Fw, 27.60.+j

I. INTRODUCTION

The series of semimagic Sn isotopes have long attracted a particular interest in nuclear structure research both from an experimental as well as a theoretical point of view. With the 33 experimentally accessible isotopes between the two double-magic cornerstones ^{100}Sn and ^{132}Sn, it allows for systematic and stringent tests of the validity of theoretical models across an entire span of a large major neutron shell and beyond, from the proton dripline with $N = Z$ to the isotope which has 10 neutrons more than the most neutron-rich stable tin isotope. In the upper half of the major neutron shell the filling of the unique-parity $h_{11/2}$ orbital gives rise to the observation of seniority isomers. Indeed in all even Sn isotopes in the range $A = 116$–130 10^+ $\nu h_{11/2}^{-2}$ isomeric states have been observed using deep-inelastic reactions, the β decay of long-lived isomeric states in the In isotopes, as well as fragmentation and fission at relativistic energies [1–4]. In the odd isotopes the experimental information on the corresponding $27/2^-$ $\nu h_{11/2}^{-3}$ isomer has been recently extended up to the ^{129}Sn isotope [5]. These complete sets of excitation energies as well as decay properties allowed us to study in detail the filling of the $h_{11/2}$ orbital and to determine the effective $E2$ charges. In addition to the $\nu h_{11/2}^{-n}$ states, other long-lived levels involving the $d_{3/2}$ neutron orbital, which is lying close in energy to the $h_{11/2}$ orbit, have been observed in all $A = 116$–130 Sn isotopes. In detail these are $\nu h_{11/2}^{-1} d_{3/2}^{-1}$ states with spin 7^- in the even and $\nu h_{11/2}^{-2} d_{3/2}^{-1}$ levels with spin $23/2^+$ in the odd Sn isotopes. However, what is still lacking is the information from seniority $v > 3$ states involving both orbitals. The purpose of the present article is to report on the identification of the first $v = 4$, $\nu h_{11/2}^{-3} d_{3/2}^{-1}$ isomeric state with spin (15^-) in the nucleus ^{128}Sn.

*Corresponding author: andrea.jungclaus@iem.cfmac.csic.es
†Present address: GANIL, Caen, France.
‡Present address: RIKEN, Japan.
§Present address: Universidad de Vigo, Spain.
‖Present address: Wright Nuclear Structure Laboratory, Yale University, Princeton, NJ.

II. EXPERIMENT AND RESULTS

Isomeric states in the $A = 128$–130 Sn isotopes were populated by means of relativistic fragmentation of a ^{136}Xe beam at an energy of 750 A·MeV on a 4 g/cm^2 thick ^{9}Be target within the RISING campaign at GSI, Darmstadt. The fragment separator (FRS) [6] was set to optimize the transmission of ^{126}Cd and the reaction products were identified ion by ion in the FRS via the measurement of the energy loss, the magnetic rigidity, the positions in the intermediate, and the final focal plane and the time-of-flight between the two. Finally, after being slowed down in an Al degrader, the ions were implanted in a passive stopper in the final focal plane of the FRS. The fraction of nuclei which were populated in an excited isomeric state and also implanted in this state after surviving the flight through the separator then decay to the ground state by γ-ray emission. These γ rays were detected by 15 large volume Ge cluster detectors [7] from the former EUROBALL spectrometer arranged in close geometry around the stopper [8]. With the requirement of a delayed coincidence relationship between the implanted ion and the detected γ ray the radiation can be unequivocally assigned to the decay of an isomeric state of a particular isotope. More details about the experimental setup and the data handling are given in Refs. [9–12] in which results concerning the nuclei ^{127,128,130}Cd and ^{131}In studied in the same experiment have been presented. In total 1.35×10^4 ^{128}Sn, 5.7×10^5 ^{129}Sn, and 4.8×10^5 ^{130}Sn ions have been identified and implanted in the current experiment.

A spectrum of γ rays observed in delayed coincidence with identified and implanted ^{128}Sn ions is shown in Fig. 1(a). The spectrum is dominated by two lines at 79 and 321 keV, respectively, which are known to be emitted in the decay of the $I^\pi = (10^+)$ isomeric state with a half-life of $T_{1/2} = 2.69(23)$ μs [4]. Furthermore, indications of additional lines were found in this spectrum, for example, at an energy of 426 keV. When the time range is limited to the first 1.5 μs after the implantation six previously unobserved γ transitions with energies of 119, 207, 426, 625, 1055, and 1061 keV are clearly identified in the spectrum of Fig. 1(b). They indicate the existence of an additional isomeric state with a half-life

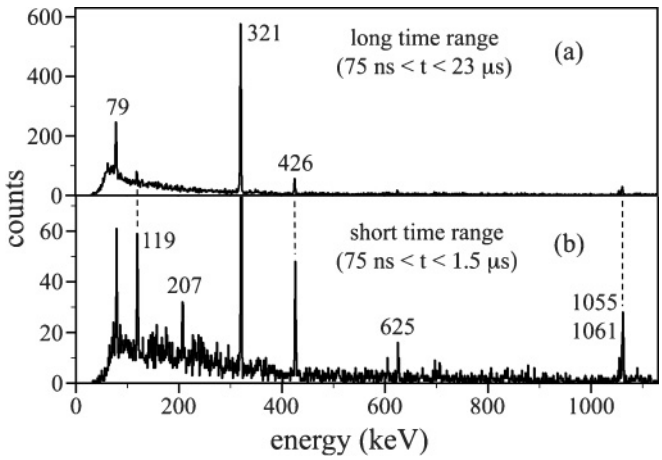

FIG. 1. Delayed γ-ray spectra in coincidence with identified ^{128}Sn ions implanted in the stopper for (a) a long (75 ns–23 μs) and (b) a shorter time range (75 ns $< t <$ 1.5 μs).

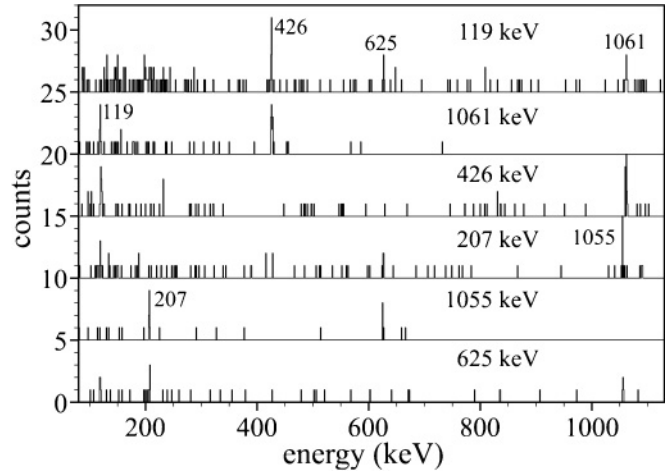

FIG. 2. γ-ray spectra observed in prompt coincidence with the 119, 1061, 426, 207, 1055, and 625 keV transitions, respectively, within the first 1.5 μs after the implantation.

in the submicrosecond range. In order to obtain information about the ordering of the newly observed transitions prompt $\gamma\gamma$ coincidence spectra were sorted for the time range 75 ns $< t <$ 1.5 μs after the implantation. The resulting spectra are shown in Fig. 2. Although the statistics of these spectra is very low there is sufficient evidence that two groups of γ rays, 426–1061 keV and 207–625–1055 keV, are observed in mutual coincidence and therefore form cascades. The 119 keV transition is observed in coincidence with members of both sequences and due to its low energy a natural candidate to be the transition depopulating the isomeric state. It is interesting to note that the sum energies of the three γ rays with 207, 625, and 1055 keV, namely 1887 keV, is equal to the sum of the 426 and 1061 keV transitions plus the known 79 and 321 keV γ rays connecting the (10^+) and (7^-) isomeric states. And indeed, when removing the prompt coincidence condition and opening the time window, the 321 keV γ rays is clearly observed in delayed coincidence with the newly identified 1061 and 426 keV transitions. We therefore place these two transitions on top of the (10^+) state leading to a new level at an excitation energy of 3979 keV and the 207–625–1055 keV cascade in parallel connecting this newly identified level to the (7^-) state at 2092 keV. The relative intensities of the newly identified transitions are summarized in Table I. They have been determined in the delayed singles spectrum to be limited to the first 1.5 μs after the implantation while the intensity of the 426 keV γ ray relative to the 79 and 321 keV transitions has been obtained from the singles spectrum without time condition. We find that the intensity of the 426–1061 keV cascade is about twice that of the 207–625–1055 keV branch. Unfortunately there is no additional experimental information that could help to fix the order of the transitions within the two cascades. The order we propose in Fig. 3 and therefore the position of the intermediate states at 3147, 3553, and 3772 keV consequently is considered to be tentative.

To determine the half-life of the new isomeric state at 4098 keV the time distributions between the ion implantation and the detection of one of the four γ rays with energies of 426,

TABLE I. Energies (E_γ), proposed initial (I_i^π), and final (I_f^π) spin values and relative intensities of the γ transitions observed in a long ($t < 23$ μs) $I_{\rm rel}^l$, respectively short ($t < 1.5$ μs) $I_{\rm rel}^s$, time window after the implantation in the present experiment.

E_γ (keV)	I_i^π	I_f^π	$I_{\rm rel}^l$	$I_{\rm rel}^s$
79	(10^+)	(8^+)	1030(80)[a]	–
119	(15^-)	(13^-)	–	190(25)[a]
207	(13^-)	(11^-)	–	55(10)[a]
321	(8^+)	(7^-)	1110(30)	–
426	(13^-)	(12^+)	100(10)	100(10)
625	(11^-)	(9^-)	–	47(8)
1055	(9^-)	(7^-)	–	33(9)
1061	(12^+)	(10^+)	–	118(14)

[a]Corrected for internal conversion assuming $E2$ multipolarity.

625, 1055, and 1061 keV have been summed and least-squares fitted by a single-exponential decay resulting in a half-life of $T_{1/2} = 220(30)$ ns. Random correlations have been taken into account in this procedure by subtracting the time distributions corresponding to background regions next to the energy peaks under study prior to the fit. The half-life of the known (10^+), 2492 keV isomer has been redetermined from the present data as $T_{1/2} = 3.00(15)$ μs by fitting the time distribution of the 321 keV transition, taking into account the feeding from the newly identified isomeric state at an excitation energy of 4098 keV. This result is in reasonable agreement with the

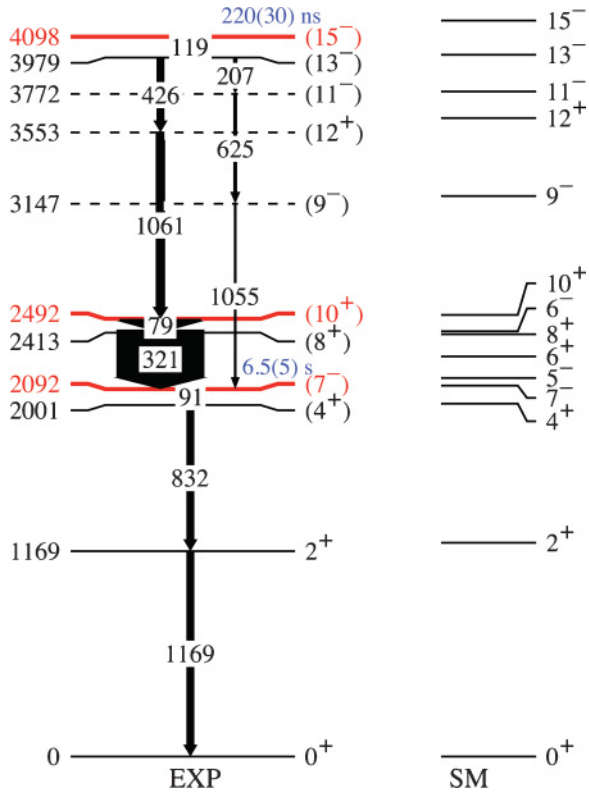

FIG. 3. (Color online) Comparison between the proposed excitation scheme of ^{128}Sn (EXP) with the results of shell-model calculations (SM).

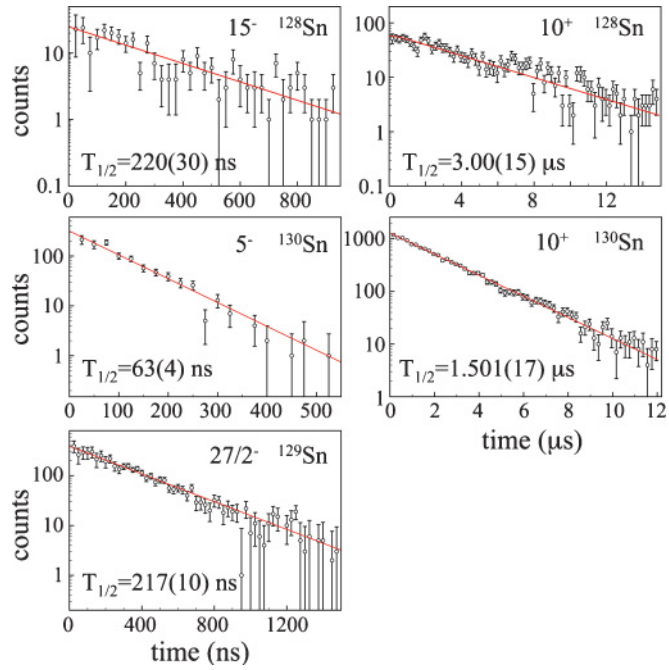

FIG. 4. (Color online) Time distributions between the ion implantation and the detection of one of the 426, 625, 1055, and 1061 keV transitions (15^-), respectively, the 321 keV γ ray (10^+) in ^{128}Sn (top row), one of the 774 and 1221 keV transitions (5^-), respectively, the 393 keV γ ray in ^{130}Sn (middle row), and one of the 145 and 605 keV transitions $(27/2^-)$ in ^{129}Sn (bottom row).

literature value of $T_{1/2}^{\rm lit} = 2.69(23)$ μs [4] and $T_{1/2} = 2.77(22)$ μs [13] deduced from the experimental data discussed in Ref. [14]. Both decay curves including the fits are shown in the top row of Fig. 4.

As mentioned before, besides ^{128}Sn the neighboring isotopes ^{129}Sn and ^{130}Sn were also produced in the present experiment with higher yields. Although no new isomeric states were found in these nuclei the half-lifes of the known $27/2^-$ level in ^{129}Sn and the (10^+) and 5^- isomers in ^{130}Sn were redetermined taking advantage of the increased statistics of the present data set. The corresponding decay curves including the fits are shown in Fig. 4. While the resulting half-lives for the $27/2^-$ state in ^{129}Sn and the (10^+) state in ^{130}Sn, $T_{1/2} = 217(19)$ ns, respectively, $T_{1/2} = 1.501(17)$ μs, agree within the experimental uncertainties with the literature values ($T_{1/2} = 270(70)$ ns, respectively, $T_{1/2} = 1.61(15)$ μs from Refs. [4,5]) a small deviation is observed for the short-lived 5^- isomer in ^{130}Sn. Our value of $T_{1/2} = 63(4)$ ns is slightly larger compared to the $T_{1/2} = 52(3)$ ns reported by Fogelberg *et al.* [4].

III. DISCUSSION

In order to interpret the new experimental information obtained from the present data set for isomeric decays in ^{128}Sn, new shell-model calculations were performed in a model space consisting of the $p_{1/2}$, $g_{9/2}$ for protons and $g_{7/2}$, $s_{1/2}$, $d_{5/2}$, $d_{3/2}$, $h_{11/2}$ for neutrons outside an inert ^{88}Sr core. It is important to note that neither proton excitations across the $Z = 50$ nor neutron excitations across the $N = 82$ gap are

considered in these calculations. The residual interaction is inferred from a realistic G matrix derived from the CD-Bonn nucleon-nucleon potential [15]. Core polarization has been corrected for following the many-body approach outlined in Ref. [16]. Monopole tuning following $A^{-1/3}$ scaling of the two-body matrix elements (TBME) was performed to reproduce the single-hole energies in ^{132}Sn as described in Refs. [5,9]. For the open proton-neutron ($\pi\nu$) space further modifications were introduced that are described in Ref. [12] but do not concern the Sn isotopes except for a -150 keV correction of the $(\nu h^2_{11/2})_{2^+}$ TBME. Modifications of individual TBME were performed maintaining the monopole of the respective multiplet and thus the ^{132}Sn single-hole energies. It should be noted that monopole tuning of the evolution of effective single-particle energies (SPE) from a closed shell nucleus to single-hole energies (SHE) in the next, here from ^{100}Sn to ^{132}Sn, is ambiguous as there are more multiplets (here $\nu\nu$) than SPE/SHE pairs. To minimize the relative shift of individual multiplets, preferably those with a high-spin partner (here $\nu h_{11/2}$) are chosen as a small monopole change creates a large SPE-SHE shift {see e.g., Eq. (2) in Ref. [17]}. The ambiguity may be reduced however by maintaining the seniority driven experimental evolution of $B(E2)$ values with changing occupation n of the high-spin orbital (here $\nu h^n_{11/2}$). Further details will be given in a forthcoming publication [18]. Effective charges of $e_\pi = 1.5e$ and $e_\nu = 0.7e$ were used for protons and neutrons, respectively [5,9]. The calculations were performed with the OXBASH code [19].

The results of the shell-model calculations with respect to the excitation energies are shown in Fig. 3 in comparison to the experimentally observed states. The agreement between experiment and calculations is extremely good for all known states up to the (10^+) isomer at an excitation energy of 2492 keV. This nice agreement together with the fact that the same interaction has already successfully been used in the past to describe other Sn and also Cd isotopes near ^{132}Sn [5,9,12,14,20] encouraged us to use the results of the shell-model calculations as a basis for a tentative spin assignment for the newly observed states above the (10^+) state. In the excitation energy range from 2.5 to 4.2 MeV the shell-model calculation predicts the existence of five states with spins of 9^-, 12^+, 11^-, 13^-, and 15^-. Experimentally two new states at 3979 and 4098 keV have been firmly established and are naturally assigned to the highest two calculated levels with spin 13^- and 15^-. Since the order of the transitions within the two parallel cascades could not be fixed on the basis of experimental information, we propose intermediate states at 3147, 3553, and 3772 keV (see Fig. 3) because of their proximity to the calculated levels at 3115, 3565, and 3700 keV, respectively. These assignments, which of course have to be considered tentative, and the resulting multipolarities of the involved transitions are consistent with the observed intensities summarized in Table I.

Besides excitation energies, reduced transition probabilities for a number of $E2$ and $E3$ transitions involved in the decay of the isomeric states in $^{128-130}$Sn were also calculated. They are compared Table II and Fig. 5 to the values deduced from the half-lives measured in the present work using the conversion coefficients from Ref. [21]. In Fig. 5 experimental and shell model $I \rightarrow I - 2$ $E2$ transition strengths in W.u. are compared for initial states with leading configurations $\nu h^{2,3}_{11/2}$; $I^\pi = 10^+$, $27/2^-$ (upper panel) and $\nu h^n_{11/2} d_{3/2}$, $I^\pi = 7^-$ ($n = 1$), $23/2^+$ ($n = 2$), and 15^- ($n = 3$) (lower panels). Data are from Refs. [5,23] and the present work. The agreement between experimental and theoretical transition probabilities is gratifying and in particular the decay of the newly observed (15^-) isomer is very well described by the shell-model calculation. The $E2$ strengths between high-spin states of rather pure configuration with the effective neutron charge used are in general a little underestimated in agreement with the conclusion drawn in Ref. [5] that a value of 0.85 e might be more appropriate. The $E3$ strengths are predicted to be hindered (see Table II) as they are dominated by the neutron $h_{11/2} \rightarrow d_{5/2}$ single-particle transition with the $d_{5/2}$

TABLE II. Half-lives $T_{1/2}$ of isomeric states in ^{128,129,130}Sn and reduced transition probabilities $B(E\lambda)$ in Weisskopf units of $E2$ and $E3$ transitions observed in their decay. The conversion coefficients α are taken from Ref. [21].

Nucleus	I^π_i	E_x (keV)	$T_{1/2}$		I^π_f	E_γ (keV)		α	$B(E\lambda)$ (W.u.)	
			This work	Literature					This work	SM
^{128}Sn	(10^+)	2492	3.00(15) μs	2.69(23) μs[a]	8^+	$E2$	79	3.69	0.341(17)	0.270
					7^-	$E3$	400	0.046	–	8.77×10^{-3}
	(15^-)	4098	220(30) ns	–	13^-	$E2$	119	0.861	1.51(21)	1.397
					12^+	$E3$	545	0.016	–	1.71×10^{-4}
	7^-	2092		6.5(5) s[b]	4^+	$E3$	91	26.5	0.133(11)[c]	0.0768
^{129}Sn	$27/2^-$	2552	217(19) ns	270(70) ns[d]	$23/2^-$	$E2$	145	0.428	0.735(64)	0.565
^{130}Sn	(10^+)	2435	1.501(17) μs	1.61(15) μs[a]	8^+	$E2$	95	1.91	0.427(5)	0.266
					7^-	$E3$	488	0.023	–	0.0320
	5^-	2085	63(4) ns	52(3) ns[a]	7^-	$E2$	136	0.537	1.16(7)	1.212

[a]From Ref. [4].
[b]From Ref. [22].
[c]From Ref. [23].
[d]From Ref. [5].

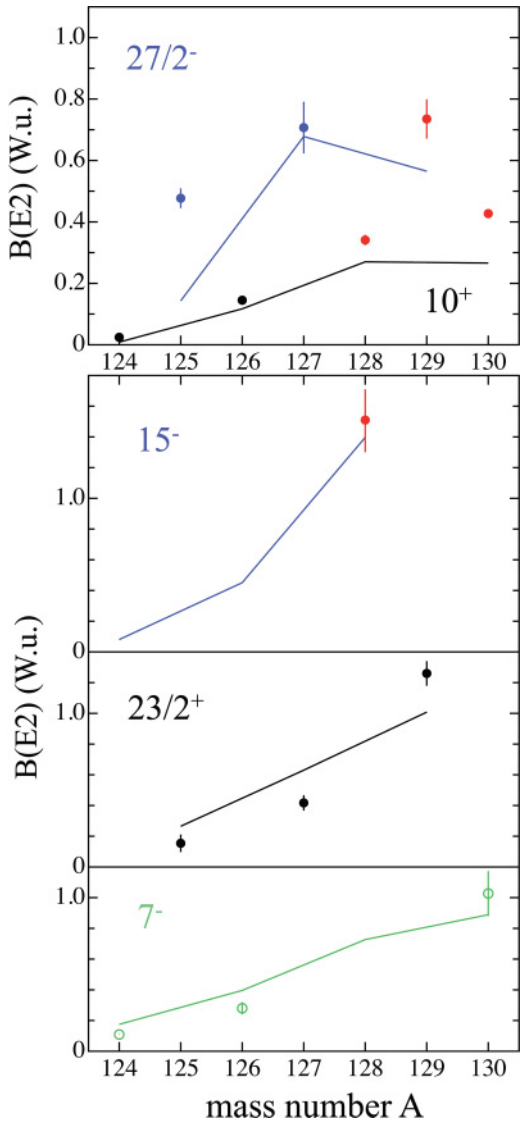

FIG. 5. (Color online) Experimental and shell model $I \rightarrow I-2$ $E2$ transition strengths in Weisskopf units for initial states with leading configurations $\nu h^{2,3}_{11/2}$; $I^\pi = 10^+$,$27/2^-$ (upper panel) and $\nu h^n_{11/2} d_{3/2}$, $I^\pi = 7^-$ $(n=1)$, $23/2^+$ $(n=2)$, and 15^- $(n=3)$ (lower panels). The experimental values for the 10^+ and 15^- states in ^{128}Sn, the $27/2^-$ level in ^{129}Sn, and the 10^+ state in ^{130}Sn have been calculated from the new lifetimes determined in the present work (red symbols) while all other values are taken from Refs. [5,23].

level lying deep in the shell. This expectation is corroborated by the nonobservation of $E3$ branches from the 10^+ and 15^- isomers.

The evolution of $E2$ strength between states of fixed configurations with decreasing occupation of the $\nu h_{11/2}$ orbital shown in Fig. 5 is well reproduced. Deviations in the slope toward midshell have been discussed in Ref. [5] and can be traced back to seniority mixing induced by proton ph excitations across $Z = 50$. The discrepancy for the $E2$ $27/2^- \rightarrow 23/2^-$ transition in ^{125}Sn is due to the fact that a second $23/2^-$ is predicted to lie 320 keV higher connected by a strong 2.8 W.u. $E2$ to the $27/2^-$. This state has dominant seniority $v = 5$ in contrast to $v = 3$ for the yrast $23/2^-$ and $27/2^-$ states. Seniority mixing induced by proton ph excitation across $Z = 50$, which is beyond the present configuration space, will improve the agreement with experiment. The phenomenon was first observed in midshell $\pi g^n_{9/2}$ $N = 50$ isotones [17].

IV. CONCLUSIONS

In conclusion, a previously unobserved isomer with a half-live of $T_{1/2} = 220(30)$ ns has been identified in ^{128}Sn at an excitation energy of 4098 keV. It decays via two parallel γ-ray cascades to the well established (7^-) and (10^+) isomeric states. Based on shell-model calculations a spin value of (15^-) and the four-neutron-hole configuration $\nu h^{-3}_{11/2} d^{-1}_{3/2}$ have been tentatively assigned to the new isomer. Reduced transition probabilities for $E2$ and $E3$ transitions involved in the decay of a number of isomeric states in ^{128,129,130}Sn have been deduced from the measured half-lives and were compared to the results of shell-model calculations. A satisfactory agreement was found for both excitation energies as well as transition probabilities. The evolution of $E2$ transitions between selected states of fixed seniority is discussed.

ACKNOWLEDGMENTS

We acknowledge financial support from the Spanish Ministerio de Ciencia e Innovación under Contracts No. FPA2007-66069 and No. FPA2009-13377-C02-02, the Spanish Consolider-Ingenio 2010 Programme CPAN (CSD2007-00042), the German Federal Ministry of Education and Research (06KY205I), the Swedish Science Council, STFC/EPSRC (UK), the Polish Ministry of Science and Higher Education (N N202 309135), and the EU Access to Large Scale Facilities Programme (EURONS, EU Contract No. 506065). We are grateful to the GSI accelerator team for the effort to provide high-quality beams.

[1] R. Broda *et al.*, Phys. Rev. Lett. **68**, 1671 (1992).
[2] C. T. Zhang, P. Bhattacharyya, P. J. Daly, Z. W. Grabowski, R. Broda, B. Fornal, and J. Blomqvist, Phys. Rev. C **62**, 057305 (2000).
[3] R. H. Mayer *et al.*, Phys. Lett. B **336**, 308 (1994).
[4] B. Fogelberg *et al.*, Nucl. Phys. A **352**, 157 (1981).
[5] R. L. Lozeva *et al.*, Phys. Rev. C **77**, 064313 (2008).
[6] H. Geissel *et al.*, Nucl. Instrum. Methods Phys. Res. Sec. B **70**, 286 (1992).
[7] J. Eberth *et al.*, Nucl. Instrum. Methods Phys. Res. Sec. A **369**, 135 (1996).
[8] S. Pietri *et al.*, Nucl. Instrum. Methods Phys. Res. Sec. B **261**, 1079 (2007).
[9] A. Jungclaus *et al.*, Phys. Rev. Lett. **99**, 132501 (2007).

[10] M. Górska *et al.*, Phys. Lett. B **672**, 313 (2009).
[11] L. Cáceres *et al.*, Phys. Rev. C **79**, 011301(R) (2009).
[12] F. Naqvi *et al.*, Phys. Rev. C **82**, 034323 (2010).
[13] L. Atanasova (private communication).
[14] L. Atanasova *et al.*, Eur. Phys. Lett. **91**, 42001 (2010).
[15] R. Machleidt, Phys. Rev. C **63**, 024001 (2001).
[16] M. Hjorth-Jensen, T. T. S. Kuo, and E. Osnes, Phys. Rep. **261**, 125 (1995).
[17] H. Grawe *et al.*, Eur. J. Phys. **27**(s01), 257 (2006).
[18] H. Grawe *et al.* (to be published) .
[19] B. A. Brown *et al.*, Oxbash for Windows, MSU-NSCL Report No. 1289 (2004).
[20] G. Ilie *et al.*, Phys. Lett. B **687**, 305 (2010).
[21] T. Kibedi *et al.*, Nucl. Instrum. Methods Phys. Res. Sec. A **589**, 202 (2008).
[22] B. Fogelberg and P. Carlé, Nucl. Phys. A **323**, 205 (1979).
[23] ENSDF database [http://www.nndc.bnl.gov/ensdf/].

High-spin isomers in ^{96}Ag: Excitations across the $Z = 38$ and $Z = 50$, $N = 50$ closed shells

P. Boutachkov,[1,*] M. Górska,[1] H. Grawe,[1] A. Blazhev,[2] N. Braun,[2] T. S. Brock,[3] Z. Liu,[4] B. S. Nara Singh,[3] R. Wadsworth,[3] S. Pietri,[1] C. Domingo-Pardo,[1] I. Kojouharov,[1] L. Cáceres,[1] T. Engert,[1] F. Farinon,[1] J. Gerl,[1] N. Goel,[1] J. Grbosz,[5] R. Hoischen,[6] N. Kurz,[1] C. Nociforo,[1] A. Prochazka,[1] H. Schaffner,[1] S. J. Steer,[7] H. Weick,[1] H.-J. Wollersheim,[1] T. Faestermann,[8] Zs. Podolyák,[7] D. Rudolph,[6] A. Ataç,[9] L. Bettermann,[2] K. Eppinger,[8] F. Finke,[2] K. Geibel,[2] A. Gottardo,[4] C. Hinke,[8] G. Ilie,[2] H. Iwasaki,[2] J. Jolie,[2] R. Krücken,[8] E. Merchán,[10] J. Nyberg,[11] M. Pfützner,[12] P. H. Regan,[7] P. Reiter,[2] S. Rinta-Antila,[13] C. Scholl,[2] P.-A. Söderström,[11] N. Warr,[2] P. J. Woods,[4] F. Nowacki,[14] and K. Sieja[14]

[1]*GSi Helmholtzzentrum für Schwerionenforschung, D-64291 Darmstadt, Germany*
[2]*Institut für Kernphysik, Universität zu Köln, D-50937 Köln, Germany*
[3]*Department of Physics, University of York, York YO10 5DD, United Kingdom*
[4]*School of Physics and Astronomy, University of Edinburgh, Edinburgh EH9 3JZ, United Kingdom*
[5]*The Henryk Niewodniczański Institute of Nuclear Physics, PL-31342 Kraków, Poland*
[6]*Department of Physics, Lund University, S-22100 Lund, Sweden*
[7]*Department of Physics, University of Surrey, Guildford GU2 7XH, United Kingdom*
[8]*Physik Department E12, Technische Universität München, D-85748 Garching, Germany*
[9]*Department of Physics, Ankara University, 06100 Tandogan, Ankara, Turkey*
[10]*Departamento de Física, Universidad Nacional de Colombia, Bogotá, Colombia*
[11]*Department of Physics and Astronomy, Uppsala University, S-75120 Uppsala, Sweden*
[12]*Faculty of Physics, University of Warsaw, PL-00681 Warsaw, Poland*
[13]*Department of Physics, Oliver Lodge Laboratory, University of Liverpool, Liverpool L69 7ZE, United Kingdom*
[14]*IPHC, IN2P3-CNRS et Université de Strasbourg, F-67037 Strasbourg, France*

(Received 12 August 2011; published 13 October 2011)

Excited states in ^{96}Ag were populated in fragmentation of an 850-MeV/u ^{124}Xe beam on a 4-g/cm^2 Be target. Three new high-spin isomers were identified and the structure of the populated states was investigated. The level scheme of ^{96}Ag was established, and a spin parity of (13^-), (15^+), and (19^+) was assigned to the new isomeric states. Shell-model calculations were performed in various model spaces, including $\pi\nu(p_{1/2}, g_{9/2}, f_{5/2}, p_{3/2})$ and the large-scale shell-model space $\pi\nu(gds)$, to account for the observed parity changing $M2$ and $E3$ transitions from the (13^-) isomer and the $E2$ and $E4$ transitions from the (19^+) core-excited isomer, respectively. The calculated level schemes and reduced transition strengths are found to be in very good agreement with the experiment.

DOI: 10.1103/PhysRevC.84.044311 PACS number(s): 21.60.Cs, 23.20.Lv, 23.35.+g, 27.60.+j

I. INTRODUCTION

There are many isomeric states predicted and observed near the doubly magic ^{100}Sn nucleus [1,2]. Their existence and properties are governed by the strong proton-neutron ($\pi\nu$) interaction between identical orbitals, and in particular the high-spin $\pi g_{9/2}$ and $\nu g_{9/2}$ orbits. Detailed shell-model calculations provide the tool to probe specific aspects of the nuclear residual interaction through comparison with key experimental data. Of particular interest are cases in the ^{100}Sn region where core-excited high-spin isomeric states may be discovered, as there is a limited number of ways of forming these states. The first and so far only known case of such a state was identified in ^{98}Cd [3]. In fact, this state has a counterpart in the $\mathcal{N} = 3$ harmonic oscillator shell in ^{54}Fe and ^{54}Ni [4]. In the present work we report on the discovery of three isomeric states in the ^{96}Ag nucleus, one of which is a core-excited isomer.

Experimentally there is little known about ^{96}Ag. The existence of an isomeric state was indicated by Grzywacz *et al.* [5], reporting two γ-ray transitions. In the experiment presented here, the power of the Rare Isotope Spectroscopic Investigation at GSI (RISING) setup [6] was used to perform detailed isomer spectroscopy of ^{96}Ag.

II. EXPERIMENT AND RESULTS

The experiment was part of the "stopped beam campaign" of the RISING project [7]. A ^{124}Xe beam with energy of 850 MeV/u and an intensity of 10^9 particles per second was produced at the GSI accelerator complex. The fragmentation reaction on a 4-g/cm^2 ^{9}Be target was employed to produce the excited ^{96}Ag residues, which were thereupon selected with the FRagment Separator (FRS) [8] using the $B\rho - \Delta E - B\rho$ technique. An event-by-event identification was performed with various detectors positioned at the middle (S2) and final (S4) focal planes of the FRS (see, e.g., Fig. 1 of Ref. [9] for the schematic setup). The nuclear charge Z was measured with two multisampling ionization chamber detectors at S4. The mass-over-charge ratio (A/Q) was determined from the measured time of flight between scintillators positioned at S2 and S4. Corrections for different trajectories through the FRS were performed based on position measurements with pairs of time-projection chambers, mounted at S2 and S4. The measured Z and A/Q were corrected for drifts in electronics

*P.Boutachkov@gsi.de

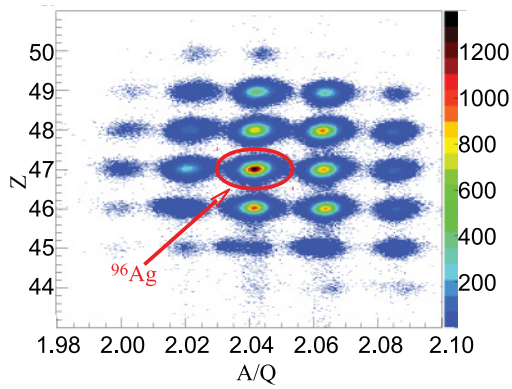

FIG. 1. (Color online) Z versus A/Q identification plot (see text for details).

and temperature and atmospheric-pressure changes during the experiment.

The fragments, including ^{96}Ag, were slowed down with an Al degrader and implanted into an array of nine double-sided silicon strip detectors (DSSSDs), 5×5 cm^2 each, with 16×16 x-y segmentation. The detectors were arranged in three rows with three detectors in each row. The DSSSDs were surrounded by the RISING HPGe detector array, with a layout described in Ref. [7]. The absolute efficiency of the Ge array in this configuration was 10% at 1.3 MeV. DGF-4C [10] modules were used to process the signals from the Ge array within 90 μs after the arrival of an ion at S4. The shortest observed half-lives were limited by the flight time through the separator, about 0.33 μs, and by the background from the prompt bremsstrahlung radiation arising from the implantation of the reaction products in the DSSSDs.

The fragment identification plot obtained in this measurement is shown in Fig. 1 with 2×10^5 ^{96}Ag nuclei identified. The correct reconstruction of Z and A/Q was verified by observing the known γ-ray transitions populated in the isomer decays of ^{96}Pd [11] and ^{98}Cd [3].

The delayed ^{96}Ag γ-ray spectrum acquired up to 90 μs after implantation is shown in Fig. 2, where the γ-ray energies

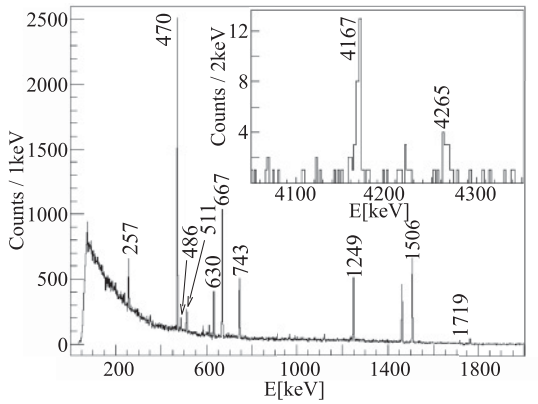

FIG. 2. A γ-ray spectrum observed from 0.075 to 90 μs after implantation of ^{96}Ag. The γ rays associated with ^{96}Ag are marked by their energies. The inset highlights the region around 4 MeV acquired in 0.075 to 0.6 μs after implantation.

of the ^{96}Ag transitions are marked. All γ-ray transitions were observed for the first time in this measurement, except for the 470-keV and 668-keV lines seen by Grzywacz *et al.* [5]. The inset highlights the region around 4 MeV acquired in 0.6 μs after the implantation.

A γ-γ coincidence analysis of the ^{96}Ag data resulted in the level scheme shown in Fig. 3. The isomeric states identified in this experiment are drawn in bold. The level energies, γ-ray energies, E_γ, relative intensities, I_γ, coincidence relations, isomeric ratios [12], R, and the half-lives, $T_{1/2}$, of the measured time distributions are summarized in Tables I and II, respectively. The half-lives for the $2643 + x$-keV and 2461-keV levels were obtained by maximum likelihood fit of the sum of the time distributions for the 470-, 1506-, 1249-, 743-, 257-, 1719-, and 486-keV γ rays (where "x" is the energy of the unobserved transition; see below) with two exponential decay curves. They are consistent with the time distributions of the 630-, 667-, and 743-keV transitions. The half-life of the $6908 + x$ level was obtained by a fit of the sum of the time distributions for the 4167-keV and 4265-keV γ rays with a single exponential decay curve. The summed time distributions are shown in Figs. 4(a) and 4(b), together with the fits. The ordering of the 470-, 1719-, 1976-, and 2461-keV levels is fixed by the cross-over transitions. A γ-ray spectrum in coincidence with the 667-keV transition and a coincidence time window of $\Delta T_c = 0.15$ μs is shown in Fig. 5(a). Because of the narrow coincidence window the γ transitions above the

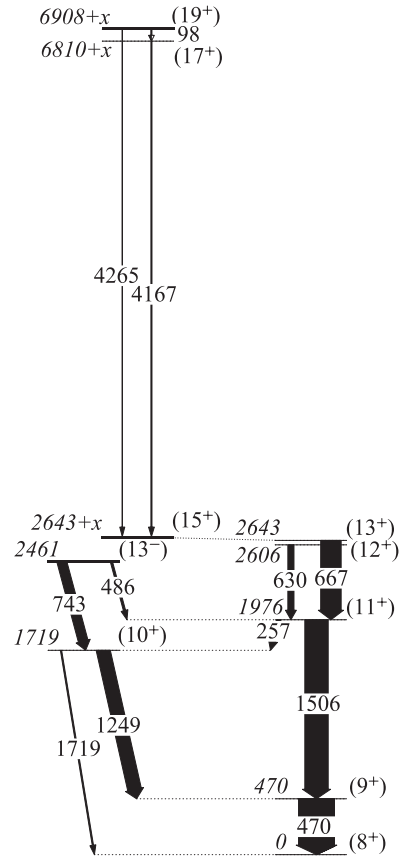

FIG. 3. Proposed level scheme of ^{96}Ag. The isomeric states identified in this experiment are drawn in bold (see text for details).

TABLE I. Level energies, γ-ray energies, relative intensities, and observed prompt coincidences.

E_x (keV)	E_γ (keV)	I_γ	Prompt coincidence transitions(keV)
469.9(2)	470.0(2)	100.0(15)	257,486,630,667,743, 1249,1506
1718.7(2)	1248.8(2)	37.7(12)	257,470,630,667,743
	1718.5(4)	3.4(5)	257,667,743
1975.6(2)	256.8(2)	12.2(8)	470,486,630,667,1249,1719
	1505.7(2)	67.1(15)	470,486,630,667
2461.2(3)	485.7(3)	5.8(6)	257,470,1506
	742.7(2)	26.6(9)	470,1249,1719
2605.7(3)	630.1(2)	18.0(8)	257,470,1249,1506
2643.0(3)	667.4(2)	60.4(12)	257,470,1249,1506,1719
6810(2) + x	4167(2)	2.9(5)	98
6908(2) + x	98(3)		4167
	4265(2)	0.7(3)	

1.56 μs isomer are not visible in this spectrum. In Fig. 5(b) a part of the coincidence spectrum is shown, when ΔT_c is increased to 3 μs and one of the γ rays was detected within 0.6 μs of implantation. The 4167-keV and 4265-keV transitions are marked. This indicates the presence of an isomeric state, with a half-life given in Fig. 4(b), which decays into the state at 2643 + x keV.

A coincidence spectrum of the 1249-keV transition with $\Delta T_c = 0.15$ μs is shown in Fig. 5(c). The 743-keV transition depopulating the 2461-keV level is clearly visible. The 486-keV γ ray is not seen, due to the branching ratios and the observational limit of the RISING array. The 486-keV transition is seen in coincidence with the 257-keV transition. Therefore, it is placed in the level scheme shown in Fig. 3.

The existence of three isomers in ^{96}Ag decaying with high γ multiplicity and partially common cascades, indicates population of high-spin yrast states. In the isotones of ^{96}Ag, ^{94}Rh, and ^{92}Tc, low-lying yrast (8^+) states were observed. These are identified as the ground state or as an isomer at low excitation energy [13,14]. The shell-model calculations in this work and in Ref. [15] predict a low-lying 8^+ state in ^{96}Ag, consistent with the systematics of the (8^+) states in ^{94}Rh and ^{92}Tc. Hence, we have assumed that the lowest state populated by the high-spin yrast cascade in Fig. 3 has $I^\pi = (8^+)$.

The spins of the excited states are assigned assuming the observed transitions follow an yrast decay. Based on the coincidence analysis, the 1719-keV transition is parallel to the 470-keV and the 1249-keV transitions. Hence, it is likely that the 1719-keV transition has an $E2$ character while the 470-keV and 1249-keV transitions have a $M1$ character. Similarly, the 1249-keV and 257-keV transitions form a parallel branch to the 1506-keV transition. There is no isomeric state in between, suggesting $E2$, $M1$, and $M1$ character for the 1506, 1249, and 257 keV transitions, respectively. Therefore, the spins of the 470-keV, 1719-keV, and 1976-keV levels are assigned as (9^+), (10^+), and (11^+). The 630-keV and 667-keV transitions are parallel [see missing coincidence in Fig. 5(a)]. They are in prompt coincidence with the discussed γ rays, and have $T_{1/2}$ of 1.52(5) and 1.54(15) μs, respectively. Hence, the 2606-keV and 2643-keV states (see Fig. 3), are fed by the 1.56-μs isomer. The isomer half-life is compatible only with $E2$ multipolarity and a transition energy close to or below the observational limit of 50 keV. Parallel primary decay branches from the isomeric state to the 2606-keV and 2643-keV levels

TABLE II. Half-lives, $T_{1/2}$, of isomeric states in ^{96}Ag, isomeric ratios, R, and reduced transition probabilities, $B(\sigma\lambda)$, of $E2$, $M2$, $E3$, and $E4$ transitions observed in their decay. One Weisskopf unit (W.u.) corresponds, respectively, to 26.11 e^2 fm^4, 34.59 μ_N^2 fm^2, 547.4 e^2 fm^6, and 12 144 e^2 fm^8 for $E2$, $M2$, $E3$, and $E4$ transitions. Electric transitions are calculated with two sets of effective charges for protons/neutrons: (1.5/0.5) e (a) and (1.72/1.44) e (b).

J_i^π	E_x (keV)	$T_{1/2}$ (μs)	R(%)	J_f^π	σL	E_γ (keV)	$B(\sigma\lambda)$ (W.u.)				
							Expt.	GF		FPG		GDS
								(a)	(b)	(a)	(b)	(a)
(19^+)	6908+x	0.16(3)	2.0(12)	(17^+)	$E2$	98	4.7(10)					3.572
				(15^+)	$E4$	4265	0.9(6)					0.697
(15^+)	2643+x	1.56(3)	10.9(6)	(13^+)	$E2$	$x = 50$	2.45(6)	2.989	4.270	2.983	4.259	3.831
						$x = 25$	6.57(16)					
(13^-)	2461	100(10)	9.0(14)	(11^+)	$M2$ [a]	486	$9.6(14) \times 10^{-5}$			3.57×10^{-5}		
					$E3$[a]		0.62(9)			0.527	0.689	
				(10^+)	$E3$	743	0.145(17)			0.0574	0.128	

[a]Alternative assumption.

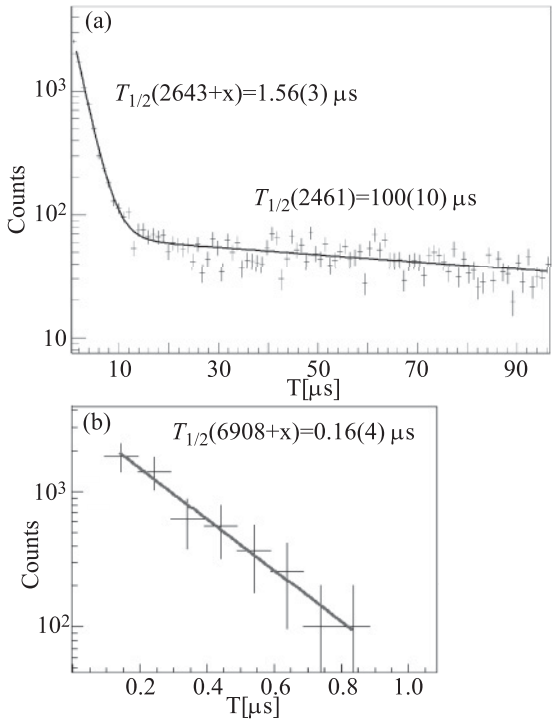

FIG. 4. (a) Summed time distributions for the 470-, 1506-, 1249-, 743-, 257-, 1719-, and 486-keV γ-ray transitions. (b) Sum of the time distributions of the 4167-keV and 4265-keV γ-ray transitions, depopulating the state at 6908 $+ x$ keV. Half-lives are shown, extracted with the maximum likelihood method.

would imply identical spin parity for these states, which is not observed in any of the $N = 49$ odd-odd isotones. Therefore, an $M1$ and $E2$ multipolarity is assigned for the 630-keV and 667-keV transitions, respectively, suggesting a parallel $M1$ cascade of a nondetectable 37-keV transition followed by the

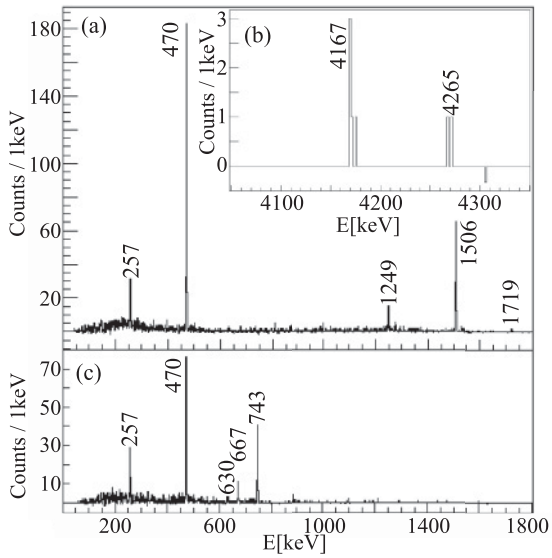

FIG. 5. (a) and (b) Coincidence spectra with the 667-keV transition within time windows of $\Delta T_c = 0.15$ μs and $\Delta T_c = 3$ μs, respectively. (c) A spectrum in coincidence with the 1249-keV transition within a time window of $\Delta T_c = 0.15$ μs.

630-keV transition. This assignment is compatible with the measured intensity ratio. Hence, the tentative spin and parity of the 2606-keV, 2643-keV, and 2643 $+ x$ keV levels [where "x" is the energy of the unobserved $E2$ transition connecting the 1.56-μs isomer to the (13^+) state] are (12^+), (13^+), and (15^+), respectively.

The core-excited 0.16-μs isomer decays by competing 98-keV $E2$ and 4265-keV $E4$ transitions, similar to the core-excited state in ^{98}Cd [16]. This is consistent with the observation of a prompt coincidence between the 98- and 4167-keV transitions. A lower multipolarity for the high-energy transitions is incompatible with the observed half-life and the level scheme. Hence, spins of (17^+) and (19^+) are assigned to the 6810 $+ x$-keV and 6908 $+ x$-keV levels.

The long decay time of the 100-μs isomer and the transition energy indicate a parity changing transition. If the 2461-keV state had a positive parity or the isomer was because of an unobserved low energy $M1$ or $E2$ transition, the 2461-keV state would have been fed from the 2643 $+ x$-keV level. Hence, the data points to a 2461-keV (13^-) state, which decays by 743-keV $E3$ and 486-keV $M2$ transitions. The strength of the $E3$ transition of 0.147(17) W.u. is similar to the $B[E3;(19^-) \rightarrow (16^+)] = 0.3$ W.u. transition strength observed in ^{94}Pd [17].

III. DISCUSSION

The standard shell-model approach to nuclei "southwest" of ^{100}Sn employs empirically fitted interactions in the $(p_{1/2}, g_{9/2})$ proton (π)-neutron (ν) model space (GF) assuming a $^{76}_{38}$Sr$_{38}$ core [18–20]. As this model space does not allow calculation of $M2$ and $E3$ γ-ray transition strengths an extension including the $\pi\nu(p_{3/2}, f_{5/2})$ orbits below $Z = N = 38$ is necessary. Recently the GF space was extended to the $\pi\nu(f_{5/2}, p, g_{9/2})$ space FPG [17] by implementing the GF two-body matrix elements (TBME) [18] with realistic interaction TBME obtained from the CD-Bonn nucleon-nucleon potential [21]. To the latter, core polarization corrections were applied assuming a $^{56}_{28}$Ni$_{28}$ core following the many-body approach of Ref. [22]. Details of tuning to experimental single-particle energies and correction to the GF TBME to avoid double counting of interaction strength are given in Ref. [17]. These approaches, however, cannot account for core excitations across the $N = Z = 50$ shell closure. Therefore, in a third approach the $\pi\nu(g, d, s)$ space GDS with a realistic interaction inferred according to Refs. [21,22] for a $^{80}_{40}$Zr$_{40}$ core was used, as detailed in Refs. [3,16]. However, such a model space cannot describe odd-parity states.

The model spaces and the respective effective interactions employed in the present work in the following are denoted by GF, FPG, and GDS. Shell-model (SM) calculations for GF and FPG were carried out with the code OXBASH [23] while the large-scale shell-model (LSSM) results in the GDS space, allowing for up to $5p$-$5h$ excitations (truncation level $t = 5$), were obtained with the codes ANTOINE and NATHAN [24,25]. Results are shown in Fig. 6 and Table II. Two sets of effective charges were used for electric transitions, namely standard values for large model spaces $e_\pi = 1.5$ e, $e_\nu = 0.5$ e (a) and

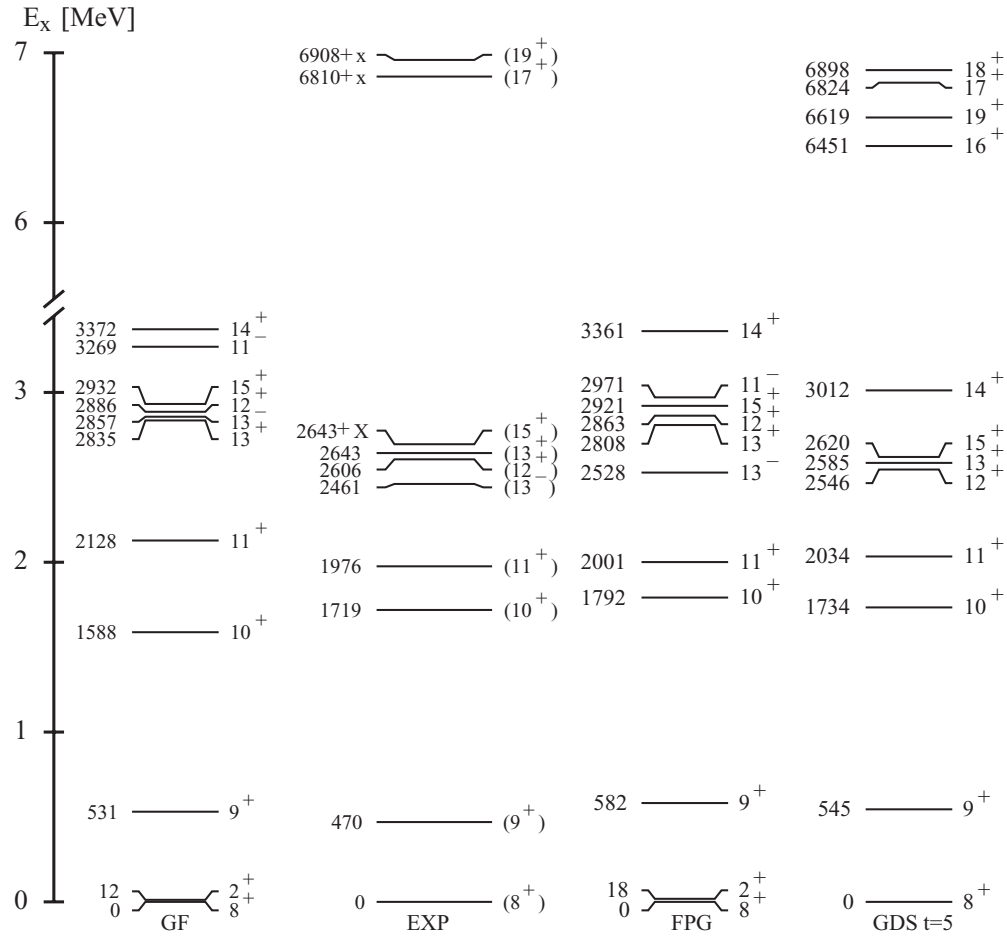

FIG. 6. Experimental and shell-model level schemes for $^{96}_{47}$Ag$_{49}$. See text for details of the shell-model approaches.

$e_\pi = 1.72\ e$, $e_\nu = 1.44\ e$ (b), which was found to be optimum for the small GF model space [20]. For magnetic transitions quenched single-particle g_s factors with $g_s = 0.7\ g_s^{\text{free}}$ were assumed.

The experimental level scheme is very well reproduced by the three approaches within their scope and predictive accuracy. Extension of the GF to the FPG model clearly improves the positions of the 10^+, 11^+, and 13^- levels. The LSSM approach accounts very well for positive parity states and reproduces both the excitation energy and correct order of the $(12\text{-}15)^+$ states including the core-excited isomer. However, it fails in the correct 17^+-19^+ sequence which may be because of details of the interaction. A similar effect was observed in ^{98}Cd for the 12^+-14^+ states [16]. Inspection of the wave functions reveals that the core-excited states in ^{96}Ag are dominated by neutron excitations across the $N = 50$ gap. Therefore, the excitation energy of the isomer is an indirect measure for the ^{100}Sn $N = 50$ neutron gap. The extracted value of 6.70(15) MeV is in fair agreement with the value of 6.46(15) MeV determined for ^{98}Cd [3], which establishes a robust $N = 50$ shell closure for ^{100}Sn. The error in the gap size is an estimate of the systematic uncertainties in the residual interaction.

Electromagnetic transition rates were extracted using the half-lives and intensities listed in Tables I and II and the conversion coefficients of Ref. [26]. The 1.56-μs isomer can be understood as a yrast trap, where a 15^+ state, the highest spin which can be obtained in the $\pi^{-3}\nu^{-1}(g_{9/2}, p_{1/2})$ space, decays by a low-energy $E2$ γ-ray transition. For the experimentally nonobserved $(15^+)\rightarrow(13^+)$ transition two values are given in Table II. The experimental observational limit of 50 keV and the value of 25 keV, below which the total conversion coefficient increases as $\alpha(E2) \sim E_\gamma^{-5}$, which makes the extracted reduced strength independent from the transition energy. Within these experimental limits good agreement with the various shell-model approaches is obtained. The parity-changing transitions, which are forbidden in the GF space, are remarkably well reproduced in the FPG approach if $E3$ multipolarity is adopted for the $(13^-)\rightarrow(11^+)$ transition. In the extended FPG model space the fairly large $E3$ width is because of excitations from the proton $p_{3/2}$ orbit across the $Z = 38$ subshell. The LSSM results in the GDS space using standard effective charges account well for transition strengths between even-parity states including the core-excited (19^+) isomer. The agreement is better than that observed for ^{98}Cd [3]. In contrast to ^{98}Cd, in ^{96}Ag the low-energy $(19^+)\rightarrow(17^+)$ $E2$ dominates over the direct $(19^+)\rightarrow(15^+)$ $E4$ transition owing to the larger $E2$ transition energy and the relative reduced transition strengths.

IV. SUMMARY

In summary, three new high-spin isomers with half-lives of 0.16(3) μs, 1.56(3) μs, and 100(10) μs were discovered in ^{96}Ag. The level scheme of ^{96}Ag was built based on coincidence analysis. The 0.16(3)-μs isomer was identified as the second known core-excited isomer in the ^{100}Sn region. The 100(10)-μs isomer is determined as a decay from a negative-parity state, giving a second data point for an $E3$ transition probability in the region. Shell-model calculations were performed in the model space $\pi\nu(p_{1/2}, g_{9/2}, f_{5/2}, p_{3/2})$, necessary to reproduce the observed $E3$, $M2$ transition probabilities, proving excitations across the $Z = 38$ subshell. A large-scale shell-model calculation within the $\pi\nu(gds)$ model space was performed to study the new data on $Z = N = 50$ core excitation. The general features of ^{96}Ag were reproduced, and the excitation energies and the transition probabilities are well described; furthermore, the robustness of the ^{100}Sn shell gap is confirmed. Fine tuning of the residual particle-hole interaction is needed to reproduce the observed (17^+), (19^+) level sequence.

ACKNOWLEDGMENTS

The authors thank the GSI accelerator staff for the excellent work and M. Hjorth-Jensen for providing the original interaction two-body matrix elements in the FPG and GDS model spaces. This work is supported by the UK STFC, the Swedish Research Council, the German BMBF under Contract Nos. 06KY205I, 06KY9136I, 06MT238, and 06MT9156, and the DFG cluster of excellence Origin and Structure of the Universe.

[1] K. Ogawa, Phys. Rev. C **28**, 958 (1983).
[2] H. Grawe *et al.*, Eur. Phys. J. A **27**, 257 (2006).
[3] A. Blazhev *et al.*, Phys. Rev. C **69**, 064304 (2004).
[4] D. Rudolph *et al.*, Phys. Rev. C **78**, 021301 (2008).
[5] R. Grzywacz *et al.*, Phys. Rev. C **55**, 1126 (1997).
[6] M. Górska *et al.*, Acta Phys. Pol. B **38**, 1219 (2007).
[7] S. Pietri *et al.*, Nucl. Instr. Meth. B **261**, 1079 (2007).
[8] H. Geissel *et al.*, Nucl. Instr. Meth. B **70**, 286 (1992).
[9] A. Garnsworthy *et al.*, Phys. Rev. C **80**, 064303 (2009).
[10] B. Hubbard-Nelson, M. Momayezi, and W. Warburton, Nucl. Instr. Meth. A **422**, 411 (1999).
[11] H. Grawe and H. Haas, Phys. Lett. **120B**, 63 (1983).
[12] M. Pfützner *et al.*, Phys. Rev. C **65**, 064604 (2002).
[13] K. Oxorn, B. Singh, and S. K. Mark, Z. Phys. A **294**, 389 (1980).
[14] C. A. Fields, F. W. N. De Boe, and B. J. Diana, Nucl. Phys. A **401**, 117 (1983).
[15] K. Schmidt *et al.*, Nucl. Phys. A **624**, 185 (1997).
[16] A. Blazhev *et al.*, J. Phys.: Conf. Ser. **205**, 012035 (2010).
[17] T. S. Brock *et al.*, Phys. Rev. C **82**, 061309 (2010).
[18] R. Gross and A. Frenkel, Nucl. Phys. A **267**, 85 (1976).
[19] F. J. D. Serduke, R. D. Lawson, and D. H. Gloeckner, Nucl. Phys. A **256**, 45 (1976).
[20] D. Rudolph, K. P. Lieb, and H. Grawe, Nucl. Phys. A **597**, 298 (1996).
[21] R. Machleidt, Phys. Rev. C **63**, 024001 (2001).
[22] M. Hjorth-Jensen, T. T. S. Kuo, and E. Osnes, Phys. Rep. **261**, 125 (1995); M. Hjorth-Jensen (private communication).
[23] B. A. Brown *et al.*, Oxbash for Windows, MSU-NSCL Report No. 1289 (2004).
[24] E. Caurier and F. Nowacki, Act. Phys. Pol. B **30**, 705 (1999).
[25] E. Caurier *et al.*, Rev. Mod. Phys. **77**, 427 (2005).
[26] T. Kibédi *et al.*, Nucl. Instr. Meth. A **589**, 202 (2008).

Isomeric states observed in heavy neutron-rich nuclei populated in the fragmentation of a ^{208}Pb beam

S. J. Steer,[1] Zs. Podolyák,[1,*] S. Pietri,[1] M. Górska,[2] H. Grawe,[2] K. H. Maier,[3,4] P. H. Regan,[1] D. Rudolph,[5] A. B. Garnsworthy,[1,6] R. Hoischen,[5] J. Gerl,[2] H. J. Wollersheim,[2] F. Becker,[2] P. Bednarczyk,[2,4] L. Cáceres,[2,7] P. Doornenbal,[2,8] H. Geissel,[2] J. Grębosz,[2,4] A. Kelic,[2] I. Kojouharov,[2] N. Kurz,[2] F. Montes,[2] W. Prokopwicz,[2] T. Saito,[2] H. Schaffner,[2] S. Tashenov,[2] A. Heinz,[6] M. Pfützner,[9] T. Kurtukian-Nieto,[10] G. Benzoni,[11] A. Jungclaus,[12] D. L. Balabanski,[13,14] M. Bowry,[1] C. Brandau,[1] A. Brown,[1,15] A. M. Bruce,[16] W. N. Catford,[1] I. J. Cullen,[1] Zs. Dombrádi,[17] M. E. Estevez,[18] W. Gelletly,[1] G. Ilie,[8,19] J. Jolie,[8] G. A. Jones,[1] M. Kmiecik,[4] F. G. Kondev,[20] R. Krücken,[21] S. Lalkovski,[16,22] Z. Liu,[1] A. Maj,[4] S. Myalski,[4] S. Schwertel,[21] T. Shizuma,[1,23] P. M. Walker,[1] E. Werner-Malento,[2] and O. Wieland[1]

[1]*Department of Physics, University of Surrey, Guildford, GU2 7XH, United Kingdom*
[2]*GSI, Planckstrasse 1, D-64291, Darmstadt, Germany*
[3]*University of West of Scotland, Paisley, PA1 2BE, United Kingdom*
[4]*The Institute of Nuclear Physics, PL-31-342, Kraków, Poland*
[5]*Department of Physics, Lund University, S-22100, Lund Sweden*
[6]*WNSL, Yale University, 272 Whitney Avenue, New Haven, Connecticut, 06520, USA*
[7]*Departmento de Fisica Teórica, Universidad Autonoma de Madrid, Madrid, Spain*
[8]*IKP, Universität zu Köln, D-50937, Köln, Germany*
[9]*Faculty of Physics, University of Warsaw, Hoża 69, PL-00-681, Poland*
[10]*Universidad de Santiago de Compostela, Santiago de Campostela, Spain*
[11]*INFN sezione di Milano, I-20133, Milano, Italy*
[12]*Instituto de Estructura de la Materia, CSIC, E-28006 Madrid, Spain*
[13]*INRNE, Bulgarian Academy of Sciences, BG-1784 Sofia, Bulgaria*
[14]*Dipartimento di Fisica, Università di Camerino and INFN-Perugia, I-62032, Italy*
[15]*NSCL, Michigan State University, East Lansing, Michigan 48824-1321, USA*
[16]*School of Engineering, University of Brighton, Brighton, BN2 4GJ, United Kingdom*
[17]*Institute for Nuclear Research, H-4001, Debrecen, Hungary*
[18]*Instituto de Fisica Corpuscular, Valencia, Spain*
[19]*National Institute of Physics and Nuclear Engineering, Bucharest, Romania*
[20]*Nuclear Engineering Division, Argonne National Laboratory, Argonne, Illinois 60439, USA*
[21]*Physik Department E12, Technische Universität München, Garching, Germany*
[22]*Faculty of Physics, University of Sofia "St. Kliment Ohridski," Sofia, Bulgaria*
[23]*Japan Atomic Energy Research Institute, Kyoto, 619-0215, Japan*

(Received 2 August 2011; published 14 October 2011)

Heavy neutron-rich nuclei were populated via the fragmentation of a $E/A = 1$ GeV $^{208}_{82}$Pb beam. Secondary fragments were separated and identified and subsequently implanted in a passive stopper. By the detection of delayed γ rays, isomeric decays associated with these nuclei have been identified. A total of 49 isomers were detected, with the majority of them observed for the first time. The newly discovered isomers are in $^{204,205}_{80}$Hg, $^{201,202,204,205}_{79}$Au, $^{197,203,204}_{78}$Pt, $^{195,199-203}_{77}$Ir, $^{193,197-199}_{76}$Os, $^{196}_{75}$Re, $^{190,191}_{74}$W, and $^{189}_{73}$Ta. Possible level schemes are constructed and the structure of the nuclei discussed. To aid the interpretation, shell-model as well as BCS calculations were performed.

DOI: 10.1103/PhysRevC.84.044313 PACS number(s): 29.30.Kv, 23.20.Lv, 25.75.−q, 27.80.+w

I. INTRODUCTION

Low-lying yrast excited states of closed shell and near-closed shell nuclei provide excellent opportunities to study specific nuclear orbitals of the nucleus [1]. This is because the dominant contributions to their wave-functions comes from only a few nuclear orbits. In the case of nuclei with a $^{208}_{82}$Pb closed core, there is relatively limited experimental information available on neutron-rich species. For example, prior to the present experiment studies on the $N = 126$ isotones below $Z = 82$ have been limited to measurements of excited states in $^{207}_{81}$Tl [2] and $^{206}_{80}$Hg [3–5] and the ground state of $^{205}_{79}$Au [6].

Moving further from ^{208}Pb, the neutron-rich W-Os-Pt nuclei are characterized by different shapes in their ground states, namely prolate, oblate, triaxial, and near $N = 126$, spherical shapes. The lighter isotopes are prolate deformed. By adding more and more neutrons, the shape becomes oblate [7–9]. The exact place where this change occurs is element dependent. Shape transitional nuclei are difficult to treat theoretically, consequently the properties of nuclei in this region are considered to provide a crucial testing ground for nuclear models.

*z.podolyak@surrey.ac.uk

Projectile fragmentation at intermediate and relativistic energies has proved to be an effective way of populating states in nuclei far from the valley of stability. The highest sensitivity is achieved with decay (both internal isomeric-decay and β-decay) spectroscopy. In this paper, experimental information obtained on a large number of heavy neutron-rich nuclei of the elements Ta→Tl ($Z = 73 \rightarrow 81$) is presented. The experiment, performed in 2006, was part of the RISING stopped-beam campaign [10].

II. EXPERIMENTAL TECHNIQUE

An $E/A = 1$ GeV $^{208}_{80}Pb^{+67}$ beam was delivered by the GSI UNILAC and SIS-18 accelerator complex. The beam was fragmented on a Be target of thickness 2.526 g/cm^2. The target was backed by a 0.223 g/cm^2-thick Nb foil, to optimize electron stripping of the outgoing fragments. The nuclei of interest, populated via fragmentation processes, were separated and identified using the fragment separator (FRS) [11]. The FRS was operated in standard achromatic mode. The matter at the midfocal plane of the FRS consisted of a 4.9 g/cm^2 Al degrader, followed by a 0.35 g/cm^2 scintillation detector used for time-of-flight (TOF) and position measurements, and another Nb foil (0.108 g/cm^2 thick) to maximize electron stripping.

At the final focal plane of the FRS, a series of detectors characterized the beam. The nuclei passed through two multi-wire detectors for position measurements; two multi sampling ionization chamber (MUSIC) detectors to measure the rate of energy loss of particles, ΔE ($\propto Z^2$); and three scintillation detectors, for timing, position, and energy measurements. A variable thickness homogeneous Al degrader was used to slow down the beam particles, which were finally implanted into a passive plastic stopper. A schematic view of the experimental setup is shown in Fig. 1. The scintillation detectors placed in front of and behind the catcher allowed the offline suppression of the majority of fragments undergoing secondary reactions in the slowing-down process or those which were not stopped in the catcher.

The catcher was surrounded by the high-efficiency, high-granularity stopped RISING γ-ray spectrometer [10,12], which has a full-energy peak efficiency of 15% at 662 keV. Time-correlated γ decays from individually identified ions have been measured, allowing unambiguous identification of isomeric decays.

Multiple electronic branches recorded the time of emission of γ rays. XIA digital γ finder (DGF) modules recorded γ-ray information with 25-ns resolution for up to 380 μs following implantation. Two other timing circuits were also used. These are termed the short-range (SR) timing circuit, operating with 0.293-ns resolution for an effective 850 ns and long-range (LR) circuit, operating with 0.7629-ns resolution for 100 μs following implantation. The use of the short-range timing is advantageous in the case of short-lived isomeric decays (<300 ns).

From synthesis of the fragmentation products at the target to implantation in the stopper approximately 300 ns elapsed. During this in-flight period, electron conversion branches of excited states were suppressed by the high degree of ionization of the nuclei. This had the effect of extending the half-life of the excited states for the in-flight period. Therefore, the experiment was sensitive to the decay of metastable states that are transmitted through the FRS and then decayed in the 380 μs following implantation. In general, this experimental setup can measure isomers with half-lives in the range 10 ns–1 ms.

During the experiment, nine different magnetic rigidity settings of the FRS were used. The results from six of these, dealing with heavy neutron-rich nuclei, are presented in this paper. In these cases, the magnetic rigidities were set to transmit fully stripped ions of ^{206}Hg, ^{203}Ir, ^{202}Os, ^{199}Os, ^{192}W, and ^{185}Lu. An average of 20 h of beam time was dedicated to each setting, with a primary beam intensity of $\sim 10^9$ ions/22 s spill. Details summarizing which species and how many nuclei were implanted during the experiment are information given in Ref. [13], with a more detailed breakdown of this information is given in the PhD thesis [14]. The other three settings, centered at $^{188}_{82}$Pb, $^{186}_{82}$Pb, and $^{147}_{64}$Gd [15,16], aimed at the study of the fragmentation reaction mechanism, and in particular the angular momentum population probability [17].

As a first step in the identification of the nuclei, a charge state selection had to be performed. Charge state calculations with the GLOBAL code [18] show that when exiting the Be/Nb target approximately 94% of the fragmentation products of interest were fully ionized (i.e., $q = Z$, also referred to as "fully stripped") and that the remaining 6% had one electron bound to the nucleus ($q = Z - 1$, referred to as being in a "H-like" charge state). Following energy losses at the midfocal

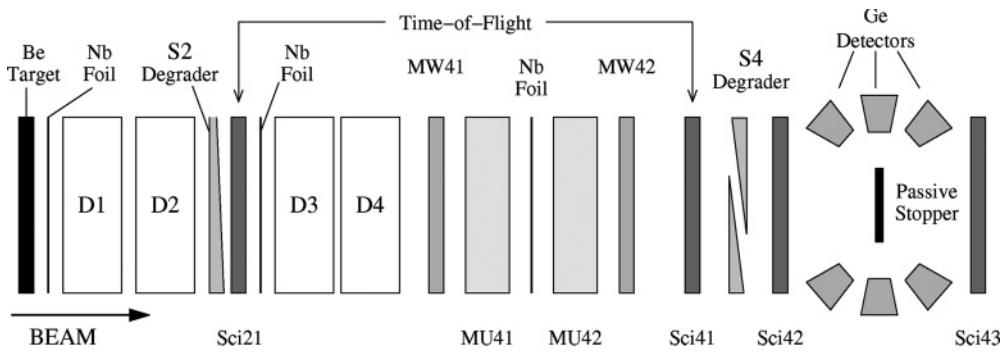

FIG. 1. Schematic of the fragment separator including the used detectors. For details see the text.

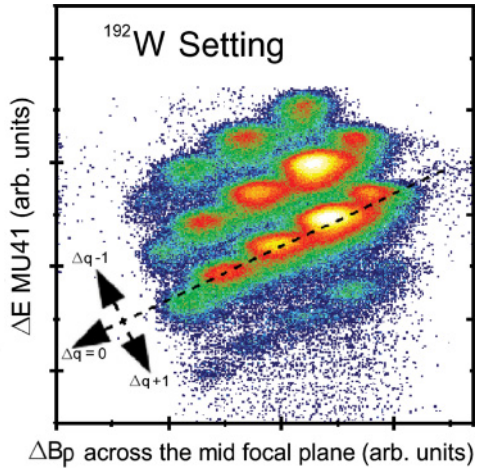

FIG. 2. (Color online) Charge state selection for the ^{192}W setting. The change in the magnetic rigidity at the mid-focal plane, $\Delta B\rho$, is plotted against ΔE ($\propto Z^2$) at the final focal plane measured by the MUSIC detectors. Changes in charge state are identified by the diagonally correlated data.

plane, 77% of the beam was fully stripped of electrons, 22% was in a H-like state, and 1% was in a He-like state ($q = Z - 2$). The matrix energy loss at the final focal plane versus change in magnetic rigidity, $\Delta B\rho$ ($\propto q^2$), at the intermediate focal plane can be used for charge state selection (see Fig. 2). This distinguishes nuclei that do not change charge state in the middle of the FRS (approximately all $\Delta q = 0$ correspond to $q = Z$ for the entire FRS flight time) from those which pick up one or two electrons ($\Delta q = -1$ and $\Delta q = -2$) or lose one electron ($\Delta q = +1$).

The identification plot corresponding to the $^{192}_{74}$W setting is shown in Fig. 3. The analogous pictures for the $^{203}_{77}$Ir and $^{199}_{76}$Os settings can be found in Refs. [19,20], respectively. All identification plots are available in Ref. [14]. Each

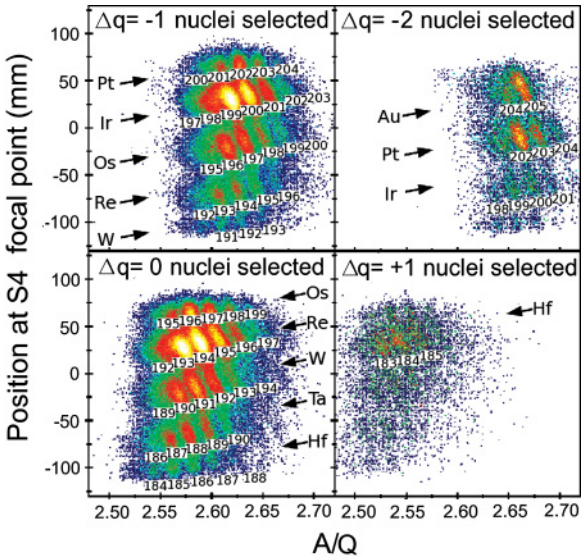

FIG. 3. (Color online) Identification plot for the FRS setting centered on $^{192}_{74}$W. The four figures correspond to different charge state combinations through the fragment separator.

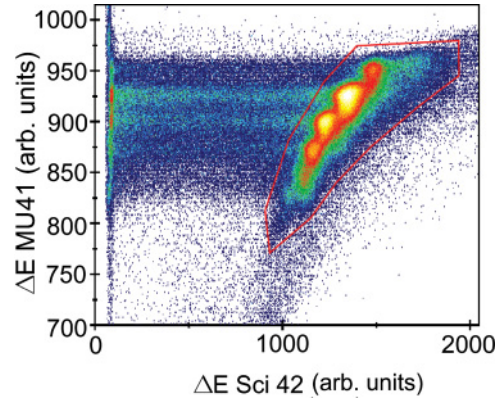

FIG. 4. (Color online) Rate of energy loss of identified beam nuclei before (ΔE MUSIC41) and after (ΔE Sci42) the homogeneous degrader at the final focal plane. The closed line encompasses those nuclei that did not react during the slowing down process.

identification plot has been confirmed by the observation of γ-ray transitions following the decay of previously reported isomers.

Following their identification, the nuclei were slowed down in the homogeneous Al degrader, before being implanted in a passive stopper. In the degrader, the ions were slowed down from an energy of $E/A \sim 400$ MeV to $E/A < 100$ MeV. In the slowing-down process, a number of the nuclei of interest were lost due to reactions in the degrader. A comparison of a ΔE measurement by a MUSIC chamber located upstream from the degrader and one made by the scintillation detector placed immediately following the degrader (Sci42) identifies nuclei that react inside it (see Fig. 4). The latter are removed from further analysis. It was found that ≈18% of the nuclei react at this stage.

In the $^{206}_{80}$Hg, $^{203}_{77}$Ir, and $^{202}_{76}$Os settings, the selected beam nuclei were implanted in a 7-mm-thick perspex stopper. For the other three settings, a 9-mm-thick perspex stopper was used. One final scintillation detector (Sci43), placed after the stopper, acted as a veto on events where particles were detected after the stopper, this accounted for ≈0.2% of the identified nuclei.

As each nucleus decelerates and comes to a halt in the stopper, bremsstrahlung is emitted, causing the so-called "prompt flash" [21,22]. The prompt flash is measured to have a FWHM $\sim$ 20 ns when using the SR devices at γ-ray energies, $E_\gamma > 500$ keV; this width includes the uncertainty associated with synchronizing the independent time circuits of the 105 Ge crystals. Isomers with half-lives comparable to this width are subject to a large background contribution.

III. RESULTS

The analysis of the data collected in this experiment has identified 49 isomers in 39 nuclear species between Ta ($Z = 73$) and Tl ($Z = 81$). The nuclei with isomeric states are indicated in Fig. 5 and the experimental observables are summarized in Table I. The experimental observables include the intensity of the γ rays, the isomeric lifetime, and the

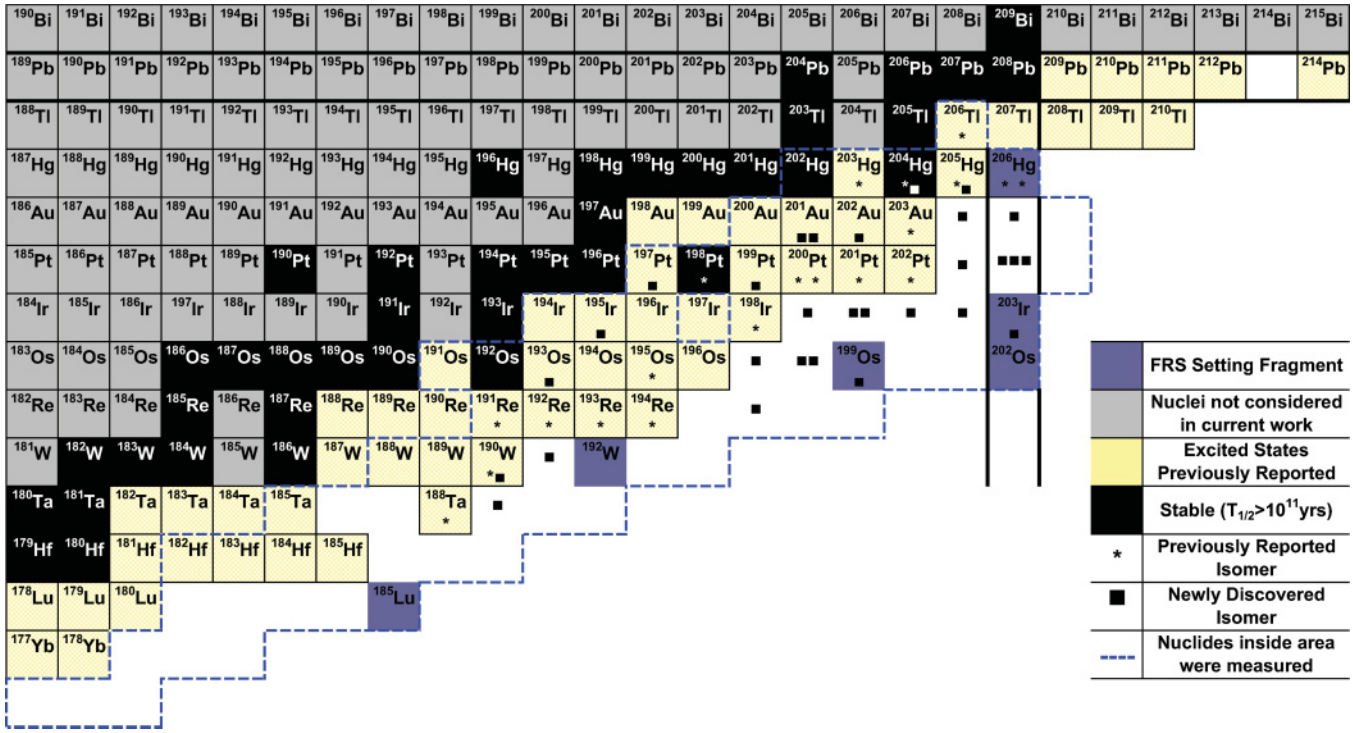

FIG. 5. (Color online) Section of the nuclide chart indicating the nuclei studied in the present experiment. The figure shows the nuclei with observed isomers as well as the nuclei with knowledge on excited states prior to the present experiment.

isomeric ratio. Of the observed isomers, 20 have been already reported prior to performing the described experiment and 29 were observed for the first time.

An isomeric ratio is defined as the number of times a nuclide is populated in an excited state that decays through a given isomer, divided by the total number of times that the nuclide has been populated. A detailed explanation of how this is determined is given in Ref. [23]. Where more than one isomer has been observed in a nucleus, the isomeric ratio of the lower-lying isomer is *inclusive* of any feeding from the higher-lying isomer. If the same nucleus was transmitted in different settings and in different charge states, the isomeric ratios were determined for each charge-state combination separately. The final values are given in Table I. Isomeric states often decay via low-energy highly converted unobserved transitions. Without knowing the energy of the decaying transition, one cannot calculate how many of them decay while flying through the fragment separator. Therefore, only a lower isomeric ratio limit could be determined in these cases, assuming no decays (infinite conversion electron coefficient) during flight through the FRS.

A. Theoretical calculations

We performed shell-model calculations on the nuclei in the vicinity of ^{208}Pb. The OXBASH code [24] was employed. The model space considered consisted of the proton orbitals $3s_{1/2}$, $2d_{3/2}$, $1h_{11/2}$, $2d_{5/2}$, and $1g_{7/2}$ below the $Z = 82$ closed shell and the neutron orbitals $3p_{1/2}$, $2f_{5/2}$, $3p_{3/2}$, $1i_{13/2}$, $2f_{7/2}$, and $1h_{9/2}$ below the closed $N = 126$ shell. Except for ^{202}Au, where the $\pi g_{7/2}$ and $\nu h_{9/2}$ orbitals were kept filled, no further truncation was applied. Therefore, no core excitations across the ^{208}Pb double-shell closure are allowed. The single proton-hole and neutron-particle energies are taken from the experimental spectra of ^{207}Tl and ^{207}Pb, respectively. The two-body interaction matrix elements (TBMEs) are from Ref. [25]. They are based on the Kuo-Herling interaction [26] including core polarization, with decisive elements adjusted to the experimental data available at the time. We shall refer to this as the standard parametrization.

In addition to the aforedescribed standard parametrization, a modified parametrization was also used. These modifications were introduced to get better agreement between theory and experiment for the new ^{204}Pt and updated ^{206}Hg data [5]. As explained in Ref. [19], the Rydström interaction [25] was modified in three points: (i) the $(d_{3/2}\ h_{11/2})_{7^-}$ TBME was increased by +135 keV as needed for ^{206}Hg; (ii) the $(s_{1/2}\ d_{5/2})$ monopole was increased by +230 keV, which accounts for the 4^+ level energy in ^{204}Pt and the increased blocking of the $h_{11/2} \otimes 3^-$ coupling lowering the effective $d_{5/2}$ single hole energy; (iii) following a systematic search of the influence of nondiagonal TBME on the $E2$ strength evolution from ^{206}Hg to ^{204}Pt, the $(s_{1/2}\ h_{11/2};d_{3/2}\ h_{11/2})_{6^-}$ TBME was changed to +160 keV, close to the value for the corresponding 5^- TBME.

Here we examine whether these modifications needed by ^{204}Pt and ^{206}Hg improve the predictive power of the calculations for other nuclei in the region. This is especially important, since such shell-model calculations are used to predict the properties of the $N = 126$ r-process path nuclei [27].

TABLE I. Summary of the observed isomeric states. Half-lives and isomeric ratios, as well as γ-ray energies and relative intensities are given. For details see the text.

Nucleus, I^π, $T_{1/2}$, IR (%) E_γ (keV)	I_γ
^{206}Tl, $I^\pi = (5)^+$ [30], $T_{1/2} = 71(4)$ ns, IR $= 14.2^{+21}_{-32}$	
265.4	89(6)
452.9	90(6)
685.8	100(7)
^{206}Hg, $I^\pi = (10^+)$ [30], $T_{1/2} = 112(4)$ ns, IR $= 2.2^{+7}_{-8}$	
100.9	3(3)
363.4	21(1)
1156.3	28(1)
1257.2	8(1)
^{206}Hg, $I^\pi = 5^-$ [30], $T_{1/2} = 2.09(2)$ μs, IR $= 21.9^{+12}_{-29}$	
1033.7	100(2)
1068.0	99(2)
^{205}Hg, $I^\pi = (23/2^-)$, $T_{1/2} = 5.89(18)$ μs, IR $= 3.3^{+2}_{-4}$	
227.6	8(1)
722.6	11(1)
810.0	100(3)
950.2	87(3)
^{205}Hg, $I^\pi = 13/2^+$, $T_{1/2} = 1.09(4)$ ms [36], IR $= 20.5^{+25}_{-40}$	
378.9	37(2)
967.0	10(2)
1014.7	33(2)
^{204}Hg, $I^\pi = (14^+)$, $T_{1/2} = 20(2)$ ns, IR < 10	
422.7	35(7)
597.2	100(14)
964.8	61(14)
1013.9	30(15)
^{204}Hg, $I^\pi = 7^-$ [38], $T_{1/2} = 6.7(5)$ ns [38]	
436.6	59(10)
691.8	36(9)
1062.7	36(10)
^{203}Hg, $I^\pi = (13/2^+)$ [39], $T_{1/2} = 21.9(10)$ μs, IR $= 11.8^{+11}_{-20}$	
341.0	57(2)
591.1	100(3)
^{205}Au, $I^\pi = (19/2^+)$, $T_{1/2} = 163(5)$ ns, IR $= 6.5^{+10}_{-15}$	
34.2	–
243.4	4(2)
736.9	39(2)
928.3	23(2)
946.1	94(4)
962.5	100(5)
962.5	11(4)
980.2	24(2)
1171.5	32(2)
^{204}Au, $I^\pi = (16^+)$, $T_{1/2} = 2.1(3)$ μs, IR $= 0.6(2)$	
839.0	100(15)
976.6	93(15)
^{203}Au, $I^\pi = 11/2^-$, $T_{1/2} = 140(44)$ μs, IR $= 2.5^{+8}_{-10}$	
562.8	100(6)
^{202}Au, $I^\pi =$ unknown, $T_{1/2} = 13.1(5)$ ns	
137.8	21(21)
414.2	100(5)

TABLE I. (*Continued*)

Nucleus, I^π, $T_{1/2}$, IR (%) E_γ (keV)	I_γ
^{201}Au, $I^\pi = 11/2^-$, $T_{1/2} = 340^{+900}_{-290}\mu$s, IR $= 13^{+36}_{-11}$	
553	100(51)
^{201}Au, $I^\pi =$ unknown, $T_{1/2} = 5.6(24)\mu$s, IR $= 5(3)$	
378.2	58(17)
638.0	100(34)
^{204}Pt, $I^\pi = (10^+)$, $T_{1/2} = 146(14)$ ns, IR $= 9.2^{+25}_{-32}$	
96.1	2(2)
1060.8	20.7(11)
1157.5	3.7(5)
^{204}Pt, $I^\pi = (7^-)$, $T_{1/2} = 55(3)$ μs, IR $= 27^{+7}_{-9}$	
$<$78.4	–
^{204}Pt, $I^\pi = (5^-)$, $T_{1/2} = 5.5(7)$ μs, IR $= 40^{+17}_{-20}$	
872.4	100(2)
1122.7	97(2)
^{203}Pt, $I^\pi = (33/2^+)$, $T_{1/2} = 641(55)$ ns, IR $= 1.3(2)$	
1104.0	100(8)
^{202}Pt, $I^\pi = 7^-$ [67], $T_{1/2} = 141(7)$ μs, IR $= 12^{+1}_{-2}$	
534.3	95(2)
534.3	95(2)
718.8	100(3)
^{201}Pt, $I^\pi = (25/2^-, 27/2^-)$, $T_{1/2} = 18.4(13)$ ns, IR $\geqslant 4(2)$	
353.6	76(6)
373.9	80(5)
726.9	100(6)
^{200}Pt, $I^\pi = (12^+)$ [68], $T_{1/2} = 13.9(10)$ ns, IR $\geqslant 2(1)$	
318.4	16(2)
542.5	17(2)
708.6	22(3)
^{200}Pt, $I^\pi = 7^-$ [68], $T_{1/2} = 17.0(5)$ ns, IR $\geqslant 7(4)$	
298.9	8(2)
397.5	8(2)
401.0	8(2)
463.6	72(3)
470.1	87(3)
633.0	100(4)
^{199}Pt, $I^\pi = (25/2^-, 27/2^-)$, $T_{1/2} = 18.6(34)$ ns, IR $\geqslant 5(3)$	
318.9	84(19)
419.6	86(15)
597.4	100(15)
^{198}Pt, $I^\pi = 7^-$,$T_{1/2} = 3.4(2)$ ns [47]	
382.0	54(16)
407.2	100(29)
577.8	65(25)
^{197}Pt, $I^\pi = (25/2^-, 27/2^-)$, $T_{1/2} = 10.2(13)$ ns, IR $\geqslant 5(2)$	
374.5	100(12)
432.2	72(14)
546.9	66(12)
^{203}Ir, $I^\pi = (23/2^+)$, $T_{1/2} = 798(350)$ ns, IR $= 5^{+3}_{-4}$	
207.0	18(8)
841.3	73(21)
894.7	100(25)
^{202}Ir, $I^\pi =$ unknown, $T_{1/2} = 3.4(6)$ μs, IR $= 0.7^{+2}_{-3}$	
311.5	41(13)

TABLE I. (*Continued*)

Nucleus, I^π, $T_{1/2}$, IR (%) E_γ (keV)	I_γ
655.9	54(17)
737.2	100(29)
889.2	51(17)
967.6	44(15)
^{201}Ir, I^π = unknown, $T_{1/2}$ = 10.5(17) ns, IR $\geqslant$ 3(2)	
439.6	39(9)
452.0	51(9)
680.9	100(13)
^{200}Ir, I^π = unknown, $T_{1/2}$ = 17.1(12) ns, IR = 22(12)	
120.0	30(2)
^{200}Ir, I^π = unknown, $T_{1/2}$ = 28.5(15) ns, IR = 3.5(14)	
126.6	100(3)
^{199}Ir, I^π = unknown, $T_{1/2}$ = 8.9(5) ns,	
448.5	100(7)
500.2	67(5)
500.2	14(1)
547.2	82(7)
596.6	38(6)
^{198}Ir, I^π = unknown, $T_{1/2}$ = 73(11) ns, IR = 5(4)	
116.4	100(17)
^{195}Ir, I^π = unknown, $T_{1/2}$ = 4.4(6) μs, IR = 1.1^{+2}_{-3}	
268.4	76(19)
404.4	90(30)
476.7	61(28)
537.8	96(29)
566.7	100(30)
^{199}Os, I^π = unknown, $T_{1/2}$ = 25.2(20) ns, IR $\geqslant$ 1.4(7)	
379.3	57(18)
401.8	100(19)
424.8	49(13)
736.5	47(25)
970.6	48(28)
^{198}Os, $I^\pi = (12^+)$, $T_{1/2}$ = 18.0(28) ns, IR $\geqslant$ 0.4(2)	
446.8	11(2)
526.9	10(2)
544.0	6(2)
^{198}Os,$I^\pi = (7^-)$, $T_{1/2}$ = 16.1(8) ns IR $\geqslant$ 5(3)	
329.9	27(3)
412.1	16(3)
465.4	100(4)
473.1	13(2)
607.3	80(4)
608.2	80(4)
885.6	19(3)
^{197}Os, $I^\pi = (25/2^-, 27/2^-)$, $T_{1/2}$ = 78.2(66) ns, IR = 4(2)	
204.4	62(12)
415.9	92(9)
486.5	100(10)
628.8	96(11)
^{195}Os, $I^\pi = (25/2^+, 29/2^-)$, $T_{1/2}$ = 34.0(23) ns, IR $\geqslant$ 2.4(8)	
438.6	100(11)
493.0	73(10)
533.1	73(10)
714.0	90(12)
^{193}Os, I^π = unknown, $T_{1/2}$ = 132(29) ns, IR $\geqslant$ 7(4)	
242.0	100(26)
^{196}Re, I^π = unknown, $T_{1/2}$ = 3.6(6) μs	
x rays	–
^{194}Re, I^π = unknown, $T_{1/2}$ = 45(18) μs, IR = 5(3)	
86.3	100(25)
^{193}Re, $I^\pi = (9/2^-)$, $T_{1/2}$ = 65(9) μs, IR = 16^{+4}_{-5}	
145.2	100(11)
^{192}Re, I^π = unknown, $T_{1/2}$ = 85(10) μs, IR = 3(1)	
159.3	100(9)
^{191}Re, I^π = unknown, $T_{1/2}$ = 77(33) μs	
134.5	42(11)
139.9	40(11)
158.3	57(13)
224.6	100(19)
418.5	65(18)
443.7	42(15)
^{191}W, I^π = unknown, $T_{1/2}$ = 0.36(2) μs	
67.5	100(25)
167.4	50(10)
^{190}W, I^π = unknown, $T_{1/2}$ = 0.35(4) μs	
x rays	–
^{190}W, $I^\pi = (8^+)$, $I^\pi = (10^-)$ [64], $T_{1/2}$ = 108(9) μs	
206.8	81(10)
358.3	92(10)
484.3	100(11)
694.0	71(10)
^{189}Ta, I^π = unknown, $T_{1/2}$ = 0.58(22) μs	
153.9	100(19)
283.7	73(17)
342.5	47(13)
388.7	80(19)
481.6	97(21)
^{188}Ta, I^π = unknown, $T_{1/2}$ = 3.5(4) μs, IR = 8(2)	
291.9	100(7)

Shell model calculations with both the standard and the modified parametrization have been performed for all cases. As the changes involve only proton orbitals, the energy spectra of both calculations are presented only for the $N = 126$ nuclei. In $N < 126$ nuclei, the differences in the energy spectra are generally small and only the energy spectra of the modified parametrization are given. Transition rates were calculated using effective operators as listed in Table II. The effective charges and g factors were adjusted to transitions in the one- and two-hole neighbors of ^{208}Pb. The measured transition strengths are compared with both shell model calculations for all nuclei for which such calculations could be performed (see Table II).

TABLE II. Experimental and calculated transition strengths. Both the calculated Rydström [25] shell model $(SM)_{standard}$ and the new TBMEs (SM_{mod}) values are given. The following effective operators were used: $e_\pi = 1.5e$ and $e_\nu = 0.85e$ for E2 and E5 transitions, $e_\pi = 2.0e$ and $e_\nu = 2.5e$ for E3 and E4 transitions, $g_s = 0.7 g_s^{free}$ for M1 and M2 transitions, and $g_s = 0.35 g_s^{free}$ for M4. See the text for details.

Nucleus	Transition	B(EL) (W.u.)		
		exp.	$SM_{standard}$	SM_{mod}
^{206}Hg	$B(E3: 10^+ \to 7^-)$	0.25(3) [5]	0.17	0.21
^{206}Hg	$B(E2: 10^+ \to 8^+)$	0.94(15) [5]	0.87	0.87
^{206}Hg	$B(E3: 5^- \to 2^+)$	0.18(2) [5]	1.17	0.90
^{205}Au	$B(E3: 19/2^+ \to 13/2^-)$	0.3(1)	0.004	0.02
	or			
	$B(E3: 19/2^+ \to 15/2^-)$	0.3(1)	1.0	1.10
^{205}Au	$B(E2: 19/2^+ \to 15/2^+)$	1.2(2)	2.99	1.70
^{205}Au	$B(M4: 11/2^- \to 3/2^+)$	$\leqslant$1.7(7) [34]	1.92	2.46
^{204}Pt	$B(E3: 10^+ \to 7^-)$	0.19(3)	0.21	0.21
^{204}Pt	$B(E2: 10^+ \to 8^+)$	0.80(8)	2.64	1.22
^{204}Pt	$B(E2: 7^- \to 5^-)$	0.017+ $\to$0.0034[a]	1.21	0.0037
^{204}Pt	$B(E3: 5^- \to 2^+)$	0.039(5)	0.713	0.612
^{203}Ir	$B(E2: 23/2^+ \to 19/2^+)$	0.020(9)	3.58	0.013
	or			
	$B(E3: 19/2^+ \to 15/2^-)$	1.3(6)	0.39	0.44
	or			
	$B(E3: 19/2^+ \to 13/2^-)$	1.3(6)	0.144	0.50
^{205}Hg	$B(E3: 23/2^- \to 17/2^+)$	0.10(1)	1.80	1.34
^{205}Hg	$B(M2: 23/2^- \to 19/2^+)$	$8(1)\times10^{-5}$	0.008	0.009
^{205}Hg	$B(E3: 13/2^+ \to 7/2^-)$	1.14(7) [36]	3.50	3.38
^{205}Hg	$B(M2: 13/2^+ \to 9/2^-)$	$4.7(3)\times10^{-4}$ [36]	0.03	0.03
^{204}Au	$B(M2: 16^+ \to 14^-)$	$4.7(8)\times10^{-4}$	3.5×10^{-4}	21×10^{-4}
	or			
	$B(E3: 16^+ \to 14^-)$	0.28(5)	0.80	0.83
^{203}Pt	$B(E3: 33/2^+ \to 27/2^-)$	0.38(4)	0.30	0.32
^{203}Hg	$B(M2: 13/2^+ \to 9/2^-)$	0.0457(21)	0.05	0.045
^{203}Au	$B(M2: 11/2^- \to 7/2^+)$	0.03(2)	0.035	0.034
^{202}Pt	$B(E3: 7^- \to 4^+)$	0.268(13)	0.09	0.058

[a]Assuming a transition energy between 10 $\to$ 78 keV.

In the case of deformed nuclei, multi-quasi-particle calculations were performed with a BCS blocking code [28]. The deformation parameters were taken from Ref. [29].

B. N = 126 nuclei

Isomeric decays were observed in four $N = 126$ nuclei: ^{206}Hg, ^{205}Au, ^{204}Pt, and ^{203}Ir. The associated delayed γ-ray spectra are shown in Fig. 6.

Previously, experimental information existed only on the excited states of ^{206}Hg, where two isomeric states were identified. These are an $I^\pi = 5^-$, $T_{1/2} = 2.15(21)$ μs state [3–5,30] and an $I^\pi = (10^+)$, $T_{1/2} = 92(8)$ ns state [5,30], which has 100% feeding to the lower-lying isomer. Our measured half-lives of $T_{1/2} = 2.09(2)$ μs and $T_{1/2} = 112(4)$ ns agree with the previously published values. The determined isomeric ratios, given in Table I, are in fair agreement with the predictions of two nucleon removal reaction theory, as discussed in Ref. [31]. In addition, the dependence of the isomeric ratio of the 5^- state on the transferred longitudinal momentum was compared with the theoretical calculations [32].

In ^{205}Au, an isomeric state with $T_{1/2} = 163(5)$ ns was observed. In ^{204}Pt three isomeric states with half-lives of 146(14) ns, 55(3) μs, and 5.5(7) μs were identified. The data on these nuclei have already been discussed in detail in Refs. [19,20], respectively.

In the case of $^{203}_{77}$Ir two γ-ray transitions were observed, with energies of 841 and 895 keV. The half-life of the isomer is measured to be $T_{1/2} = 0.8(4)$ μs. There is a candidate for a third γ-ray transition with 207 keV energy.

The shell-model predictions and interpretation of experimental data are presented in Fig. 7. In the case of ^{204}Pt [19], based on similarities with ^{206}Hg as well as shell model predictions, the three isomeric states were interpreted as $I^\pi = (5^-)$, (7^-), and (10^+) with $\pi h_{11/2}^{-1} s_{1/2}^{-1}$, $\pi h_{11/2}^{-1} d_{3/2}^{-1}$, and $\pi h_{11/2}^{-2}$ predominant configurations, respectively.

In ^{205}Au, the yrast structure has been established up to spin-parity $(19/2^+)$ via the observation of the decay of an isomeric state with configuration $\pi(h_{11/2}^{-2})_{10}(s_{1/2}^{-1})$ (for details see Ref. [20]). This isomer feeds into the long-lived $11/2^-$ state

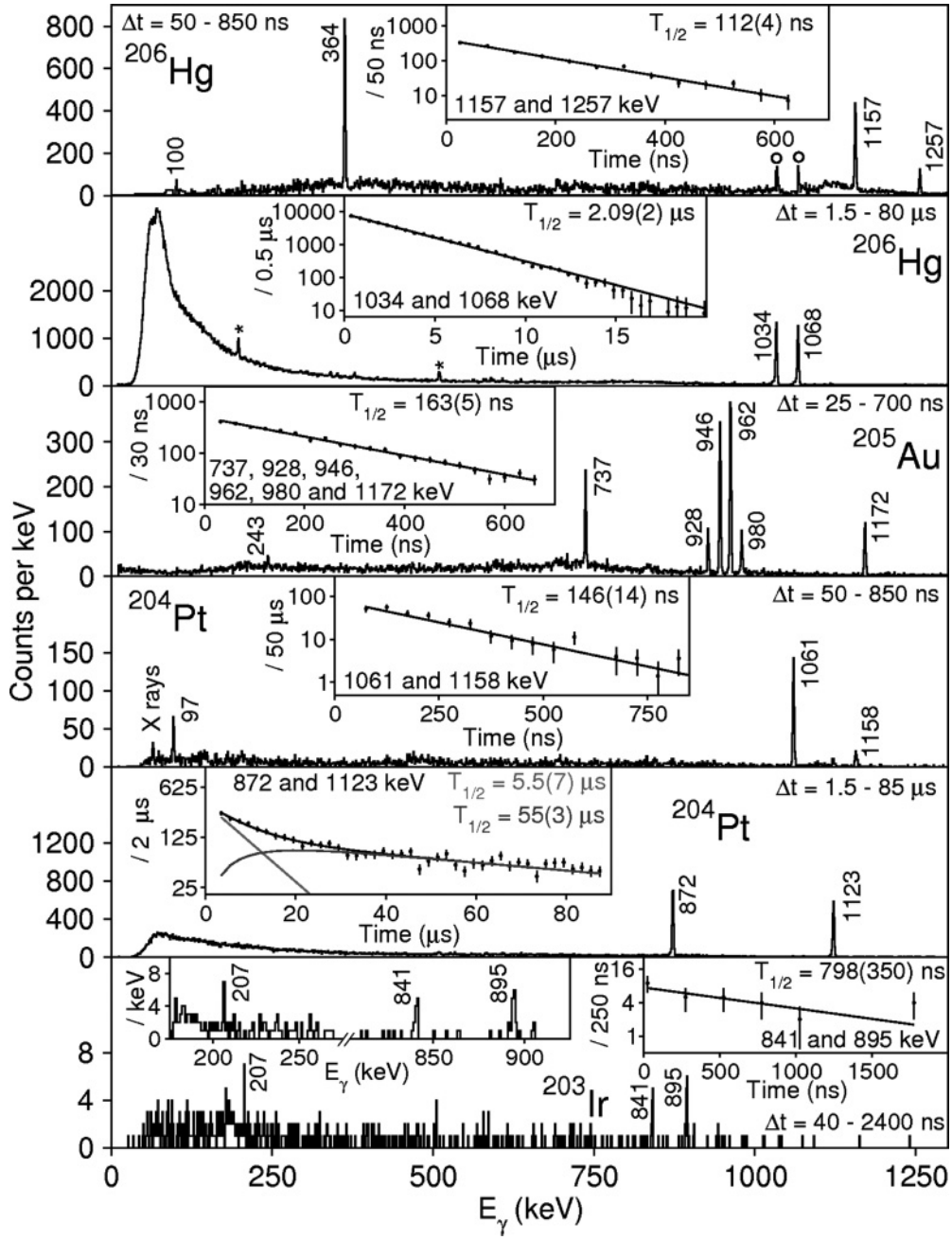

FIG. 6. Delayed γ-ray energy spectra for $N = 126$ nuclei. Background peaks are indicated by $\star$. The peaks indicated by $\circ$ belong to the nucleus of interest, but originate from a different isomeric state than that for which the time limits of the γ spectrum are optimised. Inset spectra are time curves associated with the decay of the observed isomers. The transitions used to measure half-lives are indicated in the time spectra. For ^{203}Ir, the inset presents an expanded γ-ray energy spectrum to highlight the observed energy peaks.

with $\pi h_{11/2}^{-1}$ configuration. This latter state has been identified and its lifetime measured in a later RISING experiment using an active Si stopper [33], by observing the conversion electron associated with the $\pi h_{11/2}^{-1} \rightarrow \pi d_{3/2}^{-1}$ transition [34]. The higher-lying, $19/2^+$, isomer decays into the yrast $15/2^+$ state by a low-energy E2 transition. In addition, it decays by a 963 keV transition into a state that can have spin-parity of either $13/2^-$ or $15/2^-$. The shell-model calculations predict that even if it is $15/2^-$, the transition will have predominantly E3 character with only a very small, $\sim 10^{-5}$ W.u., M2 admixture. The $15/2^+$ state decays by three high-energy transitions to states with $I^\pi = (13/2^-, 15/2^-)$.

In ^{203}Ir, similarly to ^{205}Au, the observed isomeric state is expected to decay into the $11/2^-$ long-lived level. The isomer is likely to have a spin in the 19/2–23/2 range. There are two possible scenarios. One is that the isomer is similar to that in ^{205}Au, so has $I^\pi = 19/2^+$ and it decays to the $15/2^+$ state by a low energy E2 transition. Alternatively, the isomer

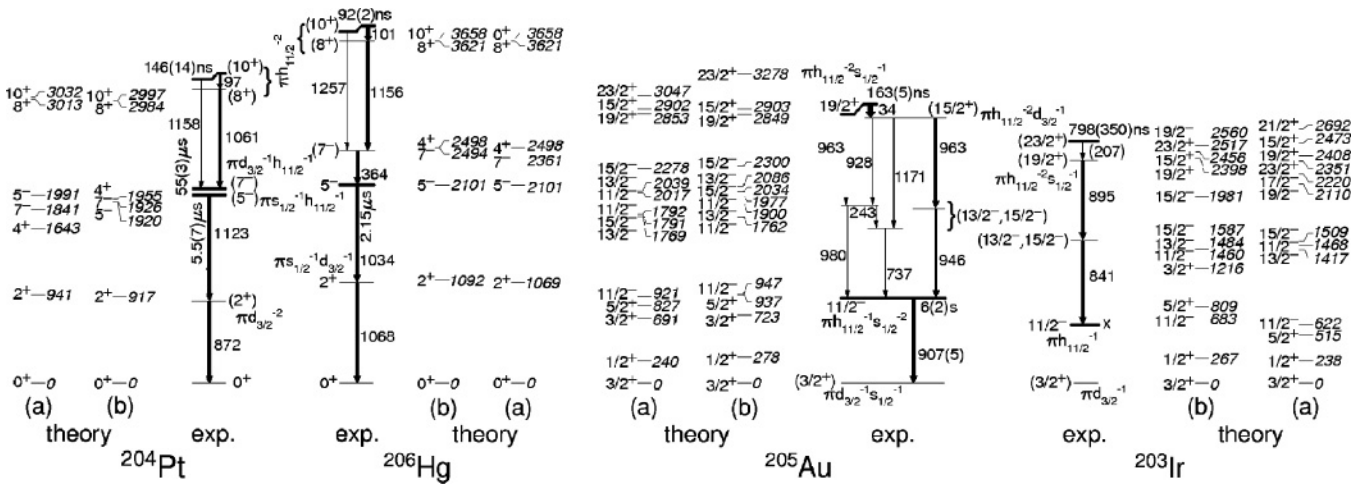

FIG. 7. Experimental and calculated partial level schemes of the $N = 126$ ^{206}Hg [5], ^{204}Pt, ^{205}Au and ^{203}Ir nuclei. Arrow widths denote relative intensities of parallel decay branches. The dominant state configurations are indicated. Theory (a) represents calculations using the Rydström matrix elements, while (b) are with the modified ones, as described in the text.

has $I^\pi = 23/2^+$ and it decays to the $19/2^+$ state, possibly via the 207 keV tentative γ-ray transition. In this case, the $19/2^+$ state is most likely isomeric as well, decaying by a strong E3 into either a $13/2^-$ or $15/2^-$ state. Based on the shell-model calculations, we are inclined toward this second scenario. The existence of two isomeric states would explain the lower intensity of the tentative 207 keV transition. The transition strength was determined assuming the same half-life for both metastable states (Table II).

We compare the standard and the modified shell model calculations with the experimental data, with the energy spectra presented in Fig. 7, and with the reduced transition strengths in Table II. The main differences are: (i) the modified shell model gives a better description of the decay of the long-lived $11/2^-$ isomer in ^{205}Au. According to the calculations, the isomer should decay via an E3 transition into the yrast $5/2^+$ state with a partial half-life of the order of $\sim$0.1 s. This is contradicted by the experiment as the measured half-life is much longer [34]. The $5/2^+$ state cannot be as low as predicted by the standard shell model, it is likely that it lies above the $11/2^-$ state; (ii) the B(E2 :$19/2^+ \rightarrow 15/2^+$) transition strength in ^{205}Au is described much better by the modified shell model; (iii) in ^{203}Ir the modified shell-model gives a low B(E2) transition strength for the transition depopulating the isomer, in agreement with the experiment. (iv) the modified shell model calculation predicts a much longer half-life (when compared with the standard calculations) for the $11/2^-$ state in ^{203}Ir. However, in this case we do not have experimental information. Based on the above evidence, (i), (ii), and (iii) we conclude that the modifications of the shell-model TBMEs improve the description of the odd-A ^{205}Au and ^{203}Ir nuclei.

C. $N = 125$ nuclei

Isomeric decays were observed in five $N = 125$ nuclei: ^{206}Tl, ^{205}Hg, ^{204}Au, ^{203}Pt, and ^{202}Ir. The corresponding delayed γ-ray spectra are shown in Fig. 8.

Two of the observed isomers and their decay have been reported previously. These are the $I^\pi = (5)^+$, $T_{1/2} = 78(1)$ ns [30,35] isomeric state in ^{206}Tl, and the $I^\pi = 13/2^+$, $T_{1/2} = 1.09(4)$ ms [36] isomer in ^{205}Hg. The lifetime of $T_{1/2} = 71(4)$ ns for ^{206}Tl measured in the present experiment agrees with the published value. We could not determine the half-life of the above mentioned isomeric state in ^{205}Hg since our correlation time, 85 μs in this case, was much shorter than the lifetime.

In ^{205}Hg a previously unreported isomer has also been detected. Transitions with energies of 228, 723, 810, and 950 keV have been observed. The isomer has a lifetime of $T_{1/2} = 5.89(18)$ μs. Time differentiated γ-γ coincidence analysis proves that this newly discovered isomer feeds the previously observed $I^\pi = 13/2^+$ isomer. Within experimental uncertainties the sum of the energies of the 228 and 723 keV transitions is equal to the 950 keV transition, indicating that these are parallel decay pathways, which was confirmed by γ-γ coincidence analysis. All these three transitions are in coincidence with the 810 keV line.

In ^{204}Au excited states have been observed for the first time. Transitions are detected at the energies 839 and 977 keV. The half-life of the isomer is $T_{1/2} = 2.1(3)$ μs. There are other, tentatively identified γ-ray transitions at energies of 97, 277, 427, and 704 keV [14]. We note that recently the β decay of ^{204}Pt was studied and γ rays belonging to ^{204}Au, with energies of 165 and 305 keV, in mutual coincidence, were reported [37].

In ^{203}Pt, one transition has been identified, with an energy of 1104 keV and associated half-life of $T_{1/2} = 641(55)$ ns.

In ^{202}Ir, no experimental observation was available prior to this work. γ rays with energies of 312, 656, 737, 889, and 968 keV and Ir K x rays were detected. A parallel decay branch is likely as the sum of the energy of the 312 and 656 keV transitions is equal to 968 keV, within experimental uncertainties. The half-life of the isomer is determined to be $T_{1/2} = 3.4(6)$ μs.

The experimental and calculated level schemes of the $N = 125$ nuclei are shown in Fig. 9. In ^{205}Hg, the low

energy part is dominated by single-neutron orbitals. The $p_{1/2}$, $f_{5/2}$, $p_{3/2}$, and $i_{13/2}$ neutron holes are associated with the 0, 379, 468, and 1556 keV states. The latter one is isomeric. All the yrast states above 2 MeV must involve at least three unpaired holes. The calculations suggest that the $23/2^-$ state should be isomeric and decaying into the yrast $17/2^+$ and $19/2^+$ states. The $23/2^-$ and $19/2^+$ states have predominant $\pi(s_{1/2}^{-1}h_{11/2}^{-1})5^-\nu i_{13/2}^{-1}$ and $\pi(d_{3/2}^{-1}h_{11/2}^{-1})7^-\nu f_{5/2}^{-1}$ configurations, respectively, while the $17/2^+$ state has a leading $\pi(s_{1/2}, d_{3/2})^{-2}2^+\nu i_{13/2}^{-1}$ configuration. Therefore, the parity changing M2 and E3 transitions will be hindered as they proceed via minority components in the wave functions. We associate these decay out transitions with the observed 950 and 723 keV γ rays. Assuming that both transitions are stretched, the deduced transition strengths are B(E3; 950 keV) = 0.10(1) W.u. and B(M2; 723 keV) = $8(1)\times10^{-5}$ W.u. The E3 transition is mediated by the $\pi h_{11/2} \rightarrow \pi d_{5/2}$ conversion; i.e., the weak $d_{5/2}$ content in

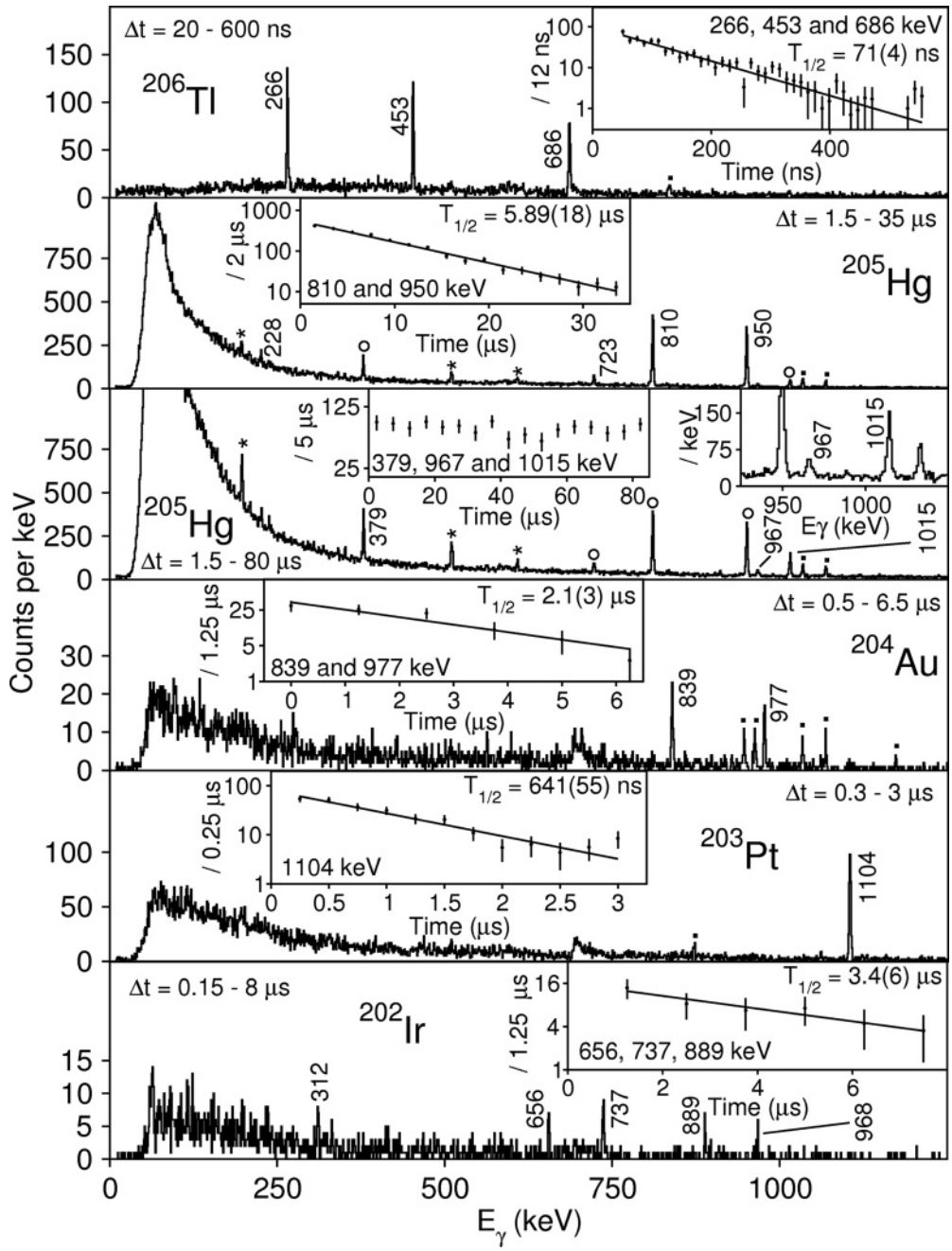

FIG. 8. Delayed γ-ray spectra for $N = 125$ nuclei. Background peaks are indicated by $\star$, transitions arising due to contaminant nuclei are indicated by, ■. The peaks indicated by ○ belong to the nucleus of interest, but originate from a different isomeric state than that for which the time limits of the γ spectrum are optimised. Inset spectra are time curves associated with the decay of the observed isomers. The transitions used to measure half-lives are indicated in the time spectra.

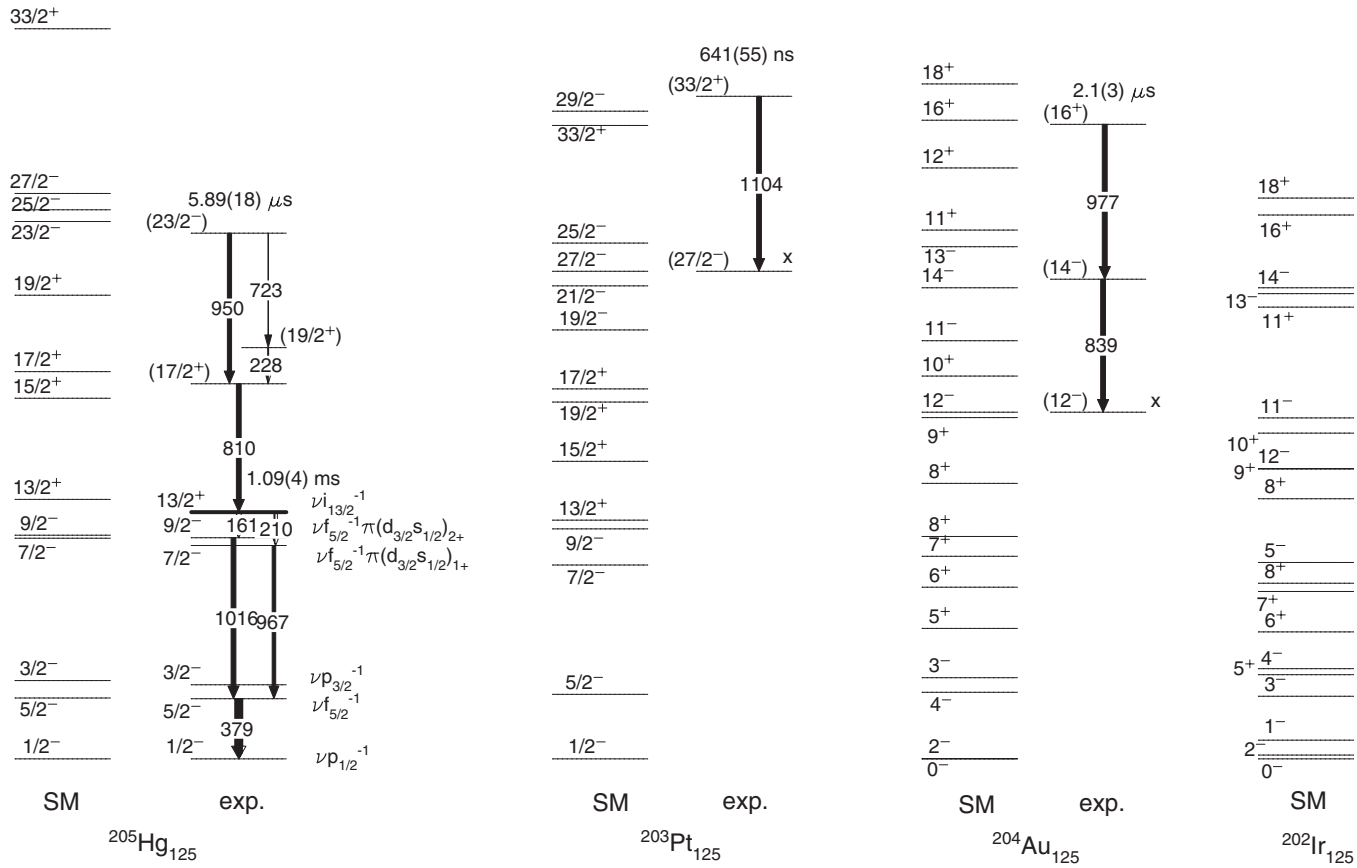

FIG. 9. Calculated and experimental level schemes for N = 125 nuclei ^{205}Hg, ^{203}Pt, ^{204}Au and ^{202}Ir. The experimental level scheme below the $13/2^+$ isomer in ^{205}Hg, as well as its half-life is from Ref. [36].

the wave function of the final state is crucial. Analogue E3 transitions with similar transition strengths have been observed in the $N = 126$ nuclei ^{204}Pt, ^{205}Au, ^{206}Hg (see Table II), supporting our interpretation.

The level schemes of ^{203}Pt and ^{205}Hg are expected to be very similar, as shown by the calculated level schemes of Fig. 9. The obvious difference is that the negative parity three-hole states (involving the $\pi h_{11/2}$ orbital) are at lower excitation energy in ^{203}Pt, which is analogous with the ^{204}Pt–^{206}Hg case. The interpretation of the sole ^{203}Pt γ ray observed in the experiment is far from straightforward. Its submicrosecond lifetime indicates that this transition cannot be associated with the predicted $\nu i_{13/2}^{-1}$ $13/2^+$ isomer. Similarly, the lifetime of the predicted $27/2^-$ state ($\nu i_{13/2}^{-1}\pi h_{11/2}^{-1}d_{3/2}^{-1}$) should be much longer than the measured one and should decay through a cascade of observable transitions. Most likely the observed 1104 keV transition populates this predicted long-lived $27/2^-$ isomeric state. The shell model suggests that the observed 1104 keV transition is the transition connecting the yrast $33/2^+$ isomeric state with the much longer lived $27/2^-$. The transition strength, B(E3) = 0.38(4) W.u., is in line with other octupole transitions in the region. The determined isomeric ratio of 1.3(2)% is low, as expected for high-spin isomers.

In the odd-odd ^{204}Au and ^{202}Ir nuclei, the shell model predicts isomers with spin-parity 12^- and possibly 5^+. The 5^+ is expected to be very short lived, no longer than its counterpart in ^{206}Tl with $T_{1/2} = 78$ ns (it decays via a hindered E1, and E1 transitions are forbidden in the used shell-model space). On the other hand, the 12^- state with $\pi h_{11/2}^{-1}\nu i_{13/2}^{-1}$ configuration should have a much longer lifetime than the observed μs isomers, because it has to decay by E3/M4 transitions (in ^{206}Tl it has $T_{1/2} = 3.74$ min). Consequently, it is likely that the observed transitions feed the long-lived 12^- isomer, again a spin trap. The observation of γ rays with similar intensity at 600–1000 keV supports this interpretation, as the 12^- and 5^+ isomers should have very different decay patterns. In ^{204}Au, it is most likely that the two observed transitions correspond to the decay of the 16^+ isomer into the 14^- state via an M2 + E3 and a consequent E2 into the long-lived 12^- state. The ordering of the two transitions cannot be determined from the experiment and is guided by the shell model calculations. Assuming a stretched M2 decay from the 16^+ isomer, the transition strength is B(M2; 977 keV) = $5(1)\times10^{-4}$ W.u.; assuming a stretched E3, the transition strength is B(E3; 977 keV) = 0.28(5) W.u. We note that the very low isomeric ratio, below 1%, supports the idea of the high-spin isomer.

In ^{202}Ir, the shell model predicts the same isomeric states and decay patterns as in its ^{204}Au isotone. Due to the larger number of observed transitions, we cannot suggest an experimental level scheme. The isomeric ratio is below 1% in this case as well, suggesting that the isomer has a high spin.

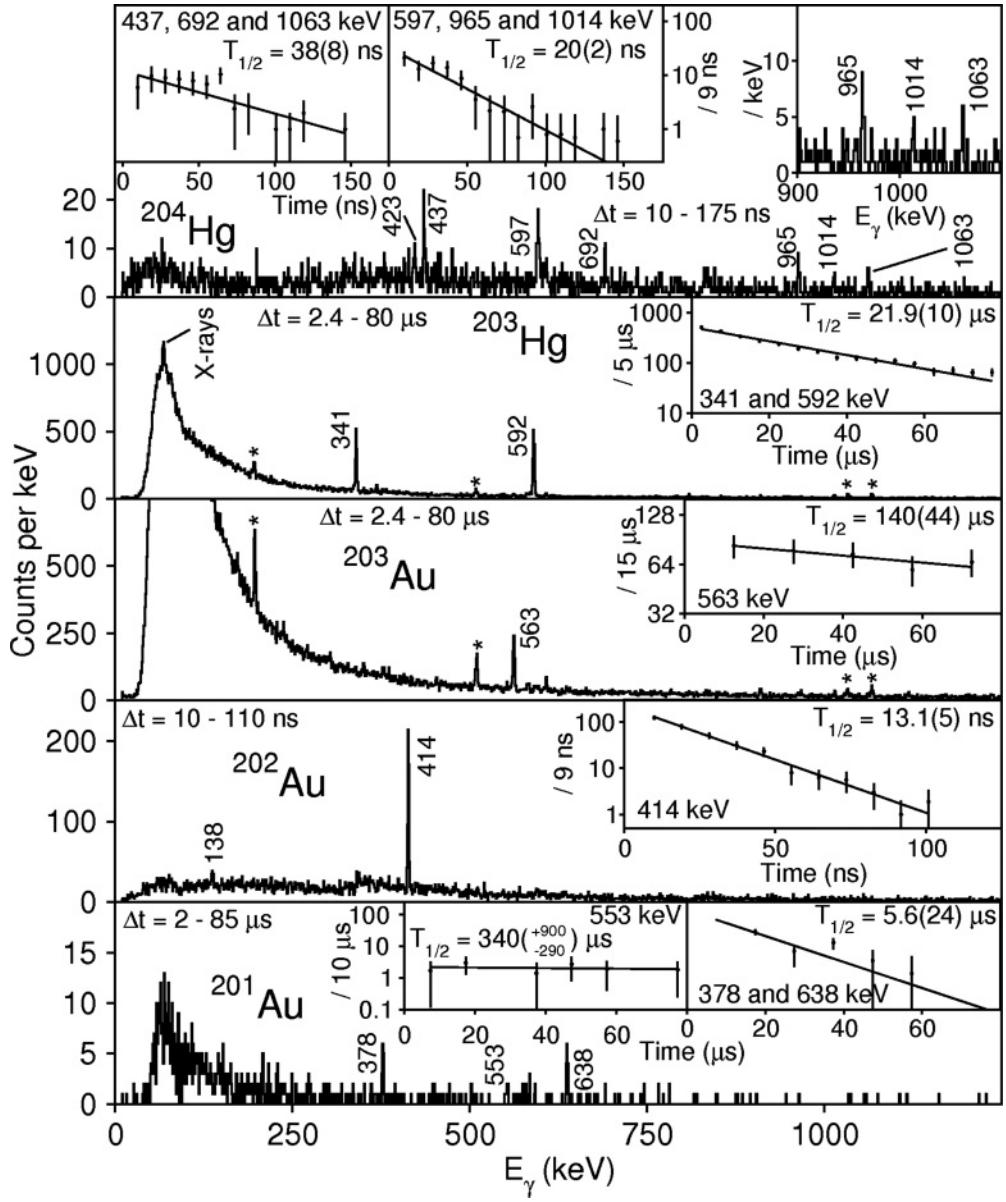

FIG. 10. Gamma-ray spectra for Hg and Au nuclei with $N < 125$ measured in the described experiment. Background peaks are indicated by ⋆. Inset spectra are time curves associated with the decay of the observed isomers. The transitions used to measure half-lives are indicated in the time spectra.

We note that the transition strengths calculated with the two shell model parametrizations are close to each other for the $N = 125$ nuclei(Table II).

D. $^{204,203}_{80}$Hg and $^{203,202,201}_{79}$Au

Delayed γ-ray spectra associated with ^{204,203}Hg and ^{203,202,201}Au are shown in Fig. 10.

In ^{204}Hg, in addition to the transitions depopulating a very short lived $I^\pi = 7^-$, $T_{1/2} = 6.7(5)$ ns [38] isomeric state, new γ lines were identified at 597, 965, and tentatively at 423 and 1014 keV (note that a 423 keV line is known to decay into the 7^- isomeric state [38]). These have equal half-lives within experimental uncertainties, $T_{1/2} = 20(2)$ ns. The effective half-life of the transitions depopulating the 7^- isomer (437, 692, and 1063 keV) is 38(8) ns (see Fig. 10), longer than the real half-life of this metastable state. This suggests that the newly identified transitions decay into the previously known isomer. The proposed level scheme is shown in Fig. 11. Shell model calculations predict a 14^+ isomeric state decaying via a low-energy E2 transition. Due to the low statistics, we cannot establish the decay sequence from this higher-lying isomeric state.

In ^{203}Hg, the previously reported $I^\pi = (13/2^+)$ $\nu i^{-1}_{13/2}$ isomer [39] has been observed in the present work (see Fig. 11). The half-life is measured to be $T_{1/2} = 21.9(10)$ μs, which is consistent with and more accurate than the accepted value of

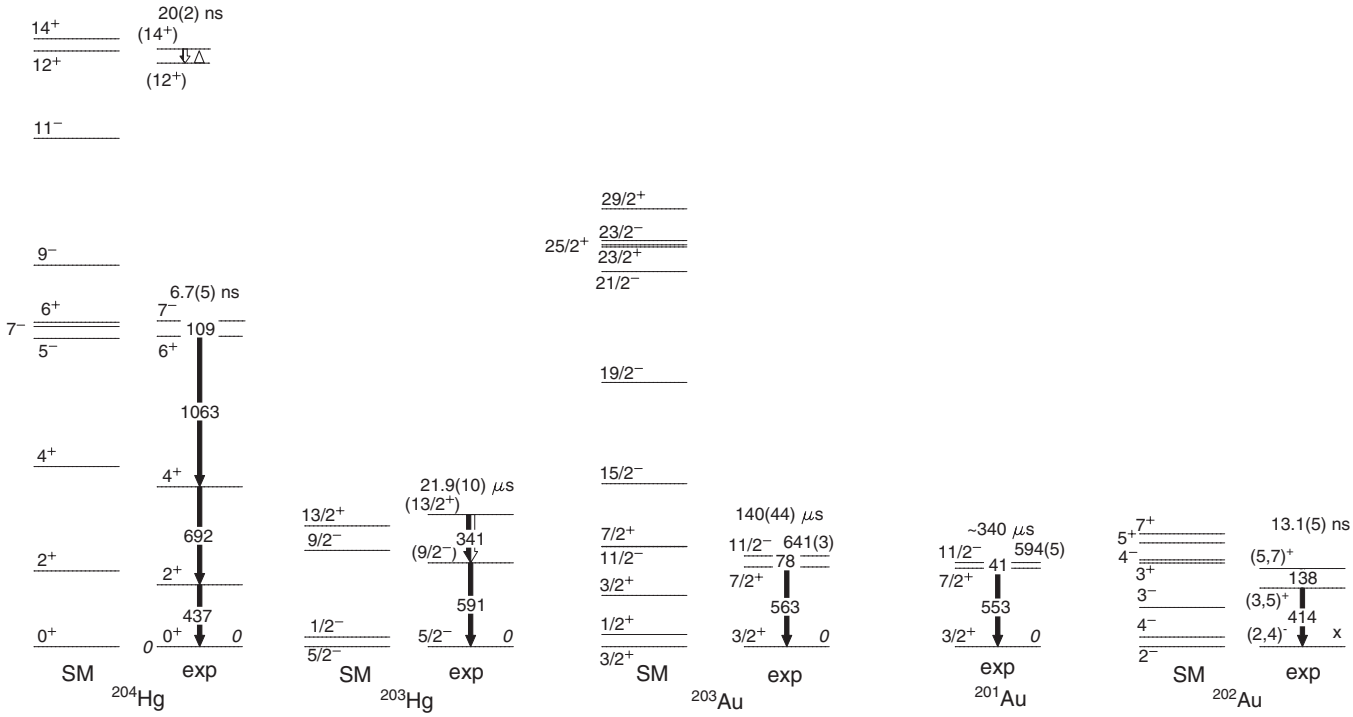

FIG. 11. Level schemes of ^{204}Hg, ^{203}Hg [39], ^{203}Au, ^{201}Au and ^{202}Au. The low-lying levels up to the 7^- isomer in ^{205}Hg [36] and the energies of the $11/2^-$ isomeric states in ^{203,201}Au [39,42] are taken from the literature.

$T_{1/2} = 24(4)$ μs. The isomer decays by an M2 transition with B(M2) = 0.0457(21) W.u. strength, which is reproduced by the shell model (see Table II).

In $^{203}_{79}$Au$_{124}$, Caamaño *et al.* [40] identified a single transition (563 keV) with a half-life of 40^{+7000}_{-20} μs. Our half-life, $T_{1/2} = 140(44)$ μs, is consistent with and more precise than the published value. The error bars are large because in this case the γ-ray correlations following implantation were limited to a maximum time of 85 μs. Nevertheless, the improved lifetime measurement is the key to the interpretation of this decay (Fig. 11). It is expected that the $\pi h^{-1}_{11/2}$ state is isomeric. A charged particle reaction experiment pinned down this state as being at 641(3) keV [38,41]. The half-life of the isomer suggests a low-energy M2 transition and rules out a low-energy E3. (Note, that while the standard shell model calculation does predict an inverse ordering of the $11/2^-$ and $7/2^+$ states, the modified one agrees with the experiment.) The observed 563 keV transition connects the $7/2^+$ state with the $3/2^+$ $\pi d^{-1}_{3/2}$ ground state. The B(M2) transition strength of the unobserved 78(3) keV γ ray is 0.03(2) W.u., in excellent agreement with the shell model prediction. The lack of strong K x rays indicates that the energy of the M2 transition is below the K-electron binding energy of 80.725 keV. The rather low isomeric ratio, 2.5^{+8}_{-10}% here and >1% in Ref. [40], suggests the existence of a higher lying long-lived isomer in this nucleus.

In $^{202}_{79}$Au$_{123}$ no excited states were reported before. Two transitions are identified at 138 and 414 keV. The half-life is $T_{1/2} = 13.1(5)$ ns. γ-γ coincidences confirmed that the two transitions are in coincidence [14]. The intensity balance supports an M1 or possible E2 assignment for the 138 keV transition. Based on the shell model calculations we propose the tentative level scheme shown in Fig. 11. Either the 7^+ or the 5^+ state could be isomeric. The isomer decays by the 138 keV E2 transition, followed by a fast 414 keV E1. The measured transition strength, B(E2) = 5.0(2) W.u., is consistent with the ∼11 W.u. value predicted by the shell model.

In ^{201}Au, three new delayed transitions are identified at 378, 553, and 638 keV. The half-life of the 553 keV transition is $T_{1/2} = 340^{+900}_{-290}$ μs, while the other two transitions originate from a shorter lived isomeric state with $T_{1/2} = 5.6(24)\mu s$. Previously, excited states of ^{201}Au were studied experimentally in the ^{202}Hg($\vec{t}$,α) reaction [41,42]. The yrast $11/2^-$ state with $\pi h^{-1}_{11/2}$ configuration was identified at 594(5) keV [42]. Below this state only low-spin states ($3/2$ and $1/2$) and a tentative level with no spin-parity assignment at 549(5) keV were observed. Based on the lifetime, and the similarity between the observed γ-ray energy of 553 keV and the 549(5) keV excitation energy, we propose the level scheme shown in Fig. 11. The $11/2^-$ isomer at 594(5) keV decays by an unobserved low-energy 41(6) keV M2 transition into the $7/2^+$ state, which decays into the $3/2^+$ ground state by the 553 keV γ ray. This decay pattern, as well as the M2 transition strength of $B(M2)$ ∼0.02 W.u. is similar to that observed in the neighboring ^{199}Au [43] and ^{203}Au (this paper) odd-mass isotopes. This interpretation fits with the conclusions of a recent ISOLDE experiment [44]. There it was concluded [45] that the $11/2^-$ state cannot have a half-life of the order of seconds; i.e., it does not decay directly into the $3/2^-$ ground-state by an M4 transition (the case in ^{205}Au). The 638 and 378 keV transitions are associated with a higher lying isomeric state which decays into the $11/2^-$ one. The intensity balance and lifetime are compatible with the 378 keV

transition being an M2 transition decaying from the isomer with a strength of $B(M2) = 0.014(7)$ W.u. Note that due to the large number of holes outside the ^{208}Pb core, no shell model calculations were performed for ^{201}Au.

E. Platinum isotopes $^{202,201,200,199,198,197}_{78}$Pt

In $^{202}_{78}$Pt$_{124}$, an $I^{\pi} = (7^{-})$ isomer was previously observed by Caamaño *et al.* [40]. Our half-life of $T_{1/2} = 141(7)$ μs is consistent with and more accurate than the previous value of $T_{1/2} = 280^{+420}_{-190}$ μs. γ-γ coincidence analysis has confirmed the doublet nature of the 535 keV peak [14]. This is consistent with the interpretation made by Caamaño *et al.* [40].

In $^{201}_{78}$Pt$_{123}$, the previously reported isomer [40] has been observed in the current work. In addition to the three known transitions, we searched for a possible low-energy one, without success. The isomeric half-life is measured to be $T_{1/2} = 18.4(13)$ ns, which is consistent with the previous measurement of $T_{1/2} = 21(3)$ ns [40].

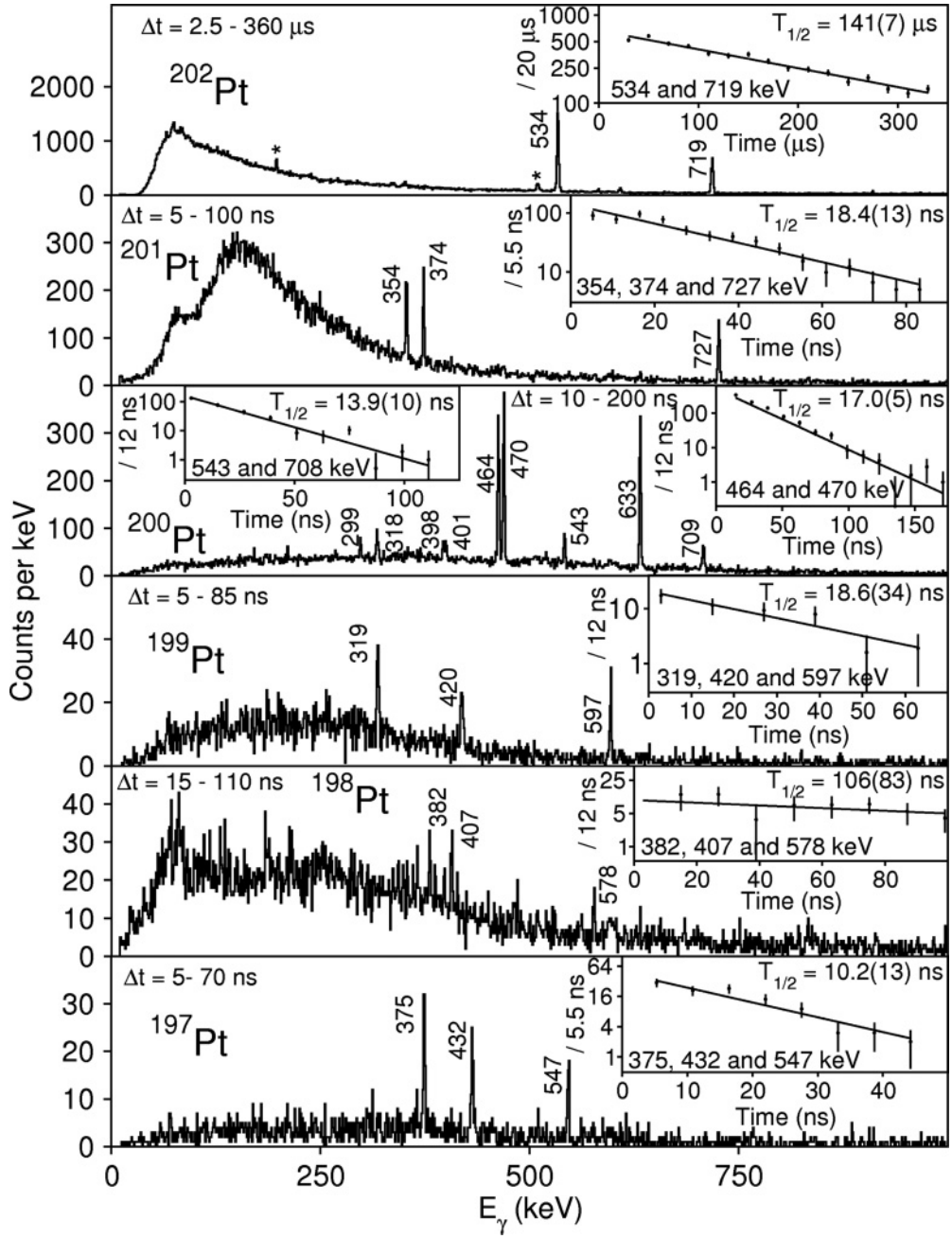

FIG. 12. Gamma-ray spectra for Pt nuclei with $N < 125$ measured in the described experiment. Background peaks are indicated by $\star$. Inset spectra are time curves associated with the decay of the observed isomers. The transitions used to measure half-lives are indicated in the spectra.

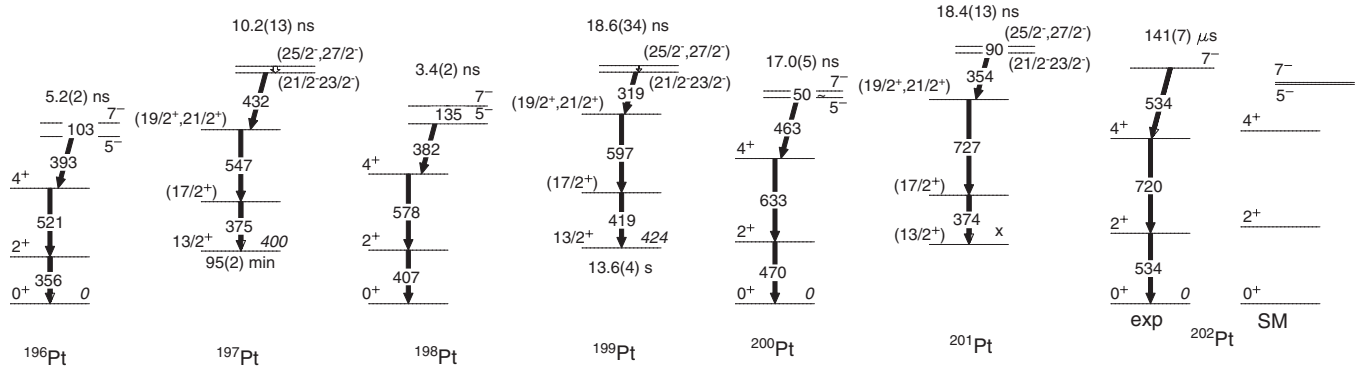

FIG. 13. Partial experimental level schemes of the $^{198-202}$Pt nuclei. The level schemes of the even-even isotopes are from [40,46,47,51,56]. The $13/2^+$ states were identified in ^{197,199}Pt before [43,54]. The half-lives are from the present work with the exception of ^{196}Pt [56] and ^{198}Pt [47]. The shell-model level scheme of ^{202}Pt is also given.

In $^{200}_{78}$Pt$_{122}$, two previously reported isomers were observed. The lower-lying $I^\pi = (7^-)$ isomer has a half-life of $T_{1/2} = 14.3(6)$ ns, which is the weighted average of the previous measurements [40,46]. This work reports a half-life of $T_{1/2} = 17.0(5)$ ns. The other isomer has only been reported by Caamaño *et al.* [40], it has a spin-parity $I^\pi = (12^+)$ and it feeds the $I^\pi = (7^-)$ isomer. The current work agrees with the previous findings and reports a half-life of $T_{1/2} = 13.9(10)$ ns; it was previously reported to be $T_{1/2} = 10.3(24)$ ns.

In $^{199}_{78}$Pt$_{121}$, we observe an unreported isomeric state. γ-ray transitions have been detected at the energies 319, 420, and 597 keV. All three transitions exhibit the same decay lifetime, within experimental uncertainties. The half-life of the isomer is $T_{1/2} = 18.6(34)$ ns.

In $^{198}_{78}$Pt$_{120}$, we observe three transitions that follow the decay of the previously reported $I^\pi = 7^-$, $T_{1/2} = 3.4(2)$ ns isomer [47]. A higher-lying isomer with $T_{1/2} = 36(2)$ ns was also reported [48,49], feeding the lower-lying $I^\pi = 7^-$ isomer. The data evaluators of Ref. [47] suggested $I^\pi = (12^-)$ for this isomer. There is weak evidence in the γ-ray energy spectrum (see Fig. 12) for the presence of the 135-, 752-, and 823-keV transitions that feed the $I^\pi = 7^-$ state; therefore, the half-life determined from the present experiment has a large uncertainty due to the poor statistics, and it is consistent with previous measurements.

In $^{197}_{78}$Pt$_{119}$, three transitions emitted following the decay of a previously unreported isomer have been detected with energies of 375, 432, and 547 keV. The three transitions are in mutual coincidence [14] and the half-life is $T_{1/2} = 10.2(13)$ ns.

The partial level schemes of the $^{196-202}$Pt nuclei are shown in Fig. 13. The even-even Pt nuclei are characterized by a 7^- isomeric state with a predominantly $\pi(h^{-1}_{11/2}d^{-1}_{3/2})7^-$ configuration. g-factor measurements [50] in lighter, $^{190-194}$Pt, isotopes support this interpretation. Due to the large number of nucleons outside the closed shell, theoretical calculations were done for ^{202}Pt only. These were performed with a truncated model space, i.e., with closed $\pi g_{7/2}$ and $\nu h_{9/2}$ orbitals. The calculations predict predominantly two-proton character for the 7^- state. (In contrast, the 7^- state in ^{204}Hg is of mixed $\pi h^{-1}_{11/2}d^{-1}_{3/2}$ and $\nu i^{-1}_{13/2}p^{-1}_{1/2}$ character.) In the case of ^{196,198,200}Pt, the 7^- isomer decays by a low-energy E2 transition into the $\pi(h^{-1}_{11/2}s^{-1}_{1/2})5^-$ state and has a half-life of the order of nanoseconds. In the case of ^{202}Pt, the half-life is much longer, $T_{1/2} = 141(7)$ μs. This is explained by the lowering of the 7^- state below the 5^- [40,51]. The reduced transition strength is $B(E3) = 0.268(13)$ W.u. According to the interpretation proposed here, the isomers observed in the odd-mass Pt isotopes have similar structure to that in the neighboring even-even Pt isotopes, with an added neutron in the $i_{13/2}$ orbital. Isomeric states with similar structure were previously identified in lighter Pt isotopes, such as ^{191,193}Pt [52,53]. This interpretation differs from the previously suggested one [40] for ^{201}Pt (the data on the isomers in ^{197,199}Pt is new). Previously, it was proposed that the isomer populates the $5/2^-$ ground state. The present interpretation is based on the similarities between the isomers observed in these nuclei: there are always three strong transitions in similar energy regimes; and the half-lives are of the order of tens of nanoseconds (with the exception of ^{202}Pt). The scenario is also supported by the E2 strengths, which for ^{200}Pt is $\sim$13 W.u. close to the value of 11 W.u. calculated for ^{202}Pt, the last one accessible to shell model calculations. With increasing distance from $N = 126$ an increase to twice this value is observed for both the even-A and odd-A isotopes.

We note that the $13/2^+$ state is known in ^{197}Pt [54] and ^{199}Pt [43] but was not observed in ^{201}Pt. The ordering of the three transition in the odd-mass nuclei is based on the systematics. The exception is the $17/2^+$ state in ^{197}Pt, where a $(17/2^+)$ state at 767(10) keV was previously identified in a (^{3}He,α) reaction [54,55].

F. Iridium isotopes $^{201,200,199,198,195}_{77}Ir_{124}$

The delayed γ-ray and time spectra of $^{201,200,199,198,195}_{77}Ir_{124}$ are shown in Fig. 14.

In $^{201}_{77}$Ir$_{124}$, no experimental information on the excited states was previously available. Presently, an isomer has been observed, emitting three transitions: 440, 452, and 681 keV. The half-life is $T_{1/2} = 10.5(17)$ ns.

No experimental information on the excited states of $^{200}_{77}$Ir$_{124}$ was previously available. Two transition were

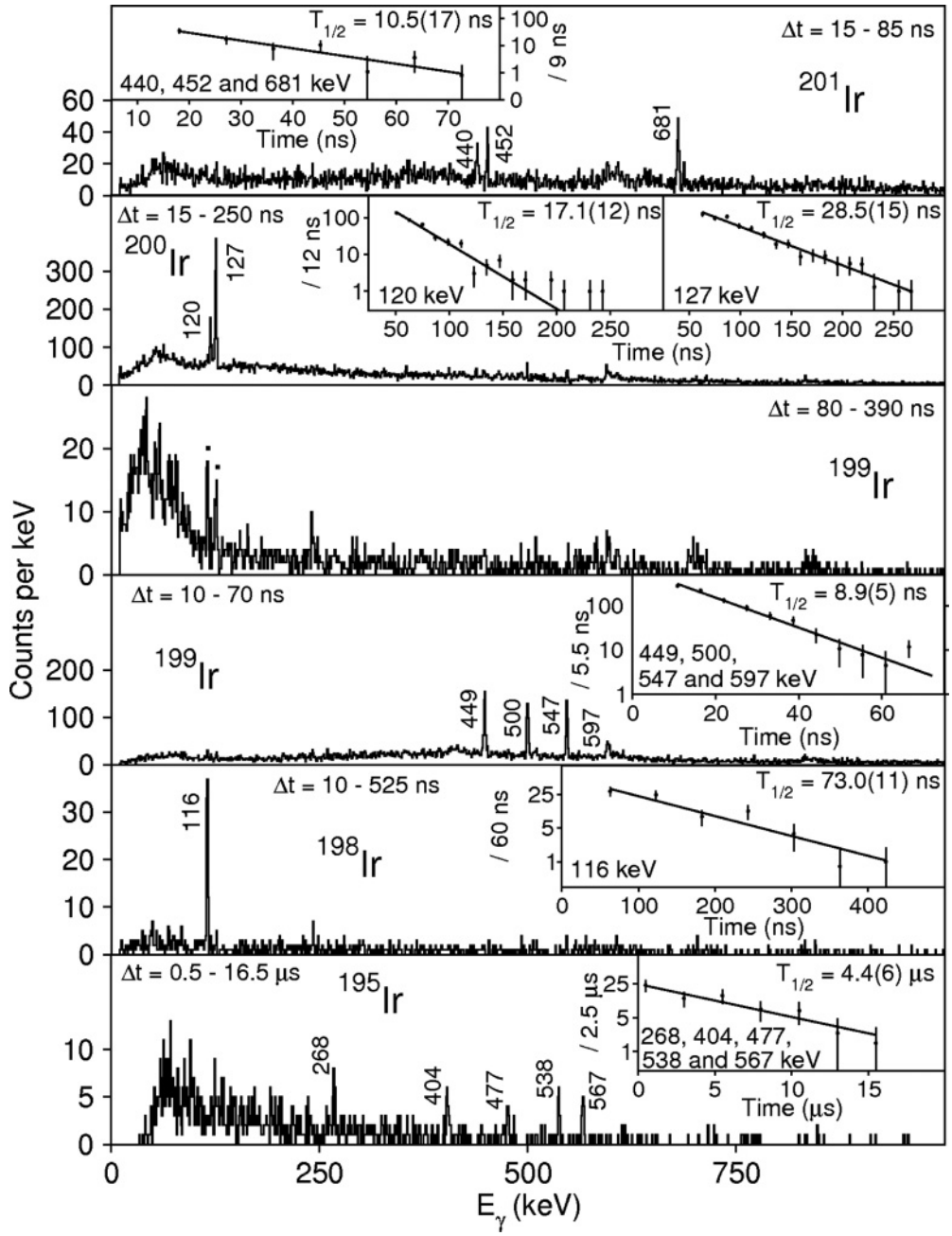

FIG. 14. Gamma-ray spectra for Ir nuclei with $N < 125$ measured in the described experiment. Transitions arising from contaminant nuclei are indicated by, ■. Inset spectra are time curves associated with the decay of the observed isomers. The transitions used to measure half-lives are indicated in the spectra.

observed, at energies of 120 and 127 keV. The transitions are not in coincidence with each other [14]. The half-lives associated with the decay of these two transitions are $T_{1/2} =$ 17.1(12) and 28.5(15) ns, respectively.

In $^{199}_{77}\mathrm{Ir}_{122}$, a new isomeric state has been observed decaying by 449-, 500-, 547-, and possibly 597-keV transitions. The intensity of the tentative 597-keV transition (its energy is similar to that from the ^{74}Ge(n,n′) reaction) is distinctly less than the intensity of the other three. γ-γ coincidence analysis shows that the three stronger transitions are in mutual coincidence. In addition, the 500 keV is a doublet, since it is in coincidence with itself. The 597-keV transition is tentatively observed to be in coincidence with the other three transitions. Based on the presently available experimental data, it is interpreted that all of the transitions are emitted following the decay of a single isomer with a half-life of $T_{1/2} = 8.9(5)$ ns. Caamaño *et al.* [40] have previously tentatively reported the existence of an isomer in $^{199}_{77}\mathrm{Ir}_{122}$. Candidate transitions were suggested at the energies 104, 112, 122, and 162 keV. Our spectrum, with the same time range $\Delta t = 80 \rightarrow 390$ ns is shown in Fig. 14. No indication of the tentatively observed isomer has been detected in this work.

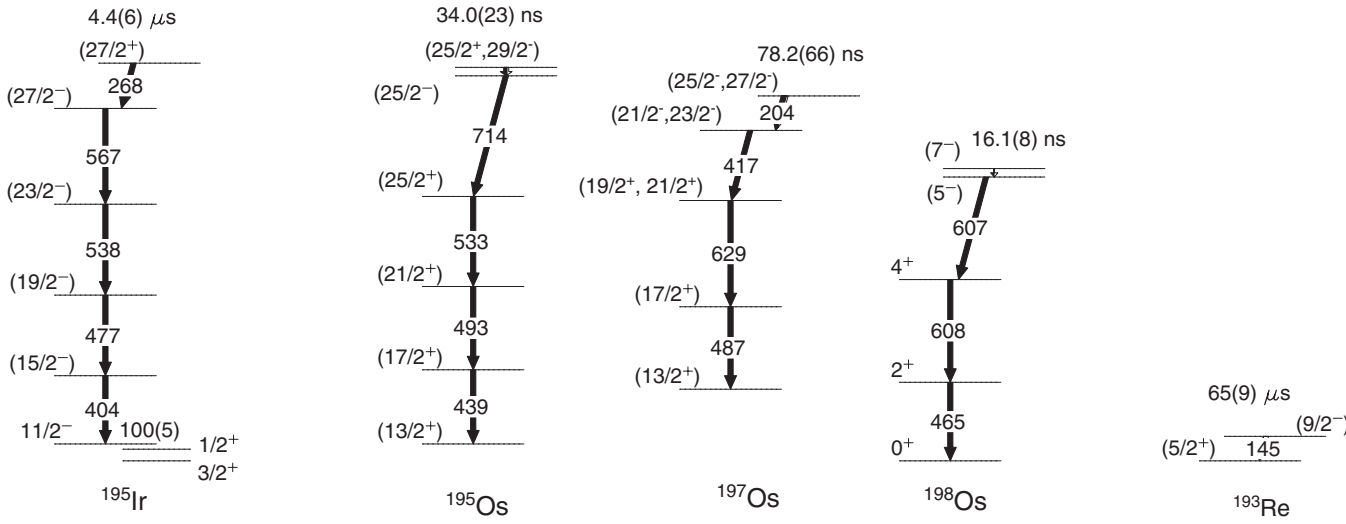

FIG. 15. Tentative level schemes for iridium, osmium and rhenium isotopes. The single particle states in ^{195}Ir are from literature [54,57]. For a more complete level scheme of ^{198}Os see [58].

An isomer has previously been identified in $^{198}_{77}\mathrm{Ir}_{121}$ with a half-life of $T_{1/2} = 77(9)$ ns [40]. Our measured half-life of $T_{1/2} = 73.0(11)$ ns is in agreement with the previous value.

A previously unreported isomer has been identified in $^{195}_{77}\mathrm{Ir}_{118}$. The transitions are observed to have energies 268, 404, 477, 538, and 567 keV. None of these transitions were known before [57]. The half-life of the isomer measured from the combined statistics of all of the transitions is found to be $T_{1/2} = 4.4(6)$ μs.

The odd-mass ^{193,195,197}Ir nuclei have a remarkably similar single quasiparticle level structure [53,54,57]. The ground-state is $\pi 3/2^+[402]$, followed by the $\pi 1/2^+[400]$ at ∼60-keV excitation energy and by $\pi 11/2^-[505]$ at ∼100 keV. The $11/2^-$ is isomeric with very long half-life (e.g., 10.5 days in ^{193}Ir). The similarity indicates that these isotopes must have very similar deformation. This, and the further similarity to less neutron-rich ^{189,191}Ir nuclei suggests that they all exhibit prolate deformation (note that the calculations of Möller *et al.* [29] suggest that Ir isotopes up to ^{196}Ir are prolate, and become oblate from ^{197}Ir onwards). The proposed level scheme for ^{195}Ir is shown in Fig. 15. Based on BCS calculations, we suggest for ^{195}Ir that a three-quasiparticle $27/2^+$ isomer with configuration $\pi 11/2^-[505]\nu 3/2^-[512]13/2^+[606]$ decays into the rotational band built on $\pi 11/2^-[505]$. The transition energies within the band fit into the systematics of the lighter odd-mass Ir isotopes. The transition strength of the 268-keV E1 transition is $\mathrm{B(E1)} = 2.3(3)\times 10^{-9}$ W.u.

In ^{198}Ir and ^{200}Ir, the lack of x rays in the spectra suggests that the observed low-energy transitions are of E1 character. In the case of ^{198}Ir, following the previous suggestion [40] that the observed transition is E1 in nature and it depopulates the isomer directly, a transition strength of $\mathrm{B(E1)} = 1.4(3)\times 10^{-6}$ W.u. and an isomeric ratio of IR = 5(4)% is measured. This is lower than the previous $\mathrm{IR} = 19^{+5}_{-3}$ value [40]. With the same assumptions for ^{200}Ir, we get $\mathrm{B(E1)} = 2.8(2)\times 10^{-6}$ W.u and $\mathrm{B(E1)} = 5.4(4)\times 10^{-6}$ W.u, IR = 3.5(14)% and IR = 22(12)%, for the 127- and the 121-keV transitions, respectively.

The lifetimes, of order of tens of nanoseconds, in ^{201}Ir and ^{199}Ir are compatible with decays via low-energy E2 transitions. Both nuclei are predicted to be almost spherical, with small, $\beta_2 < 0.1$, oblate deformation [29]. The observed γ-ray spectra do not resemble rotational bands, in agreement with the above prediction. No level schemes are proposed for these nuclei.

G. Osmium isotopes $^{199,198,197,195,193}_{77}$Os

The delayed γ-ray and time spectra for $^{199,198,197,195,193}_{77}$Os nuclei are shown in Fig. 16.

A previously unreported isomer has been observed in ^{199}Os. Five transitions have been detected with energies 379, 402, 425, 737, and 971 keV. The half-life of the isomer is measured to be $T_{1/2} = 25.2(20)$ ns.

Two new isomers were found in $^{198}_{76}\mathrm{Os}_{122}$. These results have been discussed in detail by Podolyák *et al.* [58]. In supplement to the previous publication, we present here limits on the isomeric ratios of the observed $I^\pi = (12^+)$ and (7^-) metastable states (see Table I).

No states have previously been reported in $^{197}_{76}\mathrm{Os}_{121}$. Presently, four transitions have been observed, these are at energies 204, 416, 487, and 629 keV. The half-life is found to be $T_{1/2} = 78.2(66)$ ns. All four transitions are in mutual coincidence [14].

In $^{195}_{76}\mathrm{Os}_{119}$, we confirm the isomeric state previously observed both in fragmentation [40] and deep-inelastic [48] experiments. Our half-life is $T_{1/2} = 34.0(23)$ ns, similar to the previously determined values of $T_{1/2} = 26(4)$ ns [40] and $T_{1/2} = 26(9)$ ns [48].

An isomer is reported for the first time in $^{193}Os_{117}$. One transition with 242 keV is associated with the decay of the isomer that has a half-life of $T_{1/2} = 132(29)$ ns. This energy does not fit into the known low-spin-level scheme [53] and we are unable to propose a level scheme.

The observed isomer in ^{195}Os was interpreted [48] to have $I^{\pi} = (27/2^{-})$ with $\nu 13/2^{+}[606]3/2^{-}[501]11/2^{+}[615]$ character. Here we suggest an alternative interpretation, as shown in Fig. 15. The $I^{\pi} = (29/2^{-})$ with $\nu 13/2^{+}[606]\pi 11/2^{-}[505]5/2^{+}[402]$ (or, alternatively, the $I^{\pi} = (25/2^{+})$ with $\nu 13/2^{+}[606]3/2^{-}[501]9/2^{-}[505]$) isomer decays via a low-energy E2 (or E1) transition into the $25/2^{-}$, $\nu 13/2^{+}[606]11/2^{-}[505]1/2^{+}[411]$ band-head, which decays via the 714-keV transition into the $\nu 13/2^{+}[606]$ band. We note that the $\nu 13/2^{+}[606]$ and $\nu 3/2^{-}[501]$ states are expected to be close in energy, one of them being the ground state and the other a long-lived isomer.

Theoretical calculations predict a weakly deformed oblate shape for $^{197-199}$Os [29,59], similar to the platinum isotopes. From the experimental side, the similarity between the excitation spectra of ^{198}Os and ^{200}Pt [58] suggests that the neighboring odd-mass nuclei are also similar. Consequently, a low-energy $13/2^{+}$ state, with a long half-life, is expected in the odd-mass Os isotopes. Most likely, the isomers observed in ^{197,199}Os decay into this yrast $13/2^{+}$ state. Possible isomeric states should have the $i_{13/2}$ neutron coupled with $\pi h_{11/2}^{-1} d_{3/2}^{-1}$ and/or $\pi h_{11/2}^{-2}$. For ^{197}Os, we suggest a level scheme similar to that of its ^{199}Pt isotone, with the isomer having $\nu i_{13/2}^{-1} \pi h_{11/2}^{-1} d_{3/2}^{-1}$ configuration (see Figs. 15 and 13). In ^{199}Os, the number of observed γ rays suggests a higher spin isomer, possibly with $\nu i_{13/2}^{-1} \pi h_{11/2}^{-2}$ character; however, we are unable to propose a level scheme.

We note that no isomeric state was observed in ^{196}Os [58]. This suggests that ^{196}Os has a different shape from the slightly

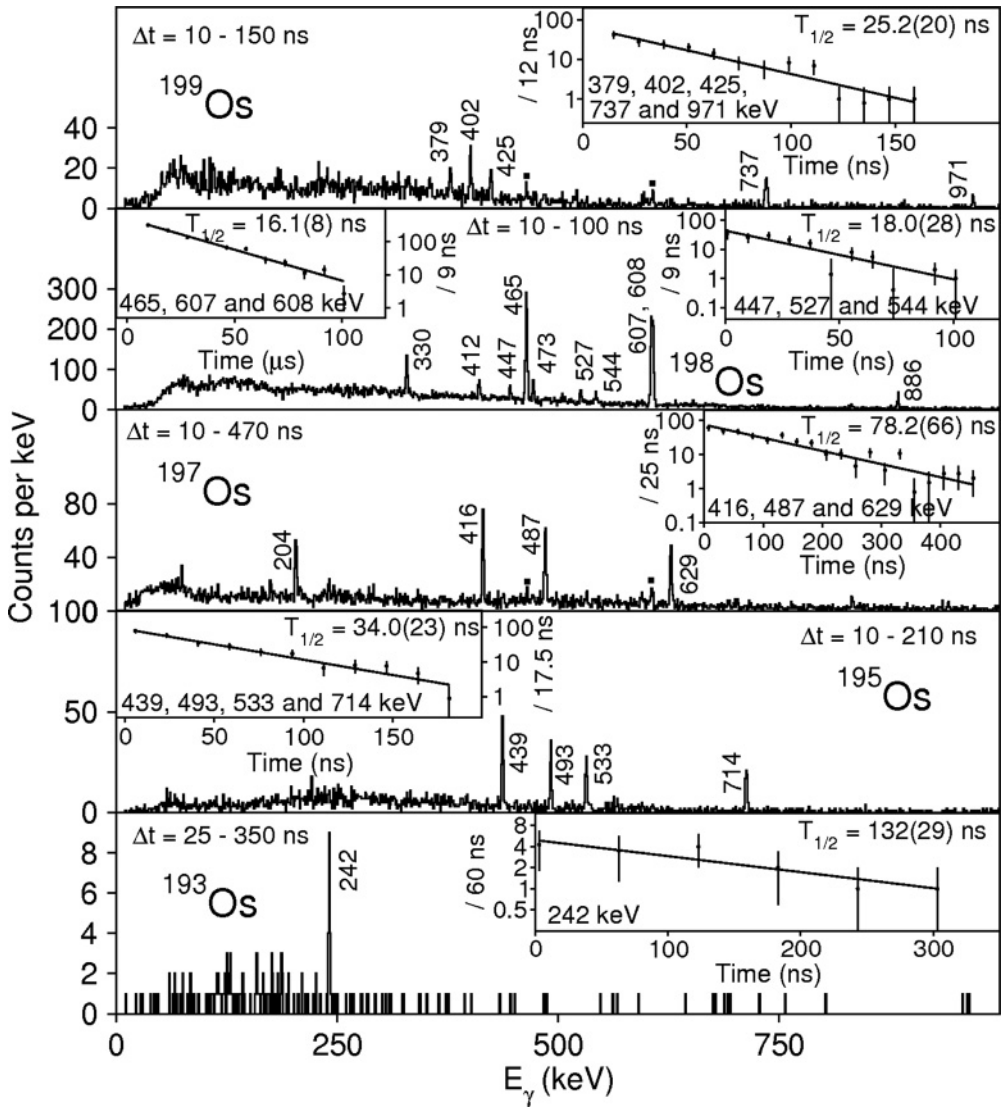

FIG. 16. Gamma-ray spectra for Os nuclei measured in the described experiment. Inset spectra are time curves associated with the decay of the observed isomers. The transitions used to measure half-lives are indicated in the spectra.

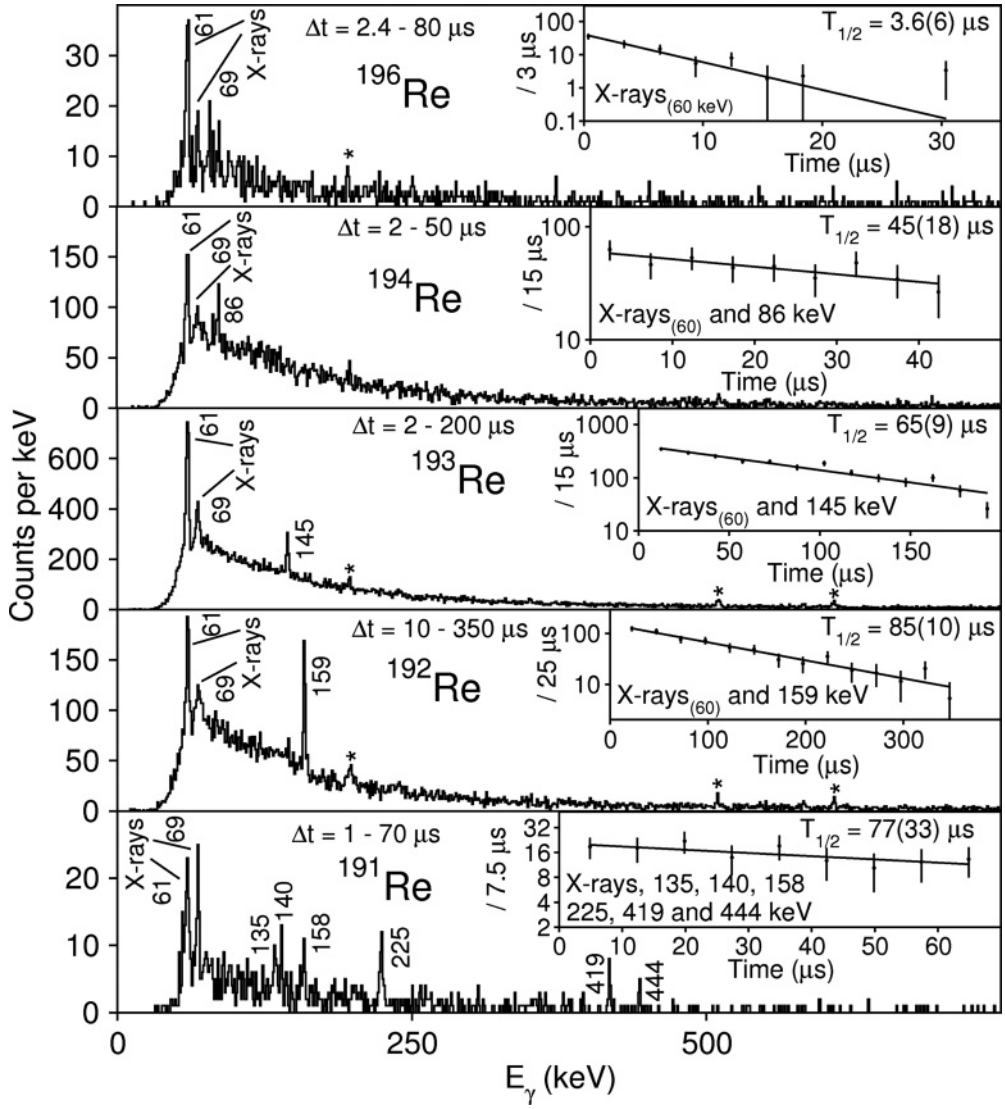

FIG. 17. Gamma-ray spectra for Re nuclei measured in the described experiment. Background peaks are indicated by ⋆. Inset spectra are time curves associated with the decay of the observed isomers. The transitions used to measure half-lives are indicated in the spectra.

oblate ^{198}Os [58] and the platinum isotopes. Here we propose that the shape transition to oblate happens after ^{196}Os.

H. Rhenium isotopes $^{196,194,193,192,191}_{75}$Re

The delayed γ-ray and time spectra of $^{196,194,193,192,191}_{75}$Re nuclei are shown in Fig. 17.

For the first time an excited state is reported to be observed to decay in ^{196}Re. Characteristic rhenium K_α and K_β x rays are observed following the decay through an unobserved highly converted transition. The half-life associated with the K_α x rays is measured to be $T_{1/2} = 3.6(6)$ μs.

In $^{194}_{75}$Re$_{119}$, Caamaño *et al.* [40] tentatively reported an isomeric state by observing possible transitions at 128, 148, and 464 keV and rhenium K_α and K_β x rays. The current report confirms the existence of an isomer with a measured half-life of $T_{1/2} = 45(18)$ μs. We observe the x rays and the 86-keV γ ray. The 128-, 148-, and 464-keV transitions have not been observed.

In ^{193}Re previous work by Caamaño *et al.* [40] identified the emission of a 145-keV γ-ray transition and characteristic rhenium K_α and K_β x rays following the decay of an isomer with a half-life of $T_{1/2} = 75^{+300}_{-40}$ μs. We confirm the existence of this isomer. The determined half-life, $T_{1/2} = 65(9)$ μs, is consistent with and more precise than the previous value. A more recent experiment also detected this isomer and gave $T_{1/2} = 72(8)$ μs [60].

In $^{192}_{75}$Re$_{117}$ Caamaño *et al.* [40] have previously identified the decay of an isomer. We confirm the existence of this isomer by detecting a 159 keV, γ ray, as well as characteristic rhenium K_α and K_β x rays. The determined half-life, $T_{1/2} = 85(10)$ μs, is consistent with and more precise than the previous value of $T_{1/2} = 120^{+210}_{-50}$ μs. A more recent experiment also detected this isomer and reported $T_{1/2} = 93(15)$ μs [60].

In $^{191}_{75}Re_{116}$, an isomer has tentatively been identified by Caamaño *et al.* [40] with possible transitions at 53, 139, 225, 308, 360, 419, and 444 keV with Re x rays as well. We confirm the existence of this isomer. There are differences between the transitions observed in this and the previous work. The suggested transitions at 53, 308, and 360 keV have not been observed in this work, although the others have. In addition, in this work a transition of 135 keV is tentatively identified, which was not previously observed. The intensity of the 225-keV line is double compared to the others, suggesting a doublet nature. The half-life of the isomer is $T_{1/2} = 77(33)\ \mu s$.

Odd-mass ^{187}Re [61] and ^{189}Re [61] are characterized by an $\pi 5/2^+[402]$ ground state with a low-lying $\pi 9/2^-[514]$ excited state. Our BCS calculations predict the same situation for ^{193}Re. We propose that the observed 145-keV transition connects these states and has an M2 transition strength of $B(M2) = 0.0175(25)$ W.u. The intensity of the observed x rays is in agreement with this scenario.

In ^{191}Re, we are unable to suggest a level scheme. Most likely the isomer feeds the $\pi 9/2^-[514]$ band head as the energy of the 140-keV transition is in agreement with the $(11/2^-) \rightarrow (9/2^-)$ energy difference [52]. The strong x rays as well as the lifetime suggest an M2 decay from the isomer, possibly arising from the same proton configuration change (with a broken neutron pair) as in ^{193}Re. We note that the $9/2^-$ band head at 145(3) keV [52] is likely to be isomeric with a similar lifetime, decaying into the $5/2^+$ band head at 97(3) keV (but the observed x rays are not from this decay and the 97(3)-keV transition is not observed).

The odd-odd ^{192,194,196}Re nuclei all exhibit strong x rays and similar microseconds lifetimes. These would suggest a low-energy M2 decay, similarly to the odd-mass nuclei. However, the x rays in ^{192}Re and ^{194}Re are too weak for the 159- and 86-keV transitions to be of M2 character, respectively. Consequently, no level schemes are suggested for the odd-odd rhenium nuclei. The isomeric ratios were determined assuming M1 character for the 159- and 86-keV transitions.

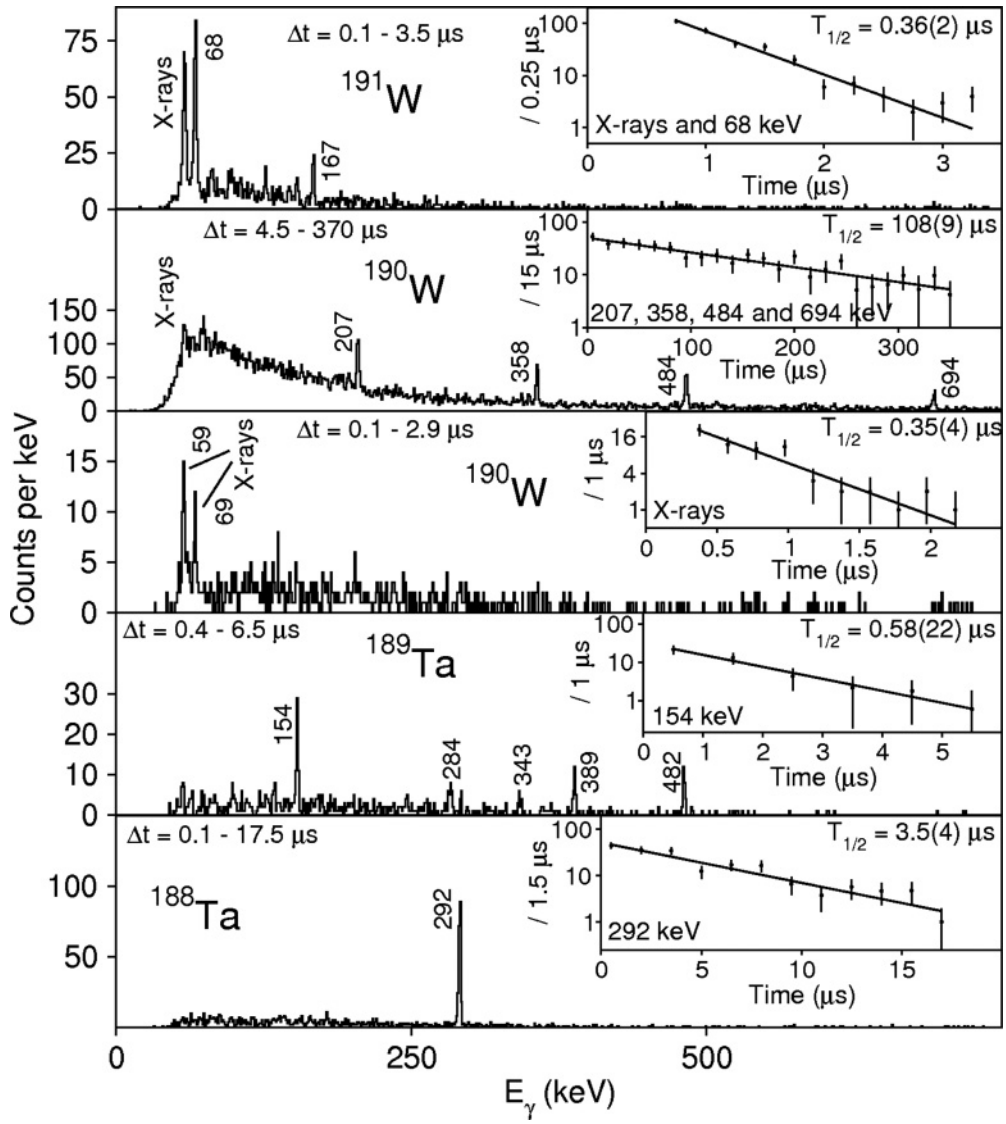

FIG. 18. Gamma-ray spectra for W and Ta nuclei measured in the described experiment. Inset spectra are time curves associated with the decay of the observed isomers. The transitions used to measure half-lives are indicated in the spectra.

I. The $^{191,190}_{74}$W and $^{189,188}_{73}$Ta nuclei

The delayed γ-ray and time spectra of ^{191,190}W and ^{189,188}Ta nuclei are shown in Fig. 18.

The first observation of excited states in $^{191}_{74}$W have been made in the present work [13,14]. γ-ray transitions at 68 and 167 keV and characteristic tungsten x rays are observed. The half-life is $T_{1/2} = 0.36(2)$ μs. This isomer is confirmed by Alkhomashi *et al.,* who in a subsequent experiment performed one year later measured $T_{1/2} = 0.32(2)$ μs [60]. We are unable to propose a level scheme.

In $^{190}_{74}W_{114}$, an isomeric state has been previously reported [40,62]. The results from the present experiment and possible interpretations were discussed in detail in Ref. [63]. The half-life of the isomer has been measured to be $T_{1/2} =$ 108(9) μs. We note that a subsequent experiment confirmed this isomer and reported a half-life of $T_{1/2} = 106(18)$ μs [60]. In addition, there are indications for a previously unreported isomer with a much shorter life-time. Characteristic tungsten x rays have been observed, but no γ-ray transitions, with an associated half-life of $T_{1/2} = 0.35(4)$ μs. There are insufficient statistics available for γ-γ analysis to identify whether there is any feeding between this newly discovered isomer and the previously observed one. Very recently, results from an experiment employing deep-inelastic collisions were published by Lane *et al.* [64]. They deduce that a 10^- $T_{1/2} =$ 166(6) μs isomer decays by a low-energy M2 transition into the 8^+ 110(17) ns isomer. The lower-lying isomer decays via the γ-ray transitions observed in the present experiment. Our experimental data supports the level scheme suggested by Lane *et al.* (see Fig. 1 of Ref. [64]). However, our short-lived x-ray spectrum cannot be explained by that level scheme. It was previously noted that a possible cause of the low $E(4^+)/E(2^+)$ ratio in ^{190}W is shape coexistence [9]. Consequently, it might be that the observed x rays are from the $0^+ \rightarrow 0^+$ shape-changing transition. This has to be isomeric also because its decay has to proceed via conversion electron as the γ-ray transition is forbidden.

Excited states have been measured in $^{189}_{73}Ta_{116}$ for the first time. γ-ray transitions have been observed at energies of 154, 284, 343, 389, and 482 keV. The half-life is $T_{1/2} = 0.58(22)$ μs. γ-γ coincidence analysis shows that all of the γ rays are in mutual coincidence [14]. A more recent experiment has also detected this isomer. γ rays with energies 57 (x ray), 83, 134, 154, 199, 264, 284, 389, and 481 keV were reported with a half-life of $T_{1/2} = 1.6(2)$ μs [60]. The additional, lower intensity γ rays show up in our spectrum as tentative lines (also 99 keV). It seems that two isomers are involved, and we are unable to propose a level scheme

In $^{188}_{73}Ta_{115}$, we confirm the previous observation of an isomeric state by Caamaño *et al.* [40]. A single 292-keV transition is observed with half-life of $T_{1/2} = 3.5(4)$ μs, which is in agreement with the previous value of $T_{1/2} = 5(2)$ μs. A subsequent fragmentation experiment has also seen this isomer and reported a $T_{1/2} = 4.4(10)$ μs half-life [60]. No level scheme is proposed.

J. Lighter nuclei

The experiment covered a number of nuclei in the $Z =$ 69−72 (Tm-Hf) region, as shown in Fig. 5. The yields of these nuclei were rather low [13]. Therefore, no conclusion can be drawn from the nonobservation of isomeric states in the region. To some extent, the above is valid for tantalum isotopes as well. Actually, we know that this region is characterized by K isomerism, and some K isomers have been identified. For example, fragmentation experiments populate isomeric states in ^{190}Ta [60] and ^{183,184,186}Hf [65], while deep-inelastic reactions made them in ^{182}Hf [66].

IV. SUMMARY

Isomeric states were observed in a large number of heavy neutron-rich nuclei in the Ta-Hg region. In the case of nuclei close to the doubly magic ^{208}Pb, the results were interpreted with the aid of the shell-model. It was found that the modifications introduced in order to obtain a better description of ^{204}Pt and ^{206}Hg improved the agreement with experiment for the whole region.

Information on the prolate-oblate shape transition was obtained. It is suggested that osmium isotopes with mass $A \geqslant 197$ are slightly oblate and have isomeric states similar to those in the platinum nuclei. The lighter osmium isotopes such as ^{193,195}Os exhibit isomeric states characteristic of prolate shapes. The lack of isomeric transitions in ^{196}Os are interpreted as an indication that this nucleus is still prolate deformed. The spectra obtained from iridium isotopes indicate that up to ^{197}Ir they are prolate while the ^{199,201}Ir isotopes are oblate.

Several isomeric states with half-lives beyond the sensitivity of the technique used here are predicted. It may be possible to identify them using other methods, such as the GSI storage ring.

ACKNOWLEDGMENTS

The excellent work of the GSI accelerator staff is acknowledged. This work is supported by the EPSRC (UK) and AWE plc. (UK), the EU Access to Large Scale Facilities Programme (EURONS, EU Contract No. 506065), The Swedish Research Council, The Polish Ministry of Science and Higher Education, The Bulgarian Science Fund, The US Department of Energy (Grant No. DE-FG02-91ER-40609), The Spanish Ministerio de Ciencia e Innovacion under Contract No. FPA2009-13377-C02-02, The German BMBF, The Hungarian Science Foundation, and the Italian INFN.

[1] J. H. D Jensen, Rev. Mod. Phys. **29**, 182 (1957).
[2] D. Eccleshall and M. J. L. Yates, Phys. Lett. **19**, 301 (1965).
[3] J. A. Becker *et al.*, Phys. Rev. C **26**, 914 (1982).
[4] K. H. Maier *et al.*, Phys. Rev. C **30**, 1702 (1984).
[5] B. Fornal *et al.*, Phys. Rev. Lett. **87**, 212501 (2001).

[6] Ch. Wennemann *et al.*, Z. Phys. A **347**, 185 (1994).
[7] K. Nomura *et al.*, Phys. Rev. C **83**, 054303 (2011).
[8] P. Sarriguren, R. Rodriguez-Guzman, and L. M. Robledo, Phys. Rev. C **77**, 064322 (2008).
[9] P. D. Stevenson, M. P. Brine, Z. Podolyak, P. H. Regan, P. M. Walker, and J. R. Stone, Phys. Rev. C **72**, 047303 (2005).
[10] S. Pietri *et al.*, Nucl. Instrum. Methods Phys. Res., Sect. B **261**, 1079 (2007).
[11] H. Geissel *et al.*, Nucl. Instrum. Methods Phys. Res., Sect. B **70**, 286 (1992).
[12] S. Pietri *et al.*, Acta Phys. Pol. **38**, 1255 (2007).
[13] S. J. Steer *et al.*, Int. J. Mod. Phys. E **18**, 1002 (2009).
[14] S. J. Steer, Ph.D. Thesis, University of Surrey, unpublished (2008).
[15] S. Myalski *et al.*, Acta Phys. Pol. B **40**, 879 (2009).
[16] Zs. Podolyák *et al.*, Eur. Phys. J. Special Topics **150**, 165 (2007).
[17] Zs. Podolyák *et al.*, Phys. Lett. B **632**, 203 (2006).
[18] C. Scheidenberger *et al.*, Nucl. Instrum. Methods Phys. Res., Sect. B **142**, 441 (1998).
[19] S. J. Steer *et al.*, Phys. Rev. C **78**, 061302(R) (2008).
[20] Zs. Podolyák *et al.*, Eur. Phys. J. A **42**, 489 (2009).
[21] Zs. Podolyák *et al.*, Nucl. Phys. A **722**, 273c (2003).
[22] P. Detistov, D. L. Balabanski, and Zs. Podolyák, Acta Phys. Pol. B **38**, 1287 (2007).
[23] M. Pfützner *et al.*, Phys. Rev. C **65**, 064604 (2002).
[24] B. A. Brown *et al.*, MSU-NSCL report 1289 (2004).
[25] L. Rydström, J. Blomqvist, R. J. Liotta, and C. Pomar, Nucl. Phys. A **512**, 217 (1990).
[26] T. T. S. Kuo and G. H. Herling, US Naval Research Laboraotory, Report No. 2258, unpublished (1971).
[27] H. Grawe, K. Langanke, and G. Martínez-Pinedo, Rep. Prog. Phys. **70**, 1525 (2007).
[28] K. Jain *et al.*, Nucl. Phys. A **591**, 61 (1995).
[29] P. Moller, J. R. Nix, W. D. Myers, and W. J. Swiatecki, At. Data Nucl. Data Tables **59**, 185 (1995).
[30] F. G. Kondev, Nucl. Data Sheets **109**, 1527 (2008).
[31] E. C. Simpson, J. A. Tostevin, Zs. Podolyák, P. H. Regan, and S. J. Steer, Phys. Rev. C **80**, 064608 (2009).
[32] E. C. Simpson, J. A. Tostevin, Zs. Podolyák, P. H. Regan, and S. J. Steer, Phys. Rev. C **82**, 037602 (2010).
[33] R. Kumar *et al.*, Nucl. Instrum. Methods Phys. Res., Sect. A **598**, 754 (2009).
[34] Zs. Podolyák *et al.*, Phys. Lett. B **672**, 116 (2009).
[35] O. Häusser, J. R. Beene, T. K. Alexander, A. B. McDonald, and T. Feastermann, Phys. Lett. B **64**, 273 (1976).
[36] F. G. Kondev, Nucl. Data Sheets **101**, 521 (2004).
[37] A. I. Morales *et al.*, Acta Phys. Pol. B **40**, 867 (2009).
[38] C. J. Chiara and F. G. Kondev, Nucl. Data Sheets **111**, 141 (2010).
[39] F. G. Kondev, Nucl. Data Sheets **105**, 1 (2005).
[40] M. Caamaño *et al.*, Euro. Phys. J. A **23**, 201 (2005).
[41] E. R. Flynn *et al.*, Phys. Lett. B **105**, 125 (1981).
[42] F. G. Kondev, Nucl. Data Sheets **108**, 365 (2007).
[43] B. Singh, Nucl. Data Sheets **108**, 79 (2007).
[44] Zs. Podolyák *et al.*, CERN-INTC-2006-021, INTC-P-212, unpublished (2006).
[45] M. Bowry, ISOLDE newsletter, Spring (2011).
[46] S. W. Yates *et al.*, Phys. Rev. C **37**, 1889 (1988).
[47] Huang Xiaolong, Nucl. Data Sheets **110**, 2533 (2009).
[48] J. J. Valiente-Dobón *et al.*, Phys. Rev. C **69**, 024316 (2004).
[49] P. H. Regan *et al.*, Laser Phys. Lett. **1**, 317 (2004).
[50] A. I. Levon, Y. V. Nosenko, V. A. Onischuk, A. A. Shevchuk, and A. E. Stuchbery, Nucl. Phys. A **764**, 24 (2006).
[51] Zs. Podolyák *et al.*, Prog. Theor. Phys. Suppl. **146**, 467 (2002).
[52] V. R. Vanin *et al.*, Nucl. Data Sheets **108**, 2393 (2007).
[53] E. Achterberg, O. A. Capurro, G. V. Marti, V. R. Vanin, and R. M. Castro, Nucl. Data Sheets **107**, 1 (2006).
[54] X. Huang and C. Zhou, Nucl. Data Sheets **104**, 283 (2005).
[55] T. F. Thorsteinsen, J. S. Vaagen, G. Lovhoiden, N. Blasi, M. N. Harakeh, and S. Y. Van Der Werf, Nucl. Phys. A **435**, 125 (1985).
[56] Huang Xiaolong, Nucl. Data Sheets **108**, 1093 (2007).
[57] C. Zhou, Nucl. Data Sheets **86**, 645 (1999).
[58] Zs. Podolyák *et al.*, Phys. Rev. C **79**, 031305(R) (2009).
[59] L. M. Robledo, R. Rodríguez-Guzmán, and P. Sarriguren, J. Phys. G: Nucl. Part. Phys. **36**, 115104 (2009).
[60] N. Alkhomashi *et al.*, Phys. Rev. C **80**, 064308 (2009).
[61] M. S. Basunia, Nucl. Data Sheets **110**, 999 (2009).
[62] Zs. Podolyák *et al.*, Phys. Lett. B **491**, 225 (2000).
[63] G. F. Farrelly *et al.*, Acta Phys. Pol. B **40**, 885 (2009).
[64] G. J. Lane *et al.*, Phys. Rev. C **82**, 051304(R) (2010).
[65] M. W. Reed *et al.*, Phys. Rev. Lett. **105**, 172501 (2010).
[66] R. D'Alarcao *et al.*, Phys. Rev. C **59**, R1227 (1999).
[67] S. Zhu and F. G. Kondev, Nucl. Data Sheets **109**, 699 (2008).
[68] F. G. Kondev and S. Lalkovski, Nucl. Data Sheets **108**, 1471 (2007).

16^+ Spin-Gap Isomer in ^{96}Cd

B. S. Nara Singh,[1] Z. Liu,[2] R. Wadsworth,[1] H. Grawe,[3] T. S. Brock,[1] P. Boutachkov,[3] N. Braun,[4] A. Blazhev,[4] M. Górska,[3] S. Pietri,[3] D. Rudolph,[5] C. Domingo-Pardo,[3] S. J. Steer,[6] A. Ataç,[7] L. Bettermann,[4] L. Cáceres,[3] K. Eppinger,[8] T. Engert,[3] T. Faestermann,[8] F. Farinon,[3] F. Finke,[4] K. Geibel,[4] J. Gerl,[3] R. Gernhäuser,[8] N. Goel,[3] A. Gottardo,[2] J. Grębosz,[9] C. Hinke,[8] R. Hoischen,[3,5] G. Ilie,[4] H. Iwasaki,[4] J. Jolie,[4] A. Kaşkaş,[7] I. Kojouharov,[3] R. Krücken,[8] N. Kurz,[3] E. Merchán,[3] C. Nociforo,[3] J. Nyberg,[10] M. Pfützner,[11] A. Prochazka,[3] Zs. Podolyák,[6] P. H. Regan,[6] P. Reiter,[4] S. Rinta-Antila,[12] C. Scholl,[4] H. Schaffner,[3] P.-A. Söderström,[10] N. Warr,[4] H. Weick,[3] H.-J. Wollersheim,[3] P. J. Woods,[2] F. Nowacki,[13] and K. Sieja[13]

[1]*Department of Physics, University of York, Heslington, York, YO10 5DD, United Kingdom*
[2]*School of Physics and Astronomy, University of Edinburgh, Edinburgh, United Kingdom*
[3]*GSI Helmholtzzentrum für Schwerionenforschung, D-64291 Darmstadt, Germany*
[4]*IKP, Universität Köln, D-50937 Köln, Germany*
[5]*Department of Physics, Lund University, S-22100 Lund, Sweden*
[6]*Department of Physics, University of Surrey, Guildford, GU2 7XH, United Kingdom*
[7]*Department of Physics, Ankara University, 06100 Tandoğan, Ankara, Turkey*
[8]*Physik Department E12, Technische Universität München, D-85748 Garching, Germany*
[9]*The Institute of Nuclear Physics PAN, Kraków, Poland*
[10]*Department of Physics and Astronomy, Uppsala University, SE-75120 Uppsala, Sweden*
[11]*Faculty of Physics, University of Warsaw, PL-00-681 Warsaw, Poland*
[12]*Department of Physics, Oliver Lodge Laboratory, University of Liverpool, Liverpool, United Kingdom*
[13]*IPHC, IN2P3-CNRS et Université de Strasbourg, F-67037 Strasbourg, France*

(Received 10 August 2011; published 18 October 2011)

A β-decaying high-spin isomer in ^{96}Cd, with a half-life $T_{1/2} = 0.29^{+0.11}_{-0.10}$ s, has been established in a stopped beam rare isotope spectroscopic investigations at GSI (RISING) experiment. The nuclei were produced using the fragmentation of a primary beam of ^{124}Xe on a ^{9}Be target. From the half-life and the observed γ decays in the daughter nucleus, ^{96}Ag, we conclude that the β-decaying state is the long predicted 16^+ "spin-gap" isomer. Shell-model calculations, using the Gross-Frenkel interaction and the $\pi\nu(p_{1/2}, g_{9/2})$ model space, show that the isoscalar component of the neutron-proton interaction is essential to explain the origin of the isomer. Core excitations across the $N = Z = 50$ gaps and the Gamow-Teller strength, B(GT) distributions have been studied via large-scale shell-model calculations using the $\pi\nu(g, d, s)$ model space to compare with the experimental B(GT) value obtained from the half-life of the isomer.

DOI: 10.1103/PhysRevLett.107.172502 PACS numbers: 21.60.Cs, 23.20.Lv, 23.35.+g, 26.20.−f

The nuclear landscape around the heaviest known bound doubly magic self-conjugate nucleus ^{100}Sn, which resides far from the valley of stability, exhibits a rich variety of nuclear structure phenomena [1–15]. A feature of great interest in this region is the presence of isomeric states, especially those which may undergo particle decay. Indeed, early work by Peker *et al.* was paramount in motivating studies of such states based on three or four particle/hole configurations in nuclei. This included the 16^+ isomeric state in ^{96}Cd, which was suggested to result from a four-hole configuration relative to a ^{100}Sn core that may decay via proton radioactivity [1].

A particularly interesting issue in this region is the role played by the neutron-proton, np, interaction in leading to the existence of the isomers. The isovector ($T = 1$) component of the interaction between like-nucleons is known to dominate in all non-self-conjugate nuclei while the $T = 1$ np interaction has been shown to have a major influence on the $N = Z$ line below mass 80 due to the large overlap of the proton and neutron wave functions [16]. Although calculations suggest an important influence of the isoscalar ($T = 0$) np interaction on the structure of medium-heavy $N = Z$ nuclei, its role has been less clear and often debated [17–20]. Very recent experimental work has claimed the first indications for the crucial role of this interaction at low spins in ^{92}Pd, that are supported by shell-model (SM) calculations [2]. In order to establish or dispute the expected strong influence of the $T = 0$ np interaction for self-conjugate nuclei close to ^{100}Sn, it is of paramount importance to obtain further evidence for its effects.

Long standing SM calculations for the self-conjugate nucleus ^{96}Cd predict the presence of a 16^+ state at an energy lower than that of the first 12^+ and 14^+ states [10]. This situation arises from the strong influence of the $T = 0$ np interaction and results in "spin-gap" isomerism [4] for the 16^+ state, since its $E6$ γ decay to the next available 10^+ state is highly hindered. Consequently, β-,

β-delayed proton and proton decays may be expected to become favorable modes of deexcitation [1,10]. The identification of such decay characteristics, along with the evolution of single-particle energies, provides a sensitive probe of the residual interactions seen by the nucleons and can serve as critical tests of nuclear models. Studies related to the predicted "spin-gap" isomerism in $N \approx Z \approx 50$ nuclei around the proton drip line also have been of great interest due to the purity of the wave-functions and the possibility to describe their properties using only a few orbitals [4–7,21]. Apart from providing important data on the np interaction, the structural properties of these nuclei also serve as key inputs to the astrophysical rp-process calculations [22].

In this Letter, we report on the identification of an isomeric state in ^{96}Cd that β decays mainly to the (15^+) isomeric state in ^{96}Ag [21]. From the observed Gamow-Teller (GT) strength and the decay γ rays, we conclude that this provides evidence for the existence of the long predicted 16^+ "spin-gap" isomer in ^{96}Cd [10]. This is the second highest spin (the 21^+ isomeric state in ^{94}Ag being the highest [3]) observed for a state preceding β decay.

^{96}Cd nuclei were produced at GSI by fragmentation of an 850 MeV/u ^{124}Xe primary beam with an intensity of 10^9 particles/s from the SIS-18 synchrotron on a 4 g/cm^2 ^{9}Be target. The nuclei of interest were separated using the fragment separator (FRS) [23] and transported to its $S4$ focal plane, where the RISING [24,25] stopped beam setup was located. The ions, fully stripped ($Q = Z$) due to their relativistic energies, were identified on an event-by-event basis [21,23–25]. Figure 1 shows the Z versus A/Q identification plot for the implanted ions. Here, A, Q and Z are the mass, charge state and the atomic number of the fragments, respectively.

The ^{96}Cd nuclei were slowed down using an aluminum degrader at the $S4$ focal plane. Subsequently, the ions were stopped in an "active stopper" (AS) that detected the implantation position of nuclei as well as the particles

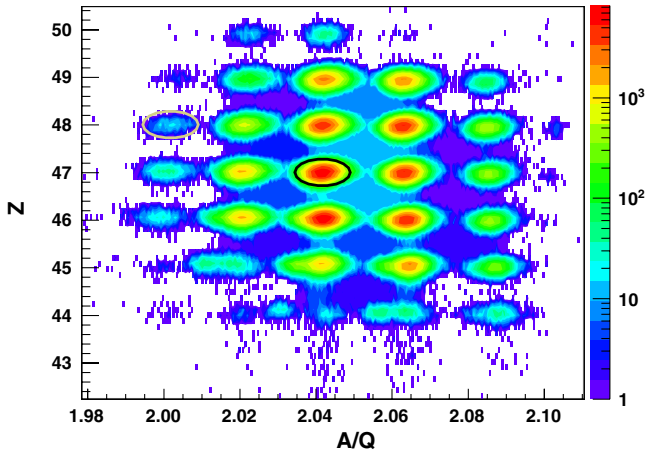

FIG. 1 (color online). Z versus A/Q identification plot. $^{96}_{48}$Cd and $^{96}_{47}$Ag nuclei are circled.

from their decays [26]. The AS consisted of nine double sided silicon strip detectors (DSSSD) arranged in three horizontal rows perpendicular to the beam direction, with three detectors in each row. Each DSSSD was 1 mm thick with an area of 5×5 cm^2 and had 16 X and 16 Y strips [27]. This geometrical arrangement also had an optimal solid angle coverage for the decays from the nuclei implanted in the central detector. The primary beam and FRS settings were optimized so as to stop the ^{96}Cd nuclei in the center of the AS. To detect the γ rays from the fragments, the AS was surrounded by 15 EUROBALL cluster detectors, each cluster comprising seven individual HPGe crystals. A timing signal from a scintillator placed down-stream to the $S4$ focal plane, corresponding to the instance of fragment implantation (see [24,28] for details), was used for time correlations with subsequent decays.

A total of 630 ^{96}Cd nuclei were identified by the FRS focal plane detectors in the current experiment in a period of close to 8 days. In the analysis presented here, we used approximately 95% of these events that were implanted into the detector located in the middle of the AS. The endpoint energies, for the β decay of the ground and 16^+ states in ^{96}Cd, are expected to be in the range of 8 to 10 MeV [29,30] and most of the resulting β particles are estimated to deposit an energy of up to 600 keV in a single strip of a Si detector. Figure 2(a) shows the prompt γ-ray events which follow within a time window of up to 200 ns after a β-decay event, that deposited an energy of up to $\simeq$ 600 keV in the AS and has been identified within a correlation time of up to 1 s after ^{96}Cd implantation. The latter are defined by a contour line in Fig. 1. A γ ray at 421 keV is observed, next to the dominant 511 keV line arising from positron annihilation.

SM calculations for ^{96}Ag, using the Gross-Frenkel (GF) interaction and the $\pi\nu(p_{1/2}, g_{9/2})$ model space, predict the lowest 1^+ and 2^+ states at excitation energies of 356 and 12 keV, respectively, above an 8^+ ground state [31]. Experimentally, spins or parities of 2^+, 8^+ have been tentatively assigned to two low-lying states based on the β^+/EC decay [32,33]. Low-lying 1^+ states of odd-odd $N = 49$ isotones are populated in β^+/EC GT decay from the ground states of their even-even neighbors and are connected to the 2^+ states by $M1$ transitions [34]. Therefore, we tentatively assign the observed 421 keV γ line to a $(1^+) \rightarrow (2^+)$ transition in ^{96}Ag fed by β^+/EC decay of the ^{96}Cd ground state (see Fig. 3). The time distribution of the 421 keV γ ray with respect to the implantation of ^{96}Cd is shown in the inset of Fig. 2(a). An analysis based on the maximum likelihood method yields $T_{1/2} = 0.67 \pm 0.15$ s. This is in good agreement with the known value of $1.03^{+0.24}_{-0.21}$ s reported for the ground state decay of ^{96}Cd [8]. From the observed γ intensities in Fig. 2(a), we estimate an upper limit of 10% population for the 16^+ isomeric state implying $\sim$90% population for the ground state. This "isomeric

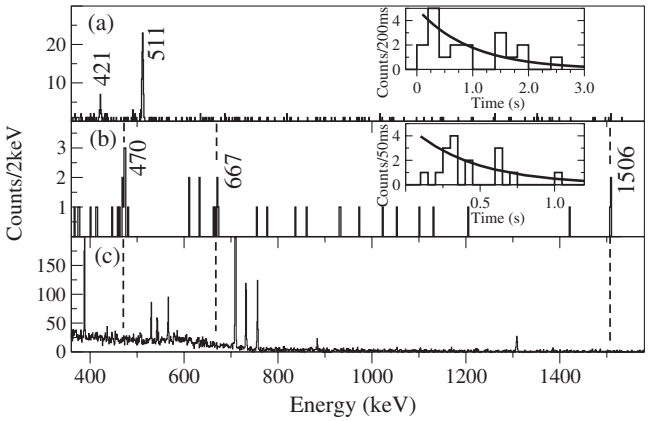

FIG. 2. Gamma-ray spectra associated with the decays following implantation into the geometrically central DSSSD of the "active stopper." (a) ^{96}Cd events with γ-ray times restricted to be between 0 to 200 ns following the β-decay signal detected in the DSSSD. In the inset the time distribution of the 421 keV γ ray with respect to the ^{96}Cd implantation time is shown for the data (histogram) and the calculations (smooth curve) using $T_{1/2} = 0.67 \pm 0.15$ s. (b) Same as (a) except the γ-ray times are restricted to be between 200 ns to 4 μs. The inset shows the combined correlation time distribution of the 470, 667, 1506 keV γ rays which gives $T_{1/2} = 0.29^{+0.11}_{-0.10}$ s for the 16^+ isomer. (c) Same as (b) for all nuclei other than ^{96}Cd. In the above spectra, the 511 keV line arises from the positron annihilation while the remaining lines with labels correspond to the transitions in ^{96}Ag (cf. Fig. 3). See text for details. The dashed lines are merely to guide the eye to particular energy coordinates.

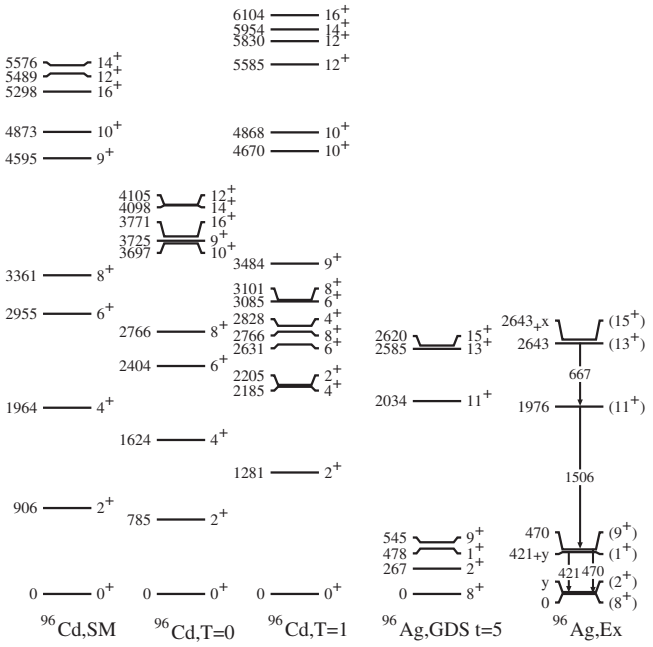

FIG. 3. Shell-model calculations for ^{96}Cd. ^{96}Cd, SM: All isovector nn, pp, np and isoscalar np interactions are included. ^{96}Cd, $T = 0$: Only the isovector np interaction is switched off. ^{96}Cd, $T = 1$: Only the isoscalar np interaction is switched off. Large-scale shell-model calculations for ^{96}Ag. ^{96}Ag, GDS $t = 5$: Up to 5 ph core excitations across the $N = Z = 50$ shell gap are included. Only the lowest states are shown for each spin. EX: Partial experimental scheme and the transitions observed in the decay of ^{96}Cd [21,37]. Here, x and y correspond to the unobserved transition energies.

ratio" is similar to that observed for the 15^+ isomeric state in ^{96}Ag, but somewhat higher than our theoretical estimation of $\sim$2% [21,35].

Figure 2(b) shows the γ-ray spectrum that was obtained with the same conditions as those for Fig. 2(a), except that the events are delayed by 200 ns to 4 μs with respect to the β-decay signal. In this case there is evidence for γ rays at 470, 667, and 1506 keV, two of which were first observed by Gryzwacz *et al.* [36]. These are identical to the main observed transitions following the decay of the (15^+) isomer in ^{96}Ag (see Fig. 3), which has $T_{1/2} = 1.5$ μs [21,37]—a value which is about twice that inferred in Ref. [36]. To investigate other possible contributions from random coincidences Fig. 2(c), using the same conditions as those for Fig. 2(b), shows γ rays which are in coincidence with all fragments other than ^{96}Cd that are stopped in the central detector. This spectrum shows no evidence for the 470, 667, or 1506 keV γ-ray lines. We therefore conclude that the γ rays observed in Fig. 2(b) result directly from the β decay of the 16^+ "spin-gap" isomer in ^{96}Cd, since β-decay selection rules for GT decays ($\Delta I = 0, 1$) exclude the possibility of the 0^+ ground state in ^{96}Cd populating such a high-spin isomer in its daughter ^{96}Ag. The extracted time distribution of the β-decay events when the three γ decays are simultaneously detected is shown in the inset to Fig. 2(b). The maximum likelihood method gives $T_{1/2} = 0.29^{+0.11}_{-0.10}$ s for the distribution. This is in good agreement, within the uncertainties, with the expected value of 0.5 s from Ref. [10] for the GT decay of the 16^+ "spin-gap" isomer.

Figure 3 (left column) shows the results of SM calculations for ^{96}Cd using the GF interaction and the $\pi\nu(p_{1/2}, g_{9/2})$ model space [31]. Further details on our SM approach can be found in Refs. [7,21]. The 16^+ isomer has a $\pi\nu(p^2_{1/2}g^8_{9/2})$ particle configuration within $\pi\nu(p_{1/2}, g_{9/2})$ model space, leaving two proton ($\pi(g^{-2}_{9/2})$) and two neutron ($\nu(g^{-2}_{9/2})$) holes coupled to the maximum possible spin $I = 16$.

Figure 3 (center) shows the results of our SM calculations performed with either the $T = 0$ or $T = 1$ np interaction switched off. Here, the original proton and neutron particle/hole energies for both, ^{88}Sr and ^{100}Sn are maintained by using a monopole correction [38]. The 16^+ state moves up substantially to lie above the 12^+ and 14^+ states and no longer forms a "spin-gap" isomer when the $T = 0$ np interaction is switched off. Our identification of the 16^+ β-decaying isomer therefore provides additional evidence for the importance of the $T = 0$ np interaction at high spins in $A \simeq 90$–100 $N = Z$ nuclei.

The 15^+ isomeric state in ^{96}Ag (cf. Fig. 3) has a pure $\pi\nu(p^2_{1/2})\pi(g^7_{9/2})\nu(g^9_{9/2})$ configuration within the $\pi\nu(p_{1/2}, g_{9/2})$ model space with the $\pi(g^{-3}_{9/2})\nu(g^{-1}_{9/2})$ holes coupled to the maximum possible spin [21]. This scenario results in the full GT strength for a $g_{9/2}$ proton (projection $5/2$) $\rightarrow$ $g_{9/2}$ neutron (projection $7/2$) transition that is illustrated schematically in Fig. 4 (left). This is similar to the decay of the 12^+ isomeric state in ^{52}Fe to the 11^+ state in its daughter ^{52}Mn, one major harmonic oscillator shell below, with a small B(GT) value of 0.061 [34,39].

The experimental GT strength in standard units is related to the half-life via $B(\mathrm{GT}) = \frac{3860(18)I_\beta}{fT_{1/2}}$ [40], where I_β is the branching ratio and f is the phase space function tabulated for various Q_{EC} values in Ref. [41]. We obtain $B(\mathrm{GT}) = 0.19^{+0.10}_{-0.06}$, using $T_{1/2} = 0.29^{+0.11}_{-0.10}$ s, 100% for I_β and $Q_{EC} = 11.51 \pm 0.26$ MeV. The latter is extrapolated from the ground state-to-ground state value [30] and the GF shell-model calculations. This is in good agreement with the SM result for the $\pi\nu(p_{1/2}, g_{9/2})$ model space of $B(\mathrm{GT}) = 0.14$, where we have used 0.6 for the GT quenching taken from Ref. [30].

In order to investigate the effects in an extended model space, we carried out large-scale shell-model (LSSM) calculations in a $\pi\nu(g, d, s)$ space using a ^{80}Zr core and including up to $t = 4$ (^{96}Cd) or $t = 5$ (^{96}Ag) particle-hole (ph) core excitations across the $N = Z = 50$ shell gap [5,21]. In this case a quenching factor of 0.75 was used for the GT operator [42]. The relevant calculated level scheme for ^{96}Ag is shown in the next to the last column of Fig. 3. The calculations in Fig. 4 (right) show the decay of the parent 16^+ state. This contains 76% content of the $(\pi g^{-2}_{9/2}\nu g^{-2}_{9/2})_{16}$ configuration and decays to the first 15^+ (isomeric) state at 2.62 MeV and the 15^+, 16^+, and 17^+ GT resonance states, which have $\simeq 2$ MeV width at centroid energies of 10.2, 10.6, and 9.5 MeV, respectively. The B(GT) values for these states are calculated to be 0.07, 2.78, 2.33, and 1.41, respectively. Clearly, in these calculations, the 15^+ state at 2.62 MeV is predicted to have a factor two smaller value for B(GT) compared to the GF estimate of 0.14. Both these estimates agree, within the uncertainties, with our experimental result. Future measurements with better statistics will be needed to study all the decay branches that should validate the calculations. It should be noted that the observed difference in the estimates is due to the core excitations included in LSSM calculations. A similar effect of core excitations is found for the ^{100}Sn case. A large GT strength is entirely concentrated in the $\pi(g_{9/2}) \rightarrow \nu(g_{7/2})$ transition to the 1^+ state in ^{100}In, when no core excitations are considered. The strength to this state is reduced by 19% for SM calculations performed in the (g, d, s) space at low truncation levels, $t = 2$ for ^{100}Sn and $t = 3$ for ^{100}In [11]. Further reduction is anticipated from an LSSM calculation at $t = 5$ due to the fragmentation of B(GT) to several 1^+ states [43].

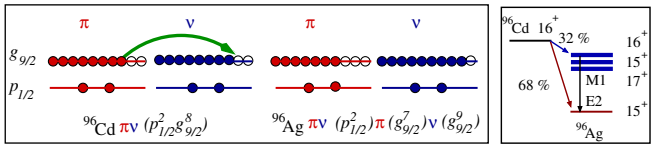

FIG. 4 (color online). Left: The proton and neutron occupations lined up in the sequence of increasing projection in the $p_{1/2}$ and $g_{9/2}$ orbitals representing the 16^+ "spin-gap" isomer in ^{96}Cd and the 15^+ isomer in ^{96}Ag [21]. The GT β-decay process ($\pi g_{9/2} \rightarrow \nu g_{9/2}$) is depicted by the arrow that receives the full GT strength within the $\pi\nu(p_{1/2}, g_{9/2})$ space. Right: Decay branches are shown from the large-scale shell-model calculations with core excitations allowing different transitions including the one depicted on the left. Overlaps of the resonances, due to their $\simeq 2$ MeV width, are not shown for the clarity. See text for details.

The decay energies from the 16^+ state to the GT resonance states in the daughter are smaller, therefore the phase space is smaller, compared to that for the 15^+ isomeric yrast state. Consequently, the 15^+ state is predicted to receive about 68% branching. The remaining 32% feeds the predicted 15^+, 16^+ and 17^+ GT resonance states, which lie at energies above the proton threshold. These are expected to decay via competing β-delayed proton and γ decays with 33% and 67% branching ratios, respectively. As shown in Fig. 4 (right), the latter are expected to feed the 15^+ state at 2.62 MeV via $M1$ and $E2$ transitions. However, due to the limitations in the detection efficiencies and statistics in our data, the corresponding high energy γ transitions could not be observed. The γ branch creates a pandemonium problem [44], since the nonobserved feeding via $M1$ and $E2$ transitions [see Fig. 4 (right)] to the 15^+ daughter state has a larger value for the B(GT) which is not accounted for in the experimental B(GT) based on the assumption of $I_\beta = 100\%$. This warrants a caution when comparing our experimental value with the theoretical estimates for the B(GT) strength to the 15^+ state or for the total B(GT) strength. Future experiments with better statistics will be useful in understanding the hindrance factor in GT strengths in this region [45].

Recent work [15] identified the $25/2^+$ "spin-gap" isomer in ^{97}Cd and pointed out that when multiple β-decaying states are present, the measured half-lives need to be carefully analyzed to deduce the half-life of the ground state, which is usually the important quantity for nuclear astrophysics. Bazin *et al.* reported on the decay half-life of ^{96}Cd [8]. However, it was not known whether their result was for the ground state, the isomeric state, or a combination of the two states. Our work allows us to deduce $T_{1/2} = 0.67 \pm 0.15$ s for the ground state in ^{96}Cd. This value is smaller but, within the uncertainties, agrees with the result from Ref. [8] and thereby supports their conclusion that the x-ray bursters are not the main source for the large abundance of ^{96}Ru in the solar system.

In summary, evidence for the existence of the 16^+ $E6$ "spin-gap" isomer in ^{96}Cd is presented for the first time and supported by SM calculations on the level structure and GT strengths. This result provides important evidence for the strong influence of the isoscalar neutron-proton interaction not only at low-spins as in the case of ^{92}Pd [2], but also at high-spin in the region around ^{100}Sn.

This work has been supported by the UK STFC, the German BMBF under Contracts No. 06KY205I, No. 06KY9136I, and No. 06MT9156, the Swedish Research Council, and the DFG cluster of excellence Origin and Structure of the Universe.

[1] L. E. Peker *et al.*, Phys. Lett. B **36**, 547 (1971).
[2] B. Cederwall *et al.*, Nature (London) **469**, 68 (2011).
[3] I. Mukha *et al.*, Phys. Rev. Lett. **95**, 022501 (2005); Nature (London) **439**, 298 (2006).
[4] H. Grawe *et al.*, Eur. Phys. J. A **27**, 257 (2006).
[5] A. Blazhev *et al.*, Phys. Rev. C **69**, 064304 (2004).
[6] M. Górska *et al.*, Phys. Rev. Lett. **79**, 2415 (1997).
[7] T. S. Brock *et al.*, Phys. Rev. C **82**, 061309(R) (2010).
[8] D. Bazin *et al.*, Phys. Rev. Lett. **101**, 252501 (2008).
[9] I. G. Darby *et al.*, Phys. Rev. Lett. **105**, 162502 (2010).
[10] K. Ogawa, Phys. Rev. C **28**, 958 (1983).
[11] B. A. Brown and K. Rykaczewski, Phys. Rev. C **50**, R2270 (1994).
[12] A. Juodagalvis and D. J. Dean, Phys. Rev. C **72**, 024306 (2005).
[13] M. Honma *et al.*, Phys. Rev. C **80**, 064323 (2009).
[14] S. Zerguine and P. Van Isacker, Phys. Rev. C **83**, 064313 (2011).
[15] G. Lorusso *et al.*, Phys. Lett. B **699**, 141 (2011).
[16] A. Afanasjev and S. Frauendorf, Phys. Rev. C **71**, 064318 (2005), and the references therein.
[17] J. Engel *et al.*, Phys. Lett. B **389**, 211 (1996).
[18] A. L. Goodman, Adv. Nucl. Phys. **11**, 263 (1979); Phys. Rev. C **60**, 014311 (1999).
[19] W. Satula and R. Wyss, Phys. Lett. B **393**, 1 (1997); Phys. Rev. Lett. **86**, 4488 (2001).
[20] E. Caurier *et al.*, Phys. Rev. C **82**, 064304 (2010).
[21] P. Boutachkov *et al.*, Phys. Rev. C **84**, 044311 (2011).
[22] H. Schatz *et al.*, Phys. Rep. **294**, 167 (1998).
[23] H. Geissel, Nucl. Instrum. Methods Phys. Res., Sect. B **70**, 286 (1992).
[24] D. Rudolph *et al.*, Eur. Phys. J. Special Topics **150**, 173 (2007); D. Rudolph, Acta Phys. Pol. **42**, 567 (2011).
[25] H.-J. Wollersheim *et al.*, Nucl. Instrum. Methods Phys. Res., Sect. A **537**, 637 (2005); S. Pietri *et al.*, Nucl. Instrum. Methods Phys. Res., Sect. A **261**, 1079 (2007).
[26] Zs. Podolyak *et al.*, Phys. Lett. B **672**, 116 (2009).
[27] R. Kumar *et al.*, Nucl. Instrum. Methods Phys. Res., Sect. A **598**, 754 (2009); N. Alkhomashi *et al.*, Phys. Rev. C **80**, 064308 (2009).
[28] S. Pietri *et al.*, Eur. Phys. J. Special Topics **150**, 319 (2007).
[29] G. T. Biehle and P. Vogel, Phys. Rev. C **46**, 1555 (1992).
[30] H. Herndl and B. A. Brown, Nucl. Phys. **A627**, 35 (1997).
[31] R. Gross and A. Frenkel, Nucl. Phys. **A267**, 85 (1976).
[32] W. Kurcewicz *et al.*, Z. Phys. A **308**, 21 (1982).
[33] L. Batist *et al.*, Nucl. Phys. **A720**, 245 (2003).
[34] ENSDF database, http://www.nndc.bnl.gov/ensdf/.
[35] M. Pfützner *et al.*, Phys. Rev. C **65**, 064604 (2002).
[36] R. Grzywacz *et al.*, Phys. Rev. C **55**, 1126 (1997).
[37] A. D. Becerril *et al.*, Phys. Rev. C **84**, 041303(R) (2011).
[38] H. Grawe *et al.*, Rep. Prog. Phys. **70**, 1525 (2007).
[39] D. F. Geesaman *et al.*, Phys. Rev. Lett. **34**, 326 (1975); Phys. Rev. C **19**, 1938 (1979).
[40] A. Plochoki *et al.*, Z. Phys. A **342**, 43 (1992).
[41] N. B. Gove and M. J. Martin, Nucl. Data Tables **10**, 205 (1971).
[42] E. Caurier *et al.*, Rev. Mod. Phys. **77**, 427 (2005).
[43] Ch. Hinke *et al.* (to be published).K. Sieja (private communication).
[44] J. C. Hardy *et al.*, Phys. Lett. B **71**, 307 (1977).
[45] I. S. Towner, Nucl. Phys. **A444**, 402 (1985).

ARTICLE

doi:10.1038/nature11116

Superallowed Gamow–Teller decay of the doubly magic nucleus ^{100}Sn

C. B. Hinke[1], M. Böhmer[1], P. Boutachkov[2], T. Faestermann[1], H. Geissel[2], J. Gerl[2], R. Gernhäuser[1], M. Górska[2], A. Gottardo[3], H. Grawe[2], J. L. Grębosz[4], R. Krücken[1,5], N. Kurz[2], Z. Liu[6], L. Maier[1], F. Nowacki[7], S. Pietri[2], Zs. Podolyák[8], K. Sieja[7], K. Steiger[1], K. Straub[1], H. Weick[2], H.-J. Wollersheim[2], P. J. Woods[6], N. Al-Dahan[8], N. Alkhomashi[8], A. Ataç[9], A. Blazhev[10], N. F. Braun[10], I. T. Čeliković[11], T. Davinson[6], I. Dillmann[2], C. Domingo-Pardo[12], P. C. Doornenbal[13], G. de France[14], G. F. Farrelly[8], F. Farinon[2], N. Goel[2], T. C. Habermann[2], R. Hoischen[2], R. Janik[15], M. Karny[16], A. Kaşkaş[9], I. M. Kojouharov[2], Th. Kröll[17], Y. Litvinov[2], S. Myalski[4], F. Nebel[1], S. Nishimura[13], C. Nociforo[2], J. Nyberg[18], A. R. Parikh[19], A. Procházka[2], P. H. Regan[8], C. Rigollet[20], H. Schaffner[2], C. Scheidenberger[2], S. Schwertel[1], P.-A. Söderström[13], S. J. Steer[8], A. Stolz[21] & P. Strmeň[15]

The shell structure of atomic nuclei is associated with 'magic numbers' and originates in the nearly independent motion of neutrons and protons in a mean potential generated by all nucleons. During β$^+$-decay, a proton transforms into a neutron in a previously not fully occupied orbital, emitting a positron–neutrino pair with either parallel or antiparallel spins, in a Gamow–Teller or Fermi transition, respectively. The transition probability, or strength, of a Gamow–Teller transition depends sensitively on the underlying shell structure and is usually distributed among many states in the neighbouring nucleus. Here we report measurements of the half-life and decay energy for the decay of ^{100}Sn, the heaviest doubly magic nucleus with equal numbers of protons and neutrons. In the β-decay of ^{100}Sn, a large fraction of the strength is observable because of the large decay energy. We determine the largest Gamow–Teller strength so far measured in allowed nuclear β-decay, establishing the 'superallowed' nature of this Gamow–Teller transition. The large strength and the low-energy states in the daughter nucleus, ^{100}In, are well reproduced by modern, large-scale shell model calculations.

Gamow–Teller transitions, in which a proton is transformed into a neutron or vice versa, while possibly flipping its spin, represent an important spin–isospin degree of freedom in atomic nuclei. They are important in many astrophysical processes: they govern, for example, electron capture during the core collapse of supernovae. Furthermore, a detailed understanding of Gamow–Teller transitions will provide an essential constraint on the neutrino mass, in the event that neutrinoless double β-decay is ever observed. Most of the Gamow–Teller strength is found in the collective Gamow–Teller giant resonance (GTGR) of the neighbouring nucleus, which is typically a broad structure composed of many states. Whereas in charge-exchange reactions in stable nuclei the full GTGR is accessible, the Gamow–Teller strength in unstable nuclei can, so far, only be studied through β-decay. However, β-decay studies can observe only the fraction of the total Gamow–Teller strength within the decay energy window. Towards more proton-rich nuclei, this window becomes larger. Nevertheless, it is still experimentally challenging to detect all small components of the Gamow–Teller strength[1,2]. Thus, in most nuclei, measuring the full Gamow–Teller strength is difficult because it is fragmented and only partly accessible in β-decays.

^{100}Sn has $N = 50$ neutrons and $Z = 50$ protons, and as a result has completely occupied shells. It is therefore called 'doubly magic' and is particularly suited both experimentally and theoretically to the study of Gamow–Teller transitions. The closed $N = Z = 50$ shells reduce the effect of long-range correlations, thus decreasing the amount of fragmentation of the GTGR. Theoretical predictions suggest that a single state is dominantly populated in this decay. At the same time, the energy window for β-decay is ~7.4 MeV (ref. 3), and most of the GTGR is therefore accessible. Such a situation for a doubly magic system is realized nowhere else in the Segrè chart (a two-dimensional lattice in which all known nuclei are arranged with N and Z on the x and y axes, respectively): ^{16}O and ^{40}Ca are stable nuclei; ^{56}Ni has too small a Q_{EC} value (the energy available for β$^+$-decay or electron-capture decay) to make the Gamow–Teller resonance observable in β-decay; and doubly magic nuclei with $N = Z$ that are heavier than ^{100}Sn are unbound. Also, a recent experiment shows that ^{56}Ni has a much more fragmented Gamow–Teller strength[4] as a result of a less robust $N = Z = 28$ doubly magic shell closure as well as subtle differences in the shell structure (Methods Summary and Supplementary Information).

In an extreme, pure single-particle picture, the only possible Gamow–Teller transition of ^{100}Sn is the decay of a proton in the completely filled $g_{9/2}$ shell to a neutron in the empty $g_{7/2}$ shell because the $g_{9/2}$ neutron orbital is filled and no levels above $Z = 50$ are occupied. The large energy separation (shell gap) between these spin-parallel ($g_{9/2}$) and spin-antiparallel ($g_{7/2}$) orbitals, for which the orbital angular momentum is $L = 4$, is responsible for 50 being a magic number. The β-decay of ^{100}Sn is supposed to be enhanced as a result of the large

[1]Physik Department E12, Technische Universität München, D-85748 Garching, Germany. [2]GSI Helmholtzzentrum für Schwerionenforschung GmbH, D-64291 Darmstadt, Germany. [3]Istituto Nazionale di Fisica Nucleare, Laboratori Nazionali di Legnaro, 35020 Legnaro, Italy. [4]The Henryk Niewodniczanski Institute of Nuclear Physics (IFJ PAN), 31-342 Krakow, Poland. [5]TRIUMF, Vancouver, British Columbia V6T 2A3, Canada. [6]School of Physics & Astronomy, The University of Edinburgh, Edinburgh EH9 3JZ, UK. [7]Université de Strasbourg, IPHC, 67037 Strasbourg Cedex, France. [8]Department of Physics, University of Surrey, Guildford GU2 7XH, UK. [9]Physics Department, Faculty of Science, Ankara University, 06100 Tandogan, Ankara, Turkey. [10]Institute of Nuclear Physics, University of Cologne, D-50937 Köln, Germany. [11]Institute Vinca, University of Belgrade, 11000 Belgrade, Serbia. [12]IFIC, CSIC-University of Valencia, E-46071 Valencia, Spain. [13]RIKEN Nishina Center, Wako, Saitama 351-0198, Japan. [14]Grand Accélérateur National d'Ions Lourds, CEA/DSM-CNRS/IN2P3, 14076 Caen, France. [15]Comenius University, 818 06 Bratislava 16, Slovakia. [16]Institute of Experimental Physics, University of Warsaw, PL-00681 Warsaw, Poland. [17]Institut für Kernphysik, Technische Universität Darmstadt, D-64289 Darmstadt, Germany. [18]Department of Physics & Astronomy, Uppsala University, SE-75120 Uppsala, Sweden. [19]Departamento de Fisica i Enginyeria Nuclear, Universitat Politecnica de Catalunya (EUETIB), E-08036 Barcelona, Spain. [20]KVI, University of Groningen, 9747AA Groningen, The Netherlands. [21]National Superconducting Cyclotron Laboratory, Michigan State University, East Lansing, Michigan 48824-1321, USA.

number of protons occupying the $g_{9/2}$ shell, which can decay to the mostly empty neutron $g_{7/2}$ shell. This would lead to a GTGR consisting of only a single $I^{\pi} = 1^{+}$ level (I, spin; π, parity) with a large Gamow–Teller strength of about $B_{GT} = 10$, taking into account the standard renormalization factor (0.75) of the Gamow–Teller matrix element due to configurations outside the model space[5]. This unique situation has been termed 'superallowed' Gamow–Teller decay[6]. Even in more realistic models, including particle–hole correlations, the Gamow–Teller decay of the ground state of ^{100}Sn is predicted to populate with more than 95% probability a single 1^{+} state in ^{100}In at an excitation energy of about 3 MeV. In these calculations, a Gamow–Teller strength of around 8–14 is obtained[7–10], leading to renormalized predictions of 5–7 (refs 8, 10). These theoretical results are summarized in Methods Summary and Supplementary Information.

The production of ^{100}Sn, and the study of its decay properties, has been the aim of several experiments[11–16], but in these only a few ^{100}Sn nuclei were uniquely identified. Here we report a new measurement of the half-life and Q_{EC} value from 259 identified ^{100}Sn nuclei, which yields the smallest log(ft) value of any known β-decay (here t is the half-life and f is a phase space factor that takes into account the trivial decay energy dependence of the half-life). The Gamow–Teller strength is inversely proportional to ft and thus is greatest for the ^{100}Sn decay establishing the robustness of $N = Z = 50$ shell closures. The experimentally observed Gamow–Teller strength is well described in modern, large-scale shell model (LSSM) calculations, which are able to handle an unprecedentedly large degree of configuration mixing in the case of ^{100}Sn. This ^{100}Sn doubly magic shell closure is the benchmark for various topics currently discussed in this mass region, such as spin-aligned pairing in $N = Z$ nuclei, alpha clustering and quadrupole collectivity in the Sn isotopic chain.

Experimental details

The experiment was performed at the GSI Helmholtzzentrum für Schwerionenforschung, Germany. A ^{124}Xe beam with a kinetic energy of 1.0A GeV (A, nucleon number) and 1-s-long spills of 3×10^9 ions every 3 s was directed onto a beryllium target placed in front of the fragment separator[17]. Neutron-deficient nuclei were produced through relativistic projectile fragmentation, transmitted to the final focal plane of the fragment separator, and identified event by event (Fig. 1). The correct identification was verified by observing the γ-radiation depopulating known isomers, for example the 8^{+} isomer in ^{98}Cd. In total, 259 ^{100}Sn nuclei were unambiguously identified.

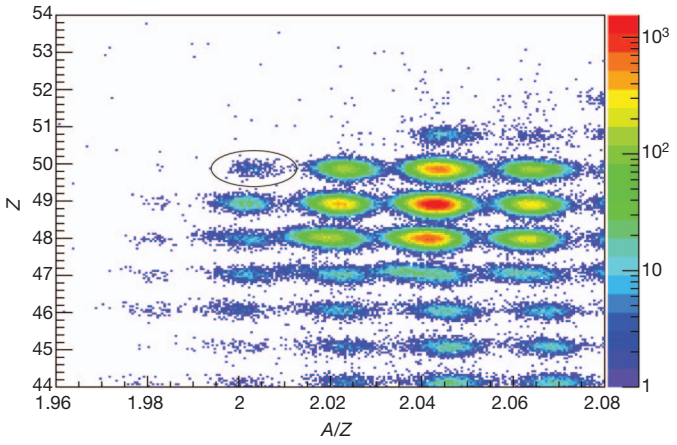

Figure 1 | Particle identification plot. Events are plotted with respect to Z and the mass-to-charge ratio, A/Z, for the full statistics of the ^{100}Sn fragment separator setting. In total, 259 ^{100}Sn nuclei (those indicated in the figure) were unambiguously identified. Resolutions (full-widths at half-maximum) in mass of $\Delta A = 0.32$ ($A = N + Z$) and in nuclear charge of $\Delta Z = 0.25$ were obtained. The colours indicate the number of events per bin in a logarithmic scale as indicated on the right-hand side.

This corresponds to a production rate of 0.75 per hour and a cross-section of 5.8 ± 2.1 pb. All uncertainties correspond to one standard deviation.

The ions were implanted into a stack of highly segmented silicon strip detectors surrounded by the RISING array, which consists of 105 germanium detectors arranged in the stopped-beam configuration[18] to detect γ-rays with high efficiency. Of the 259 identified ^{100}Sn nuclei, 163 were stopped in the 2.1-mm-thick implantation layer.

Analysis and results

Following a ^{100}Sn implantation in a pixel of the implantation zone of the silicon detector, all decay events were recorded that occurred within 15 s in that pixel or in the directly neighbouring ones. During this correlation time, it was possible to assign 126 decay chains to the 163 ^{100}Sn implantations. A maximum-likelihood (MLH) analysis with a maximum of three decay events during the correlation time was used to analyse these decay chains. The half-life of ^{100}Sn was deduced to be 1.16 ± 0.20 s in the MLH analysis using established values for the lifetimes of the daughter nuclei. The measurement is much more precise than previous experiments yielding $0.94^{+0.54}_{-0.27}$ s (ref. 14) and $0.55^{+0.70}_{-0.31}$ s (ref. 16). In Fig. 2, we show the decay curve for ^{100}Sn.

Figure 3 shows the γ-ray spectrum observed in coincidence with decay events following ^{100}Sn implantations. Notably, discrete γ-transitions from the ^{100}Sn decay could be observed. The five transitions denoted in Fig. 3 are associated with the depopulation of excited states in the daughter nucleus ^{100}In.

The statistics were sufficient only to establish a coincidence between the 436-keV and 96-keV transitions, and it is thus impossible to deduce an unambiguous level scheme for ^{100}In. Within the uncertainties, the transitions could have the same intensity, which would allow for a single cascade of five transitions from the excited 1^{+} state to the ground state. However, this would lead to an excitation energy of more than 4 MeV, which is higher than the value of about 2.5 MeV predicted with realistic shell model calculations (see, for example, refs 19, 20). The large uncertainties in the observed intensities also allow for two parallel cascades originating from this 1^{+} state.

Figure 4 shows the relevant level scheme for ^{100}In obtained from LSSM calculations. In this approach, ^{100}Sn is not treated as an inert, doubly magic core but instead excitations across the $N = Z = 50$ shell closures were allowed within the fifth ($4\hbar\omega$) harmonic oscillator shell (Methods Summary and Supplementary Information).

The states of two multiplets that are relevant for the decay are shown. The states originate in the coupling of proton (π) holes in the $g_{9/2}$ orbital either to neutron (ν) particles in the $g_{7/2}$ orbital ($\pi g_{9/2}^{-1} \otimes \nu g_{7/2}^{1}$) with total spin and parity $I^{\pi} = 1^{+}$–8^{+} or to neutron

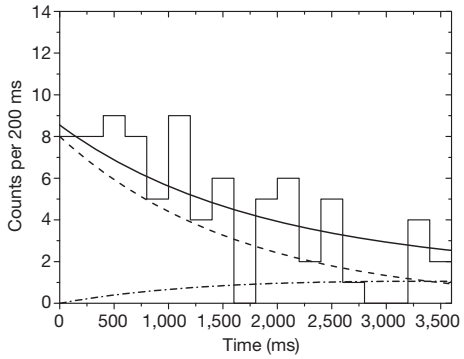

Figure 2 | Time distribution of first decay events. The histogram shows the observed time distribution of all first decay events in the nearest-neighbouring pixels after implantation of ^{100}Sn nuclei. Decay curves resulting from the MLH analysis are shown individually for ^{100}Sn (dashed) and its daughter nucleus ^{100}In (dash–dot). The solid line shows the sum of these decay curves and takes into account a small amount of random background.

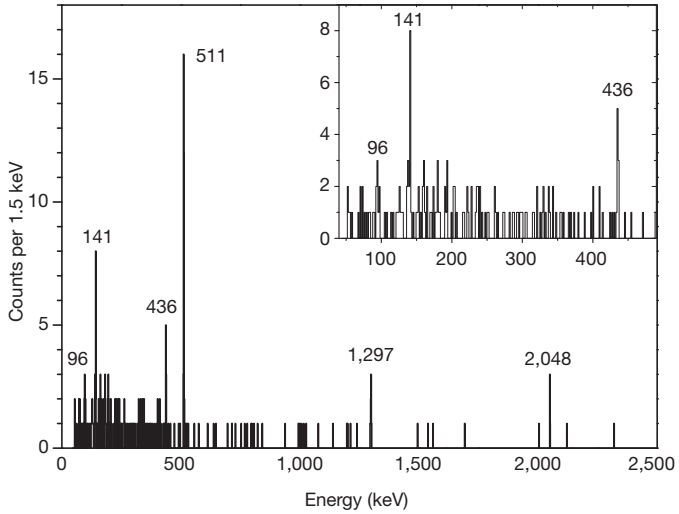

Figure 3 | Spectrum of γ-radiation. Energy distribution of the γ-radiation observed within 4 s after implantation of ^{100}Sn. With 65% probability these are directly following the ^{100}Sn decay. The other contributions are uncorrelated background decays and daughter decays of ^{100}In. None of the observed lines corresponds to known transitions from these minor contributions. The line at 511 keV is due to positron annihilation radiation. The measured absolute numbers of transitions of the five lines with the energies 96, 141, 436, 1,297 and 2,048 keV are respectively 79 ± 40, 100 ± 31, 59 ± 22, 72 ± 26 and 53 ± 26 corrected for electron conversion assuming M1 (magnetic dipole) transitions. Inset, enlarged view of the energy range up to 500 keV.

particles in the $d_{5/2}$ orbital ($\pi g_{9/2}^{-1} \otimes \nu d_{5/2}^{1}$) with $I^{\pi} = 2^{+}$–7^{+}. The predictions reflect the observed γ-ray transitions well if the high-energy, 2,048-keV, transition populates the lowest 2^{+} state, this then decays to lower-lying states via the 436-, 141- and 96-keV transitions, and the decay chain ends either in the 6^{+} ground state or a low-lying isomeric state with unobserved decay. In this picture, the second 2^{+} state is populated by the 1,297-keV transition and decays to the lower-lying 2^{+} and 3^{+} states. This may lead to a fragmentation of the intensities, making it impossible to observe these transitions in the present experiment. This picture is supported by three experimental facts: the measurement of the total γ-ray energy ($E^{*}_{1+} = 2.76 \pm 0.43$ MeV) in a previous experiment with a bismuth germanate detector[14]; the known mass difference between ^{100}Sn and ^{100}In[13], combined with our measured β-decay end-point energy ($E^{*}_{1+} = 2.6 \pm 1.0$ MeV); and our observation of a single event of β-delayed proton emission ($E^{*}_{1+} = 2.93 \pm 0.34$ MeV). It is fully consistent with the expectation that a single 1^{+} state is dominantly populated in the decay. Further details are given in Methods Summary and Supplementary Information.

As a key feature of this experiment, we measured the kinetic energy of the decay positrons fully absorbed in the compact silicon detector array. The spectrum resulting from the summed energies deposited by a β-particle in the pixels of the calorimeter up to 3 s after a ^{100}Sn implantation is shown in Fig. 5. It was fitted using a MLH analysis based on a single-component β-decay phase space function to determine the end-point energy in the decay of ^{100}Sn. For the fit of the end-point energy, only data in the energy region between 400 and 2,600 keV were used. In the analysis, corrections were applied to account for the emission of conversion electrons instead of low-energy γ-rays during the de-excitation of the daughter nucleus ^{100}In, for bremsstrahlung emitted when the positrons are slowed down and for the annihilation of positrons in flight before the deposition of their total kinetic energy. The end-point energy of the β-decay, if populating a single final state in the daughter nucleus ^{100}In, was determined to be 3.29 ± 0.20 MeV. The corresponding fraction of electron-capture decays is 13% of all ^{100}Sn decays.

Discussion

Using the measured half-life and the end-point energy, we calculated a log(*ft*) value of $2.62^{+0.13}_{-0.11}$, which is the smallest such value found so far for any nuclear β-decay. Thus, the Gamow–Teller decay of ^{100}Sn has a much larger strength than the known $0^{+} \rightarrow 0^{+}$ superallowed Fermi decays of $N = Z$ nuclei and can indeed be considered a superallowed Gamow–Teller decay[21]. This finding is also illustrated in Fig. 6, which shows the distribution of log(*ft*) values for allowed Gamow–Teller and Fermi transitions.

The extracted Gamow–Teller strength of the ^{100}Sn ground-state decay to the single excited 1^{+} state in ^{100}In is $B_{GT} = 9.1^{+2.6}_{-3.0}$. The measured value is extraordinarily large but consistent with the value of $B_{GT} = 5.8^{+5.5}_{-3.2}$ deduced from previous results for Q_{EC} and half-life[22], within the large error bars of the earlier measurement. The uncertainty in the new B_{GT} value is dominated by the uncertainty in the β-decay end-point energy. The extraction of the strength was done under the assumption that the Gamow–Teller decay was into only one final 1^{+}

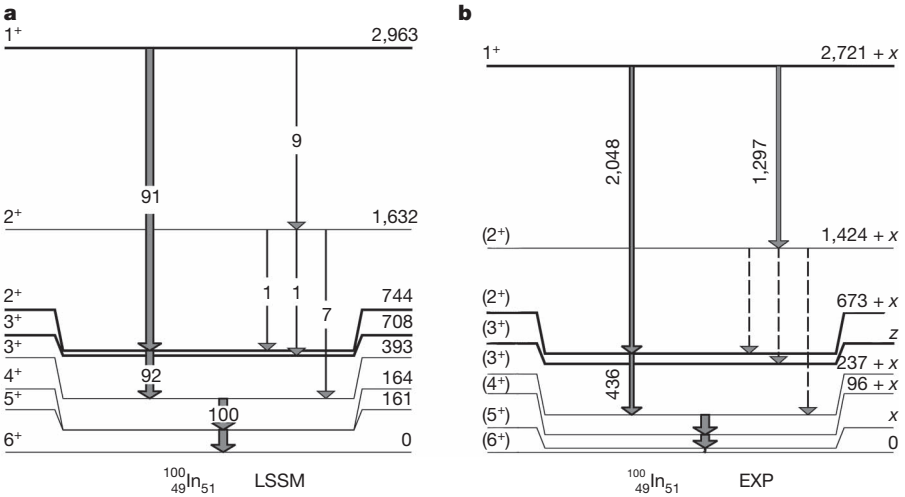

Figure 4 | Tentative level scheme of ^{100}In. **a**, LSSM calculation of the low-lying excited states in ^{100}In. Spin and parity (I^{π}) are shown on the left and energy (keV) is shown on the right. Populated levels with an almost pure $\pi g_{9/2}^{-1} \otimes \nu g_{7/2}^{1}$ configuration are indicated with bold lines, and the remaining levels are part of the $\pi g_{9/2}^{-1} \otimes \nu d_{5/2}^{1}$ multiplet. Gamma-transitions with their relative intensities (in per cent and indicated by arrow width) are shown for selected transitions. **b**, Most likely level scheme for the five observed γ-transitions in ^{100}In (three with energies (keV) shown). Because one low-energy transition might have been missed, the energy of the levels might have a systematic shift of up to $x = 80$ keV. The dashed transitions and level *z* were not observed. The assignment of spin and parity is certain only for the 1^{+} state; the others are tentative assignments based on theory.

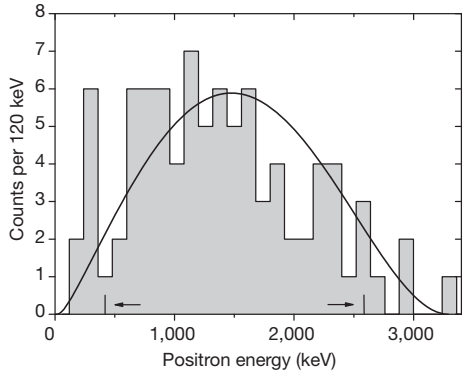

Figure 5 | Distribution of the positron energies emitted in the β-decay of ^{100}Sn. The spectrum contains only decay events that can be assigned to ^{100}Sn decays with a probability of at least 75%. The MLH fit was applied to the region between 400 and 2,600 keV, which is indicated with markers. The solid curve illustrates the shape of the best-fitting single-component β-decay phase space function determined by MLH analysis.

state in ^{100}In. However, if 1^+ states at excitation energies above the observed state were also populated, the summed Gamow–Teller strength would increase while the strength of the decay into the first excited 1^+ state would decrease. It would have been difficult to observe such higher-energy states because the reduced phase space for lower-energy β^+-particles would have led to a strongly reduced population.

The LSSM calculations, which within the *gds* harmonic oscillator shell take into account most of the long-range correlations across the $N = Z = 50$ doubly magic shell closure and include up to five particle–hole excitations (Methods Summary and Supplementary Information), yield a total summed Gamow–Teller strength of $B_{GT} = 8.19$ for all possible final states in the daughter nucleus up to 60 MeV. The standard renormalization due to correlations beyond the 0*g*, 1*d*, 2*s* model space has been applied[5]. The distribution of strength up to an excitation energy of 10 MeV is shown in Methods Summary and Supplementary Fig. 1.

A Gamow–Teller strength of $B_{GT} = 7.82$ is predicted in the experimental Q_{EC} window of 7.03(20) MeV. This corresponds to a reduction in the total renormalized Gamow–Teller strength of the extreme single-particle estimate ($B_{GT,ESPM} \approx 10$) by 18% for excitation energies up to 60 MeV and by 22% in the Q_{EC} window. It is due to mixing in the *gds* harmonic oscillator shell, that is, emptying of the proton $g_{9/2}$ orbital, pre-filling of the neutron $g_{7/2}$ orbital and destructive interference of the four possible combinations of Gamow–Teller transitions within the *g* orbital ($L = 4$). The occupation numbers of the two orbitals that are linked by the Gamow–Teller operator, which acts on spin and isospin but does not change *L*, directly influence the strength of the transition matrix element.

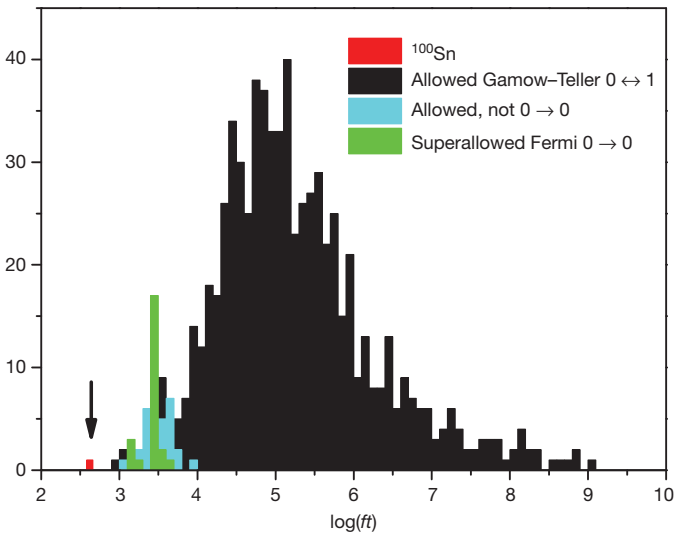

Figure 6 | Log(*ft*) values of allowed nuclear β-decays. Number distribution of log(*ft*) values for allowed β-transitions (obeying the selection rules). The data are from ref. 26. The values are for generally allowed Gamow–Teller transitions between 0^+ and 1^+ states (black), mixed Fermi/Gamow–Teller transitions (blue) and the well-established pure, superallowed Fermi transitions from 0^+ to 0^+ states (green). The decay of ^{100}Sn is unique because it has the smallest known log(*ft*) value (red) of any nuclear β-decay.

The calculation predicts that the largest fraction of the strength remains located in the first excited 1^+ state, in agreement with earlier calculations[7,21]. Nevertheless, according to our LSSM calculations it is reasonable to consider that several 1^+ states in ^{100}In are populated in the decay of ^{100}Sn. If, as an exercise, we take from the LSSM calculation the four lowest 1^+ states in ^{100}In with their energy splittings and relative Gamow–Teller strengths (Methods Summary and Supplementary Information), the value of $B_{GT}(1_1^+) = 9.1^{+2.6}_{-3.0}$ (assuming a single 1^+ state) would be reduced to $B_{GT}(1_1^+) = 7.6^{+2.2}_{-2.5}$ for the first excited 1^+ state using the experimental half-life and β-spectrum. The corresponding summed Gamow–Teller strength would be $\sum_{i=1}^{4} B_{GT}(1_1^+) = 9.9^{+2.8}_{-3.2}$. Because this exercise served only to gauge the effect of branching on the experimental B_{GT} value, no error for the branching ratios is included.

The LSSM result of $B_{GT} = 5.7$ for this first excited 1^+ state agrees within the statistical uncertainty with the value, $B_{GT} = 7.6^{+2.2}_{-2.5}$, extracted from the experimental log(*ft*) value under the above assumptions. The experimental concentration of most of the Gamow–Teller strength in the first excited 1^+ state clearly classifies the ^{100}Sn Gamow–Teller decay as superallowed. This large experimental Gamow–Teller strength of the transition to the first excited 1^+ state proves that both the ^{100}Sn ground state and the first excited 1^+ state in ^{100}In have relatively pure wavefunctions. As expected, the LSSM calculation reveals that the respective wavefunctions consist predominantly of the $\pi g_{9/2}^{10} \otimes \nu g_{7/2}^{0}$ (82% probability) and $\pi g_{9/2}^{9} \otimes \nu g_{7/2}^{1}$ (54% probability) components. The high purity of the wavefunctions within the *gds* model space establishes the simultaneous robustness of the $Z = 50$ and $N = 50$ shell closures in ^{100}Sn, which is only ~3 MeV from the proton drip line, corroborating for $N = 50$ the results of refs 23, 24, and excludes the need for explicitly treating the unbound proton orbits as continuum states.

The LSSM calculations allow enough configuration mixing in the *gds* shell that convergent results are obtained, leading to meaningful conclusions in this exotic region far from the valley of stability. This indicates that it should be possible to obtain reliable, more accurate results for nuclei in the neighbourhood of ^{100}Sn, especially close to the proton drip line.

The underlying shell structures of nuclei in the vicinity of ^{100}Sn have to be determined with the highest possible accuracy to address the important issues in nuclear structure, such as the possibility of a new coupling scheme developing in the $N = Z$ nuclei in the vicinity of ^{100}Sn (ref. 25). The present measurement is a stringent test for LSSM calculations, in which the realistic character of such a coupling scheme still needs to be probed.

A better understanding of the nuclear structure is of major importance for modelling weak interaction rates in nuclei, which depend on the underlying shell structure and are important in many astrophysical processes. For example, Gamow–Teller transitions govern electron capture during the core collapse of supernovae. Also, Gamow–Teller transitions are an essential constraint on the theoretical calculations of neutrino-less double-β-decay matrix elements, the knowledge of which is necessary to relate the neutrino mass to the rate of this yet undiscovered process. Further interest in the decay rates of nuclei around ^{100}Sn comes from the study of certain astrophysical processes, as this region has been considered the end of the rapid proton capture process due to the Sn-Sb-Te cycle.

METHODS SUMMARY

^{100}Sn and neighbouring nuclei were produced by fragmentation of a 1.0A-GeV ^{124}Xe beam from the GSI accelerators, separated in the fragment separator and identified by multiple energy-loss, magnetic rigidity and time-of-flight measurements. The nuclei were stopped in an implantation detector with high spatial resolution to correlate implantations with succeeding decays. The device was surrounded by the stopped-beam RISING array of 15×7 germanium detectors in close geometry. In this configuration, the set-up enabled us to do nearly 4π spectroscopy of the emitted γ-radiation and particle-decay radiation. With a photopeak efficiency of about 10% (1 MeV) for γ-ray detection and nearly 100% for full energy detection of decay particles up to 5 MeV, this high-resolution set-up allowed for a maximum use of the secondary beam.

The ^{100}Sn half-life and the β-decay end-point energy were calculated in the framework of a MLH analysis applied respectively to the time distribution of β-decays after implantation and the energy distribution of emitted positrons. This analysis also considered the daughter decays and the presence of uncorrelated random background decays from previous implantations.

To interpret the measured Gamow–Teller strength and the observed γ-rays emitted from ^{100}In, we carried out LSSM calculations. The valence space used in the LSSM consists of the fifth ($4\hbar\omega$) harmonic oscillator shell, that is, proton and neutron $\pi\nu(g,d,s)$ orbitals outside the ^{80}Zr core. The calculations included up to five particle–hole excitations from the $g_{9/2}$ proton and neutron orbitals to the rest of the shell, which made it possible for us to obtain convergent results for excitation spectra and the Gamow–Teller strength.

Received 28 October 2011; accepted 2 April 2012.

1. Ichimura, M., Sakai, H. & Wakasa, T. Spin-isospin responses via (p,n) and (n,p) reactions. *Prog. Part. Nucl. Phys.* **56,** 446–531 (2006).
2. Hardy, J. C., Carraz, L. C., Jonson, B. & Hansen, P. G. The essential decay of pandemonium: a demonstration of errors in complex beta-decay schemes. *Phys. Lett. B* **71,** 307–310 (1977).
3. Audi, G., Wapstra, A. H. & Thibault, C. The Ame2003 atomic mass evaluation: (II). Tables, graphs and references. *Nucl. Phys. A* **729,** 337–676 (2003).
4. Sasano, M. *et al.* Gamow-Teller transition strengths from ^{56}Ni. *Phys. Rev. Lett.* **107,** 202501 (2011).
5. Caurier, E., Martínez-Pinedo, G., Nowacki, F., Poves, A. & Zuker, P. A. The shell model as a unified view of nuclear structure. *Rev. Mod. Phys.* **77,** 427–488 (2005).
6. Brown, B. A. The nuclear shell model towards the drip lines. *Prog. Part. Nucl. Phys.* **47,** 517–599 (2001).
7. Brown, B. A. & Rykaczewski, K. Gamow-Teller strength in the region of ^{100}Sn. *Phys. Rev. C* **50,** R2270–R2273 (1994).
8. Dean, D. J., Koonin, S. E., Kuo, T. T. S., Langanke, K. & Radha, P. B. Complete $0\hbar\omega$ shell model Monte Carlo calculations of ^{94}Ru, ^{96}Pd, ^{96,98}Cd and ^{100}Sn. *Phys. Lett. B* **367,** 17–20 (1996).
9. Bobyk, A., Kaminski, W. & Borzov, I. N. Gamow-Teller beta-decay strengths of neutron-deficient tin isotopes: comparison of FFST and pnBCS+QRPA results. *Acta Phys. Pol. B* **31,** 953–963 (2000).
10. Batist, L. *et al.* Systematics of Gamow-Teller beta decay "Southeast" of ^{100}Sn. *Eur. Phys. J. A* **46,** 45–53 (2010).
11. Schneider, R. *et al.* Production and identification of ^{100}Sn. *Z. Phys. A* **348,** 241–242 (1994).
12. Lewitowicz, M. *et al.* Identification of the doubly-magic nucleus ^{100}Sn in the reaction ^{112}Sn+^{nat}Ni at 63 MeV/nucleon. *Phys. Lett. B* **332,** 20–24 (1994).
13. Chartier, M. *et al.* Mass measurement of ^{100}Sn. *Phys. Rev. Lett.* **77,** 2400–2403 (1996).
14. Sümmerer, K. *et al.* Identification and decay spectroscopy of ^{100}Sn at the GSI projectile fragment separator FRS. *Nucl. Phys. A* **616,** 341–345 (1997).
15. Stolz, A. *et al.* Projectile fragmentation of ^{112}Sn at E_{lab} = 1A GeV. *Phys. Rev. C* **65,** 064603 (2002).
16. Bazin, D. *et al.* Production and beta-decay of rp-process nuclei ^{96}Cd, ^{98}In, and ^{100}Sn. *Phys. Rev. Lett.* **101,** 252501 (2008).
17. Geissel, H. *et al.* The GSI projectile fragment separator (FRS): a versatile magnetic system for relativistic heavy ions. *Nucl. Instrum. Methods B* **70,** 286–297 (1992).
18. Pietri, S. *et al.* Recent results in fragmentation isomer spectroscopy with rising. *Nucl. Instrum. Methods B* **261,** 1079–1083 (2007).
19. Plettner, C. *et al.* Beta decay of ^{100}In. *Phys. Rev. C* **66,** 044319 (2002).
20. Coraggio, L., Covello, A., Gargano, A. & Itaco, N. Structure of particle-hole nuclei around ^{100}Sn. *Phys. Rev. C* **70,** 034310 (2004).
21. Hamamoto, I. & Sagawa, H. Gamow-Teller beta decay and isospin impurity in nuclei near the proton drip line. *Phys. Rev. C* **48,** R960–R963 (1993).
22. Faestermann, T. *et al.* Decay studies of N ≈ Z nuclei from ^{75}Sr to ^{102}Sn. *Eur. Phys. J. A* **15,** 185–188 (2002).
23. Blazhev, A. *et al.* Observation of a core-excited E4 isomer in ^{98}Cd. *Phys. Rev. C* **69,** 064304 (2004).
24. Boutachkov, P. *et al.* High-spin isomers in ^{96}Ag: excitations across the Z = 38 and Z = 50, N = 50 closed shells. *Phys. Rev. C* **84,** 044311 (2011).
25. Cederwall, B. *et al.* Evidence for a spin-aligned neutron–proton paired phase from the level structure of ^{92}Pd. *Nature* **469,** 68–71 (2011).
26. Singh, B., Rodriguez, J. L., Wong, S. S. M. & Tuli, J. K. Review of log*ft* values in β-decay. *Nucl. Data Sheets (N.Y. N.Y.)* **84,** 487–563 (1998).

Supplementary Information is linked to the online version of the paper at www.nature.com/nature.

Acknowledgements We thank the staff of the GSI ion source and accelerator for the preparation of a stable, high-intensity ^{124}Xe beam, and we thank the fragment separator technicians for setting up the beamline detectors. We acknowledge discussions with G. Martínez-Pinedo, K. Langanke and A. Zuker. We are also grateful to the EUROBALL Owners Committee for the use of the Euroball Cluster Detectors. This work was supported by the BMBF under contracts 06MT238, 06MT9156, 06KY205I and 06KY9136I; by the GSI; by the DFG Cluster of Excellence 153 'Origin and Structure of the Universe'; by the EC within the FP6 through I3-EURONS (contract no. RII3-CT-2004-506065); and by the Swedish Research Council.

Author Contributions Fragment separator: H.W., P.B., H. Geissel, M.G., Zs.P. and C.N.; particle detectors: C.B.H., K. Straub, R.G., T.F., L.M. and F. Nebel; RISING γ-array: P.B., M.G., S.P., J.G., I.M.K. and H.-J.W.; data acquisition and analysis software: M.B., R.G., J.L.G., N.K. and L.M.; data analysis and interpretation: C.B.H., K. Straub, T.F., M.G., H. Grawe, R.K., K. Steiger, F. Nowacki and K. Sieja; shell model calculations: F. Nowacki and K. Sieja; writing of manuscript: C.B.H., T.F., R.G., H. Grawe, R.K., F. Nowacki and K. Sieja. All authors except H. Grawe, F. Nowacki and K. Sieja took part in the preparation and the experiments, and all authors commented on the final paper.

Author Information Reprints and permissions information is available at www.nature.com/reprints. The authors declare no competing financial interests. Readers are welcome to comment on the online version of this article at www.nature.com/nature. Correspondence and requests for materials should be addressed to T.F. (thomas.faestermann@ph.tum.de).

APPLICATION OF DIAMOND DETECTORS IN TRACKING OF HEAVY ION SLOWED DOWN RADIOACTIVE BEAMS*

P. Bednarczyk[a,b], E. Berdermann[a], J. Gerl[a], M. Górska[a]
I. Kojouharov[a], M. Pomorski[a], M. Rębisz[a], B. Voss[a], L. Acosta[c]
R. Berjillos[c], I. Martel[c], M.A.G. Alvarez[d], J.M. Espino[d]
J.L. Flores[d], I. Mukha[d], R. Wolski[b,e]

[a]GSI Darmstadt, Germany
[b]IFJ PAN Kraków, Poland
[c]University of Huelva, Huelva, Spain
[d]University of Seville, Seville, Spain
[e]JINR, Dubna, Russia

(Received November 6, 2006)

Results of irradiation of thin Chemical Vapor Deposition (CVD) diamond detectors with low energy: p, α and ^{7}Li beams are presented. Energy resolution: $\Delta E/E < 1\%$ of a single crystal detector was achieved. A coincident measurement with two diamond detectors showed time resolution of 100 ps and efficiency above 70%. Despite a high beam flux reaching 10^9 particles/s cm^2 the tested detectors showed low dead-time and satisfactory radiation hardness. Perspectives of applying thin CVD diamond detectors in monitoring of a slowed down radioactive beam (RIB) are discussed.

PACS numbers: 29.30.Ep, 29.40.–n, 29.40.Gx, 29.40.Wk

1. High resolution γ-ray spectroscopy at slowed down RIBs

Significant progress in prompt γ-ray spectroscopy of rare nuclei was achieved at the RISING setup in GSI due to availability of relativistic RIBs produced in flight [1]. In addition, delayed γ-decay studies of stopped fragments at RISING were successful [2]. However, use of RIBs slowed down to a Coulomb barrier energy would open a new perspective in in-beam γ-spectroscopy studies of nuclei far off stability accessible by transfer reactions, deep inelastic collisions and, in some cases, fusion–evaporation reactions.

* Presented at the Zakopane Conference on Nuclear Physics, September 4–10, 2006, Zakopane, Poland.

At the planned radioactive beam facility NUSTAR [3] we aim at high resolution γ-spectroscopy measurements with secondary RIBs at energies close to the Coulomb barrier limit of 5AMeV. Relativistic radioactive fragments created in flight will be selected in the Low Energy Branch of the SFRS separator [4] and slowed down in a series of degraders. In turn, they will induce a nuclear reaction on a target. Due to the superior SFRS transmition, the secondary beam intensity can reach 10^8 particles/s. However, a significant spread in the projectile energy and position is expected. Detection of prompt γ-radiation emitted from the reaction target will employ novel techniques that incorporate pulse shape analysis and tracking of scattered photons. Nonetheless, for efficient Doppler shift compensation exact information about the velocity vector and the position of every projectile at the target has to be determined. Detectors suitable for the RIB tracking shall provide: *(i)* good energy resolution and minimum ion energy absorption, *(ii)* excellent timing properties, *(iii)* high efficiency and low dead-time, *(iv)* radiation hardness. In this context, thin diamond polycrystalline (PC) or single crystal (SC) CVD detectors [5] attract lots of attention. Recently, it was shown that SC CVD diamonds permitted of detection of α-particles from a ^{241}Am source with good energy resolution, comparable with Si detectors [6]. On the other hand, time of flight measurements of relativistic heavy ions demonstrated that a time accuracy of PC and SC CVD diamond sensors is significantly better than 100 ps [7, 8].

2. Performance of CVD diamond detectors in beam

Here, we report on an in-beam evaluation of a CVD diamond detector sensitivity on low energy and high intensity ion beams: p, α and ^{7}Li at energies of 5.8 MeV, 8.7 MeV and 11.2 MeV, respectively, delivered by the CNA-Seville 3 MV tandem accelerator [9]. SC and PC CVD diamond detectors of a size of $4\times4\,\mathrm{mm}^2$ and $1\times1\,\mathrm{cm}^2$ respectively, and various thicknesses were tested. The projectiles, were Rutherford scattered on thin Al, Pb and Au targets. A SC CVD diamond detector of 500 μm thickness was positioned at 70° with respect to the beam direction. Output signals were shaped in a standard charge sensitive preamplifier. The measured energy spectra of the scattered protons are presented in Fig. 1(A). The peak shift and broadening resulted from the target element composition and the energy spread due to the target thickness, as indicated in the picture. However, the spectrum measured for the 1μm Al target demonstrates rather narrow distribution of 50 keV at the FWHM, reaching the energy of 5.55 MeV. These values correspond rather well to the calculated energy spread and the maximum scattered proton energy. Therefore, one may conclude that the intrinsic energy resolution of the SC CVD diamond is better than 50 keV.

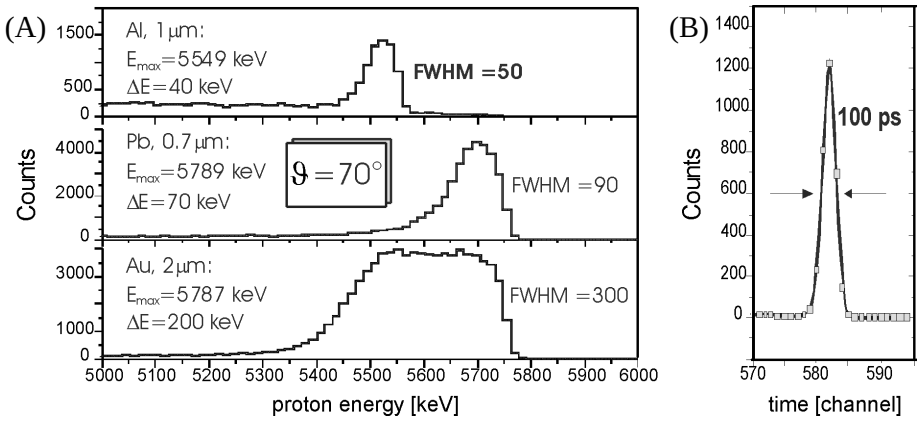

Fig. 1. (A) Energy spectra of 5.8 MeV protons elastically scattered from different targets, detected by a 500μm SC CVD diamond detector at 70°. The calculated maximum energy and the peak broadening are indicated. The intrinsic detector energy resolution is below 50 keV, thus better than 1%. (B) Time correlation spectrum of two SC CVD diamond detectors of 110μm and 300μm thickness, mounted in a stack, irradiated by the scattered proton beam. The time resolution of 100 ps at the full width half maximum and efficiency above 70% were measured.

A stack consisting of a 110μm and 300μm SC CVD diamond detectors was mounted at the angle of 90°. The protons scattered on the Pb target crossed over the thinner detector, loosing half of the kinetic energy and were stopped in the second diamond. Pulses from both detectors were fed into broad band voltage-sensitive preamplifiers DBA2 [10] that provided signals with a few tens ps rise-time. The coincidence rate was 70% of singles, in part due to the detectors misalignment. Leading edge discriminators were used to determine the signal timing. The telescope time correlation spectrum is shown in Fig. 1(B). One clearly sees a coincident peak of only 100 ps at the FWHM, even though a walk correction for such fast signals was not feasible.

The scattering setup was used to measure a time correlation between a PC CVD diamond detector of 13μm thickness and the 300μm SC CVD diamond, mounted in a stack. The ^{7}Li beam irradiated the Pb target. The projectile range in diamond was 16μm, the distance comparable with the PC detector thickness. Therefore, one expected high energy deposition of about 10 MeV in this detector. Indeed, despite low charge collection efficiency in a PC diamond, a signal of sufficient amplitude was generated. Although ^{7}Li ions entered into the second SC CVD diamond with energy below 1 MeV, one could clearly see coincident signals from the two detectors. As in the previous case, the PC and the SC diamonds exhibited very good correlation with the time resolution within the 10^2 s range.

To clarify the diamond detectors ability of detecting ions at high rates the 300 μm SC CVD diamond detector was exposed to direct proton and α-particle beams. The minimum stable current extracted from the accelerator corresponded to a beam flux of the order of 10^7–10^9 particles/s cm^2. Although the irradiation lasted several minutes, DBA2 preamplified signals monitored on a fast digital oscilloscope exhibited no signs of degradation or noisiness. Negligible leakage current was registered. The detector allowed for a clear distinction of two consecutive signals separated by 10 ns that would correspond to a continuous rate of 100 MHz.

3. Summary of obtained results and further perspectives

In the course of the described experiment SC and PC CVD diamond detectors were tested in low energy ion beams. The SC detectors showed excellent performance revealing the energy and time resolution being of 1% nad 100 ps respectively and efficiency above 70%, even at very low energies of the impinging particles. In this respect, PC detectors have comparable timing properties if the charge induced in the diamond was high. The tested detectors showed low dead-time and satisfactory radiation hardness allowing for effective operation even at 100 MHz charged particle rate. In the light of the current work use of SC CVD diamonds in low energy ion beam tracking is promising. However, availability of very thin single crystal diamond films of surfaces larger than 1 cm^2 is still limited. On the other hand, heavier ions may generate a charge in a PC diamond sufficient for measurements with satisfactory energy resolution. This issue needs a further clarification.

This work was partially supported by the Spanish Ministry of Education and Science (MEC) projects: FFPA2003-05958 and PA-2005-04460.

REFERENCES

[1] M. Górska *et al., Acta Phys. Pol. B* **38**, 1219 (2007), these proceedings.
[2] S. Pietri *et al., Acta Phys. Pol. B* **38**, 1255 (2007), these proceedings
[3] B. Rubio, T. Nilsson, *Nucl. Phys. News Int.* **16/1**, 9 (2006).
[4] H. Geissel *et al., Nucl. Instrum. Methods* **B204**, 71 (2003).
[5] W. Adam *et al., Nucl. Instrum. Methods* **A514**, 79 (2003).
[6] M. Pomorski *et al., Phys. Status Solidi* **A202**, 2199 (2006).
[7] A. Stolz *et al., Diamond Relat. Mater.* **15**, 807 (2006).
[8] M. Pomorski *et al., Phys. Status Solidi* **A203**, 3152 (2006).
[9] J. Garcia Lopez *et al., Nucl. Instrum. Methods* **B161**, 1137 (2000).
[10] P. Moritz *et al., Diam. Relat. Mater.* **10**, 1765 (2001).

DEVELOPMENT OF SLOWED DOWN BEAMS AT THE FRAGMENT SEPARATOR FOR FAIR*

F. Naqvi[a,b], P. Boutachkov[b], M. Górska[b], J. Gerl[b], F. Farinon[b]
E.T. Gregor[b,c], K. Hadynska[d], A. Jhingan[b,e], R. Janik[f]
I. Kojouharov[b], N.A. Kondratyev[g], M.A.G. Alvarez[h]
I. Mukha[b], P. Napiorkowski[d], C. Nociforo[b], D. Pietak[d]
W. Prokopowicz[b], S. Pietri[b], A. Prochazka[b], H. Schaffner[b]
P. Strmen[f], H. Weick[b], H.J. Wollersheim[b]

[a]Institut für Kernphysik, Universität zu Köln, Köln, Germany
[b]Helmholtzzentrum für Schwerionenforschung, Darmstadt, Germany
[c]Technische Universität Darmstadt, Darmstadt, Germany
[d]Faculty of Physics, University of Warsaw, Warsaw, Poland
[e]Inter-University Accelerator Centre, New Delhi, India
[f]Comenius University, Bratislava, Slovakia
[g]Flerov Laboratory of Nuclear Reactions, JINP, Dubna, Russia
[h]Centro Nacional de Aceleradores CNA, Seville, Spain

(Received February 10, 2011)

The feasibility studies of the slowed down beam setup involving deceleration of a ^{64}Ni beam at 250 MeV/u to 13 MeV/u in a thick Al degrader was performed at the FRagment Separator (FRS) at GSI. The experimentally measured energy spread and the nuclear reaction yields in the degrader are in good agreement with simulations.

DOI:10.5506/APhysPolB.42.725
PACS numbers: 07.05.Fb

1. Introduction

The GSI/FAIR [1] facility will provide high-intensity beams of relativistic ions. Secondary beams of radioactive nuclei can be produced by in-flight projectile fragmentation or fission. With the beam currents planned for FAIR we expect radioactive beams at the final focal plane of the Super-FRS [2] with intensities sufficient for nuclear spectroscopy and reaction studies at energies around the Coulomb barrier. The low beam energy will be obtained

* Presented at the Zakopane Conference on Nuclear Physics "Extremes of the Nuclear Landscape", August 30–September 5, 2010, Zakopane, Poland.

by slowing down relativistic beam ions in a thick degrader. In contrast to the ISOL facilities, in experiments involving such slowed down beams, short lived fragments can be accessed with high survival rate after the deceleration. The high angular momentum transfer at Coulomb barrier energies opens a new field of high-spin investigations at the in-flight separation facilities. In the presented feasibility study, the characteristics of a primary ^{64}Ni beam after deceleration were investigated with a detector system optimized for an event-by-event identification at Coulomb barrier energies.

2. Simulations

Interactions of fragments penetrating through the matter govern the energy and angular straggling of the slowed down beams. The simulated values given by the MOCADI code [3] for a primary ^{64}Ni beam at 250 MeV/u, slowed down to 13 MeV/u in a homogeneous Al degrader of 3.95 g/cm^2 are shown in Fig. 1. A typical initial energy spread (σ_E/E) of 0.1% was assumed for the beam. The considerable energy and angular spread makes it necessary to track the ions after the degrader on an event-by-event basis. During the deceleration nuclear reactions also occur which lead to the production of unwanted isotopes. The simulated yields of the reaction products in the degrader are illustrated in Fig. 2 as a function of the beam energy. The integrated background contribution amounts to $\sim$ 1% of the slowed down ^{64}Ni ions in an energy window of $\pm$0.5 MeV/u at 13 MeV/u. This energy window corresponds to the time resolution of the TOF detectors used in the present experiment. All the parameters of the simulation take into account the detailed technicalities of the experimental setup discussed in next section.

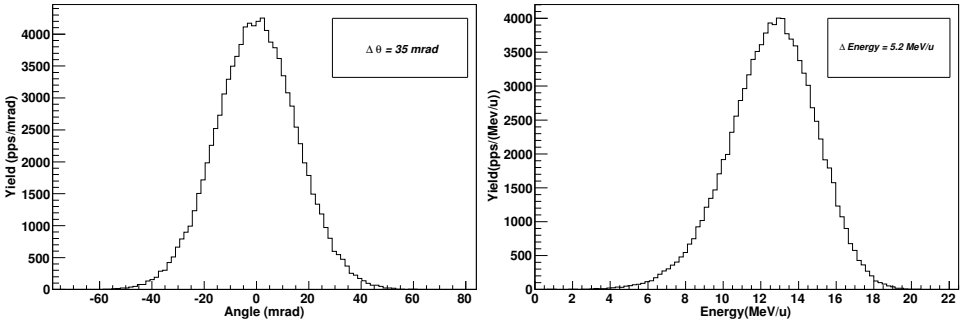

Fig. 1. Simulated angular spread (left) and energy straggling (right) of a ^{64}Ni beam after slowing down from 250 MeV/u to 13 MeV/u in a 3.95 g/cm^2 Al degrader.

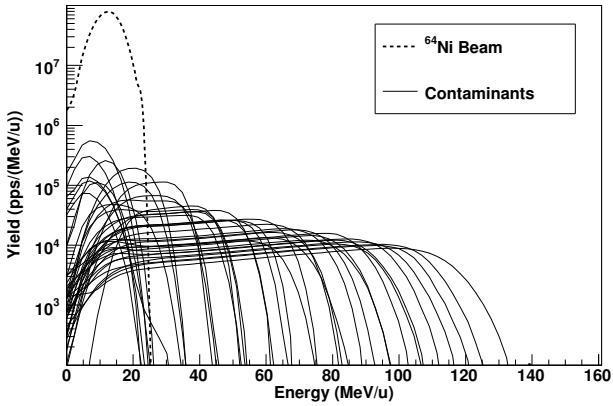

Fig. 2. The dominant curve (dashed) represents slowed down ^{64}Ni ions and the contaminants from nuclear reactions in Al degrader are shown in solid curves.

3. Experimental setup and results

In the present experiment a primary ^{64}Ni beam at 250 MeV/u was slowed down in a 3.95 g/cm^2 Al degrader at the FRS. The experimental setup is shown in Fig. 3 which consists of a plastic scintillator, a degrader, two position sensitive micro-channel plate (MCP) [4] detectors and a silicon (Si) detector. The Si detector was used for a rough estimate of the beam en-

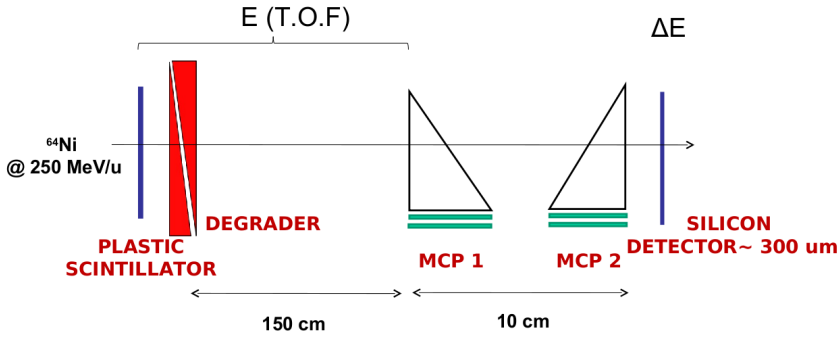

Fig. 3. Schematic setup for the slowed down beam experiment.

ergy during the measurement. The proper beam velocity after the degrader was obtained from the Time-of-Flight (TOF) measurement between the fast scintillator and the MCP detectors. The extracted energy distribution (from TOF measurement) of the ^{64}Ni ions after the degrader is shown in Fig. 4. The width of the energy distribution is 8 MeV/u (FWHM). In order to estimate the background underneath the ^{64}Ni energy peak, the simulated background distribution (see Fig. 2) was scaled to the observed distribution

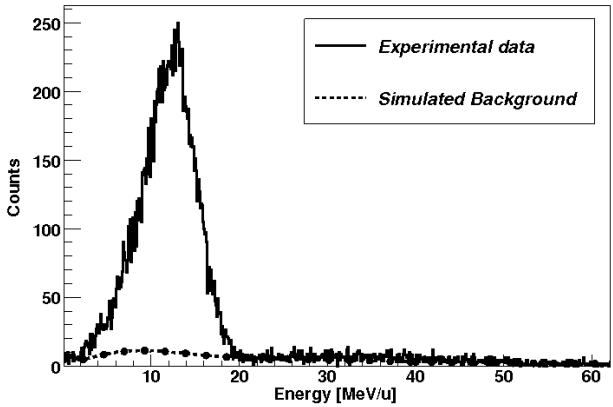

Fig. 4. Energy distribution of ^{64}Ni ions after slowing down in Al degrader. A final energy of 13 MeV/u was obtained with a width of 8 MeV/u. The dashed curve represents the simulated background.

in the range of 20–60 MeV/u. This resulted in a peak-to-background ratio of 2% in an energy range of 13 ± 0.5 MeV/u. The survival rate of the ^{64}Ni ions after passing through the degrader was 80% which agrees well with the simulations [5]. Unfortunately, the angular straggling could not be determined in the present experiment due to the limited size of the tracking detectors, positioned downstream from the degrader. In the final experimental setup the Si detector will be replaced by a $\Delta E - E$ telescope to identify the reaction products.

In conclusion, the presented experimental results are in good agreement with the performed simulations and hence, support the suitability of the slowed down beams for secondary reactions.

REFERENCES

[1] www.fair-center.org
[2] www.gsi.de/GSI-Future/cdr/
[3] N. Iwasa *et al.*, *Nucl. Instrum. Methods Phys. Res.* **B126**, 284 (1997).
[4] G. Montagnoli *et al.*, *Nucl. Instrum. Methods* **A547**, 455 (2005).
[5] P. Boutachkov *et al.*, Annual report 2007, GSI, p. 215.